## UC Berkeley
**UC Berkeley Electronic Theses and Dissertations**

**Title**
Static and Seismic Performance of California Levees

**Permalink**
https://escholarship.org/uc/item/0t8051w3

**Author**
Shriro, Michelle Jennifer

**Publication Date**
2014

Peer reviewed|Thesis/dissertation

Static and Seismic Performance of California Levees

By

Michelle Jennifer Shriro

A dissertation submitted in partial satisfaction of the

requirements for the degree of

Doctor of Philosophy

in

Engineering - Civil and Environmental Engineering

in the

Graduate Division

of the

University of California, Berkeley

Committee in charge:

Professor Jonathan Bray, Chair
Professor Nicholas Sitar
Professor Douglas Dreger

Spring 2014

Abstract

Static and Seismic Performance of California Levees

by

Michelle Jennifer Shriro

Doctor of Philosophy in Engineering - Civil and Environmental Engineering

University of California, Berkeley

Professor Jonathan D. Bray, Chair


This study has two main thrusts. The first part of the study addresses static seepage and stability of California levees as related to the presence of woody vegetation. The second part of this study addresses seismic deformations related to California levees through calibration, validation, and sensitivity analysis of a constitutive model implemented to capture seismic embankment deformations.

Two field tests were conducted to investigate the effects of seepage in the vicinity of live and decaying tree root systems to examine the effects of live and decaying root systems on levee seepage and slope stability. The first field test involved the construction of parallel trenches in the vicinity of a eucalyptus stump located along the landside of the northern levee bordering the American River adjacent to the California Exposition and State Fair. A live hackberry tree with healthy roots was present at the toe of the levee. A control set of parallel trenches was constructed away from the eucalyptus stump. During the test, the upslope trench was flooded and maintained at constant head to induce slope-parallel seepage and the downslope trench was used to make observations and collect any intercepted seepage. Piezometers and tensiometers were installed to measure positive and negative pore water pressures within the zone of flow to describe the wetting and flow patterns as they evolved within the levee. Instrumentation was installed to assess the influence of the stump and its decomposing root system. Live roots, mammal burrows, and other features added complexity to the system. In addition to instrumentation data, visual observations were recorded during the 6 day flow test. During the flow test, wetting front and water flow patterns appeared to be dominated by flow through a network of shallow mammal burrows. Physical observation of the saturation front, as seen from the lower wall, confirmed that the area below the stump was the last location to saturate during the wetting test. Ground-based tripod light detection and ranging (T-LiDAR) was used to complement traditional logging and for constructing a 3D model of the root system,

burrows and stratigraphy. Preliminary computer simulations of the advance of the wetting front support the basic patterns observed in the field test.

The second field experiment was conducted along the crown of a bypassed levee along an oxbow segment of the Sevenmile Slough on Twitchell Island, Rio Vista, California. An 8-foot deep crown trench was excavated into the levee crown to intersect the root system of a land side live oak tree, a water side valley oak tree, and a control section. The test was designed to evaluate the effects of seepage in the vicinity of live tree root systems. During the test, the crown trench was flooded and maintained at constant head to simulate a flood condition with water delivered from the center of the levee. Piezometers and tensiometers were installed to measure positive and negative pore water pressures, respectively, within the zone of flow to describe the wetting and flow patterns as they evolved within the levee. Burrow networks, fracturing, and void space within the levee soil matrix, as well as variability of stratigraphic conditions across the site added complexity. Visual observations were made during the flow test to view surficial seepage and flow patterns from the surface in addition to continuous monitoring of subsurface instruments. The site contained an extensive network of muskrat burrows in addition to burrows by other species and the initial advance of the wetting front appeared to be related to burrowing activity. With increased time and saturation of levee soils, flow through macropores appeared to diminish. The levee appears to have been founded on overbank deposits composed of lower permeability soils than the overlying levee fill. Water appeared to accumulate on this stratigraphic layer, driving seepage patterns on the landside of the levee. A discontinuity in these low permeability overbank deposits affected flow patterns, while the slope of this layer toward the discontinuity appears to have added a three dimensional aspect to flow patterns. Cracking was observed in the crown road along the levee crest within the first 24 hours of the flow test. After approximately 40 hours of flow, the waterside oak tree, initially leaning at an angle of approximately 44 degrees from horizontal, rotated an additional approximately 20 degrees into the adjacent slough, creating cracks and deformation along the waterside slope. A dye test was performed as a part of the experiment to better understand the extent of the burrows, their effect on flow patterns, and to better evaluate the role of these burrow networks in the deformations observed on the waterside slope during the flow test. Ground-based tripod light detection and ranging (T-LiDAR) technology was used to complement our efforts related and track deformations during the test.

Based on calibrated numerical simulations, trees were found not to play a significant role in seepage-induced rotational or block failure of the levee slopes. However, where trees exhibit significant lean (center of mass extends beyond the fulcrum of the root plate), horizontal roots extending into the levee may place additional loads on the levee embankment. Loading of this type can be incorporated into two dimensional slope stability

analyses, using mass-averaging to capture the three-dimensional impact of the tree. Tree overturning was evaluated at the waterside oak tree. Root forces were represented as a single horizontal force and a single vertical force. Horizontally oriented tree root loading increased faster than vertical loading in response to increasing slope angle, while the reverse was true for tree lean where vertical root forces increased more rapidly with increasing tree lean. The method was implemented and successfully captured the observed landside and waterside tree responses during the Crown Trench Seepage Test.

The second part of this research focused on seismically induced permanent displacement of earth levees, embankments, and earth-fill slopes resulting from liquefaction below these earth structures. Deformations of this nature are not well captured in current seismic design practice. Ground remediation can be employed to reduce the hazards resulting from soil liquefaction for cases where the analytical tools predict poor seismic performance. There are not sufficient funds to repair all vulnerable levees in the system. Thus, robust analytical procedures are required to evaluate sections of levees where liquefiable foundation materials may lead to significant damage.

Inertially driven ground movements of intermediate levels are the primary focus of this study. In these cases, the post-liquefaction static stability of the earth slope is greater than one, and seismically induced permanent displacements result primarily from earthquake shaking after liquefaction is triggered. Limited lateral spreads involving liquefaction of medium dense sand can produce seismic displacements on the order of several centimeters to a meter or more. These levels of seismic displacements are sufficient to damage severely levees. The most commonly employed simplified method for evaluation of seismic deformation at these intermediate levels relies on the concept post-liquefaction residual shear strength. For many practical cases, residual shear strength is ill-defined due to the ever changing resistance provided by soils that undergo repetitive dilative responses during cyclic loading. Where liquefied soils are sufficiently strong to resist flow failures, engineers lack satisfactory tools to evaluate the seismic performance of earth structures that overlie liquefiable soils.

A nonlinear soil constitutive model (UBCSAND), which was developed by Professor Byrne and implemented in the finite difference program FLAC, is employed to evaluate seismic deformations of earth structures resulting from liquefaction-induced lateral movements. Analyses of one-element laboratory tests are performed first to develop trends within the UBCSAND soil model calibration parameters. The basic model parameters are correlated to $(N_1)_{60}$ values. The UBCSAND model also has four "fitting" parameters. Two of the four model parameters are varied in this study to evaluate the sensitivity of the results to these variations. Triggering is captured with values of the m_hfac1 parameter with a typical range of 0.5 to 2.0 depending on relative density, CSR, and initial static shear stress.

The trends identified are implemented in the back-analysis of several case histories, and the ability of the UBCSAND model within the program FLAC to capture observed deformations is evaluated. The numerical simulations of seismic performance at Moss Landing Marine Laboratory and Monterey Bay Aquarium Research Institute during the 1989 Loma Prieta Earthquake and at the Juvenile Hall Facility during the 1971 San Fernando Earthquake are shown to capture well the key features of these case histories.

The study was generalized through a broader sensitivity study to investigate the seismic performance of earthen embankments built atop potentially liquefiable soils. Several representative levee sections on differing foundations are analyzed, wherein key characteristics, such as the thickness of the liquefiable layer and its relative density, are systematically varied to develop useful insights. The thickness of the liquefiable foundation layer impacted displacements in a non-linear pattern where displacement increased more rapidly as the liquefiable material layer thickness increases. As would be expected, combinations of thicker deposits of liquefiable foundation soils combined with higher embankments yielded the maximum displacement of the cases analyzed in this study.

A suite of nine near-fault, forward-directivity, fault-normal soil earthquake ground motions and seven intermediate-field soil earthquake ground motions are used to reflect the seismic hazards most likely to control the design of levees within the San Joaquin-Sacramento delta region of California. The intense forward-directive 1994 Northridge Sylmar Converter Station motion yielded approximately twice as much displacement as the lower intensity backward-directive 1992 Landers Joshua Tree motion. The rate of increase of the calculated liquefaction-induced displacement with increasing Arias intensity was roughly linear for these embankment configurations for the entire suite of earthquake ground motions

# TABLE OF CONTENTS

## LIST OF FIGURES

vi

viii

xvii

## LIST OF TABLES

## APPENDICIES

Appendix 2A – Soil Borings and Instrumentation Logs ; Cal Expo Test Site

Appendix 2B – Regional Soil Data; Cal Expo Test Site

Appendix 2C – Trench Logs; Cal Expo Test Site

Appendix 2D – Instrument Data; Cal Expo Test Site

Appendix 2E – Field Characterization Test Logs; Cal Expo Test Site

Appendix 3A – Soil Borings and Instrumentation Logs; Twitchell Island Test Site

Appendix 3B– Laboratory Testing; Twitchell Island Test Site

Appendix 3C– Cone Penetration and Pore Pressure Dissipation Testing; Twitchell Island Test Site

Appendix 3D – Regional Soil Data; Twitchell Island Test Site

Appendix 3E – Trench Logs; Twitchell Island Test Site

Appendix 3F– Instrument Data; Twitchell Island Test Site

Appendix 4A – Slope Stability Model Results; Twitchell Island Test Site

# CHAPTER 1

## Introduction

The devastating flooding of New Orleans resulting from Hurricane Katrina brought to light the fragility of levee systems across the United States. The years following this disaster have brought a renewed focus on public safety and a closer look at policies, standards, and conditions of existing levee systems.

In California, there are approximately 1,345 miles of levees protecting 750,000 acres of lowland in the Sacramento-San Joaquin Delta and the Suisun Marsh, about a third of which are Project Levees (eligible for federal flood control funding). The remaining levees are considered local levees maintained by local reclamation districts with supplemental financing for maintenance and emergency response through the State of California. Given the proximity of the Delta to the highly seismic San Francisco Bay Area, a major earthquake in the region could have extensive consequences for California's water supply as well as impacts to the environment, recreation, agriculture, local residents and businesses and other infrastructure.

In 2006, a statewide effort was initiated in California to evaluate levee risk, spawning the ongoing urban and non-urban levee evaluations programs (ULE and NULE, respectively). The California Department of Water Resources is evaluating 470 miles of urban and 1620 miles of non-urban levees as part of these programs (DWR, 2014).

In 2009, the United States Army Corps of Engineers (USACE) released the document "Guidelines for Landscape Planting and Vegetation Management at Levees, Floodwalls, Embankment Dams, and Appurtenant Structures", ETL 1110-2-571, recently released an update with minor changes (USACE, 2014). The guidelines show a vegetation-free zone across the levee surface and extending 15 feet from the toe of both the land and water sides (Figure 1-1). The vegetation-free zone is expanded where stability berms or other structures are present near the toe. This policy has been the subject of debate in states where levees were built close to adjacent to the rivers and as a result critical riverine habitat shares space with structures providing flood protection (Harder et al., 2011).
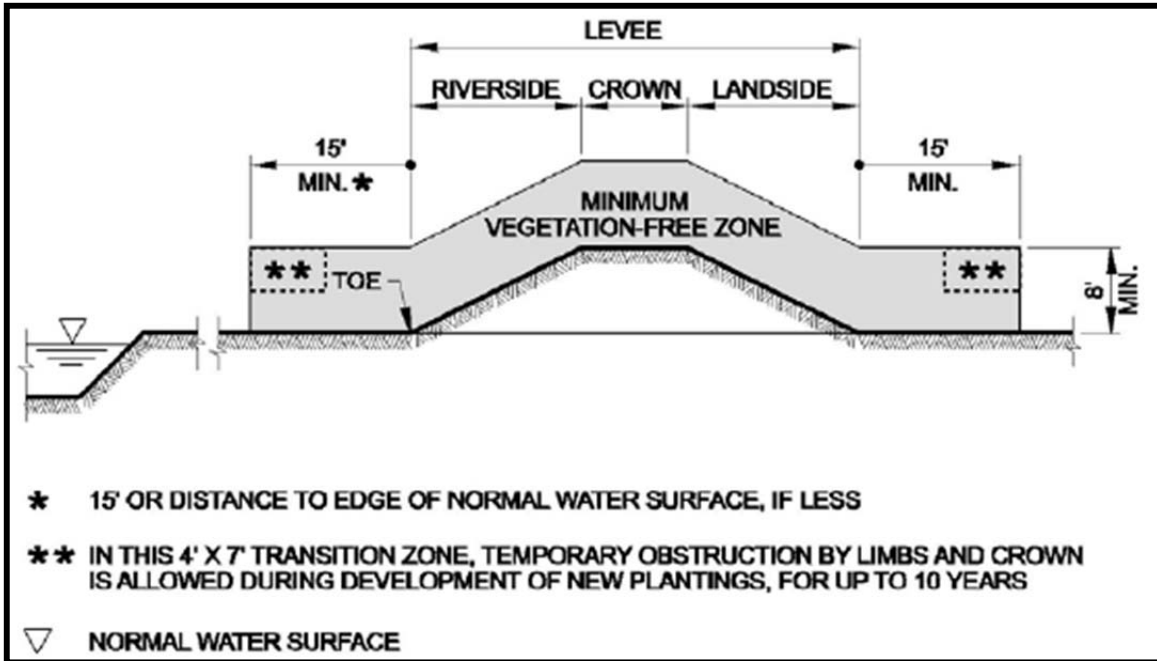
Figure 1-1. USACE Vegetation-Free Zone (Source: USACE ETL 1110-2-571).

## 1.1 SCOPE AND OBJECTIVE PART I: EFFECTS OF WOODY VEGETATION ON LEVEE SEEPAGE AND SEEPAGED-INDUCED STABILITY

Consensus has not been reached with regard to the impact of woody vegetation on levee integrity (Corcoran et al., 2010). The presence of woody vegetation can introduce uncertainty in the reliability of levee performance. Trees and their roots have been suggested to possibly undermine the integrity of compacted earthen levees by providing enhanced and focused seepage through the levees. It is argued that tree roots could potentially provide paths that water could more easily flow through which could bring the full water pressure of the water retained by the levee to locations within the levee (Pierson, 1983). These high water pressures within the levee could produce piping and erosion of the levee materials, which could undermine levee integrity and stability (ASDSO, 2002). Further, windthrow of levee trees during large storms or hurricane events leading to concentrated flow through the levee or erosion and scour present additional concerns (ASDSO, 2002). Maintenance and access for inspectors is another stated reason for the USACE policy on vegetation.

Alternately, live tree roots are believed to strengthen the levee and improve slope stability in many cases (e.g., Shields and Gray, 1992; Ziemer, 1981). It is not known whether the documented benefits of roots in terms of reinforcing earth slopes and strengthening the slopes may more than offset the potentially damaging effects of any localized regions of higher pore water pressure within the levee. The effects of roots of healthy woody vegetation on seepage patterns through levees are not well understood. Additionally, the removal of trees from levees may destabilize levees due to the decay of roots that remain after the trees are cut down (Ziemer, 1981). Decomposed and decayed roots could provide enhanced seepage that might degrade long-term levee performance.

2

The above issues have spawned debate as to the hazards and benefits associated with vegetation on levees. The agencies of the California Roundtable for Central Valley Flood management (formerly the California Levees Roundtable) are conducting research that will determine the extent to which woody vegetation, such as trees, may affect the safety and integrity of levees in California's Central Valley.

These studies include:

1. A national research program implemented by the U.S. Army Engineer Research and Development Center (ERDC).
2. Parallel and complementary effort initiated in California referred to as the California Levee Vegetation Research Program (CLVRP).

ERDC and the CLVRP have been collaboratively coordinating their research efforts. As part of the CLVRP research effort, researchers from several universities along with expert consultants and advisors were brought together to investigate the effects of woody vegetation on levee performance. The overall objective of the CLVRP research effort is to gain the technical knowledge needed for the development of sound vegetation management policies.

The first part of this work is focused on developing and understanding of the effects that live and decaying root systems have levee seepage and slope stability as part of the overall research effort of the CLVRP. The research is funded through the Sacramento Area Flood Control Agency (SAFCA) and the California Department of Water Resources (DWR). Two field tests were designed and performed to evaluate the effects of live and decayed tree roots on seepage through earthen levees and the resulting potential for seepage-induced instability. The first field test was performed at the site of a decomposing tree stump located on the landside of the north levee of the American River in Sacramento, California.

The second field test was designed around the roots systems of two oak trees (both live) on the land and water sides of the south levee of the Sevenmile Slough on the northern side of Twitchell Island in Rio Vista, California.

Flow tests were conducted where a flood condition was simulated over an instrumented section of the levee embankment. Following the flow test, each field effort was modeled using the Geostudio software package. Finite element seepage modeling was performed by Cobos-Roa (2014) and Cobos-Roa et al. (2014). Transient and steady state seepage models included in Cobos-Roa et al. (2014) were validated against test conditions and served as inputs to limit equilibrium stability models presented herein.

1.2 SCOPE AND OBJECTIVE PART II: SEISMIC ASSESSMENT OF EARTH STRUCTURES OVER POTENTIALLY LIQUEFIABLE SOILS

Another levee potential performance issue for California's levee systems is vulnerability under seismic loading. The liquefaction of soils presents a significant hazard to the built

environment. Whereas much attention has been devoted over the past four decades towards developing liquefaction triggering procedures to evaluate the likelihood of liquefaction occurring, relatively less attention has been devoted to understanding liquefaction-induced ground movements. In particular, the seismically induced permanent displacement of earth levees, embankments, and fill slopes due to liquefaction below these earth structures is not well captured in current seismic design practice (e.g., EERI 2003, Seed et al. 2003).

There are several levee systems that are potentially vulnerable to liquefaction-induced ground failure. This project is particularly important to the new studies of the seismic fragility of the levees in the San Joaquin-Sacramento delta region. This levee system provides drinking water for over 66% of Californians as well as water for agriculture, recreation, and environmental purposes (CADWR 2007). Unacceptable liquefaction-induced deformations to this system could lead to devastating consequences. However, there is not sufficient funding available currently to repair all vulnerable levees in the San Joaquin-Sacramento Delta.

Many of the prevalent procedures for evaluating liquefaction are discussed in the document "Recommended Procedures for Implementation of DMG Special Publication 117: Guidelines for Analyzing and Mitigating Liquefaction Hazards in California" edited by Martin and Lew (1999). This important guidance document separates liquefaction-related slope movement hazards into two categories:

1. Flow slides wherein the post-liquefaction static factor of safety (FS) is below unity so that large displacements that are greater than a few meters occur after the cessation of earthquake shaking; and
2. "Limited" lateral spreads of the order of a meter or so triggered and sustained by the earthquake ground shaking."

Flow slides could potentially be the most catastrophic liquefaction-induced slope movement. The expected range of displacement for a flow slide (i.e., post-liquefaction FS < 1) is typically large and current prediction methods are well suited to predict their occurrence. Once identified, these levee or embankment sections would require remediation in most cases as the amount of permanent ground displacement that could occur would be too large. As summarized in Finn (1990), large liquefaction-induced levee crest settlements on the order of several meters are possible as the post-liquefaction factor of safety approaches a value of about 0.8. However, Finn also indicates that crest settlements of a meter or so are possible when the post-liquefaction factor of safety is slightly greater than one. Movements of a meter or so can produce significant damage to earth structures, so reliable procedures for estimating seismic displacements within this range of movements are also required.

"Limited" lateral spreads involving liquefaction of moderately dense clean sand or silty sands can produce seismic displacements in earth levees, earth embankments, and earth slopes on the order of several centimeters to a meter or more. These levels of seismically

induced displacements are sufficient to damage water retention structures in the following ways:

- Deformations can cause cracking that can lead to piping of water through the structure.
- Deformations resulting in a loss of freeboard can lead to overtopping.

The post-liquefaction static stability of the earth slopes for these cases are greater than unity; therefore, significant deviatoric-induced seismic displacements are not expected after the cessation of ground shaking. The seismically induced permanent displacement for these cases occurs primarily during earthquake shaking but after liquefaction is triggered. Hence, there are three important aspects of the problem to capture: (1) the point in which liquefaction is triggered; (2) the seismic response of the sliding mass during continued shaking; and (3) the post-liquefaction cyclic response of these soils.

These are not easy aspects of nonlinear soil response to capture. Robust analytical procedures are required to evaluate sections of levees where liquefiable foundation materials exist to evaluate:

1. If large flow slides will occur, which will require relatively expensive remediation;
2. If negligible seismic displacements will occur, which will require no expenditures; or
3. If intermediate seismic displacements will occur, which may require some level of remediation depending on the consequences of the estimated level of seismic displacement.

To meet this objective, a promising, popular nonlinear soil constitutive model (UBCSAND) has been implemented in a widely available finite difference program (FLAC) for evaluating seismic deformations of earth structures resulting from liquefaction-induced lateral movements focusing on ground conditions that lead to inertially driven ground movements of intermediate levels. The results of this research will also be applicable to earth structures other than San Joaquin-Sacramento Delta levees. It is our hope that with these improved analytical tools, earthquake losses can be reduced through effective screening and remediation of those earth slopes that would likely perform poorly in a future seismic event.

Part II of this research focuses on another potential hazard impacting California's levees: seismic vulnerability. This research, funded by the USGS, involved implementing a promising soil constitutive model that is implemented in a widely used finite difference program is employed to analyze seismic deformations of levees resulting from liquefaction-induced lateral movements in foundation soils. It is important to note that the cases to be analyzed will have post-liquefaction static slope stability factors of safety greater than unity, so inertially driven "limited" lateral spreads is this study's focus. An assessment of this commonly employed advanced seismic displacement model is required to evaluate its ability to capture inertially driven liquefaction-induced lateral deformation effects. One

such timely application is the high priority seismic vulnerability studies of the earth levees in the San Joaquin-Sacramento delta region of California.

The scope of the study is divided into four phases: (1) perform analyses of one-element laboratory tests to demonstrate proficiency with the FLAC/UBCSAND numerical simulations; (2) perform back-analyses of key case histories to calibrate the numerical model; (3) conduct a systematic numerical sensitivity study of a simplified case

Characterization of the seismic hazard and the geotechnical conditions at a particular site will always remain critical factors. No amount of sophistication in the analytical method employed can compensate for shortcomings in one's understanding of the local site conditions and the seismic hazard at a site. However, there are cases where advanced analyses based on an enhanced characterization of the site will be required. The goal is to advance a reliable numerical method for cases in which refined assessments are required to evaluate seismic performance.

## 1.3 ORGANIZATION OF CHAPTERS

Chapters 2 through 4 are related to work performed as part of the California Levee Vegetation Research Program. These chapters relate to the impacts of woody vegetation on levee integrity. Chapters 5 and 6 relate to evaluating seismic vulnerability of California levees. Chapter 7 presents conclusions of this research program. A detailed breakdown of content by chapter is as follows:

PART I:

- Chapter 2: Methods and results of a full scale wetting front test are presented. The test was performed at the site of a decomposing tree stump located on the landside of the north levee of the American River at the California Exposition and State Fair (Cal Expo) in Sacramento, California. The test investigated the impact of a decomposing root system on levee seepage. The stump was excavated and the conditions documented following the study.
- Chapter 3: Methods and results of a full scale seepage test are presented. The test was constructed to study the impact of waterside and a landside oak trees, both live, through simulation of a flood event via a trench through the levee crown. The test was performed on the north levee of Twitchell Island on the Sevenmile Slough in Rio Vista, California.
- Chapter 4: At the Cal Expo test site, two-dimensional limit equilibrium methods were employed to investigate the impact of a decaying root system on slope stability. At the Twitchell Island test site, observed levee performance deficiencies under test conditions are explored using two-dimensional limit equilibrium modeling, mass averaged to capture three-dimensional effects. Modeling of tree root systems, static tree loading with variable lean, and wind loading are explored.

PART II:

- Chapter 5: A popular soil constitutive model, UBCSAND, is implemented within the finite difference program FLAC. Single element laboratory tests are modeled to demonstrate proficiency of the model and generate a series of calibration parameters. Key case histories are then siumulated to validate the calibration.
- Chapter 6: FLAC/UBCSAND is implemented to analyze seismic deformations of earthen embankments resulting from liquefaction-induced lateral movements in foundation soils.

CONCLUSIONS

- Chapter 7: Conclusions of the study are presented.

# CHAPTER 2

## Parallel Trench Wetting Front Test, North Levee of the American River at Cal Expo Sacramento, California

2.1 PARALLEL TRENCH WETTING FRONT TEST – SACRAMENTO, CALIFORNIA

The Parallel Trench Wetting Front Test was as part of an overall research effort with the CLVRP. A conceptual sketch, prepared by Professor Jonathan Bray, illustrated a conceptual design for a test to explore the effects that live and decaying root systems have levee seepage and slope stability (Figure 2-1). The concept of the test involves excavating small parallel trenches above and below the root system of a tree on a levee slope. The upslope trench is supplied with water and held at a constant hydraulic head, imposing a two-dimensional flow path from the upslope trench to the downslope trench. Instrumentation installed within the zone of flow captures positive and negative pore water pressures before, during, and after flow.
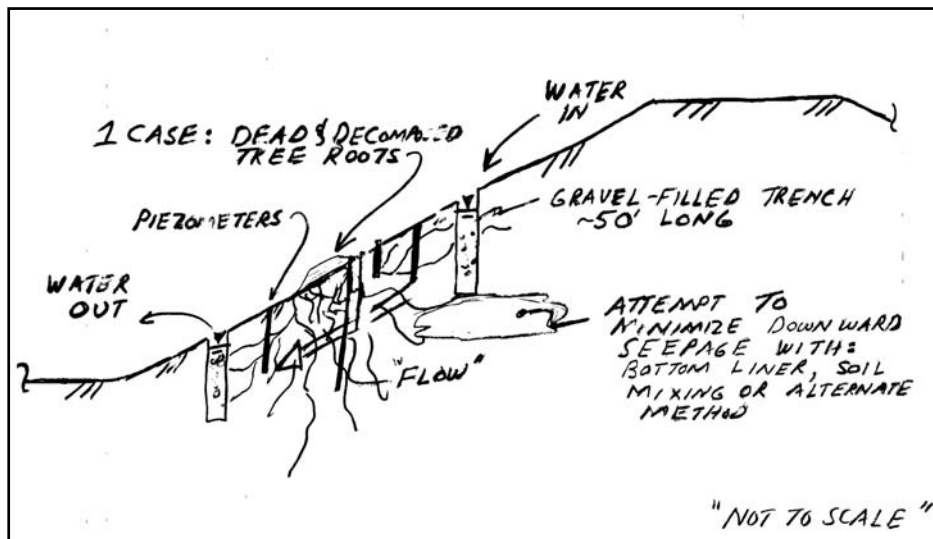


Figure 2-1. Conceptual Sketch of Parallel Trench Wetting Front Test.

Conceptual sketches began to evolve into a design phase as site selection began. Each site viewed possessed unique qualities with its own set of advantages and disadvantages. The final was ultimately customized to adapt to the conditions of the most suitable site.

2.1.1 Site Selection – California Exposition and State Fair (Cal Expo)

Selection of an appropriate site to study was an important element of the field effort and involved the combined efforts of the UC Berkeley team, DWR and SAFCA to contact reclamation and flood control districts within areas known to maintain

levees with vegetative cover. Individual districts provided information regarding possible stump sites and promising sites were viewed and evaluated for suitability.

The primary considerations in selecting a test site were soil conditions, age of stump, position of stump on slope, and proximity to 'control' conditions. Additionally, the reclamation districts needed to allow access to the levees for a large-scale excavation effort in the months just prior to flood season. A mid-slope stump was important in order to accomplish the Parallel Trench Wetting Front Test and keep both upper and lower trenches within levee soils rather than foundation soils. Soils exhibiting no cohesion were determined to be undesirable for reasons of temporary stability during the flow test. In terms of stump age, we were seeking a stump that was likely to be undergoing significant decomposition, but without having achieved complete decomposition within the root system at the time of the study. Gray and Leiser (1982) provide a discussion of tensile resistance of roots with time after felling. They cite the work of Burroughs and Thomas (1977) where 75 percent of root tensile strength for a 1 cm root is lost over 4 years after felling of a Pacific Coast Douglas fir. The tensile resistance of this root was approximately a tenth of its fresh strength at 10 years after felling. A Rocky Mountain Douglas fir lost only 10 percent of fresh tensile strength in a 4 year period following felling and took about 10 years for the root strength to drop to 70 percent of fresh strength. Based on discussions with the CLVRP advisory panel, including Professor Gray, a target age of stump was determined to be on the order of 5 to 10 years with an understanding that this may vary based on a number of factors including tree species and size. Other factors considered were tree species, observed animal activity, and proximity to other trees and stumps.

Based on the criteria presented above, we selected a site within the American River Flood Control District (ARFCD). The site is located along the landside of the northern levee bordering the American River adjacent to California Exposition and State Fair ('Cal Expo') and was selected due to the presence of the decaying eucalyptus stump shown on Figure 2-2. The stump was well positioned on the slope, appeared to be significantly decayed, and exhibited minimal signs of animal activity in the immediate vicinity of the stump. The northern levee of the American River in the vicinity of Cal Expo has a crest elevation approximately 16 feet above adjacent grades with a landside horizontal to vertical slope gradient of approximately 2 to 1.

Figure 2-2. California Exposition and State Fair (Cal Expo) site. Source of base aerial imagery: Google Earth.

### 2.1.2  Cal Expo Site Description

As previously discussed, the selected site is located along the landside of the northern levee bordering the American River. A site walkover was performed to evaluate site conditions from the surface. Professor Dirk Van Vuren of UC Davis served as the CLVRP team expert on burrowing mammals. Professor Van Vuren viewed the site with our team and burrow locations were flagged and categorized based on his experience. A total of 17 surface expressions of burrows were found within 20 feet of the test (to the east and west) on the landside slope face. Based on Professor Van Vuren's visual observations, the burrows consisted of abandoned and some collapsed burrows of the California ground squirrel and the pocket gopher (Figure 2-3).

Figure 2-3. Aerial view of the site showing the scatter of burrows relative to the study area. Base photo source: Google Earth, September 19, 2010.

The landside of the levee is inclined at approximately 2H:1V (horizontal:vertical). The eucalyptus stump selected for study was positioned approximately 6 feet from the crown and 10 feet from the toe of the levee, measured vertically (Figure 2-4).

A second stump was found just east of the study area adjacent to the lower trench. The stump was observed by Professor Alison Berry of UC Davis, and determined to be a eucalyptus stump. Trench construction revealed two additional stumps, both north (downslope) of the control trench that were not previously visible from the ground surface. Figure 2-5 shows the configuration of all stumps found within the study area overlain onto a 1973 aerial photograph. A live hackberry tree with a 36 inch trunk diameter is located at the toe of the levee on an alignment 4 feet west of the stump as shown on Figure 2-3 through Figure 2-5. Aerial imagery shows the tree to have a canopy diameter of approximately 55 feet at the time of our study in 2010.

The history of trees and stumps within the study area was explored by examination of aerial photography. Cal Expo has an extensive library of photography and construction documents, including a planting plan showing trees proposed for planting on the levee at the time of construction of Cal Expo between 1967 and 1968. Cal Expo retains aerial photos flown on a nearly annual basis, typically during the state faire each year in late August. Many photos were not high enough quality in the study area to identify individual trees with certainty.

Figure 2-4. Photos of the study site at the Eucalyptus stump.

Figure 2-6 shows Cal Expo under construction in 1968 at which time trees has not yet been planted along the levee. A planting plan prepared by Lawrence Halprin and Associates and dated November 27, 1967 was provided by Cal Expo for our review. Figure 2-7 shows an approximately 1500 foot stretch of the planting plan aligned with an aerial photo taken in 1973. The plan shows many trees that do not exist in the 1973 photograph, while trees actually seen in the 1973 aerial photograph do not appear to have been planted in the precise locations proposed. Nevertheless, a mass planting took place and many more trees are present in 1973 than in 1968. According to Ron King, the head of grounds maintenance for Cal Expo, many of the initial trees planted at that time did not survive. This observation is consistent with our review of planting plans as compared with aerial photography in the years following construction.

Figure 2-8 shows a close-up of the aerial photo from 1973 with the tree identified as the stump under study indicated. Four trees are shown within the study area and street lights are used to pinpoint the location of our Eucalyptus stump. The planting plan shows the two trees to the east are *Eucalyptus rostrata*, while the two trees to the west are *Pinus radiata*. The position of trees does not seem to correlate exactly with the plan. In general, the species of the trees onsite currently seem to match those planted and consist primarily of eucalyptus and pine. Based on a visual evaluation, CLVRP root architecture research expert, Dr. Alison Berry of UC Davis identified the two stumps to the east as Eucalyptus. Stumps to the west were not evaluated for species as they were not visible from the surface, were highly

decomposed and generally downslope of the study area. Additional stumps were found during trench construction and may have been remnants of the trees shown on Figure 2-8.
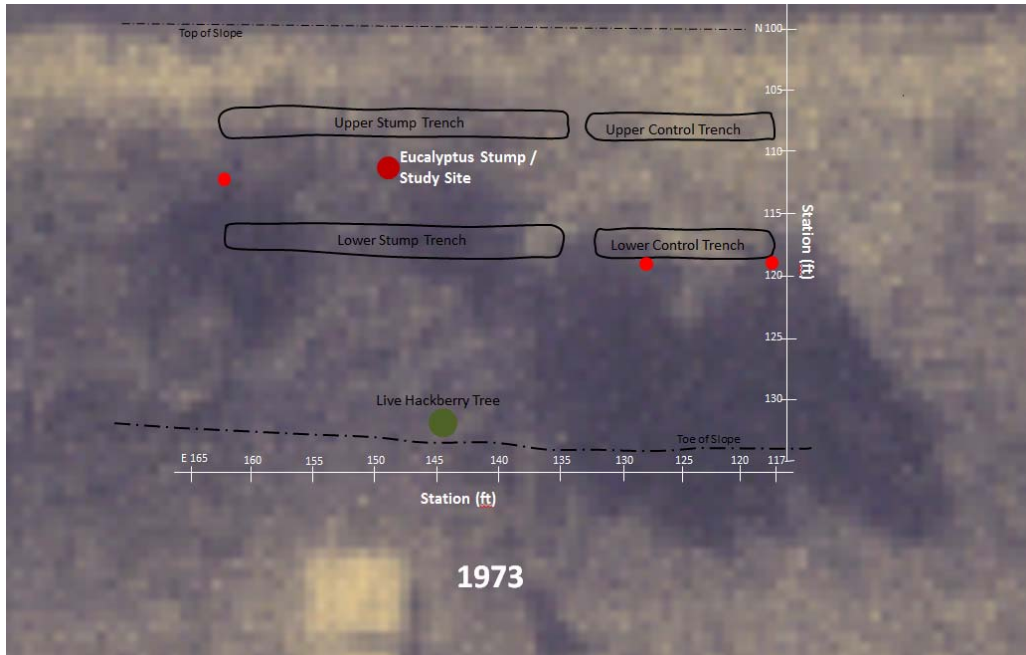


Figure 2-5. Plan view showing trench configuration and stump locations identified during construction. Base photo provided by Cal Expo, 1973.



Figure 2-6. Aerial view of Cal Expo and the north levee of the American River in 1968 during the construction of Cal Expo. Aerial image provided by Cal Expo.

Figure 2-7. 1973: Approximate alignment of planting plan with aerial photo of site. Aerial image provided by Cal Expo.
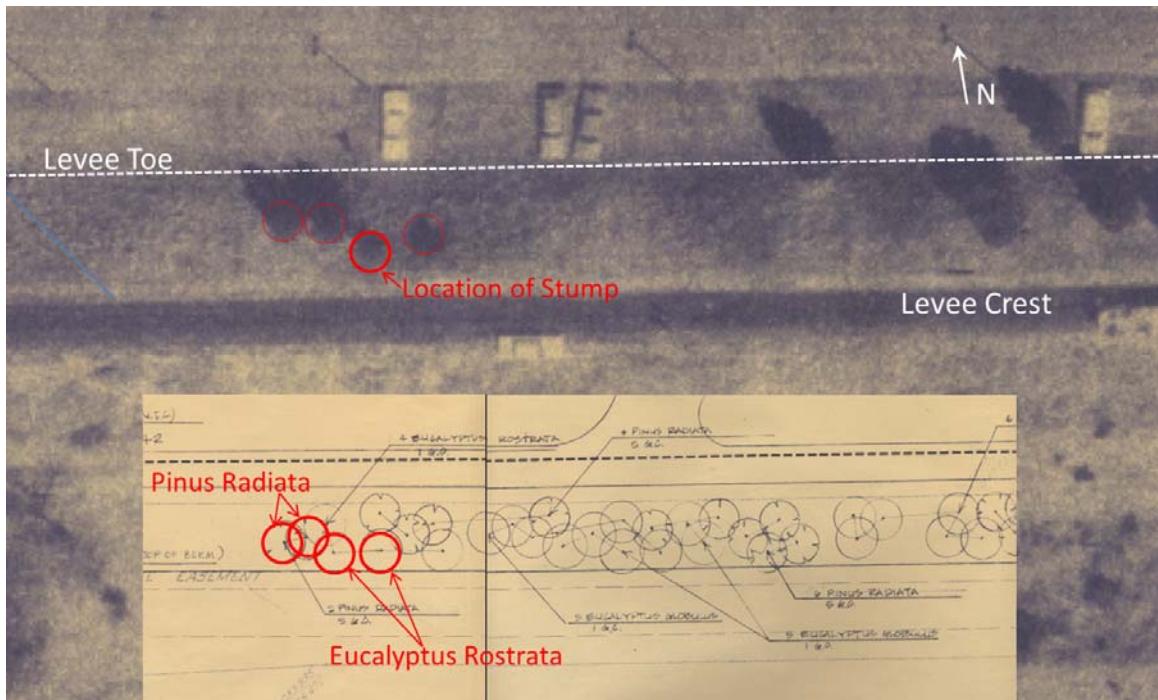


Figure 2-8. A view of the four trees on site as of 1973 with corresponding planting plan showing proposed planting for those trees. Aerial images provided by Cal Expo.

Based on our review, we estimate the Eucalyptus tree studied was cut between 1994 and 1998. Figure 2-9 shows the site in 1975, 1979, 1983, and 1990. In 1975, four trees can be seen at site. In 1979, a small shadow could be the hackberry tree. In 1983, both the hackberry and the eucalyptus trees are clearly visible. In 1990, it is clear that there is at least one tree with multiple main branches or possibly two trees upslope of the hackberry tree. In Figure 2-9 and Figure 2-10, the Eucalyptus tree(s) can be seen in 1990 and 1994 and appear to be two trees. The following year in 1995, the aerial photograph appears to have been taken at a similar time of day and the shadow of the Eucalyptus tree shown in 1994 is not present in 1995 (Figure 2-10). Trees may have been cut back or removed between 1994 and 1995.

Figure 2-11 shows the site in 1996, 1997, 1998, and 2010. The 2010 image shows the hackberry tree during our flow test. In 1996 and 1997, the shadow patterns, overlapping canopies, and poor image quality make it difficult to discern whether the Eucalyptus trees are present. In 1997, leaves of the hackberry are beginning to change color, while the uphill segment of the canopy appears a slightly different shade of green, possibly indicative of a tree that does not lose leaves in the winter, such as a Eucalyptus. Between 1997 and 1998, a number of trees, including those just west of our stump, were removed. The removal was likely part of the 1998-1999 American River Watershed Improvements project that involved construction of a slurry wall within the levee crown. The eucalyptus trees upslope of the Hackberry may have been removed between 1997 and 1998 in preparation for this work. The USACE's plans approved in April of 1999 (USACE, 1999) and prepared by the Sacramento District, Central Valley Section show the hackberry tree, the eucalyptus tree(s) and other nearby trees to be present in the background aerial photograph (Figure 2-12). Also shown is the water pipeline found during trench excavation (N3-10 as shown on the plan) and further discussed in Appendix 2B. Many trees are noted as requiring removal for construction, but the eucalyptus is not specified, perhaps because it had already been removed.

A summary of information gained from our review of aerial photography follows:

- The eucalpytus stump under study was likely the remains of a tree removed in 1998 prior to the installation of the slurry wall along the north levee of the American River. It is also possible that the tree was aggressively cut back or removed between 1994 and 1995, making the stump 12 to 16 years old at the time of our study.
- The two trees west of the stump under study may be *Pinus radiata*, planted around 1968 and removed between 1983 and 1990.
- The eucalyptus west of the stump under study was planted during or shortly after 1968. This tree may have been removed in 1994 or 1998 with the stump being studied.
- The hackberry tree at the toe of slope was not planted and appears in the late 1970's and is clearly visible in a 1983 aerial photograph. The age at the time of study is estimated at 31 years. This is consistent with estimates by Dr.

Alison Berry of UC Davis based on her visual evaluation.
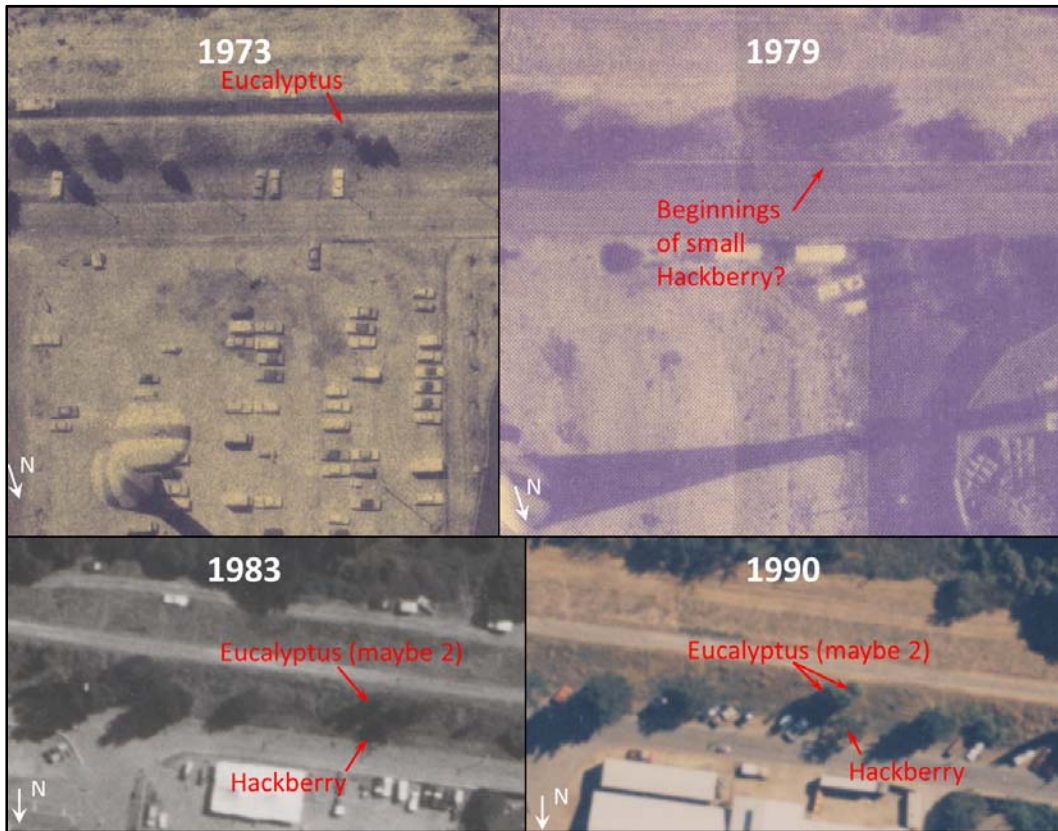


Figure 2-9. View of the site in 1973, 1979, 1983, and 1990. Aerial images provided by Cal Expo.
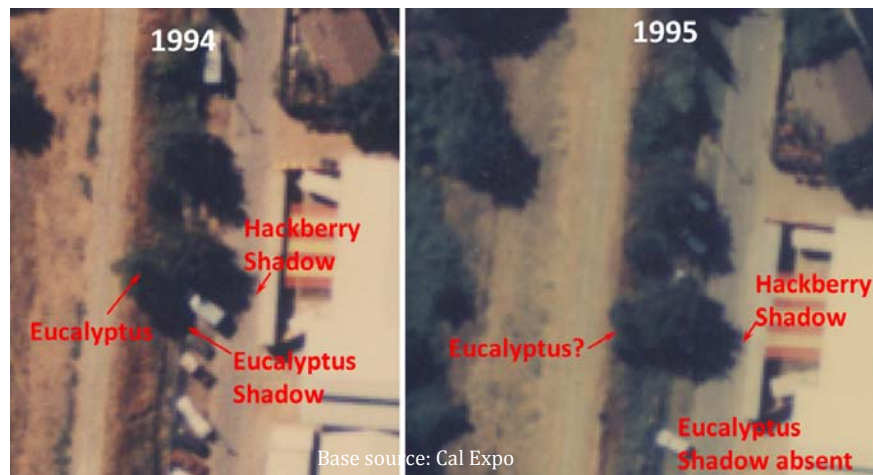


Figure 2-10. Aerial photo comparison of the site in 1994 and 1995. In 1994, a distinct shadow of the eucalyptus tree(s) is seen. In 1995, the shadow is absent.
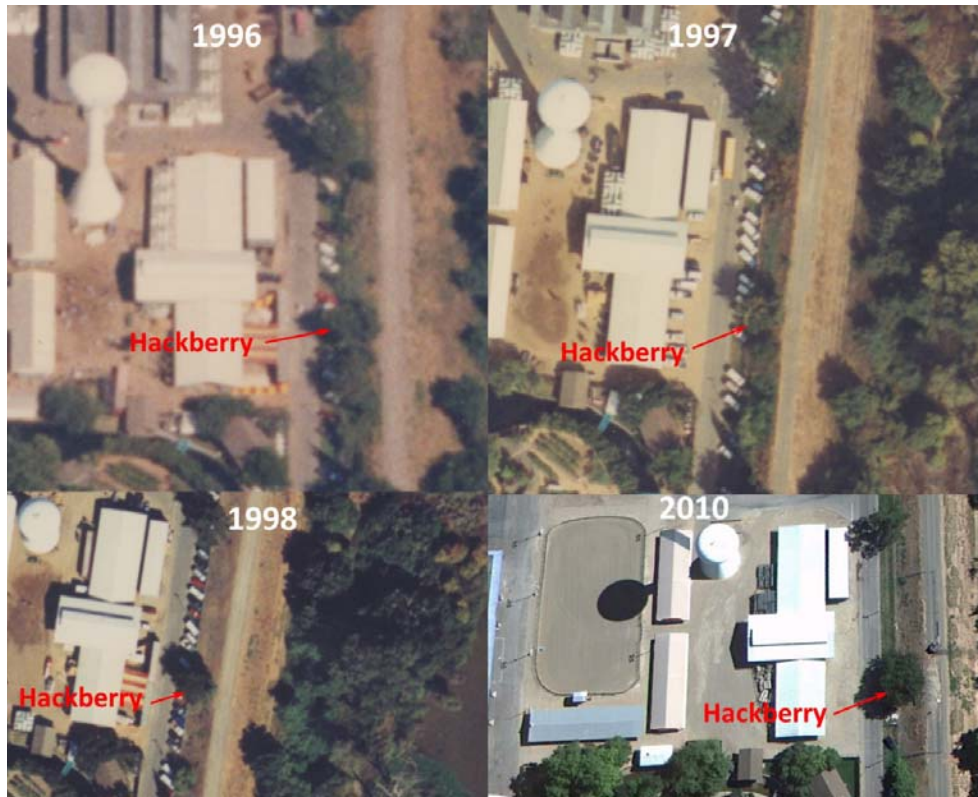
Figure 2-11. Aerial view of the site in 1996, 1997, 1998, and 2010. Source: 1996-1998, Cal Expo; 2010, Google Earth.
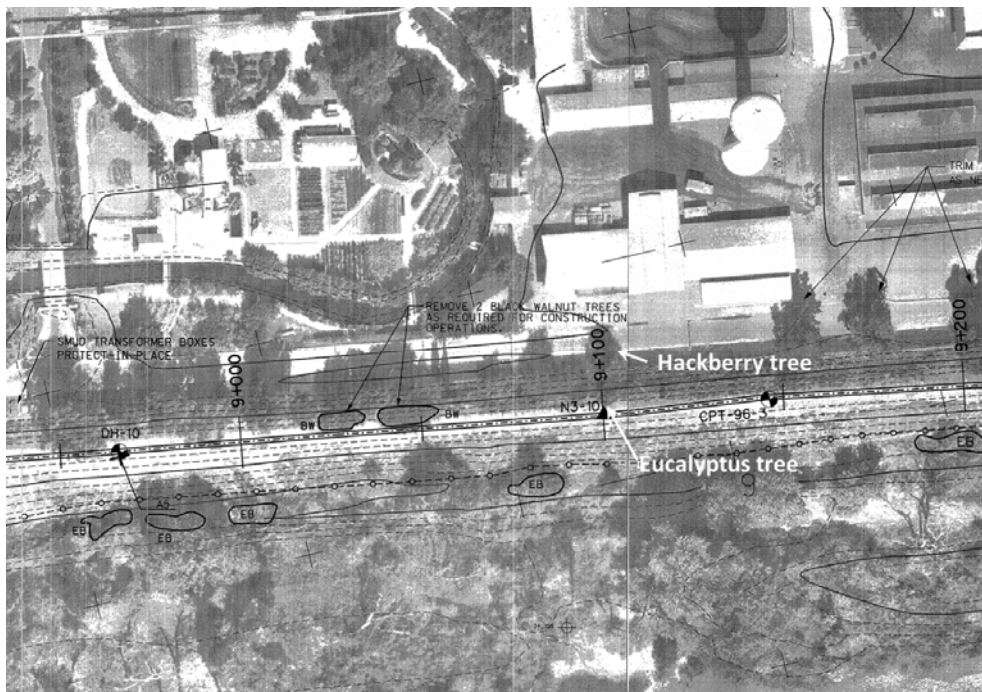


Figure 2-12. Aerial image from 1998-1999. Source: American River Watershed Improvements project (USACE, 1999).

### 2.1.3 Subsurface Stratigraphy

Soil conditions were an important factor in the selection of the site, in the implementation of the test, and in the interpretation of test results. The site soils were characterized using the Unified Soil Classification System (USCS) prior to and during test construction. Test borings and instrument holes were augered and conditions logged and summarized in Appendix 2A. We reviewed available regional and local soil information in the American River Common Features General Re-evaluation Report (URS, 2009), the American River Watershed Project Right (North) Bank Levee Strengthening plans dated April 1999 (USACE, 1999), and the American River Levee General Design dated June of 1956 (USACE, 1956). In Appendix 2B, we included relevant plans, soil boring logs, cross sections and excerpts.

During construction and after the flow test, trench walls and excavations were observed and observations were recorded onto field logs. These field logs are provided in Appendix 2C. Our post-flow characterization effort included excavation of the zone surrounding the stump with observations recorded through both traditional field logging and tripod-based light detection and ranging (T-LiDAR) imaging (Cobos-Roa et al., 2012). A cross section showing the stratigraphy in the area of the eucalytus stump under study is provided as Figure 2-13. T-LiDAR was used only in the area around the stump and root system. At the control section, a backhoe test pit was excavated at instrument Line C in order to view the and log the stratigraphy (Figure 2-14). Site soils consisted of interbedded silts, silty sands, sandy silts, and lean clay.

The site soils generally consisted of clayey and sandy silts and silty sands. Pockets and lenses of low fines content sands were observed during excavation and characterization efforts. Relatively horizontal layering was found within localized excavation areas. Based on our excavations, site soils consist of roughly continuous layering of heterogeneous blends of materials where pockets of homogeneity are encountered. Material 3 is comprised of materials 3a and 3b in a heterogeneous blend. Material 4, lean clay with zones of clayey silt, is found to be about 1 foot deeper in the control than in the stump section. Like all onsite materials, the layer is heterogeneous and contains pockets of sands and silts. Additional information is provided in Appendix D. In general, our findings are consistent with general levee profiles for the region by URS (showing layered silts and lean clays to the west of our study site and layered sandy silts and silty sands to the east) as well as available boring and Cone Penetration Test (CPT) data for the American River Watershed Project Right (North) Bank Levee Strengthening plans (USACE, 1999).

① Sandy silt with clay (ML), brown, moist, occasional rounded to sub-rounded gravels; sand is fine-grained and uniform. Fine roots.

② Sandy silt/silty sand (ML/SM), brown, moist, occasional sub-rounded gravels, sand very fine grained and uniform, trace clay.

③ Clayey silt (ML) with sand, mottled dark brown and brown, moist, light cementation, trace sand

③a Clayey silt (ML), dark brown, light cementation and soils structure

③b Sandy silt (ML) with clay, brown

④ Silty clay/clayey silt (ML/CL), olive brown with reddish oxidation stains

⑥ Silty sand (SM), olive brown, fine uniform sand, lightly cemented

⑩ Silty sand (SM) with clay, brown, moist

Figure 2-13. Statigraphic section between upper and lower trenches at the eucalyptus stump.
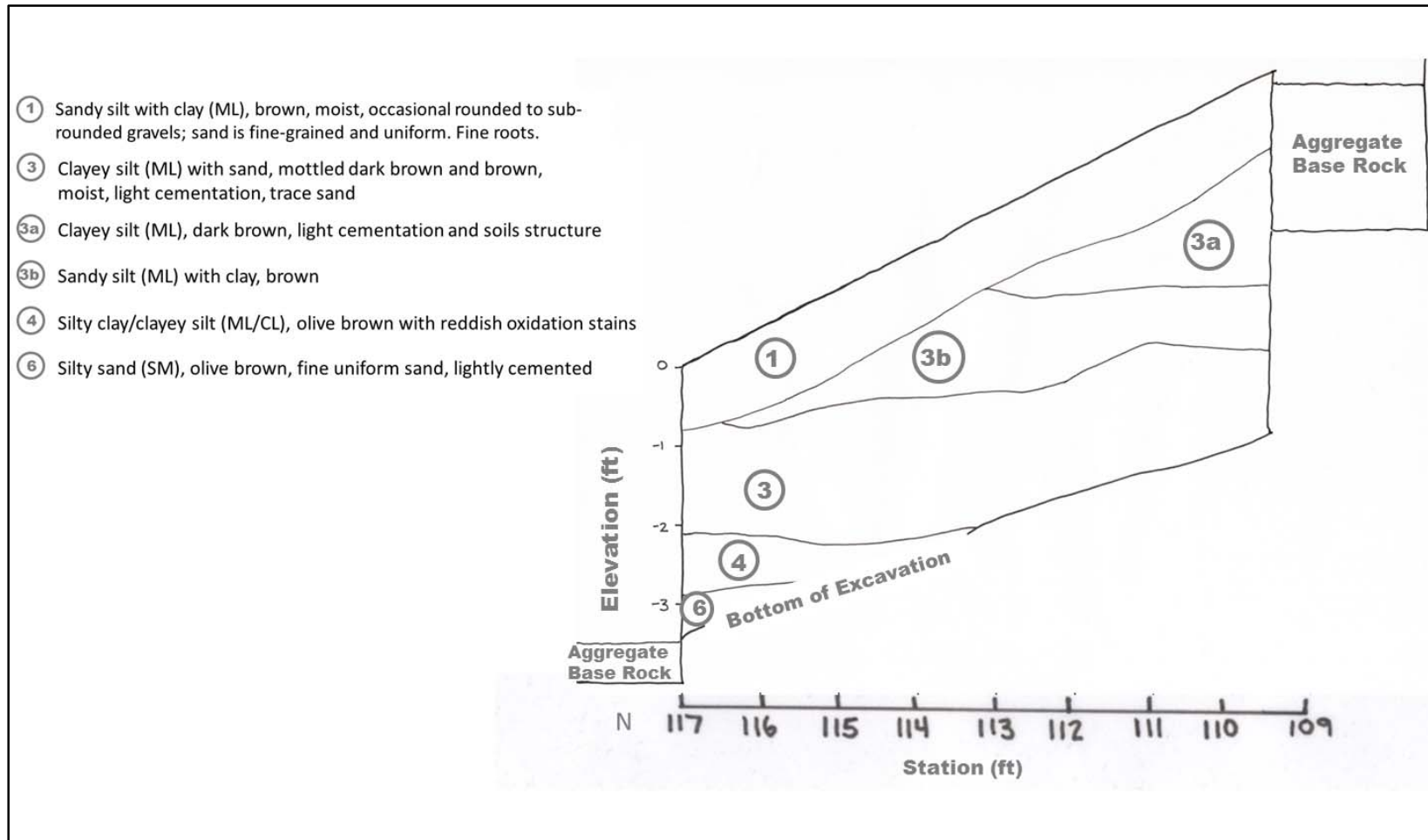
Figure 2-14. Stratigraphic section at control trenches, located just west of instrument Line C (see Figure 2-21).

2.1.3.1   Test Layout

As previously discussed, the flow test was designed to deliver water above the decomposing root system of the eucalyptus stump, inducing a wetting front and a flow net that could be monitored through observation and instrumentation. Water was delivered to an upper trench, constructed above the stump, and held at a constant head during the test (Figure 2-15 and Figure 2-16). A lower trench was constructed below the stump for viewing the exposed trench wall face and to capture seepage flowing downslope during the flow experiment. The walls of the trench were braced with shoring to prevent collapse. The uphill side and base of the upper trench as well as the base of the lower trench were lined with plastic sheeting to minimize water losses outside the study area. Stockpiled gravel was available to rapidly infill the lower trench in the event of instability prior to the equilibration of flow patterns.
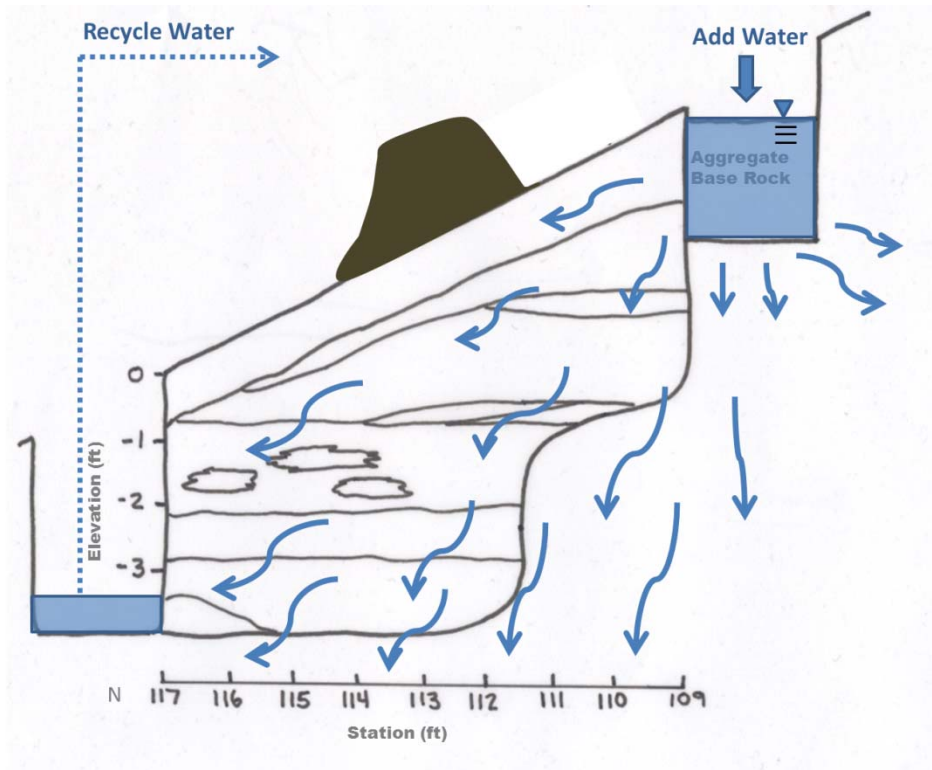


Figure 2-15. Cross section between upper and lower trenches at eucalyptus stump showing concept of proposed wetting front flow test.

Figure 2-16 shows the configuration of trenches constructed above and below the stump. An approximate 30-foot long zone around the stump was deemed the 'stump zone' and a 'stump trench' was constructed above and below this segment. The water delivery trench above the stump will be referred to as the 'Upper Stump Trench' while the viewing trench below the stump will be known as the 'Lower

21

Stump Trench'. As seen on the figure, the stump and control trenches were separated by a small gap in excavation in order to control water flow and volumes to the two trenches separately.
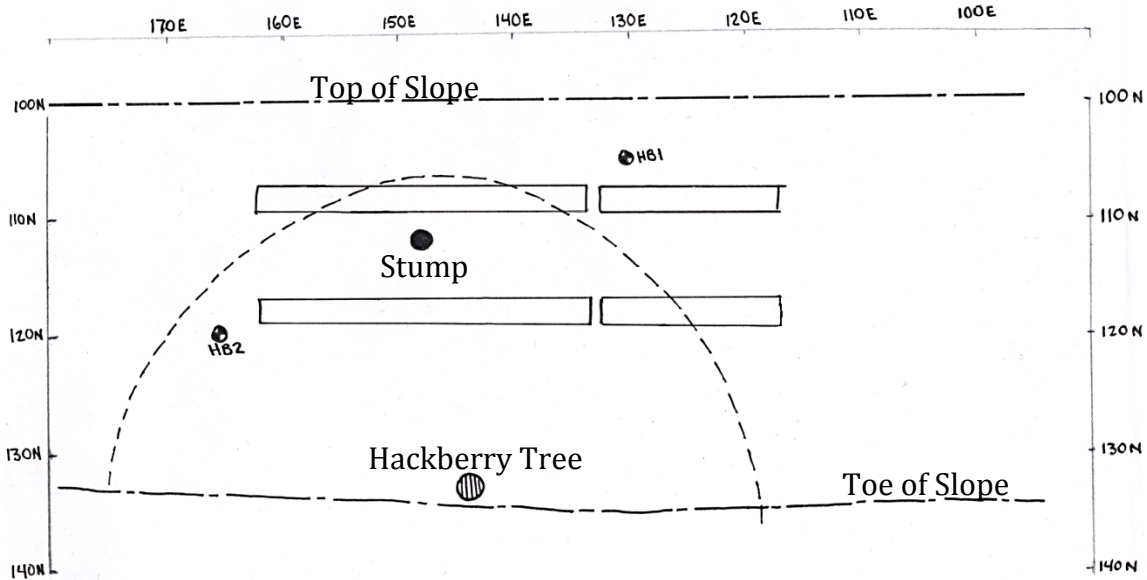


Figure 2-16. Site plan with coordinate grid showing the stump and trenches under study, and the location of hand auger borings HB1 and HB2.

A detailed site design began with development of a plan view layout consistent with observed conditions. Three levee cross sections were surveyed with increasing distance from the tree stump using handheld tools such as a compass, measuring tape, and hand level with collapsible survey stick. Based on the sections, a decision was made to align the trenches and coordinate system with the hinge point of the landside slope at the levee crest and lay out the site from that line. This decision minimized topographic differences between instrument lines. Figure 2-17 shows the site in cross section with the root system as scanned with T-LiDAR after the completion of the test. The T-LiDAR scan contains points throughout the study area and the thickness of the point cloud in cross section is a measure of the topographic variations across the site. The image shows that topographical variations between cross sections are on the order of 6 to 12 inches. Layout of the site was completed by establishing a grid of northings and eastings, beginning with an arbitrarily selected station number at north 100 ft and east 100 feet (N100, E100) and with increasing station numbers to the north and east. For the purposes of a practical coordinate system, north was defined as the downslope direction rather than true north (Figure 2-16). When not noted otherwise, station numbers used in this report are eastings (i.e. along the reference line parallel to the levee hinge).

The separation between upper and lower trenches was 10 feet on center, measured horizontally. Each trench was 2 feet wide, leaving an 8-foot wide mass of soil (measured horizontally) from the downhill wall of the upper trench to the uphill

wall of the lower trench. To the west of the stump trenches, a 15-foot long levee segment was identified as a 'control' area. Both an upper and lower trench were constructed spanning this zone. Measured trench dimensions and coordinates are shown on Table 2-1. In Figure 2-18, the stump is shown in relation to the upper and lower trenches. An as-built plan showing trenches, soil borings, stumps (those visible from the surface and those found during trench construction), the hackberry tree at the toe, surface expressions of burrows, as well as the top and toe of slope is provided in Figure 2-19.



1 ft
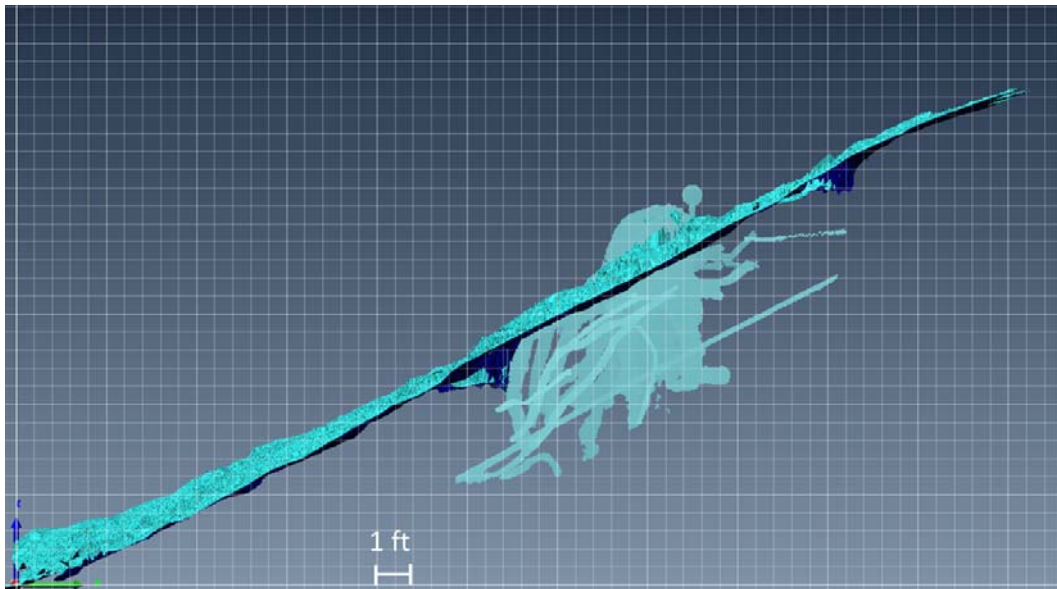
Figure 2-17. T-LiDAR image looking east at the eucalyptus stump and root system. Base T-LiDAR Image provided by Gerald Bawden of the USGS.

Table 2-1. Trench Dimensions and Coordinates

| | Uphill Depth (ft) | Downhill Depth (ft) | Width (ft) | Length (ft) | Coordinates (ft) |
|---|---|---|---|---|---|
| Upper Control Trench | 3 | 2 | 2 | 15.5 | (N107.5, E132.5), (N109.5, E132.5), (N107.5, E117), (N109.5, E117) |
| Upper Stump Trench | 3 | 2 | 2 | 28.5 | (N107.5, E133.5), (N109.5, E133.5), (N107.5, E162), (N109.5, E162) |
| Lower Control Trench | 4 | 3 | 2 | 15.5 | (N117.25, E132.5), (N119.25, E132.5), (N117.5, E117), (B119.5, E117) |
| Lower Stump Trench | 4 | 3 | 2 | 28.5 | (N117.25, E133.5), (N119.25, E133.5), (N117, E162), (N119, E162), |

Figure 2-18. Eucalyptus stump is shown A) close in, B) from the east end of the trenches looking west, C) from below the stump trench looking southeast, and D) from the west end of the stump trench looking east.
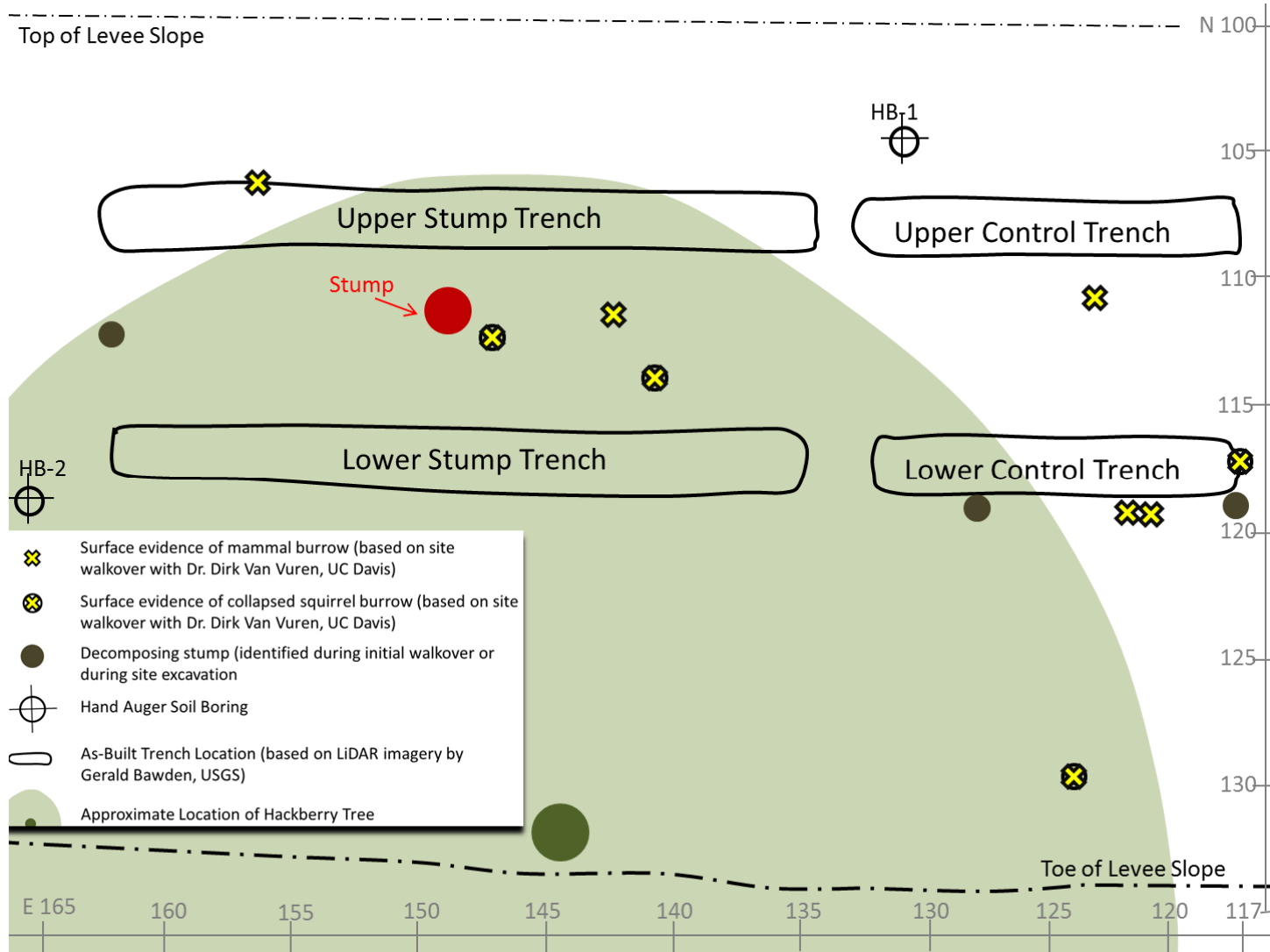
Figure 2-19. Plan view of field test layout.

Photos showing an overview of the overall site are shown on Figure 2-20. As can be seen in the photographs, the site design concept includes three instrument lines to monitor the progression of the wetting front and pore pressures at increasing distance from the stump center. Instrument Lines A, B, and C were placed a distance of 0, 7, and 23 feet west of the stump center, respectively (Figure 2-21).



Figure 2-20. Field test layout looking west (upper left), east (upper right), and south (bottom left). Lower right is a site overview looking east and showing the hackberry tree in relation to trench excavations.

Piezometers and tensiometers were installed to measure positive and negative pore water pressures, respectively, within the zone of flow to monitor the wetting and flow patterns with increasing distance from the decomposing root system. A complete instrument line consisted of 7 tensiometers with electronic transducers installed to depths of 18 to 60 inches as well as two vibrating wire piezometers installed to depths of 60 to 84 inches. Instrument Line A was located in the vicinity of the decomposing stump (Section A of Figure 2-21). Instrument Line C was located approximately 23 feet from the stump (Section C of Figure 2-21). Supplemental instrumentation consisting of 5 tensiometers were installed a distance of 7 feet from the stump, between Instrument Lines A and C. The supplemental line is referred to as Instrument Line B and was installed a distance of 7 feet from the stump at Section B as shown on Figure 2-21.
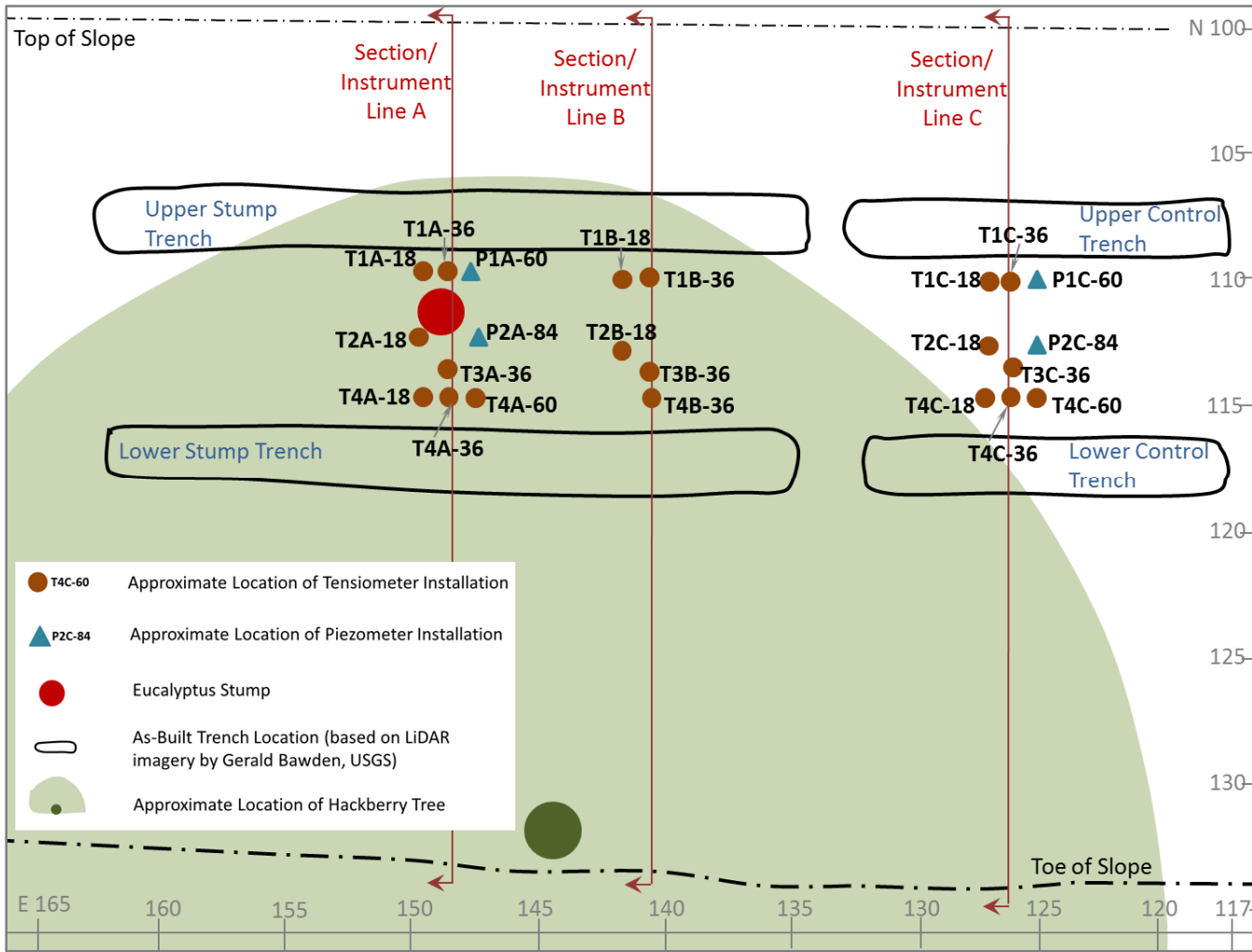
Figure 2-21. Instrument layout plan showing the locations of piezometers and tensiometers.

Transducers continuously recorded suction values during the flow test. Piezometers were read manually at varied intervals determined in the field based on the rate of change of the data. Figure 2-22 shows a typical instrument line as well as a photographic view of the three installed instrument lines. Tensiometer locations are named to reflect the type of instrument, the row number, the section number, and the depth in inches (i.e., T4A-18 is a tensiometer located in row 4 within Section A, and was installed to a depth of 18 inches below grade). The naming convention is illustrated in Figure 2-22. Figure 2-23 shows the layout of instrument Line A in cross section relative to the upper and lower trenches. Instrument Line C, within the control area, has an identical instrument layout.
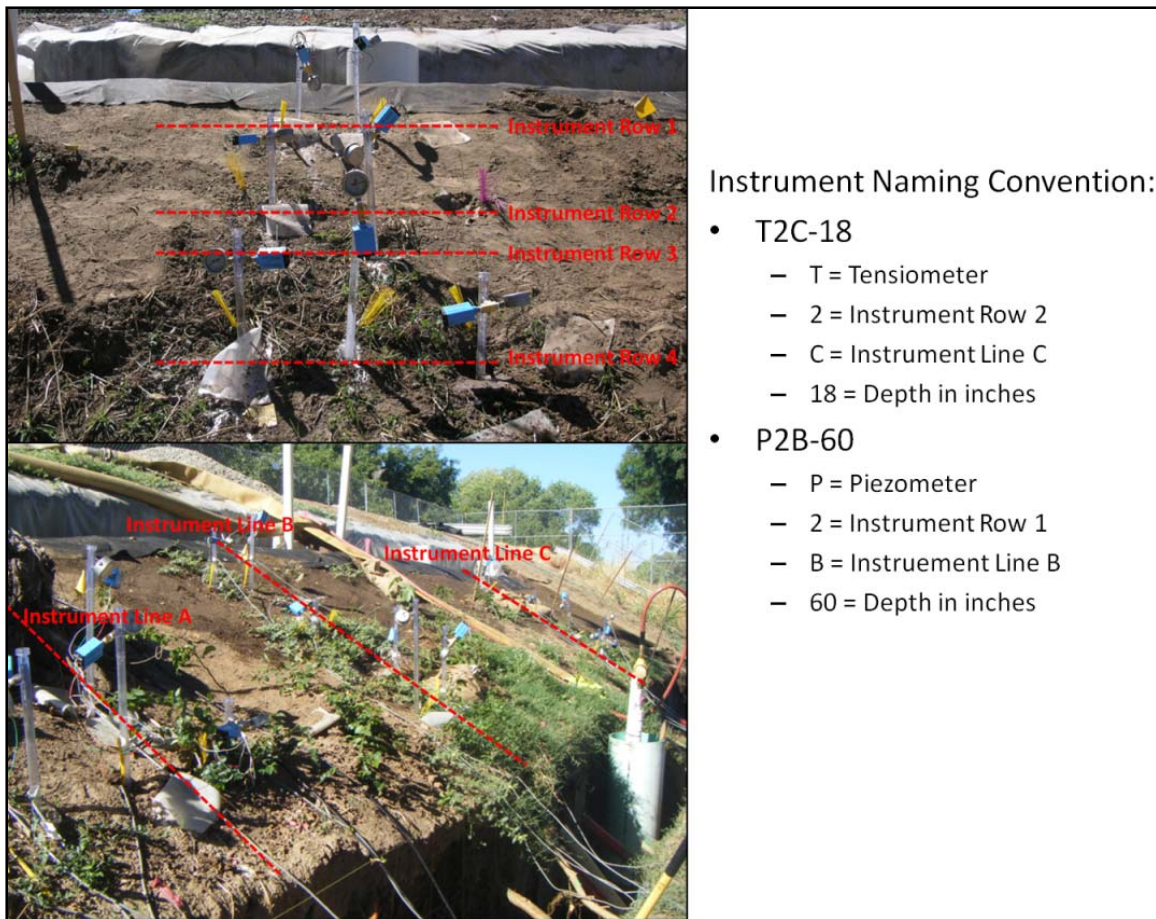


Figure 2-22. Photographic instrument plan showing the locations of piezometers and tensiometers as well as the naming conventions.
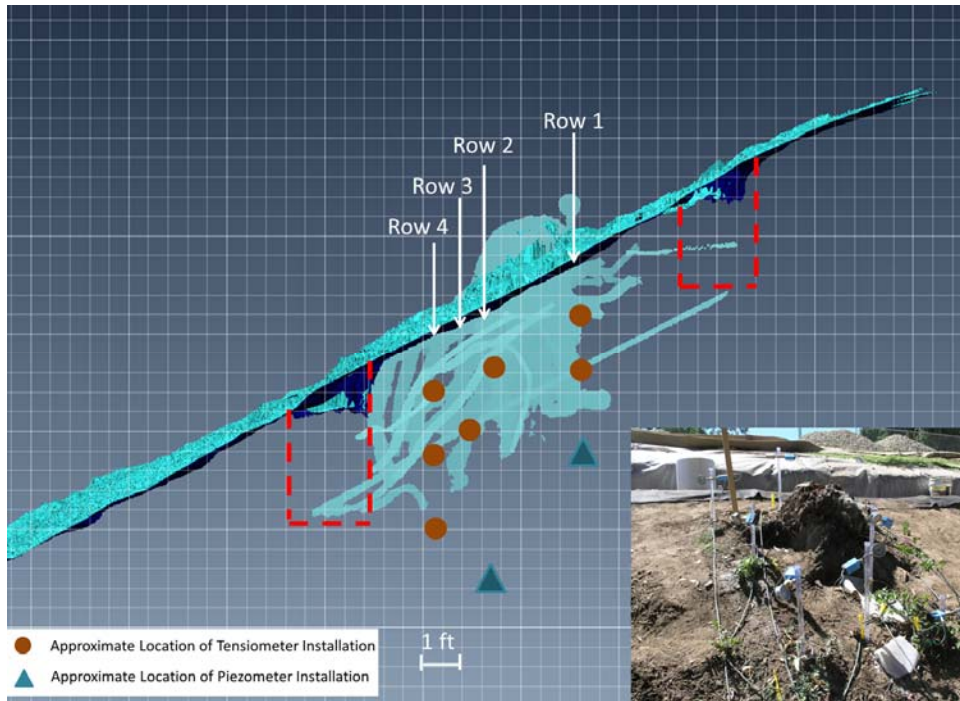
Figure 2-23. Instrument layout at Line A at the eucalyptus stump in photograph and cross section. Base T-LiDAR image provided by Gerald Bawden, USGS.

### 2.1.4    Site Construction

#### 2.1.4.1   Trench Excavation

Upper and lower trenches were constructed to depths of 3 and 4 feet, respectively, using primarily manual efforts to loosen soils (shovels, digging bars, and trowels) and a vacuum trailer to remove spoils (Figure 2-24). Where decomposing roots were found, manual excavation allowed them to be viewed photographed and appropriately characterized. Where live roots were encountered, an air knife operating with a compressor capable of compressing 375 cubic feet of air per minute (CFM) was used to excavate around roots. Most areas were excavated with a lower compressor setting in order to minimize disturbance to sidewalls and fragile areas where decomposing roots were suspected.

Live roots were sketched onto logs and photographed prior to being gently cut with hand tools to avoid disturbance in the vicinity of roots. Roots were more abundant in the stump trenches relative to the control trenches (Figure 2-25 and Figure 2-26).

29

Figure 2-24. Construction equipment used during excavation. A) hand excavation with vacuum to remove spoils; B) a vacuum trailer; C) air knife used to excavate around live roots; D) 375 CFM compressor to run the air knife.
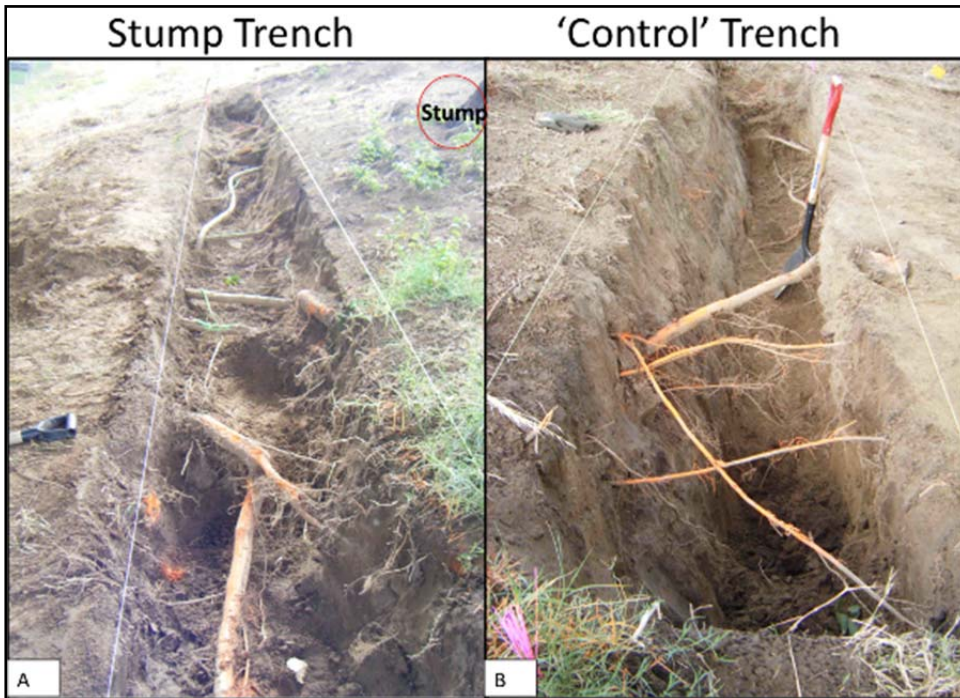


Figure 2-25. View of trenches, A) looking east at stump trench and; B) looking west at control trench.

Figure 2-26. View of upper trenches, A) looking west at stump trench and; B) looking east at control trench.

String was stretched across the trenches in 1 foot increments to facilitate plan-view sketches and photographic documentation of the root system (Figure 2-27 and Figure 2-28). Not all roots in the logs are visible in the photograph as shallow roots were removed as needed to achieve depth. Appendix 2C provides a complete set of similar plan view site logs and spliced photography. Roots are shown to be more abundant in the lower trenches than the upper. The lower trenches are closer to the live hackberry at the toe, which is the source of the live roots. Decomposing roots also appear to be more abundant in the downhill direction than the uphill direction.

Decomposing roots were found in the upper and lower trenches in the vicinity of the eucalyptus stump. Additional decomposing roots were found outside of the study area at the periphery of the excavations. Figure 2-29 and Figure 2-30 show an example of a segment of the control trench where a stump was uncovered on the downhill side during excavation. As discussed in Section 2.1.2, this may have been an original tree planted during Cal Expo construction in 1968 that was seen in aerial photographs to have disappeared between 1983 and 1990. The stump would have been decaying for 20 to 27 years at the time of our study there was no significant trace of a root system found to be associated with this stump within the trench.

Figure 2-31 provides another example of field logs correlated to photographic documentation of the roots encountered. When roots prevented excavation, they were carefully logged and cut prior to proceeding with additional excavation and documentation efforts. Figure 2-32 shows the same section of trench excavated to full depth. The photo shows roots and a metal pipe that are not visible in the photographs of Figure 2-31.
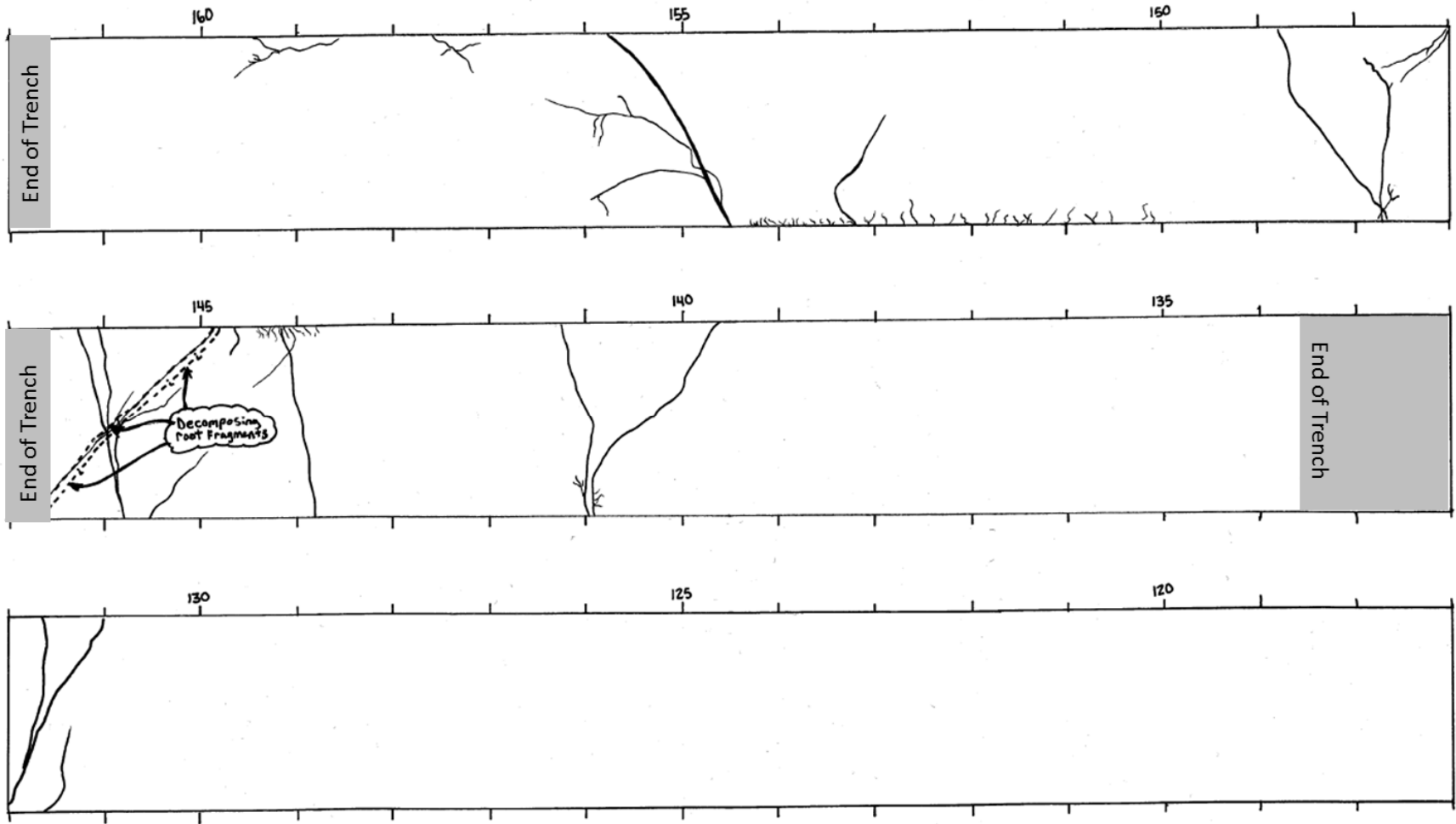
Figure 2-27. Upper stump and control trench plan view logs (Stations 117-162).
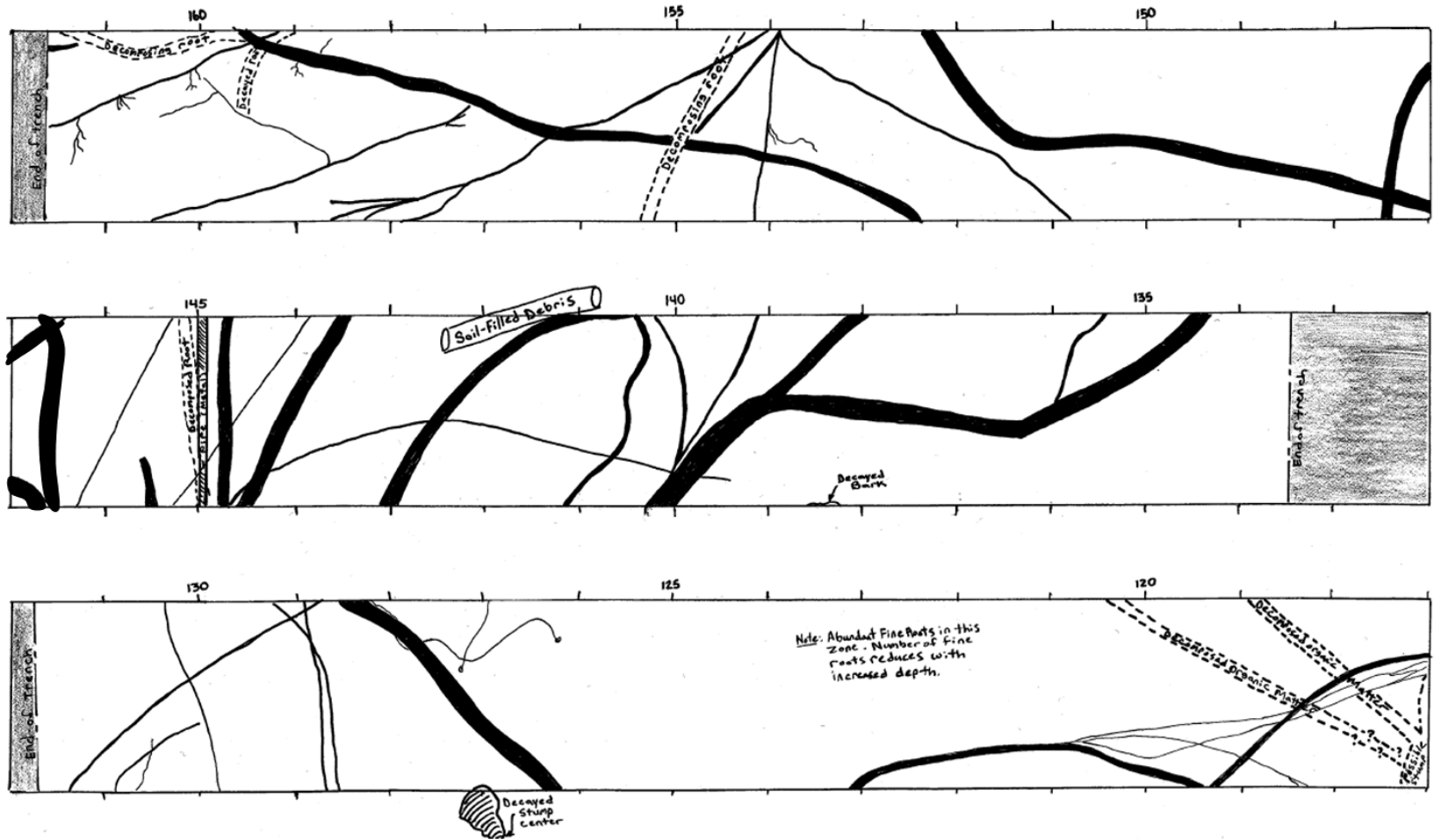
Figure 2-28. Lower stump and control trench plan view logs (Stations 117-161.5).

Figure 2-29. Lower control trench Stations 124-132. Spliced plan view photos (top) during excavation of lower control trench and log of analogous segment below.



Figure 2-30. Stump found on downhill side of control trench at Station 127 as shown on Figure 2-29.
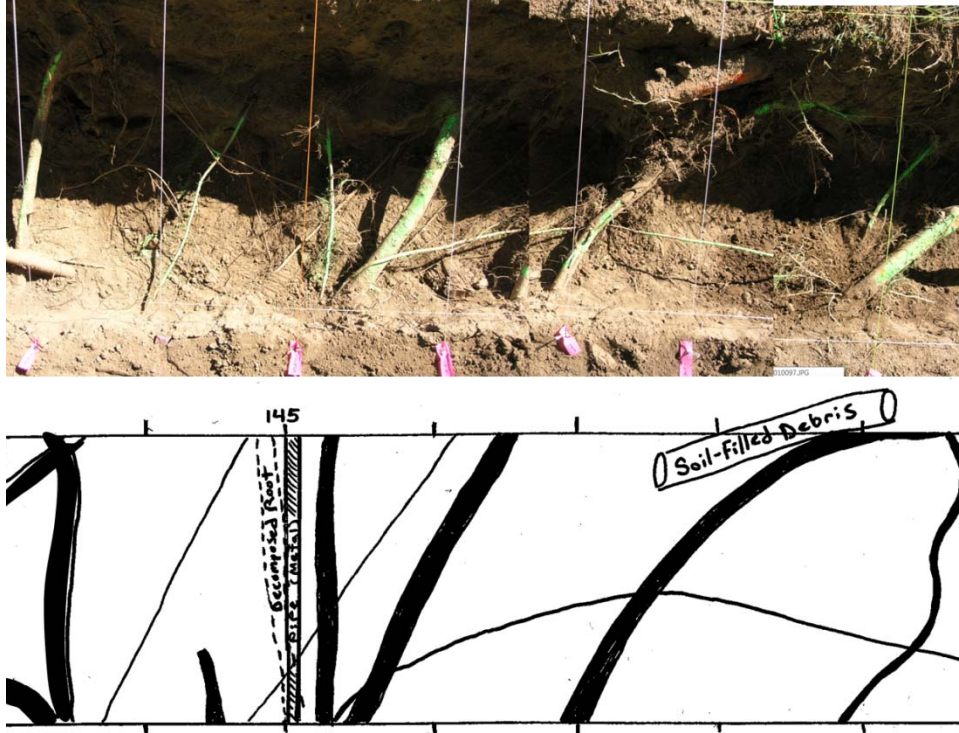
Figure 2-31. Lower stump trench Stations 140.5-146 (increasing to left). Spliced plan view photos (top) during excavation of lower stump trench and log of analogous segment below. Excavation not shown to full depth.
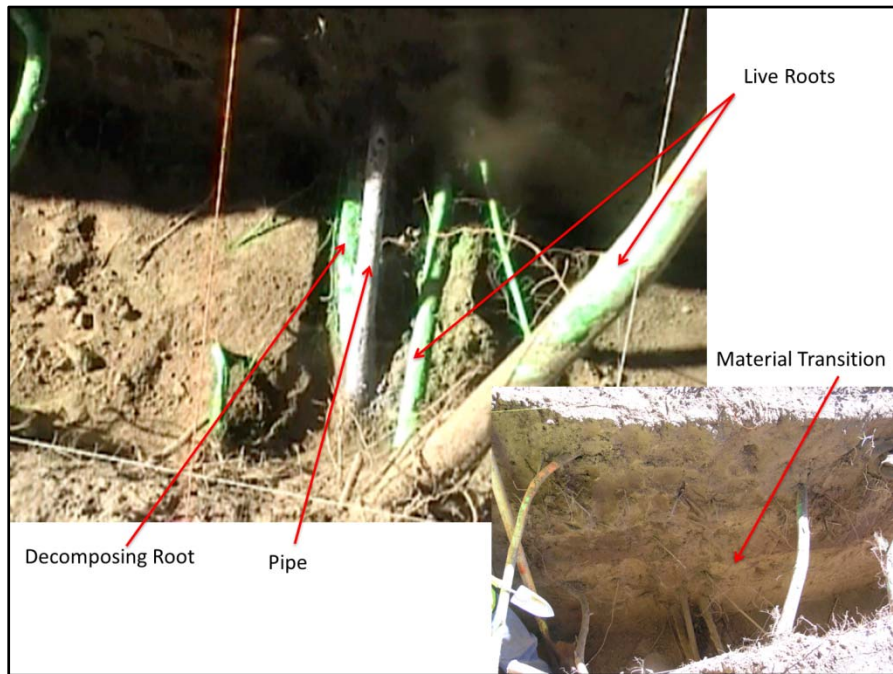


Figure 2-32. View looking south of 4' deep trench at Station 145. Upper left photos are a cluster of live and decomposing roots and a 1" diameter pipe. Bottom right is a larger view of the same trench segment.

Upon completion of trench excavation and plan view documentation, roots were cut flush with the wall face, a grid with 1-foot contours was placed over the uphill wall face in order to facilitate documentation (Figure 2-33).

Figure 2-34 shows a typical wall face field log including decomposing and live roots, animal burrows, and the metal pipe shown on Figure 2-31 and Figure 2-32 above. Complete trench wall logs are provided in Appendix 2C along with the plan view logs previously discussed.
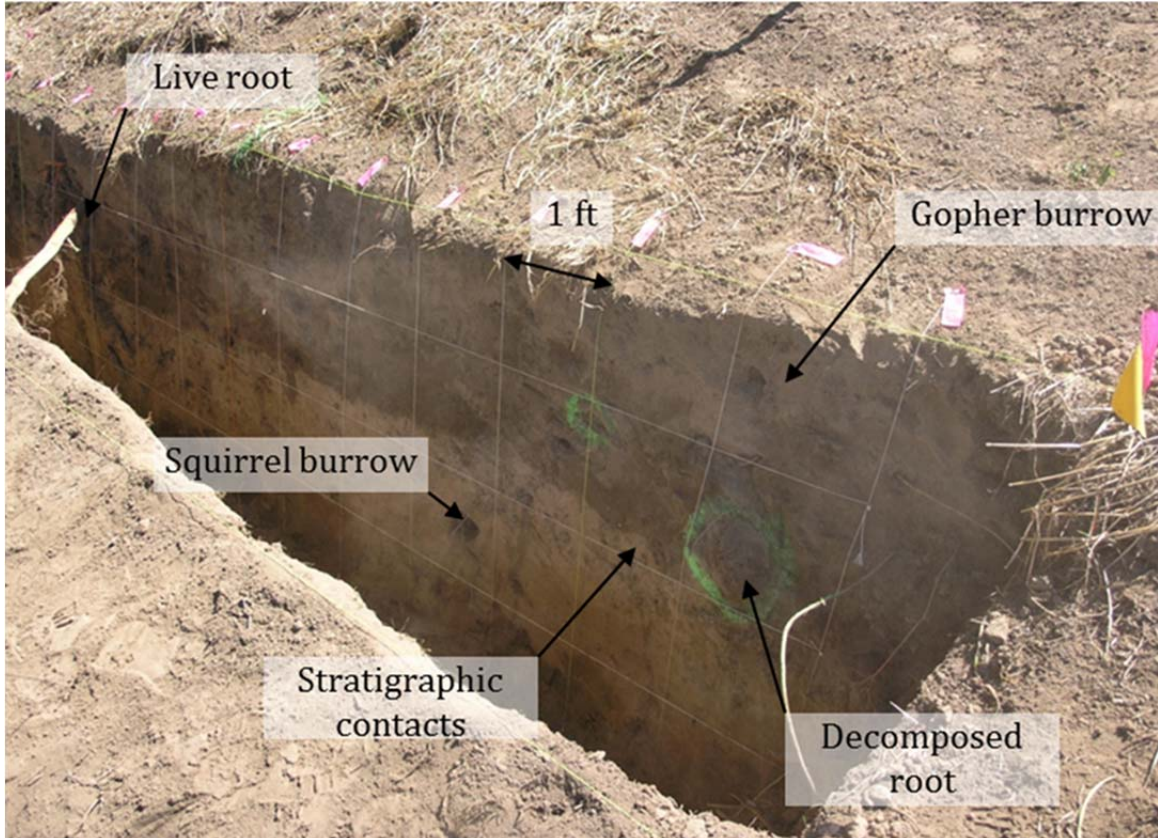


Figure 2-33. A 1-foot by 1-foot square grid was constructed to aid in logging and documentation of observations during the flow test. Source: Cobos-Roa et al. 2012.
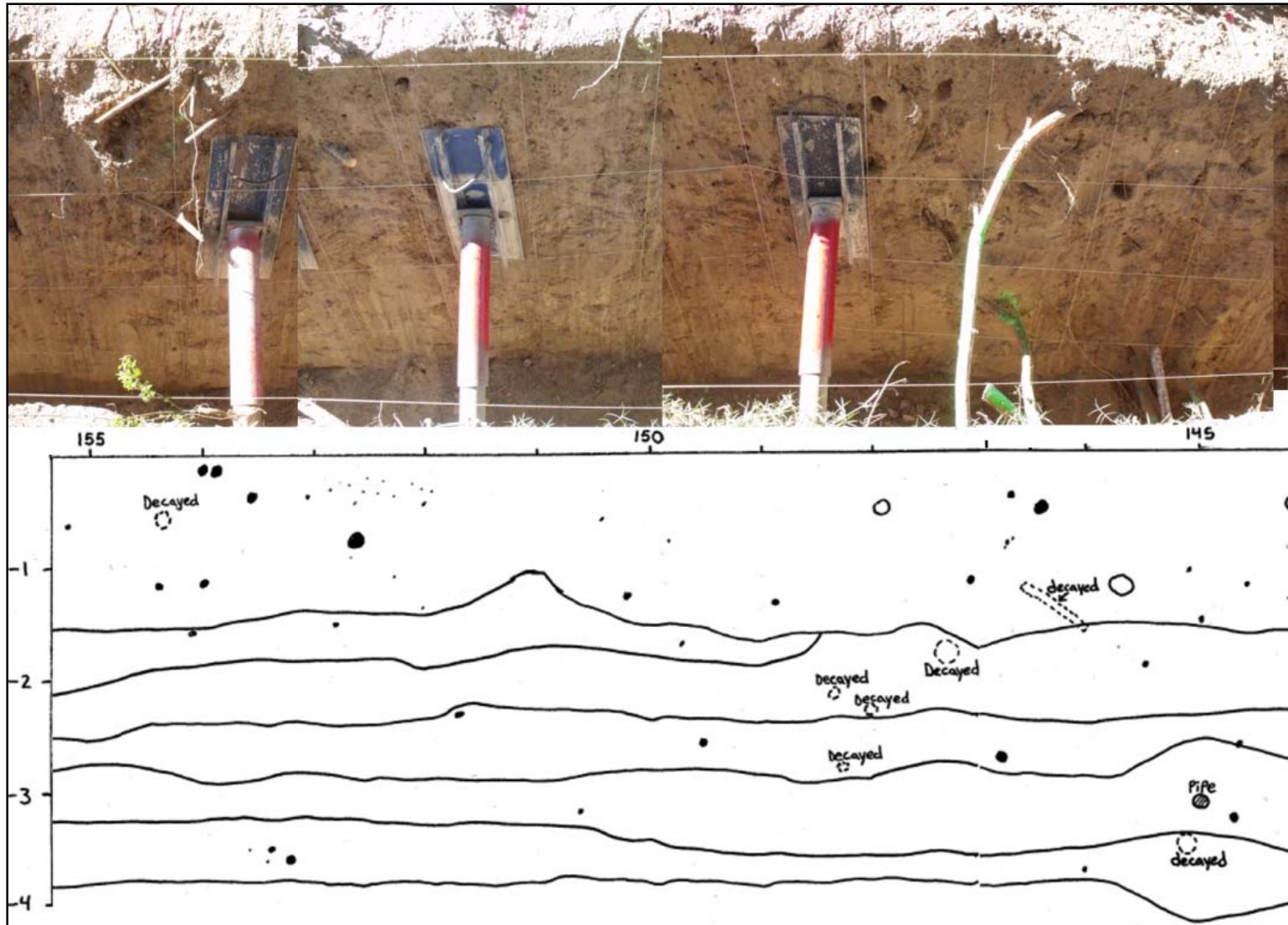
Figure 2-34. Field log of uphill trench wall of lower stump trench, Stations 144-155 with corresponding photos above.

During trench construction, consideration was given to grouting burrows onsite prior to the flow test. Field logs of the lower trench wall revealed 15 burrows in the uphill wall, while the downhill wall of the uphill trench did not reveal any burrows. As previously discussed and shown on Figure 2-3 and Figure 2-19, surface expressions of mammal burrows were observed across the site. The holes were viewed by a member of the CLVRP team, Dr. Dirk Van Vuren, a burrowing mammal expert from UC Davis. All of the locations were considered either abandoned ground squirrel burrows, which were partially collapsed and had not been in use for some time, or burrows of the pocket gopher.

Pocket gophers burrow day and night, using the burrow as a protective residence, a base for foraging, for feeding on roots encountered and to pull vegetation into the tunnel for food (Reichman et al., 1982). They may kick soil behind them as they dig, push soil to the surface, or backfill old tunnels as they make new excavations (Reichman and Smith, 1990). Holes are not much larger than the animal and are relatively horizontal and paralleling the ground surface (Reichman and Smith, 1990). Based on field discussions with Dr. Van Vuren, the work of Reichman et al (1982), and Reichman and Smith (1990), the pocket gopher leaves behind a shallow network of holes (1 to 2 inches in diameter), often slightly oval shaped, and partially filled with loose soil. On this basis, most holes in the trench walls were identified to be gopher burrows.

California ground squirrels make use of burrows for essential protection from predators, in inclement weather, for refuge at night, or for rearing offspring (Van Vuren and Ordeñana, 2012). These burrows have the potential to penetrate the width of a levee depending on burrow age and soil conditions, or could partially enter from both sides and full penetrate the levee (Van Vuren and Ordeñana, 2012). In the lower trench wall, Dr. Van Vuren was able to identifiy California ground squirrel burrows by their diameter (3 to 4 inches as opposed to 1 to 2 inches for the pocket gopher), as well as having a round, well-traveled appearance.

Of the fifteen (15) burrows logged in the lower trench wall, two (2) were considered squirrel burrows and thirteen (13) were identified as gopher burrows. One squirrel burrow extended back 10 inches into the uphill wall of the lower trench and the other 18 inches. A firm end was felt in these holes. The gopher burrows were small and exhibited many curves, making an accurate assessment of depth difficult. In generating field logs of the upper wall of the lower trench, numerous irregular features were documented, including:

- 1.5 to 2-inch holes (likely pocket gopher) in the shallow zones extending back a distance of a few inches to a little over a foot (Figure 2-35 A).
- Two holes of approximately 4 inches in diameter (believed to be ground squirrel burrows) extending back a distance of 10 and 18 inches from the upper wall of the lower trench.
- Live roots as shown on Figure 2-35C and in Sections 3.5.1 and 3.7.

- Decayed roots (of various levels of decomposition and some with small holes bored in them) as shown on Figure 2-35A and B and in Sections 3.5.1 and 3.7.
- A 1.5 inch diameter metal pipe at a depth of nearly 4 feet in the lower trench (pipe points downhill at approximately 11 degrees from horizontal) as shown previously in Figure 2-32.
- Small holes of ½ to ¼ inch in diameter. Based on observations with Dr. VanVuren, we believe the holes may be related to ant activity at the site (Figure 2-36). During excavation, worms were also seen creating and traveling through small holes in the trench walls as shown on Figure 2-37.
- Differing material types ranging from loose sandy silts and discontinuous pockets of clean sand to clayey silts and occasional lean clays.
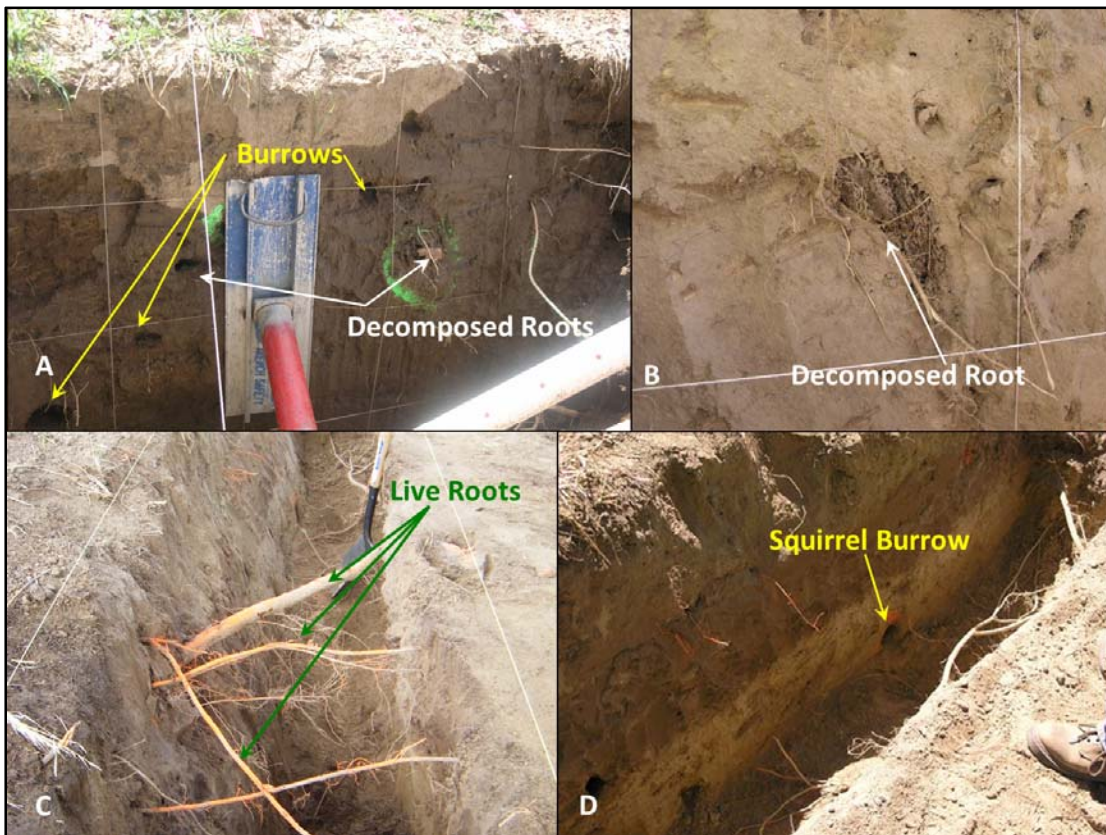


Figure 2-35. Lower trench photos with A) burrows and decomposing roots, B) a decomposing root, C) live roots, and D) a squirrel burrow and a material change.

With a range of irregular features present and no clear or unobstructed input locations to provide a natural place for grouting, we elected not to grout. During Dr. Van Vuren's visit, we explored several locations along the northern levee of the American River and found that gopher and ground squirrel activity would be difficult to avoid altogether. At the time of trench logging, no one hole appeared to act as a through pathway for seepage, or "pipe" from the top trench to the bottom

trench. Accordingly, we decided to view the relative influence of the live and decaying root systems in a real levee system rather than fill visible holes when uncertain which would become preferred pathways.



Figure 2-36. Ants encountered during trenching activities (left). Small holes (1/2 to ¼ inch) found in trench wall could be related to ant activity (right).



Figure 2-37. Worm activity was observed to be responsible for some of the small holes (<¼ inch diameter) encountered during trenching.

### 2.1.4.2 Preparation of Trenches for Flow Test

Upon completion of trench excavation, the upper trench was lined with a plastic membrane along the upslope wall, base, and sides to minimize flow of water to areas outside of the study area. The upper trenches were then filled with ¾ inch of clean crushed rock to maintain stability throughout the test. Lower trenches were lined with plastic sheeting along the base and a thin layer of rock was placed to hold

the sheeting in place. The upslope wall was left open for viewing during the test (Figure 2-38). An effort was made to place hydraulic shoring such that key features observed in the wall during the logging phase were not obscured from view.

Figure 2-38A shows the 1 foot wide band of soil that separated the 'control' and 'stump' trenches. The band of soil was not expected to fully prevent flow between the zones. The upper trench was separated to allow the flexibility of inflow into the two trenches separately in the event that one or the other needed to be shut off due to unforeseen conditions. The lower trench was separated so that outflow volumes from water entering the two trenches could be separately tracked. In photo B, the lower trenches are shown shored for stability with hydraulic vertical shores placed at intervals of 2 to 5 feet across the lower trench, taking care not to obscure visible irregularities such as decaying or live roots or mammal burrows. Slopes and trench walls were periodically moistened to aid in air knife excavation and prevent cracking prior to the flow test as shown on photo C.



Figure 2-38. Trench preparation prior to commencement of flow. A) Upper trenches lined with plastic sheeting (uphill and base walls) and permeable fabric (downhill wall); B) shored lower trench lined with plastic sheeting and gravel (base); C) water truck moistens site to prevent cracking prior to flow test.

Once trench excavations were complete, the water delivery and pumping systems were installed to deliver water into the upper trench. A 2500-gallon polyethylene tank was placed on the levee crown and filled prior to commencement of the test. Figure 2-39 shows the water delivery and recycling system installed at the site. Water was delivered into the upper trenches via a 15-inch well casing connected to

a perforated pipe embedded in the gravel-filled upper trench. The pipes acted as a water delivery manifold rapidly distributing the water throughout the upper trenches (Figure 2-39A). Perforated riser pipes at the trench ends provided points along the trench to confirm water levels. Fire hoses were used to deliver water (Figure 2-39B and D) into a 15-inch diameter perforated pipe through a mechanical float valve (Figure 2-39D). The float valve is shown mounted into the well casing and used to maintain a constant head in the upper trenches during the flow test. The water tank was refilled throughout the test and the level of water in the tank as well as flow volumes of water into the tank were measured and used to approximate the amount of water delivered into the upper trenches with time. Water collected from the lower trenches was recycled into the delivery tank. All flows into the tank were tracked using ¾ inch flow meters (Figure 2-39C).
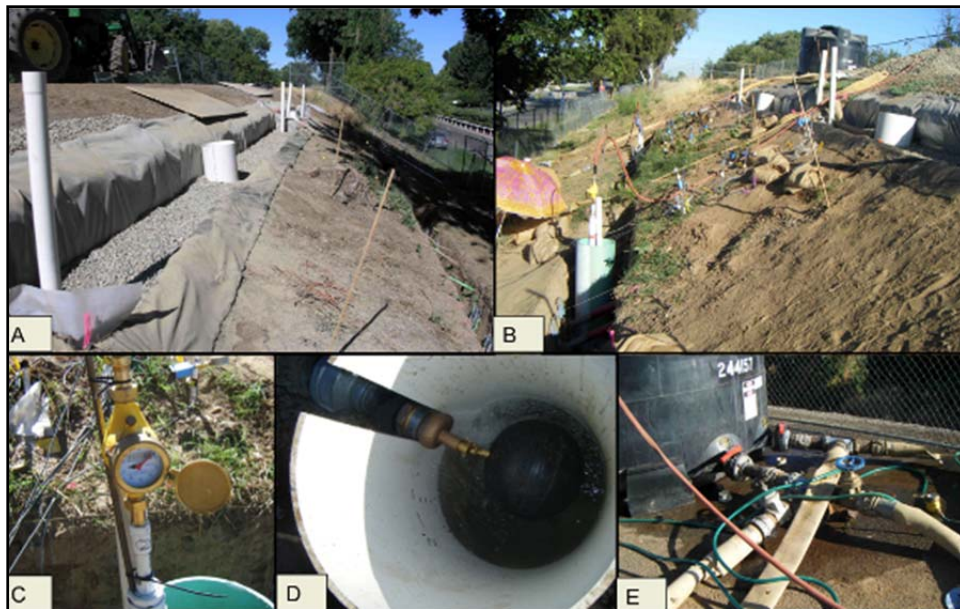


Figure 2-39. A) Upper gravel-filled trenches; B) Water delivery system; C) ¾" flow meter for monitoring flows into water storage tank; D) Mechanical float to maintain constant head in upper trenches;  E) Control valves at tank

### 2.1.4.3   Instrument Installation

Tensiometers were obtained from Soil Moisture, Inc. and equipped with a mechanical pressure gauge and a pressure transducer with maximum suction capacity of 100 kpa (Figure 2-40). Tensiometers of 24, 48 and 60 inches were installed to depths of 18, 36, and 60 inches, respectively. All instruments were installed in accordance with the manufacturer's specifications. Holes were advanced with a gauge auger (provided by the manufacturer) with a diameter slightly larger than the instrument diameter of ¾ inch. The instrument holes were logged for soil conditions prior to installation.

Figure 2-40. A typical tensiometer is shown including a mechanical gauge and pressure transducer. White silica sealing material is seen at the hole entrance.

Tensiometers were pre-assembled and saturated prior to installation. All connections were cleaned, and the gauge and transducer ensemble were connected to the tensiometer, taking care to properly achieve a seal on each connection. The porous tips were pre-saturated and brought to the site in de-aired water. In a lab, the porous stones that communicate with the soil were pre-saturated in a vacuum with de-aired water and connected to the tensiometer onsite just prior to installation. De-aired water was brought into each instrument through a suction pump attached at the top. Once the tensiometer was filled, the suction pump was used, along with tapping action, to remove trapped pockets of air from the gauge and transducer connections.

With all seals checked and no observed leaks, a silica slurry was mixed to create a seal between the soil and the tensiometer. This step is optional according to the manufacturer if the hole is snug to the tensiometer, but proved helpful in our soil conditions. A seal was established between the porous ceramic tip of each tensiometer and the surrounding soil using a slurry of water and silica flour with silt-sized particles (Figure 2-30). The tensiometer then communicates with the surrounding soil by allowing water in the instrument to flow into the surrounding soils until the tension in the instrument matches the tension in the surrounding soils. The suction created by the column of water in the instrument is subtracted from recorded suction values. Water is periodically refilled by opening the

43

instrument, losing tension, refilling, closing the instrument, and allowing time for re-establishment of tension.

During installation of instrument Line A in the vicinity of the Eucalyptus stump, 6 of 6 tensiometers encountered decomposing roots in the auger holes, 3 instruments encountered live roots, and 2 instrument tips were placed partially within decomposing roots. While augering holes for tensiometer installation at Line C, two holes encountered live roots. See Figure 2-21 for instrument locations. A detailed summary follows:

- T4A-18 and T4A-36 encountered live roots at their tip
- T1A-18, T3A-36, T4A-18, T4A-36, T4A-60, P2A-84 encountered decomposing roots during augering
- P1A-60, T4A-36, P2A-84, T4C-18, P2C-84 encountered live roots during installation

Instruments installed within row 4 of instrument Line A (below the Eucalyptus stump) were among those encountering decomposing roots during installation (T4A-18, 36, and 60). The tensiometers were located approximately 16 inches from the uphill wall face of the lower trench (measured horizontally). Within 1 hour of installation, silica slurry was observed trickling out of two exposures of one of the decomposing roots. Photos were taken and observations were recorded (Figure 2-41). Excavation of the root system at the end of the flow test revealed a number of locations where silica slurry flowed for distances of a few inches to approximately 5 feet along a decomposing root within a cavity observed between the decaying bark and the inner woody core (*xylem*) of the root.
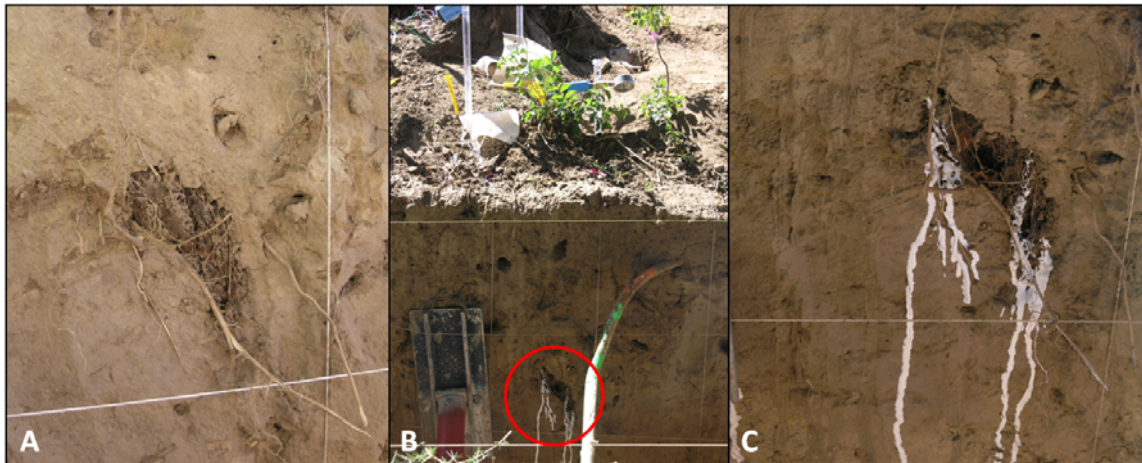


Figure 2-41. Silica flour migration pattern below the stump (red circle) following installation of tensiometers.

## 2.1.5    Flow Test

Following instrument installation, instruments were monitored for several days with stable readings prior to the beginning of the flow test. On September 7, 2010 at 11:57 am, the valve from the 2500 gallon polyethylene water storage tank located at the crown of the levee was opened and water was channeled via gravity flow into the upper trenches via the input hoses connected to mechanical float valves located at two input sites at the approximate centers of the upper stump and control trenches (Figure 2-39). The flow test ran for approximately 6 days after which the trench was allowed to drain and monitoring continued as measured soil suction values began to increase with the drying of site soils. A detailed timeline showing the duration of each phase of testing as well as key observations is presented as Figure 2-42.
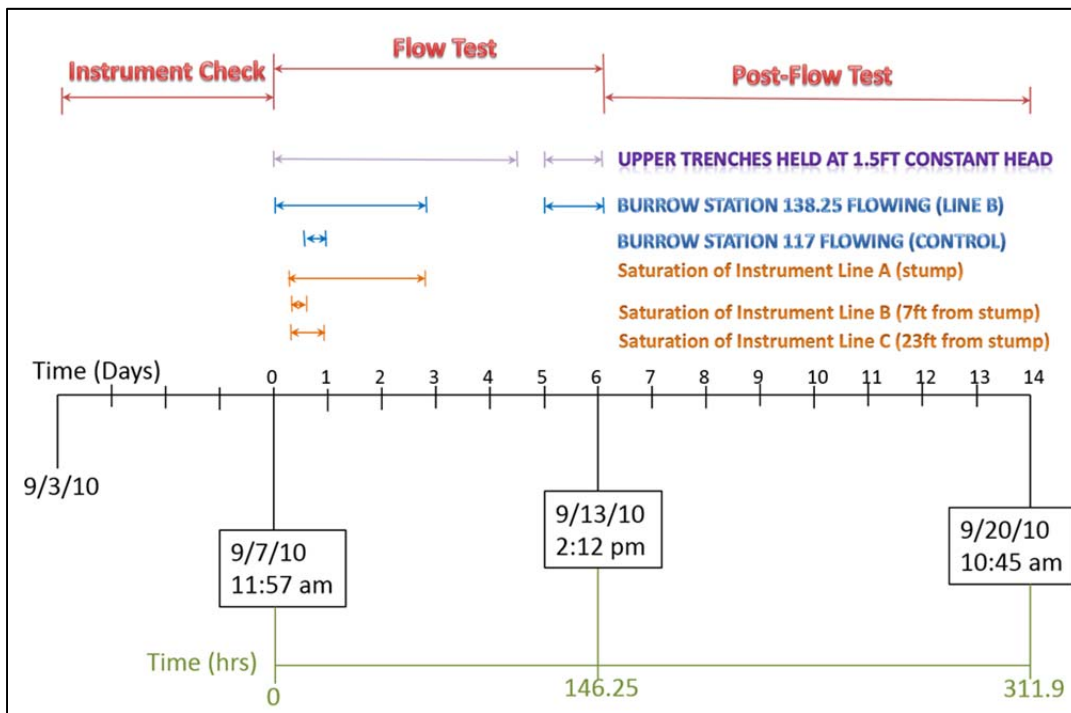


Figure 2-42. Flow test timeline.

The upper trench was approximately 2 feet deep on the downhill side. The constant head height in the upper trench was set to 1.5 feet above the base to avoid overflow or failure of the trench wall. A constant head was held for 4 days after which a nighttime malfunction caused the water to temporarily stop flowing. On the morning of September 12, water in the trenches was brought back up to a constant 1.5 feet above the trench base and held for the remainder of the flow test. When water in the lower trench reached 5 inches in depth, a pump recycled the water into the storage tank. Visual observations and measurements of soil suction and pore pressure between the trenches were recorded during the 6 day flow test.

Upon the commencement of water flow into the upper trench, early observations in the first 24 hours were primarily surficial seeps along the face of the levee slope between the two trenches, and flow from animal burrows. When surficial seeps were first observed, the location and time of seep was noted in field logs and then photographed. If the seep was rapid or threatened to erode the slope surface, it was slowed through use of a gravel bag placed over the seep.

On days 2 and 3 of the flow test, we saw seepage locations expanding and saturating the slope face and by day 3 we saw a reduction and then stoppage of flow from the gopher burrows. On days 2 through 4, our observations gradually shifted from the saturation and seepage patterns of the slope face to the arrival of the wetting front in the uphill wall face of the lower trench. The wetting front began to slowly move up the trench wall from the bottom up. The uphill face of the trench wall saw the wetting front climbing faster than the lower trench wall, indicating that the water was not purely a result of capillary action from the standing water that had accumulated in the base of the lower trench (from gopher burrow flows). This capillary action from the standing water in the trench masked any arrival of the wetting front in the lower 1 foot of the wall trench on day 1. By day 2, however, wetting patterns began to climb above the wet zone at the base of the trench and patterns were recorded.

Photographic timelines are provided below detailing levee slope face seepage and wetting patterns, the seepage observed related to two gopher burrows that played prominent roles in the flow test, and the wetting front patterns observed on the wall faces of the lower trenches.


2.1.5.1   Levee Slope Face Seepage

Seeps along the levee slope face between the upper and lower trench were the first sign of water movement between the two trenches and began happening within 30 minutes of turning on the water to the upper trench. The stump trench reached the pre-determined constant head of 1.5 feet of water in the upper trench at 12:22pm after the water had been turned on at 11:57am. Water was observed seeping out of the slope face at 12:21pm (Time=0.45 hrs) at Station 140. A gravel bag was placed over the seep within a few minutes of the initial seep and within seconds water began flowing from the lower wall face through a gopher burrow at Station 138.25. This burrow will be discussed in detail in Section 3.6.2. Figure 2-43 through Figure 2-45 follow the slope seepage patterns at instrument Lines B and C at 9.25 hours, 19.5 hours, and 55 hours into the flow test, respectively. A detailed timeline of slope face seepage is provided below in Table 2-2.

Figure 2-43. View of instrument line C (left) looking west and instrument Lines A and B looking east (right) 9.25 hours into the flow test. Note isolated seeps (darker spots) and gravel bags (covering seeps) at the top of Line C and extending down Line B.
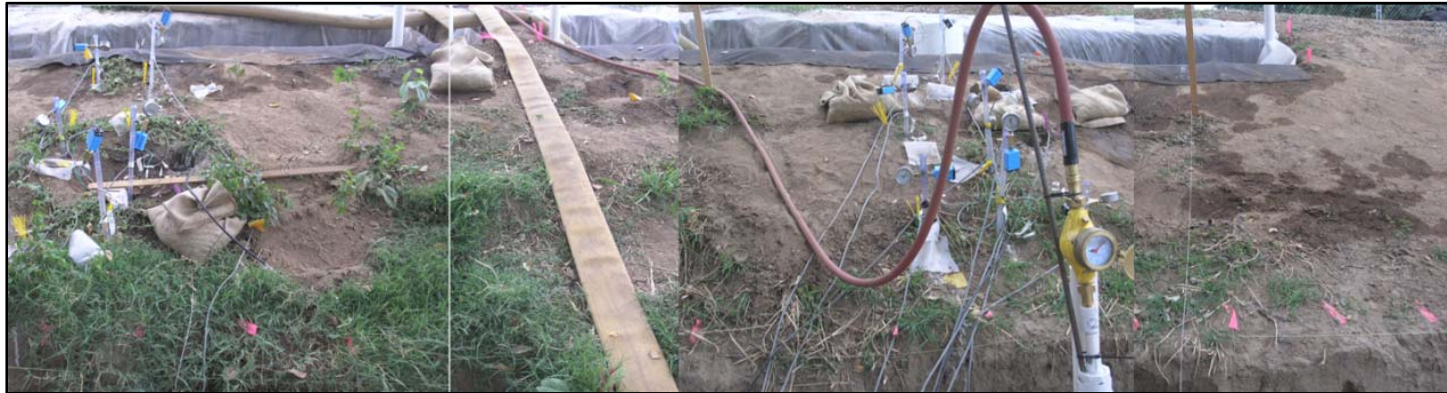
Figure 2-44. View of instrument Lines B and C looking south 19.5 hours into the flow test. Note wet zones in slope face (darker spots) and gravel bags (covering seeps).
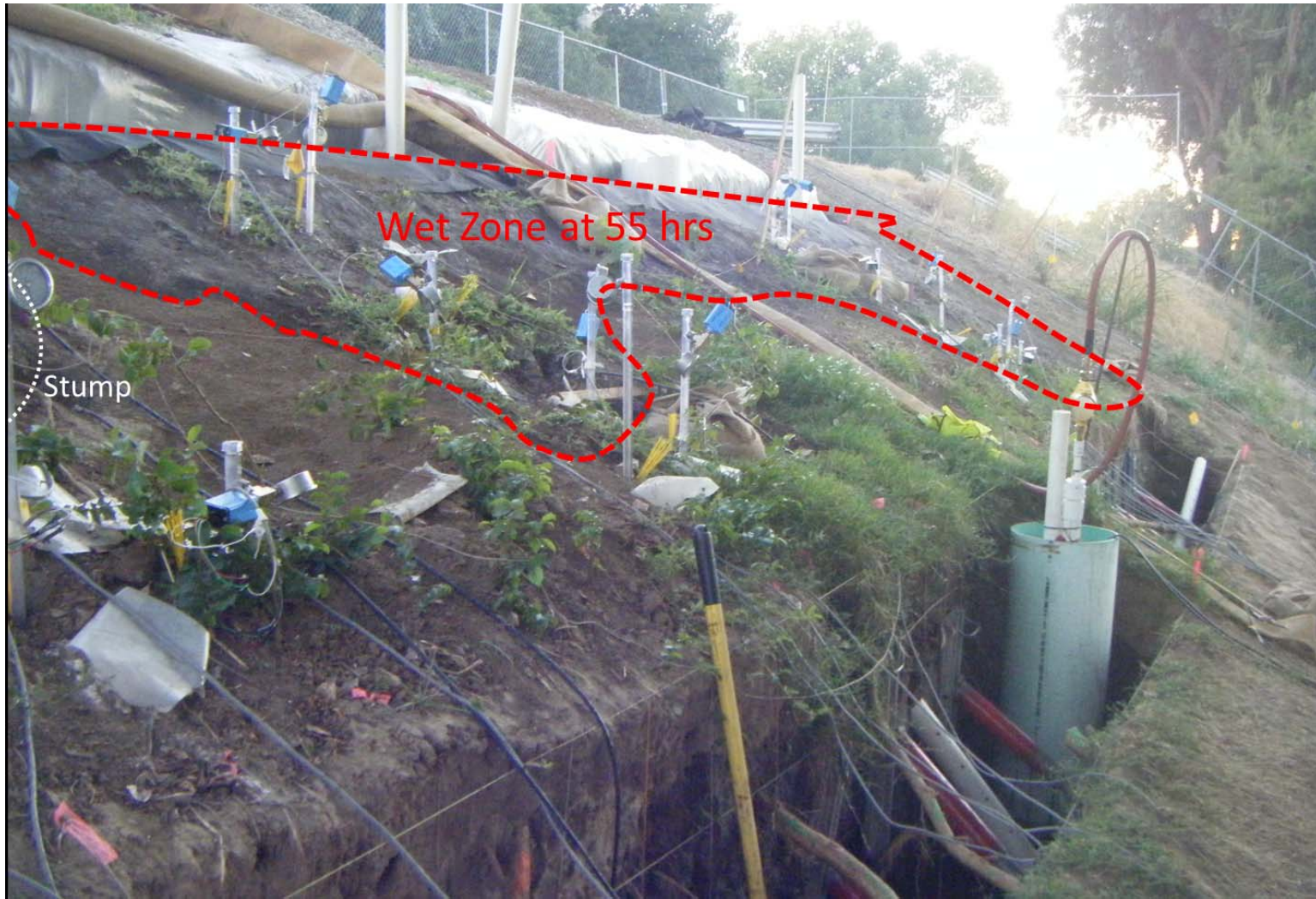
Figure 2-45. View looking west from instrument Line A at stump at 55 hours into the flow test. Note the outline (red) of the growing wet zone observed at the levee slope face.

Table 2-2. Photographic Timeline of Slope Face Seepage

| Time (hrs) | Observation | Photo or Illustration |
|---|---|---|
| 0 | Water flow begins | |
| 0.45 | Sta. 140 (Instrument Line B) at 2.3 feet upslope of lower wall face, water seeping out of slope near T4B-36, P2B-24, and T3B-36; water began pouring down the face of the lower wall threatening to erode; gravel bag was placed over each seep |  |
| 0.60 | Seep at Sta. 123, 125, 127 (Instrument Line C – Control). Gravel bags were placed |  |
| 0.73 | Seep Sta. 116 (west of control and 7" uphill of lower trench) |  |

| 0.9 | Seep at Sta. 135, 1.8 ft down from upper trench |  |
|-----|-----|-----|
| 1.4 | New seeps between old seeps at instrument rows 1 and 2 at Stations 121, 122, 125 (Instrument Line C). Instrument rows increase from top trench to bottom trench. | No photo available. |
| 2.3 | Sta. 120-122 seeps observed between upper trench and instrument row 2 (just west of seeps at Instrument Line C) |  |
| 3.7 | Sta. 120-128 existing seeps expanding in size while adjacent new small seeps form between gravel bags |  |

| 5.2 | Sta. 141 a 7" diameter seep southeast of tensiometer T3B-36 |  |
|---|---|---|
| 10.3 | Seep at Sta. 117 at western limit of lower trench and extending down the western end wall of the trench as it grows |  |
| 15.7 | Sta. 117 to 125; Seeps growing larger and pipe placed at area of rapid flow to prevent erosion |  |
| 19.8 | Moisture seeping from eastern-most leg of equipment table below lower trench (outside of study area) | No photo |
| 23.6 | New seep at Sta. 127 at 1 ft above tensiometer T4C-18 | No photo |
| 54.4 | New seep near Sta. 131 |  |

| 54.4 | Seep near upper trench at Sta. 155 and greater |  |
|------|------------------------------------------------|---------------------|
| 67.6 | Pattern of small seeps observed about 10 feet west of western limit of control trench, following a line of gopher burrows visible from surface |  |

As shown in Table 2-2, burrow patterns were found to have a major influence on slope face seepage patterns and flows throughout the test. For this reason, burrows influencing flow patterns are discussed in detail in Section 3.6.2.

2.1.5.2   Burrows at Instrument Lines B and C

During the flow test, wetting front and water flow patterns appeared to be dominated by flow through a network of shallow gopher burrows in the vicinity of instrument Lines B (7 feet west of the stump) and C (in the control trench). Figure 2-46 shows the alignment of the burrows. The burrow pathways were grouted, excavated, and mapped after the flow test. The burrow at Line B extended all the way from the upper water delivery trench down to the lower stump trench. The burrow at instrument Line C began at the upper control trench but did not appear to continue all the way to the lower control trench. Both burrows connected to the upper trench and neither was detected prior to the flow test, despite careful documentation. Figure 2-46 shows the excavated burrow alignments.
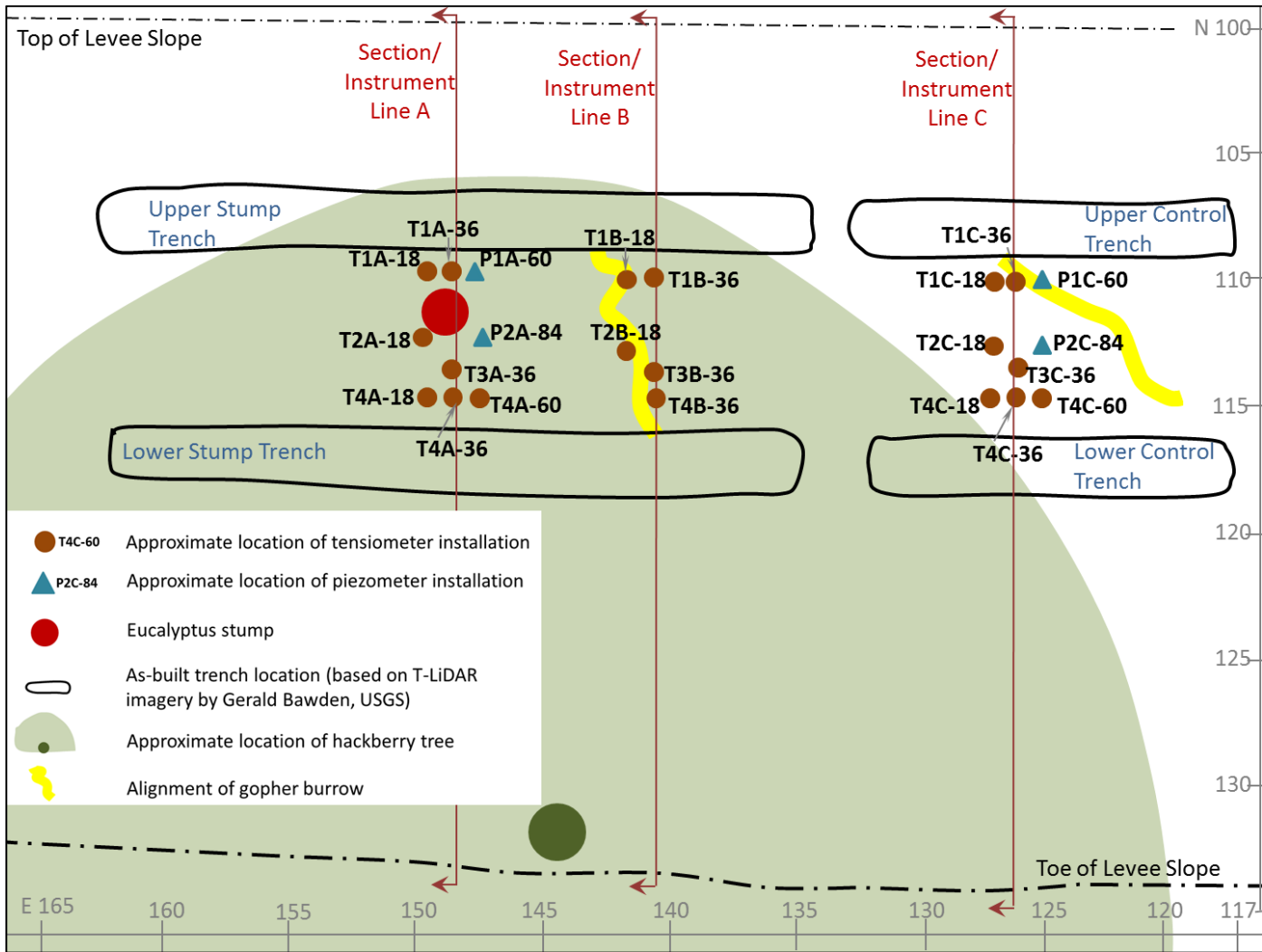
Figure 2-46. Location of mammal burrows in relation to Instrument Lines A, B, and C.

The gopher burrow at Line B produced water at the lower trench approximately 30 minutes following the beginning of water flow to the upper trench, about the time needed to fill the trench. Flow began as a small seep at the levee surface and proceeded to flow through a gopher burrow at the face of the lower wall upon placement of a gravel bag at the location of the initial seep (Figure 2-47). Table 2-3 provides a detailed account of observations associated with the flow of water through the gopher burrow at instrument Line B, Station 138-140. Table 2-4 provides a similar account for a gopher burrow encountered near instrument Line C that extended down toward the western corner of the control trench. Based on post-test grouting of the burrow adjacent to instrument Line C, the hole did not connect directly to the lower trench. A preferred flow pathway appears to have been established via another gopher burrow at the western extent of the lower control trench. It is possible that the gopher burrow networks once connected and a collapsed or plugged segment did not allow the grout to fill the full extent of the burrow. Instrument test results presented later in this report will detail the arrival of the wetting front in the vicinity of these burrows compared to the vicinity of the eucalyptus stump.
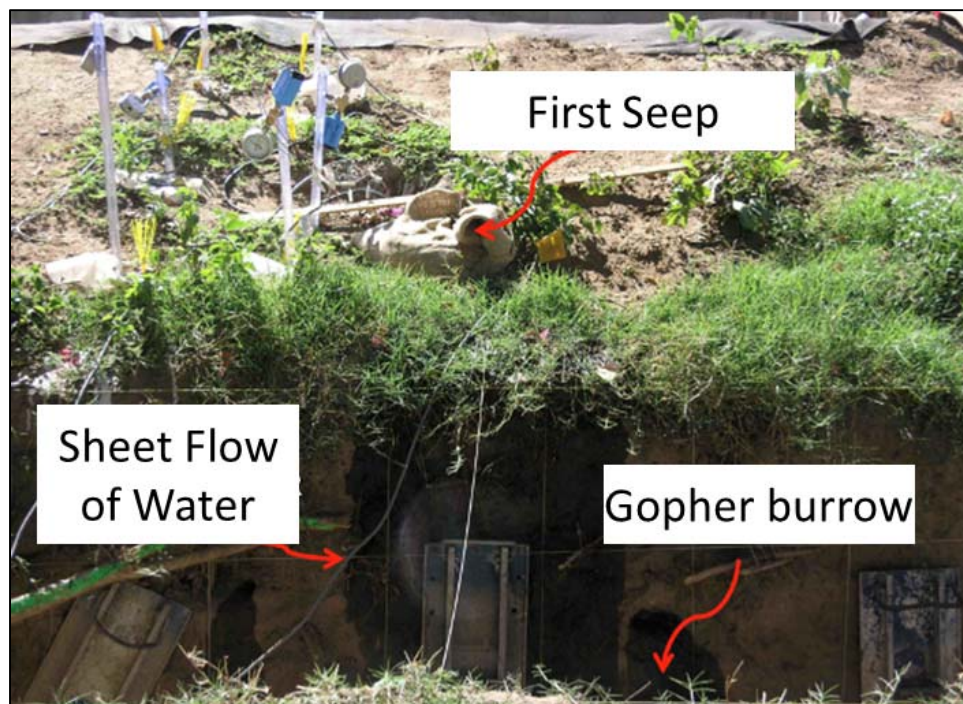


Figure 2-47. Water seepage at lower trench wall near gopher burrow at instrument Line B minutes after first water appeared on the levee slope face.

Table 2-3. Summary of observations at animal burrow at Station 138-140 (Line B)

| Time (hrs) | Observation | Photo or Illustration (if available) |
|---|---|---|
| 0 | Begin water flow. | No photo |
| 0.45 | Water seeping out of slope face at tensiometers T4B-36, P2B-24, T3B-36. |  |
| 0.52 | Gravel bag placed on slope seep. | Figure 2-47 |
| 0.53 | Water burst from gopher burrow at Sta 138-139 and Sta 141 (both about 1.2 feet down from top of wall). Station 138-139 produced the majority of free water. |  |
| 1.2 | Measured 4.3 inches standing water in lower stump trench due entirely to water flow through gopher burrow at Sta 138-139. | No photo |
| 4.7 | Water level in lower stump trench at Sta 138 is 0.65 ft above bottom. |  |

| | | |
|---|---|---|
| 5.85 | Water seeping out of saturated zone east of gopher hole at Sta 138-139. |  |
| 55.1 | Flow through gopher hole at Sta 138-139 slowing rapidly between 53.1 (rate = 2 gal/min) and 55.1 hrs (rate = 1.7 gal/min). |  |
| 67.1 | Flow has stopped and all that remains is moisture seeping through as seen in the photo to the right. This observation was made early in the morning and no observations were made between the last recorded observation at time = 55.1 hours. |  |
| 97.6 | Left site for the night; tank full and upper trenches at constant head 1.5 ft above trench bottom. | No photo |
| 118.4 | Arrived onsite in the morning (Sept. 12) to find the tank empty and upper trenches below 0.5 ft. | No photo |
| 122.1 | Tank full and upper trenches back to constant head. Gopher burrow at Sta 138.25 begins to flow water. | See photo at 125.9 hours |

| 125.9 | Water seeping out of wall face near burrows at Station 138.25. Much of the walls appear to be saturated. |  |
|---|---|---|

Table 2-4. Summary of observations at gopher burrow, Station 117 (control trench)

| Time (hrs) | Observation | Photo or Illustration (if available) |
|---|---|---|
| 0 | Begin water flow | |
| 0.73 | Seep Sta. 116 (west of control and 7" uphill of lower trench). Original seep location is under the gravel bag in the photo below (time =10.27 hrs). | See photo at time = 10.27 hours. |
| 10.27 | Seep observed at the western end of the control trench at Sta. 117 |  |

| | | |
|---|---|---|
| 10.52 | Water burst through trench wall at Sta. 117 and began to flow through gopher burrow (< 2" in dia). Some decomposed root fragments came out of the hole, likely from old stump and root system. Water begins ponding in control trench. |  |
| 22.6 | Water stops flowing through gopher burrow. Seep continues to produce moisture and water wicks up the lower trench walls adjacent from the standing water in the base. |  |
| 28.4 | No water observed free flowing through gopher burrow but saturation zone continues to expand around zone of seep. |  |
| 97.6-122.1 | Left site with full water tank and trenches at 97.6 hours. Trenches nearly empty by 118.4 hrs and re-filled by 122.1. | No photo |

| 125 | Small seep seen producing a trickle of water at squirrel burrow in control trench (Sta. 121.5). Photo to the right is of the squirrel burrow |  |
|---|---|---|

### 2.1.5.3  Wall Surface Saturation Progression

As previously discussed, on the first day of the flow test, observations primarily consisted of surficial slope seeps and flow into the lower trenches via conduits identified as gopher burrows. In these initial hours, saturation patterns in the lower trenches were mostly related to capillary action of water moving up the trench walls from the standing water in the base delivered by the flowing burrows. On days 2 and 3 of the flow test, saturation patterns began to emerge on the uphill wall of the lower trenches.

Figure 2-48 through Figure 2-52 show sketches of wetting front patterns in the uphill wall of the lower trench beginning at 29.1 hours from the time of initial inundation of the upper trench to 51.7 hours from inundation. Sketches were made to support observations during this time window as changes in site conditions were occurring rapidly. Figure 2-53 and Figure 2-54 show photographs of the site (both stump and control trenches) at 67.9 hours and 140 hours, respectively. Some visual changes can be detected between photos at 67.9 hours and 140 hours (the end of the test), but the site had essentially achieved a steady state by 67.9 hours into the flow test. These figures show only minor changes in the arrival of the wetting front at the uphill wall of the lower trench.
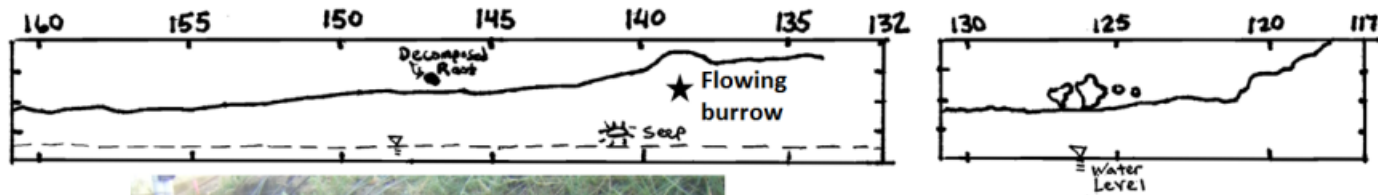
Figure 2-48. Saturation patterns in lower wall face at 29.1 hours after inundation of the upper trench with water. The lower stump (top left) and control (top right) trench wall seepage patterns are documented by station with corresponding photos below.
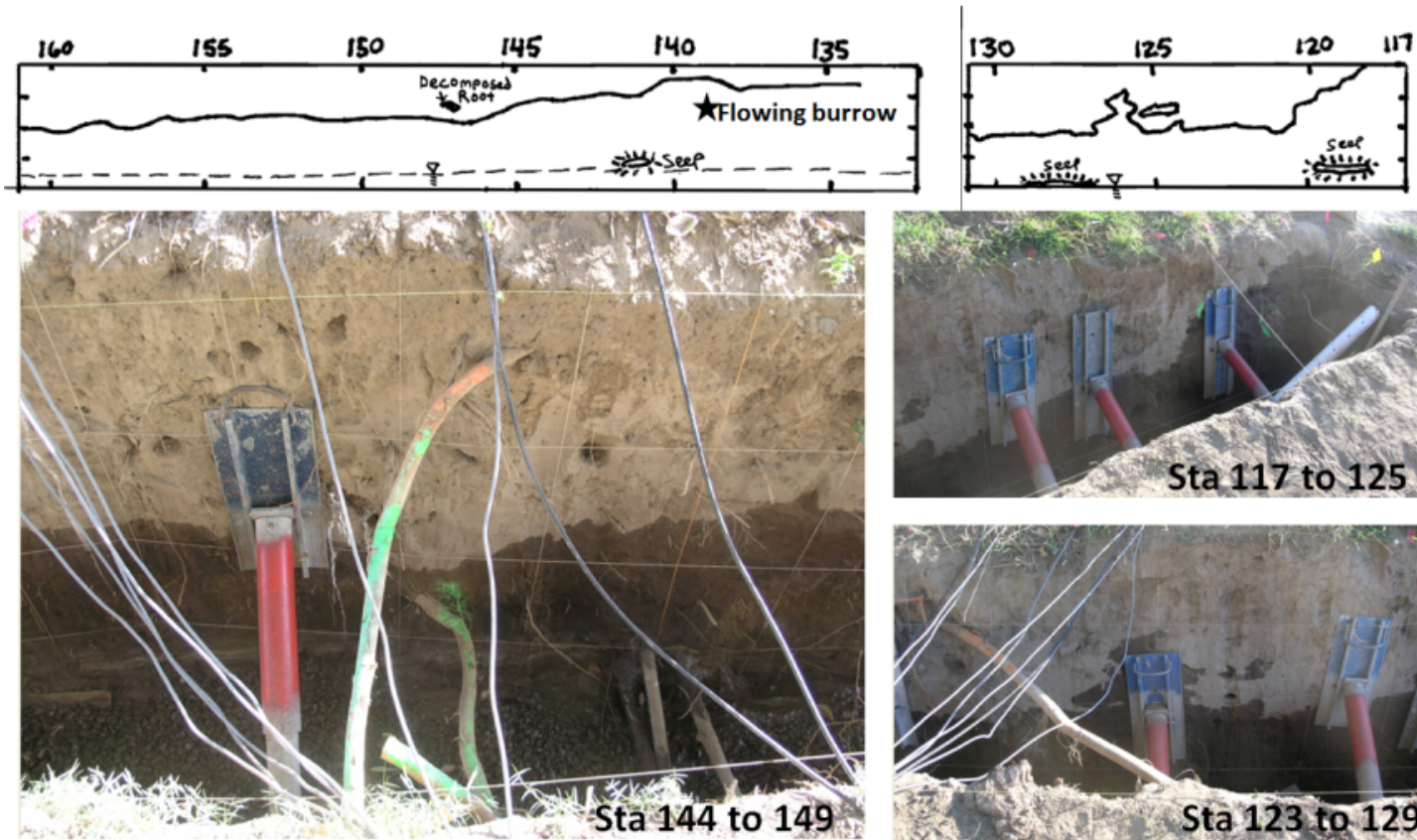
Figure 2-49. Saturation patterns in lower wall face at 29.4 hours after inundation. Note the appearance of seeps in permeable zones near the trench bottom. The lower stump (top left) and control (top right) trench wall seepage patterns are documented by station with corresponding photos below.
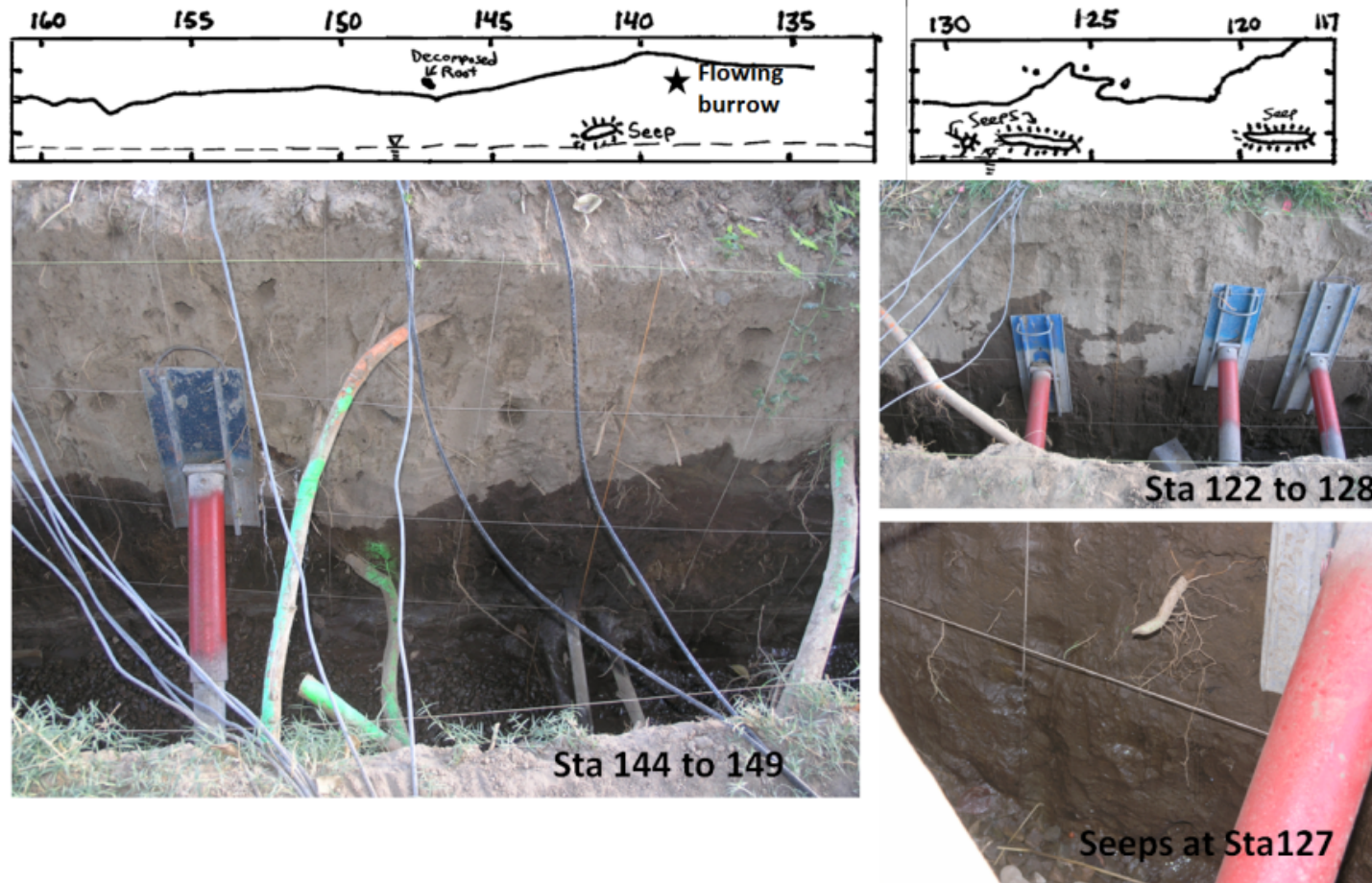
Figure 2-50. Saturation patterns in lower wall face at 29.9 hours after inundation. Note that seeps seem to be related to permeable material types. The lower stump (top left) and control (top right) trench wall seepage patterns are documented by station with corresponding photos below.
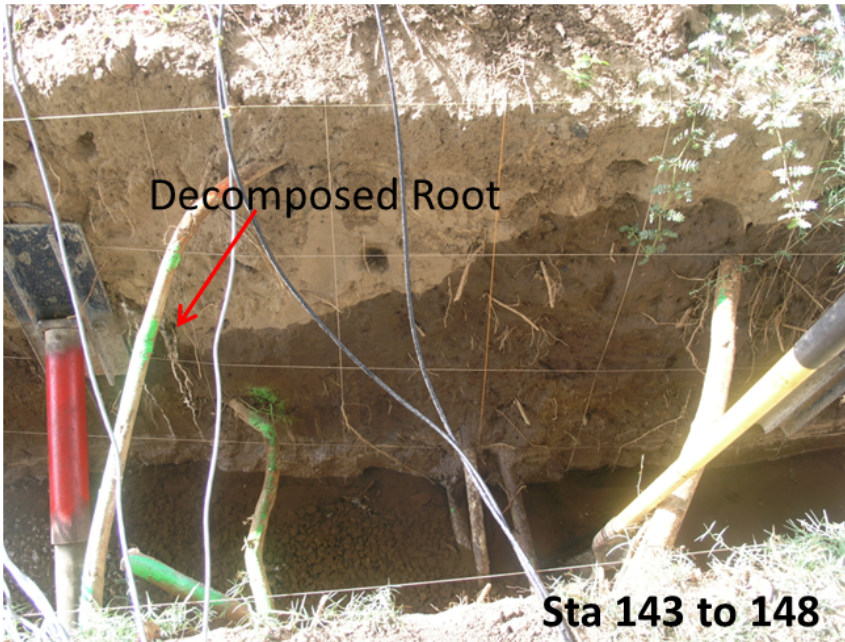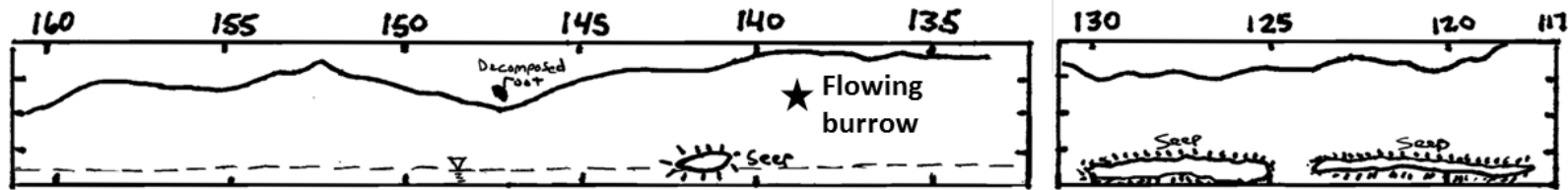
Figure 2-51. Saturation patterns in lower wall face at 46.6 hours after inundation. Note the depression in the saturation pattern in the area of the decomposed root at Station 147. The lower stump (top left) and control (top right) trench wall seepage patterns are documented by station with corresponding photos below.
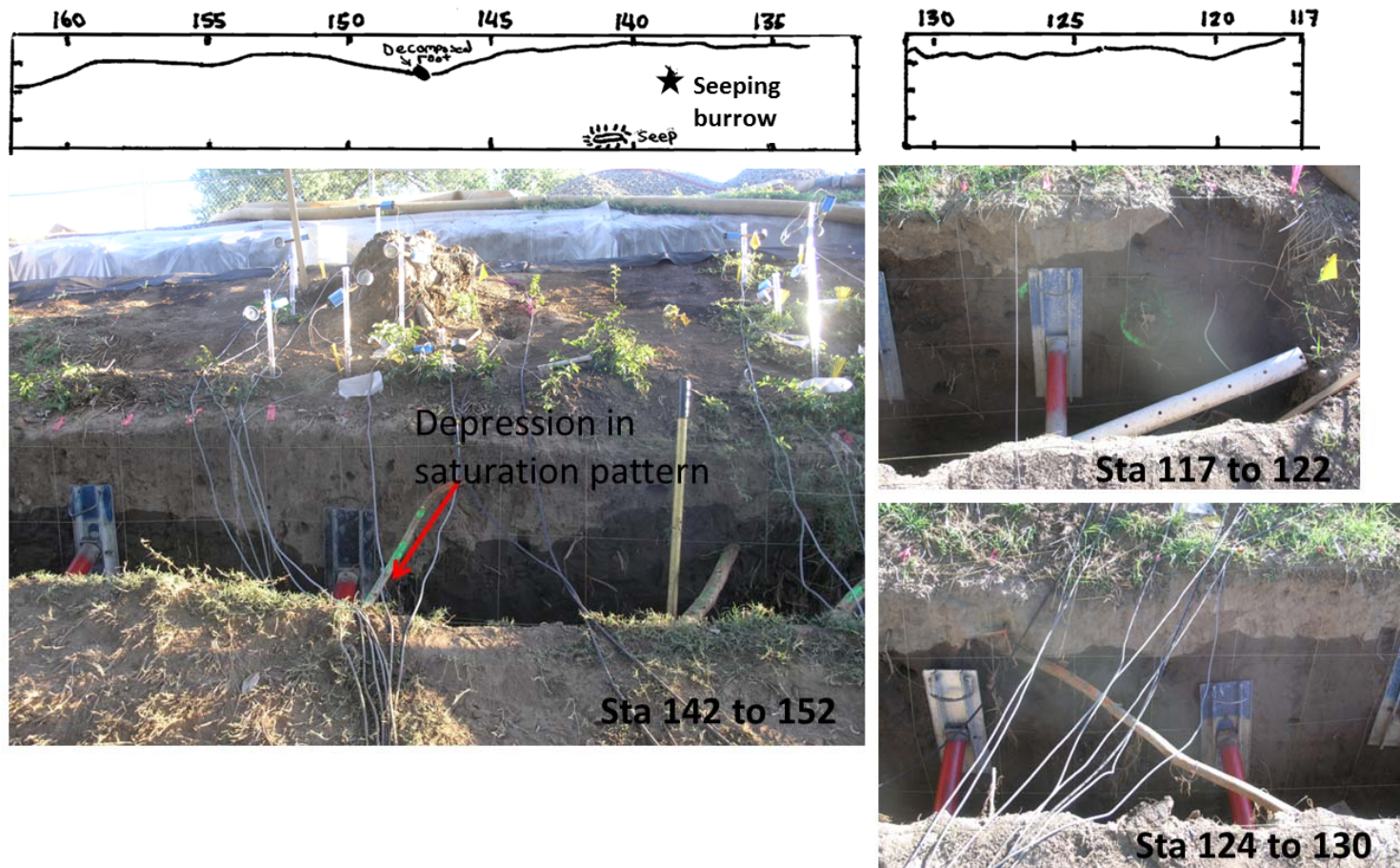
Figure 2-52. Saturation patterns in lower wall face at 51.7 hours after inundation. Note the wetting front continues to rise near the stump at Stations 145-150, though a depression is still visible indicating the stump is the last zone to saturate. The lower stump (top left) and control (top right) trench wall seepage patterns are documented by station with corresponding photos below.

Figure 2-53. Wide angle view of saturation patterns at 67.9 hours into the flow test. The area below the stump has begun to saturate.

Figure 2-54. Saturation patterns in the stump and control trenches at 140 hours into the flow test, just before the end of the test. Only small changes were observed in saturation patterns between 67.9 hours and 140 hours.

Figure 2-55 shows a direct comparison between the stump and control trenches showing a delayed wetting front in the vicinity of the decaying stump. Possible reasons include a reduced permeability in soils surrounding the stump, a physical obstacle to saturation and flow is created by the stump and root system, or the water is being redirected beneath the test through permeable layers or anomalies. Adding further complexity, the saturation of instrument Lines B and C are influenced by the presence of animal burrows, making a direct comparison between the instrument results and observations increasingly complex. Observations were made with regard to factors which may be influencing the pattern of the wetting front.
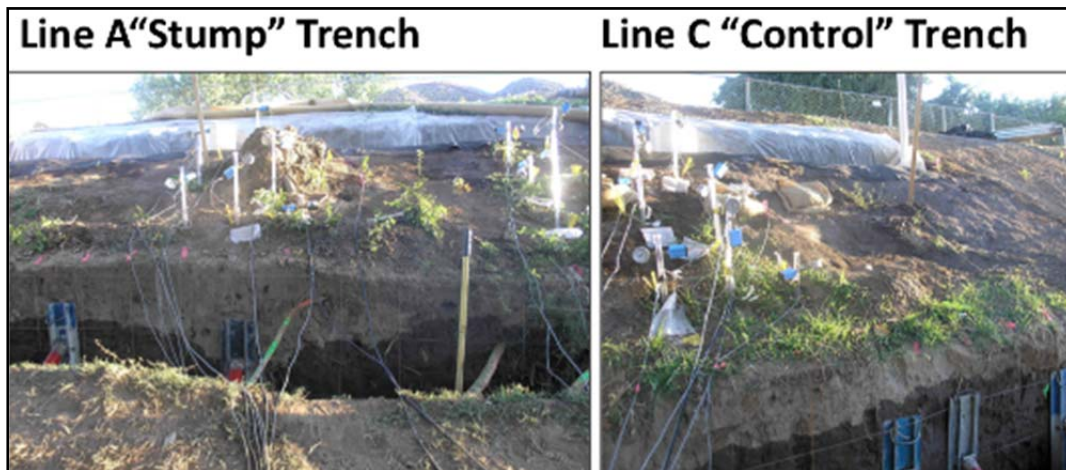


Figure 2-55. Comparison after 51.7 hours of flow. The zone in front of the stump was the last to saturate.

Figure 2-56 combines approximate gopher burrow alignments, outlet locations and wetting front patterns at 50 hours into the flow test to better understand the effect of these burrows on the wetting front at the lower trench. During a post-flow test site characterization effort, the gopher burrow at Line C was found to not connect directly to the lower trench, while the gopher burrow at Line B connected directly to both the upper and lower trenches. The influence of these gopher burrow patterns on the wetting front at the lower wall is shown in Figure 2-57 and Figure 2-58. Gopher burrows that did not connect directly with the upper trench, also did not conduct water preferentially (Figure 2-59) – at least not until saturation was achieved in surrounding soils. As shown in Table 2-3 at a time of 125 hours, the squirrel burrow shown in Figure 2-59 did eventually produce water once the surrounding walls had saturated. The small metal water pipe encountered during trench excavation at Station 145 was found to extend beyond our study area on each end and did not conduct visible free water along the zone of backfill (consisting of gravel within a fine-grained soil matrix). The pipe can be seen on Figure 2-49, Figure 2-50, and Figure 2-51 at times 29.4, 29.9, and 46.6 hours into the flow test, respectively.

Figure 2-56. View looking west at the uphill wall of the lower stump trench 50 hours into the flow test. Gopher burrow outlet locations at Stations 138.25 and 117 are identified on the diagram as well as approximate alignments of burrows.
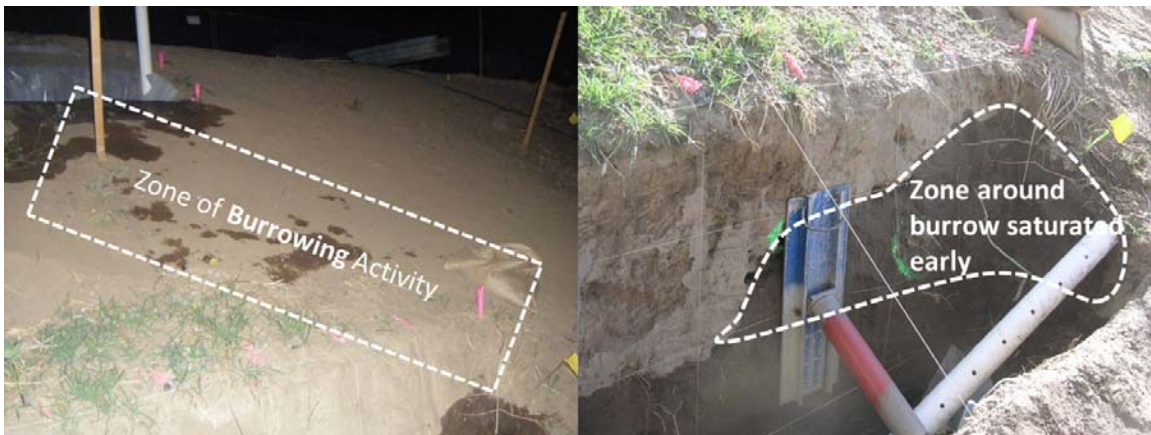


Figure 2-57. Control trench gopher burrow advances the wetting front (left) tracing a pathway to the outlet location at Station 117 (right). The outlet flowed briefly.
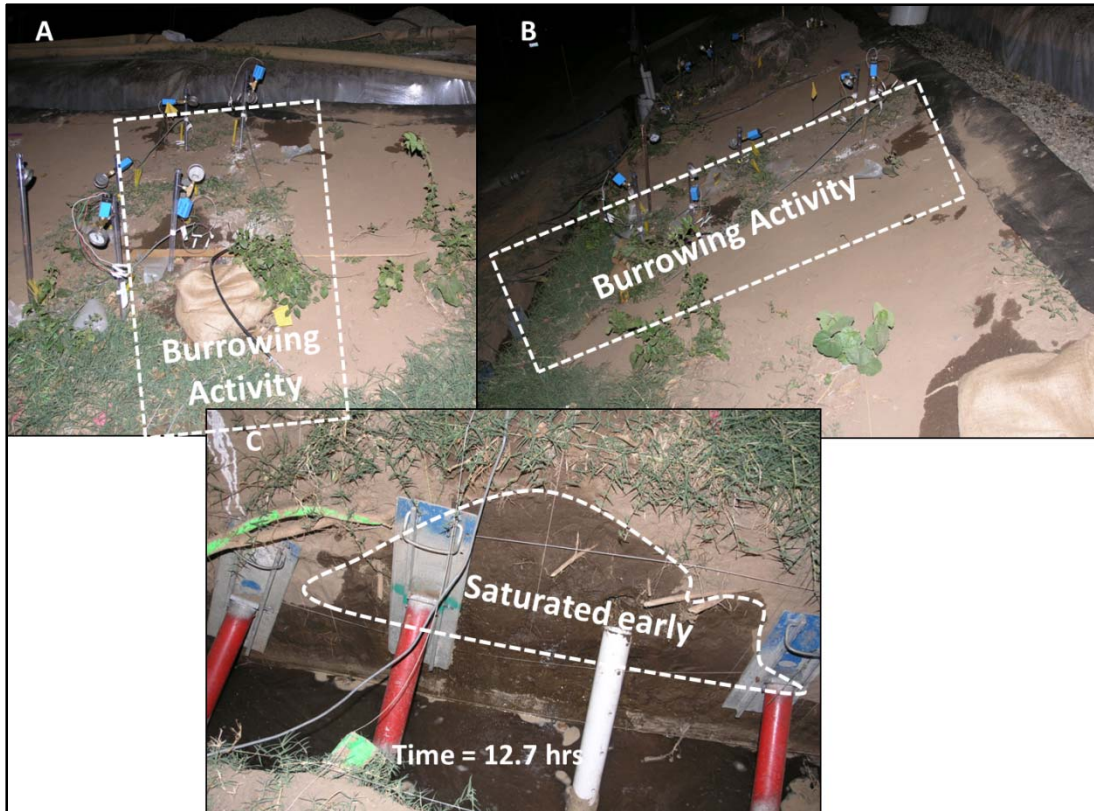
Figure 2-58. The wetting front is advanced by gopher burrow at Station 138.25. Slope saturation patterns looking A) south; and B) east. Photo C traces zone of early saturation due to the gopher burrow at a time of 12.7 hours into the flow test



Figure 2-59. Squirrel burrow extending at least 18 inches into the uphill wall of the lower trench at A) the time of trench construction and B) 50 hours into the flow test. No free water flows until a seep upon saturation at 125 hours (See Table 2-2)

Neither live roots nor decomposing roots were observed to conduct water preferentially during the flow test. Figure 2-60 and Figure 2-61 show how the wetting front progressed in the vicinity of the decomposing roots. In particular, the root shown on Figure 2-60 was initially observed to conduct silica slurry during the installation of tensiometers. Preferential flow of water was not observed through the annular space between the bark and the woody core of the root during the flow test, despite an intermittent annular space which was found and explored in the post flow test site characterization effort.  As previously discussed, the area of the stump was the last zone to saturate.
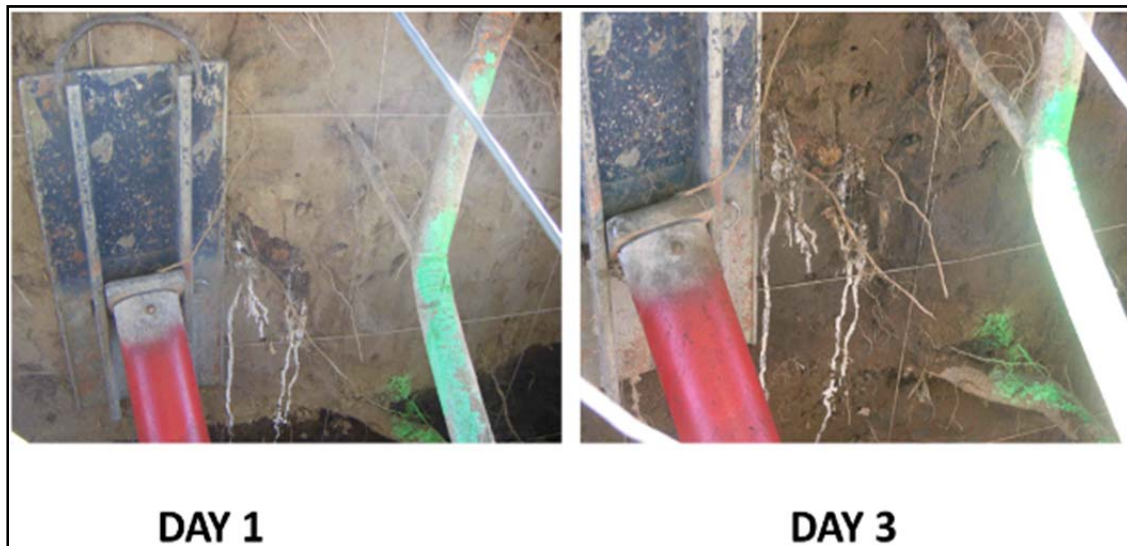


Figure 2-60. Progression of wetting at the decomposed root at Station 147.5.
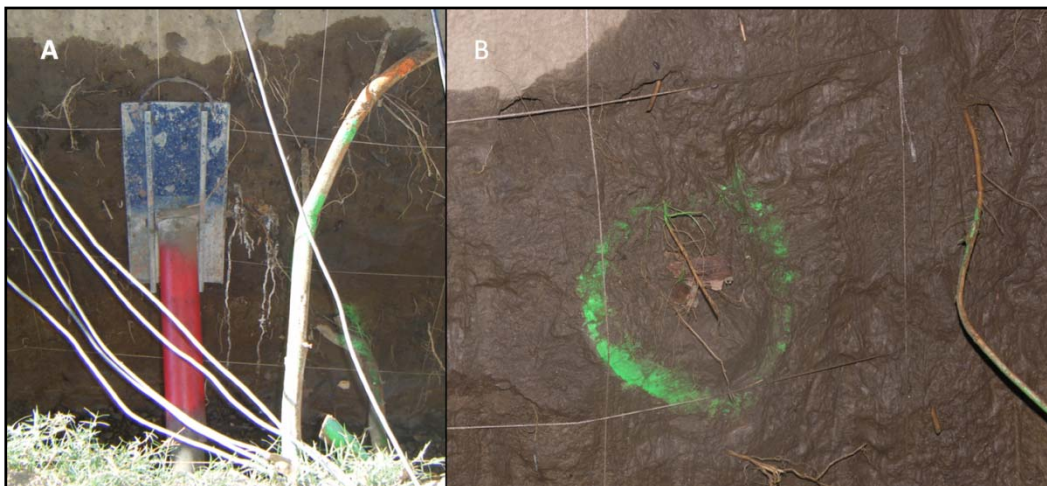


Figure 2-61. Progression of wetting at decomposed roots showing no preference to flow through the root zone or surrounding loose soil zones surrounding the roots.

No impact on flow or wetting front patterns was observed to be connected with live roots. No voids or annular spaces were observed in connection with the live roots extending radially from the hackberry tree located at the toe of the levee. Figure 2-62 shows water preferentially flowing through the gopher burrow at Station 138.25 while no flow is observed through nearby live roots. Even as the wetting front arrived, observations of numerous live roots during the duration of the flow test show no preference for water to flow through or around these live root systems (Figure 2-63).
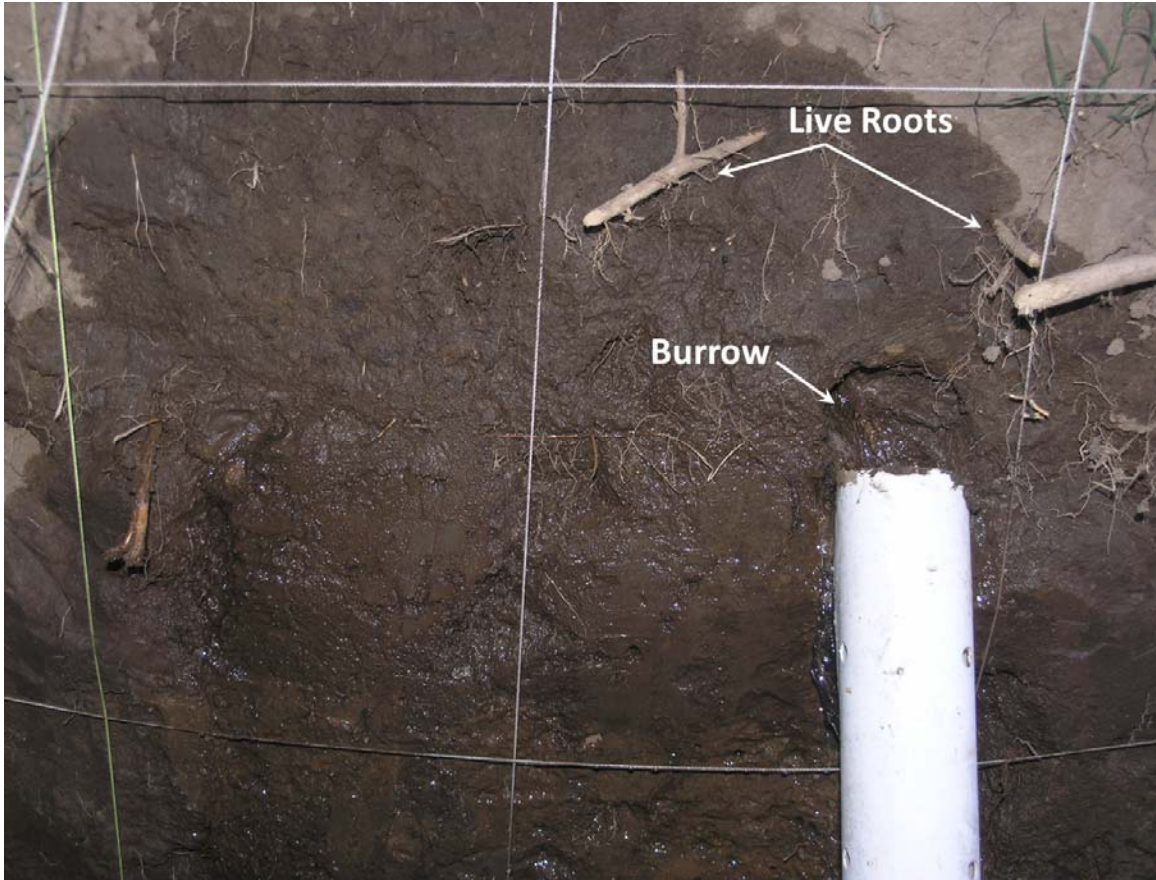


Figure 2-62. During the flow test water is shown flowing through the gopher burrow and seeping out of permeable soils within the wall face, though no flow was observed through the adjacent live roots.
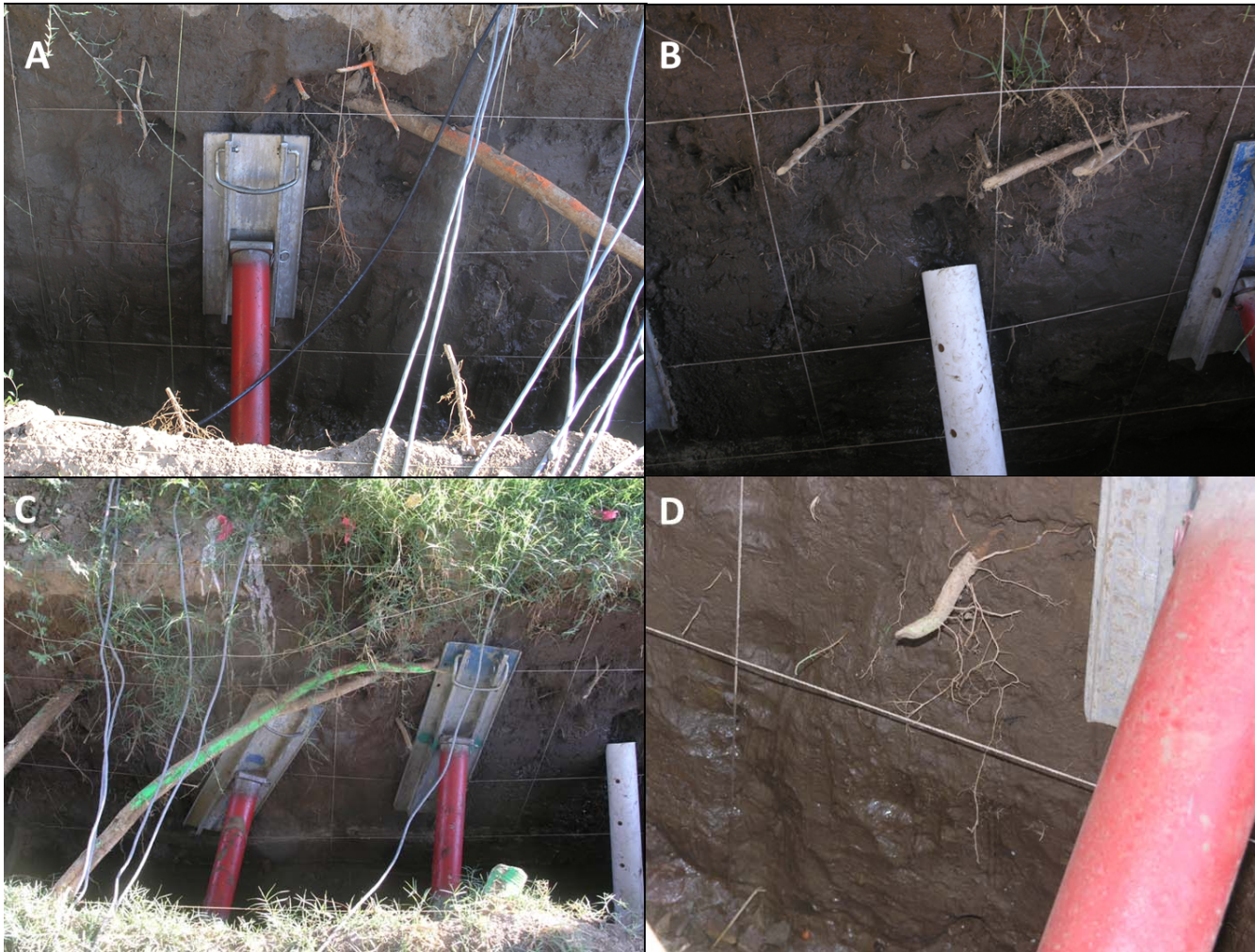
Figure 2-63. Live roots are shown during the flow test throughout the lower stump trench. At no time during the flow test were live roots observed to conduct water.

## 2.1.5.4   Instrument Results

Tensiometers and piezometers measured negative and positive pore water pressures before, during, and after the flow test. Complete results of all instruments including a discussion of instruments used and their calibration are presented in Appendix 2D. The results recorded by each tensiometer during the first four days of the flow test are summarized by instrument line and presented below. This time interval was selected because the wetting front had reached each instrument by this time. All piezometer data is presented together on a single plot.

Tensiometers were installed one week prior to the flow test and were connected to a continuously reading datalogger for several days prior to the inundation of the upper trenches to establish baseline values in the instruments and to check functionality. Initial moisture contents of surficial soils are presented in Shriro et al. (2014) and results of initial testing is presented in Appendix 2D. These moisture contents resulted in observed initial suction values of approximately 8 to 60 kPa.

Typical tensiometer results showing values of soil suction measured with time are shown on Figure 2-64. An initial drop in suction and recovery is seen during refilling of the instruments with water. Stable values drop suddenly indicating the time corresponding to the arrival of the wetting front at the instrument tip. The drop in suction values beginning at 30 hours indicates the arrival of the wetting front.
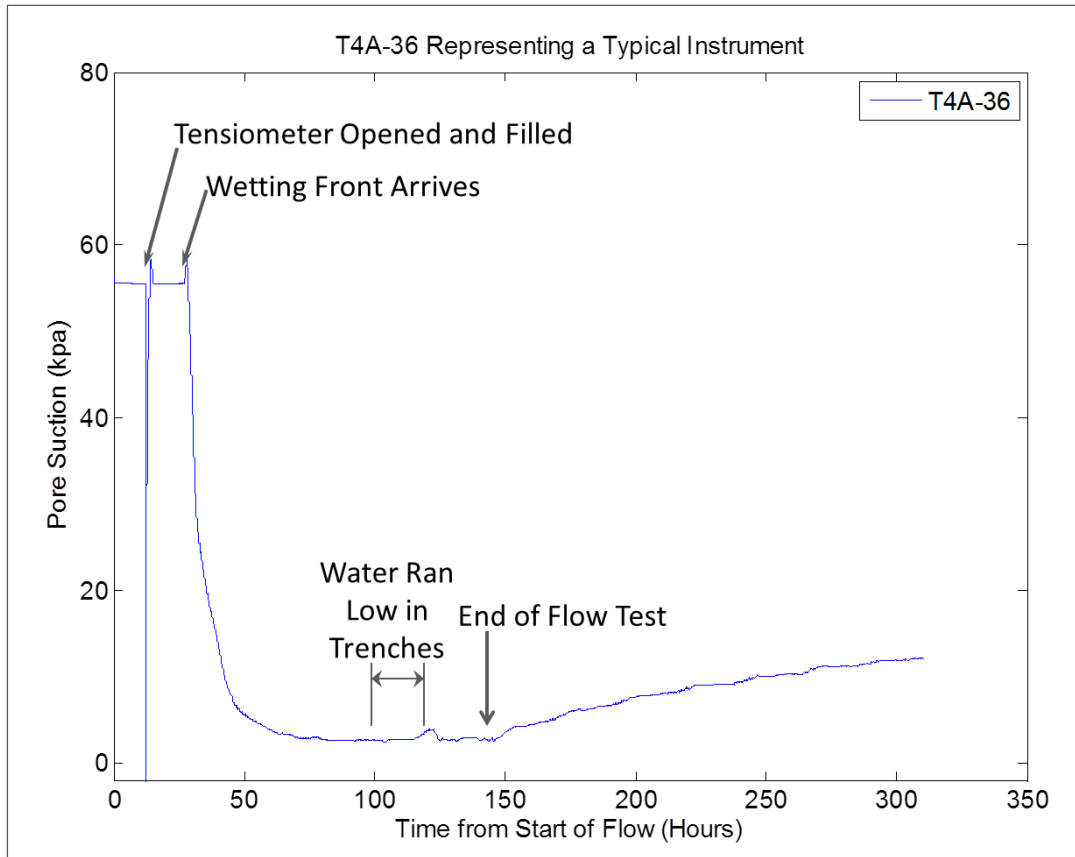
Figure 2-64. Typical tensiometer result plot.

The saturation front in the vicinity of instrument Line A was observed to progress more slowly than in instrument Lines B and C. In particular, Line A instruments in the area below the stump showed the arrival of the wetting front at approximately 70 hours after the start of the test. In contrast, analogous instruments of Lines B and C recorded no suction approximately 10 and 20 hours, respectively, from the start of the test, indicating rapid saturation in comparison to Line A. Physical observation of the saturation front, as seen from the lower wall, confirmed the area below the stump was the last location to saturate during the wetting test.

Figure 2-65 through Figure 2-67 show tensiometer data by instrument line. Figures showing comparisons of similarly positioned instruments across the various instrument lines are provided in Appendix 2D. As discussed previously, gopher burrows at Lines B and C appear to have accelerated the progression of the wetting front and the stump at Line A appears to have retarded the progression of the wetting front. Tensiometer T4A-60 (Line A) was observed to saturate more quickly than surrounding shallower instruments. This is likely due to free water present in the base of the lower stump trench flowing through the gopher burrow at Station 138.25. Tensiometers T2B-18 (Line B) and T2C-18 (Line C) were very proximal to the path of the gopher burrow which likely acted as a water conduit with patterns

74

extending radially from the burrow. This accelerated the arrival of the wetting front at these tensiometers. The relative effects of these competing influences will be evaluated in future seepage modeling.
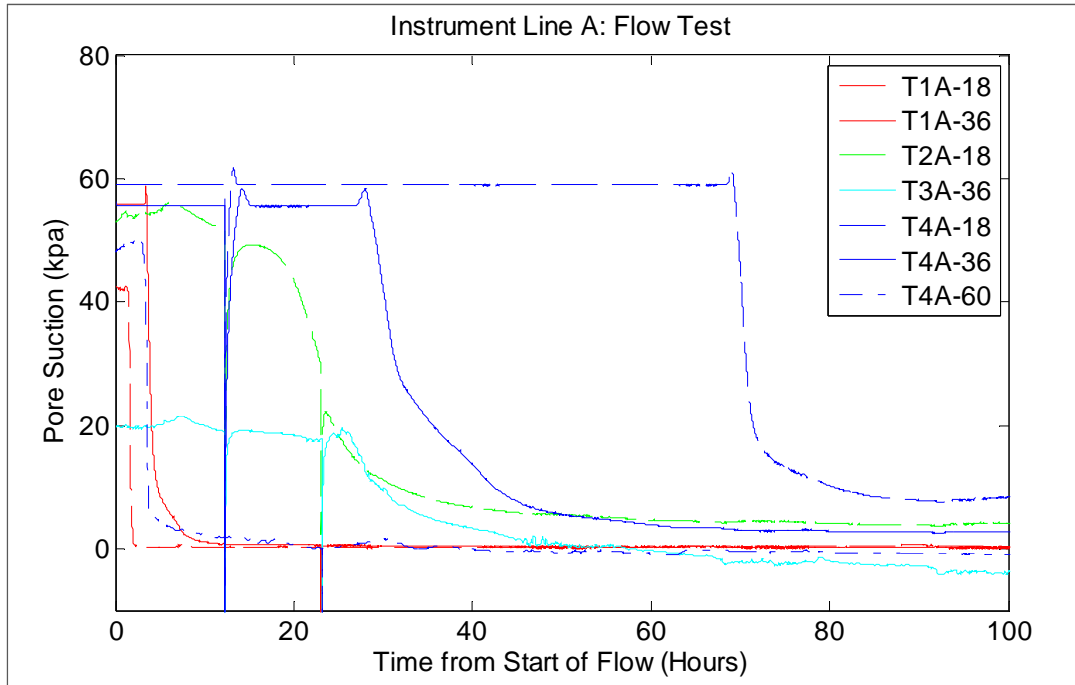


Figure 2-65. Tensiometer data for instrument Line A (at stump).
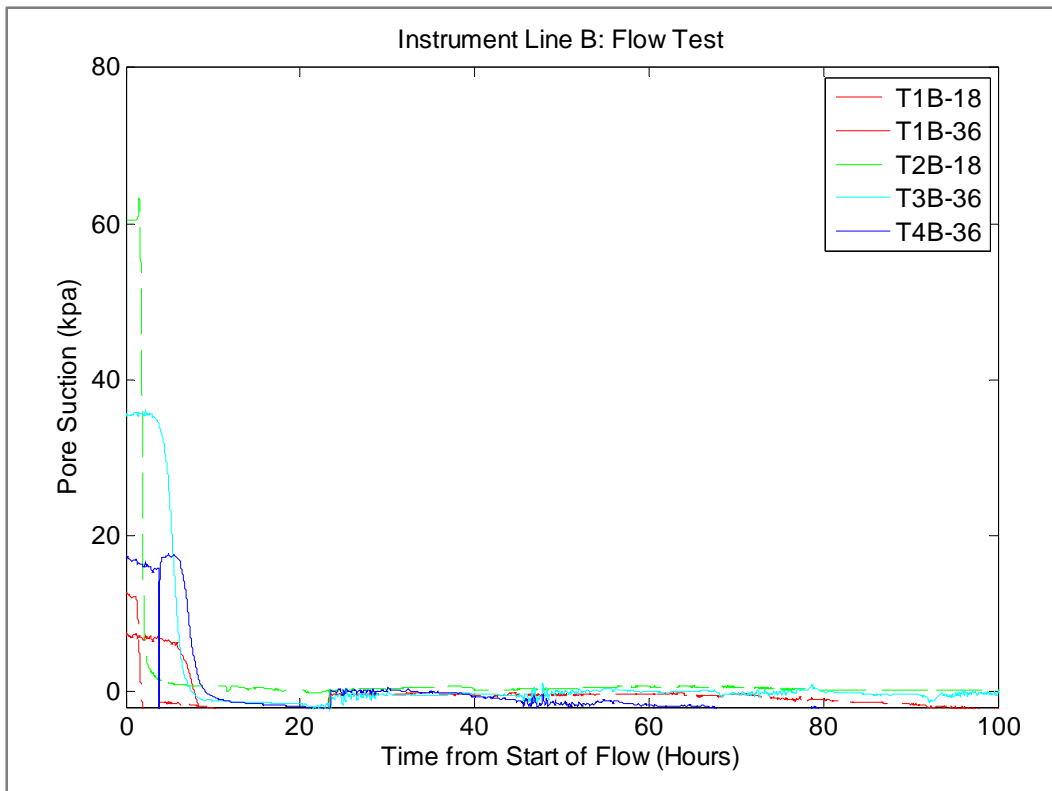
Figure 2-66. Tensiometer data for instrument Line B (7 ft from stump).
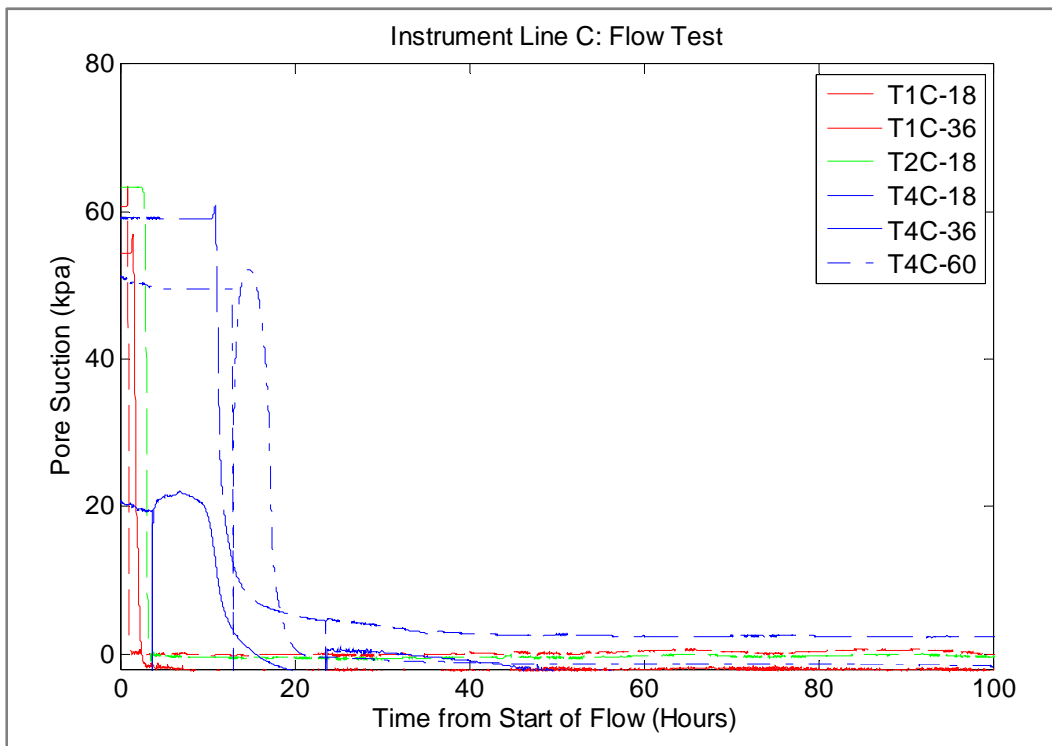


Figure 2-67. Tensiometer data for instrument Line C (23 ft from stump).

Piezometers were installed into 4-inch diameter auger holes and grouted in place with a mix of Portland cement and bentonite in accordance with the specifications of the manufacturer (Slope Indicator). Due to initially unsaturated conditions and the likelihood of low measured pressures throughout the flow test area, the Slope Indicator 10 psi Low Pressure Vibrating Wire model was selected. The constant head in the trench was held a maximum of 9 feet above the porous stone of the deepest piezometer (84 inches from surface grade, installed at mid-slope) resulting in a maximum possible pressure of 3.9 psi. The 10 psi low-pressure instrument was the most sensitive available for this application. The instruments were pre-saturated in a water bath and grouted into the hole upside down in order to minimize loss of saturation in its porous element due to the unsaturated conditions.

Based on piezometer data, saturation of the instruments was achieved within 1 to 2 days of flow. Pore pressures of less than 10 kPa (1.45 psi) developed following saturation (Figure 2-68) for 3 of the 4 instruments. High initial and final pressures in Piezometer P2A-84 did not fit with physical observations and available data. The piezometer was not able to be recovered for laboratory calibration testing and therefore data from this instrument was excluded from our analysis.
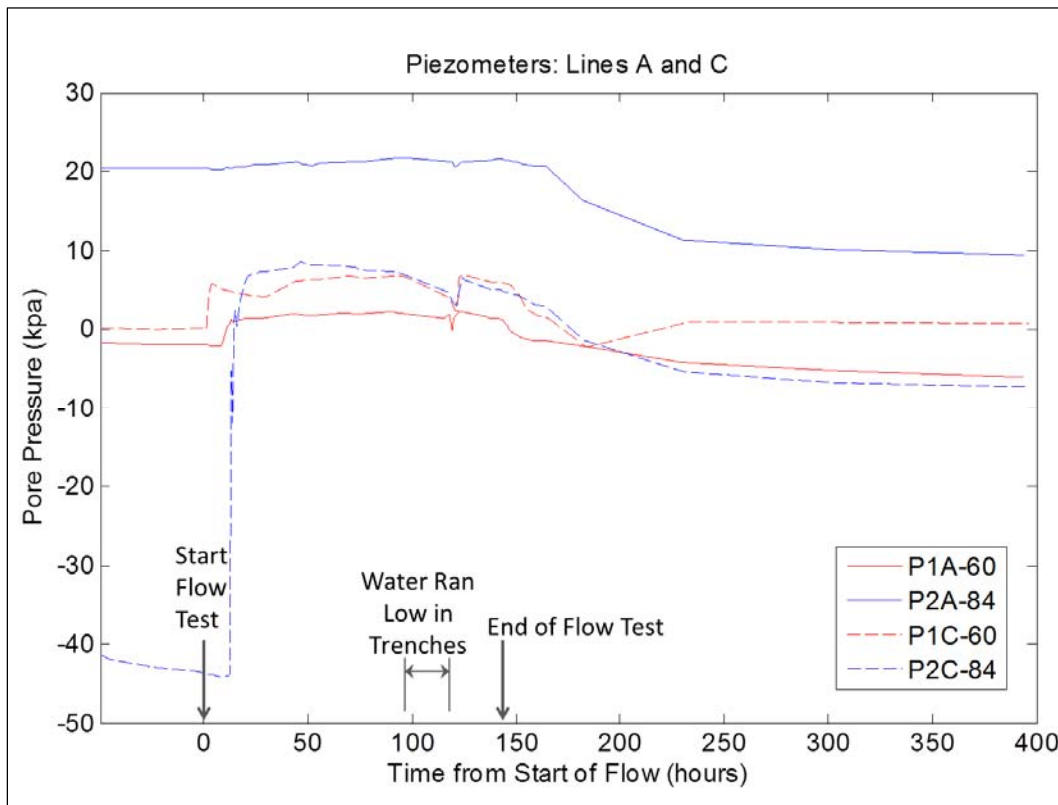


Figure 2-68. Pore pressures measured during flow test at instrument Lines A and C.

### 2.1.5.5  Water Volume Usage During Flow Test

During the 6-day flow test, approximately 45,000 gallons of water were released by gravity into the upper trenches.  Two flow meters were installed in total on the two lines supplying water from a nearby source into the 2500 gallon reservoir. Two additional flow meters were installed at the two electric pumps controlled by float valves. The pumps were set up to recycle water back into the reservoir and volumes were recorded for each. Initially, one pump was placed in the stump trench and one in the control trench. Once the gopher burrow at Station 117 stopped flowing in the lower control trench on Day 2, the pump in the lower control trench was relocated into the lower stump trench to help control large flows coming through the gopher burrow at Station 138.25. All flow meters were read at regular intervals and at the same time. The water level in the reservoir was also measured at this time and we estimated and recorded the volume of water flowing by gravity into the upper trenches. Inflow volumes for water flowing into the trenches are therefore combined volumes.

The volume of water that flowed from the gopher burrow at Station 117 was not enough to actvate the control trench pump and the burrow stopped flowing before the water in this trench was ever pumped. The total volume of water pumped from the lower stump trench during the flow test was approximately 19,000 gallons, virtually all of which flowed through the gopher burrow at Station 138.25. The volume that flowed through this burrow was underestimated by the amount lost to the surrounding soil of the lower trench. Figure 2-69 shows the balance of water during the flow test. Approximately 23,000 gallons of water were lost outside of the study section based on the assumption that the soil in the zone of study (assumed unit weight 120 pcf and 17 to 22% moisture content) would take approximately 2,300 to 3,700 gallons to achieve saturation (calculation based on 3,000 gallons for Figure 2-69).
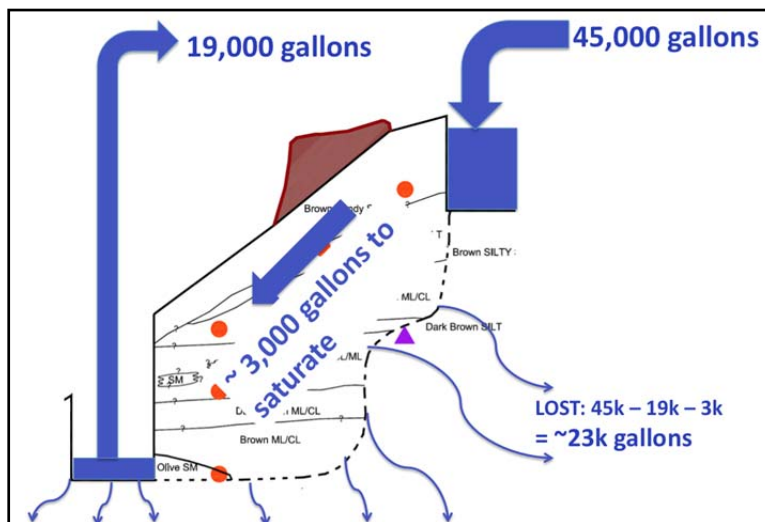


Figure 2-69. Calculation of flow volumes into and out of trenches. Note that a significant fraction of the input water was lost to areas outside of the study zone.

Figure 2-70 shows the cumulative volume of water delivered to the upper trenches and cumulative water recycled/pumped from the lower stump trench as a function of time during the flow test. Note the slope of the water delivery curve changes over the course of the test.
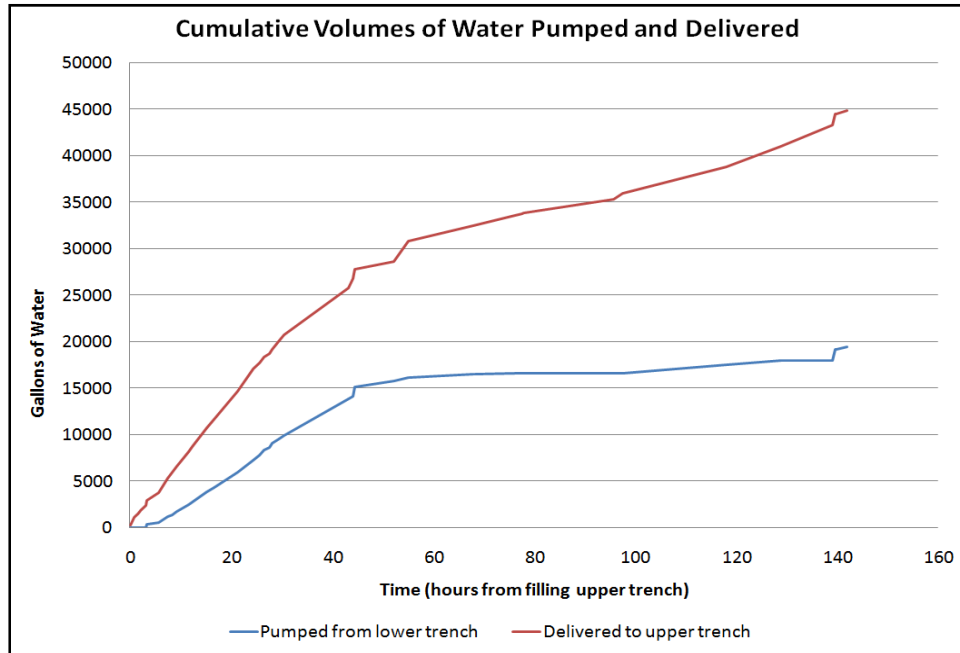


Figure 2-70. Plot of cumulative water delivered to the upper trenches from the 2,500 gallon reservoir and water recycled from the lower stump trench to reservoir.

Figure 2-71 breaks the curve into segments and the slope of each segment is calculated with a linear regression. The slope of each segment is the rate of water flow over that time period. Table 2-5 provides a summary of flow rates along with a reminder of key observations relevant within each interval.

During field observations, at approximately 55 hours, we observed a rapid decline in the rate of flow from the gopher burrow in the lower stump trench at Station 138.25. It appears that flow began slowing at 30 hours, though the decline in flow rate became apparent after a time of 55 hours. The recycle rate refers to the number of gallons of water pumped from the lower stump trench into the 2500 gallon reservoir over a period of 1 hour. Virtually all of this water was delivered to the lower trench via the gopher burrow at Station 138.25. This rate underestimates the actual rate of flow through the burrow. Water lost through the lower trench due to standing water percolating into surrounding soils arrived through the burrow and was lost outside of the study area prior to being recycled into the reservoir. In the first 30 hours of the flow test, a minimum of 367 gph flowed through the burrow, while 321 gph was saturating soils between the trenches, or was lost outside of the study zone.

79
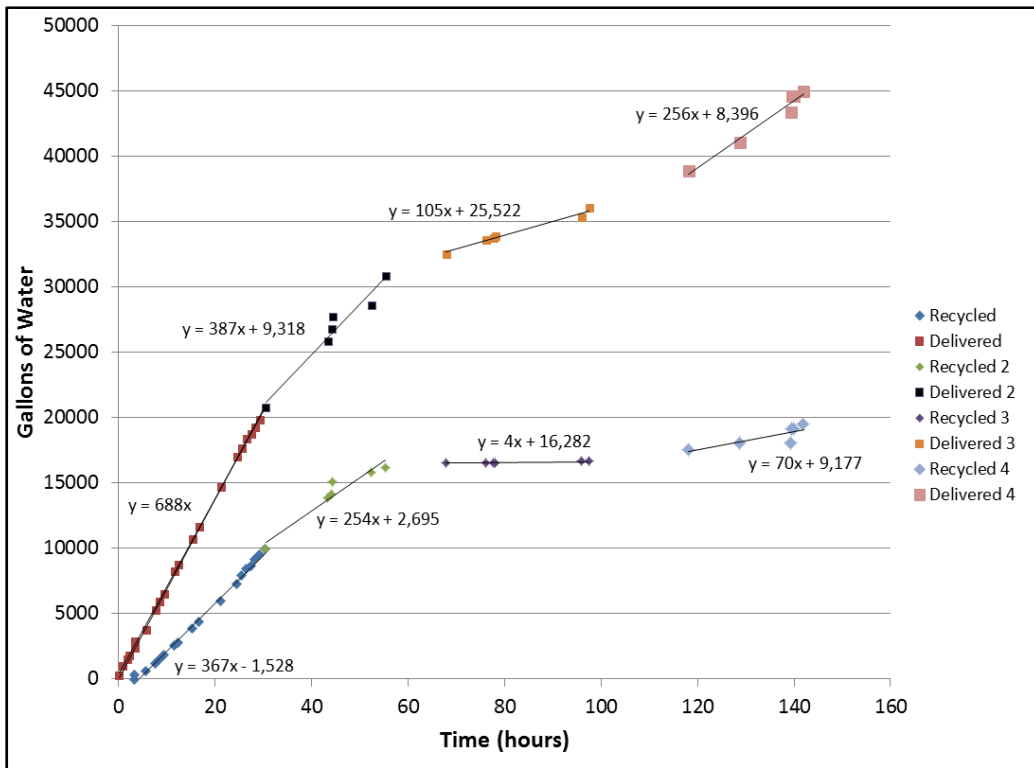
Figure 2-71. Cumulative gallons of water either delivered to the upper trench from the reservoir or recycled from the lower trench back to the reservoir. Curves are broken into segments with slopes representing the rate of flow.

Table 2-5. Flow Rate Breakdown

| Time (hrs) | Delivery Rate (gal/hr) | Recycle Rate (gal/hr) | Water Loss Rate to Soils (gal/hr) | Notes |
|---|---|---|---|---|
| 0 to 30 | 688 | 367 | 321 | Burrows flowing Sta. 138.25, Sta. 117 |
| 30 to 55 | 387 | 254 | 140 | Burrow flowing Sta. 138.25 |
| 55 to 67 | - | - | - | Burrow Sta.138.25 flow slowing; no data |
| 67 to 97 | 105 | 4 | 101 | Burrow Sta. 138.25 stopped flowing |
| 97 to 118 | - | - | - | Water tank ran dry; trenches ran low |
| 118 to 142 | 256 | 70 | 186 | Burrow Sta. 138.25 began flowing again |

Between hours 30 and 55, the rate of recycled water pump, which flowed through the gopher burrow at Station 138.25 decreased from 367 to 254 gph. The loss rate for water declined from 321 to 140 gph. Between 55 and 97 hours into the flow test, burrow flow slowed and then stopped and the loss rate for water dropped to 101 gph. When the reservoir ran out of water at 97 hours and was refilled at 118 hours, the burrow at Station 138.25 began to flow again, but resulting in only 70 gph, available for recycle while the loss rate of water to surrounding soil was 186 gph.

80

Two burrows were observed to stop flowing over the course of the test. A reduction in macropore flow is expected as losses to surrounding soils rise with increased saturation of surrounding soils (Figure 3-71). This is consistent with observations by Beven and Germann (1982), who note that the rate of input into the hole must exceed losses to the surrounding soils and continuity must be maintained for the macropores to preferentially flow water. Collapse, siltation, or plugging may also have occurred over the course of the flow test. The gopher burrows may have been partially backfilled with loose soils, aiding in siltation or plugging of the burrows during the flow test. The overall reduction in water losses from the beginning of the flow test to the end is indicative of the reduction in flow through macropores as hydraulic conductivity of soil is expected to rise with increased degree of saturation (Figure 2-72), increasing rather than decreasing the flow rates.
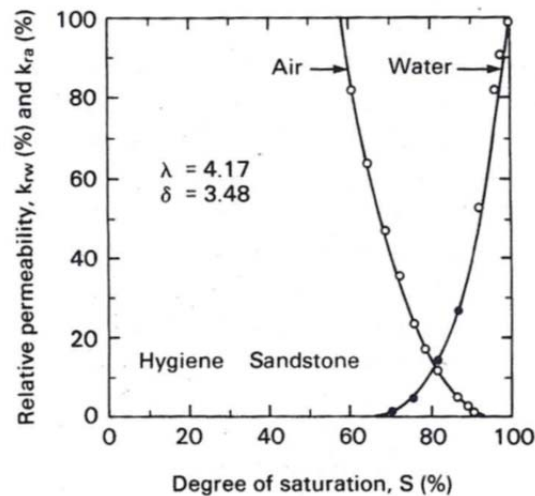


Figure 2-72. Relative permeability of water and air as a function of degree of saturation during drainage (Freudlund and Rahardjo, 1993; originally from Brooks and Corey, 1964). Note: Diagram intended for the illustration of concepts only. Actual relative permeability is expected to vary by soil or rock type.

2.1.6    Post-Flow Test Site Characterization Effort

After completion of the flow test, the site was allowed to dry for two weeks prior to the characterization phase that began on October 1, 2010. The work was overseen by the UC Berkeley team, and excavation work was logged by Professor Richard Evans of UC Davis and John Lichter of Tree Associates, Consulting Arborists. The effort incorporated Ground-Based Tripod Light Detection and Ranging (T-LiDAR) technology in order to capture the root architecture. The T-LiDAR imaging (performed by Gerald Bawden of the USGS) was also adapted for use in capturing the soil stratigraphy and mammal burrow locations (Cobos-Roa et al., 2012).

2.1.6.1    Written and Photographic Documentation of Stump Excavation

Soil surrounding the eucalyptus stump was excavated in vertical slices extending back from the upslope side of the lower stump trench wall face as shown on Figure 2-73. When the last segment of soil was removed and the stump was removed to view the roots beneath. Segments of approximately 1.5 to 2 feet in thickness (measured into the trench wall) were removed with an air knife (connected to a compressor as described earlier). In the vicinity of delicate, decomposing roots, hand excavation was necessary to observe and document the *in-situ* condition. Areas of decomposing roots were carefully hand excavated, logged, photographed, and shot with T-LiDAR. Original logs prepared by Richard Evans and John Lichter are provided in Appendix 2E. The mammal burrow at Instrument Lines B and C were grouted, uncovered, photographed, and shot with T-LiDAR.



Figure 2-73. Excavation was completed around the stump in a series of vertical slices from Stations 138 to 153 as shown.

Grouting of burrows was performed by the American River Flood Control District (ARFCD) using a Chemgrout plant and trailer equipped with a moyno pump for grout delivery. Jim Warner, PE was retained as a grout expert to consult with our team on the grouting approach. At his recommendation, a grout mix was prepared with 10 percent bentonite and blended to a consistency that maximized thickness while remaining flowable. The mix was placed under low pressure (less than 10 psi) and injected slowly with enough pressure to move the grout to maximize filling of the hole while minimizing upheaval of the shallow surface soils covering the burrow. Burlap gravel sacks were positioned near the burrow outlet and were used to plug the burrows when grout began to flow from the lower trench wall (Figure 2-74).

Figure 2-74. ARFCD grout plant and trailer combination is shown (left). To the right, burrows are plugged with burlap sacks using a rod leveraged against the ground in order to prevent loss of grout.

The mammal burrow in Lines B and C were grouted and the soil covering them was excavated to expose the alignment extending from the upper trench. Figure 2-75 shows the exposed mammal burrows at Lines B and C.



Burrow at Station 138.25
(Instrument Line B)

Burrow at Control Trench
(Instrument Line C)

Figure 2-75. Mammal burrows at instrument Lines B and C following post-flow grouting and characterization efforts.

Excavation began by removing the downslope wall of the lower stump trench for access and in doing so gently following the remains of a decomposing root extending downslope of the lower trench from Station 155 (Figure 2-76). Careful excavation around the root revealed no gap between it and the soil. The root was sufficiently decomposed such that a distinction could not be made between bark and woody center. Figure 2-77 shows a sandy silt soil matrix directly against the root.

Figure 2-76. View of decomposing root encountered in the lower stump trench, Station 155.



Figure 2-77. Close in view of decomposing root at Station 155. No gap was observable around this friable and highly decomposed root.

Figure 2-78 shows the final excavation of the upper wall of the lower trench, revealing the uphill wall to be scanned with T-LiDAR. Though field logs of this wall had already been generated, the wall was labeled with a consistent system for consistency and for the purposes of collecting T-LiDAR data (Figure 2-79). Visible live and decomposing roots as well as burrows were given labels and a reflective strip affixed proximally to aid in location of features that were difficult to isolate with T-LiDAR data.

Figure 2-78. View looking southeast at the trenches following excavation of the downhill wall of the lower stump trench.
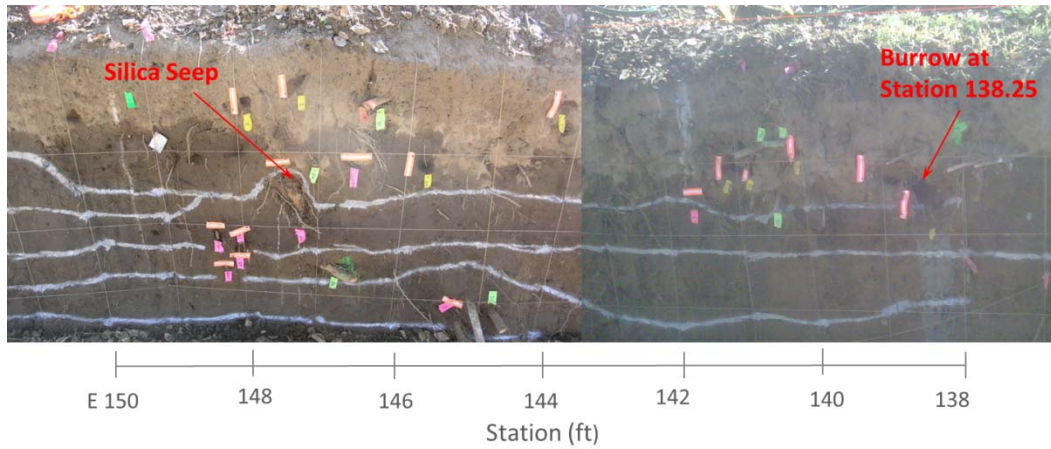


Figure 2-79. View of the uphill wall of the lower stump trench between Stations 138 and 151 just prior to scanning with T-LiDAR.

Excavation of the first slice began with removal of overburden and soils surrounding the stump using the air knife (Figure 2-80). As excavation proceeded, a prominent root emerged between tensiometers T4A-36 and T4A-60 (Figure 2-81). The excavation revealed this root to be the conduit for the silica seen flowing through a decomposing root at Station 147 during installation of tensiometers in the 4th row of Line A. Figure 2-82 shows the location of that root relative to the approximate installation position of tensiometers T4A-36 and T4A-60 and the seep location. The figure also shows the completed the first slice –'Slice 1' - excavation wall with roots exposed in the vicinity of the observed seep as compared with the

initial lower trench wall. The silica slurry had traveled down the back of the root and a small volume turned to the west following the bend in the root. The silica traveled a tortuous path of approximately 5 feet in total length. Another prominent root was revealed to the east and silica staining was also found on this root likely originating from its connection with Tensiometer T4A-18. Typical decomposing roots encountered are shown on Figure 2-83. Examples of annular spaces were most common in larger roots, likely because these spaces were larger and more noticeable. Figure 2-84 shows some examples of annular spaces and hollowed roots.



Figure 2-80. View of air knife operation during post-flow test site characterization effort.
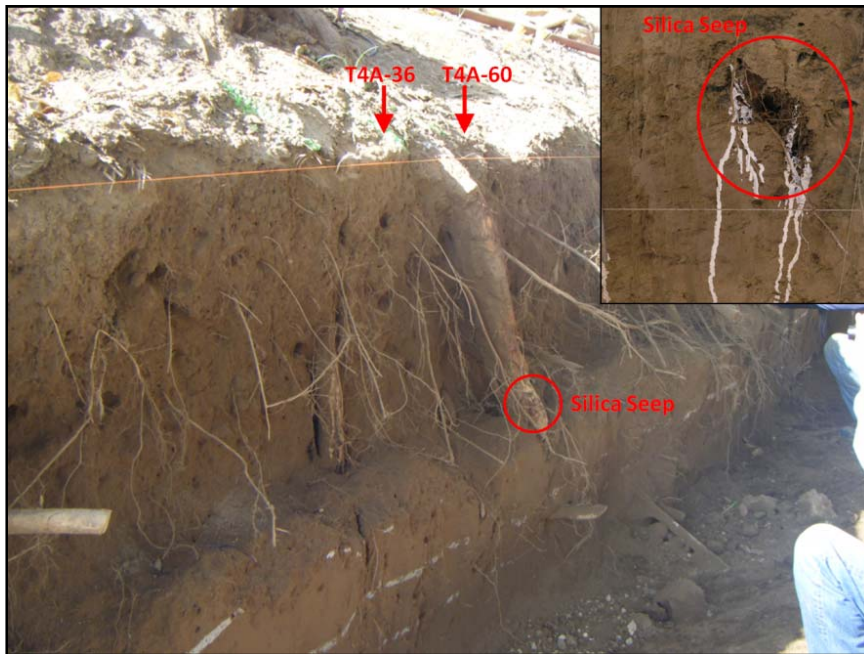


Figure 2-81. View of uphill wall of the lower stump trench as excavation of Slice 1 began. The root that was a conduit for silica slurry to the face of the lower wall during tensiometer installation is pictured.
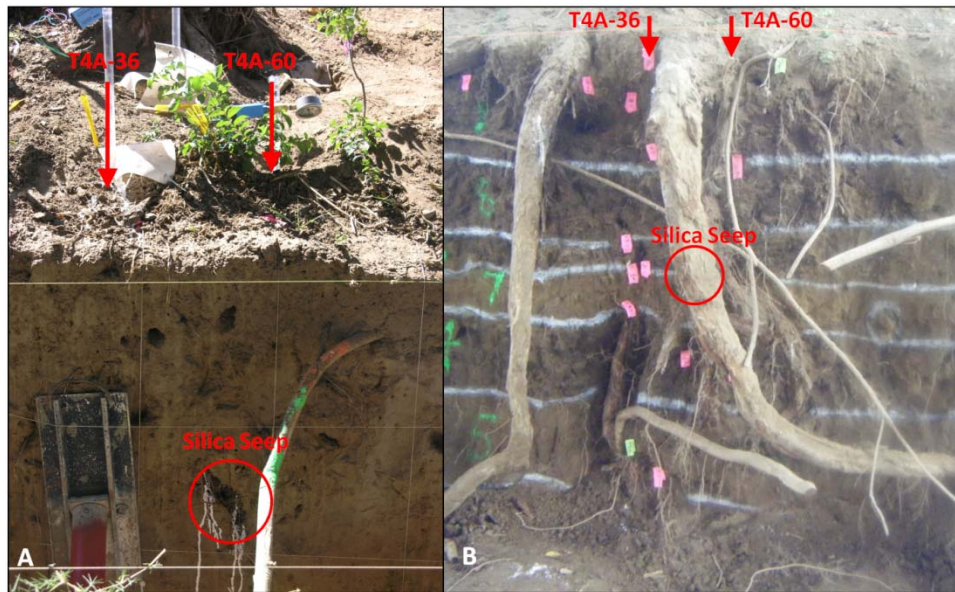
Figure 2-82.View of upper wall in lower trench below the stump A) during the flow test, and B) following the completion of 'Slice 1' excavation.



Figure 2-83. Typical appearance of decomposing roots encountered. Bark was fragile and discontinuous in many places. Annular spaces are seen on larger roots. Photos by Richard Evans.
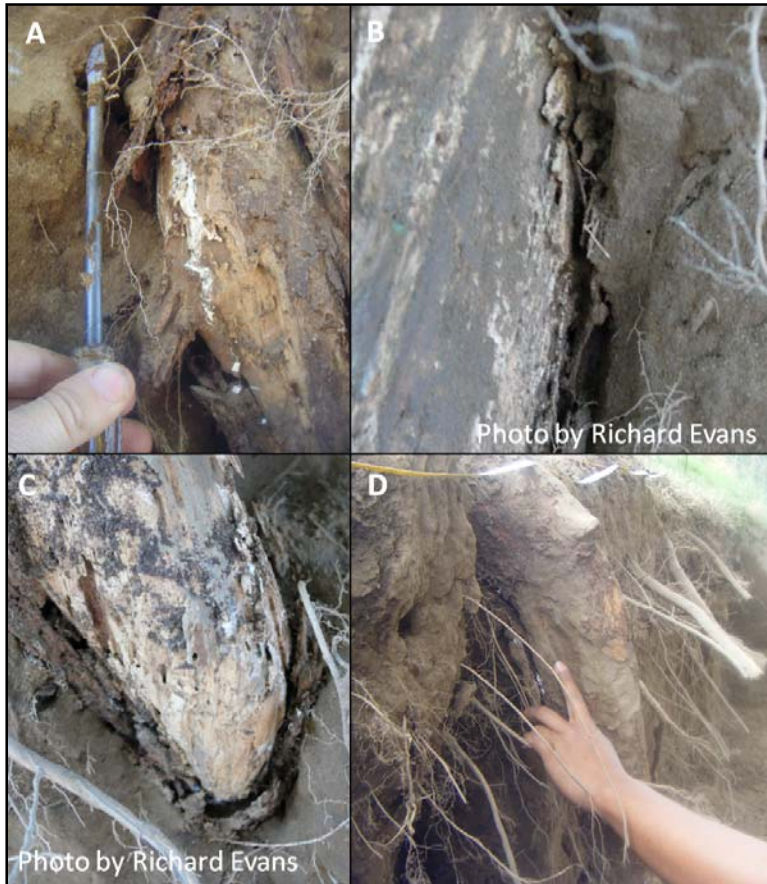
Figure 2-84. Examples of discontinuous annular space found in some decomposing roots. Many decomposing roots did not display this gap

Figure 2-85 provides an overview of findings from the excavation of 'Slice 1'. Live roots smaller than about ½ inch in diameter were cut as they interfere with T-LiDAR data collection. Figure 2-85B shows the excavation team exposing the decomposing root system through manual excavation. In Figure 2-85C, the burrow can be seen prior to removal of overburden soils. Portions of the burrow could not be grouted as seen in the photograph.

Excavation of 'Slice 2' proceeded, revealing the entry points of the silica (used in sealing tensiometers into the ground) into the decaying roots. Each instance of silica observed within the annular spaces around decaying roots were traced to a tensiometer instrument. The silica slurry generally did not flow far absent a direct connection to a void space. Figure 2-86 shows that though both T4A-36 and T4A-60 were installed on either side of a prominent decomposing root, it was tensiometer T4A-60 that was the conduit (or source) for silica that flowed that flowed out the lower trench wall face. Likewise, T4A-18 was found to connect directly to another prominent root and flow of silica was observed through annular spaces associated with this root also.

Figure 2-85. Slice 1 wall surface

Throughout excavation, examples were uncovered of silica slurry flowing in animal burrows, in burrows within the woody core of the root (Figure 2-87), and even for short distances into loose soils (Figure 2-87A and C). With the exception of mammal burrows, the annular spaces were generally not sufficiently continuous to permit liquid silica slurry to flow far or to conduct large volumes. In general, the decomposition process of a root was found to be heterogeneous and segments where a clear gap was visible were followed by segments where the bark (Figure 2-88) or even the entire root (Figure 2-89) were so decomposed that all that remained was a hole with a loose fill of organic matter and soil. Depending on the stage of decomposition, voids may fill with surrounding soils and decomposed organic matter. Figure 2-90 illustrates examples of decaying roots exhibiting a space between the woody center and the bark and where sand has infilled the annular space of these root sections.

In addition to sand infilling/occupying these gaps, live roots were present at the site from the nearby hackberry tree located at the levee toe. Live roots observed did not conduct fluid or function as a preferred seepage pathway during our flow test or during instrument installation. Annular spaces were not observed between the bark and the woody core of these roots or between the soil and the root. Live root growth within the decomposing roots was very common (Figure 2-91). At times, the live root networks around the decomposing roots held root fragments together as a single unit. Live roots seemed to occupy the void spaces and thrive in the mixture of decomposed organic matter and soil. Small live roots were growing 'opportunistically' through bark and the woody cores of decomposing roots.
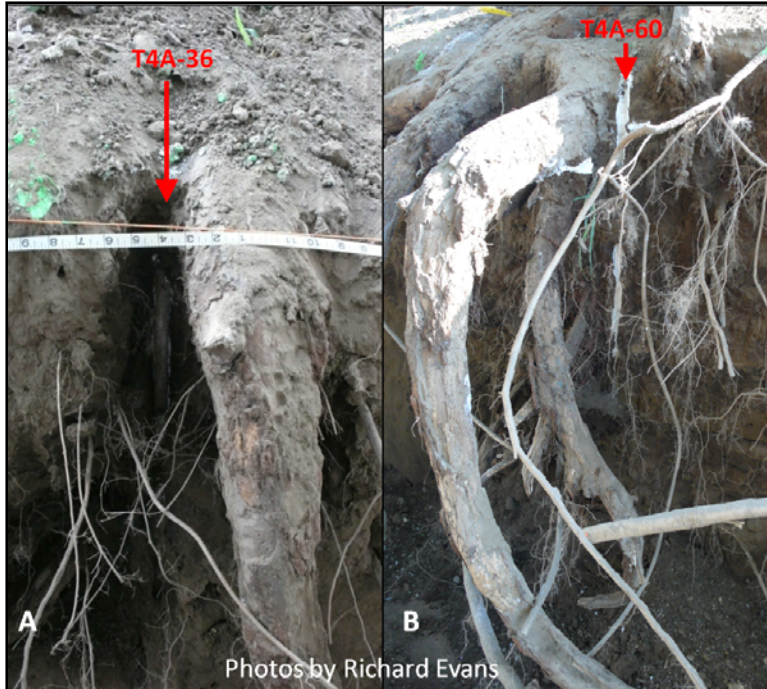
Figure 2-86. Hardened silica slurry associated with tensiometers T4A-36 (left) and T4A-60 (right) is discovered. Flow paths were observed showing that silica flowed through a burrow or void when a direct hydraulic connection was present.



Figure 2-87. Silica slurry freely flowed in burrows (as shown in A) and void spaces within roots (as shown in B) when a direct hydraulic connection was available (or present).
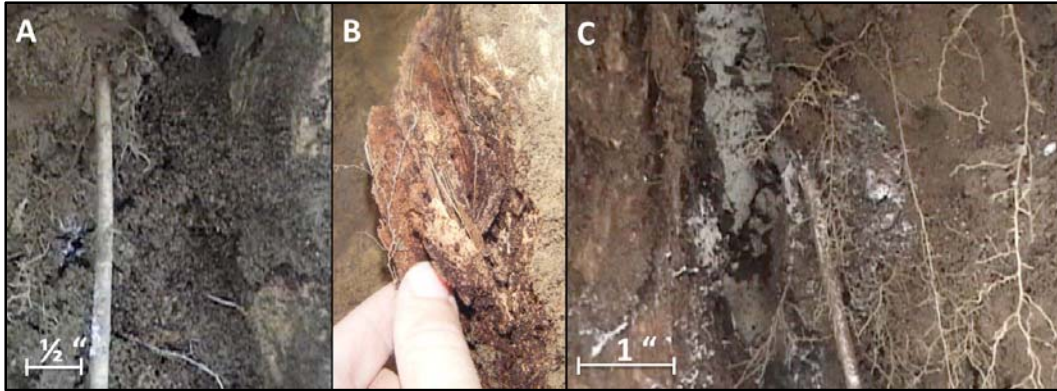
Figure 2-88. Bark fully decomposed with annular space between the woody core and bark, loosely filled with decomposed organic matter and soil (A and B). White silica slurry in Photos A and C are from a tensiometer intersecting loose organic soils and the silica slurry permeating the void space for a short distance.



Figure 2-89. Roots can leave a void where they become completely decomposed and surrounding soils and live roots have not yet in filled the void. The root in Photo D has likely been subjected to decomposition from biological activity.
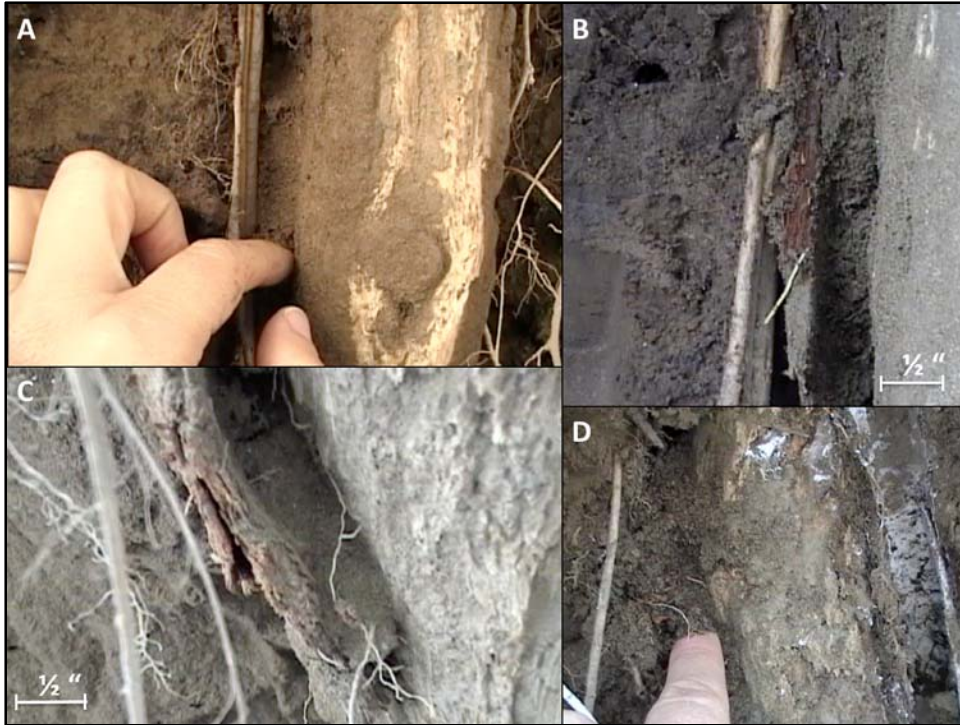
Figure 2-90. Photos A through D are examples of sands in-filling void spaces present between the decaying roots woody center and the bark. In Photo B, from right to left we see the woody core, an infill sand layer, a layer of decomposing bark, a live root, and then the surrounding soil matrix.



Figure 2-91. Live roots frequently observed growing within the decomposing organic matter of old root systems.

Figure 2-92 illustrates the final wall face following excavation of Slice 2. At this time, the gopher burrow (grouted) at Station 138.25 has been revealed and the root architecture of the stump has begun to take shape. Burrows were present in the vicinity of the stump, though animal burrows were present in large numbers throughout the site and did not seem to be more common at the stump than in other areas of the site, as discussed in a subsequent section. Once uncovered, the gopher burrow casting at Station 138.25 was cleaned and undermined slightly in several places to capture its dimension with a T-LiDAR scan. The casting was painted orange for photographs.



Figure 2-92. Final position of 'Slice 2' at the time of logging and before T-LiDAR scanning. Note presence of burrow networks between the root system in Photo B (indicated by vertically-oriented orange nylon strips). Photo C shows the newly revealed burrow casting at Station 138.25.

Slice 3 more fully revealed the architecture of the stump. As excavation proceeded, creating a 'wall log' became challenging as the wall became increasingly thin and formed the support soils beneath the stump. For the last slice, logs were generated on the sides of the stump. Below the stump soils were strategically left in place in order to make a final T-LiDAR image before the stump was undermined and

removed. A segment of soil was left behind (Figure 2-93A) and below the stump, supports rods added, and additional soils were removed just prior to the final T-LiDAR scan. Figure 2-93 shows the final slice from multiple angles. Figure 2-93D shows the final wall face of Slice 3 and provides a perspective of the proximity of the stump and root system to the burrow (cast painted orange) that allowed over 19,000 gallons to pass from the upper to lower stump trench during the 6 day flow test.



Figure 2-93. View of stump excavation following removal of 'Slice 3' soils. Photo A is a view of the stump from the crest of the levee looking down into the upper trench. Photos B through D show the stump from varying angles. Photo D also shows T-LiDAR scanning in progress.

Once the final logs and T-LiDAR scanning were complete, additional excavation was performed behind the stump and then beneath the stump to reveal and photograph more of the root system. The excavation effort behind the stump revealed few roots extending into the levee uphill of the stump (Figure 2-94 and Figure 2-95). Figure 2-94 shows another example of a root that had been pierced by a tensiometer on the uphill side of the stump. This root had begun to decompose inside the woody core of the root. When a tensiometer installation pierced this friable root, the silica slurry used to seal the instrument into the hole filled voids traceable to the tensiometer (Figure 2-94).

Figure 2-94. View root system of the decomposing stump looking north from the upper trench (top). Note migration of silica flour through a path directly traceable to a location where the installation of a tensiometer penetrated the root.

Figure 2-95. View of the excavated eucalyptus stump looking A) southwest from the former location of the lower trench, B) north from the upper trench, C) south at the roots at base of stump, and D) west from between the upper and lower trenches as Richard Evans, UC Davis, inspects the roots system from the uphill side.

In summary, careful excavation around the decomposing elements of the root system of the eucalyptus stump led to a number of observations as follows:

- Discontinuous annular spaces found within some decomposing roots between bark and woody core.
- Bark that was completely decomposed with an intact woody core.
- Entire roots completely decomposed.
- Void spaces loosely filled with sand.
- No annular spaces or voids observed associated with decomposing root.
- Decomposing roots exhibit small, discontinuous voids and holes throughout, likely a result of biological activity.
- Live roots opportunistically growing around and through decomposing root systems.
- Silica slurry/flour flowed into burrows and voids in roots, but only where a direct hydraulic connection existed with the silica source.
- Stratigraphic layering of soils were found to be essentially horizontal.

### 2.1.6.2 Post Flow Test Site Characterization – Analysis of Data

The site excavation phase revealed qualitative data that was used to better understand the state of decomposition of the root system as well as the discernible root architecture. Qualitative data in the section are analyzed to gain insights to stability and seepage implications of a complex, decomposing root system at a snapshot in time.

As previously discussed, the site characterization effort consisted of excavation around the decaying stump in a series of slices/soil segments. Root conditions were photographed and logged at 4 wall faces as shown on Figure 2-73. Detailed logs were created through a collaborative effort of our team with Professor Richard Evans of UC Davis and John Lichter, consulting arborist with Tree Associates. The logs are provided in Appendix 2E and are examined herein.

The soil 'slices' were placed in the coordinate system developed for the site (Figure 2-96) and radial distances from the stump center were calculated for each of the decomposing roots logged in each slice. The data was merged into a single database and categorized by root size, radial distance from stump, degree of weathering and presence or absence of void spaces creating a potential hydraulic conduit through the root.
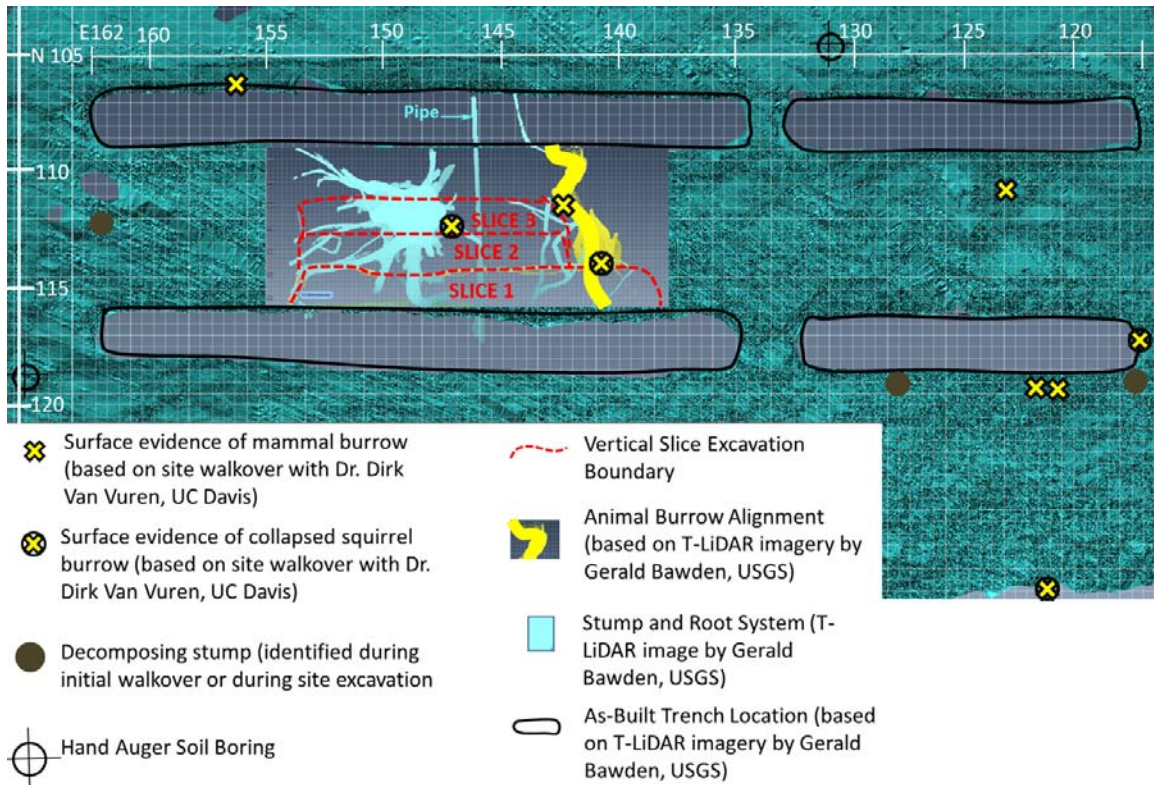


Figure 2-96. As-built site plan showing T-LiDAR scans of root system and burrow (provided by Gerald Bawden, USGS) at Station 138.25.

Annular spaces or voids, as shown on Figure 2-84, were observed in some form in approximately 39% of the roots intersected. This included roots hollowed or cored in sections by biological activity as well as spaces between the woody root center (xylem) and the bark, or the bark and the soil. In general, annular spaces were not noted in roots smaller than 1 inch in diameter. These spaces can be difficult to positively identify for smaller roots. Annular spaces were noted to be absent in 24% of the roots intersected. while for 37% the presence or absence of these spaces was not clear and therefore not noted.

Root size was found to be an important factor in degree of decomposition. An estimated 22% of roots 2 inches in diameter and smaller were described as very or completely decomposed, while 18% of roots in this range were described as 'intact'. In the category of roots larger than 2 inches in diameter, 8% were described as very or completely decomposed while 25% of roots in this range were described as 'intact'. In general, smaller roots displayed a greater degree of weathering than larger ones. These observations are consistent with the findings of Gray and Leiser (1982).

Our final analysis examined total root area with distance from the center stump. Total root area is calculated for each root based on diameter and an assumption that the root is circular. The area of all roots intersected within a given radius is summed and plotted with increasing radius from the stump center. The total intersected area of root as a ratio with total area of soils being studied is a commonly used measure of root density within a soil (Bischetti et al., 2005; Shields and Gray, 1992).

Root area was calculated for all roots within a given radius and the areas were summed and plotted. Roots were then segregated into three size categories:

1. Roots with a diameter larger than 2 inches
2. Roots with a diameter larger than 1 inch
3. Roots with a diameter larger than ½ inch

Figure 2-97 provides a plot of the total root area with distance for each size category. It should be noted that roots smaller than about ¼ inch were not logged. Removal of all roots down to ½ inch in diameter would require excavation of up to twelve (12) feet in diameter around this Eucalyptus stump. Removal to a radius of eight (8) feet is estimated to remove 98% of root matter, while a removal radius of five (5) feet would result in a 92% removal of root matter. These estimates assume an excavation depth of six (6) feet.
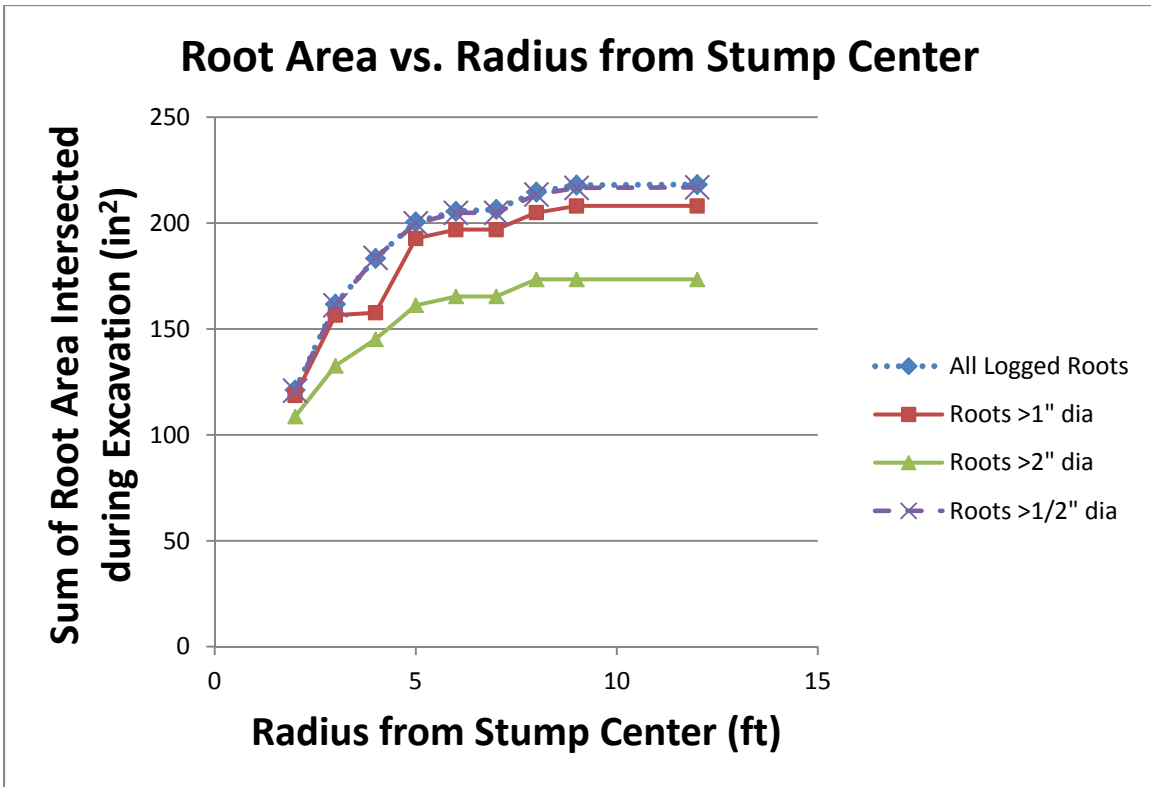
Figure 2-97. The area of each root intersected was calculated and sorted by distance from the stump center. The chart shows the cumulative sum of root area from the center of the stump extending radially outward

In addition to decomposing roots, the flow test site characterization effort documented burrows encountered during excavation. Burrows were counted for each soil segment, or 'slice', excavated and compared to the number of burrows recorded along the uphill wall of the lower control trench. A summary of results is provided as Table 2-6.

Table 2-6. Burrow density at excavated stump and control trenches.

| | Station (ft) | Number of Burrows | Wall Area (ft$^2$) | Burrow Density (burrows/ft$^2$) | Average Burrow Density (burrows/ft$^2$) |
|---|---|---|---|---|---|
| Control Trench | 117-131.5 | 6 | 58 | 0.10 | 0.10 |
| Stump Trench, uphill wall of lower trench | 138-153 | 8 | 60 | 0.13 | |
| Stump Trench, 'Slice 1' | 138-153 | 5 | 60 | 0.08 | 0.10 |
| Stump Trench, 'Slice 2' | 138-153 | 6 | 60 | 0.10 | |
| Stump Trench, 'Slice 3' | 143-153 | 3 | 40 | 0.08 | |

Five burrows were initially identified along the control trench, while an additional burrow appeared during the flow test at Station 117, bringing the total count to 6 burrows in 15 feet stretch as shown on Table 2-6. Based on average burrow densities, it was concluded that burrowing occurred onsite at a similar rate adjacent to and away from the stump.

### 2.1.6.3 T-LiDAR Applied to Flow Test Characterization

T-LiDAR scans were taken to generate a three-dimensional model of the pre-test site condition, excavation walls and flow test site, and throughout excavation efforts to expose the root system. Reflective targets were placed next to roots and burrows (Figure 2-98) and metallic paint was used to highlight the different stratigraphic contacts, thus allowing the T-LiDAR to capture these features given the reflectance contrast between the reflective strips, metallic paint and moist soil (Cobos-Roa et al., 2012).

Figure 2-98 shows a comparison between a T-LiDAR image and a photograph of the site at the same time, following removal of the first segment of soil - 'Slice 1'. Stratigraphic contacts, live and decomposing roots, and reflective targets are visible in the T-LiDAR image. The points gathered can be digitally processed into 3D images of the entire root system. In addition the technology facilitates taking measurements or making calculations that would be difficult to capture using other methods. Data can be managed in a 3D environment in the KeckCAVES at University of California Davis shown on Figure 2-99. Personnel from the USGS-Sacramento Western Remote Sensing and Visualization Center and the UC Davis KeckCAVES were able to use the center's facilities to isolate decomposing roots, burrows, and geologic layers so that they may be viewed separately.

Figure 2-98. Slice 1 comparison between T-LiDAR image (left) and photograph (right). Note reflectors in T-LiDAR image indicating burrows (vertically oriented) and decomposing roots (horizontally oriented). Source: Cobos-Roa et al. 2012.



Figure 2-99. T-LiDAR data is viewed in 3D at the UC Davis KeckCAVES. Point clouds are selected and isolated, separated, relocated, and rotated through this user-friendly 3D interface. Gerald Bawden of the USGS gives the UC Berkeley team a tour. Photos courtesy of Mick Klasson.

Figure 2-100 provides a view of the completed excavation looking south with a corresponding T-LiDAR scan and a view where the live and decomposing root systems, pipe, and burrow are isolated for easier interpretation. Figure 2-101 is useful to visually understand the extent (in plan-view) of the decomposed root system. Fully decomposed roots are not included in this image. Scans were viewed in the KeckCAVE as a means of enhancing field documentation, sketches, and measurements. In Figure 2-102, the root system of the stump is isolated and this plan view image is useful in illustrating the path of silica flow during installation of tensiometers. Figure 2-103 and Figure 2-104 are additional T-LiDAR images generated from different vantage points to illustrate the different geometric characteristics of the root system. The T-LiDAR image in Figure 2-105 shows a view of the stump looking west as compared with a vectorized version of the root system generated from the data.
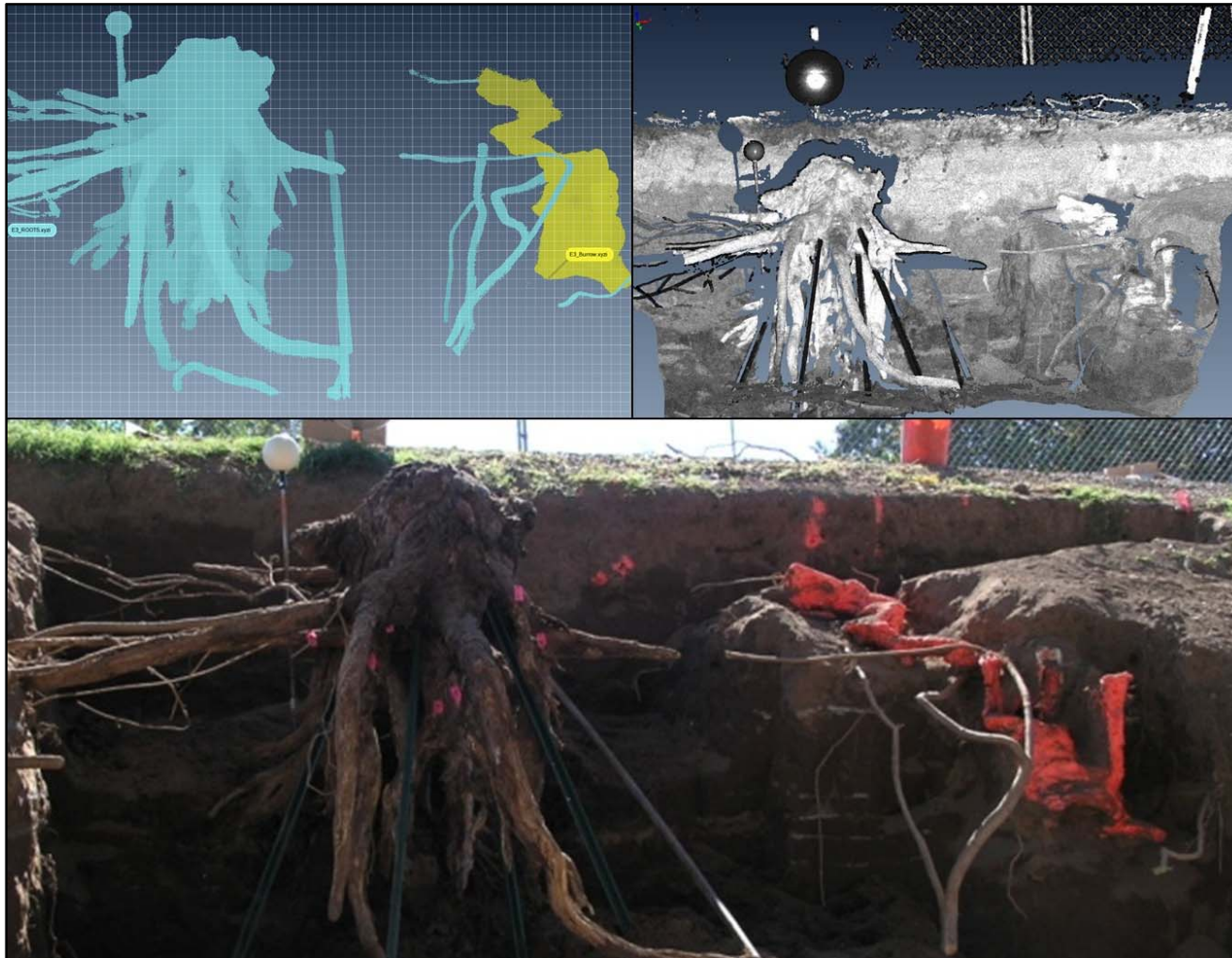
Figure 2-100. T-LiDAR images provided by Gerald Bawden of the USGS (top) looking south compared with photograph of root system (bottom) and burrow at Station 138.25.
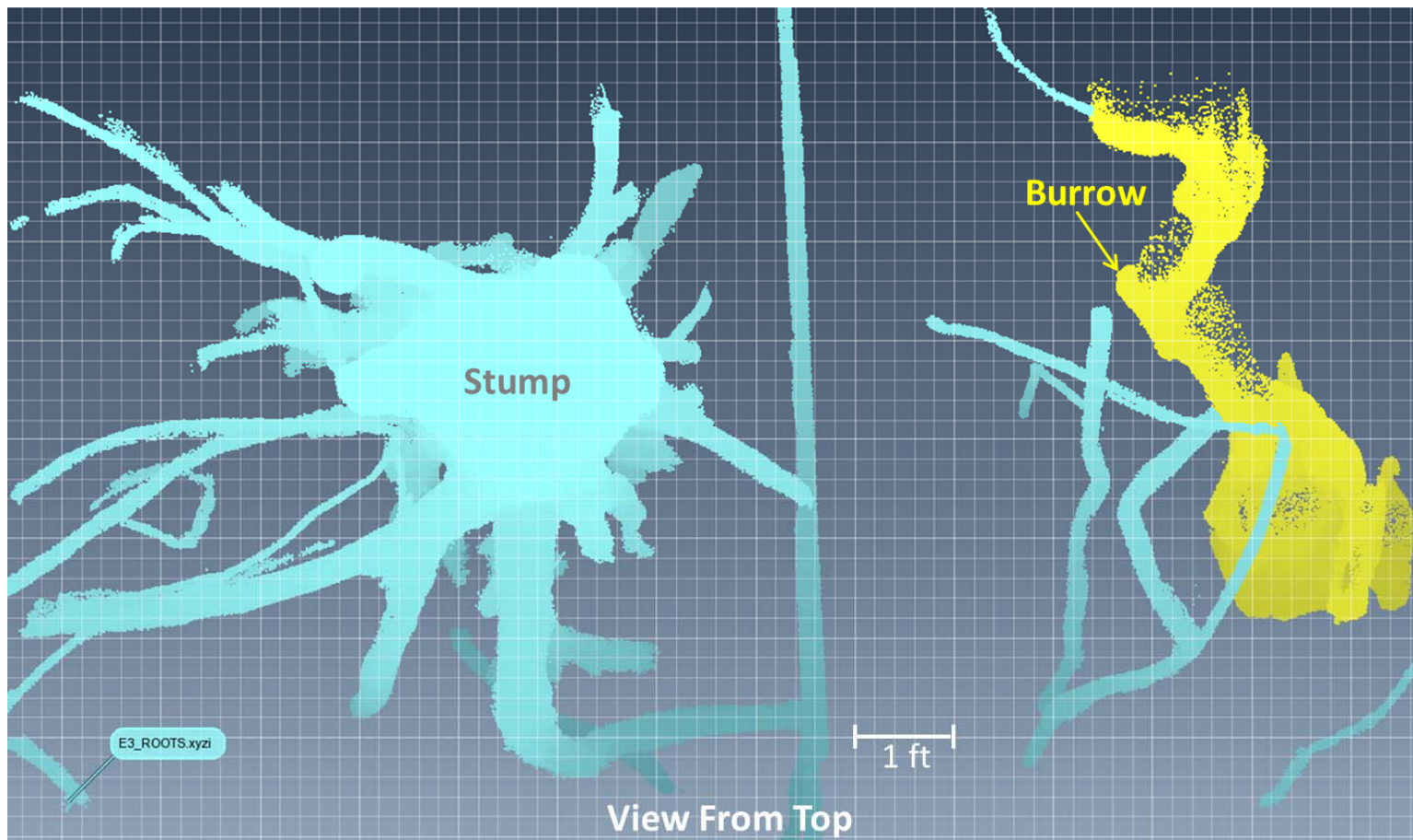
Figure 2-101. T-LiDAR scan of root system and burrow at Station 138.25 (provided by Gerald Bawden of the USGS). View is from the top. Most roots are decomposing roots related to the eucalyptus stump, but live roots are present, particularly in the vicinity of the burrow.
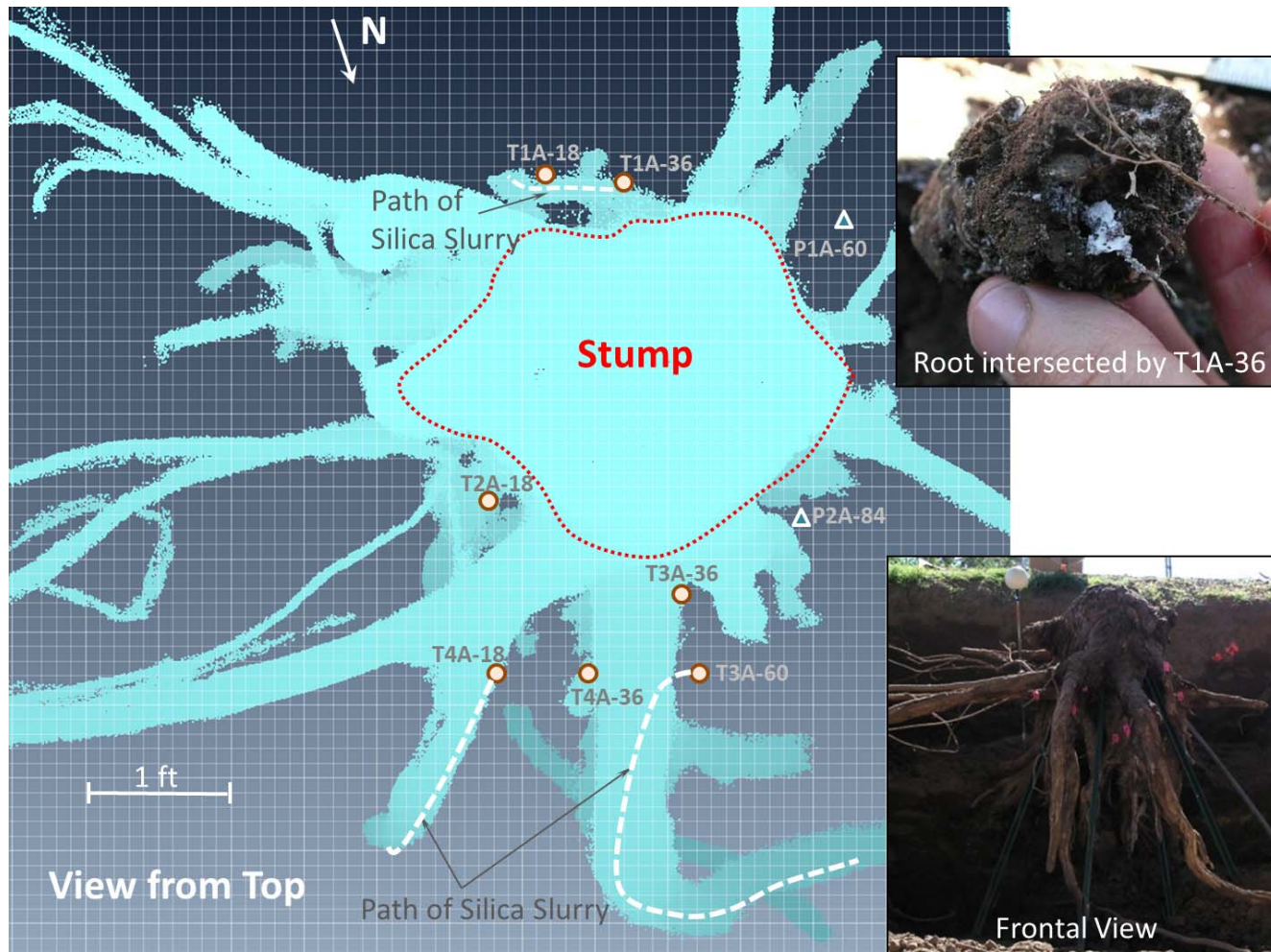
Figure 2-102. View of the decomposing eucalyptus root system from above as scanned with T-LiDAR. The image is used here to show the path of silica flow from the tensiometers and instrument positions within the root system. Photographs show silica flow through the root intersecting with tensiometer T1A-36 (upper right) and a south-facing frontal view of the stump and root system. T-LiDAR image courtesy of Gerald Bawden of the USGS.

Figure 2-103. A south-facing view of eucalyptus stump and root system (right) and the corresponding point cloud image (left) derived from combining data from a series of T-LiDAR scans. T-LiDAR image courtesy of Gerald Bawden of the USGS.
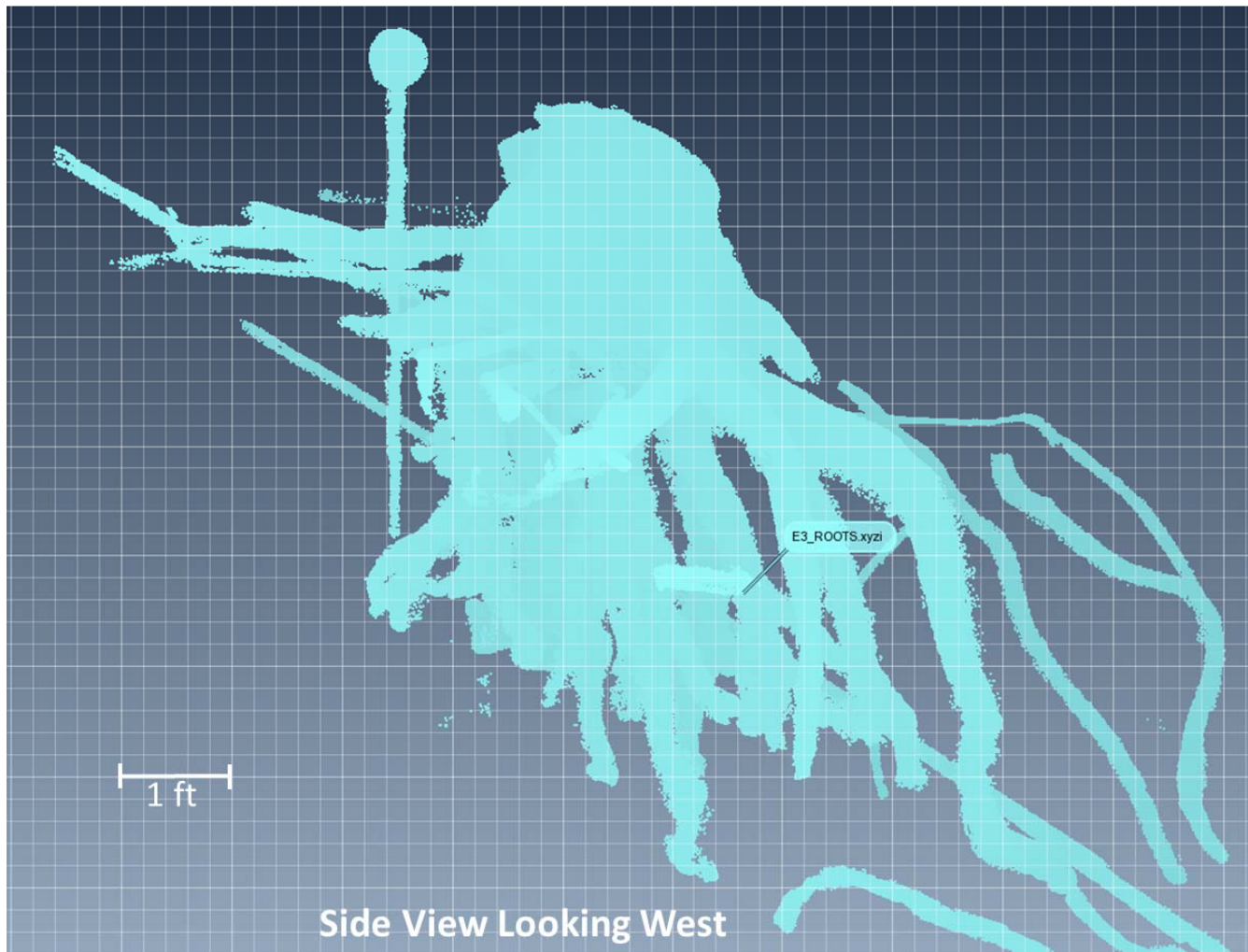
Figure 2-104. A west-facing view of the Eucalyptus stump and root system stitched together from a series of T-LiDAR scans (provided by Gerald Bawden, USGS).
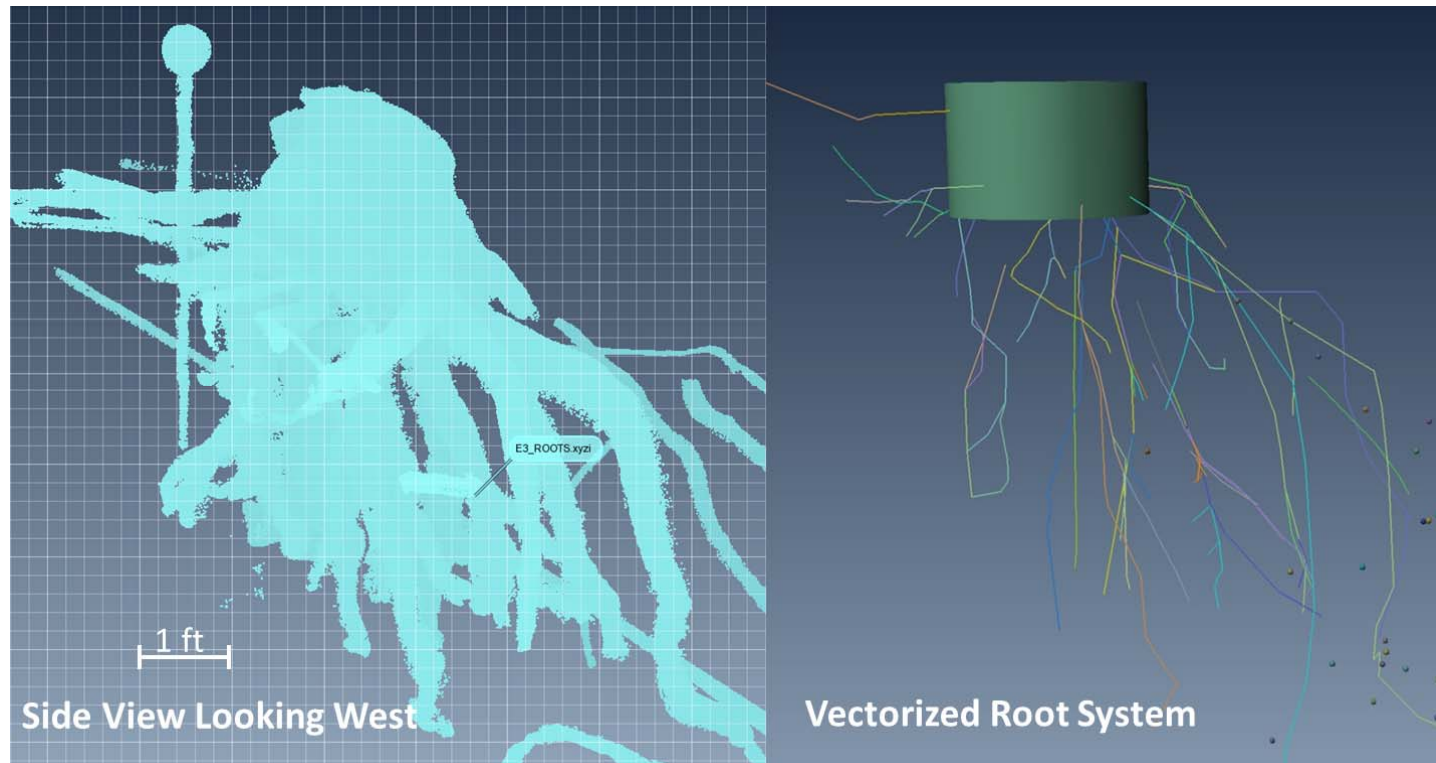
Figure 2-105. A view of the Eucalyptus root system as a point cloud generated from T-LiDAR scans (left) and a vectorized plot of the root system to aid in modeling efforts. Base source: Gerald Bawden, USGS.

## 2.2  DISCUSSION OF FINDINGS

The parallel trench wetting front test subjected the levee site to an imposed flow of water over a period of 6 days during which time positive and negative pore pressures were monitored within the study area. As noted, the test site was generally composed of silty soils and the test was focused around a decomposing eucalyptus stump and root system. The tree was cut sometime between 1994 and 1998 and the stump left decomposing for 12 to 16 years prior to the field test. Decomposing roots, excavated following the flow test, displayed varying degrees of decomposition with voids or annular spaces in 39 percent of roots intersected by the excavation. Annular spaces were continuous over short distances, and many were partially or loosely filled with organic matter. Some roots had voids that were partially filled with both organic matter and soil. Live roots growing from a hackberry tree located at the toe of the levee, mammal burrows, ant and worm holes, and a water pipeline added complexity to the system and the study. Small live roots were observed to be concentrated in the decomposing root channels. The field test benefited from the complexity of this site as these diverse conditions represent the reality of a levee system.

Tensiometer installation revealed the sealant materials (a silica slurry) could flow through a gap between the bark and woody core of a decomposing root at the lower trench wall face downhill from the stump. Silica slurry was found in several other roots as well as in loose soil pockets and cracks, but only where the tensiometer hole made a direct hydraulic connection with the void space.

Beven and Germann (1982) assert that for a macropore to flow, the supply of water must be in excess of the lateral losses to the surrounding matrix and the macropore must be sufficiently connective to transport the water downslope. Absent a direct hydraulic connection, pore suction would prevent flow from smaller pores into larger macropores or voids. However, eventual saturation of smaller pores allows flow into larger pores as pore suction is eliminated and pore pressure is generated, driving flows. As full saturation is achieved in the surrounding matrix, however, lateral losses are increased and supply must keep pace for flow to continue. Further, continuity of void space is also necessary for flow. We observed that where voids are shallow, seeps can form at the slope surface. Burrow networks, including gopher burrows (which are often partially backfilled as gophers excavate new tunnels) were found to be sufficiently continuous to flow once water enters the macropore/burrow. In this case, water entered the macropore through a direct hydraulic connection to the water source. During the flow test, these influences dominated flow and wetting patterns.

Initially, the burrow at instrument Line C resulted in observed seeps at the levee slope face. For a window of about 12 hours, water supply was sufficient and the burrow was sufficiently connective to allow for slow flows emerging through the upper wall of the lower control trench at Station 117. After that time, flow stopped, possibly due to collapse of the hole or saturation patterns causing the lateral losses

to exceed inflow. Even though burrows dominated flow patterns and brought seepage to the slope surface in many locations, flow eventually diminished and stopped in the burrows. Rapid flow was initially observed through the gopher burrow at Station 138.25. Flow eventually slowed, then stopped, and began to flow again following a brief period of drying (when the water delivery system malfunctioned). A decrease in permeability of the burrow walls, and therefore infiltration volumes, following drying could cause inflow volumes to exceed lateral losses to surrounding soils. Alternatively, a blockage developed within the burrow during the study may have cleared upon re-establishment of flows. The presence of two gopher burrow greatly impacted flow patterns during the test and both were hydraulically connected to the water source.

The two (2) ground squirrel burrows encountered did not exhibit a direct hydraulic connection with the water source (the upper control trench). Flow can, however, concentrate into a macropore but only at the rate that the surrounding soils can deliver water to the hole. At approximately 125 hours into the flow test, a small amount of water was seen seeping from the ground squirrel burrow at Station 121.5 of the lower control trench.

Similarly, excavation of the root system revealed intermittent annular spaces or voids in about 39 percent of decomposing roots intersected during the site characterization effort. These voids were found to be discontinuous, at times loosely filled with decomposed bark or sand, or simply not present in segments of the root. Flow was not observed through these known voids during the flow test, though flow of silica slurry was observed when a direct hydraulic connection was made by intersection of a root with a tensiometer installation. The 6 day flow test, however, did not result in visible flow through the voids. A direct hydraulic connection did not exist between the upper and lower trenches via root conduits and the system of voids associated with the decomposing root system lacked sufficient inflow of water and continuity of void spaces to flow water. The soil segment between the stump and the uphill wall face of the lower trench was the last to saturate, despite the presence of voids associated with decaying roots in that segment.

2.3  RESULTS IN THE CONTEXT OF PREVIOUS STUDIES

A better understanding of our findings can be gained by viewing our results in the context and findings of similar studies. In 1971, Aubertin performed field and laboratory scale seepage testing on forest soils within Tuscarawas County, Ohio. Trees primarily consisted of white oak, beach, and hickory. Field scale testing occurred at two sites - a sandy loam and silt loam site – where simulated rainfall was introduced to an undisturbed soil surface just above an observation pit. Water was observed to flow through many root channels (macropores remaining following the decomposition of roots) and burrows, though the author noted soils immediately around the root channels were very low permeability, proposing a theory that vertical macropores (possibly from earthworms) may have influence the introduction of water into the macropore. Macropores observed by Aubertin (1971)

were primarily shallow with the number and diameter of open channels decreasing at depths greater than 12 inches. Mitchell et al. (1995), discusses how, in expansive soil conditions, smaller macropores such as those associated with earthworms tended to close as soils swelled under saturation. Beven and Germann (1982) suggest that undisturbed forest environments are more conducive to the preservation of macropores than sites experiencing more intensive land use. According to Whipkey (1965), leaf litter covers the forest surface and acts to maintain permeability in forest soils.

Aubertin (1971) observed lower flow through channels in a sandy loam site as compared to a silt loam and found that 'channels' tended to fill with soils at the sandy loam site. Similarly, an abundance of root channels were discovered in a coarse textured test site studied by Gaiser (1952), though most were found to be loosely filled with soil. Beven and Germann (1982) conclude that channels tend to persist in soils with clay contents greater than 30 percent, but could be destroyed by the in-washing from one large rainstorm. Similarly, in an agricultural context, Green and Askew (1965) found that macroporosity had a significant influence on hydraulic conductivity where soils had clay content greater than 40 percent. Our study consisted of lean clays, various silts, and silty sands where annular spaces around some decomposing roots were discontinuous and loosely filled with sands while others were not filled.

Beven and Germann (1982) assert that the volume of water entering the pore must exceed the volume lost laterally for flow to occur. In a study by De Vries and Chow (1978), disturbance of a surface layer, where macropores were initially open to the atmosphere, resulted in a shift of flow to the soil matrix over the macropores. Similarly, Beasley (1976) found that for channels to flow, the channel needed to be open to the environment and offer a depression as a means for water to gather and be channeled into the macropore. Aubertin (1971) demonstrated, through dye testing, the need for a direct hydraulic connection to a water source for through flow and for advancement of a wetting front through a pore. Channels without a direct hydraulic connection did not flow as indicated by an absence of dye. Similarly, our field study found that a direct hydraulic connection to a water source facilitated advancement of the wetting front through a network of gopher burrows.

Barley (1954) asserts that roots decrease permeability of the soils around roots by compacting them as they grow. According to Aubertin (1971), this compaction can result in a decreased permeability of soils directly around root channels. Barley (1954) also found that decaying roots can increase overall soil permeability but this depends on which of the opposing processes of growth and decay tend to dominate based on seasons and conditions. Where live roots continue to grow, studies have shown that these roots tend to grow preferentially within the organic matter and void spaces of decomposing roots, often filling those voids (Parker and Van Lear, 1995; McKee, 2001). Similarly, live roots of a nearby hackberry tree were observed growing preferentially within the decaying root system of the eucalyptus stump that was excavated.

The fraction of water flowing through a macropore network is expected to be reduced as the soils surrounding the macropore become saturated and later losses to the soil matrix are increased (Beven and Germann, 1982). This behavior was observed in our study as flow rates decreased with time and burrow flow either slowed or stopped as the soil matrix approached saturation.

# CHAPTER 3

## Crown Trench Seepage Test, Northern Levee of Twitchell Island in Rio Vista, California

### 3.1 CROWN TRENCH SEEPAGE TEST – TWITCHELL ISLAND, CALIFORNIA

A second field test focusing on achieving saturation of levee embankment soils through the root systems of live trees was conceived to further explore the effects of these root systems on the integrity of a levee. The concept of the Crown Trench Seepage Test involved excavation of an 8 foot deep trench through the levee crown and supplying the trench with water held at a constant head, simulating a flood condition where water is delivered from the center rather than the side. Instrumentation installed within the zone of flow captures positive and negative pore water pressures before, during, and after flow. A conceptual sketch of the second field test is provided as Figure 3-1. While the focus of the first field test was on the study of decomposing tree roots, the second field test was modified slightly to focus on the effects of live, native root systems to levee seepage and stability under conditions approximating steady state flow.
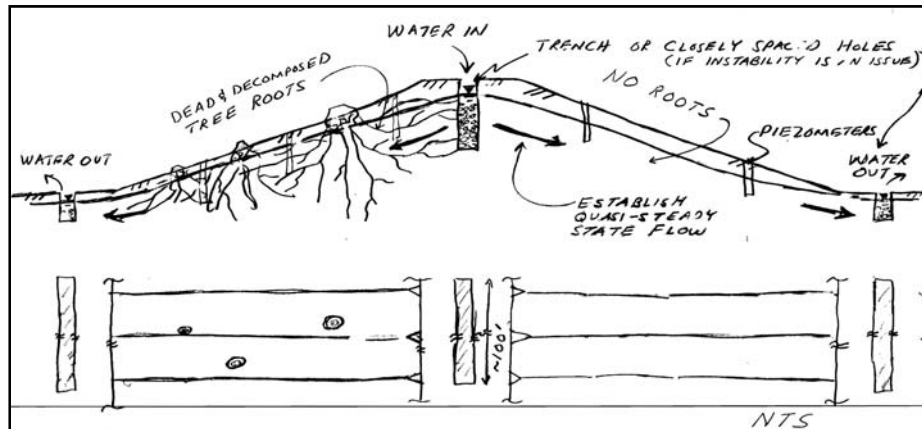


Figure 3-1. Conceptual sketch by Professor Jonathan Bray illustrating concept of crown trench seepage test.

### 3.1.1 Site Selection

Conceptually, the crown trench seepage test (Figure 1-1) is quite simple and elegant. However, the large scale and depth of the crown trench test combined with the destructive nature of the work involved in the experiment presented concerns for many reclamation districts maintaining active flood control levees. As a result, inactive or bypassed levees, or those with low consequences of failure were sought in site selection. Further, during the parallel trench wetting front test at the California Exposition and State Fair site in Sacramento ('Cal Expo') the majority of water was lost outside of the study area. Large water demands expected for a test of this size established a need for a water source near the test location. To minimize losses of water outside of the study area, a shallow water table or a low permeability layer below the study zone was sought in order to meet the objective of developing saturated flow within the study area. A site with soils sufficiently cohesive to

114

allow for construction with vertical shores was sought, allowing safe entry and while maintaining trench wall visibility for logging and data collection. Tree species, position, and site configuration were also considered important factors. Valley Oaks (Quercus lobata) and cottonwoods (Populus fremontii) were sought out as the most appropriate species to include in our study as they are native to California and occur in abundance on levees throughout the State.

After a review of candidate sites, a site was selected within Reclamation District 1601 along an oxbow segment of the Sevenmile Slough, on the northern levee of Twitchell Island (Figure 3-2). This site lies within the Sacramento San Joaquin Delta. The paved levee served as the primary access road along the northern border of the island until a segment of levee about a third of a mile in length (including the study site) was bypassed in 2008. The levee is no longer maintained but retains water, protecting an approximately 8 acre stretch of unimproved land between it and the new flood control levee (Figure 3-3).  The Sevenmile Slough is a gated channel used for irrigation of the island. Gates are operated from the neighboring Brannan Island at the eastern end of the slough at high tide and closed at low tide to allow farmers to siphon water for irrigation. Water levels within the slough are relatively stable, typically fluctuating only a few inches to a foot day-to-day. The slough was deemed suitable as a water source and the candidate levee segment had a suitable landside oak tree near a control segment with no trees on the land side and small trees and bushes on the water side (Figure 3-4). The site was selected primarily for the landside tree and uniform appearance of the landside levee. A waterside oak located between the landside oak and the control was included in the study due to a favorable site configuration that could easily accommodate the study of both, though topographic non-uniformity and limited access of the waterside levee made the landside tree the focus of the study design.



Figure 3-2. Site Vicinity Map.
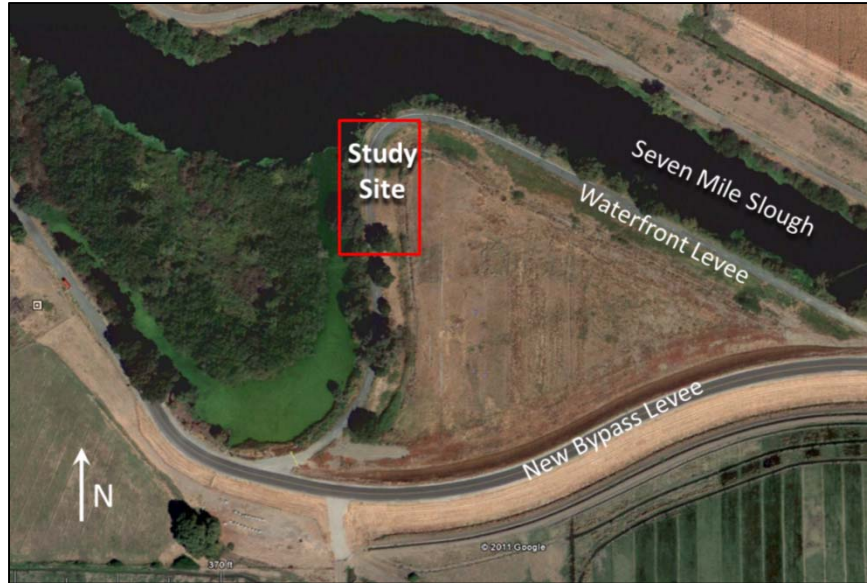
Figure 3-3. Location of the study site along the Sevenmile Slough.
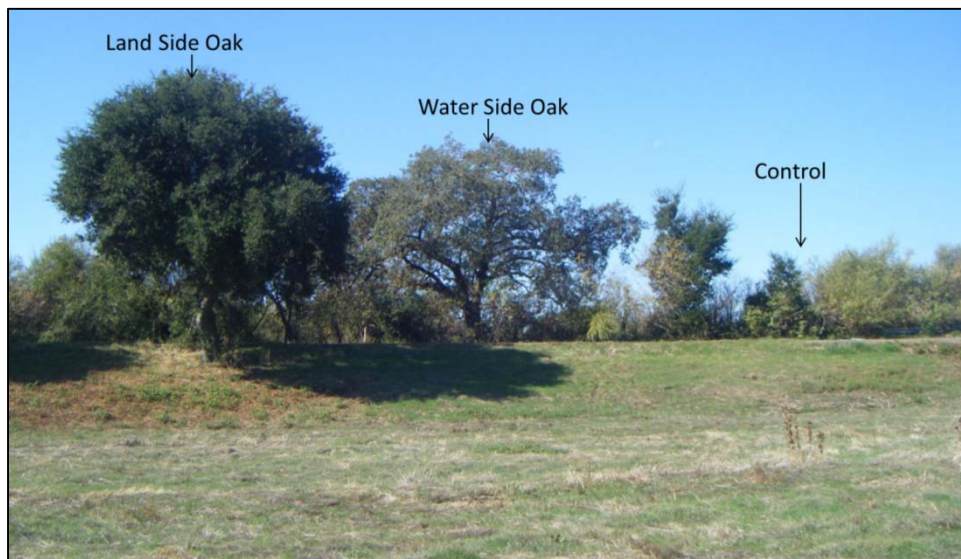


Figure 3-4. View looking west at landside oak, waterside oak, and study control section.

### 3.1.1   Site Description

A 2001 topographic map of the selected site (KSN, 2001) showing the landside and waterside oak trees is provided as Figure 3-5. An additional, site specific topographic map was shot with a surveyor's level on June 1, 2012, just following the flow test.  This map provides a higher degree of topographic detail for interpretation of site data. The limits of the topographic map are provided on Figure 3-6 and a detailed view of the study area topography is provided as Figure 3-7.
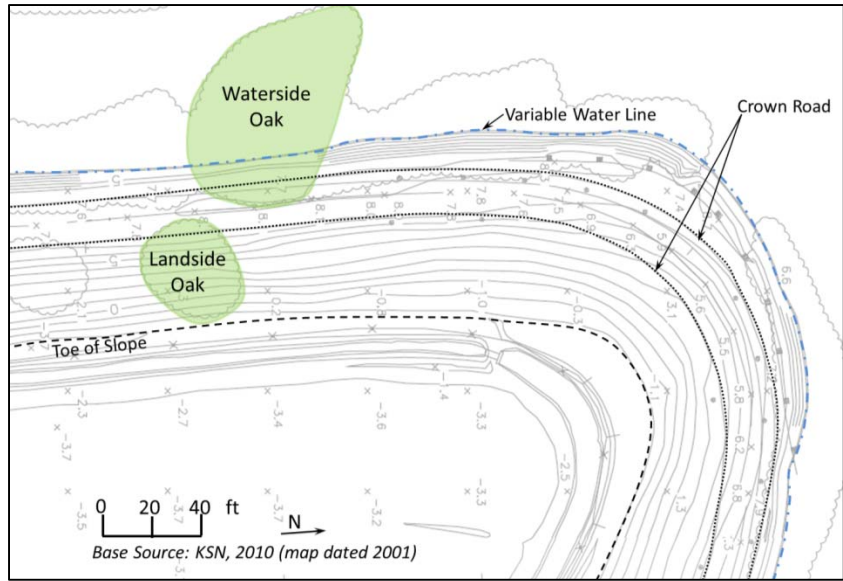
Figure 3-5. Topographic map of the site as shot by KSN in 2001.
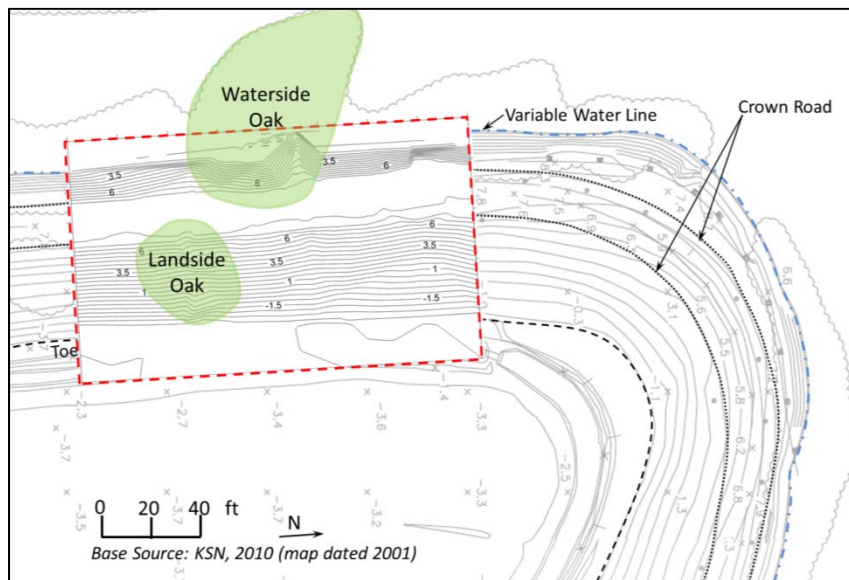


Figure 3-6. Topography of the study area following the flow test was captured with a surveyors level and outlined in red and inset over 2001 topography by KSN.
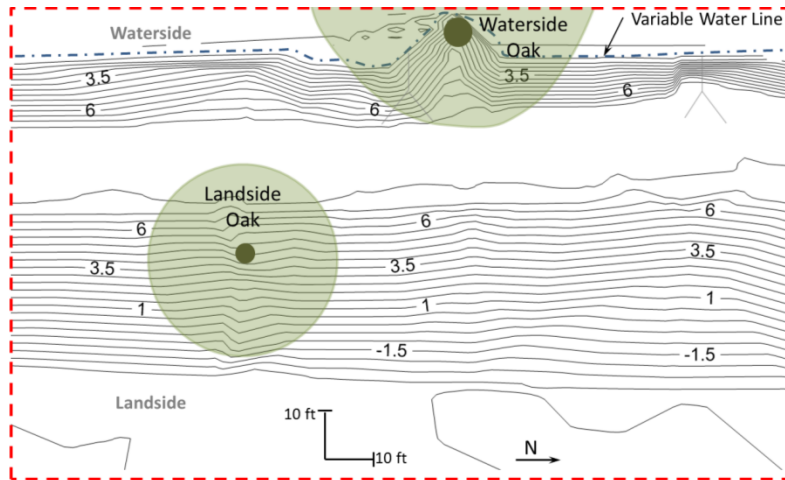
Figure 3-7. Topography following the flow test shot on July of 2012.

Figure 3-8 shows cross sectional topography of three identified sections across the site representing the landside oak tree, the waterside oak tree, and the proposed control area. The landside of the levee is inclined at a relatively consistent gradient of 4:1 (horizontal:vertical) with a total vertical height from crown to toe of just over 10 feet. The waterside slope has a variable gradient ranging from 4H:1V near the top and steepening to 1H:1V near the base. Section C is flatter than Sections A and B near the top with a larger portion of the slope inclined at a gradient of 1H:1V or steeper. Section C topography was difficult to capture due to access constraints associated with dense vegetation and overly steepened slopes.
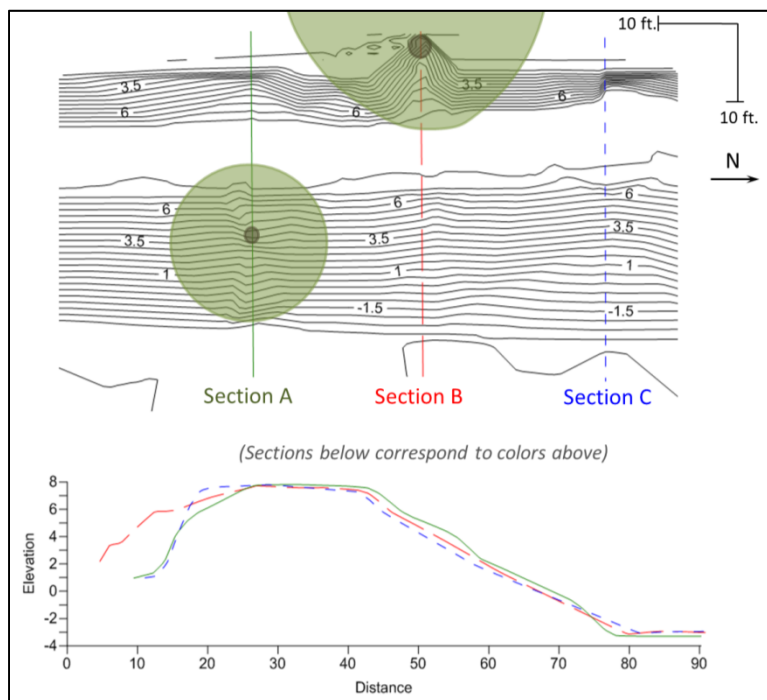


Figure 3-8. Cross-sectional topography at the landside oak tree (Section A), the waterside oak tree (Section B), and the proposed control section (Section C).

118

Historic topography and available historical documents were reviewed to provide an understanding of the age, construction methods, and materials used to construct the site levees. A historical account of reclamation of Twitchell Island and surrounding islands is provided by Thompson (2006). Twitchell Island, originally marshland, was reclaimed in 1869. Due to the presence of peat soils and high flows in the San Joaquin River at the southern border, the island suffered frequent floods between 1869 and 1875 and was temporarily abandoned. Levees were originally constructed to a height of 3 ½ to 5 feet with a 2 to 4 foot crown width. When this was found to be inadequate, levees increased in height by about 3 feet with a crown width of at least 6 feet and a base of 12 to 20 feet. Levees to the south were more problematic due to construction on peat foundation soils. Reclamation began again in 1894 and portions of the island were being leveed through 1904. Flooding problems continued in 1906, 1907, and 1909. In a 1910 topographic map, the levees appear to be in their current configuration. Flood impacts to northern levees, on firmer soils than southern levees, are not detailed. Figure 3-9 shows topographic maps of the site in 1932 and 1952. The Sevenmile Slough has been gated within this time window. High waters occurred in 1937 and 1950 (Paulson, 1988-89). Based on discussions with Mr. Rick Carter of RD1601, the gate was installed in part due to problems with scour. According to URS (2011), their engineer noted during a field reconnaissance interview that gate structures were constructed around 1950. The URS summary document also states that data related to levee segment improvements occurring between 1920 and 1960 were not available for review.

Figure 3-10 shows mapped soil conditions for Twitchell Island based on USDA mapping (1935), which indicates the site is underlain by alluvial soils, specifically Columbia silty clay (Co) with nearby deposits of Ryde silty clay loam (Rd).



Figure 3-9. Historic topographic maps: USGS (1932) and USGS (1952). Note the position of structures have changed along the Sevenmile Slough between 1932 and 1952. A flow control gate has been installed by 1952 and the oxbow section appears to be wetland.
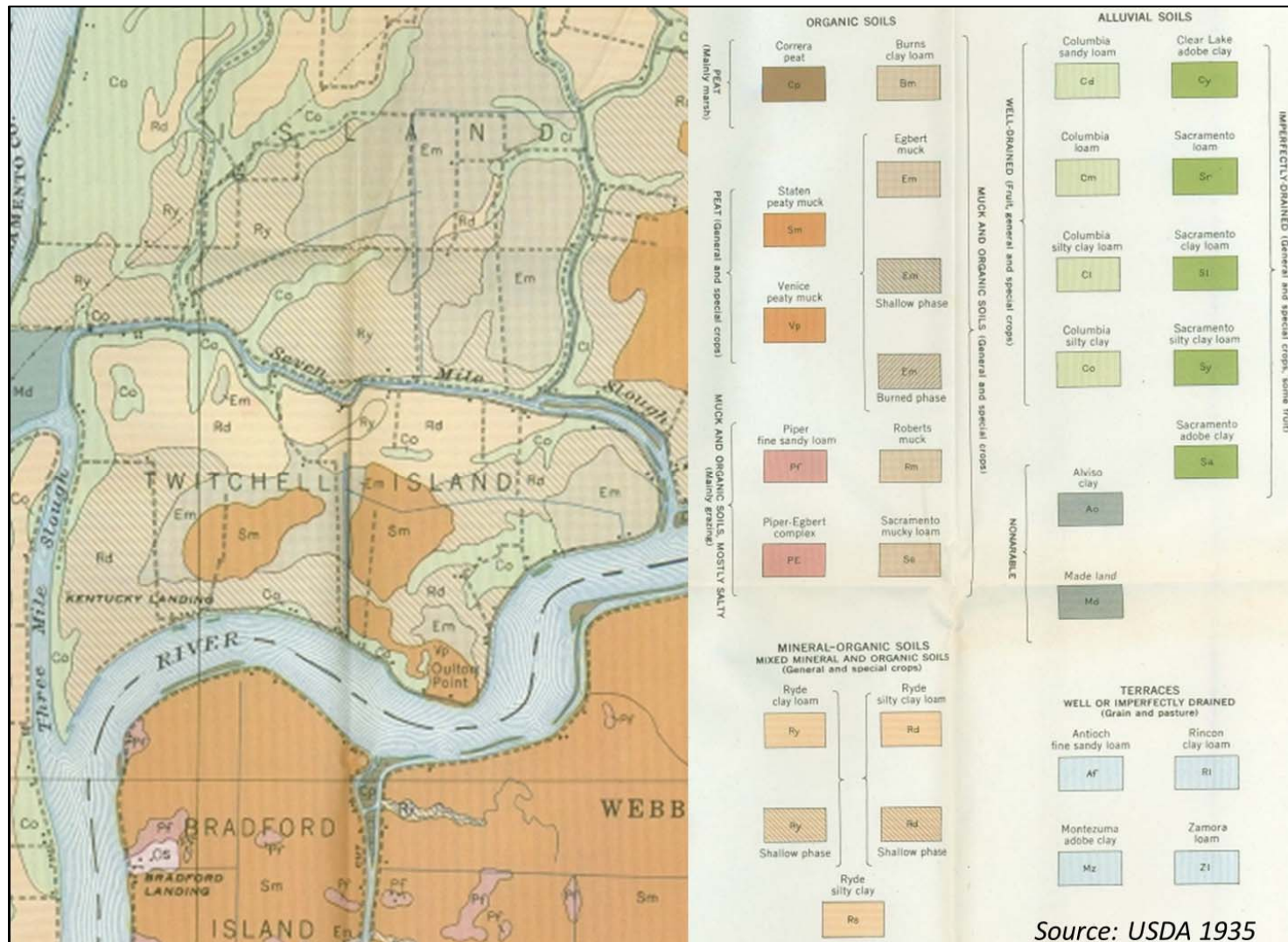
Figure 3-10. Soil conditions at Twitchell Island as mapped by the USDA in 1935.

The landside vegetation consisted primarily of low grass cover with patches of mowed and returning blackberry and included one oak tree (Figure 3-11), while the waterside was found to be densely vegetated, as shown on Figure 3-12. During the site reconnaissance, rustling sounds and moving vegetation were indicators of animal activity just north of the control site within a patch of blackberry brush.

Dr. Dirk Van Vuren of UC Davis visited the site as the CLVRP team expert to evaluate the potential for burrowing mammals at the Twitchell Island study site. During a site walkover on May 2, 2012, Dr. Van Vuren identified evidence of vole activity on the landside (Figure 3-13A and B) and noted that pocket gophers are likely present at this site as well.  He suggested both are likely to dig shallow burrows with exits on the landside of the levee. Blackberry makes for a protected burrow entrance as well as a food source (Ordeñana et al., 2012). Evidence of gophers appeared during trench construction (Figure 3-13C).



Figure 3-11. Landside vegetation; views looking west (top) and north (bottom).

Figure 3-12. Waterside vegetation looking: south from the water (left); south from the waterside oak tree (top right); and north from the waterside oak tree (lower right).

Access to the waterside was limited due to dense vegetation and because trimming of elderberry was not allowed within the conditions of our permits. Access became somewhat easier when water levels in the slough were lowest. On the day of Dr. Van Vuren's walkover, access was possible from the waterside oak tree. Several locations of likely abandoned muskrat burrows were identified during the reconnaissance (Figure 3-13D and E). Based on our discussion, muskrats typically enter their burrows below the water and excavate their burrows up from the water to create a dry den above the water line. Mr. Rick Carter, in charge of maintenance for RD1601, confirmed that muskrats had been a past problem, but had not been seen in that area in recent years.

Figure 3-13. Evidence of burrowing animals on the landside consisting of voles (A and B) and gophers (C) and evidence of muskrats found on the waterside (D and E).

The type, size and location of onsite vegetation was noted prior to commencement of construction. Professor Alison Berry of UC Davis assisted in vegetation identification. The landside oak tree was determined to be a Coast live oak based on its leaves and bark (Figure 3-14), native to California (Cooper, 1926). Based on our review of aerial photographs, no trees existed on the landside of the levee in 1978. By 1993, a small but established landside oak can be seen, along with several other landside trees. The even spacing and apparent simultaneous appearance on the levee suggests the trees were planted between 1978 and 1993. The landside oak tree has a canopy diameter of approximately 40 feet and is likely to have been approximately 25 years old at the time of our study.

Waterside vegetation within the study site consisted primarily of a blend of willow and elderberry. Just north of the waterside oak tree was a small Coast live oak amongst dense willow and elderberry. Figure 3-15 shows examples of typical waterside vegetation found within the study area. The waterside oak tree was identified by Professor Berry as a Valley Oak based on its leaves and bark (Figure 3-16). The tree was leaning at an angle of about 44 degrees from the horizontal with a large branch extending out over the water as shown on Figure 3-16 and Figure 3-17. The tree age was estimated at 60 years at the time of our study based on historic aerial photography and a growth ring count following the removal of the tree at the end of the project. The tree canopy had a diameter of approximately 80 feet in its maximum direction, however, the width of the canopy along the levee road was estimated at 60 feet.

123

Figure 3-14. Landside Coast live oak tree bark (left), leaves (top right), and from a distance looking south (lower right).



Figure 3-15. Waterside vegetation consisting of primarily elderberry (A and B) and willow (E and F) with north-facing views of dense waterside vegetation (C and D).

Figure 3-16. View of the waterside Valley oak branches, leaves, and bark.


Figure 3-17. View of waterside oak looking west (left), north from a distance (top right), and north from close in (lower right).

The waterside Valley oak can be seen in the 1993 aerial image as shown in Figure 3-18. The tree appears to extend farther into the levee road in 1993 than in subsequent years which may indicate an increasing lean angle or pruning. Figure 3-18 shows the construction of the bypass levee in 2008, serving as both flood protection and a paved primary access road along the north side of Twitchell Island and diverting traffic flows from the site under study.

In September of 2008, an irrigation ditch interrupted by the bypass levee can be seen abandoned. Figure 3-19 shows the ditch intact in 2010 and overgrown or possibly removed by July of 2011. The site appears to have undergone minor re-grading by September of 2011 with the toe ditch completely removed in this photograph. The ditch was located at the toe of the landside levee within our study site.



Figure 3-18. Image of the study site in 1993 showing a small, but present, landside oak. Images between March and September of 2008 show the construction of the levee bypass.
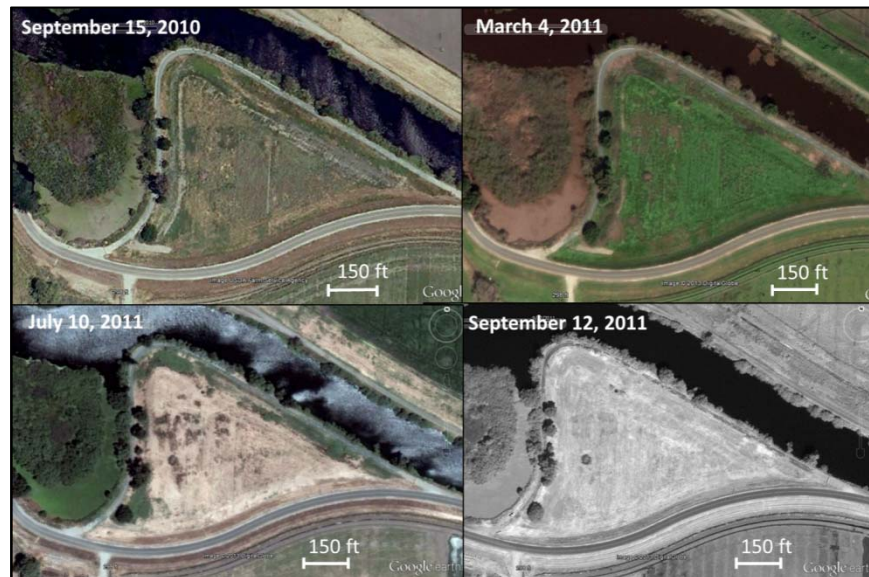


Figure 3-19. Aerial imagery in the years before the flow test show minor re-grading in 2011 to remove a toe ditch abandoned during the bypass installation.

## 3.1.2  Test Layout and Design

As discussed, the conceptual test design intended to simulate a flood condition where water is delivered into a trench through the levee crown rather than from the side. Upon site selection, the team modified the test concept slightly from that shown on Figure 3-1 to account for differences between waterside and landside site conditions. A control section and a study tree, the landside oak that was the focus of the study, exhibited the uniformity appropriate for a reasonable comparison to be made. As previously mentioned, given the layout of the site, with a waterside tree existing between the landside oak tree and a control section, the experiment was extended to include study of a waterside tree to be evaluated against a waterside control section. With the landside as the primary study site, the trench was shifted from the levee centerline toward the landside. A location was selected where the wall of the trench would be positioned approximately 3 feet from the hinge point of the landside slope. The new configuration allowed the 'tree trench' to intersect the root systems of both land and water side levee trees. In addition, a separate 'control' trench was constructed north of the tree trench, as shown on Figure 3-20.

The trenches were excavated to a width of 2 feet and a depth of 8 feet. The as-built length of the control trench was approximately 31.5 feet while the as-built length of the tree trench was 95 feet with an approximate 5 foot separation between them. Water was pumped from the main channel of the slough and delivered to the trenches via gravity from a 4900 gallon polyethylene water reservoir placed at the highest location at the southern end of the trenches (Figure 3-21).
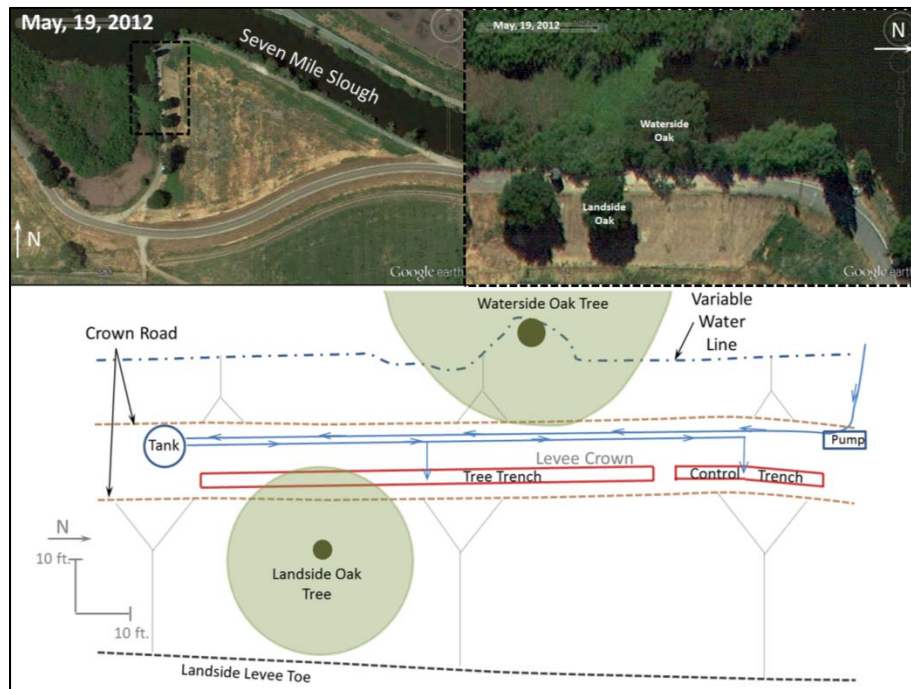


Figure 3-20. Layout of Twitchell Island Crown Trench Seepage Test. Aerial photos (top) taken on May 19, 2012, capture the flow test setup.

Figure 3-21. Pump and tank system (A and B). Image C shows valves used to control rate of flow into the trenches.

The water supply pump was a model DV-100c diesel unit with a minimum pump rate at idle of approximately 500 gallons per minute. The pump was activated by an automatic switch installed in the water tank that indicated when the water reached a maximum level. The reservoir was equipped with an overflow pipe with an outlet to the slough in the event of switch malfunction. Flow meters were installed on the water tank inflow pipe as well as th delivery lines into the trenches (Figure 3-22).



Figure 3-22. Typical flow meter (left) as installed on pipes flowing into and out of the 4900 gallon reservoir. Water delivery pipes and hoses are pictured to the right.

The trenches were filled with clean crushed gravel for stability during the experiment. A manifold of perforated pipes was installed to encourage rapid delivery of water throughout the trench and vertical risers were used to monitor water levels (Figure 3-23). Delivery of

water into the trenches was via a 4-inch diameter fire hose. The hose was equipped with 2-inch diameter removable adapter hoses connecting to mechanical float valves to maintain a constant head in each trench once flow volumes were sufficiently reduced (Figure 3-23D and E).

An instrumentation layout was designed to monitor positive and negative pore pressures in the vicinity of the landside and waterside oak trees and the control section. Sections A, B, and C represent the landside oak tree, the waterside oak tree and the control zones, the primary areas of study for this test. In the interest of evaluating the effect of distance from the tree center on seepage through a root system, supplemental instruments were placed at Lines D and E. Line D is placed at approximately two-thirds of the canopy radius to the north of the landside oak trunk. Similarly, Line E is placed at an approximate distance of ½ of the canopy radius to the south of the waterside oak tree as shown on Figure 3-24.



Figure 3-23. Gravel filled A) Control trench and B) Tree trench. The water delivery manifold (photo C), the constant head mechanical float (photo D), and the delivery hoses (photo E) are shown.
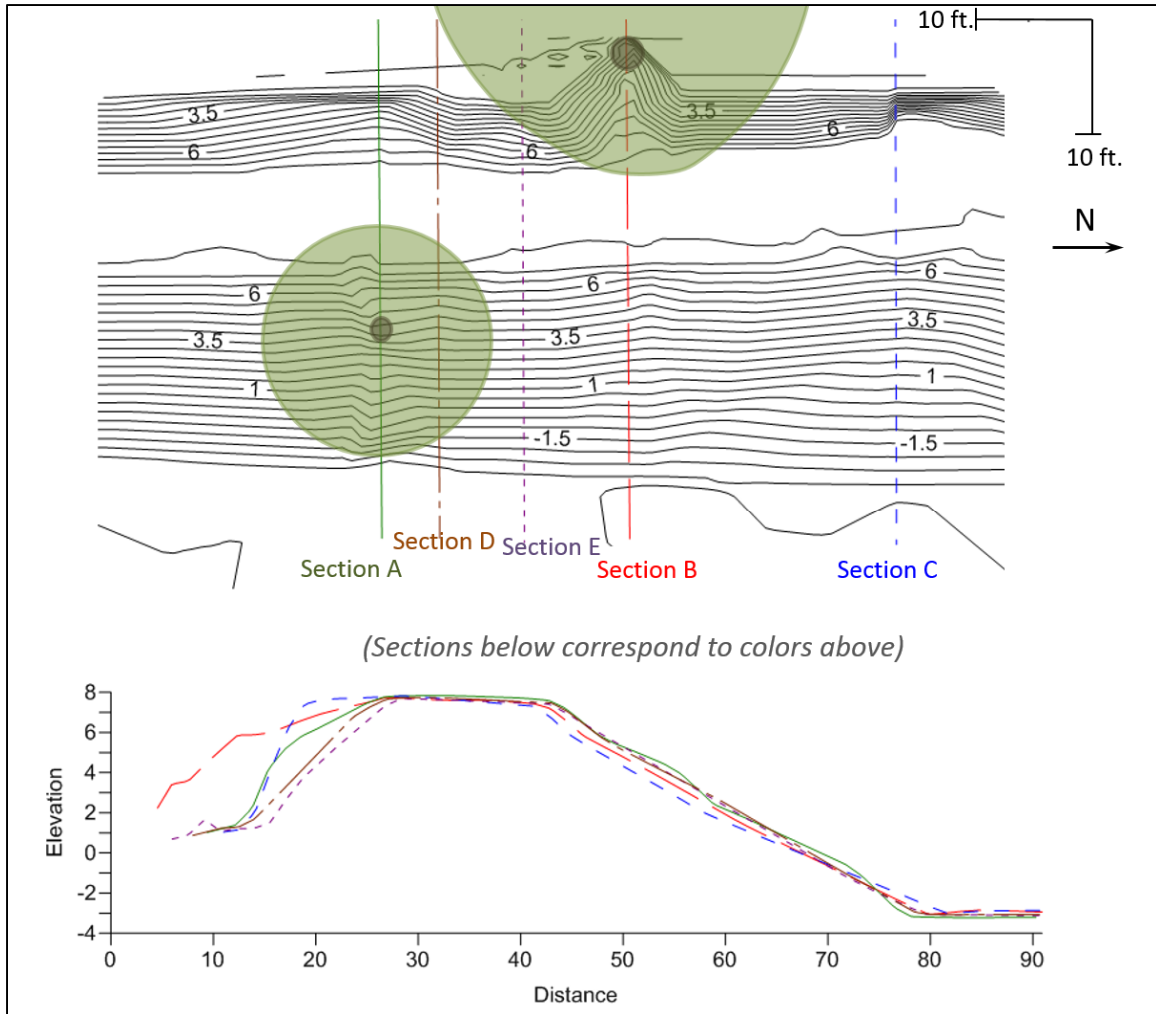
Figure 3-24. Location and topography of instrument lines showing supplemental lines D and E at a distance from the tree center of approximately half to two-thirds of the canopy radius.

Instrumentation was placed in rows with similar configuration at each primary line for ease of comparison. Instruments consisted of vibrating wire piezometers and tensiometers with electronic transducers. Piezometer Rows 1, 2, and 3 were placed earlier than other instruments as these borings provided early stratigraphic soil data needed to make modifications to the final instrument plan. Remaining piezometers – in Rows 4 through 6 – and all tensiometers were installed after construction of both trenches to minimize damage to the instruments. Figure 3-25 and Figure 3-26 show the position of instruments as well as the naming convention which calls out the row and line number for each and the depth for tensiometers. Piezometer depths are provided in Table 3-1.

The intent of Lines A and D was to understand the effects of the landside oak tree on levee seepage and stability, therefore waterside instrumentation was limited at these lines. Lines A and C had matching instrument layouts on the land side. Lines B and C had matching instrument layouts on the waterside and Line E was established to supplement data for the zone around the waterside tree. A nearly complete landside instrument line was placed at Line B as redundancy to the control Line C. All instruments were wired into continuously

reading recorders, as shown on Figure 3-27 and discussed further in a subsequent section of this report.
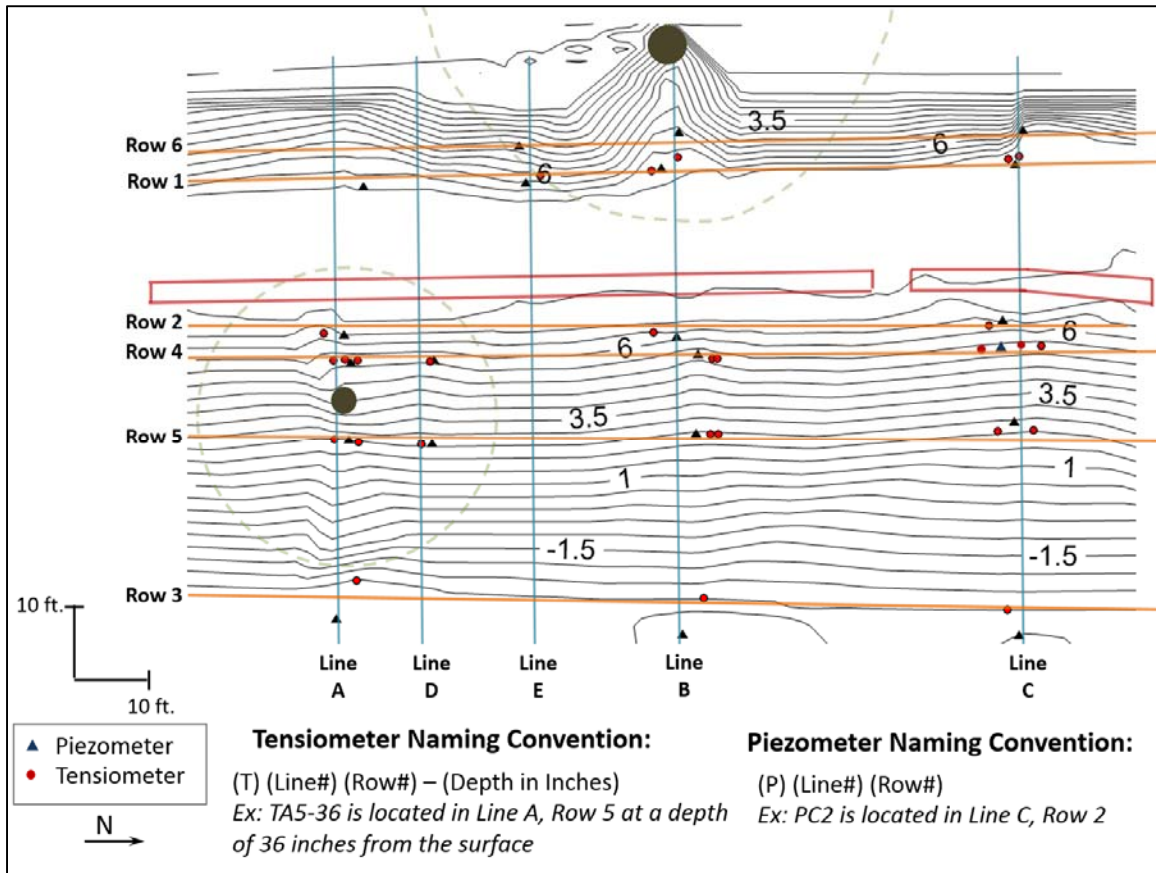


Figure 3-25. Instrument layout and naming convention.
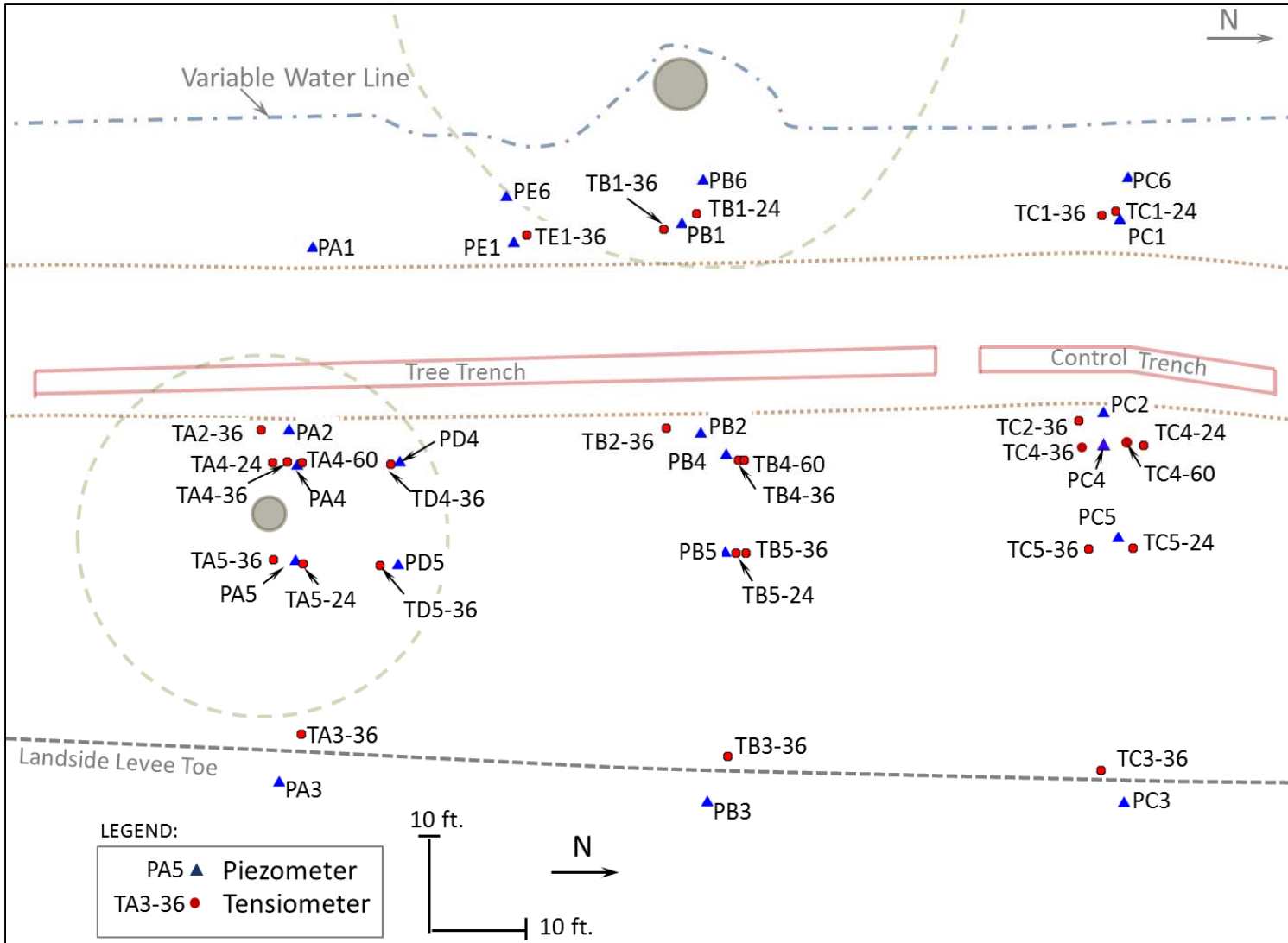
Figure 3-26. Instrument location plan.

Figure 3-27. Instruments (photos A through C), once installed, are wired into readout boxes (D) for continuous readings during the flow test.

Table 3-1. Piezometer model numbers and depths.

| Instrument Number | Instrument Model | Depth (ft) | Instrument Number | Instrument Model | Depth (ft) |
|---|---|---|---|---|---|
| PA1 | Geokon 4500AL (70 kPa) | 5.9 | PD4a | Geokon 4500AL (70 kPa) | 2.4 |
| PB1 | Geokon 4500AL (70 kPa) | 6.5 | PD4b | Geokon 4500AL (70 kPa) | 5.7 |
| PC1 | Geokon 4500AL (70 kPa) | 6.2 | PB4 | Geokon 4500AL (70 kPa) | 5.7 |
| PE1 | Geokon 4500AL (70 kPa) | 6.5 | PC4a | Geokon 4500AL (70 kPa) | 2.4 |
| PA2 | Geokon 4500AL (70 kPa) | 15.0 | PC4b | Geokon 4500AL (70 kPa) | 5.7 |
| PB2 | Geokon 4500AL (70 kPa) | 15.9 | PA5 | Geokon 4500AL (70 kPa) | 3.0 |
| PC2 | Geokon 4500AL (70 kPa) | 12.4 | PD5 | Geokon 4500AL (70 kPa) | 3.0 |
| PA3 | Geokon 4500AL (70 kPa) | 7.9 | PB5 | Geokon 4500AL (70 kPa) | 3.0 |
| PB3 | Slope Indicator (150 kPa) | 13.5 | PC5 | Geokon 4500AL (70 kPa) | 3.0 |
| PC3 | Geokon 4500AL (70 kPa) | 8.5 | PB6 | Geokon 4500AL (70 kPa) | 3.4 |
| PA4a | Geokon 4500AL (70 kPa) | 2.4 | PC6 | Geokon 4500AL (70 kPa) | 3.4 |
| PA4b | Geokon 4500AL (70 kPa) | 5.7 | PE6 | Slope Indicator (150 kPa) | 3.4 |

### 3.1.2 Subsurface Stratigraphy and Groundwater Conditions

Soil conditions are a critical part of the implementation of the test and interpretation of results. The site soils were characterized using the Unified Soil Classification System (USCS). Our exploration of the site included drilling nine soil borings with a conventional auger drilling rig (equipped with 8 inch diameter hollow stem augers) advancing 3 cone penetration tests (CPT) with frequent pore pressure dissipation readings, and hand auger borings at each instrument location. Test borings and instrument hole logs are summarized in Appendix 3A with associated laboratory testing presented in Appendix 3B. CPT logs and pore water pressure dissipation tests are presented as Appendix 3C. We reviewed available regional and local soil information in the Reclamation District 1601 Twitchell Island Five Year Plan (KSN, 2010) and the Sevenmile Slough Sites 1, 2, & 3 Levee Improvements report prepared by Neil O. Anderson and Associates (NOA, 2007). In Appendix 3D, we included relevant plans, logs and excerpts of these reports. During construction, trench walls were logged and are summarized in Section 3.1.3.2 and Appendix 3E.

Levee soils generally consisted of clayey and sandy silts and silty sands. In many locations, the silts were found to be thinly bedded with randomly oriented and variable bedding angles. These silts appeared to have retained much of the structure of a native deposit of fluvial soils, however the heterogeneity of the deposit and variable bedding angles would imply a method of construction that did not involve the proper blending and compaction, such as placement by a clamshell dredge. As such, voids were apparent in a number of locations, likely associated with construction techniques no longer meeting modern standards. Detailed photographs of soils and conditions encountered during trenching are provided in a subsequent discussion of trench construction in Section 3.1.3.2. Deposits on the waterside slope were found to be loose. A piece of old farming equipment was seen protruding from the waterside slope at Station 70 as if the material was either dumped there or arrived in a flood (Figure 3-28). The waterside oak tree was rooted within these loosely dumped deposits and had developed a lean of about 43 degrees prior to commencement of our work onsite.

At deeper elevations, about 4 to 6 feet within the levee, a layer of stiff to very stiff clayey plastic silt was encountered, which was relatively homogeneous and consistently present throughout most of the site. This deposit was named Material 4 during trench logging and it may be the Columbia clay silty clay deposit mapped by the USDA (1935) and shown on Figure 3-10. This soil is encountered in foundation soils and forms the shape of a small levee within the existing levee, as shown on the detailed stratigraphic sections at A, B, and C, provided as Figure 3-29, Figure 3-30, and Figure 3-31, respectively. According to the Twitchell Island 5-year plan:

> *"The peat accumulations eventually formed peat islands, with river channels and sloughs established around them and within some of the larger islands. During floods, rivers would overtop the banks of the peat islands, and as the water receded, would leave deposits of sand and silt that formed natural levees along the edges of the islands. Many of the levees currently in the Delta are founded on these natural levees, including most of the levees on Twitchell Island". (KSN, 2010)*

Based on field observations of Material 4, the material is certainly older than overlying fills and may indeed be a natural deposit. This irregular layer is consistently present throughout

the trench up to Station 37 at which point the layer dips below the bottom of the trench. The layer reappears at Station 42 and angles sharply up (shown on trench logs presented in Section 3.1.3.2). The discontinuity in the Material 4 layer was filled with a loose mix of alluvial soils suggesting the discontinuity may be related to past excavation activity (e.g. - pipeline installation) or it may be the result of past scour during a flood or a small break in the old levee.

Foundation soils encountered generally consisted of silts of low and high plasticity with some zones of lean clay overlying sands at depths of 20 to 30 feet below the crown of the levee. Sands ranged from relatively clean and poorly sorted (USCS classification SP) to silty sands (USCS classification SM).

The water table was encountered during exploration at a depth of approximately 24 feet below the crown of the levee at an approximate elevation of -16 feet. Pore water pressure dissipation tests performed during cone penetration testing provided an initial estimate of the groundwater table onsite (Appendix 3C). The water table was encountered during installation of piezometer PB3 and was consistent with the pore water pressure dissipation data. The elevation of water in the slough was found at an approximate elevation of 1 ft during testing (Figure 3-29 through Figure 3-31). It was determined that the low permeability plastic silt (Material 4) or the sediment within the base of the slough may be consistently present and functioning as a limiting layer allowing for a perched water condition above. This condition was considered beneficial for the purpose of achieving saturation within the root zone of the landside oak tree.

Surface soils extending into the water are loose silts, not strong enough to support the weight of a human without sinking. The depth of the oxbow section adjacent to the sites is generally on the order of 2 to 3 feet away from shore, shallowing to about 6 inches near shore for the typical water levels encountered during the flow test. The depth to the base of the slough is about 25 feet at the center of flow, about 9 feet at the entrance to the oxbow section, and shallowing quickly with distance into the oxbow. As shown on Figure 3-9, prior to installation of the flow control gates within the slough, the oxbow section was still part of the primary flow channel. The section is shown as wetland by the time the flow control gate is installed (shown in 1952 topographic map), implying that the shallow sediment currently present had arrived either via filling or via a flood in that timeframe.

Figure 3-28. The wheel of what appears to be horse-drawn farming equipment protruding from the waterside of the levee (Sta TT 70). The axle and possibly the other wheel extend into the levee slope.
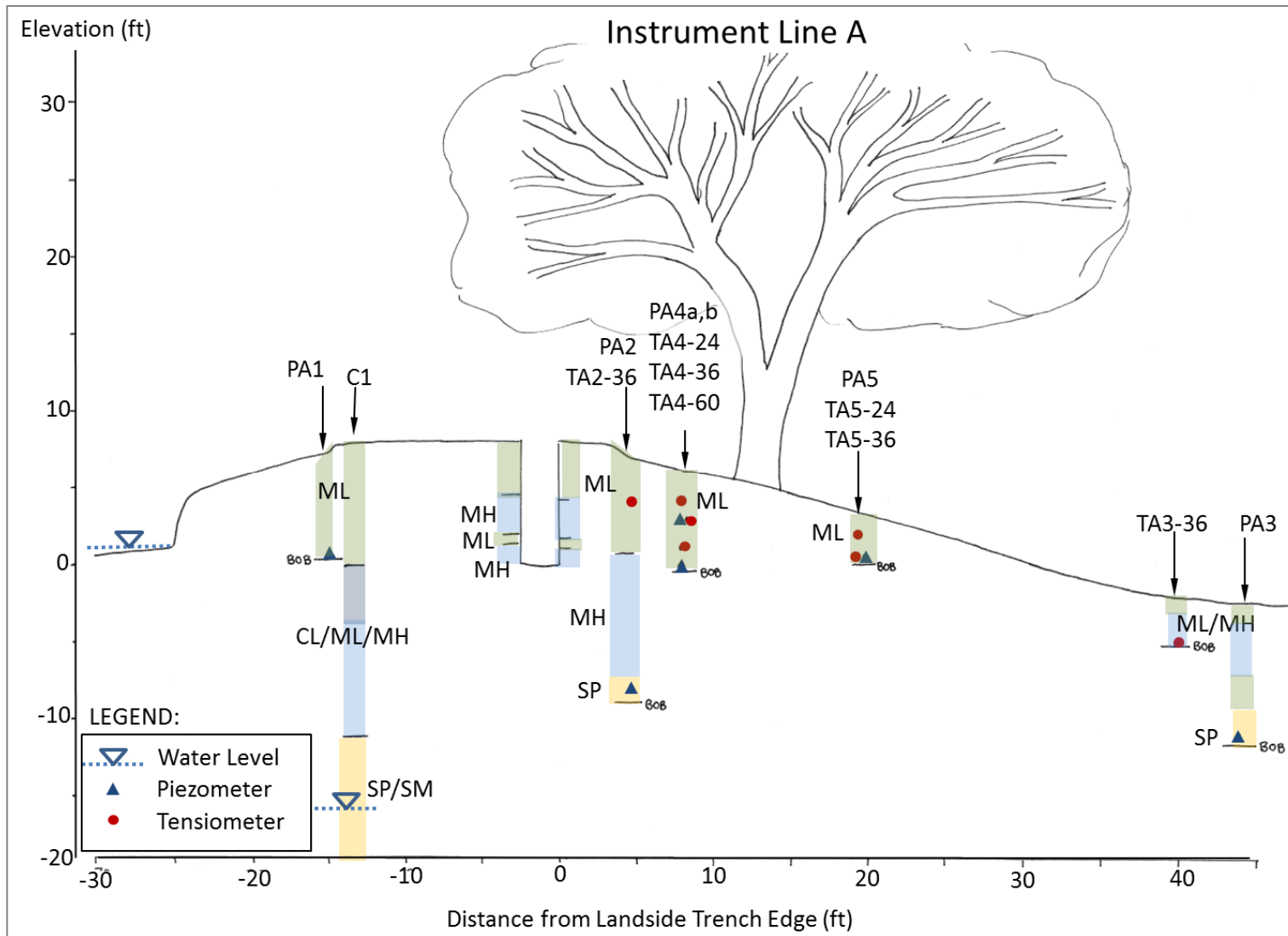
Figure 3-29. Levee section view of Instrument Line A (landside oak) showing instrument locations and generalized soil stratigraphy.
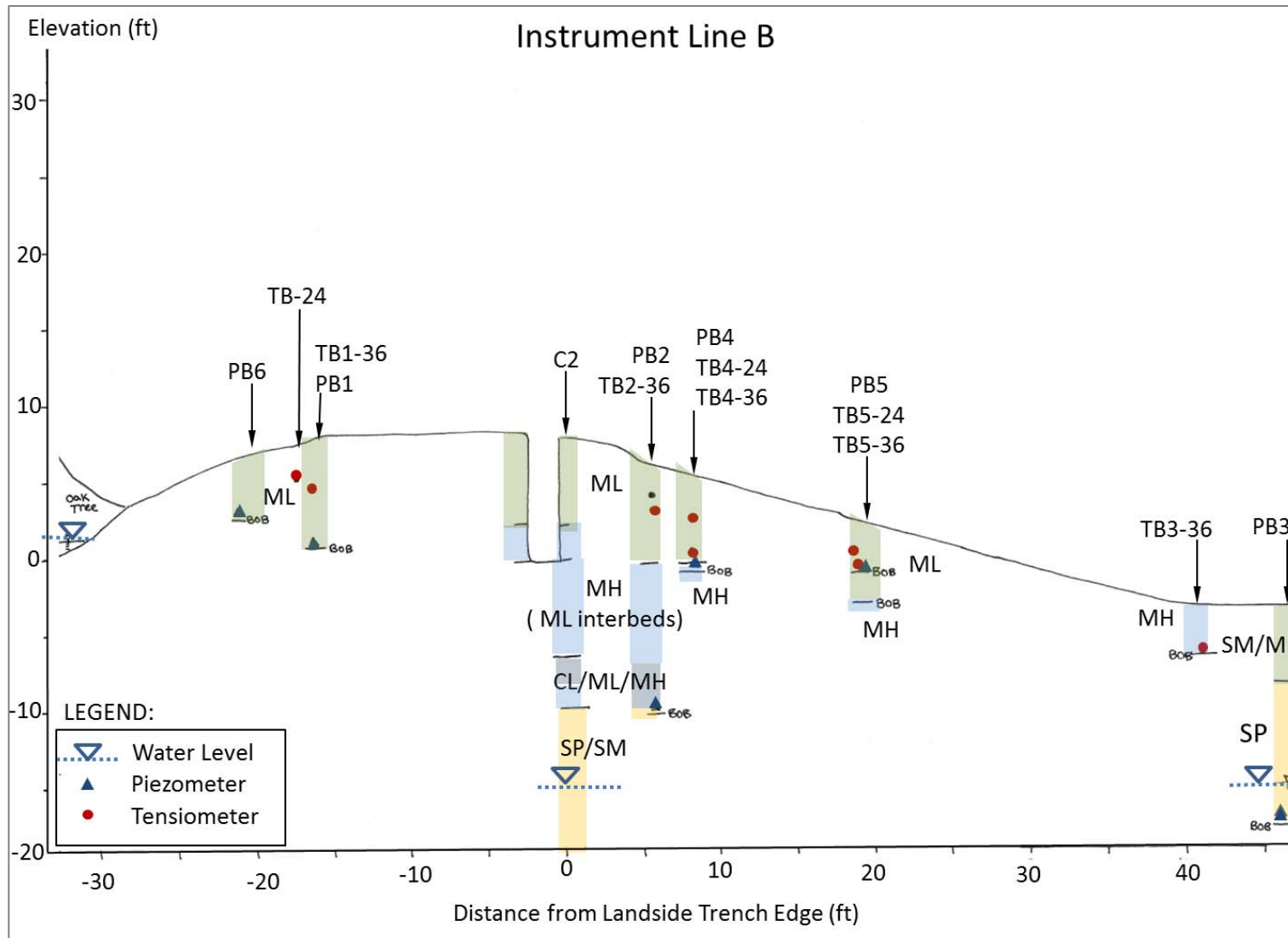
Figure 3-30. Levee section view of Instrument Line B (waterside oak) showing instrument locations and generalized soil stratigraphy.
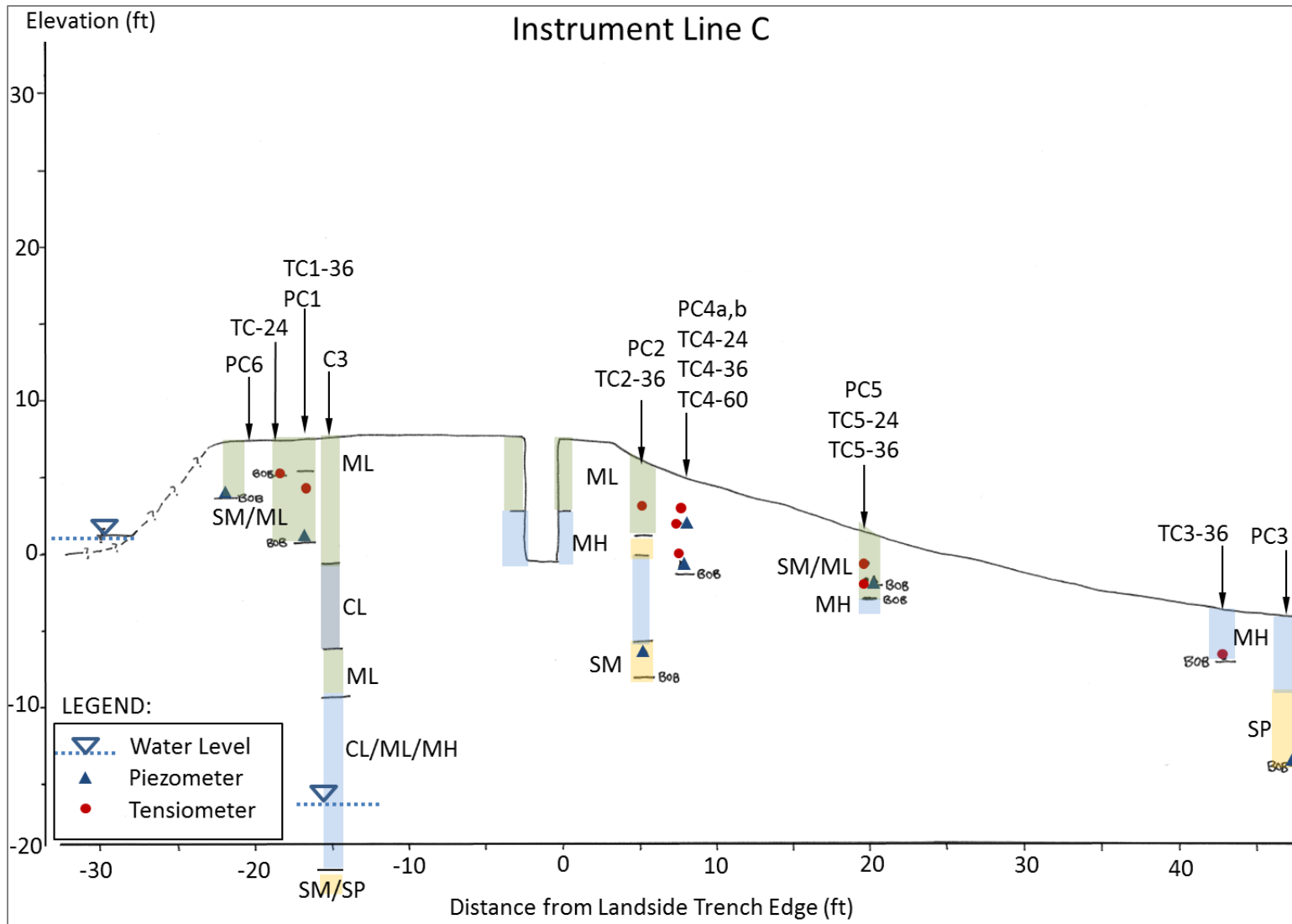
Figure 3-31. Levee section view of Instrument Line C (control) showing instrument locations and generalized soil stratigraphy.

### 3.1.3 Experiment Construction

Construction for the proposed flow test began with excavation and logging of the trenches, followed by backfill of each trench with clean crushed rock for stability during the flow test. The water delivery system was then assembled and tested for functionality and the instruments were installed. Observations were made throughout construction and during instrument installation consisting primarily of the logging of test borings and the generation of the cross sections detailing the stratigraphic conditions discussed in the previous section. These observations made during trenching provide a unique and broad picture of the heterogeneity of levee soils that cannot be made from soil borings or cone penetration testing.

#### 3.1.3.1 Method of Trench Construction

Determining an appropriate method of trench construction was a challenge and critical to the successful execution of the experiment. The objective was to avoid disturbing roots and facilitate accurate mapping to better understand the nature of the root systems under study. Disturbances to the root system during excavation with heavy equipment could create void space between the root and surrounding soil. This type of disturbance could affect the natural relationship between the soil and the root, potentially affecting flow patterns and flow test results.

At our first flow test site near Cal Expo on the American River in Sacramento, where live and decomposing roots were encountered, an air knife operating with a compressor capable of compressing 375 cubic feet of air per minute (CFM) was used to excavate around live roots. In this manner, live roots were revealed, logged, and then cut prior to the flow test. It was elected that this method would used at this site where possible and safe, given the trench depth of 8 feet.

Prior to trench construction, the trenches were stationed with Control Trench stationing (CT) or Tree Trench stationing (TT). The control trench was stationed from CT 0 to CT 31.5. The five-foot separation zone between the tree and control trenches was stationed as CT 31.5 to CT 36.5 where CT 36.5 is equal to TT 0 at the northern end of the tree trench as shown on Figure 3-32.
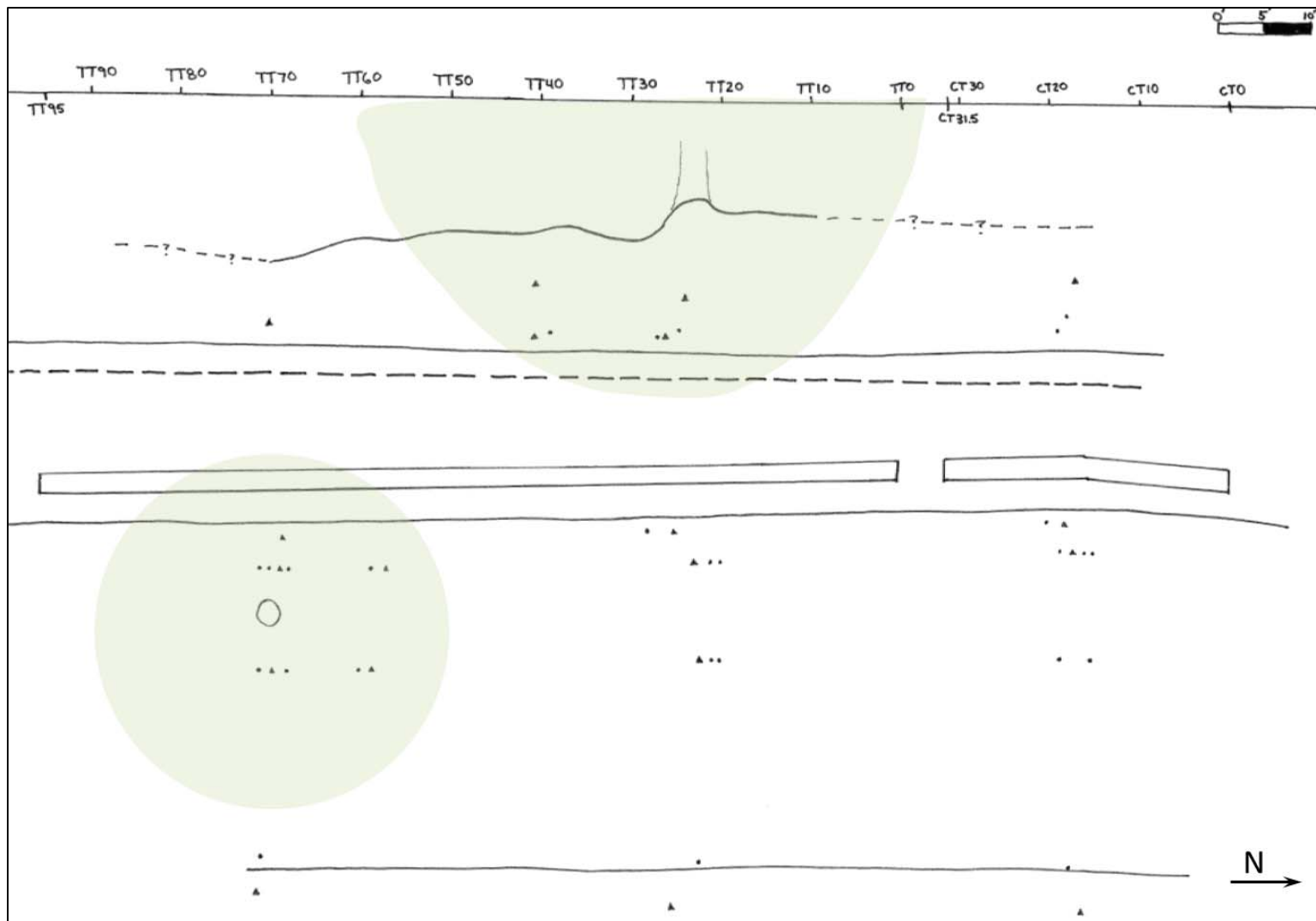
Figure 3-32. Field site plan showing stationing associated with control trench logging (CT) and tree trench logging (TT). Approximate instrument locations are shown as triangles (piezometers) and circles (tensiometers) for reference.

### 3.1.3.1.1 Control Trench

The control trench was completed prior to the tree trench to test and develop a suitable excavation technique prior to entering into a zone with abundant roots. Excavation began by excavating a segment from the northernmost end of the control trench (Station CT 0 to 5) with an excavator. This step was required as a pit was needed to blow the spoils of the air knife. Once the segment was excavated and no significant roots were found, slow excavation to a depth of 4 feet proceeded throughout the trench (Figure 3-33). The land side and water side walls of the upper 4 feet of the control trench were carefully cleaned and logged (logs provided in Appendix 3E).



Figure 3-33. A) The control trench excavated to 4 foot depth; B) Walls are logged; C) Walls are sampled ahead between 4 and 8 feet; D) Excavation of small segments proceeds to 8 feet.

The walls were then shored, cleaned, and logged to a depth of 8 feet in the first segment. Additional control trench segments of 5 feet long were excavated to 8 feet in depth using the excavator and encountering only small isolated roots near the base of the excavation (Figure 3-34A,C, and D). Each 5 foot segment was mapped first in plan view for roots (when applicable), and then the walls were mapped for soil conditions.

The last 5-foot increment of the control trench (station CT 25 to 31) encountered a cluster of large roots requiring manual excavation (Figure 3-34B). Upon close inspection, some of the roots had been broken in excavation and the area was carefully evaluated for damage to the walls from the root breakage. The location where the root entered the trench was revealed and found to be undamaged. The remainder of the segment was shored and hand excavated to reveal the root cluster (Figure 3-34B).



Figure 3-34. A) The control trench is shored for logging; B) Station 26 to 31.5 is shored for manual excavation and logging of first large roots; C) and D) Smaller roots are logged and trimmed from above prior to proceeding with excavation.

Once completed, the entire trench was backfilled to a depth of 4 feet with ¾ inch clean crushed rock. The manifold of perforated pipes was installed at a depth of 4 feet to facilitate even water delivery throughout the trench (Figure 3-35). No compaction efforts were made other than light tamping and smoothing with the excavator bucket. From start to finish, the control trench was excavated and backfilled between April 12 and April 17 of 2012.

Figure 3-35. The control trench is partially filled with gravel, a manifold installed, and backfill with gravel is completed.

### 3.1.3.1.2    Tree Trench

An air knife was selected as the most appropriate tool for the excavation of the tree trench and was incorporated where possible, preserving the root systems of the waterside and landside oak trees for logging and avoiding disturbance to trench walls. A procedure for excavation was developed that evolved based on conditions encountered.

Beginning at north end of tree trench, an 'initial pit' was cut with an excavator prior to use of the air knife such that spoils could be aimed into the pit and then removed by excavator, revealing intact roots in adjacent segments. The 'initial pit' encountered some significant roots near the base and these roots were revealed through manual excavation. A root was broken during this excavation (Figure 3-36), the walls were carefully inspected for evidence of disturbance or void spaces, and none were not found (Figure 3-36C and D). The segment was completed to a depth of 8 feet, shored and logged prior to the placement of spoils.

Figure 3-36. A) Root encountered during excavation of initial spoils pit at Station TT 0 to TT5; B) Trench is shored; C) and D) Roots damaged by excavation are carefully inspected at walls and found to be intact at connection to the wall.

Roots from the 'initial pit' were trimmed flush with the walls and spoils generated by air knife from the upper 4 feet of the adjacent 20 foot segment were directed into the pit (Figure 3-37). Spoils were periodically removed by excavator to make room for new spoils (Figure 3-38). The 4 foot deep segment was logged in plan view for roots. The roots were then cut flush and the walls cleaned to log soils on the landside and waterside walls.

The 20 foot segment (excavated to 4 feet deep) was deepened to 8 feet in 5 foot increments to minimize the length of open trench. Each segment was logged in plan view for roots, then shored, roots cut, and walls cleaned and logged for soil conditions and other observations (e.g. - burrowing activity). Once logged, each segment became the spoils pit for the next segment under excavation. It was possible for the air knife operator to stand on the ledge of the 4 foot trench and excavate to a depth of 8 feet by blowing the soils into the spoils pit as he backs up, removing the ground where he was previously standing (Figure 3-38A). Excavation permits required that no trench or segment deeper than 4 feet remain open overnight. Each evening all trench segments were temporarily backfilled with loose spoils for safety and preserve moisture in the trench walls.

Excavation proceeded in a similar manner for the entire 100 foot trench. The tree trench excavation was completed over a three week period between April 17th and May 7th of 2012.

Figure 3-37. Initial spoils pit (left) and air knife operation revealing the upper 4 feet within Stations TT 5 to TT 15.

Rock backfill and manifold installation proceeded on May 8, 2012, beginning with excavation of temporary spoils placed within the trench, then placement of 4 feet of rock throughout the trench. A single perforated pipe was installed to the full trench depth (at the southern end) to view water levels and provide a way to pump water from the trench if necessary. A perforated manifold delivery system similar to that used in the control trench was installed at a depth of 4 feet and the trench backfilled with ¾ inch clean crushed rock to the surface.

Figure 3-38. A) Air knife operator stands in 4 foot deep trench excavating to 8 feet; B) and C) New roots revealed as air knife spoils are blown in the previously logged segment; C) Spoils are used to stabilize previously excavated sections as new excavation proceeds.



Figure 3-39. A) Large root at Station TT 17; B) Logging; C) Burrow found during air knife excavation; D) Burrow patched prior to flow test.

### 3.1.3.2 Observations during Trench Excavation

Given that post-flow test excavation of the site was not planned, the excavation of the control and tree trenches provided an important window into the heterogeneity of site conditions. In addition to providing insight into the nature of the soils and the structure of the levee, this type of logging sheds light on the strengths and limitations of the common practice of geotechnical characterization of a heterogeneous system.

#### 3.1.3.2.1 Materials

Soils encountered during excavation were categorized into 7 material types to aid in logging (Figure 3-40). In general, all of the material types found within the levee were sandy and clayey silts. Materials 1 through 3 generally represented the shallower soils within the levee (Figure 3-41, Figure 3-42, Figure 3-43, and Figure 3-44), typically within the upper 4 feet but extending deeper in some areas.

Material 4, a plastic silt, is an important soil as it is believed to have acted as a low permeability barrier to flow during the flow test (Figure 3-44 and Figure 3-45). Further, the consistency, density and apparent age of the material imply that the soil may have been a natural overbank deposit, as already indicated.

Material 5 was a lighter colored and lower plasticity silt layer that was found typically as a thin sublayer (less that about 6 inches to 1 foot thick) within the Material 4 soils near the base of the tree trench (Figure 3-47 and Figure 3-48).

Material 6 represented changes in Material 3 as trenching extended to the south. Materials 6 and 3 frequently occurred together in heterogeneous pockets of light brown and olive colored sandy silts.

Finally, Material 7 represented a variable but at times loose, unstable or unpredictable blend of Materials 2, 3 and 4 (Figure 3-46). This material was encountered between at depth between Stations TT 37 to 42, but pockets were encountered between Stations TT 37 and TT 85 (for reference the landside oak was at Station TT 70 and the waterside oak was at Station 20).

Materials 2 and 7 are the most notable of the surficial silts as these deposits seem to have a potential for sloughing, void space, and heterogeneity, while materials 4 and 5 tend to be more stable and consistent soils.

SOIL TYPES:

(1) Clayey silt (ML), olive mottled with oxidation staining, moist, blocky structure with light cementation.

(2) Clayey silt (ML), light brown, moist, thinly bedded, easily cleaves along bedding of variable orientation, gaps and cracks observed, prone to sloughing and instability, bed thickness 1-5mm (typ.) .

(3) Sandy silt (ML) with pockets and lenses of silty sand (SM), light brown, moist.

(4) Clayey silt (MH), dark olive brown with oxidation staining, moist.

(5) Clayey silt (ML), reddish brown, moist

(6) Sandy silt (ML), olive brown with oxidation staining, occasional silty sand pocket.

(7) Sandy silt with clay (ML), pockets of olive with oxidation mixed with pockets of reddish brown with fine sand at cleavage planes in structure, material is highly unstable and consists of a mixture of soil types 2, 3, and 4.

Figure 3-40. Description of materials encountered during trenching. USCS classification and description of Materials 1 through 7 are provided.
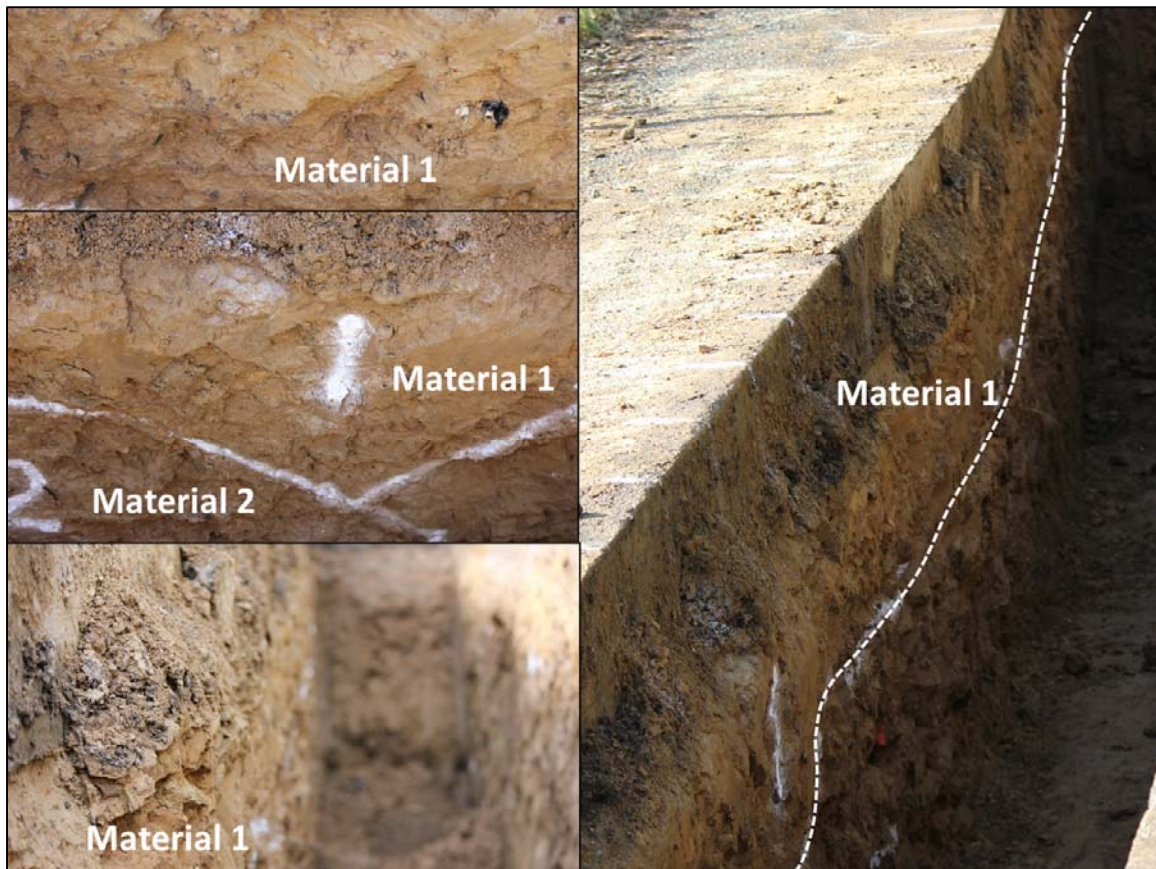


Figure 3-41. Photographs of Material 1, clayey silt found near the surface of the levee.

149
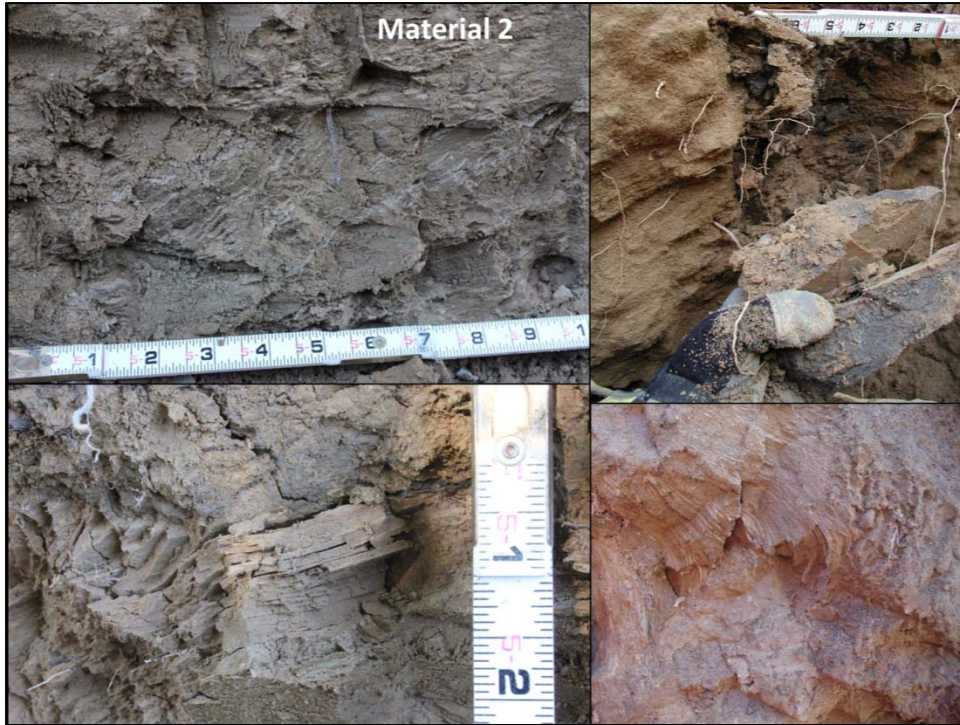
Figure 3-42. Photographs of Material 2, the thinly bedded silt. Notice variable bedding angles (upper left) and occasional voids within the material (lower photos).



Figure 3-43. Materials 1 and 2. Material 2 was prone to sloughing (right and lower left).
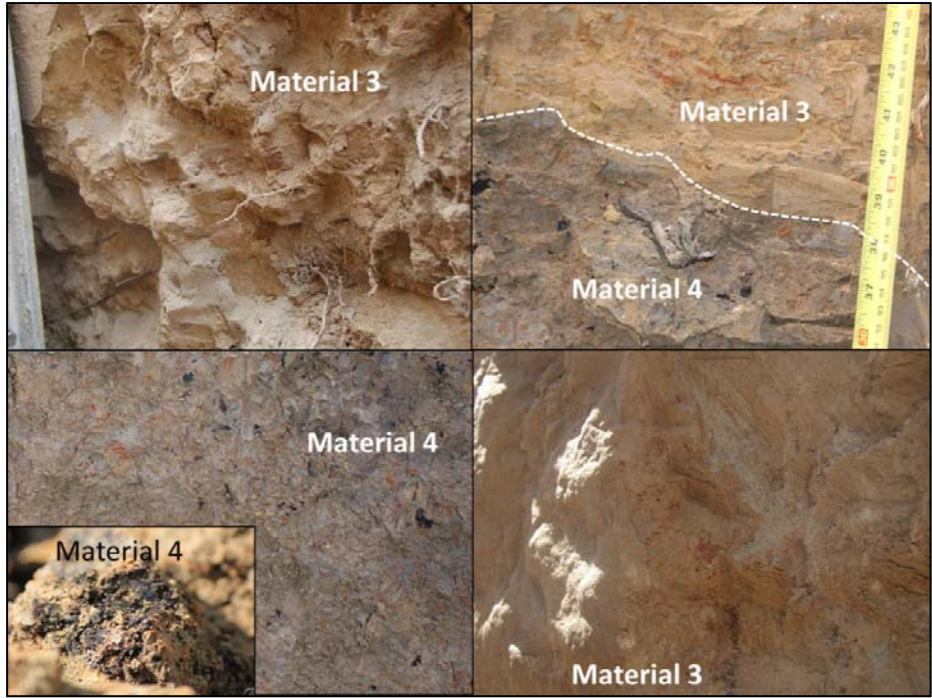
Figure 3-44. Material 3, a light brown sandy silt (USCS ML) with pockets of silty sand, is seen overlying Material 4, a plastic silt (USCS MH). Material 4 contains pockets of decomposed organic matter (lower left).



Figure 3-45. Pockets of Materials 3 and 6 (light brown and olive sandy silts, respectively) frequently occur together (left) and underlain by the plastic silt layer, Material 4.
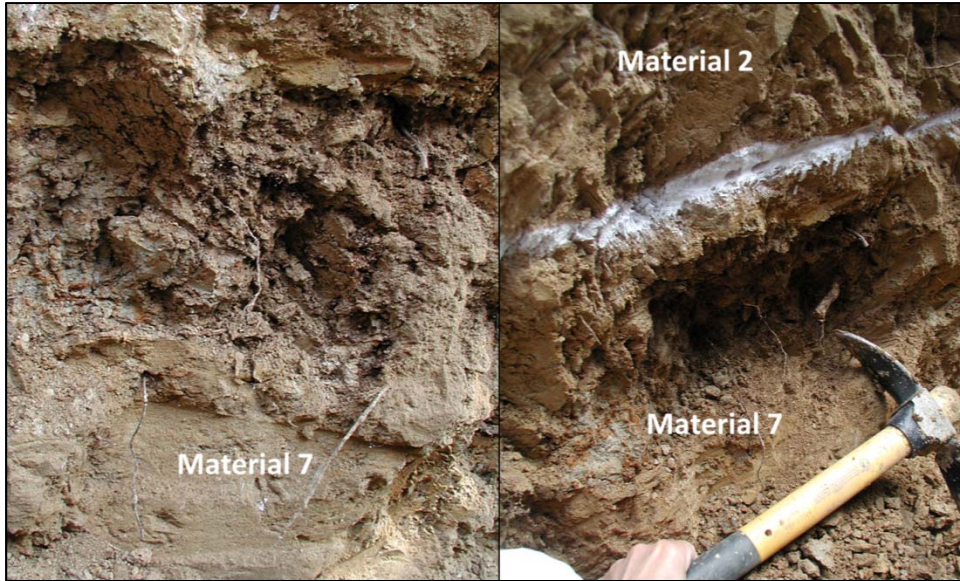
Figure 3-46. Material 7, encountered between Station TT 37 and TT 85, was highly unstable when encountered at depth and was comprised primarily of Materials 2, 3 and 4.
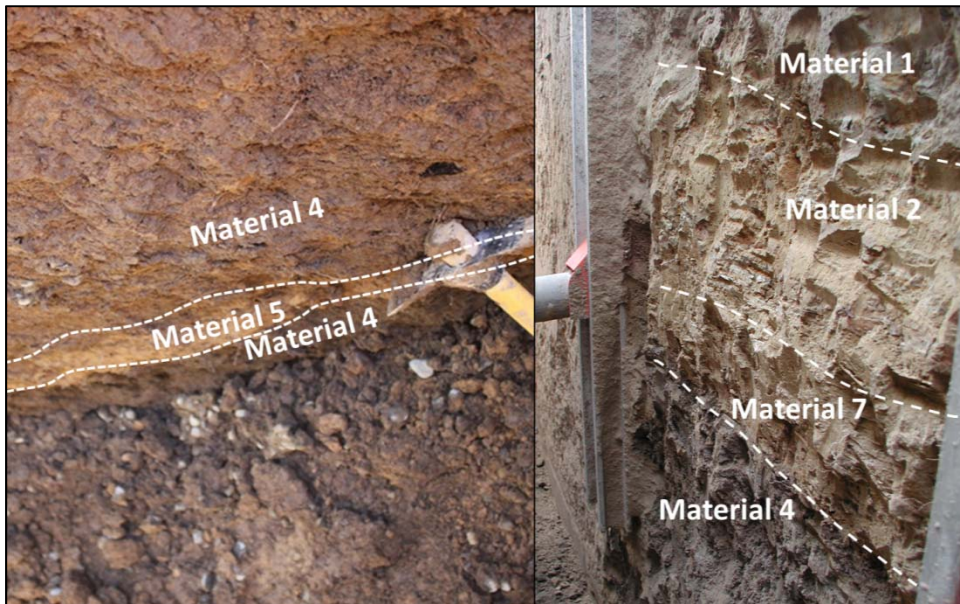


Figure 3-47. Near Station TT 70 to 75, Material 4 became slightly lighter in color (left). A thin lift of Material 5 (USCS ML) commonly occurs between zones of Material 4. Photo to the right shows typical layering with variable low plasticity silts (Materials 1, 2 and 7) overlying the plastic silt (Material 4) near the base of the 8 foot trench.
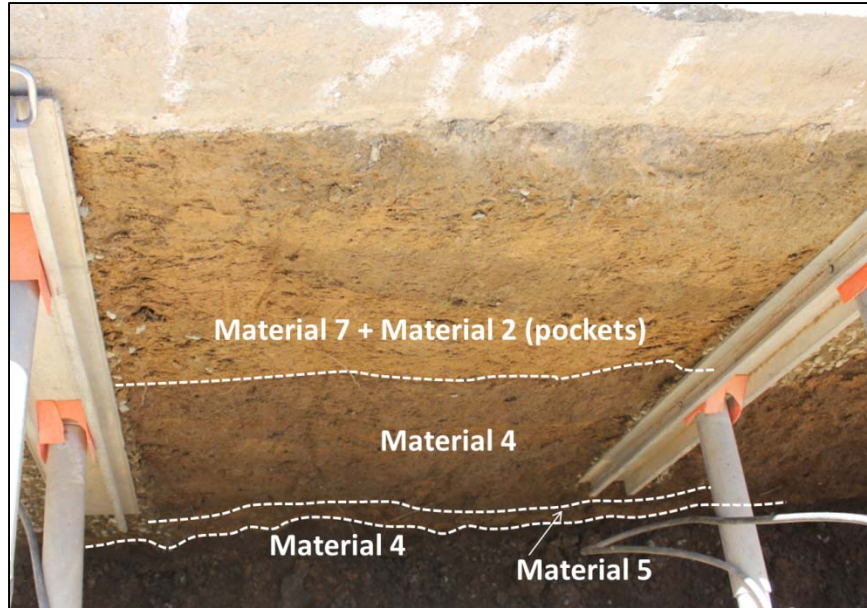
Figure 3-48. Typical layering with low plastic silts overlying plastic silt (Material 4) with a thin lense of Material 5 shown within the Material 4 layers.



Figure 3-49. Materials 1 and 3 (left) and Material 2 (right) exhibit manganese oxide staining on what appear to be fractures within the levee soils.

3.1.3.2.2   Control Trench

The control trench excavation began with excavation of the shallow zone between 0 and 4 feet below grade. Complete trench logs are provided in Appendix 3E. A 1 ½ inch diameter burrow was discovered between Stations 11 and 12 at a depth of about 2 ¼ to 2 ½ foot below grade (Figure 3-50). A single ½ inch diameter root was encountered. The size and depth were consistent with either gopher or vole activity based on discussions with burrowing animal advisor to the CLVRP Dr. Dirk Van Vuren of UC Davis. Surficial evidence of both animals was found in the vicinity as previously discussed.
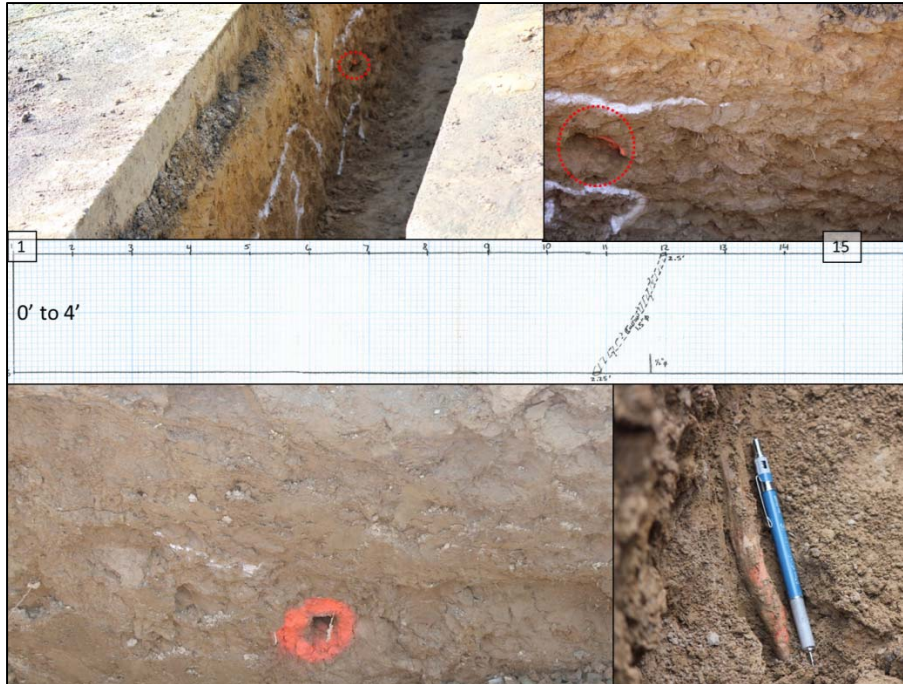
Figure 3-50. Notable features of control trench 0 to 4 foot depth: A burrow at Station CT 11 to CT 12 (diameter 1 ½ inch) and a single ½ inch diameter root at CT 12 (lower right).

Figure 3-51, Figure 3-52, and Figure 3-53 illustrate that Stations CT 0 to 27 of the control trench had very few roots or other anomalous features with the exception of one burrow. As discussed previously, the thinly bedded silt (Material 2) was found to be sloughing on the waterside Stations CT 0 to 5 (Figure 3-43).



Figure 3-51. A single ½ inch diameter oak root is found and cut when excavating to full depth of 8 feet within the control trench Stations CT 1 to 15.
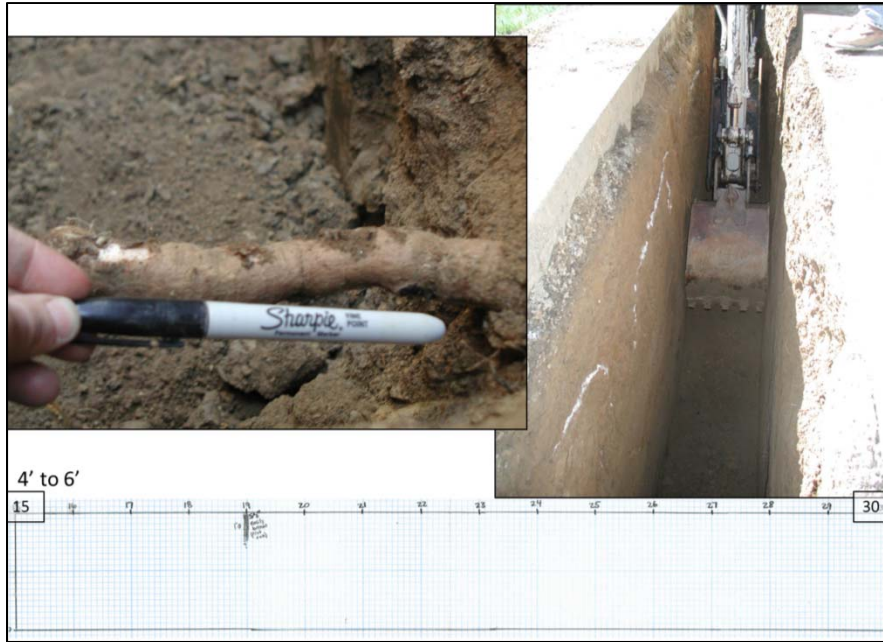
Figure 3-52. A 1" diameter root is encountered at Station CT Station 19. The inner core of the root is not woody and is assumed not to have originated from either oak tree.
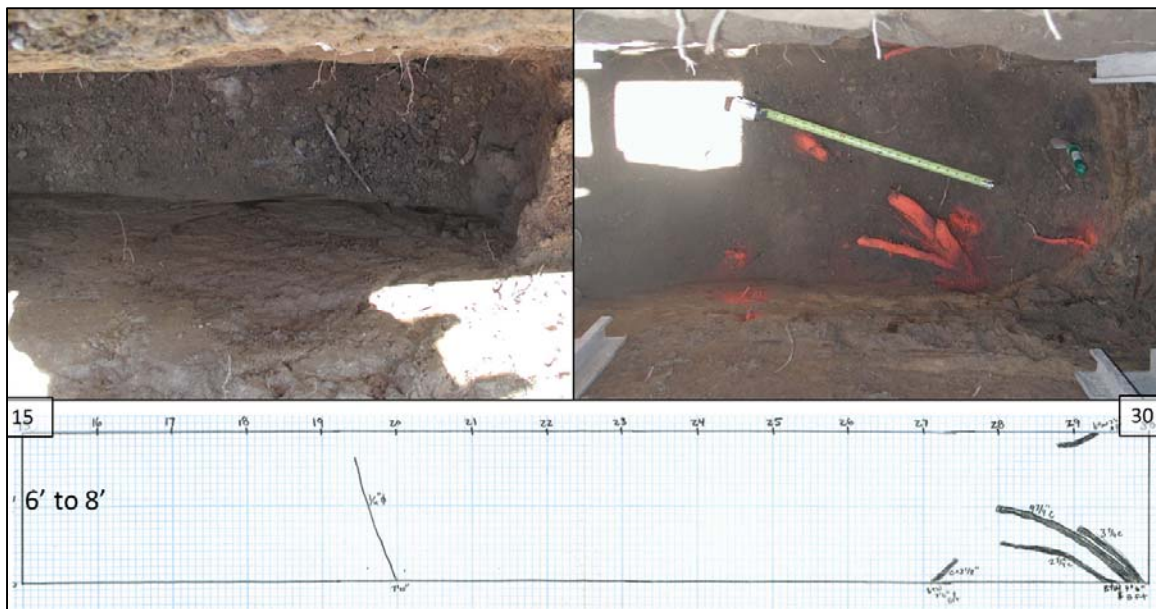


Figure 3-53. A cluster of roots ranging from about ¾ inch to 1 ½ inch diameter are encountered at Stations CT 27 to CT 30.

Trench logs for the land and water side walls of the control trench are provided on Figure 3-54. The figure is based on material types outlined in Section 3.1.3.2.1 titled Materials.
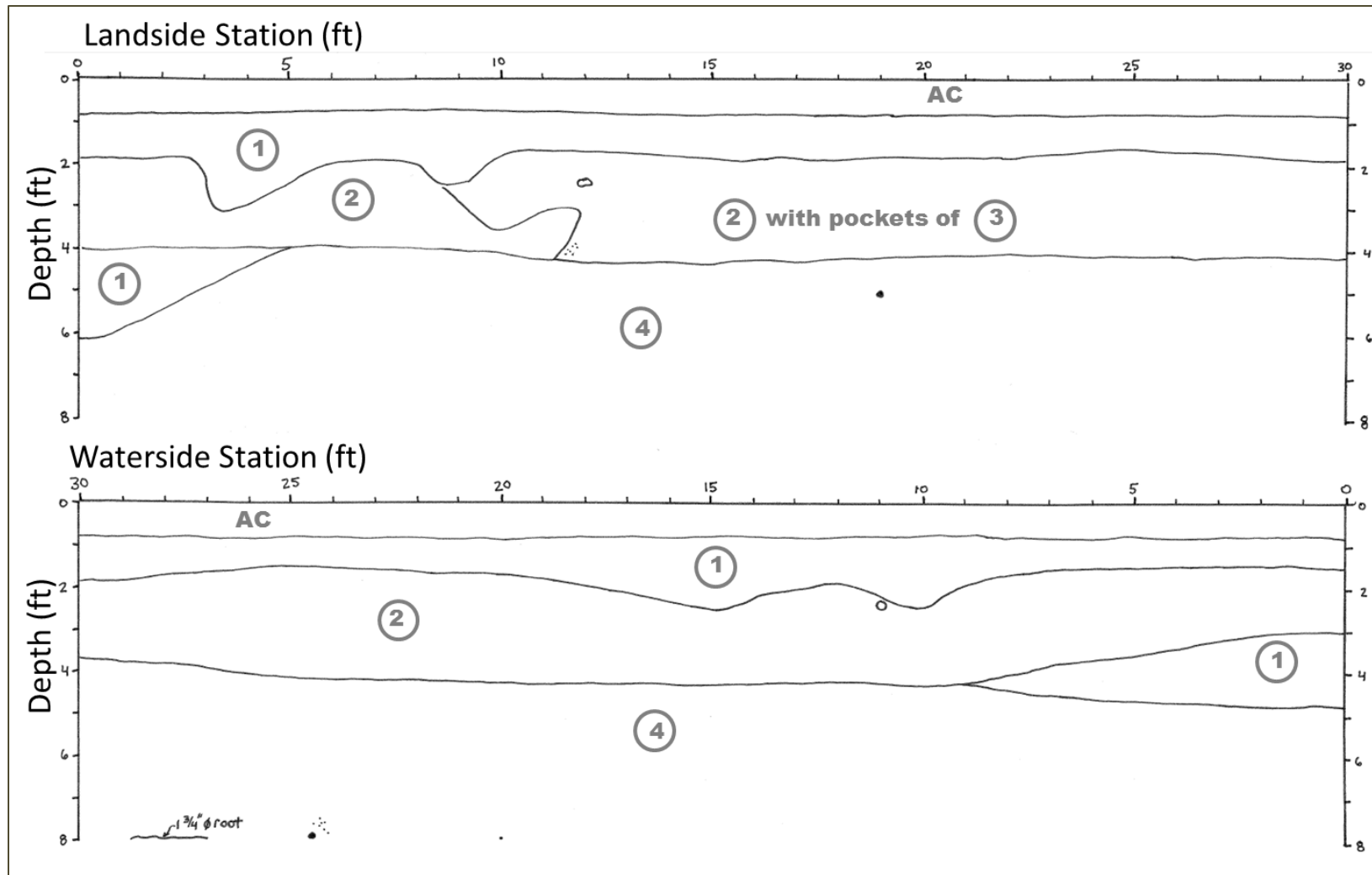
Figure 3-54. Landside and waterside trench log for Stations CT 0 to 30. Hollow circles are burrows, while solid dots represent roots.

### 3.1.3.2.3   Tree Trench: 0 to 4 Foot Depth

The maximum root diameter found within the upper 4 feet of the tree trench was 1 ¼ inch. In general, roots smaller than about ½ inch in diameter were not logged. Root and burrow locations are shown on plan view logs discussed below and provided as complete field logs in Appendix 3E. Plan view field sketches were logged in depth categories of 0 to 4 feet, 4 to 6 feet, and 6 to 8 feet. Stations TT 6 through TT 17 encountered abundant roots ranging from about ¼ inch to about 1 ¼ inch in diameter (Figure 3-55 and Figure 3-56). The directionality of the roots was not readily apparent, but roots in the 4 to 6 foot depth range in the same segment had branching indicative of a waterside origin and no other trees were nearby other than the waterside oak tree. Between Stations 33 and 49 (Figure 3-57 and Figure 3-58), two roots on the order of ½ inch diameter were logged. Again, the origin of the roots was unclear but deeper roots in the vicinity originated from the waterside. Stations TT 62 to TT 86 (the vicinity of the landside tree) encountered abundant roots smaller than 1 inch in diameter (Figure 3-60 and Figure 3-61). Branching of these roots indicated a landside origin.  Roots were not found at stations TT 0 to 6 (Figure 3-55), TT 19 to 33 (Figure 3-56 and Figure 3-57), TT 49 to 62 (Figure 3-58 and Figure 3-59), and TT 86 to 95 (Figure 3-61). No burrows were found in the upper 4 feet of the tree trench during logging.

Roots encountered were cut after logging. Some live roots wept upon cutting. No void space for flow around the root was observed, but the weeping occurred from the inside of the root (Figure 3-62). When reviewing logs below landside is always facing up and station numbers increase to the right (or to the south).
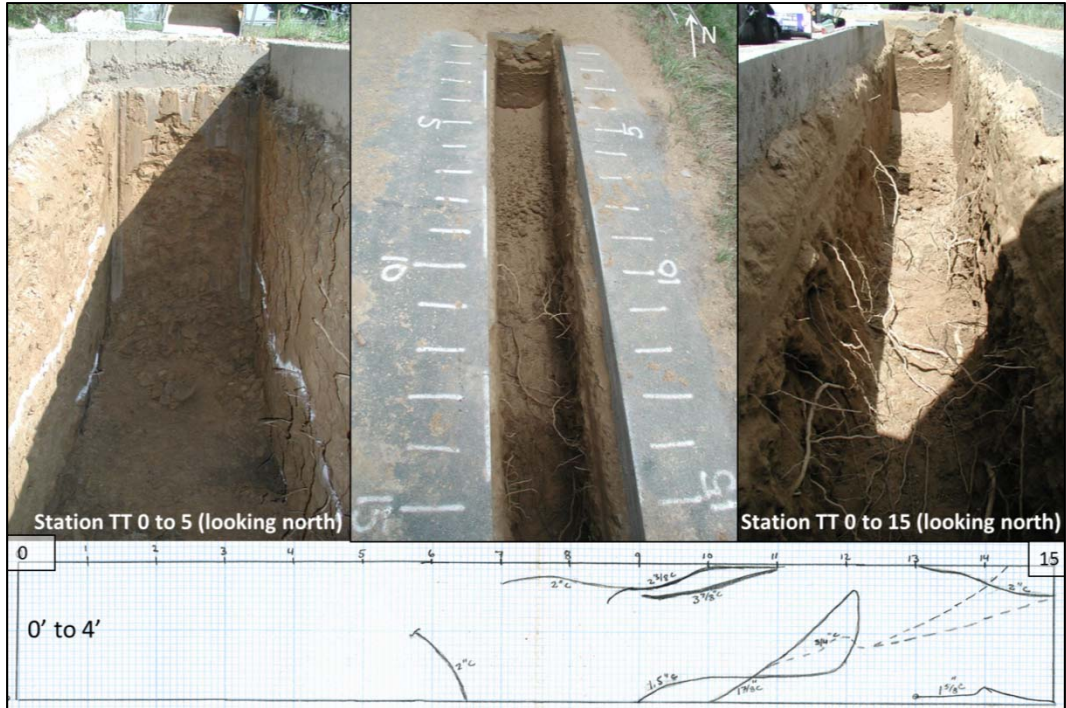
Figure 3-55. Root log at 0 to 4 foot depth Station TT 0 to 15.



Figure 3-56. Root log at 0 to 4 foot depth Station TT 15 to 30.
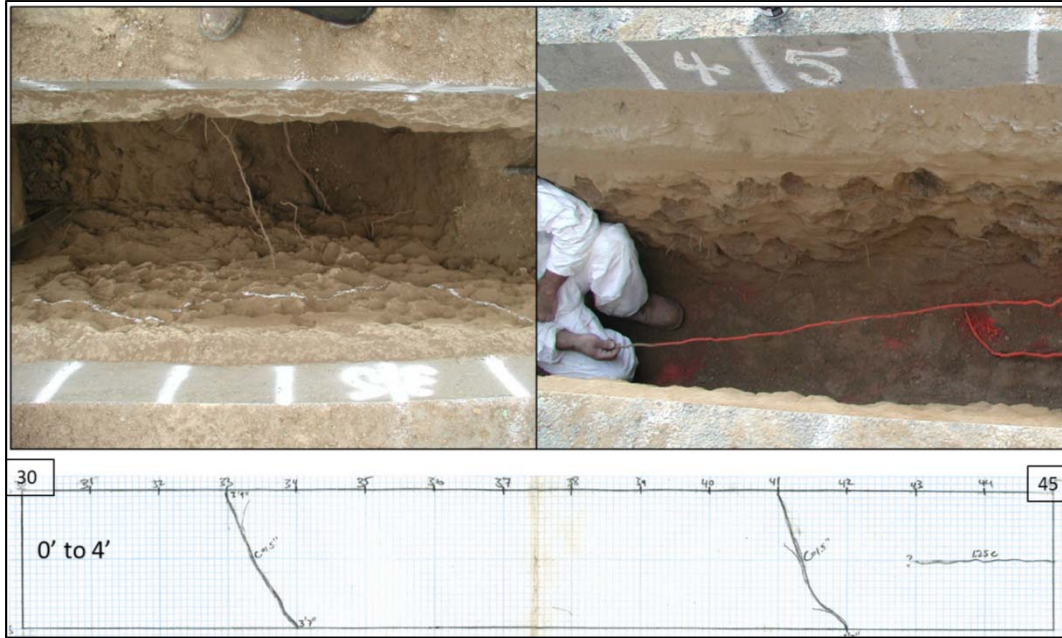
Figure 3-57. Root log at 0 to 4 foot depth Station TT 30 to 45.



Figure 3-58. Root log at 0 to 4 foot depth Station TT 45 to 60.
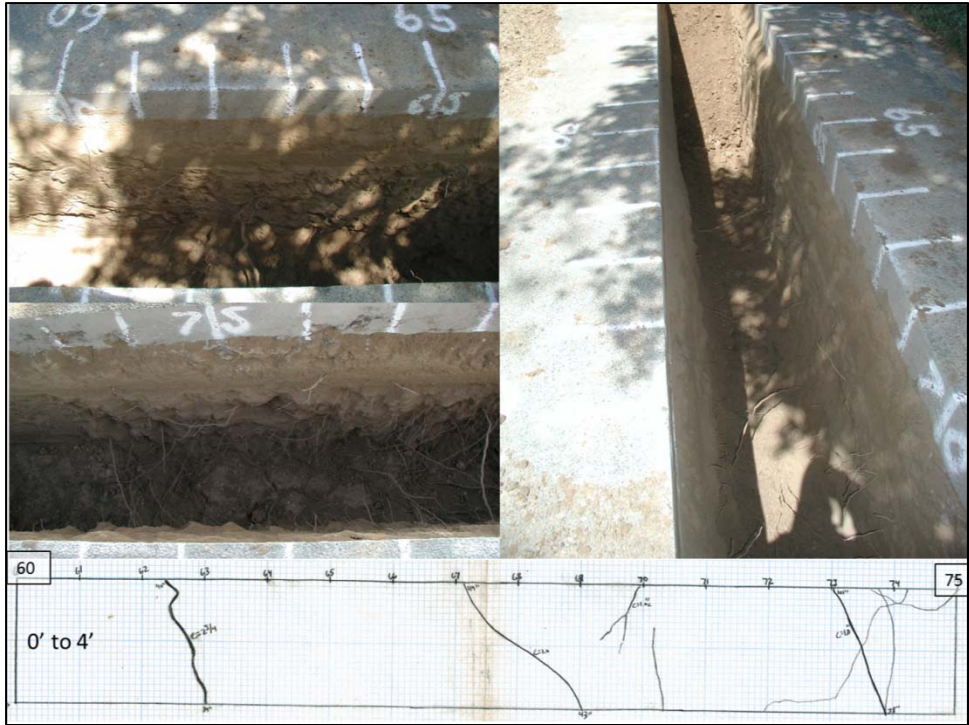
Figure 3-59. Root log at 0 to 4 foot depth Station TT 60 to 75.
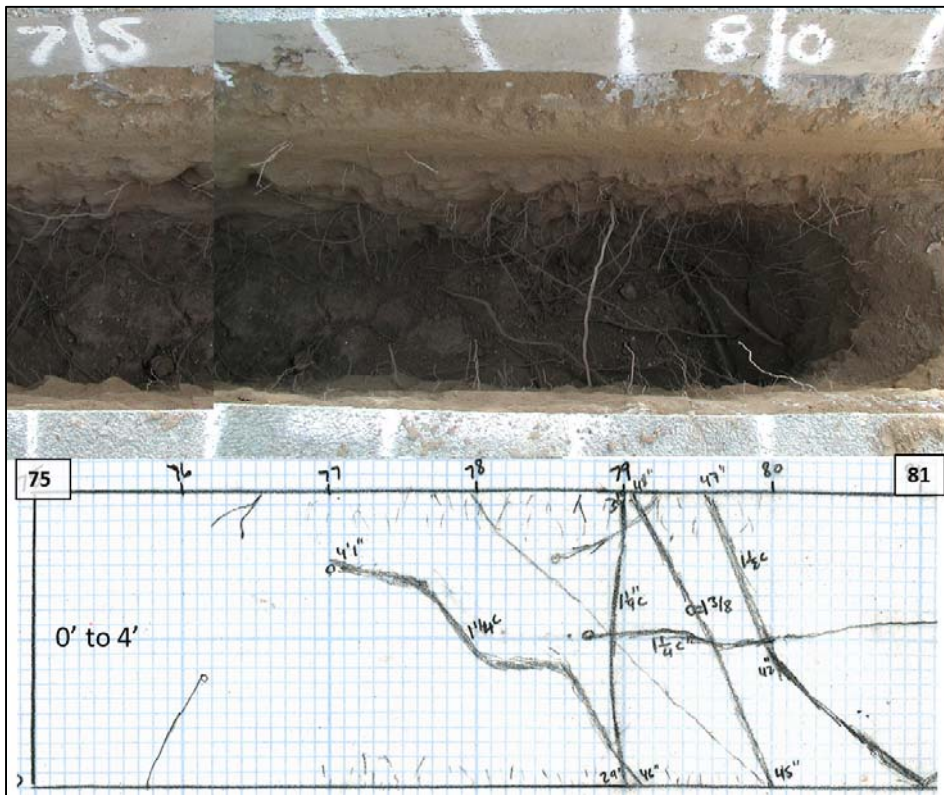


Figure 3-60. Root log at 0 to 4 foot depth Station TT 75 to 81.
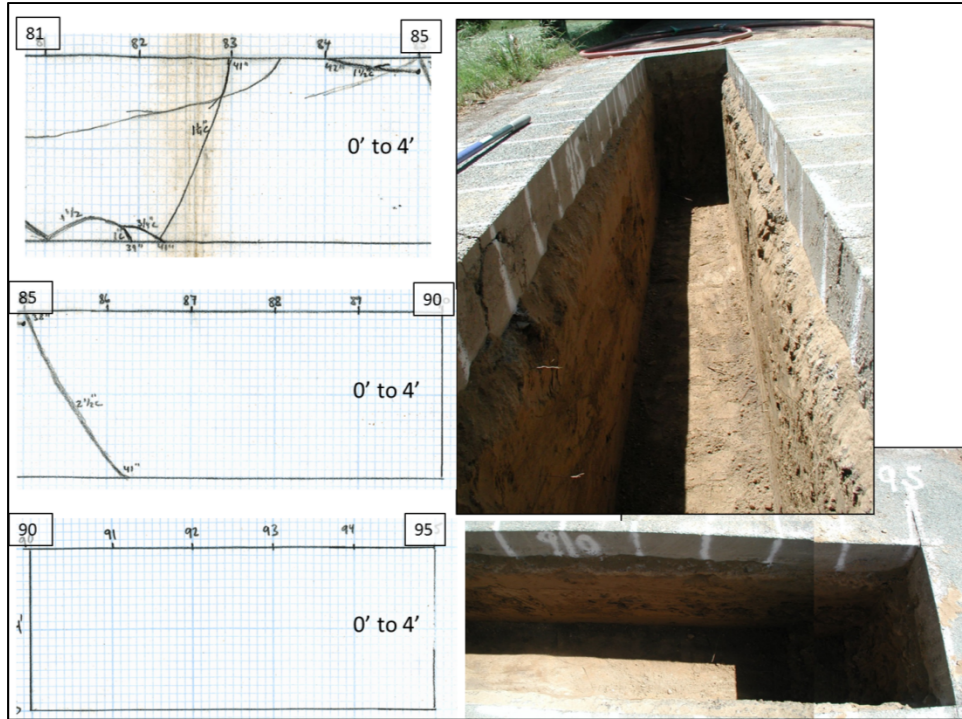
Figure 3-61. Root log at 0 to 4 foot depth Station TT 81 to 95.



Figure 3-62. Some live roots wept from the inside of the root upon cutting. No void space around the root was observed.

### 3.1.3.2.4   Tree Trench: 4 to 8 Foot Depth

In general, the root zone for the waterside oak tree (Station TT 20) extends from Station CT 27 to Station TT 50 (30 feet on either side of the trunk) with a few small (< ½ inch diameter) roots extending 7 feet beyond this zone to the south to Station TT 57. Root size in the upper 4 feet was never larger than 1 ½ inch in diameter. Roots became larger with depth. It should be noted that the tree is located at an elevation approximately 7 feet lower than the levee crown and so roots encountered at a depth of 7 to 8 feet in the tree trench are growing approximately horizontally from the tree. At depths of 4 to 6 feet below grade, the root system of the waterside oak extended from Station TT 9 to 42 with root sizes typically on the order of ½ to 1 ¼ inch in diameter but growing as large as 2 ½ inches between Stations TT 15 and 26. Detailed logs and photographs of roots associated with the waterside oak tree at depths greater than 4 feet are shown on Figure 3-63 through Figure 3-73.

The deeper roots from 6 to 8 feet in depth were the most extensive, beginning at Station CT 27 and extending to Station TT 57. Roots were generally larger to the north (typically up to 2 inches in diameter) with the largest root being 3 ½ inches at Station TT 17 to 18 (Figure 3-66 and Figure 3-67). This larger root was slightly below the 8 foot base of the trench but a decision was made to excavate it out to prevent the excavator from pulling on it when preparing the final trench. The bottom was locally excavated to a depth of 8 foot 9 inches at this location, which is below the surface water level in the adjacent slough. The root appeared to originate from the waterside tree whose root system extended from the waterline of the slough to the trench. It was noted that the conditions around the root did not differ from surrounding conditions and water was not observed traveling around the roots.

The largest roots were found in the vicinity of Stations TT 17 and 18 (up to 3 ½ inches in diameter). Root sizes between Stations TT 18 and 45 were on the order of 1 to 2 inches with many smaller than 1 inch (Figure 3-68 through Figure 3-71). Between Stations TT 45 and and 57, roots were on the order of ½ inch or smaller (Figure 3-72 and Figure 3-73).

Burrowing activity began at Station 57 (Figure 3-74) and was extensive in the zone between Stations TT 64 and 81 (Figure 3-75 through Figure 3-82). Burrow diameters ranged from tiny holes on the order of ¼ to ½ inch, to moderately sized holes of 1 to 1 ½ inch, up to holes 2 to 3 ½ inch. Based on discussions with Dr. Van Vuren of UC Davis, the 1 to 1 ½ inch diameter holes were likely due to gopher or vole activity originating on the land side, but the depth of 6 to 8 feet was unusual. The larger holes were suggested to be related to muskrat activity originating on the water side. Dr. Van Vuren suggested that perhaps the smaller rodents were taking advantage of pre-existing abandoned burrows created by the muskrat, explaining the range in size of the burrows as well as the unusual depth of the smaller rodent burrows.

The root system of the landside tree (centered at Station TT 70) was found to extend from Station TT 62 to TT 89 (Figure 3-77, Figure 3-79 through Figure 3-84). All roots extending from the landside oak tree that were encountered in the tree trench were 1 inch in diameter or smaller. Unlike the waterside oak tree roots, the larger roots were found between 3 and 8 feet deep and did not show a notable increase in size at any particular depth but rather were distributed throughout the depth profile. Roots were generally not found at depths above 3 feet.

The last 5 feet of trench from Station TT 90 to 95 were devoid of roots (Figure 3-85). Trench wall logs for the tree trench show the material types (from Section 3.1.3.2.1, Materials) encountered on the waterside and landside walls of the tree trench. These logs are provided as Figure 3-86 through Figure 3-89. Of note is the sharp dip of the Material 4 layer at Stations 37 to 42 on the land and water side of the trench. This material is believed to be an older, possibly natural levee as discussed previously. The surface of Material 4 dips along with Material 5, implying that perhaps this was a low point, or a point that settled to become a low point, in the overbank deposits. This depression is filled with the loose, highly variable Material 7, suggesting later infilling. The observations in this area are consistent with an old excavation or possibly a deep scour or breach location, backfilled with loose fills. Poor performance records were kept prior to the 1950s. A deep scour or breach may have occurred during one of the flood events in the late 1800s or early 1900s, possibly breaching from the landside from the flooding on the San Joaquin River.
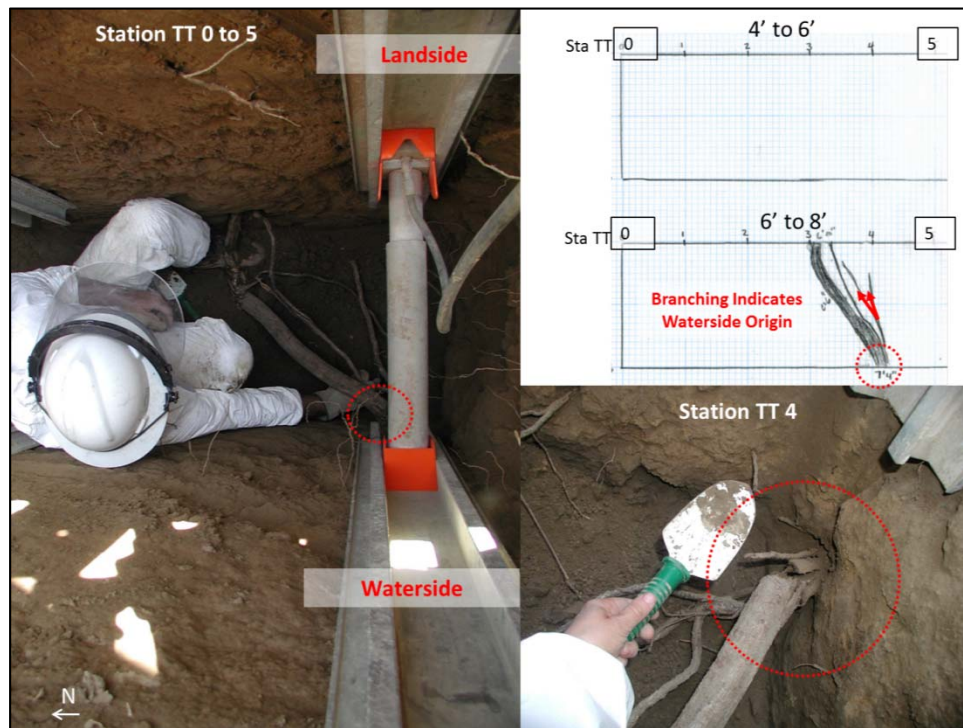


Figure 3-63. Root logs at 4 to 8 foot depth Stations TT 0 to 5.

Figure 3-64. Roots at Station TT 5 to TT 10.
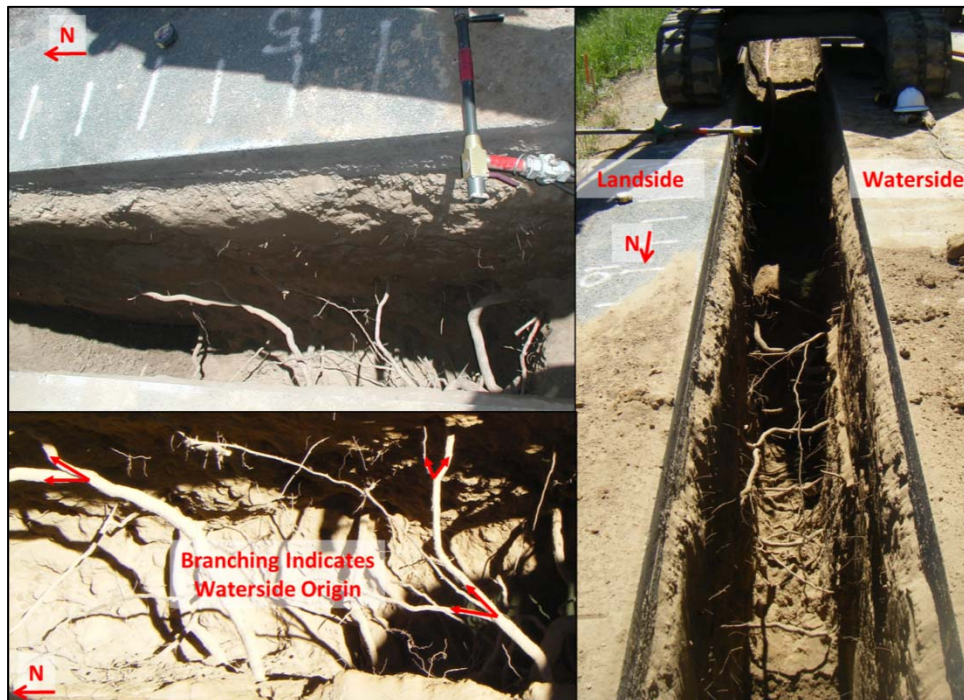

Figure 3-65. Roots at depths of 4 to 8 feet at Station TT 10 to 15.
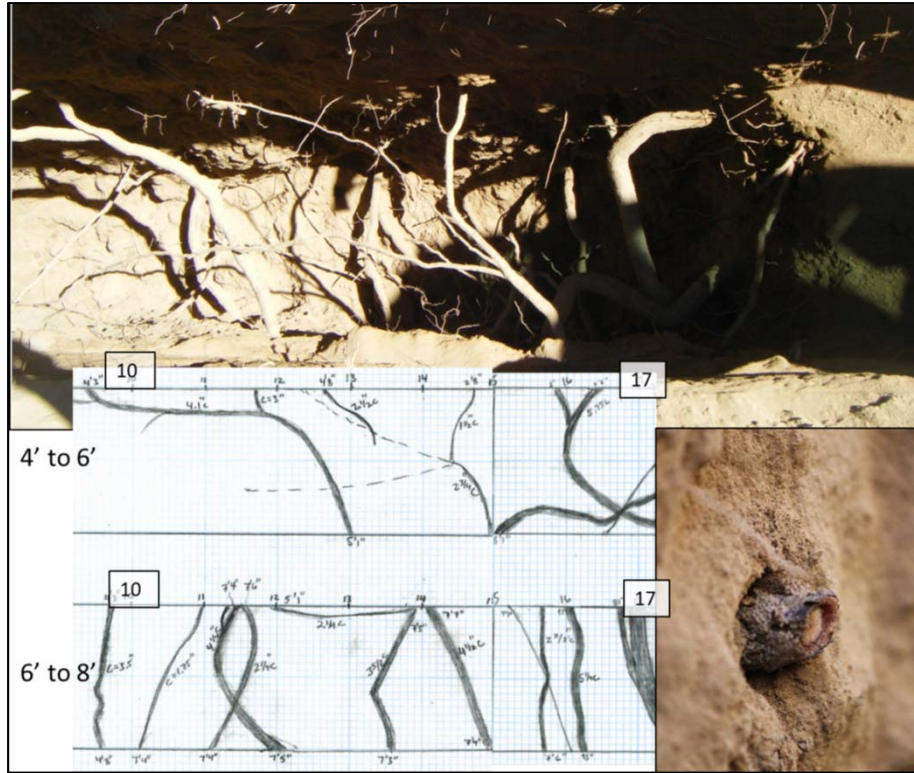
Figure 3-66. Root logs at 4 to 8 foot depth Stations TT 10 to 17.



Figure 3-67. Station TT 15 to 20. Excavation extended below 8 feet to remove a 3.5 inch diameter root for constructability concerns (upper right, lower left). Void space was found in the soils at Station TT17 waterside (bottom center).
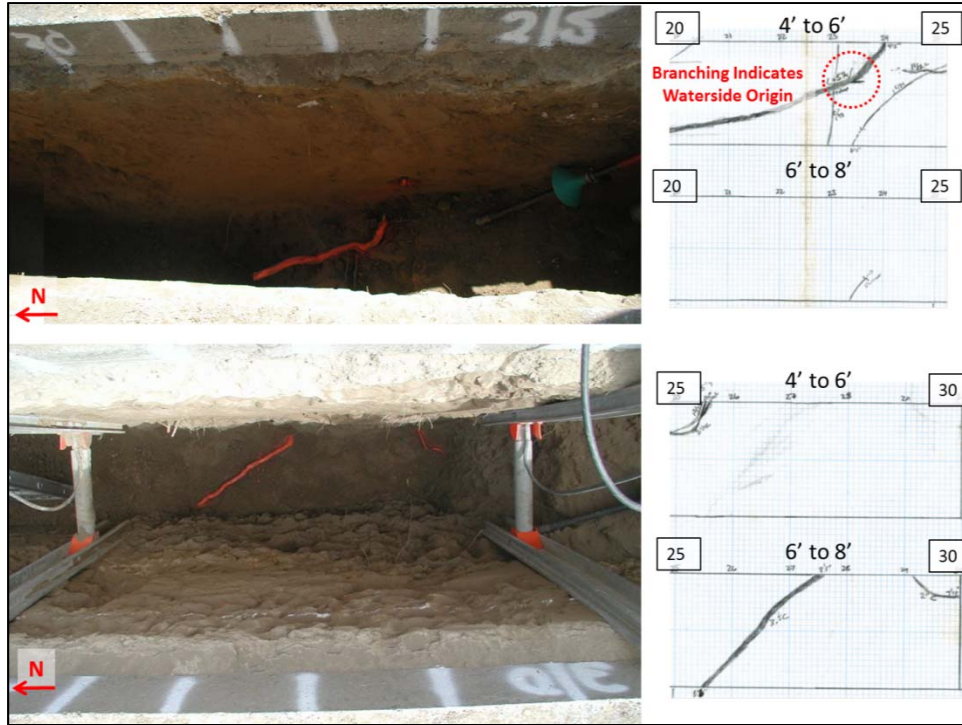
Figure 3-68. Root logs at 4 to 8 foot depth Stations TT 20 to 30.
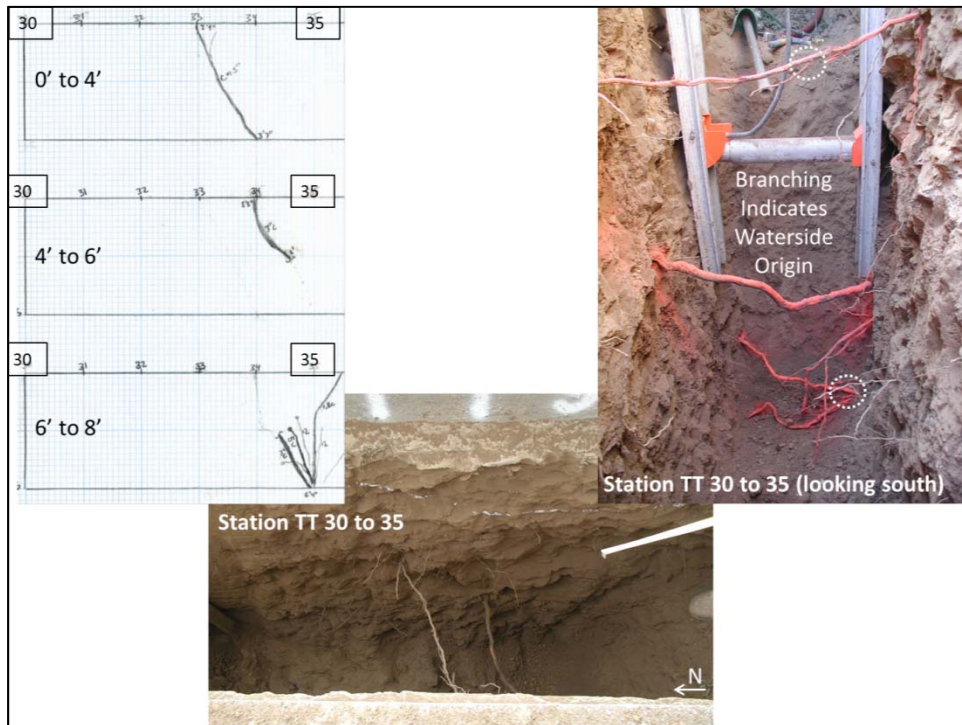


Figure 3-69. Root logs at 0 to 8 foot depth Stations TT 30 to 35. Plan view log compared with view from above and inside trench. The difficulty of capturing three dimensional aspects of a root system in plan view logs is illustrated.
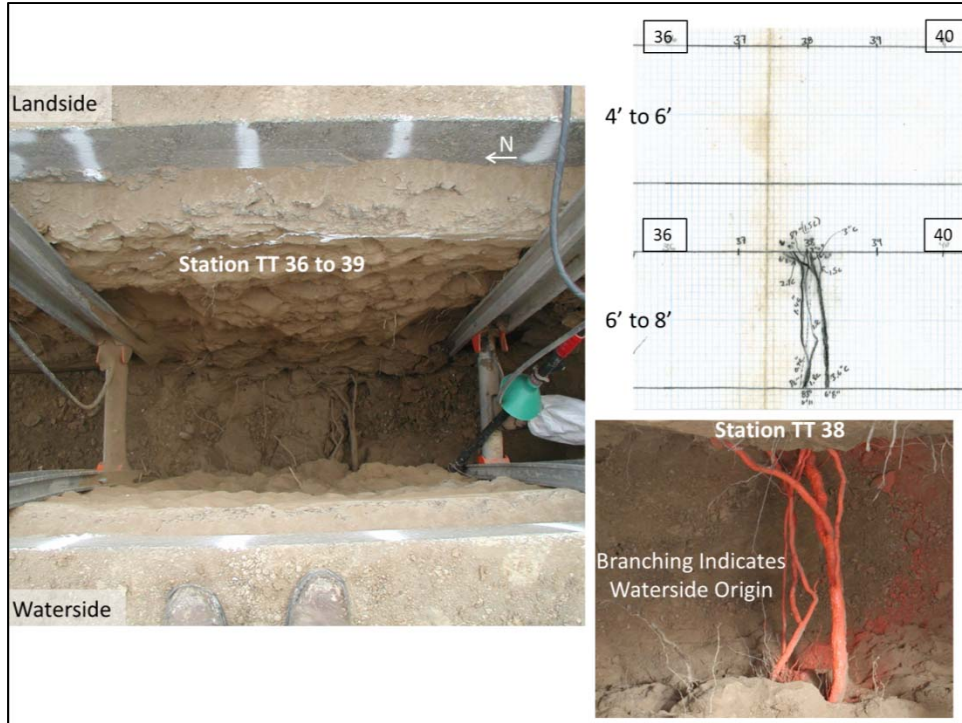
Figure 3-70. Root logs at 4 to 8 foot depth Stations TT 35 to 40.
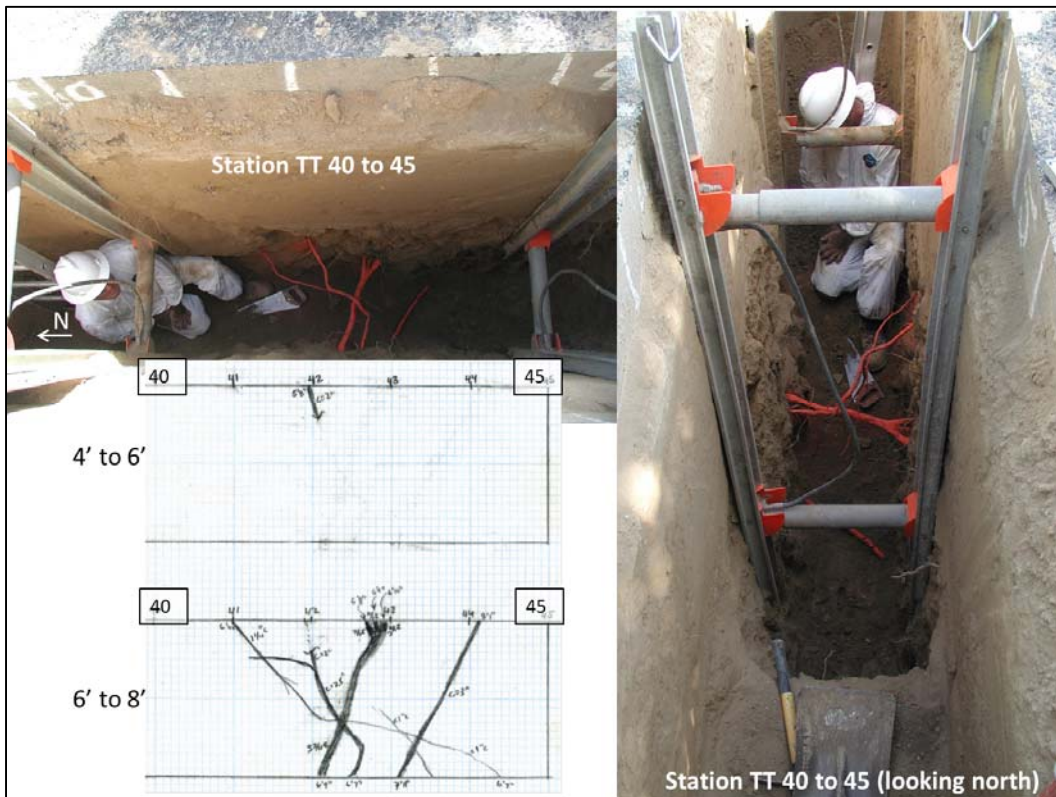


Figure 3-71. Root logs at 4 to 8 foot depth Stations TT 40 to 45.
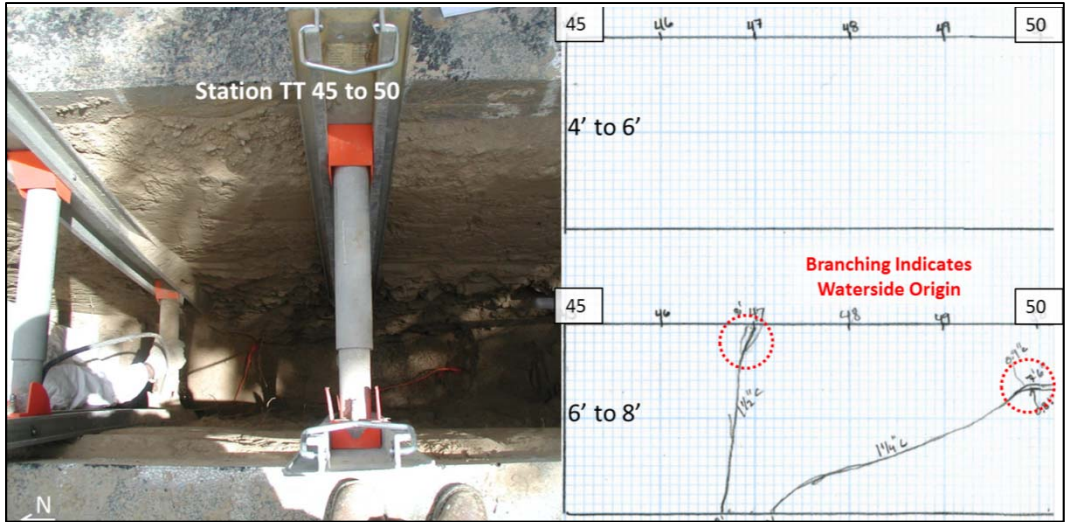
Figure 3-72. Root logs at 4 to 8 foot depth Stations TT 45 to 50.
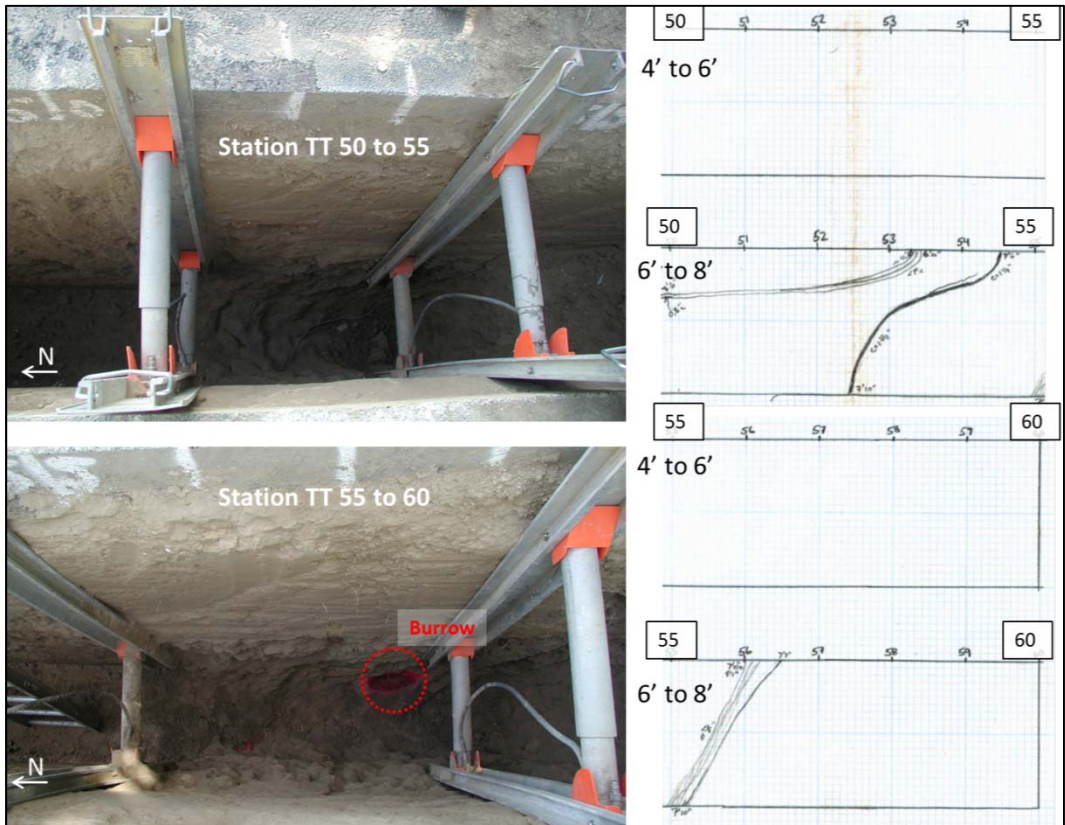


Figure 3-73. Root logs at 4 to 8 foot depth Stations TT 50 to 60. Note the first burrow of the tree trench was encountered at landside Station TT 57 at a depth of 7 feet.

Figure 3-74. Burrow on landside of Station TT 57 at 7 foot depth. Vegetative debris and live root growth found inside 2 ½ diameter hole (left, top right). A plug of grout is placed (bottom right).



Figure 3-75. A burrow is encountered during air knife work. The burrow is painted pink in photographs. Burrow diameter varies from 2 to 2 ½ inches.
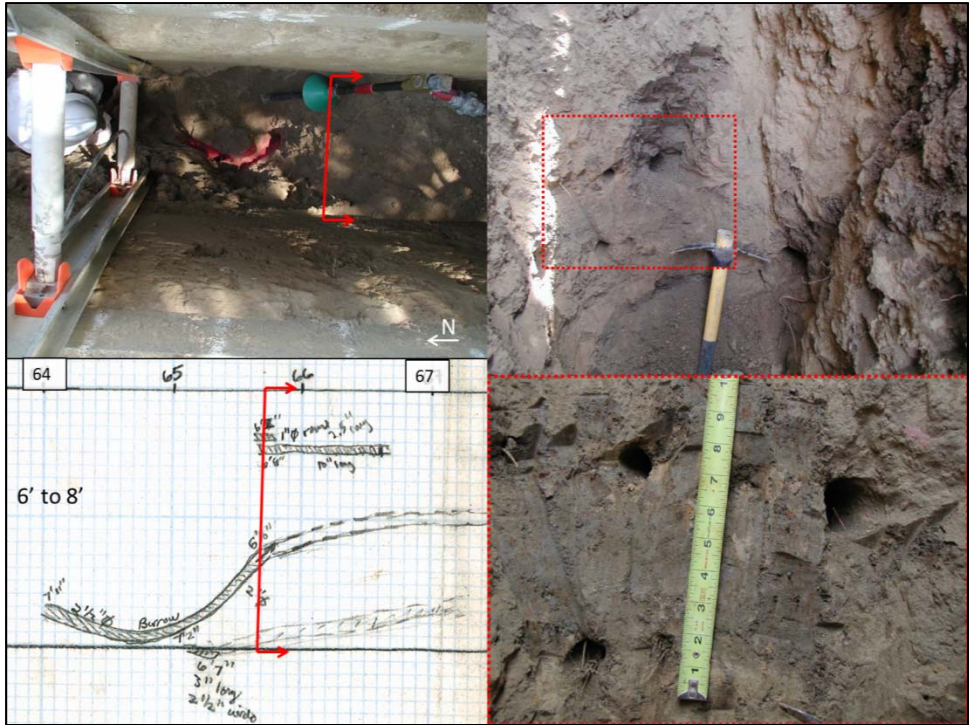
Figure 3-76. Views of burrow network extending south from Station TT 66 (right). Burrows ranging from 1 inch to 2 inches in diameter.
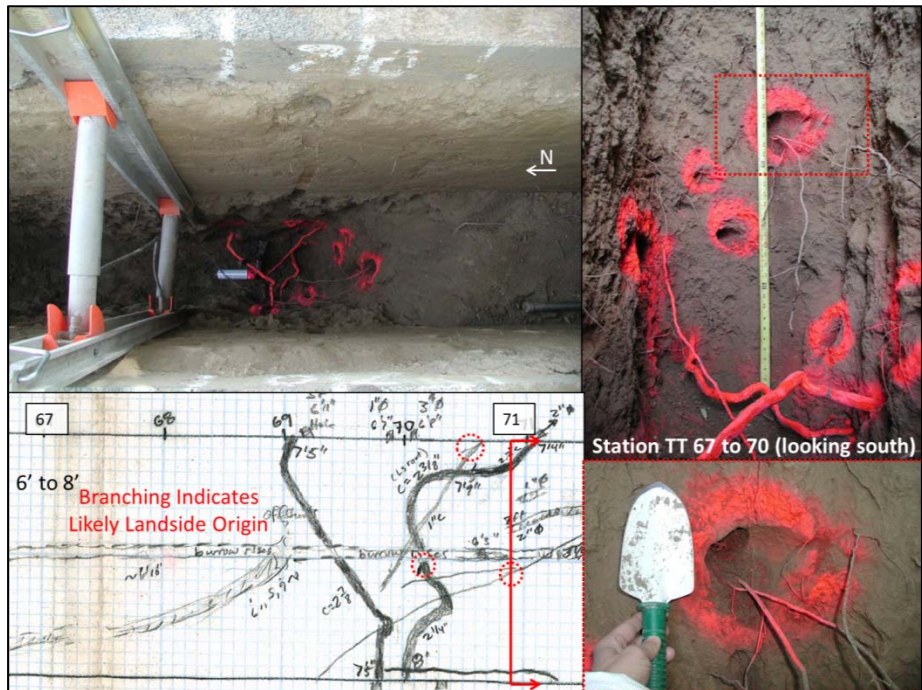


Figure 3-77. Root and burrow log at depth of 6 to 8 feet at Stations 70-71. Live root growth in burrows of 2 to 3 ¼ inch diameter.

Figure 3-78. Small holes, less than ½ inch in diameter observed near mammal burrows.
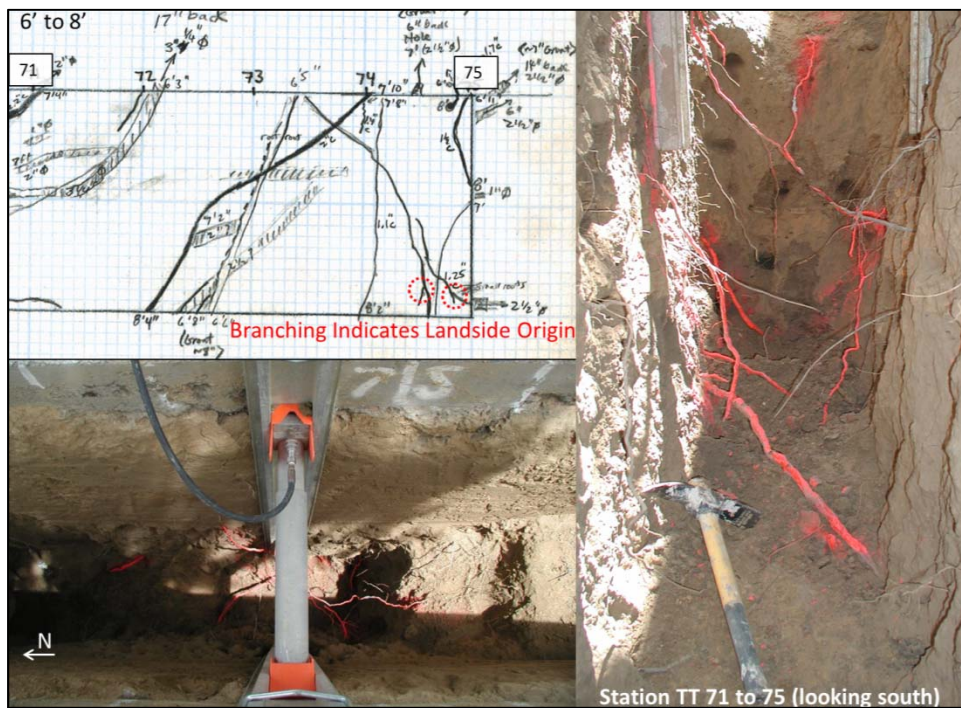


Figure 3-79. Root log for Stations TT 71 to 75 including plan view photo (bottom left) and trench view (right).
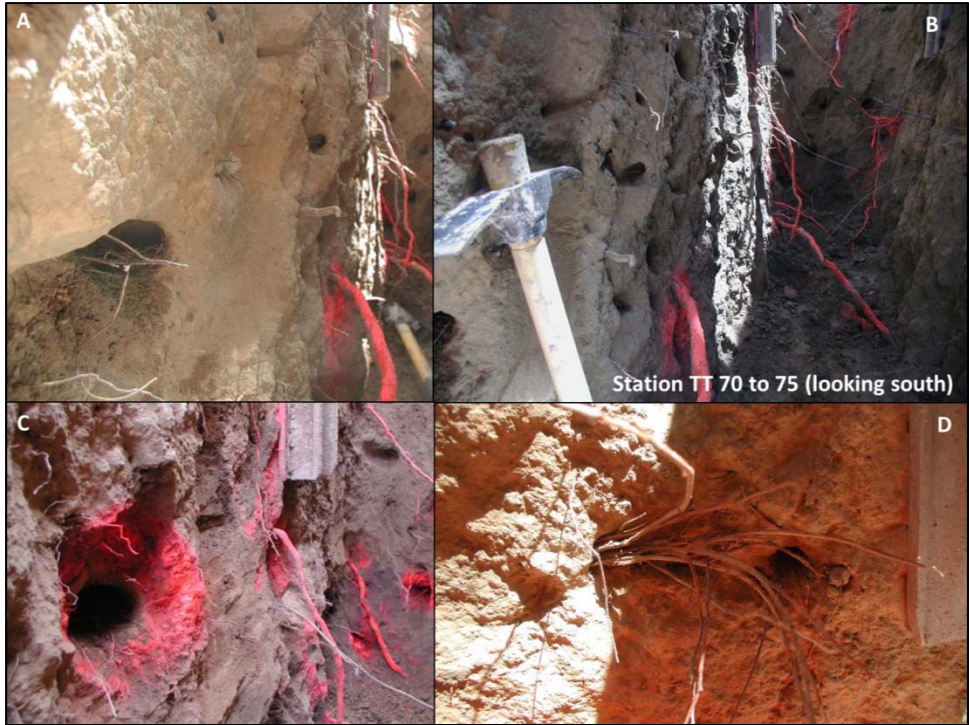
Figure 3-80. Close in view of mammal burrows with root growth and vegetative litter left by mammals (A, C, D) and an overview of extensive burrowing activity between Stations TT 70 and TT 75 (B). Burrows range in diameter from 1 to 2 ½ inches.
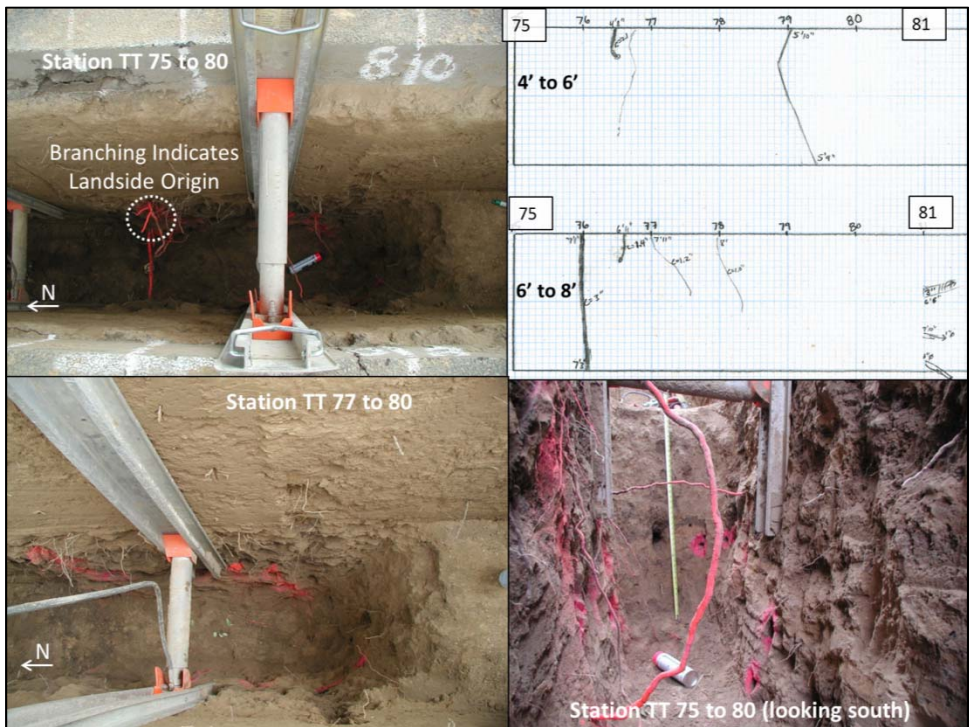


Figure 3-81. Burrowing activity and live root logs between Stations TT 75 and 80.

Figure 3-82. A) Overview of roots and burrowing activity (diameters from 1 to 3 inches) from Stations TT 77 to 80. B) View of 1 to 1 ½ in diameter holes at Station TT 81 waterside wall; C) View of 3 inch diameter burrow at Station TT 81.
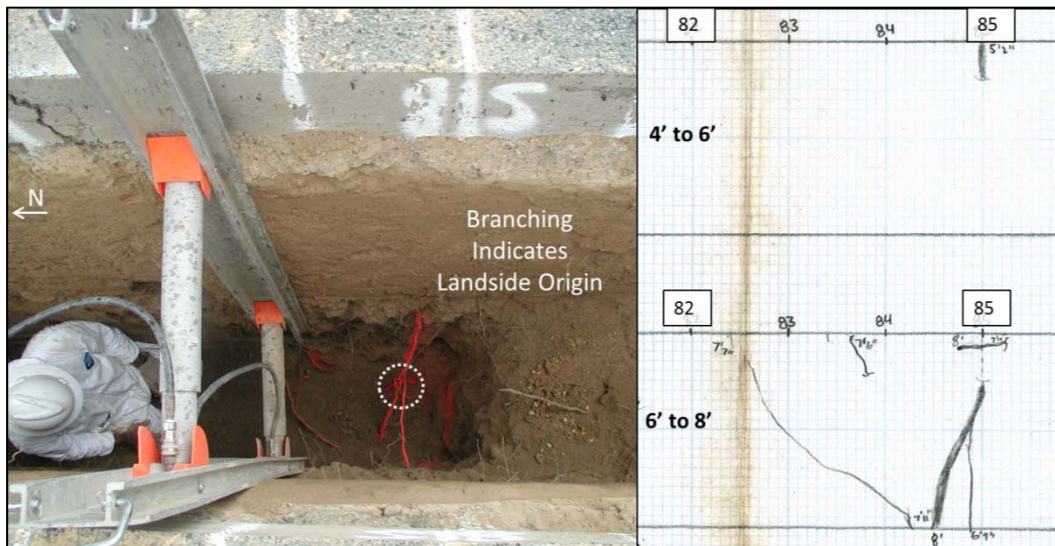


Figure 3-83. Root logs at depths 4 to 8 feet at Stations TT 82 to 85 showing a 1 inch diameter root originating from the land side of the trench.
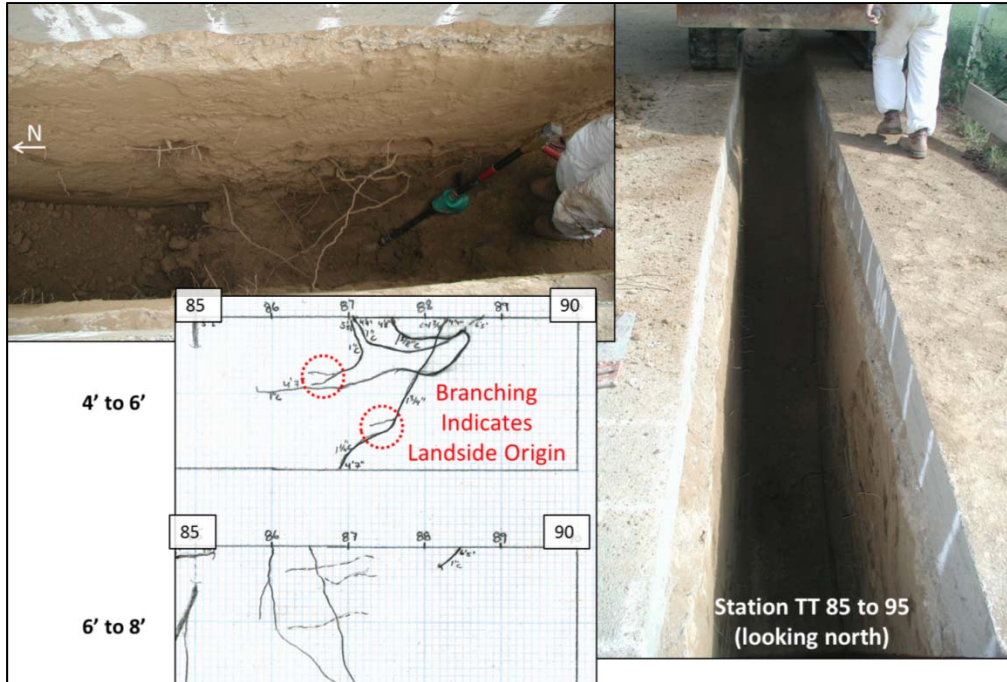
Figure 3-84. Root logs at depths of 4 to 8 feet at Stations 85 to 90 showing the last cluster of roots (approx. ½ inch and smaller) that appear to originate from landside oak tree.
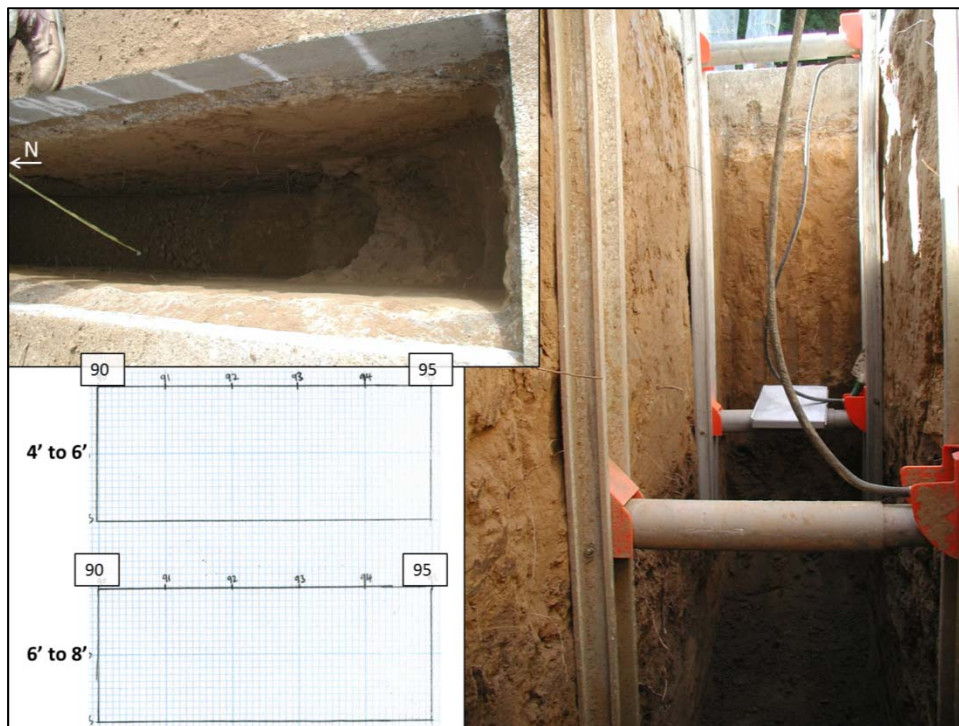


Figure 3-85. Root logs and photographs of the 4 to 8 foot depth range at Station 90 to 95 show an absence of roots and burrows. A clean transition from low plasticity silts (Materials 2, 3, 5, and 7) to plastic silts (Material 4) is seen visible as a shift to darker material midway down the trench (right).
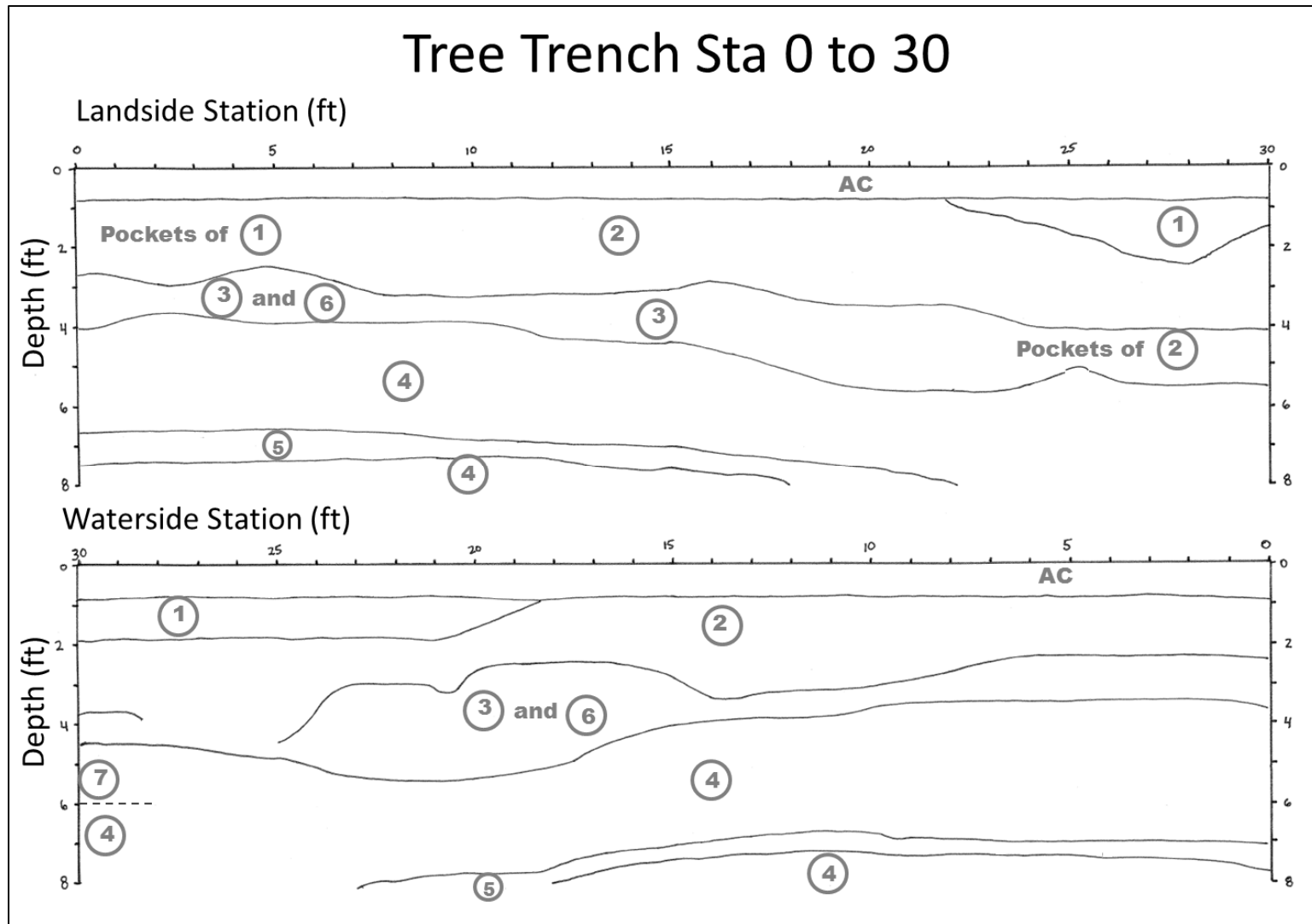
Figure 3-86. Tree trench landside and waterside wall logs, Station TT 0 to 30. Material types are described in detail in Section 3.1.3.2.1.
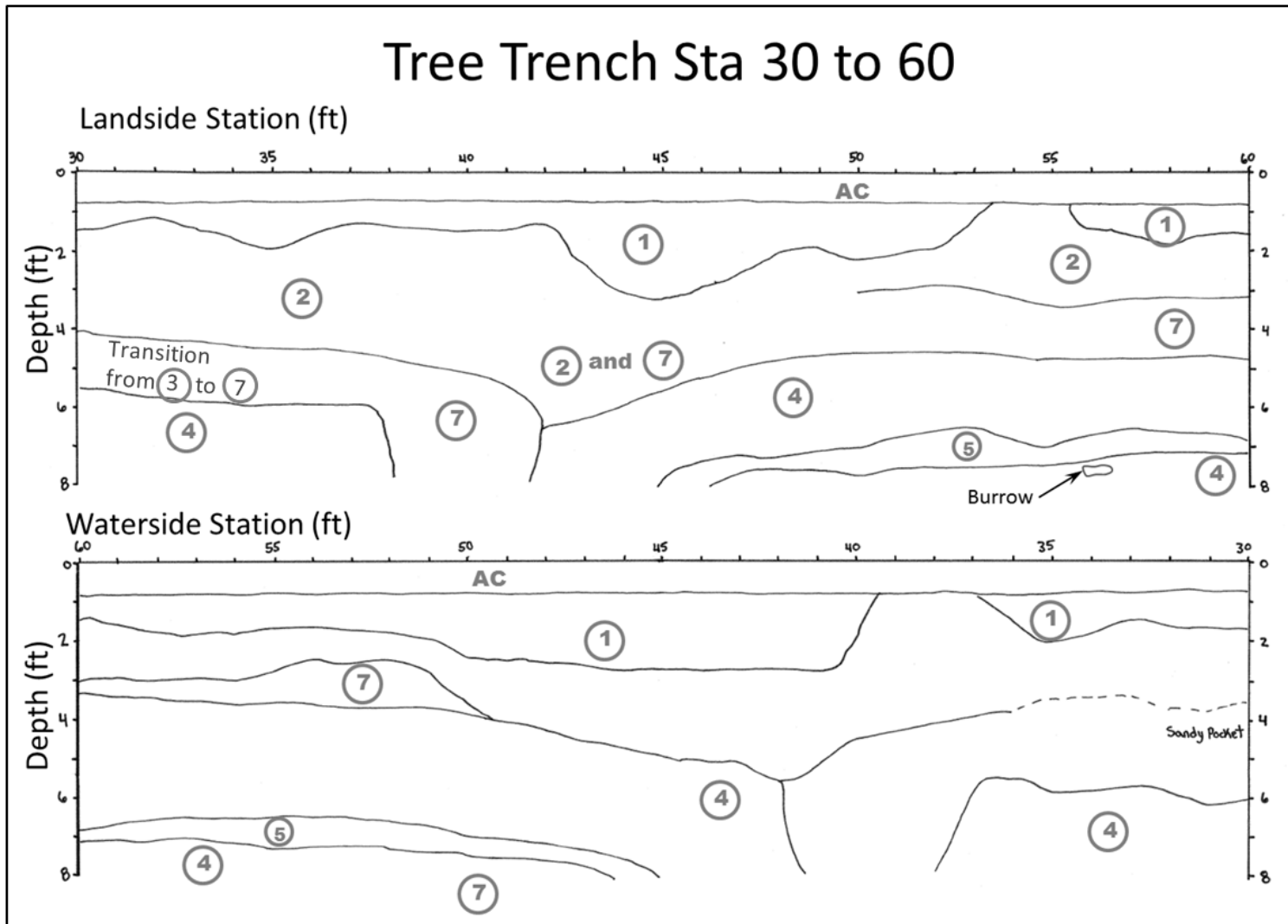
Figure 3-87. Tree trench landside and waterside wall logs, Station TT 30 to 60. Material types are described in detail in Section 3.1.3.2.1.
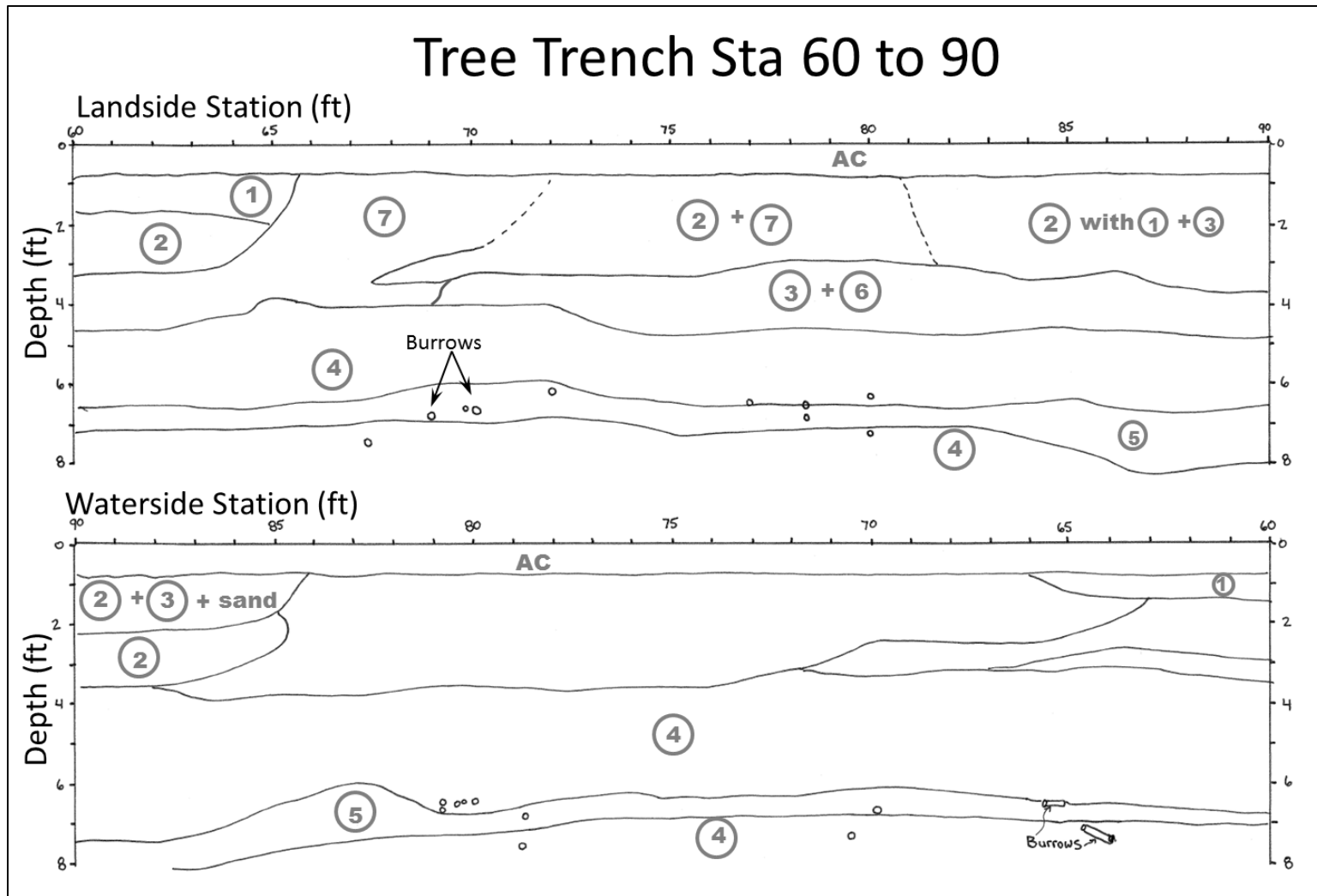
Figure 3-88. Tree trench landside and waterside wall logs, Station TT 60 to 90. Material types are described in detail in Section 3.1.3.2.1.
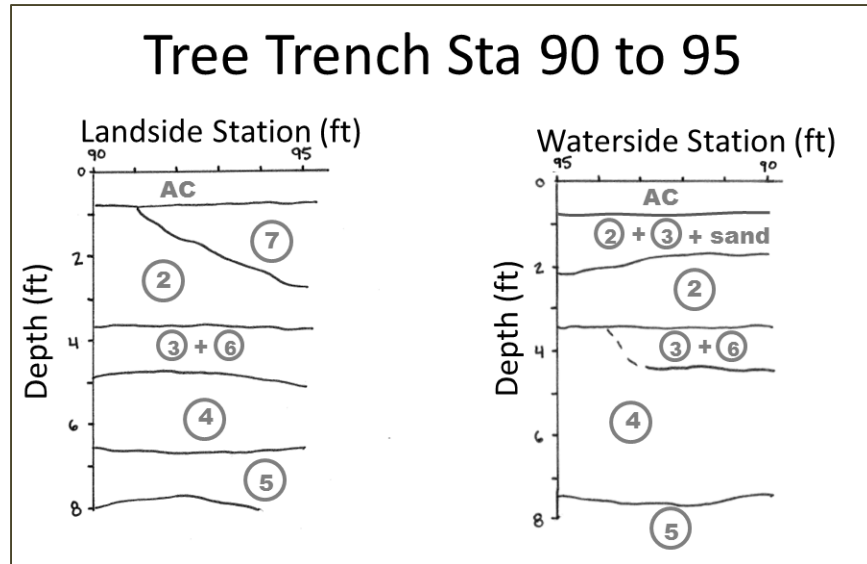
Figure 3-89. Tree trench landside and waterside wall logs, Station TT 90 to 95. Material types are described in detail in Section 3.1.3.2.1.

### 3.1.3.3    Installation of Instrumentation

Initial instrument equilibration and additional installation details are provided in Appendix F. Tensiometers were obtained from Soil Moisture, Inc. and equipped with a mechanical pressure gauge and a pressure transducer with maximum suction capacity of 100 kPa. They were pre-assembled and saturated prior to installation (Figure 3-90). All connections were cleaned, the gauge and transducer ensemble connected to the tensiometer, taking care to properly achieve a seal on each connection. The porous tips were pre-saturated in vacuum with de-aired water and brought to the site in de-aired water. They were connected to the tensiometers onsite just prior to installation. De-aired water was brought into each instrument through a suction pump attached at the top. Once the tensiometer was filled, the suction pump was used, along with tapping action, to remove trapped pockets of air from the gauge and transducer connections.

Tensiometers of 24, 48 and 60 inches were installed to depths of 18, 36, and 60 inches, respectively. All instruments were installed in accordance with the manufacturer's specifications. Holes were advanced with a gauge auger (provided by the manufacturer) with a diameter slightly larger than the instrument diameter of ¾ inch. The instrument holes were logged for soil conditions prior to installation.

With all seals checked and no observed leaks, silica slurry (a mixture of water and silica flour with silt-sized particles) was used to create a seal between the soil and the tensiometer. This step is optional according to the manufacturer if the hole is snug to the tensiometer, but proved helpful in our soil conditions. De-aired water was periodically refilled by opening the instrument, losing tension, refilling, closing the instrument, and allowing time for re-establishment of tension. For convenience, many of the instruments were equipped with a reservoir cap to facilitate refilling (Figure 3-90B), however the effect on soil tension was the same. The functionality of the instruments was checked after each refilling.

178

Figure 3-90.  Tensiometer is leak-checked, saturated (A) and sealed into the ground (B and C). Grout is mixed (D) and piezometers are grouted into the ground (E).

Vibrating wire piezometers were pre-saturated and grouted into place upside down to prevent desaturation of the porous stone in accordance with the recommendations of the manufacturer, consultation with Mr. Eric Mikkelson, and available literature (Mikkelsen 2002; Mikkelsen and Green, 2003; McKenna, 1995). Piezometers were read continuously with two 16 channel Geokon LC-2 Series Model 8002-16 dataloggers. Frequency of readings was determined based on the observed rates of change in recorded pore pressures. Table 3-5 and Table 3-7 provide summaries of recorded piezometer data on the land and water sides. Data results are discussed in Section 3.1.4.4.

Approximate alignments of instrument lines are shown overlain onto site photography in Figure 3-91. Figure 3-92 through Figure 3-95 show photos of installed instrument lines on the landside and waterside. Piezometers are difficult to see in photographs as the only visible element is a wire protruding from the ground unlike tensiometers which have an above grade mechanical gauge and transducer.

Figure 3-91. Photographic view of landside and waterside instrument line locations.



Figure 3-92. Instrument line A looking west from toe (left) and east from top of slope. (right)

Figure 3-93. Instrument Line B at waterside oak tree looking west (upper left, right) and north (lower left).



Figure 3-94. Waterside instrument line B (top images) and line E (bottom images).

Figure 3-95. Instrument line C from the toe of slope looking west (left) and from the crest looking west at waterside instruments.

### 3.1.4 Flow experiment

Following instrument calibration and monitoring, the flow test experiment was initiated by filling the levee crown trenches with water on May 21, 2012. The experiment ran for approximately 4 days after which the water was shut off to the tree trench while the control trench continued to run for 6 additional days. Some instruments were not fully saturated in the control trench, yet instruments showed that seepage in the vicinity of the tree trench had achieved steady state conditions. On May 31, 2012, approximately 10 days after the start of the flow test, a dye test was introduced to better understand where water was being lost during the test, particularly on the water side. Following the dye test, water to both trenches was shut off and suction was allowed to build within the tensiometers as soils dried. All working instruments were monitored through June 5, 2012, approximately 15 days after the start of the flow test. Some instruments were no longer functioning for a portion of this time period due to vandalism and theft of some of our equipment. A detailed timeline showing the duration of each phase of testing as well as key observations is presented as Figure 3-96.

On May 21, 2012 at 1:47 pm, the valve from the 4900 gallon polyethylene water storage tank located at the crown of the levee was opened and water was channeled via gravity flow into the control and tree trenches via the input hoses connected to mechanical float valves located at two input sites at the approximate centers of the tree and control trenches. Shortly after turning the water on, the 2 inch hoses were disconnected from the mechanical float valves to increase flow rates during filling of the trenches. Trenches seemed to be losing significant water and the level at one point was not rising. Ultimately water as delivered directly from the 4 inch fire hose. A constant

head of water was reached in 3 hours from the start of the test in the control trench, and after nearly 5 hours in the tree trench.
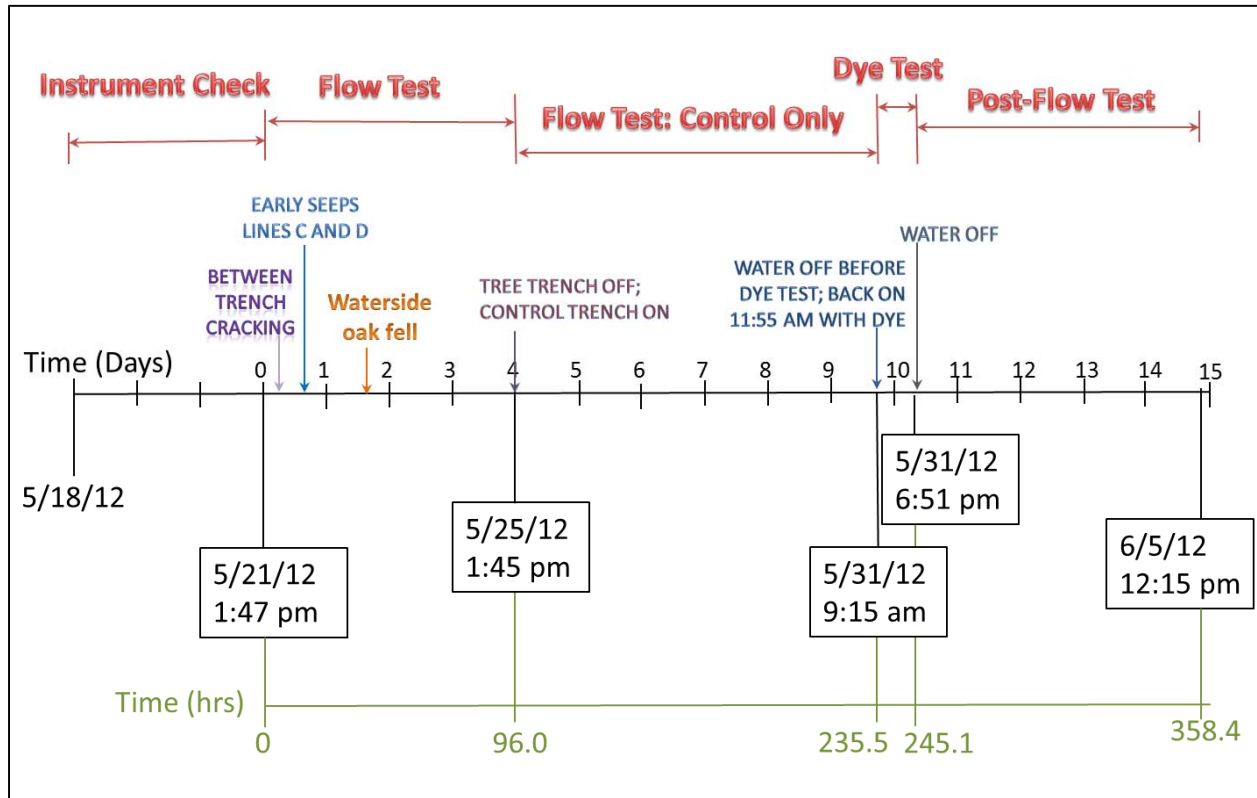


Figure 3-96. Timeline for Twitchell Island crown trench seepage test.

The constant head water surface elevation was set to approximately 9 inches below the edge of the pavement, or about 7 ¼ feet from the base of the trench to avoid overflow. The water level in the control trench, once full, was maintained using the mechanical float valve, as planned. The water volumes required to maintain constant head in the tree trench in excess of the capacity of the valve to deliver water under the available head. Water was delivered via the 4 inch hose while mechanically adjusting the volumes using valves on the delivery tank. At night, fine adjustments were made and visits were made every 4 to 6 hours to maintain water levels and make brief site inspections during the primary flow test.

Upon the commencement of water flow into the upper trench, a crack occurred between the control trench and the tree trench within about 2 ½ hours of the test start. The crack was monitored for changes throughout the duration of the flow test as discussed in a subsequent section. The first seep occurred at the waterside oak tree about 9 hours into the flow test. Seeps began to appear on the landside near the control line C in the middle of the night, about 13.3 hours into the flow test. By morning, more seeps were appearing in this area and also near instrument Line D, downslope from the extensive burrowing activity that was encountered during trenching. Within a few hours, large seeps were appearing under instrument line D and also instrument line A below the landside oak tree. The area of seepage correlated well with the area of extensive burrowing encountered in the tree trench between Stations TT 56 and 82. Upon post-flow test inspection of the seepage areas on the slope, the surface expressions of the burrows were not apparent. The water at the slope face was observed to be exiting the slope through ¼ inch to ½ inch diameter macropores.. These holes

were later inspected and are believed to be associated with a very active earthworm population. The earthworm burrows appear to have allowed for concentration of flows in the near-surface soils. It is not known whether these small holes were interconnected with mammal burrow networks.

Within the first 25 hours of the test, a pattern of seepage began to develop in a linear alignment extending across the slope at a vertical elevation about 2 feet higher than the toe of slope. This pattern continued throughout the test, where seepage and flow seemed to appear either along this alignment or from areas known to be riddled with burrows.
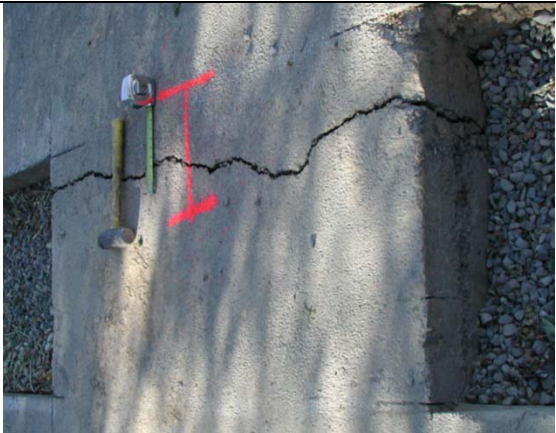
After a little over 39 hours of testing, and the monitoring of a growing seep at the base of the waterside oak tree, the tree rotated approximately 20 degrees and came to rest with the long branch of the tree providing support within the shallow oxbow section of the slough. Cracking and deformation was monitored around the tree, the waterside slope, and the pavement at the crown throughout the duration of the test. T-LiDAR scans were performed by Gerald Bawden and his team at the USGS to document deformations at the site. A pre-flow scan was taken as well as a scan following the primary flow test, and a scan following the final dye test. His results and deformation analysis are summarized in Bawden et al. (2013).

The constant head was held for 4 days at which time water flow to the tree trench was turned off. Steady state appeared to have been achieved in the area of the tree trench, based on instrument data, and Rows 3 and 5 of the control trench had not yet saturated. It was not clear if these instruments in the vicinity of the control trench would saturate or if steady state had been achieved without the wetting front reaching all of instrument line C. Flow to the control trench was allowed to continue. The tree trench was found not to drain completely upon turning the water off on the tree trench, while flow rates pumped into the control trench increased during this time period. The morning of May 31, 2012, water in both trenches was shut off for a few hours to allow levels to drop prior to a dye test. Blue Cole Parmer tracer dye was mixed into the tank and delivered into the trenches to determine the path of water losses, particularly those on the waterside. A series of land and waterside observations were made. Water levels in the slough were kept low by the operators of the gate in order to facilitate our inspections of waterside burrows. These burrows were difficult to access up close during the primary test due to soft soil conditions, high water levels, and dense brush, including Elderberry bushes that could not be cut for access due to permit restrictions.

Visual observations were made over the 4 day primary flow test and during the dye test. Limited observations were made during the 6 days when water was delivered only into the control trench. The instruments were disconnected on June 5, 2012 and removed shortly thereafter. The site was allowed several weeks to dry out prior to the repair phase.

A photographic timeline is provided below detailing the primary events that occurred throughout the test (Table 3-2). Detailed discussions and photos of landside seepage patterns, waterside deformations and monitoring, the waterside oak tree, the dye test, and the findings of the T-LiDAR survey are summarized in the following sections. Instrument data is presented and discussed in the context of these observations. Detailed instrument data is presented in Appendix F.

Table 3-2. Overview Chronology of Observations
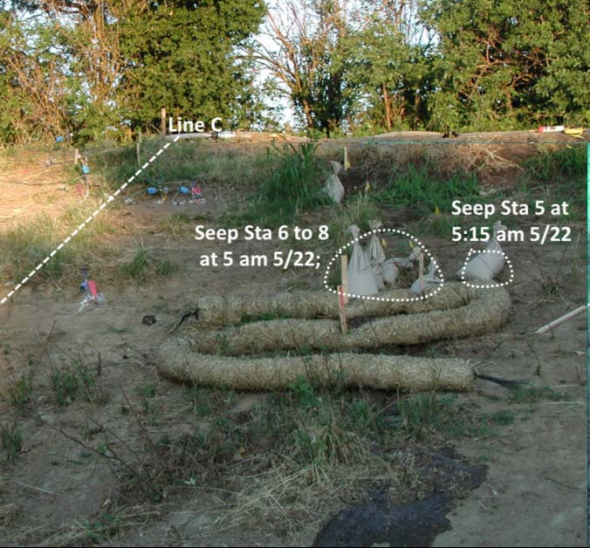
| Time (hrs) | Date | Time | Observation | Photo or Illustration |
|---|---|---|---|---|
| 0 | 5/21 | 13:43 | Water flow begins at 1:43pm on 5/21/12.<br><br>Mechanical float introduces bottleneck and is removed. |  |
| 1.32 | 5/21 | 15:02 | 2" diameter hose (connection to float) removed to allow flow through 4" diameter delivery hose. Flows were not sufficient to fill the trenches with 2" diameter hose. |  |
| 2.6 | 5/21 | 16:16 | Noticed crack between Control and Tree Trenches. Nails installed to monitor separation.<br><br>(also see Figure 3-112 through Figure 3-117). |  |
| 3.0 | 5/21 | 16:45 | Control Trench nearly to target water surface elevation. Cannot maintain sufficient flows with float. | No photo |

| 4.3 | 5/21 | 18:01 | Crack between trenches grows and begins to develop vertical offset . |  |
|-----|------|-------|---|---|
| 4.8 | 5/21 | 18:30 | Flows in Control Trench have stabilized and reduced to where the head can be maintained with the float. |  |
| 4.8 | 5/21 | 18:30 | Tree Trench nearly to target water surface elevation, but capacity of mechanical float insufficient to maintanin constant head. Must use valve on tank to maintain target water surface elevation. |  |

| 7.3 | 5/21 | 21:00 | ¼ inch vertical offset measured at crack between the trenches. |  |
|---|---|---|---|---|
| 9.0 | 5/21 | 22:40 | A seep was noticed at the waterside oak tree. |  |
| 13.3 | 5/22 | 03:00; photo at 05:30 | Seep at oak had grown; Traced with string for photograph at 5:30am (shown)<br><br>Seep recorded on the landside at Control Trench (CT) Stations 7 to 10 (no photo). Gravel bags not needed to contain. |  |

| 15.3 | 5/22 | 05:00 | Seeps open at CT Sta 6 and 8 mid-slope landside; confirmed burrow (possible vole or gopher). Gravel bags placed.<br><br>Two gravel bags added to seep at Stations 7 to 10. |  |
|------|------|-------|------|------|
| 15.5 | 5/22 | 05:15 | Sta CT 5 opened when gravel bag placed on seeps at CT Sta 6 and 8 midslope (at Time = 15.3 h); wattles and gravel bags required to prevent erosion. |  |

| 15.8 | 5/22 | 05:30 | Seep at Sta TT 57 to 59 (Instrument Line D); no gravel bags placed. |  |
|------|------|-------|---------------------------------------------------------------------|----------------------|
| 16.6 | 5/22 | 06:20 | Crack width reaches a maximum; vertical offset continues to grow. |  |

| | | | | |
|---|---|---|---|---|
| 19.3-20.0 | 5/22 | 09:00-09:45 | Seep below landside oak Sta TT 68 to 77;<br><br>Landside Sta 50 to 63 also seeping and expanding to the north. |  |
| 25.5 | 5/22 | 15:10 | New cracking in pavement near landside oak tree. New monitor installed at Sta TT 58.5. |  |
| 26.3 | 5/22 | 16:00 | Three new seeps between Sta TT 34 and 44 on the landside mid-slope. |  |

| 27.9 | 5/22 | 17:35 | New seep landside Sta 24 to 27; mid-slope in line with seeps at Sta TT 34 to 44. |  |
|---|---|---|---|---|
| 28.3 | 5/22 | 18:00 | Visible flow is observable in waterside seeps, Sta TT 13 to 24. |  |
| 28.3 | 5/22 | 18:00 | Cracks opening in pavement near Sta 82 to 88. |  |

| 28.6 | 5/22 | 18:20 | Seeps on landside Sta TT 55 to 58 are flowing; suspect macropores. |  |
|---|---|---|---|---|
| 28.9 | 5/22 | 18:34 | Widening Pavement Cracks at Sta TT 82 to 88.<br><br>Gusting winds. |  |
| 38.5-38.8 | 5/23 | 04:15-04:30 | New seeps Sta TT 17 to 21 landside;<br><br>Moderate wind no gusts. |  |

| 38.8-39.0 | 5/23 | 04:30-04:45 | Waterside seep at oak grown somewhat; photo taken shortly before departing site at 4:45 am. |  |
|---|---|---|---|---|
| 39.25-39.75 | 5/23 | 05:00-05:30 | Based on instrument data, waterside oak tree likely fell within this time window. |  |
| 42.2 | 5/23 | 08:00 | Inspected landside prior to discovering tree failure on waterside. Noticed seeps near control line on land side (Sta CT 5 to 10) had stopped flowing. |  |

| 43.5 | 5/23 | 09:15 | Noted flow in seeps in vicinity of Instrument Line D, Stations 57 to 59. <br><br> Flow seemed to be coming from small holes from ¼ to ½ inch in diameter. |  |
|---|---|---|---|---|
| 43.5-43.8 | 5/23 | 09:15-09:30 | Waterside oak tree observed to have fallen; photographed site. |  |

| 51.8 | 5/23 | 17:30 | Visit from team advisor Dr. Les Harder. Additional cracking observed beneath an erosion protection wattle and leaf litter. Cracking was mapped, photographed and further explored. Monitors were installed to track movements. |  |
|---|---|---|---|---|
| 54.3 | 5/23 | 20:00 | New crack monitors installed between Stations TT 11 and 25. |  |
| 57.3 | 5/23 | 23:00 | Small seep at landside TT 10; in line with seeps at Stations TT 20 to 85. | See photo at Time = 62.9 hours. |
| 62.9 | 5/24 | 04:35 | Mid-slope landside seeps have spread across the site all beginning at the same elevation on the slope. The seep at Station TT 10 is beginning to connect together with other seeps. |  |

| 92.3 | 5/25 | 10:00 | Onsite meeting of the CLVRP funders and advisory team prior to completion of the flow test. |  |
|---|---|---|---|---|
| 96.0 | 5/25 | 13:45 | Turned off water on tree trench while leaving the control trench running. |  |
| 235.5-245.1 | 5/31 | 09:14-18:51 | Dye Test. | See Section 3.1.4.3 |
| 245.1 | 5/31 | 18:51 | Water off; begin falling head test. |  |

### 3.1.4.1    Landside: Surficial Seeps and Macroporosity

As shown on Table 3-2, observations on the landside of the levee consisted of mapping the locations of seeps on the face of the slope and noting those that appeared to exhibit flows through macropores. Figure 3-97 through Figure 3-109 show sketches and associated photographs of wetting front patterns on the face of the landside slope between 15.8 and 92.8 hours from the time of initial inundation of the trenches. Sketches were made to support observations and photographs during this time window as visual changes were occurring rapidly, particularly over the first 48 hours.

Early seeps appeared to be related to macroporosity and likely burrowing activity. The earliest seeps were just north of the control instrument line C and by late morning (10 am on 5/22/12), the

mid-slope seeps were rapidly flowing. Gravel bags were piled on to slow down the flow and an erosion control wattle was installed beneath the zone of rapid flow to prevent rilling of the slope. This rapid flow had begun to slow later in the afternoon and stopped by 8 am the following morning on May 23.

Another early seep was encountered just after those found north of instrument line C in the vicinity of instrument line D just north of the landside oak tree. The seeps started small and grew throughout the day on 5/22/12, the second day of the flow test. Later that morning flow from the seeps began and gravel bags were placed. By 9 am that same morning, another seep had appeared under the landside oak tree along instrument line A. By 3:40 pm (26 hours into the flow test), gravel bags were added to these seeps to control water flows. Shortly after, at 4 pm (time = 26.3 hours), three new seeps were discovered at Stations TT 34, 39, and 44. By 5:35 pm, another seep appeared at Station TT 25. All seeps appeared in a linear alignment about 2 feet (measured vertically) from the base of the slope (Figure 3-100 and Figure 3-101).

Figure 3-110 shows a sketch of seepage patterns observed plotted with a simplified log of the contact between the older levee (lower permeability clayey silt named Material 4 in Section 3.1.3.2.1) and the higher permeability, heterogeneous and sometimes loose and more recent silt fills above. Instrument data show that saturation occurred in deeper instruments before shallower ones. Further, the linear pattern of seepage that occurred implied that water may was traveling along this low permeability layer and flowing out the face along that contact. The Material 4 contact dips to the east as we saw in Figure 3-29 through Figure 3-31, but also dips from the control trench toward Station TT 37 where the layer disappears and reappears at Station TT 42. In general, there is also a dip from Station TT 50 to Station TT 42. Localized but distinct dips in the Material 4 contact were observed where water accumulated and was channeled out to the surface, especially where burrow networks accelerated flows. Such response was observed between Stations TT 70 and 85 and TT 50 and 65, which corresponds to early seeps as shown on Figure 3-99. The spatial gap between these seeps and those appearing to the north in Figure 3-100 may be related to the sudden drop in elevation or lack of a Material 4 contact. Figure 3-111 shows the 5/25/12 seepage patterns overlain with the original location of blackberry at the site. Locations where macroporosity was observed correlate well to these areas. Though an extensive burrowing area was near the landside oak tree, the tree did not appear to play a significant role in the flow test.
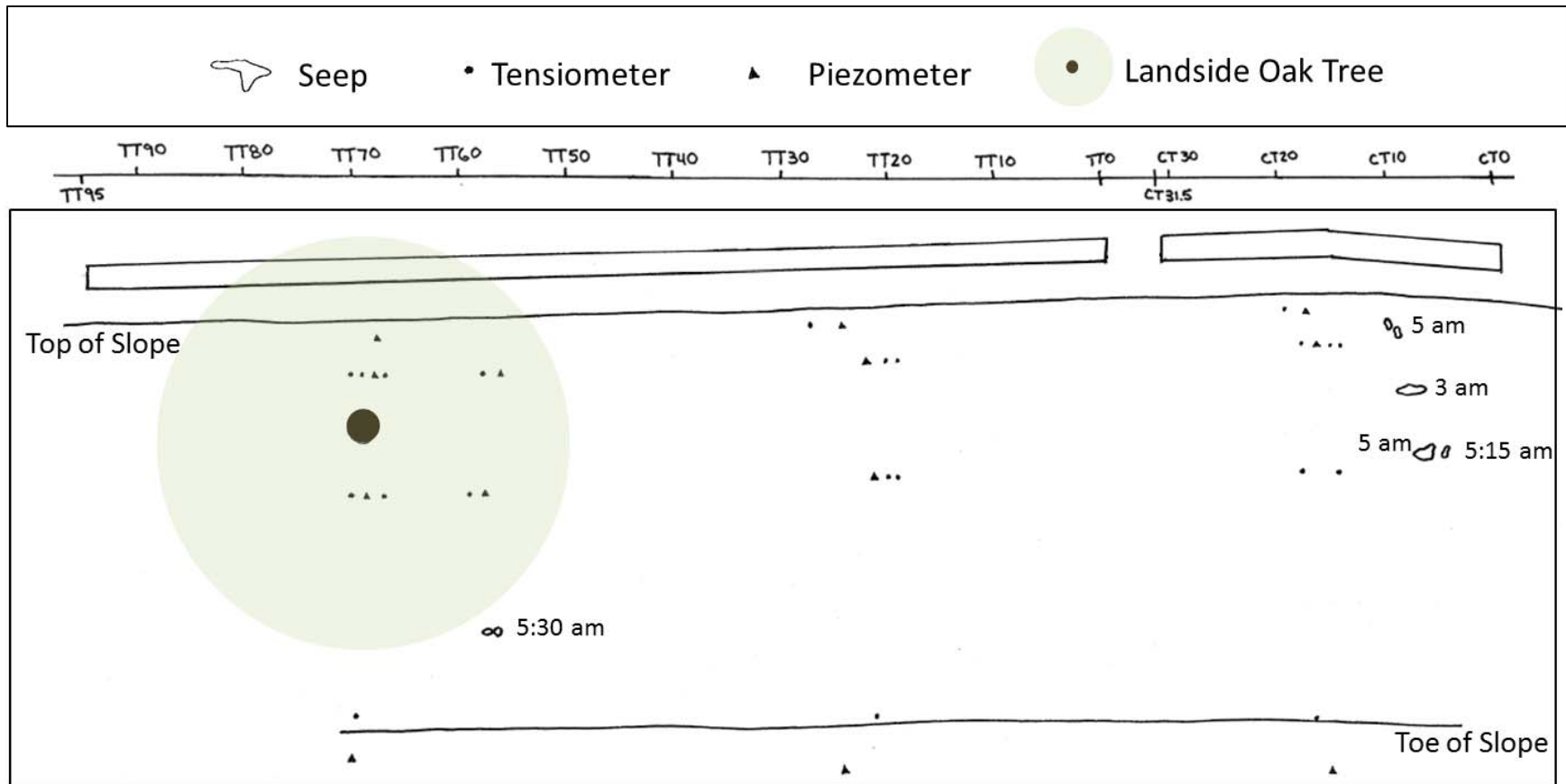
Figure 3-97. Sketch of landside seepage patterns: Time=15.8 hrs (5:30 am on 5/22/12). Time of seep appearance listed next to seep.

Figure 3-98. Time = 15.8 hours (5:30 am 5/22/13): Seeps at Line D (left), macropore flow near Line C (top right), and active gopher activity to north of control line (lower right).
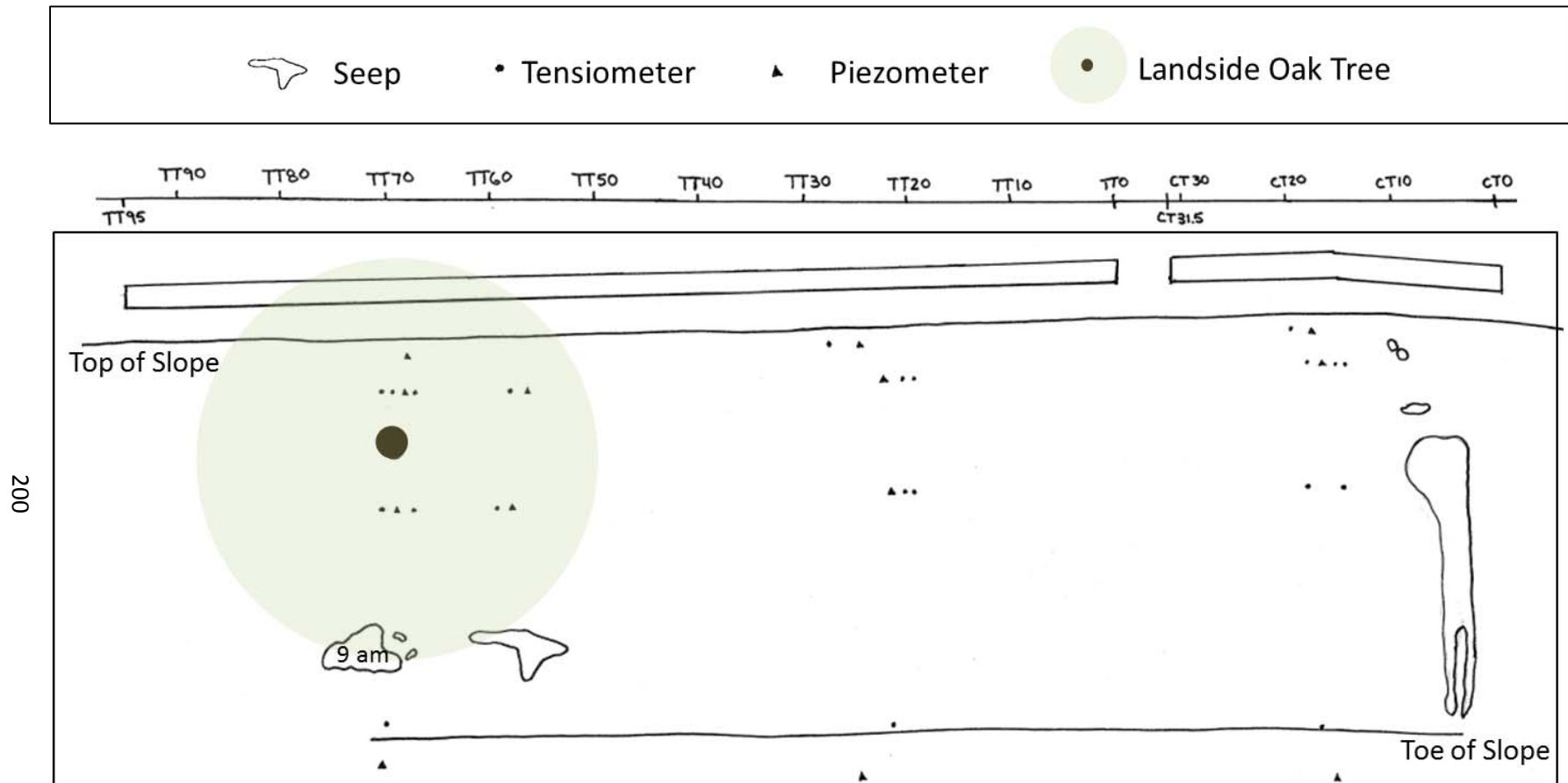
Figure 3-99. Sketch of landside seepage patterns: Time=20 hrs (9:45 am on 5/22/12).
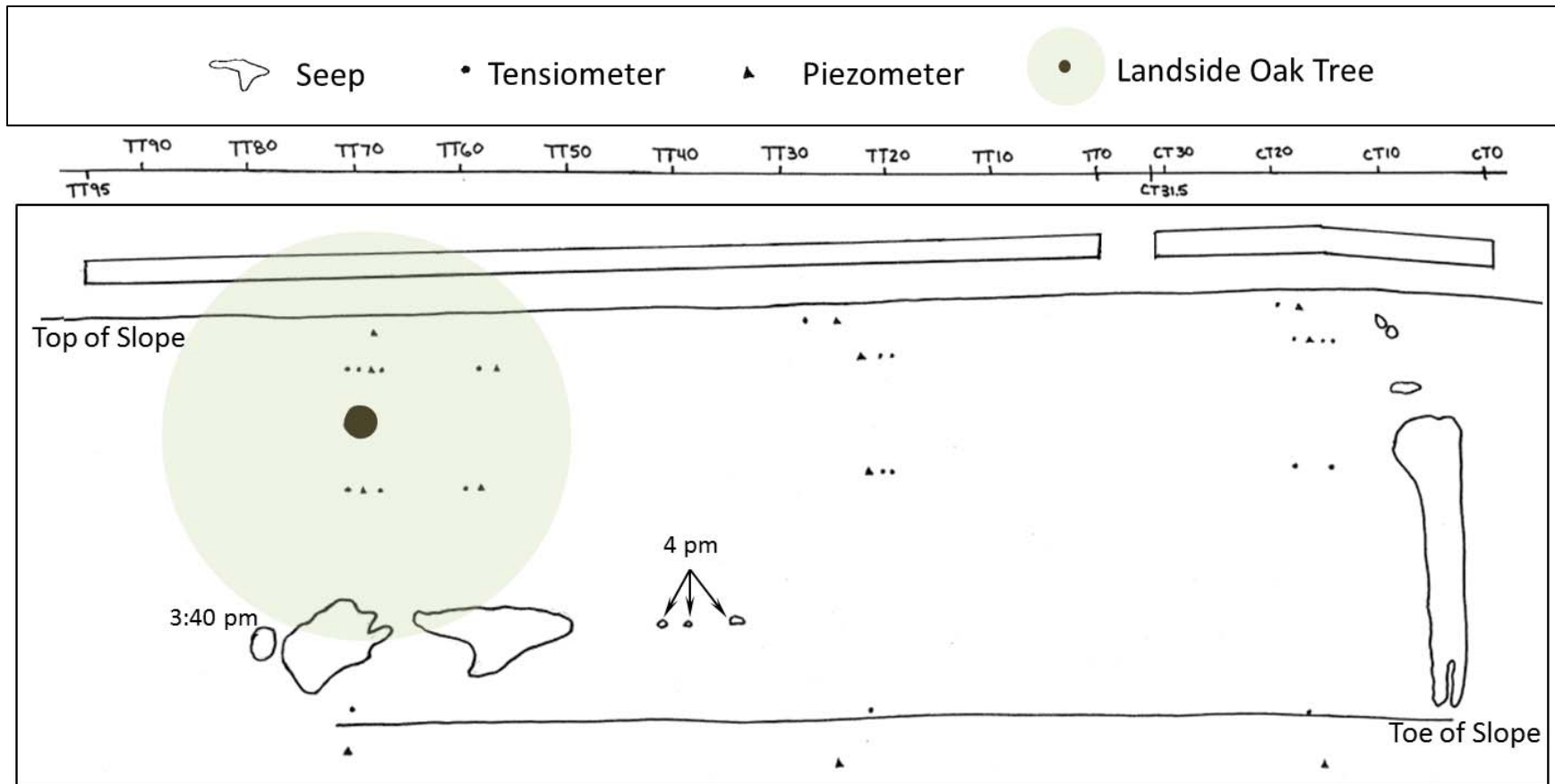
Figure 3-100. Sketch of landside seepage patterns: Time=26.3 hrs (4:00 pm on 5/22/12); Seep to the north of control line C has begun to produce less flow.
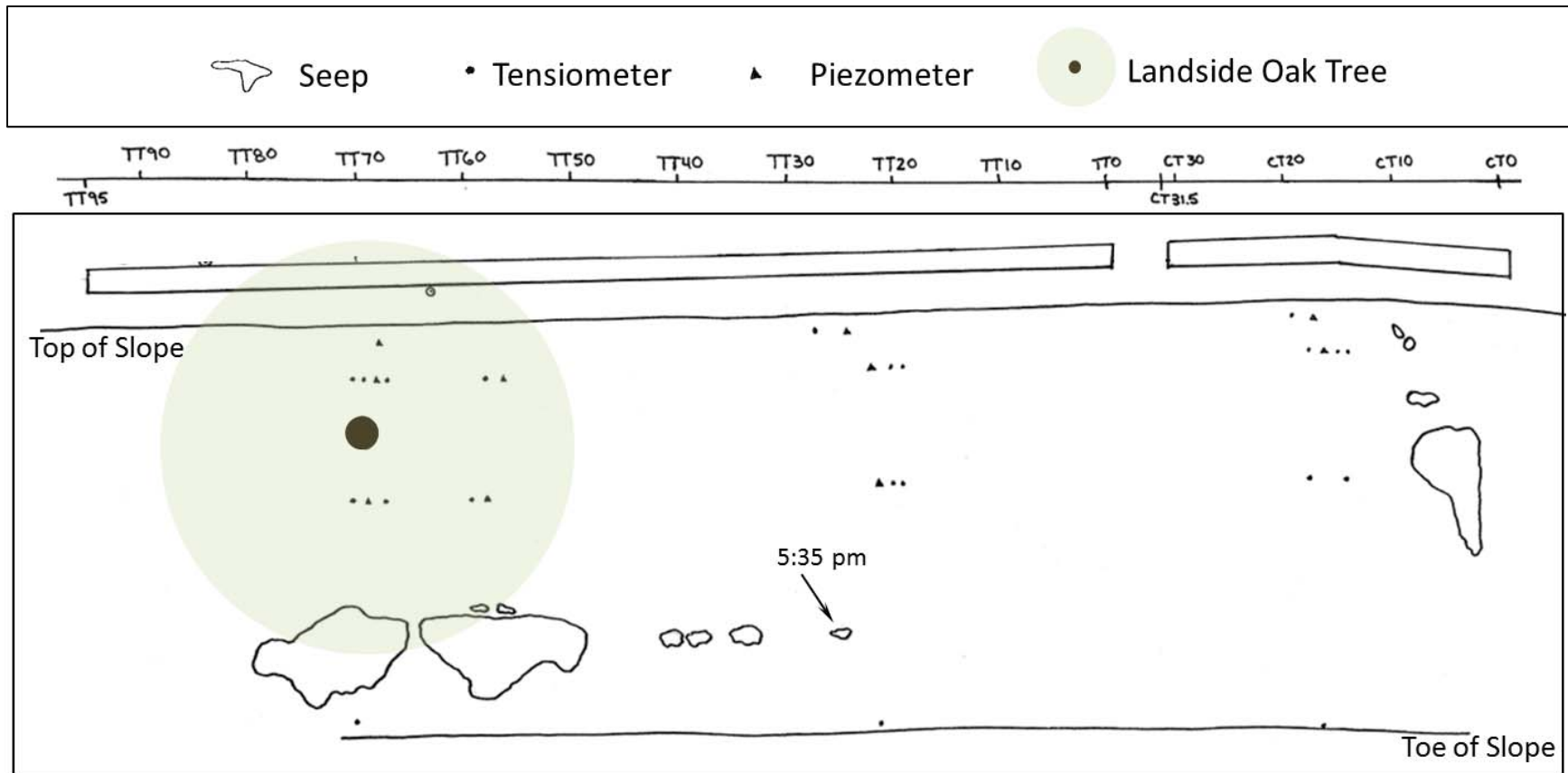
Figure 3-101. Sketch of landside seepage patterns: Time=28.3 hrs (6:00 pm on 5/22/12); Rills from seep to the north of control line C have begun to dry up.
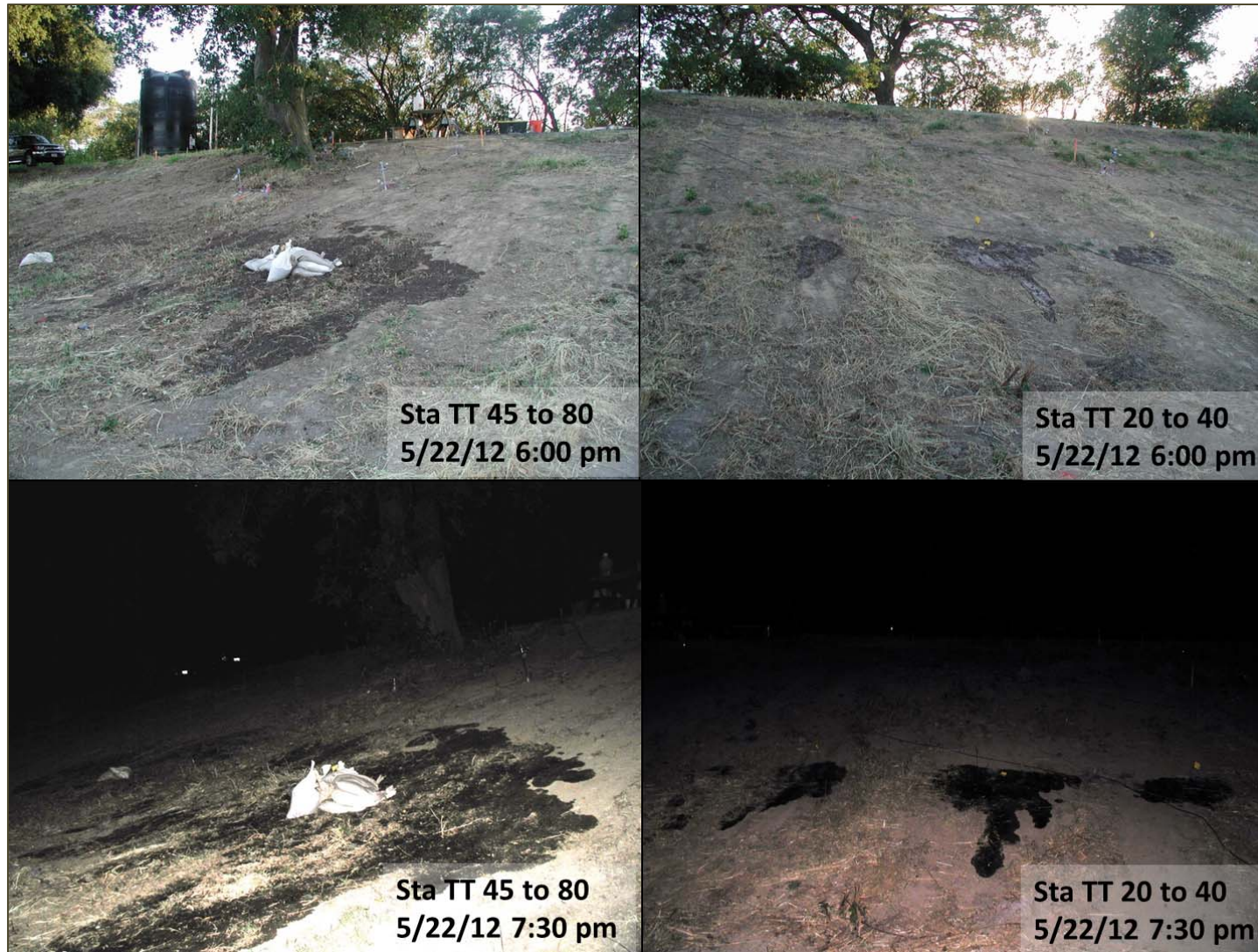
Figure 3-102. Time = 28.3 to 29.8 hours. Seeps continue to expand slowly, growing closer together with a small amount of free water flow from the newer seeps at Sta. TT 20 to 40 (right) as well as continued steady seepage from larger seeps at Sta. TT 45 to 80 (left).
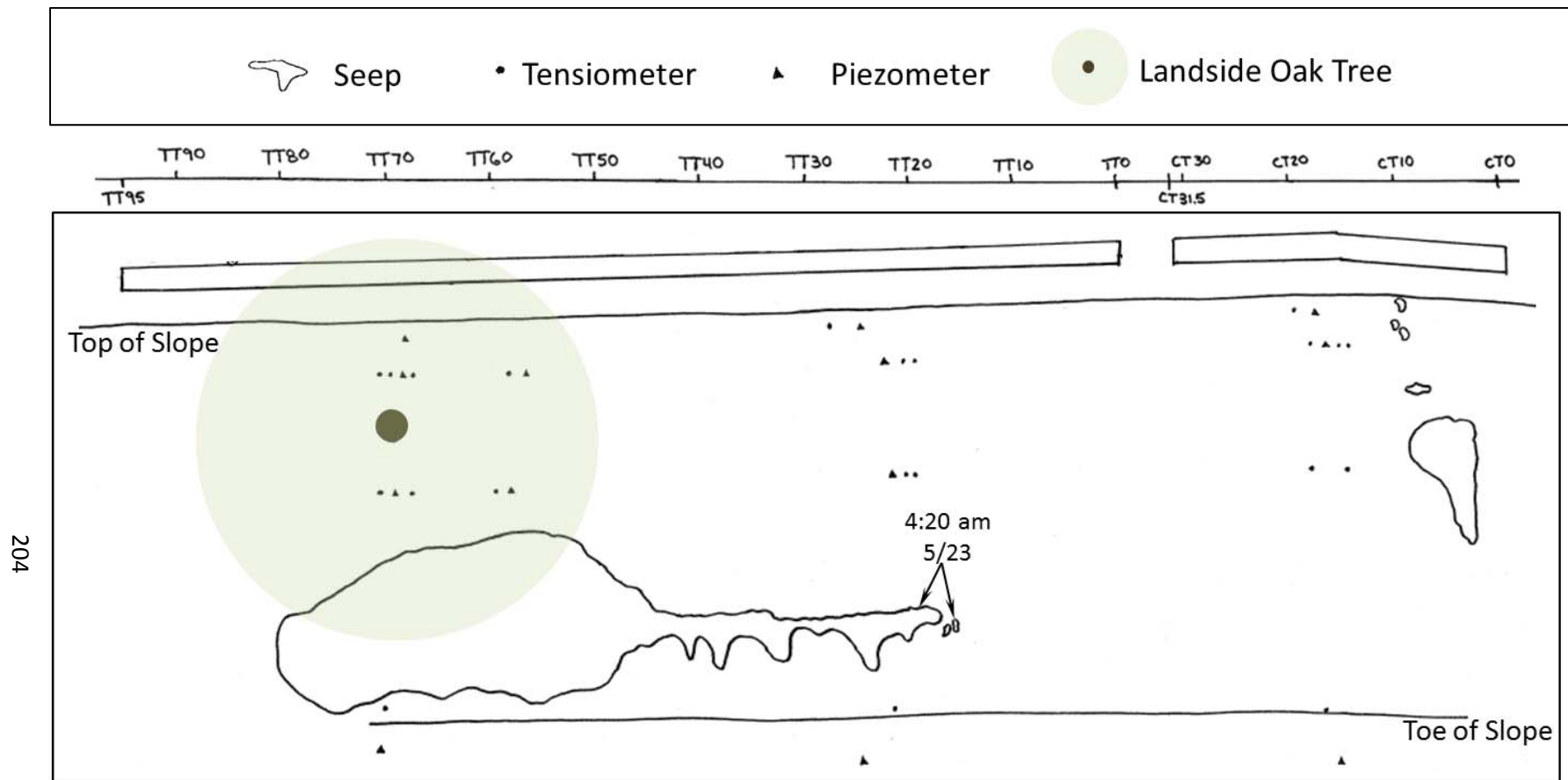
Figure 3-103. Sketch of landside seepage patterns: Time=43.8 hrs (9:30 am on 5/23/12).
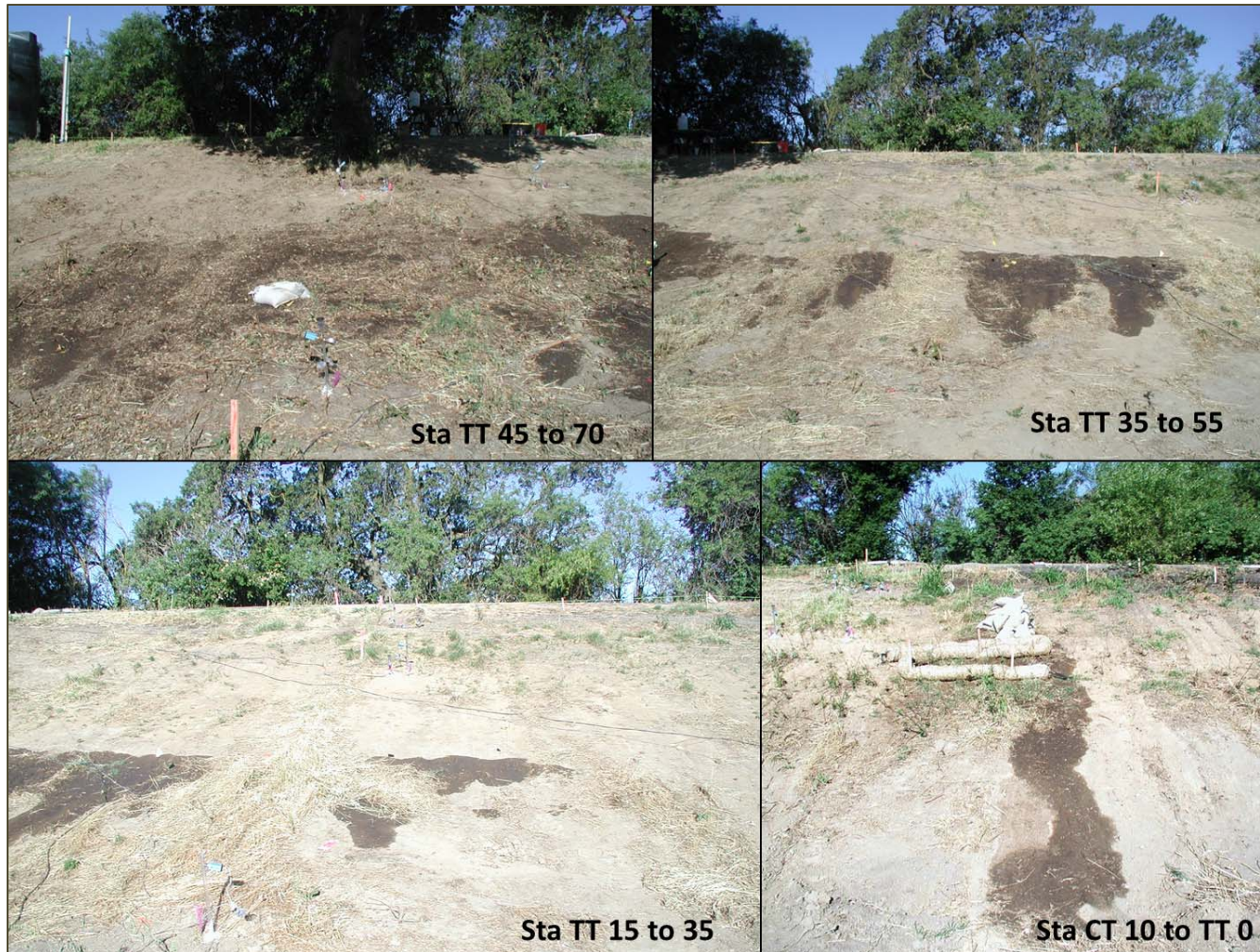
Figure 3-104. Time = 43 hours (8:45 am on 5/23/12) Seepage on the landside Line C has significantly slowed in concentrated flow at macropores. Notice the waterside oak looks different in this series (top right, lower left) – it had rotated 20 degrees into the slough and was discovered just after this series of photographs was taken.

Figure 3-105. Time = 43 hours (8:45 am on 5/23/12). In the vicinity of Stations TT 45 to 60, seeps are observed to be flowing from tiny holes on the order of ¼ to ½ inch in diameter (lower photos). Later exploration revealed worm burrows in these locations as discussed in subsequent sections.
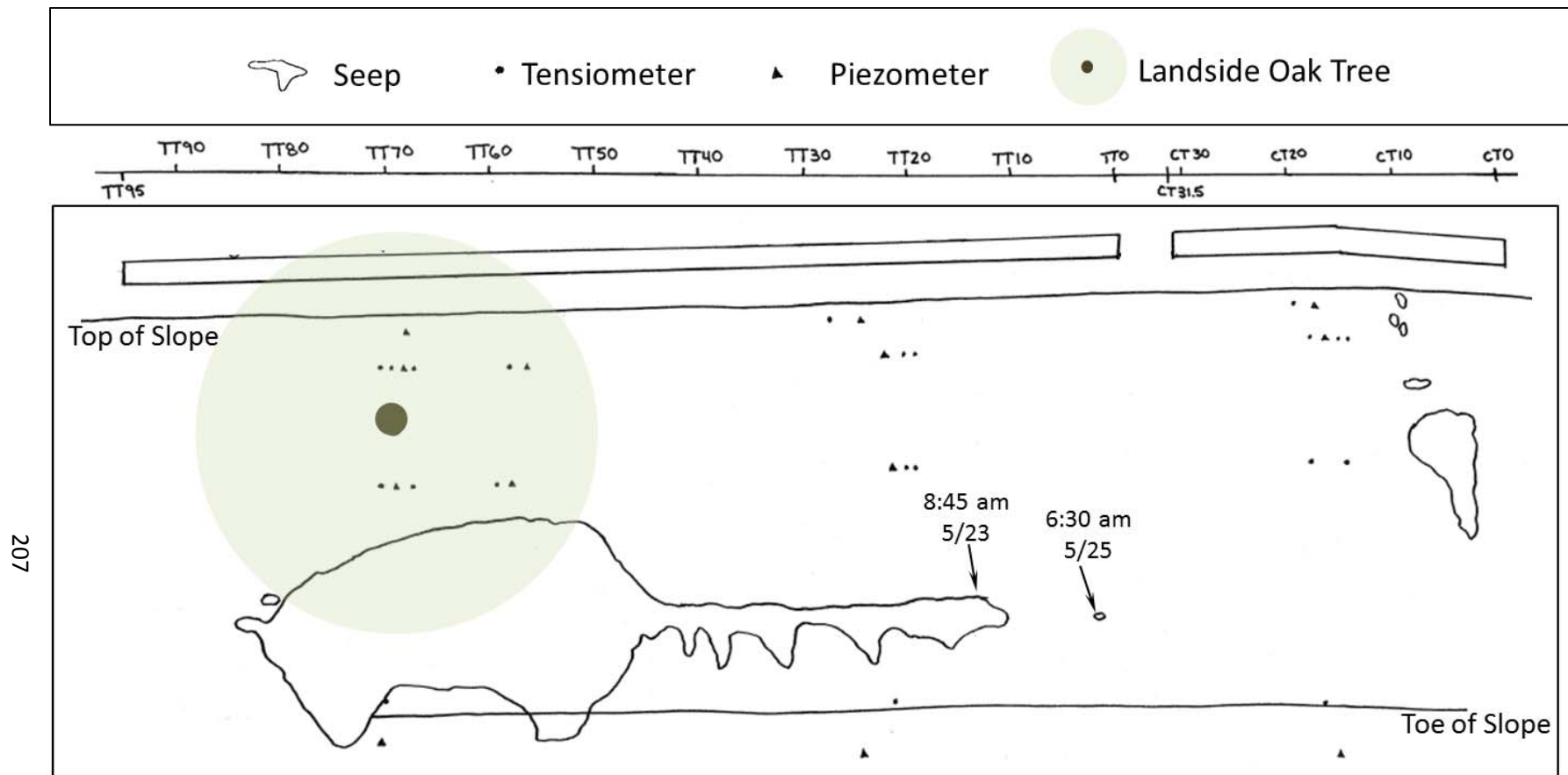
Figure 3-106. Sketch of landside seepage patterns: Time=92.8 hrs (6:30 am on 5/25/12).

Figure 3-107. Time = 93 hours (6:45 am on 5/25/12); Small new seep near Station TT 3 while seeps to the south expand.

Figure 3-108. Time = 93 hours (6:45 am on 5/25/12). View west of Stations TT 45 to 90 (top) and Stations TT 60 to CT 10.
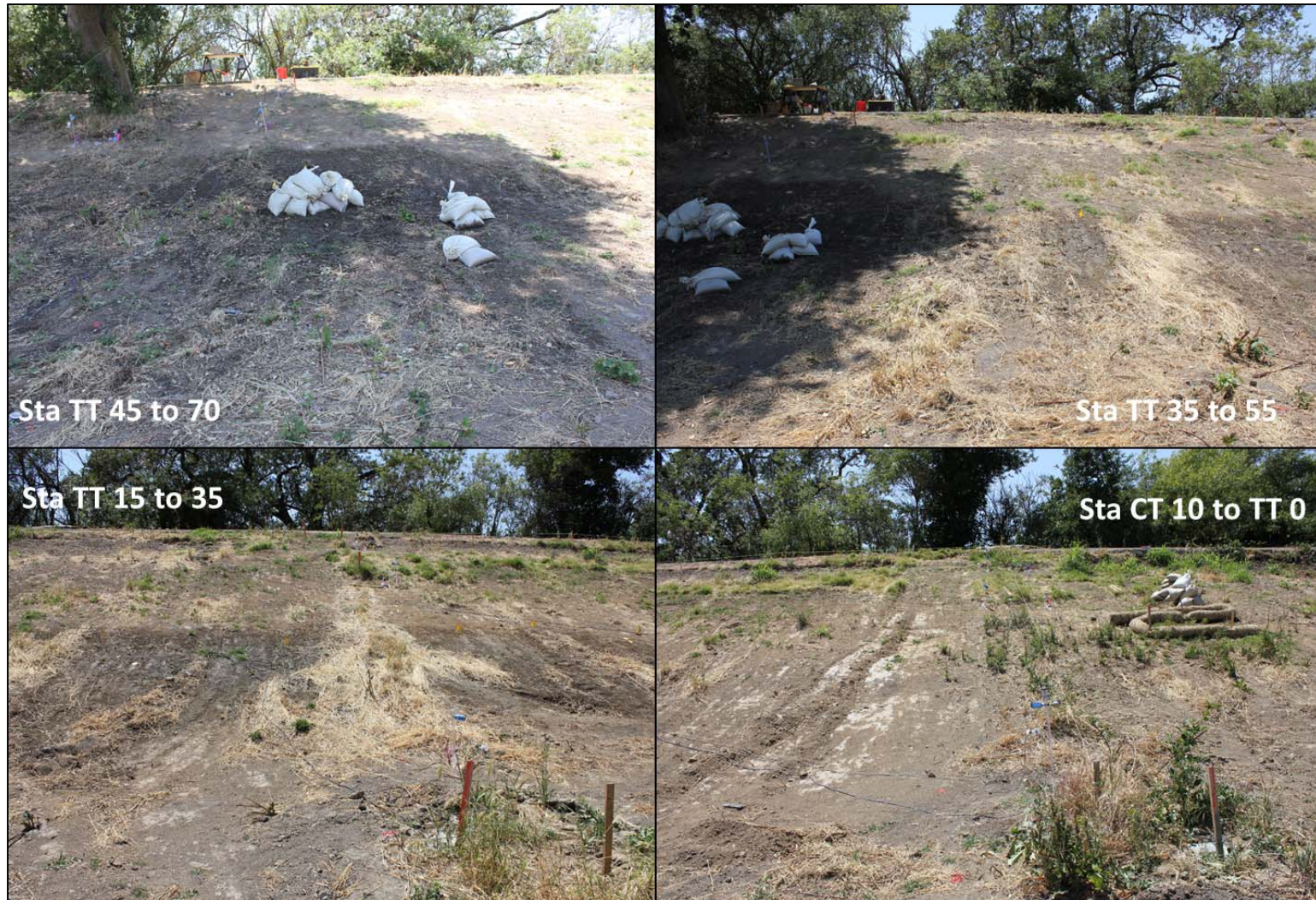
Figure 3-109. Time = 168.9 hours (5/28/12 at 2:35 pm). Tree trench was turned off on 5/25 at 1:45 pm and site has begun to dry up despite the fact that water has not fully drained from the tree trench. Note the blackberry vegetation beginning to grow back around the seepage areas north of instrument line C (lower right).

## Landside Trench Wall: Location of low permeability layer

Depth (ft)

TT90  TT80  TT70  TT60  TT50  TT40  TT30  TT20  TT10  TT0  CT30  CT20  CT10  CT0

CT31.5

0

(ML)

Material 4 (MH)

Material 4 (MH)

8

Top of Slope

8:45 am
5/23

6:30 am
5/25

Toe of Slope
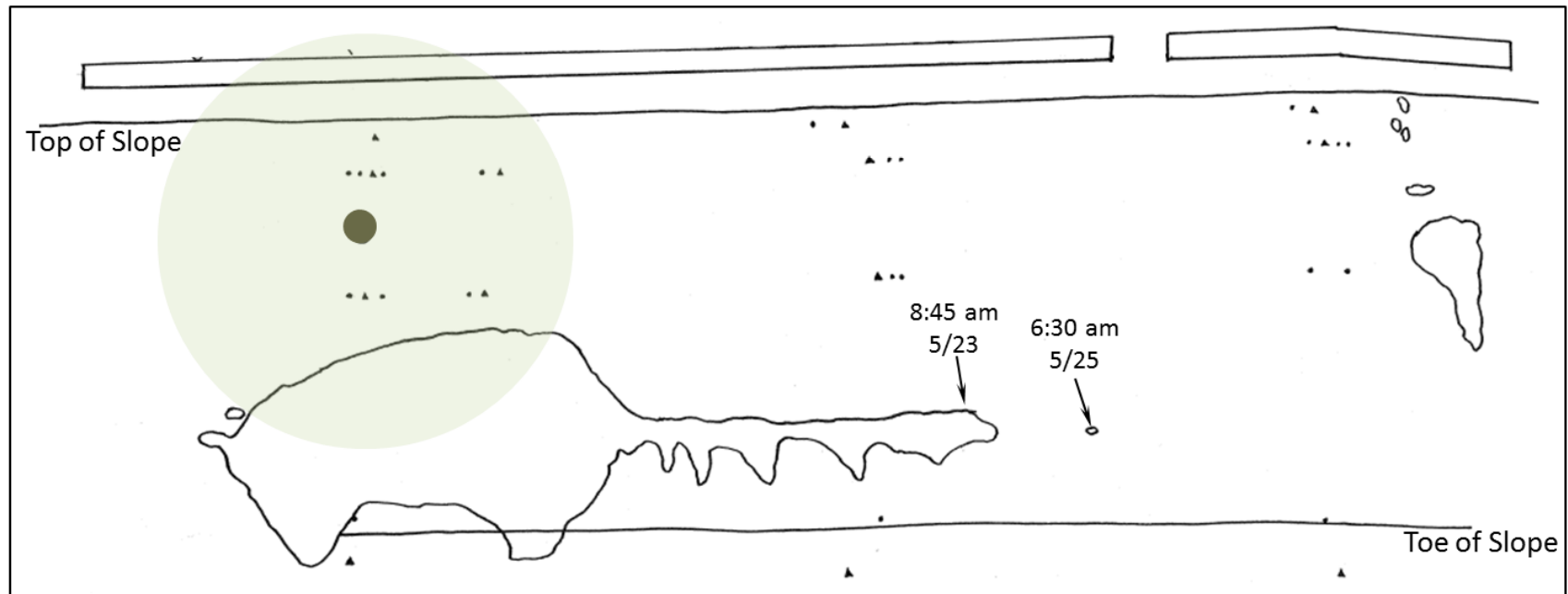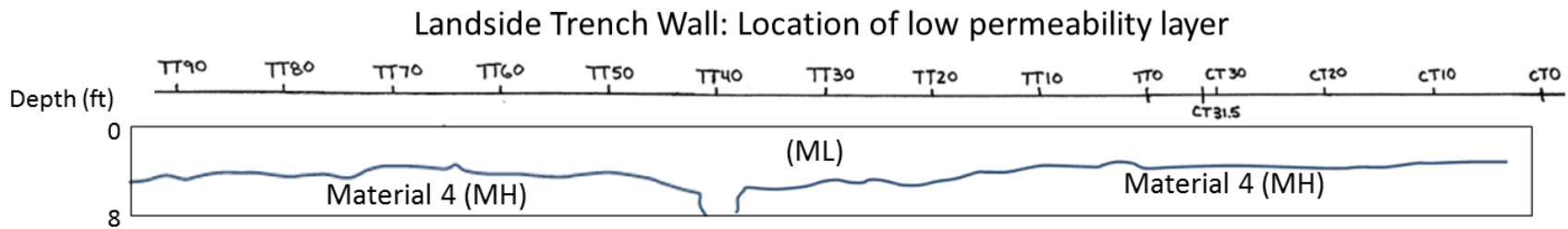
## Landside Seepage Patterns : Time = 92.8 hrs (6:30 am on 5/25/12)

Figure 3-110. Simplified trench wall log showing the pattern of Material 4, the plastic silt that may be acting as a low permeability layer. The contact begins to dip to the south at Station TT0, disappears below the trench bottom between TT 37 and 42, and dips from Station TT 50 toward Station TT 40.
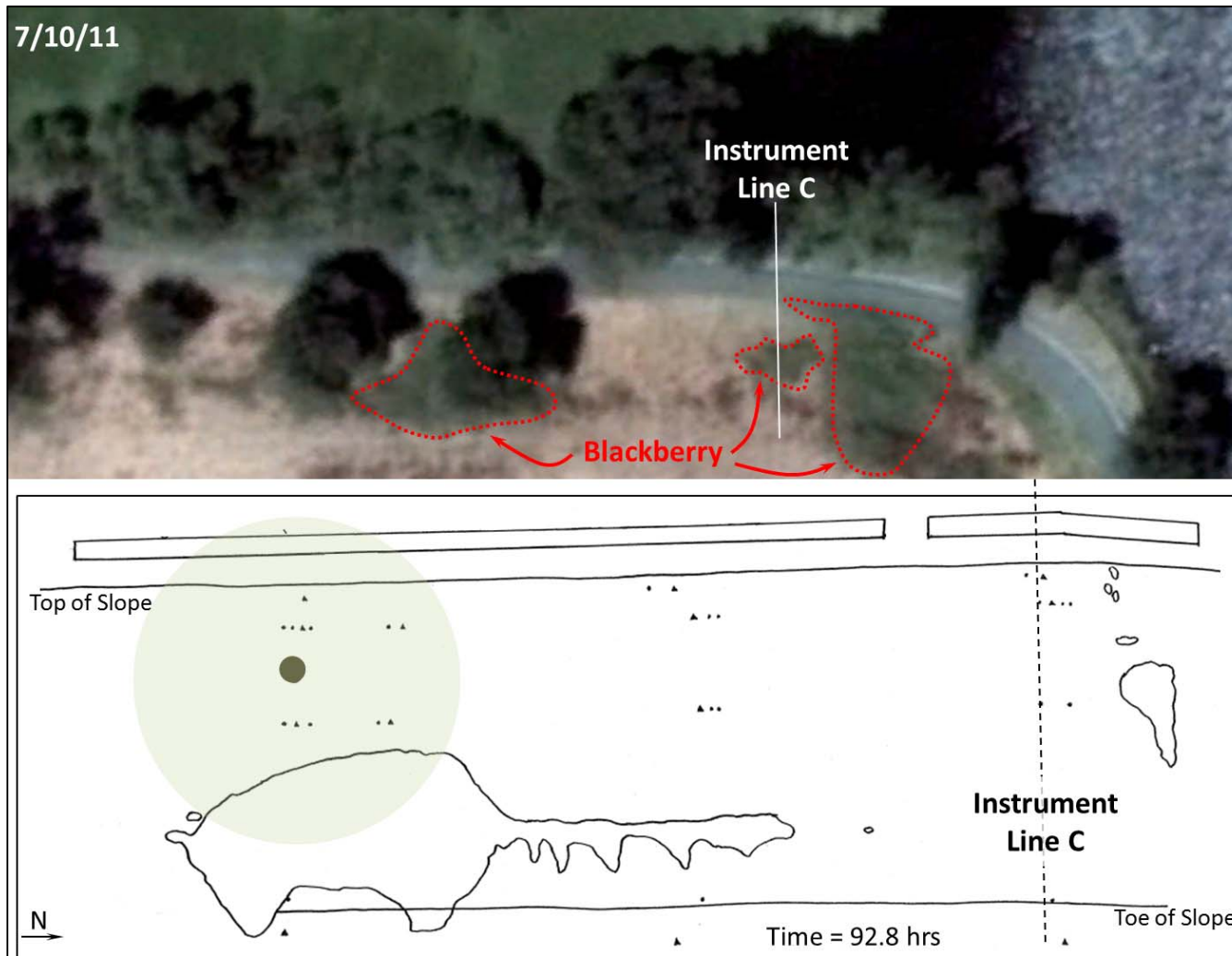
Figure 3-111. Seepage patterns at time = 92.8 hrs as compared with patterns of blackberry growth in the pre-test condition in July of 2011. Blackberry was dense in the locations indicated prior to our testing. Burrowing activity in areas north of the control instrument line C could be heard during the construction phase. Burrow activity was observed in both locations during trench construction.

### 3.1.4.2 Waterside: Seepage, Macroporosity, and Deformations

Deformations were observed at the site within the first 3 hours of flow and the first seep on the waterside, at the waterside oak, was observed about 9 hours into the test. Deformations consisted of those observed in pavements and slopes through observable cracks. Seepage records include those observed during the primary flow test. Access to the water side was limited due to high water levels during the flow test. Water levels were lower during the dye test (Section 3.1.4.3), allowing for a closer examination of seepage patterns and flow through macropores.

### 3.1.4.2.1 Pavement Crack Development and Monitoring

Figure 3-112 shows the location of a crack that appeared between the tree trench and the control trench less than 3 hours into the flow testing program. The crack continued to grow throughout the first day and began to develop a visible vertical offset by the end of the first day, about 9 hours into the flow test (Figure 3-113). Overnight, crack growth continued, reaching a maximum width of just under 0.6 inch and a vertical offset of $^3/_8$ inch at 13.3 hours into the flow test (Figure 3-114 and Figure 3-115).
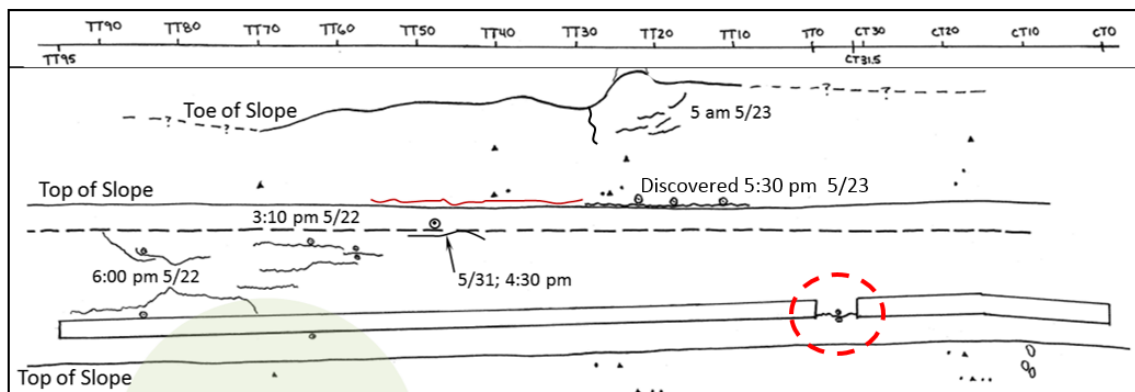


Figure 3-112. Cracking was observed in the pavement between the trenches (between Station CT 31.5 and TT 0) at 4:16 pm on the first day of the flow test (Time = 2.6 hours)

213
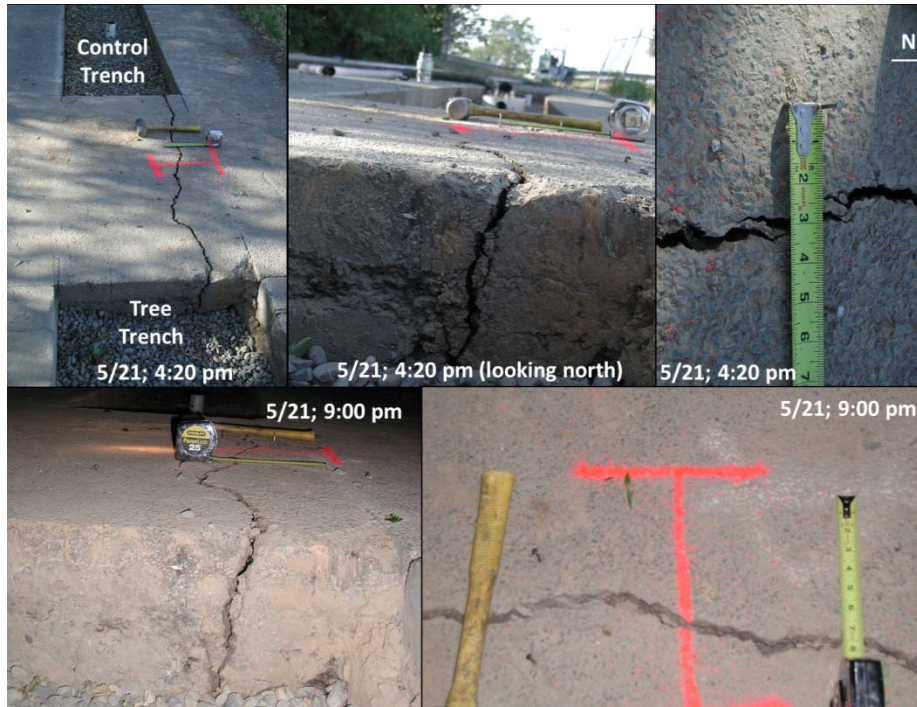
Figure 3-113. Cracking between tree trench on the first day of the field test (Time = 2.6 hours to 7.3). The crack grew and the waterside began to drop relative to the landside
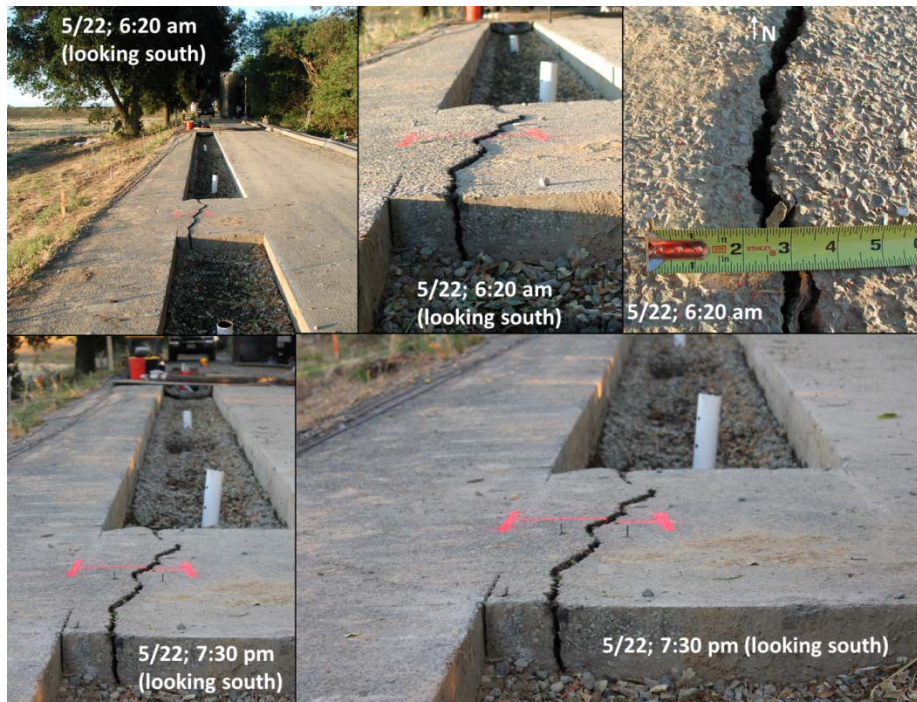


Figure 3-114. Crack between trenches on the second day of the field test (Time = 16 to 30 hours). The crack achieved maximum size early in the morning and began to shrink throughout the day
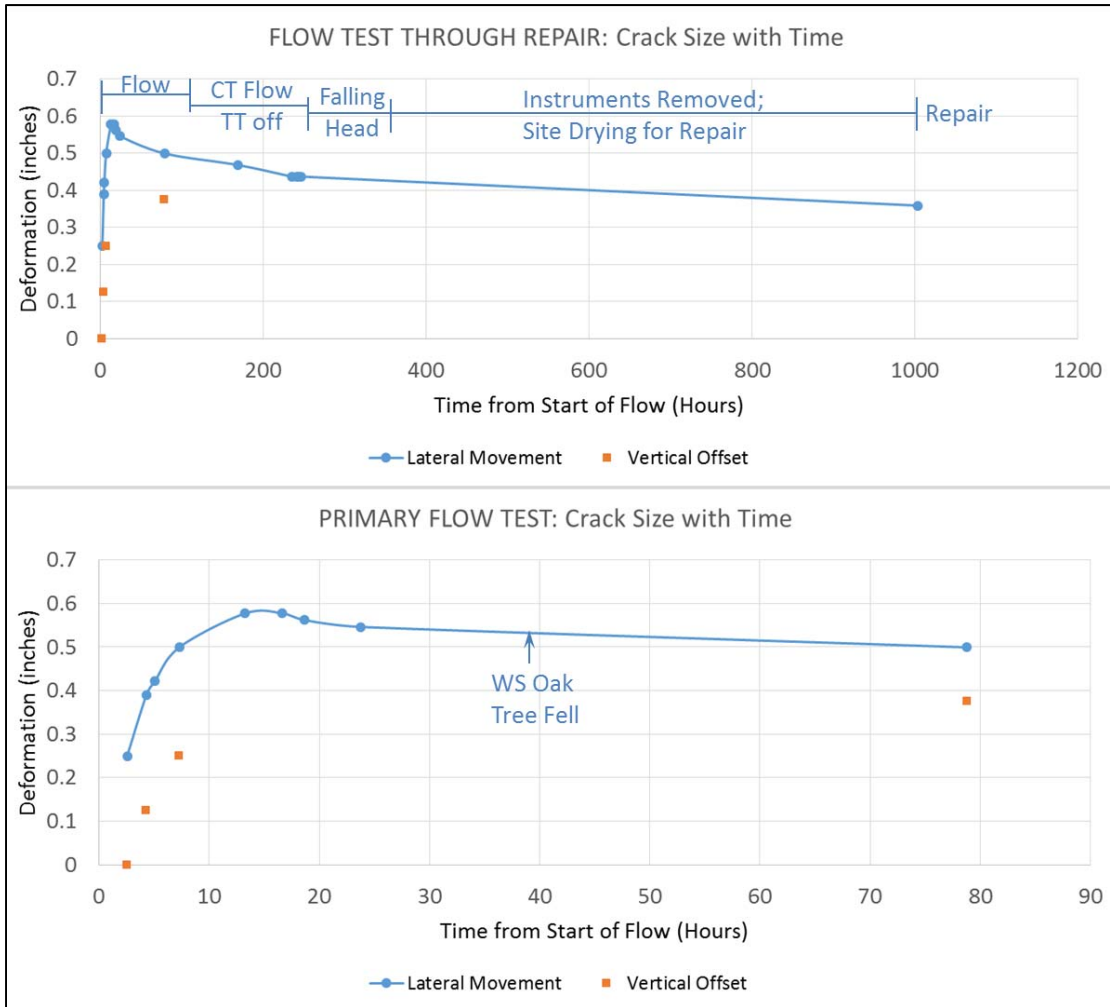
Figure 3-115. The size of the crack between the tree trench and the control trench was monitored as it grew to a maximum size and then began to get smaller. The crack peaked in size at about 13 hours into the flow test.

It was determined through analysis of photographs taken during construction that the crack may have been pre-existing. In Figure 3-116, the lower right photograph, taken after a rain, shows a dark spot appearing to be water in a crack in a location corresponding to the area moving during the flow test. The photo to the left shows the pavement, which looks like it may have an old crack in the appropriate location. Figure 3-117 shows a view of the cracking during the repair phase in July of 2012, after the flow test, as compared to the same section of pavement during trench construction. Based on the photo, the crack is more apparent on the control side than it is on the side of the tree trench. Further, in the photos, it appears as if the pavement has been overlain with a thick (approximately 6 inch) overlay. This type of overlay implies that the original pavement section was distressed, though implies nothing of the locations of the distress.
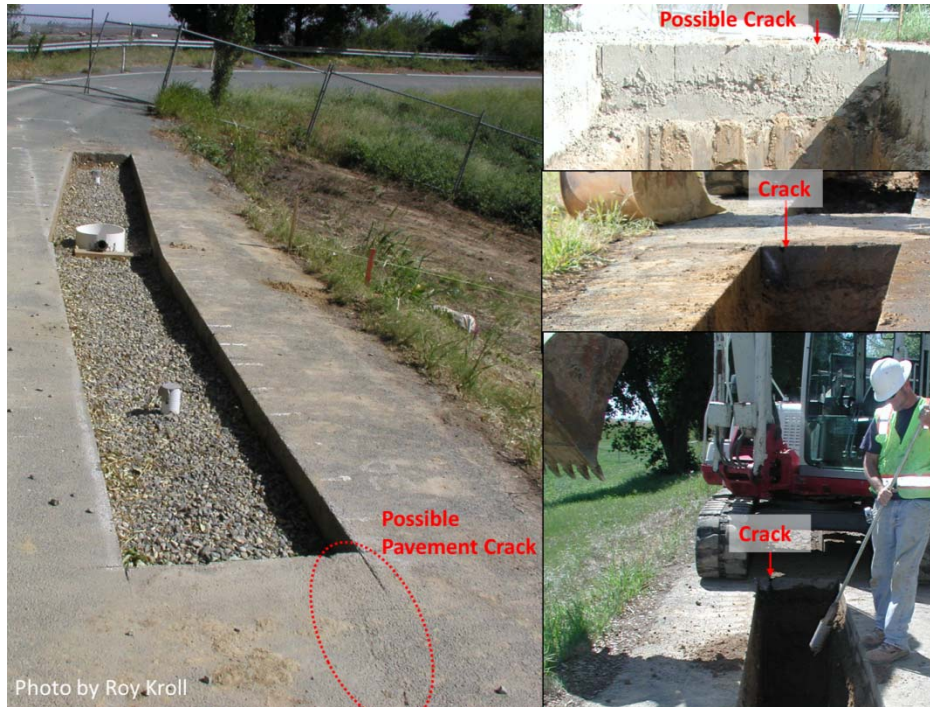
Figure 3-116. A crack may have existed between the trenches (left) prior to the flow test. Photos during trench construction show a clear crack on the control trench side (right middle and bottom) but it may not have extended to the tree trench side (upper right).
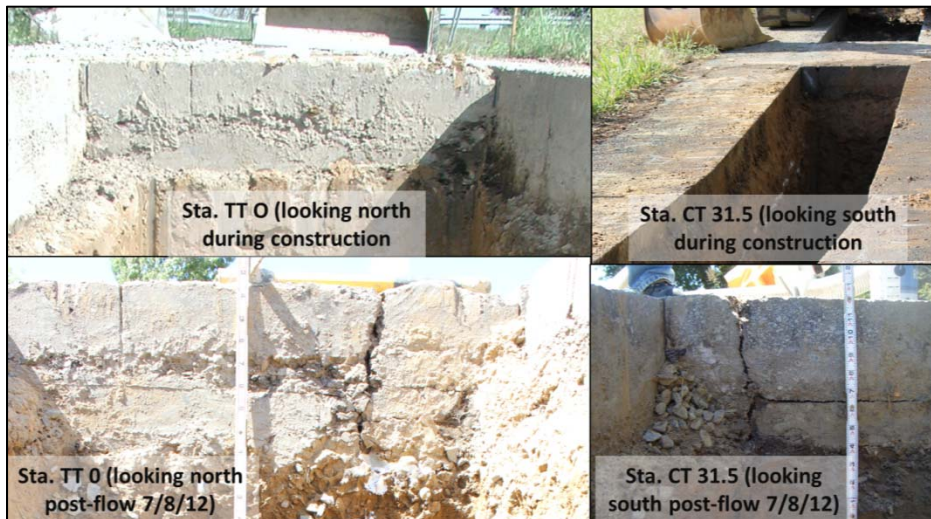


Figure 3-117. A close-in view of cracking in the asphalt between the trenches before (top) and after (bottom) the flow test. The pavement appears to have been overlaid as evidenced by the horizontal splitting of the lower section from the upper section (lower right).

In the afternoon of 5/22/12, a little over 25 hours into the flow test, a series of fine cracks opened up in the vicinity of Station TT53 to 73 ranging in size from hairline to $1/8$ inch (Figure 3-118). Monitors were installed (Figure 3-119) but did not yield measureable movements after the cracks were observed. The cause of the cracking was not entirely clear, as discussed later.

216
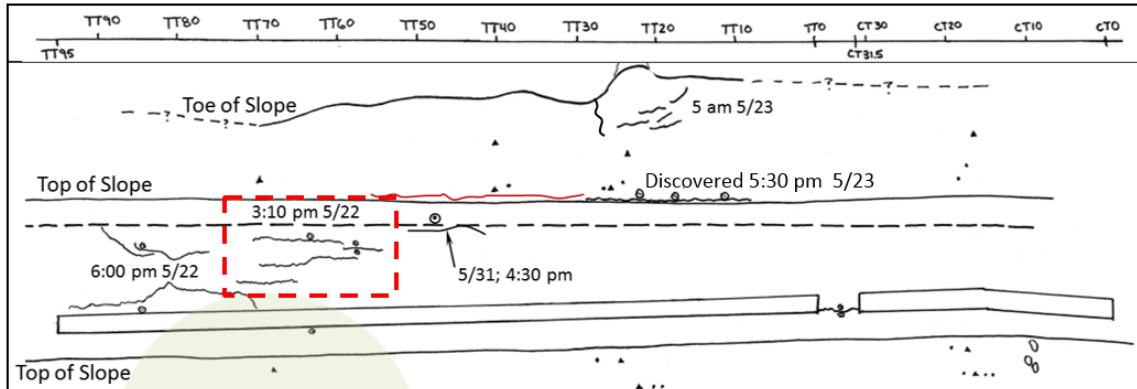
Figure 3-118. Cracking was observed in the pavements at approximate Stations TT 53 to 73 at 3:10 pm on the second day of the flow test (Time = 25.5 hours).



Figure 3-119. View of Stations TT 57 to 62 where cracking was observed in pavement 25.5 hours into the flow test. A monitor was installed at Station TT 58.5.

Figure 3-120 highlights cracking in the vicinity of Stations TT 70 to 95 first observed at 6 pm on 5/22/12, a little over 28 hours into the flow test. Cracking along the west side of the crown road appeared that it may continue into the waterside slope. Once the flow test was over, pipelines moved, and vegetation trimmed to allow for access, the area was inspected and a trace of the crack could not be found located (Figure 3-121).

217

The crack adjacent to the trench within this zone was first noticed during construction (Figure 3-120 and Figure 3-122). The crack may have been pre-existing, but grew during trench construction to have an offset of about $^3/_8$ inch before the flow test began (Figure 3-123). At the time of construction, there was a question as to whether the pavement had slid on the soils under equipment loading or if a segment of soil had moved with the pavement. Walls were cleaned and inspected along this segment of trench with special focus placed on the zones extending down the wall from where the cracks intersected the trench. Cracking extended a few inches into the soil and soils beneath appeared to be intact (Figure 3-123D and E). At a time of 28.3 hours into the flow test, signs of fresh movement were observable, though it was unclear whether movements were occurring towards the trench or whether the waterside block of soil was moving to the west.
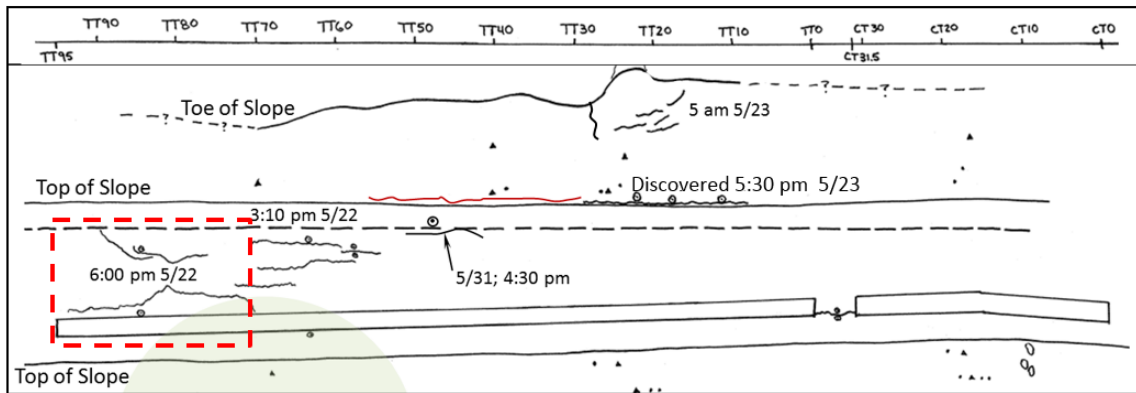


Figure 3-120. Cracking was observed in the pavements at approximate Stations TT 70 to 95 at 6 pm on the second day of the flow test (Time = 28.3 hours).

Figure 3-121. Waterside Station TT 85 to 90 on 6/8/12 after the tank, pipes, and wattles had been removed. Vegetation was locally cleared and the crack was not found extending outside of pavements.



Figure 3-122. Crack at Stations TT 70 to 95 seen through wide angle lens on 5/31/12 facing south. Cracking observed during original excavation but grew slightly (<1/8") during flow testing.

Figure 3-123. During trench construction Stations TT 70 to 95. A) Original crack appeared during 0 to 4 foot excavation but showed no offsets; B) During backfill with rock, 3/8" offset visible; C) Cracking may have been present before construction as it is seen on landside and waterside at Station TT 80-81; D) and E) Wall inspection at Station 70; crack not continuous down wall face.

Though the cause of movements between Stations TT 70 to 95 during the flow test is difficult to determine, Figure 3-124 shows this section during site repair after equipment loads collapsed the segment between Station TT 65 and 88. A clear failure plane is visible and in many locations the failure followed weak zones within the thinly bedded silt material (Material 2 as described previously) and along zones with dark staining appearing to be manganese oxides, commonly indicating previously existing fractures. Manganese oxide staining along fractures was discussed in an earlier description of materials encountered during trench construction. These stains were encountered throughout trenching activities, particularly in the most unstable wall sections. Dark staining can be seen in the overall wall failure photographs on Figure 3-124 with a close-in view on Figure 3-125.

Figure 3-124. Station TT 65 to TT 88 failed under equipment loading during repair. Dark staining appearing to be manganese oxides appear along the failure plane in numerous locations indicating possible pre-existing fracturing within the leve

Figure 3-125. Trench wall failure at Stations 65 to 88. Close in view at Station 75 shows fractures focused within weak zones of Material 2, thinly bedded sandy silt (top), and zones stained with manganese oxide, indicating previous fractures (bottom).

A crack of about $^1/_8$ to $^1/_4$ inch in size opened between the water delivery pipelines between Stations TT 40 and 52 on 5/31 in the afternoon of the dye test just a couple of hours before the end of the test (Figure 3-126 and Figure 3-127). A crack monitor was installed and the crack was inspected several times post-flow, displaying no additional movements.
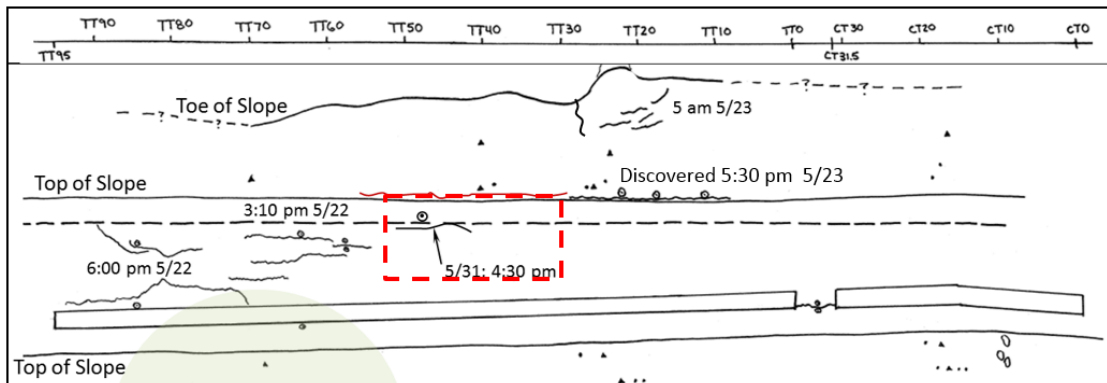


Figure 3-126. Cracking was observed in the pavements at approximate Stations TT 40 to 52 at 4:30 pm on 5/31, the last day of flow (Time = 242.8 hours)

Figure 3-127. Crack discovered on 5/31/12. No additional movement was recorded on the monitoring device (Stations TT 40 to 52).

3.1.4.2.2    Water Side Oak Tree, Slope Deformation, Seepage, and Burrows

On 5/23/12, the third day of the flow test, between about 4:45 am and 8:00 am (39 to 42.3 hours into the flow test), the waterside oak tree rotated approximately 20 degrees toward the oxbow section of the Sevenmile Slough, leaving a set of slope cracks that were apparent upon morning inspection of the site (Figure 3-128 through Figure 3-130). The likely time of the fall is somewhere between 5 and 5:30 am based on instrument data (discussed in subsequent sections). Figure 3-131 shows the study site from a distance before and after the tree fell.
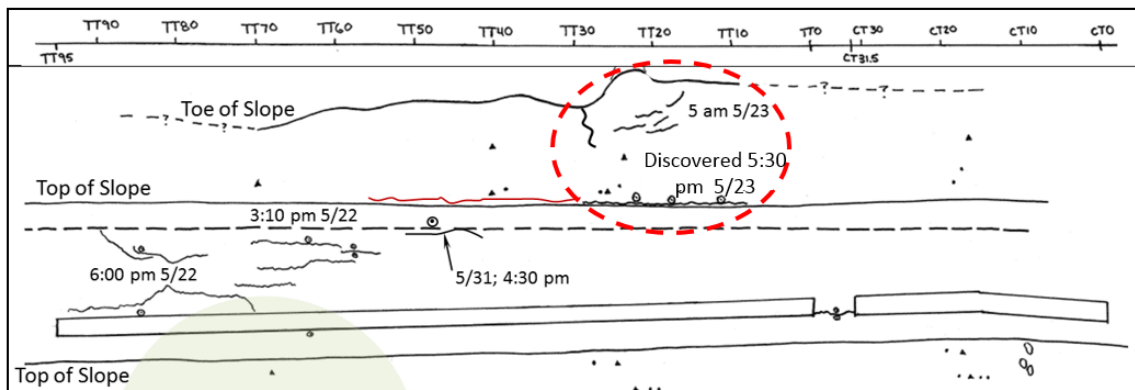


Figure 3-128. On 5/23, the third day of flow, the waterside oak tree was found to have fallen between 4:45 and 8 am (Time = 39 to 42.3 hours). Based on instrument readings, this may have been at about 5:00 to 5:30 am.
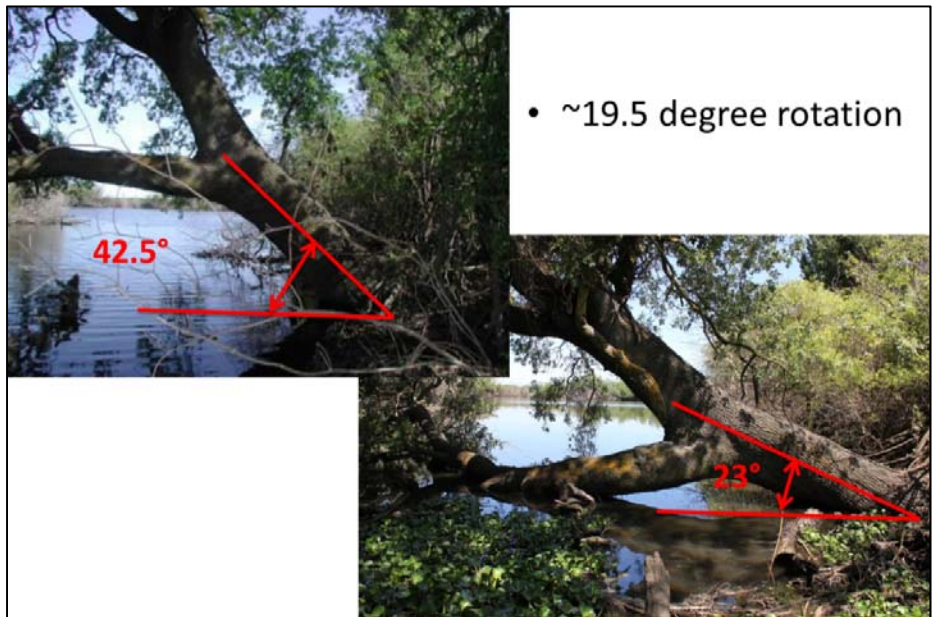
Figure 3-129. The waterside oak rotated just under about 20 degrees to rest the long waterside branch in the shallow oxbow section of the Sevenmile Slough.



Figure 3-130. The fallen waterside oak photographed from land (left) and the water (right).

Figure 3-131. View of the site from a distance showing the waterside tree before (top) and after (bottom) it had fallen.

A stake was placed in the slough just north of the waterside oak tree prior to the beginning of the flow test and was photographed periodically to track small variations in water level throughout the test. Based on discussions with the operator of the gate structure controlling flows into the Sevenmile Slough, the water levels typically vary not more than 2 feet but are based on tides and water uses of the local residents (as discussed under section titled Site Description). Gates are opened at high tide and closed as the tide retreats, trapping water for use by residents and farmers of Brannan and Twitchell Islands. As seen on Figure 3-132, the water level was relatively constant on 5/21/12 and 5/22/12 with an approximate water depth at the stake of 6 to 7 inches. The water level appears to have risen 5 inches to a depth of 11 inches by 4:30 am the morning of 5/31/12, just before the tree failure. The role that water level may have played is unclear, but saturation of the slope can soften soils and reduce strengths (Duncan and Wright, 2005), as discussed later.

Figure 3-132. The water level in the slough had been about 6-7 inches deep prior to the failure. In the last photograph taken before the tree fell, the water level in the slough has risen 5 inches overnight.

Figure 3-133 through Figure 3-135 detail the deformation of the waterside slope that are believed to be directly associated with the movement of the waterside tree. Large cracks, one displaying about 12 inches of vertical offset, were present in the loose soils on the pathway leading down to the waterside tree, directly around the root ball (Figure 3-133). Figure 3-134 shows a view of these cracks taken from the fallen tree looking east at the levee access road, including a sketch of cracking found to the south of the tree. Figure 3-135 provides a detailed view of this cracking as well as a sketch of the approximate location. As shown on Figure 3-128 as well as Figure 3-134 through Figure 3-138, a crack was uncovered at the top of slope, running parallel to the levee just off the paved crown road. A small blackberry bush marked the end of the fresh crack and where an old crack extended along the same alignment, not displaying movement in this event (Figure 3-137). The fresh crack intersected the grout of a piezometer that was installed prior to testing (Figure 3-138).

The size of the crack along the top of slope was initially 1 to 1 ½ inches in width at the time of discovery and was monitored for changes in size throughout the remainder of the flow test and repair effort with results presented as Figure 3-139. The crack grew throughout the primary flow test (ending at about 96 hours from the start of flow) and either retreated slightly or stayed the same size once the water to the tree trench was turned off. The crack began to grow again during the dye test, but all segments of the fresh crack had reduced in size at the time of repair in July of 2012.

Figure 3-133. The fallen waterside oak as seen from the crown road (left and upper right) and the access path to the water at instrument line E.
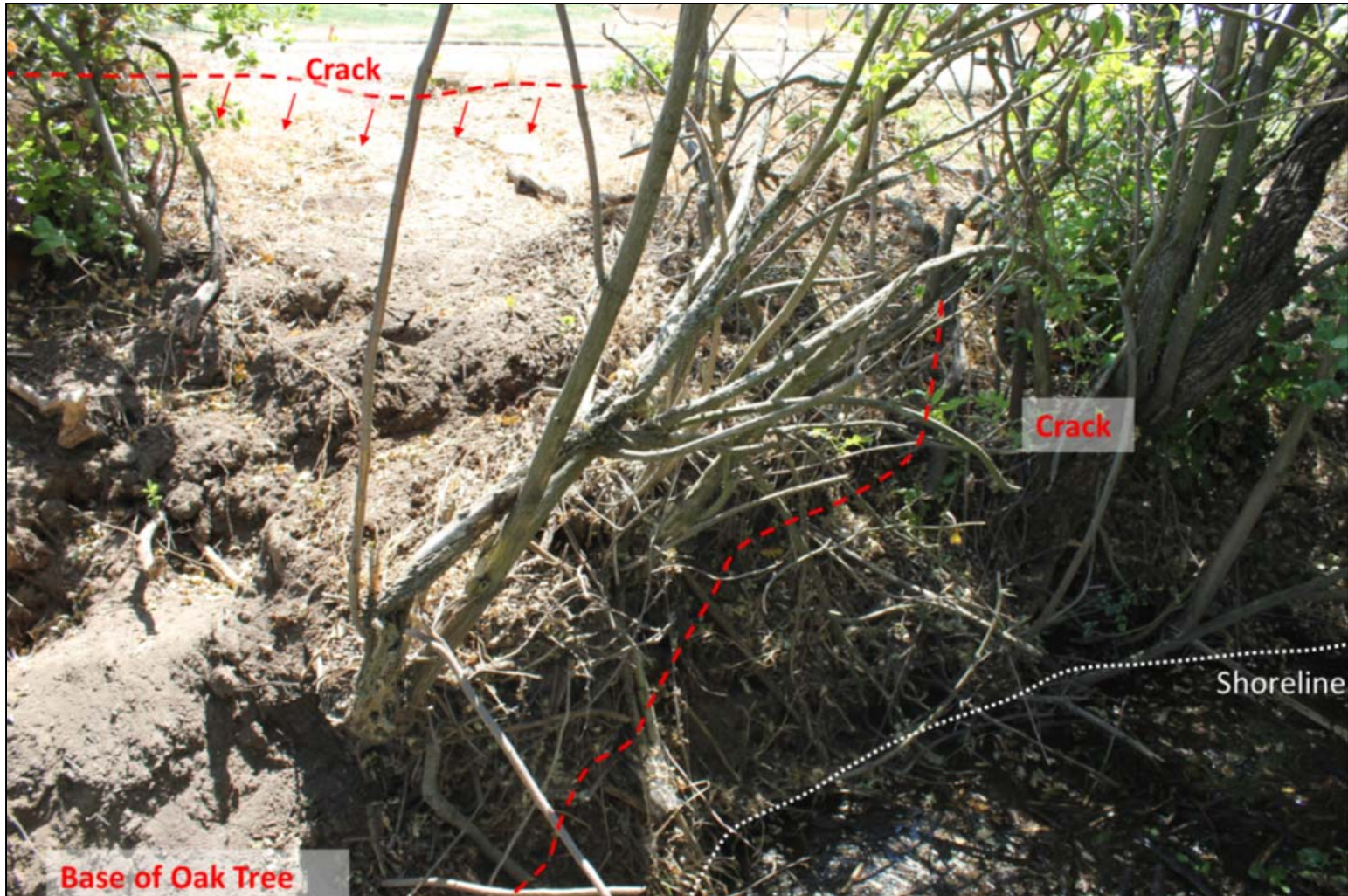
Figure 3-134. View of from the fallen waterside oak showing cracking patterns at the base of the tree and at the top of the slope.
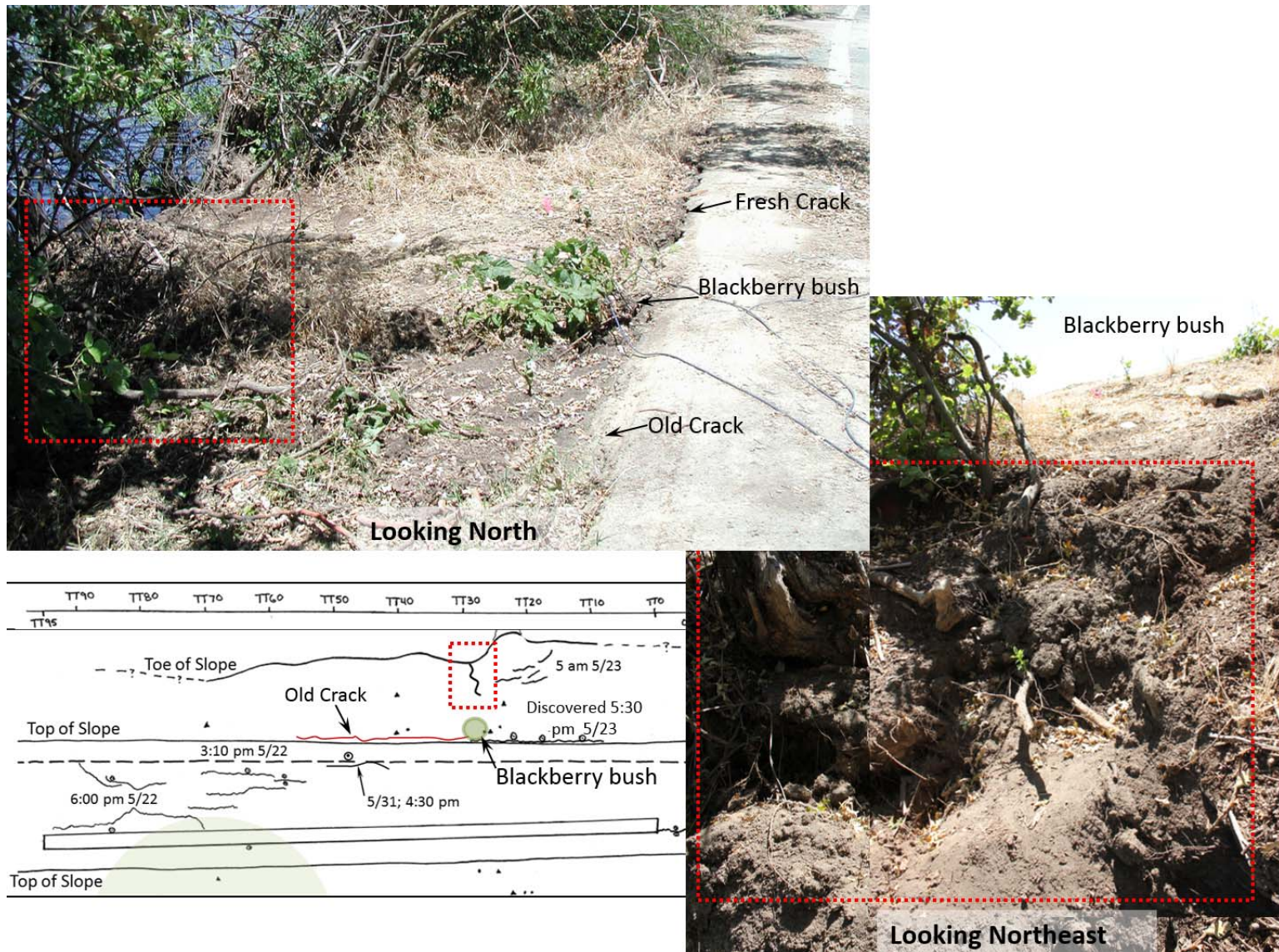
Figure 3-135. A view of the cracking within the loose waterside soils surrounding the fallen tree (right). Surficial excavation did not reveal a connection between this crack and cracking at the top of slope (upper and lower left).

Figure 3-136. In the afternoon of 5/23, during a visit from Dr. Les Harder of HDR, a fresh crack was revealed along the top of slope, previously concealed by leaves and an erosion control wattle.



Figure 3-137. A blackberry bush is the transition point between the fresh crack (left) and an older crack (right).

Figure 3-138. The grout of piezometer PB1 is intersected by the crack at the top of slope at the waterside oak.
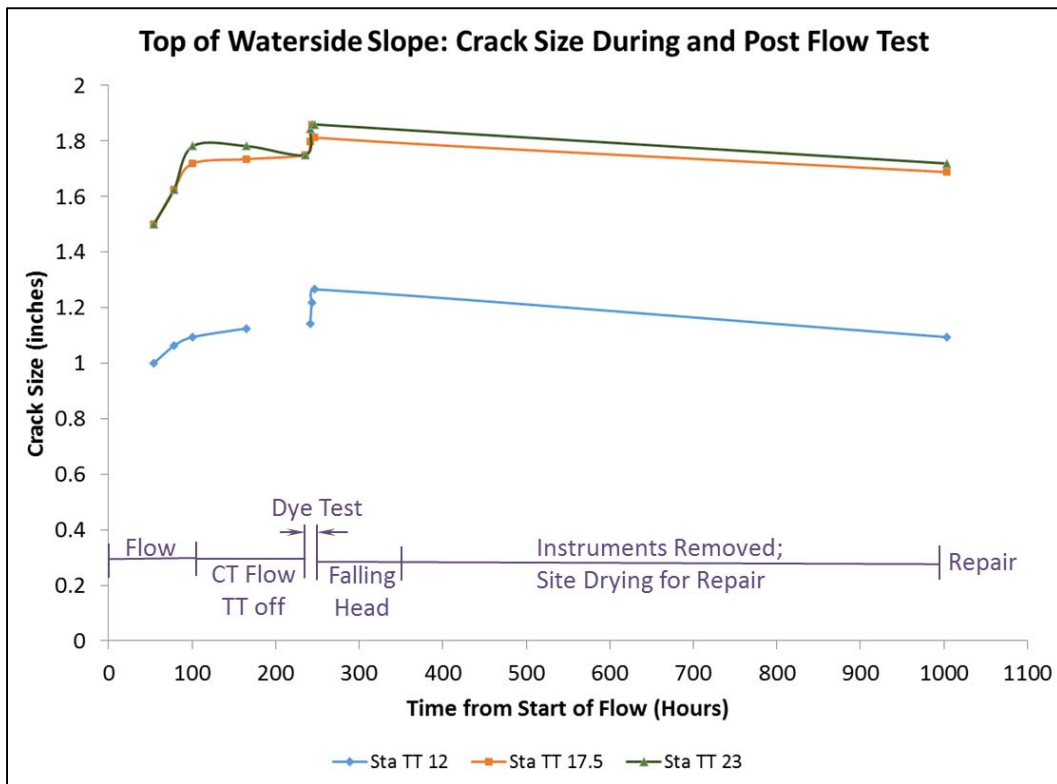


Figure 3-139. The crack at the top of the waterside slope was discovered on 5/23/12, the day the tree fell. The size of the crack was monitored throughout the flow test and just prior to repair.

An old crack was discovered extending along the top of slope just south of the actively moving top of slope crack as shown on Figure 3-140. The crack began at the southern end side of the blackberry

bush shown on Figure 3-135 and Figure 3-137. Dead vegetation was found growing out of portions of it (Stations TT 49 to 55) as shown on Figure 3-141. Crack widths ranged from ½ to ¾ inch on this segment. Other segments appear to be little more than distressed pavement at the edge of the road (Figure 3-141), but showing small amounts of lateral offset toward the waterside (on the order of ½ inch or less). Fresh movement was not observed in these cracks during or in the weeks following our flow test.
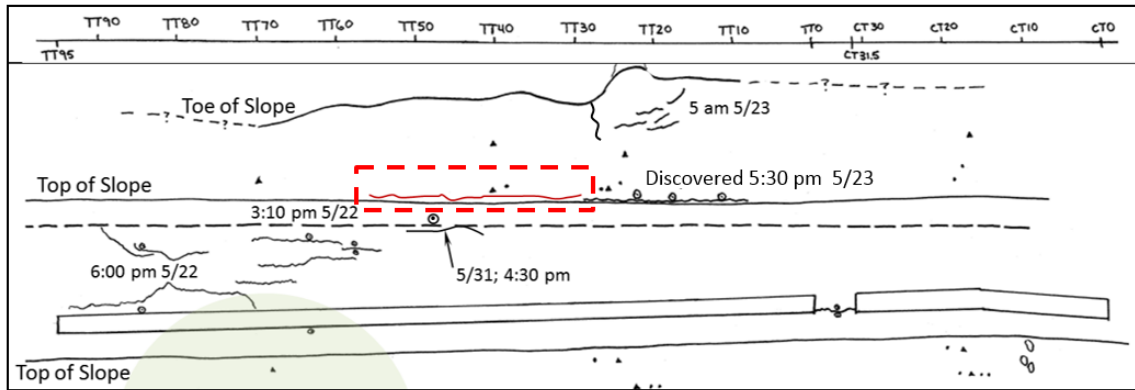


Figure 3-140. A crack at the top of slope (Stations TT 30 to TT 55) was found on 5/25. The crack did not exhibit signs of recent movement but rather is evidence of past deformation.



Figure 3-141. An older crack at Stations TT 30 to 55. Note dead plants rooted into the crack. Seepage at the waterside oak tree was the first location that moisture was observed coming out of the slope at approximately Station TT 20. The seep was first spotted at 10:40 pm on 5/21/12, 9 hours into the flow test, at the location shown on Figure 3-142. By 6 pm the following day, nearly 29

hours into the flow test, seeps were encountered at Station TT 13 (just north of waterside oak) and TT 24 (just south of waterside oak). These seeps were coming from burrows that had been identified as likely muskrat burrow entrances during a visit by Dr. Van Vuren. Photographs of these burrow entrances are shown on 5/2/12 (the day of the walkover with Dr. Van Vuren) and on 5/23/12 at 1:40 pm, 48 hours into the flow test (Figure 3-143). The rate of flow within the burrows had slowed from the day prior, particularly the burrows to the south of the tree at Station TT 24.

Figure 3-144 shows the first seep, located at the waterside oak tree, just prior to the movement of the tree, as compared with photos of that location approximately 12 hours after the tree failure. The seep at that location appears to have subsided or the path of water outlet changed due to the tree movements. Water was not observed to seep from that location for the remainder of the experiment.
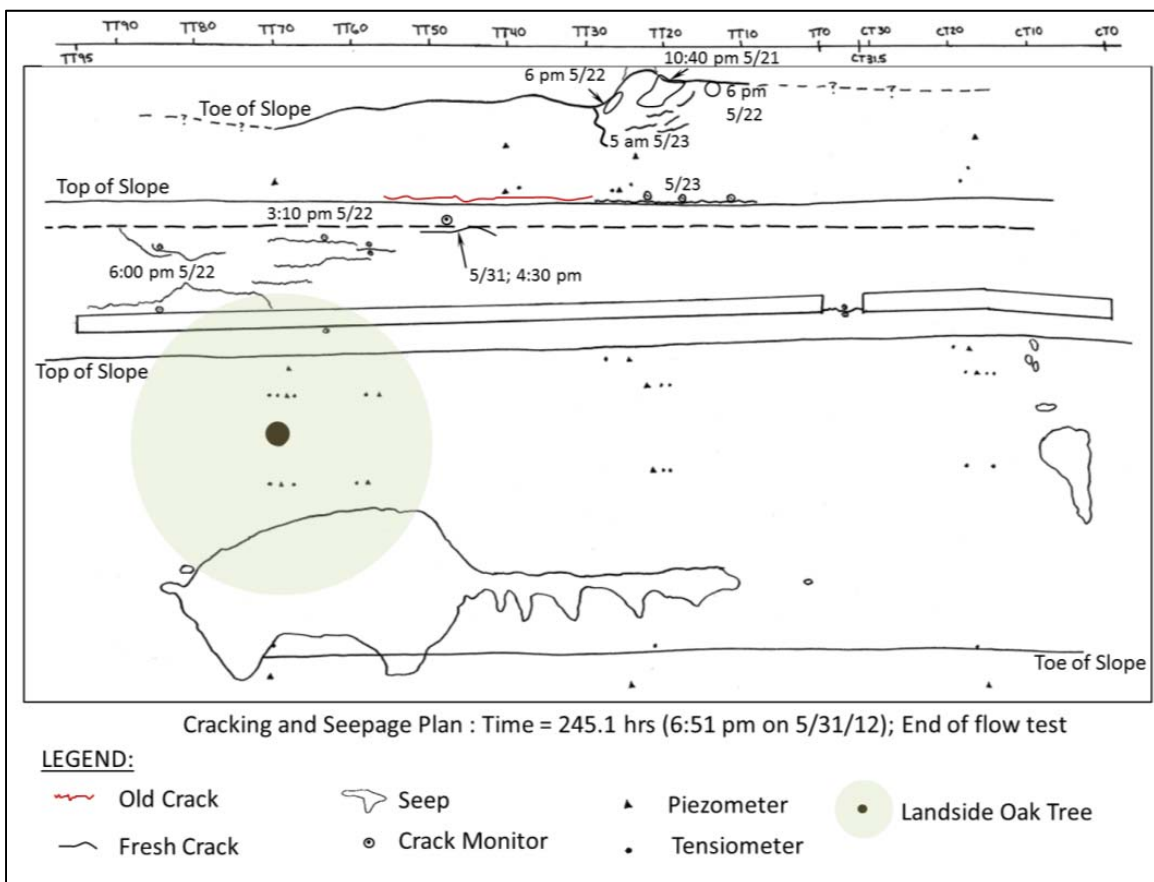


Figure 3-142. Cracking and seepage locations at the end of the flow test (Time = 245.1 hrs). Details for landslide seeps were presented previously.
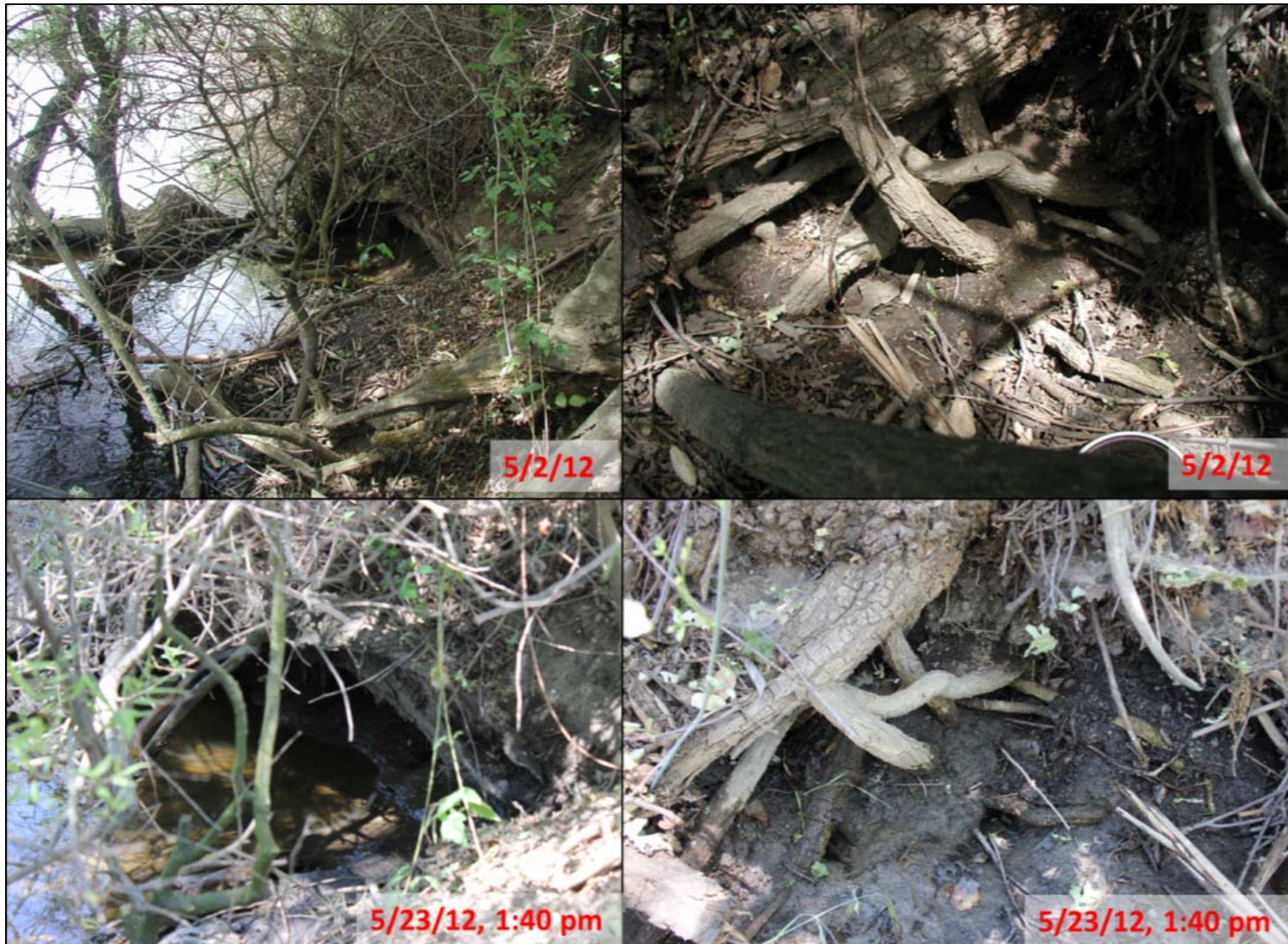
Figure 3-143. Top photos show locations of suspected muskrat burrows identified by Dr. Dirk Van Vuren on 5/2/12. Photos below show corresponding locations (Station TT 13, left and Station TT 24, right) seeping during the flow test.

234

Figure 3-144. Location of first seep (found at 10:40 pm on 5/21) at the base of the waterside oak tree before (5/22 at 1:44 pm) and after the oak tree fell (6 pm on 5/23). Seepage at this location had ceased and begun to dry 12 hours after the tree fell.

### 3.1.4.3    Dye Test

The flow rates during the test were on the order of 7300 gallons each hour during the primary flow test. These rates were higher than expected for the 100-foot long 8-foot deep trench. In an effort to better understand the water losses at the site, a dye test was devised to improve our ability to identify locations where large water losses were occurring. Two gallons of Cole Parmer blue dye concentrate were used to perform the test. The water was turned off to both trenches between 9:15 am and 11:55 am on 5/31/12. The dye was mixed slowly into the water reservoir, one cup at a time, and the dye-tinted water was released into the trenches at 11:55 am. Figure 3-145 shows the location of seepage observed throughout the day. Generally, landside seepage patterns during the dye test mimicked those encountered during the primary flow test (Figure 3-146). Blue tinted water emerged from the landside at the locations and times indicated on Figure 3-145.  Each of the locations correspond with burrowing activity observed within the trench excavation or at the slope surface, as further discussed in a photographic timeline of the dye test included as Table 3-3 at the end of this section.

Waterside seeps observed between Stations TT 13 and 24 during the primary flow test began to dry up following the fall of the waterside oak tree, as previously discussed. Figure 3-147 shows an early seep location, drying after the waterside oak has fallen and almost completely dry 4 hours into the dye test. The seeps surrounding the waterside oak tree did not flow during the dye test, while seepage was observed away from the tree. The water level in the Sevenmile Slough was held low during the dye test, by request of our team to the gate operator at Brannan Island. Access was possible with waterproof boots and careful footing. A boat was also made available by Mr. Rick Carter of RD 1601. Given these factors, we were able to make observations of seepage during the dye test in areas that were inaccessible during the primary flow phase. Seeps were photographed between Stations CT 15 and TT 0 as well as from Stations TT 45 to TT 70. Seeping burrows could be seen north of Station CT 15 and south of Station TT 70, but the locations could not be accessed.

Figure 3-148 provides photographic examples of seeping waterside burrows observed during the dye test. Blue dye was not observed flowing from the majority of the burrows during the limited timeframe of our dye test. Figure 3-149 shows a burrow at Station TT 70 that flowed blue-tinted water at a rate of approximately ½ gallon per minute. The burrow flow rate was measured with a graduated cup and timer at 6:30 pm (5/31/12). This burrow displayed the fastest flow rate observed in any burrow that was seen during our inspections, while the majority of burrows were found to slowly weep. Figure 3-150 shows burrows along the waterside slope toe on 6/1/12, the day after the dye test. Weeping of water had stopped. The photographs indicate the density of burrows along the toe of slope, typically out of view due to higher water levels. According to Dr. Van Vuren, muskrats prefer entry under the water. A detailed photographic timeline is provided for the events and key observations associated with the dye test on 5/31/12 (Table 3-3) while dates are provided for previously observed features.
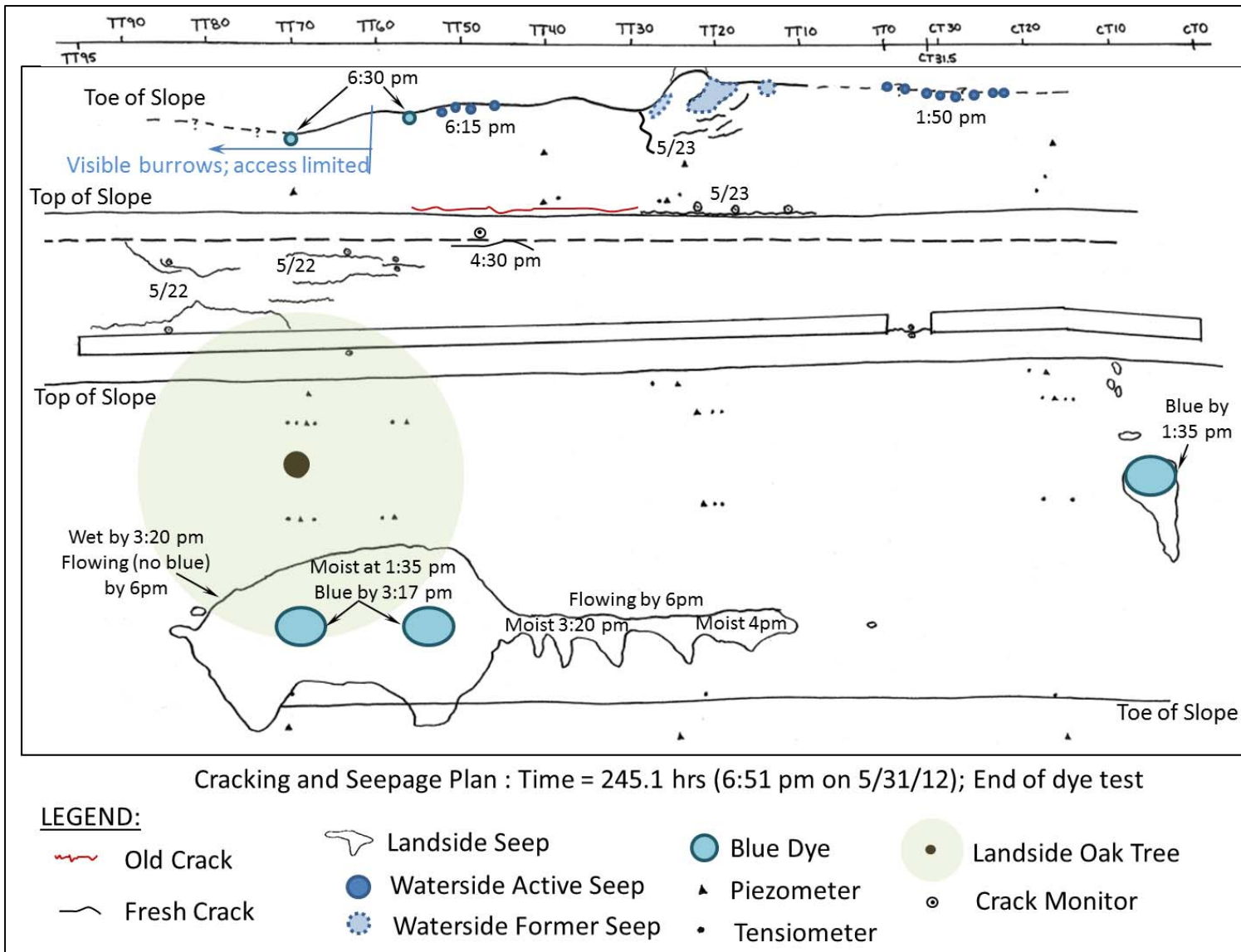
Figure 3-145. Cracking and seepage plan showing findings of dye test on 5/31/12. Dye began at 11:55 am (Time = 238.2 hours).

Figure 3-146. Flow on the landside at the end of the dye test (Time = 245.1 hours).

Figure 3-147. Several hours into the dye test, early seep discovered at waterside oak ceased flowing once the tree fell (left) and did not begin flowing again during the dye test on 5/31 (right).

Figure 3-148. Burrows were observed flowing during the dye test both to the north and south of the waterside oak tree. Note a crawdad at the entrance to a burrow (top right).

Figure 3-149. Burrow at Station TT 70 flows blue-tinted water at a measured rate of about ½ gallon per minute from a 2 ½ inch diameter burrow, likely muskrat.

Figure 3-150. Photos taken on 6/1/12, the day after completion of the flow test. The waterside burrows are photographed and observed to have stopped flowing.

Table 3-3. Observational timeline during the dye test on 5/31/12

| 235.5 | 5/31 | 09:14 | Turned off water to control trench in an effort to concentrate the pulse of dye injected into the test |  |
|---|---|---|---|---|
| 238.2 | 5/31 | 11:55 | Turn on water to both control and tree trenches using visible range blue dye to help determine locations of concentrated water flow |  |
| 239.7 | 5/31 | 12:38 | Trenches filled with dye-infused water |  |

| | | | | |
|---|---|---|---|---|
| 239.9 | 5/31 | 13:35 | Seep observed with blue dye at Stations CT 3 to 7 in area where gravel bags were placed during the primary flow test |  |
| 169.6 | 5/31 | 15:17 | Seep Station TT 70 appears blue (photo right) while Stations TT 75 to 84 are running clear. Stations TT 48 to 84 appearing wet and Stations TT 20 to 48 appear to have moistened |  |
| 244.8 | 5/31 | 18:30 | Blue dye is found in water seeping from a waterside burrow at Station TT 56. |  |
| 245 | 5/31 | 18:43 | Flow rate is measured at ½ gallon per minute in burrow at Sta. TT 70. | See Figure 3-149 |
| 245.1 | 5/31 | 18:51 | Water off; begin falling head test |  |

3.1.4.4    Instrument Data

Tensiometers and piezometers measured negative and positive pore water pressures before, during, and after the flow test. For this discussion, results are broken into landside instruments and waterside instruments. Complete results of all instruments including a discussion of instruments used and their calibration are presented in Appendix F.

3.1.4.4.1    Landside

Landside tensiometer results during the 4-day primary flow test and the complete 15-day flow test with post flow period are summarized by instrument line and presented below. The primary flow test represents the time when both trenches were filled to a constant head. Figure 3-151, Figure 3-152, Figure 3-153 and Figure 3-154 show results of instrument lines A, B, C, and D, respectively, during primary flow. Some instruments experienced problems retaining water and sustaining suction, possibly due to an imperfect seal. Tensiometers TC3-36, TB5-36, TA3-36, TC4-24, and TA5-24 began to drop water levels and suction potentially while the instrument is still re-gaining suction after the instrument was opened for filling. In many cases, the data are sufficient to determine the arrival of the wetting front, but the peak values of suction may not have been reached and, therefore, reported values may not be reliable other than to provide a lower bound on the suction value.

Landside piezometer results are presented as analogous rows plotted together beginning with row 2 at the top of the levee (Figure 3-155) followed by row 4, just above the landside oak (Figure 3-156 and Figure 3-157), row 5, just below the landside oak (Figure 3-158), and row 3 at the toe of slope (Figure 3-159).   For ease of comparison, summaries of time of arrival of the wetting front and saturation are provided for each landside tensiometer on Table 3-4.  Similarly, time to wetting front arrival, the value of and time of steady state pore pressure for each piezometer are provided on

Table 3-5.

Instrument line C, at the control trench, began with saturation of the 36 inch deep instrument at row 2 and the 60 inch instrument at row 4. Looking at Figure 3-31, these instruments are in close proximity to one another. They may be connected by a sand lens, a burrow, or fracture as they saturated at close to the same time. TC4-24 is the only shallow instrument on site that saturated before the adjacent instrument at a depth of 36 inch. This 24 inch deep tensiometer was positioned closest to the burrow encountered during trenching as well as those discovered in post-flow exploration, as will be discussed in a subsequent section. In row 4, the 60 inch deep tensiometer saturates at 3.9 hours, the 24 inch instrument saturates in 9.8 hours, and the 36 inch instrument between them saturates in 11 hours. This is an indication of non-uniform flow, likely related to the burrowing activity that we have seen evidence of. Burrows seen at this location have been shallow, in the upper 3 feet of the control trench.

In comparison, row 2 of instrument lines A and B takes 2.5 to 3 times longer to arrive at TB2-36 and TA2-36 than TC2-36. Arrival of the wetting front is again faster at line C for Row 4 at 24 inch and 60 inch depths. Arrival times at row 4 between all three instruments are comparable at 36 inch depth. Comparison of piezometer PA4a and b, PD4 a and b,  and PC4a and b show pore water pressures at steady state to be increased by about 40 percent in the zone behind the landside tree root system. This was calculated by averaging the steady state pore water pressure for instrument lines A and C and comparing it against analogous instruments of Lines B and C.

Within a few hours of saturation at row 4, instrument line A sees a progression of the wetting front to row 5, below the landside tree. Wetting front arrival times and pore water pressures are very consistent between lines A and D. All line A and D instruments show an arrival of wetting about 12.5 hours into the flow test. Three hours later, water was seen seeping from the slope below row 5 instruments.

Row 5 of instrument lines B and C exhibited different behavior. Although instrument Line C saturated at Rows 2 and 4 ahead of line A, row 5 never saturated and took nearly 6 days for the wetting front to arrive at TC5-36 and over 8 days to arrive at TC5-24. As discussed previously, stratigraphic sections show a low permeability layer that appears to be an original levee, or possibly a natural levee (Material 4), beneath loosely placed, more recent silt fills. A steeply dipping gap in the otherwise consistent Material 4 is shown on trench logs (Figure 3-87) dipping toward this gap segment (Station TT 37 to 42). The shape and loose backfill of this feature are indicative of a possible historic breach or scour event or excavation at this location. The older levee embedded within the existing levee may have features and contours that affect flow patterns, possibly developed and erosion rills from past flooding. The water may be re-directed through such a feature, or through macroporosity within the shallower soil layers. There does, however, in viewing trench logs (Figure 3-86 to Figure 3-89) seem to be a general tilt in the material 4 layer toward this possible breach, which could be affecting flow patterns at instrument lines B and C. Steady state at instrument line C was not a saturated condition for rows 5 and 3, indicating that stratigraphy may have added a three dimensional effect to data interpretation.

Row 3, at the toe of slope, yielded little in the way of results at the tensiometer instruments as instrument line A shows zero suction throughout the test and seems to not be able to maintain suction. TB3 eventually saturates at 65 hours, while TC3 maintains the same suction throughout the test.

Piezometers located in row 3 at the toe of slope are not all the same depth. PB3 was installed deeper and under the groundwater so that effects on the groundwater table could be monitored. The instruments were building pore water pressure steadily and had not achieved steady state. PB3 predictably begins to build water pressure before PA3 and PC3. PA3, however, begins to build pore pressure prior to the arrival of hydrostatic water pressures as measured by PB3.

It should be noted that there is a gap in the data of some of the piezometers between 72 and 99 hours into the field test due to an equipment difficulty. Most instruments have reached steady state before this data gap, but pore water pressures at piezometers P3B and P3C were still rising. The comparison of total head provided in Table 3-5 is based on the readings at 99 hours for PA3, PB3, and PC3 rather than 96 hours (when the water was turned off) for best comparison between the instruments.
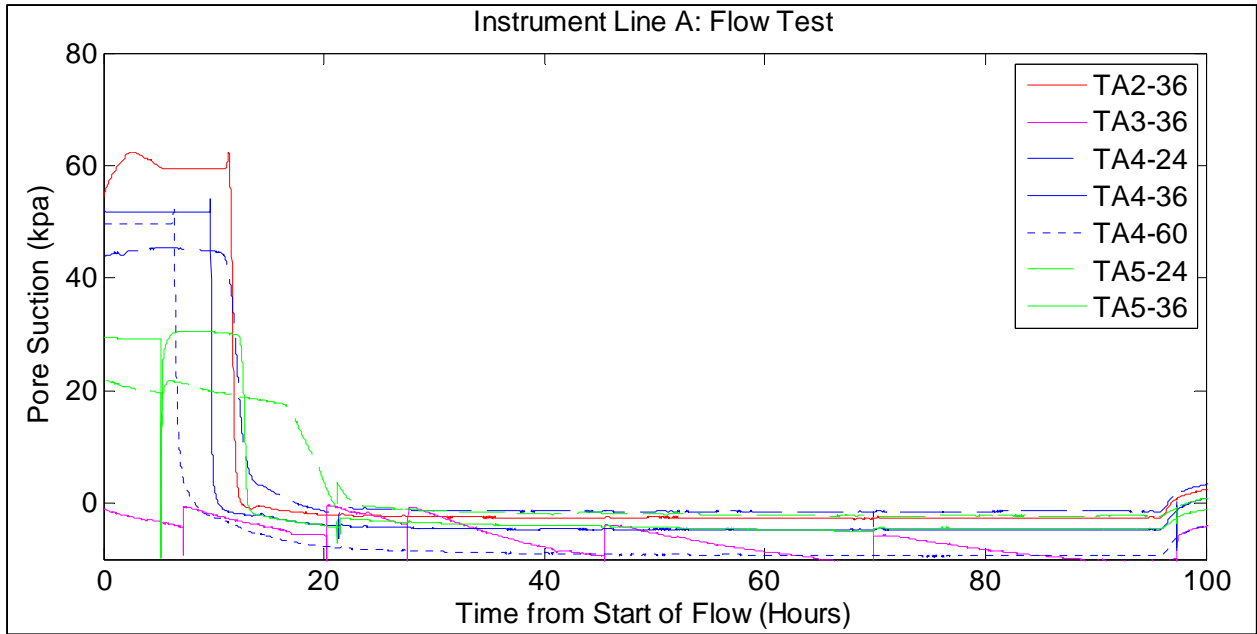
Figure 3-151. Tensiometer data for the primary flow test at instrument line A.
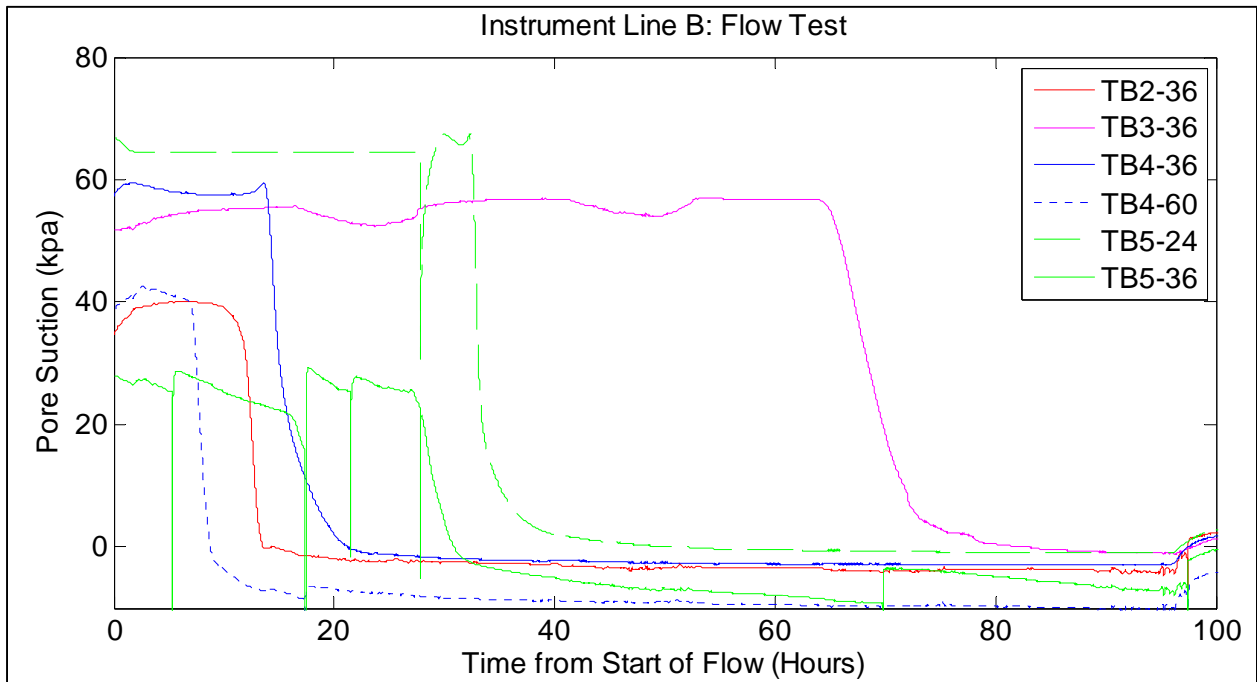

Figure 3-152. Tensiometer data for the primary flow test at instrument line B.

247
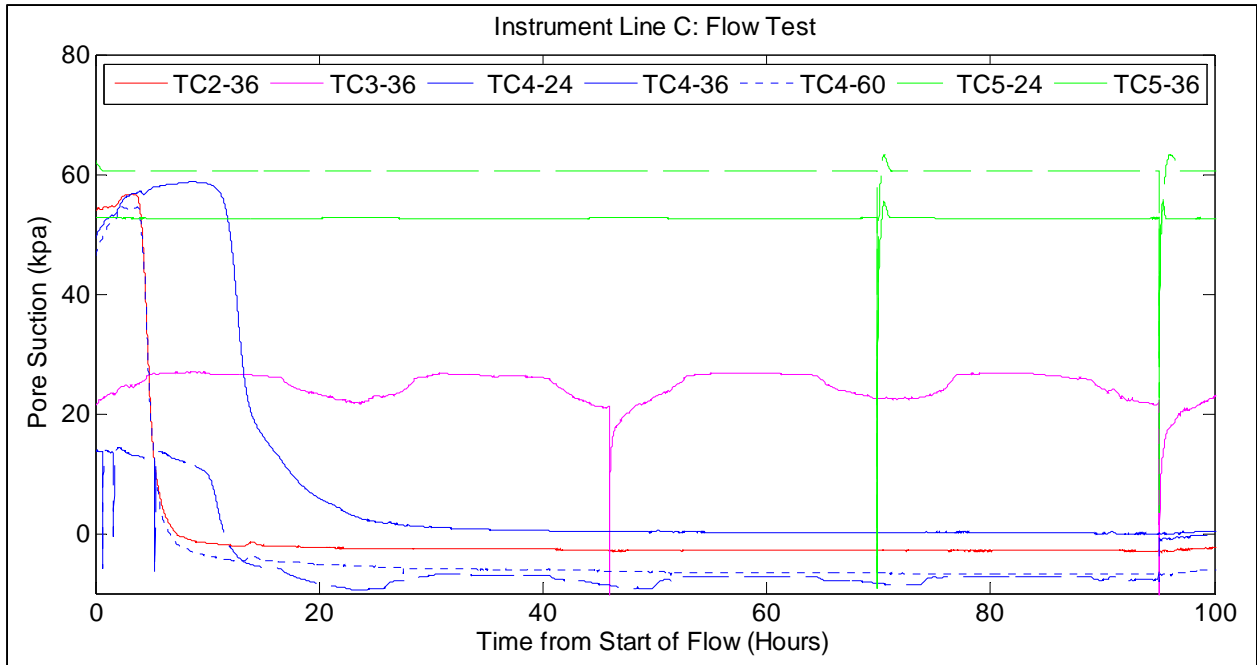
Figure 3-153. Tensiometer data for the primary flow test at instrument line C.
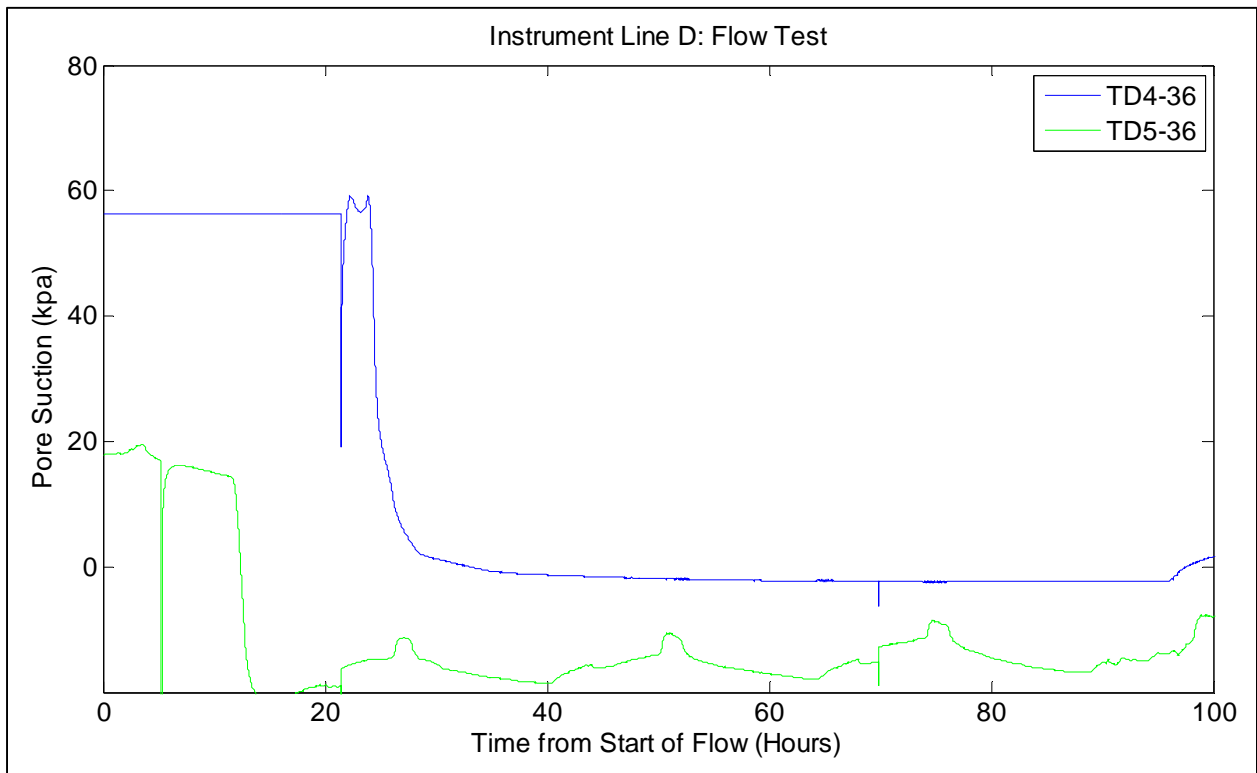


Figure 3-154. Tensiometer data for the primary flow test at instrument line D.
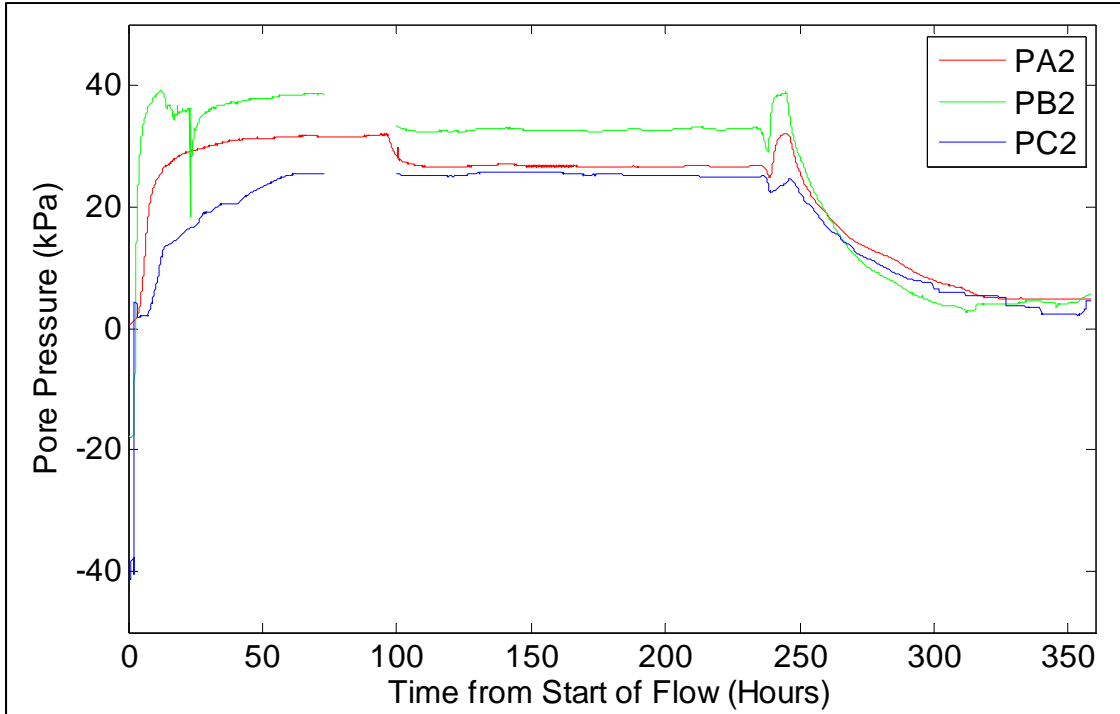
Figure 3-155. Piezometer data for the 10-day flow test and post flow at instrument row 2 (at the top of the slope) at depths of 15, 15.9, and 12.4 feet for lines A, B, and C, respectively.
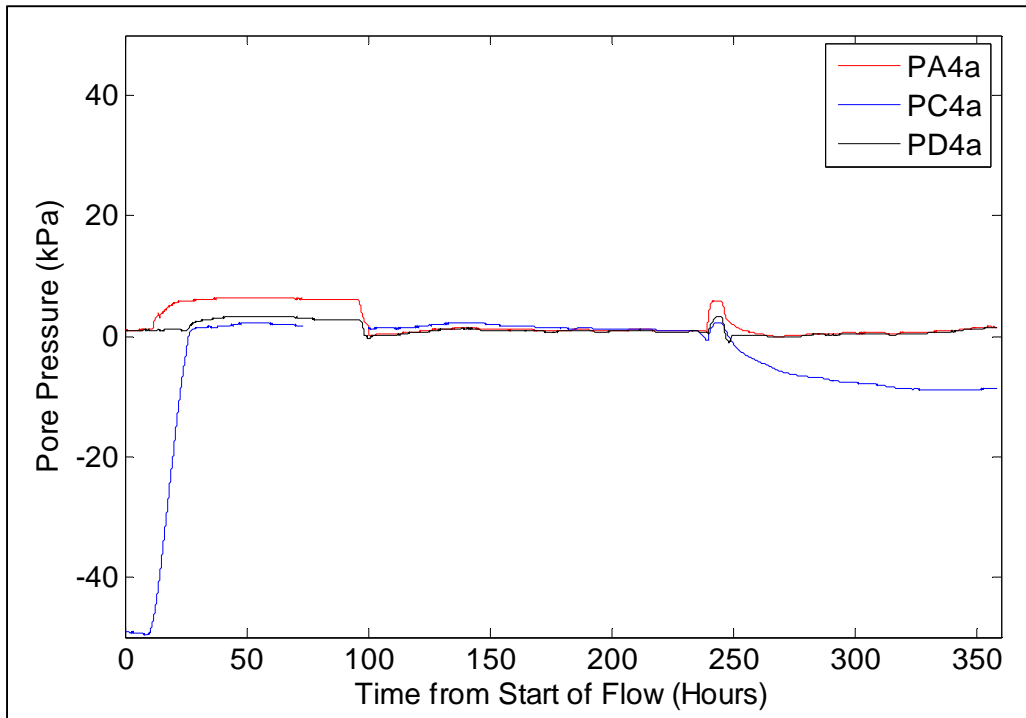


Figure 3-156. Piezometer data for the 10-day flow test and post flow at instrument row 4 (elevation just above the landside oak) at depths of 2.4 feet below grade.
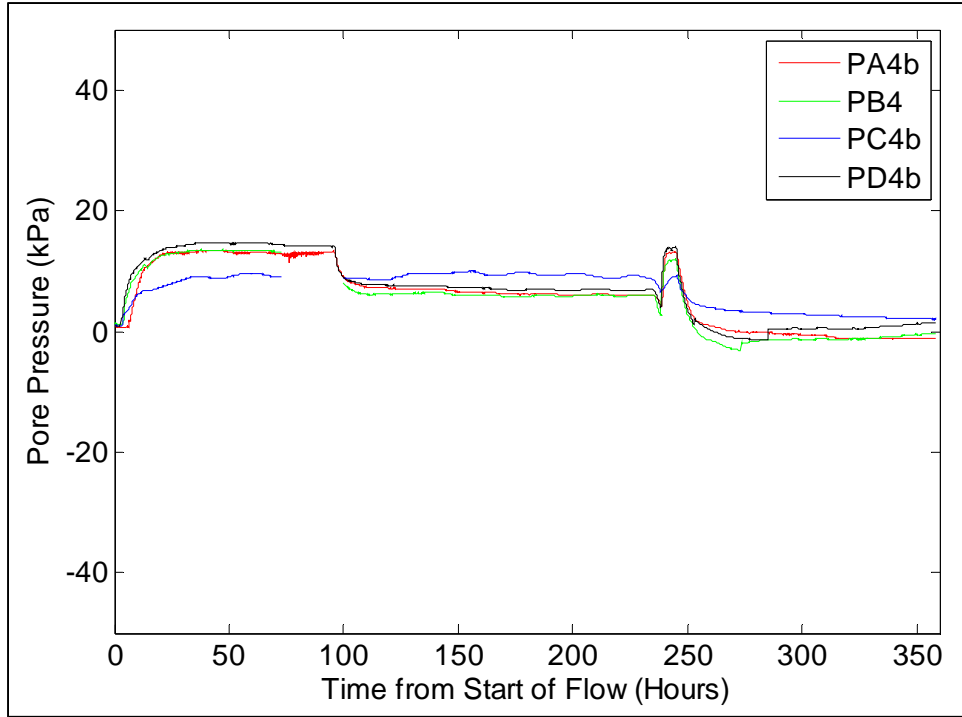
Figure 3-157. Piezometer data for the 10-day flow test and post flow at instrument row 4 (elevation just above the landside oak) at depths of 5.7 feet below grade.
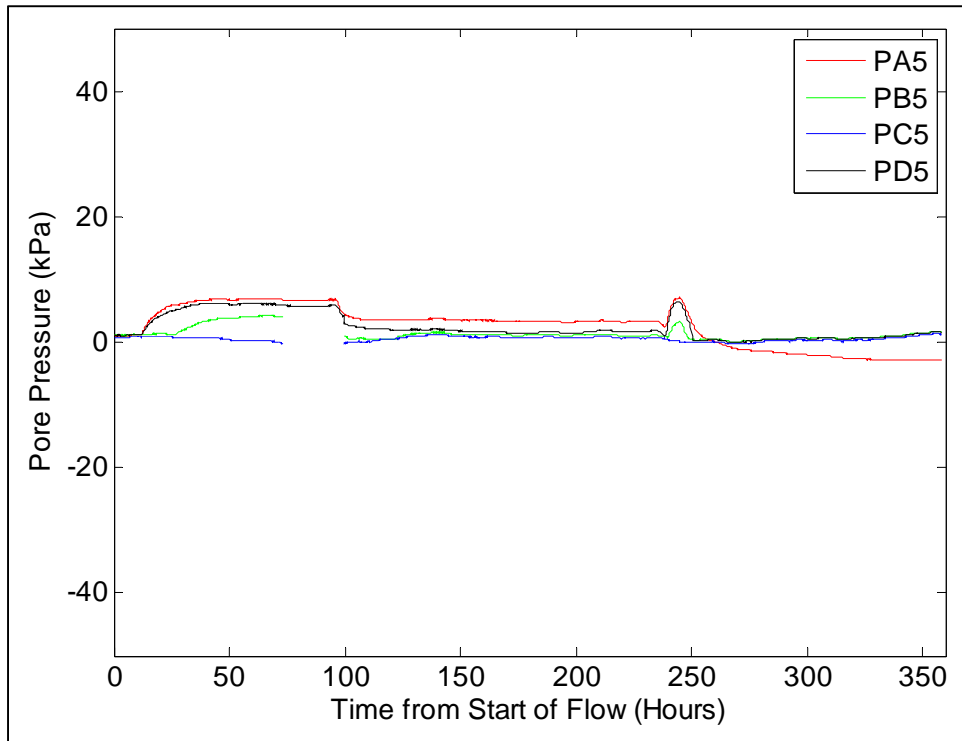


Figure 3-158. Piezometer data for the 10-day flow test and post flow at instrument row 5 (elevation just below the landside oak) at depths of 3 feet below grade.
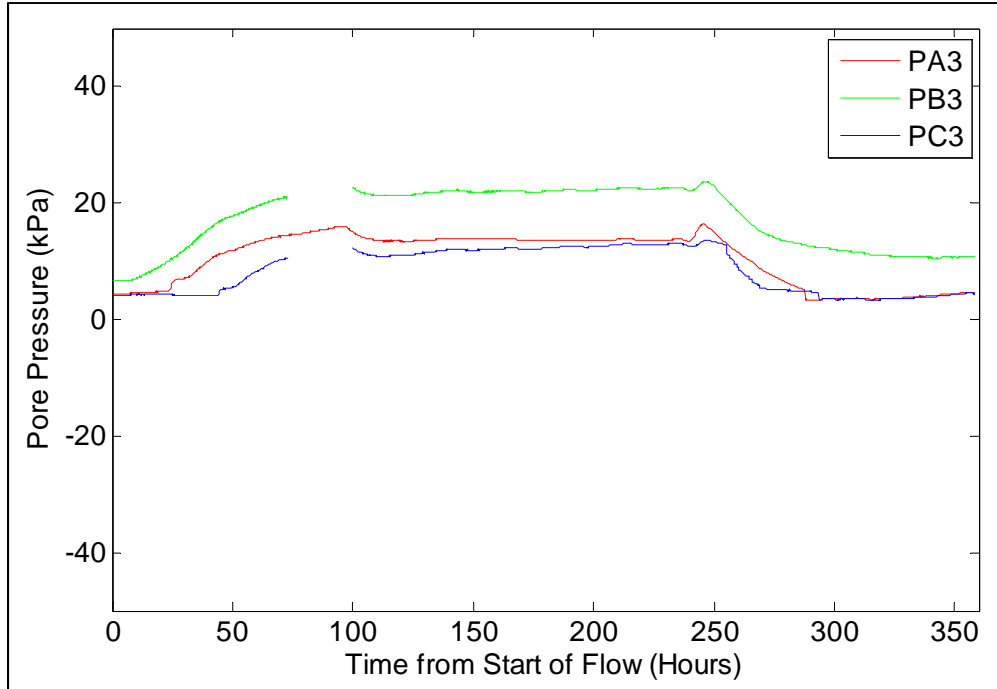
Figure 3-159. Piezometer data for the 10-day flow test and post flow at instrument row 3 (at the toe of slope) at depths of 7.9, 13.5, and 8.5 feet below grade for lines A, B, and C, respectively.

Table 3-4. Landside tensiometer result summary table.

| Instrument Name | Wetting Front Arrival (hrs) | Time to Saturation (hrs) | Steady State Suction for Unsaturated Instruments (kpa)* | Saturation Achieved? (y/n) | Time of Steady State (hrs) |
|---|---|---|---|---|---|
| TA2_36 | 11.5 | 12.5 | Pressure | y | - |
| TA4_24 | 11.0 | 17.4 | Pressure | y | - |
| TA4_36 | 9.7 | 10.4 | Pressure | y | - |
| TA4_60 | 6.4 | 8.3 | Pressure | y | - |
| TA5_24 | 16.8 | 20.9 | Pressure | y | - |
| TA5_36 | 12.4 | 13.1 | Pressure | y | - |
| TA3_36 | Not Reached | - | - | - | - |
| TD4_36 | 24.1 | 33.0 | Pressure | y | - |
| TD5_36 | 11.9 | 12.4 | Pressure | y | - |
| TB2_36 | 10.2 | 13.6 | Pressure | y | - |
| TB4_36 | 13.9 | 21.2 | Pressure | y | - |
| TB4_60 | 7.0 | 8.8 | Pressure | y | - |
| TB5_24 | 32.5 | 51.5 | Pressure | y | - |
| TB5_36 | 27.3 | 30.9 | Pressure | y | - |
| TB3_36 | 65 | 82.7 | Pressure | y | - |
| TC2_36 | 3.8 | 7.2 | Pressure | y | - |
| TC4_24 | 9.8 | 11.6 | Pressure | y | - |
| TC4_36 | 11.0 | - | 0.2 | n | 51 |
| TC4_60 | 3.9 | 6.6 | Pressure | y | - |
| TC5_24 | 195 | Not reached | lowest suction: 24.7 | n | not reached |
| TC5_36 | 133 | Not reached | lowest suction: 7.5 | n | not reached |
| TC3_36 | Not Reached | - | - | - | - |

*Some instruments indicated pressures which are not reported. Instrument calibrations do not support pressures

Table 3-5. Landside piezometer result summary table.

| Instrument Name | Wetting Front Arrival (hrs) | Time to Steady State (hrs) | Steady State Pressure (kpa)* | Elevation of Instrument (ft) | Total Head (ft) |
|---|---|---|---|---|---|
| PA2 | 1.5 | 45.6 | 31.3 | -8.2 | 2.2 |
| PA4a | 11.9 | 24.7 | 5.9-6.3 | 3.2 | 5.2 |
| PA4b | 6.5 | 20.2 | 12.7-13.4 | -0.1 | 4.2 |
| PA5 | 12.3 | 37.9 | 6.7-6.9 | -0.6 | 1.7 |
| PA3 | 24.1 | Not reached | - | -11.2 | -6.1 |
| PD4a | 25.9 | 32.9 | 2.7-3.3 | 3.2 | 4.2 |
| PD4b | 3.3 | 27.9 | 14.1-14.8 | -0.1 | 4.7 |
| PD5 | 12.4 | 38.9 | 6.1 | -0.4 | 1.7 |
| PB2 | 1.6 | 45 | 37.6- 38.6 | -9.6 | 3.2 |
| PB4 | 3.9 | 33.7 | 13.4 | -0.5 | 4.0 |
| PB5 | 27.7 | 62 | 4.2 | -0.6 | 0.8 |
| PB3 | 6 | Not reached | - | -16.3 | -8.9 |
| PC6 | Not reached | - | 3.8-4.3 | 4.3 | 5.7 |
| PC2 | 2 | 60.1 | 25.2 | -6.0 | 2.5 |
| PC4a | 10.7 | 47.2 | 2.1 | 2.9 | 3.6 |
| PC4b | 3.4 | 35.8 | 8.8-9.6 | -0.4 | 2.6 |
| PC5 | Not reached | - | 0 | -0.6 | -0.6 |

* Data not corrected for barometric pressure

Figure 3-160, Figure 3-161 and Figure 3-162 show the entire 10-day flow test (including 4 days of primary flow, 5 ½ days of control trench flow only and ½ day of dye testing) and 5 days of post-flow readings as site soils begin to dry and rebuild suction.
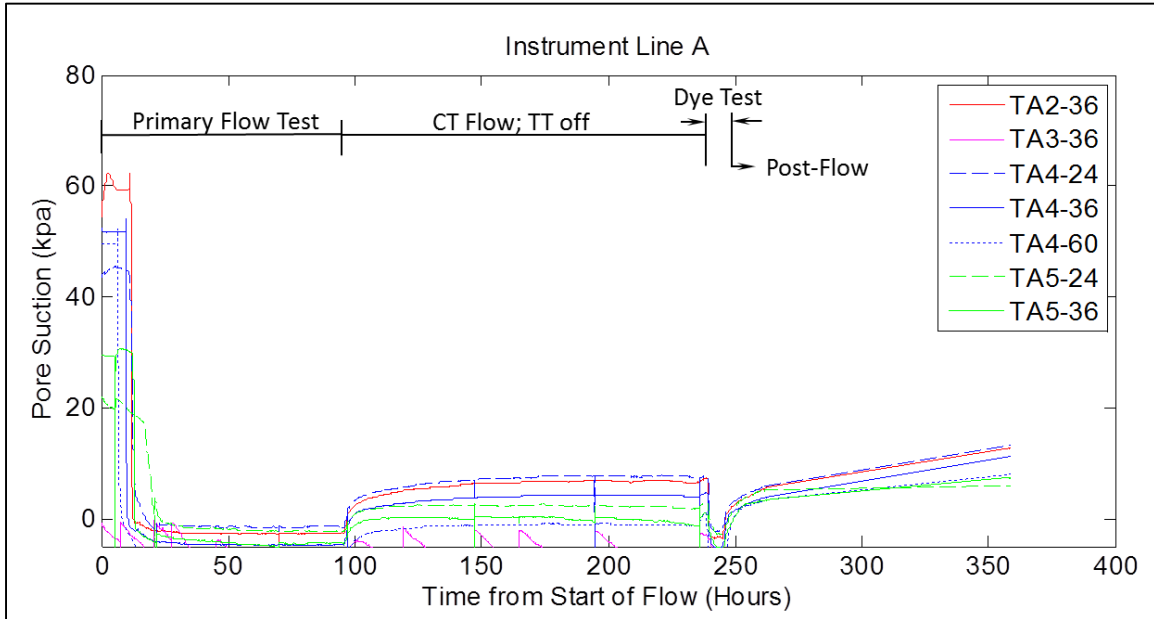


Figure 3-160. Tensiometer data for 10-day flow test and post flow at instrument line A.
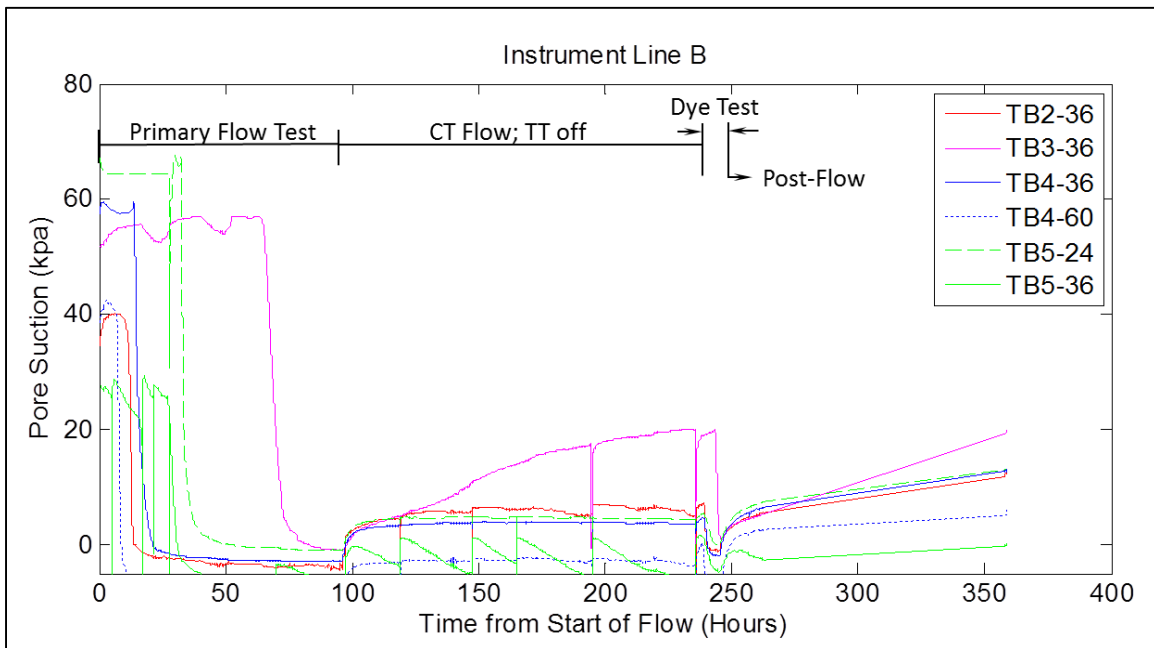


Figure 3-161. Tensiometer data for 10-day flow test and post flow at instrument line B.
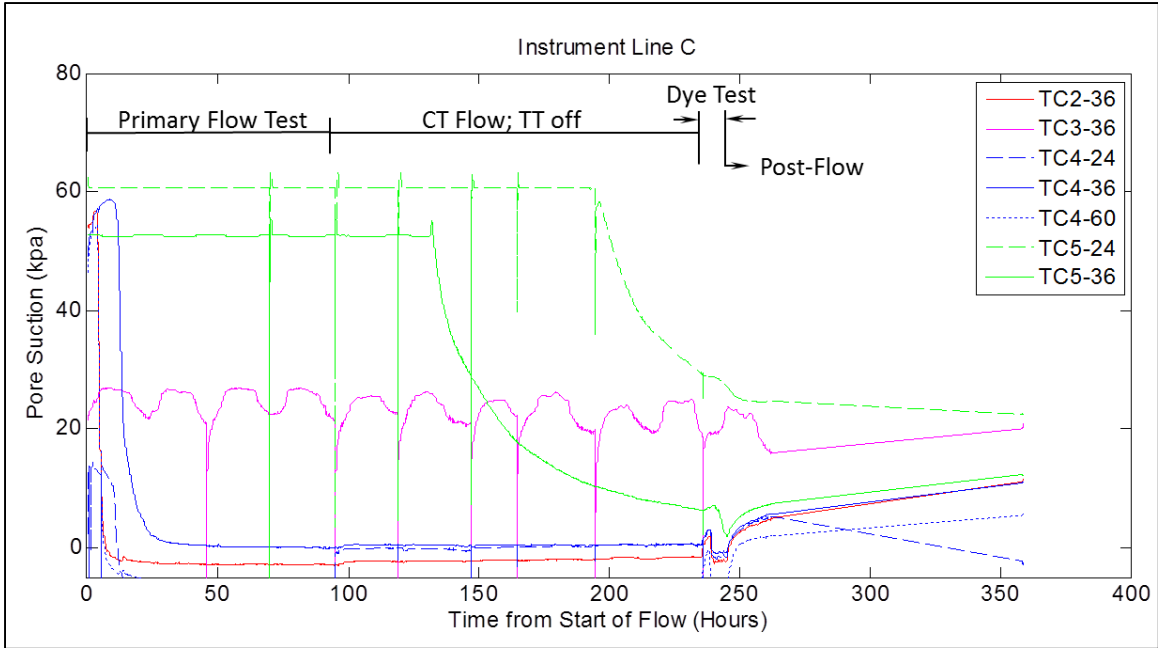
Figure 3-162. Tensiometer data for the 10-day flow test and post flow at instrument line C.
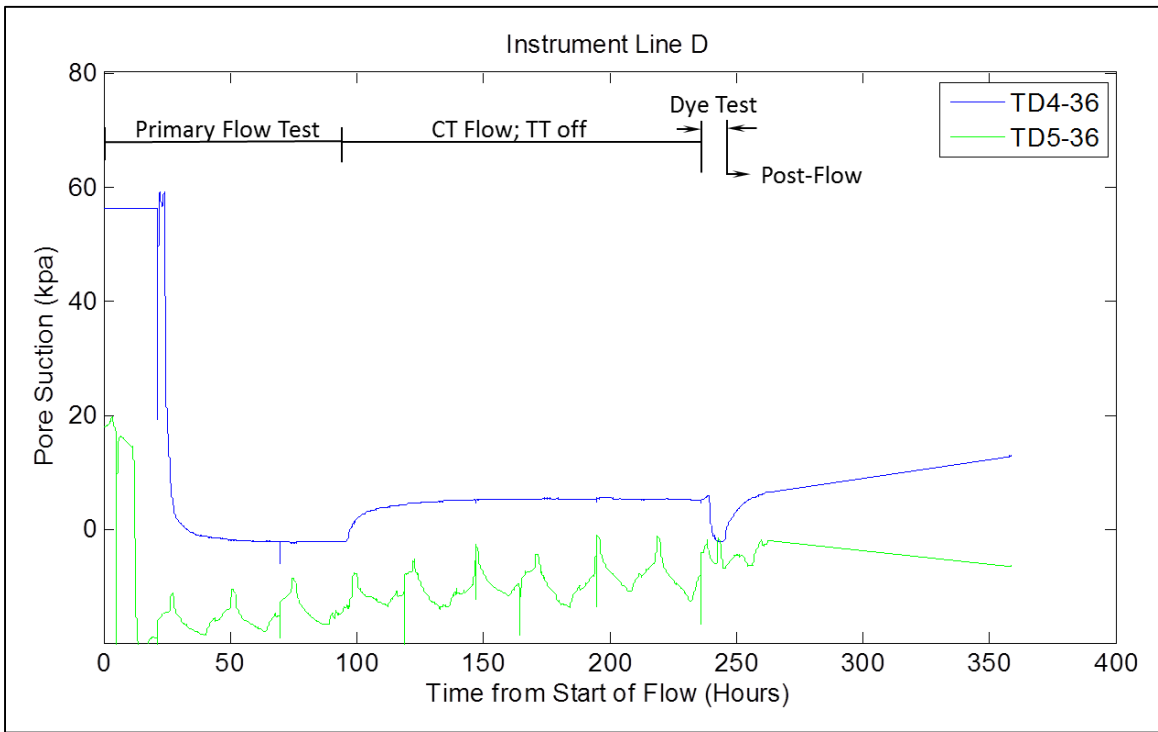


Figure 3-163. Tensiometer data for the 10-day flow test and post flow at instrument line D.

### 3.1.4.4.2   Waterside

Waterside tensiometer results during the 10-day flow test with post flow period are summarized by row and instrument depth and presented below on Figure 3-164 and Figure 3-165. Waterside

255

piezometer data are plotted by row (1 and 6) and provided as Figure 3-166 and Figure 3-167. For ease of comparison, summaries of time of arrival of the wetting front and saturation are provided for each waterside tensiometer on Table 3-6. Similarly, time to wetting front arrival, the value of and time of steady state pore water pressure for each piezometer are provided on Table 3-7.

At line E, tensiometer TE1-36 appears to have problems maintaining suction, however sufficient suction is able to be maintained to estimate the time of saturation as evidenced by the low (below zero) value following re-filling of the instrument and regaining of suction. This instrument saturates at 6.8 hours as compared to analogous instruments at line B (9.6 hours) and line C (16.4 hours). Piezometer time to wetting follows the same pattern where line E experiences wetting at 1.5 hours (PE1), line B in 4 hours (PB1), and line C in 9 hours (PC1). Row 6 displays a different pattern where PB6 is wetted by 6 hours, and PE6 is wetted in 9.2 hours. A number of factors could be at play here including higher permeability through the possible breach zone backfilled with loose soils at Stations TT 37 to 42, fractured levee soils, and burrowing activity (particularly muskrat). Water arrived later to PA1, and PC1. The path of macroporosity in unknown and the degree to which each factor affects flow is not clear.
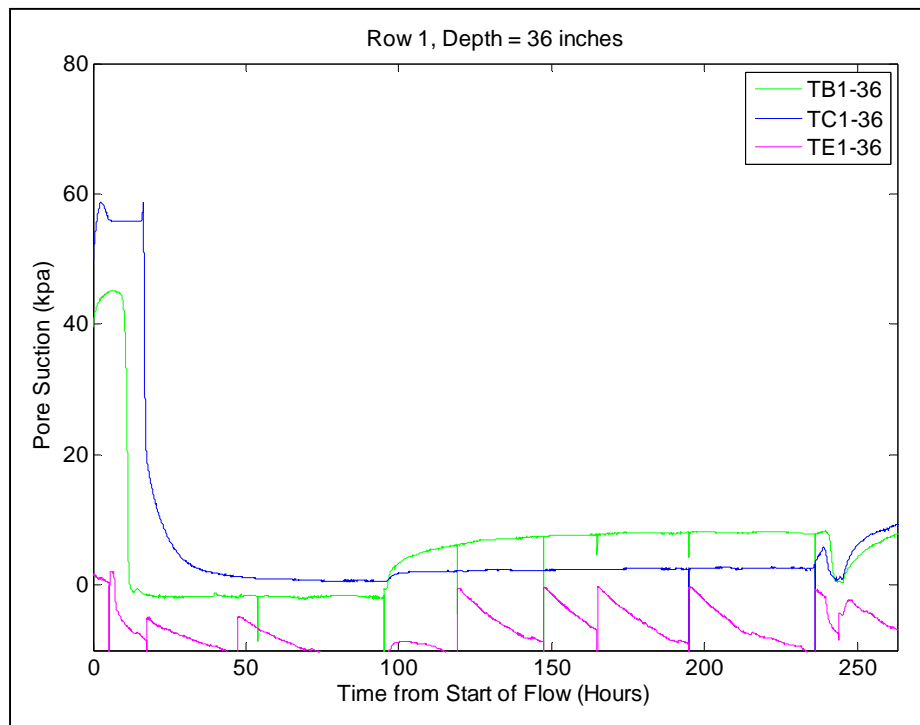


Figure 3-164. Tensiometer results for Row 1, 36 inch depth, for the 10-day flow test and early post-flow.
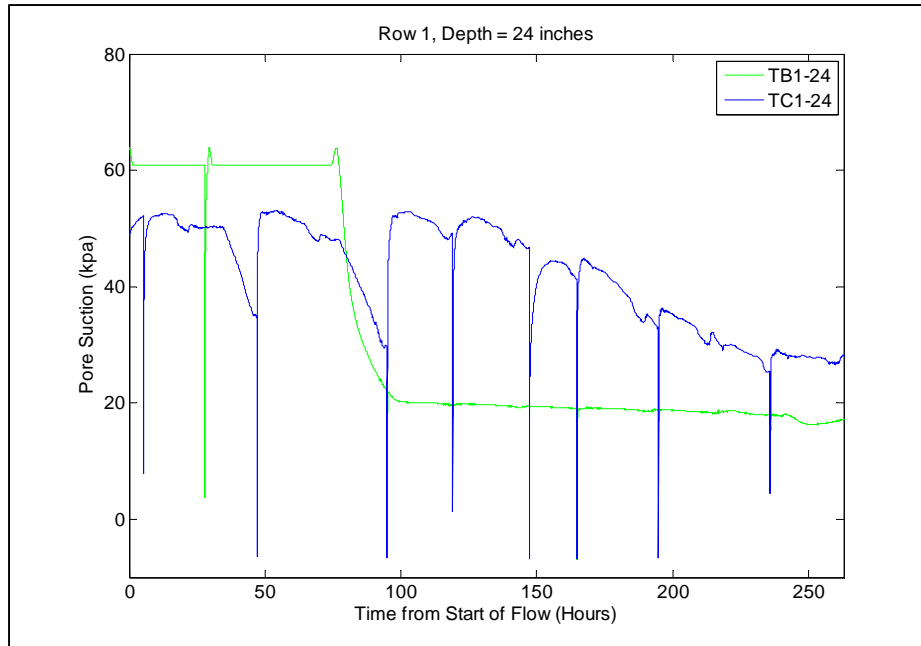
Figure 3-165. Tensiometer results for Row 1, 24 inch depth, for the 10-day flow test and early post-flow.
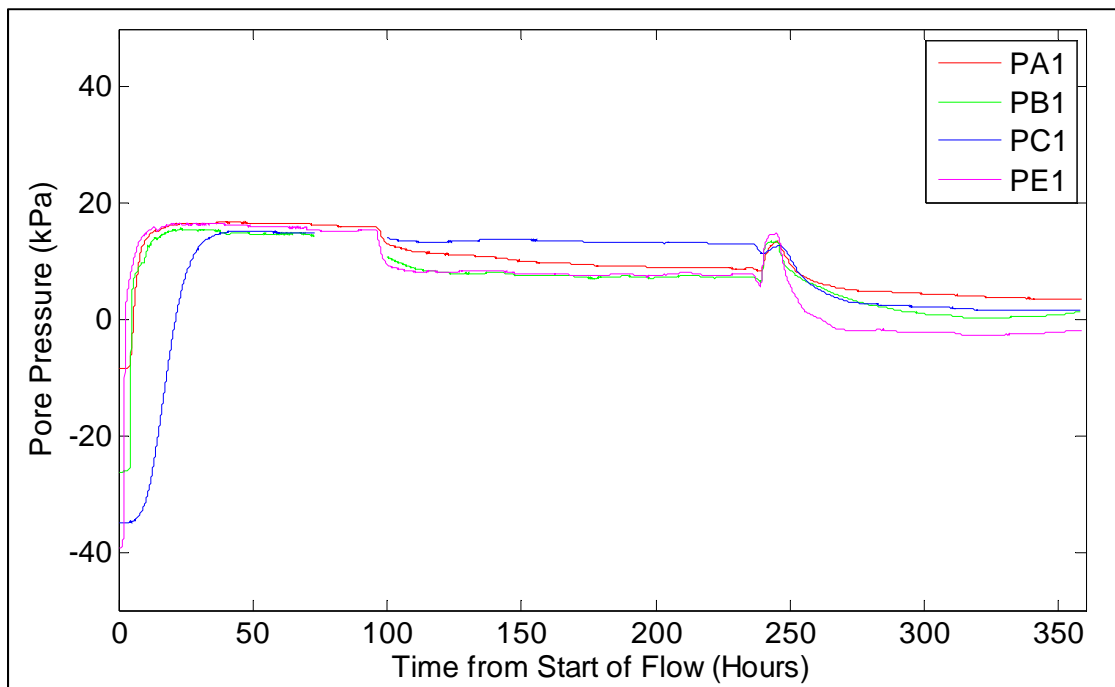


Figure 3-166. Piezometer data for the 10-day flow test and post flow at instrument row 1 (top of waterside slope) at a depths of 5.9, 6.5, 6.2, and 6.5 feet below grade for lines A, B, C, and E, respectively.
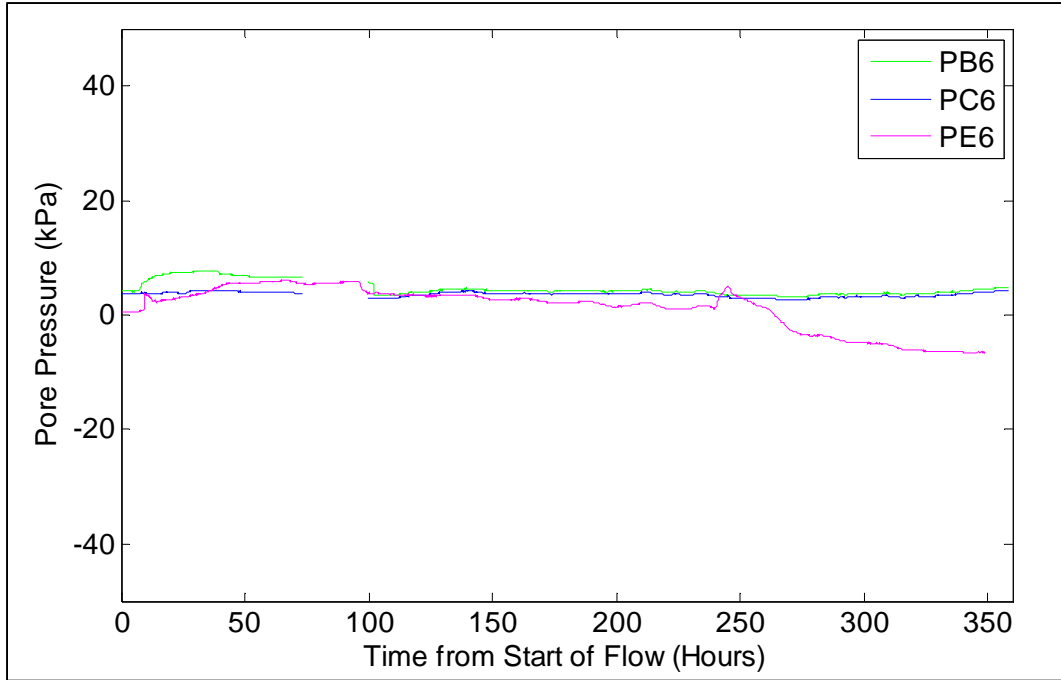
Figure 3-167. Piezometer data for the 10-day flow test and post flow at instrument row 3 (middle of waterside slope) at depths of 3.4 feet below grade.
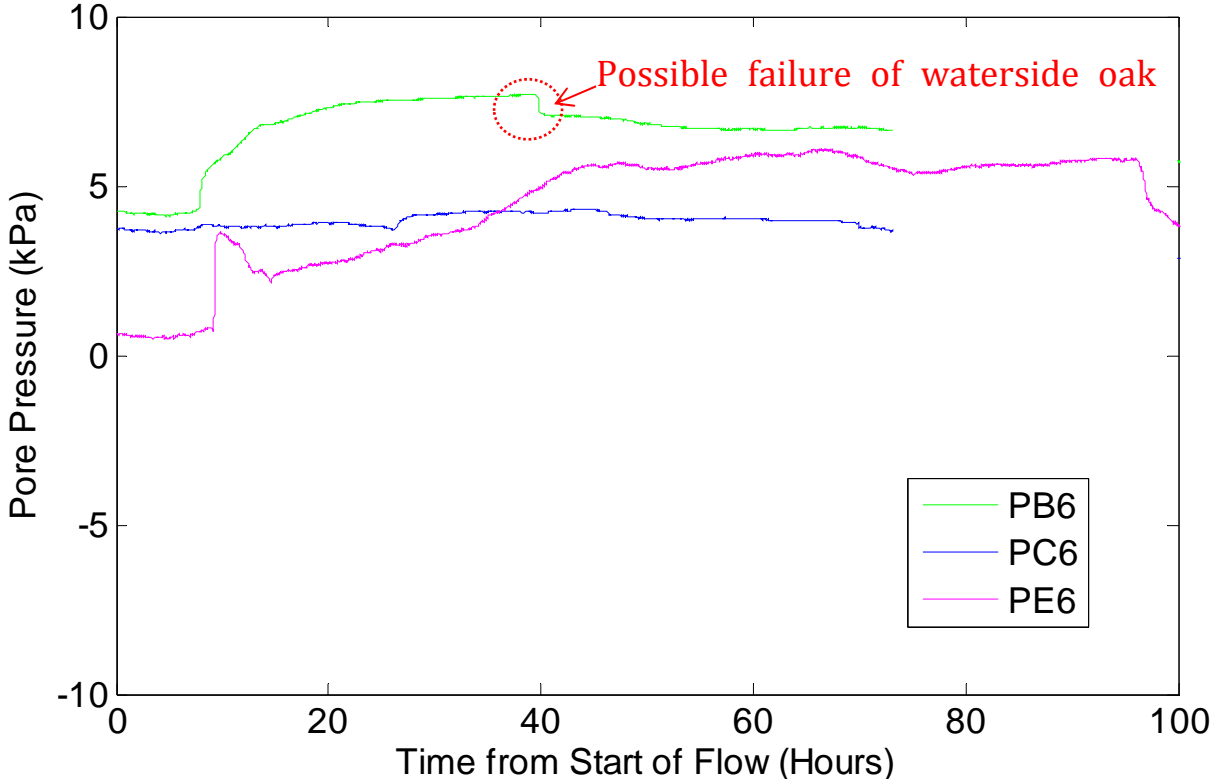


Figure 3-168. Piezometer PB6, at the waterside oak, shows a notable dip in pore pressure. The time of the dip is 39.7 hours, or 5/23/12 at 5:25 am and could be the time of tree failure.

Table 3-6. Waterside tensiometer result summary table.

| Instrument Name | Wetting Front Arrival (hrs) | Time to Saturation (hrs) | Steady State Suction for Unsaturated Instruments (kpa)* | Saturation Achieved? (y/n) | Time of Steady State (hrs) |
|---|---|---|---|---|---|
| TC1_24 | 140 | - | 28 | n | not reached |
| TC1_36 | 16.4 | - | 2 | n | 69 |
| TB1_24 | 77.3 | - | 20-21 | n | 95 |
| TB1_36 | 9.6 | 12.1 | Pressure | y | - |
| TE1_36 | 6.8 | 7.1 | Pressure | y | - |

*Some instruments indicated pressures which are not reported. Instrument calibrations do not support pressures

Table 3-7. Waterside piezometer result summary table.

| Instrument Name | Wetting Front Arrival (hrs) | Time to Steady State (hrs) | Steady State Pressure (kpa)* | Elevation of Instrument (ft) | Total Head (ft) |
|---|---|---|---|---|---|
| PA1 | 3.7 | 23.3 | 16.5 | 1.4 | 6.9 |
| PE1 | 1.5 | 15.5 | 15.9-16.6 | -0.1 | 5.3 |
| PE6 | 9.2 | 41.4 | 5.4-6.0 | 1.2 | 2.8 |
| PB6 | 6 | 25 | 7.5 | 3.2 | 5.7 |
| PC1 | 7 | 42.8 | 15.2 | 1.5 | 6.6 |
| PC6 | - | - | 3.8-4.3 | 4.3 | 5.7 |

* Data not corrected for barometric pressure

3.1.4.5    Flow Volumes

During the 10-day flow test, a total of 1,212,500 gallons of water was pumped into the reservoir and released by gravity into the control and tree trenches (Figure 3-169). As previously described, flow monitoring devices were installed on the inlet pipeline into the reservoir as well as both outlet lines into the control and tree trenches.

Monitoring gauges were designed so as not to be a limiting factor in water delivery into the trenches. Delivery lines were somewhat oversized and as a consequence, flows into the trenches were not high enough to turn the volume-tracking wheel within the meter reliably. As a result, the inflow meter from the pump to the tank was considered the most reliable meter for estimation of total water delivered. Based on the first day of data, the mechanical flow meters (which track total flow volume through each meter) showed that about 82 percent of the total water was going to the tree trench and 18 percent to the control trench. The problem with the flow meter not having enough water to turn the meter is exacerbated in the control trench, which is smaller and requires less water than the tree trench. Flow gauges showed flow rates to be 80 gallons per minute to the control trench and 200 gallons per minute into the tree trench, a breakdown of 71 percent to the tree trench and 29 percent to the control trench. A simple ratio based on the size of each trench would yield a breakdown of 76 and 24 percent for the tree and control trenches, respectively. This estimate seems reasonable in the absence of better data. The control trench delivery line volume trip meter and flow rate gauge stopped functioning completely after the first day of flow. Given inaccuracy issues, it was not replaced. Volumes were calculated from the total inlet volume readings, read periodically, and combined with levels of water in the tank at the time of the readings. A detailed plot of flow rates and cumulative volumes of flow into the trenches is provided with time on Figure 3-169.  A volume breakdown of flow into the control trench and tree trench during the primary flow test, when both trenches are full, is assumed to be 76 percent delivered to the tree trench and 24 percent delivered to the control trench.

Total flow during each test phase is broken out in Table 3-8. Best estimates are provided for the breakdown of flow rates between the control trench and the tree trench in Table 3-9. During trench filling, flow rate estimates to each trench were not made. In the primary flow phase and during the dye test, the breakdown discussed above was assumed. Flow to the tree trench was turned off after 4 days of flow while water continued to be delivered to the control trench for over 5 days until the beginning of the dye test. During the timeframe when only the control trench was running, delivery volumes to the control trench increased, as observed by the fact that the mechanical float valve could no longer maintain a constant head in the trench. The valve was bypassed and controlled manually until the morning of the dye test. When we returned for the dye test, the control trench was about 4 inches low and the water in the tree trench contained about 3 feet of water at the base that had not drained.

Reviewing Figure 3-169 and Table 3-9, flow rates are seen to decrease at about 40 hours into the flow test. This corresponds to the failure of the waterside oak tree. Observations of reduced seepage to this area following the tree failure could mean that the tree falling introduced discontinuities in the previously active flow pathways leading to a reduction in overall flow through the network of macropores at the site. The flow rate into the trenches was higher at the beginning of the dye test after water to the tree trench had been cut off for several days and then restarted. Once the test had run for several hours, the flow rate decreased to a similar rate observed at steady state during the primary flow phase, a little over 100 gallons per minute.

During post-flow inspection of the trenches (Section 3.1.4.6), a burrow was found to have opened between the tree trench and the control trench, allowing the trenches to share flows during this phase. If the control trench is assumed to have a constant flow once the tree trench is turned off, it the flow through the burrow can be approximated. The total flow rate increased over time, possibly due to the growing size of the hole between the trenches allowing for increased delivery of water from the control trench into the tree trench. The most reliable value for understanding volumes is the total flow volumes and rates, while breakdowns between trenches are best estimates based on available data.

Based on assumed unit weights of onsite soils of 110 to 115 pounds per cubic foot, and measured moisture contents ranging from about 20 to 40 percent, the fraction of void space in the materials is estimated to be on the order of 40 to 45 percent with 10 to 15 percent capacity to take on moisture to reach saturation. If all soils within 5 feet of the levee toe on land and water side and extending to the depth of the water table were to become completely saturated, the total volume of water require to accomplish this saturation is estimated to be just under 150,000 gallons of water. If site soils had been completely dry at the beginning of the project, the volume to accomplish saturation would be about 660,000 gallons. The volume of the trench is about 13,700 gallons. The volume of water that flowed through the site was 1,212,500 gallons of water, with estimated water losses offsite of 1,062,500 gallons.
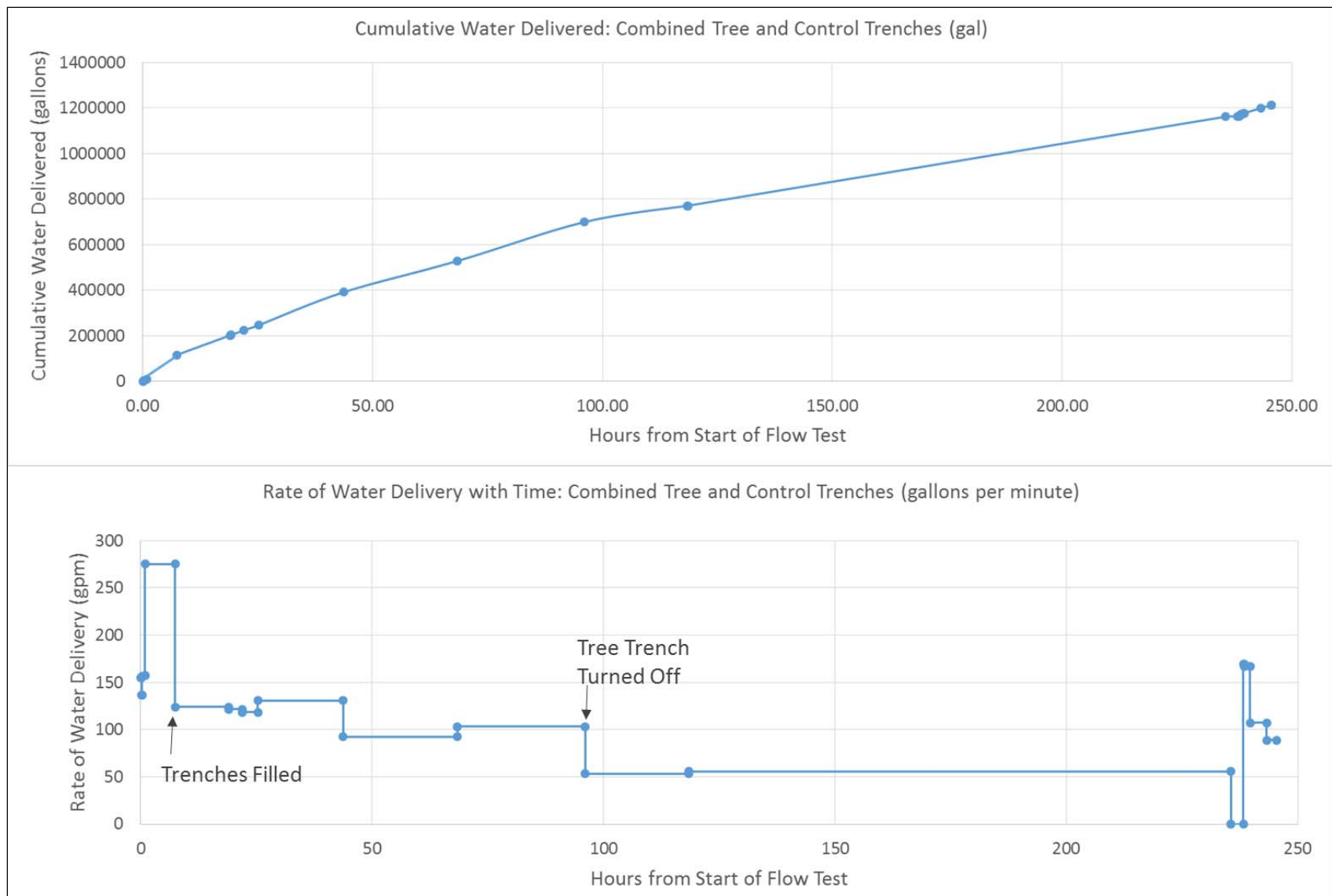
Figure 3-169. Water flow cumulative volumes over time (top) and corresponding flow rates (below).

Table 3-8. Flow volume breakdown by flow phase

| Flow Phase | Flow Volume (gallons) | Time Interval (hrs) |
|---|---|---|
| Primary Flow | 699,500 | 96 |
| CT on, TT off | 462,600 | 139.5 |
| Dye Test | 50,400 | 10 |

Table 3-9. Flow rate breakdown with flow phase

| Flow Phase | Time Interval (hrs) from start of flow | | Calculated Flow Rate (gpm) | Estimated Water Delivery Breakdown | | Comments |
|---|---|---|---|---|---|---|
| | Start | End | | Control Trench | Tree Trench | |
| Primary Flow | 0 | 0.95 | 150 | - | - | Trench filling, 2" delivery pipe |
| | 0.95 | 5 | 368 | - | - | Trench filling, 4" delivery pipe |
| | 5 | 25.2 | 123 | 30 | 93 | CT and TT filled |
| | 25.2 | 43.7 | 131 | 31 | 100 | |
| | 43.7 | 68.4 | 92 | 22 | 70 | |
| | 68.4 | 96 | 105 | 25 | 80 | |
| CT on, TT off | 96 | 118.5 | 53 | 25 | 28 | TT receiving water through burrow |
| | 118.5 | 235.5 | 56 | 27 | 29 | between CT and TT |
| Dye Test | 235.5 | 238.2 | 0 | 0 | 0 | Water turned off before pulse of dye |
| | 238.2 | 238.9 | 169 | - | - | Filling trenches |
| | 238.9 | 239.7 | 167 | - | - | Filling trenches |
| | 239.7 | 243.3 | 108 | 26 | 82 | Trenches are full |
| | 243.3 | 245.5 | 89 | 21 | 68 | Water turned off at Time = 245.5 hrs |

### 3.1.4.6    Post Flow Test Observations

After completion of the flow test, instruments were left in to monitor the beginning of the drying phase as pore pressures dropped and soils began to dry and rebuild suction. On June 5, 2012, the instrument monitoring phase ended. Tensiometers were removed on June 8, 2012. During this visit, gravel bags were removed and zones of high flow were inspected in an effort to determine what caused the concentrated flow.

On the landside slope of the control trench, between Stations CT 6 and 10, mid-slope and top of slope gravel bags were placed to prevent erosion of the slope under concentrated flows. Near the top of slope, at Stations CT 7 to 10, two seeps were encountered at 3 am on 5/22, a little over 13 hours into the flow test. A photograph of the findings at that location is provided as Figure 3-170. Two burrows were encountered (1 ½ inch diameter each) consistent in size with gopher or vole. Similarly, Figure 3-171 shows the mid-slope burrow beneath the pile of gravel bags at Station CT 7. Upon lifting the gravel bags, worms and traces of worms were found through the soils under the bag. Armadillidiidae, also known as pill bugs, were abundant and disappeared into the burrows and worm traces when the gravel bags were lifted.



Figure 3-170. Two burrows (left) encountered at Station CT 9 near the top of slope (upper right). The burrows were about 1.5 inches in diameter.

Figure 3-171. The gravel bags were parted (lower right) and a single burrow was revealed at Station CT 7. The burrow was about 1 ½ inch in diameter and the top of the burrow extended into the slope.

The seep areas at instrument lines A and D were inspected and no traces of mammal burrows could be found in this area. Similar to the burrow at instrument line C, however, earthworms and pill bugs were observed to be in abundance as shown on Figure 3-172 through Figure 3-174. Occasional holes on the order of ¼ inch diameter and traces of earthworms, some still occupied by a worm, were seen under each gravel bag. These were noted, as no other mammal burrow could be located. Further, water had been recorded about 19 hours into the flow test flowing from small holes (¼ to ½ inch diameter) at the location of these seeps near Station 56 at instrument line D. The small holes were found beneath gravel bags at all locations where gravel bags had been placed, but it is unclear whether the holes had been present during the flow test or were created post-flow.

Figure 3-172. Station TT 57 to 59 seepage location upon lifting gravel bags. Worm traces were abundant and ¼ inch diameter holes entering into the slope were occasional.



Figure 3-173. View beneath gravel bags at Station TT 50, 8 days post-flow. Note earthworm traces and pill bugs in abundance.

Figure 3-174. Gravel bag Station 73 below landside oak tree. Pill bugs seemed to disappear into a cavity that, upon excavation, did not seem to extend anywhere or resemble a burrow. Worm traces were found to be abundant as in other locations.

After the site had been allowed one month to dry, the restoration phase occurred between July 2 and July 6, 2012 to remove the gravel in the trench and refill with compacted backfill. A decision was made not to repair site cracking and slope deformations as the levee is not considered a flood control structure due to the bypass levee constructed in 2008. The fallen waterside oak tree was slated for removal following the backfill work and at the convenience of RD 1601 and DWR.

During the removal of gravel, an effort was made to preserve the condition of the walls and base of the trench so that key observations could be made. Gravel was carefully removed with a vacuum truck or backhoe bucket centered such that the walls were not disturbed within zones to be inspected. All walls were inspected to a depth of 4 feet and selected sections were viewed to 8 foot depth looking for holes, fractures, roots of interest, or other anomalies that may have affected flow patterns. Features were logged and photographed.

 The crack between the trenches was explored. White paint was funneled into the crack prior to excavation of the gravel in an effort to reveal the pattern and depth of cracking. The crack had partially closed by the time of repair as discussed previously and shown on Figure 3-115. The crack did not follow a clean path as the soils are heterogeneous and may pull apart along several planes rather than forming a single clean crack. Figure 3-175 and Figure 3-176 show the trench wall at Station CT 31.5 looking south, while Figure 3-177 shows the trench wall at Station TT 0 looking north. A burrow was encountered connecting the trench walls positioned a distance of 43 inches from the top of the asphalt at Station CT 31.5 and a distance of 24 inches from the top of pavement at Station TT 0 (size = 2.5 inches high, 3.5 inches wide). A crack was seen on the control trench end wall extending down to a depth of 82 inches from the surface, beginning at the crack between the trenches (Figure 3-175 and Figure 3-176). In some places the crack becomes very visible and in

other places concealed within looser deposits. On the tree trench endwall at Station TT 0, the visible crack extends down to the burrow location and then transitions into as deposit of Material 2, the thinly bedded silt material, which cleaves readily along predefined planes. Figure 3-177 shows cracking at the end wall of Station TT 0 with the lower right photo showing Material 2 with vertical bedding, exhibiting small separations along beds of fine sand between silt layers. Evidence of soil deformation could not be found at depths below 43 inches as the stratigraphy transitioned into Material 4, a plastic silt material discussed previously.



Figure 3-175. View looking south at the upper 4 feet of control trench end wall at Station CT 31.5 (left) with close-in views of cracking near the top of the trench (upper right) and just above and to the left of the burrow.

Figure 3-176. View looking south of 8 foot deep trench at end wall of control trench at Station CT 31.5 showing cracking to a depth of 82 inches.



Figure 3-177. View north of tree trench end wall at Station TT 0 showing a burrow (2 feet deep) and a series of vertical tension cracks along bedding planes of Material 2 (thinly bedded silt).

The area at Station TT 17 to 18, particularly the waterside wall, was inspected for the condition of roots and the condition of the trench bottom. The trench bottom was inspected looking for cracks extending below the trench (Figure 3-178). No cracking was found along the walls or base in this area. Large roots had been encountered and cut prior to the flow test. These roots were viewed and nothing abnormal was discovered. The roots did appear to have begun to decay between the time of excavation and the post-flow repair (about 2 months), but did not show clear signs of pullout or deformation due to falling of the waterside tree (Figure 3-178).
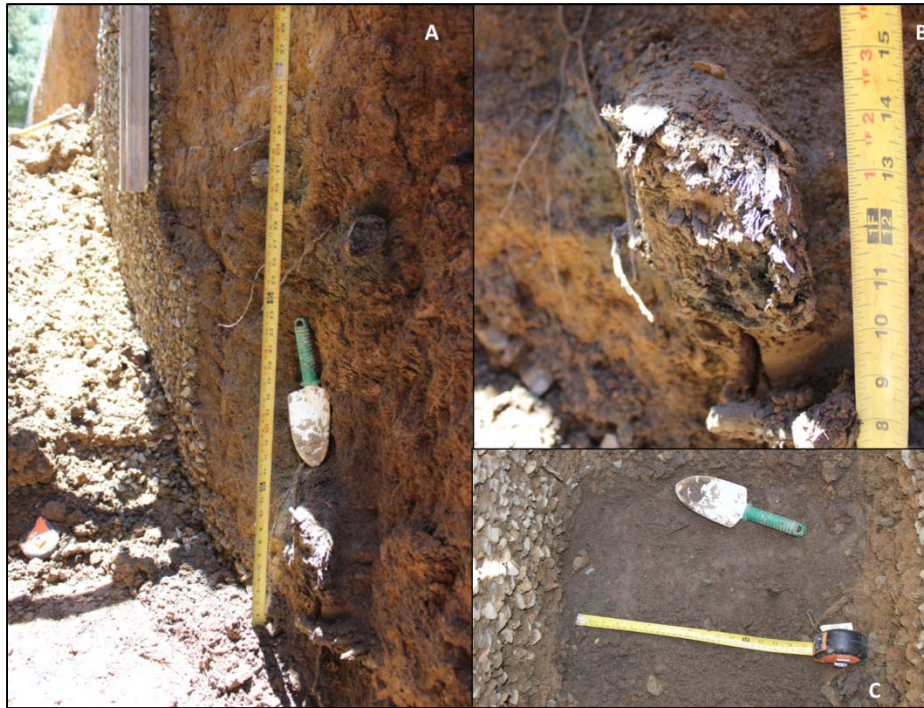


Figure 3-178. Roots at Sta 17; and bottom inspection for cracks at base of trench.

Burrowing activity is believed to have played a key role in influencing the flow patterns during the flow test. Inspections determined whether additional burrows had opened or whether plugs that had been placed during construction had held up over the 10 day flow test. Figure 3-179 shows the locations of two new burrows within the control trench that were not found or plugged during trenching operations. Both burrows were on the land side at Station CT 10 (depth 18 inches, diameter 1 ½ inch) and at Station CT 3 (depth 3 feet, diameter $3/_8$ inch). Figure 3-180 shows a zone of burrow patches located within Stations 70 to 73. For reference, the landside tree is centered at Station 70 with the canopy spanning from approximate Stations TT 50 to TT 90. Three burrows can be seen in the photo and all are intact following the flow test. All burrow patches are found intact except one waterside burrow at Station 11 within the control trench. At this burrow, the burrow patch was missing and the hole had grown in size since initial discovery during the trenching phase (Figure 3-181).

Figure 3-179. New burrow landside Station CT 10 at 18 inches deep (left) and new small burrow at landside CT 3 (right).



Figure 3-180. Patched burrows Station TT 70 to 73. A) overview of patched burrows, B) and C) Initially intact burrow patch is removed and viewed; D) intact landside burrow patch; E) intact waterside burrow patch.

Figure 3-181. Open burrow at waterside Station CT 11 (top images) and intact patch on burrow at landside Station CT 12 (bottom images).

Once the site repair had been completed, temporary fencing was removed and photographs were taken showing the site after vegetation returned several weeks following the flow test (Figure 3-182). Patterns of aggressive blackberry growth within the zones of highest burrowing activity are apparent in the photographs.

Figure 3-182. Vegetation patterns post-flow show blackberry growing back aggressively and coinciding with areas of observed burrowing activity.

### 3.1.4.7    T-LiDAR Findings

Baseline scans with tripod-based light detection and ranging (T-LiDAR) equipment were performed prior to trench construction. This work was performed by Dr. Gerald Bawden and his team with the USGS. The USGS team subsequently scanned the site following the primary flow phase of the test and the dye test for the purpose of improving upon standard field data gathering methods to monitor deformations associated with the flow testing at the site. The USGS team has compiled their findings and published a report summarizing their work under separate cover (Bawden et al., 2013-DRAFT). Figure 3-183 shows a T-LiDAR image from the pre-scan condition shot on April 9, 2012 before trenching began overlain with an image shot on May 29th, 2012 following the primary flow test and failure of the waterside oak tree. The image shows the rotation of the waterside oak tree.
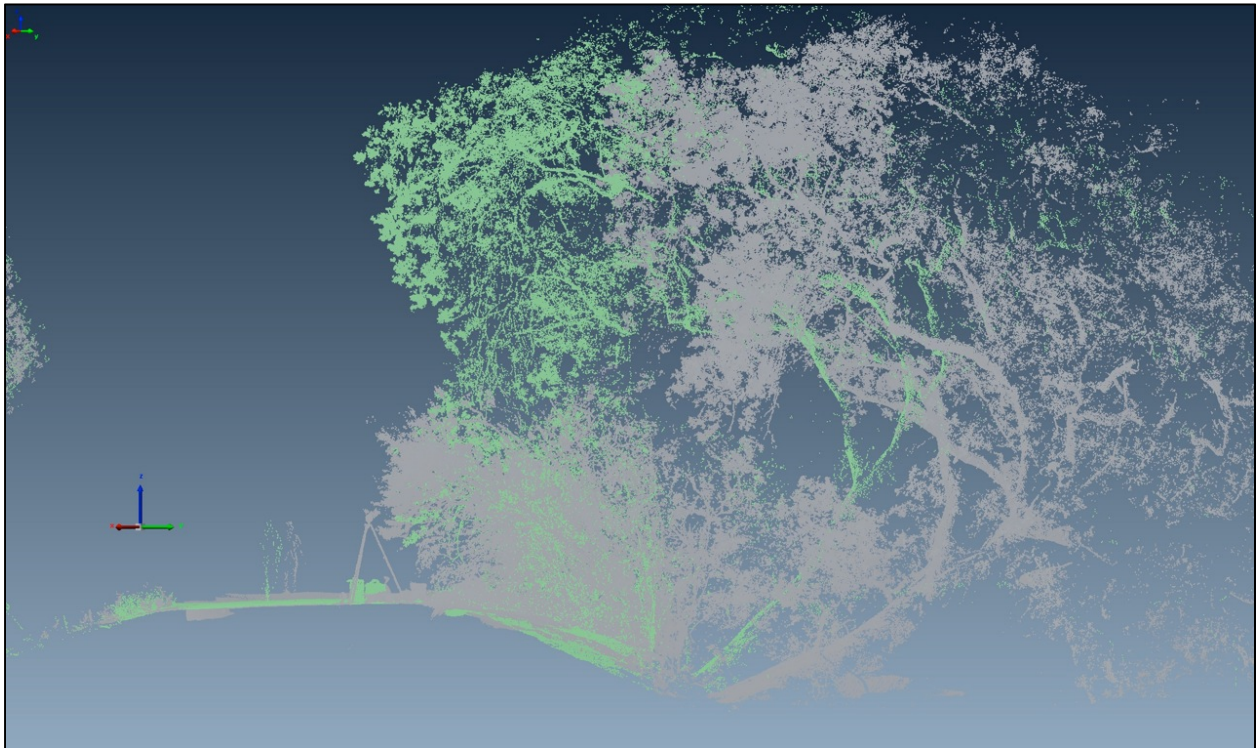
Figure 3-183. T-LiDAR images shot and analyzed by Gerald Bawden and his team from the USGS. The image shows the rotation of the waterside oak tree between April 2012, prior to construction of the trenches, and May 29, 2012, after the failure of the tree on May 23.

Figure 3-184 shows the vertical deformation across the study area as determined by the USGS T-LiDAR study (Bawden et al, 2013-DRAFT). Subsidence on the order of 6 cm (2.5 in) is seen in a semi-circular pattern on the waterside between trench Stations TT 20 and 50. Smaller deformations on the order of 1.5 cm (0.6 in) are visible on the landside of the trench between Stations TT 35 and 45. The unstable trench zone that eventually failed during trench backfill (Figure 3-125) can be seen on Figure 3-184 and Figure 3-185 to have undergone subsidence on the order 3 ½ cm (1.4 in). These deformations appear to be moving in the direction of the trench. Given that the T-LiDAR study has captured these as total deformations that occurred between scans before and after the study, it is unclear when exactly these deformations occurred. Surface expression of the deformations was not visually apparent as these deformations were apparently occurring over the span of the entire road.

Figure 3-185 is a similar figure to Figure 3-184, but limits the scale to 2 cm of displacement to focus in on areas of smaller displacements. A subsidence of 1 ½ to 2 centimeters (0.6 to 0.8 inch) of the waterside trench wall is seen relative to the landside wall in the vicinity of the crack located between the control and tree trenches. Field measurements found the crack to have a vertical offset of 0.5 to 0.6 inch, relatively consistent with determinations by the USGS team.

Cracking was noted on the west side of the crown road during the dye test on 5/31/12, the last day of flow (Figure 3-126 and Figure 3-127). It can be seen on Figure 3-184 and Figure 3-185 that this cracking is just on the outer edge of the movement area and may be associated. During trench

construction, the zone between Station TT 37 to 42 was noted to have a zone of highly unstable soils where the most stable competent soils (Materials 4 and 5) were found to dip below the trench bottom (Figure 3-87). While other deformations onsite were visually apparent and measured in the field, the discovery of subsidence within this zone by the USGS team will provide aid in the interpretation of the study, as this deformation was very gradual, over a broad area, providing few visual clues to be detected by eye in the field.

Additionally, the USGS team noted that a small rotation of the landside oak tree, on the order of 5 cm (2 inches) at a height of 2 meters up the tree (about 6.5 feet), was detected in the study. For a mid-slope tree experiencing saturation of its root system and gusting winds (as were observed on May 22, 2012), a rotation of this nature is not unexpected given the softening of soils within the root zone and the existing lean angle of the tree, slightly off vertical in the downhill direction. With pruning and the tree's natural ability to maintain balance in response to small deformations, this type of deformation may be considered tolerable, depending on the situation, with proper maintenance and inspection. The rotation could not be visually detected, nor were there any signs of distress in the zone around the landside oak tree.
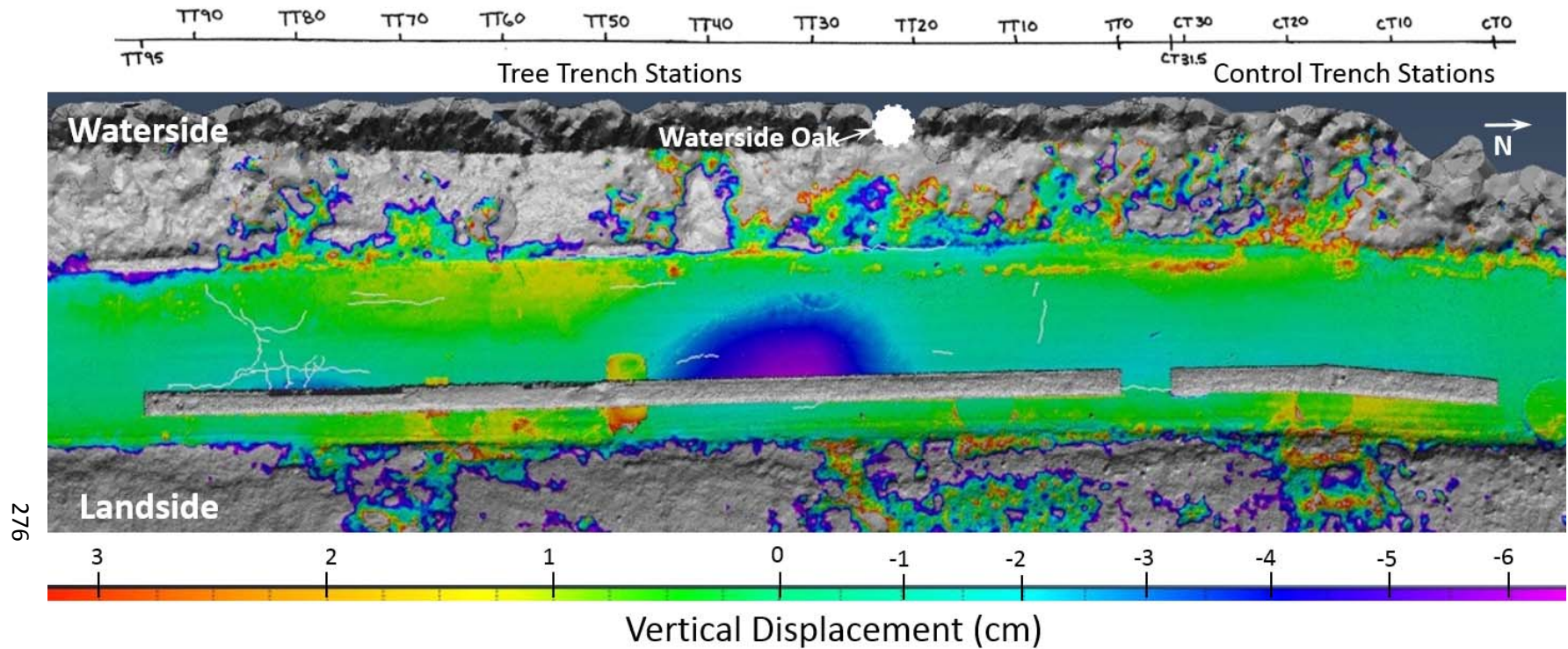
Figure 3-184. Image showing vertical deformations along the length of the trench. Settlements of up to 6 cm (2.4 inches) were observed at Stations TT 20 through 48 through comparison of T-LiDAR scans (4/9/12 and 6/4/12). These movements were not visually apparent during testing. Image provided by Gerald Bawden of the USGS.
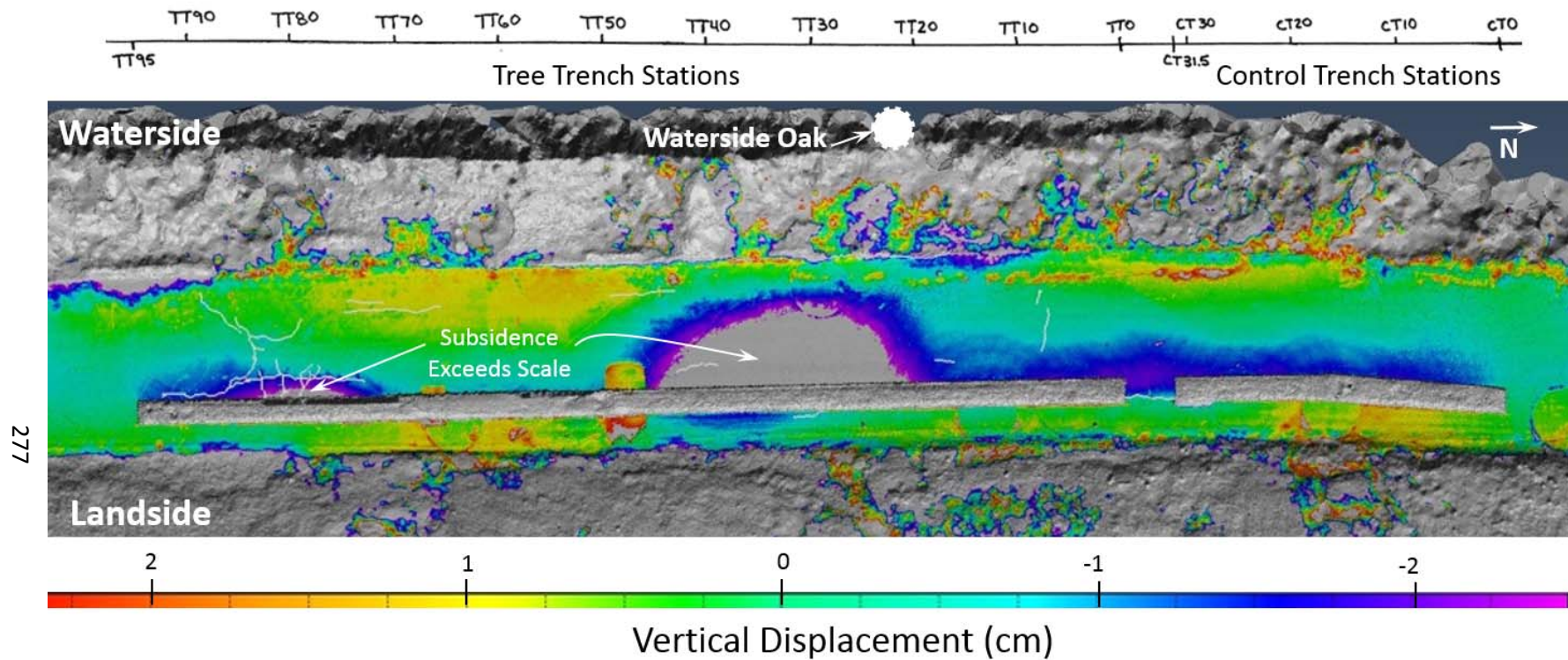
Figure 3-185. T-LiDAR scan comparison of 4/9/12 and 6/4/12 images. Similar to Figure 3-184 but zoomed in to focus on vertical movements less than 2 cm to better define deformations associated with cracking between the control and tree trenches. Image provided by Gerald Bawden of the USGS.

## 3.2 DATA INTERPRETATION

### 3.2.1 Discussion of Observations

Observations and data collection were made before site construction, during trenching, throughout the 10-day flow test, after flow, and during restoration of the levee and backfill of the trenches. Data collected included:

- A 130 foot stretch of a delta levee logged in detail to a depth of 8 feet (10-foot levee height). Logs include detailed sketches of the root systems of nearby trees, burrows, and variable soil conditions.
- Pre-flow test inspection with Dr. Dirk Van Vuren of UC Davis to look at burrowing animal activity at the site.
- Soil borings and logging for each instrument location as well as 3 cone penetration tests along the levee crown.
- Continuous monitoring of positive and negative pore water pressures before, during, and after the flow test using a network of 48 instruments, including piezometers and tensiometers.
- Field observations of time and location of observed seeps along the surface of the levee.
- Field observations and monitoring of cracks and their progression throughout the test. This included observations associated with a fallen tree on the water side of the levee.
- Deformations associated with the studied trees and the crown road, analyzed through T-LiDAR analysis by Dr. Gerald Bawden and his team with the USGS.
- Manual monitoring of flow volumes through reading of a mechanical gauge connected to the pump system.
- Observations of seepage and preferential pathways during a 1-day tracer dye test.
- Post-flow site inspections to evaluate conditions that may have affected flow and to evaluate the age (60 years) of the fallen waterside tree.

Figure 3-186 summarizes the most notable site observations including the profile of the old (possibly natural) levee on which the existing levee is founded, cracking associated with the failure of the waterside oak tree, zones of discontinuity in the old levee and loose backfill of the void, zones within the trench where burrowing was abundant, landside and waterside seepage areas, delineation of T-LiDAR-detected subsidence between 1.5 and 6 cm, and extent of blackberry vegetation. Information is presented in the context of the test layout, including locations of the landside and waterside oak trees, the position of the trenches, and the limits of the levee slopes, and crown road (at top of slope).
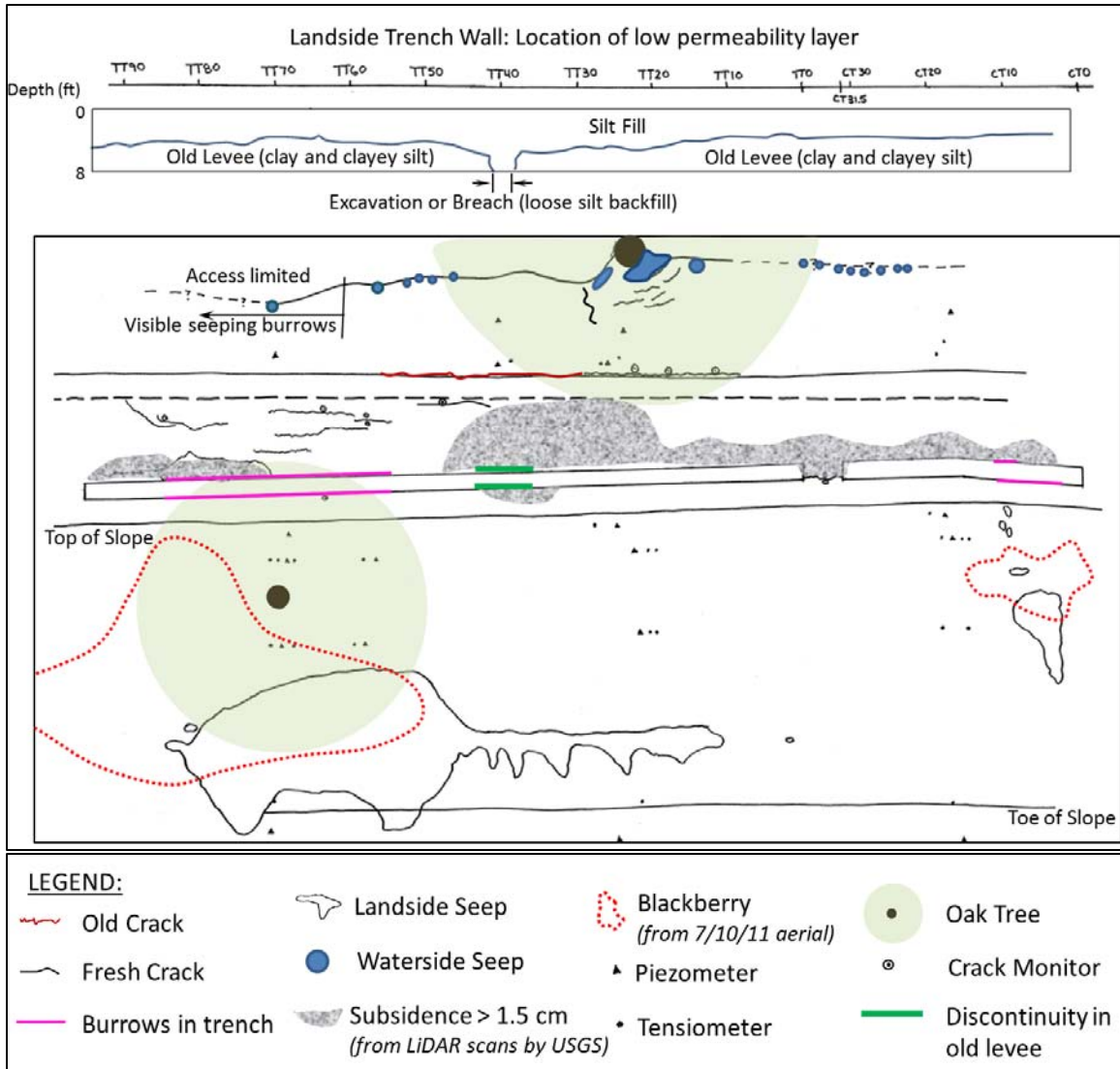
Figure 3-186. Overlay of relevant features of the crown trench seepage test. Includes site layout and instrumentation, relevant vegetation, burrow and stratigraphic data recorded during trenching, cracking and seepage observed during the entire 10 day flow test.

In addition to data collected during the test, available reports and soil data, historical records, aerial photography, and historic topography were reviewed and incorporated into the analysis of the crown trench seepage test.  The documents revealed:

- Twitchell Island was first reclaimed in 1869 (Thompson, 2006). Many of the levees at Twitchell Island were founded on natural levees (KSN, 2010). The southern levees, bordering the San Joaquin River are vulnerable due to their peat foundation, while northern levees more stable due to their foundation on alluvial soils (Thompson, 2006).  Twitchell Island is reported to have flooded repeatedly between 1870-1875, and 1894 to 1909, while the island was temporarily abandoned between 1875 and 1894.

- The oxbow section of Sevenmile Slough flowed as part of the slough as of 1932. Around 1950, the Sevenmile Slough was gated. Topography in 1952 shows the flow channel of the oxbow section at the study site as a wetland. Two structures and an access road are present in the vicinity of the study area in 1932 and gone by 1952. Poor records exist for the period between 1920 and 1960 (URS, 2011).
- Aerial photography shows that the levee under study was bypassed in the summer of 2008. A toe ditch at the study site was rendered inactive at that time and appears to have been filled by 2011.
- Aerial images were used to date vegetation and determine extent. The approximate age of the landside oak tree is estimated to be on the order of 25-30 years old. Blackberry groundcover corresponds well to where burrowing was most abundant at the site and aerial images helped to delineate the limits.

Figure 3-187 shows the study area overlain on 1932 topography in order to create interpreted stratigraphic sections of the levee for the purposes of seepage and slope stability modeling. Sections are shown extending across the former flow channel. Depth to sediment within the main channel of the slough was measured at 25 feet below the water line at the time of study, while shallow, loose sediments were found at depths of 2 to 3 feet from the water line within the oxbow section of the slough. Exploration to define site stratigraphy and geotechnical conditions did not extend into the slough. Interpreted stratigraphic sections are shown on Figure 3-188 through Figure 3-190. Where geologic contacts are bounded by exploratory points, solid contacts are shown, while queried contacts are shown in areas where contacts were approximated. It is unknown whether the current depth of the slough represents the original depth of the oxbow section, but it was considered to be an upper bound on the depth for the purpose of our analysis. The natural levee and sand deposits were extended in the stratigraphic sections based on available data. The natural levee clays and clayey silts may disappear beneath the channel, but a low permeability layer exists, separating the flow of water in the slough from the groundwater at depth, and so the layer is shown beneath the sediment.
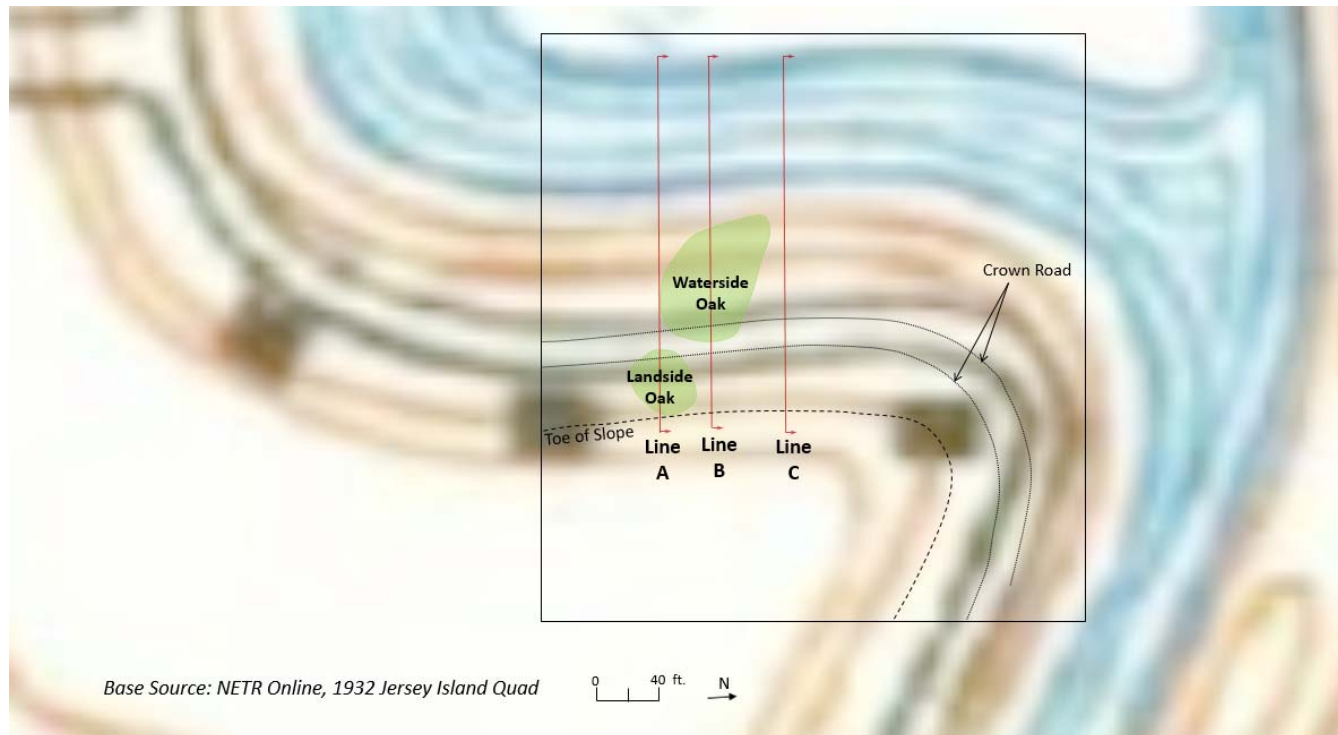
Figure 3-187. Section locations and oak trees under study overlain onto 1932 Jersey Island Quadrangle to estimate waterside channel geometry for interpreted sections.
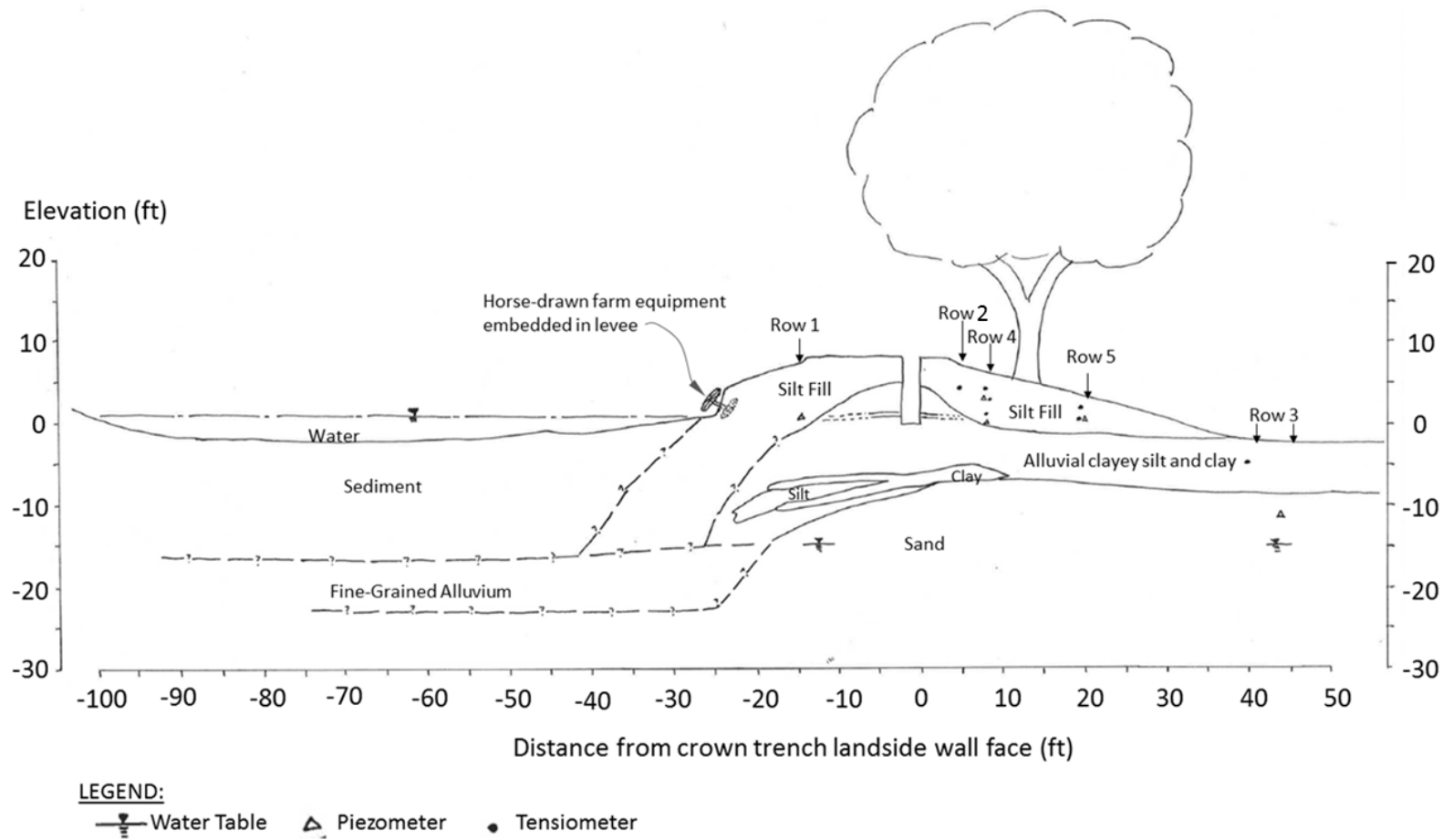
Figure 3-188. Interpreted stratigraphic section at instrument line A, through the landside oak tree. Instrument rows 1 through 5 are shown.
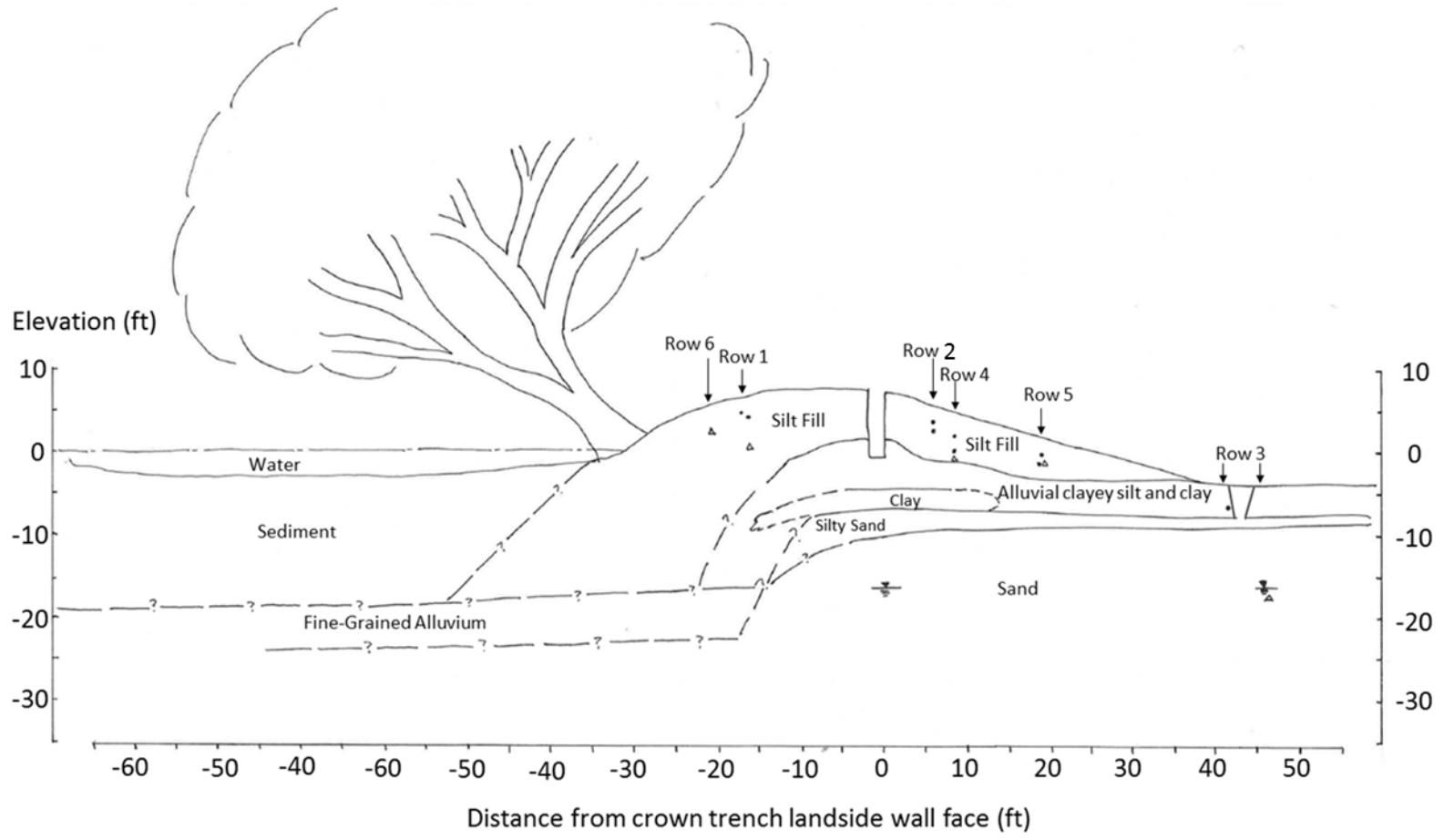
Figure 3-189. Interpreted stratigraphic section at instrument line B, through the waterside oak tree. Instrument rows 1 through 6 are shown.
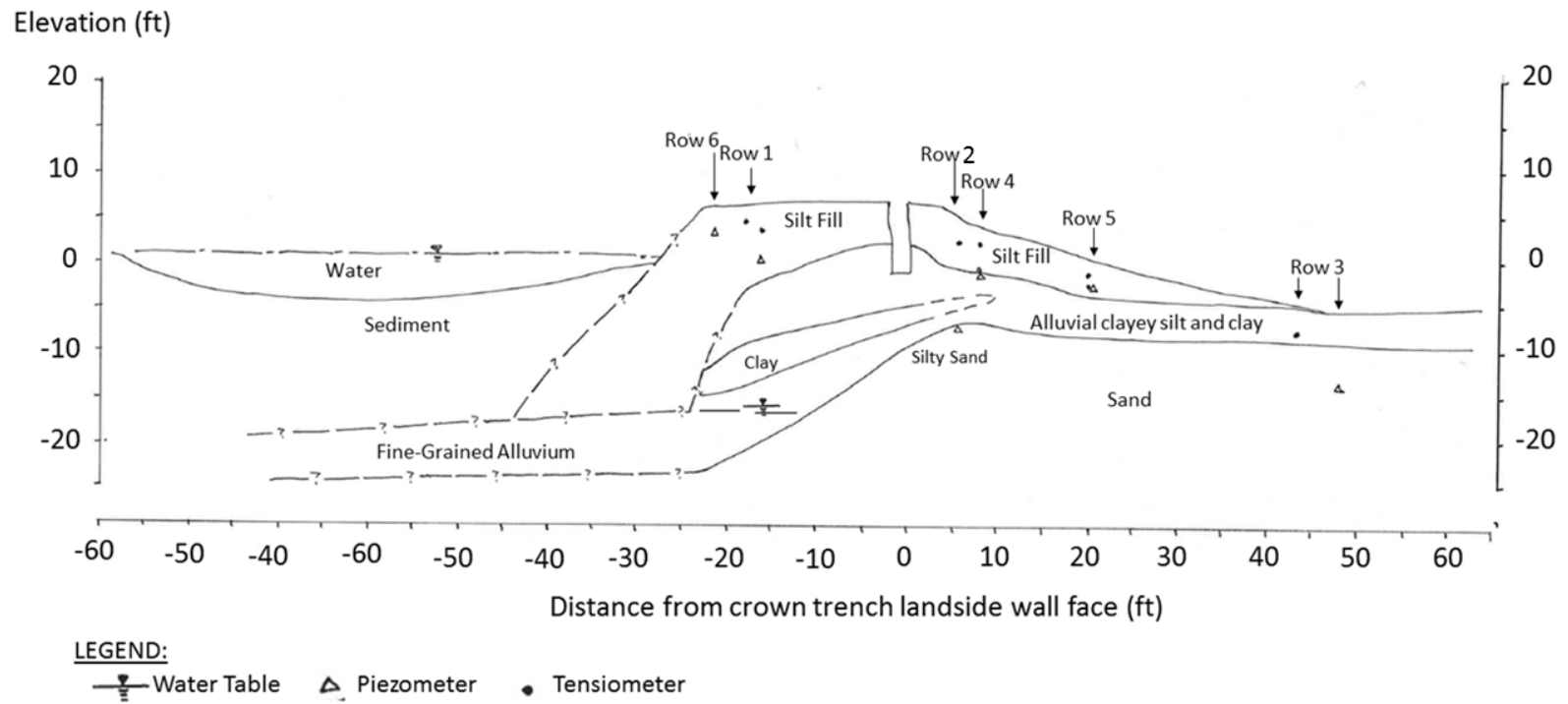
Figure 3-190. Interpreted stratigraphic section at instrument line C, within the control trench. Instrument rows 1 through 6 are shown.

### 3.2.1.1 Landside Flow Patterns

Landside flow patterns were found to be heavily influenced by (1) macroporosity associated with burrowing activities, and (2) site stratigraphy and heterogeneity.

Early seeps on the landside were observed to flow rapidly in the vicinity of Stations 8 to 10. Active mammal populations were observed just north of this area before construction began, and burrows were found at the slope surface at these locations following testing. Gravel bags placed on the seeps slowed flow, and the burrow flow slowed with time as permeability of the burrow walls increased with increased wetting which allowed the water to be absorbed by levee soils faster than it could flow into the burrow, consistent with Beven and Germann (1982).

Early seeps in the vicinity of instrument Lines A and D produced flows less rapidly than near the control instrument Line C, but they seemed to advance the wetting front over a broad area. In general, the primary seepage areas correlated well with where burrows were encountered in the trenches and with areas of blackberry groundcover (Figure 3-186). Based on flow observations, seeps in the vicinity of instrument Lines A and D, are likely influenced by burrows (intersected by the tree trench and plugged but not seen to outlet at the slope face) that do not form a direct pipe between the water source and the seepage points. The only holes that were found to outlet to the slope surface in this zone are worm holes. These small and relatively shallow holes were seen to concentrate flows within the shallow, surficial levee soils.

At the landside oak, pore water pressures were found to be elevated in piezometer PA4a relative to comparable instruments on other lines. This instrument is at a depth of 3 feet and located between the water source and the root ball of the landside oak tree. PA4b at a depth of 6 feet was not elevated. It is unclear whether there was a local effect from the root ball or from another anomaly, such as one of the numerous burrows in the vicinity.

Numerous researchers have found that the influence of macropores on flows through a soil matrix are greater in soils with higher clay content than in soils that are more granular in nature (Beven and Germann, 1982; Green and Askew 1965). Macropores require inflows into the pore that exceed lateral losses through the walls of the pore for flow to occur (Beven and Germann, 1982). Unless saturation is achieved, capillary forces within the soil matrix tend to hold water within the pores of the soil rather than allowing for flow into a macropore. Upon saturation of the area around the macropore, inflows into the pore are limited by the permeability of the pore walls. Rapid flows were observed north of the control instrument line C (Station CT 6 to 10) where a burrow was found to be rapidly flowing, likely connected directly to the control trench. In general, the landside of the levee performed well despite burrowing activity that appeared to advance the wetting front in the vicinity around instrument lines A and D. Flood fighting efforts were effective and, though water seeped from the levee slope face, visible signs of distress were not apparent during the test.

The water delivery trench was located within the crown of an early, and possibly natural, levee of lower permeability than soils used in raising the levee (Figure 3-29 through Figure 3-31 and Figure 3-188 through Figure 3-190). A discontinuity in the natural overbank

deposits (Material 4 of Section 3.1.3.2.1) extends below the explored depth of the 8 foot deep trench at Stations TT 37 to 42, between the landside and waterside trees. This gap suggests a possible old breach or an area that was locally excavated and then loosely refilled (Figure 3-186). The old levee appears to slope toward this discontinuity from the north and south between Stations TT 2 and TT 50. The slope of this material may divert water from the control instrument Line C, providing a possible explanation for instruments failing to saturate in this area.

The limits of this loose zone were well defined by the subsidence zone detected by T-LiDAR between Stations 22 and 47 (Figure 3-184 and Figure 3-186). To the south of this possible breach or previously disturbed area, burrowing activity within the old levee soils was found beginning at Station TT 56 and extending to Station TT 82 (Figure 3-186). The reason for such active burrowing activity at this location is unclear as is the role of the landside vegetation, both the landside oak tree and the blackberry groundcover around and below the tree. Smaller burrows within the 8 foot deep zones of the tree trench are consistent in size with those of voles and gophers, but not in typical behavior according to Dr. Van Vuren. These rodents enter from the landside and may have taken advantage of existing burrows, but in Dr. Van Vuren's opinion would be unlikely to themselves have burrowed to these depths. Muskrats enter from the waterside and inactive muskrat entrances were found in abundance along all accessible and visible areas we were able to inspect. Loose backfill of the gap in the old levee may have affected muskrat burrow patterns, since burrows were observed to occur preferentially in more stable soils where collapse is less likely. Given that the evidence of burrowing within the trench was only found within the old levee soils in this area and burrows had roots growing through them and were deemed inactive, it is possible that these burrows predate the tree. The age of the burrowing activity at this location is unknown and, according to Dr. Van Vuren, burrows can persist in stable cohesive soils for many years, and can be re-activated by animals over generations.


### 3.2.1.2    Landside Slope Stability

In general, signs of slope instability or distress were not observed on the landside of the levee during trench construction, the 10 day flow test, or repair of the site. T-LiDAR scans noted a small rotation of the landside tree, on the order of 0.12 degrees (or about 2 inches measured 6.5 feet up from the base of the tree). Given the deformations that occurred onsite, lining up the various T-LiDAR scans involved significant judgement, as spheres used to align scans fell within areas that had experienced deformation. Additional analysis may be required to resolve whether these deformations, as well as upward movements at the waterside top-of-slope, could be related to these challenges in data alignment.

### 3.2.1.3    Waterside Flow Patterns

Patterns of water flow and saturation on the waterside of the levee show that water arrived at the waterside oak tree to instrument line E (Stations TT 38 to 40) before arriving at instrument line B (Station TT 20 to 25). Burrows may have played a role in these flow patterns, as burrow entrances were observed all along the waterside toe. A single individual burrow could skew saturation results, however burrows were not found in these zones extending to the trench. As discussed previously, burrows that outlet to the slope face and are not connected to the water source may concentrate seepage but are less likely to

advance the wetting front. Waterside flow patterns may have been advanced by the zone of loose soil filling the gap in the old levee between Stations TT 37 to 42 and subsidence was observed in the T-LiDAR scans (Figure 3-186 and Figure 3-184). These loose and relatively more permeable soils may have allowed the wetting front to arrive at piezometer PE1 before other nearby instruments. Instruments at the control line were slower to saturate, with muskrat burrow entrances observed along the shoreline but without knowledge of how deeply they penetrate into the site. The control line is more uniform in soil conditions than the tree trench, without obvious pockets of loose soils or rapid changes in stratigraphy like those observed in the tree trench.

Pore water pressures in row 6 instruments (at the toe of the waterside oak tree as shown on Figure 3-188 through Figure 3-190) were evaluated to determine whether elevated values could be found upslope of the waterside oak tree, and no discernible pattern was found. Seepage was observed at the waterside oak tree at about 9 hours into the flow test. Water appeared to be seeping out of burrow entrances all along the waterside toe, and the area adjacent to and upslope of the tree trunk. When the tree fell, the pore water pressure dropped by about 0.25 feet of head at PB6 (Row 6 of Figure 3-189). Seepage stopped from the areas around the oak tree and pore pressures never returned to the level previously achieved prior to the fall of the tree. The fall of the tree seemed to render previously preferred macropore pathways inactive, possibly by introducing discontinuities. During they dye test on the tenth day of flow, seepage was seen flowing only from burrow sites outside of the area of the waterside oak tree (Figure 3-145; discussed in detail in Section 3.1.4.3). The complexity of preferred pathways created by muskrat burrow networks along the waterside slope seem to have a larger effect on pore water pressure accumulation than the presence of the root ball of the waterside oak tree.

### 3.2.1.4 Waterside Slope Stability

A series of deformations were observable during the 10 day flow test. These deformations are discussed in detail in Section 3.1.4.2 and summarized on Figure 3-186. The following primary areas of deformation are of interest:

- <u>Cracking between control and tree trench</u>: This crack began opening a little over 2 hours into the flow test, before trenches were full. The crack peaked in size 13 hours into the test and began to shrink after 15 hours. It is unclear whether these early cracks were connected to movements associated with the waterside oak tree prior to failure. The waterside oak tree fell 39 hours into the test.
- <u>Older and fresh cracking observed at the top of the waterside slope</u>: The cracks were buried under a wattle and leaves and were not discovered until after the tree fell. Once discovered, the fresh crack continued to move during the flow test
- <u>Pavement cracking (Stations TT 55 to 90):</u> Minor cracking was observed near southern end of tree trench. Crack patterns appear to outline movements toward the waterside, though T-LiDAR data shows upward movements of 1 to 1.5 cm. Thick pavement overlay (6" on a 4" original section) provides evidence of past poor performance and cracking. A localized section of the trench wall failed into the tree trench upon repair (Stations 65 to 88), revealing manganese oxide staining on a possible pre-existing fracture planes within the levee fills.

- Subsidence of up to 6 cm between Stations TT 20 and 50:  An area subsided up to 6 cm (observable in the T-LiDAR scans but not noted during testing), coincident with loose soils associated with the dip in the natural levee (Material 4) and the gap at Stations TT 37 to 42 (Figure 3-186). Timing of deformation is unknown, but a crack at Stations TT 40 to 50 opened late in the test (day 10 of flow). The crack lies near the zone of subsidence captured by analysis (Figure 3-186). The subsidence could be caused by settlement of the loose materials at this location toward the trench, as implied by the semicircular patterns on both land and water sides. Lateral offsets of pavement at the trench was not observed at this location, and trench walls did not collapse during the repair phase as they did at Stations 65 to 88 (Figure 3-124).
- Cracking in the area of the tree rootball after failure of the tree (Stations TT 16-28): Observed at 9:30 am on 5/23/12, coincident with the discovery of the tree failure

Cracking in the localized area of the root ball of the waterside tree between Stations TT 16 to 28 appeared when the tree fell and is considered attributable to the tree failure. Movement was seen in the embankment prior to observable tree movements. The extent to which deformations of the embankment (cracking at the top of slope and cracking between the control and tree trenches) were influenced by the presence of and movement of the waterside oak tree is unclear and will be discussed below and explored further through modeling.  Waterside fills were observed to be loose, with farm equipment embedded into the levee in one location (Figure 3-188 and Figure 3-28) and buried barbed wire fencing at the control section. The waterside tree is 60 years old (by ring count on the fallen tree that has since been cut), indicating that the tree did not appear on the loose soils of the waterside edge until after the slough was gated in 1950. As discussed above, historical data in combination with exploratory data were used to arrive at interpreted sections for modeling. These sections are presented on Figure 3-188 through Figure 3-190. The sections show the extent of the loose silt fills as well as a zone of weak clay within the old levee that was found in boring and CPT data.

The instability of loose soils along the waterside slope as well as potential sliding along the weak clay seam will be considered to explain the cracking observed at the southern end of the tree trench. A photograph taken just following a rain at the beginning of trench construction is shown on Figure 3-191. The photograph shows zones of water ponding in linear patterns west of the centerline of the levee crown road and tapering toward the waterside pavement edge near the southern end of the tree trench. Cracking patterns observed in the field follow a similar pattern. Subsidence may have occurred at pre-existing crack locations from past movements along the waterside slope. An old crack was found at the top of the waterside slope at Stations TT 28 to 55.

Vertical deformations on the order of 1.5 to 2 cm (0.6 to 0.8 inch) were captured by T-LiDAR (Figure 3-184) along the entire length of the control trench and extending to the previously discussed deformation zone at Station TT 20 to 50 (Figure 3-186). These deformations were tracked as they were able to be monitored at the gap between the trenches. The deformations began early in the flow test and grew as the wetting front progressed through the waterside instruments (TC1-36 saturated at 16.4 hours into the flow test). After about 13 to 15 hours of flow, deformations tapered and the crack began to stabilize and then decrease in size (Figure 3-115).  In this same timeframe, piezometer P2B was recording a sharp dip in recorded pressure, consistent with a sudden event opening a

new avenue for water flow and causing a rapid loss in building pore water pressures (Figure 3-155). Perhaps a previously blocked avenue for water flow suddenly opened at that time, such as a burrow or a crack. We do not know the time when the top of slope crack opened (Figure 3-136 through Figure 3-139) and if it was before the tree was observed to have fallen or in the same event. A seep was observed at the waterside oak at 9 hours into the flow test which may have relieved some pore water pressures. Other waterside seeps could not be inspected at that time as the water surface elevation in the slough was too high to allow for  the type of access available during the dye test. The tree did not fall until about 39 hours into the flow test, after the deformations along the control and tree trench had occurred and stabilized. A progressive failure scenario will be considered in our modeling efforts where the influence of the tree (including both the static loading as well as root reinforcing) is evaluated under the following scenarios:

1) A large failure plane extending back to the control and tree trenches using transient pore pressures at 2.5 hours into the flow test when movements were first observed.
2) A smaller failure envelope extending from the crack at the top of the waterside slope at a time 13 hours into the flow test (the time when this crack would have to have opened in a progressive failure scenario)
3) A failure scenario including only the root ball at 39 hours into the test versus a scenario extending to the top of the waterside slope
4) A failure scenario of the embankment movement without the presence of a tree or reinforcing elements at 2.5, 13, and 39 hours into flow as well as at steady state

Figure 3-191. Pattern of pavement cracking (right) is similar to pattern of ponding in the pavement just following a rain event and prior to trench construction. Asphalt sections show evidence of a thick overlay, an indication of previous pavement distress.

The conditions of an individual tree can impact the stability as well. The overall embankment stability is a key factor to be considered as well as the health of the tree and root system. The waterside oak tree is a valley oak. Cooper (1926) states that "It is plain that the oaks are excluded from the subaqueous soils because of saturation and consequent lack of aeration". Valley oaks are, however, the most tolerant of the oak species to wet conditions (Cooper, 1926; Jacobs et al., 1997). Low oxygen, or hypoxia, can decrease tree vigor (Kozlowski, 1985) and pre-dispose the tree to disease, insect pests, and root rot (Heritage and Duniway, 1985; Miller and Burke, 1977). The health of the waterside valley oak tree prior to the study was not known, but given the lean and the loose fills upon which the tree was founded (uncompacted soils along the waterside slope along with thick, soft sediments within the slough), this tree was not likely to have been supported adequately on this levee.

# CHAPTER 4

## Modeling the Effects of Woody Vegetation on Levee Stability

### 4.1   INTRODUCTION

Chapters 2 and 3 presented observations during the construction and implementation of two full-scale field tests performed on California levee sites. Field test conditions at each site were simulated using the Geostudio software package to gain additional insight into the impacts of levee trees on levee seepage and stability. The results of modeling simulations of the parallel Trench Wetting Front Test ('Cal Expo Site') and the Crown Trench Seepage Test ('Twitchell Island Site') are presented.

#### 4.1.1   Limit Equilibrium Method with the Geostudio Software Package

Modeling was performed using the General Limit Equilibrium Method (GLE). The method is based on two factor of safety equations balancing moments and forces over a range of potential slide masses. For each potential slide mass, the software divides the mass into a series of slices, taking a ratio of: 1) resisting moments divided by driving moments, and 2) resisting forces divided by driving forces. To solve this otherwise statically indeterminate system, an assumption is commonly made with regard to the angle of the normal force between slices. Side force assumptions are based on Morgenstern and Price (1965).

With the limit equilibrium method, the shear strength of site soils is estimated at the base and sides of each slice. For this study, the Mohr Coulomb method was implemented to arrive at a linear failure envelope defined by:

$$\tau = c + \sigma_n \tan \phi$$

where $\tau$ is shear strength, $\sigma_n$ is normal stress, and c is the intercept of the failure envelope axis of shear stress, and $\phi$ is the slope of the failure envelope. For drained conditions, effective stress parameters, $\phi'$ and c' are specified for each material type.

### 4.2   SLOPE STABILITY MODELING – CAL EXPO TEST SITE

#### 4.2.1   Approach

Two and three dimensional transient and steady state seepage modeling of the localized zone of study during the Parallel Trench Wetting Front Test at Cal Expo was performed by Cobos-Roa (2014). Available soil boings, cone penetration tests and nearby interpreted sections were reviewed and summarized in Appendix 2B. Nearby interpreted sections were prepared by URS (2009). These sections were modified slightly based on available soil information near the site (Figure 4-1), and stratigraphic information summarized in Appendices 2A, 2B, and 2C. The slurry wall that exists at the site was omitted from the

seepage and slope stability analysis to view the impact of the decomposing root system for a levee without a slurry wall.

The site was evaluated under steady state seepage conditions under simulated flood conditions. Steady state seepage conditions with water surface elevations of 40 feet and 50 feet were simulated for input into stability models. The model geometry is presented as Figure 4-2. The root system was modeled either as a zone with lower hydraulic conductivity than surrounding soils or as a zone with voids. The models were performed in two dimensions, though the problem is three dimensional. Where three-dimensional effects are important, mass averaging of slide sections across the potential slide area, as presented in subsequent sections, or the use of three-dimensional models could be implemented to improve the analysis.

Drained friction angles for similar soil deposits at nearby locations modeled by URS (2009) were adopted to model stability at the site. Selected parameters and are summarized on Figure 4-2. Design parameters forced a failure plane to avoid intersecting the stump through use of a high friction angle. The loose nature of decomposing roots, partially in-filled with loose soils, was estimated based on an assumption that the decomposed roots may be about two-thirds filled with loose frictional soils and organic matter. A typical effective stress friction angle for a very loose sand is $\phi' < 30°$. An effective stress friction angle of 20 degrees was selected to represent the very loose infill soil and void space.
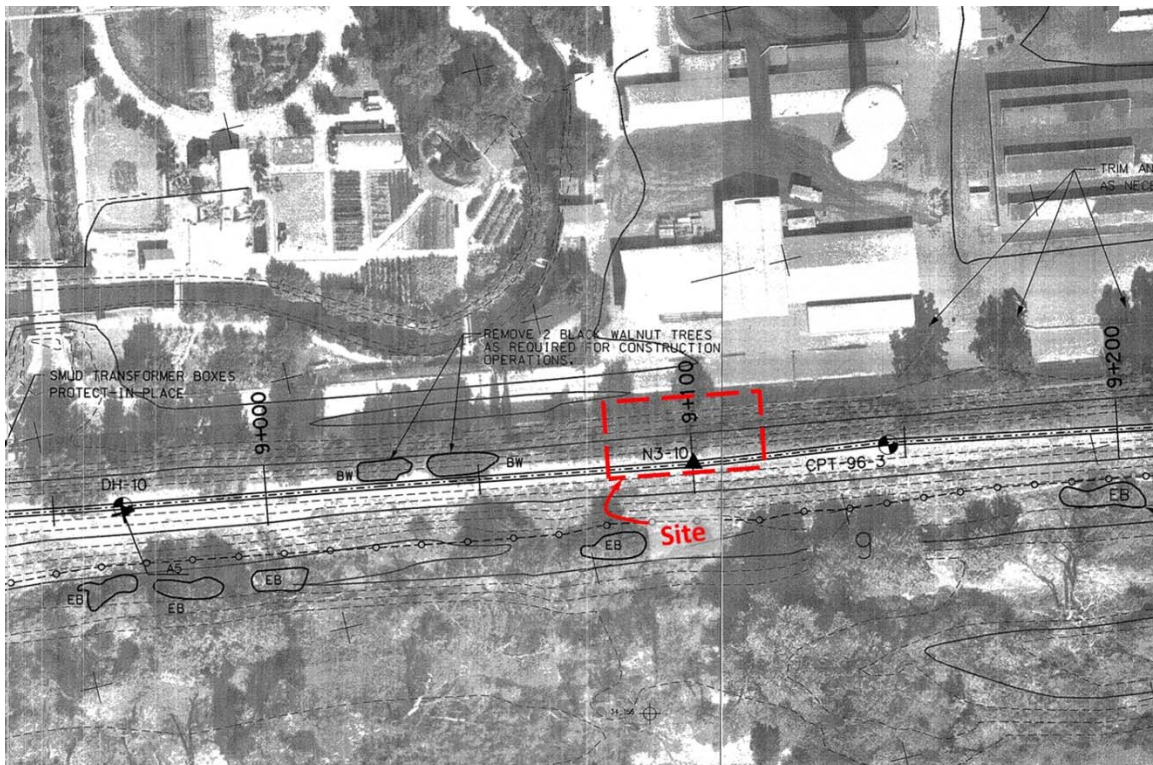


Figure 4-1. Excerpt from the American River Watershed Project. Our study site is at Station 9+100 on the plan. Source: USACE, 1999.

| | | Drained Parameters | |
| | Unit Weight (pcf) | c' | φ' |
|---|---|---|---|
| Silt (ML) | 120 | 0 | 33 |
| Silty Gravel (GM) | 135 | 0 | 45 |
| Silty Lean Clay (CL) | 110 | 0 | 33 |
| Silty Sand (SM) | 130 | 0 | 40 |
| Stump | 60 | 0 | 60 |
| Decayed Roots | 85 | 0 | 20 |
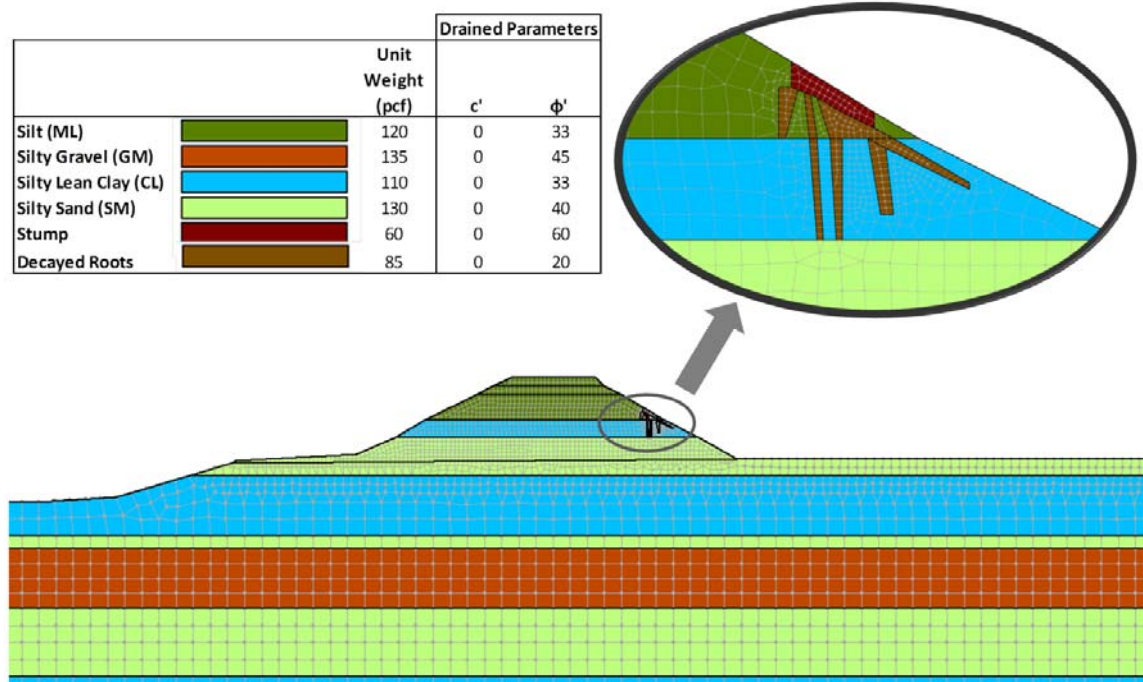
Figure 4-2. Conceptual levee section representative of the test site.

## 4.2.2 Results

The effect of a decomposing root system was explored based on the conditions noted above. Figure 4-3 presents factors of safety at a cross section extending through the root system of the decomposing stump as well as a similar section without a stump. Steady state seepage conditions were generated based on a waterside flood condition at a constant head of 40 feet and these conditions were input into the slope stability model. The water surface within the levee embankment has not risen to the level of the root system and therefore pore water pressure differences between the two models are minimal within the slide circle. Both show factors of safety of 1.34 for similar slide circles.

In Figure 4-4, the levee section is modeled with a root system acting as a barrier, acting as a drain or absent. Results show factors of safety are lowest (FS = 1.16) when the root system acts to block flow. Pressures build behind the blockage, reducing frictional strength due to decreased effective stress. In the case where the stump acts as a drain, the water surface is drawn down, reducing pore water pressures, increasing frictional shear strength, and increasing the factor of safety (FS = 1.33) against slope instability. When no stump is present, the factor of safety against instability was calculated to be 1.26. Other mechanisms of failure, such as the change in exit gradients due to the stump, were not evaluated as part of this effort. When the root system acts as a series of voids, high seepage exit gradients may present a more important failure mechanism than slope stability.
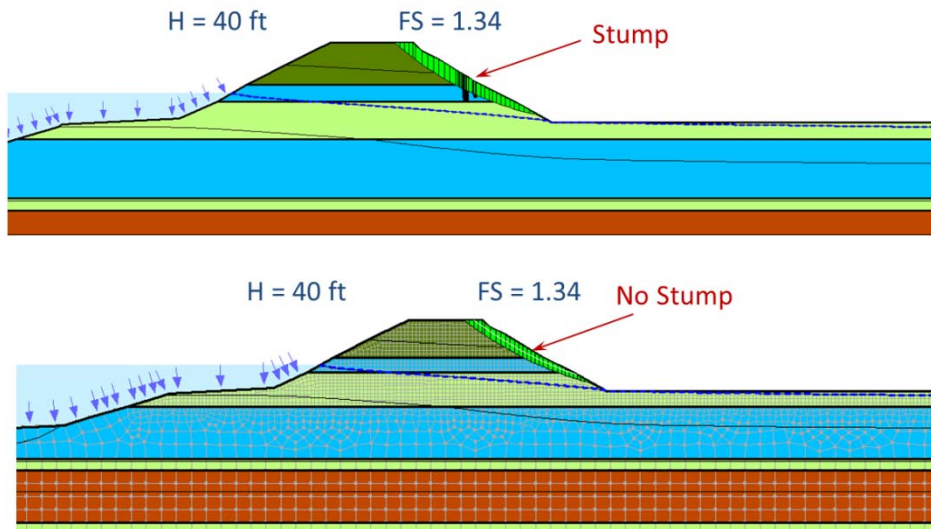
Figure 4-3.  A comparison of simulations with and without a stump yields factors of similar factors of safety for similar slide circles.
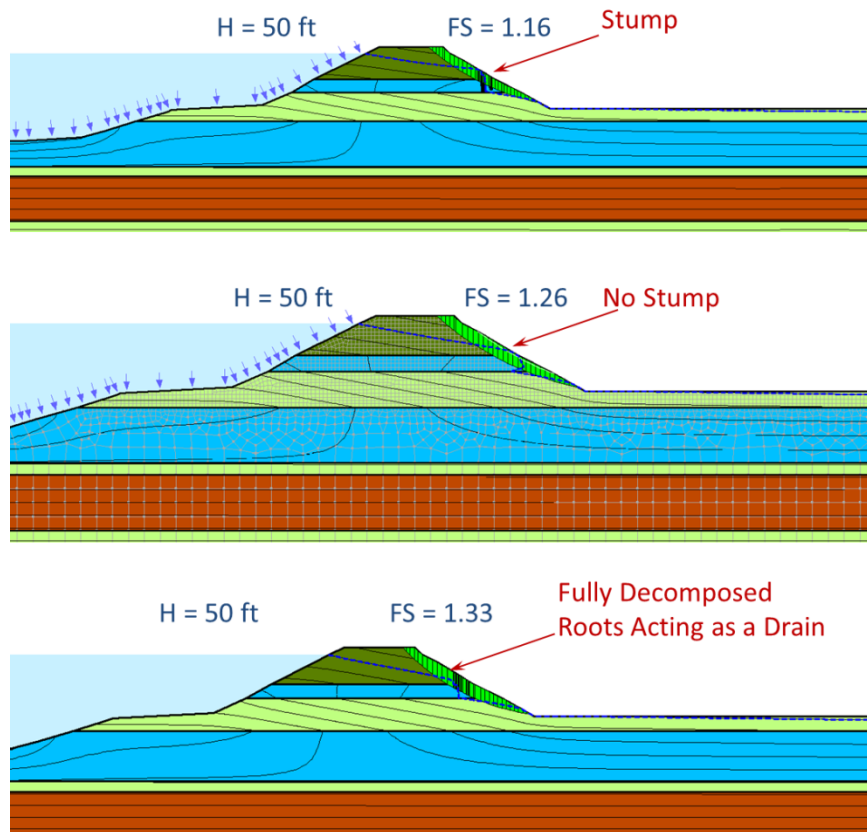


Figure 4-4. Total hydraulic head is held at 50 feet on the waterside. Three models are compared showing factor of safety with a low permeability stump and root system, no root system, or a fully decomposed root system acting as a series of voids.

## 4.3 SLOPE STABILITY MODELING – TWITCHELL ISLAND TEST SITE

As described in Chapter 3, cracks indicative of levee deformation were observed at numerous locations along the levee crown and waterside slope during the Crown Trench Seepage Test at Twitchell Island in Rio Vista, California. Based on the patterns of cracking, four possible waterside slide and two landside scenarios were identified for analysis and discussed in Chapter 3. Figure 4-5 illustrates the failure scenarios selected for modeling.
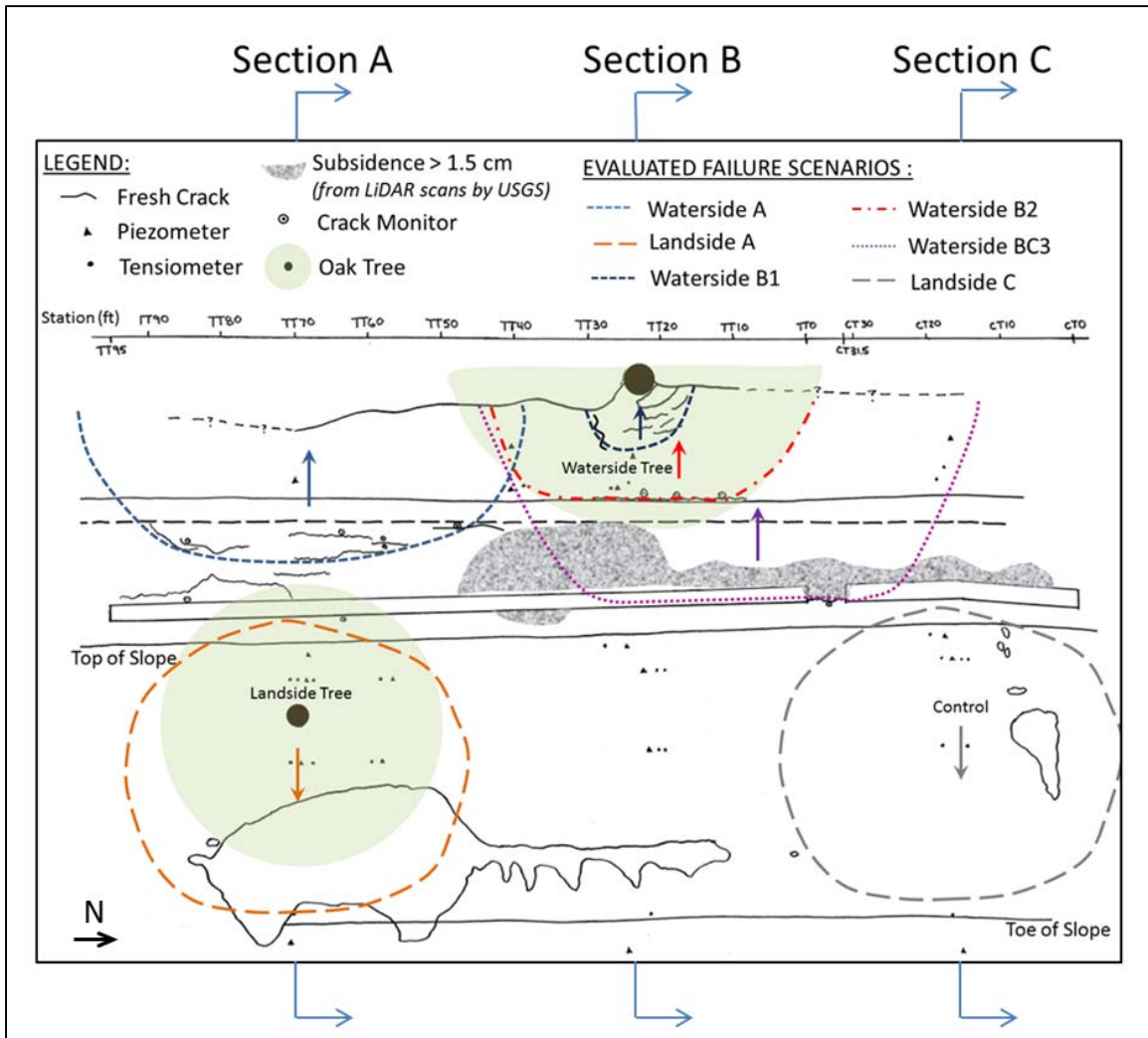


Figure 4-5. Four waterside and two landside failure scenarios are delineated for analysis.

Slope/W, the slope stability module of the Geostudio software package, is capable of analyzing two-dimensional cross sections for slope stability with limit equilibrium analysis. Isolated levee trees and their root systems are three dimensional problems. Mass averaging of 2D FS values of multiple 2D sections provides a reasonable approximation of the 3D FS (e.g., Seed et al., 1990). A simplified method is explored through mass averaged factors of safety over the slide mass as follows:

$$FS_{3D} = \frac{\sum_{i=1}^{i=n}(FS_{2D})_i(m)_i}{\sum_{i=1}^{i=n}(m)_i}$$

Three basic cross sections based on the interpreted geometry of the Twitchell Island test site, as discussed in Chapter 3, are presented as Figure 4-6, Figure 4-7, and Figure 4-8. These three basic sections are used in all models, varying the loading and reinforcement conditions the scenarios, as appropriate.
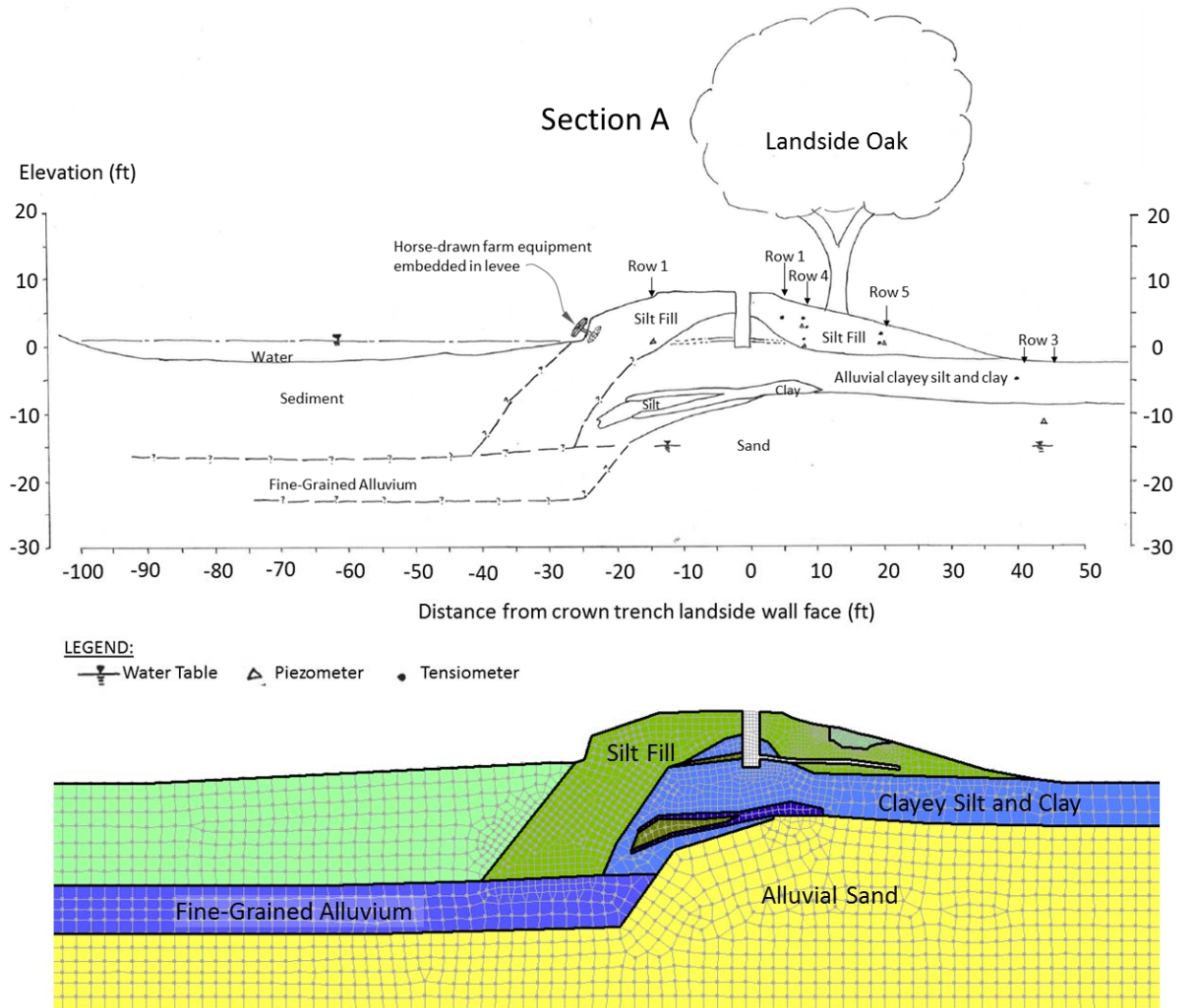


Figure 4-6. Section A interpreted section with model mesh.
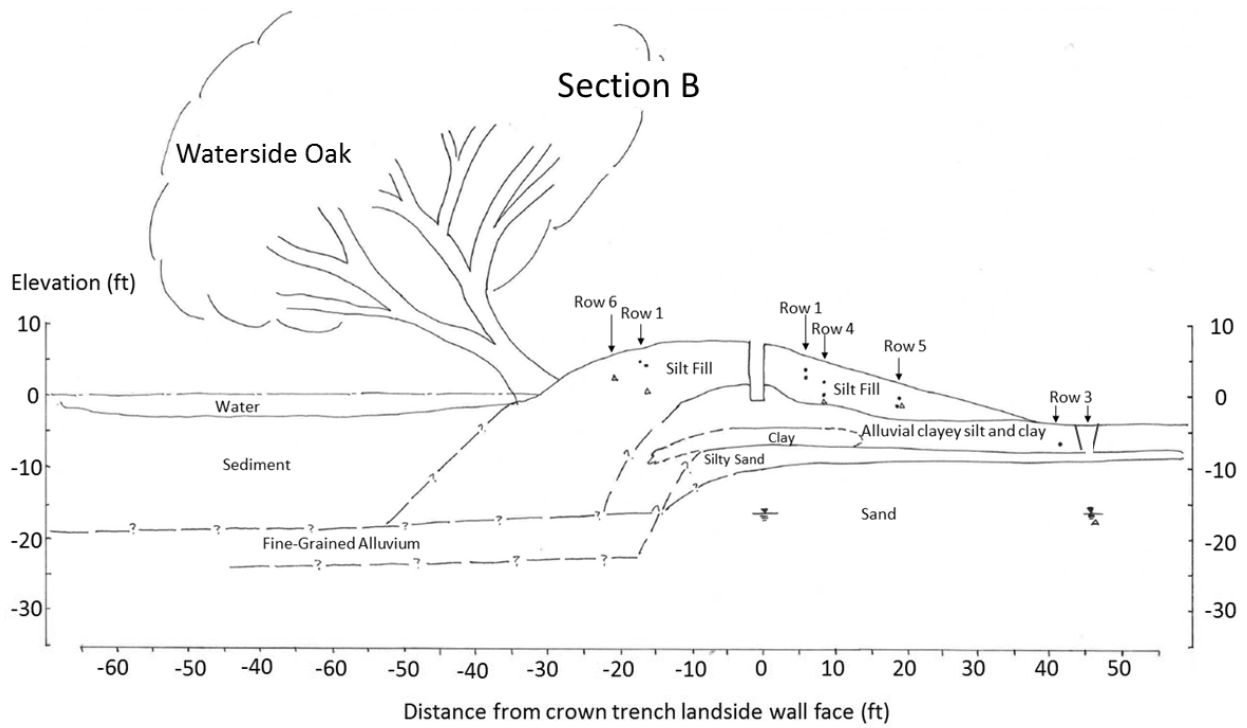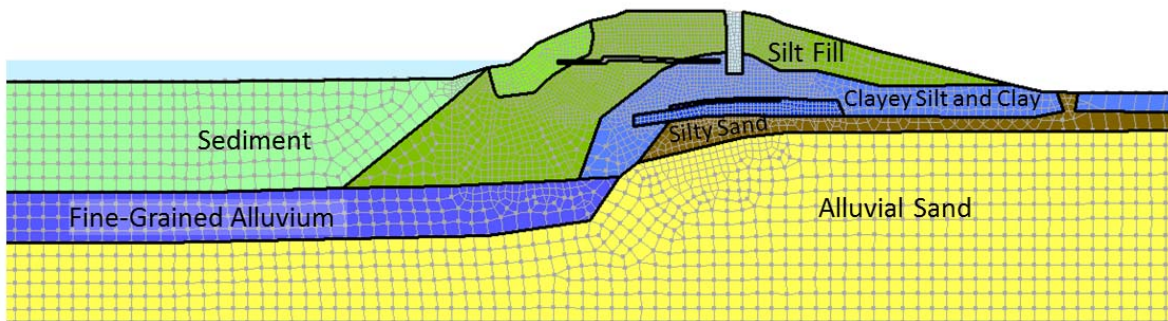
Figure 4-7. Section B interpreted section with model mesh.
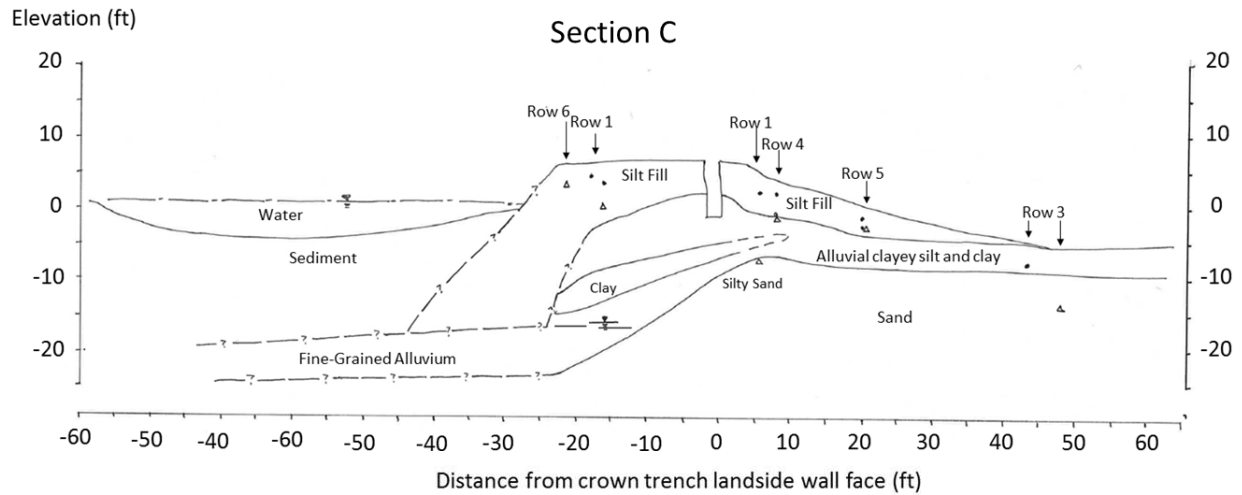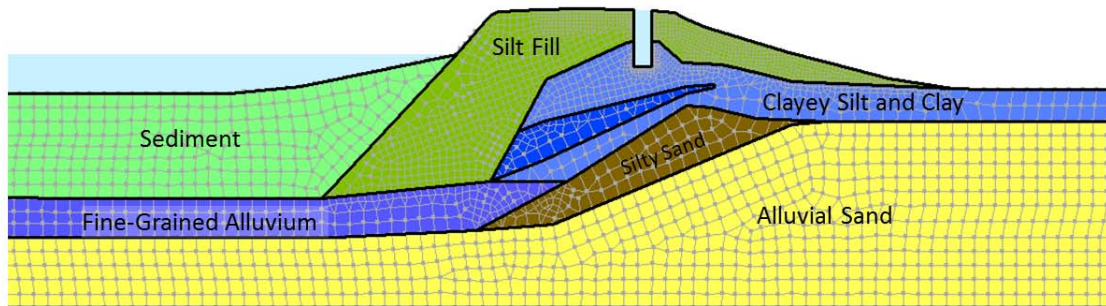
Figure 4-8. Section C interpreted section with model mesh.

### 4.3.1   Analysis of Tree Loading

To understand the potential effects of the studied trees on the integrity of the levee, the existing conditions of the waterside and landside oak trees are important. Table 4-1 shows the tree types, sizes, ages, and lean angles for the studied trees at the Twitchell Island test site. Peterson (2012) estimated critical overturning moments and pit sizes for trees of various types and plots this information with the parameter '*dbh*', or diameter at breast height. Valley Oak was one of the studied species, while Coast live oak was not. Cooper (1926) describes the root system of the Valley oak to be "characterized by a well-developed tap root, with large, comparatively numerous laterals, these penetrating to a considerable depth. It also possesses numerous superficial roots of great size-up to 70 feet in length." Comparatively, the live oak is well adapted to acquiring water from shallow sources and has "habitually shallow root systems." The critical turning moment was estimated based on *dbh* for the waterside oak a correlation presented in Peterson (2012). Based on the information provided in Cooper (1926), this curve shown for the Valley Oak is likely an overestimate for a more superficial root system such as that of the live oak. The range of trees within Peterson's study show a range of critical overturning moment from 350 to 1500 kN-m (260 to 1100 kip-ft) for trees with similar *dbh* values to those studied herein. Values are not reported for the landside oak. Tree weights were estimated for the landside

298

and waterside trees using relationships by Myers et al. (1980) developed for red oak trees and white oak trees, respectively.

Table 4-1. Estimated properties of landside and waterside oak trees

| Position | Common Name | Section | Estimated Age (yrs) | Approximate Canopy Diameter (ft) | Approximate dbh (in) | Lean Angle (deg) | Estimated Pit Size* (ft^2) | Estimated Critical Turning Moment* (kip-ft) | Estimated Weight** (kips) |
|---|---|---|---|---|---|---|---|---|---|
| landside | Coastal Live Oak | Red Oak | 25-30 | 40 | 33 | 6 | 60 | - | 11 |
| waterside | Valley Oak | White Oak | 60 | 60x80 (ave 70) | 40 | 44 | 70 | 960-1,200 | 26 |

* Estimated from Peterson (2012); ** Estimated from Myers et al. (1980)

## 4.3.1.1 Tree Lean and Dynamic Wind Loading

Tree lean and wind loading are key factors in the analysis of a root system. Figure 4-9 shows a diagram by Coutts (1983) explaining the mechanism of tree uprooting under a horizontal force. The leeward side, or 'L in Figure 4-9, the root-soil system is subject to bending with the position of the fulcrum determined by the branching of roots (Coutts, 1983) and their reduced ability to resist bending. The windward side, or 'W' in Figure 4-9 is able to stiffen soil more efficiently as roots are able to deform and develop tension without significant overburden to restrict uplift.
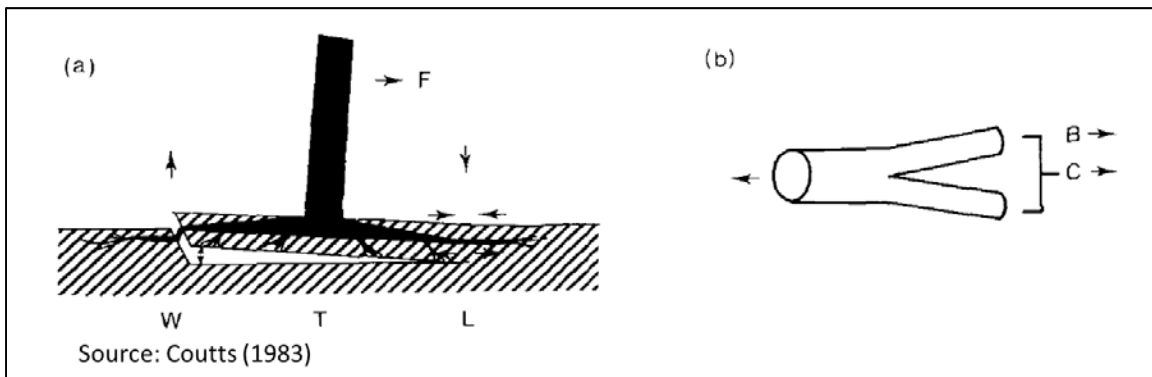


Figure 4-9. Diagram showing (a) the mechanism of overturning and (b) branching. According to Coutts (1983), branching on the leeward side can determine the position of the fulcrum on which the root plate is hinged in overturning.

The destabilizing moment due to the static loading associated with the lean angle of the waterside tree is estimated from the weight and geometry. Wind forces can add to this destabilization. Peterson (2012) estimates wind force as follows:

$$Force\ (N) = 0.5\ C_d(air\ density)\ (crown\ area)(velocity)^2$$

Where:     $C_d$ = drag coefficient, 0.4 recommended value for critical moment calculation;

air density = $1.2\ \frac{Kg}{m^3}$ ;

crown area = cross sectional area of tree in $m^2$;
velocity = wind speed in meters per second

Wind speed in the vicinity of the San Joaquin Delta during the Twitchell Island field test is shown on Figure 4-10.



Source: NOAA Tides and Currents: Port Costa Weather Station
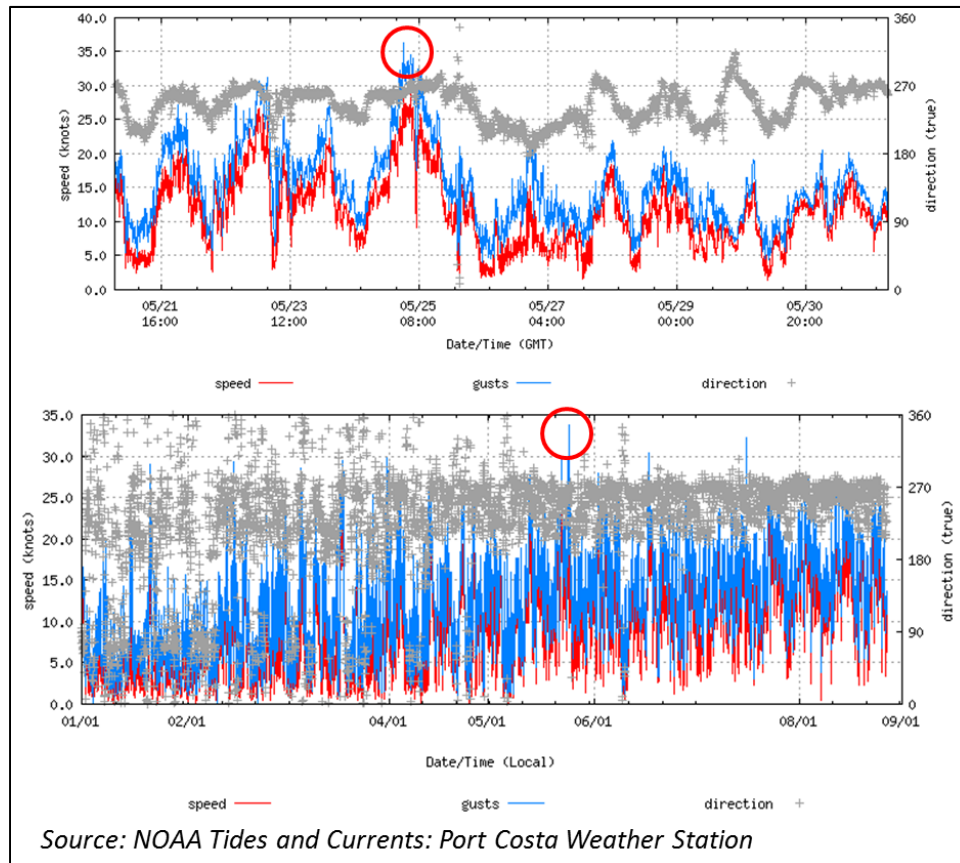
Figure 4-10. Wind speeds during the week of the field test showing peak velocities of 31 to 37 knots (16 to 19 m/s).

### 4.3.1.2   Loading for Landside Oak Tree

A free body diagram detailing the loading on the landside oak tree is presented as Figure 4-11**Error! Reference source not found.**. Based on T-LiDAR scans of the tree shape performed by Gerald Bawden of the USGS, the tree exhibited a slight lean (about 6 degrees). The diagram details wind forces, gravitational forces, a reaction force, and root tensile forces extending from a root plate. The size of the root plate was estimated from the empirically derived data associated with windthrow studies (e.g., Peterson, 2012).  Table 4-1 solves equations presented on Figure 4-11 based on assumed values of key input parameters (highlighted in green) to arrive at horizontal and vertical loading of the tree based on an assumption that the tree and root plate act as a rigid body.

$$\sum F_x = 0$$

$$T_H \sin\alpha + F_W \cos\alpha - W \sin\alpha - W_R \sin\alpha - T_V \sin\alpha = 0$$

$$\sum F_y = 0$$

$$F_W \sin\alpha - W \cos\alpha + R - W_R \cos\alpha - T_V \cos\alpha - T_H \sin\alpha = 0$$

$$\sum M_c = 0$$

$$|e|R - F_W H_2 \cos\beta - W H_1 \cos\beta - \left(\frac{t}{2}\right) W_R \sin\alpha + \left(\frac{d}{2}\right) T_H \sin\alpha - t\, T_H \cos\alpha + x\, T_V \cos\alpha + t\, T_V \sin\alpha = 0$$

*Measured along tree trunk*
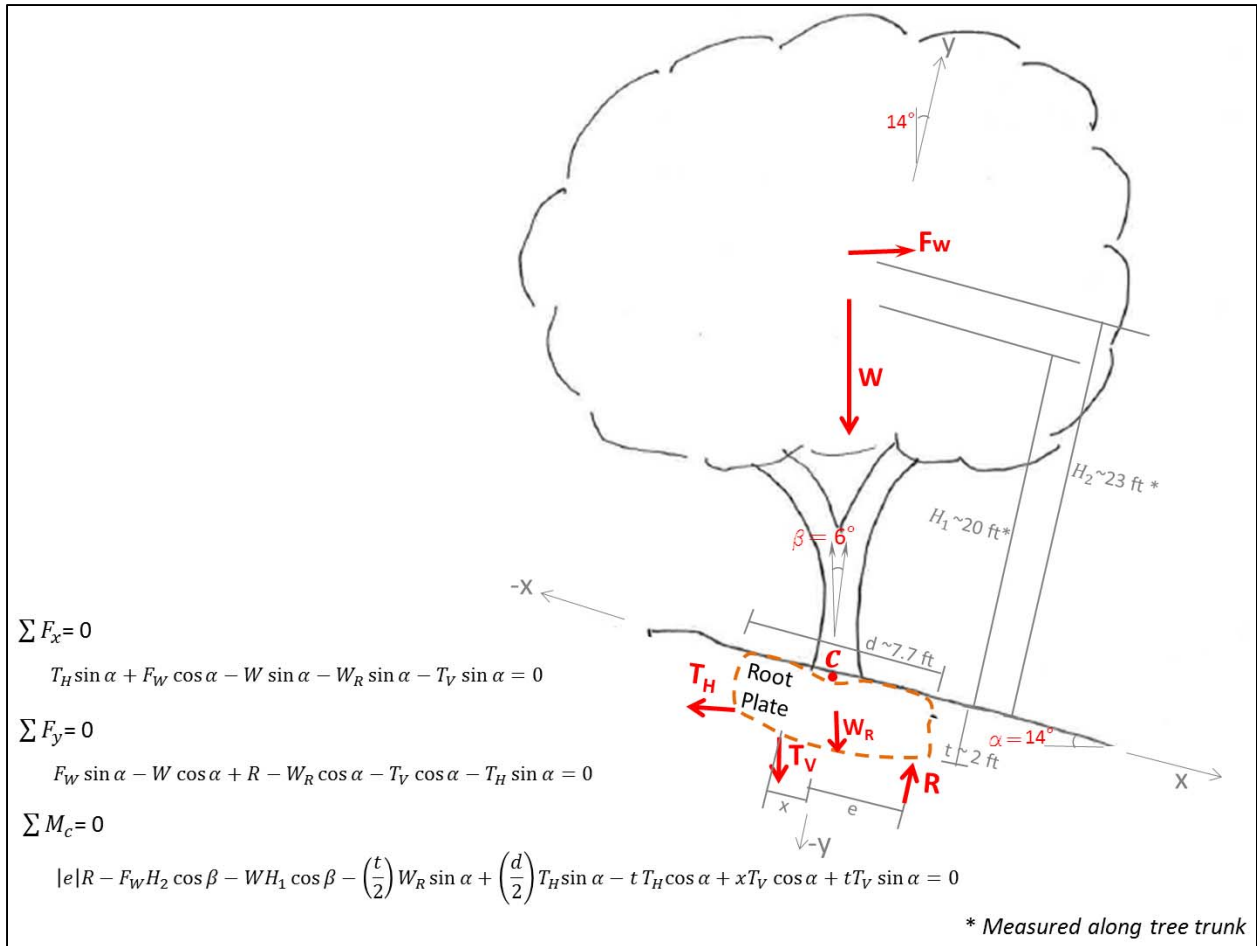
Figure 4-11. Free body diagram representing the force balance on the landside oak tree at Twitchell Island.

Table 4-2. Calculated force balance for landside oak tree.

| | | |
|---|---|---|
| **Canopy Width** | **40** | ft |
| **Canopy height** | **30** | ft |
| **Wind Speed** | **39** | mph |
| **Tree height** | **41** | ft |
| **Diameter at breast height, dbh** | **33** | in |
| **Angle of slope (from horizontal), Alpha** | **14.0** | degrees |
| **Angle of tree lean (from vertical), Beta** | **6** | degrees |
| **Thickness of root plate, t** | **2** | ft |
| **Unit weight of root plate** | **80** | pcf |
| **Height*, wind force, $H_2$** | **23** | ft |
| **Height*, center of mass, $H_1$** | **20** | ft |
| **Tap (or vertical) root offset from trunk, x** | **2.5** | ft |
| **Eccentricity of reaction force, e** | **-3.9** | ft |
| Tree Weight (white oak), W | 11,100 | lbs |
| Wind Load, Fw | 1,470 | lbs |
| Weight of Root Plate, $W_R$ | 9,570 | lbs |
| Size of root plate (assumed square), d | 7.7 | ft |
| Angle of X-axis (from horizontal) | 14 | degrees |
| **Vertical Root Tension, $T_V$** | **10,200** | lbs |
| **Horizontal Root Tension, $T_H$** | **9,170** | lbs |
| **Reaction Force, R** | **31,800** | lbs |
| *measured along the alignment of the tree trunk* | | |

### 4.3.1.3   Loading for Waterside Oak Tree

A free body diagram detailing the loading associated with the waterside oak tree is presented as Figure 4-12. Based on estimates from pre-test photographs, the waterside oak tree leaned at an angle of approximately 46 degrees from vertical prior to testing. The diagram details wind forces, gravitational forces, a reaction force, and root tensile forces extending from a root plate. As discussed for the landside oak tree, the size of the root plate was estimated from the empirically derived data associated with windthrow studies (e.g., Peterson, 2012). Table 4-3 provides input parameter (highlighted in green) and solutions to equations presented on Figure 4-12 to arrive at horizontal and vertical loading of the tree based on an assumption that the tree and root plate act as a rigid body.

Horizontal and vertical root tension loads are intended to represent total horizontal and total vertical loading associated with the anchoring demand on the root system based on the configuration of the leaning tree and wind loading. The waterside oak tree, a valley oak, is expected to have a well-developed tap root (Cooper, 1926); however, the vertical component of the root tension force includes all roots acting in the vertical direction. Roots on the windward side of the tree are expected to contribute more to resisting overturning. On this basis, the vertical tension force was assumed to act midway between the trunk

center and the edge of the root plate (i.e., a value of $x = \frac{d}{4}$ as shown on Figure 4-12). The vertical loading delivered to the root system is expected to be 25 percent smaller if the vertical root tension force, $T_V$, acts at the windward edge of the root plate, and 50 percent larger if the vertical root tension force acts at the center of the tree trunk (assumes a 27 degree slope angle). Similarly, the horizontal force, $T_H$, is also impacted by the assumed position of the vertical force. The horizontal force is reduced by 16 percent when the vertical root tension force acts at the windward edge of the root plate ($x = \frac{d}{4}$) and increased by 32 percent when the vertical root resists tree topple from the trunk center.



The figure contains the following equations:

$\sum F_x = 0$

$$T_H \cos\alpha + F_W \cos\alpha - W \sin\alpha - W_R \sin\alpha - T_V \sin\alpha = 0$$

$\sum F_y = 0$

$$F_W \sin\alpha - W \cos\alpha + R - W_R \cos\alpha - T_V \cos\alpha - T_H \sin\alpha = 0$$

$\sum M_c = 0$

$$|e|R - F_W H_2 \cos\beta - W H_1 \cos\beta - \left(\frac{t}{2}\right)W_R \sin\alpha + \left(\frac{d}{2}\right)T_H \sin\alpha - t\,T_H \cos\alpha + x\,T_V \cos\alpha + t\,T_V \sin\alpha = 0$$
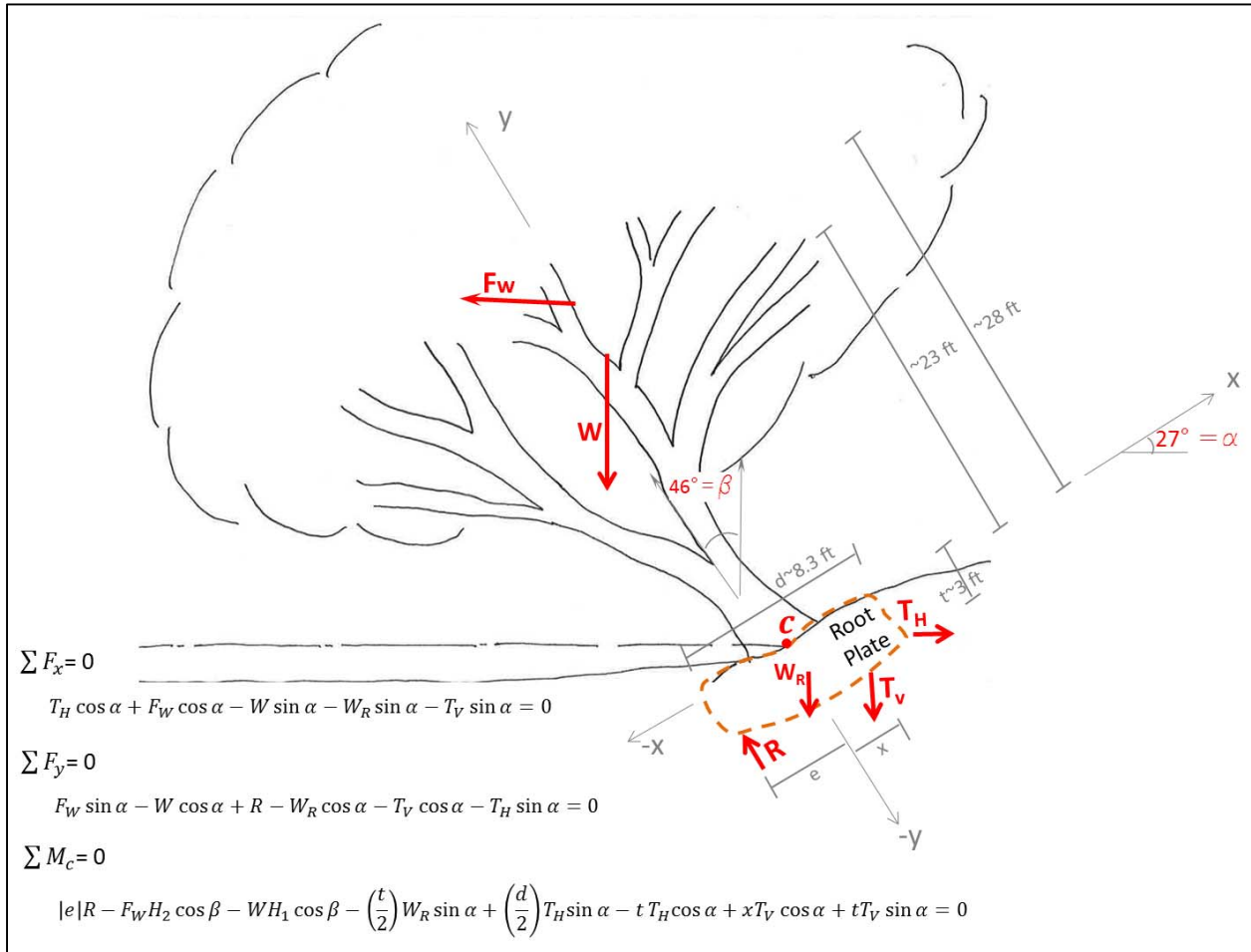
Figure 4-12. Free body diagram representing the force balance on the waterside oak tree at Twitchell Island.

Table 4-3. Calculated force balance for waterside oak tree

| | | |
|---|---|---|
| **Canopy Width** | **70** | ft |
| **Canopy height** | **35** | ft |
| **Wind Speed** | **39** | mph |
| **Tree height** | **47** | ft |
| **Diameter at breast height, dbh** | **40** | in |
| **Angle of slope (from horizontal), Alpha** | **27** | degrees |
| **Angle of tree lean (from vertical), Beta** | **46** | degrees |
| **Thickness of root plate, t** | **3** | ft |
| **Unit weight of root plate** | **80** | pcf |
| **Height*, wind force, $H_2$** | **28** | ft |
| **Height*, center of mass, $H_1$** | **23** | ft |
| **Tap (or vertical) root offset from trunk, x** | **2.0** | ft |
| **Eccentricity of reaction force, e** | **-4** | ft |
| Tree Weight (white oak), W | 26,100 | lbs |
| Wind Load, Fw | 3,300 | lbs |
| Weight of Root Plate, W$_R$ | 16,700 | lbs |
| Size of root plate (assumed square), d | 8.3 | ft |
| Angle of X-axis (from horizontal) | 27 | degrees |
| **Vertical Root Tension Force, $T_V$** | **97,000** | lbs |
| **Horizontal Root Tension Force, $T_H$** | **74,500** | lbs |
| **Reaction Force, R** | **157,000** | lbs |
| *measured along the alignment of the tree trunk* | | |

Input parameters (highlighted in green in Table 4-3) have the capacity to impact the force delivered to the root system. Understanding the forces delivered to the root system and how they may act on the levee is important in creating a representative model. To this end, a sensitivity analysis was performed examining the impact of key site conditions such as slope angle or tree lean on horizontal and vertical tree root tension loading.

Horizontal and vertical root loading associated with the waterside oak tree (estimated to weigh about 26,000 pounds) was calculated with slope angles varying from 0 to 45 degrees (measured from horizontal) and with tree lean angles of 0 to 46 degrees (measured from vertical). Root loading increases with increasing slope angle and tree lean angle. Figure 4-13 shows a steep rise in horizontal root loading for slopes steeper than 27 degrees (about 2 horizontal to 1 vertical) regardless of tree lean, while vertical root loading appears to respond more strongly to tree lean. Figure 4-14 shows the relationship between horizontal and vertical root loading with increasing tree lean. Loading calculations neglect deformations associated with the system and are estimated for a tree and root system considered as a rigid body.
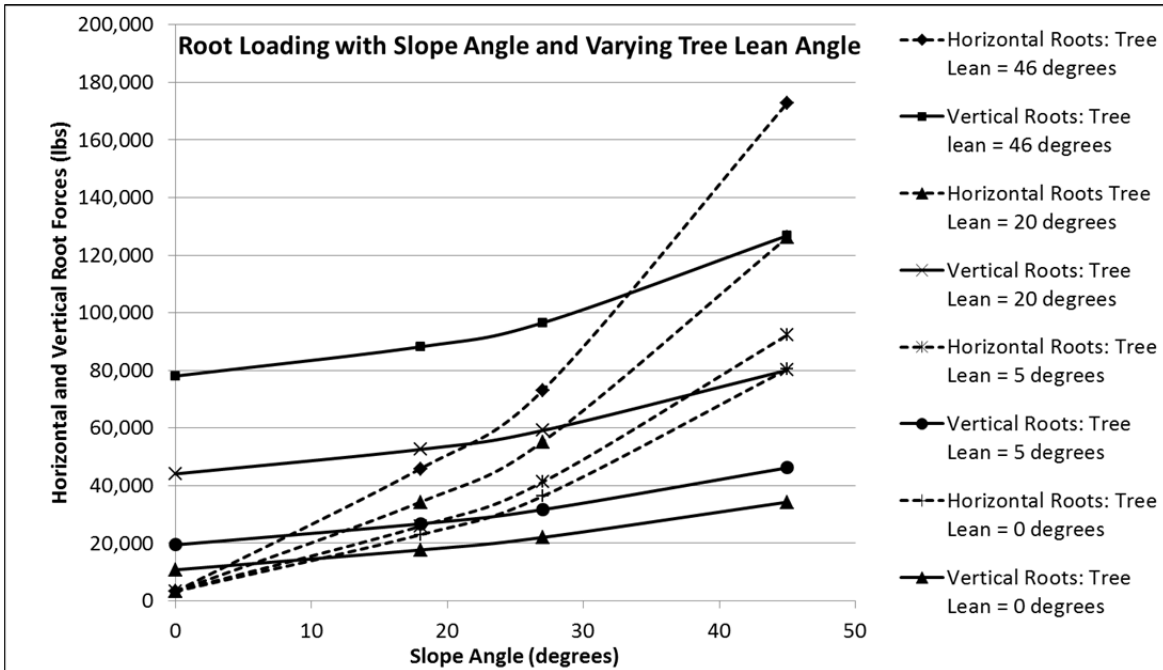
Figure 4-13. Horizontal and vertical root loading plotted against slope angle for tree lean angles ranging from 0 to 46 degrees (measured from vertical). Plots assume a 26,000 pound tree similar to the waterside oak tree with a tap root and windward roots with a vertical component (resultant acting downward from 2 feet windward of the trunk center).
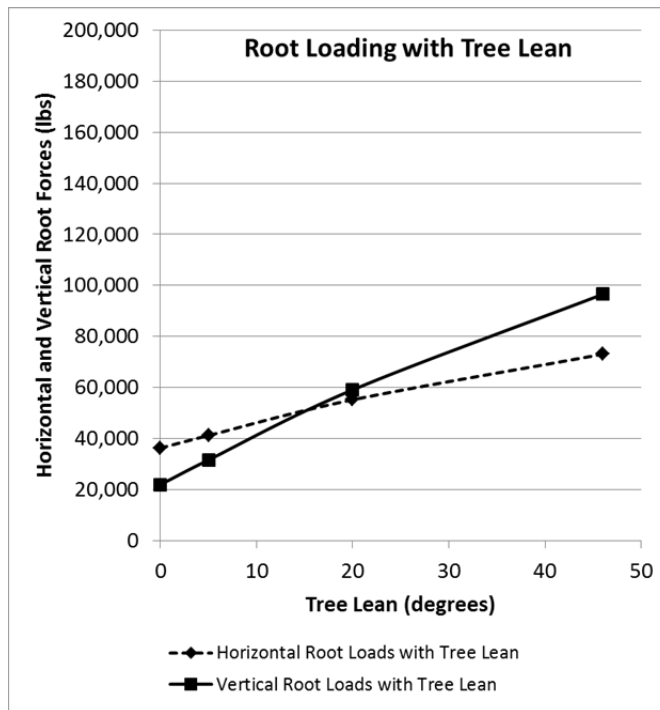


Figure 4-14. Horizontal and vertical tree root loading plotted with increasing slope angle (top) and increasing tree lean angle (bottom). Assumes a tree similar to the waterside oak tree, weighing approximately 26,000 pounds with a tap root and windward roots with a vertical component (resultant acting downward from 2 feet windward of the trunk center).

305

## 4.3.2   Root Reinforcement

Trench logs show that the root system of the waterside oak was significantly more extensive within the trench than the landside oak (Figure 4-15). The majority of roots of the waterside oak were found at depths of 4 to 8 feet within the trench. The waterside tree was positioned at an elevation approximately 6 feet below the levee crown and the largest roots were found to extend approximately horizontal into the levee. The landside tree shows significantly lower root area ratios and a more even distribution with depth. Our observations seem to be consistent with those reported by Cooper (1926). Figure 4-16 provides a graphical breakdown of the root size and number of occurrences within the trench wall.

Estimates for number and size of roots at closer distances to the tree were estimated based on available root architecture data. Based on a review of raw data charts for several valley oak trees excavated and data provided to us by Dr. Alison Berry and Shih-Ming Chung of UC Davis, roots were estimated to be about 5 times more abundant at distances of 25 to 50 percent of the canopy radius and about 2.5 times larger at 25 percent of the canopy radius than at 50 to 100 percent of the canopy radius. Roots intersected by the trench extending from the waterside and landside oak trees are located at approximately 65 to 100 percent of the canopy diameter.

The critical overturning moment estimated by empirical data provided by Peterson (2012) for the waterside valley oak tree is about 1,100 kip-ft.  Looking at Figure 4-16, typical root sizes are on the order of 0.8 to 1.5 inches at depths of 4 to 8 feet. Smaller and shallower roots do not provide much reinforcing. Looking at an 8 foot failure zone and the primary roots extending back from this zone, assume one root of 1.5 inch diameter and one root of 0.75 inch diameter per foot across an 8 foot section. The critical overturning moment for a one foot thick slice would be 138 kip-ft. Using Gray and Sotir (1996), each root is evaluated to determine if it fails in tension or pullout. In general, roots of 0.75 to 2 inches and an assumed 25 feet in length will not break in tension. Bond strengths are estimated using equation 3-13 of Gray and Sotir (1996):

$$\tau_b = z\gamma(1 - \sin\phi)f\,tan\phi$$

Where:        z = depth below ground surface ;
$\gamma$ = soil unit weight;
$\phi$ = friction angle of soil ;
$f$ = coefficient of friction between the soil and the root fiber


The root tensile strength was checked against equation 3-12 of Gray and Sotir:

$$T_R = \frac{4\tau_b L}{D}$$

Where:       $T_R$ = root tensile strength;
             L = root length;
             D = root diameter

Root load estimates are summarized in Appendix 4A as a series of general tables based on calculations using the above equations by Gray and Sotir. A tensile strength of 20 MPa (418 ksf) for oak was selected based on Table 3-5 of Gray and Sotir (1996). Roots are highlighted in red and capped at their tensile strength if tension is limiting. Root capacity for an oak can be estimated given root diameter, length, and effective stress. Effective stress was averaged over the bonded portion of the root zone. For roots modeled in subsequent sections, the embedment was estimated from the crown as this was the primary bonded zone. For shorter roots, an approximated average embedment was considered to arrive at the appropriate effective overburden stress.

The destabilizing moment of the waterside tree due to the static loading associated with the lean angle is estimated at about 480 kip-ft based on a weight of 26,000 lbs and a wind speed of 17.5 mph.  Based on Table 4-1, the empirically derived critical turning moment based on Peterson (2012) is on the order of 960 kip-ft to 1,200 kip-ft. In this study, trees were pulled to failure with a winch under non-flood conditions. Under pre-flood conditions, it is estimated that the initial factor of safety against overturning was on the order of 2.

Based on tables of root load capacity with effective stress provided for various root lengths in Appendix 4A, an estimate of root strength loss can be made with pore water pressure rise. The tables assume a unit weight of soil of 120 pounds per cubic foot (pcf) and no groundwater. Effective stress is equal to the total stress minus the pore water pressure. Consider the effect of pore water pressure increase on effective stress and the subsequent effect on root bond stress and load capacity. If pore water pressures rise by two (2) feet of head, the effective stress is reduced by 125 psf. When pore water pressure rises by six (6) feet of head, the effective stress decreases by about 375 psf. A reduction in bond stress on the order of 40 percent is expected. The critical overturning moment measured empirically may be expected to be reduced by 40 percent based on pore water pressure accumulation, reducing the factor of safety against tree overturning to approximately 1.2.

.
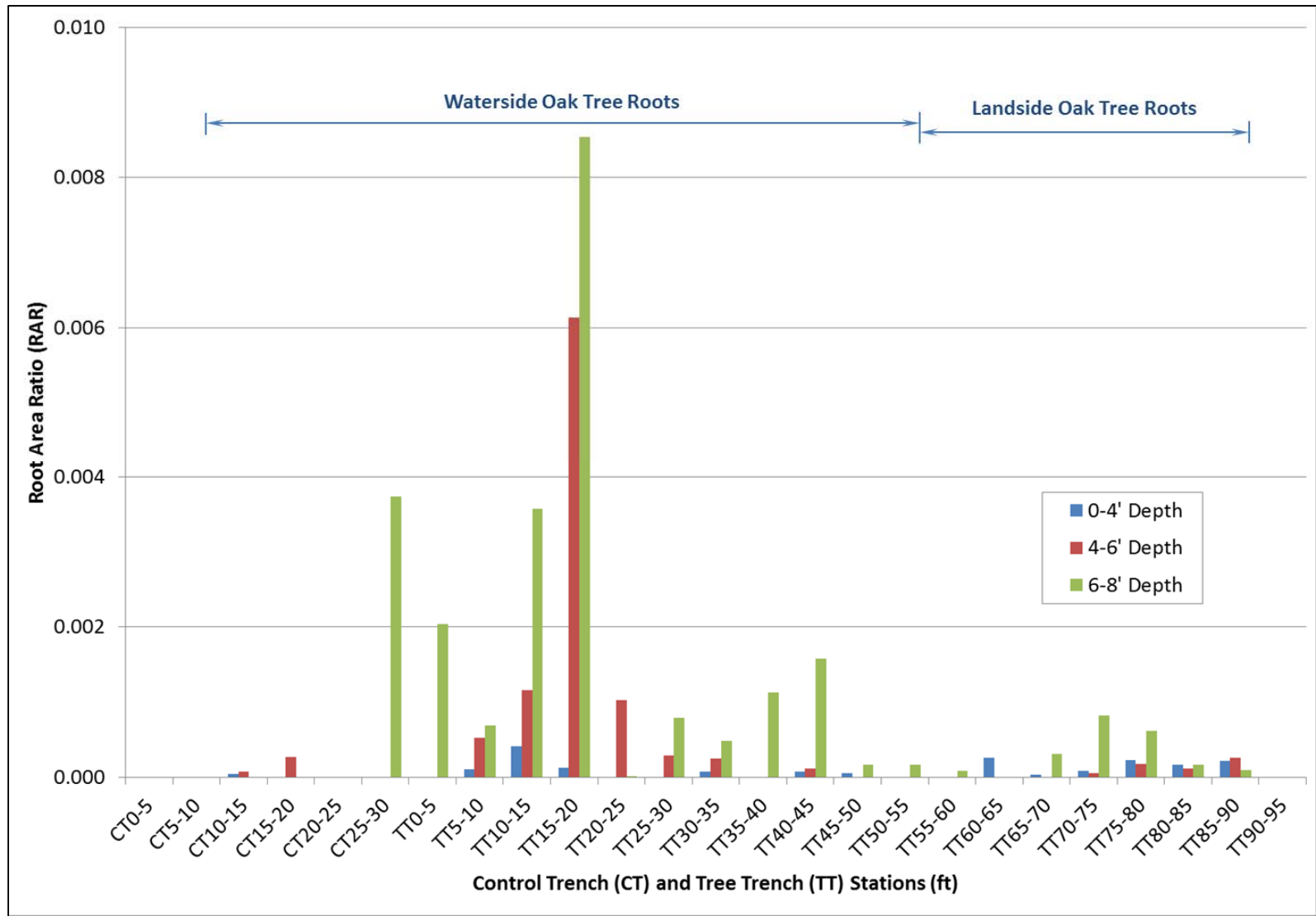
Figure 4-15. Root area ratio along the length of the control and tree trenches. Ratios are broken out for three depth categories within each 5 foot segment of trench. The waterside oak root system spans from Station CT25 to TT55, while landside oak roots were encountered between Station TT60 and TT90.
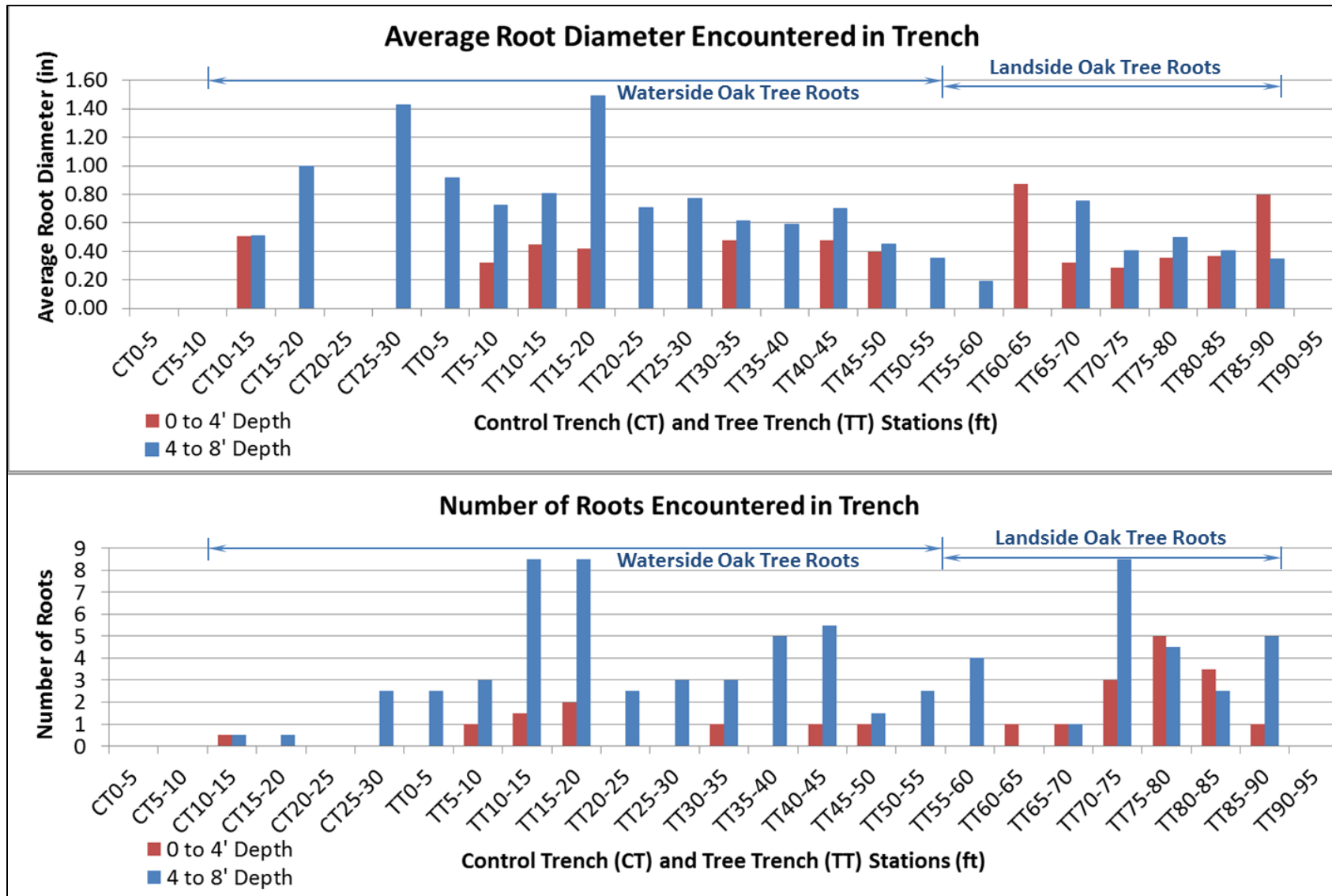
Figure 4-16. Average root diameter and number of roots encountered along the walls of the control and tree trenches. Ratios are broken out for two depth categories within each 5 foot segment of trench. Results are averaged from waterside and landside walls.

### 4.3.3 Modeling Root Reinforcement and Tree Loading

Roots within the root plate were modeled as a rigid body, similar to a footing foundation. Roots extending away from the root plate were modeled as reinforcing elements with zero shear strength in the Slope/W software. Total horizontal and vertical root loading for the landside and waterside oak trees are provided in Table 4-4 and Table 4-5, respectively.

Estimates for number and size of roots at closer distances to the tree were estimated based on available root architecture data. Roots located between the tree and the trench were not captured in trench logs. Based on a review of raw data charts for several valley oak trees excavated, which were provided by Dr. Alison Berry and Shih-Ming Chung of UC Davis, roots were estimated to be about 5 times more abundant at distances of 25 to 50 percent of the canopy radius. Roots were about 2.5 times larger at 25 percent of the canopy radius than the size at 50 to 100 percent of the canopy radius. For roots that are too short to have been intersected by trench logs, the total load capacity of these roots could be estimated from the size and number of roots encountered at the trench. The roots extending from both the waterside and landside oak trees intersected during trenching extend to approximately 65 to 100 percent of the canopy diameter. Using these relationships, root load distributions were estimated for the landside and waterside trees as shown on Table 4-4 and Table 4-5, respectively. These assumptions were used in estimating values of horizontal forces shown in Figure 4-17 and Figure 4-18 for the landside and waterside trees, respectively.

The horizontal component of force is divided over the 'slice width' to arrive at a unit horizontal force and is then further divided to create 5 forces, evenly distributed over the root zone within Slope/W model sections (Figure 4-17 and Figure 4-18). These forces represent the horizontal load on the embankment associated with the lean of the tree and a downhill wind force. Root reinforcement is modeled as a horizontal force acting into the slope, resisting movement. The bonded length of the reinforcement is equal to the length of the reinforcing element outside of the slide zone. Horizontal point loads are only active in the calculation of the factor of safety when included inside the slide circle. Combining the use of reinforcing elements with the use of horizontal forces allows for the inclusion of loading associated with wind and tree lean within the slide mass. In general, loads are higher near the tree (F1 and F2) and lower with distance.

The reaction force of the root plate on the levee slope was distributed over the root plate and entered as a unit weight for the root plate within the model. These loads were only applied through the cross section passing through the tree. This cross section is used to represent a 'slice width' equal to the square root of the root plate area.

310

Table 4-4. Horizontal and vertical root forces for landside oak tree.

| | Total Loads (lbs) | Unit Load (per 1 ft slice) (lbs) |
|---|---|---|
| $T_H$ (horizontal roots) | 9,170 | 1,200 |
| $T_{H25}$ (inner 25% of canopy radius) | 4,130 | 520 |
| $T_{H50}$ (25-50% of canopy radius) | 3,210 | 400 |
| $T_{H75}$ (outer 75-100% canopy radius) | 1,830 | 230 |
| $T_V$ (vertical roots) | 10,200 | 1,300 |

Table 4-5. Horizontal and vertical root forces waterside oak tree.

| | Total Loads (lbs) | Unit Load (per 1 ft slice) (lbs) |
|---|---|---|
| $T_H$ (horizontal roots) | 74,500 | 9,300 |
| $T_{H25}$ (inner 25% of canopy radius) | 33,500 | 4,200 |
| $T_{H50}$ (25-50% of canopy radius) | 26,100 | 3,300 |
| $T_{H75}$ (outer 75-100% canopy radius) | 14,900 | 1,900 |
| $T_V$ (vertical roots) | 97,000 | 12,100 |

A number of large roots originating from the waterside oak tree were cut during trenching. The impact of these roots on tree stability was considered using tables of root load capacity with effective stress provided for various root lengths in Appendix 4A. For the roots modeled in the root plate zone of the waterside oak tree (8-foot slice width), the additional capacity of the two roots is 1,330 lbs each if 10 additional feet were added to these roots. This load applied over the root plate width yields a total load of 10,600 lbs of capacity, discounted to 6,400 lbs due to pore water pressure rise. Roots that were cut account for approximately 9 percent of the total horizontal demand of 73,000 pounds estimated in Table 4-5. A reduction of 9 percent in the capacity of the root system added to the 40 percent loss due to strength loss in response to pore water pressure accumulation leads to a reduction of 50 percent in the original estimate of 960 kip-ft of moment capacity. With moment demand on the order of 480 kip-ft (as previously discussed), and 960 kip-ft reduced to 490 kip-ft, the factor of safety against overturning is very close to unity (factor of safety of 1.02).

Section A: Landside Oak Tree

Unit weight = 530 pcf to account for reaction force associated with static and dynamic tree loading

| Force Number | Distance from Tree (ft) | Horizontal load of Roots on Slope (lbs) |
|---|---|---|
| F1 | 1.5 | 402 |
| F2 | 4.5 | 402 |
| F3 | 7.5 | 171 |
| F4 | 11 | 51 |
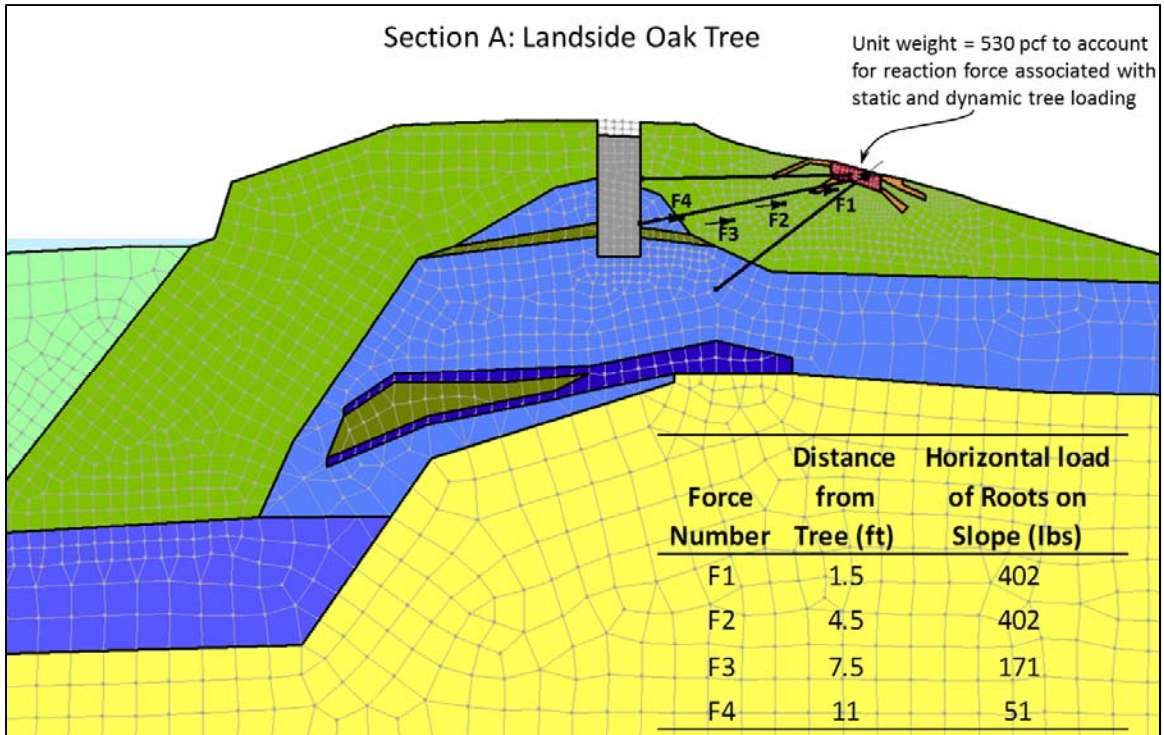
Figure 4-17. Example of root reinforcing and distributed horizontal forces at the landside oak.

Section B: Waterside Oak Tree

| Force Number | Distance from Tree (ft) | Horizontal load of Roots on Slope (lbs) |
|---|---|---|
| F1 | 2.5 | 3,314 |
| F2 | 7.5 | 3,314 |
| F3 | 12.5 | 1,360 |
| F4 | 17.5 | 347 |
| F5 | 22.5 | 347 |

Unit weight = 2200 pcf to account for reaction force associated with static and dynamic tree loading

Root 1   Root 2
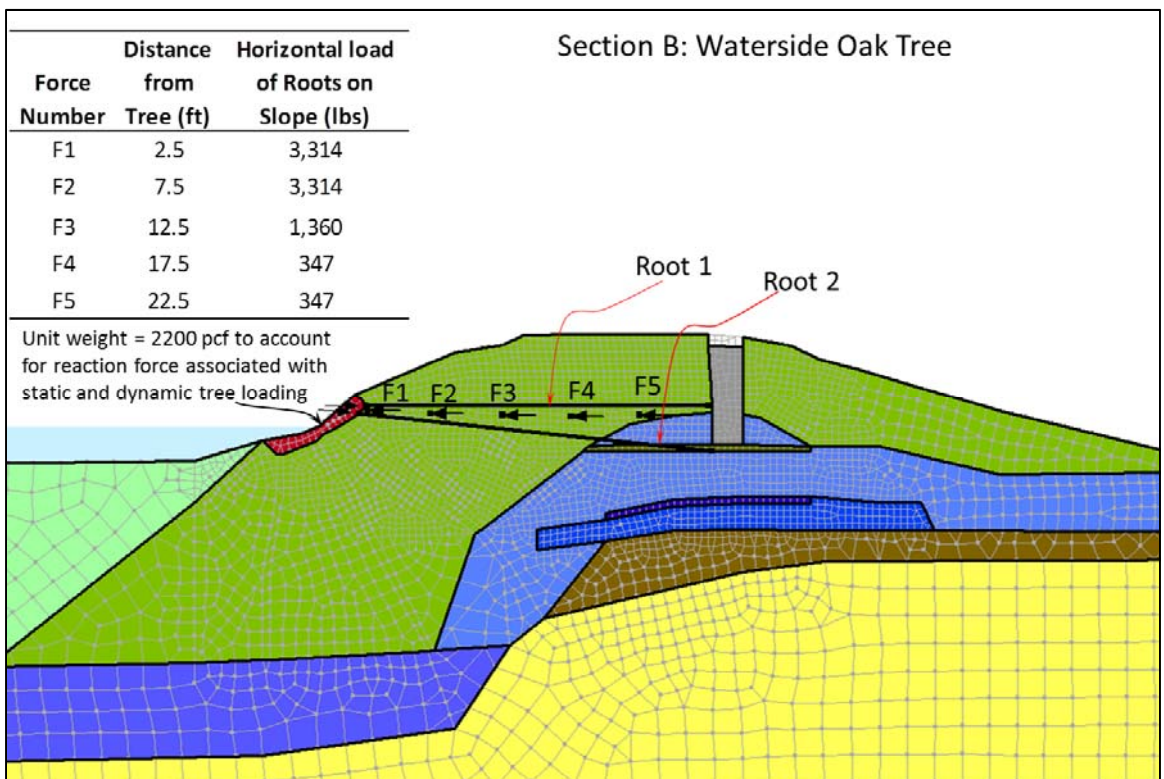
Figure 4-18. Example of root reinforcing and distributed horizontal forces at the waterside oak.

312

### 4.3.4 Shear Strength Assumptions

Coarse-grained soils were considered to be free-draining and were modeled using drained shear strength parameters. Non-free draining materials were modeled under long-term steady state conditions using drained shear strength values correlated from moisture content and index properties, standard penetration test data (SPT), and cone penetration test data (CPT).

Mayne (2007) was implemented to estimate drained friction angle for onsite soils based on normalized cone tip resistance as follows:

$$\phi' = 17.6 + 11 Log(q_{t1})$$

Where $\quad q_{t1} = normalized\ tip\ resistance = \dfrac{(q_t/\sigma_{atm})}{(\frac{\sigma'_{vo}}{\sigma_{atm}})^{0.5}}$

For silts and clays, values of drained friction angle calculated by correlation with CPT normalized tip resistance were compared with those derived using Mitchell (1976) for silts and clays with a plasticity index (PI) larger than 7:

$$\phi' = \sin^{-1}(0.8 - 0.94 \ln(PI))$$

SPT blow count values were measured during drilling and were corrected for hammer efficiency, rod length, borehole diameter, overburden stress (Youd et al. 2001). Values of corrected blow count -$(N_1)_{60}$ – were input into a correlation by Hatanaka & Uchida (1996) and summarized in FHWA (2002):

$$\phi' = (15.4(N_1)_{60})^{0.5} + 20°$$

Data were not available for waterside sediments. These sediments were given a low undrained strength with the assumption that strain compatibility may prevent full mobilization of shear strength for this material. Where site specific data was not available, typical values were used from Duncan and Wright (2005).

Strength values used in design are presented in Table 4-6: Shear strengths used in modeling effort. The shear strength of the levee fills controls the analysis, as most potential slide planes did not extend into the 'old levee soils'.

Table 4-6: Shear strengths used in modeling effort

| | Unit Weight (pcf) | c' (psf) | φ' (degrees) |
|---|---|---|---|
| Levee Silt (ML) | 120 | 0 | 32 |
| Old Clay Levee | 120 | 0 | 34 |
| Sediment | 100 | 150 | 0 |
| Silty Sand | 120 | 300 | 33 |
| Alluvial Sand | 125 | 0 | 37 |
| Alluvial Silt | 120 | 0 | 34 |
| Fine-grained Alluvium | 120 | 400 | 25 |
| Soft Clay/Weak Clay | 120 | 500 | 0 |
| Gravel | 135 | 0 | 38 |

A rapid loading condition was considered in the modeling of failure scenario BC3, a failure envelope extending to the trench that opened a little over 2 hours into the flow test. An undrained or partially drained strength envelope would need to be defined to model this condition. Supplemental exploration is recommended if a better understanding of this slide surface is sought. The program should be designed to explore the continuity of weak beds of silt and clay on the waterside as well as to collect undisturbed samples for high quality strength testing.

4.3.5    Pore Water Pressure Conditions

Transient and steady state seepage models were generated for the Twitchell Island test site by Cobos et al. (2014) and are not reproduced herein. Transient models generally captured the wetting front patterns observed during the flow test. In general, steady state in the transient model was defined as 15 days into the simulation. On the waterside, predictions matched well with 15 day 'steady state' simulation. On the landside slope, the transient model overestimated the measured steady state pore water pressures by approximately 25 percent. For landside models, steady state within the transient model simulation was defined as 2 days into the flow test to better match measured conditions.

4.3.6    Slope Stability Model Results

As discussed, a mass-averaged factor of safety was employed for each of the two landside and four waterside failure scenarios presented on Figure 4-5. A set of cross sections were placed within each mass to represent differing geometric and loading conditions. Each section represented a 'slice width'. Where trees existed within a mass, a section was drawn through the trunk representing a 'slice width' equal to the width of the root plate. Static and dynamic wind loading were applied in the area of the trunk and root system as discussed above. The width of the root plate was estimated as the square root of the pit area derived from windthrow data (Peterson, 2012).  Cross sections adjacent to the root plate represented zones of root reinforcement without static and dynamic tree loading. Trench logs and root area ratios were used to estimate the  size and placement of root reinforcement within each cross section. Each section was analyzed to calculate the factor

of safety using the two-dimensional limit equilibrium slope stability modeling software Slope/W with pore water pressures generated within the Seep/W software and discussed in Cobos et al. (2014).

4.3.6.1   Stability of Landside Failure Scenarios

Representative cross sections through failure scenarios Landside A and Landside C (Figure 4-5) are shown on Figure 4-19. Table 4-7 presents a summary by cross section of calculated factors of safety as well as the 'slice width' represented by each section, the mass of a 1-foot slice of the critical slide mass, and the mass-averaged factor of safety value of each failure scenario. Slope/W results for each section are presented in Appendix 4B.

Failure scenario Landside A was modeled under initial pore water pressure conditions (post trench construction but prior to inundation with water), and steady state flow test conditions as captured by instrumentation during the flow test. Overall, initial models found that transient seepage models over-predicted pore water pressures at steady state on the landside by about 25 percent, resulting in mass-averaged factors of safety very close to unity. Deformations or distress indicative of instability were not observed on the land side of the levee, indicating factor of safety values were likely higher than unity. These over-predictions in pore pressure were corrected by modeling with transient seepage models two days into the flow test to better match observed pore pressures.

Each pore water pressure condition was modeled with and without the loading and reinforcement of the tree. In general, the mass-averaged factor of safety was found to be similar with and without the tree for pore pressure conditions modeled. Factors of safety under initial conditions for the Landside A failure scenario are 2.52 and 2.46 with and without a tree, respectively. Similarly, under pore water pressure conditions representative of steady state conditions, factors of safety of 1.83 and 1.80 are calculated for the Landside A slide mass with and without a tree, respectively.

The factor of safety against instability under a steady state waterside flood condition (the levee is loaded with a water surface elevation 3 feet below the crest elevation) was compared with the steady state test condition. The Crown Trench Seepage Test generated higher pore water pressures within the levee than a simulated flood, resulting in a mass averaged factor of safety value of 1.83, as compared with 1.99 during simulated flood conditions.
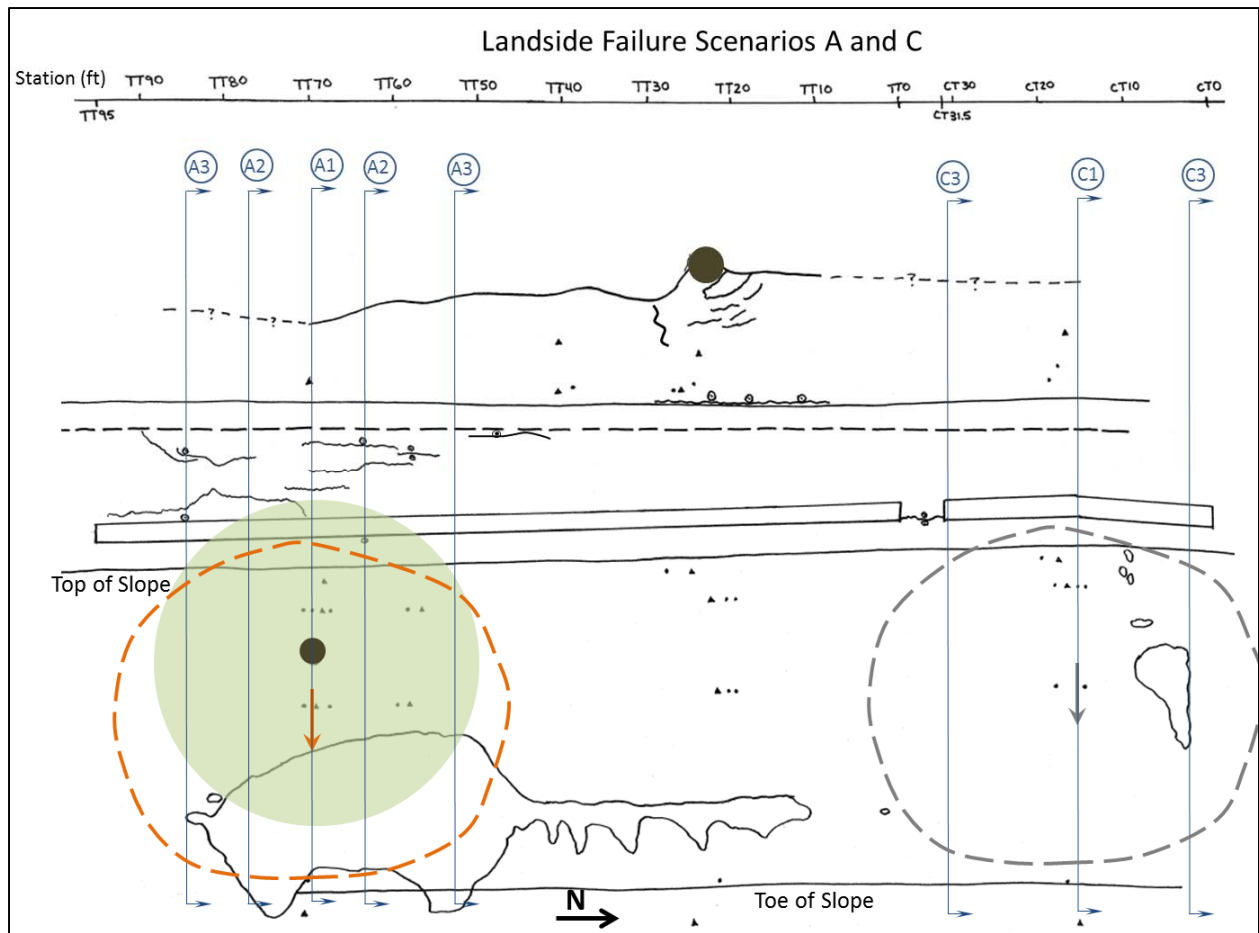
Figure 4-19. Landside failure scenarios modeled. Scenario A (orange) is in the vicinity of the landside oak tree while Scenario C (gray) is at the control section.

Table 4-7. Results of mass averaged factor of safety for landside failure scenarios

| Model | Section | Pore Pressure Condition | Slice Width (ft) | Weight of Section (lbs) | Factor of Safety (FOS) | Total mass | Total mass x FOS | Mass averaged FOS |
|---|---|---|---|---|---|---|---|---|
| Landside A | A1 | Initial pre-test without tree | 7 | 6,397 | 2.50 | 44,780 | 111,949 | 2.46 |
| | A2 | Initial pre-test without tree | 16 | 6,397 | 2.50 | 102,354 | 255,884 | |
| | A3 | Initial pre-test without tree | 24 | 5,030 | 2.41 | 120,725 | 291,188 | |
| | A1 | Initial pre-test with tree | 7 | 9,310 | 2.23 | 65,170 | 145,134 | 2.52 |
| | A2 | Initial pre-test with tree | 16 | 11,484 | 2.73 | 183,744 | 501,254 | |
| | A3 | Initial pre-test with tree | 24 | 3,830 | 2.30 | 91,920 | 211,232 | |
| | A1 (2D) | Steady state test without tree | 7 | 7,824 | 1.81 | 54,767 | 99,128 | 1.80 |
| | A2 | Steady state test without tree | 16 | 7,824 | 1.81 | 125,181 | 226,577 | |
| | A3 | Steady state test without tree | 24 | 5,563 | 1.79 | 133,512 | 238,986 | |
| | A1 | Steady state test with tree | 7 | 8,502 | 1.56 | 59,514 | 92,842 | 1.83 |
| | A2 | Steady state test with tree | 16 | 6,278 | 1.99 | 100,450 | 199,895 | |
| | A3 | Steady state test with tree | 24 | 4,804 | 1.82 | 115,296 | 209,839 | |
| | A1 | Steady state - waterside flood | 7 | 14,014 | 1.89 | 98,098 | 185,798 | 1.99 |
| | A2 | Steady state - waterside flood | 16 | 10,893 | 2.14 | 174,288 | 373,673 | |
| | A3 | Steady state - waterside flood | 24 | 8,230 | 1.91 | 197,518 | 377,851 | |
| Landside C | C1 (2D) | Steady state test | 23 | 4,548 | 1.94 | 104,597 | 202,918 | 1.98 |
| | C3 | Steady state test | 24 | 4,214 | 2.03 | 101,136 | 205,306 | |

### 4.3.6.2 Waterside Stability

The four waterside failure scenarios presented on Figure 4-5 are modeled under various pore water pressure conditions. Mass-averaged factors of safety against slope instability are presented on Table 4-8.

Waterside failures began with the observation of cracking at just over 2 hours into the flow test, with a crack forming between the control and tree trenches. The failure scenario explored at this location is Waterside BC3 as shown on Figure 4-5. The locations of representative cross sections within the Waterside BC3 failure scenario are presented on Figure 4-20. The scenario was modeled under transient pore water pressure conditions at 2 hours (when cracking first observed) and at 39 hours (the approximate time when the waterside oak fell), resulting in calculated average factors of safety of 1.88 and 1.72, respectively. Without tree loading and root reinforcing, the same slide mass yields a factor of safety of 1.67 at 39 hours into the flow test.
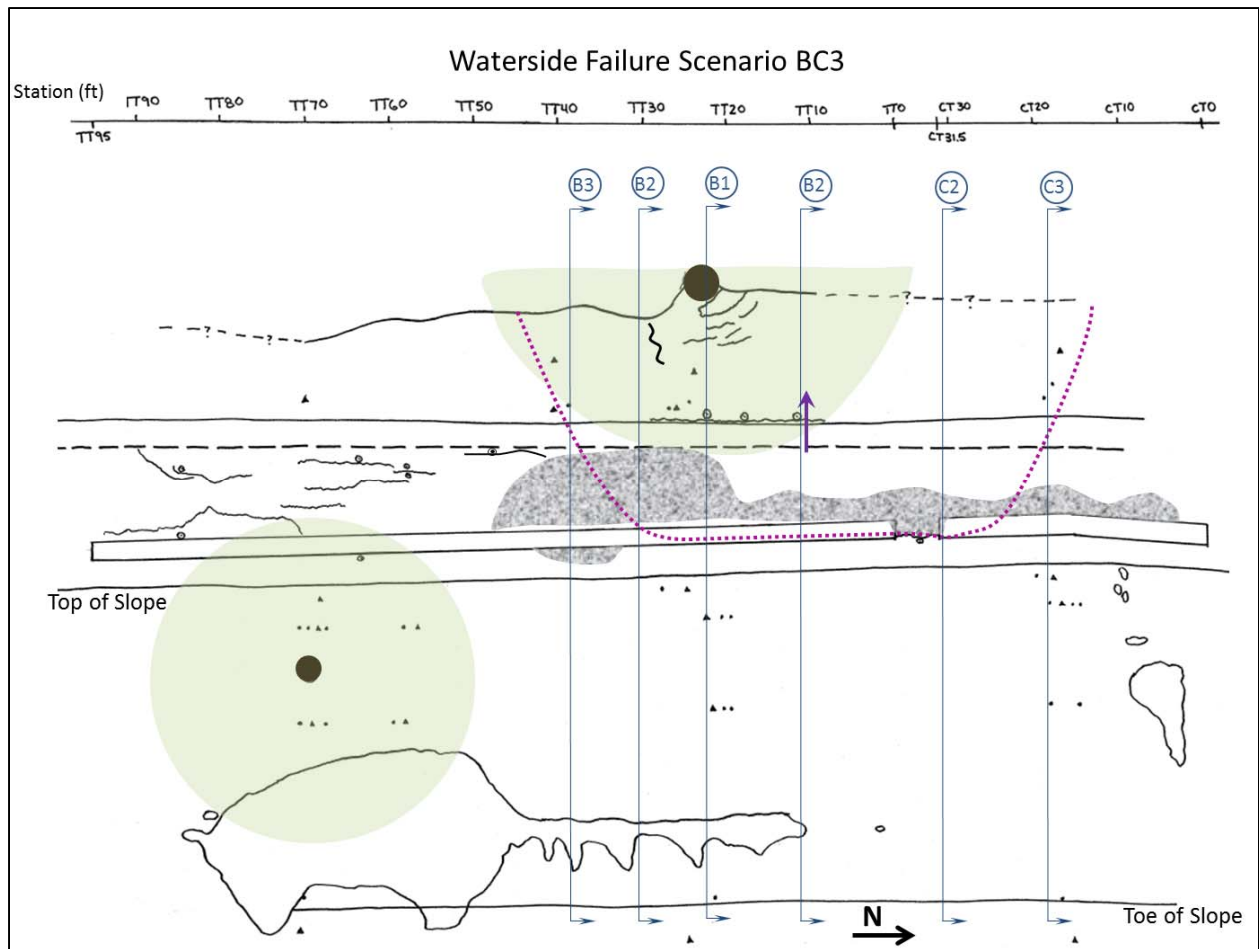
Figure 4-20. Waterside Failure Scenario BC3

The levee crown road began to show pavement cracks after about 24 hours of flow in the vicinity of Section A. Stability at this location was explored through modeling of failure scenario Waterside A (Figure 4-5) under initial and steady state conditions before and during the flow test as well as under a landside flood condition (water surface elevation 3 feet below the levee crown) with average factor of safety values of 1.88, 1.48, and 1.45, respectively.

318
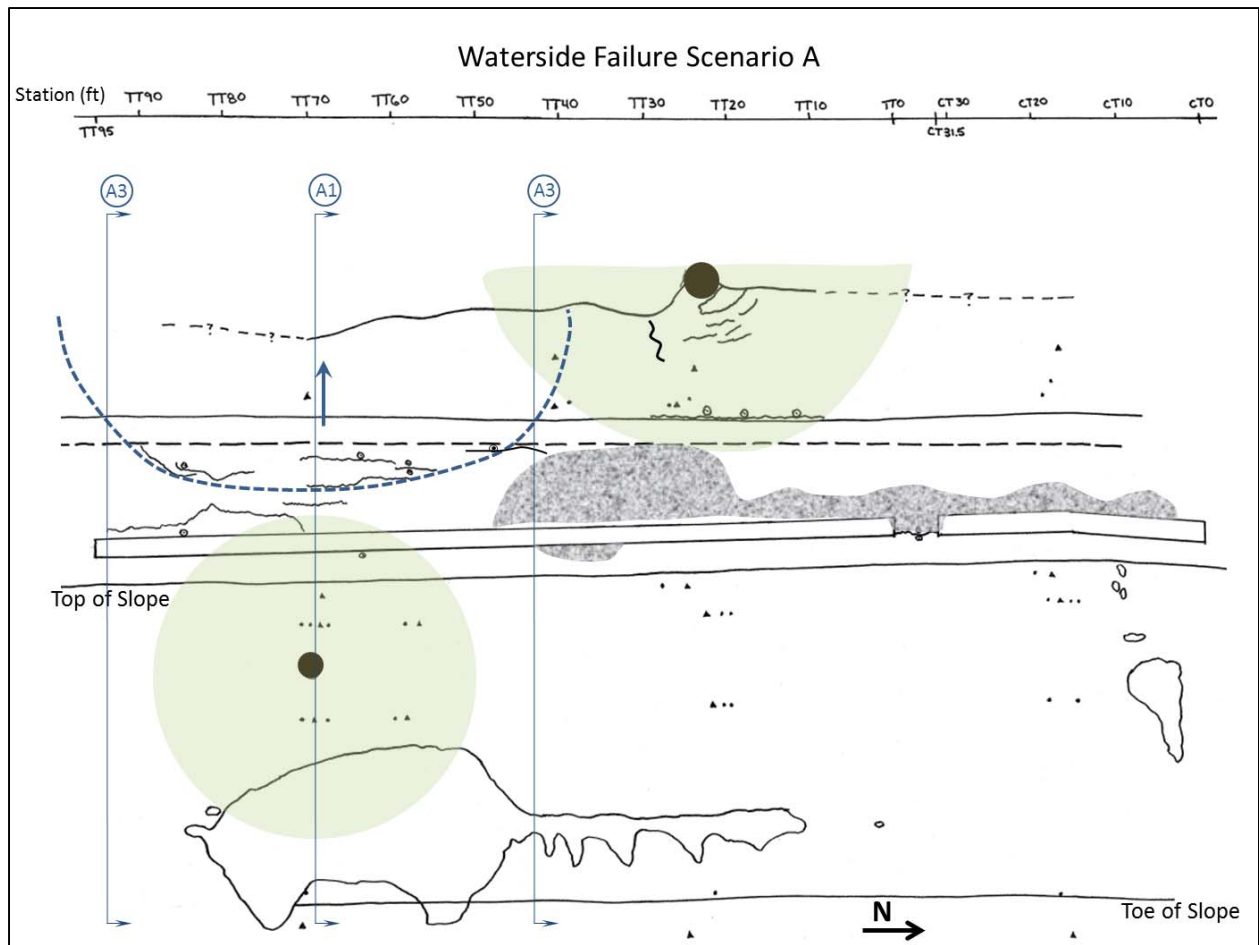
Figure 4-21 provides locations of representative cross sections modeled, results are summarized on Table 4-8, and Slope/W models are presented in Appendix 4B. Steady state test conditions produced a similar rise in pore water pressure to simulated steady state landside flood conditions (a viable flood scenario for Twitchell Island), and therefore saw similar factor of safety values.
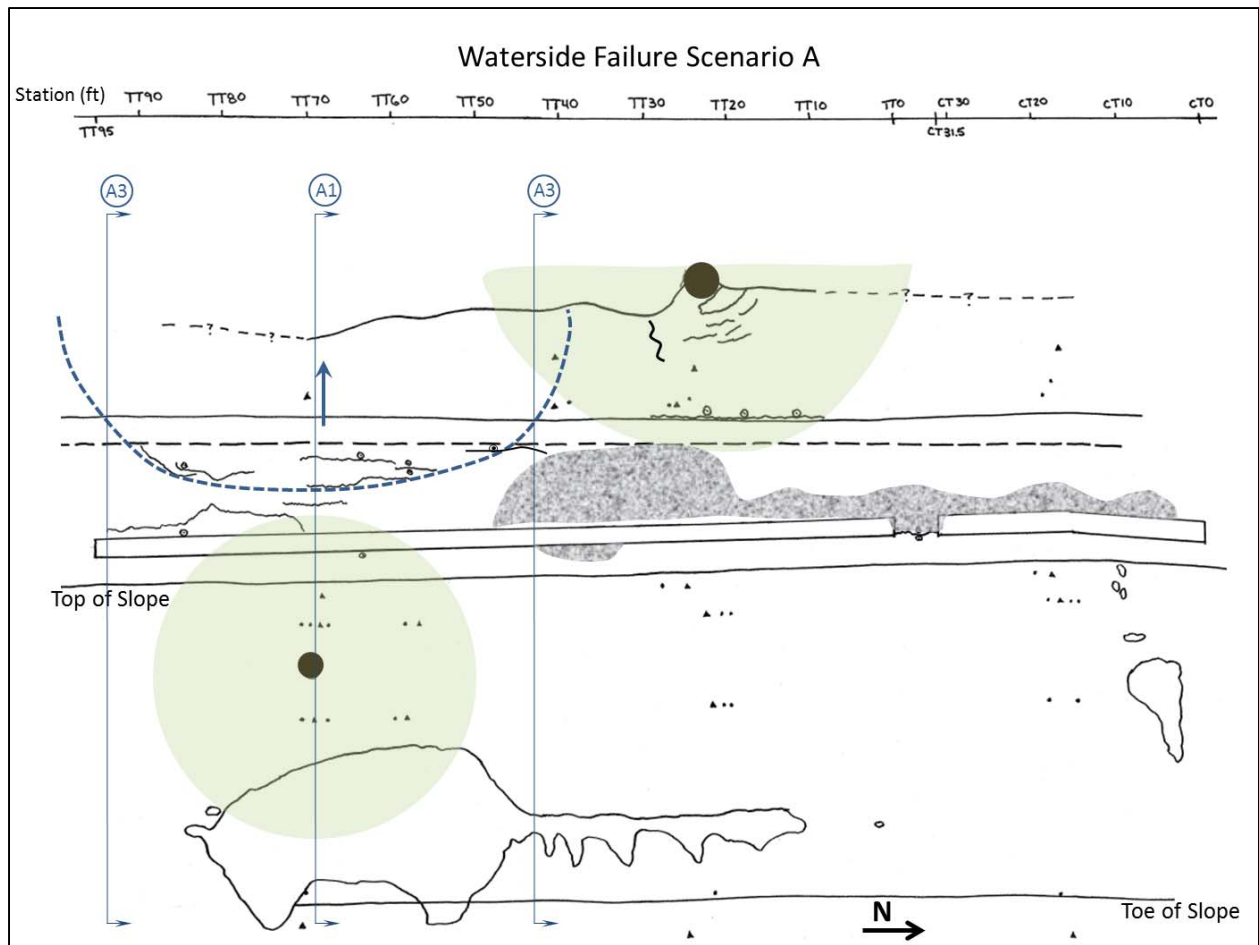
Figure 4-21: Waterside Failure Scenario A

At 39 hours into the flow test, the waterside oak tree fell. Cracking was observed in the area immediately around the fallen tree. About 8 hours later, a crack along the top of the waterside slope was discovered, previously concealed by leaf litter and erosion protection. The time that the crack originated was not known. Two failure scenarios are shown on Figure 4-22 and Figure 4-23 named Waterside B-1 (limited to local area around oak tree) and Waterside B-2 (extending up to the top of slope). The Waterside B-1 failure scenario, modeled with transient seepage conditions at 39 hours into the flow test, has a factor of safety against instability of 1.04. The B-2 failure scenario, also modeled under transient seepage conditions at a time of 39 hours, has factor of safety across the slide mass of 1.16 and 1.03 with and without the waterside oak tree, respectively. All waterside results are summarized in Table 4-8 with Slope/W results presented in Appendix 4B.
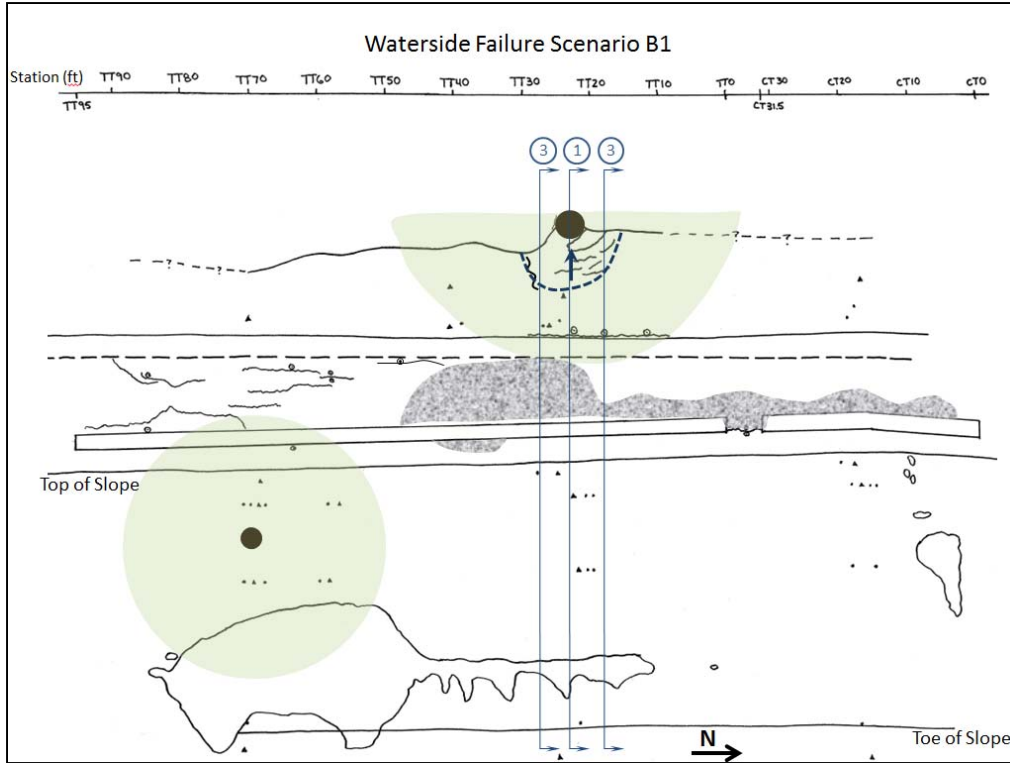
Figure 4-22. Waterside failure scenario B1.
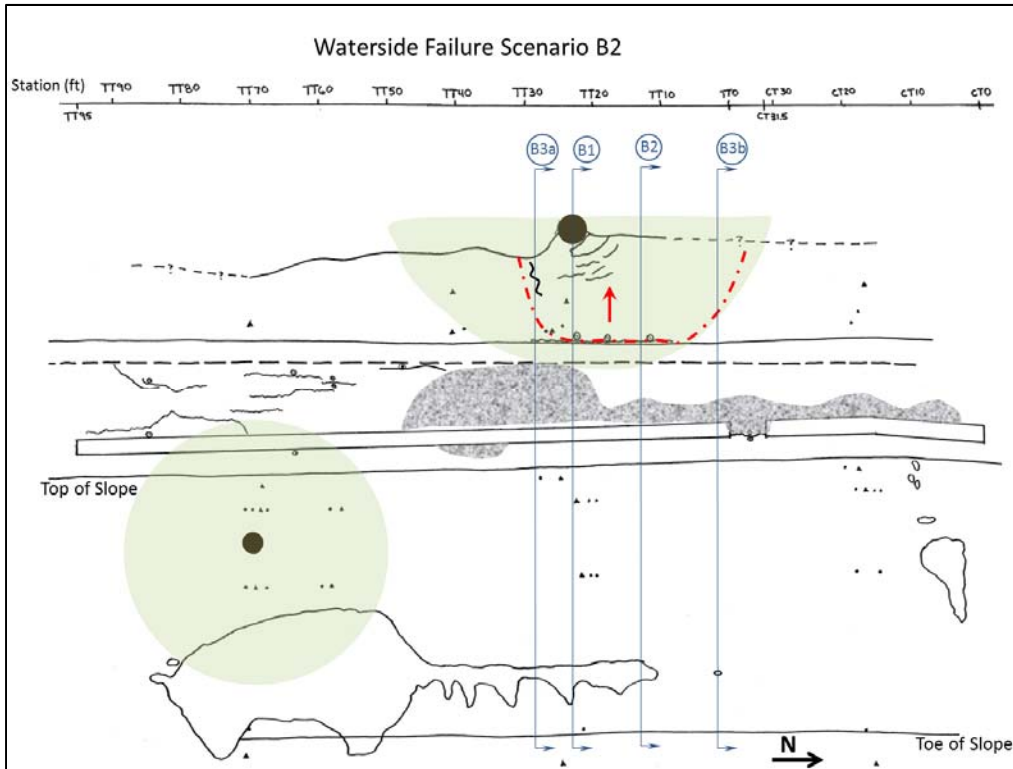

Figure 4-23. Waterside failure scenario B2.

Table 4-8: Results of mass averaged factor of safety against instability for waterside failure scenarios

| Model | Section | Pore Pressure Condition | Slice Width (ft) | Weight of Section (lbs) | Factor of Safety (FOS) | Total mass | Total mass x FOS | Mass averaged FOS |
|---|---|---|---|---|---|---|---|---|
| Waterside A | A1 | Initial pre-test | 35 | 14,804 | 1.80 | 518,140 | 932,652 | 1.76 |
| | A3 | Initial pre-test | 30 | 4,132 | 1.60 | 123,966 | 198,346 | |
| | A1 | Steady state test | 35 | 13,456 | 1.50 | 470,960 | 706,440 | 1.48 |
| | A3 | Steady state test | 30 | 4,072 | 1.40 | 122,148 | 171,007 | |
| | A1 | Steady state - landside flood | 35 | 16,014 | 1.48 | 560,490 | 829,525 | 1.45 |
| | A3 | Steady state - landside flood | 30 | 5,219 | 1.36 | 156,579 | 212,947 | |
| Waterside B-1 | B1 | 39 Hr transient - test | 8 | 26,522 | 0.96 | 212,176 | 203,689 | 1.04 |
| | B3 | 39 Hr transient - test | 8 | 4,490 | 1.50 | 35,922 | 53,884 | |
| Waterside B-2 | B1 | 39 Hr transient - test | 8 | 31,650 | 1.05 | 253,200 | 265,860 | 1.16 |
| | B2 | 39 Hr transient - test | 13 | 6,291 | 1.28 | 81,783 | 104,682 | |
| | B3a | 39 Hr transient - test | 6 | 3,802 | 1.35 | 22,811 | 30,795 | |
| | B3b | 39 Hr transient - test | 9 | 5,579 | 1.44 | 50,210 | 72,303 | |
| | B1 - No Tree (2D) | 39 Hr transient - test | 8 | 6,641 | 1.07 | 53,130 | 56,849 | 1.03 |
| | B2 - No Tree | 39 Hr transient - test | 12 | 6,641 | 1.07 | 79,694 | 85,273 | |
| | B3a - No Tree | 39 Hr transient - test | 8 | 3,561 | 0.96 | 28,489 | 27,349 | |
| | B3b - No Tree | 39 Hr transient - test | 12 | 3,561 | 0.96 | 42,733 | 41,024 | |
| Waterside BC-3 | B1 | 2 Hr Transient - Test | 8 | 44,346 | 1.36 | 314,312 | 691,486 | 1.88 |
| | B2 | 2 Hr Transient - Test | 23 | 26,984 | 2.24 | 159,997 | 262,395 | |
| | B3 | 2 Hr Transient - Test | 10 | 10,784 | 2.03 | 443,460 | 603,106 | |
| | C2 | 2 Hr Transient - Test | 16 | 39,289 | 2.20 | 431,744 | 967,107 | |
| | C3 | 2 Hr Transient - Test | 12 | 6,956 | 1.64 | 129,408 | 262,698 | |
| | B1 | 39 hrs - test | 8 | 40,161 | 1.12 | 321,288 | 359,843 | 1.72 |
| | B2 | 39 hrs - test | 27 | 22,557 | 1.76 | 609,039 | 1,071,909 | |
| | B3 | 39 hrs - test | 10 | 5,633 | 1.28 | 56,326 | 72,097 | |
| | C2 | 39 hrs - test | 16 | 36,207 | 2.08 | 579,312 | 1,204,969 | |
| | C3 (2D) | 39 hrs - test | 12 | 5,738 | 1.58 | 68,854 | 108,789 | |
| Waterside BC-3 | B1 No tree | 39 Hr transient - test | 8 | 29,926 | 1.69 | 239,408 | 404,600 | 1.67 |
| | B2 - No Tree | 39 Hr transient - test | 27 | 29,926 | 1.69 | 808,002 | 1,365,523 | |
| | B3 - No Tree | 39 Hr transient - test | 10 | 4,530 | 0.98 | 45,302 | 44,396 | |
| | C2 - No Tree | 39 Hr transient - test | 16 | 29,926 | 1.69 | 478,816 | 809,199 | |
| | C3 - No Tree | 39 Hr transient - test | 12 | 4,530 | 0.98 | 54,362 | 53,275 | |

## 4.4 DISCUSSION

The landside tree did not have an important effect on global slope stability. Under steady state test conditions, failure scenario Landside A was modeled with and without tree loading. The factor of safety of Landside A with the landside tree and root system (1.83) was slightly higher than the factor of safety of the same section without a tree (1.80). Comparing the Landside A failure scenario with the control section, Landside C, the factor of safety of Landside A at steady state with a tree (1.83) was slightly lower than Landside C (1.98) at the control section. The difference appears to be due to differences in the pore water pressure accumulation in the lower portion of the slope in the area of Landside C. Pore water pressures within the Landside A area were heavily influenced by the extensive

burrow network in the area as well as a gap in the overbank deposits on which the levee was founded that may have affected the patterns of pore water pressure accumulation. At Landside C, pore water pressures were also influenced by burrowing, but the network was far less extensive and geometry of the underlying low permeability overbank deposits are believed to have directed water away from the control instrument line (as discussed in Chapter 3).

Circular and block modes of failure were evaluated for each of the four (4) waterside and two (2) landside failure scenarios shown on Figure 4-5. In general, in the absence of horizontal loading or reinforcing, circular failure modes produced lower factor of safety values than block failure modes. Increasing the horizontal load through use of reinforcing elements or horizontal load forces (placed within the slide mass to represent the static tree lean and dynamic wind forces on the slide mass) influences the failure mode. Block failures were found to be critical for these cases with the waterside geometry.

The waterside oak tree case with various possible failure scenarios associated with observed cracking was evaluated. Based on hand calculations of the initial overturning moment of the tree, evaluated through tree weight, lean angle, and dynamic wind loading, the waterside tree initially had a pre-test factor of safety on the order of two with respect to overturning moments. Pore water pressures associated with the test conditions at steady state resulted in an estimated loss of approximately 40 percent of initial capacity, lowering the factor of safety against overturning to approximately 1.2. Shortening roots by making cuts at the crown trench during construction is estimated to have impacted capacity by about 9 percent, reducing the factor of safety to about 1.02, just above unity. Seepage and slope stability modeling revealed that test conditions put greater demands on the levee than an actual flood scenario with a high water surface 3 feet below the levee crest.

Failure scenarios Waterside B-1 and Waterside B-2 exhibited low factors of safety under transient test conditions at 39 hours (approximate time that the waterside oak tree fell). Based on models, Waterside B-2 exhibits a slightly higher factor of safety with the waterside oak tree than without it. The Waterside BC3 failure scenario was found to have a factor of safety against instability of greater than 1.5. The movements may have been related to consolidation of loose fill deposits under wetting, instability related to animal burrows or preferential planes of weakness, soft soil layers or fractures within the fill that were not captured through careful logging of site conditions.

Waterside slopes were comprised of weak, uncompacted fills of variable quality. These weak fills were found to be riddled with burrows and pockets of very loose fill. The impact of the trees on slope stability was found to be minimally helpful in improving stability of these weak fills, to the extent that the tree remains stable to overturning due to wind or static loading associated with lean or steep slope angles. Trees that lean significantly (particularly those with a center of mass extending leeward of the root plate) should be evaluated carefully and removal considered. Trees not exhibiting excessive lean should be evaluated for other potential impacts such as erosion and windthrow to determine whether the tree may remain and possibly provide a small benefit to global stability.

# CHAPTER 5

## Calibration and Validation of the UBCSAND Constitutive Model

5.1    UBCSAND CONSTITUTIVE MODEL

In the "limited" lateral spread cases examined in the proposed study, the liquefied soils undergo cyclic mobility with limited strain potential. Medium dense to dense sands and silty sands often undergo this type of cyclic response when at relatively low to intermediate effective confining stresses (e.g., Seed 1979; Seed and Idriss 1982). During the initial cycles of undrained loading, excess pore water pressures develop and the soil softens and may liquefy in terms of developing excess pore water pressures close to the effective confining stresses acting on the soil initially. However, as the soil deforms in undrained shear, the soil's tendency to dilate in drained shear is manifested through a sudden drop in the excess pore water pressure and a rapid stiffening of the soil. As noted previously, the concept of a specified post-liquefaction residual strength of the liquefied soil is a gross simplification to what is inherently a complex phenomenon. The engineering profession has analytical methods available to address this phenomenon, but these methods are still not well calibrated or accepted. To advance the state-of-the-practice, this needs to be rectified.

Soil constitutive models have been developed in attempts to capture the cyclic response of soils undergoing cyclic mobility with limited strain potential in numerical simulations. A promising nonlinear effective stress soil model is UBCSAND by Professor Peter Byrne and his colleagues (e.g., Beaty and Byrne 1998, Byrne et al. 2004, and Park and Byrne 2004). The UBCSAND soil model is employed in this study, because it is well documented, available for researchers and practitioners, implemented in the widely used finite difference programs, and offers potentially important insights into this phenomenon.

UBCSAND is implemented in the finite difference computer program FLAC (Itasca 2005), which is described at: http://www.itascacg.com/flac.html. It is relatively straightforward model that is noteworthy because it was developed to capture the undrained deviatoric response of liquefied soil and has been used to evaluate seismic displacements on several projects (e.g., Byrne and Seid-Karbasi 2003, and Seid-Karbasi and Byrne 2004). Some of its capabilities are shown in Figure 5-1. It is able to capture the cyclic build-up of excess pore water pressure and the softening and dilation of soil as it repeatedly crosses the phase transformation line during undrained cyclic shearing. Hence, it can capture the "banana-shaped" loops that occur during cyclic mobility with limited strain potential.

The UBCSAND constitutive model is a nonlinear stress-dependent effective stress model that captures the build-up of excess pore water pressure during cyclic loading and the development of "banana loops" in the shear stress versus shear strain plot once liquefaction occurs as is observed in countless laboratory experiments. Realistic soil responses are obtained by independently controlling the accumulation of permanent shear strains and volumetric strains in the model. It is one of the most popular nonlinear effective

stress soil models used in engineering practice for evaluating liquefaction-induced deformation problems. Although the UBCSAND soil constitutive model is promising for evaluating liquefaction-induced lateral deformation, every nonlinear soil model has its inherent strengths and weaknesses. An evaluation of its ability to capture inertially driven liquefaction-induced lateral spreads is required before practicing engineers can apply it confidently to study the seismic performance of earth structures situated atop potentially liquefiable soils, such as the kilometers of earth levees in the San Joaquin-Sacramento delta region of California.
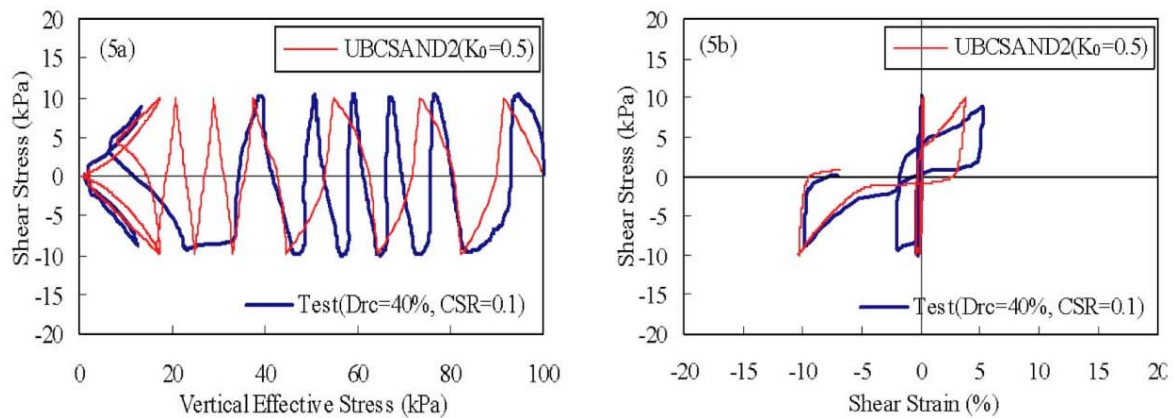


Figure 5-1. Predicted and measured stress paths and stress-strain responses for a sand with relative density of 40% at low CSR = 0.1 using UBCSAND (from Park and Byrne 2004).

## 5.2    UBCSAND MODEL CALIBRATION PARAMETERS

Several versions of UBCSAND currently exist and the model is evolving continually. Thus, calibration of the UBCSAND model may vary with changes made to the model. The version of UBCSAND employed in this study is UBCSANDCheck1 (Byrne 2009). The model input includes parameters modeling elastic stiffness, plastic shear stiffness, strength, flow rule, relative density, and four fitting parameters. Through our correspondence with Peter Byrne, the model developer, generic recommended values and relationships are provided for all but the corrected standard penetration test (SPT) blow count value, referred to as $(N_1)_{60}$, and four fitting parameters controlling triggering and post-triggering dilation. For this study, the generic correlations were not modified, and the model was evaluated for its ability to capture and predict deformations by limiting required user input to SPT blow count and the four fitting parameters discussed below.

### 5.2.1    Relative Density Index

The input parameter accounting for the relative density of the soil is the corrected SPT blow count, or $(N_1)_{60}$ value. This parameter is in wide use in industry, though laboratory testing on which model calibrations are frequently based are typically performed using the measure of relative density. A common equation used to relate relative density with $(N_1)_{60}$ blow count is:

325

$$D_R = \sqrt{\frac{(N_1)_{60}}{C_d}}$$

As summarized in Idriss and Boulanger (2008), the value of $C_d$ has been evaluated by Meyerhof (1957), Skempton (1986), Cubrinovsky and Ishihara (1999) and found to range between 35 and 65 for clean sands. A consistent conversion methodology was desirable to evaluate trends in the fitting parameters. A value of $C_d$ of 46 was used by Idriss and Boulanger (2008) in their SPT relationship, and this value falls within a reasonable range when considering the above studies. Initial modeling showed this to be a value that could capture response of the majority of tests while allowing sufficient range in the curve fitting parameters such that they could be used in fine adjustments of the response. A $C_d$ value of 46 was selected and used to relate relative density and $(N_1)_{60}$ blow count for this effort.

### 5.2.2 Elastic Stiffness Parameters

Elastic stiffness parameters include the elastic shear stiffness number (m_kGe), the bulk stiffness number (m_kb), and the stress exponents m_ne and m_me. These parameters are related in these generic equations as provided by the model developer Peter Byrne:

- m_kge = 21.7 * 15 * $((N_1)_{60})^{0.333}$
- Max. Shear Modulus = $G_{max}$ = m_kge * $P_{atm}$ * $(\sigma'_m/P_{atm})^{m\_ne}$
- m_kb = m_kge * 0.916 (assumes a small strain Poisson's ratio of 0.125)
- Bulk Modulus = K = m_kb * $P_{atm}$ * $(\sigma'_m/P_{atm})^{m\_me}$
- m_me = 0.5
- m_ne = 0.5

A plot showing the variation of normalized bulk and shear modulii with $(N_1)_{60}$ blow count is shown in Figure 5-2.
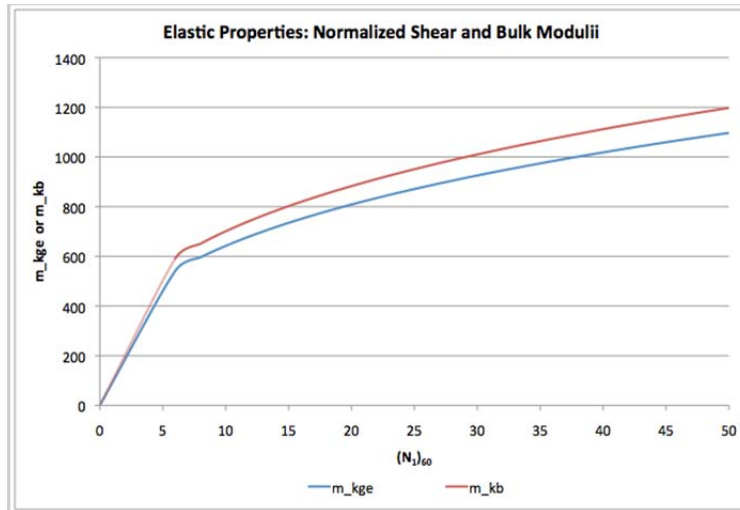
Figure 5-2. Elastic Shear and Bulk Stiffness Numbers with $(N_1)_{60}$ blow count.


### 5.2.3 Plastic Shear Stiffness Parameters

Plastic shear stiffness parameters include the plastic shear modulus number (m_kgp), the plastic shear modulus stress exponent, anisotropy parameter, and the failure ratio (m_rf). Generic correlation equations provided by the model developer were used in our analysis

and are described below and plotted on
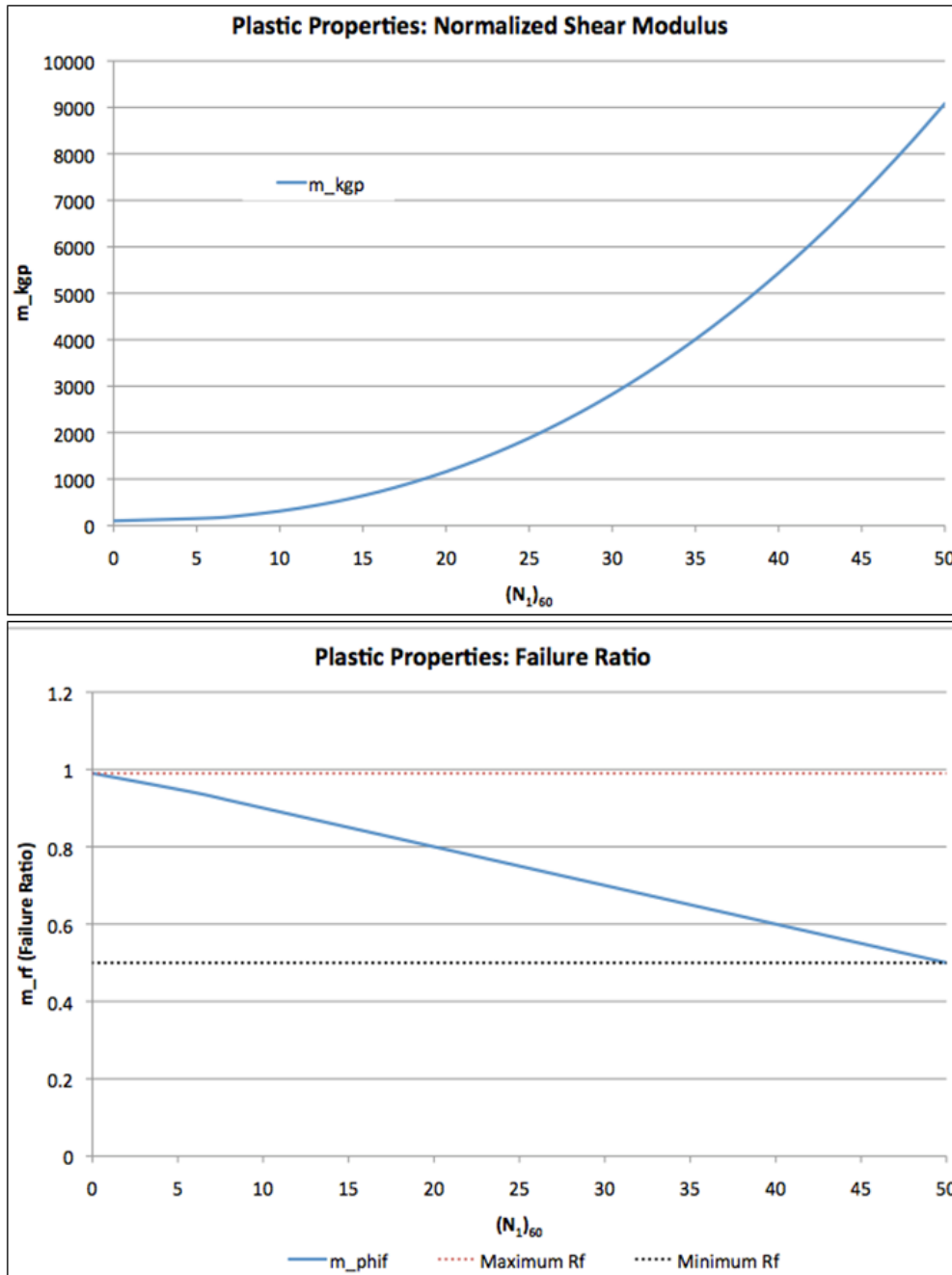


Figure 5-3. The anisotropy parameter varies linearly between 0.333 for loose pluviated soils and 1.0 for isotropic stress conditions.

- $m\_kgp = m\_kge * ((N_1)_{60})^2 * 0.003) + 100$
- Shear Modulus $= G = m\_kge * P_{atm} * (\sigma'_m/P_{atm})^{m\_ne}$
- $m\_np = 0.4$
- Failure Ratio $= m\_rf = 1.0 - m\_n160/100$
  - $0.5 < m\_rf < 0.99$

- Anisotropy parameter = m_anisofac = $0.0166 * (N_1)_{60}$
  - $0.333$ (loose pluviated) $<$ m_anisofac $< 1.0$ (isotropic)
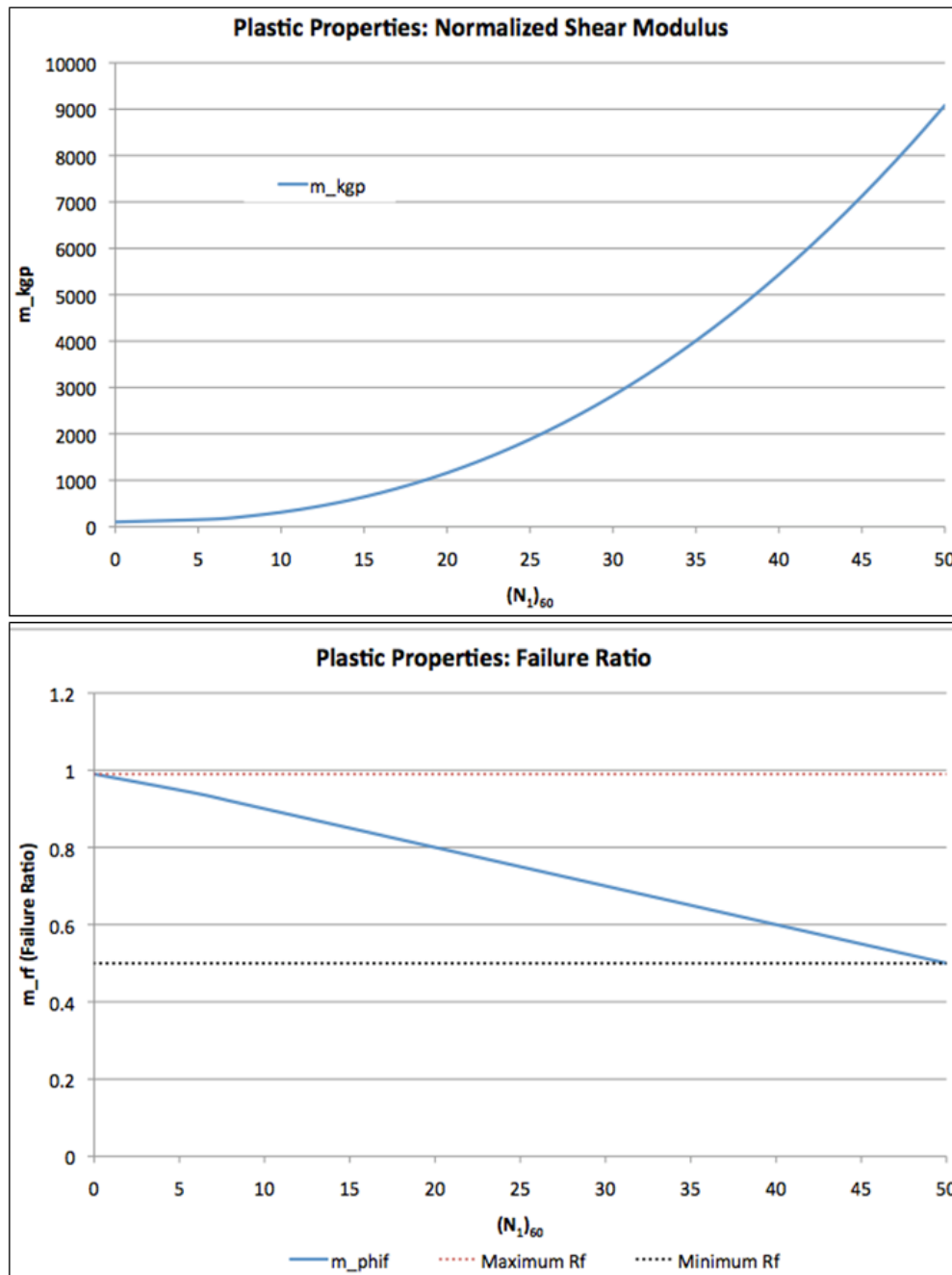


Figure 5-3. Plastic Shear Modulus Number and Failure Ratio vs. (N1)60 blow count.

### 5.2.4   Strength and Flow Rule

The constant volume friction angle is the parameter controlling the flow rule. Volumetric strain is calculated as a function of dilation angle. The dilation angle is calculated from the difference between peak friction angle and constant volume friction angle. The generic value of the constant volume friction angle is 33 degrees where the peak friction angle is calculated as a function of constant volume friction angle and blow count. Generic equations used in this study are provided below, and Figure 5-4 shows peak and constant volume friction angles plotted against blow count.

- m_phicv = 33
- m_phif = m_phicv + $((N_1)_{60})/5.0$
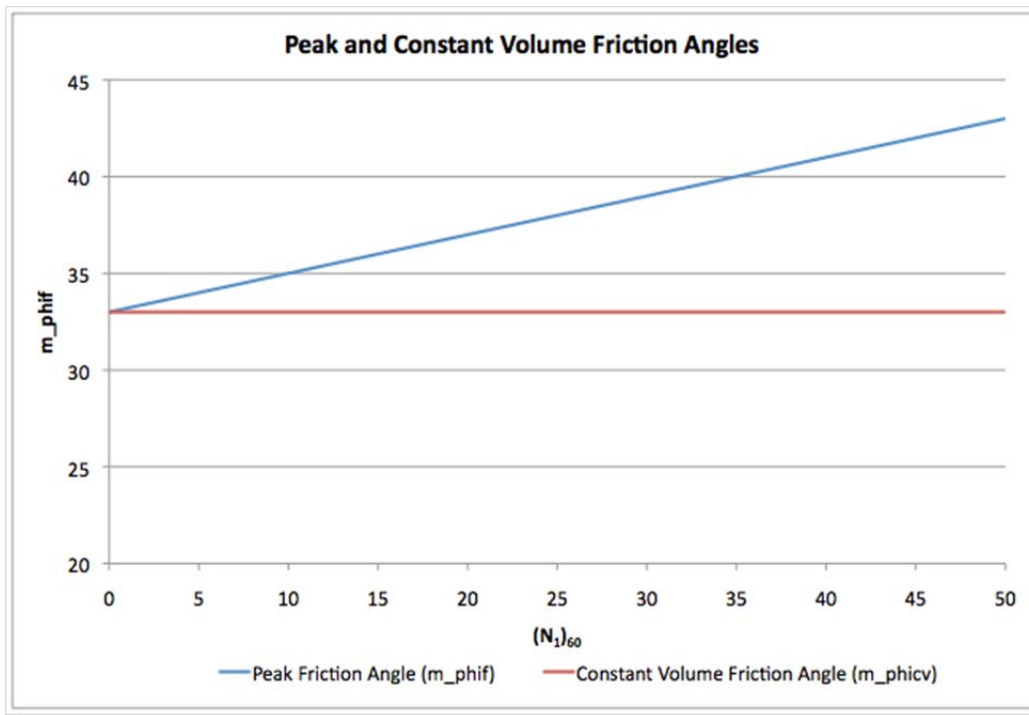


Figure 5-4. Peak and Constant Volume Friction Angles with (N1)60 blow count.

### 5.2.5   Fitting Parameters

Four fitting parameters are available within the UBCSANDCheck1 (Byrne, 2009) version of UBCSAND. The parameters and their listed function are provided below:

- m_hfac1 – Primary hardener that controls number of cycles to trigger liquefaction
- m_hfac2 – Secondary hardener that is reported to refine shape of pore water pressure rise with cycles.
- m_hfac3 – Dilation hardener, controls post-trigger response. This parameter can be set to 1 when running the model wet.
- m_hfac4 – This parameter reduces dilation after triggering.

## 5.3   MODEL CALIBRATION WITH CSS LABORATORY TEST MODELING

### 5.3.1   Selected CSS Test Set

As discussed previously, some of the difficulty the profession has had in developing simplified methods for evaluating lateral spreading is in capturing the complex phenomenon where soil resistance is changing throughout cyclic loading. Soils with low to intermediate confining stresses, which represent soil conditions appropriate for soils underlying small levees and earth embankments, eventually undergo dilation during shearing, leading to the development of "banana-shaped" loops in each half cycle of loading in the stress versus strain plots

Representative cyclic simple shear (CSS) laboratory tests were selected and modeled using a single-element numerical simulation to evaluate the proficiency of the UBCSAND soil model. Laboratory CSS tests were selected from data sets performed by Wu (2002) and Kammerer et al. (2002) on Monterey sand specimens and Nevada sand specimens, respectively. These clean sand tests were used to evaluate the ability of the model to capture the cyclic pore water pressure increase and corresponding cyclic strain response in clean sand soils. The laboratory tests listed in Table 5-1 and Table 5-2 were selected to represent flat and sloping ground conditions, and UBCSAND was then evaluated in terms of its ability to capture the seismic response of these test specimens under a range of densities, cyclic stress ratios, and initial static shear stresses.

Table 5-1. Laboratory CSS test specimens selected to represent flat ground conditions in clean sand soils.

| Test Name* | $\alpha$ $(=\tau/\sigma_v')$ | $D_r$ | $\sigma_v'$ | CSR |
|---|---|---|---|---|
| MS22J | 0.005 | 40 | 85 | 0.099 |
| MS24J | -0.001 | 43 | 85 | 0.136 |
| MS42J | 0.002 | 44 | 83 | 0.162 |
| MS17J | 0.003 | 48 | 40 | 0.164 |
| MS16J | -0.003 | 59 | 85 | 0.166 |
| MS21J | 0 | 34 | 82 | 0.174 |
| MS43J | -0.001 | 31 | 82 | 0.181 |
| MS15J | 0.004 | 54 | 95 | 0.195 |
| MS23J | 0.006 | 43 | 81 | 0.2 |
| MS59J | 0.004 | 58 | 98 | 0.223 |
| MS48J | 0.016 | 33 | 39 | 0.226 |
| MS36J | 0.004 | 70 | 80 | 0.227 |
| MS28J | -0.005 | 56 | 85 | 0.247 |
| MS20J | -0.004 | 45 | 85 | 0.249 |
| MS60J | -0.002 | 56 | 40 | 0.258 |
| MS124 | 0 | 49 | 81 | 0.312 |
| MS19J | -0.01 | 55 | 80 | 0.323 |
| MS7j | -0.004 | 58 | 33 | 0.324 |
| MS25J | -0.002 | 56 | 85 | 0.339 |
| MS30J | 0.01 | 77 | 77 | 0.364 |
| MS32J | 0.018 | 82 | 80 | 0.401 |
| MS125 | 0.012 | 64 | 79 | 0.429 |

\* Tests beginning with the MS designation are from Wu (2002) and were performed on Monterey Sand 0/30.

Table 5-2. Laboratory CSS test specimens representing sloping ground conditions in clean sand soils.

| Test Name* | $\alpha$ $(=\tau/\sigma_v')$ | $D_r$ | $\sigma_v'$ | CSR |
|---|---|---|---|---|
| NS13 | 0.05 | 47 | 38 | 0.17 |
| NS17 | 0.05 | 50 | 30 | 0.22 |
| MS118J | 0.06 | 60 | 85 | 0.175 |
| MS39J | 0.07 | 45 | 81.4 | 0.22 |
| MS117J | 0.08 | 46 | 86.2 | 0.139 |
| NS11 | 0.08 | 90 | 44 | 0.22 |
| NS16b | 0.08 | 48 | 43 | 0.24 |
| MS111J | 0.09 | 66 | 81.4 | 0.173 |
| MS113J | 0.09 | 64 | 81.4 | 0.253 |
| NS12 | 0.09 | 93 | 36 | 0.53 |
| NS16 | 0.1 | 48 | 44 | 0.1 |
| MS116J | 0.1 | 44 | 81.4 | 0.168 |
| NS4 | 0.1 | 68 | 40 | 0.24 |
| MS122 | 0.11 | 48 | 76.6 | 0.127 |
| NS10 | 0.11 | 90 | 95 | 0.26 |
| MS123J | 0.12 | 48 | 81.4 | 0.138 |
| MS119J | 0.13 | 61 | 81.4 | 0.154 |
| MS120J | 0.14 | 47 | 71.8 | 0.166 |
| NS3 | 0.14 | 62 | 39 | 0.24 |
| NS18 | 0.16 | 51 | 40 | 0.25 |
| MS114J | 0.17 | 60 | 82 | 0.24 |
| NS19 | 0.19 | 51 | 41 | 0.24 |
| NS9 | 0.21 | 90 | 102 | 0.24 |

\* Tests with MS designation were performed on Monterey Sand Specimens by Wu (2002). Test names beginning with NS were performed on Nevada Sand specimens by Kammerer et al. (2002)

A range of representative silt CSS tests were selected from data sets by Sancio (2003) and a set of CSS laboratory tests performed on non-plastic Bonnie Silt by UC Davis as part of the Verification of Liquefaction Analysis by Centrifuge Studies (VELACS) project (Arulmoli et al., 1992). These laboratory tests were evaluated through single element numerical simulations in UBCSAND to evaluate the ability of the constitutive model to capture silt behavior. The test specimens listed in Table 5-3 were utilized in this study.

Table 5-3. Laboratory CSS test Specimens selected to represent silt soils.

| Test Name* | $\alpha$ $(=\tau/\sigma_v')$ | Void Ratio (e) | $\sigma_1'$ (kPa) | $\sigma_3'$ (kPa) | $\sigma_m'$ (kPa) | CSR | Plasticity Index |
|---|---|---|---|---|---|---|---|
| CSSBS-07 | 0.035 | 0.678 | 80 | - | - | 0.213 | NP |
| A5P9B3 | 0 | 1.08 | 133 | 82 | 99 | 0.27 | 11 |
| G4P3-6 | 0.2 | 1.09 | 136.5 | 82 | 100 | 0.27 | 14 |
| G4P3-2 | 0.193 | 0.9 | 133.7 | 79 | 97 | 0.23 | 0 |

*All tests are from Sancio (2003) except test CSSBS-07 which is from Arulmoli et al., 1992.*

### 5.3.2 Sand – Flat Ground CSS Tests

Figure 5-5 through Figure 5-7 show representative 4-way plots of shear stress vs. shear strain (upper left corner), shear stress vs. effective vertical stress (upper right corner), pore water pressure increase as a ratio of initial vertical effective stress vs. cycles of shear

(lower left), and pore water pressure as a function of shear strain (lower right) for several CSS tests. In general, flat ground cases are well matched. Damping is generally overestimated as can be seen by the difference in shapes of the 'banana loops' shown in the shear stress vs. shear strain plots.

Based on the tests modeled in this study, pore water pressures were typically overestimated by UBCSAND resulting in difficulty matching strains over a range of cycles (i.e., a range of approximately 5 to 20 cycles would represent typical earthquake scenarios possible in California). As an example of this, Figure 5-6 shows an overlay of predicted vs. actual laboratory results for Monterey Sand test MS23J. As a result of overestimation of pore water pressures, softening of soils occurs earlier in the time record than observed in the actual laboratory test. Looking at plots of shear stress vs. shear strain and effective vertical stress (the two upper plots), one can see that when sufficient softening has occurred to trigger yielding in the soil under cyclic loading, the initial predicted lateral yield is larger than measured but with additional cycles the strain increment is reduced relative to measured and a match can be achieved. The range of cycles over which a suitable match to measured strains can be achieved varies with relative density, CSR, initial static shear, plasticity, and other factors as discussed in subsequent sections of this report.
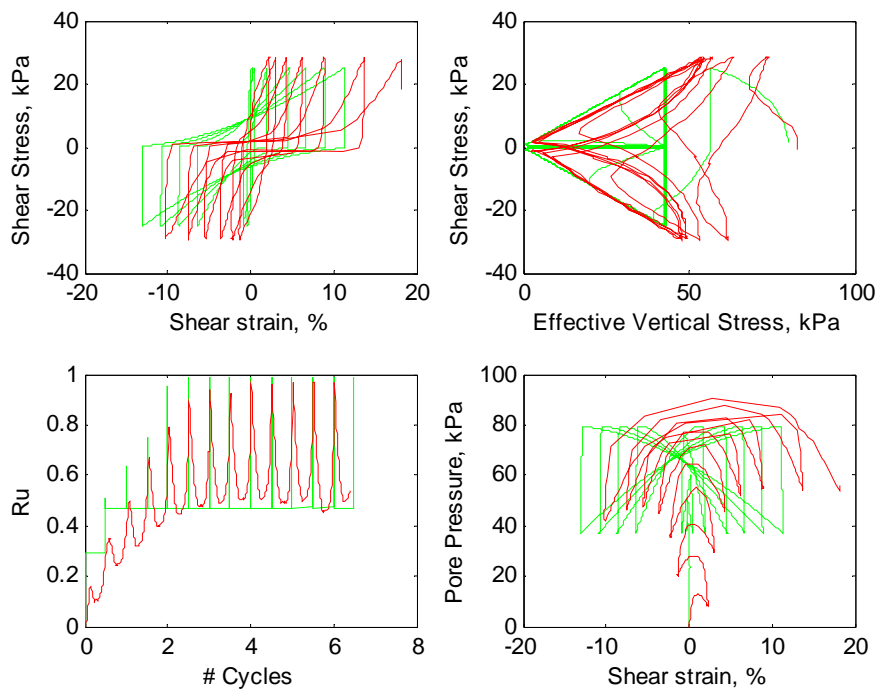


Figure 5-5. Test MS19J: $\alpha$=-0.01; Dr=55%; CSR=.24 (Wu, 2002). Test data in red and UBCSAND output in green.
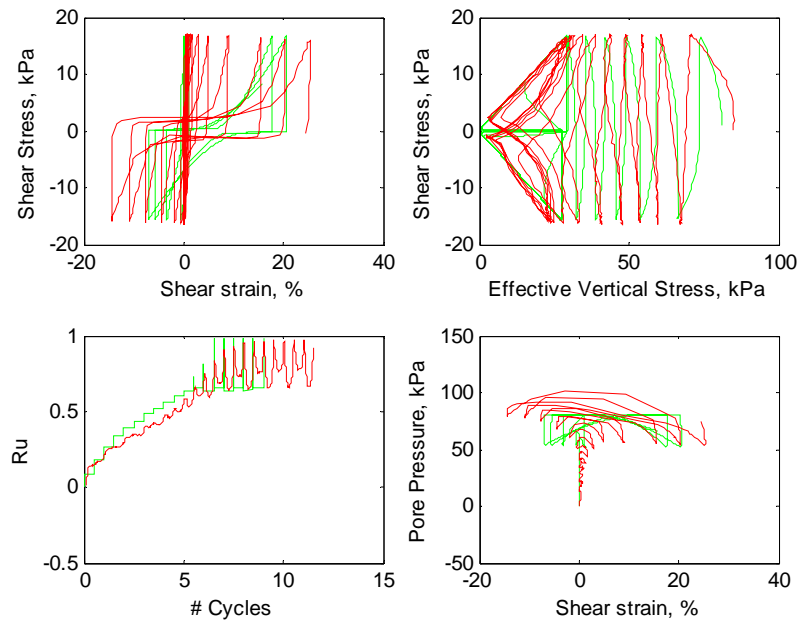
Figure 5-6. Test MS23J: α=0.006; Dr=81%; CSR=0.20 (Wu, 2002).  Test data in red and UBCSAND output in green.
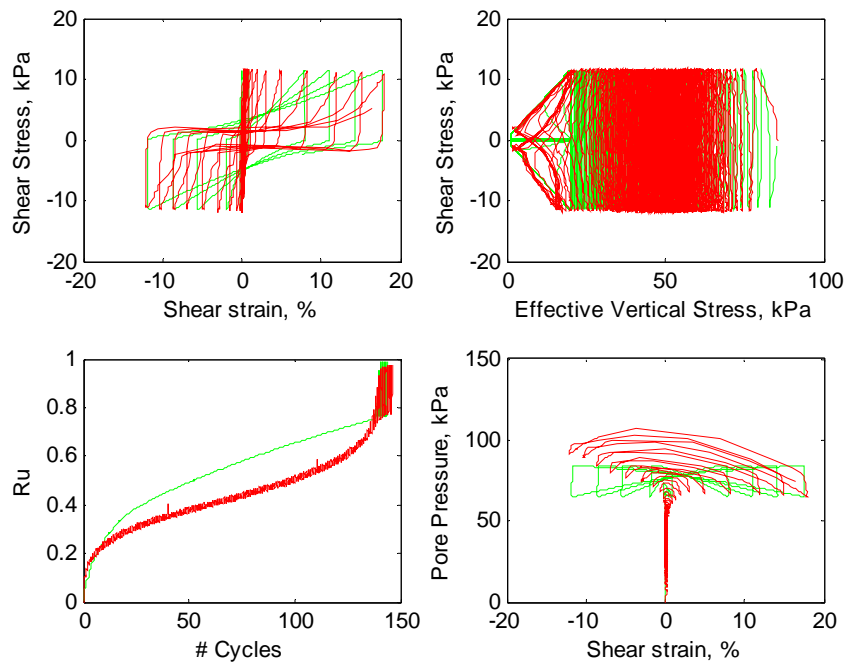


Figure 5-7. Test MS24J: α=-0.001; Dr=43%; CSR=0.136 (Wu, 2002). Test data in red and UBCSAND output in green.

### 5.3.3 Sand – Sloping Ground CSS Tests

Figure 5-8 through Figure 5-11 show examples of calculated vs. measured response of clean sand Specimens of Monterey and Nevada Sands under initial static loading conditions and subjected to cyclic loading in simple shear. The UBCSAND model can capture many key aspects of soil response. However, it has a few limitations, which will be the focus of this discussion.

Shear strain is typically not matched in both the forward and reverse directions. Instead, it is matched in only the forward direction as can be seen for tests NS3 (Figure 5-8), MS118J (Figure 5-10), and MS11J (Figure 5-11). Further, the model is unable to calculate accurately the significant shear strains that sometimes occur due to the static shear loading prior to the triggering of flow liquefaction but during the incremental building of pore water pressures. Laboratory test specimens NS9 and MS11J are excellent examples of this (Figure 5-9 and Figure 5-11, respectively). Specimen NS9 does not liquefy during the test and strains are not well captured. Similarly, Specimen MS11J exhibits cyclic mobility with limited strain potential as well as incremental movements in the downslope direction (the direction of the initial static shear stress). Looking at the plot of pore water pressure with shear strain (lower right corner) of Figure 5-11, the UBCSAND model can capture the deformation well once pore water pressures have incrementally increased to a pore water pressure ratio (Ru) of greater than about 50%. The UBCSAND model has not captured the effects of cyclic mobility with limited strain potential or the 'creeping' movements in the downslope direction driven by the initial static shear.
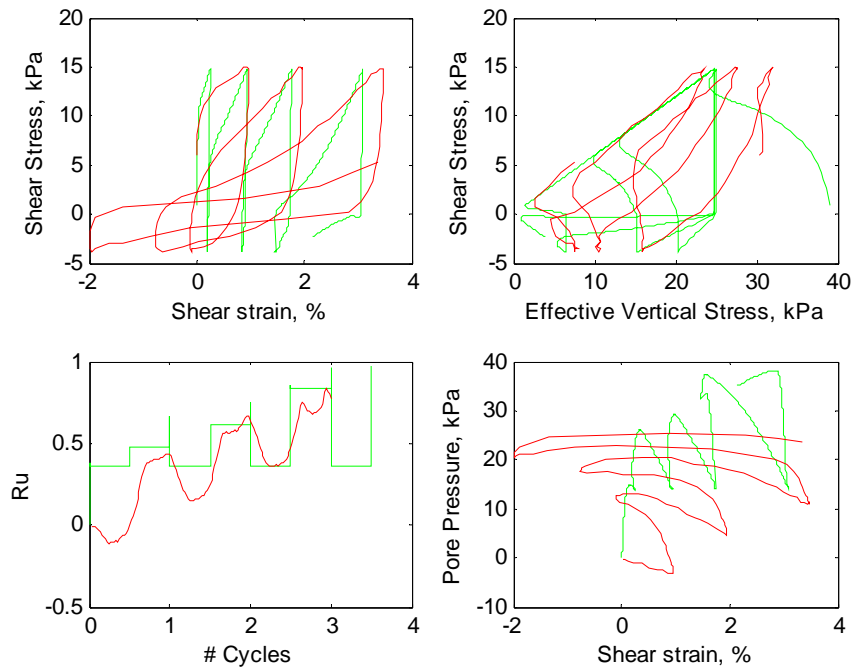


Figure 5-8. Test NS3: $\alpha$=0.14; Dr=62%; CSR=0.24 (Kammerer, 2002). Test data in red and UBCSAND output in green.

335
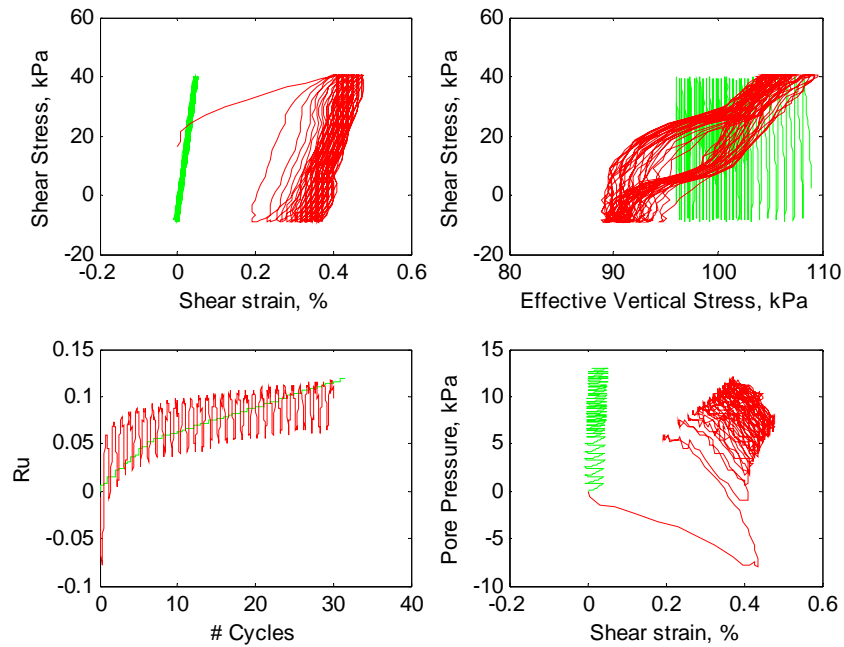
Figure 5-9. Test NS9: α=-0.21; Dr=90%; CSR=0.24 (Kammerer, 2002). Test data in red and UBCSAND output in green.
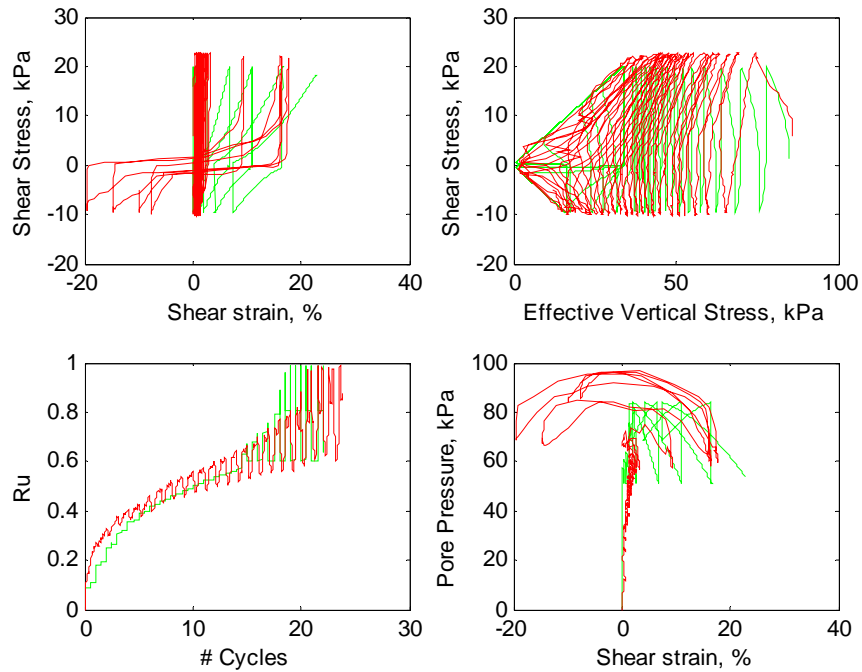


Figure 5-10. Test MS118J: α=0.06; Dr=60%; CSR=0.175 (Wu, 2002). Test data in red and UBCSAND output in green.
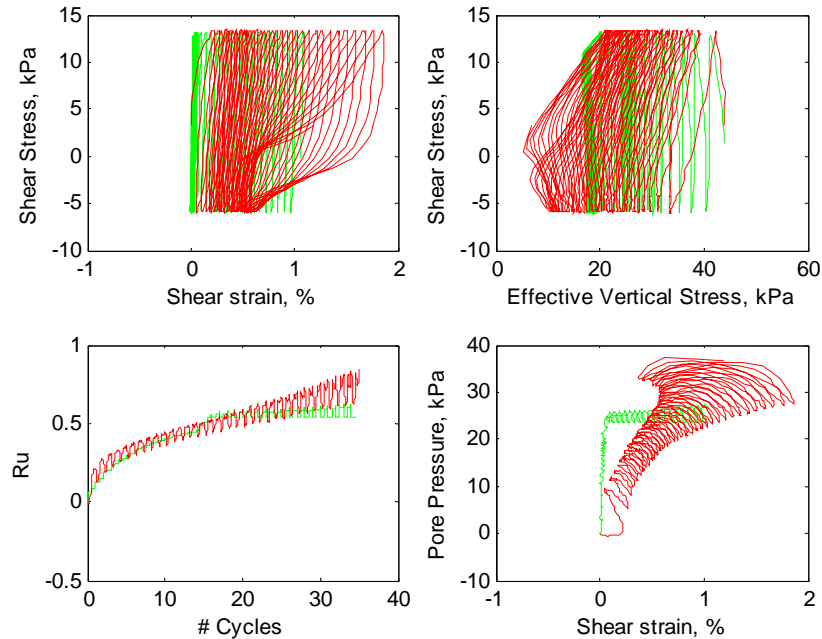
Figure 5-11. Test NS11J: α=0.08; Dr=90%; CSR=0.22 (Kammerer, 2002). Test data in red and UBCSAND output in green.

## 5.4    UBCSAND MODEL CALIBRATION PARAMETERS

### 5.4.1    M_HFAC1 and M_HFAC2

Though different functions are listed for these two parameters, we found that m_hfac1 and m_hfac2 have similar function as both affect the number of cycles to triggering. We were unable to achieve variation in the rate of pore water pressure rise with cycles through variation of the m_hfac2. In our studies we found that varying both parameters added unnecessary complication to the analysis and found best results obtained by matching m_hfac2 to m_hfac1 and treating the two parameters as a single parameter. Personal communication with the model developer, Professor Byrne, confirmed that this was an acceptable strategy. Subsequent plots refer to m_hfac1 and m_hfac2 with the assumption that the parameters were equal to one another.

Figure 5-12 shows how the m_hfac1 and m_hfac2 parameters vary with relative density ($D_r$). In general, we found that tests with lower initial static shear stress required slightly lower values of the m_hfac1 and 2 while specimens with higher initial static shear stress required higher values of these fitting parameters to achieve the best match with laboratory testing values. Specimens with higher initial static shear stress exhibited greater variation in the m_hfac1 and 2 parameters to capture the response. Larger values of the m_hfac1 and 2 fitting parameters reduce the rate of pore water pressure rise with cycles and increase the number of cycles to liquefaction.

337
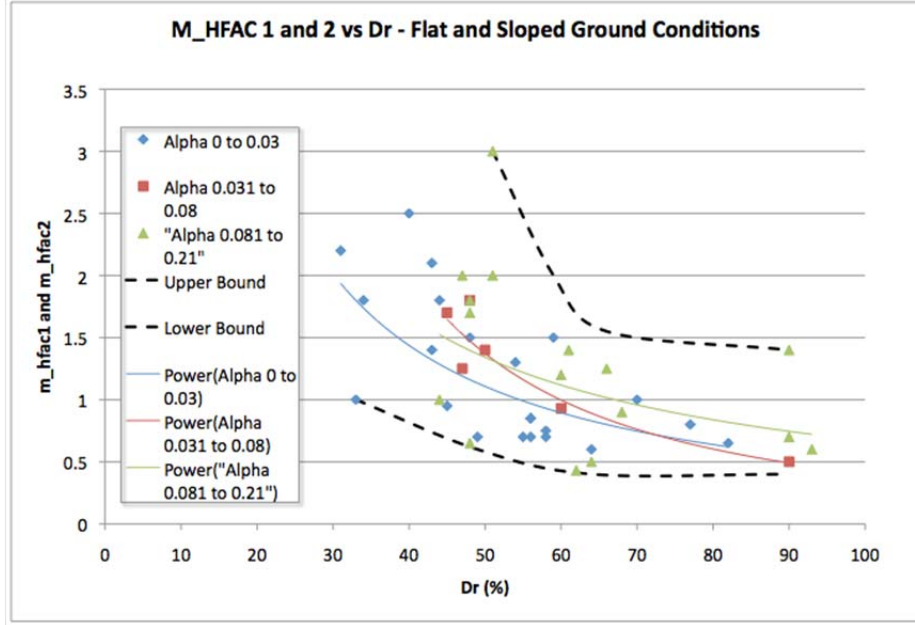
Figure 5-12. Triggering Parameters m_hfac1 and m_hfac2 vs. Relative Density (Dr).

Trends of m_hfac1 and 2 with CSR are plotted on Figure 5-13 for the flat ground condition and Figure 5-14 for sloping and flat ground conditions. A clear trend is seen with CSR for the flat ground condition. It should be noted that effects of relative density were not separated out in Figure 5-13 and Figure 5-14 and laboratory specimens prepared with a low relative density tend to be tested at low CSR, while those prepared at higher relative density tend to be tested at higher CSR in order to trigger liquefaction.

It is clear from Figure 5-14 that sloping ground conditions do not exhibit the same trend with CSR seen with flat ground specimens. The triggering parameters used to capture the liquefaction response for specimens with larger initial static shear stress exhibit trends with density as opposed to CSR. Both Figure 5-13 and Figure 5-14 were used in determining the values of fitting parameters m_hfac1 and m_hfac2 for use in back analysis of case histories as well as forward modeling of the simplified cases of our sensitivity study. Parameter selection for these models will be discussed in subsequent sections of this report.
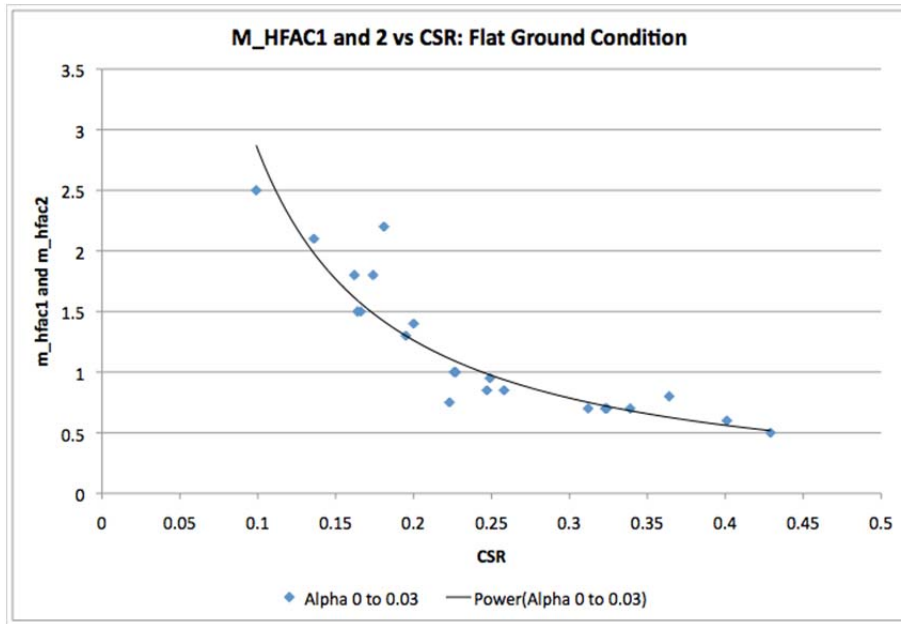
Figure 5-13. Triggering Parameters m_hfac1 and 2 vs. CSR – Flat Ground Condition.
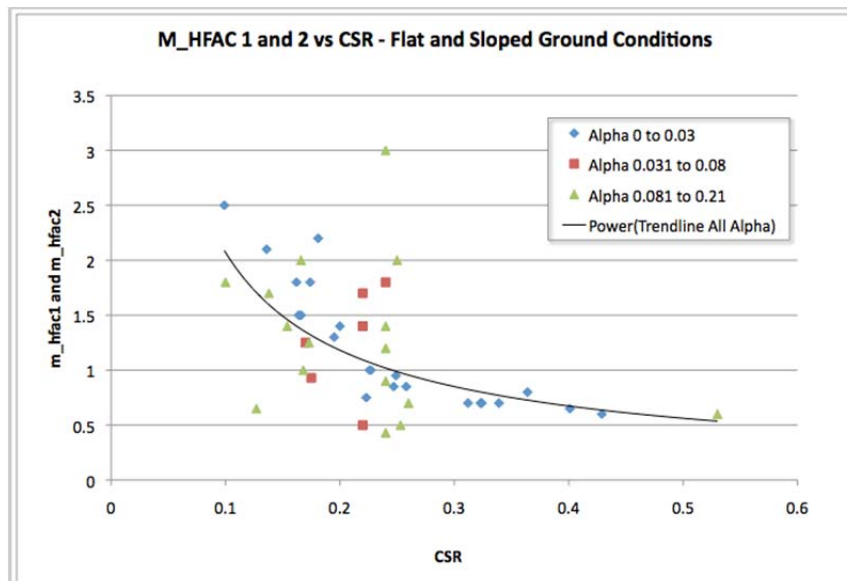


Figure 5-14. Triggering Parameters m_hfac1 and 2 vs. CSR – Flat and Sloping Ground Conditions.

### 5.4.2   M_HFAC3

The parameter m_hfac3 was not varied, but rather was set to 1.0 for analyses where the model was to be run wet. Layers above the groundwater table were modeled with the Mohr-Coulomb model.

### 5.4.3 M_HFAC4

The dilation reduction parameter m_hfac4 was varied between 0.5 and 2.7 to capture the post-triggering shear strains of clean sand and silt specimens. Silts will be discussed in a separate section, and we will discuss clean sand trends as they vary with relative density, CSR and initial static shear stress.

Figure 5-15 and Figure 5-16 show the value of m_hfac4 that was used to capture the level of shear strain in clean sand specimens with varying CSR and $D_r$ respectively for a flat ground case. The data were divided into groups of low CSR (equal to 0.2 or less) and higher CSR (greater than 0.2). Specimens subjected to higher CSR values showed a weak trend with CSR and no noticeable trend with $D_r$. The value of m_hfac4 increases with increasing CSR. Increasing m_hfac4 reduces dilation after triggering and increases incremental strains. Specimens subjected to lower CSR did not show a trend with increasing CSR, but rather exhibited a weak trend with Dr. As soils became looser, the value of m_hfac4 was decreased to match strains. Decreasing m_hfac4 increases dilation after triggering and limits the overestimation of shear strains.
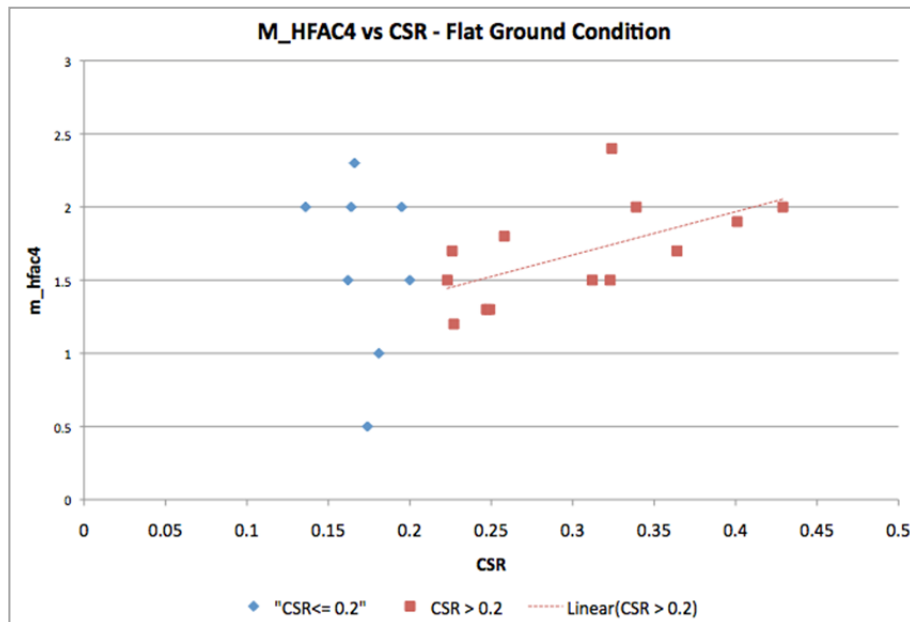


Figure 5-15. Dilation reduction parameter, m_hfac4 vs. CSR – Flat Ground Case. A weak trend with CSR is visible for values of CSR greater than 0.2. No trend is observed at CSR values of 0.2 or less.
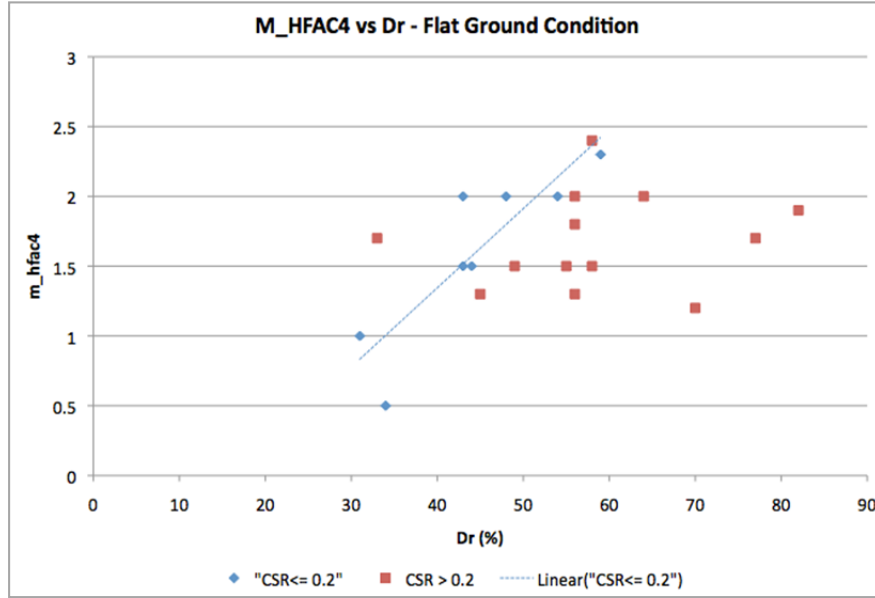
Figure 5-16. Dilation reduction parameter, m_hfac4 vs. $D_r$ – Flat Ground Case. A weak trend is visible with $D_r$ at values of CSR of 0.2 or less.

Figure 5-17 and Figure 5-18 show plots of both sloping and flat ground condition cases against relative density and CSR. A weak trend with $D_r$ can still be seen in the specimens subjected to CSR values of 0.2 or less (Figure 5-17). No trend is visible with CSR (Figure 5-18), though values typically range between 1.5 and 2.0.
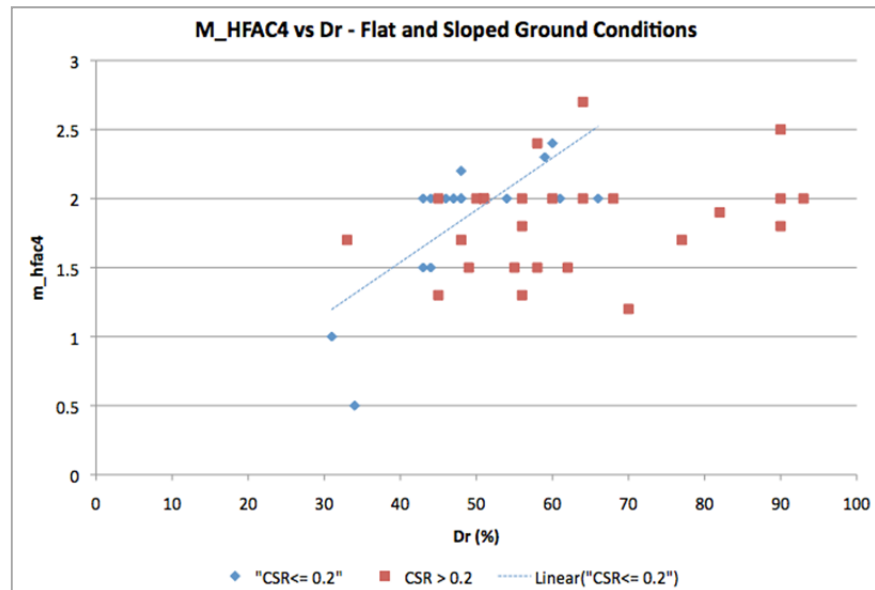


Figure 5-17. Dilation reduction parameter, m_hfac4 vs. $D_r$ – Sloping and Flat Ground Cases. A weak trend is visible with $D_r$ at values of CSR of 0.2 or less.
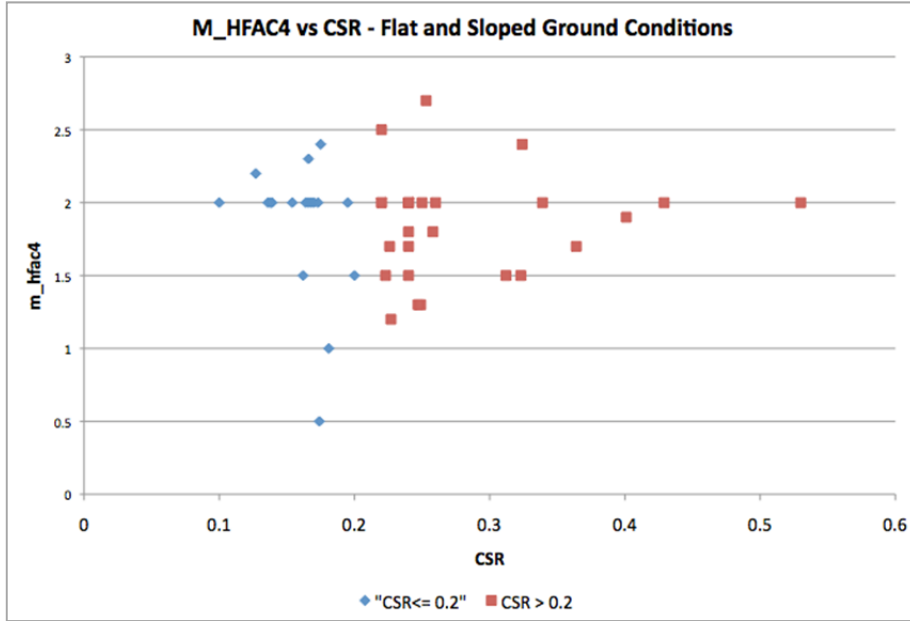
Figure 5-18. Dilation reduction parameter, m_hfac4 vs. CSR – sloping and flat ground cases.

### 5.4.4    Silt – Flat and Sloping Ground

Parameters used for modeling silts were developed by modeling laboratory tests using a series of blow count values within UBCSAND to determine a value that yielded a realistic fit to laboratory data. In general, values of m_hfac1 and m_hfac2 selected were found to be slightly higher for silts than sands of zero initial static shear stress but were found to follow a similar trend when considering the void ratio of the sample as a relative measure of blow count. Figure 5-19 shows a plot of m_hfac1 and 2 for the 4 laboratory tests considered against the selected value of blow count. The data are plotted with previously reported sand data for comparison. The values selected for m_hfac4 were lower than those selected for sands of similar fines corrected $(N_1)_{60}$ blow count.  For higher void ratio silts, a value of m_hfac4 of 0.5 was found to be appropriate. For silts of lower void ratio as well as silty sands, we selected a value of m_hfac4 of 1.5.
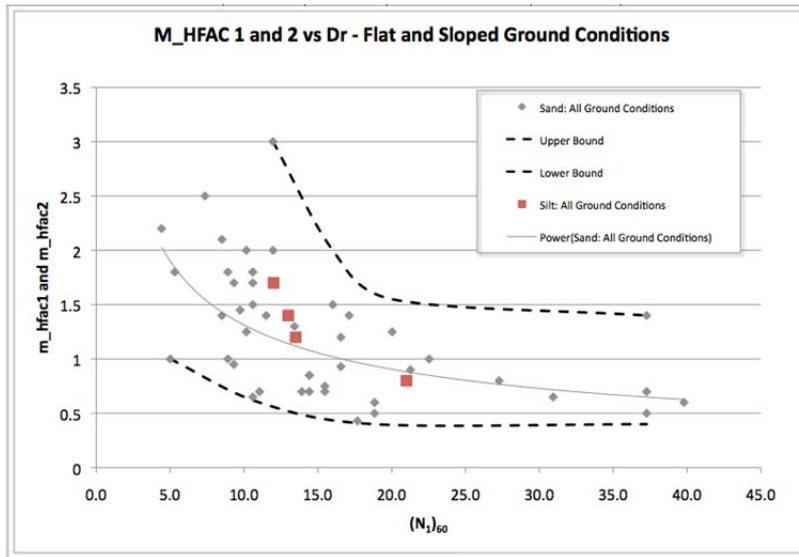
Figure 5-19. Selected values of m_hfac1 and m_hfac2 found to yield a fit to the laboratory data.

## 5.5   MODEL VALIDATION THROUGH BACK ANALYSIS

A few important case histories of "limited" lateral spreads, as defined by Martin and Lew (1999), will be performed to calibrate the numerical tools discussed previously. Excellent descriptions of lateral spread case histories are contained in Bardet et al. (1999) and Faris (2004). These descriptions will be relied upon in this study.

Due to their relatively excellent documentation and range of liquefaction-induced lateral spread displacements, these case histories will be used in this study:

- Juvenile Hall lateral spread with a maximum displacement of 2.4 m during the 1971 San Fernando Earthquake
- Moss Landing Marine Laboratory lateral spread with a maximum displacement of 1.4 m during the 1989 Loma Prieta Earthquake
- Monterey Bay Aquarium Research Institute lateral spread with a maximum displacement of 0.3 m during the 1989 Loma Prieta Earthquake

Each of these case histories will be back-analyzed with the UBCSAND model as implemented in FLAC to ensure that the analytical methods being employed in this research project provides reliable insights.

### 5.5.1   Moss Landing MBARI/Sandholdt Road – Loma Prieta 1989

Moss Landing and the surrounding region was the site of numerous examples of ground failure due to liquefaction and lateral spreading associated with ground shaking of the 1989 Loma Prieta earthquake. One such site is located along Sandholdt Road about 300 feet north of the western approach of an existing timber access bridge crossing the Old Salinas River on the Moss Landing spit in the vicinity of the Monterey Bay Aquarium Research

Institute (MBARI). Sandholdt Road runs in a north/south direction and functions as the primary access road for MBARI complex (Figure 5-20. ).

Site damage, subsurface stratigraphy, and a summary of available reports and information surrounding the case study were well documented and summarized in a comprehensive report by Boulanger et al. (1995). Inclinometers had been installed and monitored prior to the Loma Prieta earthquake and captured lateral movements with depth at three locations within the zone of lateral spreading. Section A-A' of Figure 5-20.  was selected for our analysis as a soil boring and two cone penetration tests (CPT) were performed along this section.
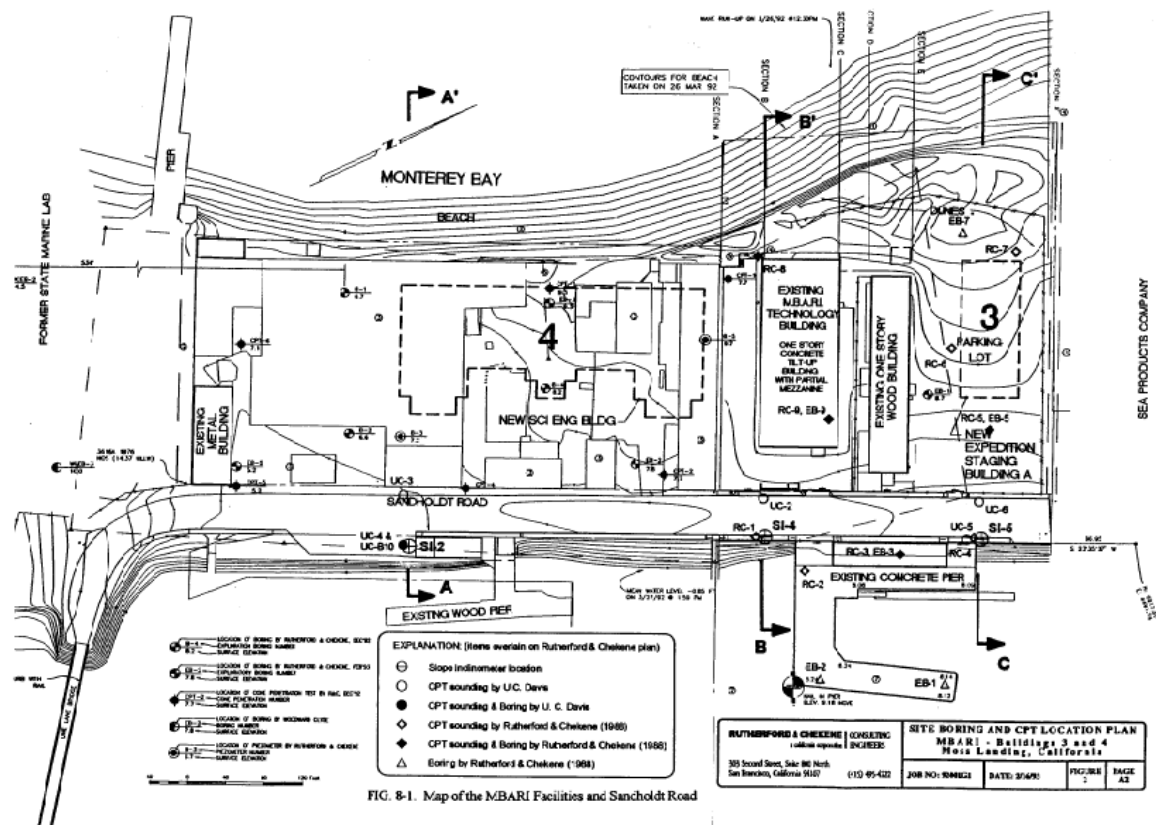


FIG. 8-1. Map of the MBARI Facilities and Sancholdt Road

Figure 5-20. Site plan showing Sandholdt Road, the MBARI complex, waterfront piers, and the former State Marine Lab site discussed in Section 3.2.

Figure 5-21 shows a cross section of the subsurface stratigraphy at Section A-A'. Inclinometer S-2 is located adjacent to boring UC-B10 and CPT UC-4. Based on Boulanger et al. (1995) the large crack within Sandholdt Road was considered to be the limit of primary deformation as shown in the photograph included in Figure 5-22. Figure 5-23 shows inclinometer S-2 data plotted with the soil profile created using soil boring B10 and CPT UC-4. Blow count data are overlain with CPT tip resistance. Inclinometer S-2 shows lateral

displacements of up to approximately 27 cm at the surface. Deformations extended to a depth of approximately 4.6 meters from the surface and stopped at the transition between the thin sand layer and the clayey silt layer below. The movement occurred gradually over a zone extending from a depth of approximately 1.5 m to a depth of 4.6 m rather than sliding as a block on a single slide plane as would be assumed by post-liquefaction stability analysis methods using residual strength assumptions.
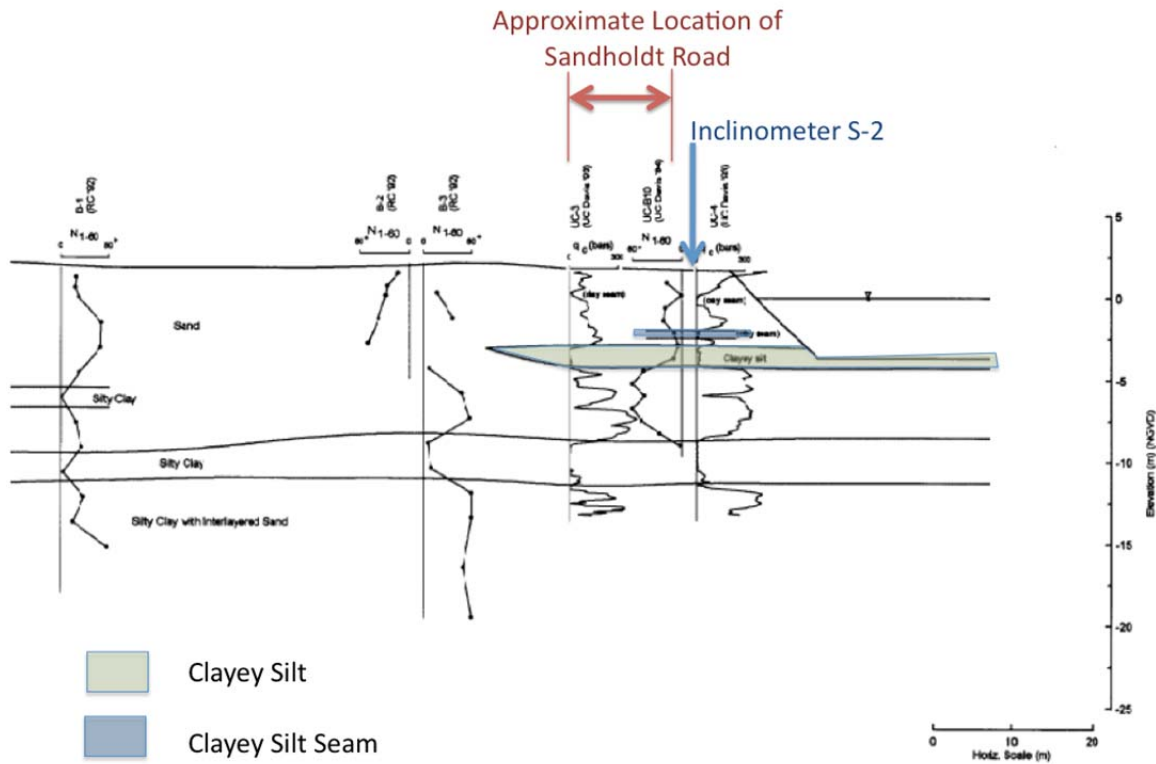


Figure 5-21. Subsurface stratigraphy at Section A-A'. The thin seam shown in blue will be referred to as a clayey silt seam to be consistent with available boring logs and laboratory test data from UC-B10.

Figure 5-22. Cracking along Sandholdt Road (looking north just south of MBARI pier; from Boulanger et al. 1995).
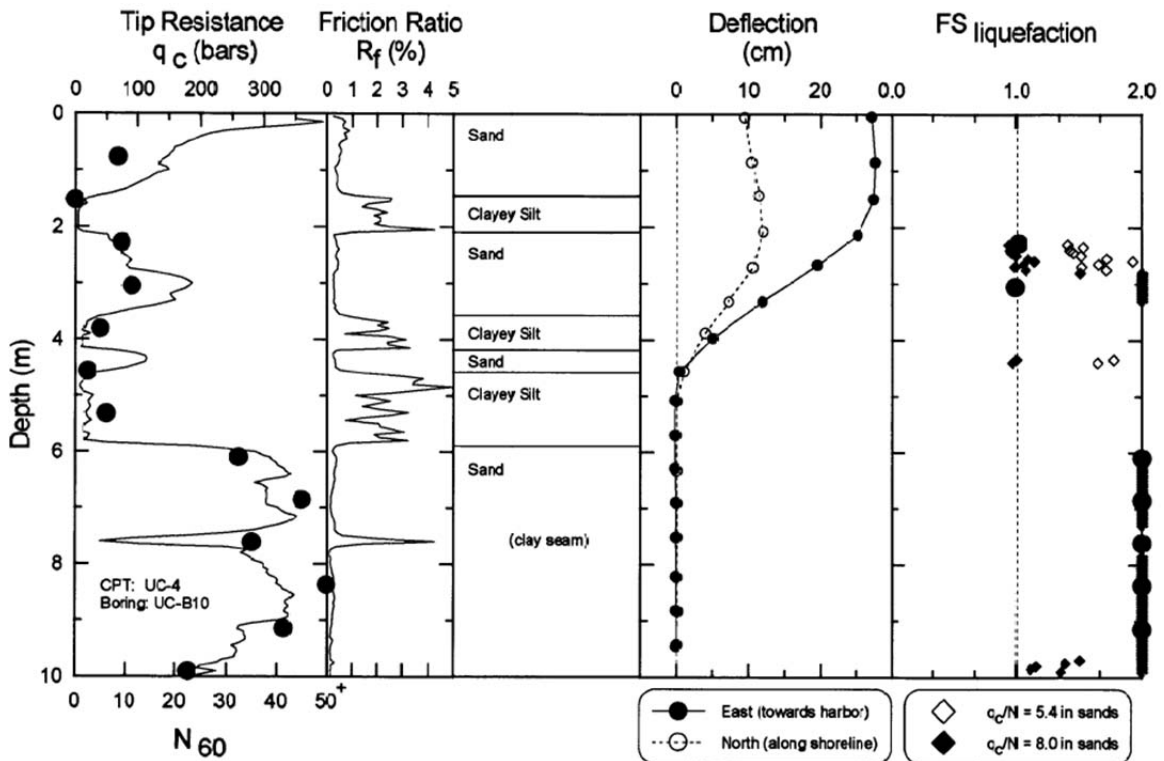


Figure 5-23. Inclinometer S-2 measured deformation data. Data is plotted with subsurface stratigraphy from boring UC-B10 and CPT UC-4 (from Boulanger et al. 1995).

Two silt layers are labeled on Figure 5-21 as 'clayey silt' and 'clayey silt seam' for the purpose of this discussion. Based on Figure 5-23, inclinometer data shows that movement occurred within the 'silt seam' but not within the 'clayey silt' layer below it. The 'clayey silt seam' may be so thin that it deformed with sand layers above and below or that the inclinometer pipe stiffness 'averaged' the deformations across thin seams of sand and silt. In deciding whether to model each silt layer with the UBCSAND or Mohr-Coulomb models, available CPT, boring, and laboratory data were evaluated in detail for each layer.

Both the 'clayey silt seam' and 'clayey silt' layers exist at the location of inclinometer S-2 and both appear in soil boring UC-B10 and CPT UC-4. Gradation testing performed on the 'clayey silt seam' found fines content to be 74% passing the number 200 sieve with 18% finer than 5 microns. Similar testing on the 'clayey silt' found a fines content of 80% and 14 percent smaller than 5 microns. Atterberg limits testing was performed only on the 'clayey silt seam' and was found to have a plasticity index (PI) of 7% and a liquid limit of 32%.

Cone penetration data (UC-4 and UC-3) are available on either side of Sandholdt road as indicated on Figure 5-20. and Figure 5-21. The 'clayey silt' layer appears in both CPTs, while the 'clayey silt seam' appears only in UC-4, adjacent to inclinometer S-2. A comparison of CPT data yielded an inconclusive result as to whether the 'clayey silt' layer at the toe of slope should be modeled as a potentially liquefiable layer with the UBCSAND model or with the Mohr-Coulomb model. Thus, both cases were considered, and the results compared. In Model A, the 'clayey silt' layer at the toe of slope is modeled as a cohesive soil with the Mohr-Coulomb model. Figure 3.1.6 shows the mesh and layers used to model the site. As summarized in Boulanger et al. (1995), the ground motion driving the observed lateral spread deformation was estimated to have a peak ground acceleration (PGA) of approximately 0.2 to 0.3 g using a bedrock motion of 0.15 g. The report concluded that 0.25 g would likely represent a median or slightly lower estimate of Loma Prieta earthquake. The Salinas ground motion record (PGA = 0.15 g) was identified as having similar soil conditions at depth and was scaled to 0.25 g. This ground motion was used as input in our analysis.
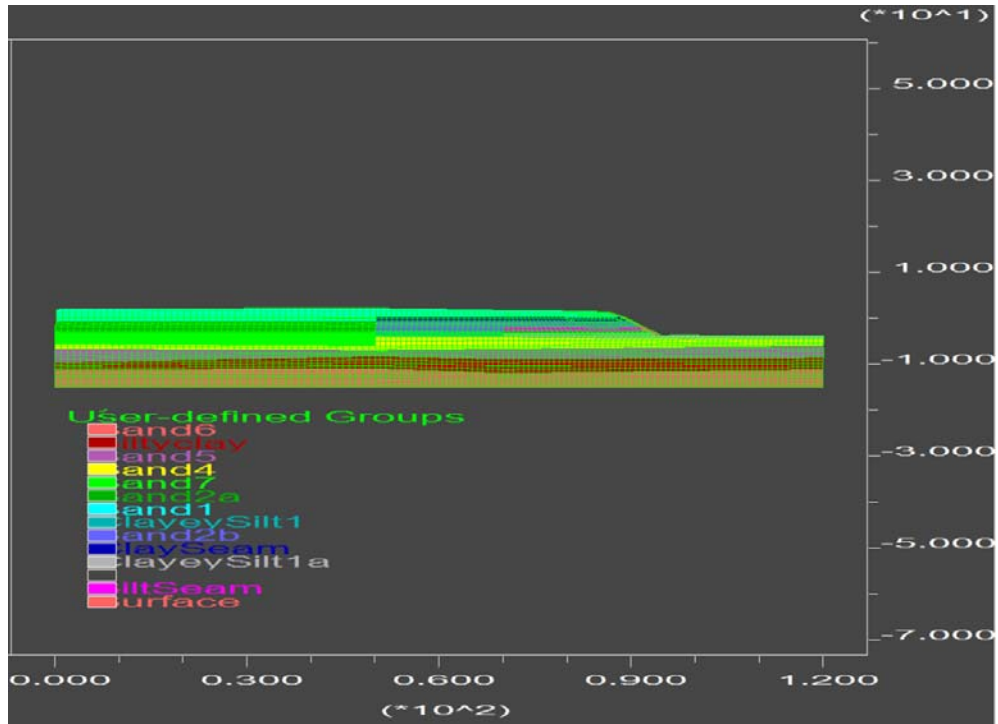
Figure 5-24. Mesh and soil groups at the site of the MBARI/Sandholdt Road lateral spread.

Figure 5-25 and Figure 5-27 show the resulting lateral deformations from each model. Figure 5-26 and Figure 5-28 show vectors of deformation showing both horizontal and vertical movements for Models A and B, respectively. Figure 5-29 shows the resulting deformations for each model plotted with measured inclinometer data. It can be seen that when the 'Clayey Silt' layer is modeled with the Mohr-Coulomb model, estimated deformations closely match observations. When the UBCSAND model is used to model the 'Clayey Silt' layer, the simulation calculates deformations in this layer that were not observed and as a consequence, the deformations are overestimated by a factor of about 2. As discussed previously, numerical models are not a substitute for detailed subsurface characterization as the model may be improved significantly with increased understanding of the subsurface conditions.

348
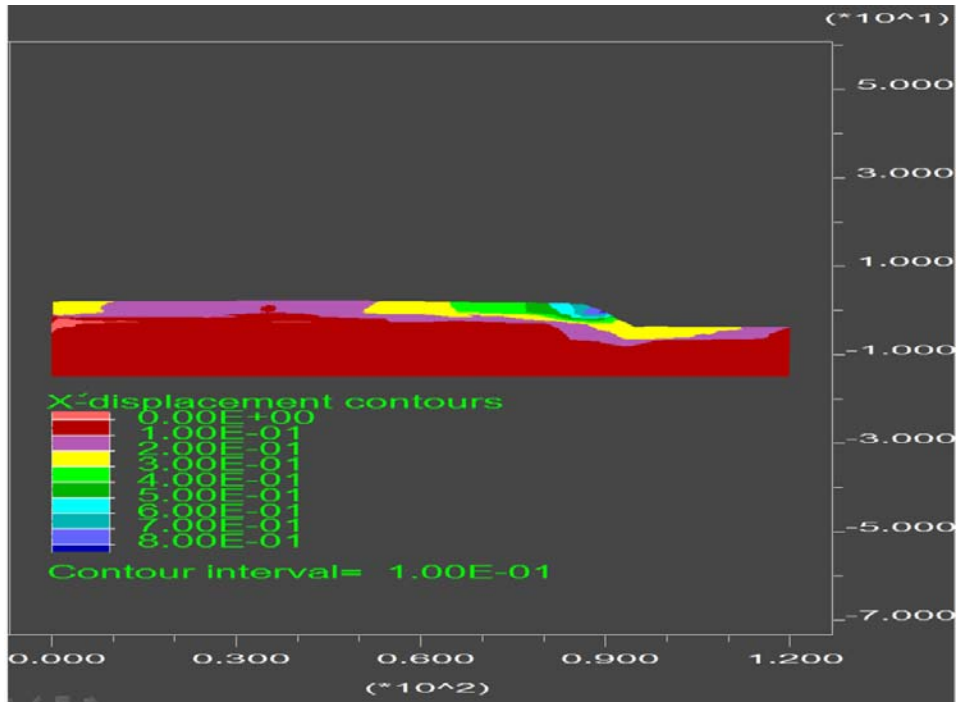
Figure 5-25. Predicted lateral displacements at MBARI/Sandholdt Road Section A-A' as predicted by Model A.
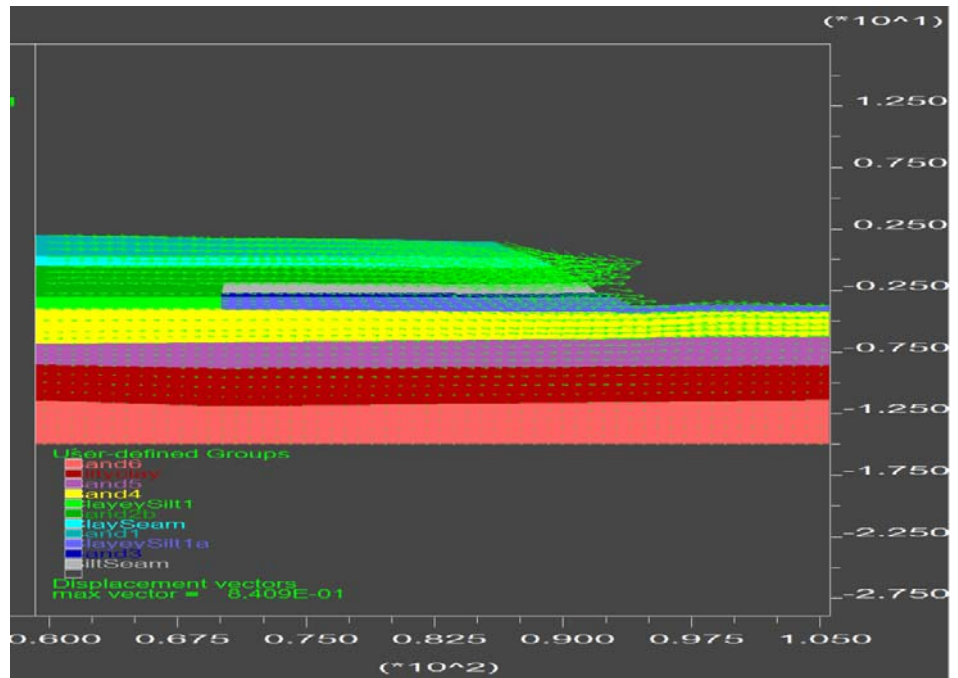


Figure 5-26.. Predicted displacement vectors plotted with soil type at MBARI/Sandholdt Road Section A-A' as predicted by Model A.
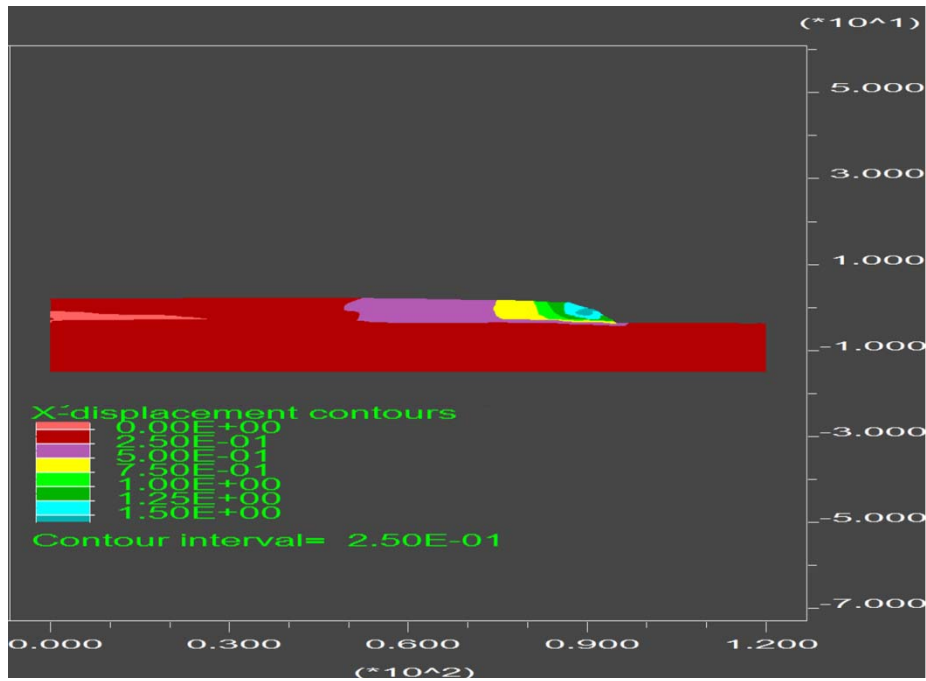
Figure 5-27. Predicted lateral displacements at MBARI/Sandholdt Road Section A-A' as predicted by Model B.
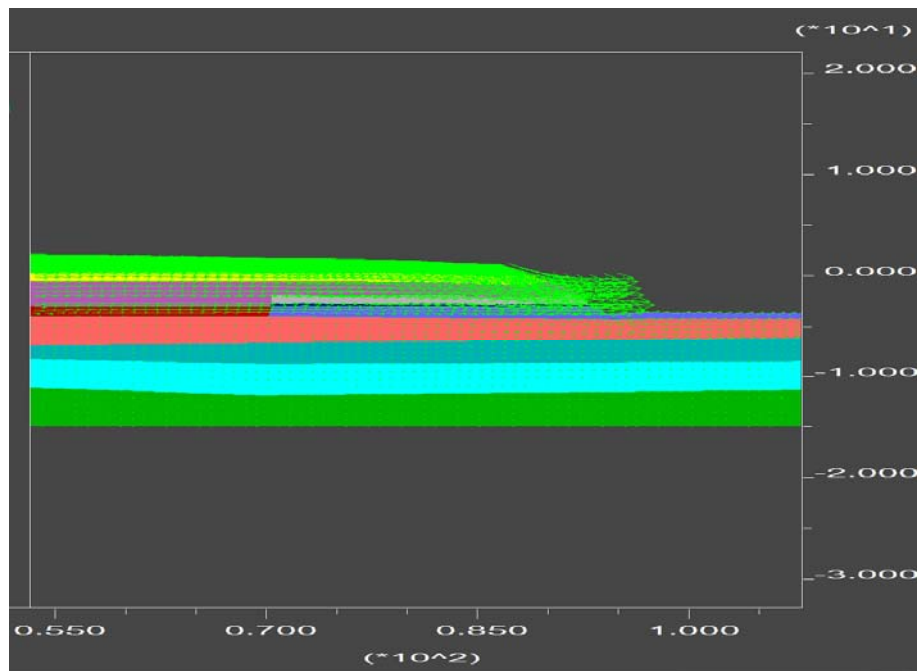

Figure 5-28. Predicted displacement vectors plotted with soil type at MBARI/Sandholdt Road Section A-A' as predicted by Model B.
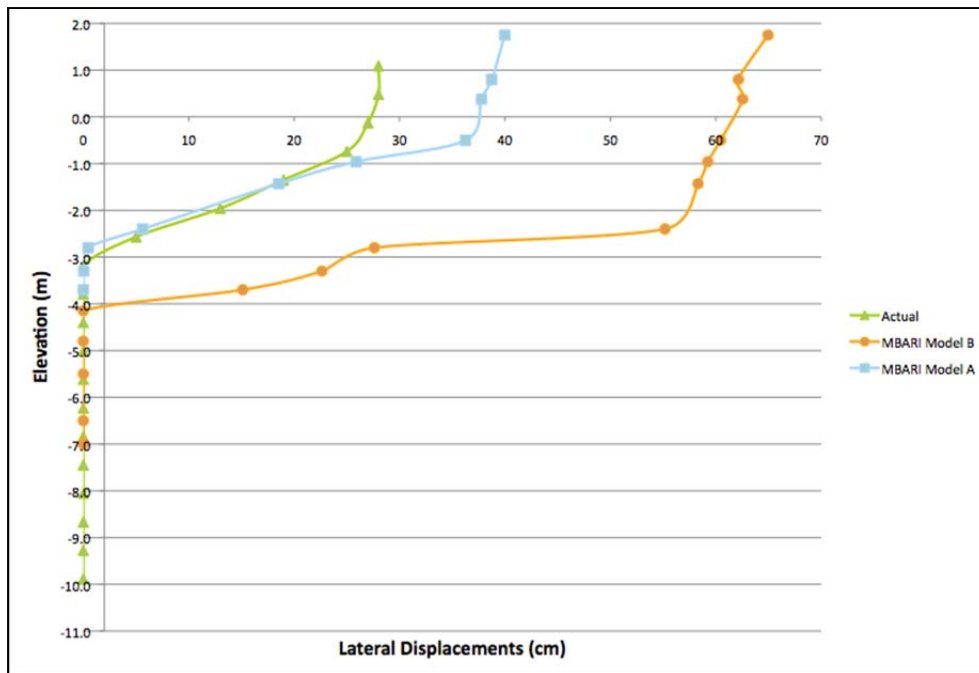
Figure 5-29. Measured and predicted lateral displacements at MBARI/Sandholdt Road. Deformations predicted by Models A and B as well as measured values are compared with depth.

### 5.5.2 Moss Landing Marine Laboratory (MLML) – Loma Prieta 1989

The Moss Landing Marine Laboratory (MLML) is located on the West side of Sandholdt road just south of the timber access bridge crossing the Old Salinas River. The location is shown on Figure 5-20. and is approximately 330 meters southwest of the MBARI/Sandholdt road case study discussed previously. The complex is shown on Figure 5-30 along with photographs of racking of one of the structures and sand boil ejecta from an area just south of the structures. The MLML facility consisted of three 1 to 2 story wood frame structures supported on spread footings constructed surrounding a center courtyard with appurtenant surface parking and a volleyball court to the south.
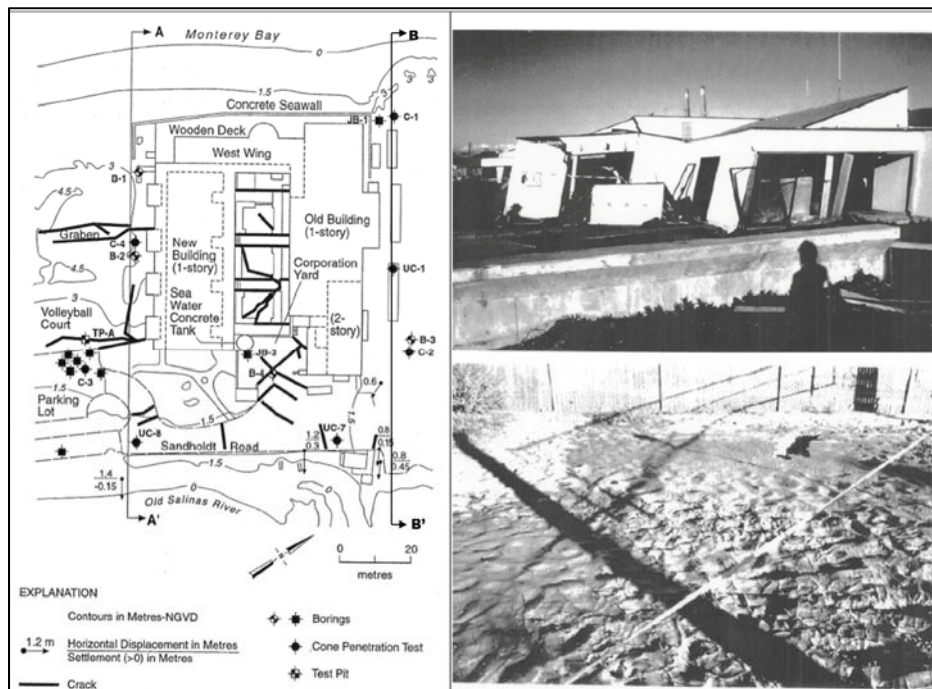


Figure 5-30. Lateral spreading damage at the Moss Landing Marine Laboratory. To the left is a map of observed cracking and deformations as well as subsurface exploratory points. Upper right shows damage to the MLML structure. Lower left photo shows sand boil ejecta at the volleyball court just south of the facility (Boulanger et al. 1995).

According to the UC Davis investigation by Boulanger et al. (1995), sand boils were observed to have ejecta shooting several feet into the air for approximately 45 minutes after ground shaking associated with the Loma Prieta earthquake had ceased. Liquefaction and lateral spreading at the site had torn the structure apart, though it did not collapse. Lateral and vertical deformations were estimated in a post-earthquake survey by Brian Kangas Foulk and summarized in Boulanger et al. (1995). A post-earthquake reconnaissance report was performed at the site by Woodward-Clyde Consultants (WCC) in 1990. Geologic cross sections were prepared as part of the Davis investigation and included subsurface data performed by WCC. Figure 5-31 shows the subsurface stratigraphy and a summary of geologic information for Section A-A', just south of the MLML facility. Similarly, Figure 5-32 details available subsurface information north of the facility.
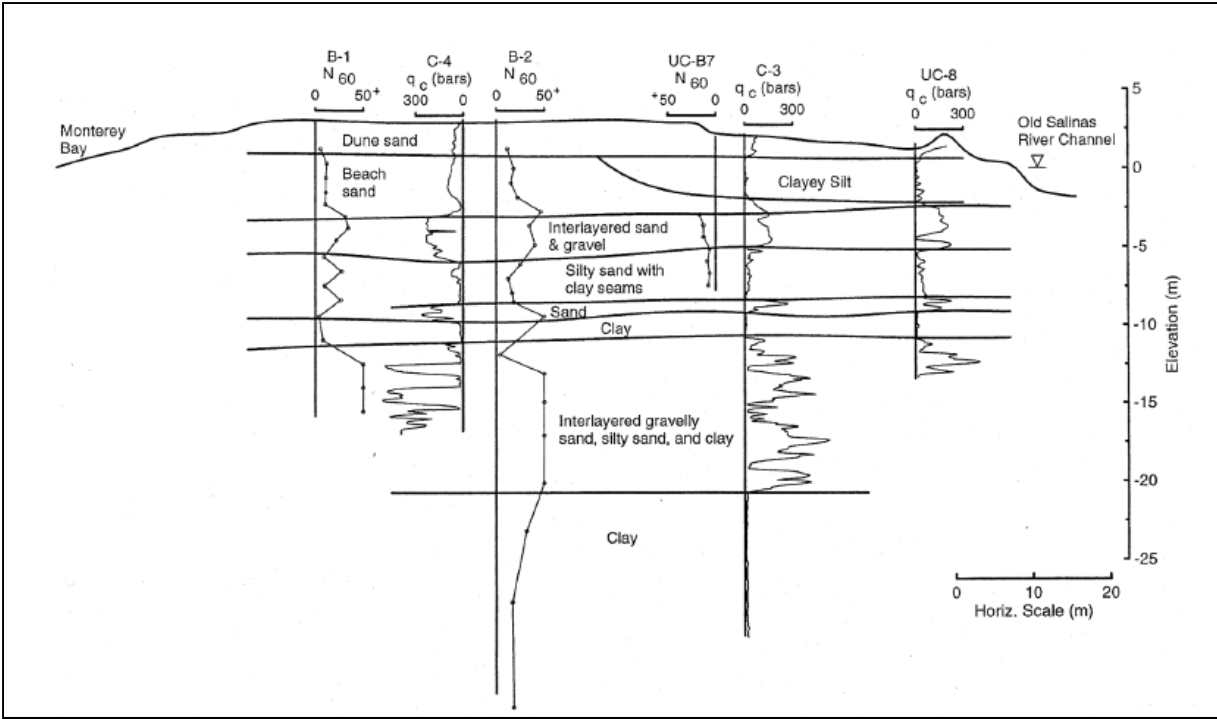
Figure 5-31. Geologic section south of MLML facility (Section A-A' of Figure 3.2.1)
(Boulanger et al. 1995).
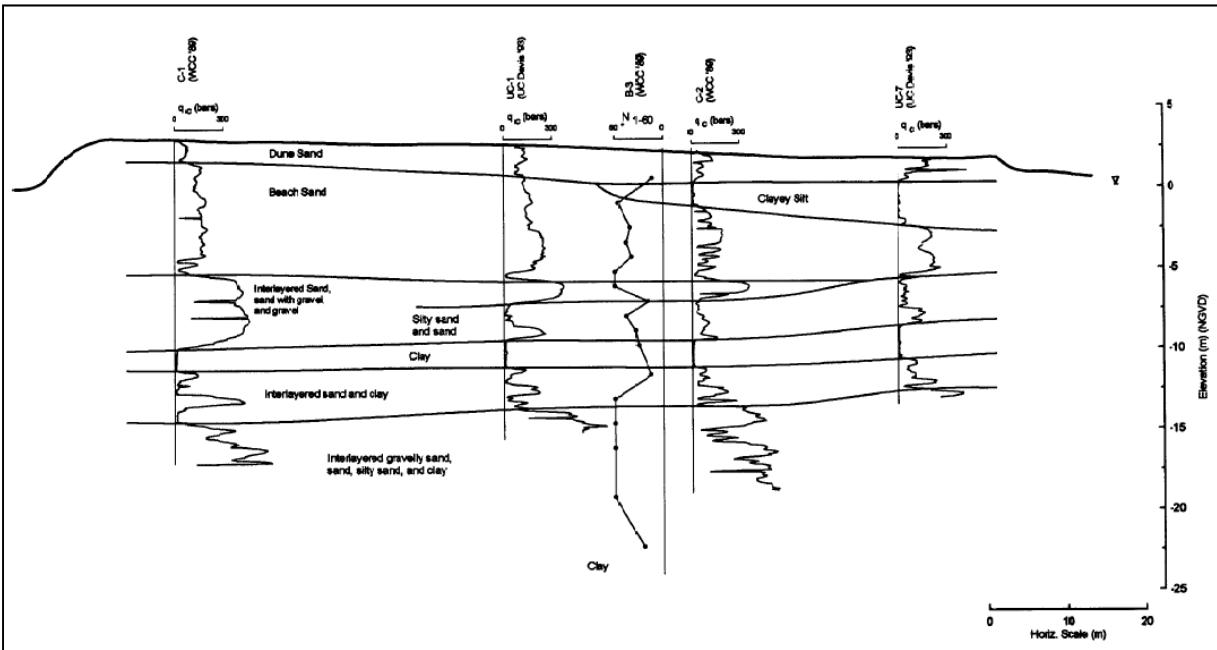


Figure 5-32. Geologic section north of MLML facility (Section B-B' of Figure 3.2.1)
(Boulanger et al. 1995).

Lateral spreading on the order of 0.75 m was estimated in the western direction, toward the Monterey Bay. Lateral spreading to the east toward the Old Salinas River was estimated

to be 0.45 m at the structure and 0.8 to 1.4 meters east of Sandholdt Road (Figure 5-30). Overall, Boulanger et al. (1995) estimates spreading of the Moss Landing spit at the MLML facility to be about 1.4 m on the north side of the structure and 2.1 m on the south side of the structure. Vertical settlements were estimated at 0.35 m on the west side of the structure and 0.3 m on the east side. Some areas of heave were also observed at the site and are detailed on Figure 5-30 (site plan).

As with the MBARI facility previously discussed in Section 3.1, the Salinas ground motion record (scaled to a PGA of 0.25 g) was used to simulate ground motions at Moss Landing during the Loma Prieta earthquake. Figure 5-33 and Figure 5-36 show the mesh and layers used to model sections A-A and B-B to the south and north of the facility, respectively. Figure 5-34 and Figure 5-35 show the horizontal and vertical displacement respectively as predicted at Section A-A'. Figure 5-37 and Figure 5-38 show contours of lateral and vertical displacement predicted for Section B-B', north of the MLML structure. A plan view summary showing contours of predicted lateral displacement extrapolated from Sections A-A' and B-B' is provided as Figure 5-39. Overall, lateral displacements were captured well as the calculated lateral spread displacements of the Moss Landing spit is approximately 2.25 m on the south side of the structure and 0.85 m on the north side of the structure. Calculated vertical displacements ranged from approximately 10 to 60 cm. Measured values of vertical displacements generally fall into this range.
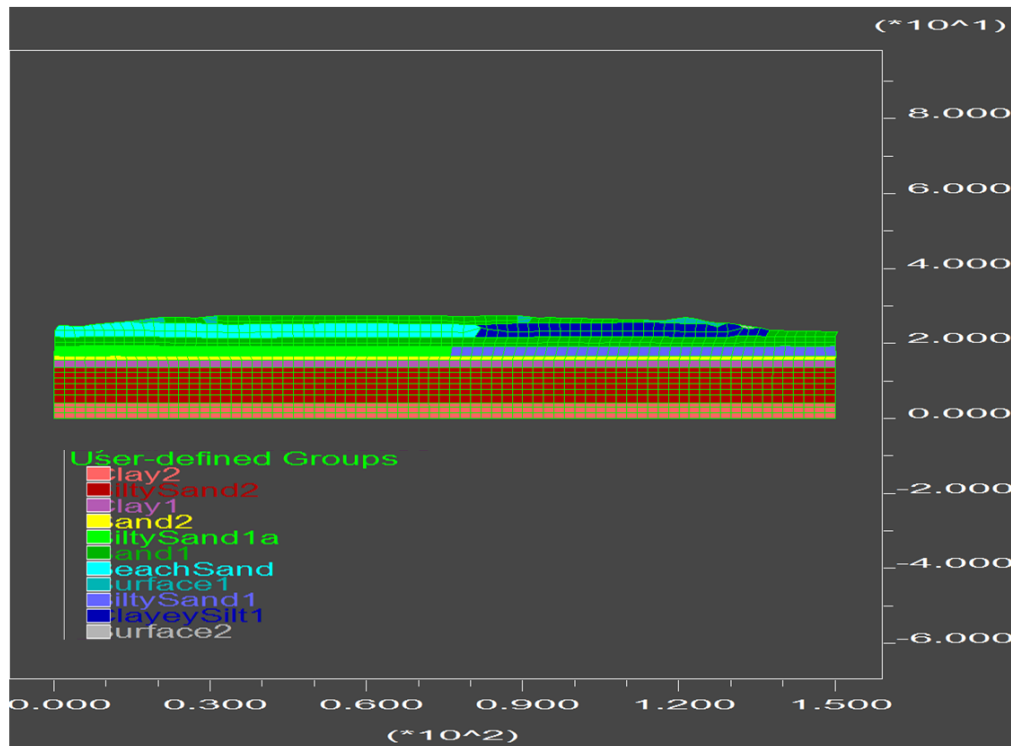


Figure 5-33. Mesh and soil types south of MLML facility (Section A-A' of Figure 5-30).
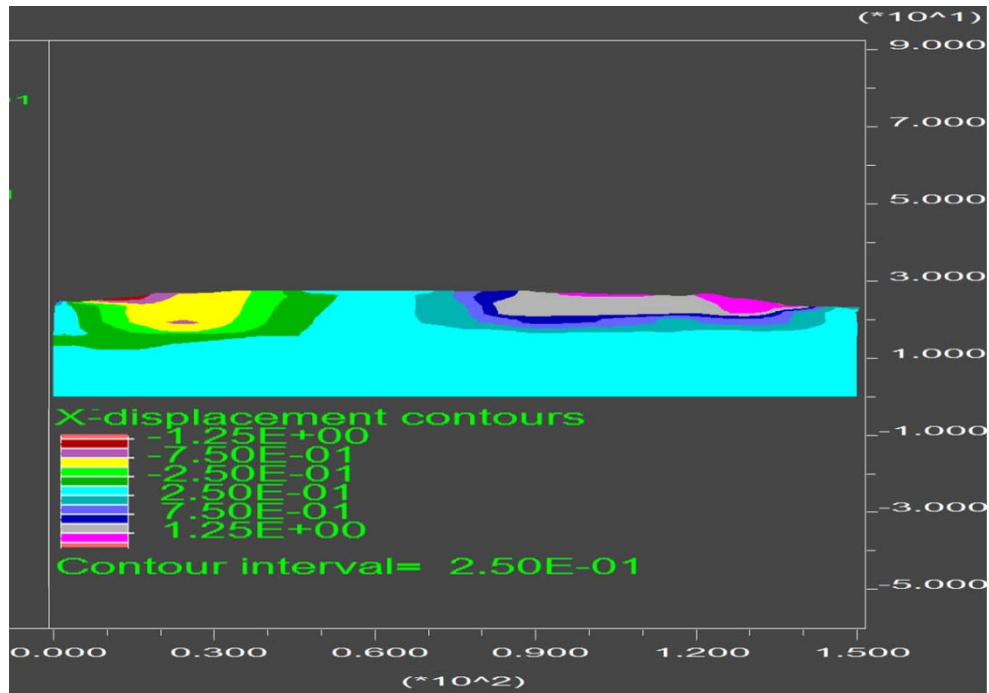
Figure 5-34. Predicted lateral displacements south of MLML facility (Section A-A' of Figure 5-30).
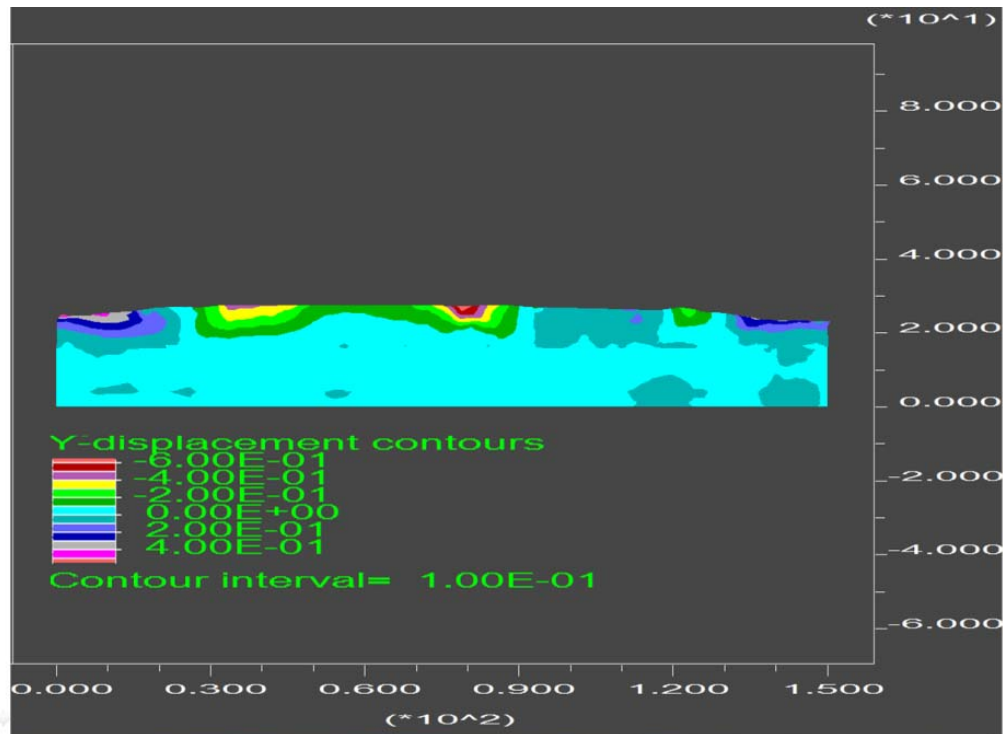


Figure 5-35. Predicted vertical displacements south of MLML facility (Section A-A' of Figure 5-30).
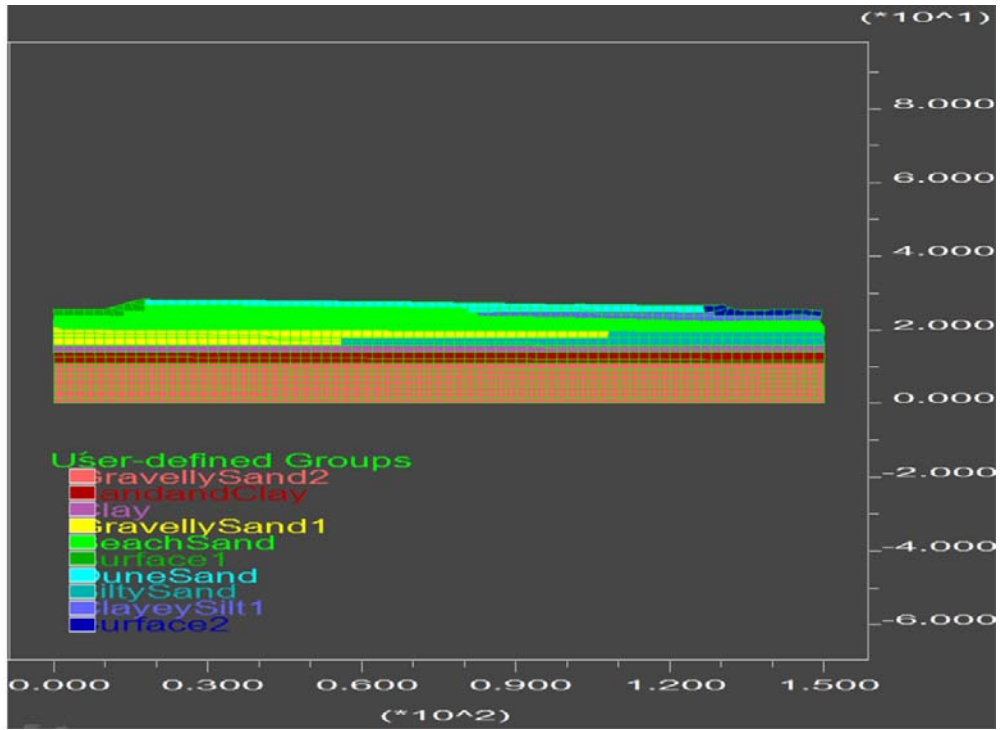
Figure 5-36. Mesh and soil types north of MLML facility (Section B-B' of Figure 5-30).
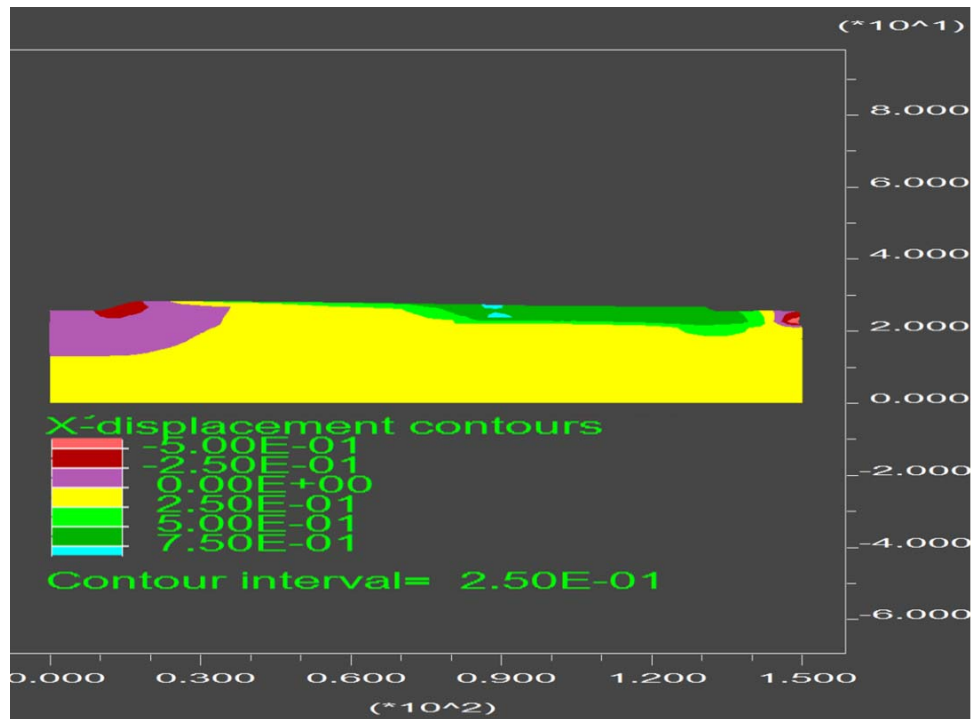


Figure 5-37. Predicted lateral displacements north of MLML facility (Section B-B' of Figure 5-30).
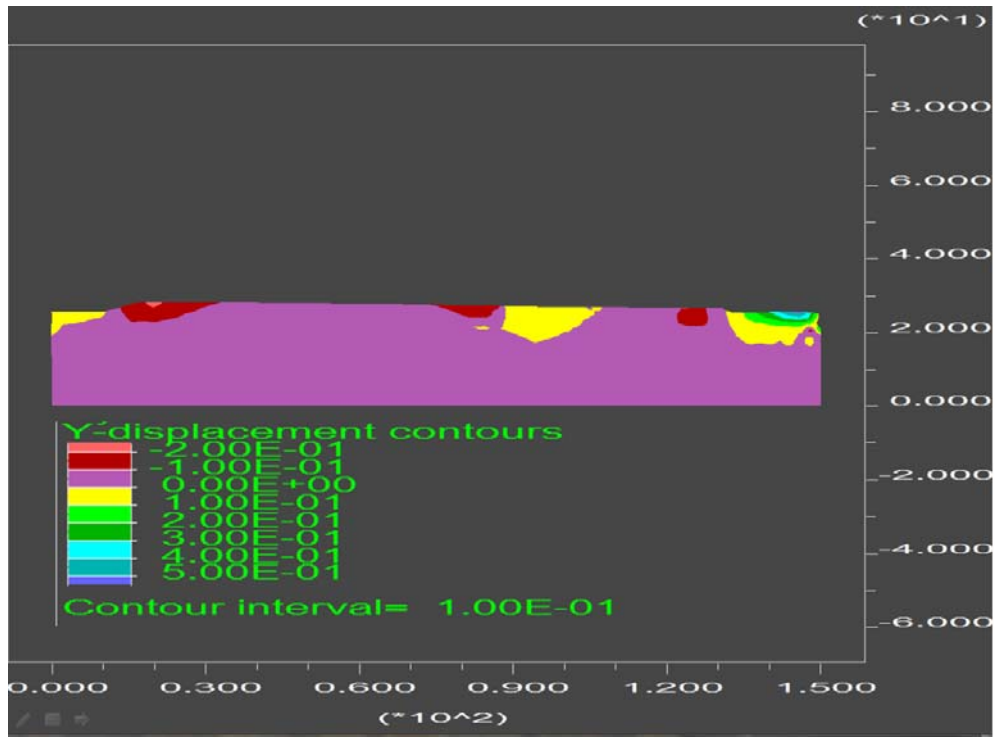
Figure 5-38. Predicted vertical displacements north of MLML facility (Section B-B' of Figure 5-30).
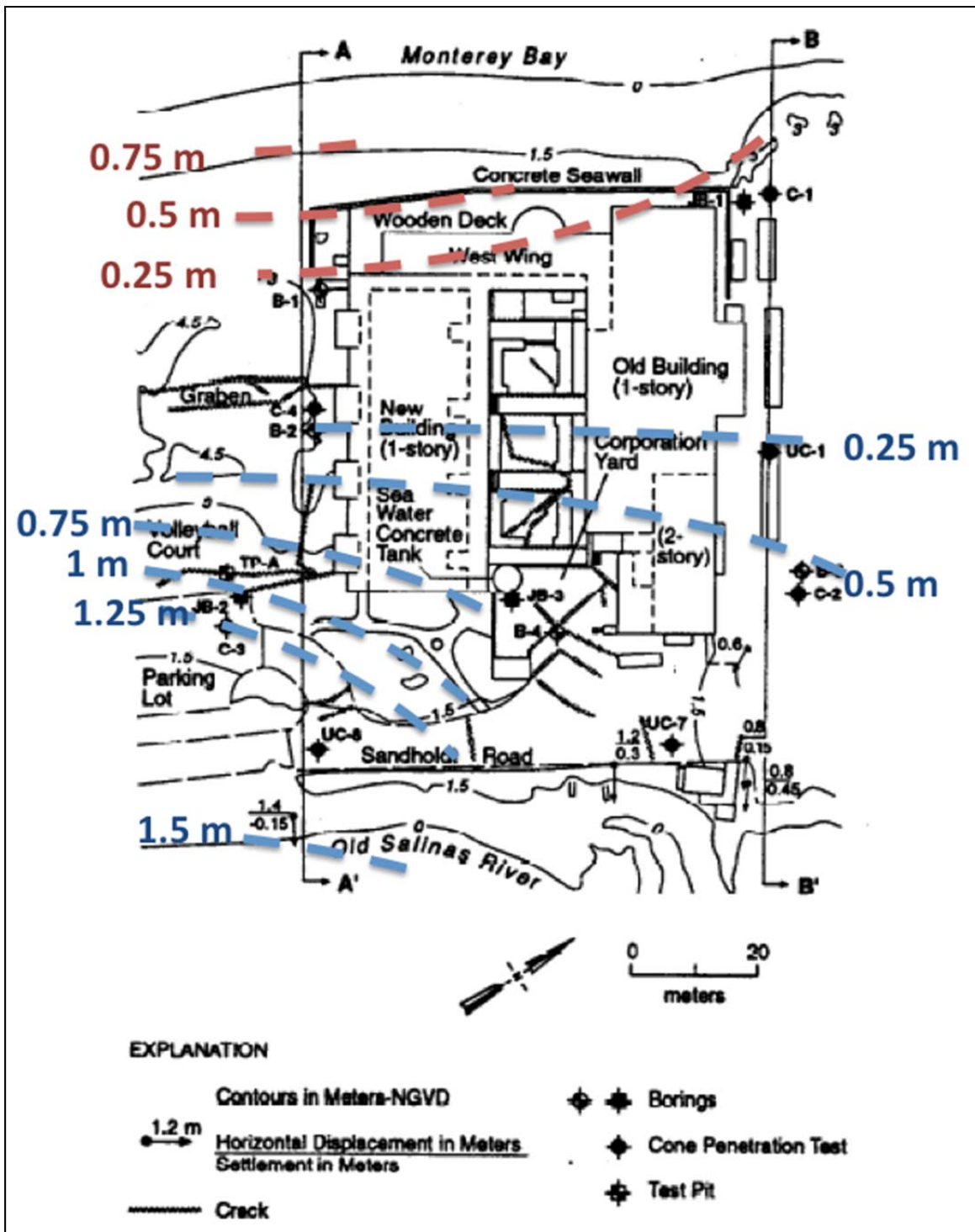
Figure 5-39.. Measured and predicted lateral deformations at the MLML Facility during the Loma Prieta Earthquake in 1989. Blue contours represent movement to the east toward the Old Salinas River. Red contours represent movement to the west toward the Monterey Bay. Prediction contours based on extrapolations from models performed at Sections A and B.

### 5.5.3   Juvenile Hall Facility – San Fernando 1971

The Los Angeles County Juvenile Hall site is located at the junction of Interstate 5 and the Foothill Freeway (210) east of the Van Norman Reservoir complex in the Sylmar region of Los Angeles, California. During the 1971 San Fernando earthquake (moment magnitude of 6.6 centered as shown on Figure 5-40), the Juvenile Hall facility experienced lateral deformations on the order of 2 meters. Displacement vectors were plotted by O'Rourke et al. (1992) and are included as Figure 5-41.  A map of cracking associated with the lateral spread by Fallgren and Smith (1973) is included as Figure 5-42. Subsurface exploratory data point locations are provided on Figure 3.3.4 (O'Rourke et al., 1992). Subsurface data were interpreted by Bennett (1989) and summarized on Figure 5-44 and Figure 5-45. A complete summary of the Juvenile Hall case study is available in Faris (2004). Faris (2004) performed a liquefaction analysis of the subsurface soils at the site and a portion of the analysis is included as Figure 5-46.

Four alluvium units, labeled A through D are shown in subsurface profiles on Figure 5-44 and Figure 5-45. Unit A consists of a 2-7 m layer of poorly sorted, loose to medium-dense silty sand located above the groundwater table. Underlying Unit A is Unit B, 2-5 m layer of very loose to loose, poorly sorted silty sand to silt. Unit C consists of medium-dense to dense, poorly sorted silty sand, while Unit D consists of stiff clayey silt. Liquefaction initiation analyses performed by Faris (2004) confirmed that the loose, saturated silty sand and sandy silt within Unit B was likely to have liquefied during the event. The precise locations of the geologic sections shown on Figure 5-44 and Figure 5-45 were not included in Faris (2004). The approximate location of the section was interpreted from the topographic map included as Figure 5-41 and the exploratory point locations shown on Figure 5-43.
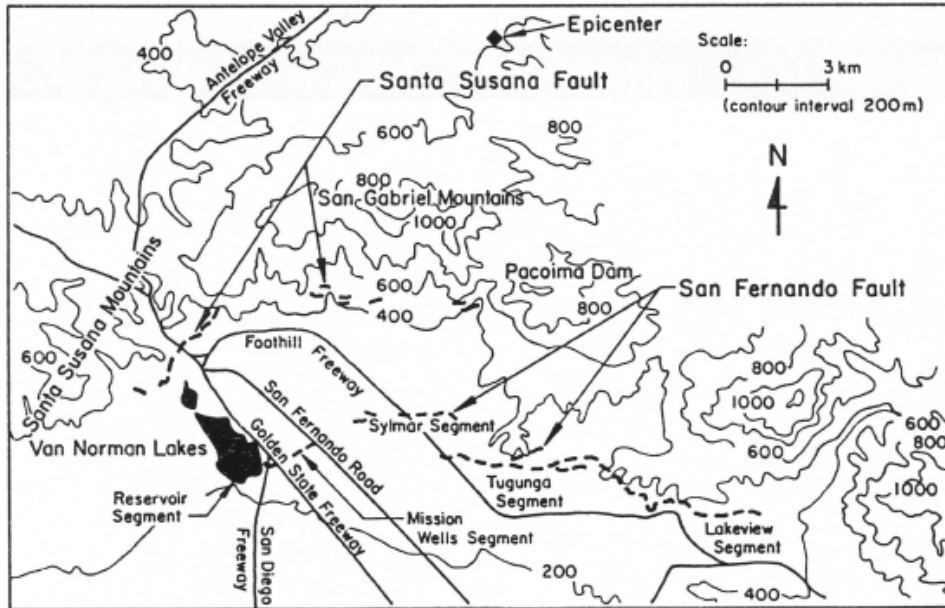
Figure 5-40. Epicenter and fault map showing Juvenile Hall site vicinity. The site is located east of the Van Norman Reservoir in the San Fernando Valley northeast of I-5 (modified from O'Rourke et al. 1992 ).
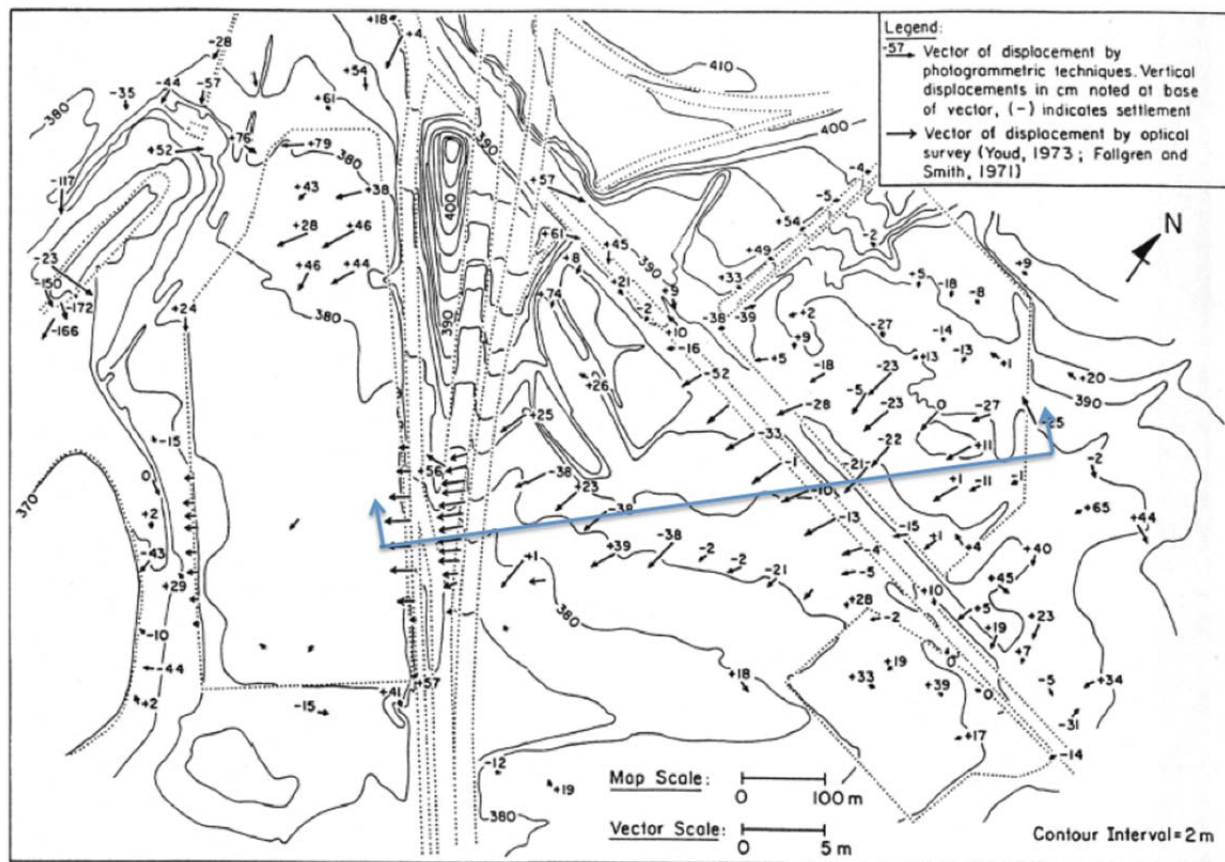


Figure 5-41. Estimated vectors of displacement at the Juvenile Hall facility during the San Fernando earthquake of 1971 (O'Rourke et al. 1992).
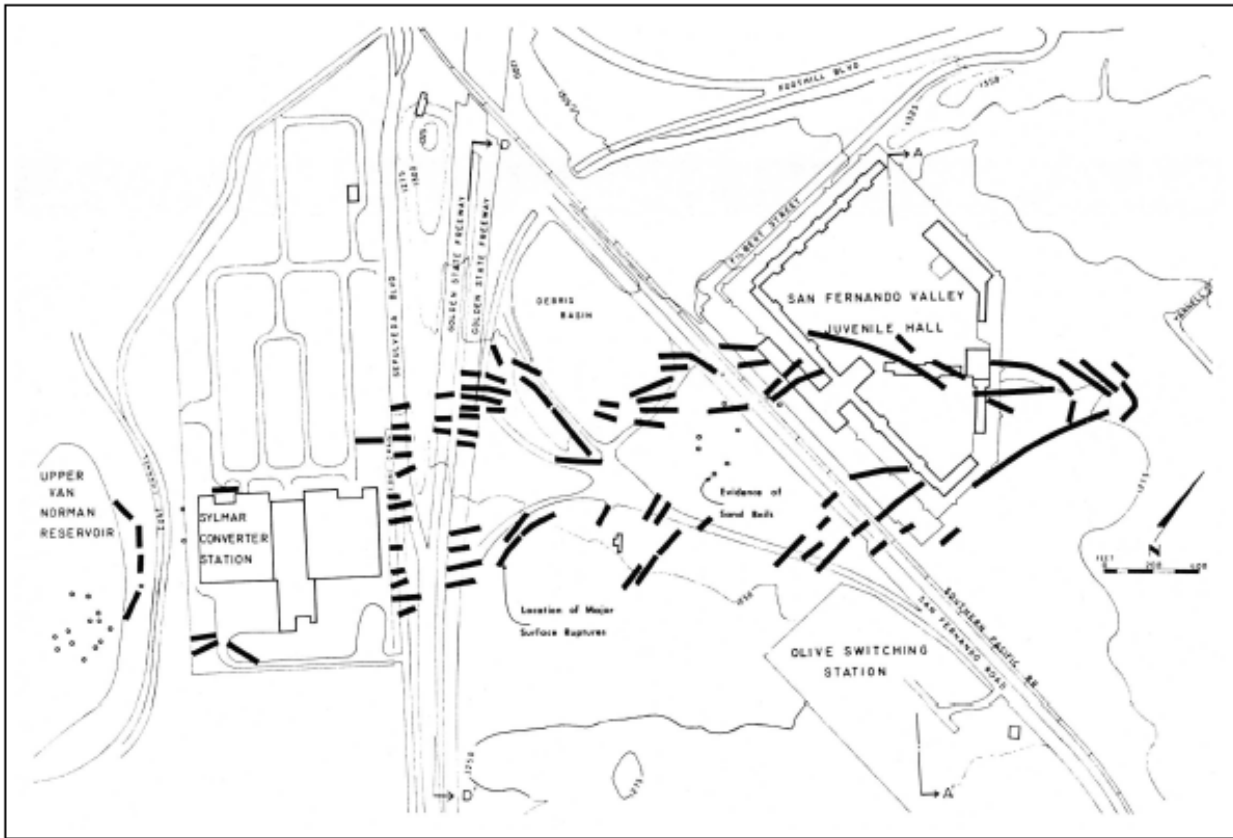
Figure 5-42. Locations of ground cracks at Juvenile Hall facility after 1971 San Fernando earthquake (Fallgren and Smith, 1973).
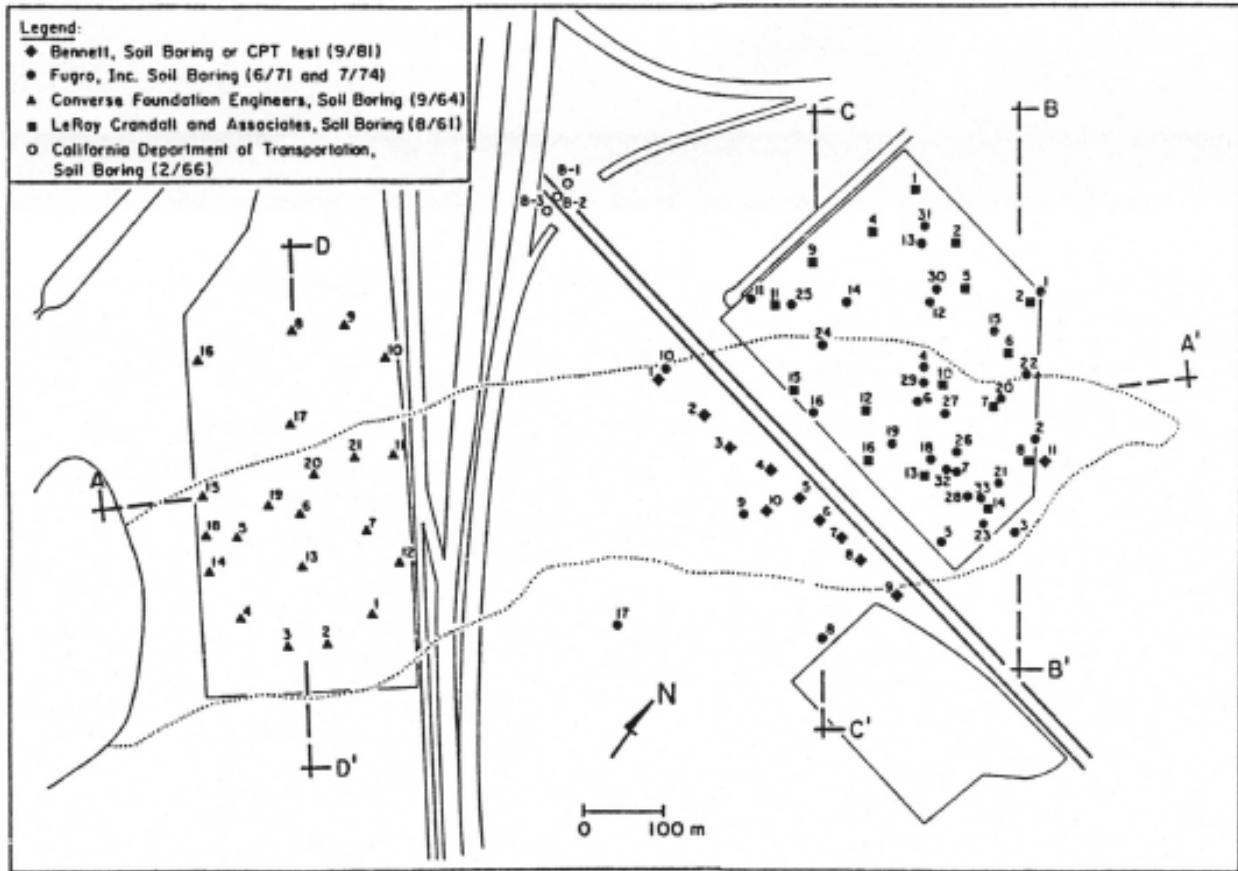
Figure 5-43. Location of subsurface exploratory points at the Juvenile Hall Facility
(O'Rourke et al., 1992 ).
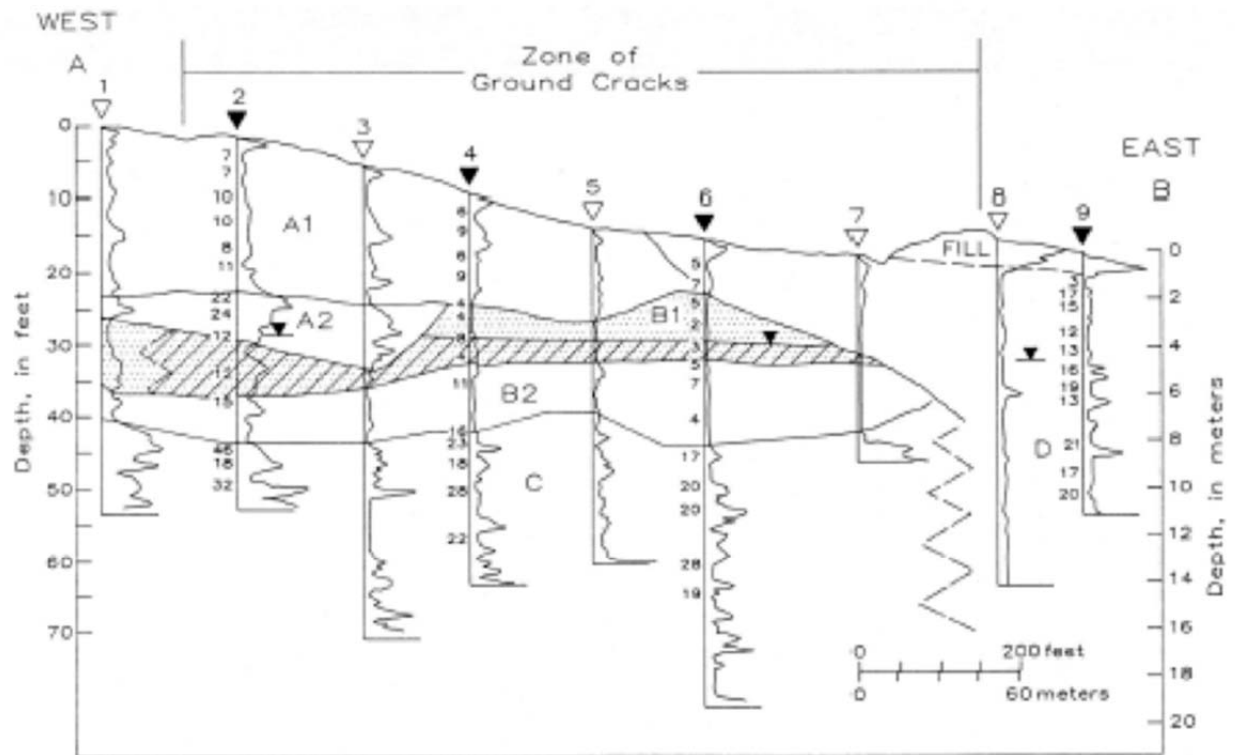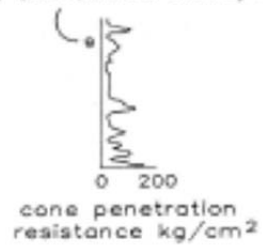
Figure 5-44. Subsurface profile at Juvenile Hall (Bennett, 1989).
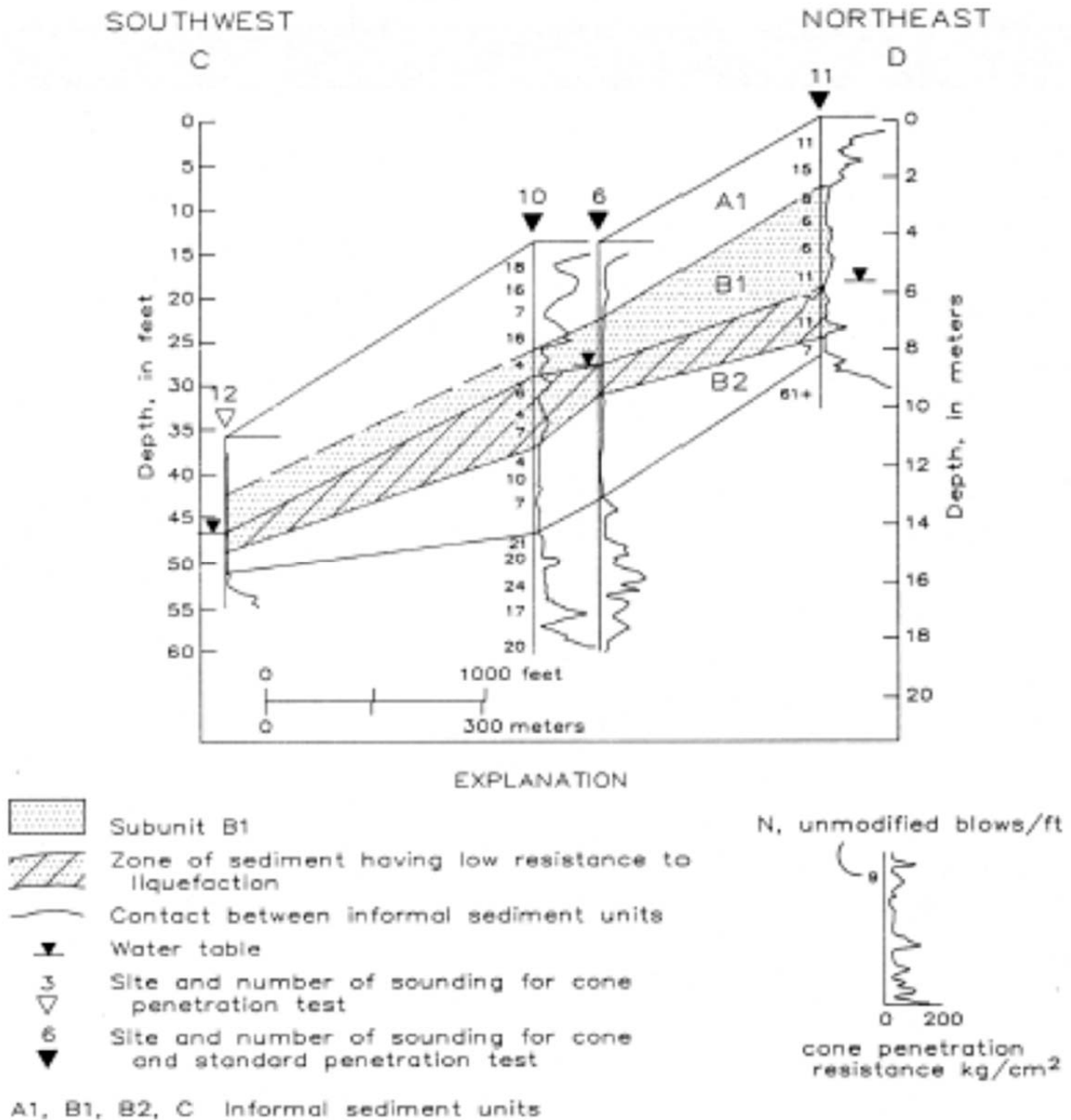
Figure 5-45.. Subsurface profile at Juvenile Hall (Bennett, 1989).
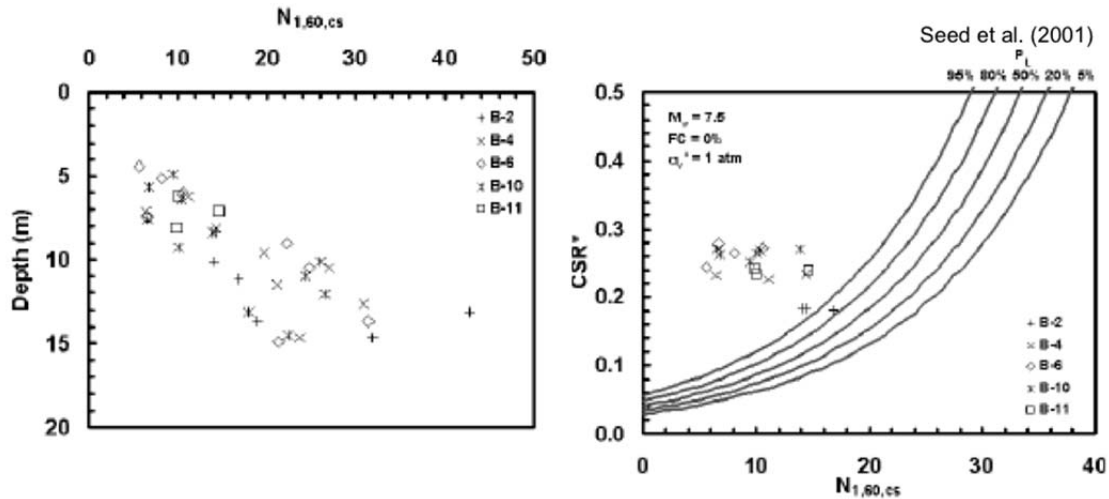
Figure 5-46. Liquefaction analysis for Juvenile Hall by Faris (2004).

No ground motion instruments were present at the site at the time of the San Fernando earthquake. Cetin (2000) estimated that the peak ground acceleration at the site was approximately 0.45 g. A limited number of ground motion recordings are available in this area for this earthquake. Ground motion records at the Upper Pacoima Dam are available for both the 1971 San Fernando earthquake and the 1994 Northridge earthquake with PGAs of 1.23 g and 1.53 g, respectively. The instrument at Lower Pacoima Dam recorded only the 1994 Northridge earthquake with a PGA of 0.45 g. Using this information, a PGA of 0.36 g was estimated for Lower Pacoima Dam during the 1971 San Fernando earthquake, and it was used as the rock input motion in SHAKE to generate a ground motion for the lower Juvenile hall site. The shear wave velocity profile of a nearby site, Olive View Community Hospital, was studied previously by Chang (1996). An idealized profile for Olive View hospital is shown on Figure 5-47. A within soil motion with a PGA of 0.45 g was the output of this analysis. Based on the agreement with estimates by Cetin (2000), this motion was used in our study.
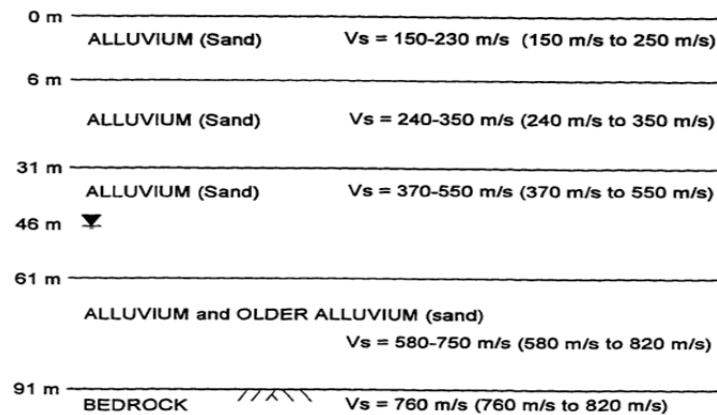


Figure 5-47. Idealized soil profile for Olive View/Sylmar County Hospital (Chang, 1996).

365

In general, the model was able to capture the magnitude of the liquefaction-induced lateral displacement. The contours of lateral displacement are provided on Figure 5-48. Measured lateral displacements at the site range between approximately 0.5 and 2 m (Figure 5-41). The model predicted lateral displacements near the lower part of the site (nearest the I-5 freeway) to be on the order of 1.5 m. Soils near the top of the movement area were calculated to displace 0.5 m to 2 m relative to the competent base materials. Measured values are consistent with calculated values as shown on Figure 5-49. Figure 5-49 shows the values of lateral displacements plotted together on an interpreted geologic cross section by Bennett (1989). Where there are large areas lacking in initial shear stress, the model calculates smaller displacements, whereas measured displacements do not show this trend. This indicates the sensitivity of the UBCSAND model to small amounts of initial static shear stress and the need for slightly increased values of m_hfac1 and 2 under initial shear. Judgment is required in this regard.

Measured vertical displacements as shown on Figure 5-31 were variable across the failure area and typically ranged from 2 to 20 cm (sometimes varying this much in adjacent measurements) of settlement with localized pockets settling as much as 38 cm along the modeled section. Calculated values were similarly erratic with typical values of settlement on the order of 5 cm and values of up to 35 cm predicted near the top of slope (the areas of largest horizontal movement).
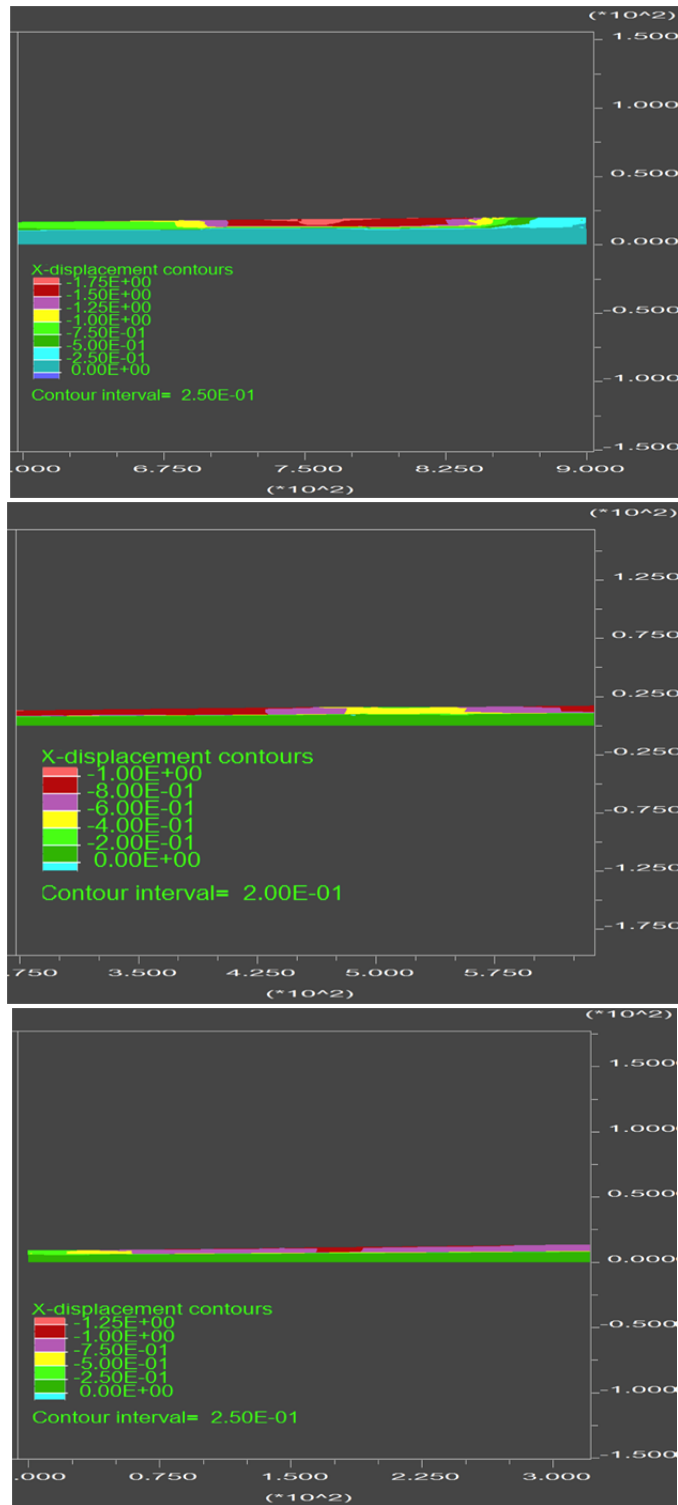
Figure 5-48. Contours of predicted lateral deformation. The deformation was on the order of 900 m in length, while liquefiable soils were located approximately 6 m below the surface. To better view the predicted deformations, the site was divided into the toe segment of 0 to 300 m (bottom), the central section of 300 to 600 m (center) and the top segment of 600 to 900 m (top).

367
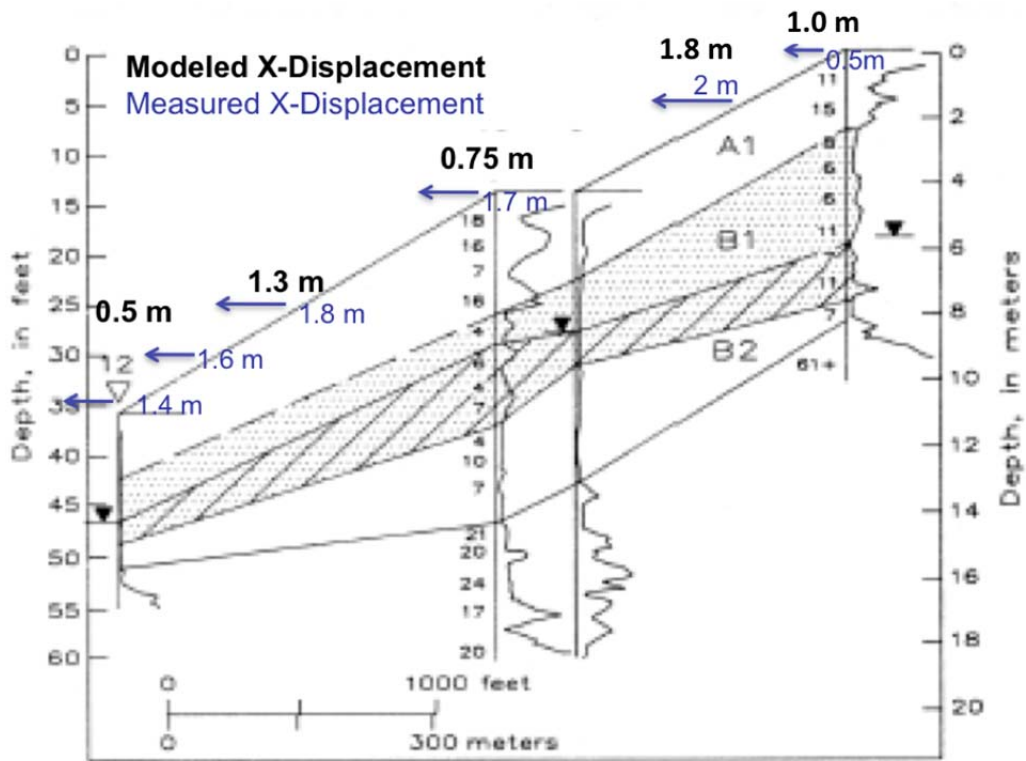
Figure 5-49. Measured and predicted lateral deformations at Juvenile Hall following the San Fernando earthquake of 1971 (modified from Bennett,1989).

# CHAPTER 6

## Sensitivity Study Using Calibrated UBCSAND Model

6.1 INTRODUCTION

After the back-analyses of the aforementioned case histories were performed, forward modeling of a simplified embankment section allowed for the use of the calibrated FLAC/UBCSAND model in calculating liquefaction-induced deformations under seismic loading in a limited lateral spread condition. The simplified baseline model is shown in Figure 6-1.
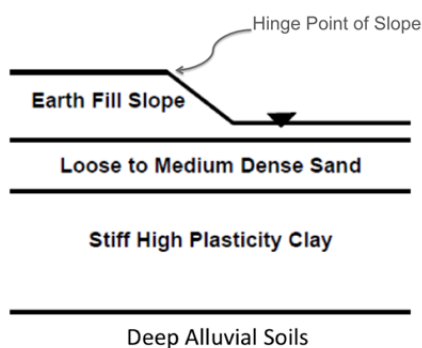


Figure 6-1. Simplified Embankment Model.

The intent is to analyze relatively simple geometries wherein key parameters, such as the thickness of the liquefiable layer and its relative density, can be systematically varied to develop useful insights. The results of the analyses will show trends in the response of liquefaction-induced lateral spreading ground. These trends were generally explored using two ground motions: 1) the 1992 Landers Joshua Tree motion was selected to represent a backward-directivity motion, and 2) the 1994 Northridge Sylmar Converter Station motion was selected to represent a forward-directivity near-fault motion. A series of additional ground motions were selected to evaluate the sensitivity of the results of a single model to a variety of motions to explore the effects of ground motion.

6.2 SENSITIVITY OF RESULTS TO VARIATIONS IN $(N_1)_{60}$

A simplified model was created in a series of configurations, varying the thickness of the liquefiable layer as well as the embankment height (discussed in subsequent sections). To explore the effects of variations in the liquefiable sand's relative density, the corrected blow count (i.e., $(N_1)_{60}$ value) was varied while embankment height and thickness of liquefiable layer were held constant. An embankment height of 9 m over a liquefiable layer thickness of 8 m was selected for the baseline model for this phase of the study. Figure 6-2 shows predicted displacement values at a distance of approximately 2 m behind the hinge point of the slope with $(N_1)_{60}$ values ranging from 8 to 25. The hinge point of a slope is defined here as the top of

slope, or the location of a dramatic change in slope near the top of the embankment (Figure 6-1). The backward-directivity motion shows significantly less lateral displacement for this case, especially at a blow count of 8. Figure 6-3 shows the variation in calculated lateral displacement at this point for two values of $(N_1)_{60}$ for the cases wherein the liquefiable soil is a clean sand or a low plasticity silt. For this model, the variation in lateral displacement is modest.



**Predicted Lateral Displacement vs. Corrected Blowcount**
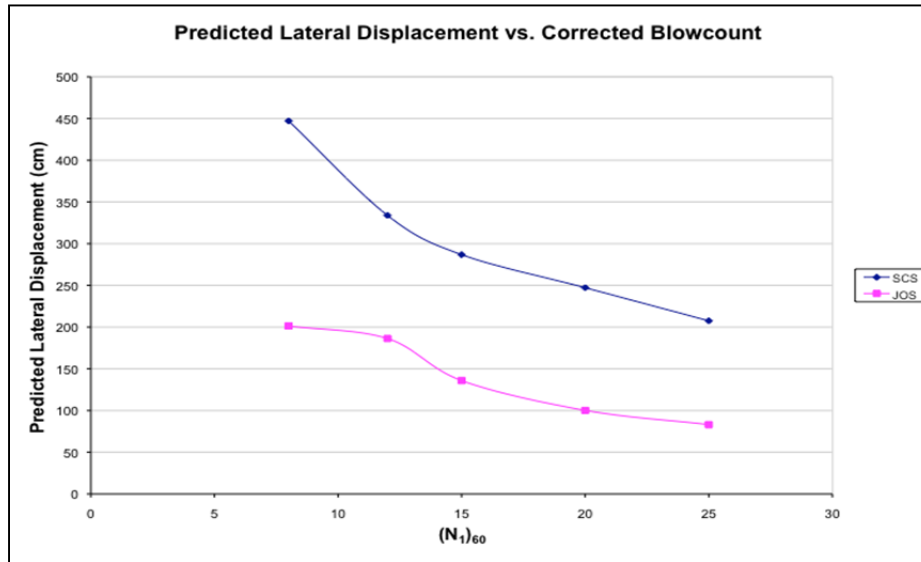
Figure 6-2. Comparisons of predicted response of 'clean sand' over similar blow count range but loaded with different ground motions. Data points marked 'SCS' were calculated using the 1994 Northridge Sylmar Converter Station motion (blue) and those labeled 'JOS' were calculated using the 1992 Landers Joshua Tree motion (pink).
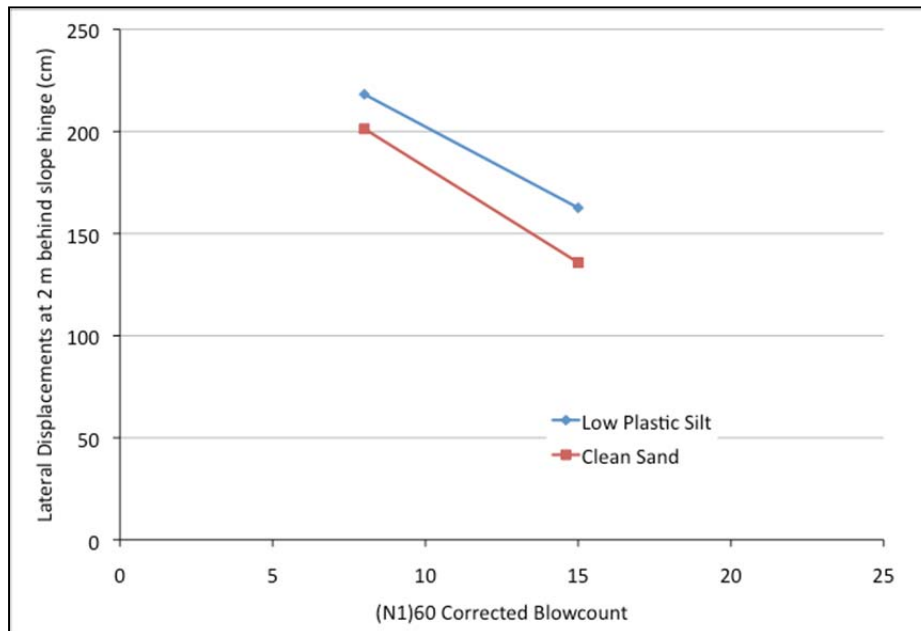


Figure 6-3. Predicted Lateral Displacement of 'low plasticity silt' and 'clean sand' as a function of blow count. Data was calculated using the 1992 Landers Joshua Tree motion.

## 6.3 SENSITIVITY OF RESULTS TO VARIATIONS IN MODEL GEOMETRY

The configuration of the simplified soil model was varied to explore the effects of different embankment heights and thicknesses of the underlying liquefiable layer. Embankment heights of 6, 9, and 12 meters were modeled overlying loose to medium dense sands of 3, 8, and 12 meters in thickness. The lateral and vertical displacements were plotted against the distance from the slope hinge point. Figure 6-4 and Figure 6-5 show the range in lateral and vertical displacement data resulting from the variation in geometry using the 1992 Landers Joshua Tree motion and the 1994 Northridge Sylmar Converter Station Motion, respectively. N8 indicates a corrected blow count of 8, E6 indicates an embankment height of 6, T3 indicates a loose to medium dense sand layer of 3 m in thickness, and 'j' or 's' at the end indicates the ground motion used (i.e., 'j' stands for 1992 Landers Joshua Tree motion while 's' stands for 1994 Northridge Sylmar Converter Station motion). The geometry was modeled assuming an $(N_1)_{60}$ blow count value of either 8 or 15 for the loose to medium dense sand.
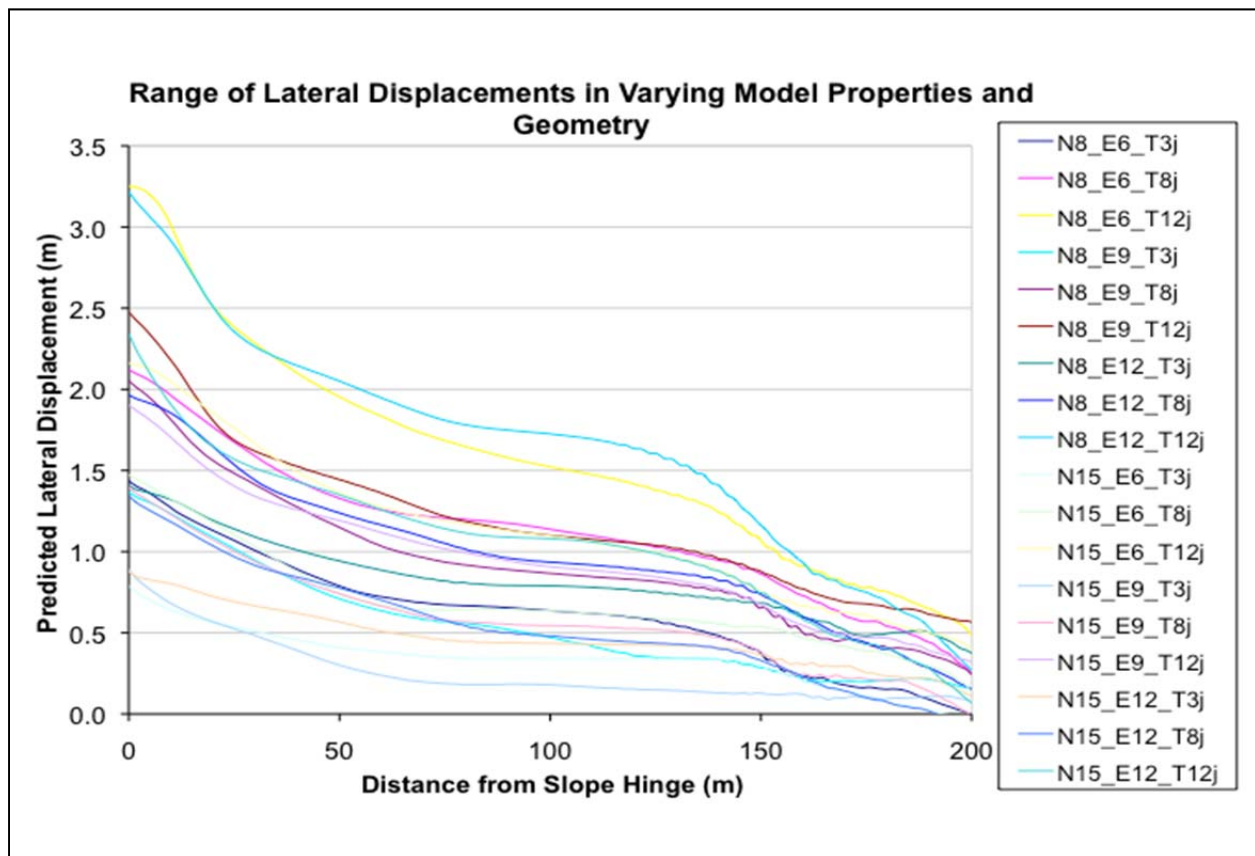


Figure 6-4. Range in liquefaction-induced lateral displacement with distance from the slope hinge point for the 1992 Landers Joshua Tree ground motion.

371
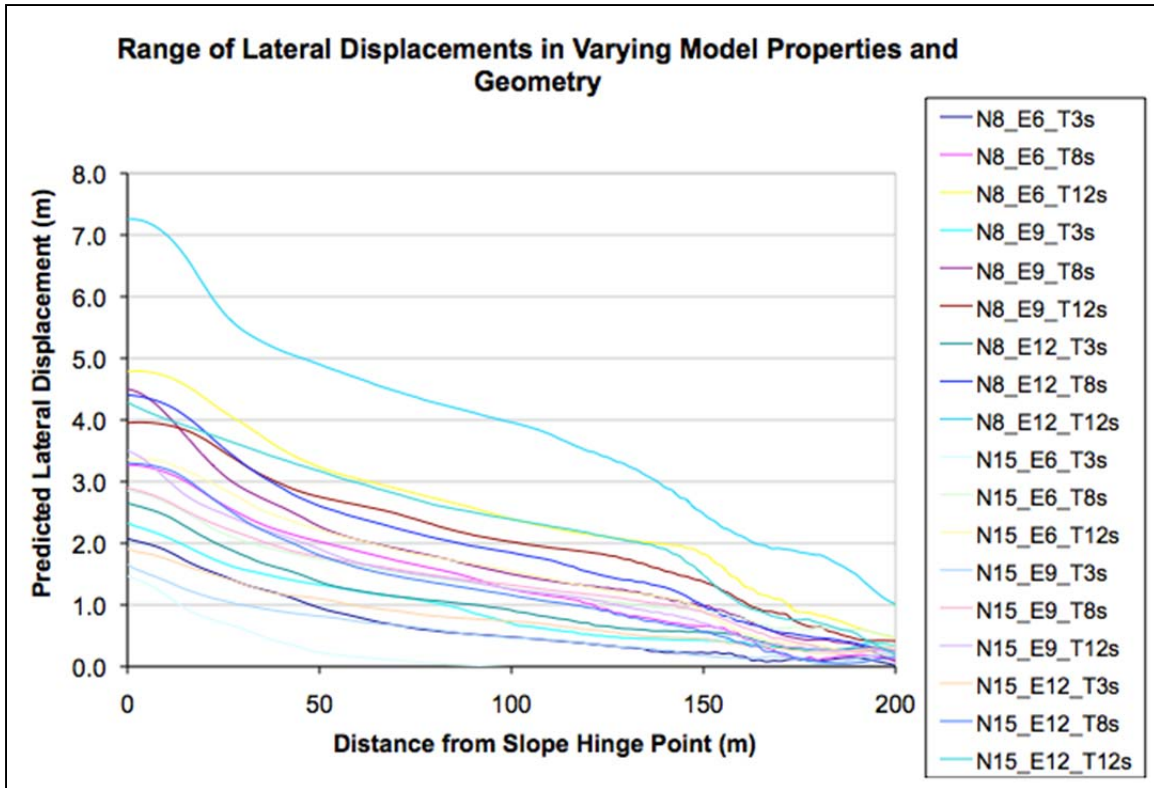
Figure 6-5. Range in liquefaction-induced lateral displacement with distance from the slope hinge point for the 1994 Northridge Sylmar Converter Station ground motion.

For the looser sandy foundation layers, the entire embankment slid as a block on the liquefied sand in several of the simulations as shown in Figure 6-6. The loose to medium dense sand layers were densified near the edges (5 m from the edge on the downslope side of the model and 15 m on the upslope side) to minimize boundary modeling errors in the program FLAC. These zones prevented the model from deforming excessively at the edge of the 300 meter long model. The simplified model is limited in that actual soils typically have a higher degree of heterogeneity in layer geometry, density, fines content, and other factors. The absence of heterogeneity built into the model may result in an unrealistic lateral extent of spreading.
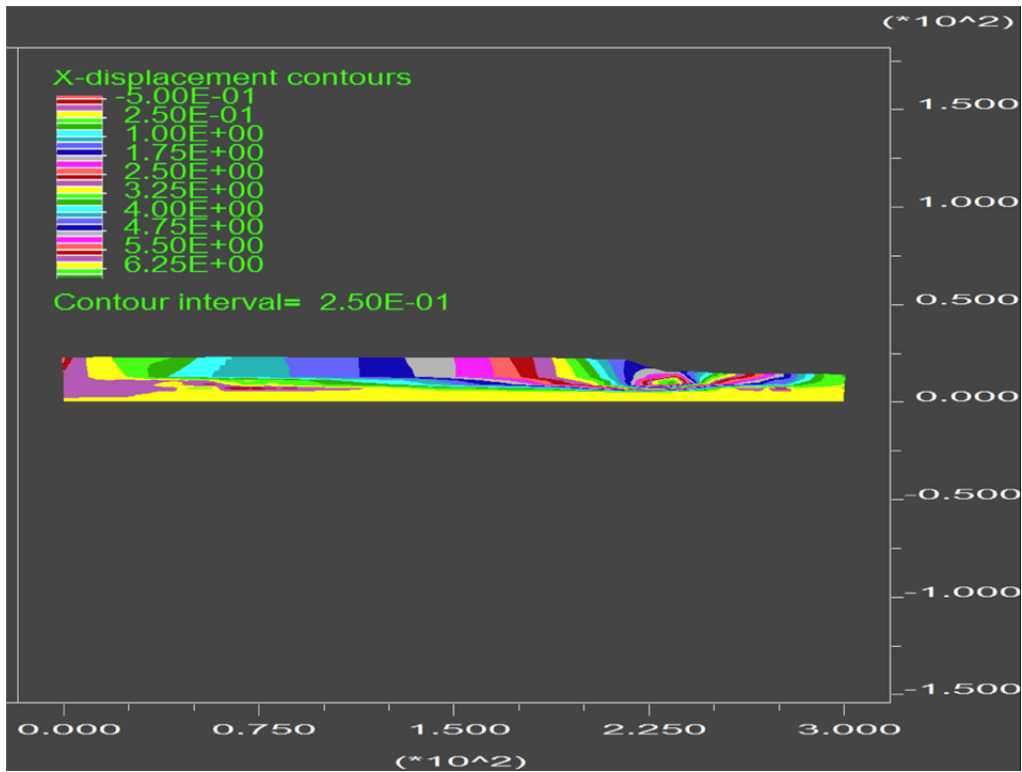
Figure 6-6. Example of predicted embankment deformation extending over 200 meters from slope hinge point. Model used in this example is a 9 foot embankment height and an 8 foot thick layer of sand with corrected $(N_1)_{60}$ blow count of 8 for the Sylmar Converter Station ground motion.

### 6.3.1 Layer Thickness

Layer thickness was found to have a significant impact on deformations. Figure 6-7 through Figure 6-12 show comparisons of models with the same embankment height and density of loose to medium dense sand, but with different thicknesses of liquefiable sand. The effects of increasing the layer thickness of the liquefiable soils can be significant. For example, increasing layer thickness while decreasing blow count can increase deformations to over 7 m as shown on Figure 6-7.

373
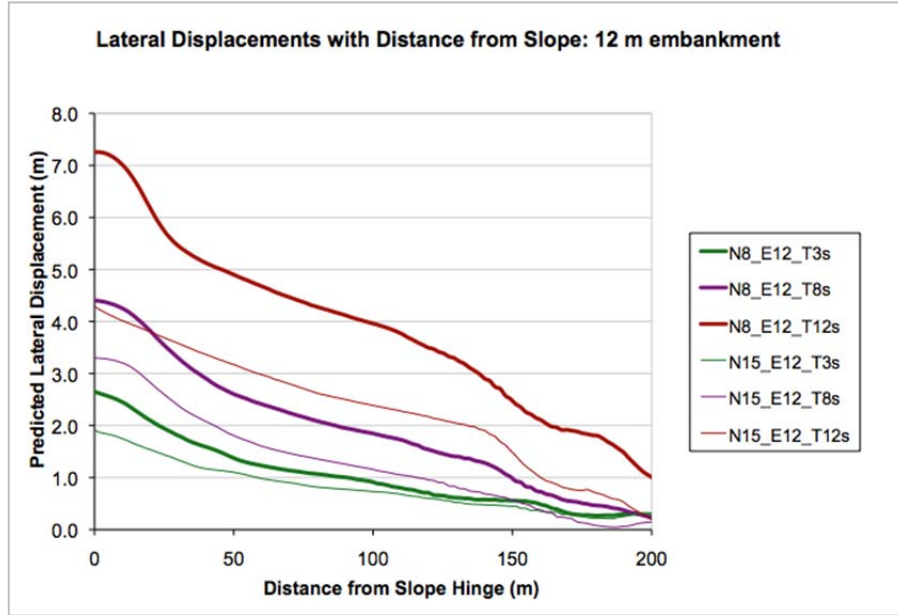
Figure 6-7. Calculated lateral displacements with distance from a slope hinge point for an embankment 12 m high founded on a sand layer of variable thickness and with $(N_1)_{60}$ blow count value of 8 and 15. (Ground Motion: 1994 Northridge Sylmar Converter Station).
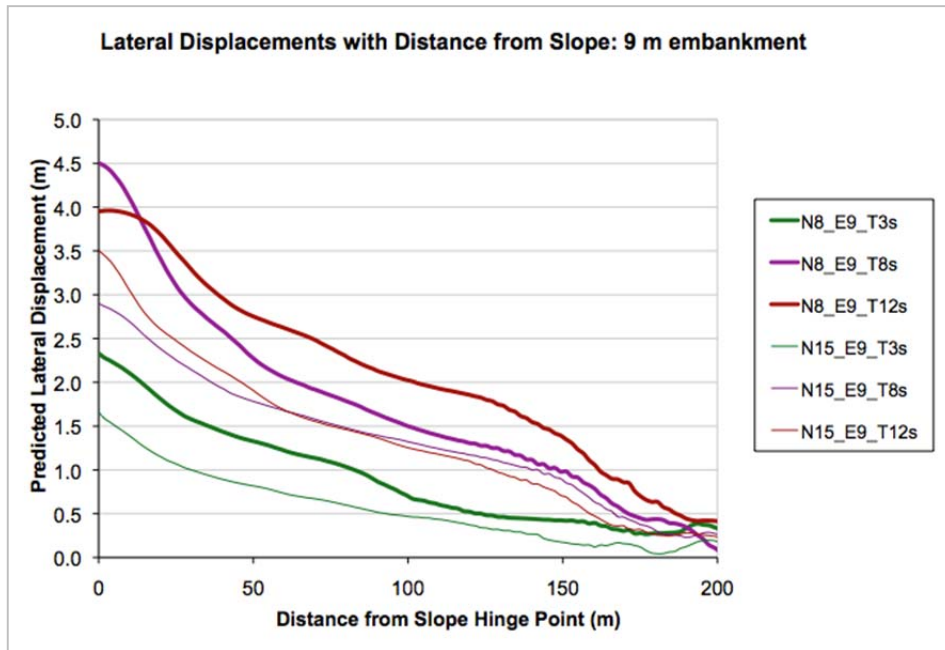


Figure 6-8. Calculated lateral displacements with distance from a slope hinge point for an embankment 9 m high founded on a sand layer of variable thickness and with $(N_1)_{60}$ blow count value of 8 and 15. (Ground Motion: 1994 Northridge Sylmar Converter Station).

374
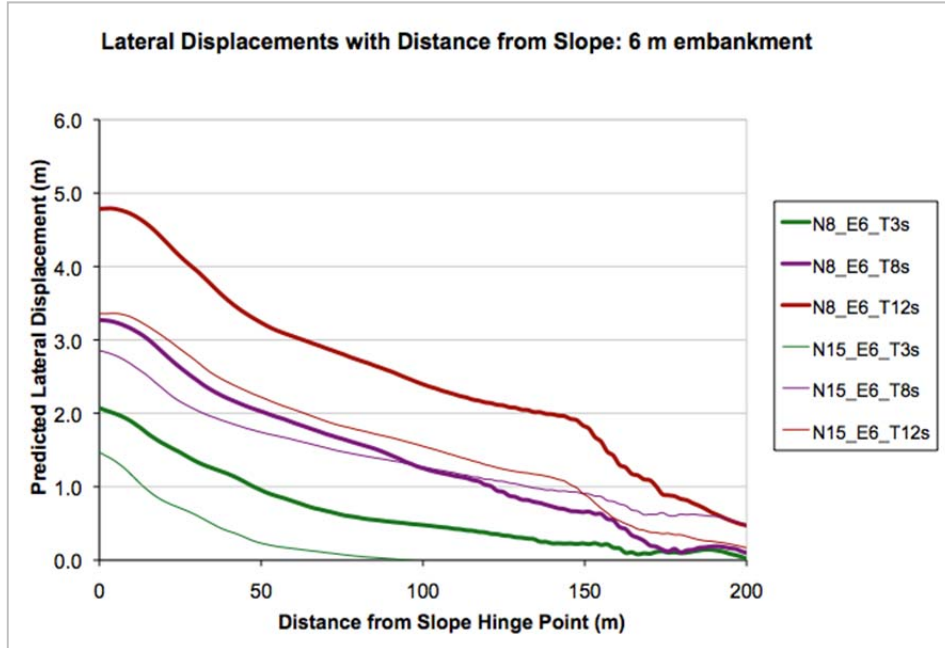
Figure 6-9. Calculated lateral displacements with distance from a slope hinge point for an embankment 6 m high founded on a sand layer of variable thickness and with $(N_1)_{60}$ blow count value of 8 and 15. (Ground Motion: 1994 Northridge Sylmar Converter Station).
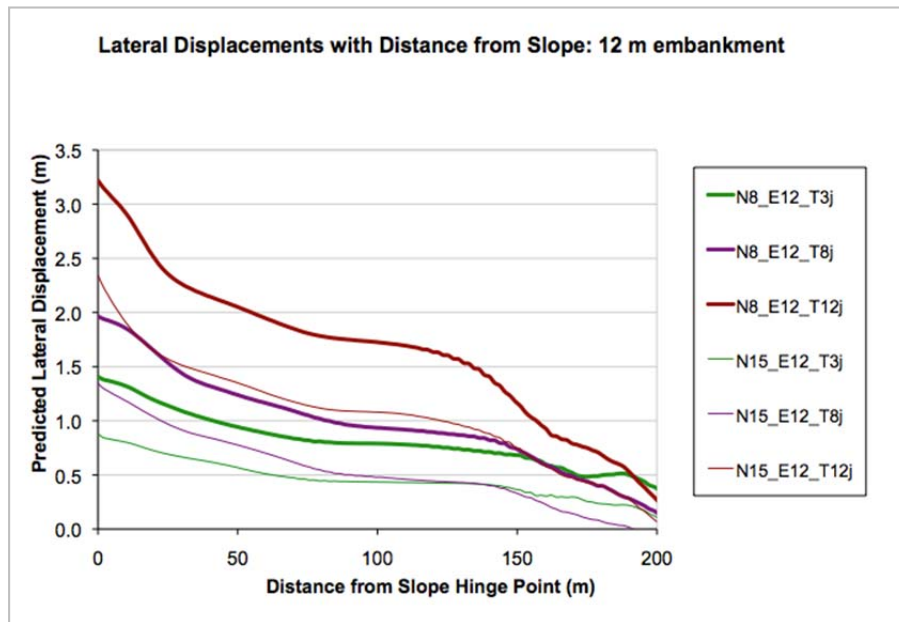


Figure 6-10. Calculated lateral displacements with distance from a slope hinge point for an embankment 12 m high founded on a sand layer of variable thickness and with $(N_1)_{60}$ blow count value of 8 and 15. (Ground Motion: 1992 Landers Joshua Tree).
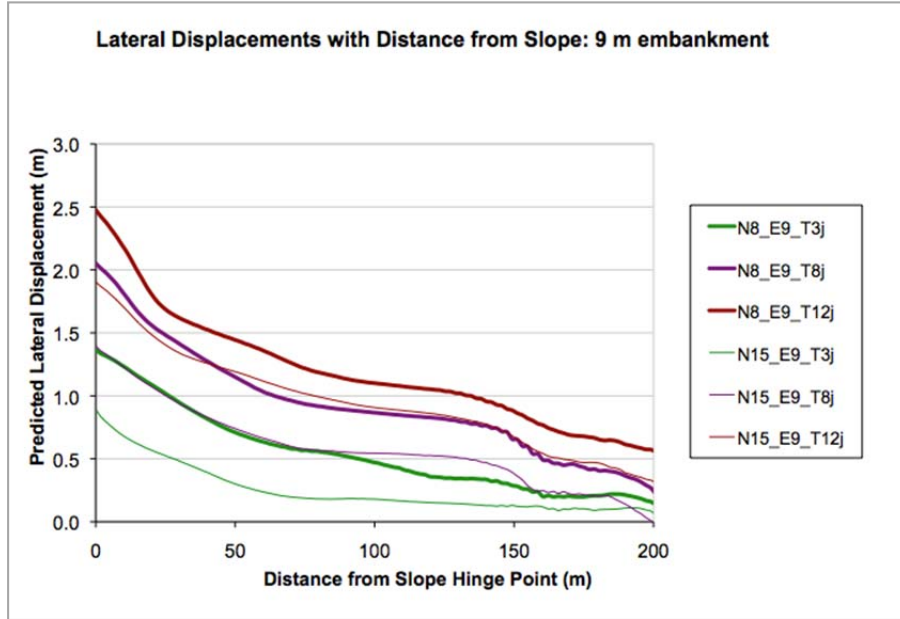
Figure 6-11. Calculated lateral displacements with distance from a slope hinge point for an embankment 9 m high founded on a sand layer of variable thickness and with $(N_1)_{60}$ blow count value of 8 and 15. (Ground Motion: 1992 Landers Joshua Tree).
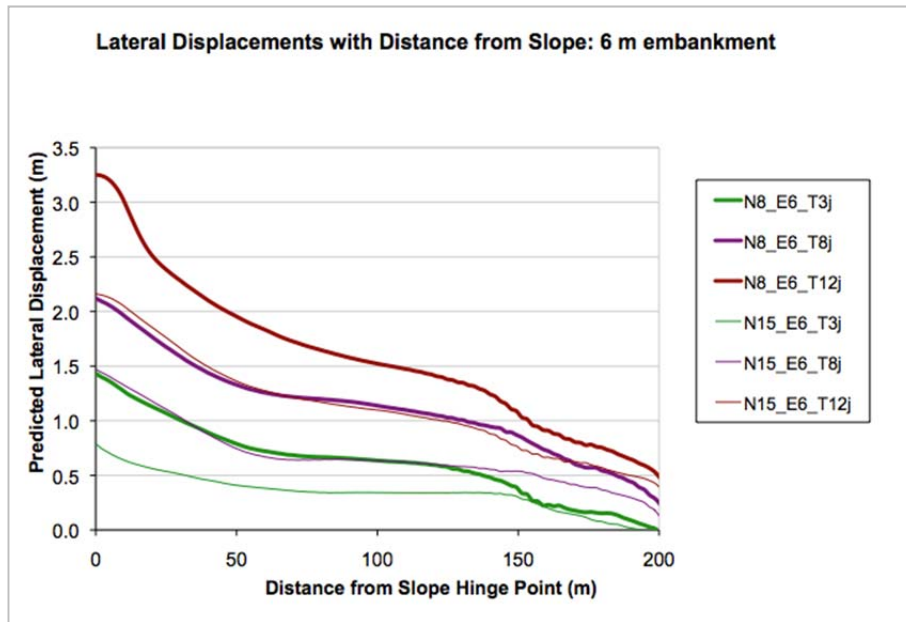


Figure 6-12. Calculated lateral displacements with distance from a slope hinge point for an embankment 6 m high founded on a sand layer of variable thickness and with $(N_1)_{60}$ blow count value of 8 and 15. (Ground Motion: 1992 Landers Joshua Tree).

## 6.3.2 Embankment Height

The embankment height of the model had a relatively minor effect on the calculated seismic displacement, though the effect became more pronounced when combined with a thicker zone of liquefiable foundation soils. Results are shown in Figure 6-13 to Figure 6-18.
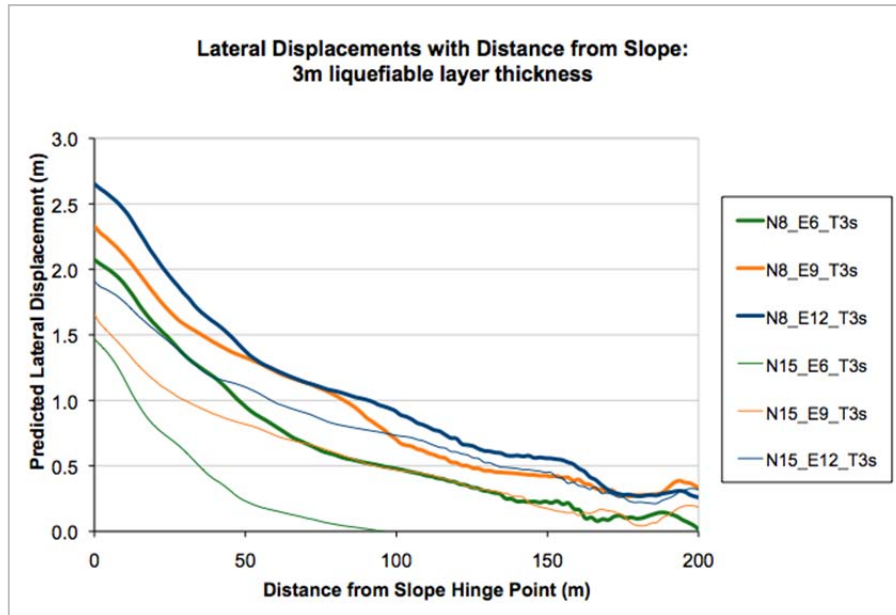


Figure 6-13. Calculated lateral displacements with distance from a slope hinge point for a variable height embankment over 3 m of liquefiable foundation soils with $(N_1)_{60}$ blow count value of 8 and 15. (Ground Motion: 1994 Northridge Sylmar Converter Station).
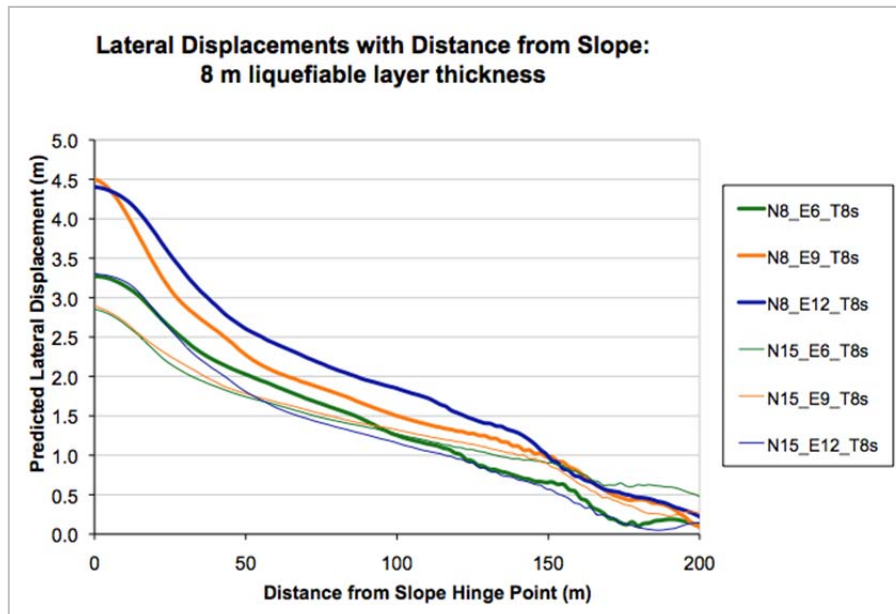


Figure 6-14. Calculated lateral displacements with distance from a slope hinge point for a variable height embankment over 8 m of liquefiable foundation soils with $(N_1)_{60}$ blow count value of 8 and 15. (Ground Motion: 1994 Northridge Sylmar Converter Station).
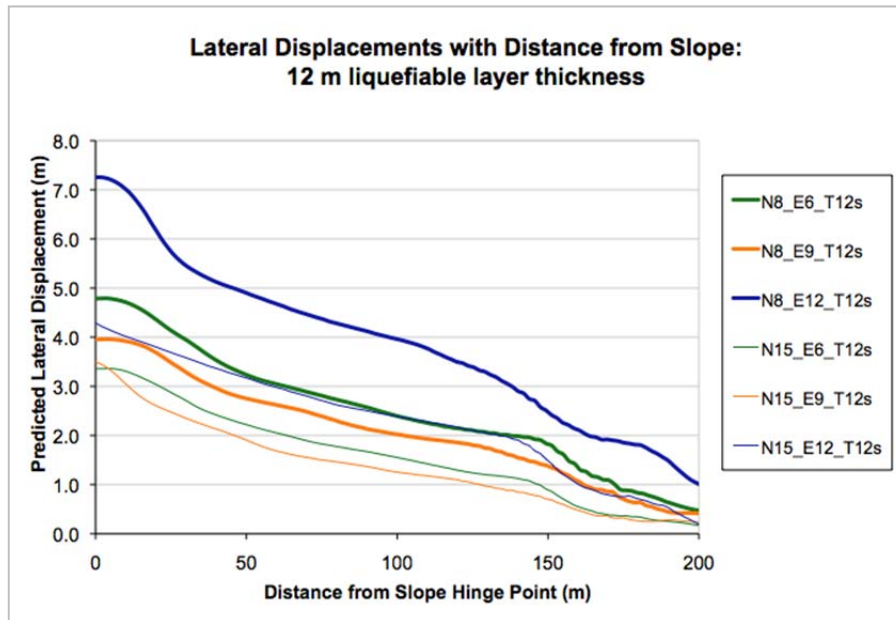
Figure 6-15. Calculated lateral displacements with distance from a slope hinge point for a variable height embankment over 12 m of liquefiable foundation soils with $(N_1)_{60}$ blow count value of 8 and 15. (Ground Motion: 1994 Northridge Sylmar Converter Station).
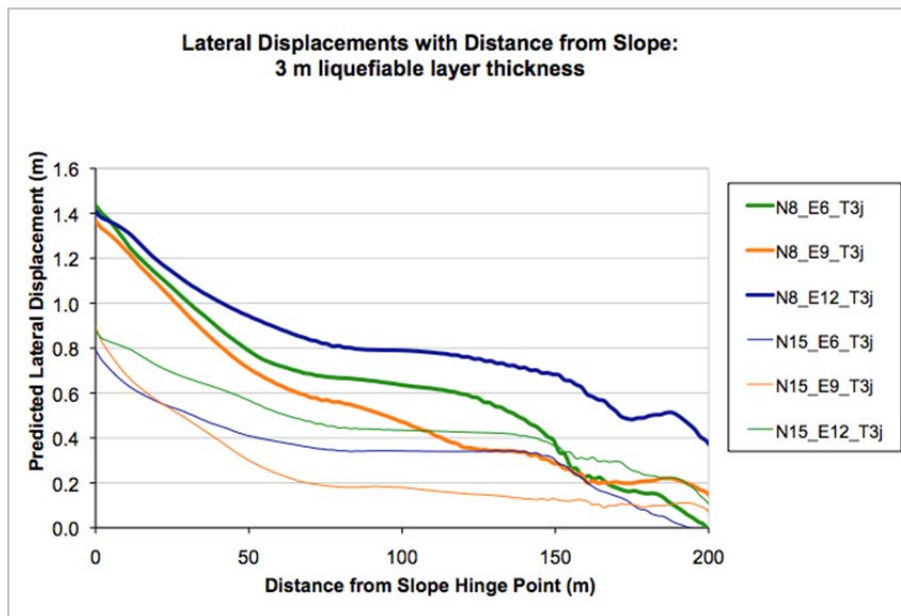


Figure 6-16. Calculated lateral displacements with distance from a slope hinge point for a variable height embankment over 3 m of liquefiable foundation soils with $(N_1)_{60}$ blow count value of 8 and 15. (Ground Motion: 1992 Landers Joshua Tree).
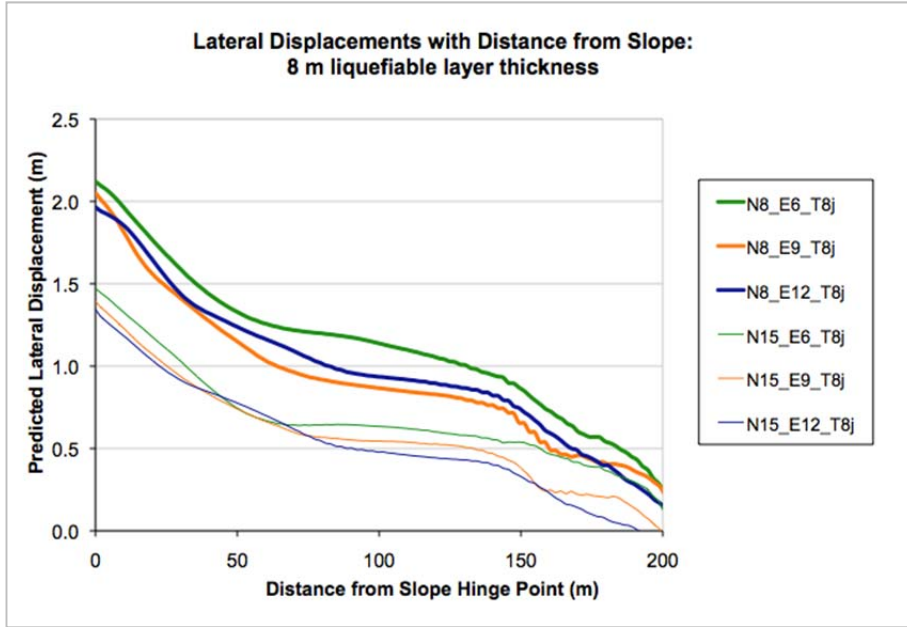
Figure 6-17. Calculated lateral displacements with distance from a slope hinge point for a variable height embankment over 8 m of liquefiable foundation soils with $(N_1)_{60}$ blow count value of 8 and 15. (Ground Motion: 1992 Landers Joshua Tree).
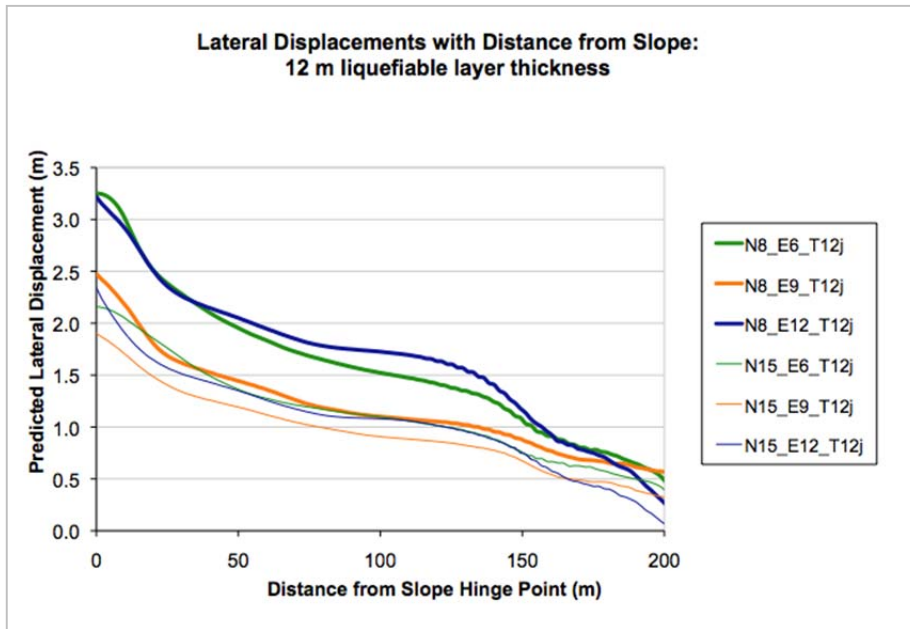


Figure 6-18. Calculated lateral displacements with distance from a slope hinge point for a variable height embankment over 12 m of liquefiable foundation soils with $(N_1)_{60}$ blow count value of 8 and 15. (Ground Motion: 1992 Landers Joshua Tree).

## 6.4 SENSITIVITY OF RESULTS TO VARIATIONS IN EARTHQUAKE GROUND MOTIONS

Earthquake ground motions for these analyses were selected from the PEER ground motion database: http://peer.berkeley.edu/nga/search.html. A suite of nine near-fault, forward-directivity, fault-normal ground motions (Table 6-1) and seven intermediate field ground motions (Table 6-2) were selected for comparisons in the sensitivity analysis. Selections were made based on a suite of motions used by Mason (2011). Ground motions were selected to reflect the seismic hazards most likely to control the design of levees within the San Joaquin-Sacramento delta region of California. Plots that describe the ground motions are provided in Appendix 6A.

Table 6-1 and Table 6-2 provide additional information for each ground motion. Table 6-3 presents the calculated lateral and vertical displacements at a distance of approximately 2 m behind the slope hinge point for each ground motion. Arias intensity proved to correlate well with predicted displacement, as shown in Figure 6-19. Peak ground acceleration (PGA) was found to have a weaker correlation with the predicted displacements, as shown in Figure 6-20. Figure 6-21 and Figure 6-22 show calculated displacements plotted with the peak ground velocity (PGV) and the square of the PGV. Arias intensity provides the best fit with displacement as can be seen below.

Table 6-1. Selected near-fault, forward directivity, fault-normal deep soil ground motions

| Station | Scale | Earthquake | $M_w$ | PGA (g) | PGV (m/s) | $I_a$ (m/s) | Tm (sec) |
|---|---|---|---|---|---|---|---|
| Brawley Airport | 1 | 79 Imperial Valley | 6.5 | 0.128 | 3.357 | 23 | 1.15 |
| Saratoga WV Coll 270 | 1 | 89 Loma Prieta | 7 | 0.293 | 5.766 | 97.9 | 0.99 |
| Newhall - W Pico Cany 046 | 1 | 94 Northridge | 6.7 | 0.421 | 0.843 | 126.6 | 1.57 |
| Sylmar - Conv Sta 052 | 0.5 | 94 Northridge | 6.7 | 0.264 | 5.282 | 115.4 | 1.16 |
| Sylmar - Conv Sta 052 | 1 | 94 Northridge | 6.7 | 0.543 | 10.646 | 478.8 | 1.15 |
| Sylmar - Conv Sta 052 | 1.25 | 94 Northridge | 6.7 | 0.684 | 13.32 | 752.2 | 1.15 |
| LGPC 090 | 1 | Loma Prieta | 7 | 0.468 | 4.697 | 239.3 | 0.59 |
| Rinaldi R Sta 228 | 1 | 94 Northridge | 6.7 | 0.747 | 15.226 | 595.3 | 0.75 |
| Lucern 260 | 1 | 92 Landers | 7.3 | 0.536 | 13.876 | 332.5 | 0.5 |

Table 6-2. Selected intermediate field ground motions

| Station | Scale | Earthquake | $M_w$ | PGA (g) | PGV (m/s) | $I_a$ (m/s) | Tm (sec) |
|---|---|---|---|---|---|---|---|
| TCU078 270 (E) | 1 | 99 Chi Chi | 7.6 | 0.354 | 3.59 | 424.6 | 0.45 |
| LA Hollywood Stor Lot 180 | 1 | 71 San Fernando | 6.6 | 0.133 | 1.333 | 26.1 | 0.42 |
| Parachute T S 315 | 1 | 87 Superstition Hills | 6.6 | 0.328 | 4.062 | 135 | 0.69 |
| Joshua Tree 090 | 0.75 | 92 Landers | 7.3 | 0.192 | 2.792 | 101.6 | 0.79 |
| Joshua Tree 090 | 1 | 92 Landers | 7.3 | 0.256 | 3.873 | 185.4 | 0.78 |
| Joshua Tree 090 | 1.5 | 92 Landers | 7.3 | 0.386 | 6.129 | 428.7 | 0.78 |
| Superstition Mtn Cam 045 | 1 | 87 Superstition Hills | 6.6 | 0.489 | 2.896 | 261.9 | 0.35 |

Table 6-3. Calculated lateral and vertical displacements for a 9 m-high embankment founded on an 8 m-thick layer of loose to medium dense sands for the suite of 16 selected ground motions.

| Station | Scale | Earthquake | $(N_1)_{60} = 8$ | | $(N_1)_{60} = 15$ | |
|---|---|---|---|---|---|---|
| | | | X-displacement at 2m from Hinge Point (cm) | Y-displacement at 2m from Hinge Point (cm) | X-displacement at 2m from Hinge Point (cm) | Y-displacement at 2m from Hinge Point (cm) |
| Brawley Airport | 1 | 79 Imperial Valley | 2 | 2 | 1 | -1 |
| Saratoga WV Coll 270 | 1 | 89 Loma Prieta | 153 | -22 | 74 | -16 |
| Newhall - W Pico Cany 046 | 1 | 94 Northridge | 186 | -34 | 89 | -30 |
| Sylmar - Conv Sta 052 | 0.5 | 94 Northridge | 209 | -32 | 144 | -27 |
| Sylmar - Conv Sta 052 | 1 | 94 Northridge | 447 | -133 | 287 | -63 |
| Sylmar - Conv Sta 052 | 1.25 | 94 Northridge | 514 | -77 | 411 | -66 |
| LGPC 090 | 1 | Loma Prieta | 136 | 30 | 105 | -24 |
| Rinaldi R Sta 228 | 1 | 94 Northridge | 268 | -29 | 221 | -55 |
| Lucern 260 | 1 | 92 Landers | 280 | -14 | 243 | -12 |
| TCU078 270 (E) | 1 | 99 Chi Chi | 300 | -36 | 180 | -24 |
| LA Hollywood Stor Lot 180 | 1 | 71 San Fernando | 3 | -3 | 2 | -2 |
| Parachute T S 315 | 1 | 87 Superstition Hills | 81 | -22 | 59 | -19 |
| Joshua Tree 090 | 0.75 | 92 Landers | 132 | -25 | 94 | -14 |
| Joshua Tree 090 | 1 | 92 Landers | 205 | -42 | 136 | -23 |
| Joshua Tree 090 | 1.5 | 92 Landers | 333 | -58 | 333 | -58 |
| Superstition Mtn Cam 045 | 1 | 87 Superstition Hills | 106 | -42 | 94 | -40 |
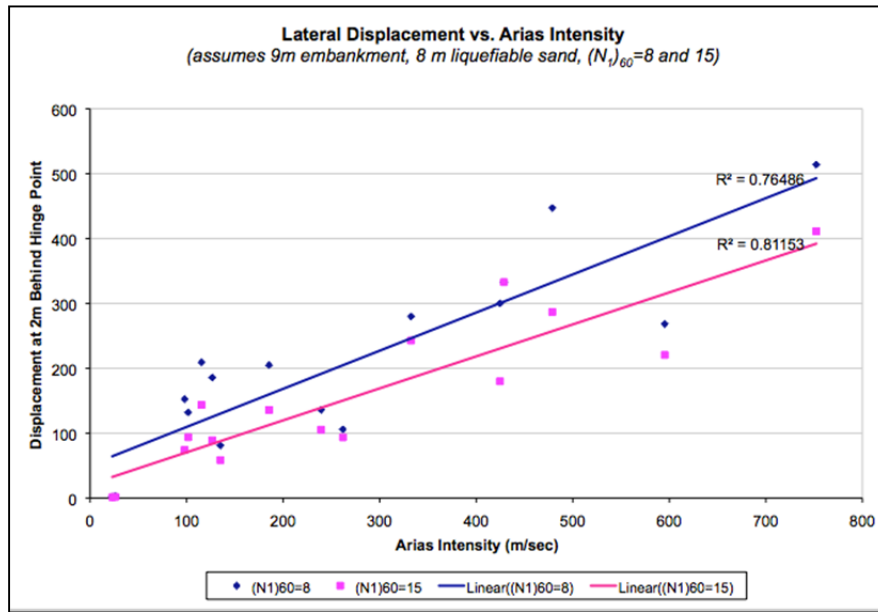


Figure 6-19. Calculated liquefaction-induced lateral displacement (cm) as a function of the Arias Intensity of the input earthquake ground motion.
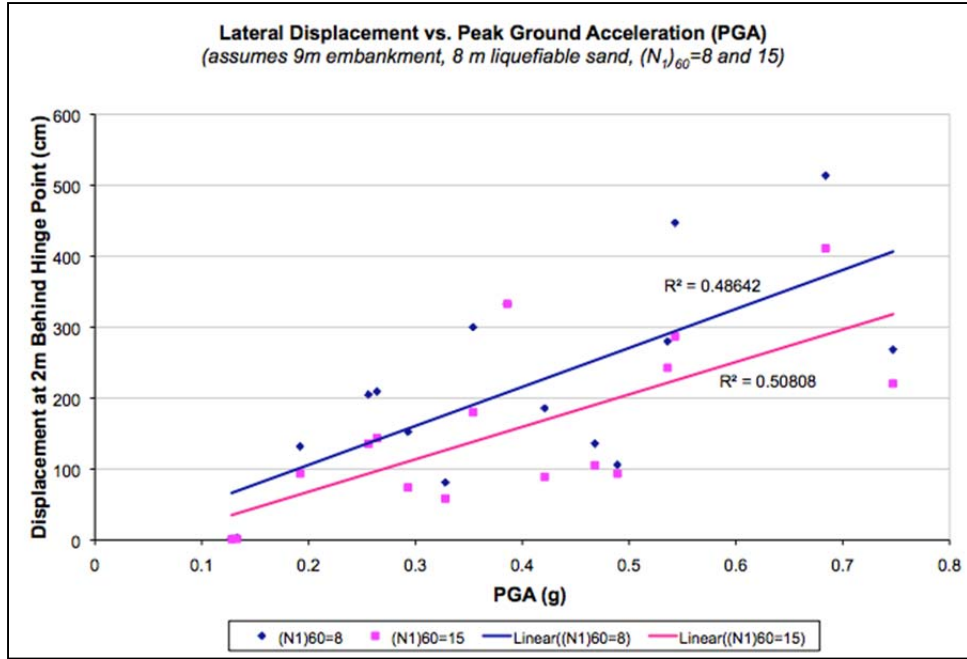
Figure 6-20. Calculated liquefaction-induced lateral displacement as a function of the peak ground acceleration of the input earthquake ground motion.
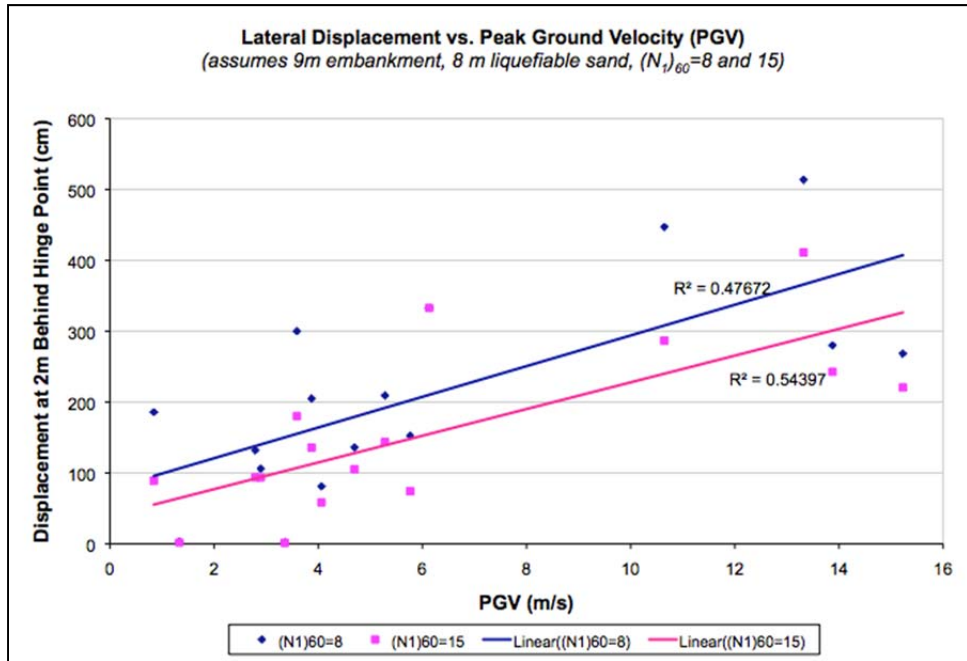


Figure 6-21. Calculated liquefaction-induced lateral displacement as a function of the peak ground velocity of the input earthquake ground motion.
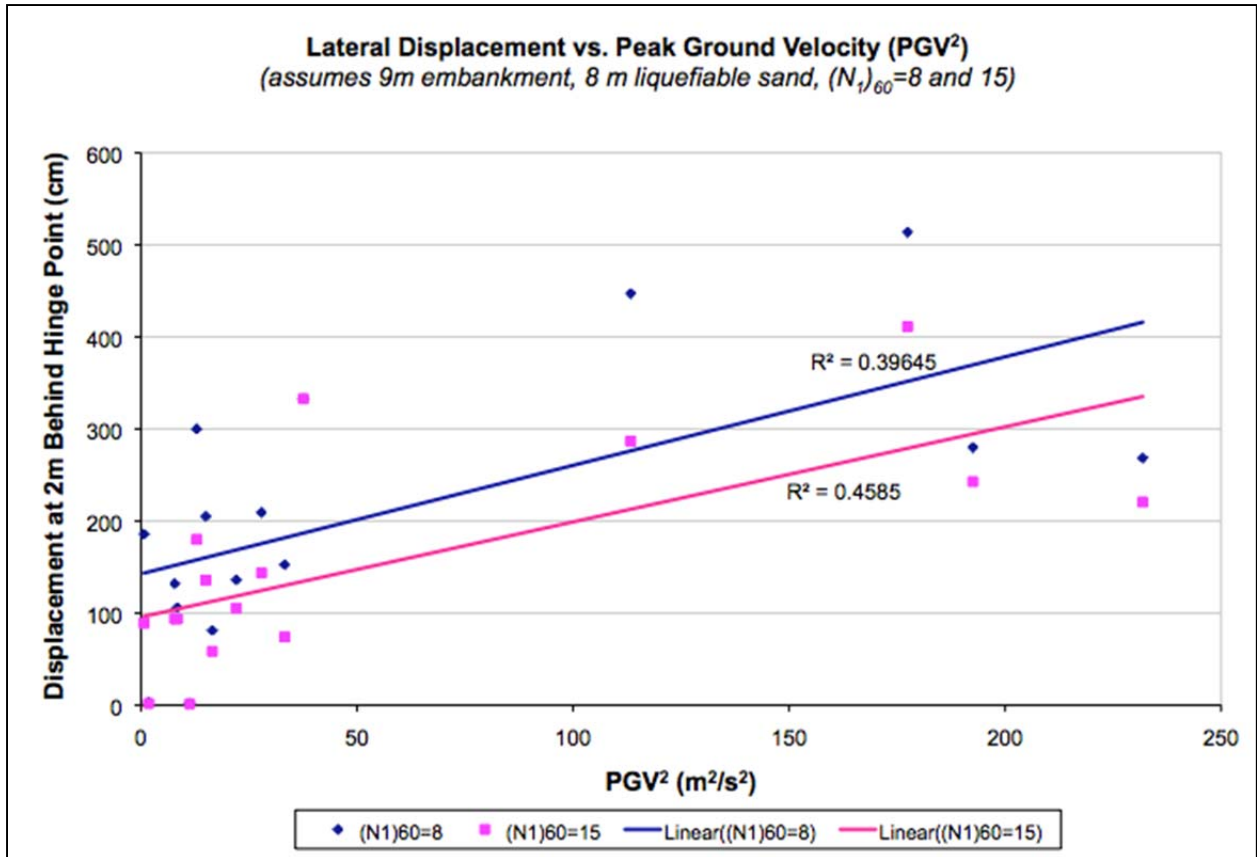
Figure 6-22. Calculated liquefaction-induced lateral displacement as a function of the square of the peak ground velocity of the input earthquake ground motion.

# CHAPTER 7

## Conclusion

7.1   SUMMARY AND FINDINGS

In the first part of this research effort, the effects of live and decomposing woody vegetation on levee seepage and seepage-induced stability were explored through a series of two field tests and subsequent numerical simulations. In both field tests, networks of macropores created by mammal burrowing activity dominated the early wetting fronts and flow patterns. Macropores require inflows into a pore that exceed lateral losses through the walls of the pore for flow to occur.

In the Parallel Trench Wetting Front test on the landside of the Cal Expo test site, which was conducted in silty soils, a direct connection to a water source was needed when the soil was in unsaturated conditions for sufficient inflow to initiate observable outflows from mammal burrows at the lower trench. Where this direct connection was continuous into the observation trench, rapid initial flow was observed, diminishing in volume with saturation of the matrix soils. For surficial seeps, gravel bags were effective as a means of initially controlling rapid flows, backing water up in the burrow until increased saturation of matrix soils increased permeability of the burrow walls, increasing losses of water to the soil matrix and reducing concentrated flows through burrow networks.

Decaying roots created sufficiently continuous void spaces for the flow of silica slurry (used in instrument installation) over short distances when the instrument hole intersected the void and created a direct hydraulic connection. These same voids along roots were not sufficiently continuous to flow water from the upper trench to the lower trench through the levee soils. The presence of the stump impeded the rate of the wetting of the soil in the zone of decomposing roots.

Flows at the Twitchell Island test site were controlled by macroporosity and stratigrapic conditions related to the presence of an old levee on which the existing levee is founded. Zones of macropores associated with burrowing activities of muskrats (from the waterside), as well as voles and gophers (from the landside) advanced the wetting front when burrows intersected (or nearly intersected) the water source. As observed at the Cal Expo test site, flow of water through macropores, which advanced the wetting front, diminished with time. Elevated pore water pressure (relative to analogous instruments in a similar position but without a tree) was observed in one piezometer located at a depth of 3 feet directly behind the landside oak tree. The instrument within the same hole at a depth of 6 feet did not show elevated pore pressure relative to comparable instruments.

A similar pattern was not found behind the waterside oak tree, though pore water pressures behind the tree were observed to drop by 0.25 feet of head when the tree fell and

pressures in an adjacent instrument increased by a similar amount. Observed seepage around the tree and surrounding muskrat burrows ceased once the tree had fallen and preferred water pathways appeared to shift to burrows to the north and south of the waterside oak tree. A leaning tree like the waterside oak tree should be evaluated for health of the tree, size, and balance of the tree with consideration to species, soil strengths, benefits to erosion resistance of the levee, consequences of failure, consequences of removal, and other relevant factors specific to each case.

At the Twitchell Island test site, four waterside and two landside failure scenarios were evaluated. Waterside failure scenarios were defined based on observed cracks visible in the field during the flow test. Each failure scenario was divided into sections and each section given a width and a series of root reinforcement and loading assumptions were implemented. Factors of safety were calculated using mass-averaging of the mass of each slide mass. Roots were modeled as reinforcing nails with zero shear strength. Portions of the nails that fell within the slide mass were not included in the analysis; yet tree lean and wind forces put a load on these roots that fall within the slide mass. Horizontal forces distributed across the root zone were added such that if these forces fall into the slide mass, they are included in the calculation of factor of safety. Slope stability analyses produced results that showed:

- The presence of a tree had little to no effect on the factor of safety against instability. Factors of safety were nearly identical or higher for the sections with a tree as opposed to those without a tree.
- The root system of a tree was considered as an eccentrically loaded footing with windward and vertically oriented roots acting as tensile forces. The root plate begins to engage significantly the roots extending beyond the root plate when the eccentric loading acts outside of its middle third. Tension loads on the root system increase and the system may become unstable when the center of gravity of the tree extends beyond the hinge-point of rotation, assumed to be half of the pit diameter.
- Loading on the root system increases with tree lean and slope angle. Horizontal forces increase more rapidly than vertical forces with increasing slope angle. Vertical forces increase more rapidly than horizontal forces with increasing tree lean. These increased horizontal and vertical forces increase significantly the loading on the tree's root system.
- The Twitchell Island field test waterside tree appears to have fallen due to horizontal forces placed on the root system associated with extensive tree lean and wind loading. Saturation of the root system reduced the bond strength on the root system by an estimated 30 to 40 percent. The most likely failure scenario for the waterside oak tree is B-2, where the failure scenario extends to the hinge-point of the waterside slope.
- Cutting tree roots at the trenches is estimated to have reduced capacity of the root system by approximately 9 percent. Though a smaller effect than that of seepage-induced instability caused by excess pore pressures induced by the simulated flood condition, this reduction in capacity also contributed to the tree failure.

- The Twitchell Island field test landside tree performed acceptably under saturated conditions and gusting wind conditions, showing a modest rotation of about 0.12 degrees (or about 2 inches measured 6.5 feet up from the base of the tree) based on LiDAR data provided by Gerald Bawden of the USGS.

In the second part of this research effort, calibration of the fully nonlinear effective stress UBCSAND soil model using CSS test results established trends in the variation of its model parameters that prove useful for employing the UBCSAND model in engineering practice. The CSS-based model parameter calibration led to the development of UBCSAND model parameterizations that were found to capture the observed performance of three well documented liquefaction-induced displacement case histories. These back-analyses of case histories demonstrate the robustness of the UBCSAND model for this application. The proposed model calibration procedure can be employed by engineers in the development of UBCSAND model parameters for liquefaction-induced deformation analysis.

In addition to the UBCSAND model parameters that depend on conventional geotechnical characterizations (e.g., $(N_1)_{60}$), there are four "fitting" parameters that are available for use in UBCSAND. In this study, two of these "fitting" parameters were used (i.e., m_fac1 and m_fac4). The model parameters m_hfac1 and m_hfac2 were found to serve a similar function. Best results were obtained by setting the parameters equal to one another. These parameters are used to model the number of cycles to liquefaction and their value has an effect on the rate of pore water pressure rise with cyclic loading. Values of 0.5 to 2.0 were typical values used in our analyses, though values can be higher and lower than this range of values. For the case of sand at low relative density, the value of m_hfac1 (which is the same as m_hfac2 for this study) must be increased to match liquefaction triggering response in CSS laboratory test results data. Increases in the initial static shear stress acting on the soil yielded a weak trend of a corresponding increase in m_hfac1 (and similarly, m_hfac2). This effect is most evident for sand at low relative density. Nonplastic or low plasticity silts were found to follow a similar trend to clean sands, though these materials required a slightly higher value of m_hfac1 (and m_hfac2) to capture their measured cyclic response. The UBCSAND m_hfac3 parameter was not used in this study. Lastly, the UBCSAND m_hfac4 parameter was found to vary between approximately 0.5 and 2.5 for sands with typical values being between 1.5 and 2.0. The m_hfac4 parameter was moderately influenced by the relative density of the sand at low CSR (i.e., CSR ≤ 0.2) and by the value of the earthquake-induced CSR at higher CSR (i.e., CSR ≥ 0.2). For silty soils, a value of 0.5 was selected for cases where the soil had a higher void ratio, and a value of 1.5 was selected for lower void ratio silty soils.

The calibrated UBCSAND model was used to estimate liquefaction-induced embankment deformations with varying foundation soil properties, layer thicknesses, as well as a range of embankment heights and ground motions. In this study, the liquefiable soils were present in the foundations of earth levees. The range of calculated displacement values for all configurations modeled with the intense forward-directivity 1994 Northridge Sylmar Converter Station motion was approximately 1.5 m to 7.5 m. The displacement resulting from the same models but with the lower intensity backward-directivity 1992 Landers Joshua Tree motion yielded displacements ranging from 0.75 m to 3.25 m, which is

approximately half those values calculated using the Sylmar Converter Station motion. The intensity of the earthquake appears to be the key factor as the calculated liquefaction-induced displacements increased significantly as the input motion's value of Arias intensity increased. The rate of increase of the calculated liquefaction-induced displacement with increasing Arias intensity was roughly linear for these embankment configurations. The rate of increase in the calculated liquefaction-induced displacement increased as the relative density of the liquefied sand decreased.

The thickness of the liquefiable foundation layer impacted displacements in a non-linear pattern where displacement increased more rapidly as the liquefiable material layer thickness increases significantly. As would be expected, looser foundation soils led to increased amounts of displacements of the overlying embankment. Additionally, for the cases analyzed in this study, higher embankments displaced more when strongly shaken. Combinations of thicker deposits of liquefiable foundation soils combined with higher embankments yielded the maximum displacement of the cases analyzed in this study, especially when shaken with the intense forward-directivity 1994 Northridge Sylmar Converter Station ground motion.

The UBCSAND model is a reliable tool for evaluating the effects of liquefaction in the foundation of earth levees. After an initial calibration effort to characterize the trends in the model response as the values of the key parameters were varied, the UBCSAND model was able to capture the performance of three case histories well. This independent evaluation of the capabilities of this soil constitutive model to capture inertially driven liquefaction-induced lateral spreads demonstrates that this model can be used in evaluations of the seismic performance of earth structures situated atop potentially liquefiable soils.

## 7.2   RECOMMENDATIONS FOR FUTURE WORK

The impacts of woody vegetation on overall levee integrity may be better understood through further research. Throughout this program of study, the author has had the good fortune to hear the opinions of numerous researchers, experts, state and federal agencies, private consultants, and local maintaining authorities on the impacts of woody vegetation on levee performance based on varied experiences. For this highly interdisciplinary subject to be well understood, the problem must be placed within a risk framework where all factors impacting levee integrity and performance can be considered and vegetation effects evaluated in terms of their relative risk. Further, given the interdisciplinary nature of the work, this research does not address all key factors needed to understand the impact of woody vegetation on levee performance. Further study to evaluate the positive and negative impacts of woody vegetation with respect to erosion would be useful, as this is an important element in understanding piping and through-seepage issues.

The UBCSAND model was shown to be a useful tool in understanding trends in embankment deformation and may be useful in evaluating levee sections to prioritize levee repairs. However, the analytical tool does require significant background knowledge and effort. Sensitivity analyses should be expanded and built upon to create a fully coupled

simplified model of deformation more appropriate for use in limited-budget studies in which thousands of miles of levees need to be evaluated.

# REFERENCES

Arduino, P., Kramer, S. and Baska, D. (2001). "UW-Sand: a simple constitutive model for liquefiable soils." In: Book of Abstracts, 2001 Mechanics and Materials Summer Conference, 27-29 June, San Diego, CA. pg. 108

Arulmoli, K., K. K. Muraleetharan, M. M. Hossain, and L.S. Fruth, 1992, "VELACS: Verification of Liquefaction Analysis by Centrifuge Studies. Laboratory Testing Program. Soil Data Report," The Earth Technology Corporation, Long Beach, CA, report for the National Science Foundation.

Association of State Dam Safety Officials (ASDSO) (2002) A Technical Manual on the Effects of Tree and Woody Vegetation Root Penetrations on the Safety of Earthen Dams, December 2002.

Aubertin, G. M. (1971). *Nature and extent of macropores in forest soils and their influence on subsurface water movement* (Vol. 192). Northeastern Forest Experiment Station.

Bardet, J.P., Hu, J., Tobita, T., and Mace, N. (1999) "Database of case histories on liquefaction-induced ground deformation," Univ. of Southern California, Department of Civil Engineering, A Report to PEER/PG&E, Task 4A, Phase 2, October 16.

Bardet, J.P., Tobita, T., Mace, N., and Hu, J. (2002) "Regional model of liquefaction-induced ground deformation." *Earthquake Spectra*. 18(1): 19-46.

Barley, K. P. (1962). The effects of mechanical stress on the growth of roots. *Journal of Experimental Botany*, *13*(1), 95-110.

Baska, D.A. (2002). "An analytical/empirical model for prediction of lateral spread displacements." Ph.D. thesis, Dept. of Civil & Environ. Engineering, Univ. of Washington, Seattle.

Bawden, G., Howle, J., Bond, S., Shriro, M. and Buck, P. (2013-DRAFT). 3D Imaging, Change Detection, and Stability Assessment along the Centerline Trench Levee Seepage Experiment at Twitchell Island, California with Ground-Based Tripod LiDAR. USGS.

Baziar, M.H., Dobry, R., and Elgamal, A. (1992). "Engineering evaluation of permanent ground deformations due to seismically-induced liquefaction." Technical Report NCEER-92-0007, National Center fo Earth-quake Engineering Research (NCEER), Buffalo, NY.

Beasley, R. S. (1976). Contribution of subsurface flow from the upper slopes of forested watersheds to channel flow. *Soil Science Society of America Journal*, *40*(6), 955-957.

Beaty, M. and Byrne, P.M. (1998) "An effective stress model for predicting liquefaction behavior of sand," Geotechnical Earthquake Engineering and Soil Dynamics III, ASCE Spec. Pub. No. 75, Edited by Dakoulos, Yegian and Holz, ASCE, Reston, VA, Vol. 1, pp. 766-777.

Beven, K., & Germann, P. (1982). Macropores and water flow in soils. *Water resources research*, *18*(5), 1311-1325.

Beven, K., & Germann, P. (1982). Macropores and water flow in soils. Water resources research, 18(5), 1311-1325.

Bischetti, G. B., Chiaradia, E. A., Simonato, T., Speziali, B., Vitali, B., Vullo, P., & Zocco, A. (2005). Root strength and root area ratio of forest species in Lombardy (Northern Italy). *Plant and soil*, *278*(1-2), 11-22.

Boulanger R.W., Mejia L.H. and Idriss I.M. (1997) "Liquedaction at Moss Landing During Loma Prieta Earthquake," *Journal of Geotechnical and Geoenvironmental Engineering*. Vol. 123(5): 453-467.

Bray, J. D., R. B. Sancio, H.T. Durgunoglu, A. Onalp, R. B. Seed, J. P. Stewart, T. L. Youd, M. B. Batu-ray, K.O. Cetin, C. Christensen, T. Karadayilar, and C. Emrem, (2001) "Ground Failure In Adapaza-ri, Turkey," in Proc., Earthquake Geotechnical Engineering Satellite Conf. of the XVth International Conference on Soil Mechanics & Geotechnical Engineering, Istanbul, Turkey, August 24-25.

Bray, J. D., R. B. Sancio, H.T. Durgunoglu, A. Onalp, T. L. Youd, J. P. Stewart, R. B. Seed, O.K. Cetin, E. Bol, M. B. Baturay, C. Christensen, and T. Karadayilar (2004b) "Subsurface Characterization at Ground Failure Sites in Adapazari, Turkey," Journal of Geotechnical and Geoenvironmental Engi-neering, ASCE, Vol. 130, No. 7, July, pp. 673-685.

Bray, J.D. and Stewart, J.P., coordinators (2000). "Damage patterns and foundation performance in Ada-pazari." Kocaeli, Turkey Earthquake of August 17, 1999 Reconnaissance Report, T.L. Youd, J.P. Bardet, and J.D. Bray, eds., *Earthquake Spectra*, Supplement A to Vol. 16, 163-189.

Bray, J.D. and Travasarou, T. (2007) "Simplified Procedure for Estimating Earthquake-Induced Deviatoric Slope Displacements," J. of Geotechnical and Geoenvironmental Engineering, ASCE, Vol. 133, No. 4, April, pp. 381-392.

Bray, J.D., and Sancio, R.B. (2006) "Assessment of the Liquefaction Susceptibility of Fine-Grained Soils," J. of Geotechnical and Geoenvironmental Engineering, ASCE, Vol. 132, No. 9, Sept., pp. 1165-1177.

Bray, J.D., Sancio, R.B., Riemer, M.F. and Durgunoglu, T. (2004a) "Liquefaction Susceptibility of Fine-Grained Soils," *11th International Conf. On Soil Dynamics and Earthquake Engineering and 3rd In-ternational Conf. On Earthquake Geotechnical Engineering,* Doolin, Kammerer, Nogami, Seed and Towhata, Eds., Berkeley, CA, Jan. 7-9, 2004, V.1, pp. 655-662.

Burroughs, E. R., & Thomas, B. R. (1977). *Declining root strength in Douglas-fir after felling as a factor in slope stability*. Intermountain Forest and Range Experiment Station, Forest Service, US Department of Agriculture.

Byrne, P.M., and Seid-Karbasi, M. (2003) "Seismic stability of impoundments," 17th Annual Symposium of VGS, Canada (http://www.civil.ubc.ca/liquefaction/Publications/VGS12R.pdf).

Byrne, P.M., Park, S-S., Beaty, M., Sharp, M., Gonzalez, L., and Abdoun, T. (2004) "Numerical modeling of liquefaction and comparison with centrifuge tests," Canadian Geotechnical Journal, Vol. 41, pp. 193-211.

California Department of Water Resources (DWR) (2013). *Levee Repair - History of Levees*. [online] Retrieved from: http://www.water.ca.gov/levees/history/ [Accessed: 12 May 2013].

California Department of Water Resources. (2007). Delta Risk Management Strategy Technical Memorandum: Levee Vulnerability, Draft 2. Sacramento, CA

California Department of Water Resources (DWR) (2013). Levee Repair - History of Levees. [online] Retrieved from http://www.water.ca.gov/levees/history/ [Accessed: 12 May 2013].

California Department of Water Resources (DWR) (2014). Delta Risk Management Strategy. [online] Retrieved from http://www.water.ca.gov/floodsafe/fessro/levees/drms/ [Accessed: 11 May 2014].

Center for Earthquake Engineering Research Center. Woodward-Clyde Consultants. Phase i - geotechnical study, Marine Biology Laboratory, California State University, Moss Landing, California. Technical report, California State University, San Jose, California, 1990.

Cobos-Roa, D. (2014, in press). *The Role of Transient Conditions on Levee Performance*. Ph.D.. University of California, Berkeley.

Cobos-Roa, D., Shriro, M., Sitar, N., Bray, J., Bawden, G., Lichter, J. and Evans, R. (2012). "3-D Stratigraphy and Root Geometry from Trench and Ground-Based LiDAR Mapping", paper presented at *GeoCongress: the State of the Art and Practice in Geotechnical Engineering*, Oakland, CA, 25-29 March. New York, NY: Currin Associates, Inc., pp. 3031-3040.

Cooper, W. S. (1926). Vegetational development upon alluvial fans in the vicinity of Palo Alto, California. *Ecology*, *7*(1), 1-30.

Corcoran, M. K., Gray, D. H., Biedenharn, D. S., Little, C. D., Leech, J. R., Pinkard, F., ... & Lee, L. T. (2010). *Literature Review-Vegetation on Levees* (No. ERDC-SR-10-2). Engineer Research and Development Center Vicksburg MS Geotechnical and Structures Lab.

De Vries, J., & Chow, T. L. (1978). Hydrologic behavior of a forested mountain soil in coastal British Columbia. *Water Resources Research*, *14*(5), 935-942.

Duncan, J. M., & Wright, S. G. (2005). *Soil strength and slope stability*.

Earthquake Engineering Research Institute (2003) "Securing Society Against Catastrophic Earthquake Losses: A Research and Outreach Plan in Earthquake Engineering."

Electric Power Research Institute (1990), Manual on Estimating Soil Properties for Foundation Design, EPRI EL-6800, August 1990.

Elgamal, A., Yang, Z., and Parra, E. (2002) "Computational Modeling of Cyclic Mobility and Post-Liquefaction Site Response," Soil Dynamics and Earthquake Engineering, ASCE, V. 22, pp. 259-271.

Faris, A.T. (2004) "Probabilistic models for engineering assessment of liquefaction-induced lateral spreading displacements," Ph.D. thesis, Dept. of Civil & Environ. Engineering, Univ. of California, Berkeley, Fall.

Faris, A.T., Seed, R.B., Kayen, R.E., and Wu. J. (2006) "A semi-empirical model for estimation of maximum horizontal displacement due to liquefaction-induced lateral spreading," Proc. 8th US Nat. Conf. EQ Engrg., 100th Anniversary Earthquake Conference Commemorating the 1906 San Francisco Earthquake, EERI, April.

Federal Emergency Management Agency (FEMA) (2005) Technical Manual for Dam Owners, Impacts of Plants on Earthen Dams, FEMA 534, Sept 2005.

Federal Highway Administration (FHWA) (2002), NHI Course No. 132031, Subsurface Explorations – Geotechnical Site Characterization.

Finn, W.D. Liam (1990) "Analysis of Post-Liquefaction Deformations in Soil Structures," Proc. H. Bolton Seed Memorial Symposium, Univ. of Calif., Berkeley, Editor J.M. Duncan, Bi-Tech Publishers, Vancouver, Canada, Vol. 2, pp. 291-311.

Finn, W.D. Liam (1998) "Seismic safety of embankment dams developments in research and practice 1988-1998," Geotechnical Earthquake Engineering and Soil Dynamics III, ASCE Spec. Pub. No. 75, Edited by Dakoulos, Yegian and Holz, ASCE, Reston, VA, Vol. 2, pp. 812-853.

Finn, W.D. Liam (2000a) "State-of-the-art of geotechnical earthquake engineering practice," Soil Dynamics and Earthquake Engineering, Vol. 20, pp. 1-15.

Finn, W.D. Liam (2000b) "Post-liquefaction flow deformations," ASCE Geotechnical Engineering Spec. Pub. No. 107, Proceedings of GeoDenver 2000, pp. 108-122.

Gaiser, R. N. (1952). Root channels and roots in forest soils. *Soil Science Society of America Journal*, *16*(1), 62-65.

GEI (2009). Twitchell Island Levee Improvement Project, San Joaquin River Reach: Geotechnical Investigation and Evaluation Report. Project 073050.

Gray, D. H., & Leiser, A. T. (1982). *Biotechnical slope protection and erosion control*. Van Nostrand Reinhold Company Inc.

Gray, D. H., & Sotir, R. B. (1996). Biotechnical and soil bioengineering slope stabilization: a practical guide for erosion control. Wiley-Interscience.

Gray, D., et al. (1991). *The Effects of Vegetation on the Structural Integrity of Sandy Levees (Technical Report REMR-EI-5)*. Repair, Evaluation, Maintenance, and Rehabilitation Research Program. [report] Vicksburg, Mississippi: United States Army Corps of Engineers Waterways Experiment Station.

Green, R. D., & Askew, G. P. (1965). Observations on the biological development of macropores in soils of Romney Marsh. *Journal of Soil Science*, *16*(2), 342-344.

Hamada, M., Yasuda, S., Isoyama, R., and Emoto, K. (1986) "Study on liquefacton induced permanent ground displacements," Report for the Association for the Development of Earthquake Prediction.

Harder, Jr., Leslie F.; Kroll, Roy, Claassen, Vic; Buck, Peter E. F.; and Berry, Alison M. (2010), *"Investigation of tree Root Penetration into a Levee Soil-Cement-Bentonite Slurry cutoff Wall,"* Proceedings of the Annual Conference of the Association of State Dam Safety Officials, Seattle, Washington, September 19-23, 2010.

Hatanaka, M. and Uchida, A. (1996), Empirical correlation between penetration resistance and effective friction of sandy soil, Soils & Foundations, Vol. 36, No. 4, Japanese Geotechnical Society.

Holzer, T.L., Bennett, M.J., Ponti, D.J., and Tinsley, J.C. (1999) "Liquefaction and Soil Failure During 1994 Northridge Earthquake," *Journal of Geotechnical and Geoenvironmental Engineering*. Vol. 125(6): 438-452.

Idriss, I.M., and Boulanger, R.W. (2008) Soil Liquefaction During Earthquakes, EERI Monograph, Oakland, California (draft available to selected persons; 2nd Edition to be published soon).

Itasca Consulting Group, Inc. (2005). FLAC, version 5.0. Itasca Consulting Group, Inc.: Minneapolis, Minnesota.

J. Wu. Liquefaction Triggering and Post Liquefaction Deformations of Monterey 0/30 Sand under Uni-Directional Cyclic Simple Shear Loading. Ph.d. dissertation, University of California, Berkeley, 2002.

J.C. Tinsley, III and W.R. Dupre. Liquefaction hazard mapping, depositional faces, and lateral spreading ground failure in the Monterey Bay Area, Central California, during the 10/17/89 Loma Prieta Earthquake. In Proceedings from the Fourth U.S.-Japan Workshop on Earthquake Resistant Design of Lifeline Facilities and Countermeasures Against Soil Liquefaction, volume I of NCEER-92-0019, pages 71 – 85, Buffalo, N.Y., 1992. National

Jacobs, K. A., MacDonald, J. D., Berry, A. M., & Costello, L. R. (1997). Rooting responses of three oak species to low oxygen stress. In *Proceedings of a Symposium on Oak Woodlands: Ecology, Management and Urban Interface Issues. Gen. Tech. Rep. PSW-GTR-160, Albany, CA. PSW Res. Station, USDA Forest Service* (pp. 91-100).

Juvenile Hall, California. Bulletin of the Association of Engineering Geologists, XXVI (2):209 – 226, 1989.

K.O. Cetin. Reliability-Based Assessment of Seismic Soil Liquefaction Initiation Hazard. Ph.D. dissertation, University of California, Berkeley, 2000.

Kammerer, A., Pestana, J., and Seed, R. (2002). "Undrained Response of 0/30 Sand Under Multidirectional Cyclic Simple Shear Loading Conditions." Geotechnical Engineering Research Report No. UCB/GT/02-01, University of California, Berkeley, July.

KSN, Inc. (2010). *Relamation District 1601, Twitchell Island, Five Year Plan*.

Lawrence Halprin and Associates (1967). *Planting Plan*. General Area Landscape Architecture, Levee Area 11, 12, 13, 14. [report] Sacramento, CA: California Exposition and State Fair, Sheet L-45.

Ledezma, C. and Bray, J.D. (2006) "A Probabilistic Design Procedure that Incorporates the Pile-Pinning Effect in Bridge Foundations Undergoing Liquefaction-Induced Lateral Spreading," Proc. 5th Nat. Seismic Conf. on Bridges & Highways, San Francisco, CA, Sept. 18-20.

Ledezma, C. and Bray, J.D. (2007) "Performance-Based Earthquake Engineering Design Evaluation Procedure for Bridge Foundations Undergoing Liquefaction-Induced Lateral Spreading," PEER Report 2007/xx, Pacific Earthquake Engineering Research Center, College of Engineering, University of California, Berkeley, November.

M.J. Bennett. Liquefaction analysis of the 1971 ground failure at the San Fernando Valley

Martin, G.R. and Lew, M., eds. (1999) "Recommended Procedures for Implementation of DMG Special Publication 117: Guidelines for Analyzing and Mitigating Liquefaction Hazards in California," Southern California Earthquake Center, Univ. of Southern Calif., March.

Mason, H. B. (2011). Seismic Performance Assessment in Dense Urban Environments. PhD dissertation, Department of Civil & Environmental Engineering, University of California, Berkeley.

McKee, K. L. (2001). Root proliferation in decaying roots and old root channels: a nutrient conservation mechanism in oligotrophic mangrove forests. *Journal of Ecology*, *89*(5), 876-887.

Mckenna, G. (1995). Grouted-in Installation of Piezometers in Boreholes. *Geotechnical Journal 32*, pp.355-363.

Mikkelsen, P. (2002). Cement-Bentonite Grout Backfill for Borehole Instruments. *Geotechnical News*, Iss. December 2002.

Mikkelsen, P., and Green, E. (2003). "Piezometers in Fully-Grouted Boreholes", paper presented at *International Symposium on Geomechanics*, Oslo, Norway, September.

Mitchell, A. R., Ellsworth, T. R., & Meek, B. D. (1995). Effect of root systems on preferential flow in swelling soil. *Communications in Soil Science & Plant Analysis*, *26*(15-16), 2655-2666.

Neil O. Anderson and Associates (2007). *Sevenmile Slough Sites 1, 2, & 3 Levee Improvements, Twitchell Island, Sacramento, California*. Project Number LFG-0229.

Newmark, N.M. (1965). "Effects of earthquakes on dams and embankments." *Geotechnique*. 15(2): 139-160.

Olson, S.M. and Stark, T.D. (2002) "Liquefied strength ratio from liquefaction flow failure case histories," Canadian Geotechnical Journal, Vol. 39, pp. 629-647.

Ordeñana, M. A., Van Vuren, D. H., & Draper, J. P. (2012). Habitat associations of California ground squirrels and Botta's pocket gophers on levees in California. *The Journal of Wildlife Management*, *76*(8), 1712-1717.

Park, S.-S. and Byrne, P.M. (2004) "Stress densification and its evaluation," Canadian Geotechnical Journal, Vol. 41, pp. 181-186.

Parker, M. M., & Van Lear, D. H. (1996). Soil heterogeneity and root distribution of mature loblolly pine stands in piedmont soils. *Soil Science Society of America Journal*, *60*(6), 1920-1925.

Paulson, R.W., Chase, E.B., Roberts, R.S., and Moody, D.W., Compilers, National Water Summary 1988-89-- Hydrologic Events and Floods and Droughts: *U.S. Geological Survey Water-Supply Paper 2375, 591 p.*

Pierson, T. C. (1983). Soil pipes and slope stability. *Quarterly Journal of Engineering Geology and Hydrogeology*, *16*(1), 1-11.

Puebla, H., Byrne, P.M., and Phillips, R. (1997). "Analysis of CANLEX liquefaction embankments: prototype and centrifuge models." *Canadian Geotechnical Journal*. 34: 641-657.

Punyamurthula, S., and Millet, R. (2012). "Forensics and Performance of California Levees with Vegetation", paper presented at *Levee Vegetation Research Symposium 2012*, Sacramento, CA, August 28-30. Sacramento: California Levee Vegetation Research Program.

Punyamurthula, S., and Millet, R. (2012). "Forensics and Performance of California Levees with Vegetation", paper presented at *Levee Vegetation Research Symposium 2012*, Sacramento, CA, August 28-30. Sacramento: California Levee Vegetation Research Program.

R.B. Fallgren and J.L. Smith. Ground displacement at San Fernando Valley Juvenile Hall during San Fernando earthquake. In The San Fernando, California, Earthquake of February 9, 1971, volume 3, pages 189 – 196. National Oceanic and Atmospheric Administration, 1973.

R.B. Sancio. Ground Failure and Building Performance in Adapazari, Turkey. Ph.d. dissertation, University of California, Berkeley, 2003.

R.W. Boulanger, I.M. Idriss, and L.H. Mejia. Investigation and evaluation of liquefaction related ground displacements at Moss Landing during the 1989 Loma Prieta earthquake. Technical Report UCD/CGM-95/02, UC Davis Center for Geotechnical Modeling, UC Davis, Davis, California, 1995.

Rathje, E.M. and Bray, J.D. (2000). "Nonlinear coupled seismic sliding analysis of earth structures." *Journal of Geotechnical and Geoenvironmental Engineering*. 126(11): 1002-1014.

Rauch, A.F. and Martin, J.R. (2000) "EPOLLS model for predicting average displacements on lateral spreads." *Journal of Geotechnical and Geoenvironmental Engineering*. 126(4): 360-371.

Reichman, O. J., & Smith, S. C. (1990). Burrows and burrowing behavior by mammals. *Current mammalogy*, *2*, 197-244.

Reichman, O., Whitham, T., and G. A. Ruffner (1982). Adaptive geometry of burrow spacing in two pocket gopher populations. *Ecology*, 63 pp.687-695.

Reid, M. E. (1997). Slope instability caused by small variations in hydraulic conductivity. *Journal of Geotechnical and Geoenvironmental Engineering*, *123*(8), 717-725.

Robertson, P.K., and Robertson, K.L. (2006) Guide to Cone Penetration Testing and it's Application to Geotechnical Engineering. *Gregg Drilling and Testing, Inc.* 126(4): 360-371.

Rutherford and Chekene. Geotechnical investigation: Moss Landing Facility (Technology Building), Monterey Bay Aquarium Research Institute. Technical report, Monterey Bay Aquarium Research Institute, 1988.

S.W. Chang. Seismic Response of Deep Stiff Soil Deposits, Ph.d. disseration, University of California, Berkeley, 1996.

Seed, H.B. (1979) "Soil Liquefaction and Cyclic Mobility Evaluation for Level Ground During Earth-quakes," J. of the Geotechnical Engineering Div., Vol. 105, No. GT2, pp. 201-255.

Seed, H. B.; Idriss, I. M. (1982) Ground Motions and Soil Liquefaction During Earthquakes. EERI Monograph, Berkeley, California, 134 pages.

Seed, R.B., Mitchell, J. K., and Seed, H.B. (1990). Kettleman hills waste landfill slope failure. II: stability analysis. Journal of Geotechnical Engineering 116 (4), 669-690.

Seed, R.B., Cetin, K.O., Moss, R.E.S., Kammerer, A.M., Wu, J., Pestana, J.M., Riemer, M.F., Sancio, R.B., Bray, J.D., Kayen, R.E., and Faris, A. (2003) "Recent Advances in Soil Liquefaction Engineering: A Uni-fied and Consistent Framework," 26th Annual ASCE Los Angeles Geotechnical Spring Seminar, Keynote Presentation, Long Beach, Calif., April 30.

Seid-Karbasi, M., and Byrne, P.M. (2004) "Embankment dams and earthquakes," J. Hydropower & Dams, Vol. 11(2), pp. 96-102.

Shields, F. D., & Gray, D. H. (1992). Effects of Woody Vegetation on Sandy Levee Integrity. *JAWRA Journal of the American Water Resources Association*, *28*(5), 917-931.

Shields, F. D., & Gray, D. H. (1992). Effects of woody vegetation on sandy levee integrity. *JAWRA Journal of the American Water Resources Association*, *28*(5), 917-931.

Shriro, M. Cobos Roa, D. Bray, J., Sitar, N. Lichter, J. Evans, R. Kroll, R. (2011)." Study of Levee Seepage and Slope Stability in Relation to Roots". *Association of State Dam Safety Official 2011 Conference Papers*.

T.D. O' Rourke, B.L. Roth, and M. Hamada. Large ground deformation and their effects on lifeline facilities: 1971 San Fernando Earthquake. In T.D. O'Rourke and M. Hamada, editors, *Case studies of liquefaction and lifeline performance during past earthquakes, volume 2 of NCEER-92-0002*, Buffalo, N.Y., 1992b. National Center for Earthquake Engineering Research.

Thompson, J. (2006). Early Reclamation and Abandonment of the Central Sacramento-San Joaquin Delta. *Sacramento History: Journal of the Sacramento County Historical Society*, VI (1-4), pp. 41-72.

United States Army Corps of Engineers (USACE) (2007), "*Treatment of Vegetation within Local Flood-Damage-Reduction Systems*," Draft Final White Paper, April 20, 2007.

United States Army Corps of Engineers (USACE) (2009). *Guidelines for Landscape Planting and Vegetation Management at Levees, Floodwalls, Embankment Dams, and Appurtenant Structures, ETL 1110-2-571*.

United States Army Corps of Engineers (USACE), Sacramento District (1956). *Design Memorandum No.1, American River Levee General Design*. American River Project. Sacramento, CA.

United States Army Corps of Engineers (USACE), Sacramento District (1999). *American River Watershed Project (Common Features), Right (North) Bank Levee Strengthening*. American River, California.

URS (2009). *General Reevaluation Report*. American River Common Features . Sacramento County, California: U.S. Army Corps of Engineers Sacramento District, Contract Number W91238-08-D-0001, Delivery Order CM04.

URS Corporation (2011), *Segment 1047 Summary*, RD 1601, April 2011.

USGS, 5499487 Jersey Island, CA 7.5X7.5 (1910, Revised 1932)

USGS, Rio Vista, CA 15X15 (1952)

Van Vuren, D., and Ordeñana, M. (2012). *Burrow Dimensions of Ground Squirrels, with Special Reference to the California Ground Squirrel* . [report] California Levee Vegetation Research Program.

Woodward-Clyde Consultants. Phase i - geotechnical study, Marine Biology Laboratory, California State University, Moss Landing, California. Technical report, California State University, San Jose, California, 1990.

Yang, Z., Elgamal, A. and Parra, E. (2003). "A computational model for cyclic mobility and associated shear deformation." *Journal of Geotechnical and Geoenvironmental Engineering*. 129(12): 1119-1127.

Yang, Z., Elgamal, A., Adalier, K., and Sharp, M.K. (2004). "Earth dam on liquefiable foundation and remediation: numerical simulation of centrifuge experiments." *Journal of Engineering Mechanics*. 130(10): 1168-1176.

Yegian, M.K., Marciano, E.A., and Ghahraman, V.G. (1991). "Earthquake-induced permanent deformation: probabilistic approach. *Journal of Geotechnical Engineering*. 117(1): 35-50.

Youd T.L., Idriss I.M., Andrus R.D., Arango I., Castro G., Christian J.T., Dobry R., Finn W.D.L., Harder Jr. L.F., Hynes M.E., Ishihara K., Koester J.P., Liao S.S.C., Marcuson III W.F., Martin G.R., Mitchell J.K., Moriwaki Y., Power M.S., Robertson P.K., Seed R.B., & Stokoe II K.H., 2001. Liquefaction resistance of soils: summary report from the 1996 NCEER and 1998 NCEER/NSF workshops on evaluation of liquefaction resistance of soils. *Journal of Geotechnical and Geoenvironmental Engineering*. Vol. 127(10): 817-903.

Youd, T.L., Bardet, J.P., and Bray, J.D. (2000). Kocaeli, Turkey Earthquake of August 17, 1999 Reconnaissance Report, in *Earthquake Spectra* Journal, Suppl. A to Vol. 16, EERI.

Youd, T.L., Hansen, C.M., and Bartleet, S.F. (2002) "Revised multilinear regression equations for prediction of lateral spread displacement," *Journal of Geotechnical and Geoenvironmental Engineering*. Vol. 128(12): 1007-1017.

Zhang, G., Robertson, P.K., and Brachman, R.W.I. (2004). "Estimating liquefaction-induced lateral spread displacements using the standard penetration test or cone penetration test." *Journal of Geotechnical and Geoenvironmental Engineering*. 130(8): 861-871.

Ziemer, R. R. (1981). Roots and the stability of forested slopes. *Erosion and Sediment Transport in Pacific Rim Steeplands, IAHS Publ*, (132).

# APPENDIX 2A

## Soil Borings and Instrument Logs – Cal Expo Test Site

Prior to site selection, available soil boring logs and geotechnical information were reviewed (see Appendix 2B) and two hand-auger soil borings to a depth of 9 feet were performed at the locations shown on Figure A-1. The logs are presented as Figures A-2 and A-3.

During installation of piezometers and tensiometers at the site, instrument holes were logged. Logs are presented on pages A-5 through A-10. Instruments P4B-84 and T4A-18 are shown on Figure A-1 and soil logs are provided for these locations, though the instruments failed to function in the field and are therefore not shown on other figures or data sheets.
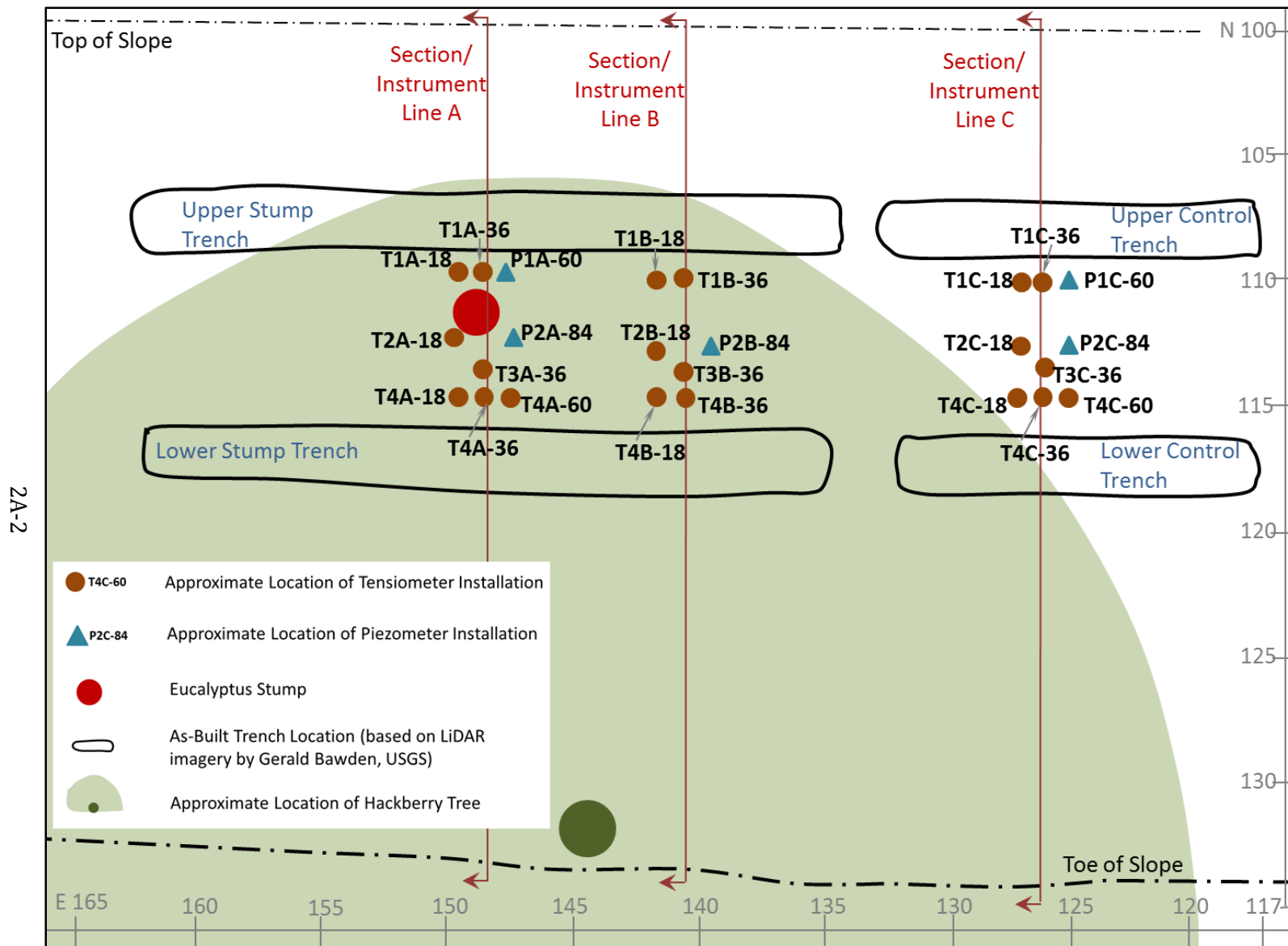
**Figure A-1**. Site plan showing locations of hand auger soil borings and logged instrument holes

| BORING LOCATION: N38.58953, W121.43249 | PROJECT NUMBER | BORING NUMBER | EX-HB1 | 6/24/2010 |
|---|---|---|---|---|
| | SAFCA-CALEXPO | SHEET | 1 OF 2 | |

## SOIL BORING LOG

| PROJECT | Cal Expo Field Investigation | DRILLED BY | J. Hollenback |
|---|---|---|---|
| ELEVATION | Levee Crest | LOGGED BY | M. Shriro |
| DRILLING METHOD AND EQUIPMENT | Hand Auger (4" Dia) | REVIEWED BY | D.Cobos-Roa |
| WATER LEVELS | n/a | START 8:30am | FINISH 10:00am |

| STANDARD PENETRATION TEST RESULTS 6-6-6" (N) | SAMPLE Number | SAMPLE BAG SAMPLE Depth | RECOVERY | LITHOLOGY | DEPTH BELOW SURFACE (ft) | SOIL DESCRIPTION SOIL NAME, USCS GROUP SYMBOL, COLOR, MOISTURE CONTENT, RELATIVE DENSITY OR CONSISTENCY, SOIL STRUCTURE, MINERALOGY | COMMENTS DEPTH OF CASING, DRILLING RATE, DRILLING FLUID LOSS, TESTS AND INSTRUMENTATION, ETC... |
|---|---|---|---|---|---|---|---|
| | | | | | 0.0 | Clayey Silt (ML), brown, moist, stiff, fine sand (FILL) | |
| | | 1/2' - 1' | | | 0.5 | | |
| | | | | | 1.0 | | |
| | | | | | 1.5 | | increased clay content at 1.5' |
| | | | | | 2.0 | | |
| | | | | | 2.5 | | |
| | | 3 1/4' - 3 1/2' | | | 3.0 | Silt (ML), brown with trace clay and fine sand (FILL) | |
| | | | | | 3.5 | | |
| | | | | | 4.0 | | |
| | | 4 1/2' - 5' | | | 4.5 | | increased clay content at 4.5' |
| | | | | | 5.0 | | |
| | | | | | 5.5 | | |
| | | | | | 6.0 | | |
| | | 6 1/2' - 6 3/4' | | | 6.5 | | |
| | | | | | 7.0 | Silty Fine Sand (SM),brown, moist with trace rootlets thinly interbedded with SILT (ML), brown mottled with yellow brown, with clay and fine sand (FILL) | fine roots at 6 3/4 feet below grade |
| | | 7 1/2 - 7 3/4 | | | 7.5 | | |
| | | | | | 8.0 | | |
| | | 8 1/4' -8 1/2' | | | 8.5 | | |
| | | | | | 9.0 | Bottom of Boring at 9 feet; No Groundwater Encountered | |

Notes:
FP - 5-inch Fixed Piston Sampler
VS - Field Vane Shear Test
BS - Bag Sample
Soil type transition
∇ Water Table (not encountered during drilling)

**Figure A-2.** Boring log for hand-auger boring 1 (HB1). For location, see Figure A-1.

| BORING LOCATION: N38.58959, W121.43233 | PROJECT NUMBER | BORING NUMBER | EX-HB2 | 6/24/2010 |
|---|---|---|---|---|
| | SAFCA-CALEXPO | SHEET 2 | OF 2 | |

## SOIL BORING LOG

| PROJECT | Cal Expo Field Investigation | DRILLED BY | J. Hollenback |
|---|---|---|---|
| ELEVATION | ~10feet down from crest | LOGGED BY | M. Shriro |
| DRILLING METHOD AND EQUIPMENT | Hand Auger (4" Dia) | REVIEWED BY | D.Cobos-Roa |
| WATER LEVELS | n/a | START 9:00am FINISH 12:00pm | |

| STANDARD PENETRATION TEST RESULTS 6-6-6" (N) | SAMPLE Number | SAMPLE BAG SAMPLE Depth | RECOVERY | LITHOLOGY | DEPTH BELOW SURFACE (ft) | SOIL DESCRIPTION — SOIL NAME, USCS GROUP SYMBOL, COLOR, MOISTURE CONTENT, RELATIVE DENSITY OR CONSISTENCY, SOIL STRUCTURE, MINERALOGY | COMMENTS — DEPTH OF CASING, DRILLING RATE, DRILLING FLUID LOSS, TESTS AND INSTRUMENTATION, ETC... |
|---|---|---|---|---|---|---|---|
| | | | | | 0.0 | Silt (ML), brown with trace clay and fine sand (FILL) | |
| | | | | | 0.5 | | |
| | | 1' - 1 1/2' | | | 1.0 | | |
| | | 1 1/2' - 1 3/4' | | | 1.5 | | |
| | | 2' - 2 1/2' | | | 2.0 | CLAYEY SILT (ML), olive brown, moist, trace fine sand, trace fine rootlets, increased soil structure (FILL) | |
| | | 2 1/2' - 2 3/4' | | | 2.5 | | |
| | | | | | 3.0 | SANDY SILT (ML) gradually grading to Silty Sand (SP), moist, olive brown, very fine sand, trace fine rootlets (FILL) | |
| | | 3 1/2' - 3 3/4' | | | 3.5 | | |
| | | | | | 4.0 | | |
| | | 4 3/4' - 5 1/4' | | | 4.5 | | |
| | | | | | 5.0 | | |
| | | | | | 5.5 | | |
| | | 6' - 6 1/2' | | | 6.0 | | |
| | | | | | 6.5 | | |
| | | | | | 7.0 | SAND (SP), yellow brown, moist, sand is clean and fine grained | |
| | | 7 1/4' - 7 1/2' | | | 7.5 | | |
| | | | | | 8.0 | | |
| | | 8 1/4' -8 1/2' | | | 8.5 | SILTY CLAY (CL), olive brown, moist | |
| | | | | | 9.0 | Bottom of Boring at 9 feet; No Groundwater Encountered | |

Notes:
FP - 5-inch Fixed Piston Sampler
VS - Field Vane Shear Test
BS - Bag Sample
Soil type transition
Water Table (not encountered during drilling)

**Figure A-3.** Boring log for hand-auger boring 2 (HB2). For location, see Figure A-1.

# Instrument Logs

**T1A-18; Coordinates = (150.3, 111)**

0 – 19.5"   Sandy Silt (ML) to silty sand (SM), trace clay, brown, moist. Decomposed root at 10".

Bottom of hole at 19.5"


**T1A-36; Coordinates = (148.5, 111)**

0 – 12"     Sandy Silt (ML) to silty sand (SM), brown, moist.

12"-37.5"  Clayey silt (ML), brown, moist.

Bottom of hole at 37.5"


**P1A-60; Coordinates = (147, 111)**

0 – 14"     Silty sand (SM) to sandy silt (ML), trace clay, brown, moist, live roots between 6"-12".

14"-19"    Sandy silt (ML) with clay, brown, moist.

19"-45"    Silty sand (ML) with clay, brown, moist, higher clay content inclusions.

              Harder drilling and roots (live) encountered at 3'. Lower clay content at 3.25 ft.

45"-60"    Sandy silt (ML), brown, moist; r

              roots less than ¼" diameter at 4'.

              Decreasing clay content to cleaner sand at 4 ¼ and siltier at the base.

Bottom of hole at 60"

**T2A-18; Coordinates = (148.75, 113.25)**

0 – 9"      Sandy Silt (ML) to silty sand (SM), trace clay, brown, moist. Loose zone between 6"-12".

9"-19.5"   Clayey silt (ML), brown, moist.

Bottom of hole at 19.5"

**P2A-84; Coordinates = (146.3, 113.25)**

0 – 48"    Silty sand (SM), trace clay, moist, brown, decayed root at 6" with pieces visible to 1.5 ft.

Small pieces of gravel and ¼" diameter live root at 2'.

Small clay pockets with silty sand matrix and live root of 5/8" diameter at 36".

48"-52"    Sandy silt (ML) with trace clay, moist, brown.

52"-68"    Silty sand (SM), light brown, moist, fine root, lightly cemented.

68"-78"    Clayey silt (ML) with trace sand, brown, moist.

78"-81"    Silty clay (CL), brown, moist.

81"-84"    Silty sand (SM), trace clay, light brown, moist, decreasing silt toward base.

Bottom of hole at 84"


**T3A-36; Coordinates = (147.7, 114.15)**

0 – 6"    Decayed root

6"-23"    Sandy silt (ML) to silty sand (SM), brown, moist

23"-37.5"  Clayey silt (ML), brown, moist.

Bottom of hole at 37.5"


**T3A-18; Coordinates = (149.5, 115.75)**

0 – 12"    Silty sand (SM), trace clay, moist, brown; decomposed organic matter at 6"-12".

12"-19.5"  Sandy silt with clay (ML), moist, brown.

Bottom of hole at 19.5"


**T4A-36; Coordinates = (148.5, 115.75)**

0 – 19"    Sandy silt (ML) with trace clay and decomposed organic matter in upper 6", brown, moist.

19"-25"    Sandy silt with clay (ML), moist, dark brown.

25"-30"    Silty sand (SM) with trace clay, light brown, moist, lightly cemented.

30"-37"    Sandy silt (ML), brown, moist, fine roots at 30-37" with decomposed organic matter at 35" that damaged gauge auger.

Bottom of hole at 37"

**T4A-60; Coordinates = (147.25, 115.75)**

0 – 12"    Sandy silt (ML) with clay, brown, moist, pyritic specs in sand fraction.

12"-18"    Clayey silt with sand (ML), brown, moist.

18"-36"    Silty sand (SM), light brown, moist, pyritic sands.

36"-60"    Clayey silt (ML), moist, brown, with very fine sand.

Bottom of hole at 60"


**T1B-18; Coordinates = (142, 111)**

0 – 19.5"   Sandy silt (ML) with clay, brown, moist.

Bottom of hole at 19.5"


**T1B-36; Coordinates = (141, 111)**

0 – 6"      Sand (SP) with clay, brown, moist, fine sand.

6"-12"      Silty sand (SM) with clay, moist, brown, very fine sand.

12"-24"     Sandy silt to silty sand (ML/SM), light brown, moist, very loose between 18" and 24".

            Auger dropped from 18" to 24" with single blow. Possible burrow.

24"-36"     Silty sand (SM) with clay, brown, moist, very fine sand.

36" – 37.5 Sandy silt (ML) with clay, brown, moist.

Bottom of hole at 37.5"


**P2B-84; Coordinates = (140, 113.25)**

0 – 16"     Silty sand to sandy silt (SM/ML) with trace clay, brown, moist.

16"-42"     Silty sand (SM) with trace clay, brown, moist, grades to almost no clay.

42"-60"     Sandy silt (ML) with clay, brown, moist.

60"-66"     Silty sand (SM), brown, moist, fine sand.

66"-75"     Sandy silt (ML) with clay, brown, moist.

75"-78"     Sand (SP), brown, moist, fine grained.

78"-84"     Silty clay (CL), brown, moist.

Bottom of hole at 84"

**T2B-18; Coordinates = (141, 113.25)**

0 – 19.5"   Silty sand with clay (SM), brown, moist, fine sand.

Bottom of hole at 19.5"


**T3B-36; Coordinates = (141, 114.2)**

0 – 6"        Silty sand (SM), brown, dry, fine sand.

6"-18"       Silty sand with clay (SM), brown, moist.

18"-30"     Sandy silt to silty sand (ML/SM), brown, moist

30"-37.5"  Silty sand (SM), brown, moist, fine sand.

Bottom of hole at 37.5"


**T4B-18; Coordinates = (142, 115.25)**

0 – 19.5"   Sandy silt (ML), brown, moist.

Bottom of hole at 19.5"


**T4B-36; Coordinates = (141, 115.2)**

0 – 24"      Sandy silt (ML) with trace clay, brown.

                 Increasing clay content with depth.

                 24"-37.5"  Silty sand (SM) with clay, brown, moist, fine sand.

Bottom of hole at 37.5"


**T1C-18; Coordinates = (126.5, 111)**

0 – 6"        Silty sand (SM) with trace clay, brown, moist, some fine gravel.

6"-19.5"     Silty sand (SM) with clay, moist, brown, sand very fine grained

Bottom of hole at 19.5"


**T1C-36; Coordinates = (125.5, 111)**

0 – 12"      Silty sand with clay (SM), brown, moist.

12"-37.5"  Silty sand to sandy silt (SM/ML), moist, brown.

Bottom of hole at 37.5"

### P1C-60; Coordinates = (124.5, 111)

0 – 12"    Silty sand (SM), moist, fine roots

12"-30"    Sandy silt with clay (ML), brown, moist, live 5/8" diameter root at 24".

30"-42"    Silty sand with trace clay (SM), brown, moist, very fine sand, root at 36" (3/8" dia).

        3/8" diameter live root at 36".

        3/8" diameter live root at 42".

42"-60"    Silty sand (SM), brown, moist, very fine sand, fine live roots.

        Clay content low near top of layer and increasing at 4.5'.

Bottom of hole at 60"


### T2C-18; Coordinates = (126.5, 113.25)

0 – 6"     Silty sand (SM), brown, moist.

6"-19.5"   Sandy silt (ML), brown, moist.

Bottom of hole at 19.5"


### P2C-84; Coordinates = (124, 113.25)

0 – 12"    Silty sand (SM) with trace clay, brown, moist.

12"-18"    Sandy silt with clay (ML), brown, moist.

18"-30"    Clayey silt (ML), brown, moist.

30"-36"    Clayey sand (SM) with silt, brown, moist, very fine sand.

36"-54"    Silty sand with clay (SM) brown, moist, very fine sand, some fine roots.

54"-66"    Silty sand (SM), moist, light brown, lightly cemented, very fine sand.

66"-72"    Sand (SP), moist, light brown, very fined grained with pockets of dark brown silty clay (CL)

72"-78"    Silty sand with clay (SM), brown, moist

78"-90"    Silty Clay (CL), brown, moist. Live root (1/4" diameter) at 7.5 ft.

Bottom of hole at 90"

**T3C-36; Coordinates = (125.5, 114.2)**

0 – 12"     Silty sand (SM), brown, moist, fine sand.

12"-37.5" Sandy silt (ML), brown, moist, increased clay content with depth.

Bottom of hole at 37.5"


**T4C-18; Coordinates = (126.5, 115.75)**

0 – 19.5"   Silty sand (SM), brown, moist, fine roots, higher silt content with depth.

Bottom of hole at 19.5"


**T4C-36; Coordinates = (125.5,115.75)**

0 – 6"      Silty sand (SM), brown, moist, fine sand.

6"-30"      Sandy silt (ML), brown, moist.

30"-37.5" Clayey silt (ML) with sand, olive brown, moist.

Bottom of hole at 37.5"


**T4C-60; Coordinates = (124.5, 115.75)**

0 – 18"     Silty sand (SM), brown, moist, fine sand.

18"-30"     Sandy silt (ML), brown, moist.

30"-42"     Sand with silt (SM), light brown, moist, fine, uniform

42"-48"     Sandy silt with clay (ML), moist, light brown with reddish stains

48"-60"     Clayey silt (ML) with sand, moist, brown

Bottom of hole at 60"

# APPENDIX 2B

## Regional Soil Data – Cal Expo Test Site

The study site bordering the California Exposition and State Fair ('Cal Expo') is located at approximately Levee Mile 0.75, Unit 3 within the American River Flood Control District (ARFCD) or approximately River Mile 3130 of the American River North Levee. URS completed a study in 2009 documenting regional soil and stability conditions for the area known as the American River Common Features, of which our study site is a part. The study is called "American River Common Features General Re-evaluation Report", or the 'ARCF GRR', dated March 24, 2009.

The report provides a detailed summary and analysis of geotechnical data within the study area. Reaches are identified and analyzed for seepage and stability behavior in a number of scenarios with representative cross sections. The closest section to the east and west of our study site were identified and the available relevant data summarized herein.

Figure 2B- 1 provides a site plan excerpted from the ARCF GRR and modified to show the Cal Expo site as well as the sections identified as most relevant to our study. Figure 2B- 2 through Figure 2B- 5 show the cross sections of soil stratigraphy closest to the site as well as graphically represented soil borings. Table 2B- 1 through Table 2B- 5 provide a summary of available index testing and soil strength assumptions for sections east and west of the study site.

In 1999, a set of design drawings for the American River Watershed project show proposed levee improvements including construction of a slurry wall in the locations shown on Figure 2B- 6. Drawings include a topographic map showing soil borings and cone penetration tests and utilities in the area of the site (Figure 2B- 7). The site is shown to be at Station 9+100 based on the stationing shown on the plans and the pipeline encountered during construction of our field test appears on the plans. The Eucalyptus tree appears to be intact in the aerial photograph on the plan, however the plans to not specify removal of the tree for construction of the slurry wall, while other trees nearby are slated for removal. The aerial photo used may not have been up to date and the tree may have already been removed at the time of the plan. Based on the aerial photo review discussed in Section 3.2 of Volume 1A of this report, the tree appears to have been removed prior to 1998. Figure 2B- 8 shows the closest soil boring log, DH-10, as shown on Figure 2B- 7. Figure 2B- 9 shows a profile view of the stratigraphy with overlain borings. This is the only information available for CPT 96-3. Figure 2B- 10 shows a close in view of the graphical logs of Boring DH-10 and CPT 96-3 as well as the legend for interpretation of the graphical log. Figure 2B-11 shows cross sections of the levee geometry in the vicinity of our study site. Figure 2B-12 provides details with regard to the history and ownership of the pipeline encountered during our excavation. The pipeline was relocated into its current position as part of the construction of the slurry wall.

In 1956, the American River Levee General Design (USACE, 1956) provides some site history and shows that the levee site was likely not raised in order to comply with Corps standards in 1956. The report shows that the levee was already at design elevation at the location of our test site (Figure 2B- 13 through Figure 2B- 14). Records for construction of the original levee were not located.

**F3 EXISTING CONDITIONS GEOTECHNICAL REPORT**
**For American River Common Features**

**AMERICAN RIVER COMMON FEATURES**
**GENERAL REEVALUATION REPORT**
**SACRAMENTO COUNTY, CALIFORNIA**

| | |
|---|---|
| **Contract No.:** | **W91238-08-D-0001** |
| **Delivery Order:** | **CM04** |

**US Army Corps**
**of Engineers**
Sacramento District

**PREPARED BY URS**                    **24 MARCH 2009**
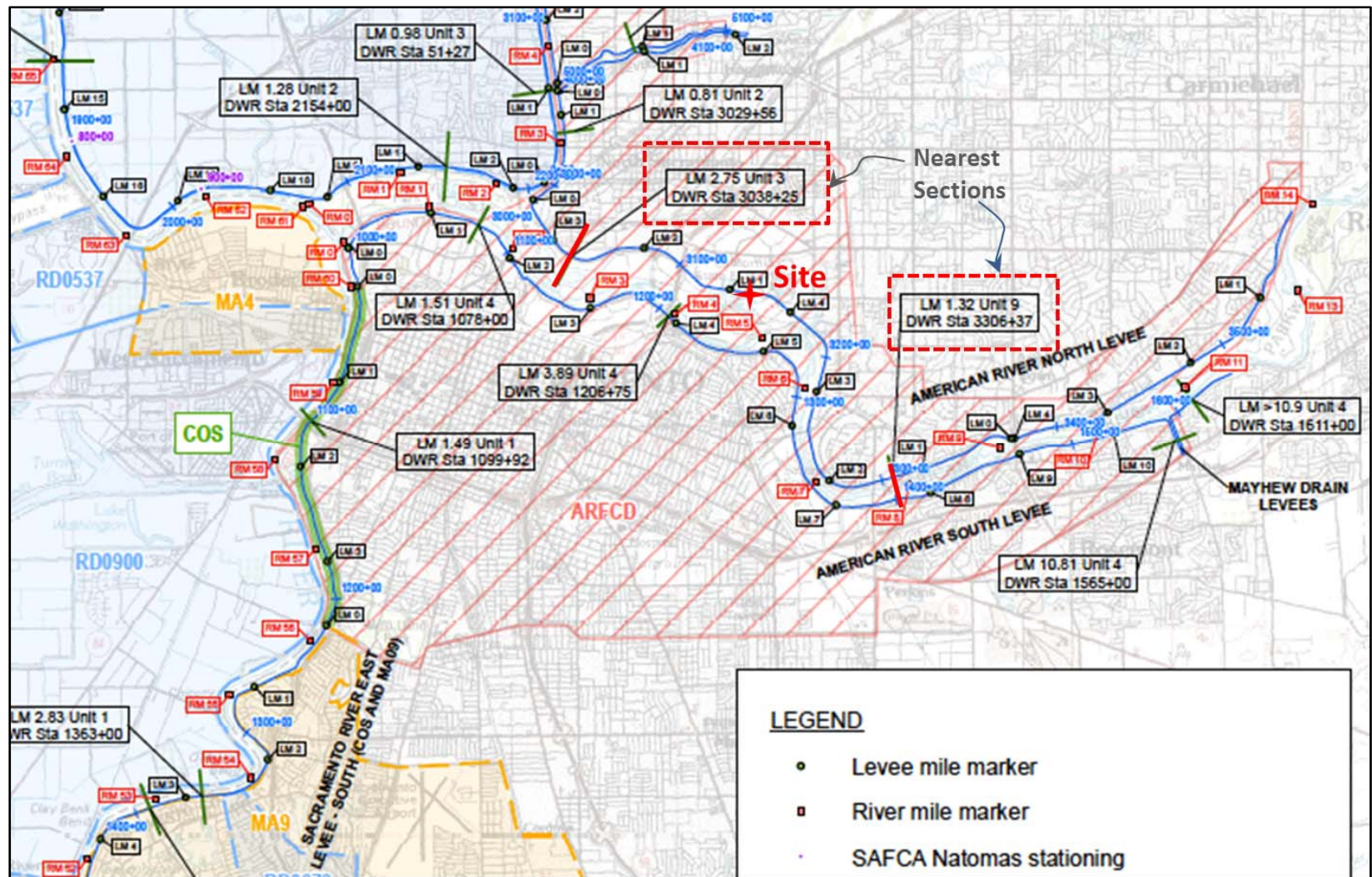
Figure 2B- 1.Vicinity map showing the Cal Expo project site, levee mile (USACE) and river mile (CDWR) stationing, and nearest URS geologic sections to the east and west of the project site. Figure excerpted and modified from URS, 2009.
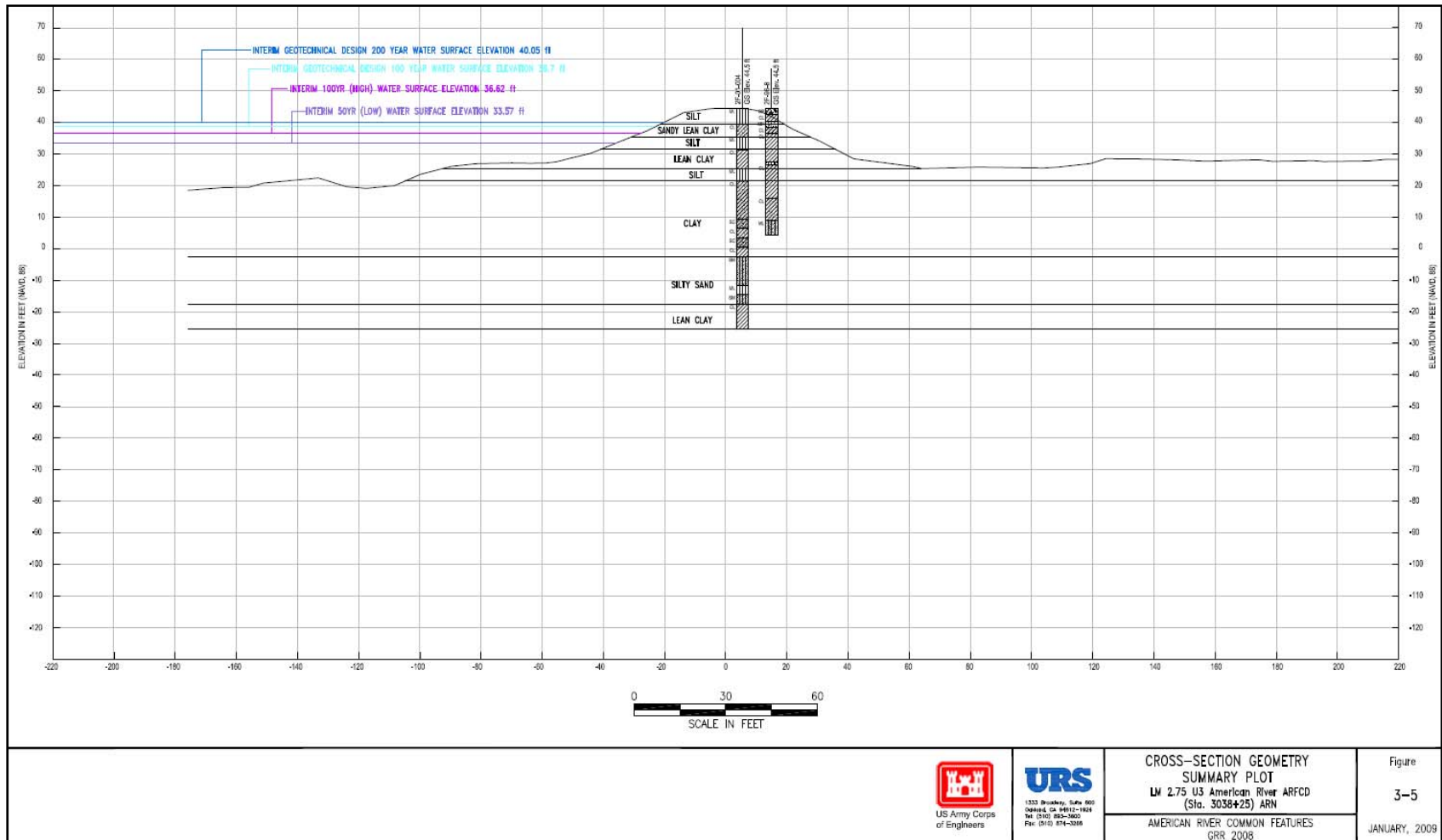
Figure 2B- 2.Geologic Section at LM 2.75, Unit 3 (RM 3038+25 of the American River North levee) within the American River Flood Control District (ARFCD). Source: URS, 2009.
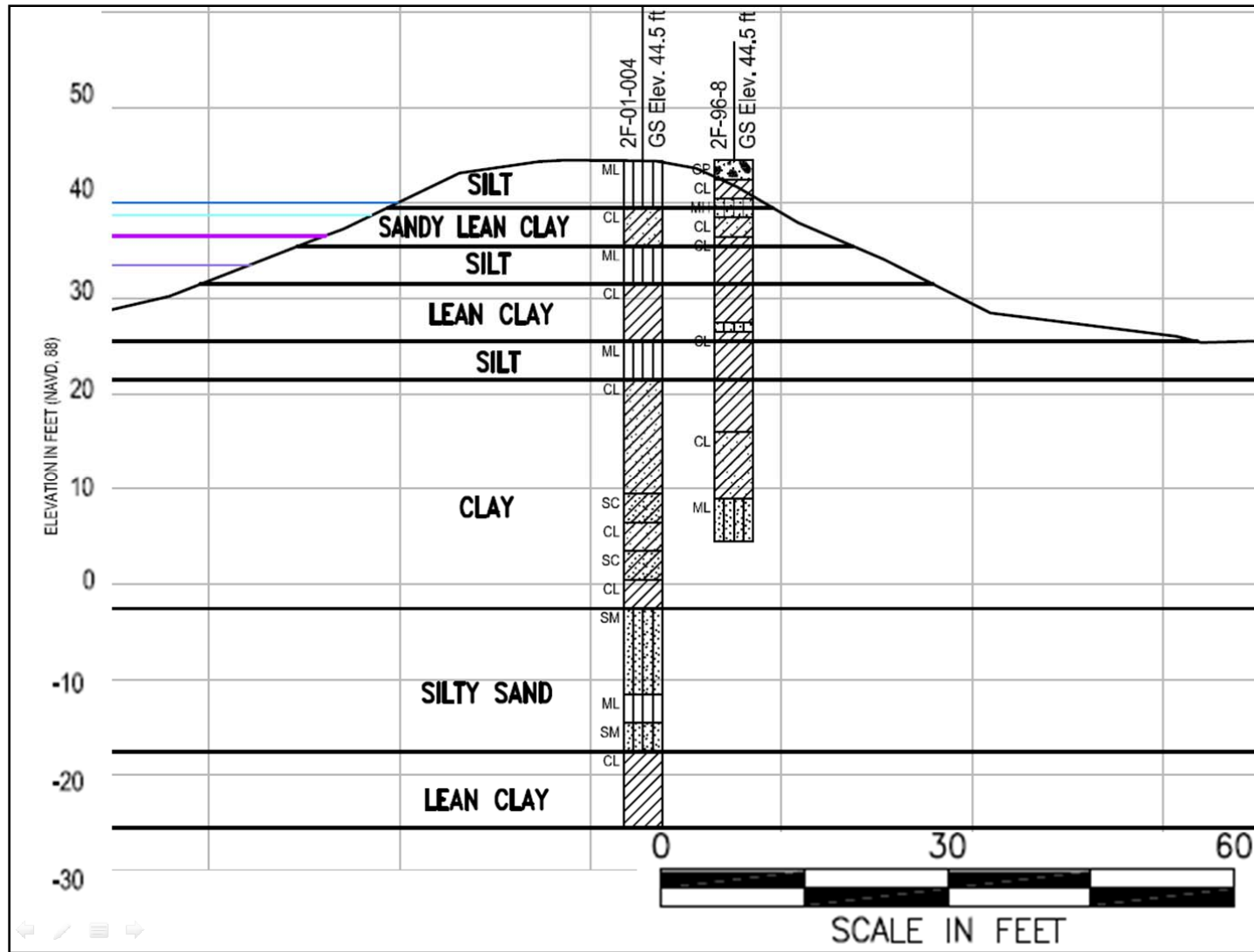
Figure 2B- 3. Close-in view of soil borings at LM 2.75, Unit 3 (RM 3038+25 of American River North levee) within the American River Flood Control District (ARFCD) as shown on Figure C.2. Excerpted and modified from URS, 2009.
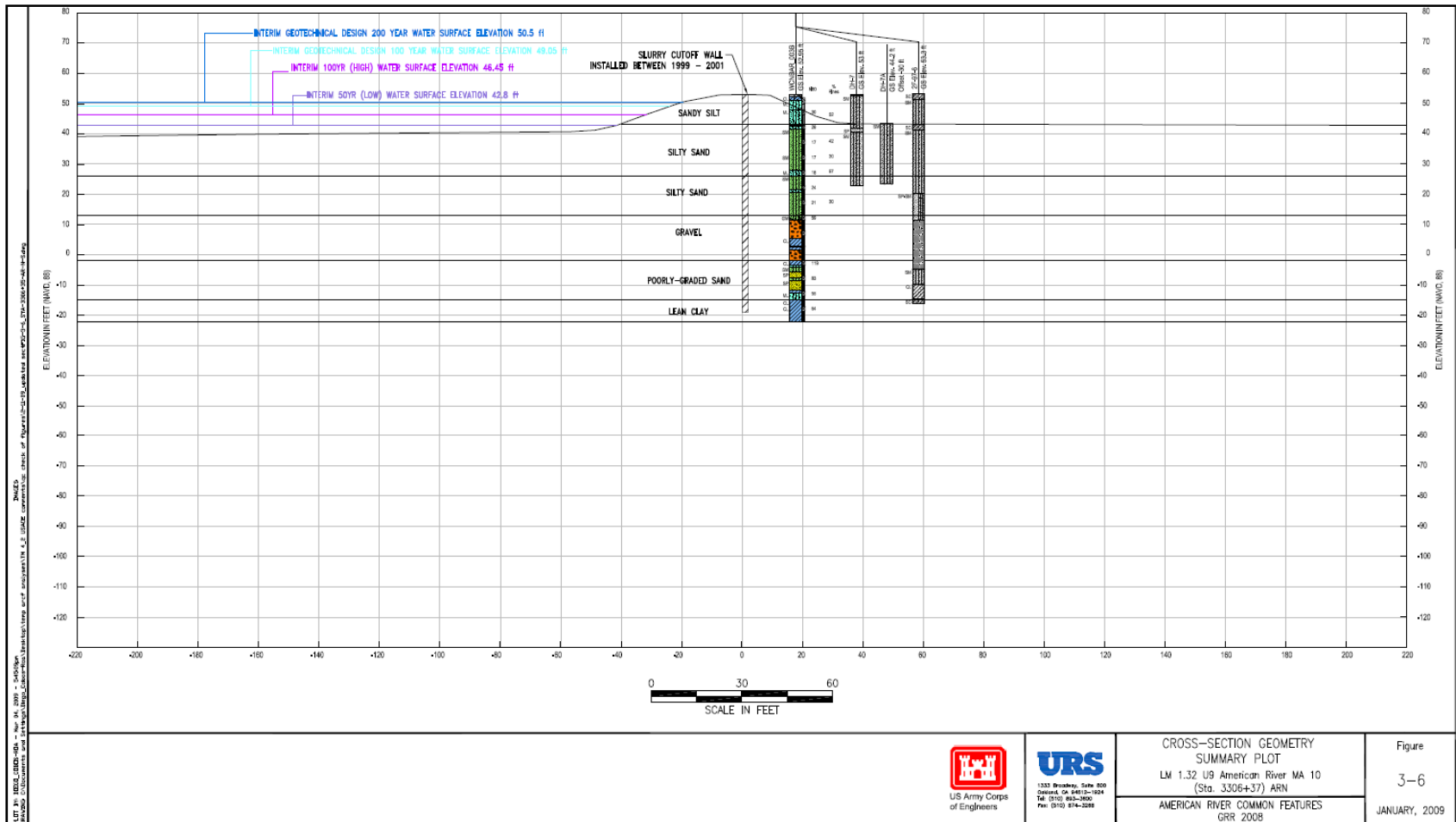
Figure 2B- 4. Close-in view of soil borings at LM 1.32, Unit 9 (RM 3306+37 of American River North levee) within American River MA 10. Source: URS, 2009.
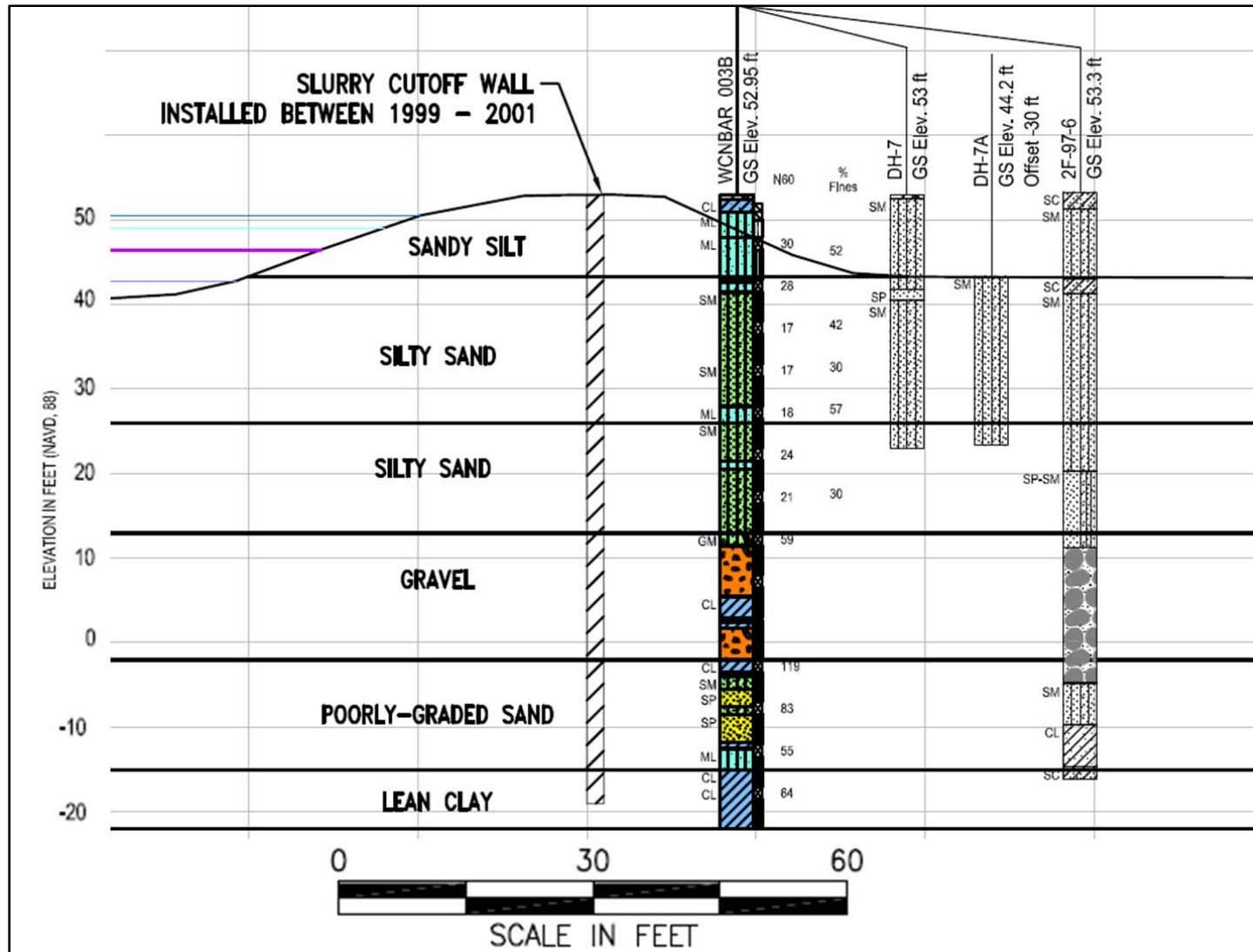
Figure 2B- 5. Geologic Section at LM 1.32, Unit 9 (RM 3306+37) within American River MA 10. Excerpted and modified from URS, 2009.

Table 2B- 1. Summary of strength parameters for sections at LM 1.32 U9 (DWR RM Sta. 3306+35) and LM 2.75 U3 (DWR RM Sta 3038+25) of the American River North levee.Source: URS 2009.

| American River North - LM 1.32 U9 (DWR Sta. 3306+35) | | | | | | | |
|---|---|---|---|---|---|---|---|
| Material Description | Material Number | Strength for Partial Pool and Steady State | | Strengths for Rapid Drawdown | | | |
| | | | | Drained ($K_c = K_f$) | | Undrained ($K_c = 1$) | |
| | | $\phi'$ | c' | $\phi'$ | c' | $\psi$ | d |
| | | (degrees) | (psf) | (degrees) | (psf) | (degrees) | (psf) |
| ML | 1 | 35 | 0 | 35 | 0 | 14.6 | 480 |
| SM | 2 | 32 | 0 | 32 | 0 | - | - |
| SM | 3 | 33 | 0 | 33 | 0 | - | - |
| GM | 4 | 46 | 0 | 46 | 0 | - | - |
| SP | 5 | 40 | 0 | 40 | 0 | - | - |
| CL | 6 | 35 | 0 | 35 | 0 | 16.9 | 5078 |

| American River North - LM 2.75 U3 (DWR Sta. 3038+25) | | | | | | | |
|---|---|---|---|---|---|---|---|
| Material Description | Material Number | Strength for Partial Pool and Steady State | | Strengths for Rapid Drawdown | | | |
| | | | | Drained ($K_c = K_f$) | | Undrained ($K_c = 1$) | |
| | | $\phi'$ | c' | $\phi'$ | c' | $\psi$ | d |
| | | (degrees) | (psf) | (degrees) | (psf) | (degrees) | (psf) |
| ML | 1 | 35 | 0 | 35 | 0 | | |
| CL | 2 | 35 | 0 | 35 | 0 | 11.5 | 551 |
| ML | 3 | 33 | 0 | 33 | 0 | | |
| CL | 4 | 35 | 0 | 35 | 0 | 11.5 | 1185 |
| ML | 5 | 33 | 0 | 33 | 0 | 11.8 | 1522 |
| CL | 6 | 33 | 0 | 33 | 0 | 10.2 | 1753 |
| SM | 7 | 40 | 0 | 40 | 0 | - | - |
| CL | 8 | 31 | 0 | 31 | 0 | - | - |

Table 2B- 2. Index testing and blowcount summary for boring 2F-96-8 at American River North 3038+25. Source: URS 2009.

| PROJECT NAME: | American River Common Features GRR |
|---|---|
| PROJECT NUMBER: | 26816760.45300 |
| Reach ID: | American River North 3038+25 2F-01-004 |

| Analysis By: | Michael Kynett | Date: | 9/30/2008 |
|---|---|---|---|
| Check By: | | Date: | |

Highlight in green any assumed value    Inputs are highlighted in grey

| | | | | | | | | | | | | | | ICU | | |
|---|---|---|---|---|---|---|---|---|---|---|---|---|---|---|---|---|
| Boring ID | Ground Surface Elevation | Ground Water Elevation | Energy Ratio | Depth to Top of Sample | USCS Group Name and Symbol | Sampler Type | γm | Blows foot, N | % finer than No200 | Liquid limit, LL | Plastic Index, PI | Moisture content | UU - su | Confining stress | su | Consol. σ'max |
| (-) | (ft) | (ft) | (%) | (ft) | (-) | (-) | (pcf) | (-) | (%) | (%) | (%) | (%) | (psf) | (psf) | (psf) | (psf) |
| 2F-96-8 | 42 | 22 | 80 | 0.5 | GP | SPT | 135 | 18 | 5 | | | | | | | |
| 2F-96-8 | 42 | 22 | 80 | 1 | CL | SPT | 110 | 24 | 90 | | | | | | | |
| 2F-96-8 | 42 | 22 | 80 | 2.5 | MH | SPT | 120 | 19 | 70 | | | | | | | |
| 2F-96-8 | 42 | 22 | 80 | 4.5 | CL | SPT | 110 | 15 | 85 | 28 | 8 | | | | | |
| 2F-96-8 | 42 | 22 | 80 | 8.5 | CL | SPT | 110 | 7 | 85 | | | | | | | |
| 2F-96-8 | 42 | 22 | 80 | 10.5 | CL | SPT | 110 | 5 | 85 | | | | | | | |
| 2F-96-8 | 42 | 22 | 80 | 12.5 | CL | SPT | 110 | 6 | 90 | | | | | | | |
| 2F-96-8 | 42 | 22 | 80 | 14.5 | CL | SPT | 110 | 6 | 90 | | | | | | | |
| 2F-96-8 | 42 | 22 | 80 | 16.5 | CL | SPT | 110 | 9 | 90 | | | | | | | |
| 2F-96-8 | 42 | 22 | 80 | 18.5 | ML | SPT | 120 | 9 | 57 | | | | | | | |
| 2F-96-8 | 42 | 22 | 80 | 22 | CL | SPT | 110 | 9 | 90 | | | | | | | |
| 2F-96-8 | 42 | 22 | 80 | 25.5 | CL | SPT | 110 | 8 | 90 | | | | | | | |
| 2F-96-8 | 42 | 22 | 80 | 29 | CL | SPT | 110 | 8 | 80 | | | | | | | |
| 2F-96-8 | 42 | 22 | 80 | 32.5 | CL | SPT | 110 | 34 | 58 | 29 | 15 | | | | | |
| 2F-96-8 | 42 | 22 | 80 | 36 | SM | SPT | 130 | 44 | 30 | | | | | | | |
| 2F-96-8 | 42 | 22 | 80 | 39 | SM | SPT | 130 | 71 | 30 | | | | | | | |

Assumed GW = 20 ft bgs and Energy Ratio =80%

Table 2B- 3.Rational for strength parameter selection for cross section at American River North 3038+25. Source: URS 2009.

< X > signifies discarded data point suspected to be unreliable

| Material Description | Material Number | Strength Type | Parameter | SPT | Boring Description | PI | CPT | Vane Shear Peak | Vane Shear Res. | Other | Selection | Unit Weight | Rationale |
|---|---|---|---|---|---|---|---|---|---|---|---|---|---|
| ML (1) | 1 | Drained | c' (psf) = | | | | | | | | 0 | 120 | |
| | | | φ' (°) = | 42 | | | | | | | 35 | | Friction angle reduced for conservatism |
| | | | σ'$_p$ (psf) = | | | | | | | | | | |
| | | Undrained | s$_u$/σ'$_{vc}$ = | | | | | | | | | | |
| | | | s$_u$ (psf) = | | | | | | | | | | |
| CL (2) | 2 | Drained | c' (psf) = | | | | | | | | 0 | 110 | |
| | | | φ' (°) = | | | 35 | | | | | 35 | | |
| | | | σ'$_p$ (psf) = | 4,920 | | | | | | | 4,920 | | OCR = 6 based on correlations with N60 |
| | | Undrained | s$_u$/σ'$_{vc}$ = | 1.20 | | | | | | | 1.20 | | |
| | | | s$_u$ (psf) = | 1,000 | | | | | | | 1,000 | | |
| ML (3) | 3 | Drained | c' (psf) = | | | | | | | | 0 | 120 | |
| | | | φ' (°) = | 33 | | | | | | | 33 | | |
| | | | σ'$_p$ (psf) = | | | | | | | | | | |
| | | Undrained | s$_u$/σ'$_{vc}$ = | | | | | | | | | | |
| | | | s$_u$ (psf) = | | | | | | | | | | |
| CL (4) | 4 | Drained | c' (psf) = | | | | | | | | 0 | 110 | |
| | | | φ' (°) = | | | 35 | | | | | 35 | | |
| | | | σ'$_p$ (psf) = | 11,400 | | | | | | | 11,400 | | OCR = 6 based on correlations with N60 |
| | | Undrained | s$_u$/σ'$_{vc}$ = | 1.20 | | | | | | | 1.20 | | |
| | | | s$_u$ (psf) = | 1,000 | | | | | | | 1,000 | | |
| ML (5) | 5 | Drained | c' (psf) = | | | | | | | | 0 | 120 | |
| | | | φ' (°) = | 33 | | | | | | | 33 | | |
| | | | σ'$_p$ (psf) = | 14,400 | | | | | | | 14,400 | | OCR = 6 based on correlations with N60 |
| | | Undrained | s$_u$/σ'$_{vc}$ = | | | | | | | | | | |
| | | | s$_u$ (psf) = | 1,600 | | | | | | | 1,600 | | |
| CL (6) | 6 | Drained | c' (psf) = | | | | | | | | 0 | 110 | |
| | | | φ' (°) = | | | 33 | | | | | 33 | | |
| | | | σ'$_p$ (psf) = | 16,000 | | | | | | | 16,000 | | OCR = 5 based on correlations with N60 |
| | | Undrained | s$_u$/σ'$_{vc}$ = | 2.00 | | | | | | | 0.83 | | su/σ'vc =0.23*5^0.8=0.83 |
| | | | s$_u$ (psf) = | 1,500 | | | | | | | 1,500 | | |
| SM (7) | 7 | Drained | c' (psf) = | | | | | | | | 0 | 130 | |
| | | | φ' (°) = | 46 | | | | | | | 40 | | Friction angle reduced for conservatism |
| | | | σ'$_p$ (psf) = | | | | | | | | | | |
| | | Undrained | s$_u$/σ'$_{vc}$ = | | | | | | | | | | |
| | | | s$_u$ (psf) = | | | | | | | | | | |
| CL (8) | 8 | Drained | c' (psf) = | | | | | | | | 0 | 110 | |
| | | | φ' (°) = | | | | | | | 31 | 31 | | |
| | | | σ'$_p$ (psf) = | | | | | | | | | | |
| | | Undrained | s$_u$/σ'$_{vc}$ = | | | | | | | | | | |
| | | | s$_u$ (psf) = | | | | | | | | | | |

Table 2B- 4. Index testing and blowcount summary for boring WCNBAR_001B at American River North 3306+35. Source: URS 2009.

| PROJECT NAME: | American River Common Features GRR |
|---|---|
| PROJECT NUMBER: | 26816760.45300 |
| Reach ID: | American River North 3306+35 WCNBAR_001B |

| Analysis By: | Michael Kynett | Date: | 9/30/2008 |
|---|---|---|---|
| Check By: | | Date: | |

Highlight in green any assumed value          Inputs are highlighted in grey

| | | | | | | | | | | | | | | INPUT DATA | | |
|---|---|---|---|---|---|---|---|---|---|---|---|---|---|---|---|---|
| Boring ID | Ground Surface Elevation | Ground Water Elevation | Energy Ratio | Depth to Top of Sample | USCS Group Name and Symbol | Sampler Type | γm | Blows foot, N | % finer than No200 | Liquid limit, LL | Plastic Index, PI | Moisture content | UU - s_u | ICU Confining stress | s_u | Consol. σ'_max |
| (-) | (ft) | (ft) | (%) | (ft) | (-) | (-) | (pcf) | (-) | (%) | (%) | (%) | (%) | (psf) | (psf) | (psf) | (psf) |
| WCNBAR_001B | 52.95 | 41.5 | 83 | 5 | ML | SPT | 120 | 22 | 35 | | | | | | | |
| WCNBAR_001B | 52.95 | 41.5 | 83 | 10 | SM | SPT | 130 | 20 | 15 | | | | | | | |
| WCNBAR_001B | 52.95 | 41.5 | 83 | 15 | SM | SPT | 130 | 12 | 35 | | | | | | | |
| WCNBAR_001B | 52.95 | 41.5 | 83 | 20 | SM | SPT | 130 | 12 | 30 | | | | | | | |
| WCNBAR_001B | 52.95 | 41.5 | 83 | 25 | ML | SPT | 120 | 13 | 35 | | | | | | | |
| WCNBAR_001B | 52.95 | 41.5 | 83 | 30 | SM | SPT | 130 | 17 | 20 | | | | | | | |
| WCNBAR_001B | 52.95 | 41.5 | 83 | 35 | SM | SPT | 130 | 15 | 30 | | | | | | | |
| WCNBAR_001B | 52.95 | 41.5 | 83 | 40 | GM | SPT | 135 | 43 | 15 | | | | | | | |
| WCNBAR_001B | 52.95 | 41.5 | 83 | 55 | CL | SPT | 110 | 86 | 35 | | | | | | | |
| WCNBAR_001B | 52.95 | 41.5 | 83 | 60 | SM | SPT | 130 | 60 | 35 | | | | | | | |
| WCNBAR_001B | 52.95 | 41.5 | 83 | 65 | ML | SPT | 120 | 40 | 35 | | | | | | | |
| WCNBAR_001B | 52.95 | 41.5 | 83 | 70 | CL | SPT | 110 | 46 | 35 | 25 | 8 | | | | | |

# Table 2B- 5.Rational for strength parameter selection for cross section at American River North 3306+35. Source: URS 2009.

**Study Section:** American River North Levee LM 1.32 U9 (DWR Sta. 3306+35). Data From borings WCNBAR_003B

< X > signifies discarded data point suspected to be unreliable

| A Material Description | B Material Number | C Strength Type | D Parameter | E SPT | F Boring Description | G PI | H CPT | I Vane Shear Peak | I Vane Shear Res. | J Other | L Selection | M Unit Weight | N Rationale |
|---|---|---|---|---|---|---|---|---|---|---|---|---|---|
| ML (1) | 1 | Drained | c' (psf) = | | | | | | | | 0 | 120 | |
| | | | φ' (°) = | 45 | | | | | | | 35 | | Friction angle reduced for conservatism |
| | | | σ'$_p$ (psf) = | 5,700 | | | | | | | 5,700 | | OCR > 10 based on correlations with N60 |
| | | Undrained | s$_u$/σ'$_{vc}$ = | 6.40 | | | | | | | 1.45 | | Assume OCR = 10 for max. past pressure calc. |
| | | | s$_u$ (psf) = | 3,800 | | | | | | | 3,800 | | su/σ'vc =0.23*10^0.8=1.45 |
| SM (2) | 2 | Drained | c' (psf) = | | | | | | | | 0 | 130 | |
| | | | φ' (°) = | 32 | | | | | | | 32 | | |
| | | | σ'$_p$ (psf) = | | | | | | | | | | |
| | | Undrained | s$_u$/σ'$_{vc}$ = | | | | | | | | | | |
| | | | s$_u$ (psf) = | | | | | | | | | | |
| SM (3) | 3 | Drained | c' (psf) = | | | | | | | | 0 | 130 | |
| | | | φ' (°) = | 33 | | | | | | | 33 | | |
| | | | σ'$_p$ (psf) = | | | | | | | | | | |
| | | Undrained | s$_u$/σ'$_{vc}$ = | | | | | | | | | | |
| | | | s$_u$ (psf) = | | | | | | | | | | |
| GM (4) | 4 | Drained | c' (psf) = | | | | | | | | 0 | 135 | |
| | | | φ' (°) = | 45 | | | | | | | 45 | | |
| | | | σ'$_p$ (psf) = | | | | | | | | | | |
| | | Undrained | s$_u$/σ'$_{vc}$ = | | | | | | | | | | |
| | | | s$_u$ (psf) = | | | | | | | | | | |
| SP (5) | 5 | Drained | c' (psf) = | | | | | | | | 0 | 130 | |
| | | | φ' (°) = | 49 | | | | | | | 40 | | Friction angle reduced for conservatism |
| | | | σ'$_p$ (psf) = | | | | | | | | | | |
| | | Undrained | s$_u$/σ'$_{vc}$ = | | | | | | | | | | |
| | | | s$_u$ (psf) = | | | | | | | | | | |
| CL (6) | 6 | Drained | c' (psf) = | | | | | | | | 0 | 110 | |
| | | | φ' (°) = | | | 35 | | | | | 35 | | |
| | | | σ'$_p$ (psf) = | <54,000> | | | | | | | 54,000 | | OCR > 10 based on correlations with N60 |
| | | Undrained | s$_u$/σ'$_{vc}$ = | 2.00 | | | | | | | 2.00 | | Assume OCR = 10 for max. past pressure calc. |
| | | | s$_u$ (psf) = | 8,200 | | | | | | | 8,200 | | |

**US Army Corps
of Engineers**
Sacramento District

# AMERICAN RIVER WATERSHED PROJECT
# (COMMON FEATURES), CALIFORNIA
# RIGHT (NORTH) BANK LEVEE STRENGTHENING

## AMERICAN RIVER
## CALIFORNIA

FY-1999

METRIC

Figure 2B- 6. Site location map showing the extent of levee improvements covered in the American River Watershed Project .
Source: USACE, 1999.

**Figure 2B- 7.** Excerpt from the American River Watershed Project involving construction of a slurry wall along segments of the American River levees. Our study site is at Station 9+100 on the plan where a pipeline labeled N3-10 is shown crossing the levee. This is likely the pipeline encountered during our study. The Eucalyptus tree under study appears to be intact in the photograph. Source: USACE, 1999.

DH-10
STA. 8+955

DEPTH

N GR SA FI LL PI MC

EL. 13.76 m (45.16') - 0

At surface, 152 mm (0.5') thick gravel and soil layer

(1.5') 0.46 m

SILT WITH SAND, ML: Stiff; moist; dusky brown; low plasticity fines; fine to medium, mostly fine sand; organic material (roots) present; easy drilling

14

At 0.70 m (2.3'), firm; sand lense present, 30 mm (0.1') thick

8

6

ML  0  20 80 31 6  -

10

At 2.22 m (7.3'), stiff; sand lense present

9

At 2.49 m (8.1'), charcoal present

11

(10.5') 3.20 m

4  - - - - - -

At 3.32 m (10.9'), as above except soft; increase of sand; abundant wood and charcoal present; possible cavity present, 152 mm (6") thick
At 3.57 m (11.7'), as above except light brown

(12.2') 3.72 m

SILTY SAND, SM: Loose; moist; moderate yellowish-brown; fine to medium, mostly fine sand; nonplastic to low plasticity fines; iron oxide staining; foundation contact at 3.72 m (12.2')
At 3.78 m (12.4'), as above except increase in plasticity; charcoal material present

9

6

0  61 39 -  -  -

SM

8

At 4.91 m (16.1'), as above except reduction in fines

7

(18.0') 5.49 m

9  - - - - - -

At 5.61 m (18.4'), as above except increase in silt

(19.3') 5.88 m

8

6

8

6  0  30 70 23 1  -

ML

7

SANDY SILT, ML: Firm to stiff; moist; dusky brown; nonplastic fines; fine to medium, mostly fine sand; organic material (roots) present; easy drilling

6

6

7

(31.5') 9.60 m

9  - - - - - -

(33.3') 10.15 m

13

GP-GM

R  - - - - - -

POORLY-GRADED GRAVEL WITH SILT, GP-GM: Firm to very dense; moist; light olive-gray; about 60% fine to coarse, subangular to rounded gravel; about 30% fine to coarse, subangular to rounded, well-graded sand; about 10% nonplastic fines; iron oxide staining; difficult drilling

R

(37.5') 11.43 m

B.O.H.

Figure 2B- 8. Boring log DH-10 as shown on Figure C.7. Source: USACE, 1999.

2B-16
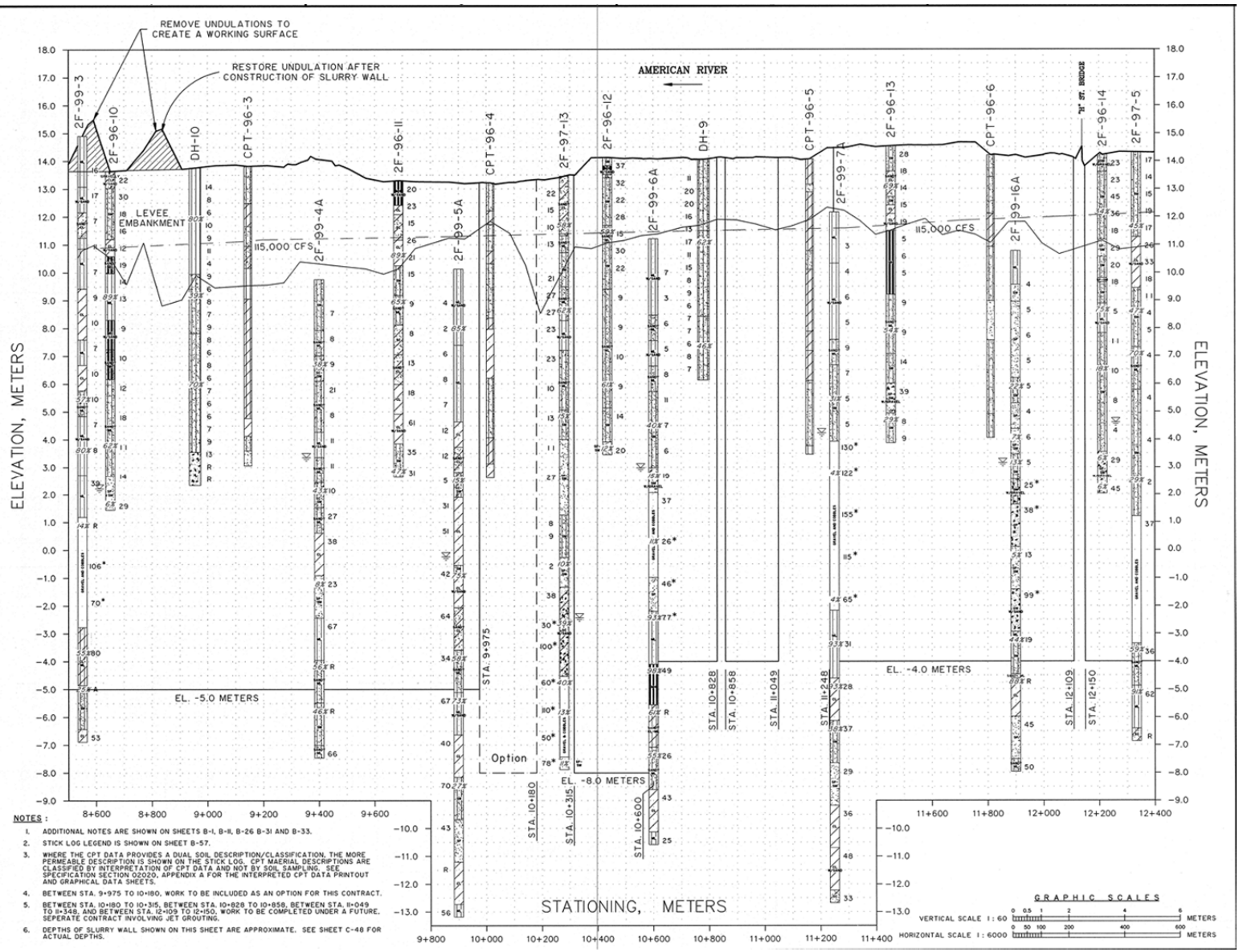
Figure 2B- 9. Profile view along levee showing available soil data. Source: USACE, 1999.
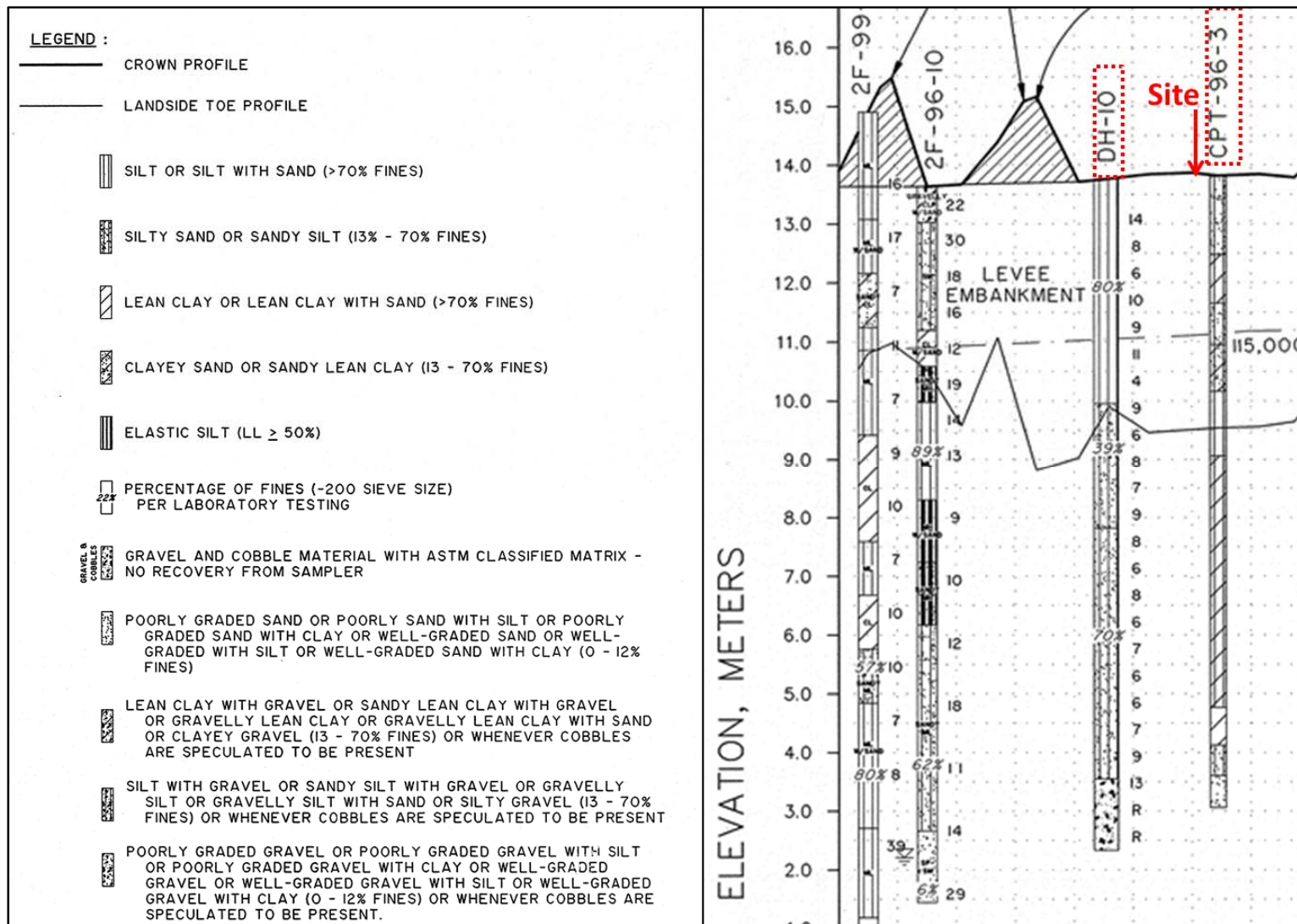
Figure 2B- 10. Legend for Figure C.9 and close in view showing our study site in the context of the closest soil boring and cone penetration test (CPT) data. Source: USACE, 1999.

GRAVEL ROAD
C/L ROAD
GRAVEL ROAD

TOE OF LEVEE

TOE OF LEVEE

Sta. 9+026.550

15    0    15

GRAVEL ROAD
C/L ROAD
GRAVEL ROAD

TOE OF LEVEE

TOE OF LEVEE

D

15

10

5

Sta. 9+272.944

15    0    15

NOTE:

1.   DEPTH OF SLURRY WALL (D) VARIES. SEE SHEET C-48 FOR DETAILS.

2.   CROSS SECTIONS ARE SHOWN LOOKING DOWNSTATION.

GRAPHIC SCALE

0    5    10    15    20    25 meters
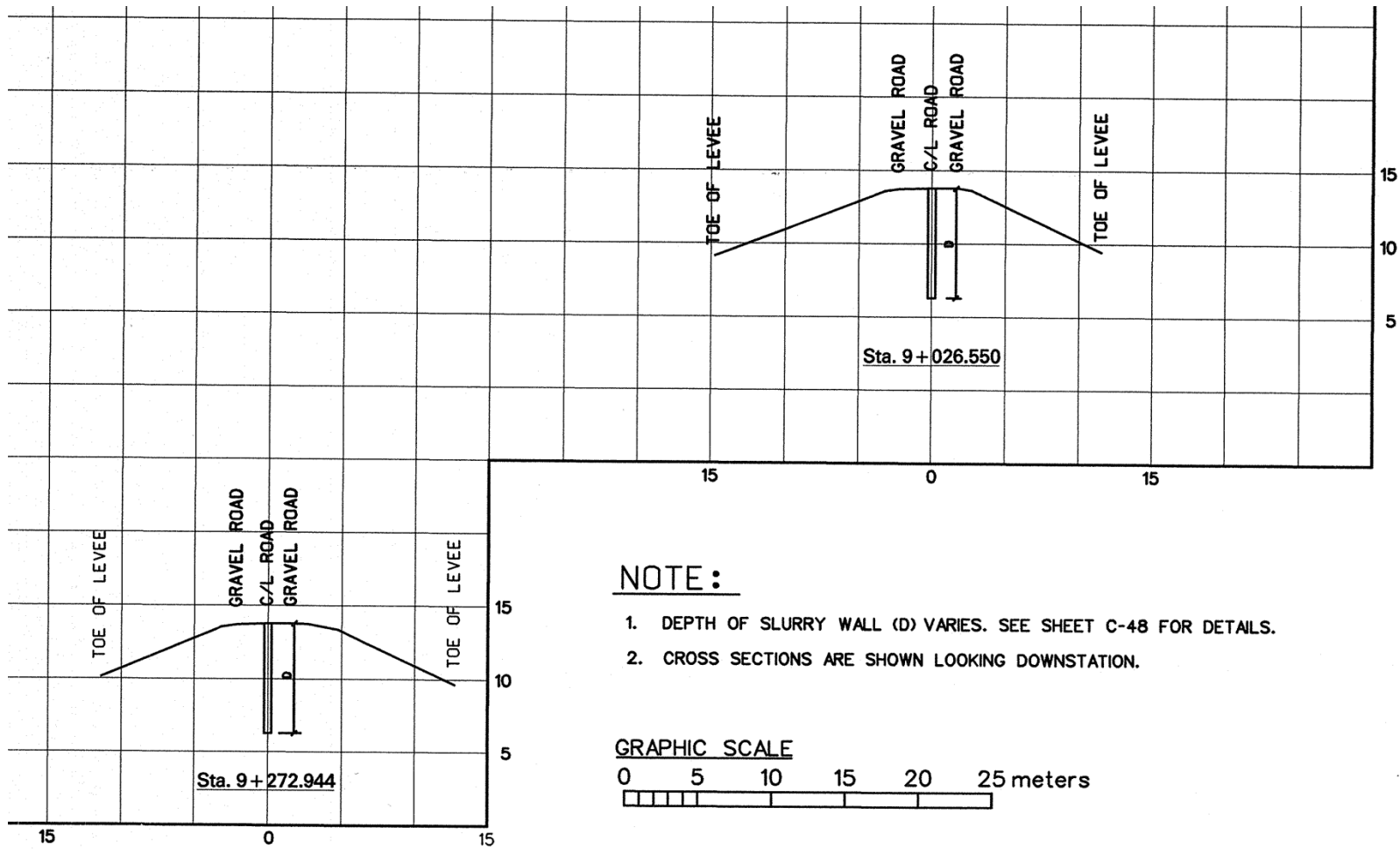
Figure 2B- 11. Levee cross sections in the vicinity of our study site. The study site is at approximately Station 9+100. Source: USACE, 1999.

| Utility Crossing Survey Point | Station (m) | Have As-Built | LS Levee Height (m) | Depth Below Crown (m) | diameter (in) | number of pipes/ distance apart (m) | Pipe Material | Utility Type |
|---|---|---|---|---|---|---|---|---|
| N3-10 | 09+100.889 | | 4.3 | 5.5 | 1. | 1 | Galvanized | Water |

| Agency of ownership and jurisdiction | | Reference to other sheets | bypass diameter if service pipe is tapped (inches) | flow rate minimum if separate hose and pump used (GPM) |
|---|---|---|---|---|
| Cal Expo | SEE NOTES 4 SHT U-6 | U-6  U-4  U-11 spec 01500-1.6.2 | 1" | N/A |

| Accommodation | Confirmation Method |
|---|---|
| COMPLETE REMOVAL OR REMOVE SEGMENTS & PLUG PIPE - RELOCATE PIPE CLOSER TO CREST | STANDARD POTHOLE PROCEDURE FROM WATER SIDE TOE |



SECTION SHOWING DEEP WATERLINES AT CAL EXPO

SEE ALSO SPECIFICATION SECTION 02730-1.7, 2.3, 2.4 & 2.5
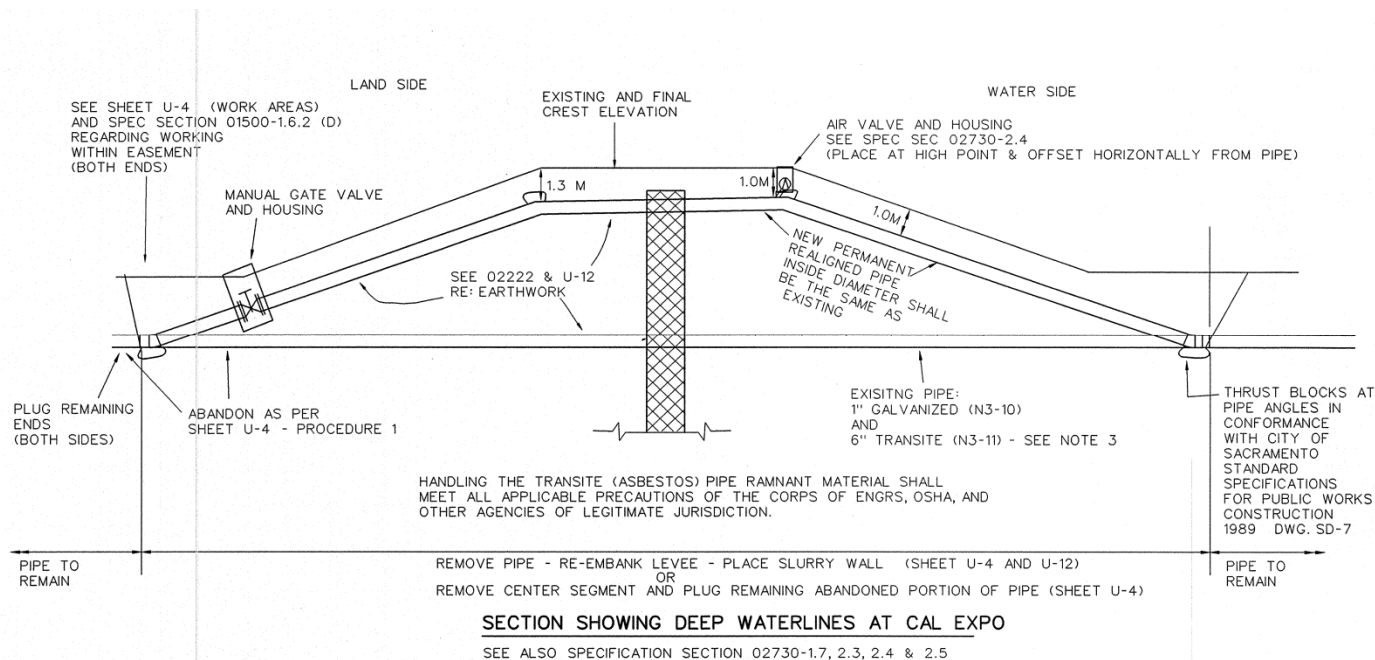
Figure 2B- 12. Notes regarding the pipeline N3-10 intersecting the study site. The pipeline is shown to be a 1 inch galvanized water line that was re-routed as shown as part of the American River Watershed Project in 1999. Source: USACE, 1999.

DESIGN MEMORANDUM NO. I

AMERICAN RIVER PROJECT, CALIFORNIA

# AMERICAN RIVER LEVEE
# GENERAL DESIGN

25 JUNE 1956

9

SACRAMENTO DISTRICT

CORPS OF ENGINEERS

U. S. ARMY

SACRAMENTO, CALIFORNIA

Paragraphs 9 and 10 were excerpted from the American River Levee General Design (USACE, 1956) and provide a discussion of what is known of the levee history at the project site. The site was completed to project standards in 1955 as summarized in paragraphs 9 and 10 below:

9. Existing Left Bank Project Levee: The existing left bank levee which protects portions of the city of Sacramento was constructed by the Sacramento District as a part of the Sacramento River Flood Control Project and completed to project standards in 1948. It extends from high ground at Mayhews downstream 10.8 miles to the mouth of the American River where it meets the left bank levee of the Sacramento River. The levee was designed and constructed to pass the Sacramento River Flood Control Project design flow (before Folsom Dam) on the American River of 180,000 c.f.s. with a freeboard of 3.0 feet and without reclamation of the north bank flood plain upstream from North Sacramento. The levee has a crown width of 20 feet, 1 on 3 riverside and 1 on 2 landside slopes and has a gravel surfacing for patrol purposes. At three locations the riverbank and levee were provided with a total of 3,000 lineal feet of bank protection as an emergency measure during and following the floods of November 1950. Intercepted interior drainage is collected by a system of ditches and is pumped over and/or through the levee at several locations. The levee and pumping plants are maintained and operated by local interests.

10. Existing Right Bank Project Levee: The existing right bank levee, which protects the city of North Sacramento, was constructed by the Sacramento District as a part of the Sacramento River Flood Control Project and completed to project standards in 1955. It extends from high ground near the junction of Howe Avenue and Arden Way downstream 3.0 miles to a junction with the left bank levee of the Natomas Canal (about 2 miles above the mouth of the American River). This levee was designed and constructed for the same flow conditions as the south levee (see paragraph 9). The levee has a crown width of 20 feet, a variable riverside slope (below the flood plane of 1 on 3 and above the flood plane of 1 on 2) and a landside slope of 1 on 2. It is gravel surfaced for patrol purposes. Intercepted interior drainage is collected by a system of ditches and is pumped over and/or through the levee at several locations. The levee and pumping plants are maintained and operated by local interests.

Figure 2B- 13 and Figure 2B- 14 show a site plan and section view, respectively, of the existing and proposed site elevations at the time of the American River Levee General Design report in June of 1956.
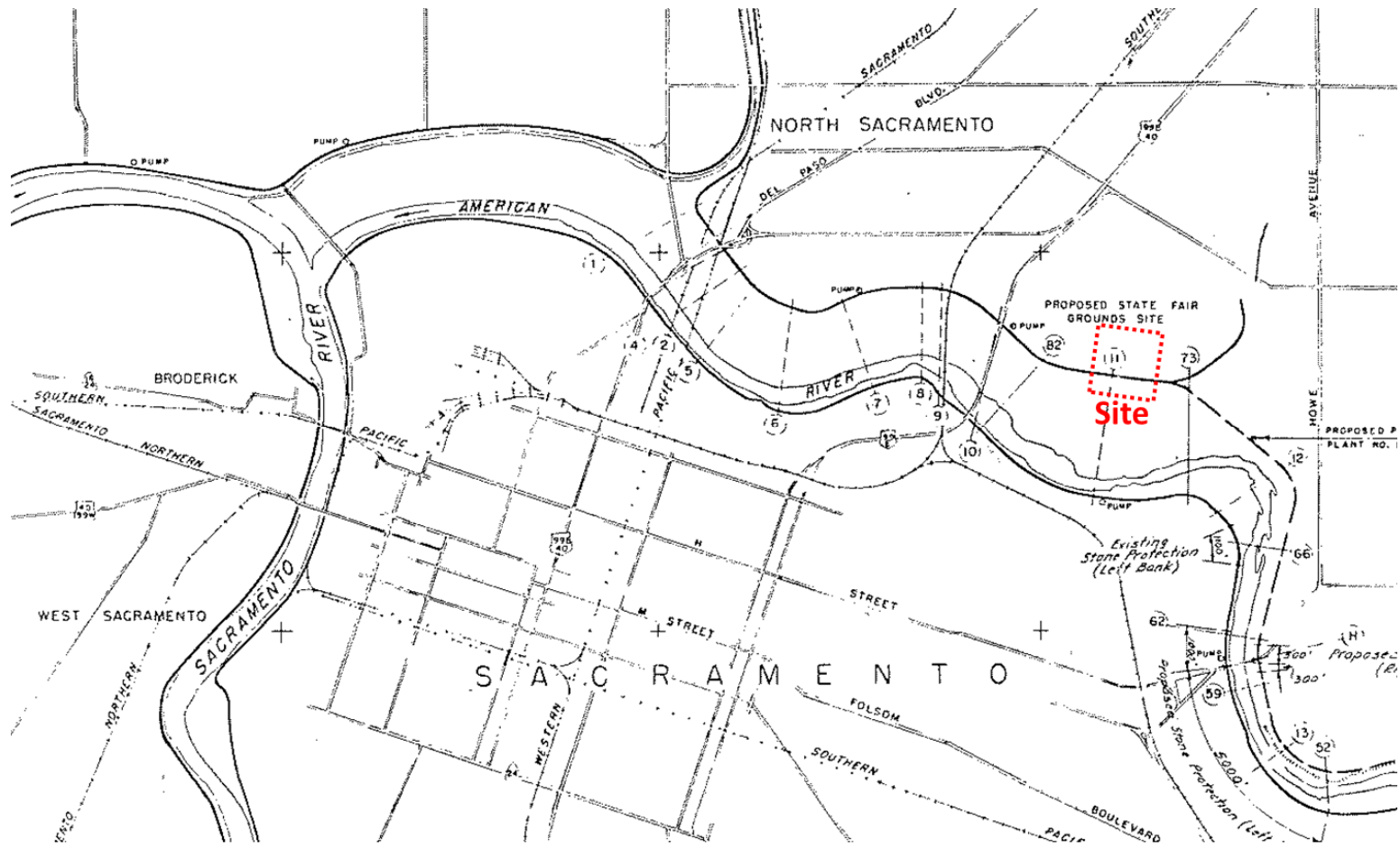
Figure 2B- 13. Plan view showing site location. The site is shown located at section 11. Source: USACE, 1956.
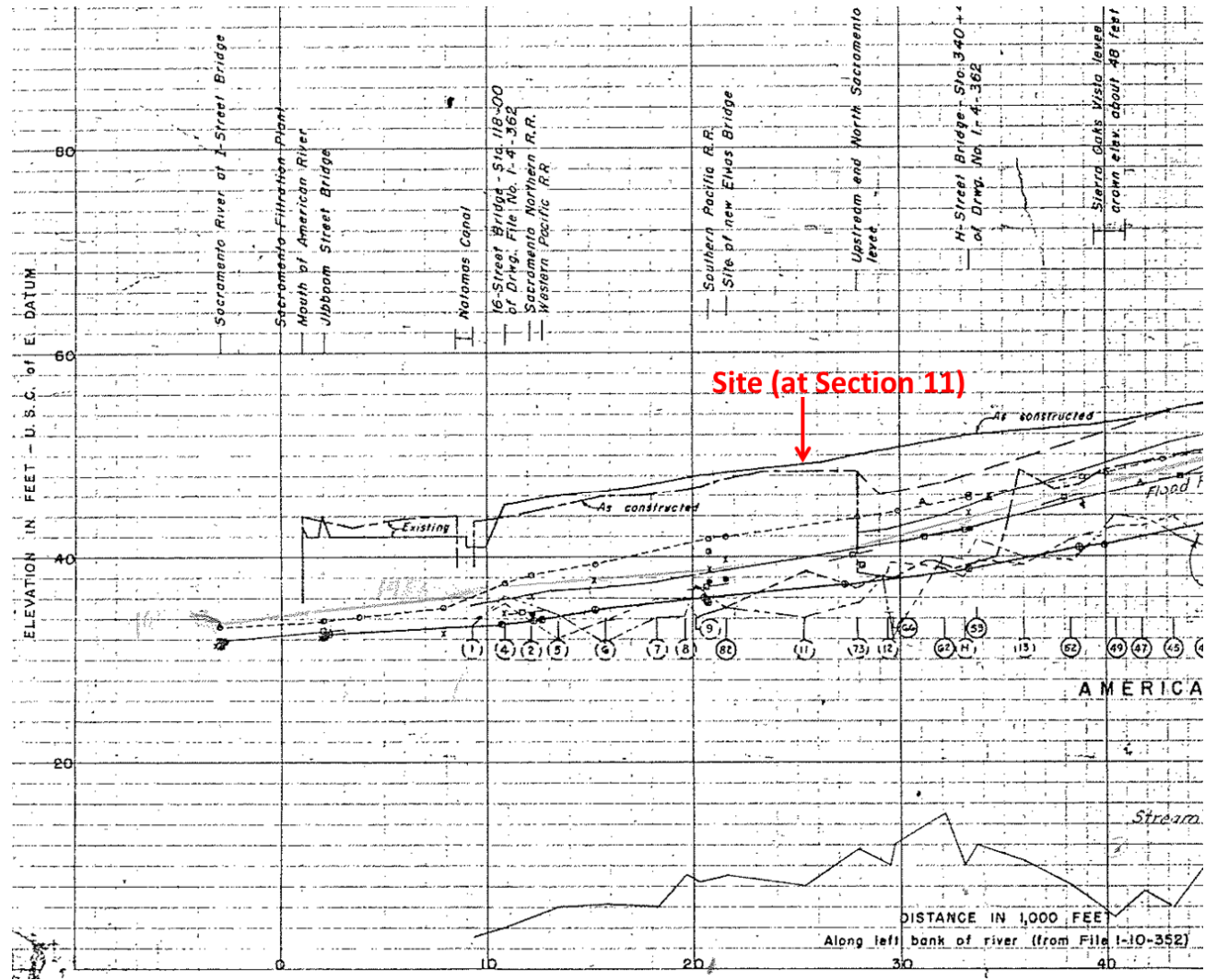
Figure 2B- 14. Cross section view along the levee showing the height existing and proposed levees at the time of the American River Levee General Design report dated June of 1956. It appears that the site, shown at section 11, was not proposed to be raised from the elevation of approximately 48.5 feet (NGVD29, or 51 feet NAVD88) as it stood at the time of the report in 1956. Source USACE, 1956.

# APPENDIX 2C

## Trench Logs – Cal Expo Test Site

Geologic sections as well as plan view and wall view trench logs are presented herein. Geologic sections are based on a set of 10 primary materials found onsite (Figure 2C- 1). Onsite materials consisted of primarily silts with varying amounts of clay and sand, silty sands, and lean clays. These findings are generally consistent with the findings of our soil borings (Appendix 2A) as well as soil information available through others (Appendix 2B). Subsurface stratigraphy for the segments between the trenches is shown for the control trench (Figure 2C- 2) and the stump trench (Figure 2C- 3).

Wall and plan view logs typically used symbols to distinguish live and decomposing roots, pipes and other findings on the field logs. A legend of symbols used is provided as Figure 2C- 4. Plan view logs of the root system encountered in the trenches is shown on Figure 2C-5 and Figure 2C- 6. Wall logs of the uphill wall of the lower trench and the downhill wall of the upper trench are presented on Figure 2C- 7 through Figure 2C- 10. Figure 2C- 11 through Figure 2C- 20break down the plan view logs into small segments and show corresponding photographs spliced together for each segment. Wall logs with corresponding spliced photographs are presented on Figures Figure 2C- 21 through Figure 2C- 31.

**SOIL TYPES:**

**(1)** Sandy silt with clay (ML), brown, moist, occasional rounded to sub-rounded gravels; sand is fine-grained and uniform. Fine roots.

**(1a)** Sandy silt with clay (ML), brown, moist, occasional rounded to sub-rounded gravels; sand is fine-grained and uniform.

**(2)** Sandy silt/silty sand (ML/SM), brown, moist, occasional sub-rounded gravels, sand very fine grained and uniform, trace clay.

**(3)** Clayey silt (ML) with sand, mottled dark brown and brown, moist, light cementation, trace sand

**(3a)** Clayey silt (ML), dark brown, light cementation and soils structure

**(3b)** Sandy silt (ML) with clay, brown

**(4)** Silty clay/clayey silt (ML/CL), olive brown with reddish oxidation stains

**(5)** Sandy silt (ML) with silty sand (SM) pockets, brown, moist, trace clay, sand is fine to medium grained

**(6)** Silty sand (SM), olive brown, fine uniform sand, lightly cemented

**(7)** Sandy silt to silty sand (ML/SM), light brown, very fine grained sand

**(8)** Sandy silt (ML), brown, moist, weakly cemented

**(9)** Heterogeneous blend of Materials 2 and 3b

**(10)** Silty sand (SM) with clay, brown, moist

Figure 2C- 1. Key to soil material types. Materials listed as ML/SM or ML/CL are materials of borderline classification where the material varies in classification somewhat across the layer.
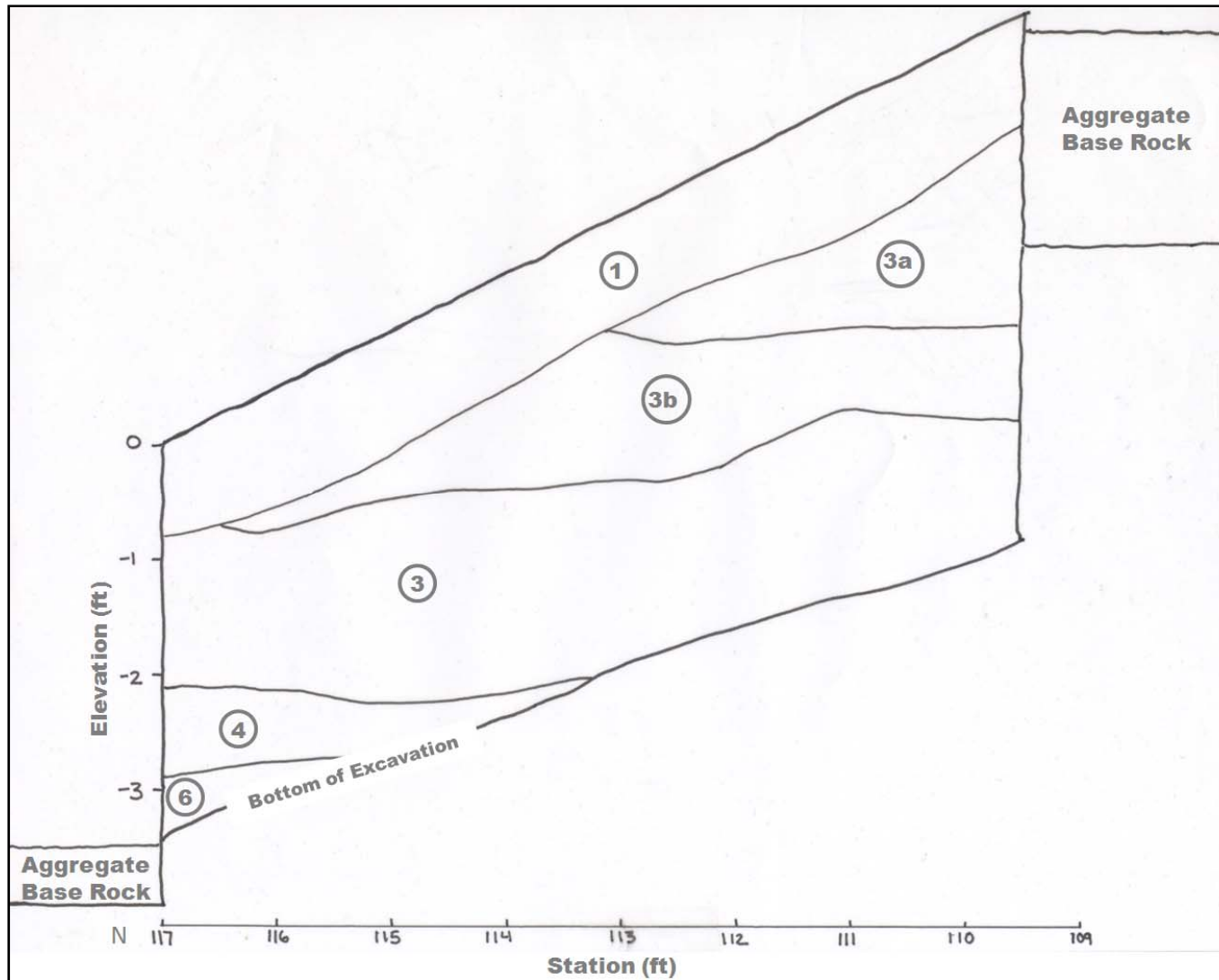
Figure 2C- 2. Trench log at Station 125 east along control trench spanning from the upper to lower trenches (Station 109.5 to 117 north). Geologic key provided on Figure D-1.
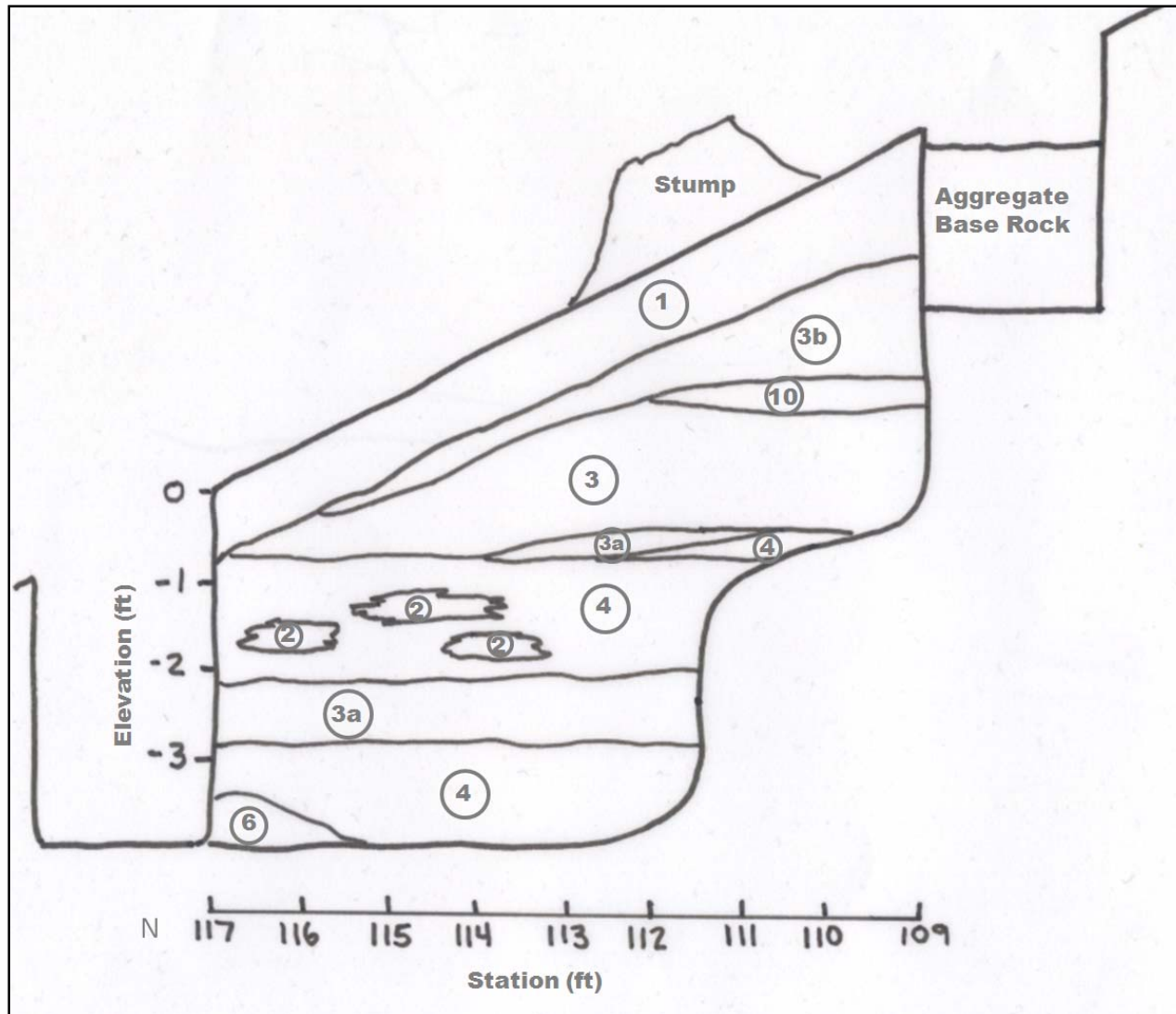
Figure 2C- 3. Trench log at Station 148 east at the eucalyptus stump and spanning between the upper to lower trenches (Station 109.5 to 117 north). Geologic key provided on Figure D-1.

**LEGEND**

**Wall Logs:**

○      Animal Burrow

◍      Pipe

•      Live Root

〰      Soil layer transition

◉      Zone of biological activity (ants burrowing)

⟳      Decomposing Root

⑩      Soil type (see list of soil types for material descriptions)

**Plan View Logs:**

∥      Decomposing Root

▬      Live Root

▊      Pipe

Figure 2C- 4**.** Key to plan view and wall view trench logs.
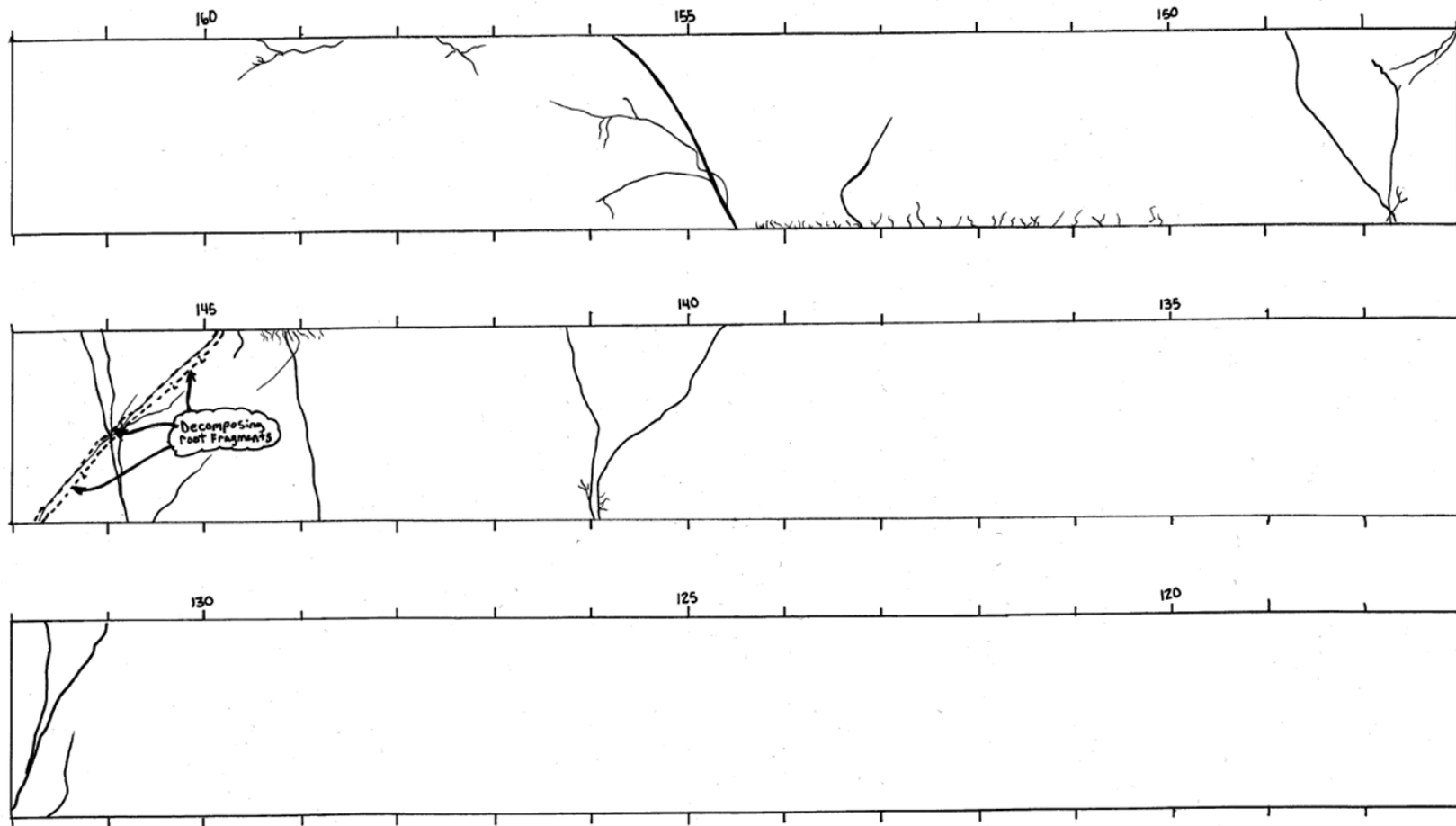
Figure 2C- 5. Upper stump and control trench plan view logs (Stations 117-162).
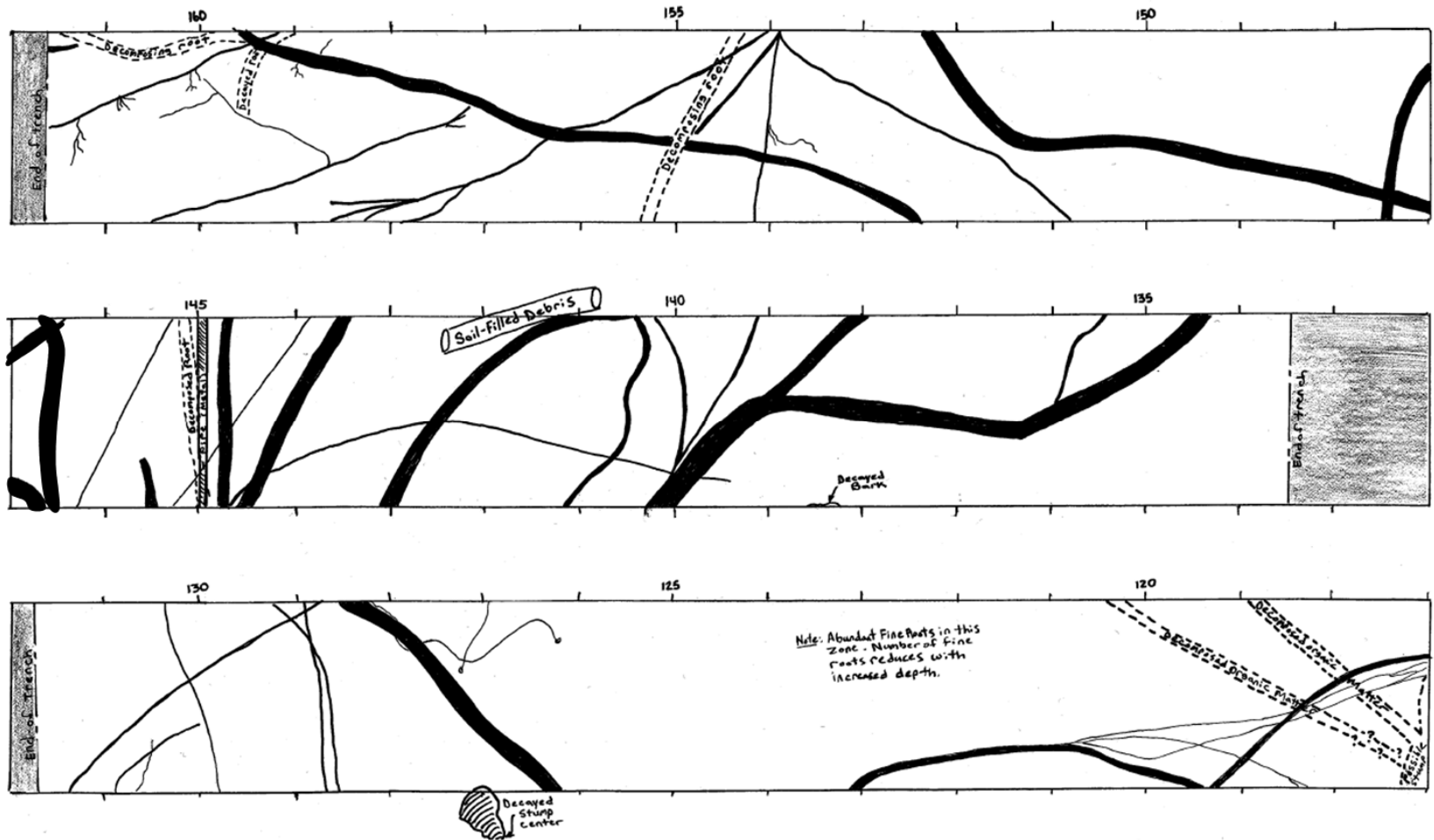
Figure 2C- 6. Lower stump and control trench plan view logs (Stations 117-161.5).
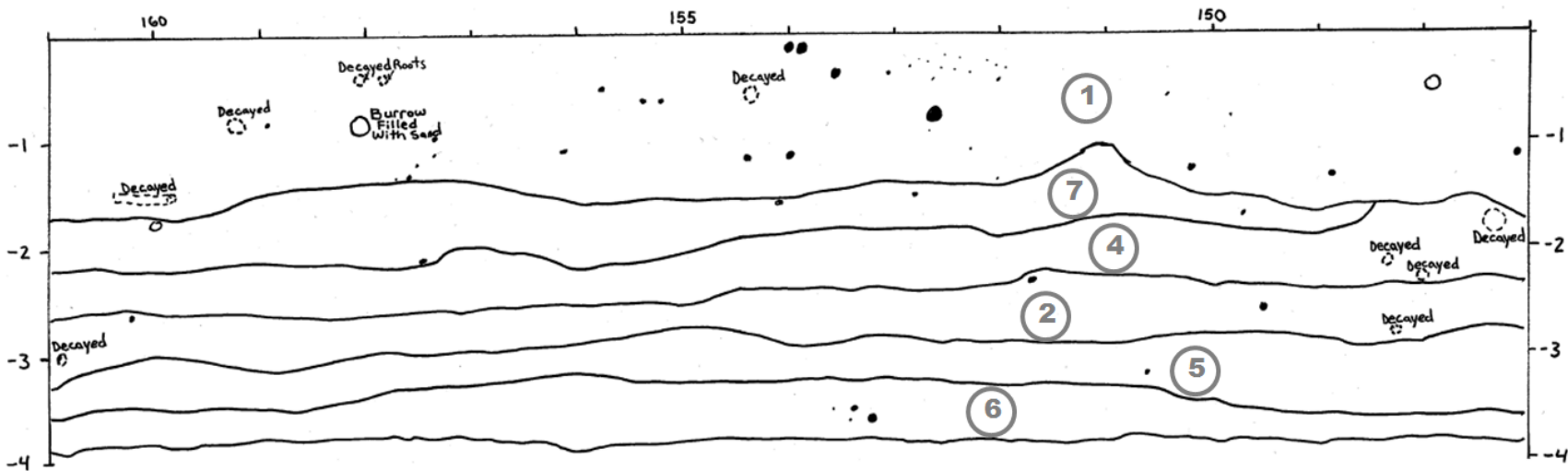
Figure 2C- 7. Log of uphill wall of the lower stump trench, Stations 147 to 161.
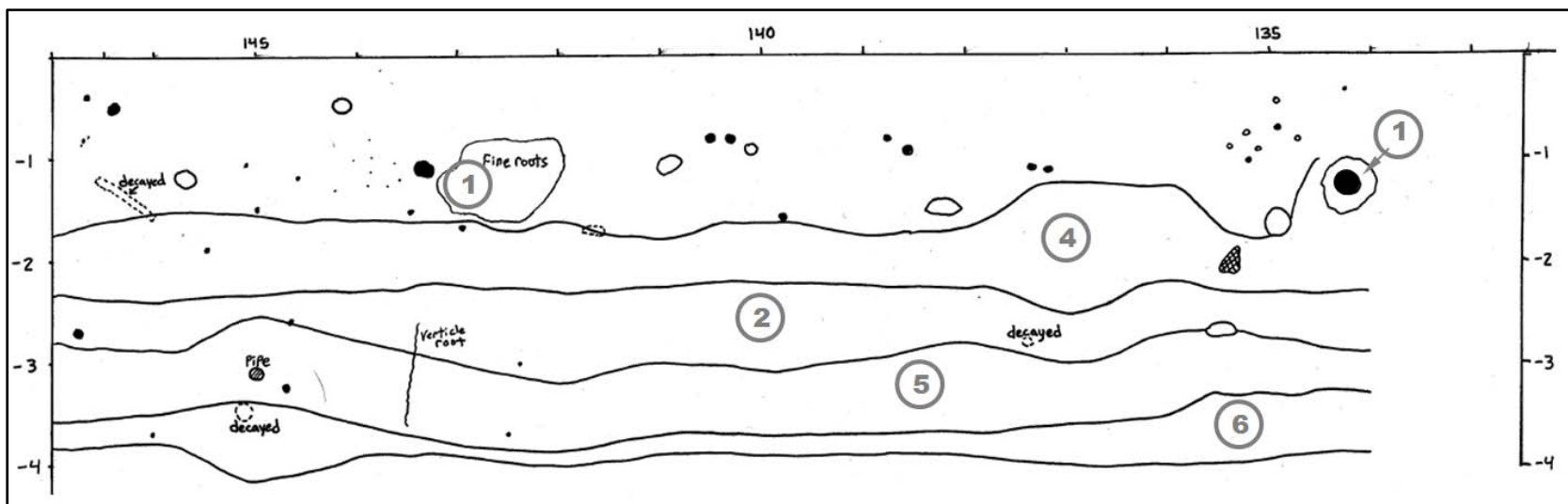
Figure 2C- 8. Log of uphill wall of the lower stump trench, Stations 133 to 147.
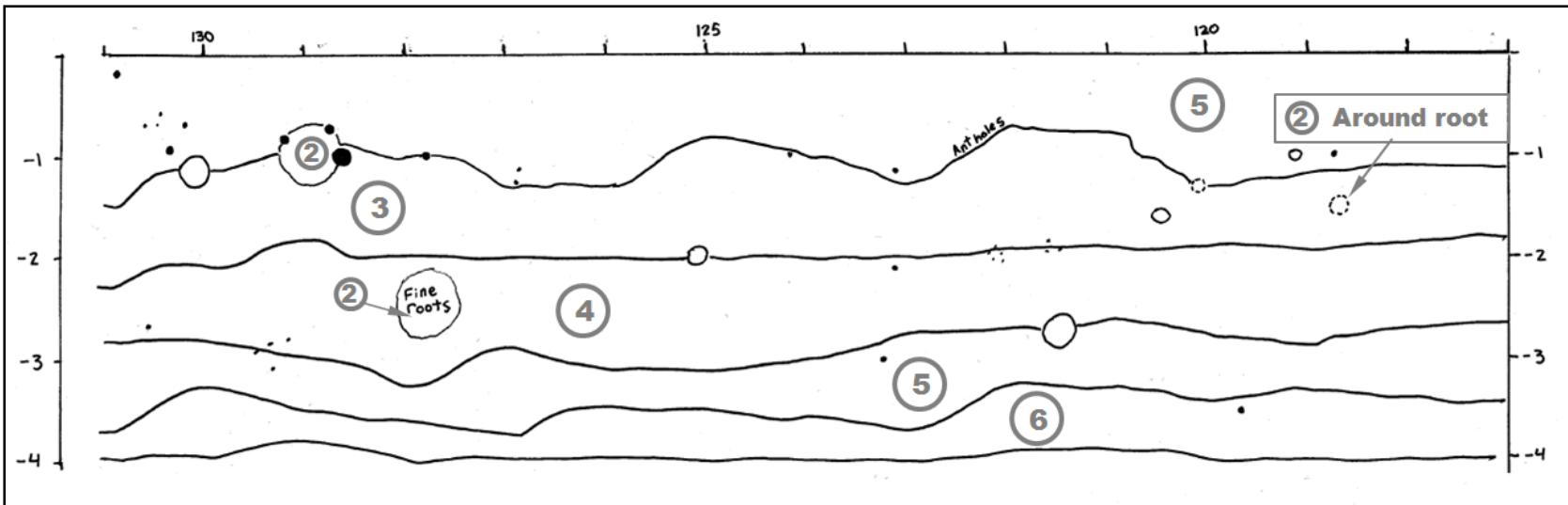
Figure 2C- 9. Log of uphill wall of the lower control trench, Stations 117 to 131.
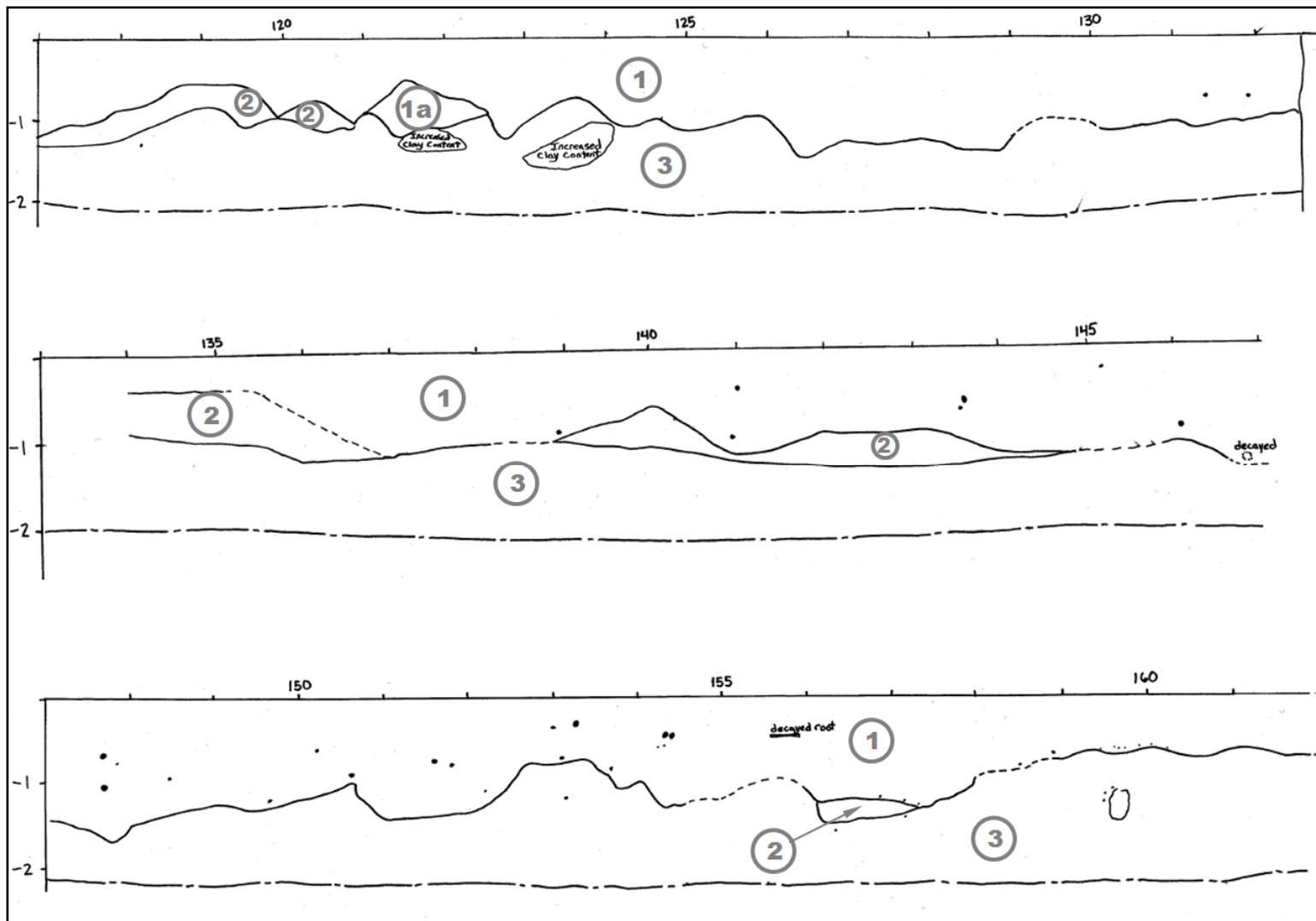
Figure 2C- 10. Log of downhill wall of the upper trenches, Stations 117 to 162.
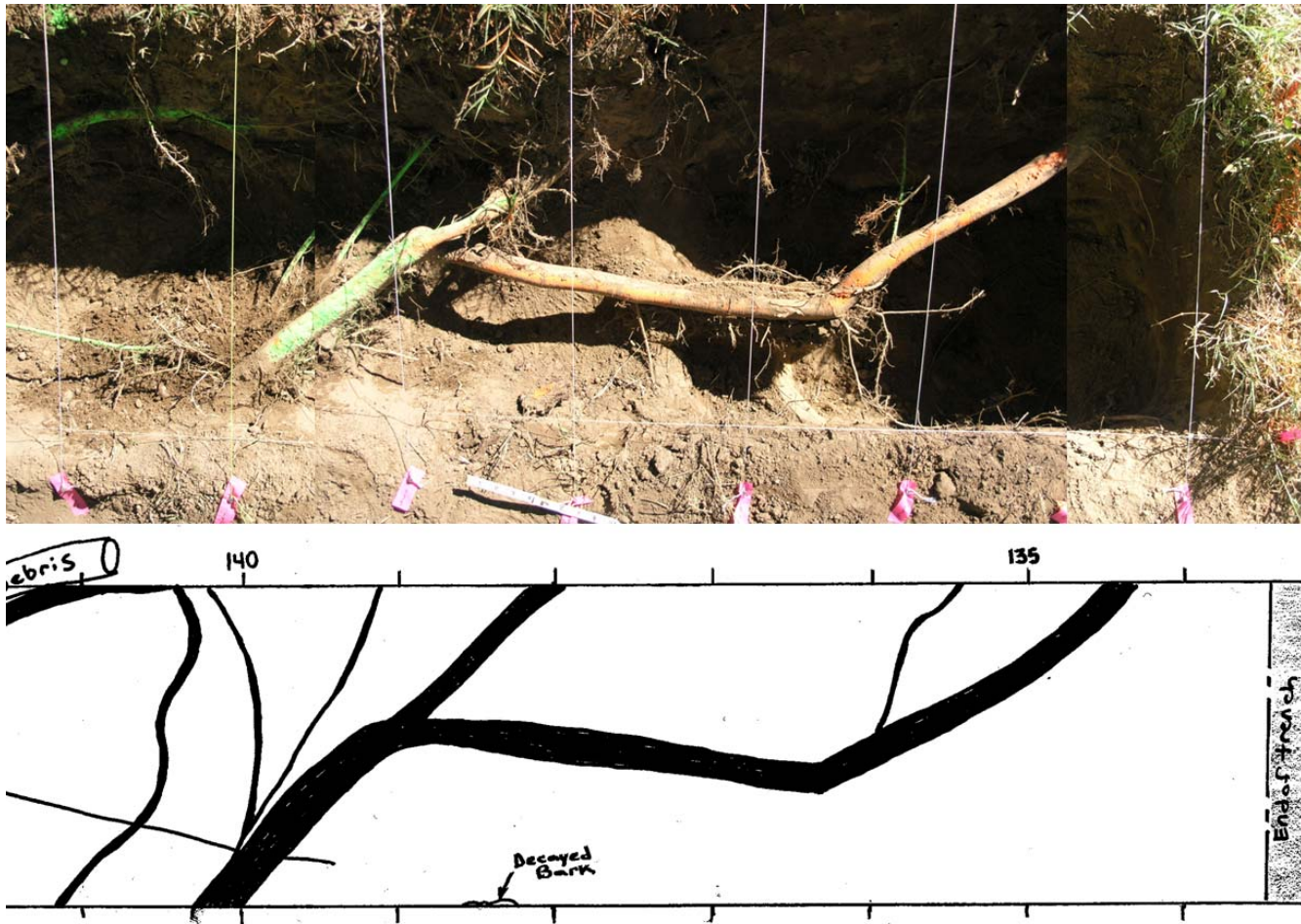
Figure 2C- 11. Lower stump trench Stations 133-141.5. Spliced plan view photos (top) during excavation of lower stump trench. Plan view log of analogous segment is below. Not all roots in the log are visible in the photograph. Additional roots may have been revealed at deeper levels.
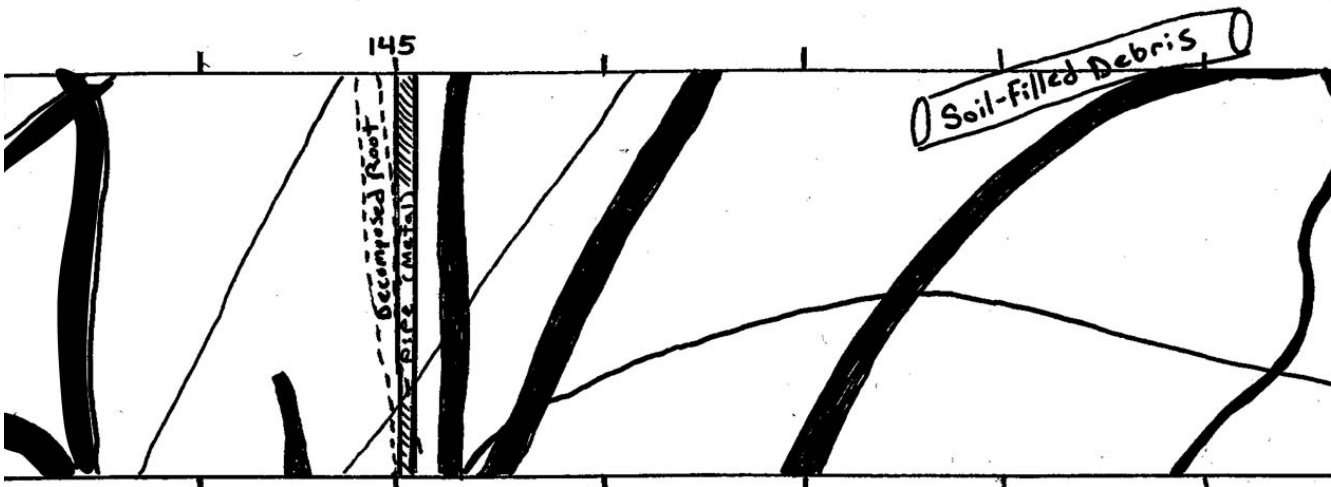
Figure 2C- 12. Lower stump trench Stations 140.5-146 (increasing to left). Spliced plan view photos (top) during excavation of lower stump trench. Plan view log of analogous segment is below. Not all roots in the log are visible in the photograph. Additional roots may have been revealed at deeper levels.

Figure 2C- 13**.** Stations 143 to 147 excavated to full depth and showing a cluster of decomposing and live roots as well as a 1.5 inch diameter pipe identified as a water line based on USACE documentation (USACE, 1999) as summarized in Appendix C.
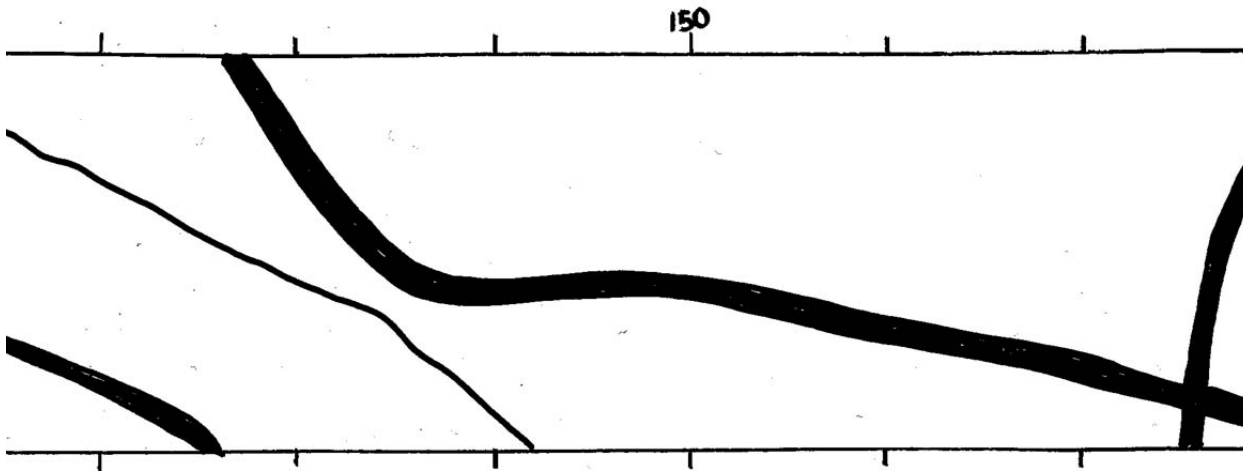
Figure 2C- 14. Lower stump trench Stations 147.5-153.5 (increasing to left). Spliced plan view photos (top) during excavation of lower stump trench. Plan view log of analogous segment is below. Not all roots in the log are visible in the photograph. Additional roots may have been revealed at deeper levels.
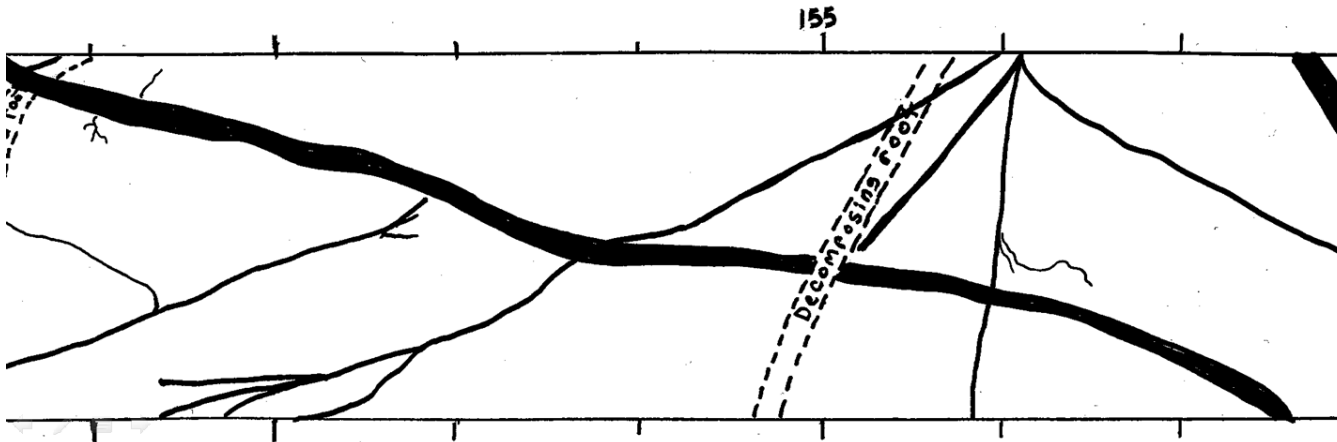
Figure 2C- 15**.** Lower stump trench Stations 153-159. Spliced plan view photos (top) during excavation of lower stump trench. Plan view log of analogous segment is below.  Not all roots in the log are visible in the photograph. Additional roots may have been revealed at deeper levels.
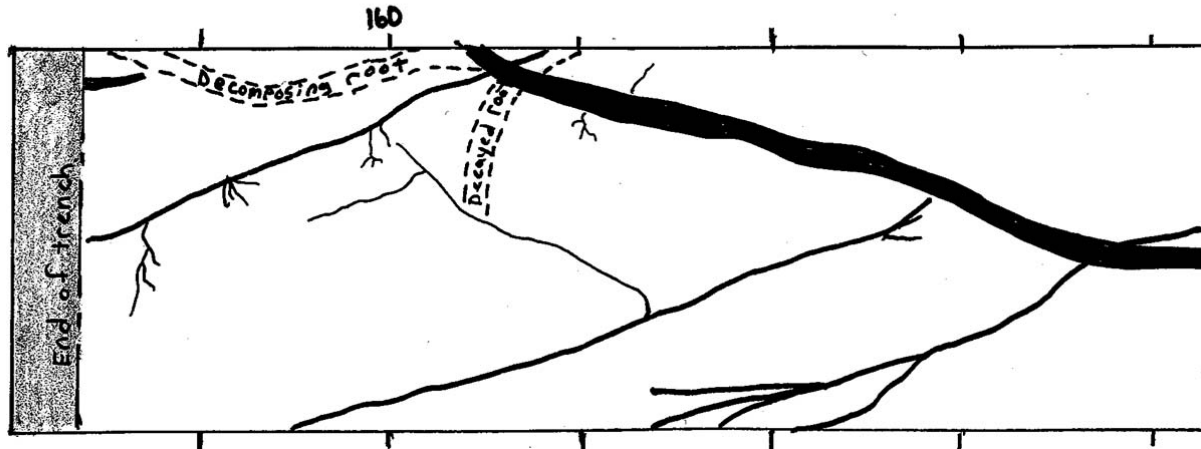
Figure 2C- 16. Lower stump trench Stations 156-161.5 (increasing right to left). Spliced plan view photos (top) during excavation of lower stump trench. Plan view log of analogous segment is below. Not all roots in the log are visible in the photograph. Additional roots may have been revealed at deeper levels.
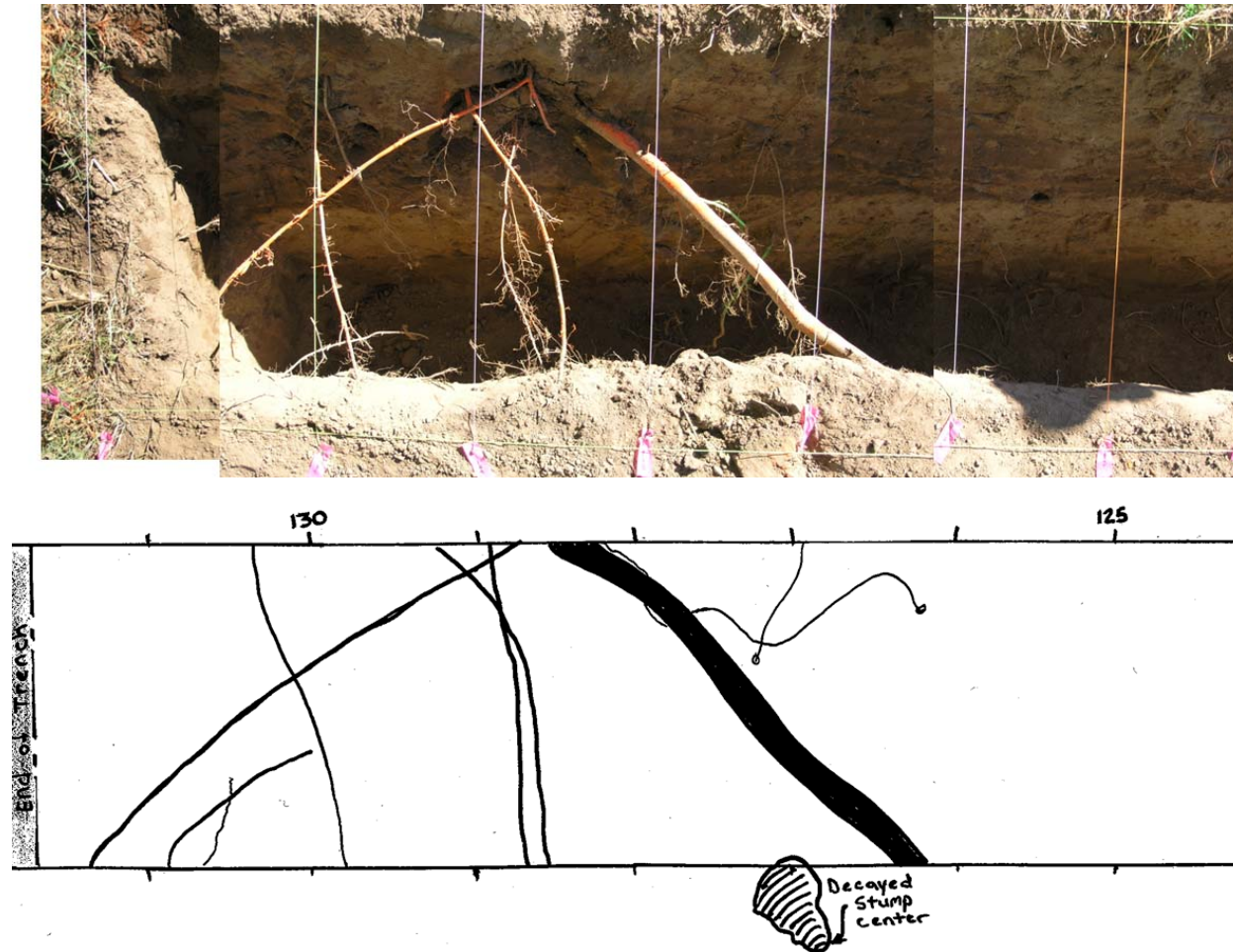
Figure 2C- 17. Lower control trench Stations 124-132. Spliced plan view photos (top) during excavation of lower control trench. Plan view log of analogous segment is below. Not all roots in the log are visible in the photograph. Shallow roots were removed as needed to achieve depth.
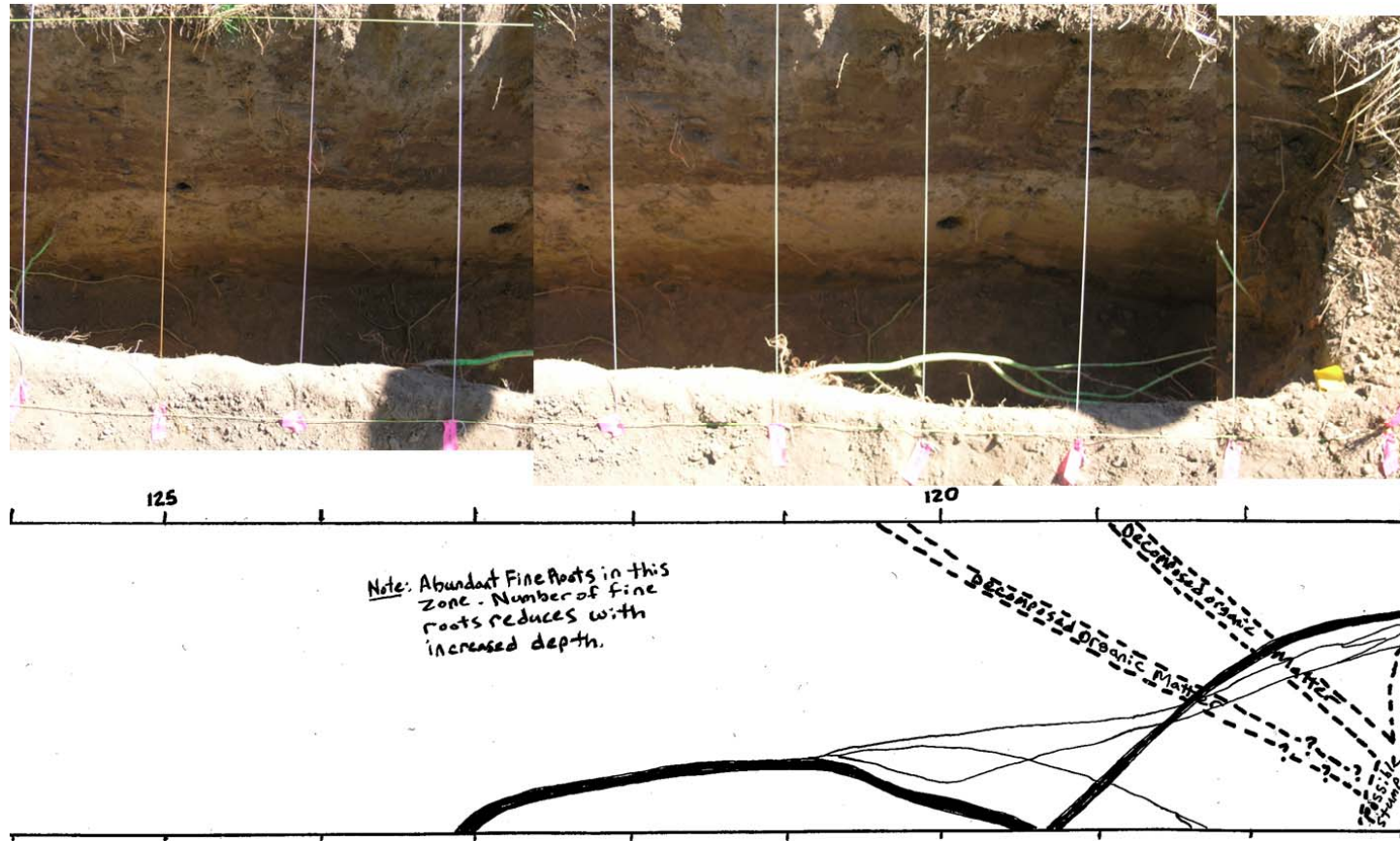
Figure 2C- 18. Lower control trench Stations 117-126. Spliced plan view photos (top) during excavation of lower control trench. Plan view log of analogous segment is below. Not all roots in the log are visible in the photograph. Shallow roots were removed as needed to achieve depth.
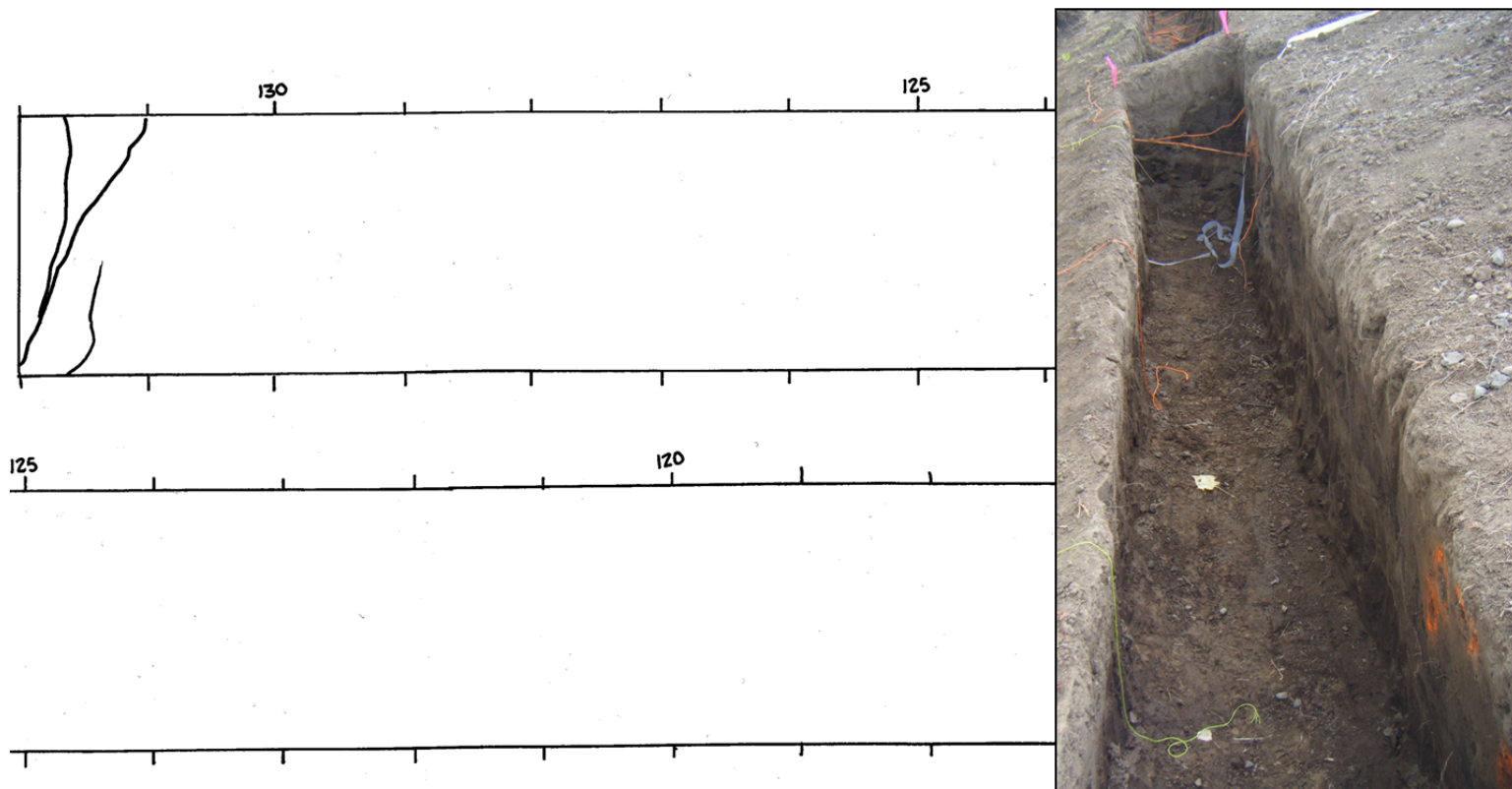
Figure 2C- 19. Photo looking east toward Station 132 from Station 118 (right) and plan view root logs (left) of upper control trench.
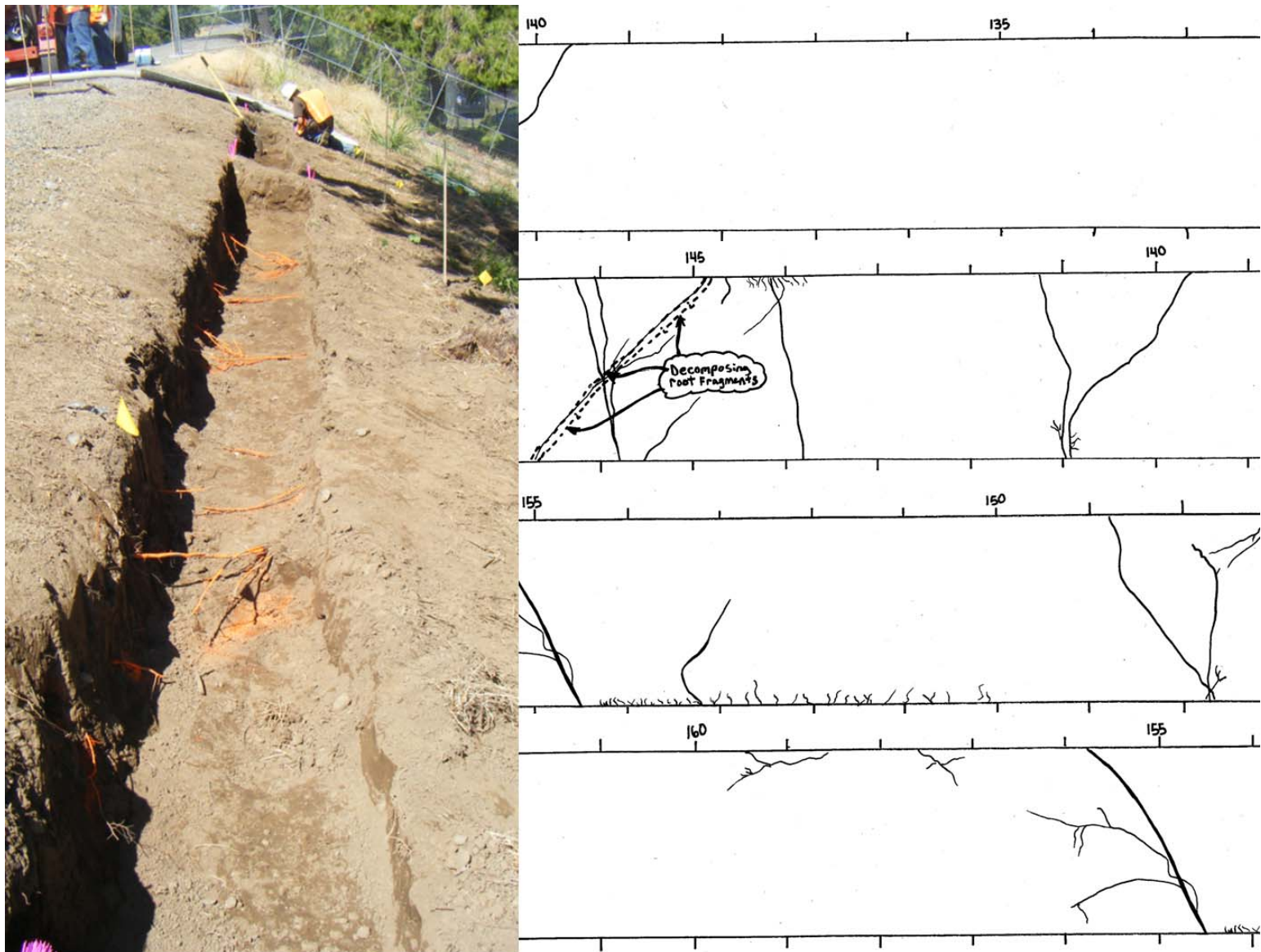
Figure 2C- 20. Photo looking west (left) and plan view logs of roots (right) of upper stump trench.
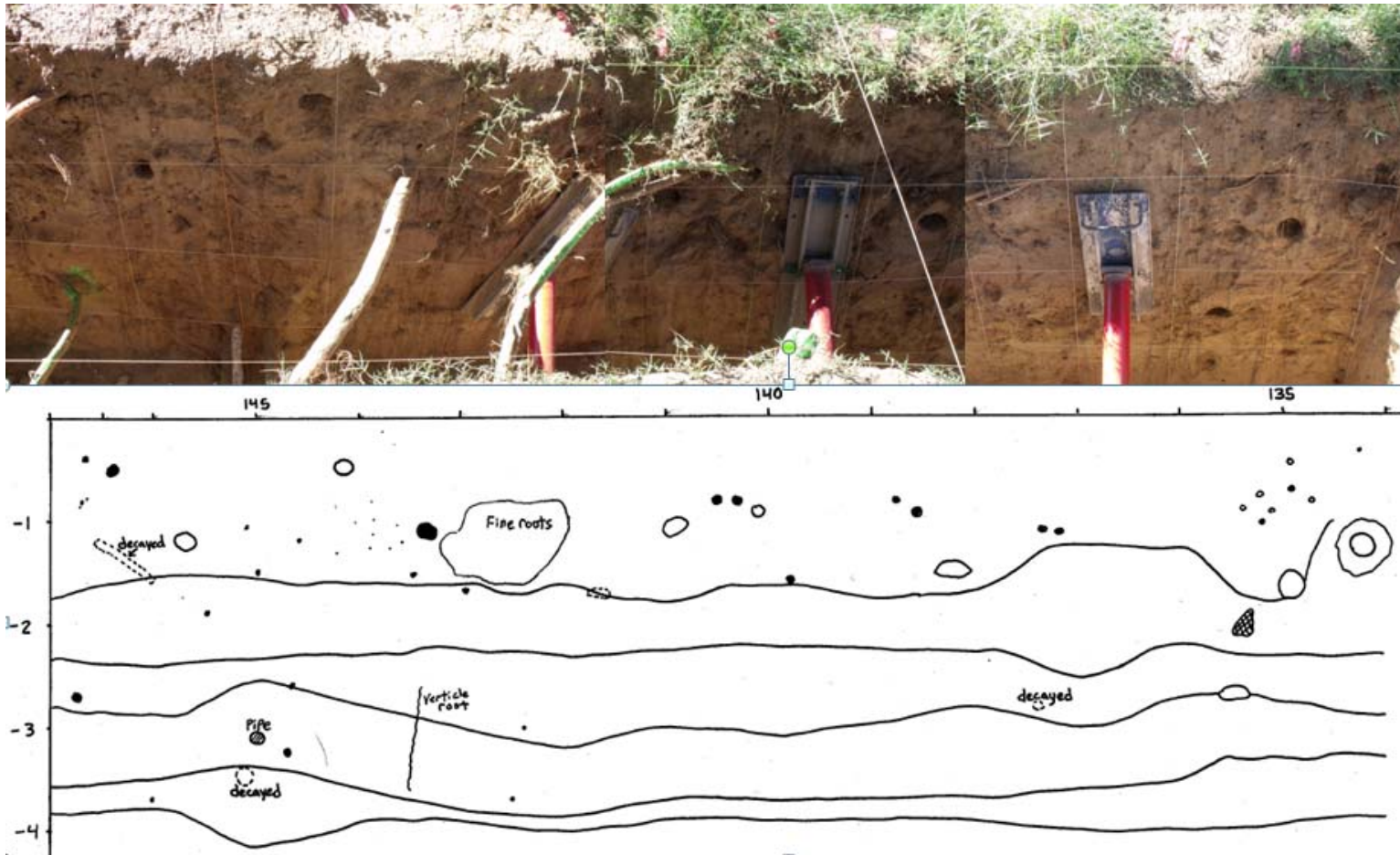
Figure 2C- 21. Spliced photos looking south (top) and analogous uphill wall log (bottom) of lower stump trench Stations 134-147.
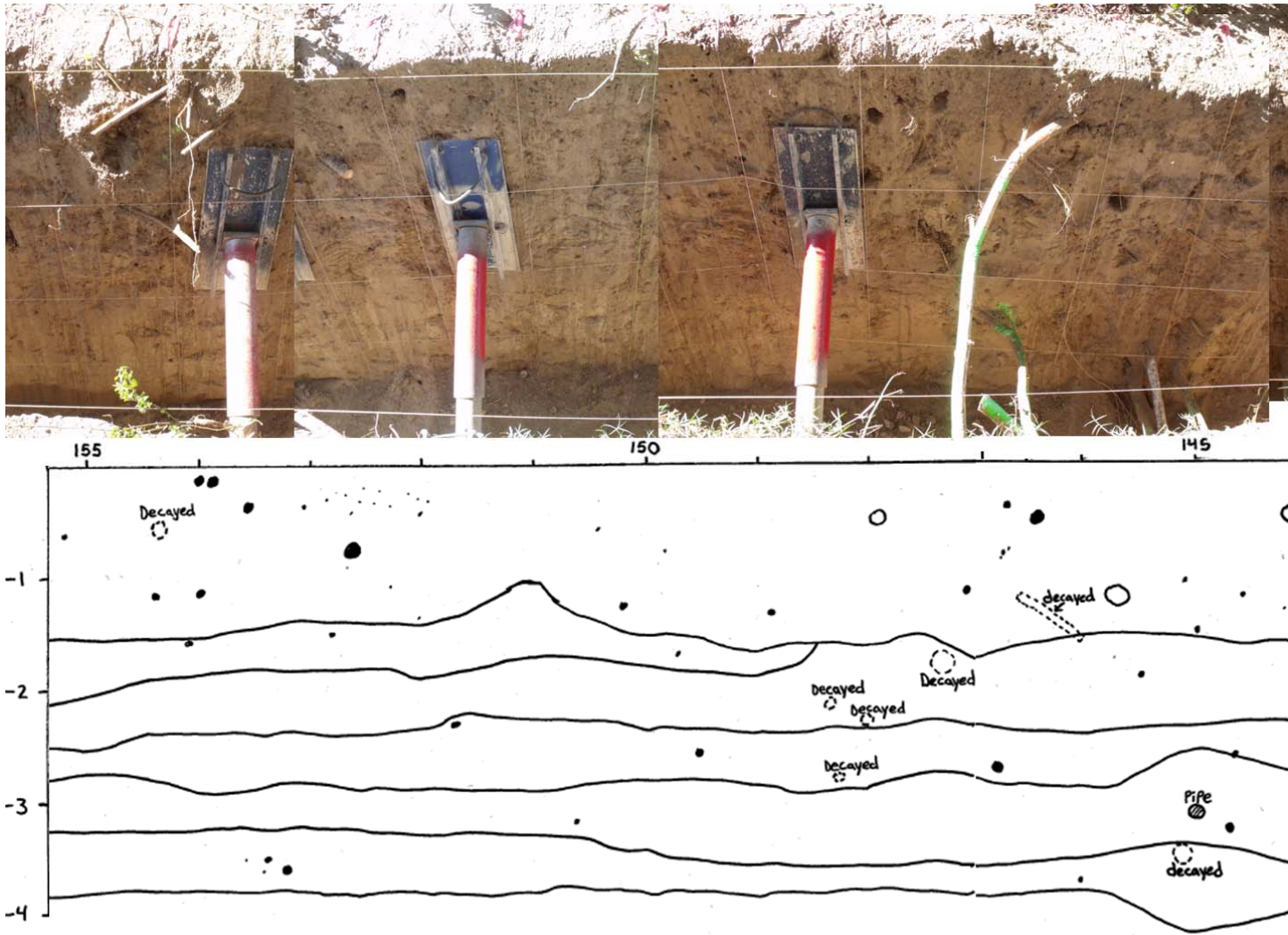
Figure 2C- 22. Spliced photos looking south (top) and analogous uphill wall log (bottom) of lower stump trench Stations 144-155.
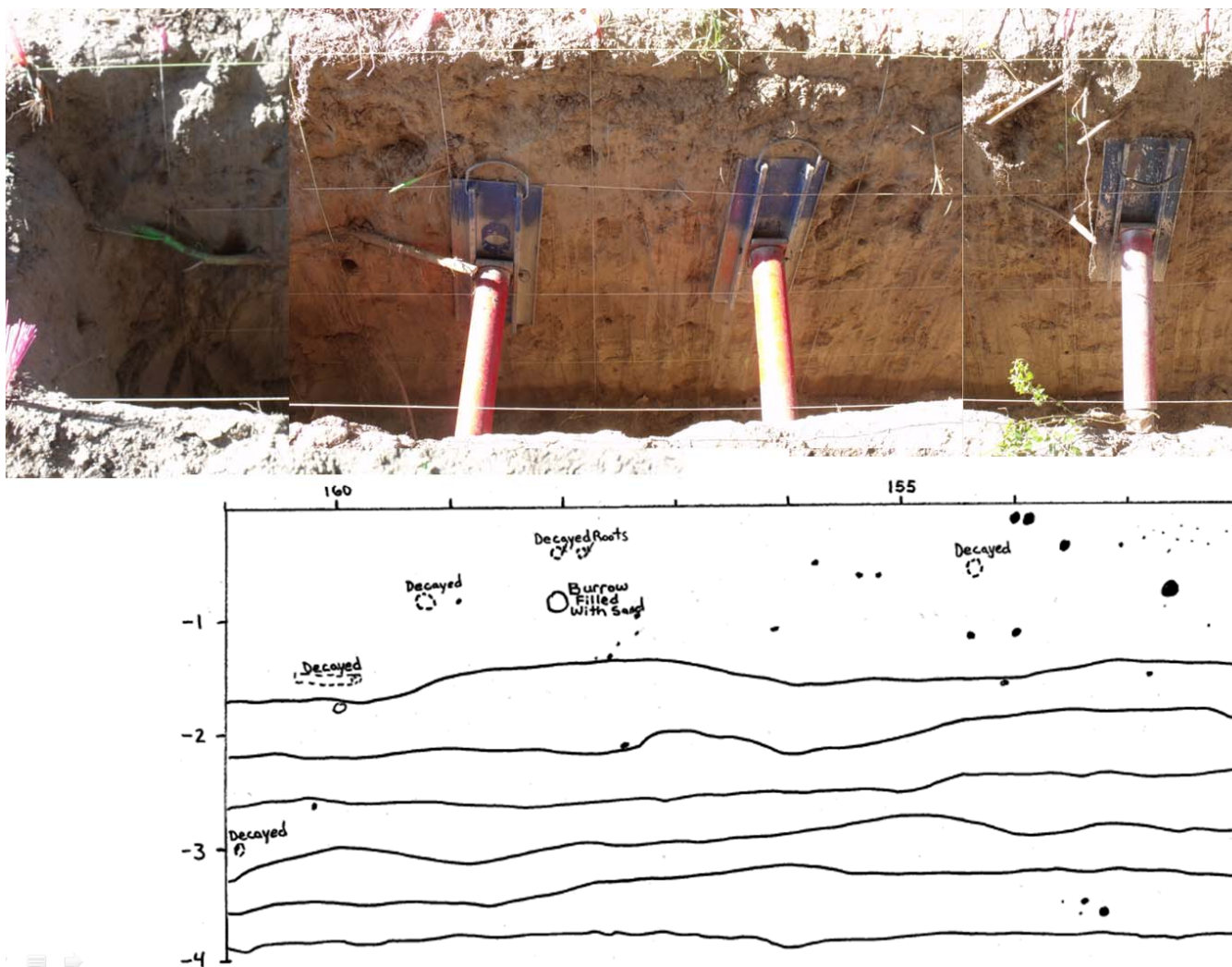
Figure 2C- 23. Spliced photos looking south (top) and analogous uphill wall log (bottom) of lower stump trench Stations 152-161.
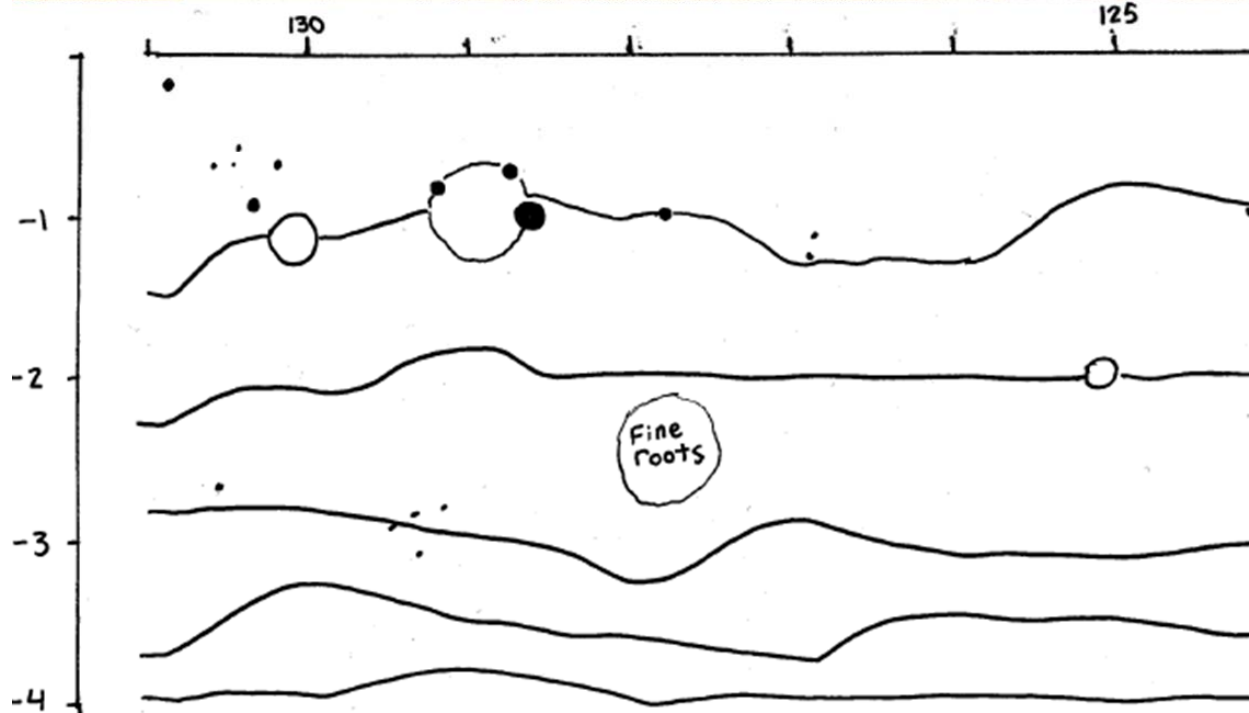
Figure 2C- 24. Spliced photos looking south (above) and uphill wall log (below) of lower control trench Stations 124-131.
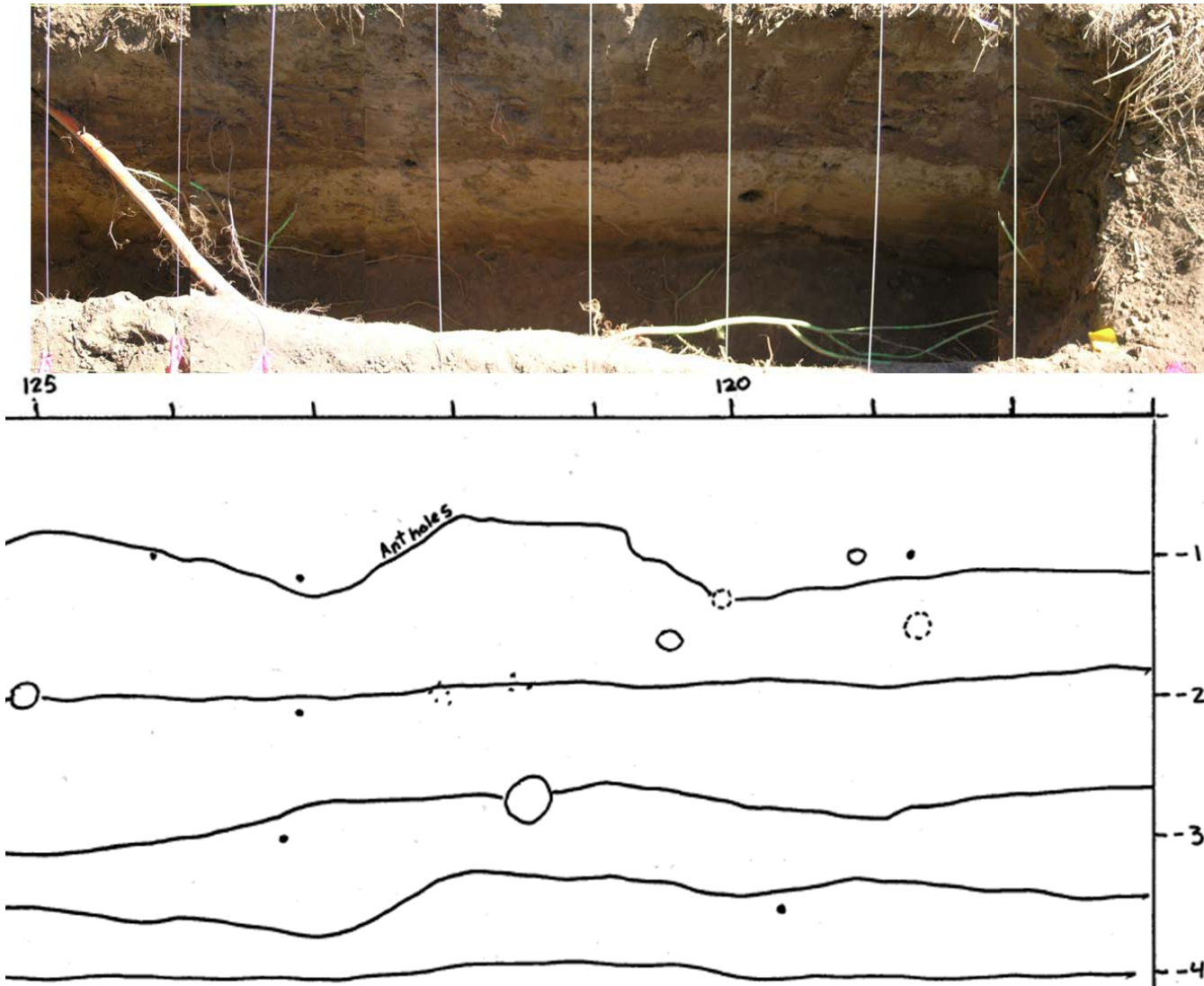
Figure 2C- 25. Spliced photos looking south (top) and analogous uphill wall log (bottom) of lower control trench Stations 117-125.
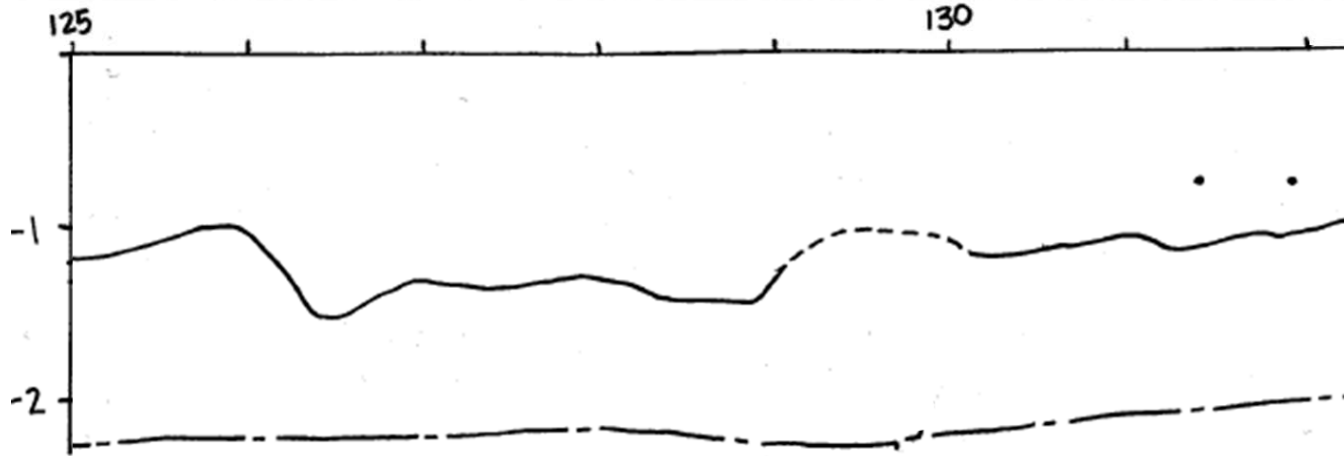
Figure 2C- 26. Spliced photos looking north (top) and analogous downhill wall log (bottom) of upper control trench Stations 125 to 132. Photos were taken prior to excavation completion.
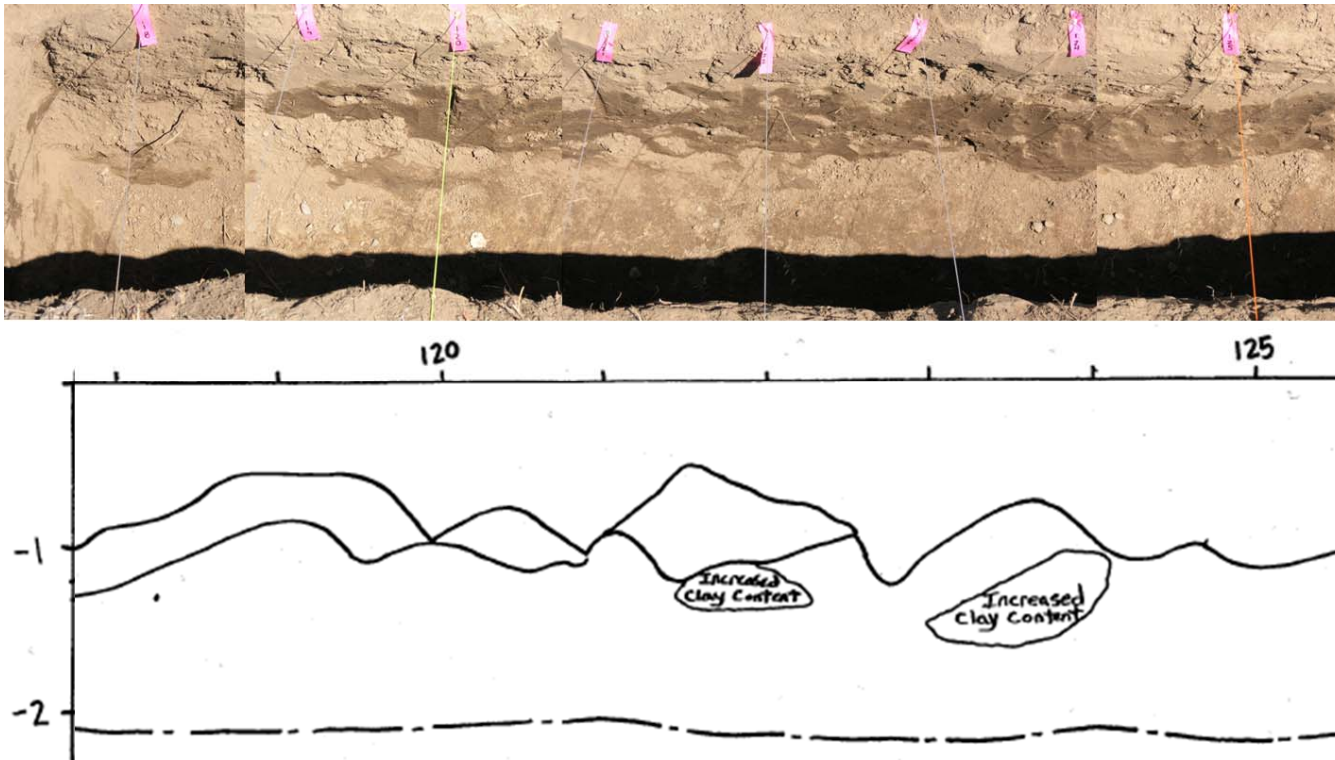
Figure 2C- 27. Spliced photos looking north (top) and analogous downhill wall log (bottom) of upper control trench Stations 118 to 125. Photos were taken prior to excavation completion.
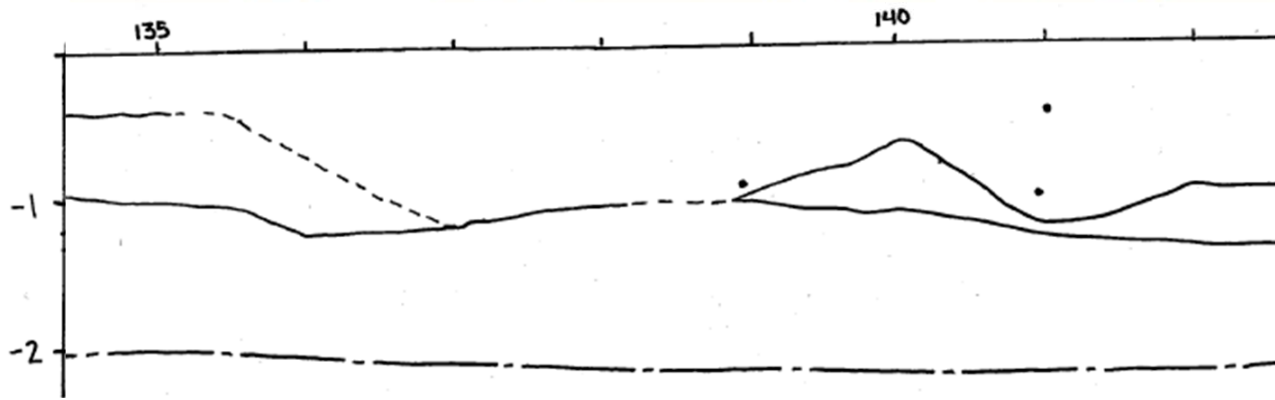
Figure 2C- 28. Spliced photos looking north (top) and analogous downhill wall log (bottom) of upper stump trench Stations 134 to 142. Photos were taken prior to excavation completion.
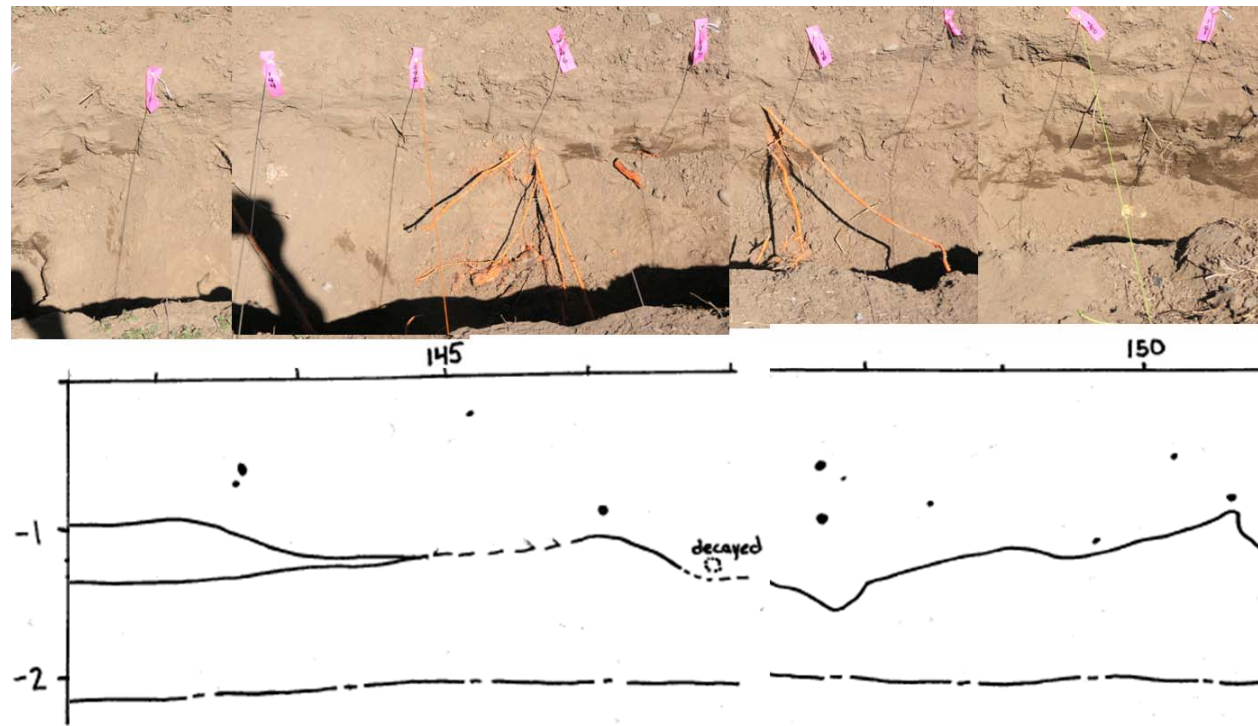
Figure 2C- 29. Spliced photos looking north (top) and analogous downhill wall log (bottom) of upper stump trench Stations 142.5 to 151. Photos were taken prior to excavation completion.
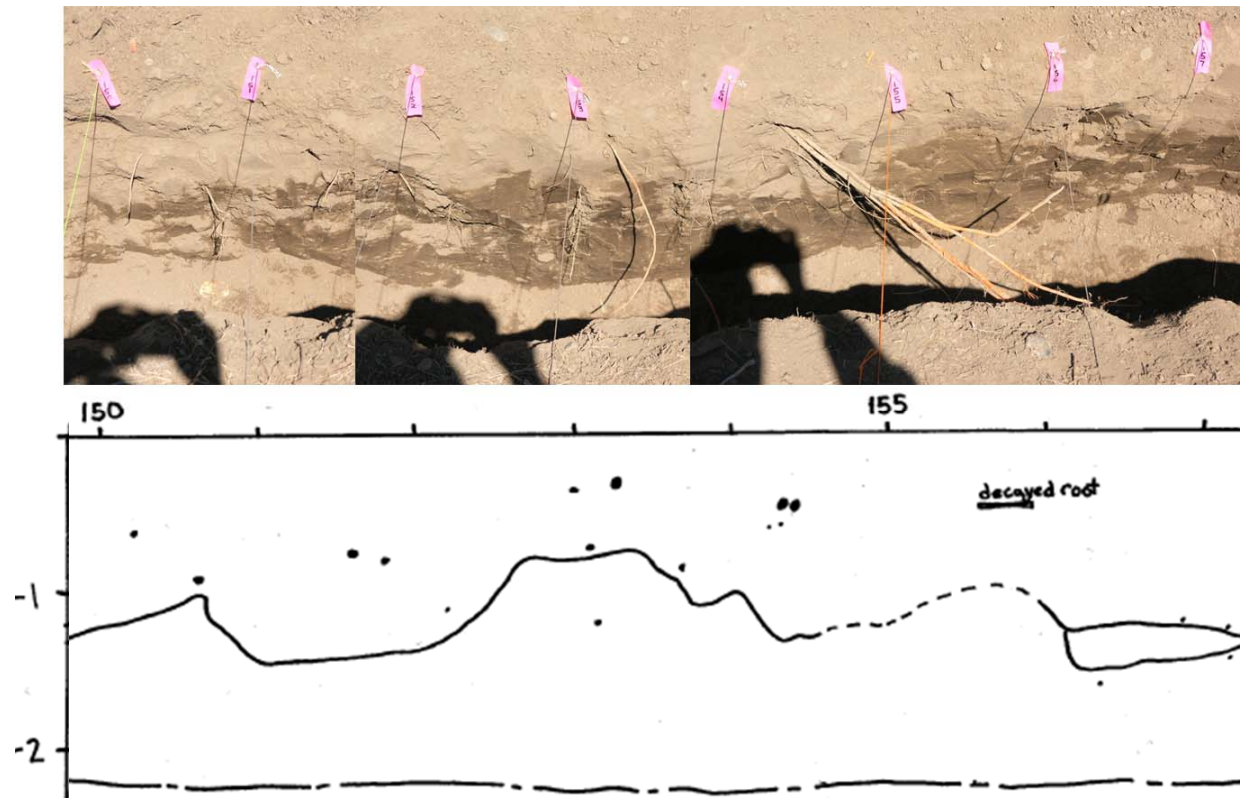
Figure 2C- 30. Spliced photos looking north (top) and analogous downhill wall log (bottom) of upper stump trench Stations 150 to 157. Photos were taken prior to excavation completion.
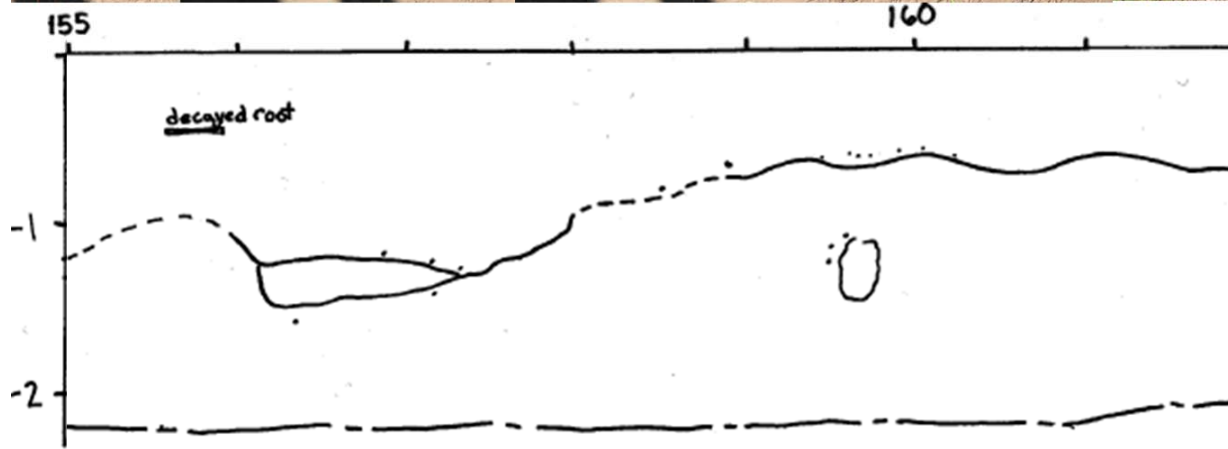
Figure 2C- 31. Spliced photos looking north (top) and analogous downhill wall log (bottom) of upper stump trench Stations 155 to 162. Photos were taken prior to excavation completion.

# APPENDIX 2D

## Instrument Data – Cal Expo Test Site

Tensiometer data is presented first, followed by piezometer data. Tensiometer data collection began with a dry run equilibration phase. During the dry run equilibration phase, tensiometers were assembled, leak checked, installed in the ground. Soil Moisture tensiometers of 24, 48, and 60 inches in length were assembled with brass 'T' adaptors to allow for connection of both a mechanical gauge and a Model 5301 current transducer by Soil Moisture. The current transducer was wired to a Campbell Scientific CR3000 datalogger in order to continuously read the instruments. The current output from each transducer was converted to voltage using a 249 ohm resister with a resistor error of 1 percent. Based on manufacturer's specifications, currents of 4 and 20 mA correspond to soil suction values of 0 and 100 kpa, respectively. The values can be scaled linearly between these values. With a resistance of 249 ohms, using Ohms Law (which states that voltage is equal to current multiplied by resistance) voltages of 996 ohms and 4980 ohms correspond to soil suction values of 0 and 100 kpa, respectively, sharing the same linear relationship.



Figure 2D- 1. Components of a tensiometer broken down by Fredlund and Rahardjo, 2005 (left) as compared with our tensiometer equipped with both vacuum gauge and transducer (right).

Figure 2D- 2 shows the locations of instruments installed at the site. Tensiometers T4B-18, and T3C-36 and piezometer P2B-84 were not functional. Tensiometers were connected to the datalogger during the days leading up to the flow test to check functionality. Tensiometer T1A-36 was selected for a calibration test. The instrument was installed in the ground, and allowed to develop tensions that seemed relatively constant based on readings of the mechanical gauge. The datalogger was observed in real time while the mechanical gauge was read periodically. Mechanical gauge suction values were compared with corresponding readings from the transducer. The results are shown on Figure 2D- 3. At high suction values, the mechanical gauge yielded higher values of soil suction than the transducer. The instrument was opened during the test, water added, and the instrument re-sealed. After 40 minutes, tension had not increased to the level prior to opening the instrument. The mechanical gauge and the transducer were generally in good agreement for much of the test. Error of the resistor is shown on the plot and does not explain the discrepancy between the gauge and the transducer at high suction values.

Regular maintenance of the tensiometers is required in the form of water additions. Water can run low in the instrument and may need to be added periodically, dropping the tension of the instrument to zero while the cap is open. In processing the data, corrections are made to subtract the weight of the water column from the reading as the weight of the water in the instrument adds to the tension. When this correction is made to all data points, data can show falsely as negative suction, or pressure, during times when this correction is made and the tensions have not yet been re-established in the instrument following a filling event. The correction is made to account for the entire instrument length, though 24 inch instruments were installed to depths of 18 inches and 48 inch instruments were installed to depths of 36 inches.  The 60 inch instruments were installed to the full instrument depth of 60 inches.
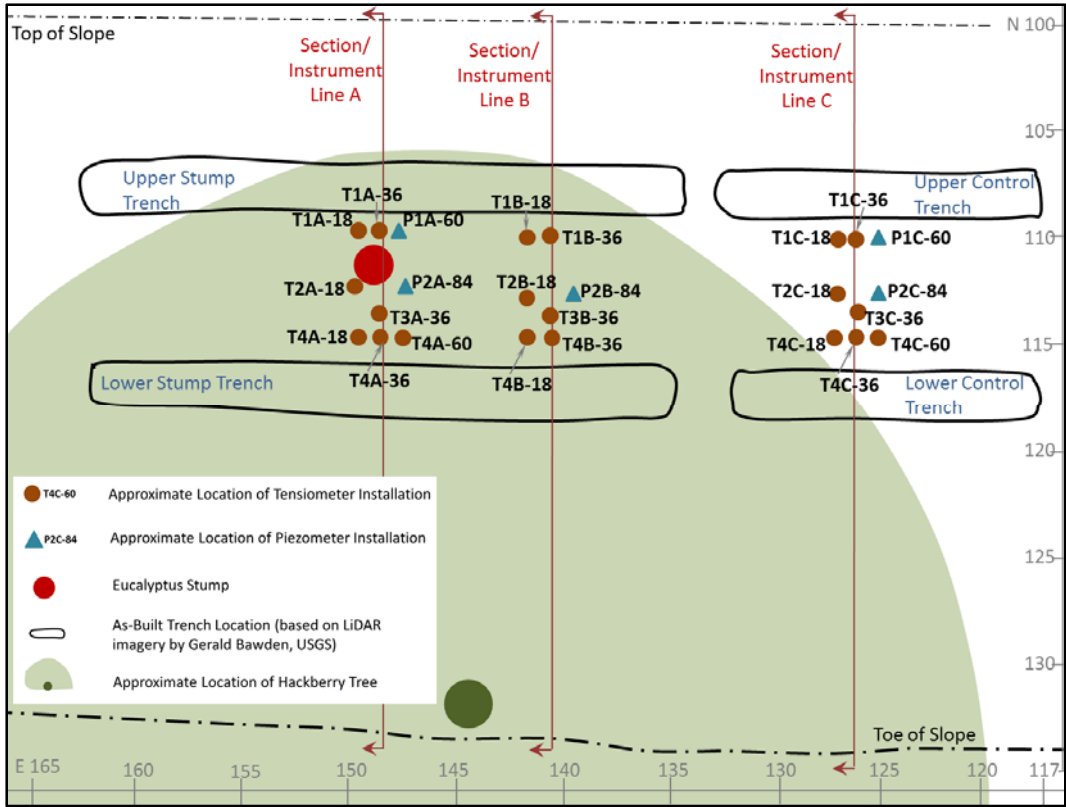
Figure 2D- 2. Location of instrument lines A, B, and C, tensiometers, and piezometers.
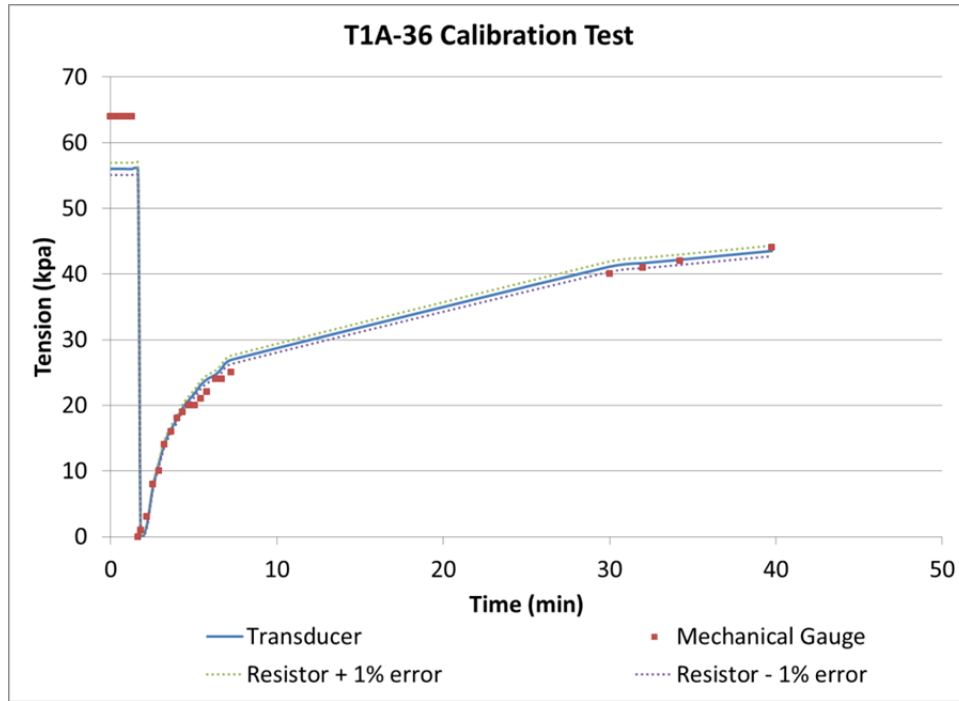
Figure 2D- 3. Calibration test correlating readings from mechanical vacuum gauge with transducer readings for tensiometer T1A-36.

Figure 2D- 4 compares mechanical gauge readings with those measured by current transducers. All instruments are shown for two time intervals on the two days just before the flow test. The flow test began on September 7, 2010 at 11:57am and comparisons between mechanical gauges and transducers were performed on September 5th and 6th. Mechanical gauge readings predicted higher values of suction than transducers in 14 of 18 tensiometers on September 5th and in 12 of 18 tensiometers on September 6th. The mean percent difference between gauge readings and transducers was 14.9 percent with a standard deviation of 11.5 percent on September 5th whereas it dropped to 13.1 percent with a 9.14 percent standard deviation the next day. Air bubbles can become trapped in the gauges and at high suction values can enter through the high air entry value ceramic cups at the base. Air content in the fill water, though minimized by boiling water in the field or bringing de-aired water from the lab prior to filling the instruments, can introduce higher errors at high suction values (approaching cavitation) as air bubbles are formed inside the instrument. Soilmoisture Equipment Corporation ceramic cups have an air entry value of about -100 kPa, however increasing this value would not improve accuracy of the instruments as the water in the tube will cavitate when the water pressure reaches -90 kPa (Fredlund and Rahardjo, 1993). Given that the height of the water column adds to the suction, the maximum value of matric suction that can be achieved with this system is 84 kPa, 78 kPa, and 75 kPa for 24 inch, 48 inch, and 60 inch instruments, respectively. Longer instruments are therefore less capable of measuring high values of matric suction.

Two days prior to the flow test, the datalogger was connected and a continuous record of soil suction was recorded for instrument lines A (Figure 2D- 5), B (Figure 2D- 6), and C (Figure 2D- 7). Water was added frequently prior to the flow test as soils were unsaturated. If air bubbles are allowed to accumulate inside the instrument, matric suctions read on the instruments can falsely trend toward zero, or atmospheric pressure (Fredlund and Rahardjo, 2005). Tensiometers T3A-36, T4A-36, T1B-18, T1B-36, T2B-18, T3B-36, T4B-36, and T4C-36 generally required more water than other instruments. These instruments show matric suction values that tend to have the lowest peak values of suction as compared to other nearby instruments or comparable depth instruments in other instrument lines. Further, curve shapes tend to be irregular, always dropping, while instruments that did not require addition of water as often developed regular curves with relatively constant values of matric suction prior to the arrival of the wetting front. It is possible that air was slowly entering the system in these instruments, either through a poor seal at the ceramic cup or through air entering through the porous ceramic cup. The results from these instruments was removed from the falling head test results as the test was conducted over a period of time when no one was onsite daily to maintain water in the instruments. Peak values of suction for these instruments are unlikely to be accurate, however a distinct drop in suction was achieved in each of the instruments indicating the arrival of the wetting front. We believe that the data is accurate for the purpose of understanding the timing of the wetting front arrival, but untrustworthy for peak values of matric suction prior to, during, and after the flow test.
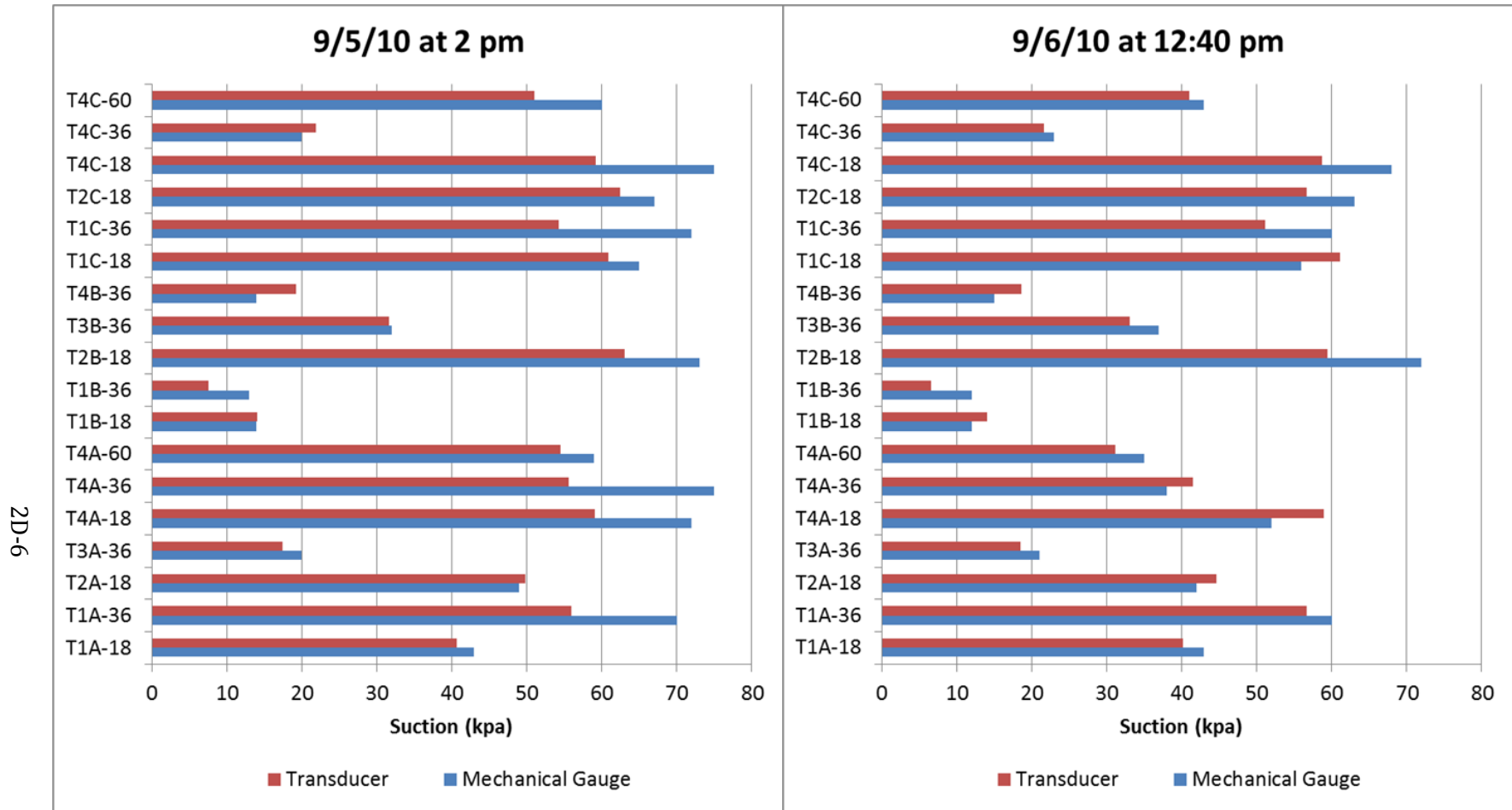
Figure 2D- 4. Comparison of mechanical vacuum gauge readings with transducer results for all instruments.
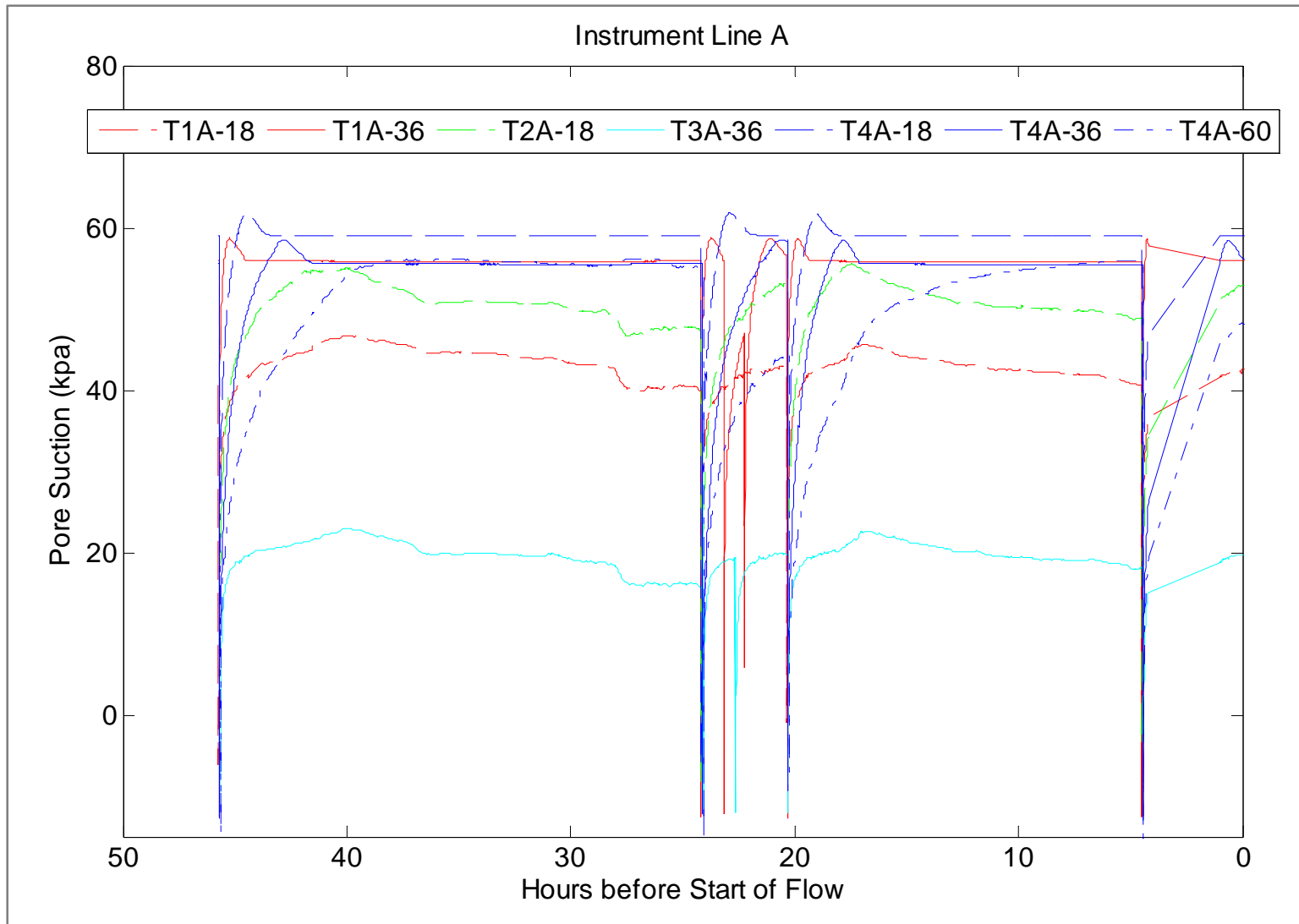
Figure 2D- 5. Matric suction values read from transducers at Line A tensiometers prior to the flow test.
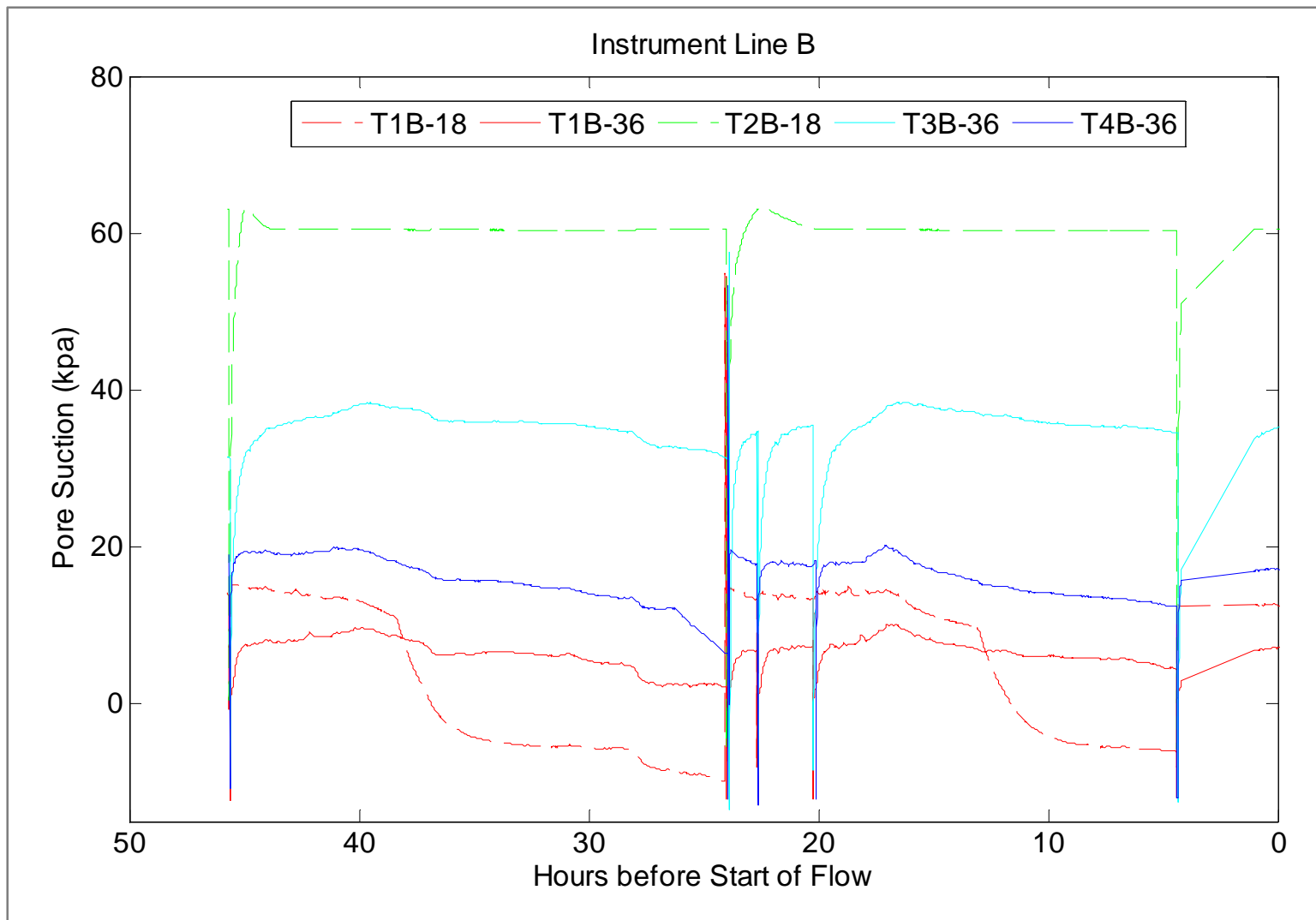
Figure 2D- 6. Matric suction values read from transducers at Line B tensiometers prior to the flow test.
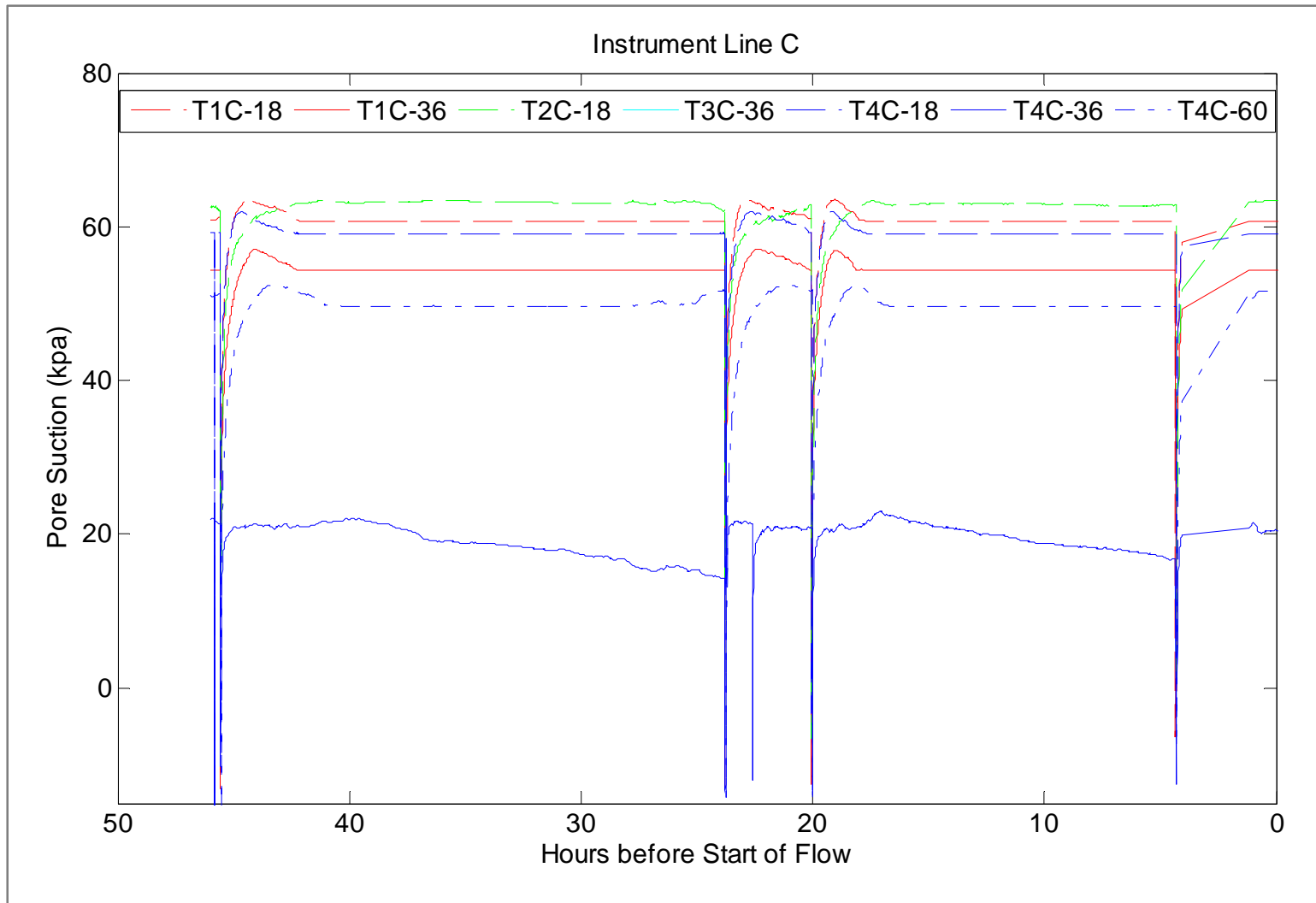
Figure 2D- 7. Matric suction values read from transducers at Line A tensiometers prior to the flow test.

Figure 2D- 8 shows a typical profile of suction with time during the flow test and the days following the test as the soil began to dry out. The plot shows the drop in tension that is expected when the instrument is opened and filled, the drop in tension associated with the arrival of the wetting front, the slight rise in soil suction when water ran low in the trenches, and the re-establishment of matric suction in the soils as drying began following the flow test.
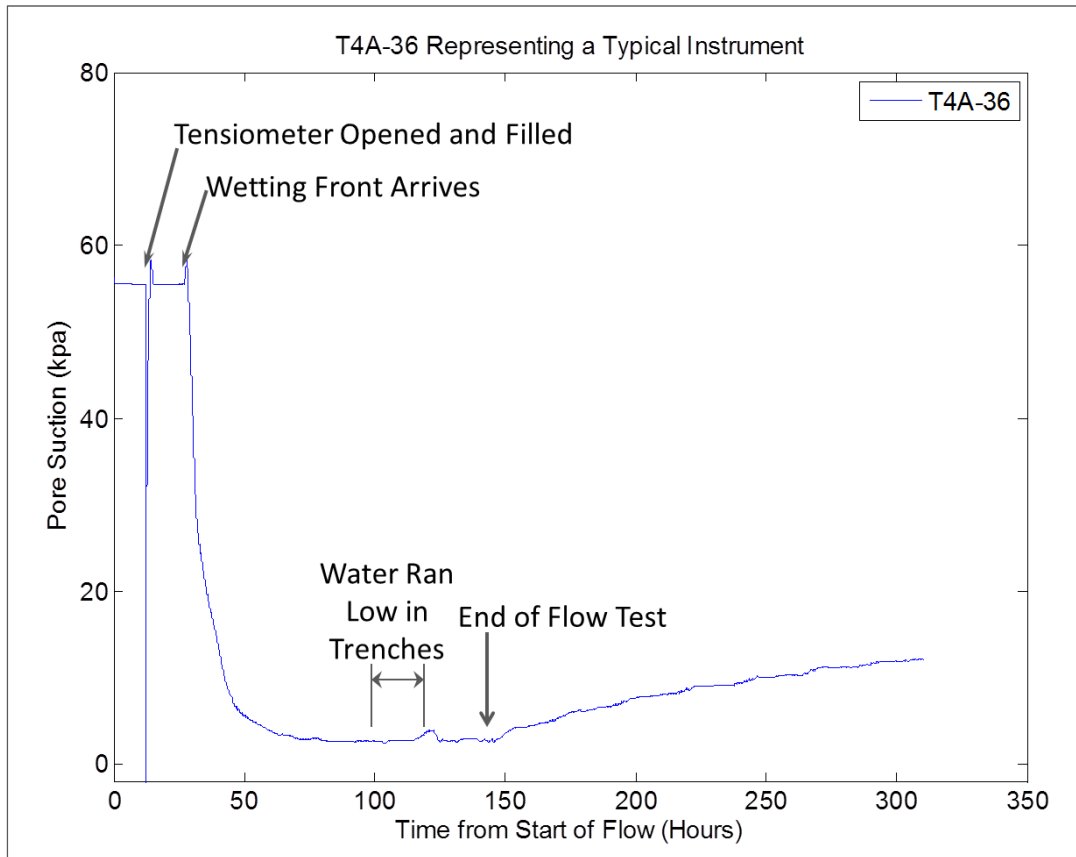


Figure 2D- 8. A typical tensiometer result for the flow test the drying period that followed.

Figure 2D- 9 provides a summary of all instrument data gathered during the flow test. Similar patterns to those of Figure 2D- 8 are seen with each instrument, however the arrival of the wetting front and the rate of decrease in suction values varies from almost immediately arriving to arriving after a period of nearly 3 days. Table E-1 provides a summary of wetting front and saturation front arrivals as well as steady state suction values for tensiometers. Table E-2 provides a summary of the saturation front arrival and buildup of pore pressures for piezometers. A discussion of instrument results in the context of the flow test observations is provided in Section 3.6.4.

Tensiometer data during the first 4 days of the flow test are provided by instrument line as Figure 2D- 10 through Figure 2D- 12.   Tensiometer data are then displaced for like instruments across all three instrument lines with results presented on Figure 2D- 13 through Figure 2D- 19.
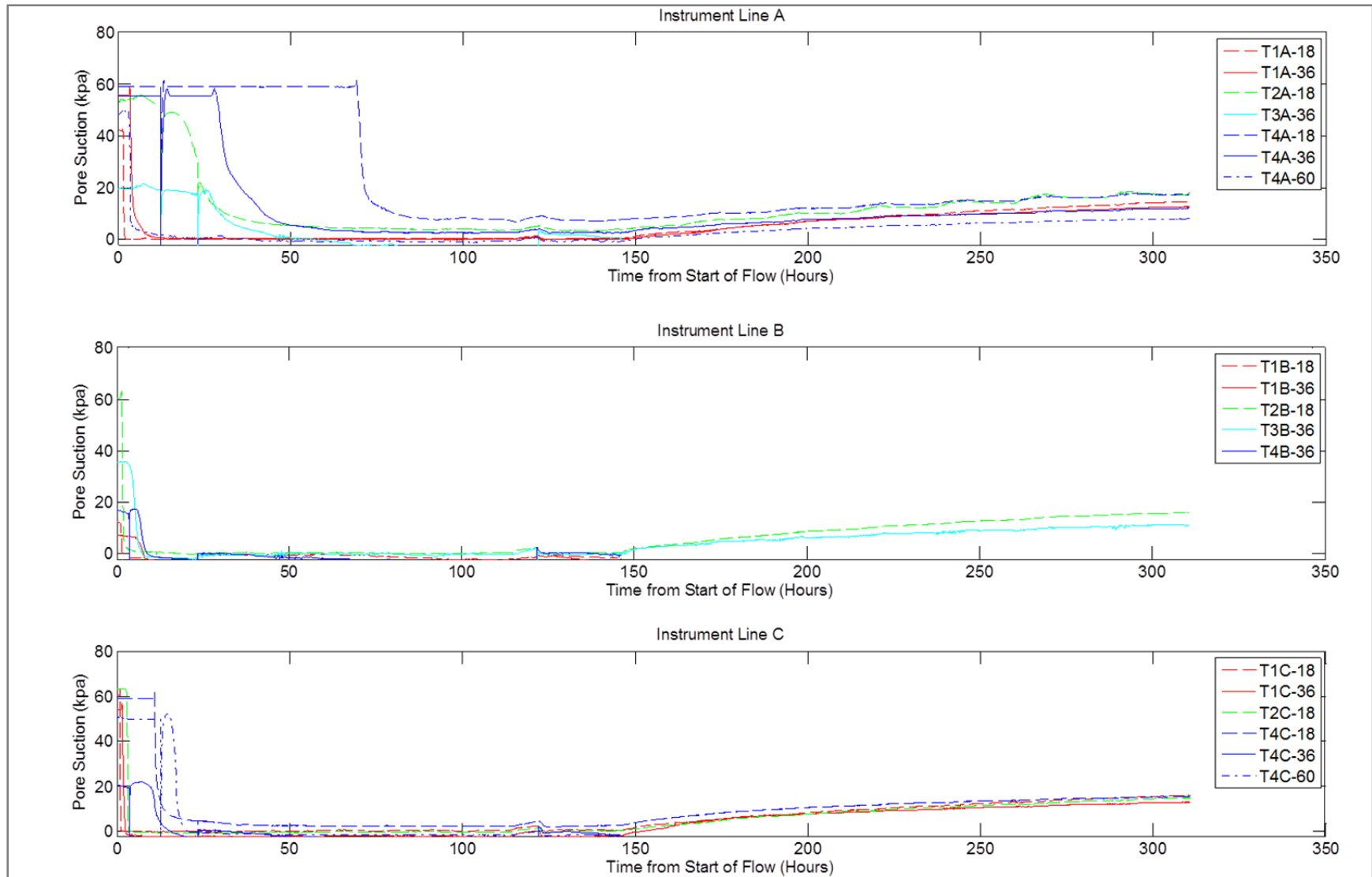
Figure 2D- 9. Tensiometer data for instrument lines A, B, and C for the duration of the flow test (146.25 hours or 6 days) and the falling head and drying phase that followed.

Table 2D-1. Tensiometer wetting and saturation fronts.

| Instrument Name | Wetting Front Arrival (hrs) | Time to Steady State (hrs) | Steady State Suction for Unsaturated Instruments (kpa)* | Saturation Achieved? (y/n) | Time of Saturation (hrs) |
|---|---|---|---|---|---|
| T1A-18 | 1.5 | 2.5 | 0 to 0.6 | near saturation | 2.5 |
| T1A-36 | 3.5 | 13.4 | 0.62 | n | - |
| T2A-18 | 15.6 | 45.5 | 5.7 | n | - |
| T3A-36 | 26.3 | 92.0 | Pressure | y | 57 |
| T4A-18 | 69.3 | 88.4 | 8.08 | n | - |
| T4A-36 | 28.5 | 69.2 | 3.08 | n | - |
| T4A-60 | 3.0 | 21.5 | 0 | y | 21.5 |
| T1B-18 | 1.1 | 2.1 | Pressure | y | 1.8 |
| T1B-36 | 6.2 | 10.2 | Pressure | y | 7.9 |
| T2B-18 | 1.6 | 7.7 | 0.7 | n | - |
| T3B-36 | 3.7 | 13.7 | Pressure | y | 9.1 |
| T4B-36 | 6.2 | 21.1 | Pressure | y | 9.1 |
| T1C-18 | 0.9 | 1.5 | 1.24 | n | - |
| T1C-36 | 1.5 | 2.8 | Pressure | y | 2.5 |
| T2C-18 | 2.7 | 3.5 | 0 | y | 3.5 |
| T4C-18 | 10.9 | 43.5 | 2.61 | n | - |
| T4C-36 | 9.6 | 23.6 | Pressure | y | 15.6 |
| T4C-60 | 15.7 | 44.9 | Pressure | y | 20.9 |

*Instruments indicated pressures on the order of 0 to 5 kpa. Pressures not reported as instrument calibrations do not support pressures

Table 2D-2. Piezometer saturation fronts.

| Instrument Name | Wetting Front Arrival (hrs) | Time to Steady State (hrs) | Steady State Pressure (kpa) |
|---|---|---|---|
| P1A-60 | 11.17 | 67.8 | 2.11 |
| P2A-84 | - | - | not reliable |
| P1C-60 | 1.55 | 69.5 | 6.7 |
| P2C-84 | 13.5 | 67.8 | 8.6 |
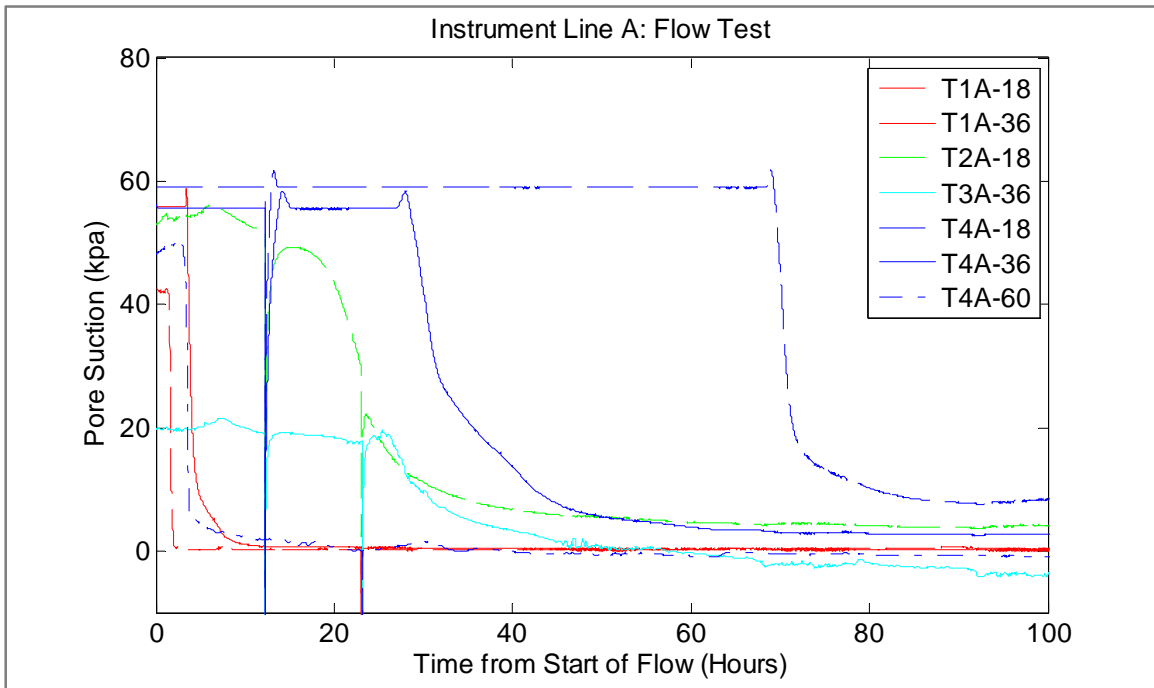
Figure 2D- 10. Summary of Tensiometer Data for Instrument Line A
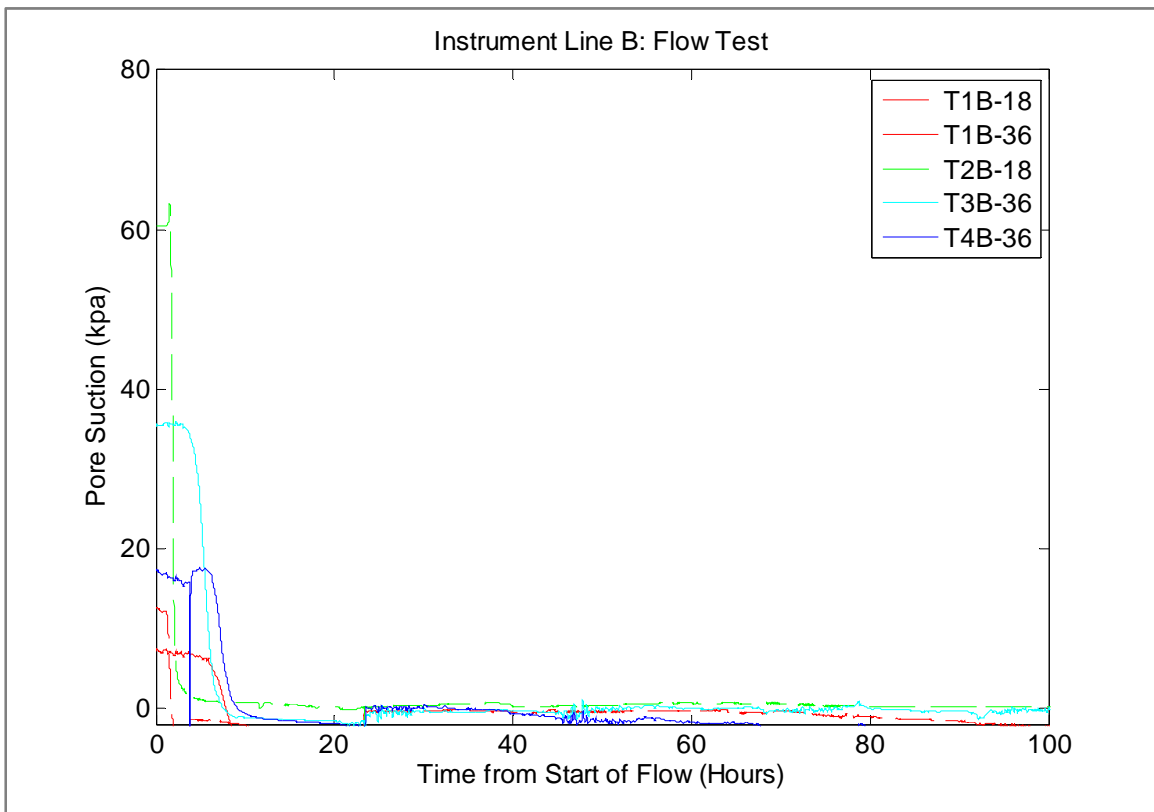


Figure 2D- 11. Summary of Tensiometer Data for Instrument Line B
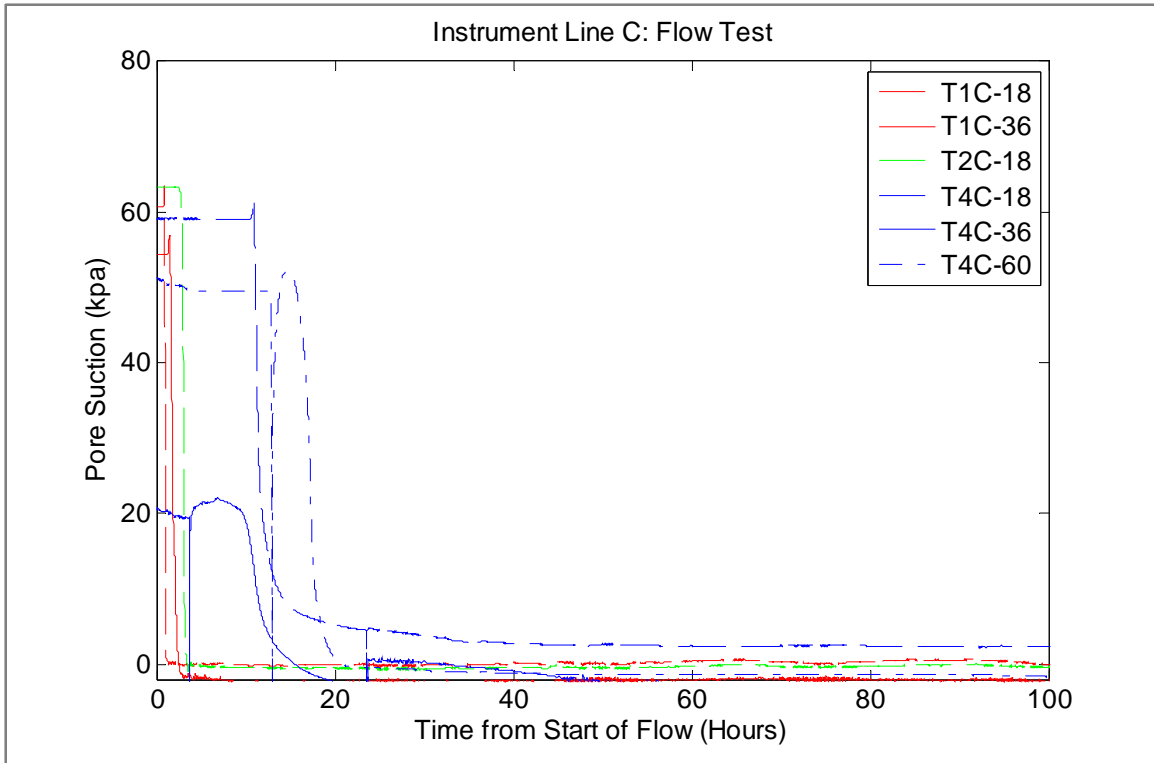
Figure 2D- 12. Summary of Tensiometer Data for Instrument Line C
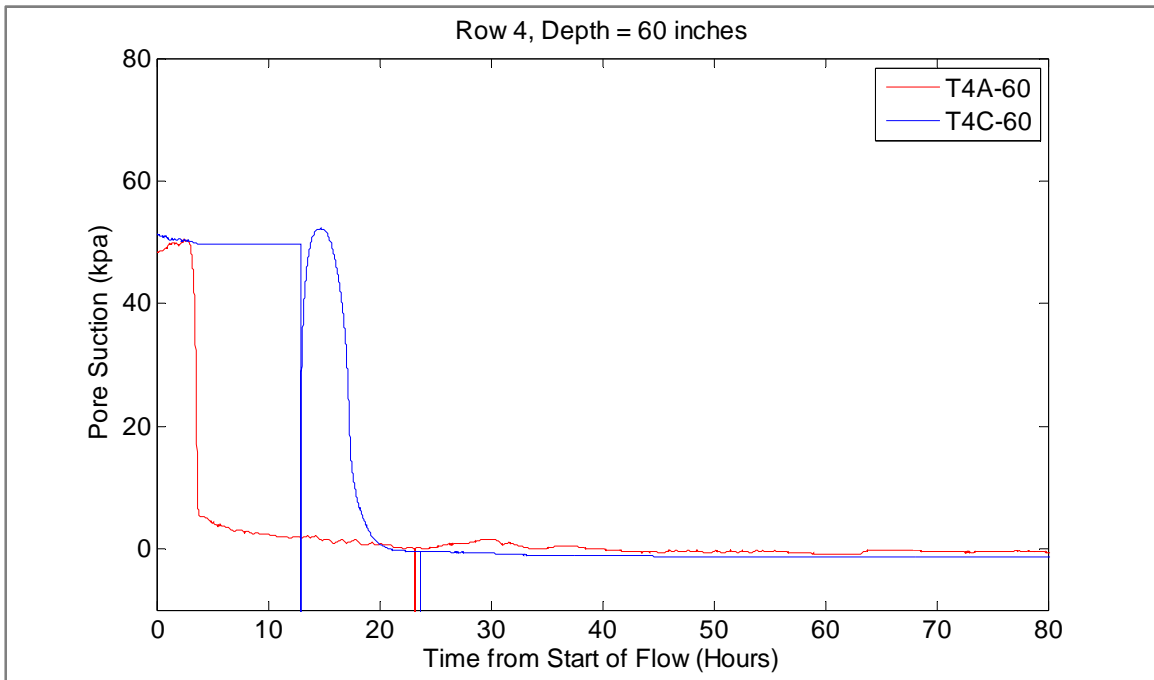


Figure 2D- 13. Comparison of Row 4 (below the stump) Lines A and C at 60 inch depth. Note the early saturation of the 60 inch tensiometer at Line A likely due to saturation flowing down from lower trench which was filling with water from the mammal burrow at Line B.
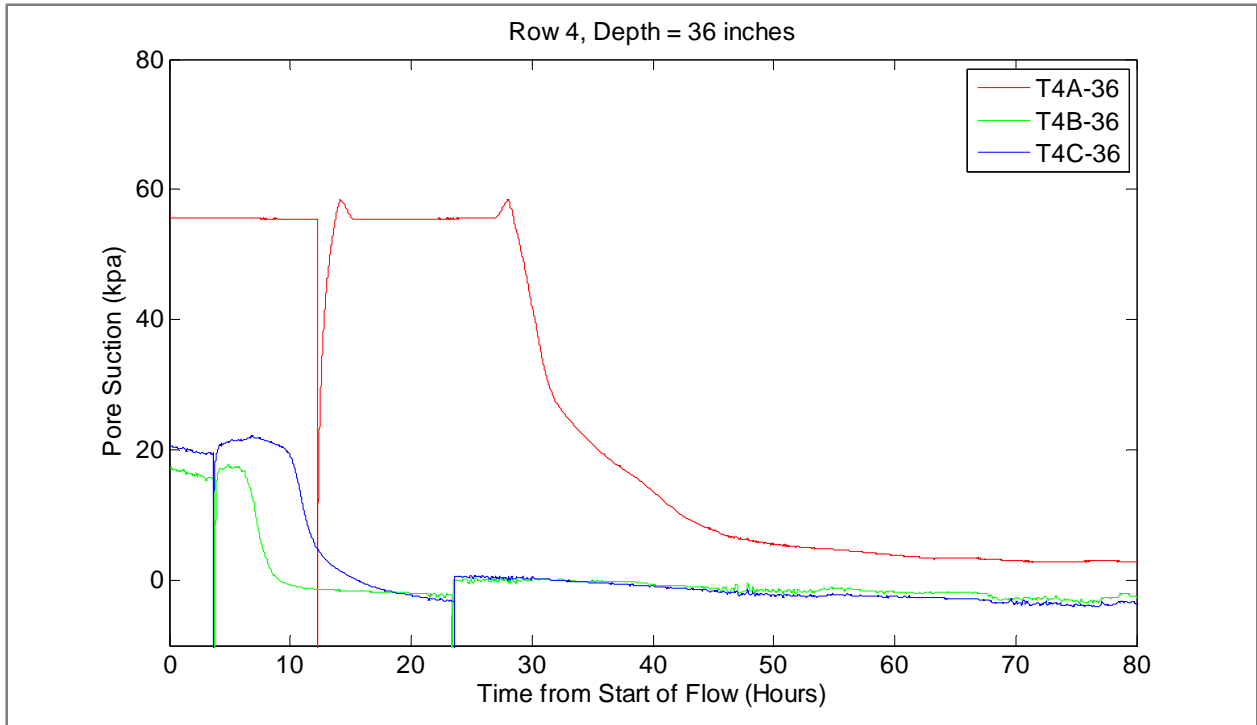
Figure 2D- 14. Comparison of Row 4 (below the stump) Lines A, B and C at 36 inch depth. Note that tensiometer T4A-36, below the stump, is the last to saturatE-
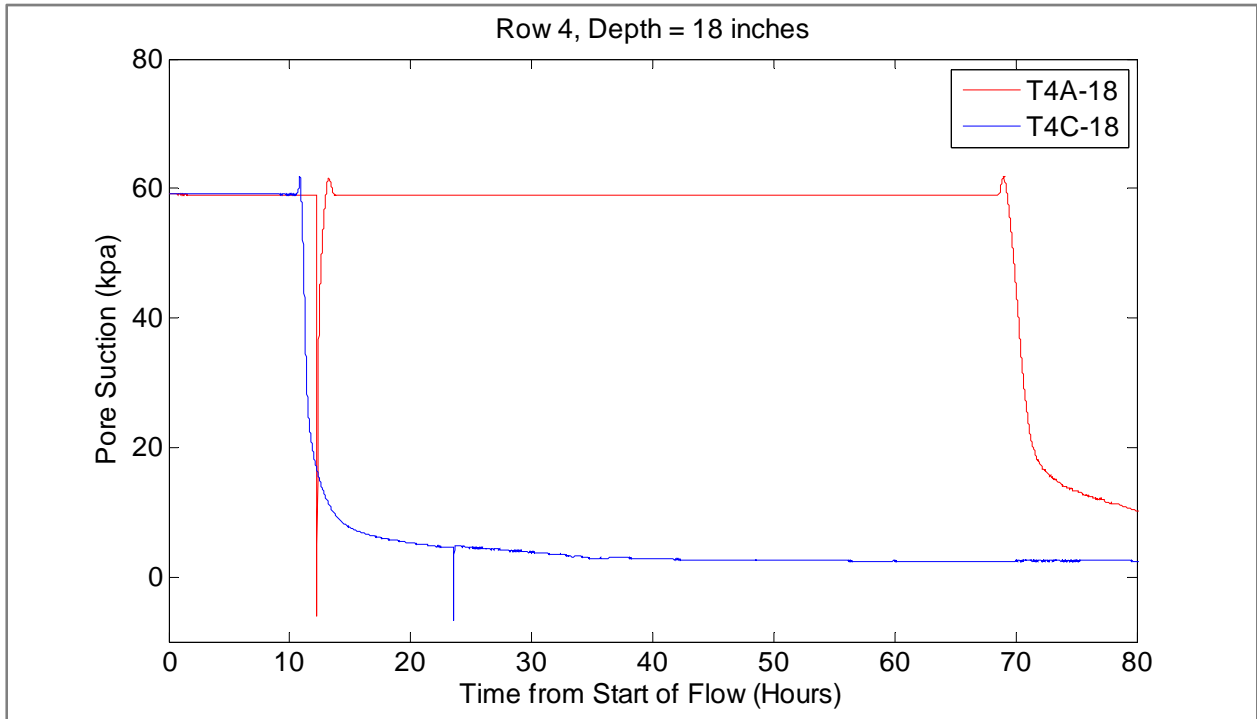


Figure 2D- 15. Comparison of Row 4 (below the stump) Lines A, B and C at 18 inch depth. Note that tensiometer T4A-18, below the stump, is the last to saturatE-
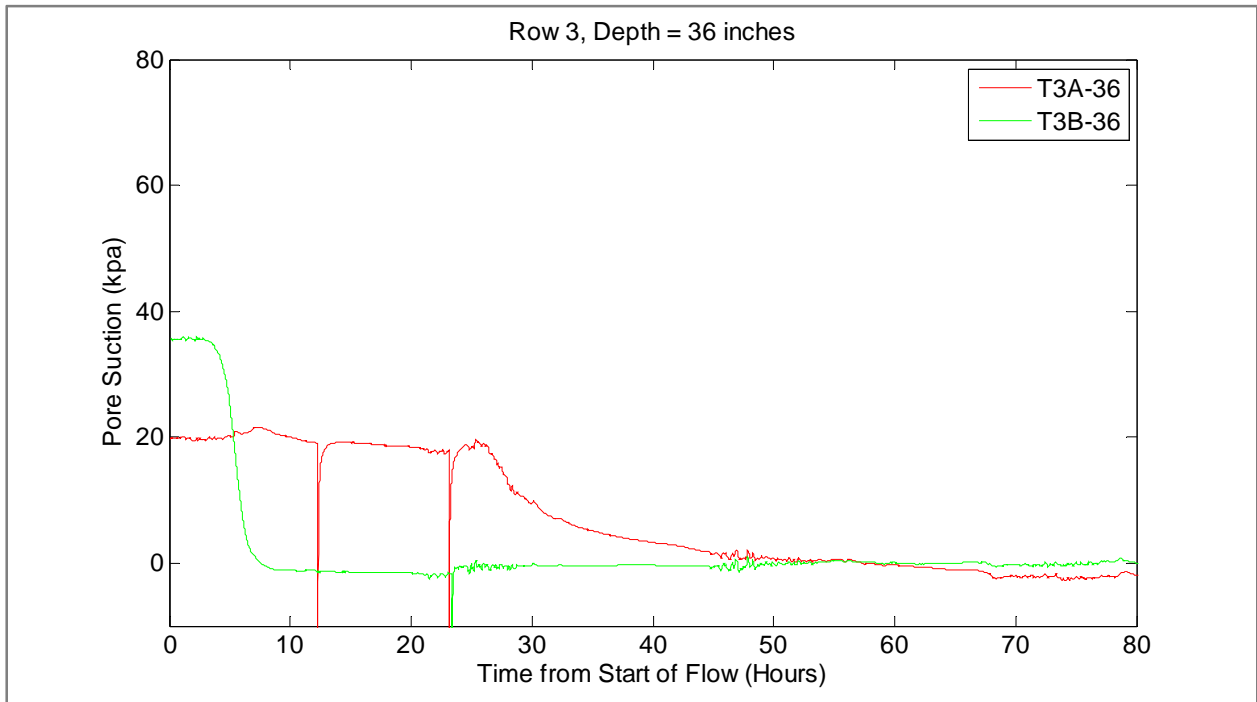
**Figure 2D- 16.** Comparison of Row 3 at Instrument Lines A and B at a depth of 36 inches. The analagous instrument at Line C was found to be non-functional during the test.
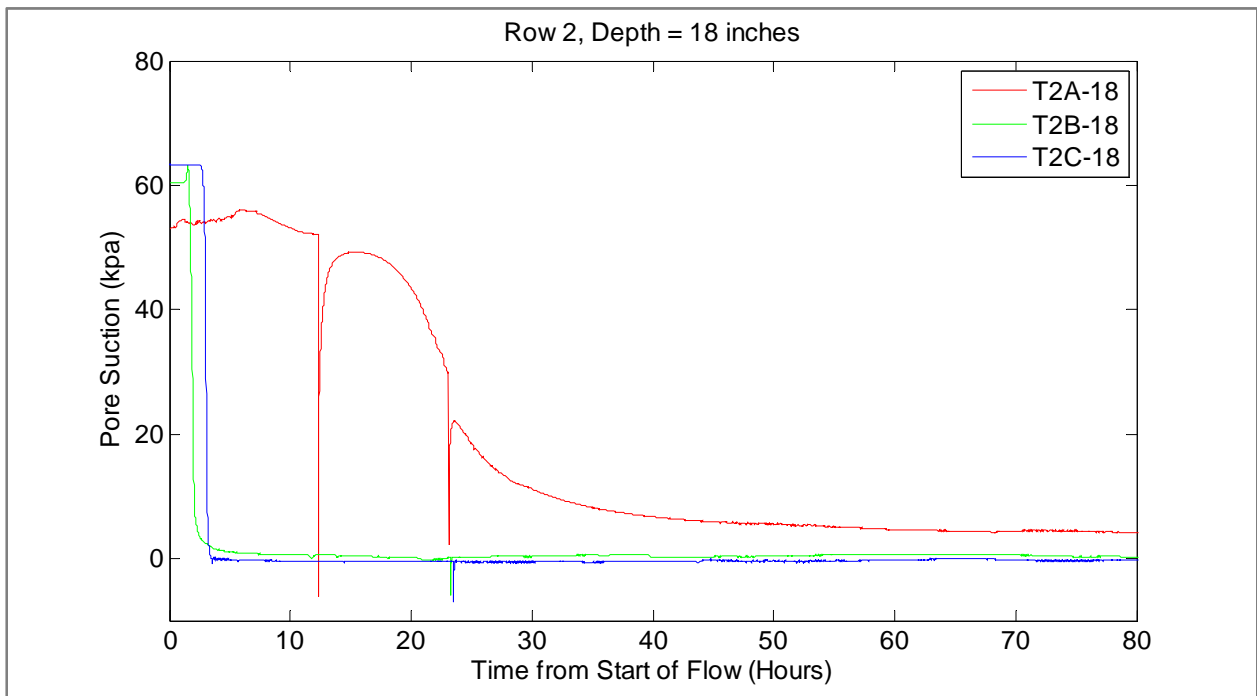


**Figure 2D- 17.** Comparison of Row 2 at Instrument Lines A, B and C at a depth of 18 inches. Note that instrument lines B and C saturate before Line A at the stump.
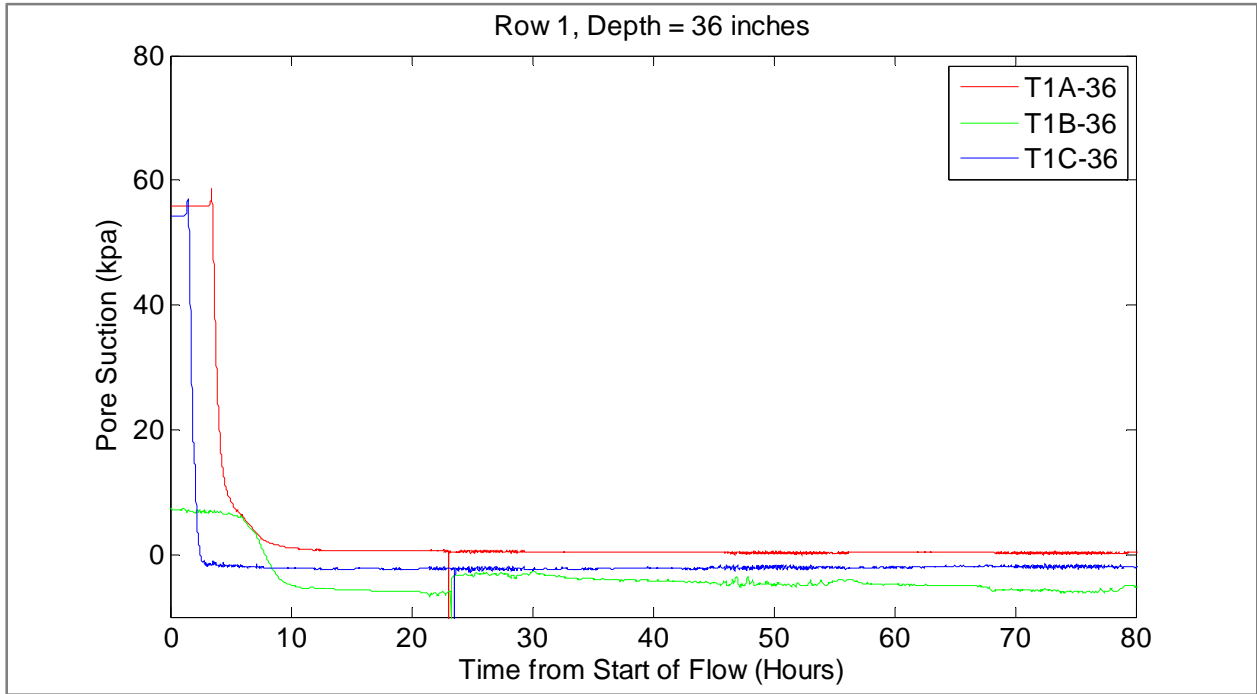
Figure 2D- 18. Comparison of Row 1 at Instrument Lines A, B and C at a depth of 36 inches
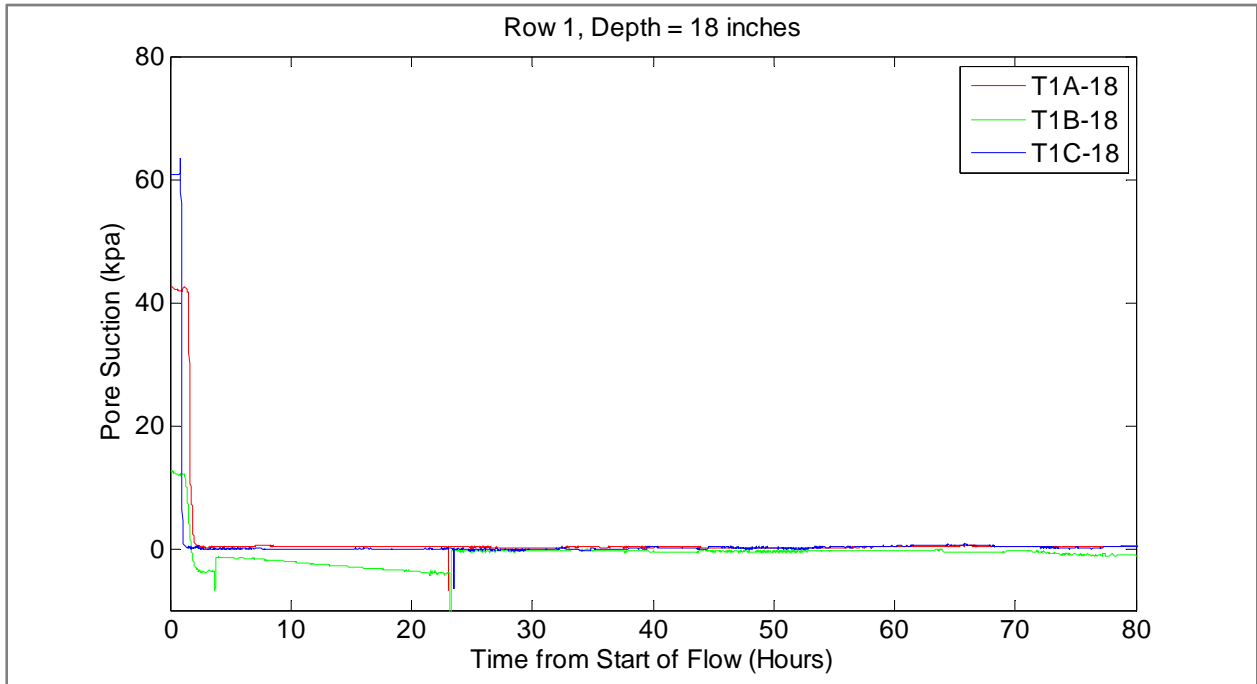


Figure 2D- 19. Comparison of Row 1 at Instrument Lines A, B, and C at a depth of 18 inches

Vibrating wire piezometers were pre-saturated and were grouted into place upside down to prevent desaturation of the porous stone in accordance with the recommendations of the manufacturer, onsite consultation with Eric Mikkelson, and available literature (Mikkelsen 2002; Mikkelsen and Green, 2003; McKenna, 1995; Vaughan, 1969; Contreras et al. 2008). Piezometers were not read continuously, but at regular intervals with a Model GK-403 vibrating wire piezometer readout box. Frequency of readings was determined based on the observed rates of change in recorded pore pressures. Figure E-11 provides a summary of recorded piezometer data at instrument lines A and C. Data results are discussed in Section 3.6.4 of the report and instrument installation is detailed in Section 3.5.3.
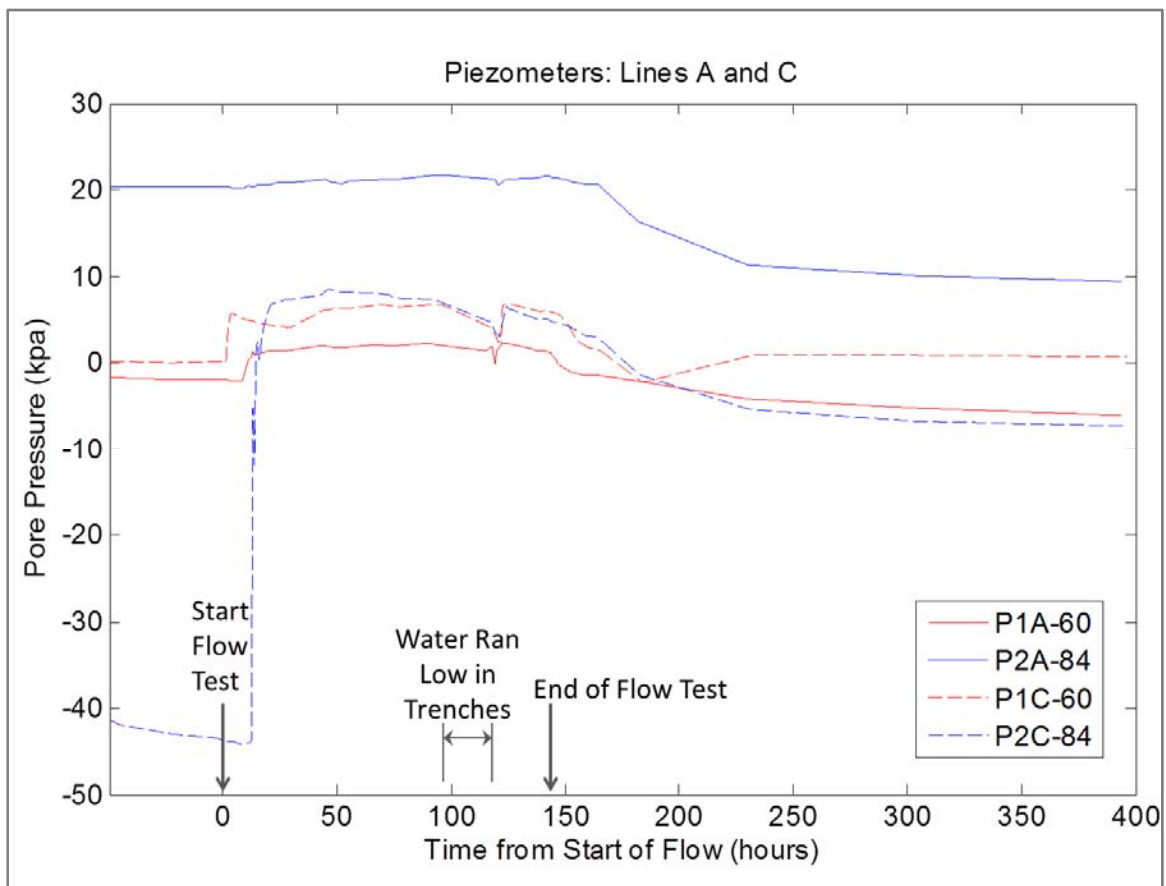


Figure 2D- 20. Pore pressures as measured during flow test through Instrument Lines A and C

# APPENDIX 2E

## Post Flow Site Characterization Logs

Root logs were created through a collaborative effort between John Lichter of Tree Associates, Richard Evans of UC Davis, and the UC Berkeley research team. Figure 2E- 1 through Figure 2E- 4 provide original root logs for the uphill wall of the lower trench (Station N117), the slice 1 wall face (Station N115), the slice 2 wall face (Station N113), and the slice 3 wall face (Station N111.5). The area around the stump was logged from Station E138 to 153. Slice 2 extended from E140 to 153, while slice 3 extended from E 143 to 153 due to the presence of the grouted animal burrow that we exposed and did not undermine. The excavation seemed to be an appropriate size to capture the decomposing root system with sufficient detail.

Abbreviations 'DR', 'LR', and 'H' were used to designate decomposed roots, live roots, and holes (or burrows) in the attached figures.

**October 1st**

| Name | Root Dia (in) | Root Area | Northing | Easting | Depth | Notes |
|------|---------------|-----------|----------|---------|-------|-------|
| DR5 | 0.5 | 0.2 | 117 | 148.3 | -2.2 | Intact, vertical orientation |
| DR6 | 0.6 | 0.3 | 117 | 148.3 | -2.7 | Intact, nearly vertical |
| DR7 | 0.7 | 0.3 | 117 | 148 | -2.3 | Intact, silica flour external |
| DR8 | 0.4 | 0.1 | 117 | 148 | -2.6 | Intact |
| DR3 | 0.4 | 0.1 | 117 | 146.6 | -1.2 | Hollow |
| DR2 | 2.0 | 3.1 | 117 | 145.2 | -3.7 | |
| DR4 | 3.2 | 8.0 | 117 | 147.5 | -1.6 | As of Oct 1 log, believe silica from T4A-36 |
| DR1 | 0.6 | 0.3 | 117 | 141.7 | -1.5 | |
| H1 | 2.3 | 4.0 | 117 | 139 | -1.3 | |
| H2 | 1.0 | 0.7 | 117 | 140 | -0.9 | |
| H3 | 0.9 | 0.6 | 117 | 140.6 | -1.2 | |
| H4 | 1.0 | 0.8 | 117 | 140.9 | -1.1 | |
| H5 | 2.6 | 5.3 | 117 | 144.3 | -0.4 | Ave dia; actual is 1.7x3.5 |
| H6 | 1.9 | 2.8 | 117 | 145.7 | -1.2 | |
| H7 | 1.4 | 1.5 | 117 | 147.3 | -0.35 | Ave dia; actual 1.5x1.25 |
| H8 | 1.5 | 1.8 | 117 | 147.8 | -0.5 | |



Figure 2E- 1. Log of original face of the uphill wall of the lower trench. Logged by John Lichter of Tree Associates and Richard Evans of UC Davis

October 5, 2010

| Name | Root Dia (in) | Root Area | Northing | Easting | Depth | Notes |
|---|---|---|---|---|---|---|
| DR1 | 0.5 | 0.2 | 114.9 | 139.5 | -0.65 | solid, no gap |
| DR2 | 2.5 | 4.7 | 114.8 | 143.8 | -0.4 | came apart in pieces, gap in places (0.25") but intermittant |
| DR3 | 1.3 | 1.2 | 114.6 | 147.9 | -0.9 | Highly decomposed with obvious gap |
| DR4 | 4.5 | 15.9 | 114.6 | 148.2 | -0.4 | intact and gapped; this is the 'nose' |
| DR5 | 1.9 | 2.8 | 114.6 | 148.7 | -0.9 | Live roots growing; root highly decomposed but no gap |
| DR6 | 1.7 | 2.3 | 114.6 | 148.2 | -1.5 | |
| DR7 | 1.0 | 0.7 | 114.6 | 148.4 | -3 | small path of silica near top of root |
| DR8 | 0.6 | 0.3 | 114.6 | 148.7 | -2.3 | |
| DR9 | 3.2 | 8.0 | 114.6 | 148.2 | -1 | intact; gapping bark; some silica; decaying bark; loose behind; 9C silica found inside and outside bark |
| DR10 | 1.0 | 0.8 | 114.6 | 148.7 | -0.4 | |
| DR11 | 0.3 | 0.1 | 114.6 | 148.5 | -2.2 | |
| DR12 | 1.2 | 1.1 | 114.6 | 148.6 | -4.2 | |
| DR13 | 1.9 | 2.7 | 114.6 | 148.8 | -3 | small gap behind filled with 'loam' |
| DR14 | 4.0 | 12.6 | 114.6 | 149.2 | -0.2 | silica flow from T4A-18; live roots growing in bark; bark mostly fully decomposed, mixed w/sand except in places |
| DR15 | 3.8 | 11.3 | 114.5 | 150.5 | -0.1 | |
| DR16 | 1.0 | 0.8 | 114.6 | 148.6 | -1.25 | |
| DR17 | 0.7 | 0.4 | 114.6 | 148.7 | -2.1 | hollow |
| DR18 | 2.0 | 3.1 | 114.7 | 146.7 | -1.2 | largely decayed; gopher hole behind |
| DR19 | 0.6 | 0.3 | 114.7 | 146 | -1.8 | |
| DR20 | 1.3 | 1.3 | 114.7 | 146.2 | -0.4 | hollow, dry |
| DR21 | 0.2 | 0.0 | 114.7 | 146.5 | -1.5 | |
| H1 | 2.5 | 4.9 | 114.9 | 139.2 | -2.7 | Actual 3x2; outlet for main burrow that flowed during test |
| H2 | 1.0 | 0.8 | 114.8 | 144.7 | -0.9 | |
| H3 | 1.5 | 1.8 | 114.7 | 146.8 | -1 | |
| H4 | 2.0 | 3.1 | 114.6 | 149.1 | -0.6 | behind DR14 |
| H5 | 1.0 | 0.7 | 114.6 | 150.2 | -0.95 | May be linked to H4 |



Figure 2E- 2. Log of wall face of Slice 1 (see Section 3.7.1). Logged by John Lichter of Tree Associates and Richard Evans of UC Davis

October 7, 2010

| Name | Root Dia (in) | Root Area | Northing | Easting | Depth | Notes |
|---|---|---|---|---|---|---|
| DR1 | 1.0 | 0.8 | 113 | 142 | -0.8 | no gap |
| DR2 | 0.7 | 0.4 | 113 | 144.9 | -0.5 | |
| DR3 | 0.4 | 0.1 | 113 | 145.4 | -2.4 | no gap |
| DR4 | 1.1 | 1.0 | 113 | 150.6 | -1 | gap at bottom |
| DR5 | 1.1 | 1.0 | 113 | 147.6 | -5.3 | gap at uphill side; no gap on part of root |
| DR6 | 1.1 | 1.0 | 113 | 147.8 | -5 | no gap; crack in soil above root |
| DR8 | 6.0 | 28.3 | 113 | 145.7 | -1 | Gap between wood and bark; bark in contact with soil |
| DR9 | 4.6 | 16.6 | 113 | 146.2 | -0.7 | |
| DR11 | 4.0 | 12.6 | 113 | 146.3 | -2 | |
| DR12 | 5.4 | 22.9 | 113 | 147.2 | -0.5 | |
| DR14 | 2.3 | 4.2 | 113 | 152 | -1.4 | |
| DR15 | 1.3 | 1.3 | 113 | 149.3 | -2.1 | No gap; small live roots (<0.1") grow at base |
| DR16 | 0.8 | 0.4 | 113 | 145.2 | -1.3 | |
| H1 | 1.0 | 0.8 | 113 | 145.7 | -0.9 | no size; assume 1" based on size drawn for analysis |
| H2 | 1.3 | 1.2 | 113 | 148.7 | -0.4 | |
| H3 | 1.0 | 0.8 | 113 | 148.9 | -0.9 | |
| H4 | 1.2 | 1.1 | 113 | 149.8 | -1.8 | |
| H5 | 1.2 | 1.1 | 113 | 150.3 | -0.6 | |
| H6 | 0.9 | 0.6 | 113 | 150.9 | -1.8 | |
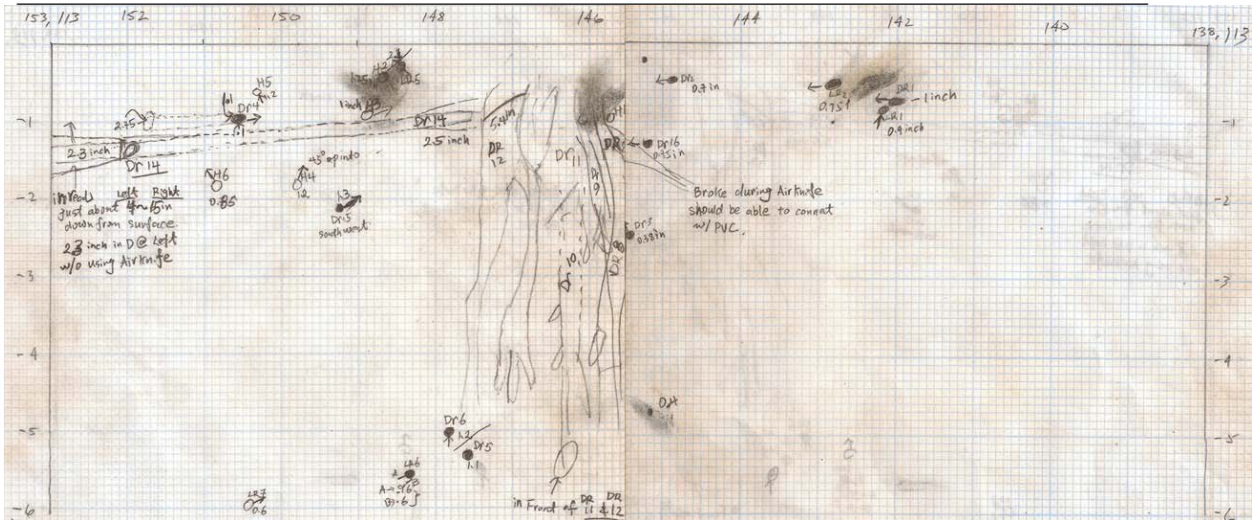


Figure 2E- 3. Log of wall face of Slice 2 (see Section 3.7.1). Logged by John Lichter of Tree Associates and Richard Evans of UC Davis.

October 11, 2010

| Name | Root Dia (in) | Root Area | Northing | Easting | Depth | Notes |
|------|--------------|-----------|----------|---------|-------|-------|
| DR1 | 2 | 3.141592654 | 111.5 | 146.5 | -2.5 | crumbly, ext. of DR8 from Oct7, appears to have been cut by trenches when pipe went in |
| DR2 | 1.15 | 1.038689071 | 111.5 | 146 | -3.7 | Powder |
| DR3 | 0.45 | 0.159043128 | 111.5 | 145 | -5.6 | decomposed, powdery |
| DR4 | 0.45 | 0.159043128 | 111.5 | 146.4 | -4.3 | breaks easily |
| DR5 | 1.3 | 1.327322896 | 111.5 | 146.7 | -4.3 | Firm |
| DR6 | 0.75 | 0.441786467 | 111.5 | 147 | -4.7 | very soft |
| DR7 | 0.78 | 0.477836243 | 111.5 | 147.5 | -4.2 | very soft |
| DR15 | 0.6 | 0.282743339 | 111.5 | 148 | -4.2 | |
| DR16 | 0.8 | 0.502654825 | 111.5 | 146.8 | -5.2 | |
| DR17 | 1.8 | 2.544690049 | 111.5 | 147 | -5 | 2.5x1.1 |
| DR18 | 0.25 | 0.049087385 | 111.5 | 146.5 | -1.7 | firm but crushable |
| DR19 | 0.21 | 0.034636059 | 111.5 | 148.4 | -4.6 | soft |
| DR20 | 0.83 | 0.541060795 | 111.5 | 148.85 | -5.8 | powder bark, wood is soft |
| DR21 | 1.4 | 1.5393804 | 111.5 | 149 | -5.3 | soft, bark is missing, some powder from bark |
| DR22 | 2 | 3.141592654 | 111.5 | 149 | -5.7 | spongy at cut face |
| DR23 | 0.88 | 0.608212338 | 111.5 | 149.5 | -5.9 | Powdery bark, very soft |
| DR24 | 0.34 | 0.090792028 | 111.5 | 150 | -4.1 | |
| DR26 | 6 | 28.27433388 | 111.5 | 147.2 | -1 | Bark increasingly decomposed or missing with depth |
| DR27 | 0.54 | 0.229022104 | 111.5 | 151.5 | -4 | soft, growing in face |
| H1 | 1.2 | 1.130973355 | 111.5 | 150.2 | -1.9 | |
| H2 | 1 | 0.785398163 | 111.5 | 151.2 | -1.8 | |
| H3 | 1.3 | 1.327322896 | 111.5 | 152 | -1.15 | |
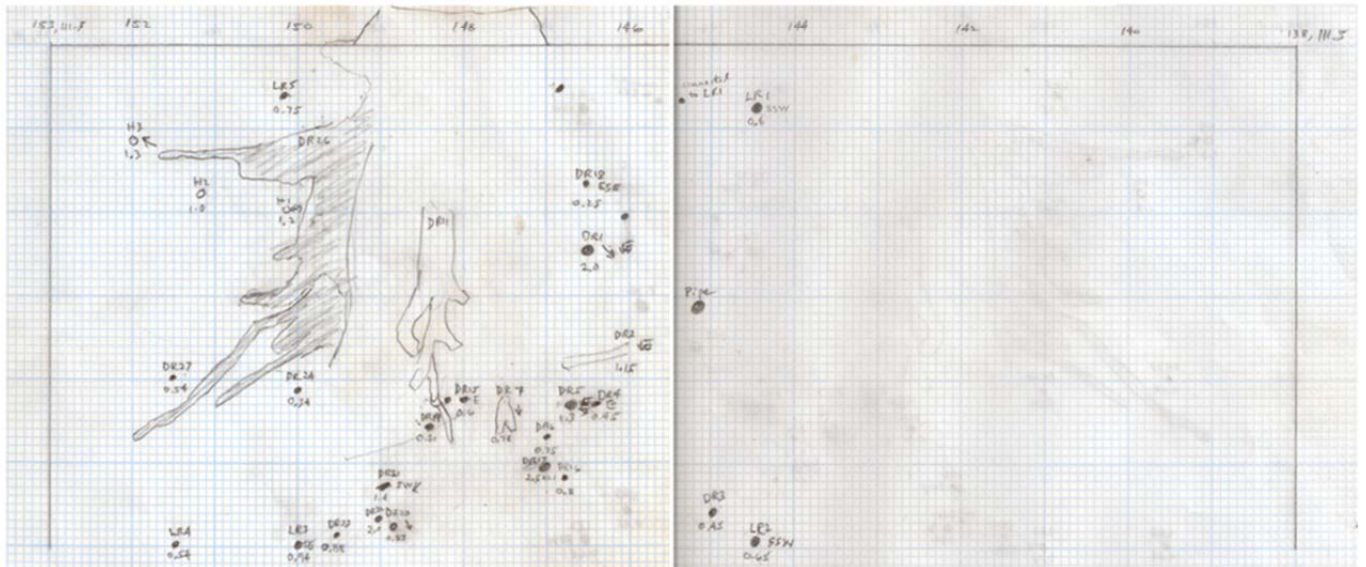


Figure 2E- 4. Log of wall face of Slice 3 (see Section 3.7.1). Logged by John Lichter of Tree Associates and Richard Evans of UC Davis.

# APPENDIX 3A

## Soil Borings and Instrument Logs

Prior to site selection, available soil boring logs and geotechnical information were reviewed and are presented in Appendix 3D. Our exploration of the site included a review of available information for the region (presented in Appendix 3D), drilling nine soil borings with a conventional auger drilling rig equipped with 8 inch diameter hollow stem augers, augering 12 soil borings with a 3 ¼ inch diameter hand auger, advancing 3 cone penetration tests (CPT) with frequent pore pressure dissipation readings, and trench logging and sampling during construction of the centerline trench.

This appendix provides a summary of all soil borings performed on the site. Material types are noted in many of the logs and are presented as Figure 3A- 1. Each hole was located at the site of a tensiometer or a piezometer, as shown on Figure 3A- 2. One to two instruments were installed as part of the backfill procedure. Boring numbers generally match instrument names except where two instruments are installed in the same hole. In this case, 'a' and 'b' are added to the boring number distinguish piezometers of different depth installed within a single boring. Piezometers were installed within each of the nine holes drilled by an auger rig. The remaining instruments, consisting of tensiometers and piezometers, were installed within the hand auger borings shown on Figure 3A- 2. Laboratory testing associated with all types of exploration are provided in Appendix 3B. CPT and pore pressure dissipation results are provided in Appendix 3C. Excerpts from available studies performed at the site including soil borings and laboratory testing by others are provided in Appendix 3D. Trench logs are provided in Appendix 3E.

Borings drilled with an auger rig were performed by Gregg Drilling. These were performed at the locations of piezometers PA1, PA2, PA3, PB1, PB2, PB3, PC1, PC2, and PC3 as shown on Figure 3A- 2. These logs are presented as Figure 3A-3 through Figure 3A-11. Hand auger boring logs are presented in list format at the back of this appendix.

**SOIL TYPES:**

(1) Clayey silt (ML), olive mottled with oxidation staining, moist, blocky structure with light cementation.

(2) Clayey silt (ML), light brown, moist, thinly bedded, easily cleaves along bedding of variable orientation, gaps and cracks observed, prone to sloughing and instability, bed thickness 1-5mm (typ.) .

(3) Sandy silt (ML) with pockets and lenses of silty sand (SM), light brown, moist.

(4) Clayey silt (MH), dark olive brown with oxidation staining, moist.

(5) Clayey silt (ML), reddish brown, moist

(6) Sandy silt (ML), olive brown with oxidation staining, occasional silty sand pocket.

(7) Sandy silt with clay (ML), pockets of olive with oxidation mixed with pockets of reddish brown with fine sand at cleavage planes in structure, material is highly unstable and consists of a mixture of soil types 2, 3, and 4.

Figure 3A- 1. Legend showing soil types 1 through 7
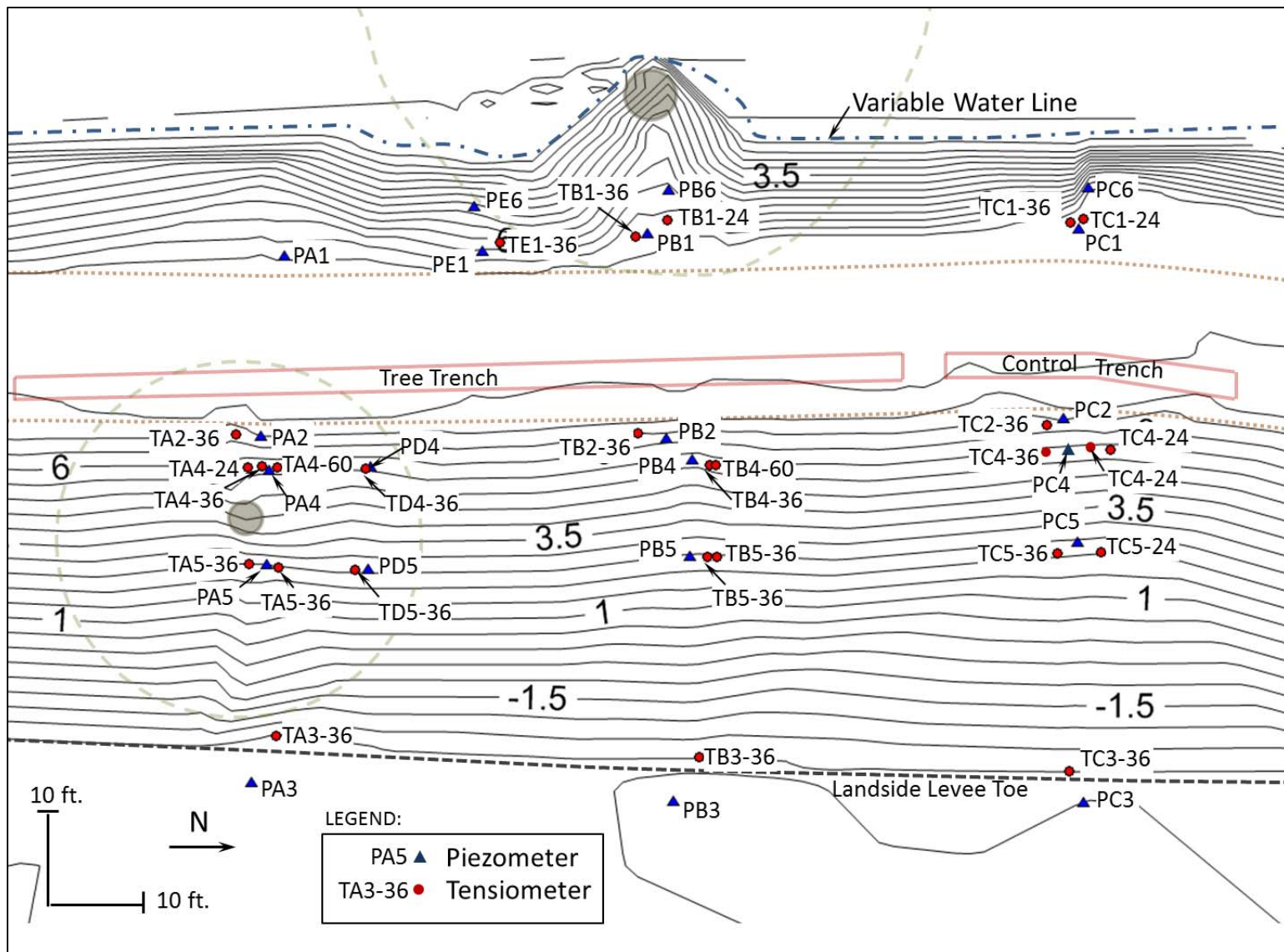
Figure 3A- 2. Site map and instrument layout

# Instrument Logs

**PA1 – Installed by drill rig with hollow stem augers**

See Figure 3A-3.

**PA2 – Installed by drill rig with hollow stem augers**

See Figure 3A-4.

**TA2-36 – Drilled with 1" gouge auger and sledgehammer**

No log of top of hole.

Log of sample at 30-36":

Sandy silt (ML), light brown, moist, sandy pockets.

Bottom of boring at 36"

**PA3 – Installed by drill rig with hollow stem augers**

See Figure 3A-5.

**TA3-36 – Drilled with 1" gouge auger and sledgehammer**

0 – 12"          Sandy Silt (ML) to silty sand (SM), brown, moist.

12"-36"          Clayey silt (MH), dark olive brown with reddish mottling, moist, stiff (Material 4).

Bottom of hole at 36"

**PA4 –Installed with a 3 1/4 inch diameter hand auger**

0"-6"          Silt (ML), light brown, loose, slightly moist, organics (topsoil).

6"-30"          Sandy silt (ML), light brown, moist (Material 3).

30"-36"     Clayey silt (ML), light brown, moist, thinly-bedded, easily cleaves along bedding planes (Material 2).

36"-48"     Sandy silt (ML), light brown, moist (Material 3).

48"-76"     Clayey silt (ML), light brown, moist, thinly-bedded, easily cleaves along bedding planes (Material 2). ¾ inch live roots at 49" and 56".

Bottom of boring at 76"

**TA4-24 – Drilled with 1" gouge auger and sledgehammer**

0"-24"     Clayey silt (ML) with sand, light brown and olive with oxidation staining, moist (Material 1).

Bottom of boring at 24"

**TA4-36 – Drilled with 1" gouge auger and sledgehammer**

0"-36"     Sandy silt (ML) with interbeds of silty sand (SM), light brown, moist lightly cemented.

Bottom of boring at 36"

**TA4-60 – Drilled with 1" gouge auger and sledgehammer**

0 – 6"          Silty sand (SM), brown, moist.

6"-32"          Sandy silt (ML) with silty sand interbeds (SM), light brown, layered structure

(Material 2).

32"-54"          Silt (ML) with clay, olive brown with reddish oxidation (Material 3).

54"-60"          Sandy silt (ML), light brown, moist, layered structure (Material 2).

Bottom of boring at 60"

**PA5 –Installed with a 3 1/4 inch diameter hand auger**

0"-22"     Sandy silt (ML) with clay, olive brown with oxidation staining, moist.

22"-43"     Silty sand (SM) with clayey silt interbeds (ML), light brown, moist.

          ½ inch live root at 35" depth.

Bottom of boring at 43"

**TA5-24 – Drilled with 1" gouge auger and sledgehammer**

0"-18"     Sandy silt (ML) with fine sand, olive with reddish mottling, some layering structure, moist, Material 3 with sandy pockets

18"-24"     Silt (ML) with clay and trace fine sand, olive with reddish mottling (Material 3 with clayey pockets).

Bottom of boring at 24"

**TA5-36 – Drilled with 1" gouge auger and sledgehammer**

0"-36"     Silt (ML) with fine sand, light brown, matrix of Material 3 with pockets of Material 2 layered bedding structure.

Bottom of boring at 36"

**PB1– Installed by drill rig with hollow stem augers**

See Figure 3A-6

**TB1-24 – Drilled with 1" gouge auger and sledgehammer**

0"-12"     Clayey silt (ML), dark brown with reddish oxidation, high organic content (topsoil)

12"-24"    Silty sand (SM), light brown with orange mottling (Material 3) with pockets of sandy silt (ML), light brown, layered structure (Material 2).

Bottom of boring at 24"

**TB1-36 – Drilled with 1" gouge auger and sledgehammer**

No log of top of hole.

Log of sample at 30-36":

Sandy silt (ML), light brown with occasional pockets of dark brown clayey silt (ML), moist, light brown matrix soils have layered structure (Material 2).

Bottom of boring at 36"

**PB2 – Installed by drill rig with hollow stem augers**

See Figure 3A-7

**TB2-36 – Drilled with 1" gouge auger and sledgehammer**

No log of top of hole.

Log of sample at 30-36":

Sandy silt (ML), light brown with reddish oxidation, moist (Material 3), blended with pockets of silt (ML) with sand in a layered structure (Material 2).

**PB3 – Installed by drill rig with hollow stem augers**

See Figure 3A-8

**TB3-36 – Drilled with 1" gouge auger and sledgehammer**

0" to 43"   Clayey silt (MH), dark olive brown with oxidation mottling, moist (Material 4).

Bottom of boring at 43"

**PB4 –Installed with a 3 1/4 inch diameter hand auger**

0"-9"        Clayey silt (ML), reddish brown, moist.

9"-30"       Clayey silt (ML), olive with reddish mottling, moist.

30"-70"      Sandy silt (ML), olive with reddish mottling, moist (Material 7).

70"-76"      Clayey silt (ML), olive brown with thin layered structure and sands at interfaces (Material 2).

Bottom of boring at 76"

**TB4-36 – Drilled with 1" gouge auger and sledgehammer**

0"-18"       Sandy silt (ML), light brown, moist, layered bedding (Material 2), organics in upper 3".

18"-36"      Sandy silt (ML) with silty sand interbeds (SM), brown with light oxidation staining.

Bottom of boring at 36"

**TB4-60 – Drilled with 1" gouge auger and sledgehammer**

0"-6"        Silty sand (ML), dark brown, slightly moist

6"-36"       Sandy silt (ML) with pockets of silty sand (SM), light brown, moist, layered structure (Material 2).

36"-54"      Sandy silt (ML) with layers of silty sand (SM), olive, moist (Material 3).

54"-60"      Sandy silt (ML), light brown, moist, layered structure (Material 2).

Bottom of boring at 60"

**PB5 –Installed with a 3 1/4 inch diameter hand auger**

0"-9"        Sandy silt (ML), reddish brown, moist.

9"-15"       Silty sand (SM) light brown, moist.

15"-43"      Clayey silt (ML), light brown, moist, pockets of silty sand (SM).

### TB5-24 – Drilled with 1" gouge auger and sledgehammer

0 – 12"   Sandy silt (ML) with pockets and lenses of silty sand (SM), light brown, moist (Material 3/6).

12"-24"   Sandy silt (ML) light brown, thinly-bedded, easily cleaves along bedding, moist.

Variation of Material 2.

Bottom of hole at 24"

### TB5-36 – Drilled with 1" gouge auger and sledgehammer

0 – 18"   Sandy silt (ML) with pockets and lenses of silty sand (SM), light brown, moist (Material 3/6).

18"-36"   Sandy silt (ML) light brown, thinly-bedded, easily cleaves along bedding, moist.

Variation of Material 2.

Bottom of hole at 36"

### PB6 –Installed with a 3 1/4 inch diameter hand auger

0"-9"   Silt (ML) with sand and clay, light brown, organics including small roots ($^1/_{16}$" to ¼")

9"-36"   Sandy silt (ML), light brown, moist, lightly cemented, barbed wire at 22".

36"-48"   Clayey silt (ML), olive brown with thin layered structure and sands at interfaces (Material 2).

Bottom of boring at 48"

### PC1 – Installed by drill rig with hollow stem augers

See Figure 3A-9

### TC1-24 – Drilled with 1" gouge auger and sledgehammer

0"-12"   Clayey silt (ML), dark brown with reddish mottling, high organic content (topsoil)

12"-24"   Sandy silt (ML), light brown, layered structure (Material 2).

Bottom of boring at 24"


### TC1-36 – Drilled with 1" gouge auger and sledgehammer

No log of top of hole.

Log of sample at 30-36":

Sandy silt (ML), light brown with occasional pockets of dark brown clayey silt (ML), moist, light brown matrix soils have layered structure (Material 2).

Bottom of boring at 36"

### PC2 – Installed by drill rig with hollow stem augers

See Figure 3A-10

### TC2-36 – Drilled with 1" gouge auger and sledgehammer

No log of top of hole.

Log of sample at 30-36":

Clayey silt (ML), olive mottled with oxidation staining, moist, sandy pockets.

Bottom of boring at 36"

### PC3 – Installed by drill rig with hollow stem augers

See Figure 3A-11

### TC3-36 – Drilled with 1" gouge auger and sledgehammer

0"-43"     Clayey silt (MH), dark olive brown with oxidation mottling, moist (Material 4).

Bottom of boring at 43"

### PC4 –Installed with a 3 1/4 inch diameter hand auger

0"-15"     Sandy silt (ML) with clay, dark olive brown, moist.

15"-30"    Clayey silt (ML), light brown, moist, thinly-bedded, easily cleaves along bedding (Material 2).

30"-62"    Clayey silt (ML), olive with reddish mottling, moist.

           Decomposing organic matter at 46.

62"-76"    Clayey silt (MH), dark brown with reddish mottling, moist (Material 4).

Bottom of boring at 76"


### TC4-24 – Drilled with 1" gouge auger and sledgehammer

0"-12"    Sandy silt (ML) with clay, dark olive brown, moist.

12"-24"    Sandy silt (ML), light brown, moist fine sand, thinly bedded layered structure (variation of Material 2)

Bottom of boring at 24"

### TC4-36 – Drilled with 1" gouge auger and sledgehammer

0"-12"    Clayey silt (ML), olive brown mottled with oxidation, slightly moist (Material 1).

12"-24"    Sandy silt (ML), light brown, moist (Material 3).

24"-36"    Sandy silt (ML), light brown, moist, layered structure (Material 2).

Bottom of boring at 36"

### TC4-60 – Drilled with 1" gouge auger and sledgehammer

0"-18"    Clayey silt (ML), brown, moist.

18"-42"    Silt (ML) with clay and sand, brown, moist, layered structure (Material 2).

42"-60"    Sandy silt (ML) with silty sand interbeds (SM), olive brown with reddish mottling (Material 3 with pockets of Material 2).

Bottom of boring at 60"

### PC5 –Installed with a 3 1/4 inch diameter hand auger

0 – 9"    Sandy silt (ML), light brown mottled with reddish brown, moist. Material 3/6.

9"-24"    Sandy silt (ML), olive with reddish mottling, moist.

24"-36"    Silty sand (SM), light brown, moist. Gradually more silt with depth.

36"-43"    Sandy silt (ML) with trace clay, light brown, weak cementation.

Bottom of hole at 43"

### TC5-24 – Drilled with 1" gouge auger and sledgehammer

0"-24"    Sandy silt (ML) with clay, light brown, moist, very fine sand, light cementation (Material 3)

Bottom of boring at 24"

### TC5-36 – Drilled with 1" gouge auger and sledgehammer

0"-36"    Sandy silt (ML) with silty sand pockets (SM), light brown, moist (Material 3).

Bottom of boring at 36 inches

### PC6 –Installed with a 3 1/4 inch diameter hand auger

0"-9"  Silt (ML) with sand and clay, light brown, moist, organics including leaf litter and live roots (sized fine to 1 ½ inch). Roots sheared easily with hand auger, likely originating from nearby bushes rather than oak trees.

9"-18"  Sandy silt (ML) brown, moist, organic matter and small roots ($1/_8$ inch diameter).

18"-48"  Sandy silt (ML), light brown, moist, lightly cemented, small roots $1/_8$ to ¼ inch diameter, ½ inch easily broken root and barbed wire at 22". Pockets of clayey silt (ML) and small roots ($1/_8$ to ¼ inch diameter) abundant at 36".

Bottom of boring at 48".

### PD4 –Installed with a 3 1/4 inch diameter hand auger

0"-8"  Clayey silt (ML), brown, moist.

8"-30"  Clayey silt (ML), olive mottled with reddish oxidation, moist, with fine sand becoming increasingly sandy with depth.

30"-48"  Sandy silt (ML), light brown, moist, layered structure (Material 2)

48"-72"  Clayey silt (ML) with pockets of sandy silt (ML), light olive with oxidation staining, moist (Material 3).

72"-76"  Clayey silt (MH), dark olive brown, moist (Material 4).

Bottom of boring at 76"

### TD4-36 – Drilled with 1" gouge auger and sledgehammer

0"-15"  Sandy silt (ML) with silty sand pockets (SM), light brown, moist (Material 3).

15"-36"  Sandy silt (ML), light brown, moist, thin lenses of sand between thin bedded thinly-bedded silt (Material 2) with pockets of Material 3.

Bottom of boring at 36"

### PD5 –Installed with a 3 1/4 inch diameter hand auger

0"-3"  Clayey silt (ML), brown, slightly moist, organics (topsoil).

3"-7"  Clayey silt (MH), dark brown, moist (Material 4).

7"-12"  Clayey silt (ML), olive brown with reddish mottling, moist.

12"-22"    Sandy silt (ML) with pockets of silty sand (SM), light olive with reddish oxidation (Material 3), gradually increasing clay content with depth.

22"-43"    Clayey silt (ML), light olive with reddish oxidation.

Bottom of boring at 43"

### TD5-36 – Drilled with 1" gouge auger and sledgehammer

0"-24"    Clayey silt (ML), olive mottled with reddish oxidation, moist.

24"-36"    Sandy silt (ML), light brown, moist, thin lenses of sand between thin bedded thinly-bedded silt (Material 2).

Bottom of boring at 36"

### PE1 –Installed with a 3 1/4 inch diameter hand auger

0"-7"      Silt (ML) with clay and sand, dark brown, moist, organics (topsoil)

7"-30"     Clayey silt (ML), yellow brown, moist, gradually becoming sandier with depth

30"-60"    Sandy silt (ML), yellow brown, moist.

60"-85"    Clayey silt (ML) with sand, olive with reddish mottling, increasing moisture content with depth, sandy pocket and ½ inch diameter root at 79".

Bottom of boring at 85"

### TE1-36 – Drilled with 1" gouge auger and sledgehammer

0"-24"     Silt (ML), light brown, dry,loose with high organic content (thick topsoil)

24"-36"    Clayey silt (ML), olive with orange mottling, moist, fine sand.

Bottom of boring at 36"


### PE6 –Installed with a 3 1/4 inch diameter hand auger

0"-9"      Silt (ML) with sand and clay, light brown, roots (1/16"-1/8" diameter) and organics (topsoil).

9"-24"     Sandy silt (ML), mottled reddish brown and dark brown, moist.

24"-28"    Clayey silt (ML), brown, moist.

28"-48"    Sandy silt (ML), light brown, moist, trace clay, gradual color change with depth to olive with orange mottling.

Bottom of boring at 48".

| | | | | | | | | | | |
|---|---|---|---|---|---|---|---|---|---|---|
| | | | | | | LOG OF BORING | | **PA1** | | |

LOG OF BORING **PA1**
SHEET 1 OF 9

DRILLER    Gregg Drilling
LOGGED BY    Michelle Shriro, UC Berkeley

BORING NO. / LOCATION      Twitchell Island, LineA, Row 1      DRY ON COMPLETION ?      Yes

DATE   March 15, 2012      SURFACE ELEV.   7.3   FT.      **WATER LEVEL DATA (IF APPLICABLE)**

START TIME   8:55 AM      END TIME   11:15 AM      DEPTH   Dry   FT.

BOTTOM OF HOLE DEPTH   6.5   FT.      ELEV. _____ FT.

BORING ADVANCED BY:    HOLLOW STEM AUGER (8" DIA)   X      ROTARY WASH _____

| DEPTH | SAMPLE DEPTH | | SAMPLE | SAMPLE | FIELD RESULTS | | LABORATORY RESULTS | | | STRATUM DESCRIPTION |
|---|---|---|---|---|---|---|---|---|---|---|
| FT. | FROM FT. | TO FT. | NO. | TYPE | Blow Count | N | LL | PI | %M | |
| | | | | | | | | | | 2" of topsoil with asphalt and organics. Clayey Silt (ML), reddish brown, moist |
| | 1.0 | 2.5 | PA1-1 | SPT | 1 2 | | | | | |
| 2.5 | 2.5 | 4.5 | PA1-2 | SS | 2 | 4 | | | 34.9 | Interbedded Sandy Silt (ML) with Clayey Silt (ML), reddish brown, moist |
| 5.0 | 5.0 | 6.5 | PA1-3 | SPT | 2 2 2 | 4 | | | 26.1 | 1/4 " root encountered at 6 feet |
| 7.5 | | | | | | | | | | Bottom of boring at 6.5 feet |
| 10.0 | | | | | | | | | | |

REMARKS: SS = Shelby sampler; SPT = Standard Penetration Test

Figure 3A-3. Boring at location of piezometer PA1 (Figure 3A- 2)

3A-14

| | | LOG OF BORING | PA2 |
|---|---|---|---|

**LOG OF BORING PA2**

SHEET 2 OF 9

DRILLER: Gregg Drilling

LOGGED BY: Michelle Shriro, UC Berkeley

BORING NO. / LOCATION: Twitchell Island, Line A, Row 2     DRY ON COMPLETION ? No

DATE: March 16, 2012     SURFACE ELEV. 6.8 FT.

START TIME: 9:30 AM     END TIME: 10:00 AM

BOTTOM OF HOLE DEPTH: 16.0 FT.

BORING ADVANCED BY: HOLLOW STEM AUGER (8" DIA) X     ROTARY WASH

**WATER LEVEL DATA (IF APPLICABLE)**

DEPTH 14.0 FT.

ELEV. _____ FT.

| DEPTH FT. | SAMPLE DEPTH FROM FT. | SAMPLE DEPTH TO FT. | SAMPLE NO. | SAMPLE TYPE | FIELD RESULTS Blow Count | N | LL | PI | %M | STRATUM DESCRIPTION |
|---|---|---|---|---|---|---|---|---|---|---|
| | 1.0 | 2.5 | PA2-1 | SPT | 1 | | | | | 2" of topsoil and organics. Sandy silt (ML) with lenses of silty sand (SM), brown, moist |
| | | | | | 2 | | | | | |
| 2.5 | | | | SS | 2 | 4 | | | 24.4 | |
| | 4.0 | 6.0 | PA2-2 | SS | | | | | | |
| 5.0 | | | | | | | | | | |
| 7.5 | 7.0 | 8.5 | PA2-3 | SPT | 3 | | | | | Clayey silt (MH), olive mottled with reddish oxidation, moist, piece of decomposed black wood/peat at 7 ft |
| | | | | | 2 | | | | | |
| | | | | | 3 | 5 | | | 23.7 | |
| 10.0 | 10.0 | 11.5 | PA2-4 | SPT | 3 | | | | | Piece of live woody root at 10 feet. Soil becomes darker olive color, more moisture, softer |
| | | | | | 4 | | | | | |
| | | | | | 5 | 9 | | | 37.9 | |
| 12.5 | 12.5 | 14.0 | PA2-5 | SPT | 2 | | | | | Clayey Silt (MH), grey, wet, soft |
| | | | | | 1 | | | | | |
| | | | | | 2 | 3 | | | 40.1 | |
| 15.0 | 14.5 | 16.0 | PA2-6 | SPT | 2 | | | | | Sand (SP), grey, wet, 2" of sample recovered |
| | | | | | 2 | | | | | |
| | | | | | 3 | 5 | | | 28.5 | |
| 17.5 | | | | | | | | | | Bottom of boring at 16 feet |
| 20.0 | | | | | | | | | | |

REMARKS: SS = Shelby sampler; SPT = Standard Penetration Test

Figure 3A-4. Boring at location of piezometer PA2 (Figure 3A- 2)

| | LOG OF BORING | PA3 |
|---|---|---|
| | SHEET 3 OF | 9 |
| | DRILLER | Gregg Drilling |
| | LOGGED BY | Michelle Shriro, UC Berkeley |

| BORING NO. /LOCATION | Twitchell Island, LineA, Row3 | DRY ON COMPLETION ? | Yes |
|---|---|---|---|

DATE   March 16, 2012    SURFACE ELEV.   -3.3   FT.     **WATER LEVEL DATA (IF APPLICABLE)**

START TIME   10:15 AM     END TIME   10:35 AM     DEPTH   Dry   FT.

BOTTOM OF HOLE DEPTH   8.5   FT.     ELEV.  _____  FT.

BORING ADVANCED BY:    HOLLOW STEM AUGER (8" DIA)   X     ROTARY WASH _____

| DEPTH | SAMPLE DEPTH FROM | TO | SAMPLE NO. | SAMPLE TYPE | FIELD RESULTS Blow Count | N | LAB LL | PI | %M | STRATUM DESCRIPTION |
|---|---|---|---|---|---|---|---|---|---|---|
| | | | | | | | | | | 2" of topsoil with grass. |
| | | | | | | | | | | Clayey Silt (ML), olive brown mottled with reddish |
| | 1.0 | 2.5 | PA3-1 | SPT | 3 | | | | | oxidation, moist, fine roots |
| | | | | | 4 | | | | | |
| 2.5 | | | | | 5 | 9 | | | 24.4 | Sandy silt (ML) with clay, yellow brown, moist |
| | 3.0 | 5.0 | PA3-2 | SS | | | | | | |
| 5.0 | 5.0 | 6.5 | PA3-3 | SPT | 3 | | | | | |
| | | | | | 3 | | | | 17.9 | |
| | | | | | 5 | 8 | | | 12.2 | Sand with Silt (SP), yellow brown, moist, weakly |
| 7.5 | 7.0 | 8.5 | PA3-4 | SPT | 5 | | | | | cemented |
| | | | | | 4 | | | | | |
| | | | | | 4 | 8 | | | 8.3 | |
| | | | | | | | | | | Bottom of boring at 8.5 feet |
| 10.0 | | | | | | | | | | |

REMARKS: SS = Shelby sampler; SPT = Standard Penetration Test

Figure 3A-5. Boring at location of piezometer PA3 (Figure 3A- 2)

| | | LOG OF BORING | **PB1** |
|---|---|---|---|
| | | SHEET 4 OF | 9 |
| | | DRILLER | Gregg Drilling |
| | | LOGGED BY | Michelle Shriro, UC Berkeley |

BORING NO. / LOCATION _____ Twitchell Island, Line B, Row 1 _____ DRY ON COMPLETION ? _____ Yes

DATE ___ March 15, 2012 ___   SURFACE ELEV. ___ 7.1 ___ FT.

START TIME ___ 11:20 AM ___   END TIME ___ 11:45 AM

BOTTOM OF HOLE DEPTH ___ 6.5 ___ FT.

BORING ADVANCED BY:   HOLLOW STEM AUGER (8" DIA) ___ X ___   ROTARY WASH _____

**WATER LEVEL DATA (IF APPLICABLE)**

DEPTH ___ Dry ___ FT.

ELEV. _____ FT.

| DEPTH | | SAMPLE DEPTH | | SAMPLE | SAMPLE | FIELD RESULTS | | LABORATORY RESULTS | | | STRATUM DESCRIPTION |
|---|---|---|---|---|---|---|---|---|---|---|---|
| FT. | | FROM FT. | TO FT. | NO. | TYPE | Blow Count | N | LL | PI | %M | |
| | | | | | | | | | | | 12" of topsoil and organics |
| | | 1.0 | 2.5 | PB1-1 | SPT | 1 | | | | | Interbedded Sandy Silt (ML) with Clayey Silt (ML), reddish brown |
| | | | | | | 1 | | | | | |
| 2.5 | | 2.5 | 4.5 | PB1-2 | SS | 2 | 3 | | | 33.7 | |
| | | | | | | | | | | | Silt (ML), yellow brown, layered structure, angled bedding, trace clay |
| 5.0 | | 5.0 | 6.5 | PB1-3 | SPT | 3 | | | | | |
| | | | | | | 2 | | | | | Higher sand content at base of sample (very fine sand) |
| | | | | | | 3 | 5 | | | | |
| 7.5 | | | | | | | | | | | Bottom of boring at 6.5 feet |
| 10.0 | | | | | | | | | | | |

REMARKS: SS = Shelby sampler; SPT = Standard Penetration Test

Figure 3A-6. Boring at location of piezometer PB1 (Figure 3A- 2)

| | | | | | | | | | | |
|---|---|---|---|---|---|---|---|---|---|---|
| DRILLER | | | | | | | | Gregg Drilling | | |
| LOGGED BY | | | | | | | | Michelle Shriro, UC Berkeley | | |

BORING NO. / LOCATION  Twitchell Island, Line B, Row 2  DRY ON COMPLETION ?  Yes

DATE  March 15, 2012  SURFACE ELEV.  6.3  FT.

**WATER LEVEL DATA (IF APPLICABLE)**

START TIME  1:35 PM  END TIME  2:15 PM  DEPTH  Dry  FT.

BOTTOM OF HOLE  DEPTH  17.5  FT.  ELEV.  FT.

BORING ADVANCED BY:  HOLLOW STEM AUGER (8" DIA)  X  ROTARY WASH

| DEPTH | | SAMPLE DEPTH | | | | FIELD RESULTS | | LABORATORY RESULTS | | | STRATUM DESCRIPTION |
|---|---|---|---|---|---|---|---|---|---|---|---|
| | | FROM | TO | SAMPLE | SAMPLE | | | | | | |
| FT. | | FT. | FT. | NO. | TYPE | Blow Count | N | LL | PI | %M | |
| | | | | | | | | | | | 6" of topsoil and organics.         Clayey silt (ML) yellow brown, moist |
| | | 1.0 | 2.5 | PB2-1 | SPT | 1 | | | | | |
| | | | | | | 2 | | | | | |
| 2.5 | | | | | | 3 | 5 | | | 35.2 | |
| | | | | | | | | | | | |
| | | 4.0 | 6.0 | PB2-2 | SS | | | | | | |
| 5.0 | | | | | | | | | | | Silt with fine sand (ML) light brown with oxidation staining, moist, stuctured in thin beds, weakly cemented |
| | | | | | | | | | | | |
| 7.5 | | 7.0 | 8.5 | PB2-3 | SPT | 3 | | | | | |
| | | | | | | 3 | | | | 18.4 | Clayey Silt (ML), olive with red oxidation mottling, moist, small pieces of black decomposed wood/peat |
| | | | | | | 4 | 7 | | | 23.6 | |
| | | 9.0 | 11.0 | PB2-4 | SS | | | | | | |
| 10.0 | | | | | | | | | | | |
| | | | | | | | | | | | |
| 12.5 | | 12.0 | 13.5 | PB2-5 | SPT | 4 | | | | | grades to higher clay content |
| | | | | | | 5 | | | | | |
| | | | | | | 7 | 12 | | | 26.2 | |
| 15.0 | | | | | | | | | | | |
| | | 16.0 | 17.5 | PB2-6 | SPT | 3 | | | | | |
| | | | | | | 4 | | | | | Sand (SP) with trace silt, olive brown, moist |
| 17.5 | | | | | | 5 | 9 | | | 14.8 | |
| | | | | | | | | | | | Bottom of boring at 17.5 feet |
| 20.0 | | | | | | | | | | | |

REMARKS: SS = Shelby sampler; SPT = Standard Penetration Test

Figure 3A-7. Boring at location of piezometer PB2 (Figure 3A- 2)

| | DRILLER | Gregg Drilling |
| | LOGGED BY | Michelle Shriro, UC Berkeley |

| BORING NO. / LOCATION | Twitchell Island, Line B, Row3 | DRY ON COMPLETION ? | No |

| DATE | March 16, 2012 | SURFACE ELEV. | -2.8 | FT. | **WATER LEVEL DATA (IF APPLICABLE)** |
| START TIME | 10:45 AM | END TIME | 11:05 AM | | DEPTH | 13.5 | FT. |
| BOTTOM OF HOLE DEPTH | 14.5 | FT. | | | ELEV. | | FT. |

BORING ADVANCED BY:      HOLLOW STEM AUGER (8" DIA)     X          ROTARY WASH _____

| DEPTH | | SAMPLE DEPTH | | SAMPLE | SAMPLE | FIELD RESULTS | | LABORATORY RESULTS | | | STRATUM DESCRIPTION |
| | | FROM | TO | NO. | TYPE | | | | | | |
| FT. | | FT. | FT. | NO. | TYPE | Blow Count | N | LL | PI | %M | |
| | | | | | | | | | | | 6" of topsoil with grass.              Silty Silty sand (SM) olive brown, moist |
| | | 1.0 | 2.5 | PB3-1 | SPT | 3 4 5 | 9 | | | 17.6 | |
| 2.5 | | | | | | | | | | | |
| | | 4.0 | 6.0 | PB3-2 | SS | | | | | | |
| 5.0 | | | | | | | | | | | Sand (SP) with silt interbedded with sandy silt (SM), yellow brown, moist, clean and very fine sand |
| 7.5 | | | | | | | | | | | |
| | | 9.0 | 9.5 | PB3-3 | SPT | 4 4 5 | 9 | | | 7.4 | Sand (SP), reddish brown, moist, clean |
| 10.0 | | 10.0 | 11.5 | PB3-4 | SPT | 3 4 4 | 8 | | | | |
| 12.5 | | 12.5 | 14.0 | PB4-5 | SPT | 2 1 1 | 2 | | | 43.9 | Sand (SP), grey brown, moist, clean  Free water encountered at 13.5 ft |
| 15.0 | | | | | | | | | | | Bottom of boring at 14.5 feet |

REMARKS: SS = Shelby sampler; SPT = Standard Penetration Test

Figure 3A-8. Boring at location of piezometer PB3 (Figure 3A- 2)

| | | | | DRILLER | Gregg Drilling |
| | | | | LOGGED BY | Michelle Shriro, UC Berkeley |

| BORING NO. / LOCATION | Twitchell Island, Line C, Row 1 | DRY ON COMPLETION ? | Yes |

DATE   March 15, 2012    SURFACE ELEV.   7.7   FT.

START TIME   12:20 PM    END TIME   12:35 PM

BOTTOM OF HOLE DEPTH   6.5  FT.

BORING ADVANCED BY:    HOLLOW STEM AUGER (8" DIA)   X    ROTARY WASH _____

**WATER LEVEL DATA (IF APPLICABLE)**

DEPTH   Dry   FT.

ELEV. _____ FT.

| DEPTH | | SAMPLE DEPTH | | | | FIELD RESULTS | | LABORATORY RESULTS | | | STRATUM DESCRIPTION |
|---|---|---|---|---|---|---|---|---|---|---|---|
| | | FROM | TO | SAMPLE | SAMPLE | | | | | | |
| FT. | | FT. | FT. | NO. | TYPE | Blow Count | N | LL | PI | %M | |
| | | | | | | | | | | | 12" of topsoil and organics consisting of sandy clay (CL) dark brown, moist |
| | | 1.0 | 2.5 | PC1-1 | SPT | 2 | | | | | Sandy silt (ML), yellow brown |
| | | | | | | 2 | | | | | |
| | | | | | | 4 | 6 | | | 25.2 | Silty sand (SM) interbedded with sandy silt (ML), yellow brown, moist |
| 2.5 | | 2.5 | 4.5 | PC1-2 | SS | | | | | | |
| | | | | | | | | | | | |
| 5.0 | | 5.0 | 6.5 | PC1-3 | SPT | 3 | | | | | |
| | | | | | | 2 | | | | | increasing soil structure with depth and streaks of orange weathering |
| | | | | | | 3 | 5 | | | 16 | |
| | | | | | | | | | | | Bottom of boring at 6.5 feet |
| 7.5 | | | | | | | | | | | |
| 10.0 | | | | | | | | | | | |

REMARKS: _____

Figure 3A-9. Boring at location of piezometer PC1 (Figure 3A- 2)

3A-20

| | | | | | LOG OF BORING | **PC2** |
|---|---|---|---|---|---|---|

| | |
|---|---|
| DRILLER | Gregg Drilling |
| LOGGED BY | Michelle Shriro, UC Berkeley |

BORING NO. / LOCATION: Twitchell Island, Line C, Row 2   DRY ON COMPLETION ?   Yes

DATE: March 15, 2012   SURFACE ELEV. 6.4 FT.

**WATER LEVEL DATA (IF APPLICABLE)**

START TIME: 12:40 PM   END TIME: 1:15 PM   DEPTH: Dry FT.

BOTTOM OF HOLE DEPTH: 14.5 FT.   ELEV. _____ FT.

BORING ADVANCED BY: HOLLOW STEM AUGER (8" DIA)  X   ROTARY WASH _____

| DEPTH FT. | SAMPLE DEPTH FROM FT. | SAMPLE DEPTH TO FT. | SAMPLE NO. | SAMPLE TYPE | FIELD RESULTS Blow Count | N | LAB LL | LAB PI | %M | STRATUM DESCRIPTION |
|---|---|---|---|---|---|---|---|---|---|---|
| | 1.0 | 2.5 | PC2-1 | SPT | 2 2 2 | 4 | | | 35.6 | 6" of topsoil and organics. Clayey silt (ML) yellow brown, moist, with occasional thin layers 1/2 inch thick of sandy silt with very fine sand |
| 2.5 | | | | | | | | | | |
| 5.0 | 4.0 | 6.0 | PC2-2 | SS | | | | | | Silty sand (SM), moist, yellow brown, weakly cemented, orange weathering veins |
| 7.5 | 7.0 | 8.5 | PC2-3 | SPT | 3 4 5 | 9 | | | 23.4 | Clayey silt (ML) olive mottled with reddish oxidation, moist |
| | 9.0 | 11.0 | PC2-4 | SS | No | | | | | Clayey Silt (ML), olive with red oxidation mottling, moist, small pieces of black decomposed wood/peat |
| 10.0 | | | | | | | | | | |
| 12.5 | 11.0 | 13.0 | PC2-5 | SS | | | | | | Silty sand (SM), olive brown, moist |
| | 13.0 | 14.5 | PC2-6 | SPT | 3 4 4 | 8 | | | 26.7 | |
| 15.0 | | | | | | | | | | Bottom of boring at 14.5 ft. |

REMARKS: SS = Shelby sampler; SPT = Standard Penetration Test

Figure 3A-10. Boring at location of piezometer PC2 (Figure 3A- 2)

| | | | | | | | | | DRILLER | Gregg Drilling |
| --- | --- | --- | --- | --- | --- | --- | --- | --- | --- | --- |
| | | | | | | | | | LOGGED BY | Michelle Shriro, UC Berkeley |

BORING NO. / LOCATION　　Twitchell Island, LineC, Row3　　DRY ON COMPLETION ?　　Yes

DATE　　March 16, 2012　　SURFACE ELEV.　-3　FT.

**WATER LEVEL DATA (IF APPLICABLE)**

START TIME　11:15 AM　　END TIME　11:35 AM　　DEPTH　Dry　FT.

BOTTOM OF HOLE DEPTH　　9.5　FT.　　ELEV.　　FT.

BORING ADVANCED BY:　　HOLLOW STEM AUGER (8" DIA)　X　　ROTARY WASH

| DEPTH FT. | SAMPLE DEPTH FROM FT. | SAMPLE DEPTH TO FT. | SAMPLE NO. | SAMPLE TYPE | FIELD RESULTS Blow Count | N | LAB LL | LAB PI | %M | STRATUM DESCRIPTION |
| --- | --- | --- | --- | --- | --- | --- | --- | --- | --- | --- |
| | 1.0 | 2.5 | PC3-1 | SPT | 3 2 3 | 5 | | | 24.1 | 2" of topsoil with grass.　　Clayey Silt (MH), dark olive brown mottled with reddish oxidation, moist |
| 2.5 | 3.0 | 5.0 | PC3-2 | SS | | | | | | |
| 5.0 | | | | | | | | | | Sand (SP), yellow brown, moist, clean |
| | 6.0 | 7.5 | PC3-3 | SPT | 5 4 6 | 10 | | | 5.7 | |
| 7.5 | 8.0 | 9.5 | PC3-4 | SPT | 3 2 3 | 5 | | | 5.6 | |
| 10.0 | | | | | | | | | | Bottom of boring at 9.5 feet |

REMARKS: SS = Shelby sampler; SPT = Standard Penetration Test

Figure 3A-11. Boring at location of piezometer PC3 (Figure 3A- 2)

# APPENDIX 3B

## Laboratory Testing – Twitchell Island Test Site

Table 3B- 1. Moisture content by depth and material number in the tree trench

| Station | Mat# | Depth (ft) | Moisture % |
|---|---|---|---|
| TT Sta 5 | 2 | 1-2.5 | 31.8 |
| TT Sta 5 | 3 | 2.5-3.5 | 37.3 |
| TT Sta 5 | 4 | 3.8-4 | 30.5 |
| TT Sta 5 | 5 | 6.8-7.4 | 17.4 |
| TT Sta 5 | 4 | 7.4-8 | 22.9 |
| TT Sta 10 | 3 | 3-3.5 | 39.0 |
| TT Sta 14 | 4 | 6.5 | 24.1 |
| TT Sta 15 | 2 | 1-3 | 34.8 |
| TT Sta 15 | 3 | 3.2-4 | 40.7 |
| TT Sta 15 | 4 | 4-4.25 | 28.5 |
| TT Sta 15 | 4 | 6 | 20.7 |
| TT Sta 15 | 4 | 6.5 | 28.3 |
| TT Sta 15 | 5 | 7.2 | 18.3 |
| TT Sta 15 | 5 | 7.7-8 | 18.8 |
| TT Sta 16 | 4 | 7.25-7.7 | 20.6 |
| TT Sta 16 | 5 | 7.7-8 | 18.1 |
| TT Sta 17 | 4 | 7.25-7.7 | 25.4 |
| TT Sta 30 | 1 | 1-1.5 | 25.8 |
| TT Sta 30 | 2 | 2-3 | 37.0 |
| TT Sta 30 | 2+3+sand | 3.5-4 | 19.3 |
| TT Sta 30 | 4 | 7-8 | 23.0 |
| TT Sta 33 | 2 | 3.5-4.5 | 16.5 |
| TT Sta 33 | 2+3+sand | 4.5-6 | 19.8 |
| TT Sta 33 | 4 | 6-8 | 24.3 |
| TT Sta 40 | 1 | 1-1.5 | 41.0 |
| TT Sta 40 | 2 | 3-4 | 25.2 |
| TT Sta 50 | 4 | 4-5 | 21.3 |
| TT Sta 50 | 5 | 7.3-7.6 | 17.9 |
| TT Sta 52 | 1 | 1 | 28.8 |
| TT Sta 53 | 7 | 3 | 30.4 |
| TT Sta 55 | 4 | 3.75-4 | 19.8 |
| TT Sta 63 | 2 | 2 | 21.2 |
| TT Sta 63 | 4 | 3.75-4 | 20.8 |
| TT Sta 65 | 7 | 1-2.5 | 24.3 |
| TT Sta 65 | 5 | 6.7-7 | 15.9 |
| TT Sta 65 | 4 | 6-6.5 | 19.8 |
| TT Sta 74 | 2 | 2-3 | 36.4 |
| TT Sta 75 | 4 | 3.75-4 | 23.4 |
| TT Sta 75 | 4 | 6-7 | 25.1 |
| TT Sta 75 | 4 | 7.5-8 | 21.5 |
| TT Sta 75 | 5 | 7 | 22.1 |
| TT Sta 77 | 3+6 | 3-4 | 36.4 |
| TT Sta 83 | 2+3+sand | 2-3 | 35.9 |
| TT Sta 83 | 4 | 3.75-4 | 23.8 |
| TT Sta 83 | 7 | 2-3 | 26.3 |

Table 3B- 2. Moisture content by depth and material number in the control trench

| Station | Mat# | Depth (ft) | Moisture % |
|---|---|---|---|
| CT Sta5 | 4 | 6-6.5 | 29.7 |
| CT Sta5 | 4+5 | 4-4.7 | 33.3 |
| CT Sta15 | 4 | 8 | 25.7 |
| CT Sta15 | 4 | 7.3-7.8 | 26.0 |
| CT Sta 5 | 4 | 7-7.5 | 25.6 |
| CT Sta 15 | 4 | 6-6.5 | 26.9 |
| CT Sta 25 | 4 | 7-7.5 | 24.7 |
| CT Sta25 | 4 | 5-5.5 | 32.5 |
| CT Sta 31.5 | 4 | 8-8.3 | 24.5 |
| CT Sta15 | 2 | 3 | 20.5 |
| CT Sta 5 | 2 | 2-4 | 38.8 |
| CT Sta 5 | 1 | 1-2 | 35.2 |
| CT Sta25 | 1 | 0.8-1.7 | 33.3 |
| CT Sta25-30 | 4 | 4.2 | 25.9 |
| CT Sta12 | 3 | 2.5 | 32.0 |

Table 3B- 3. Moisture content and material number at tensiometer tip

| Instrument# | Mat# | Moisture% |
|---|---|---|
| TA2-36 | 3+6 | 21.0 |
| TA3-36 | 4 | 18.3 |
| TA4-24 | 1 | 23.7 |
| TA4-36 | 3+6 | 18.3 |
| TA4-60 | 2 | 17.2 |
| TA5-24 | 3+6 | 20.1 |
| TA5-36 | 3+6 | 16.6 |
| TB1-24 | 2+3 | 16.6 |
| TB1-36 | 2+3 | 23.1 |
| TB2-36 | 2+3 | 25.4 |
| TB3-36 | 4 | 20.0 |
| TB4-36 | 3+6 | 29.3 |
| TB4-60 | 2 | 23.0 |
| TB5-24 | 2 | 25.1 |
| TB5-36 | 2 | 17.0 |
| TC1-24 | 2 | 14.9 |
| TC1-36 | 2+3 | 16.3 |
| TC2-36 | 3+6 | 30.5 |
| TC3-36 | 4 | 18.5 |
| TC4-24 | 2 | 32.3 |
| TC4-36 | 2 | 25.2 |
| TC4-60 | 2 | 29.4 |
| TC5-24 | 3 | 21.9 |
| TC5-36 | 3 | 19.2 |
| TD4-36 | 2 | 17.4 |
| TD5-36 | 2 | 20.8 |
| TE1-36 | 2+3 | 25.5 |
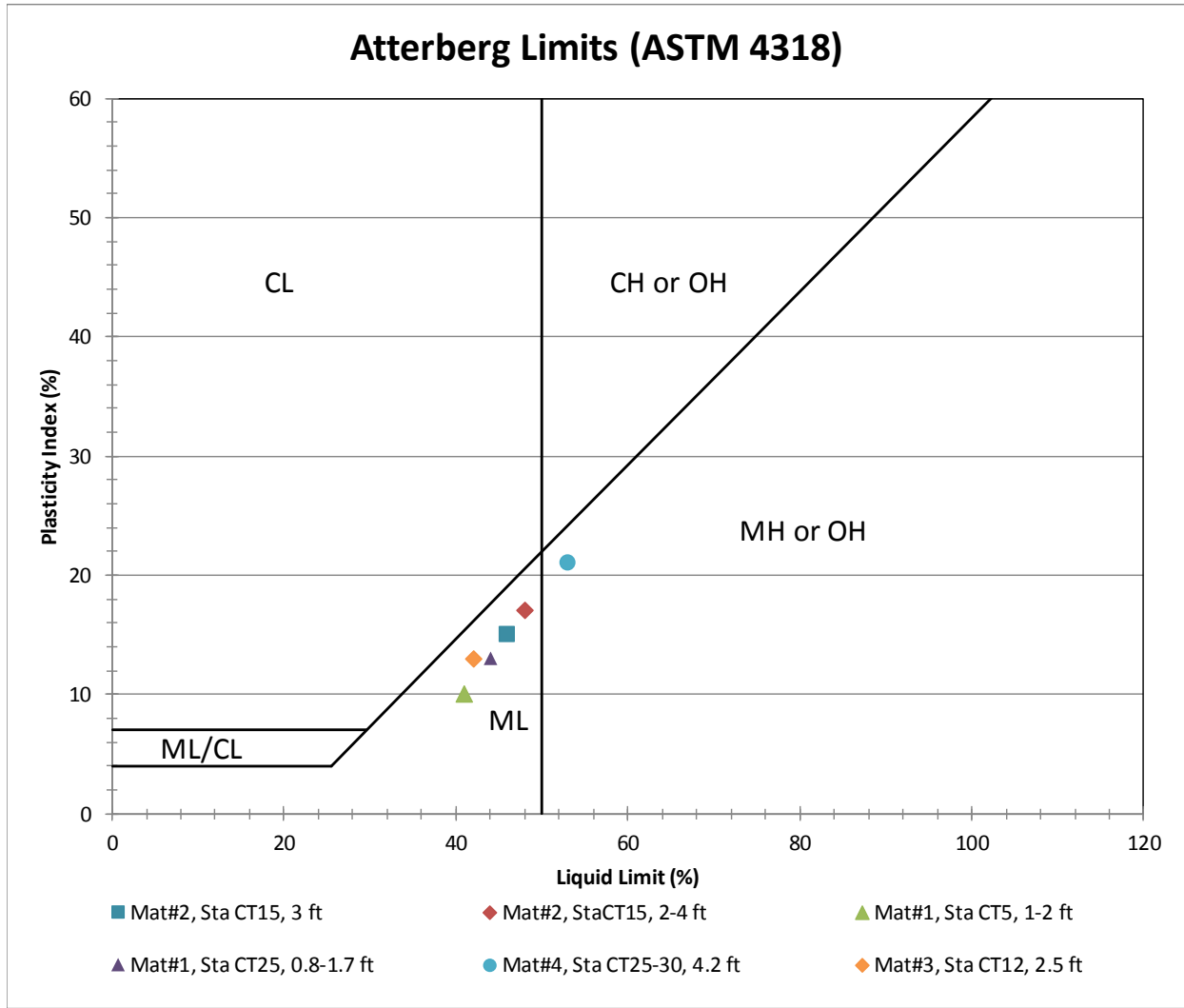
Figure 3B- 1. Atterberg limits (ASTM 4318) test results for commonly occurring onsite materials

| Material # | Station | Depth (ft) | LL | PL | PI | In-Situ w% | USCS |
|---|---|---|---|---|---|---|---|
| 2 | CT 15 | 3 | 46 | 31 | 15 | 20.5 | ML |
| 2 | CT 5 | 2 to 4 | 48 | 31 | 17 | 38.8 | ML |
| 1 | CT 5 | 1 to 2 | 41 | 31 | 10 | 35.2 | ML |
| 1 | CT 25 | 0.8 to 1.7 | 44 | 31 | 13 | 33.3 | ML |
| 4 | CT 25 - 30 | 4.2 | 53 | 32 | 21 | 25.9 | MH |
| 3 | CT 12 | 2.5 | 42 | 29 | 13 | 32.0 | ML |

# APPENDIX 3C

## Cone Penetration and Pore Pressure Dissipation Test Data

Three cone penetration tests (CPTs) were performed by Gregg Drilling at the locations shown on Figure 3C- 1. CPT C1 is located on the waterside of the levee crown road at instrument line A (Figure 3C- 2 and Figure3C- 3), C2 on the landside of the levee crown road at instrument line B (Figure 3C- 4 and Figure 3C- 5), and C3 on the waterside of the levee crown road at instrument line C (Figure 3C- 6 and Figure 3C- 7).  All tests included pore pressure dissipation testing at multiple intervals within the profile to confirm the depth to a hydrostatic groundwater table. Dissipation test results are provided on Figure 3C- 8 and Figure 3C- 9 for CPT C1, Figure 3C- 10 through Figure 3C- 14 for CPT C2 and Figure 3C- 15 through Figure 3C- 17 for CPT C3. In general, dissipation testing shows that the hydrostatic groundwater table at the time of testing was located about 23 to 25 feet below the levee crown road at the locations studied.
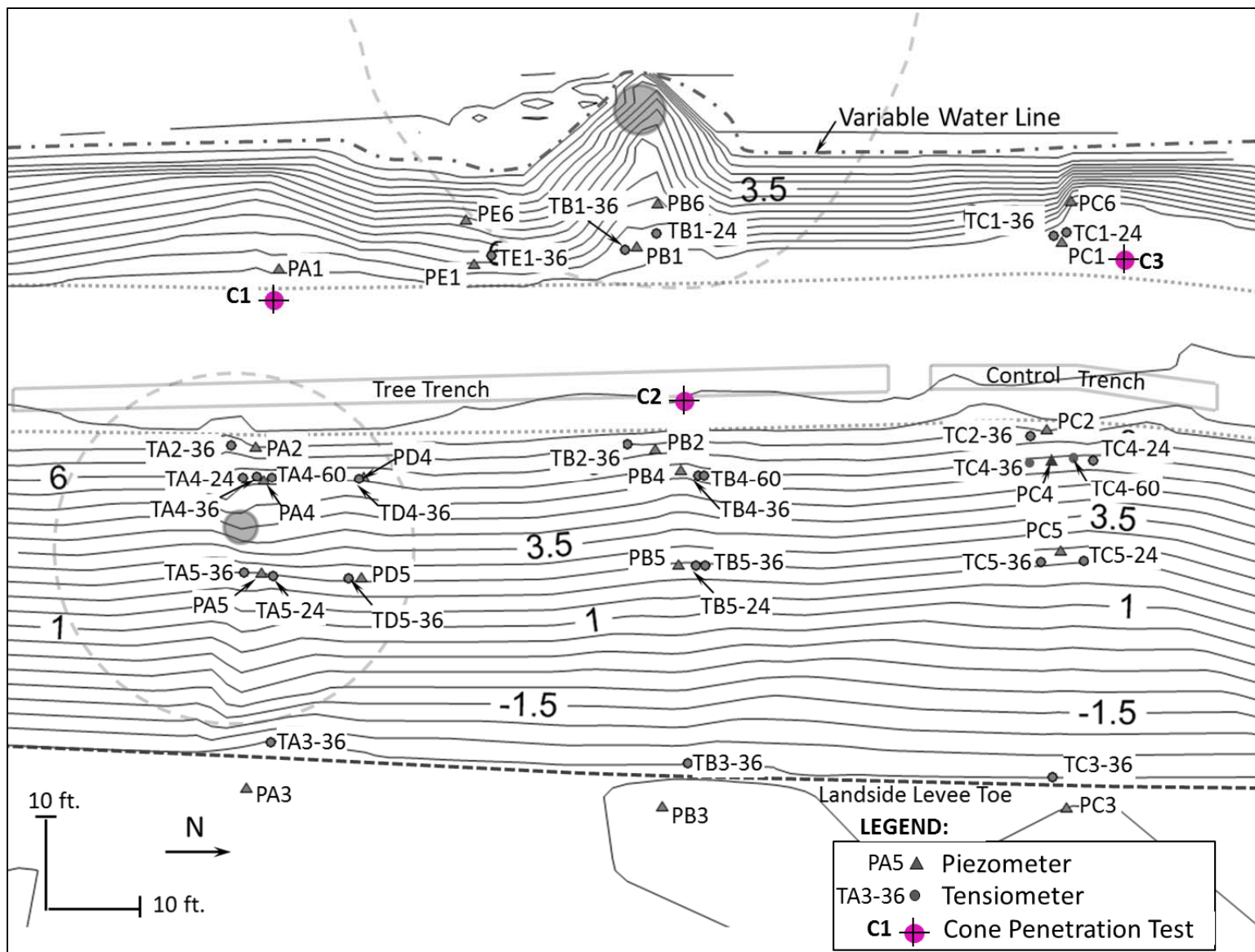
Figure 3C- 1. Cone Penetration Test (CPT) locations in the context of the site layout and instrumentation plan. Instrument locations were estimated based on nearby features
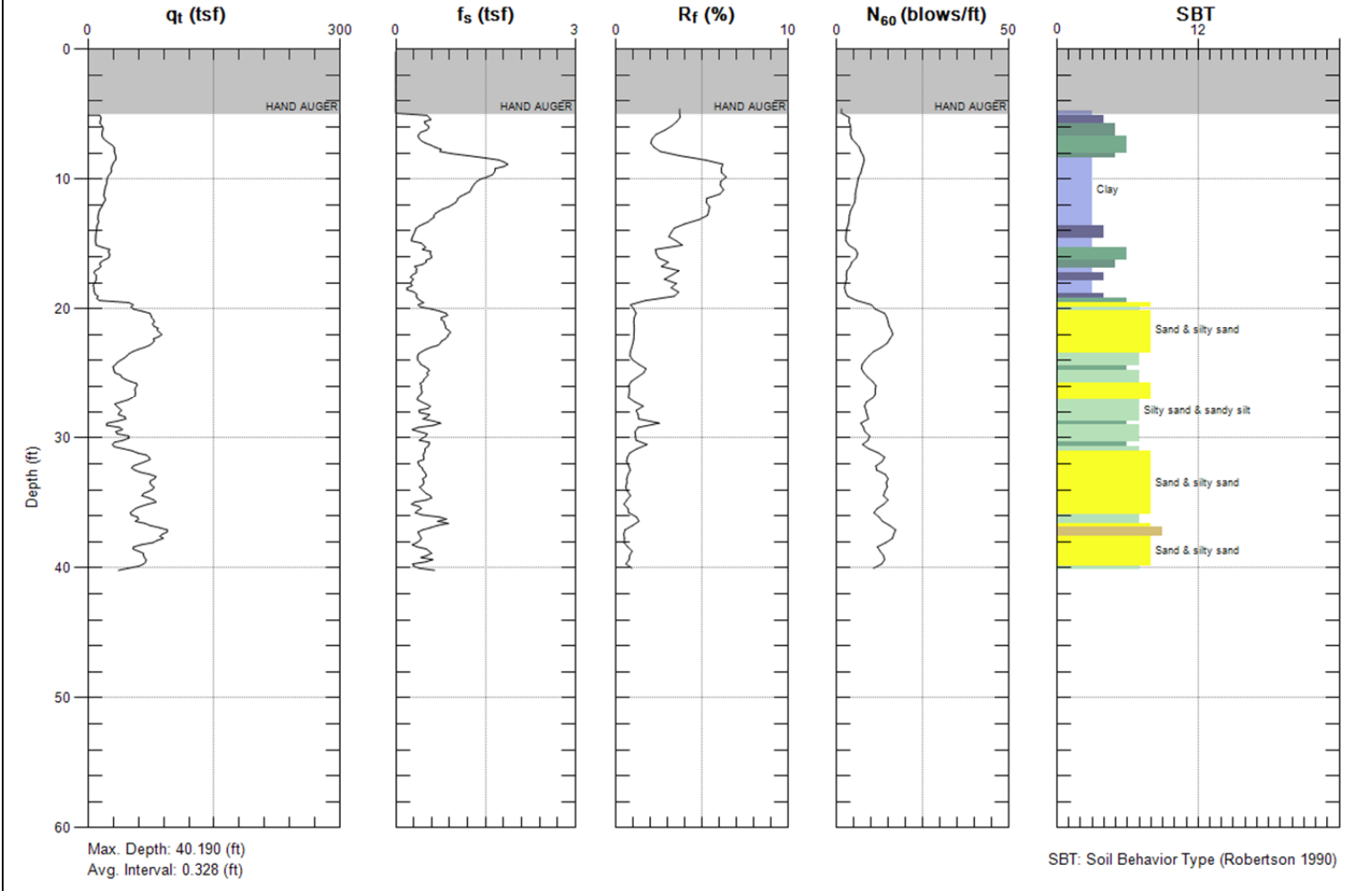
Figure 3C- 2. Cone Penetration Test Log at CPT location C1 at the waterside of the access road at instrument line A. Sheet 1 of 2.
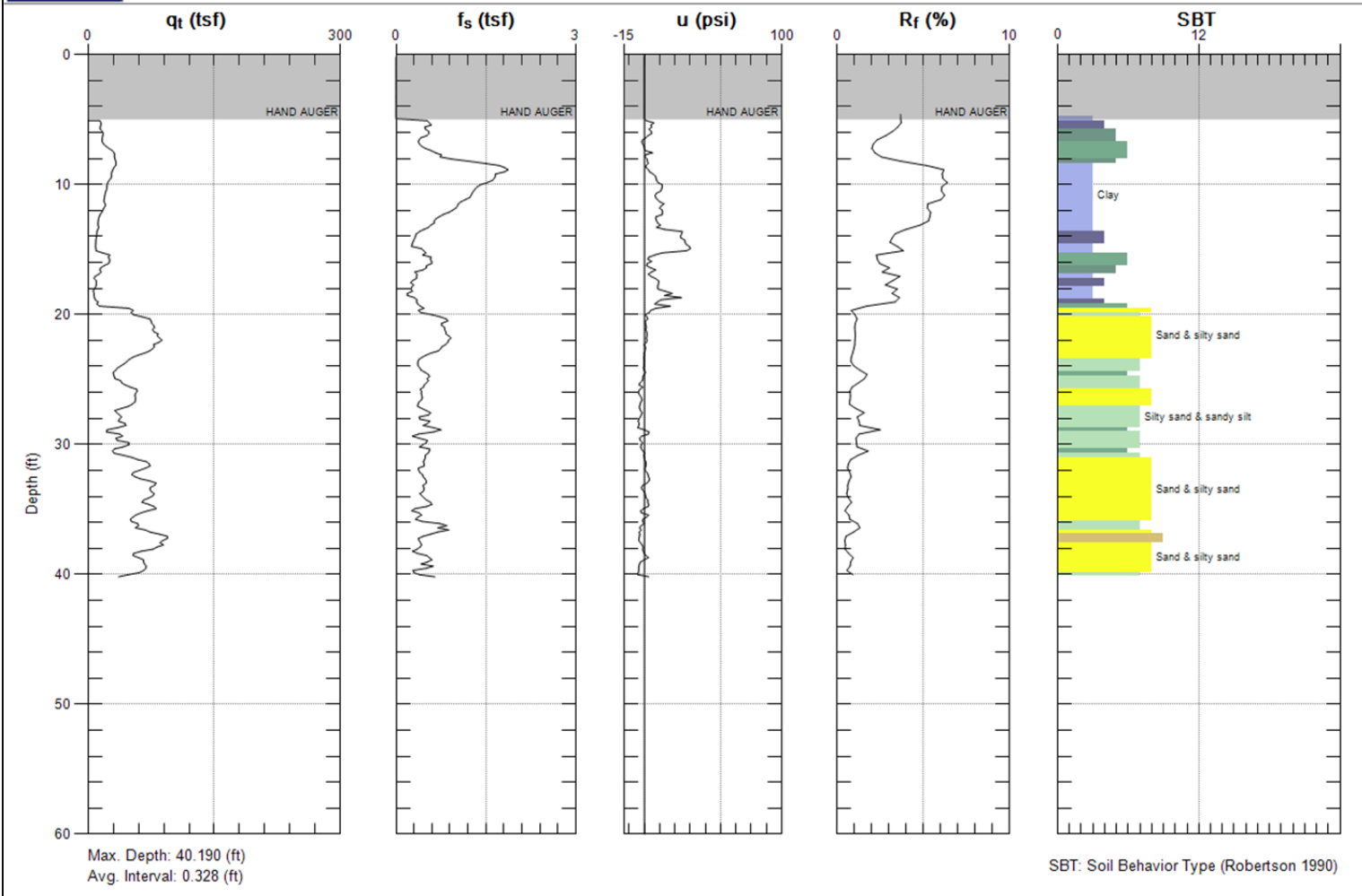
Figure3C- 3. Cone Penetration Test Log at CPT location C1 at the waterside of the access road at instrument line A. Sheet 2 of 2.
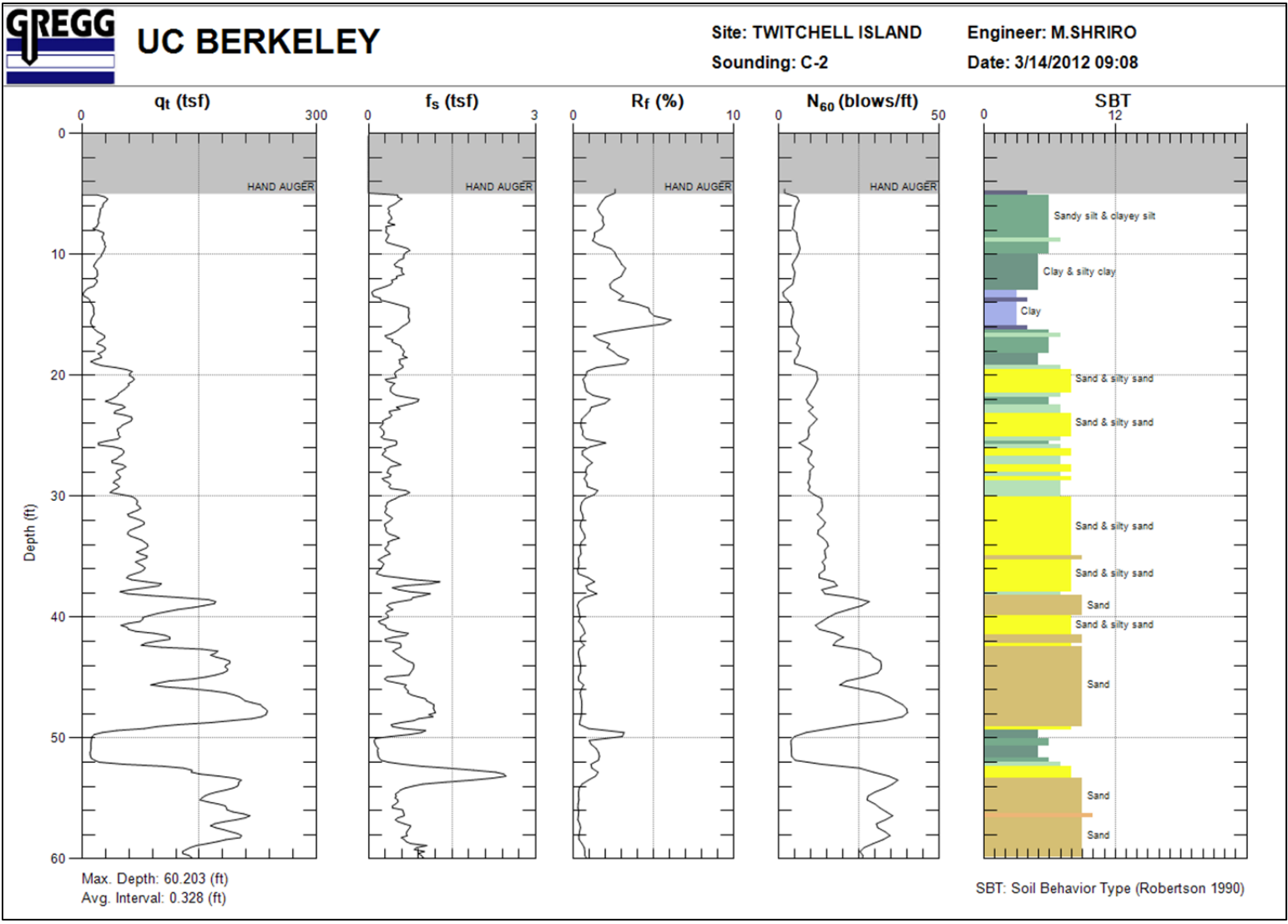
Figure 3C- 4. Cone Penetration Test Log at CPT location C2 at the landside of the access road at instrument line B. Sheet 1 of 2.
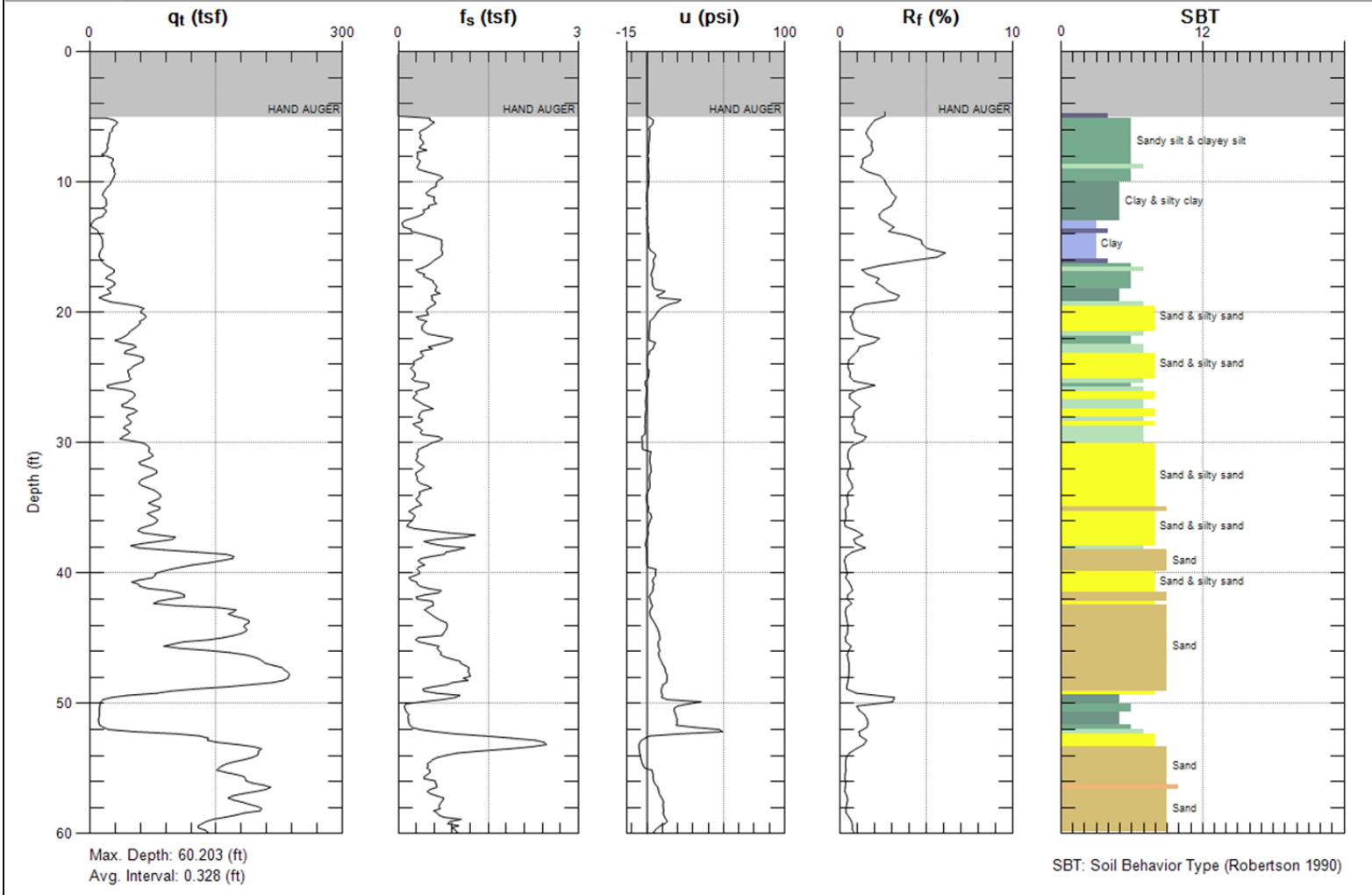
Figure 3C- 5. Cone Penetration Test Log at CPT location C2 on the landside of the access road at instrument line B.  Sheet 2 of 2.
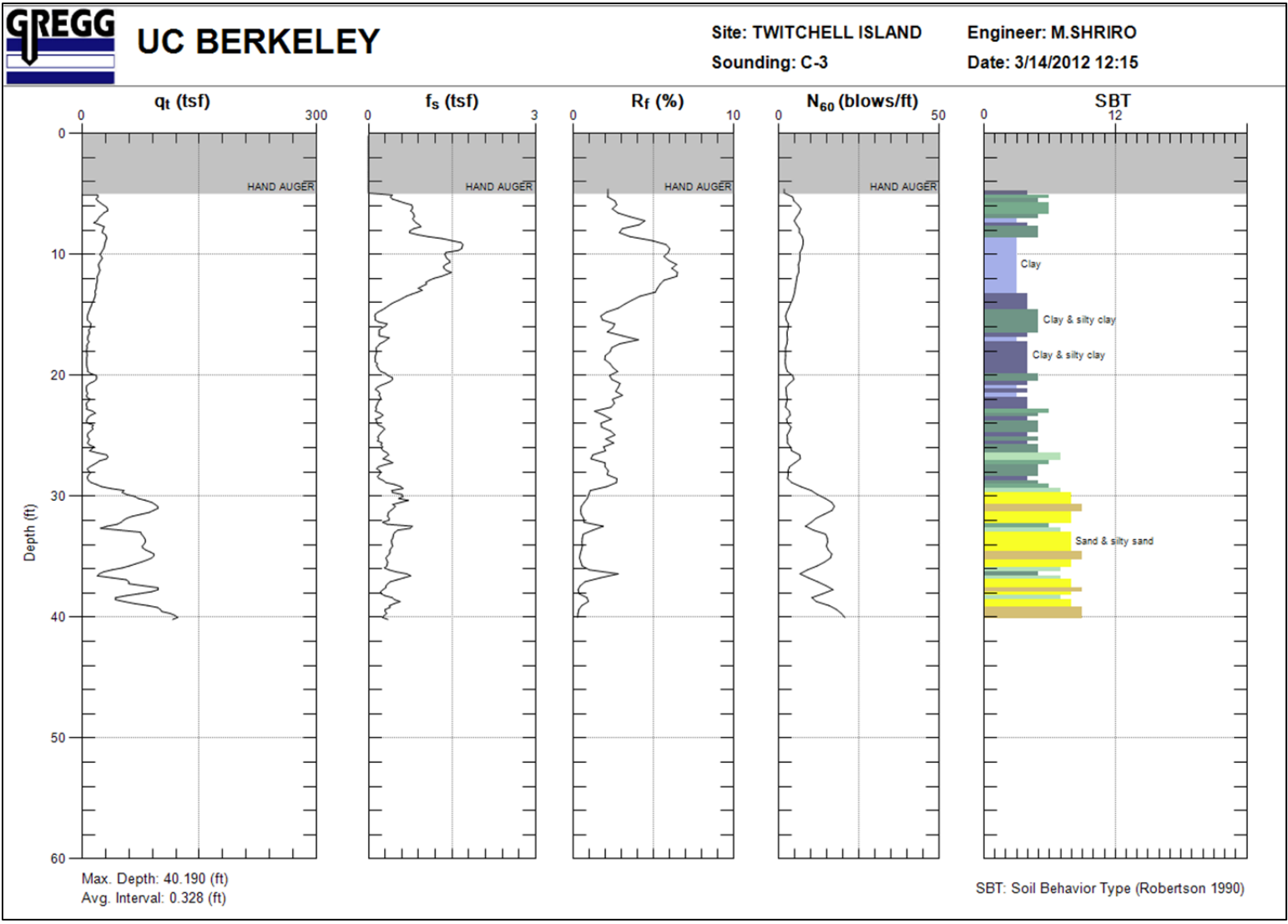
Figure 3C- 6. Cone Penetration Test Log at CPT location C3 at the waterside of the access road at instrument line C. Sheet 1 of 2.
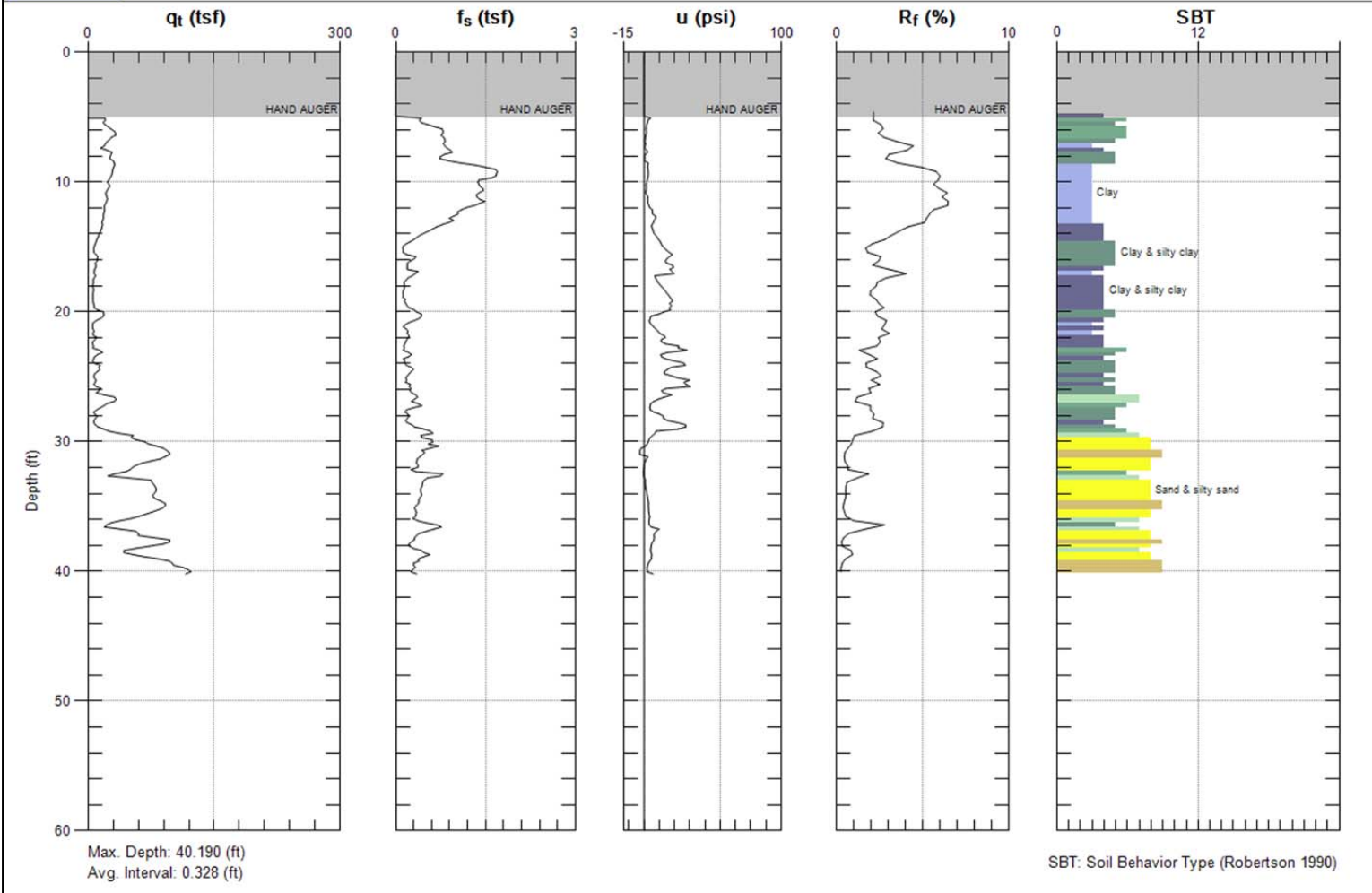
Figure 3C- 7. Cone Penetration Test Log at CPT location C3 at the waterside of the access road at instrument line C. Sheet 2 of 2.
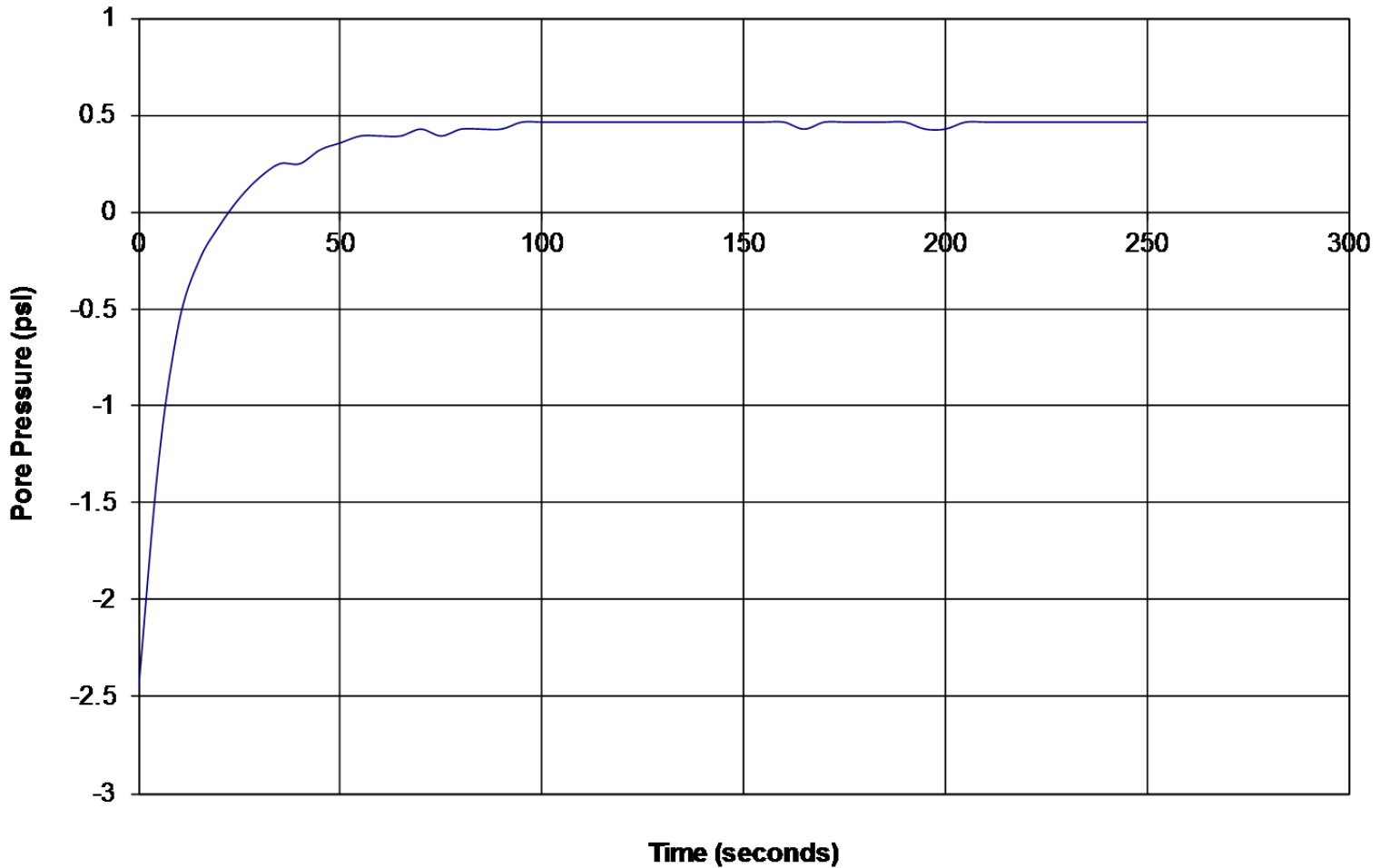
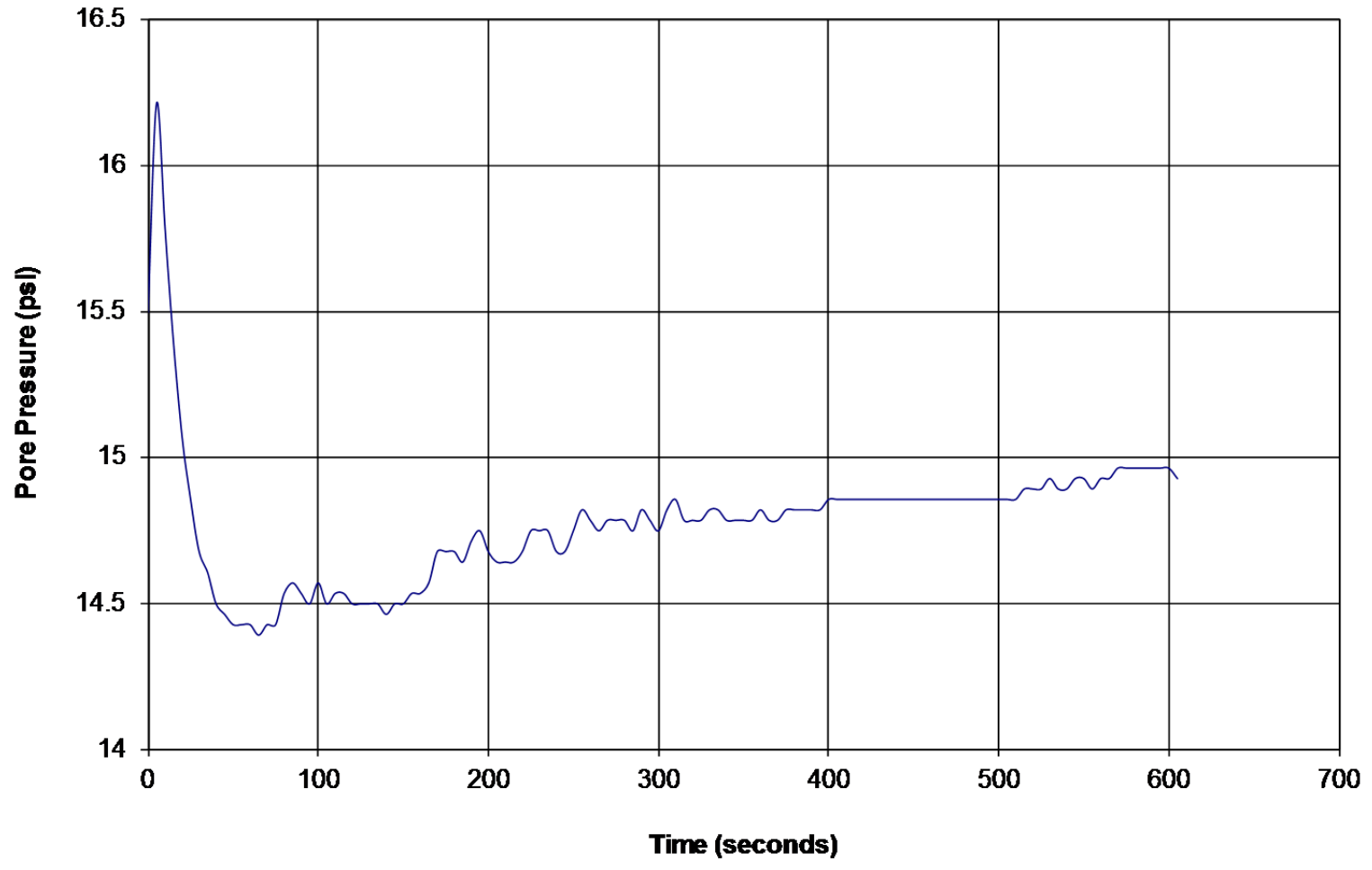Figure 3C- 8. Pore pressure dissipation test at CPT location C1 at instrument line A, depth = 25ft
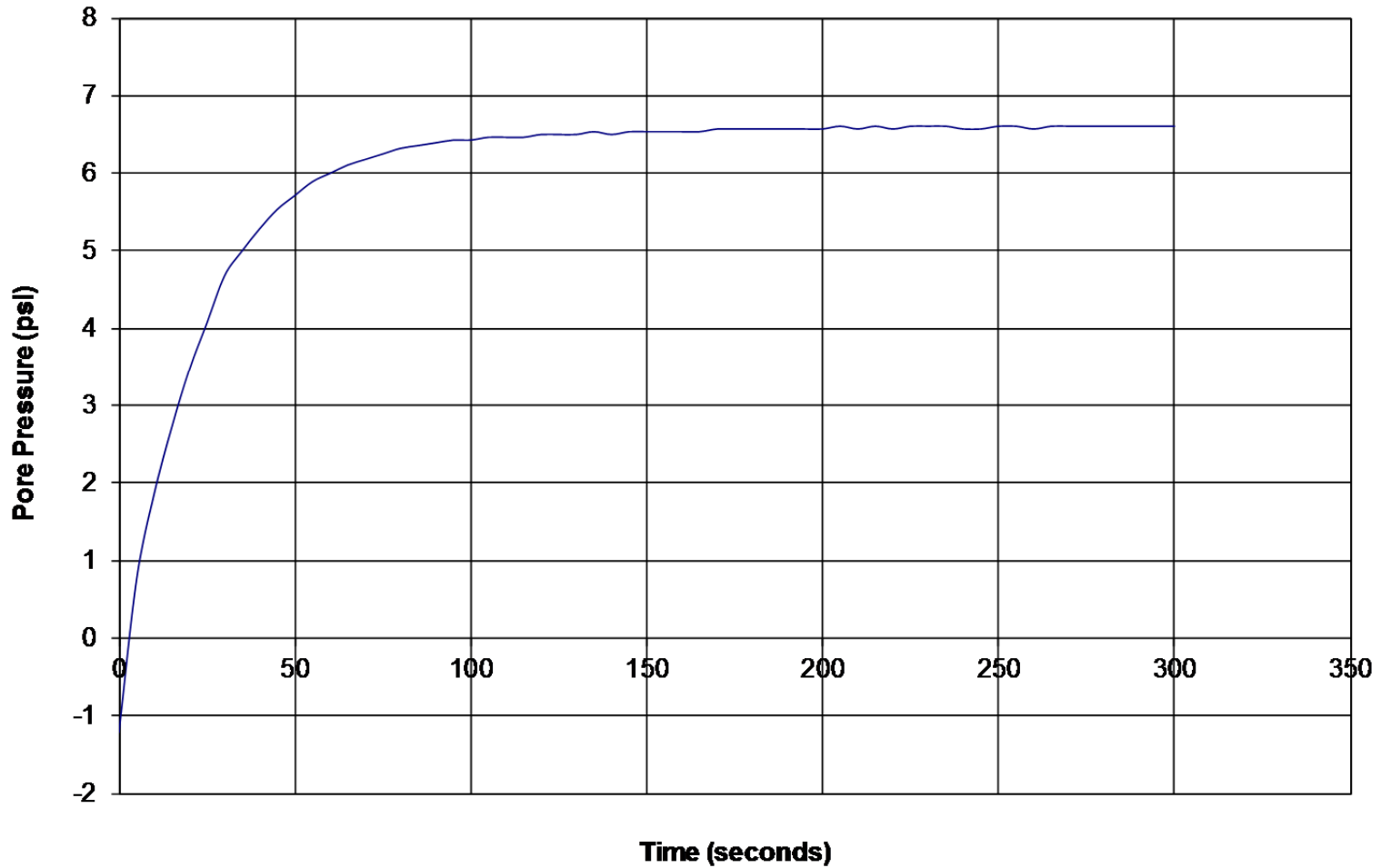
Figure 3C- 9. Pore pressure dissipation test at CPT location C1 at instrument line A, depth = 40ft
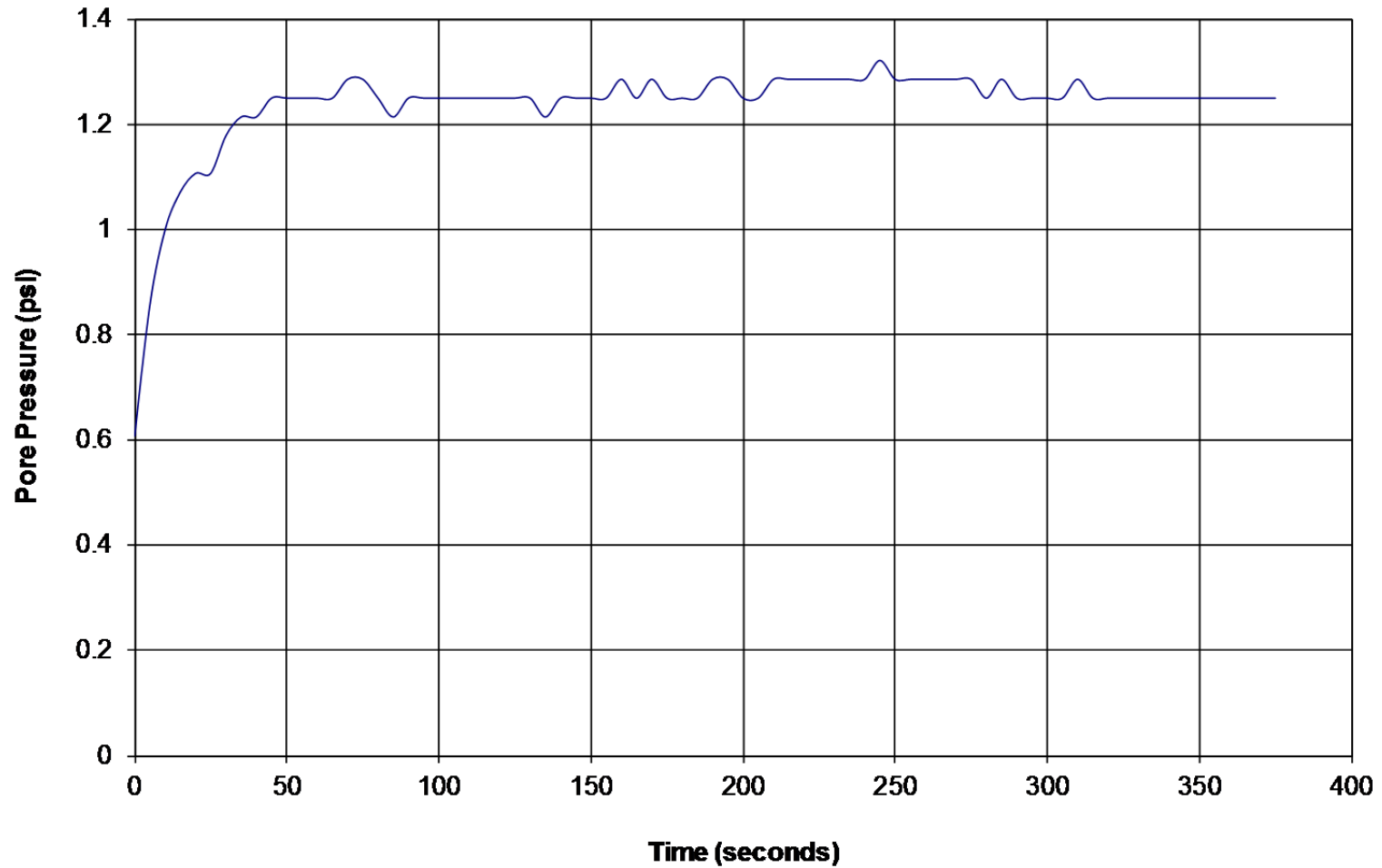
Figure 3C- 10. Pore pressure dissipation test at CPT location C2 at instrument line B, depth = 24ft
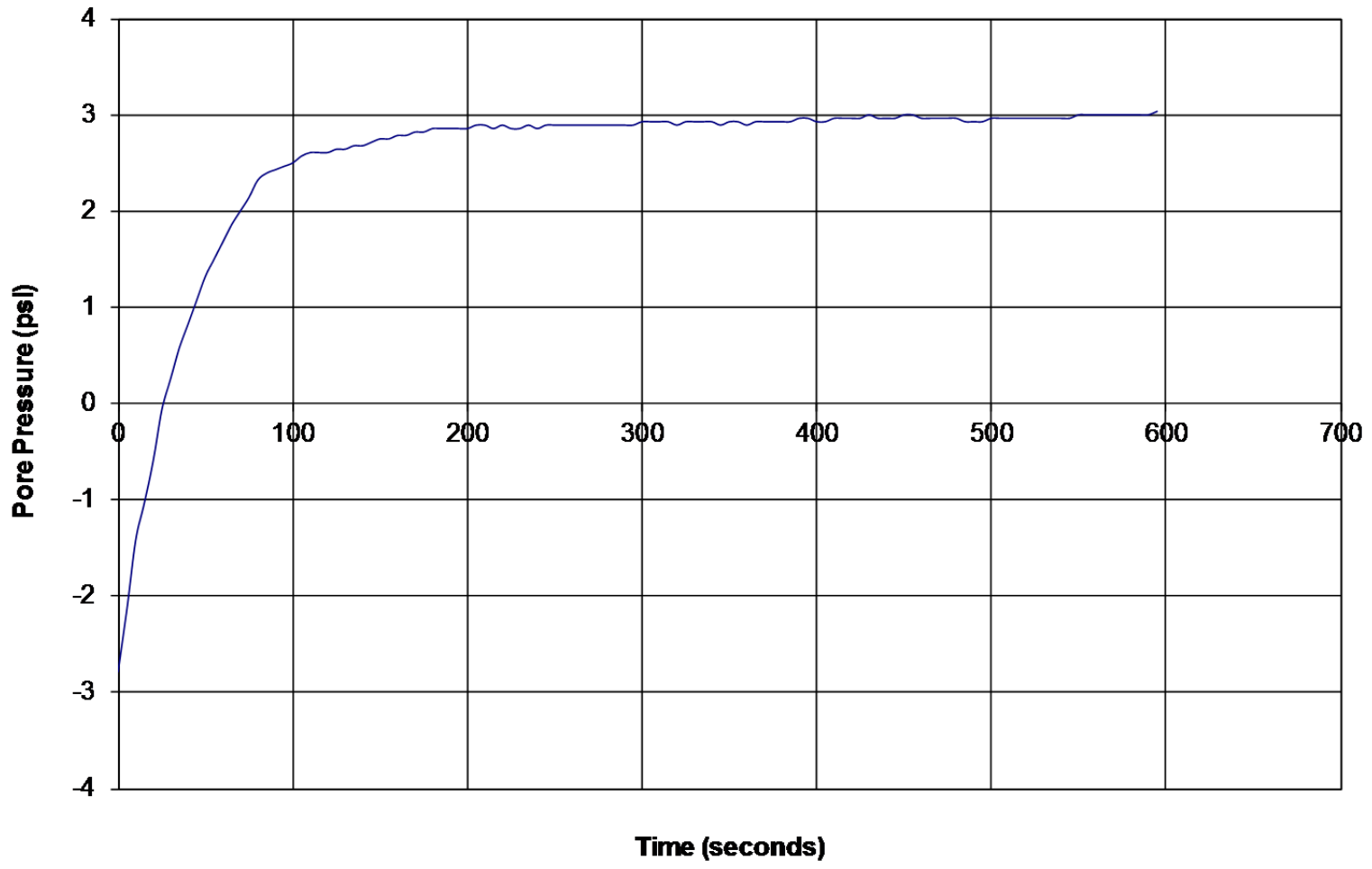
Figure 3C- 11. Pore pressure dissipation test at CPT location C2 at instrument line B, depth = 31ft
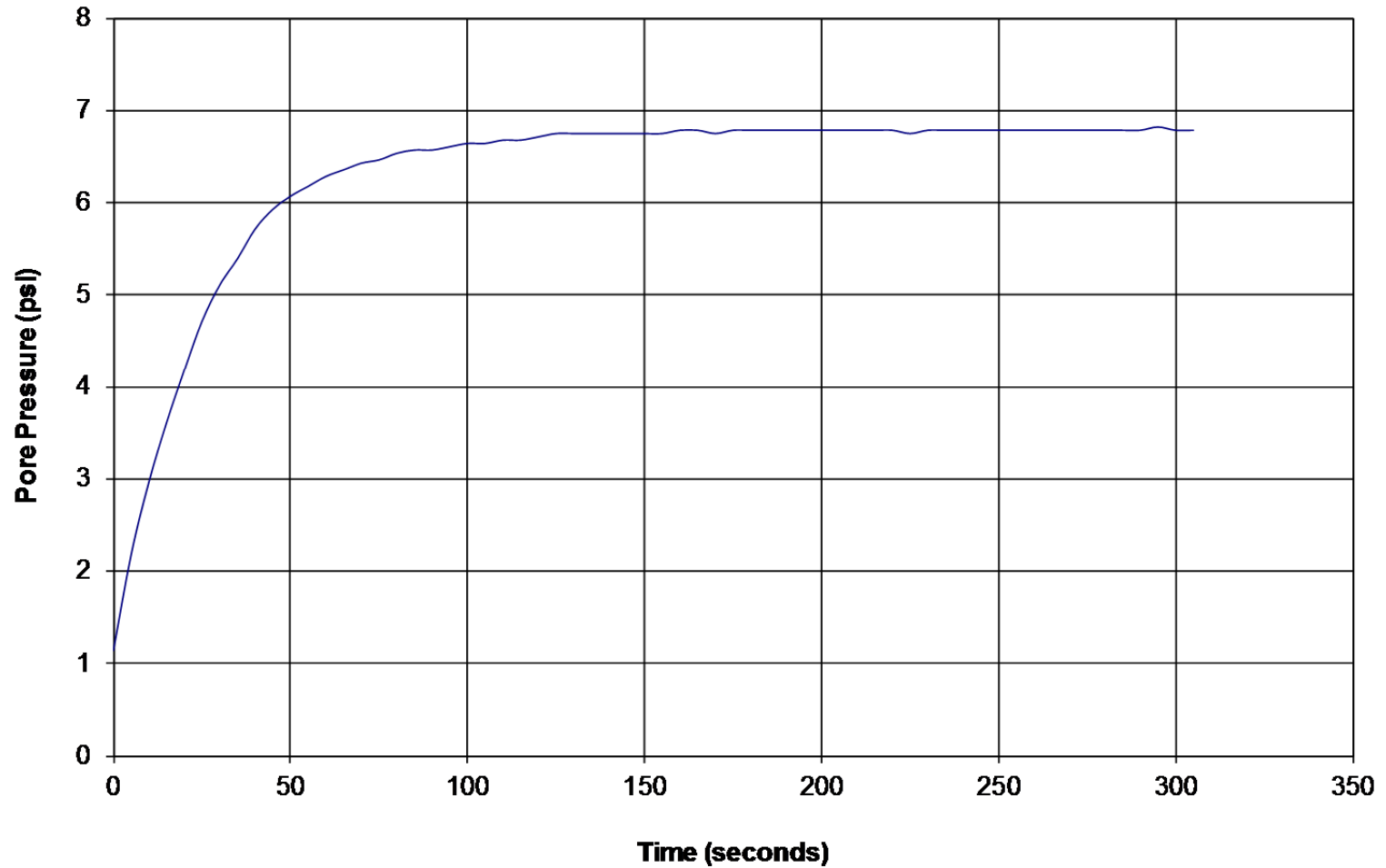
Figure 3C- 12. Pore pressure dissipation test at CPT location C2 at instrument line B, depth = 40ft
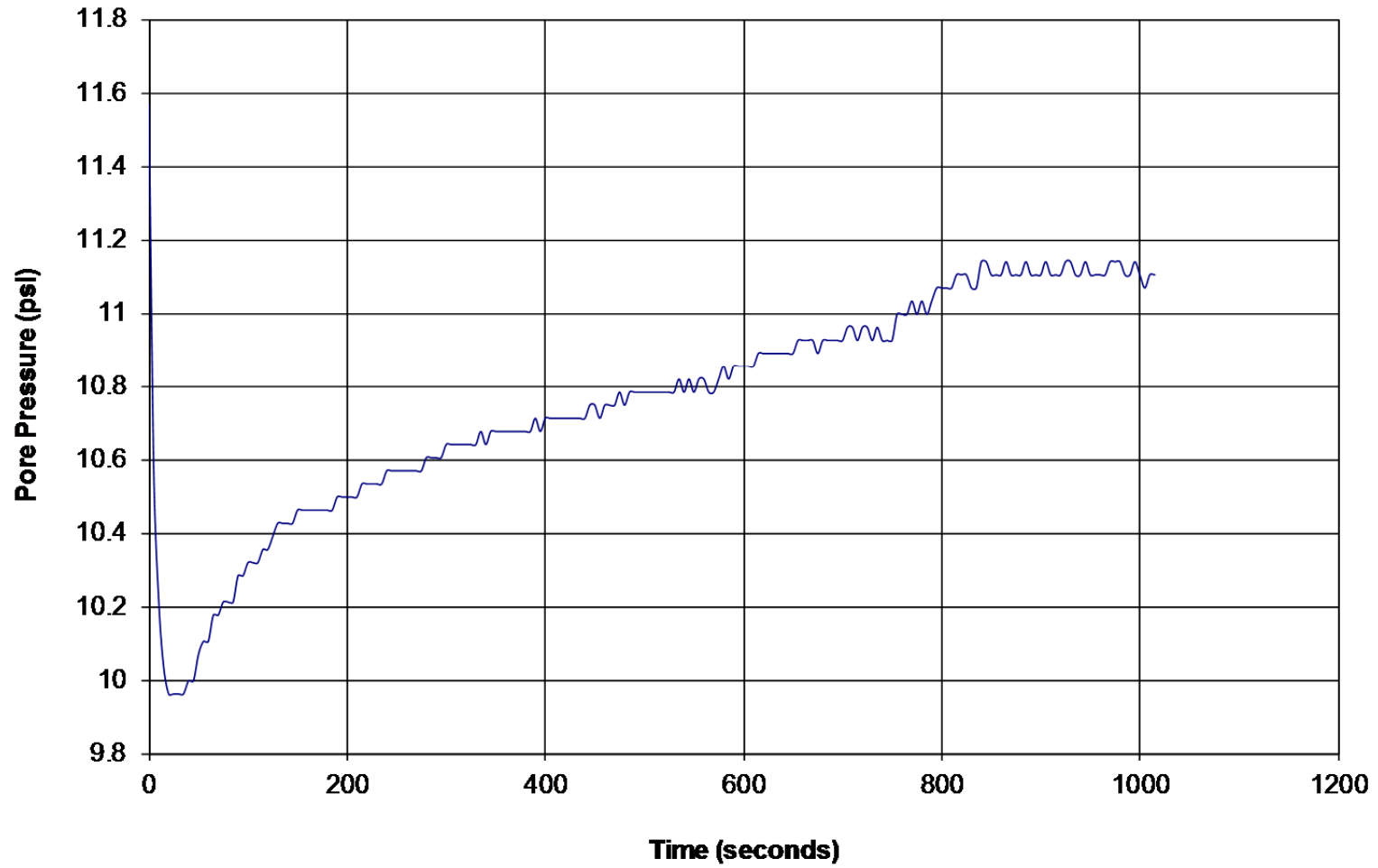
Figure 3C- 13. Pore pressure dissipation test at CPT location C2 at instrument line B, depth = 49ft

Figure 3C- 14. Pore pressure dissipation test at CPT location C2 at instrument line B, depth = 59ft
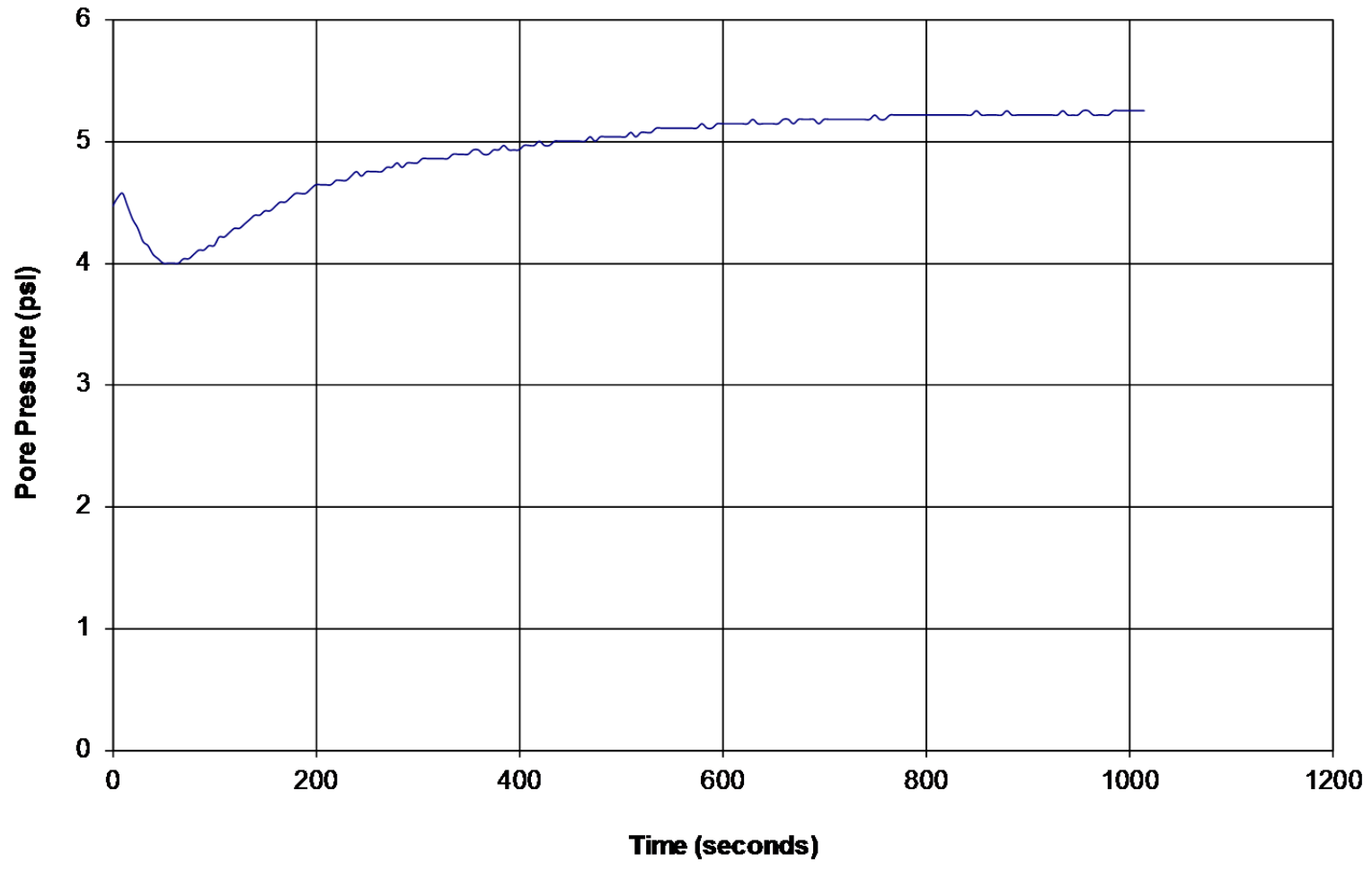
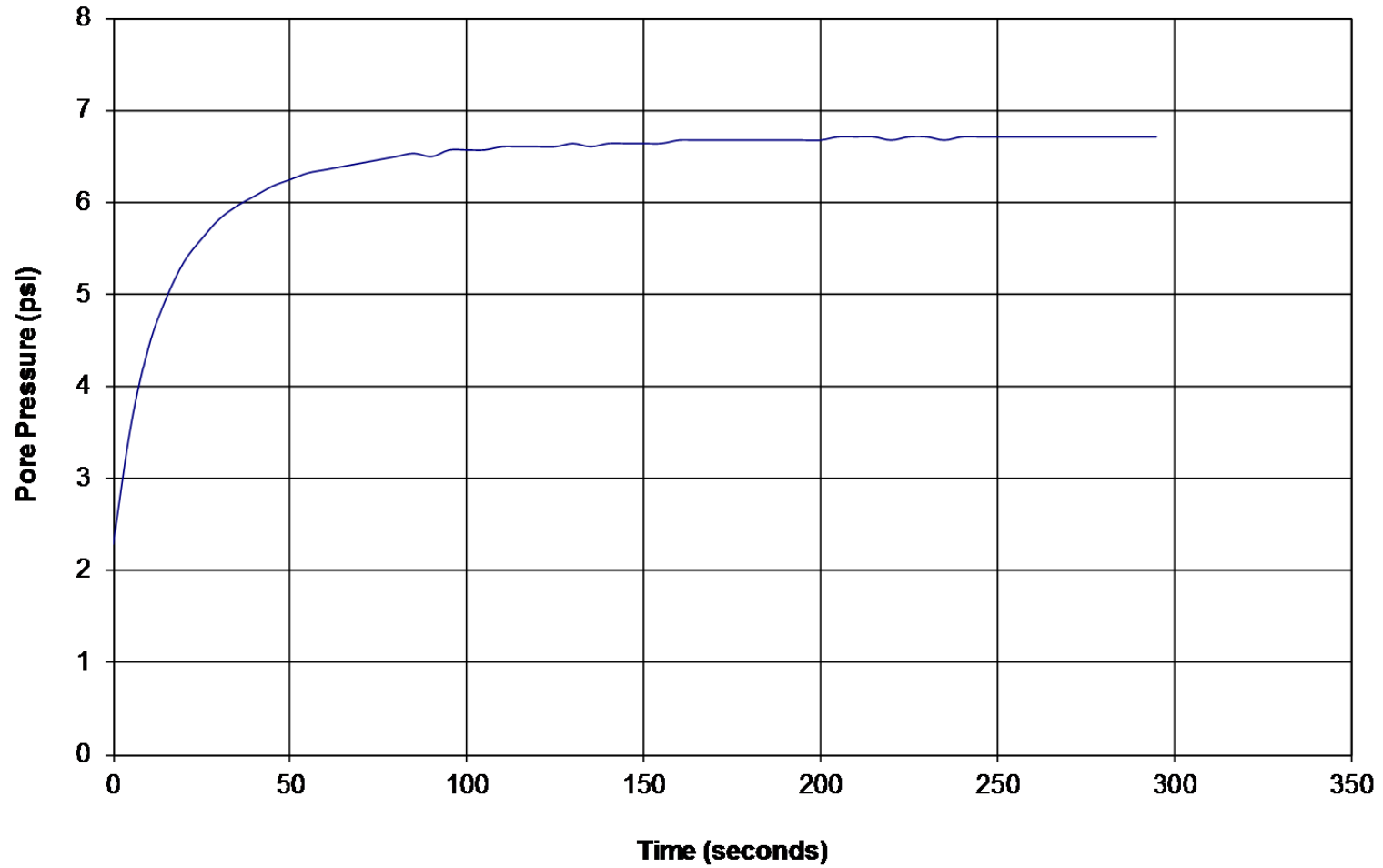Figure 3C- 15. Pore pressure dissipation test at CPT location C3 at instrument line C, depth = 27ft
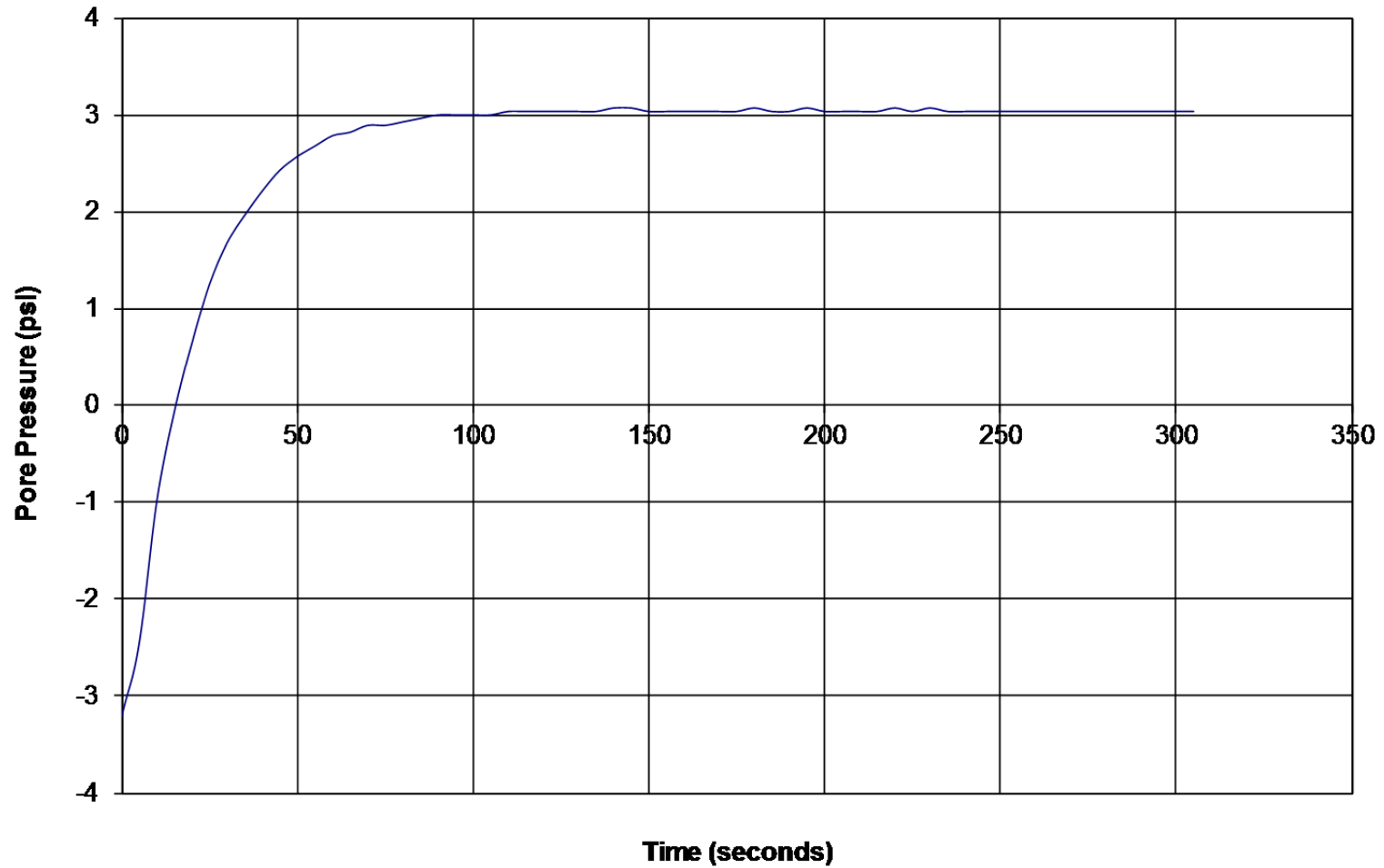
Figure 3C- 16. Pore pressure dissipation test at CPT location C3 at instrument line C, depth = 31ft

Figure 3C- 17. Pore pressure dissipation test at CPT location C3 at instrument line C, depth = 40ft

# APPENDIX 3D

## Regional Soil Data – Twitchell Island Test Site

The study site is located on the south bank of the Sevenmile Slough along the northern levee of Twitchell Island within the Sacramento San Joaquin River Delta. The site is owned by the California Department of Water Resources and maintained by Reclamation District 1601. The section of levee under study was bypassed in 2008 with construction of a new levee just south of the site. As part of our review of available documents, the document titled "Reclamation District 1601 Twitchell Island Five Year Plan" (KSN, 2010) was reviewed. The document provides a comprehensive review of site history and available civil and geotechnical data for the island. The data found to be most proximal and relevant to our site was performed as part of a study by Neil O. Anderson and Associates titled "Geotechnical Services Report: Sevenmile Slough Sites 1, 2, and 3 – Levee Improvements" and dated August 8, 2007. The study included three soil borings and three test pits within the foundation soils of the new levee that bypassed our study site. Additionally, borings and test pits were performed for two other sites along the northern levee to the north and south of our study site. A total of 9 test borings and 6 test pits were reviewed and are attached herein.

# GEOTECHNICAL SERVICES REPORT

# SEVENMILE SLOUGH SITES 1, 2, & 3 LEVEE IMPROVEMENTS

# TWITCHELL ISLAND

# SACRAMENTO COUNTY, CALIFORNIA

## REPORT PREPARED FOR:

## RECLAMATION DISTRICT 1601

## OUR PROJECT NUMBER: LFG-0229

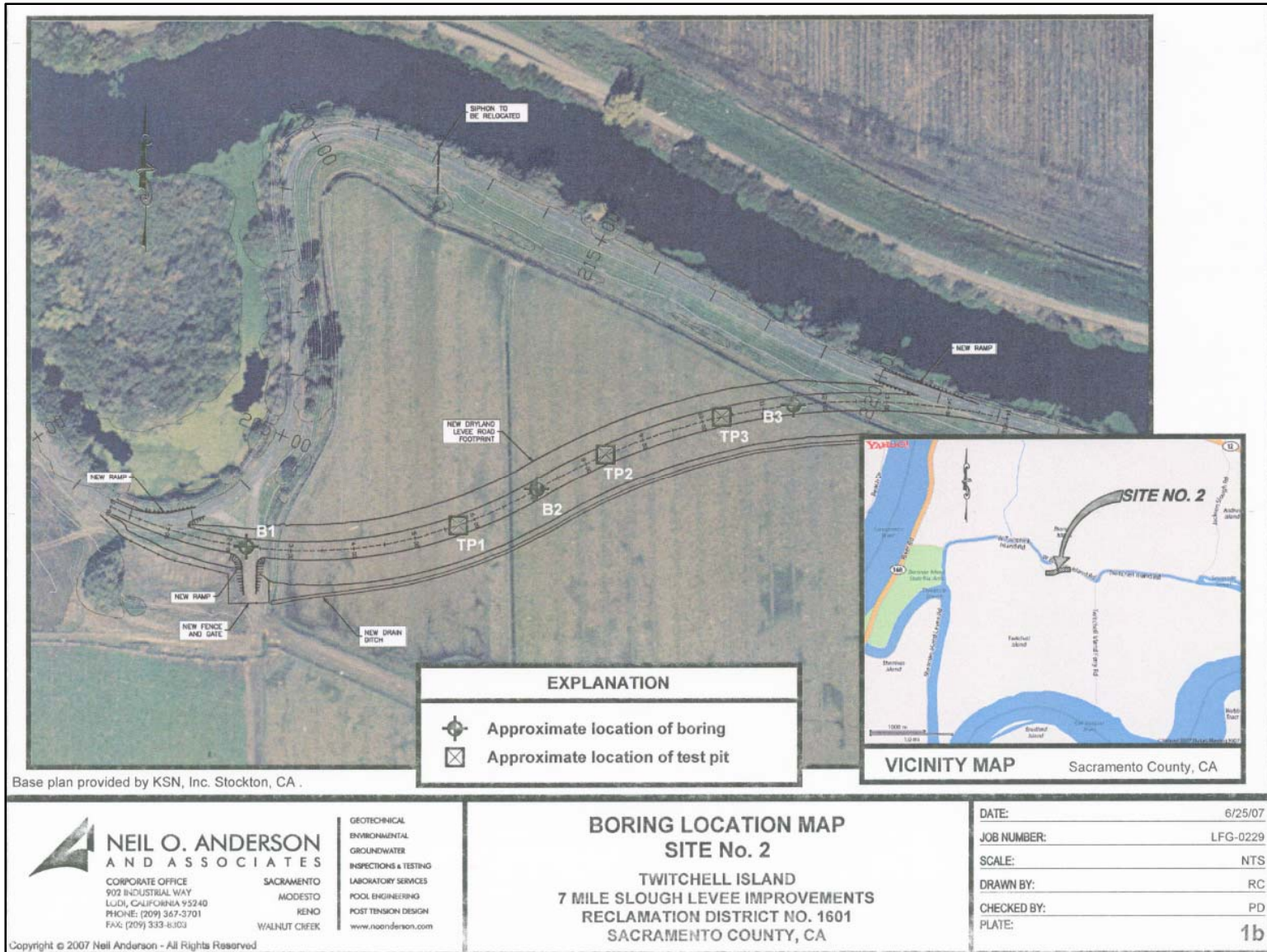## AUGUST 8, 2007

902 Industrial Way ▪ Lodi, CA 95240 ▪ 209.367.3701 ▪ Fax 209.333.8303          ©2007 Neil O. Anderson & Associates, Inc

3D-3

EXPLANATION

⊕ Approximate location of boring

⊠ Approximate location of test pit

VICINITY MAP — Sacramento County, CA

Base plan provided by KSN, Inc. Stockton, CA .
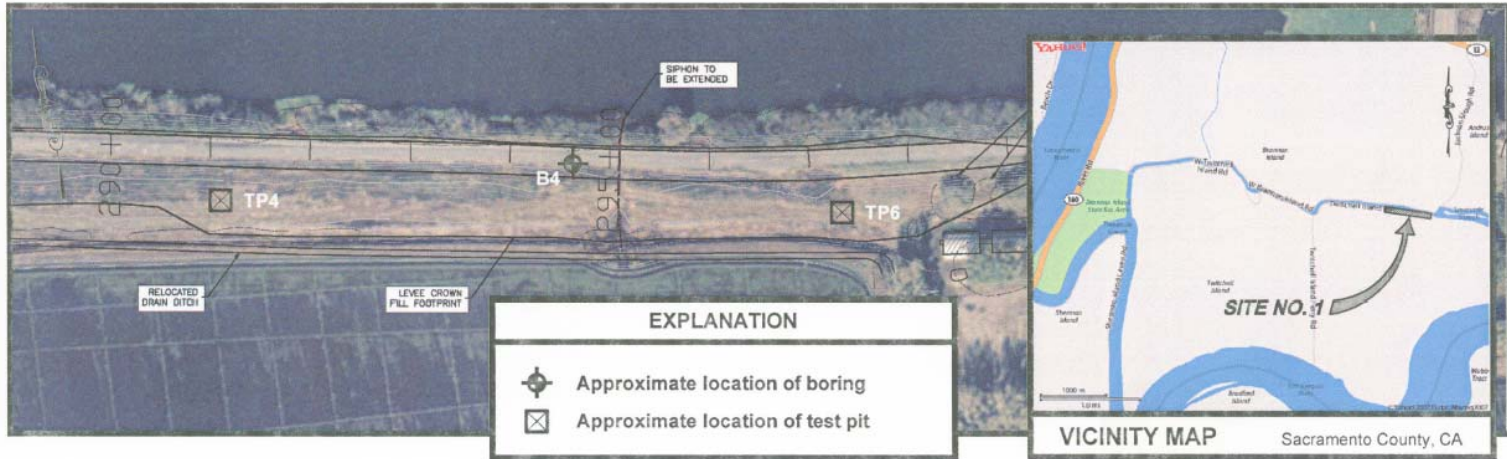
NEIL O. ANDERSON
AND ASSOCIATES

CORPORATE OFFICE
902 INDUSTRIAL WAY
LODI, CALIFORNIA 95240
PHONE: (209) 367-3701
FAX: (209) 333-8303

SACRAMENTO
MODESTO
RENO
WALNUT CREEK

GEOTECHNICAL
ENVIRONMENTAL
GROUNDWATER
INSPECTIONS & TESTING
LABORATORY SERVICES
POOL ENGINEERING
POST TENSION DESIGN
www.noanderson.com

BORING LOCATION MAP
SITE No. 2

TWITCHELL ISLAND
7 MILE SLOUGH LEVEE IMPROVEMENTS
RECLAMATION DISTRICT NO. 1601
SACRAMENTO COUNTY, CA

| DATE: | 6/25/07 |
| JOB NUMBER: | LFG-0229 |
| SCALE: | NTS |
| DRAWN BY: | RC |
| CHECKED BY: | PD |
| PLATE: | 1b |

EXPLANATION

⊕ Approximate location of boring

⊠ Approximate location of test pit

VICINITY MAP    Sacramento County, CA

Base plan provided by KSN, Inc. Stockton, CA .

NEIL O. ANDERSON
AND ASSOCIATES

CORPORATE OFFICE       SACRAMENTO
902 INDUSTRIAL WAY     MODESTO
LODI, CALIFORNIA 95240  RENO
PHONE: (209) 367-3701  WALNUT CREEK
FAX: (209) 333-8303

GEOTECHNICAL
ENVIRONMENTAL
GROUNDWATER
INSPECTIONS & TESTING
LABORATORY SERVICES
POOL ENGINEERING
POST TENSION DESIGN
www.noanderson.com

BORING LOCATION MAP
SITE No. 1

TWITCHELL ISLAND
7 MILE SLOUGH LEVEE IMPROVEMENTS
RECLAMATION DISTRICT NO. 1601
SACRAMENTO COUNTY, CA

| DATE: | 6/25/07 |
|---|---|
| JOB NUMBER: | LFG-0229 |
| SCALE: | NTS |
| DRAWN BY: | RC |
| CHECKED BY: | PD |
| PLATE: | 1a |

EXPLANATION

⊕ Approximate location of boring

**VICINITY MAP**    Sacramento County, CA

SITE NO. 3

Base plan provided by KSN, Inc. Stockton, CA .

**NEIL O. ANDERSON**
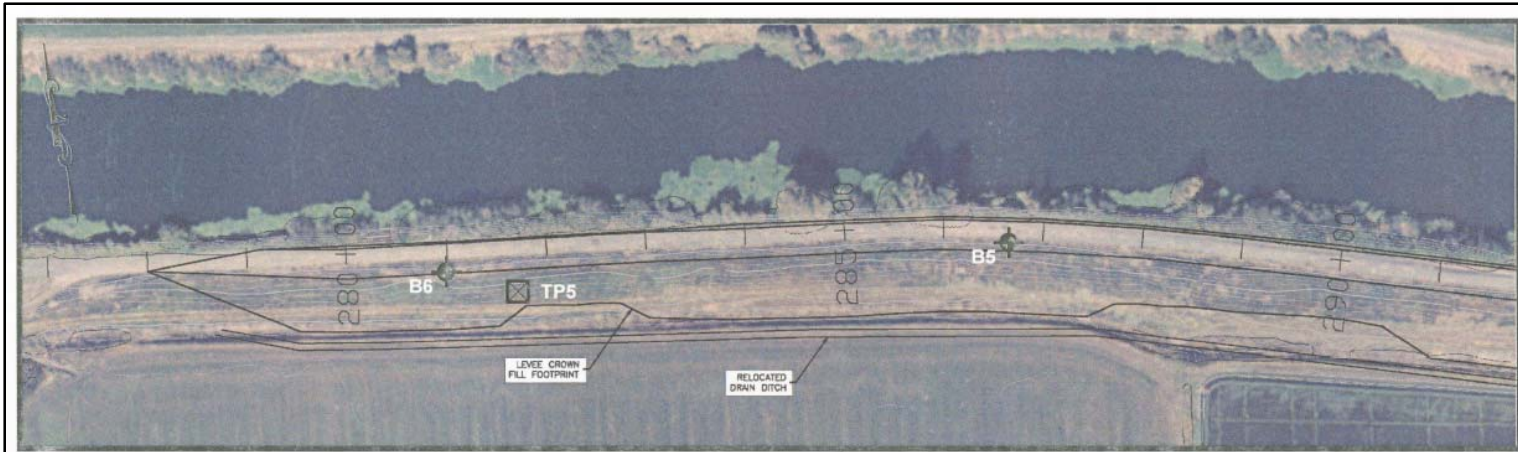**AND ASSOCIATES**

CORPORATE OFFICE
902 INDUSTRIAL WAY
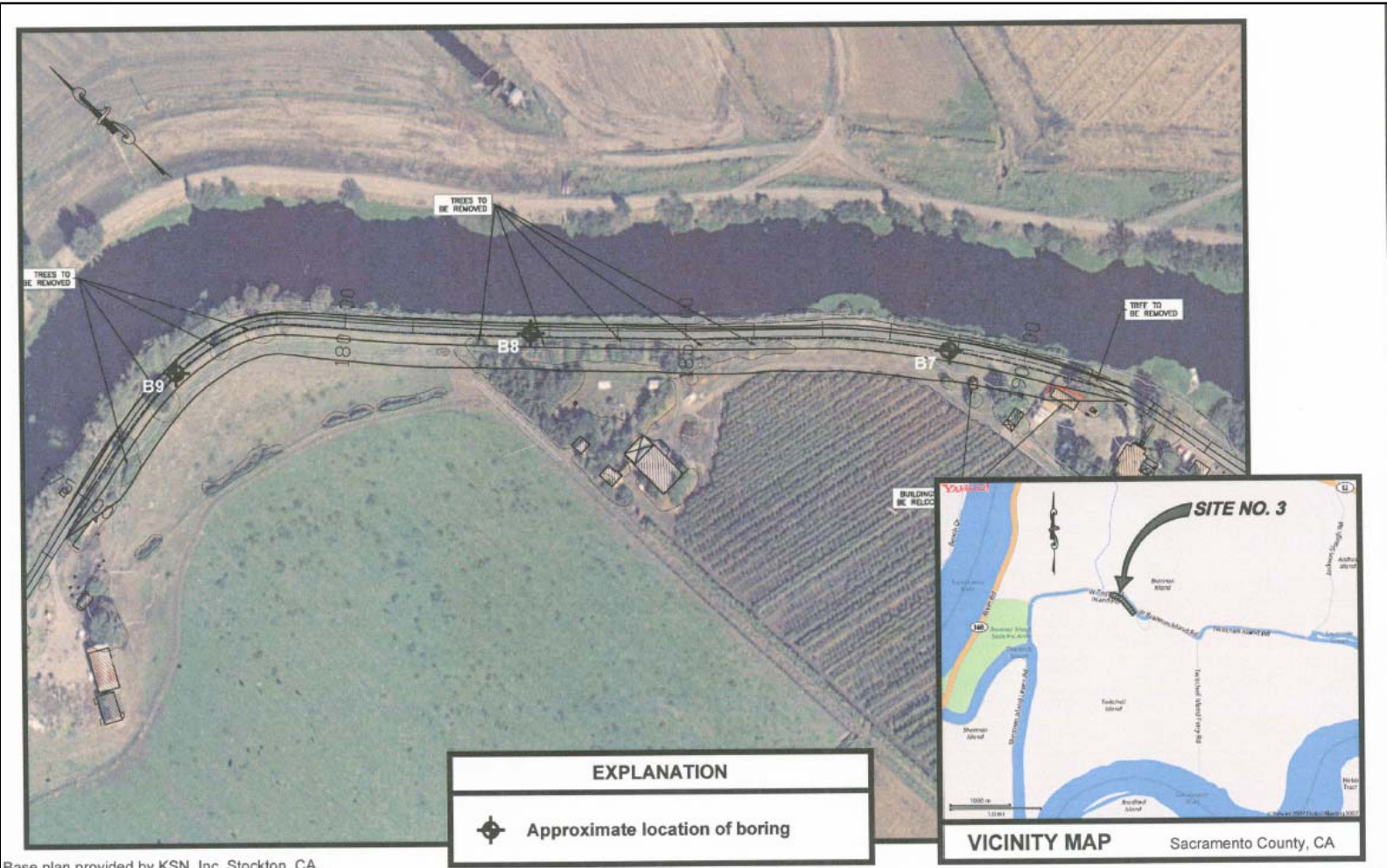LODI, CALIFORNIA 95240
PHONE: (209) 367-3701
FAX: (209) 333-8303

SACRAMENTO
MODESTO
RENO
WALNUT CREEK

GEOTECHNICAL
ENVIRONMENTAL
GROUNDWATER
INSPECTIONS & TESTING
LABORATORY SERVICES
POOL ENGINEERING
POST TENSION DESIGN
www.noanderson.com

**BORING LOCATION MAP**
**SITE No. 3**

TWITCHELL ISLAND
7 MILE SLOUGH LEVEE IMPROVEMENTS
RECLAMATION DISTRICT NO. 1601
SACRAMENTO COUNTY, CA

| DATE: | 6/25/07 |
|---|---|
| JOB NUMBER: | LFG-0224 |
| SCALE: | NTS |
| DRAWN BY: | RC |
| CHECKED BY: | PD |
| PLATE: | 1c |

## UNIFIED SOIL CLASSIFICATION SYSTEM AND BORING LOG SYMBOLS

| | DESCRIPTION | MAJOR DIVISIONS | | |
|---|---|---|---|---|
| GW | Well-graded gravels, gravel sand mixtures, little or no fines. | Clean gravels (little or no fines) | Gravel and gravelly soils | Coarse grained soils more than 50% larger than No. 200 sieve |
| GP | Poorly-graded gravels, gravel sand mixtures, little or no fines | | More than 50% of coarse fraction retained on No. 4 sieve | |
| GM | Silty gravels, gravel-sand-clay mixtures | Sands with appreciable amount of fines | | |
| GC | Clayey gravels, gravel-sand-clay mixtures | | | |
| SW | Well-graded sands, gravelly sands, little or no fines | Clean sand (little or no fines) | Sands and sandy soils | |
| SP | Poorly-graded sands, gravelly sands, little or no fines | | | |
| SM | Silty sands, sand-silt mixtures | Sands with appreciable amount of fines | More than 50% of coarse fraction passing No. 4 sieve | |
| SC | Clayey sands, sand-silt mixtures | | | |
| ML | Inorganic silts and very fine sands, rock flour, silty or clayey fine sands or clayey silts with slight plasticity | Liquid limit less than 50 | Silts and clays | Fine grained soils more than 50% smaller than No. 200 sieve |
| CL | Inorganic clays of low to medium plasticity, gravelly clays, lean clays | | | |
| OL | Organic silts and organic silty clays of low plasticity | | | |
| MH | Inorganic silts, micacious or diatomaceous fine sand or silty soils | Liquid limit greater than 50 | Silts and clays | |
| CH | Inorganic clays of high plasticity, fat clays | | | |
| OH | Organic clays of medium to high plasticity, organic silts | | | |
| PT | Peat, humas swamp soils with high organic content | Highly organic soils | | |

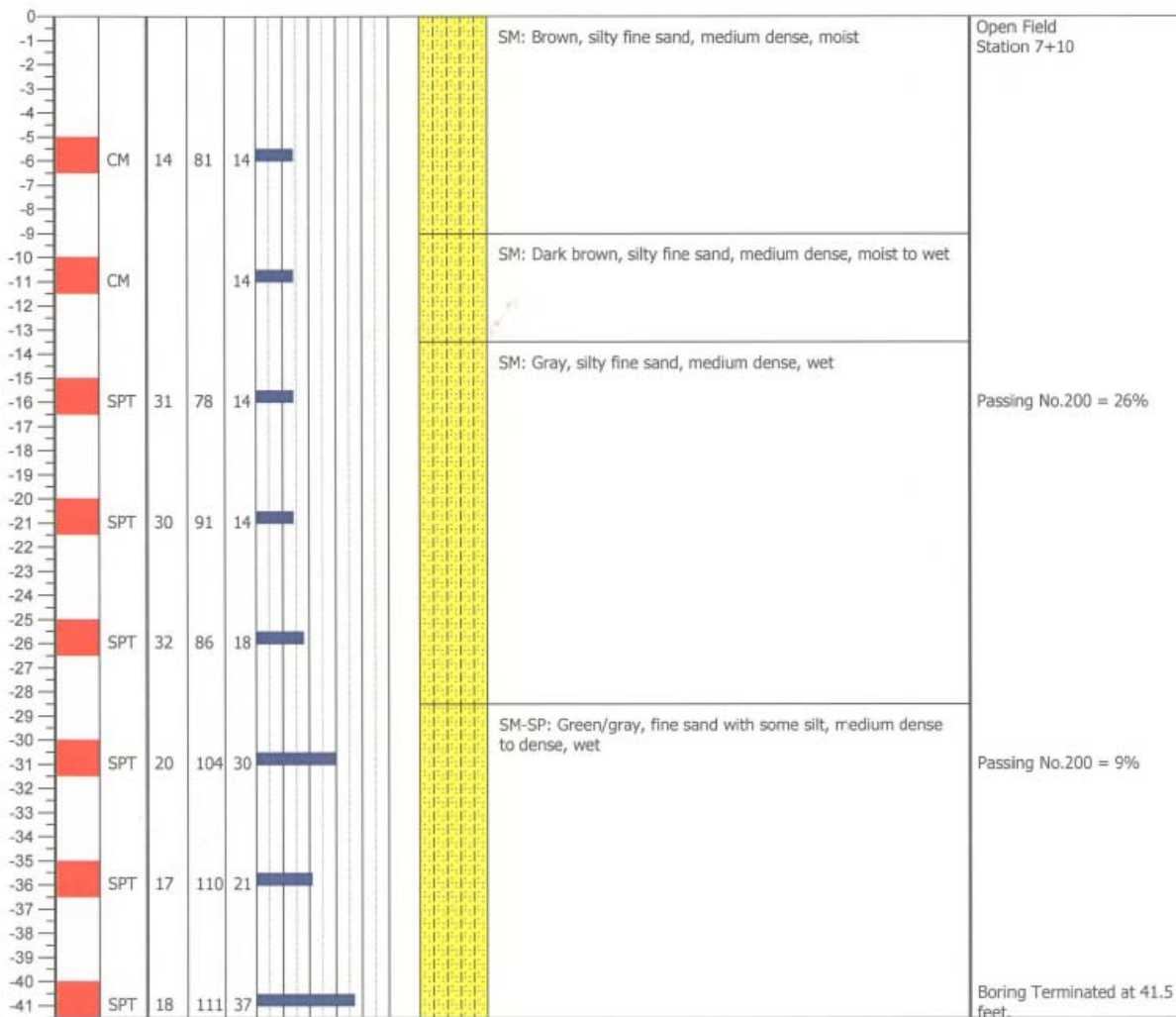| DEPTH (FEET) | SAMPLE | SAMPLE TYPE | TEST TYPE | NOTES |
|---|---|---|---|---|
| | PS | **Push Sample** | Plasticity | pi |
| | SPT | **Drive Sample**, 2.0" o.d., 1.38" i.d., sampler driven with 140 lb. hammer, 30" drop (Standard Penetration Test, SPT). | Grain Size Analysis<br>Uniformity Coefficient<br>Coefficient of Gradation | gr<br>Cu<br>Cc |
| | CM | **Drive Sample**, 2.5" o.d., 1.92" i.d., sampler driven with 140 lb. hammer, 30" drop, with 6" tube liners (California Modified, CM). | Coefficient of Consolidation<br>Specific Gravity<br>Shrink/Swell | Cv<br>sg<br>s/s |
| | ES | **Ely Sample**, Used to determine unit weight. | Direct Shear<br>Unconfined Compression | ds<br>uc |
| | HS | **Hand Sampler**, 2.0" o.d. sampler driven with 10 lb. hammer, 18" drop, with 4" tube liners. | Triaxial Compression<br>Pocket Penetrometer | tx<br>p |
| | GS | **Grab Sample**, disturbed sample taken from auger tailings and sealed in plastic bag. | Torvane Shear<br>Consolidations | ts<br>c |

**Plate Number 11**

3D-6

| | Neil O. Anderson & Assoc., Inc. | | | | | | LOG OF TEST BORING | | BOREHOLE NUMBER |
|---|---|---|---|---|---|---|---|---|---|
| | 902 Industrial Way, Lodi, CA 95240 (209)367-3701 Fax (209)333-8303 | | | | | | | | **B1** |

PROJECT NUMBER: **LFG-0229**

PROJECT NAME: **Seven Mile Slough Site 1,2, & 3 Levee**

LOCATION: **Sacramento County, CA**

DRILLING EQUIP.: **Mobile B53 Explorer**

DATE DRILLED: **12-706**

GROUND SURFACE ELEVATION: **0.0** Feet

**PLATE NO. 2**

| Depth, ft. | Sample | Sampling Method | Moisture, % | Dry Density, pcf | Blow Counts | Blow Count Histogram | Ground Water | Soil Lithology | Soil Lithology Description | Notes |
|---|---|---|---|---|---|---|---|---|---|---|
| 0 to -6 | | CM | 17 | 101 | 11 | | | | FILL: Brown, silty sand and gravel, medium dense, moist | Gravel Road Station 2+20 |
| -7 to -8 | | | | | | | | | CL: Brown, silty clay, medium stiff to stiff, moist | |
| -9 to -13 | | CM | 35 | | 4 | | | | SM: Brown, silty fine sand, very loose to loose, moist | |
| -15 to -18 | | SPT | 53 | 85 | 4 | | | | ML: Green, fine sandy silt, soft to medium stiff, wet | Passing No.200 = 71% |
| -20 to -21 | | SPT | 31 | 102 | 12 | | | | SM-SP: Green/brown mottled, fine sand with silt, medium dense, wet | |
| -26 | | SPT | 30 | 97 | 22 | | | | | Passing No.200 = 11% |
| -31 | | SPT | 27 | 103 | 19 | | | | SP: Green, fine sand, medium dense, wet | |
| -36 | | SPT | 26 | 84 | 16 | | | | | |
| -41 | | SPT | 26 | 101 | 16 | | | | | Boring Terminated at 41.5 feet. |

3D-7

<table>
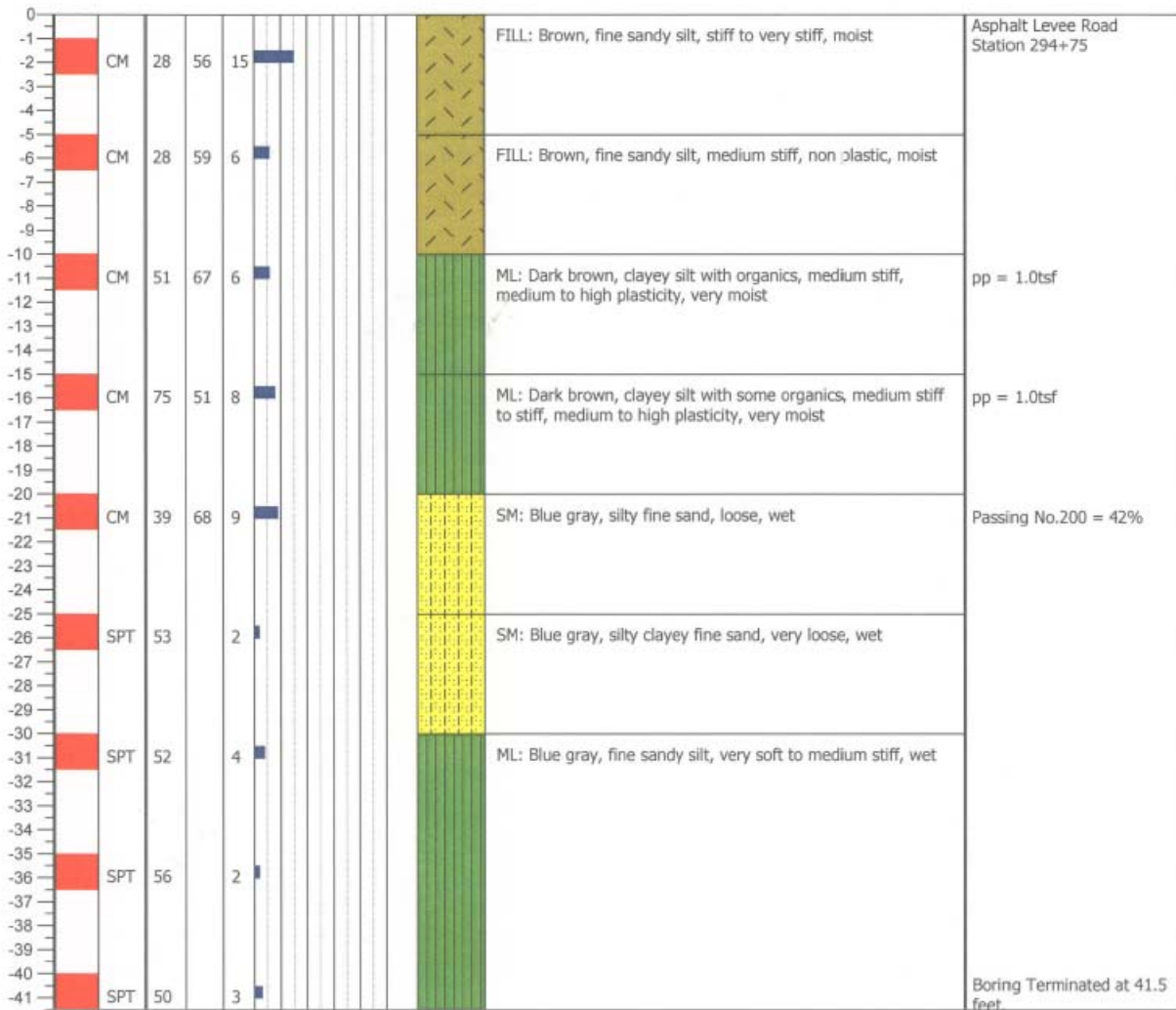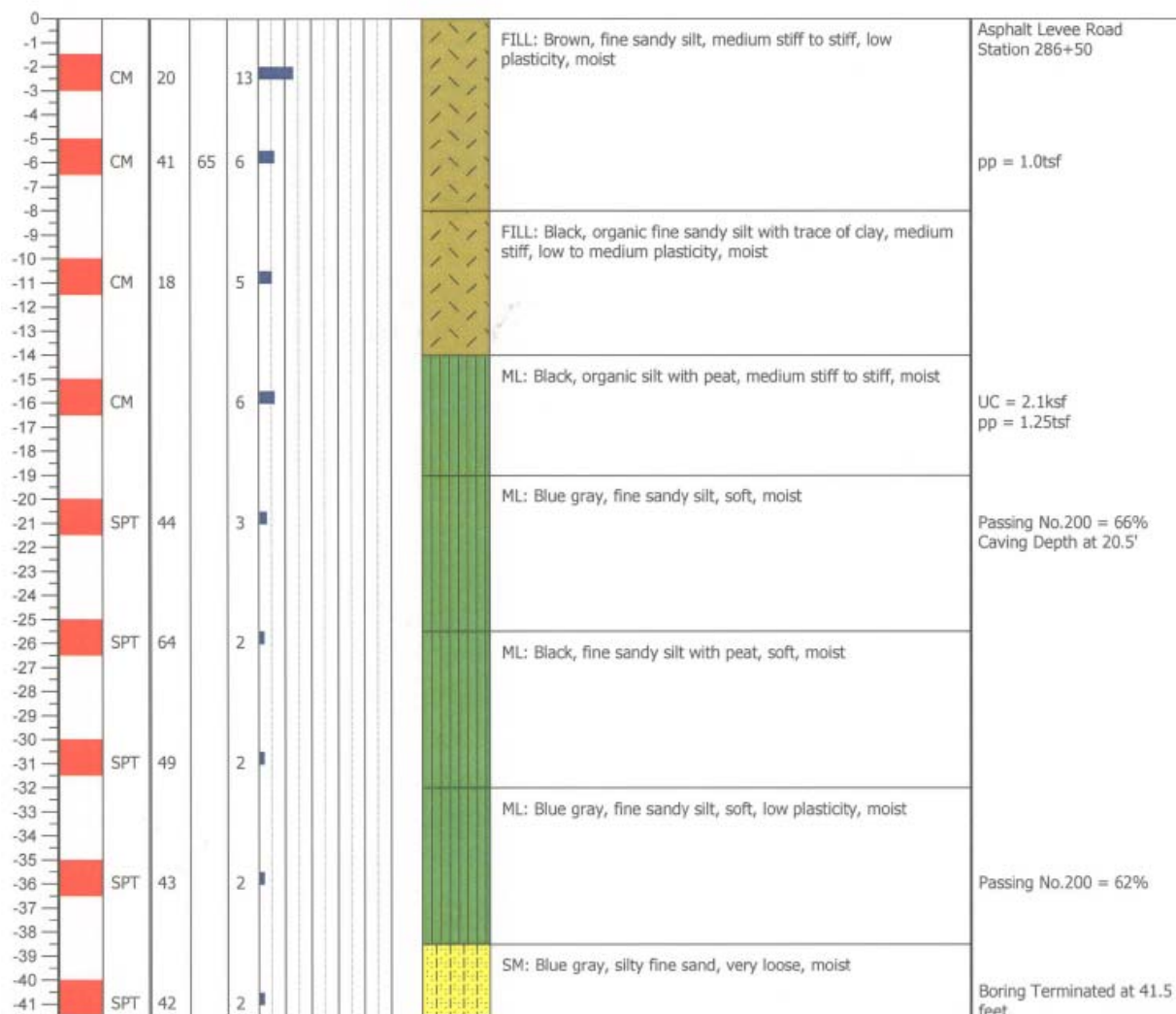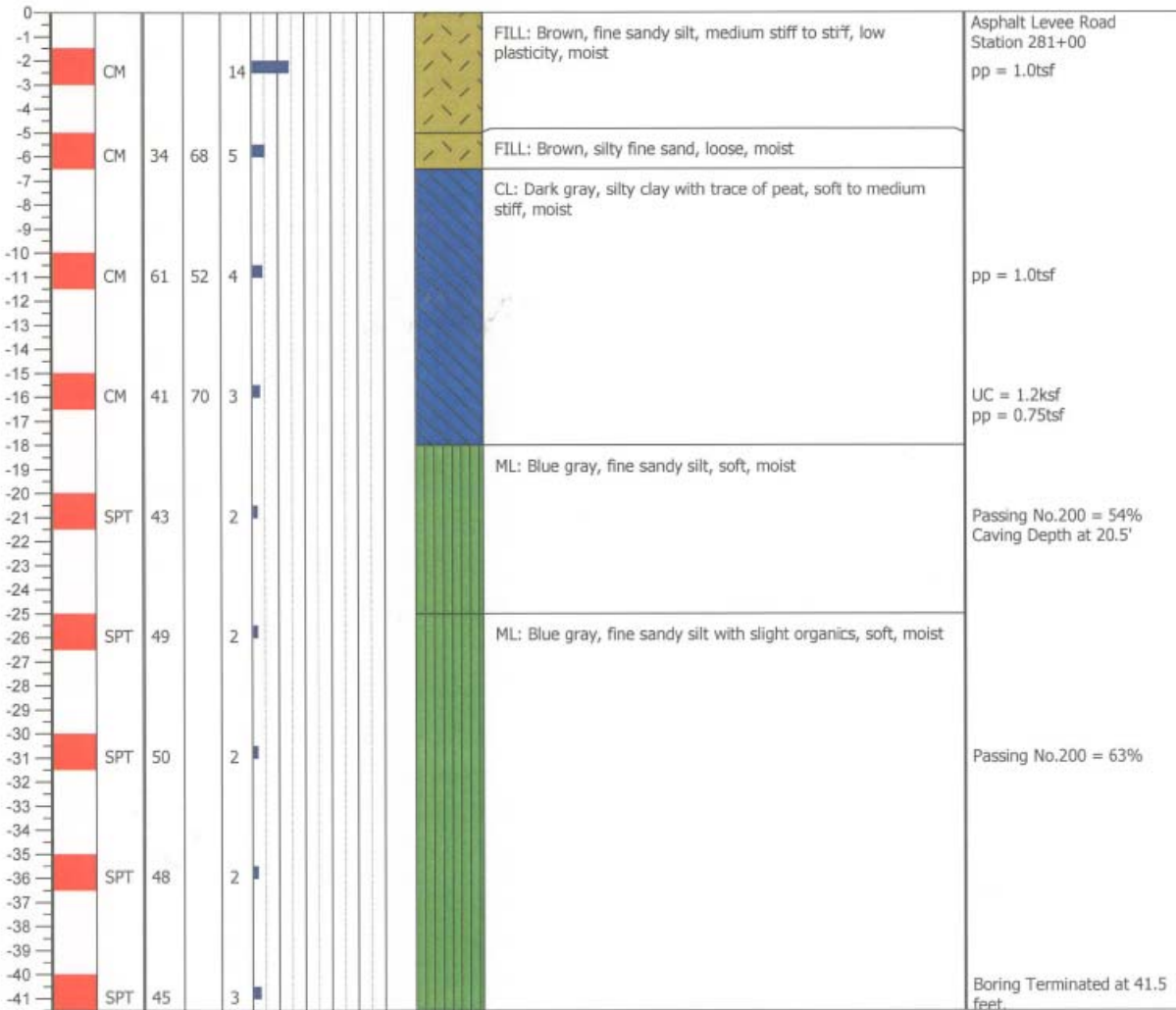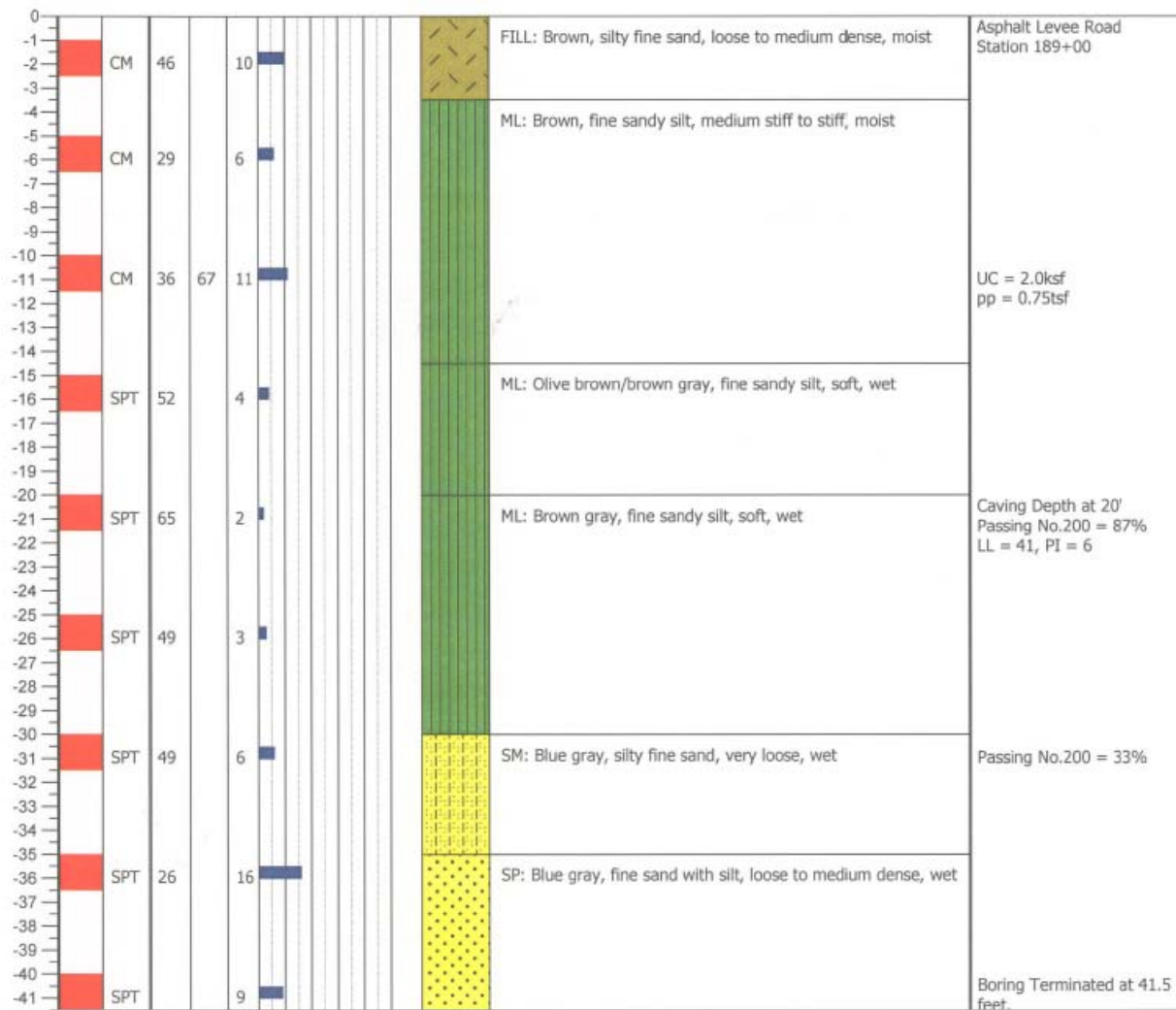<tr><td colspan="2"><strong>Neil O. Anderson & Assoc., Inc.</strong><br>902 Industrial Way, Lodi, CA 95240<br>(209)367-3701 Fax (209)333-8303</td><td><strong>LOG OF TEST BORING</strong></td><td><strong>BOREHOLE NUMBER</strong><br><strong>B2</strong></td></tr>
</table>

| | | |
|---|---|---|
| PROJECT NUMBER: **LFG-0229** | | DATE DRILLED: **12-8-06** |
| PROJECT NAME: **Seven Mile Slough Site 1,2, & 3 Levee** | | GROUND SURFACE ELEVATION: **0.0** Feet |
| LOCATION: **Sacramento County, CA** | | |
| DRILLING EQUIP.: **Mobile B53 Explorer** | | **PLATE NO. 3** |

| Depth, ft. | Sample | Sampling Method | Moisture, % | Dry Density, pcf | Blow Counts | Blow Count Histogram | Ground Water | Soil Lithology | Soil Lithology Description | Notes |
|---|---|---|---|---|---|---|---|---|---|---|
| -6 | | CM | 14 | 81 | 14 | | | | SM: Brown, silty fine sand, medium dense, moist | Open Field<br>Station 7+10 |
| -11 | | CM | | | 14 | | | | SM: Dark brown, silty fine sand, medium dense, moist to wet | |
| -16 | | SPT | 31 | 78 | 14 | | | | SM: Gray, silty fine sand, medium dense, wet | Passing No.200 = 26% |
| -21 | | SPT | 30 | 91 | 14 | | | | | |
| -26 | | SPT | 32 | 86 | 18 | | | | | |
| -31 | | SPT | 20 | 104 | 30 | | | | SM-SP: Green/gray, fine sand with some silt, medium dense to dense, wet | Passing No.200 = 9% |
| -36 | | SPT | 17 | 110 | 21 | | | | | |
| -41 | | SPT | 18 | 111 | 37 | | | | | Boring Terminated at 41.5 feet. |

3D-8

## LOG OF TEST BORING

**Neil O. Anderson & Assoc., Inc.**
902 Industrial Way, Lodi, CA 95240
(209)367-3701  Fax (209)333-8303

**BOREHOLE NUMBER**

**B3**

PROJECT NUMBER: **LFG-0229**
PROJECT NAME: **Seven Mile Slough Site 1,2, & 3 Levee**
LOCATION: **Sacramento County, CA**
DRILLING EQUIP.: **Mobile B53 Explorer**

DATE DRILLED: **12-18-06**
GROUND SURFACE ELEVATION: **0.0** Feet

**PLATE NO. 4**

| Depth, ft. | Sample | Sampling Method | Moisture, % | Dry Density, pcf | Blow Counts | Blow Count Histogram | Ground Water | Soil Lithology | Soil Lithology Description | Notes |
|---|---|---|---|---|---|---|---|---|---|---|
| -2 | | CM | 48 | 66 | 19 | | | | ML: Black, fine sandy silt with organics, stiff to very stiff, moist | Open Field Station 11+50 |
| -6 | | CM | 17 | 88 | 21 | | | | SM: Gray, silty fine sand, medium dense, moist to wet | |
| -11 | | CM | 43 | | 10 | | | | | |
| -16 | | SPT | 35 | 90 | 12 | | | | | Passing No.200 = 15% |
| -21 | | SPT | 31 | 103 | 14 | | | | | |
| -26 | | SPT | 27 | 103 | 24 | | | | | |
| -31 | | SPT | 19 | 115 | 23 | | | | SM-SP: Gray, fine sand with silt, medium dense, wet | Passing No.200 = 9% |
| -36 | | SPT | 21 | 113 | 12 | | | | | |
| -41 | | SPT | 21 | 110 | 30 | | | | | Boring Terminated at 41.5 feet. |

3D-9

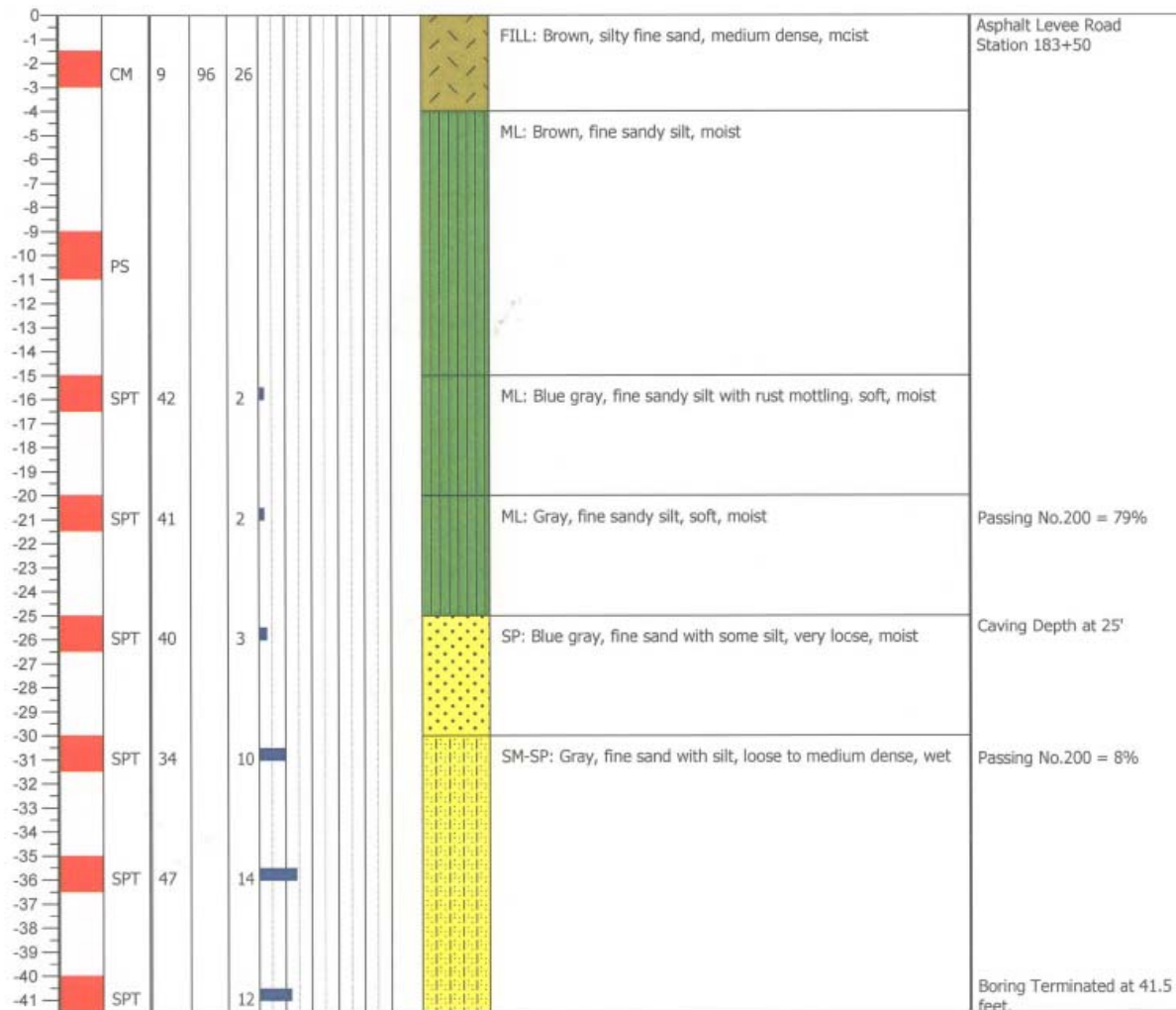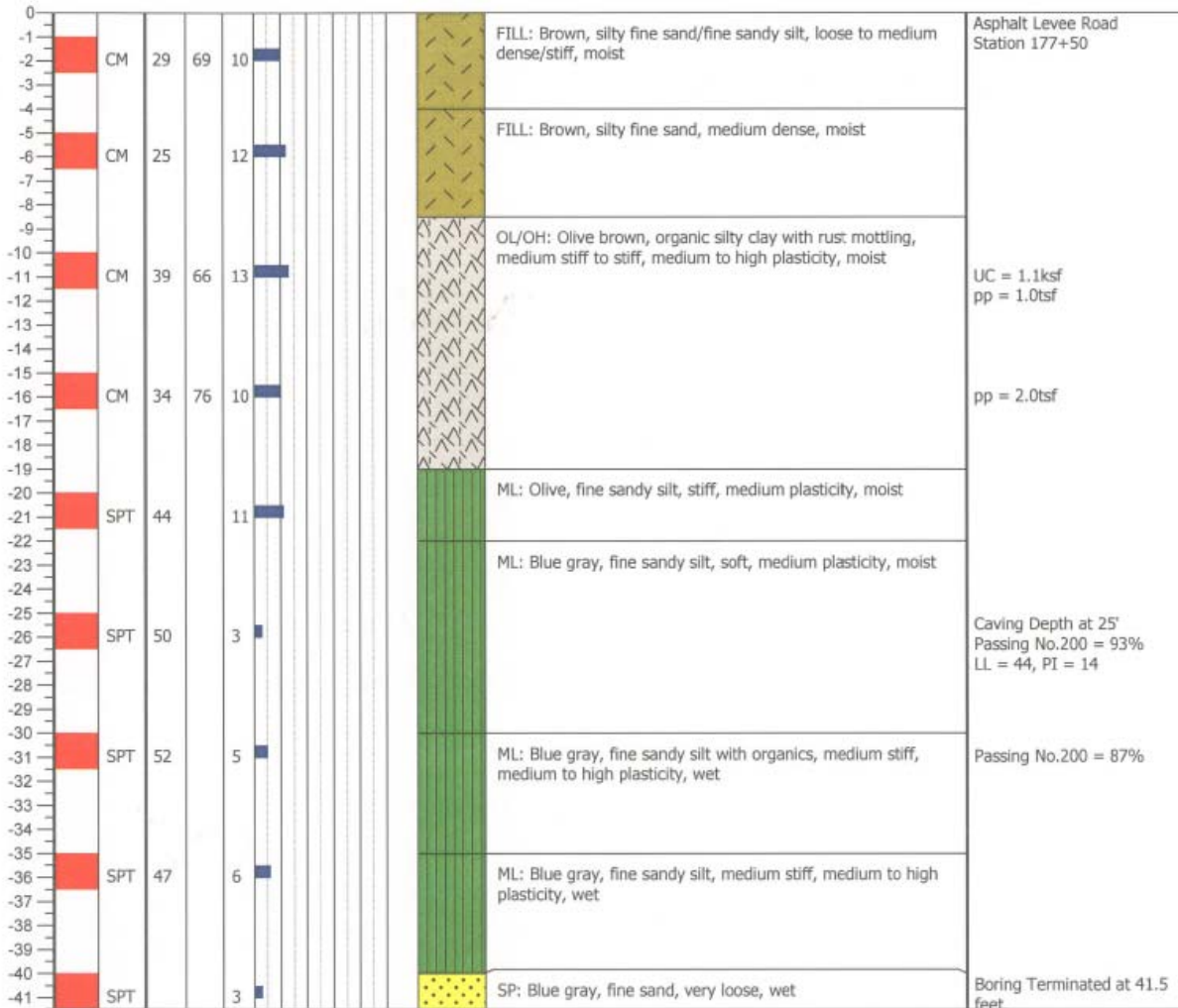## Neil O. Anderson & Assoc., Inc.

902 Industrial Way, Lodi, CA 95240
(209)367-3701  Fax (209)333-8303

# LOG OF TEST BORING

**BOREHOLE NUMBER**

**B4**

PROJECT NUMBER: **LFG-0229**
PROJECT NAME: **Seven Mile Slough Site 1, 2, & 3 Levee**
LOCATION: **Sacramento County, CA**
DRILLING EQUIP.: **Mobile B53 Explorer Mud Rotary**

DATE DRILLED: **3-13-07**
GROUND SURFACE ELEVATION: **0.0** Feet

**PLATE NO. 5**

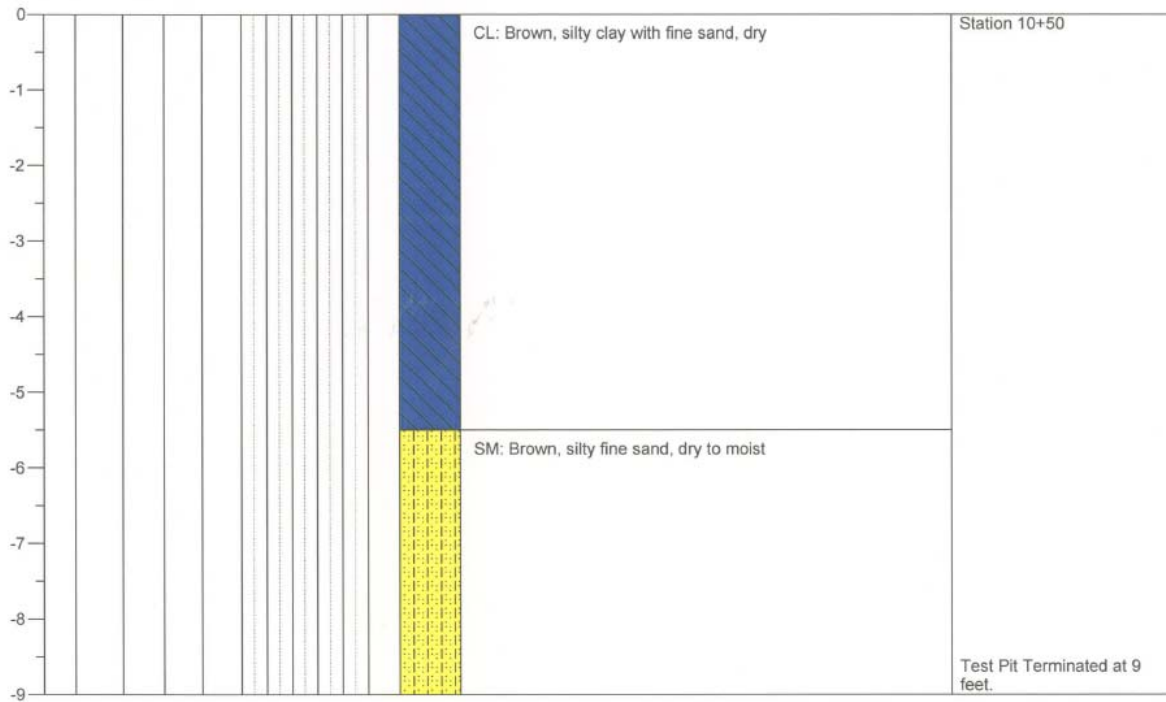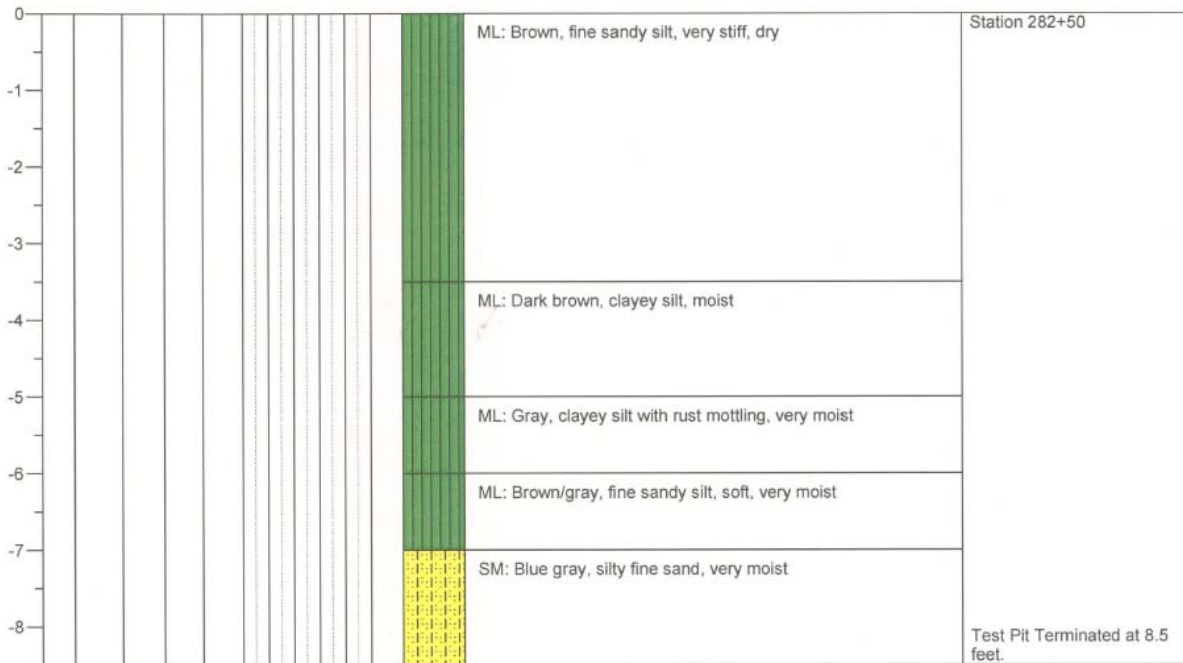| Depth, ft. | Sample | Sampling Method | Moisture, % | Dry Density, pcf | Blow Counts | Blow Count Histogram | Ground Water | Soil Lithology | Soil Lithology Description | Notes |
|---|---|---|---|---|---|---|---|---|---|---|
| -2 | | CM | 28 | 56 | 15 | | | | FILL: Brown, fine sandy silt, stiff to very stiff, moist | Asphalt Levee Road Station 294+75 |
| -6 | | CM | 28 | 59 | 6 | | | | FILL: Brown, fine sandy silt, medium stiff, non plastic, moist | |
| -11 | | CM | 51 | 67 | 6 | | | | ML: Dark brown, clayey silt with organics, medium stiff, medium to high plasticity, very moist | pp = 1.0tsf |
| -16 | | CM | 75 | 51 | 8 | | | | ML: Dark brown, clayey silt with some organics, medium stiff to stiff, medium to high plasticity, very moist | pp = 1.0tsf |
| -21 | | CM | 39 | 68 | 9 | | | | SM: Blue gray, silty fine sand, loose, wet | Passing No.200 = 42% |
| -26 | | SPT | 53 | | 2 | | | | SM: Blue gray, silty clayey fine sand, very loose, wet | |
| -31 | | SPT | 52 | | 4 | | | | ML: Blue gray, fine sandy silt, very soft to medium stiff, wet | |
| -36 | | SPT | 56 | | 2 | | | | | |
| -41 | | SPT | 50 | | 3 | | | | | Boring Terminated at 41.5 feet. |

3D-10

## Neil O. Anderson & Assoc., Inc.

902 Industrial Way, Lodi, CA 95240
(209)367-3701  Fax (209)333-8303

# LOG OF TEST BORING

**BOREHOLE NUMBER**

**B5**

PROJECT NUMBER: **LFG-0229**

PROJECT NAME: **Seven Mile Slough Site 1, 2, & 3 Levee**

LOCATION: **Sacramento County, CA**

DRILLING EQUIP.: **Mobile B53 Explorer Mud Rotary**

DATE DRILLED: **3-13-07**
GROUND SURFACE ELEVATION: **0.0** Feet

## PLATE NO. 6

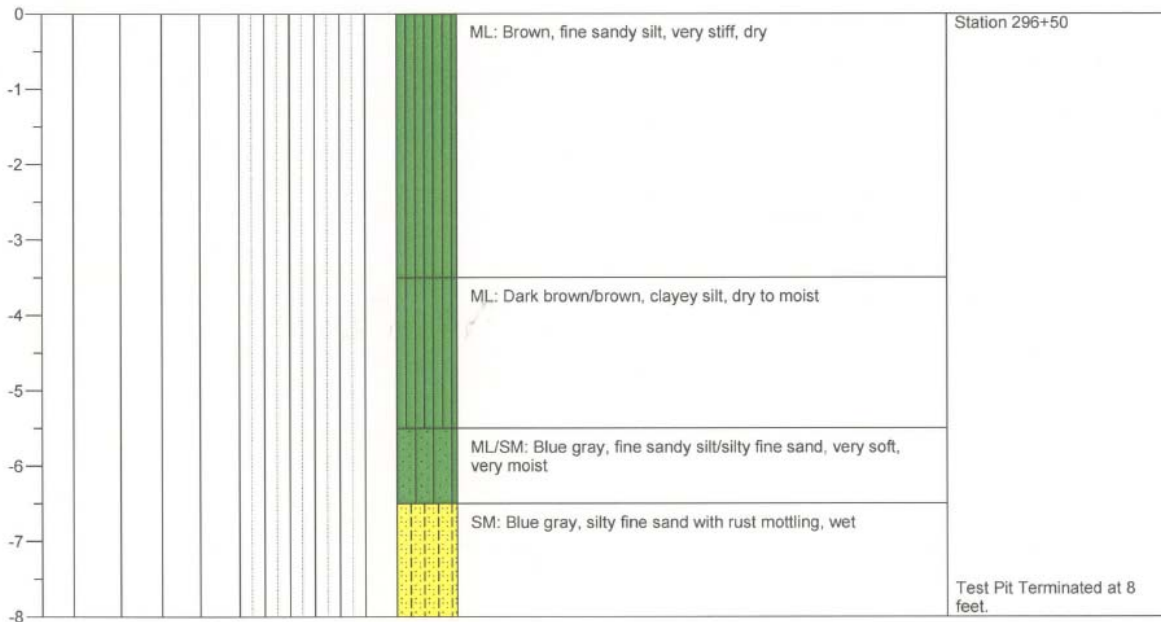| Depth, ft. | Sample | Sampling Method | Moisture, % | Dry Density, pcf | Blow Counts | Blow Count Histogram | Ground Water | Soil Lithology | Soil Lithology Description | Notes |
|---|---|---|---|---|---|---|---|---|---|---|
| -2 | | CM | 20 | | 13 | | | | FILL: Brown, fine sandy silt, medium stiff to stiff, low plasticity, moist | Asphalt Levee Road Station 286+50 |
| -6 | | CM | 41 | 65 | 6 | | | | | pp = 1.0tsf |
| -11 | | CM | 18 | | 5 | | | | FILL: Black, organic fine sandy silt with trace of clay, medium stiff, low to medium plasticity, moist | |
| -16 | | CM | | | 6 | | | | ML: Black, organic silt with peat, medium stiff to stiff, moist | UC = 2.1ksf  pp = 1.25tsf |
| -21 | | SPT | 44 | | 3 | | | | ML: Blue gray, fine sandy silt, soft, moist | Passing No.200 = 66%  Caving Depth at 20.5' |
| -26 | | SPT | 64 | | 2 | | | | ML: Black, fine sandy silt with peat, soft, moist | |
| -31 | | SPT | 49 | | 2 | | | | | |
| -36 | | SPT | 43 | | 2 | | | | ML: Blue gray, fine sandy silt, soft, low plasticity, moist | Passing No.200 = 62% |
| -41 | | SPT | 42 | | 2 | | | | SM: Blue gray, silty fine sand, very loose, moist | Boring Terminated at 41.5 feet. |

3D-11

## Neil O. Anderson & Assoc., Inc.

902 Industrial Way, Lodi, CA 95240
(209)367-3701  Fax (209)333-8303

## LOG OF TEST BORING

**BOREHOLE NUMBER**

**B6**

PROJECT NUMBER: **LFG-0229**
PROJECT NAME: **Seven Mile Slough Site 1, 2, & 3 Levee**
LOCATION: **Sacramento County, CA**
DRILLING EQUIP.: **Mobile B53 Explorer Mud Rotary**

DATE DRILLED: **3-14-07**
GROUND SURFACE ELEVATION: **0.0** Feet

**PLATE NO. 7**

| Depth, ft. | Sample | Sampling Method | Moisture, % | Dry Density, pcf | Blow Counts | Blow Count Histogram | Ground Water | Soil Lithology | Soil Lithology Description | Notes |
|---|---|---|---|---|---|---|---|---|---|---|
| -2 | ■ | CM | | | 14 | | | | FILL: Brown, fine sandy silt, medium stiff to stiff, low plasticity, moist | Asphalt Levee Road Station 281+00 pp = 1.0tsf |
| -6 | ■ | CM | 34 | 68 | 5 | | | | FILL: Brown, silty fine sand, loose, moist | |
| -7 to -8 | | | | | | | | | CL: Dark gray, silty clay with trace of peat, soft to medium stiff, moist | |
| -11 | ■ | CM | 61 | 52 | 4 | | | | | pp = 1.0tsf |
| -16 | ■ | CM | 41 | 70 | 3 | | | | | UC = 1.2ksf pp = 0.75tsf |
| -19 | | | | | | | | | ML: Blue gray, fine sandy silt, soft, moist | |
| -21 | ■ | SPT | 43 | | 2 | | | | | Passing No.200 = 54% Caving Depth at 20.5' |
| -26 | ■ | SPT | 49 | | 2 | | | | ML: Blue gray, fine sandy silt with slight organics, soft, moist | |
| -31 | ■ | SPT | 50 | | 2 | | | | | Passing No.200 = 63% |
| -36 | ■ | SPT | 48 | | 2 | | | | | |
| -41 | ■ | SPT | 45 | | 3 | | | | | Boring Terminated at 41.5 feet. |

3D-12

## Neil O. Anderson & Assoc., Inc.

902 Industrial Way, Lodi, CA 95240
(209)367-3701  Fax (209)333-8303

## LOG OF TEST BORING

**BOREHOLE NUMBER**

**B7**

PROJECT NUMBER: **LFG-0229**
PROJECT NAME: **Seven Mile Slough Site 1, 2, & 3 Levee**
LOCATION: **Sacramento County, CA**
DRILLING EQUIP.: **Mobile B53 Explorer Mud Rotary**

DATE DRILLED: **3-15-07**
GROUND SURFACE ELEVATION: **0.0** Feet

**PLATE NO. 8**

| Depth, ft. | Sample | Sampling Method | Moisture, % | Dry Density, pcf | Blow Counts | Blow Count Histogram | Ground Water | Soil Lithology | Soil Lithology Description | Notes |
|---|---|---|---|---|---|---|---|---|---|---|
| -1 to -2 | | CM | 46 | | 10 | | | | FILL: Brown, silty fine sand, loose to medium dense, moist | Asphalt Levee Road Station 189+00 |
| -6 | | CM | 29 | | 6 | | | | ML: Brown, fine sandy silt, medium stiff to stiff, moist | |
| -11 | | CM | 36 | 67 | 11 | | | | | UC = 2.0ksf pp = 0.75tsf |
| -16 | | SPT | 52 | | 4 | | | | ML: Olive brown/brown gray, fine sandy silt, soft, wet | |
| -21 | | SPT | 65 | | 2 | | | | ML: Brown gray, fine sandy silt, soft, wet | Caving Depth at 20' Passing No.200 = 87% LL = 41, PI = 6 |
| -26 | | SPT | 49 | | 3 | | | | | |
| -31 | | SPT | 49 | | 6 | | | | SM: Blue gray, silty fine sand, very loose, wet | Passing No.200 = 33% |
| -36 | | SPT | 26 | | 16 | | | | SP: Blue gray, fine sand with silt, loose to medium dense, wet | |
| -41 | | SPT | | | 9 | | | | | Boring Terminated at 41.5 feet. |

3D-13

## Neil O. Anderson & Assoc., Inc.

902 Industrial Way, Lodi, CA 95240
(209)367-3701  Fax (209)333-8303

# LOG OF TEST BORING

**BOREHOLE NUMBER**

**B8**

PROJECT NUMBER: **LFG-0229**
PROJECT NAME: **Seven Mile Slough Site 1, 2, & 3 Levee**
LOCATION: **Sacramento County, CA**
DRILLING EQUIP.: **Mobile B53 Explorer Mud Rotary**

DATE DRILLED: **3-15-07**
GROUND SURFACE ELEVATION: **0.0** Feet

**PLATE NO. 9**

| Depth, ft. | Sample | Sampling Method | Moisture, % | Dry Density, pcf | Blow Counts | Blow Count Histogram | Ground Water | Soil Lithology | Soil Lithology Description | Notes |
|---|---|---|---|---|---|---|---|---|---|---|
| -2 to -3 | | CM | 9 | 96 | 26 | | | | FILL: Brown, silty fine sand, medium dense, moist | Asphalt Levee Road Station 183+50 |
| -4 to -14 | | PS | | | | | | | ML: Brown, fine sandy silt, moist | |
| -16 | | SPT | 42 | | 2 | | | | ML: Blue gray, fine sandy silt with rust mottling, soft, moist | |
| -21 | | SPT | 41 | | 2 | | | | ML: Gray, fine sandy silt, soft, moist | Passing No.200 = 79% |
| -26 | | SPT | 40 | | 3 | | | | SP: Blue gray, fine sand with some silt, very loose, moist | Caving Depth at 25' |
| -31 | | SPT | 34 | | 10 | | | | SM-SP: Gray, fine sand with silt, loose to medium dense, wet | Passing No.200 = 8% |
| -36 | | SPT | 47 | | 14 | | | | | |
| -41 | | SPT | | | 12 | | | | | Boring Terminated at 41.5 feet. |

## Neil O. Anderson & Assoc., Inc.
902 Industrial Way, Lodi, CA 95240
(209)367-3701  Fax (209)333-8303

## LOG OF TEST BORING

**BOREHOLE NUMBER**

**B9**

PROJECT NUMBER: **LFG-0229**

PROJECT NAME: **Seven Mile Slough Site 1, 2, & 3 Levee**

LOCATION: **Sacramento County, CA**

DRILLING EQUIP.: **Mobile B53 Explorer Mud Rotary**

DATE DRILLED: **3-16-07**

GROUND SURFACE ELEVATION: **0.0**  Feet

**PLATE NO.  10**

| Depth, ft. | Sample | Sampling Method | Moisture, % | Dry Density, pcf | Blow Counts | Blow Count Histogram | Ground Water | Soil Lithology | Soil Lithology Description | Notes |
|---|---|---|---|---|---|---|---|---|---|---|
| -1, -2 | | CM | 29 | 69 | 10 | | | | FILL: Brown, silty fine sand/fine sandy silt, loose to medium dense/stiff, moist | Asphalt Levee Road Station 177+50 |
| -5, -6 | | CM | 25 | | 12 | | | | FILL: Brown, silty fine sand, medium dense, moist | |
| -10, -11 | | CM | 39 | 66 | 13 | | | | OL/OH: Olive brown, organic silty clay with rust mottling, medium stiff to stiff, medium to high plasticity, moist | UC = 1.1ksf  pp = 1.0tsf |
| -15, -16 | | CM | 34 | 76 | 10 | | | | | pp = 2.0tsf |
| -20, -21 | | SPT | 44 | | 11 | | | | ML: Olive, fine sandy silt, stiff, medium plasticity, moist | |
| -22, -23 | | | | | | | | | ML: Blue gray, fine sandy silt, soft, medium plasticity, moist | |
| -25, -26 | | SPT | 50 | | 3 | | | | | Caving Depth at 25'  Passing No.200 = 93%  LL = 44, PI = 14 |
| -30, -31 | | SPT | 52 | | 5 | | | | ML: Blue gray, fine sandy silt with organics, medium stiff, medium to high plasticity, wet | Passing No.200 = 87% |
| -35, -36 | | SPT | 47 | | 6 | | | | ML: Blue gray, fine sandy silt, medium stiff, medium to high plasticity, wet | |
| -40, -41 | | SPT | | | 3 | | | | SP: Blue gray, fine sand, very loose, wet | Boring Terminated at 41.5 feet. |

3D-15

| | | | | | | | | |
|---|---|---|---|---|---|---|---|---|
| **Neil O. Anderson & Assoc., Inc.**<br>902 Industrial Way, Lodi, CA 95240<br>(209)367-3701  Fax (209)333-8303 | **LOG OF TEST PIT** | | **TEST PIT NUMBER**<br>**TP-1** | | | | | |

| PROJECT NUMBER: | LFG-0229 | DATE EXCAVATED: | **8-8-07** |
|---|---|---|---|
| PROJECT NAME: | **Twitchell Island** | GROUND SURFACE ELEVATION: | **0.0**   Feet |
| LOCATION: | **Sacramento County, CA** | | |
| DRILLING EQUIP.: | **Case Backhoe with 30 inch Bucket** | **PLATE NO.   2** | |

| Depth, ft. | Sample | Sampling Method | Moisture, % | Dry Density, pcf | Blow Counts | Blow Count Histogram | Ground Water | Soil Lithology | Soil Lithology Description | Notes |
|---|---|---|---|---|---|---|---|---|---|---|
| 0 | | | | | | | | | CL: Brown, silty clay with fine sand, dry | Station 6+00 |
| -4 | | | | | | | | | SM: Brown, silty fine sand, moist | |
| -9 | | | | | | | | | | Test Pit Terminated at 9.5 feet. |

3D-16

| Neil O. Anderson & Assoc., Inc. | LOG OF TEST PIT | TEST PIT NUMBER |
| --- | --- | --- |
| 902 Industrial Way, Lodi, CA 95240 (209)367-3701 Fax (209)333-8303 | | TP-2 |

| PROJECT NUMBER: | LFG-0229 | DATE EXCAVATED: | 8-8-07 |
| --- | --- | --- | --- |
| PROJECT NAME: | Twitchell Island | GROUND SURFACE ELEVATION: | 0.0 Feet |
| LOCATION: | Sacramento County, CA | | |
| DRILLING EQUIP.: | Case Backhoe with 30 inch Bucket | PLATE NO. | 3 |

| Depth, ft. | Sample | Sampling Method | Moisture, % | Dry Density, pcf | Blow Counts | Blow Count Histogram | Ground Water | Soil Lithology | Soil Lithology Description | Notes |
| --- | --- | --- | --- | --- | --- | --- | --- | --- | --- | --- |
| | | | | | | | | | ML: Brown, clayey silt with fine sand, dry | Station 8+50 |
| | | | | | | | | | SM: Brown, silty fine sand, dry to moist | Test Pit Terminated at 9 feet. |



3D-17

| Neil O. Anderson & Assoc., Inc. | LOG OF TEST PIT | TEST PIT NUMBER |
|---|---|---|
| 902 Industrial Way, Lodi, CA 95240 | | TP-3 |
| (209)367-3701  Fax (209)333-8303 | | |

| | | |
|---|---|---|
| PROJECT NUMBER: **LFG-0229** | DATE EXCAVATED: **8-8-07** | |
| PROJECT NAME: **Twitchell Island** | GROUND SURFACE ELEVATION: **0.0** Feet | |
| LOCATION: **Sacramento County, CA** | | |
| DRILLING EQUIP.: **Case Backhoe with 30 inch Bucket** | **PLATE NO. 4** | |

| Depth, ft. | Sample | Sampling Method | Moisture, % | Dry Density, pcf | Blow Counts | Blow Count Histogram | Ground Water | Soil Lithology | Soil Lithology Description | Notes |
|---|---|---|---|---|---|---|---|---|---|---|

0 — CL: Brown, silty clay with fine sand, dry — Station 10+50

-5.5 (approx) — SM: Brown, silty fine sand, dry to moist

Test Pit Terminated at 9 feet.

3D-18

| Neil O. Anderson & Assoc., Inc. | LOG OF TEST PIT | TEST PIT NUMBER |
|---|---|---|
| 902 Industrial Way, Lodi, CA 95240 | | TP-4 |
| (209)367-3701  Fax (209)333-8303 | | |

| PROJECT NUMBER: | LFG-0229 | DATE EXCAVATED: | 8-8-07 |
|---|---|---|---|
| PROJECT NAME: | Twitchell Island | GROUND SURFACE ELEVATION: | 0.0  Feet |
| LOCATION: | Sacramento County, CA | | |
| DRILLING EQUIP.: | Case Backhoe with 30 inch Bucket | PLATE NO. 5 |

| Depth, ft. | Sample | Sampling Method | Moisture, % | Dry Density, pcf | Blow Counts | Blow Count Histogram | Ground Water | Soil Lithology | Soil Lithology Description | Notes |
|---|---|---|---|---|---|---|---|---|---|---|
| 0 | | | | | | | | | ML: Brown, clayey silt with fine sand, very stiff, dry | Station 291+00 |
| -1 | | | | | | | | | | |
| -2 | | | | | | | | | | |
| -3 | | | | | | | | | ML: Gray, clayey silt with slight organics, dry to moist | |
| -4 | | | | | | | | | ML: Brown, fine sandy silt with rust mottling, moist | |
| -5 | | | | | | | | | | |
| -6 | | | | | | | | | SM: Blue gray, silty fine sand, very moist | |
| -7 | | | | | | | | | | Water Seepage @ 7 feet. Test Pit Terminated at 7.5 |

3D-19

| Neil O. Anderson & Assoc., Inc. | LOG OF TEST PIT | TEST PIT NUMBER |
|---|---|---|
| 902 Industrial Way, Lodi, CA 95240 | | **TP-5** |
| (209)367-3701  Fax (209)333-8303 | | |

| | | |
|---|---|---|
| PROJECT NUMBER: **LFG-0229** | DATE EXCAVATED: **8-8-07** | |
| PROJECT NAME: **Twitchell Island** | GROUND SURFACE ELEVATION: **0.0** Feet | |
| LOCATION: **Sacramento County, CA** | | |
| DRILLING EQUIP.: **Case Backhoe with 30 inch Bucket** | **PLATE NO. 6** | |

| Depth, ft. | Sample | Sampling Method | Moisture, % | Dry Density, pcf | Blow Counts | Blow Count Histogram | Ground Water | Soil Lithology | Soil Lithology Description | Notes |
|---|---|---|---|---|---|---|---|---|---|---|
| 0 | | | | | | | | | ML: Brown, fine sandy silt, very stiff, dry | Station 282+50 |
| -1 | | | | | | | | | | |
| -2 | | | | | | | | | | |
| -3 | | | | | | | | | | |
| -4 | | | | | | | | | ML: Dark brown, clayey silt, moist | |
| -5 | | | | | | | | | ML: Gray, clayey silt with rust mottling, very moist | |
| -6 | | | | | | | | | ML: Brown/gray, fine sandy silt, soft, very moist | |
| -7 | | | | | | | | | SM: Blue gray, silty fine sand, very moist | |
| -8 | | | | | | | | | | Test Pit Terminated at 8.5 feet. |

3D-20

| Neil O. Anderson & Assoc., Inc. | LOG OF TEST PIT | TEST PIT NUMBER |
|---|---|---|
| 902 Industrial Way, Lodi, CA  95240 | | TP-6 |
| (209)367-3701   Fax (209)333-8303 | | |

| | | |
|---|---|---|
| PROJECT NUMBER: **LFG-0229** | DATE EXCAVATED: **8-8-07** | |
| PROJECT NAME: **Twitchell Island** | GROUND SURFACE ELEVATION: **0.0** Feet | |
| LOCATION: **Sacramento County, CA** | | |
| DRILLING EQUIP.: **Case Backhoe with 30 inch Bucket** | **PLATE NO.  7** | |

| Depth, ft. | Sample | Sampling Method | Moisture, % | Dry Density, pcf | Blow Counts | Blow Count Histogram | Ground Water | Soil Lithology | Soil Lithology Description | Notes |
|---|---|---|---|---|---|---|---|---|---|---|



Soil Lithology Descriptions (by depth):

- ML: Brown, fine sandy silt, very stiff, dry (0 to ~3.5 ft)
- ML: Dark brown/brown, clayey silt, dry to moist (~3.5 to ~5.5 ft)
- ML/SM: Blue gray, fine sandy silt/silty fine sand, very soft, very moist (~5.5 to ~6.5 ft)
- SM: Blue gray, silty fine sand with rust mottling, wet (~6.5 to 8 ft)

Notes:
- Station 296+50
- Test Pit Terminated at 8 feet.

3D-21

# APPENDIX 3E

**Plan View Trench Logs – Twitchell Island Field Test**

Partial plan view trench logs with photographs as well as complete wall logs are provided with discussion in the primary report. Complete field plan view logs are provided herein unedited. Where measured, root circumference is provided adjacent to the root (ex – 2.5 C means 2.5 inch circumference) with a depth in feet and inches noted at the location where the root intersected the wall. Roots are shown shaded and approximately to scale with solid lines, while burrows are lightly hatched. Diameters, where measured are noted with the ∅ symbol.

**Tree Trench (Sta TT 0 to TT 15):**

**Tree Trench (Sta TT 15 to TT 30):**

**Tree Trench (Sta TT 30 to TT 45):**
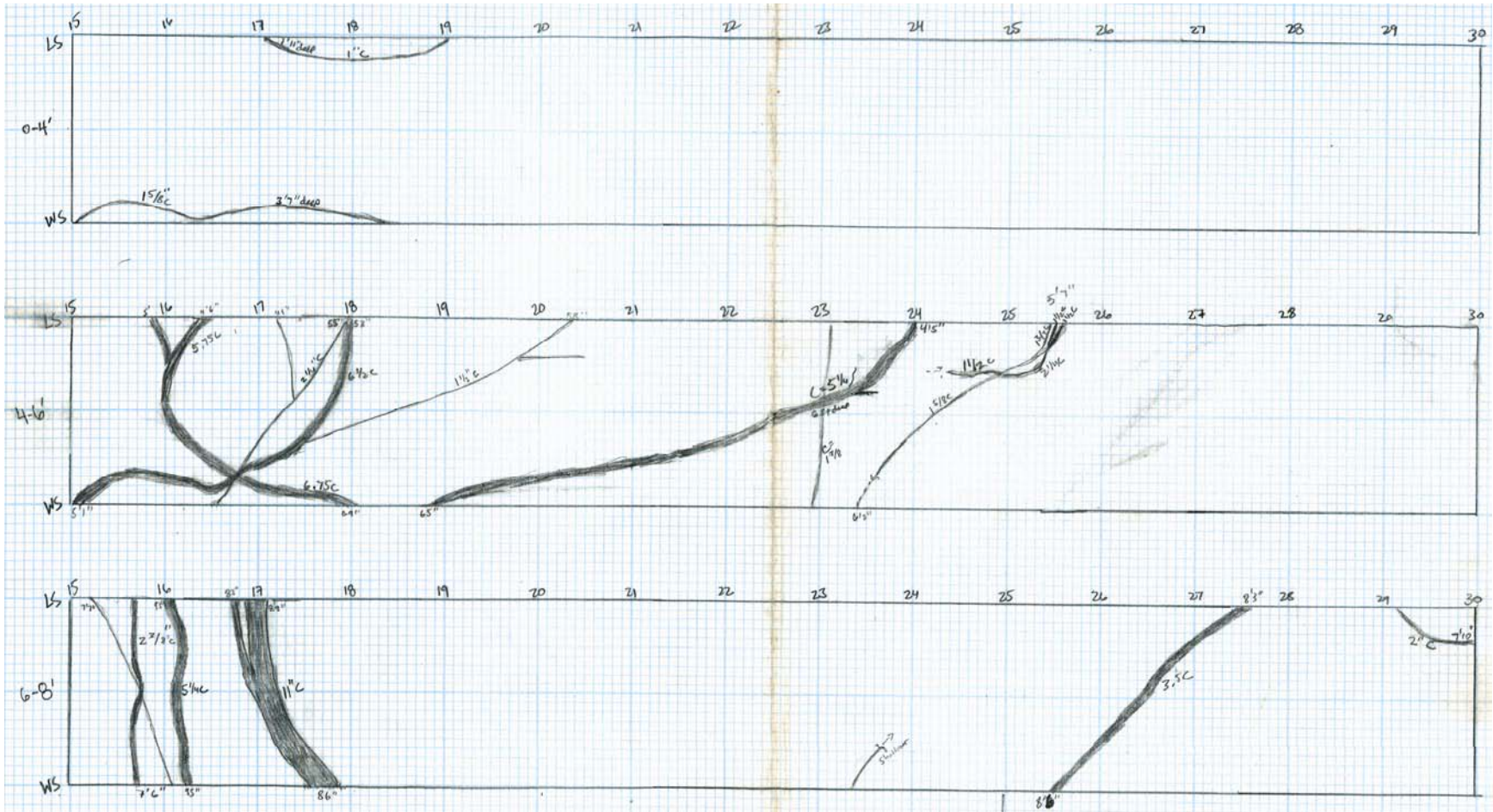
**Tree Trench (Sta TT 45 to TT 60):**

**Tree Trench (Sta TT 60 to TT 75):**
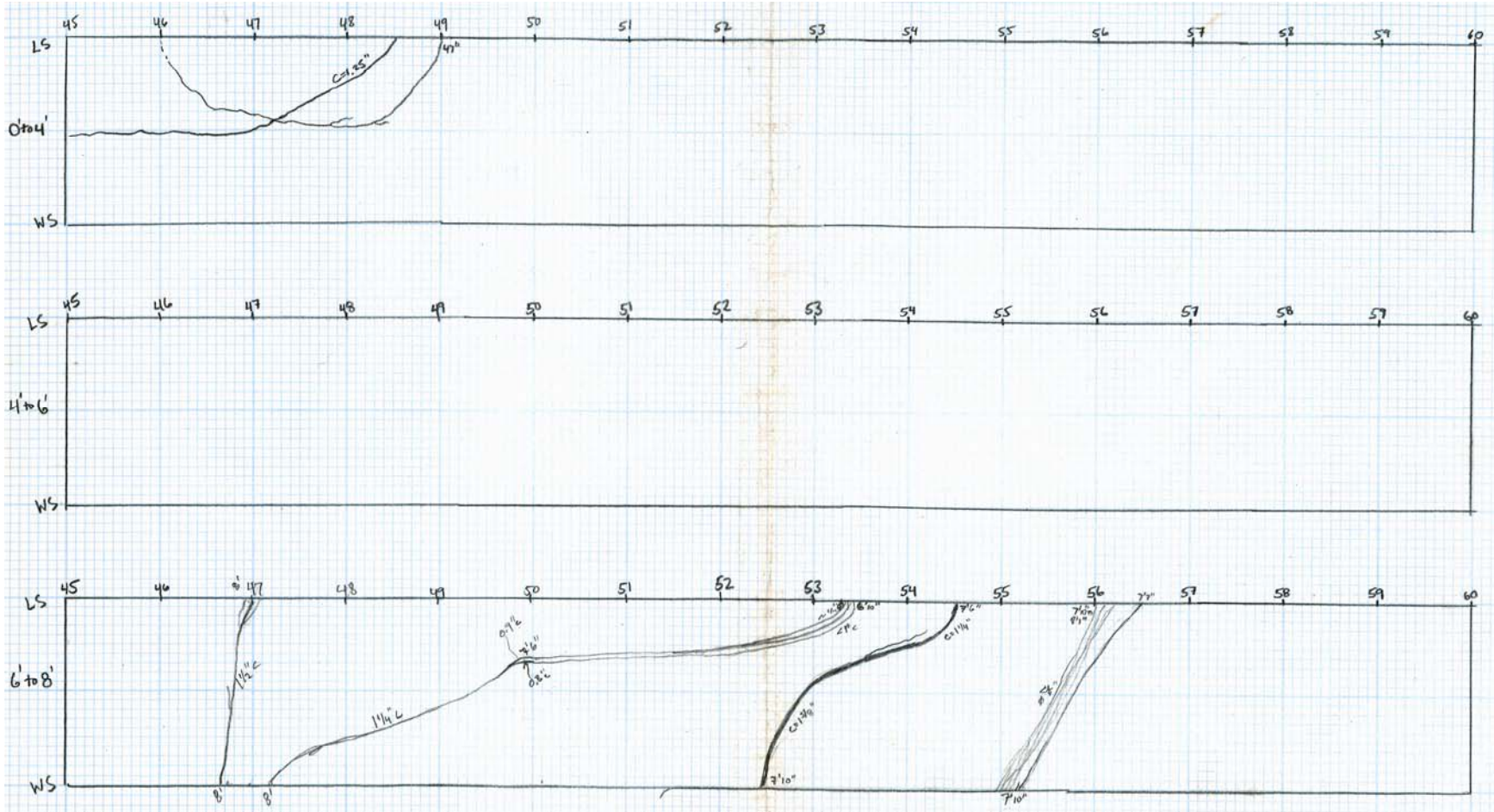
**Tree Trench (Sta TT 75 to TT 90):**
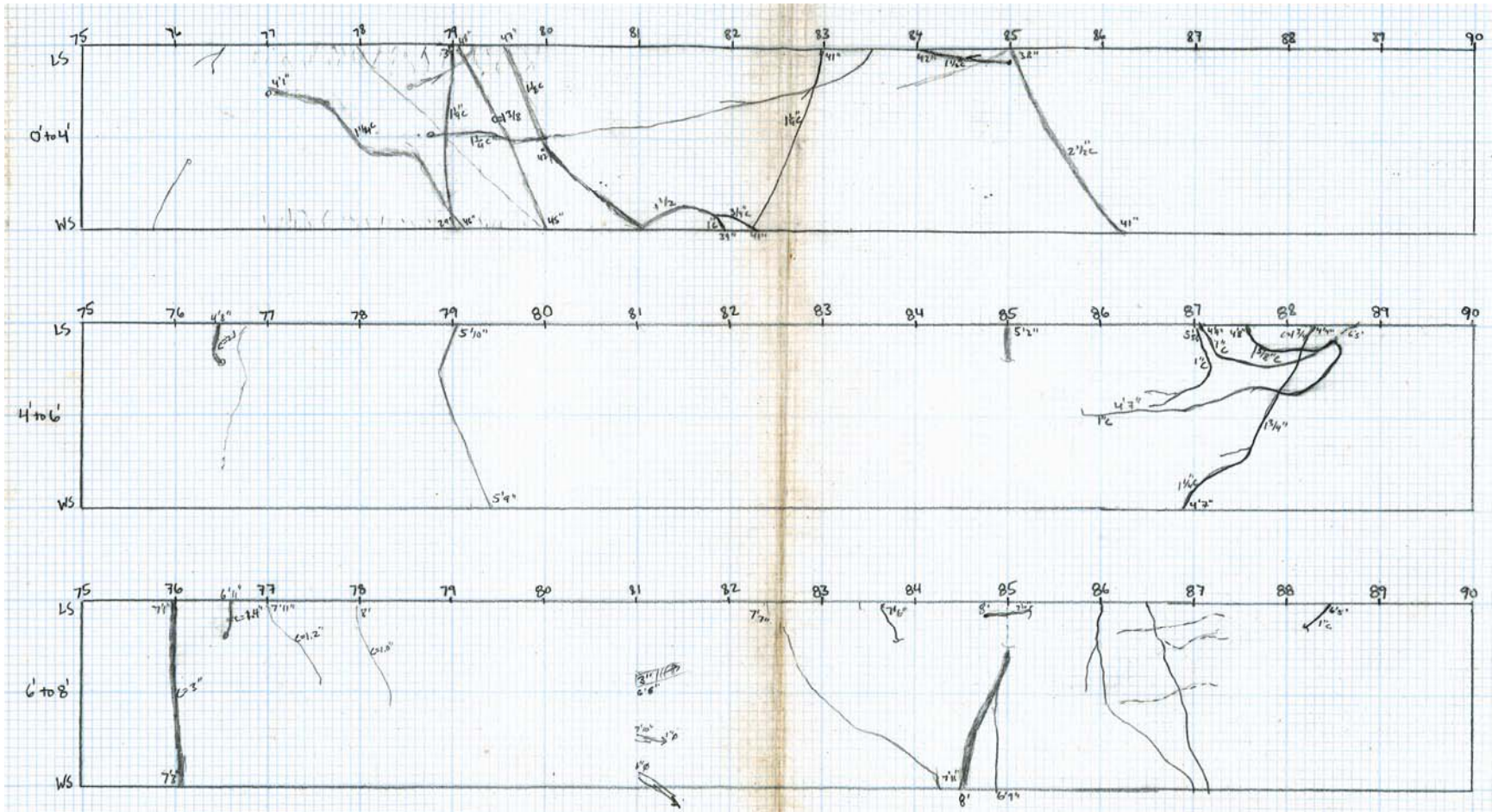
**Tree Trench (Sta TT 90 to TT 95):**
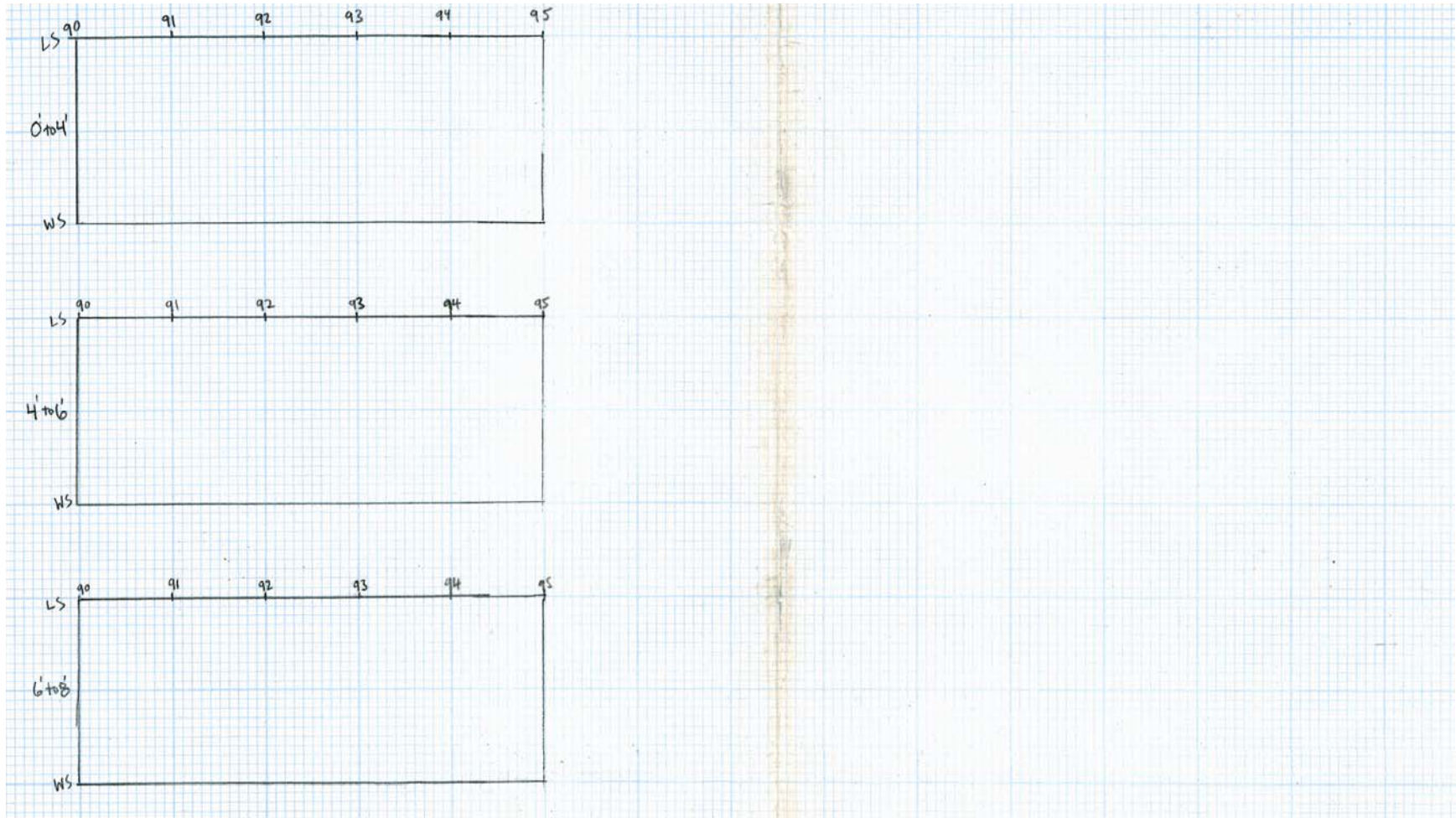
**Control Trench (Sta CT 0 to CT 15):**
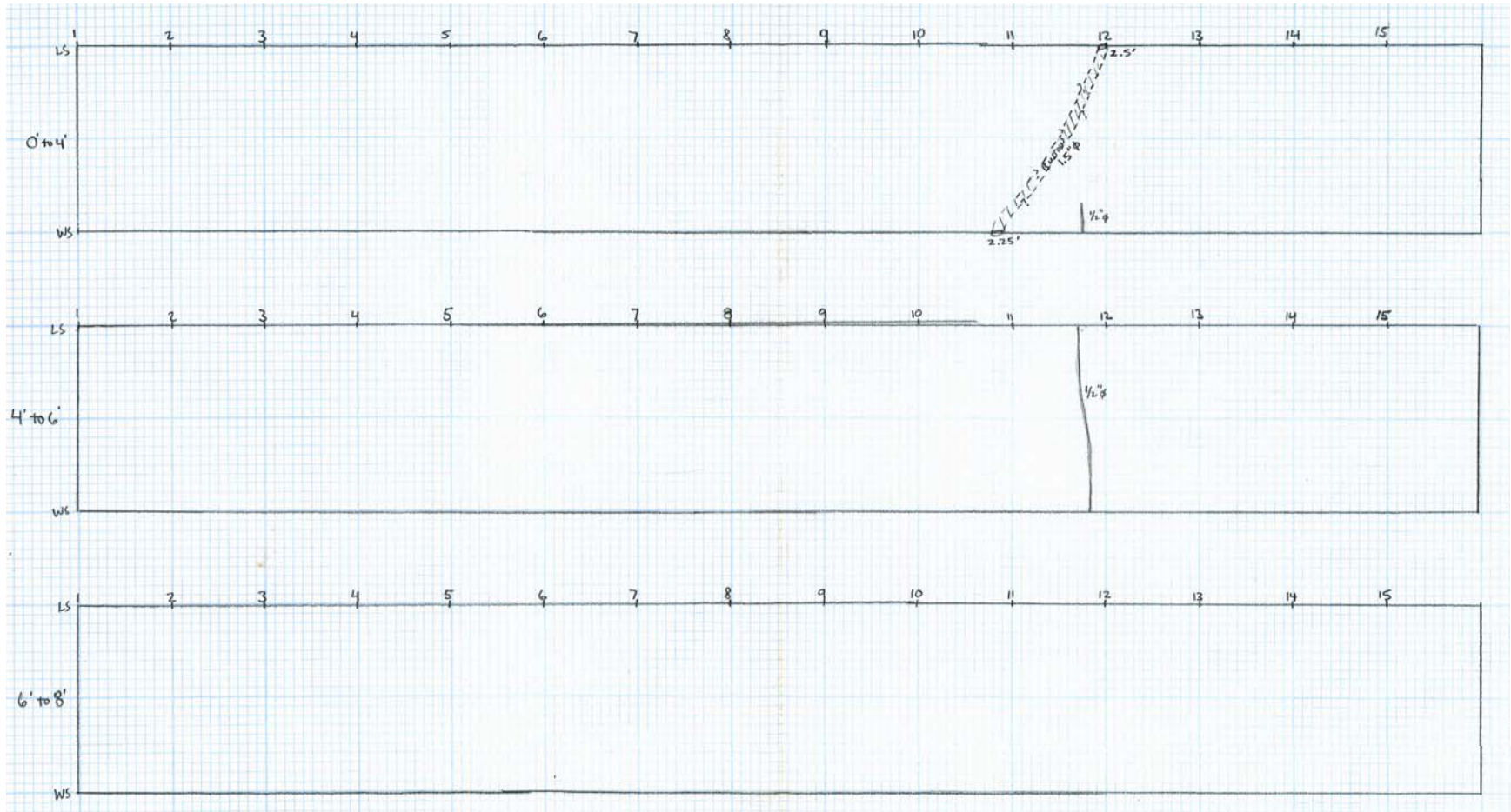
**Control Trench (Sta CT 15 to CT 30):**
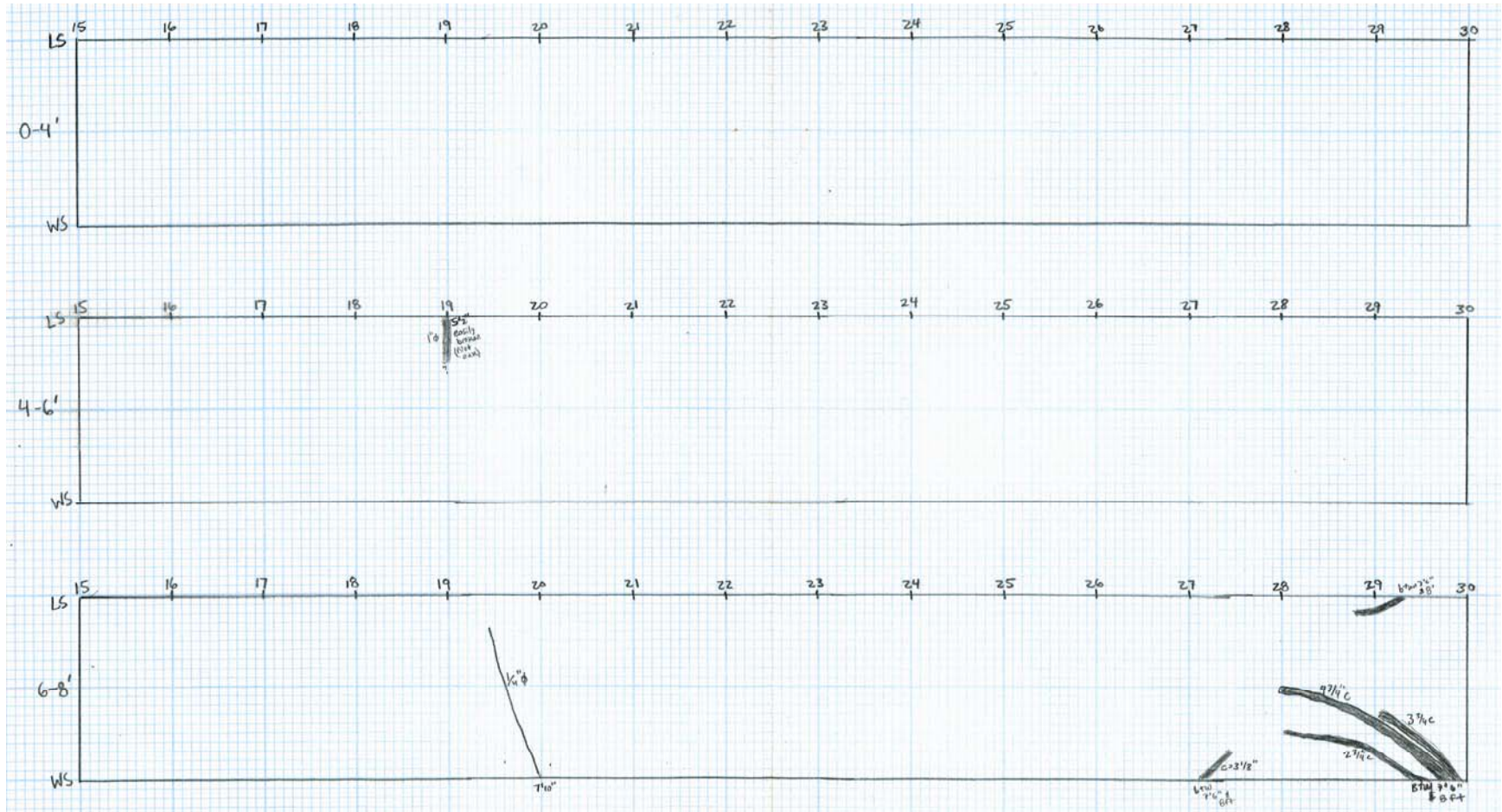
# APPENDIX 3F

## Instrument Data – Twitchell Island Test Site

Tensiometer data is presented first, followed by piezometer data. Tensiometer data collection began with a dry run equilibration phase. During the dry run equilibration phase, tensiometers were assembled, leak checked, and installed in the ground. Soil Moisture tensiometers of 24, 48, and 60 inches in length were installed to depths of 24, 36 and 60 inches, respectively (). The instruments were assembled with brass 'T' adaptors to allow for connection of both a mechanical gauge and a Model 5301 current transducer by Soil Moisture. The current transducer was wired to a Campbell Scientific CR3000 datalogger in order to continuously read the instruments. The current output from each transducer was converted to voltage using a 249 ohm resister with a resistor error of 1 percent. Based on manufacturer's specifications, currents of 4 and 20 mA correspond to soil suction values of 0 and 100 kpa, respectively. The values can be scaled linearly between these values. With a resistance of 249 ohms, using Ohms Law (which states that voltage is equal to current multiplied by resistance) voltages of 996 ohms and 4980 ohms correspond to soil suction values of 0 and 100 kpa, respectively, sharing the same linear relationship.



Figure 3F -1. Components of a tensiometer broken down by Fredlund and Rahardjo, 2005 (left) as compared with our tensiometer equipped with both vacuum gauge and transducer (right).

Tensiometers were installed ahead of the flow test and were connected to a continuously reading datalogger for a few days prior to the inundation of the trenches to establish baseline values in the instruments and to check functionality. Initial moisture contents of surficial soils are presented in Appendix B and results of initial testing are presented in Figure 3F -2 through Figure 3F -6. These moisture contents resulted in observed initial suction values of approximately 0 to 64 kPa. Results during the flow test are presented in Section 2.6.4. Values reported are not corrected for barometric pressure, though this parameter was recorded at the surface and values are presented on Figure 3F -7.

Piezometers were installed into 4 to 8-inch diameter auger holes and grouted in place with a mix of Portland cement and bentonite in accordance with the specifications of the manufacturers, Geokon and Slope Indicator. A grout mix compatible with soft soils as discussed in Mikkelsen (2002) and Mikkelsen and Green (2003). Due to initially unsaturated conditions and the likelihood of low measured pressures throughout the test, the Geokon 4500 AL (70 kPa) and the Slope Indicator Low Pressure (10 psi) Vibrating Wire models were selected. The constant head in the trench is held a maximum of 9 feet above the porous stone of the deepest piezometer (84 inches from surface grade, installed at mid-slope) resulting in a maximum possible pressure of 3.9 psi. The 10 psi low-pressure instrument was the most sensitive available for this application. The instruments were pre-saturated in a water bath and grouted into the hole upside down in order to minimize loss of saturation in the porous element due to the unsaturated conditions.

Figure 3F -8 includes data from piezometer during the dry run equilibration period prior to the flow test. Instruments show steady pressures, typically near zero. Waterside instruments in Row 6, nearest the water, show small initial pressures of less than 5 kPa, as do the deeper instruments near the landside toe in Row 3. Initial suction values are recorded in several instruments within Rows 1 and 2 on the waterside and landside of the levee crown road, respectively. Gray and Leiser (1982) discuss the ability of trees to deplete soil moisture due to transpiration through their leaves. The extent to which the presence of roots has contributed to increased initial suction values in these instruments is unclear. Suction in these instruments was lost upon inundation of the site with water.
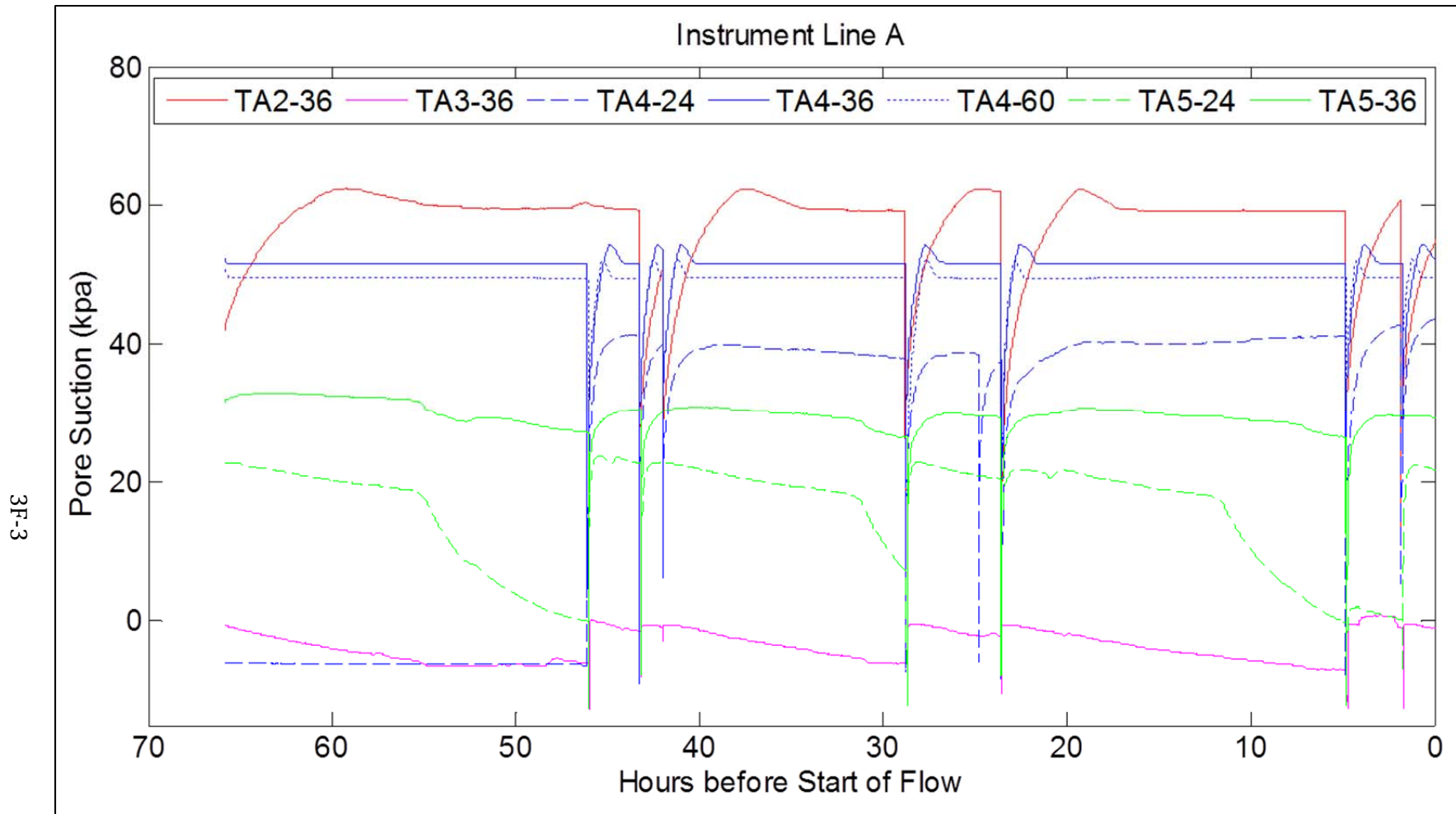
Figure 3F -2. Initial values of soil suction at instrument line A, measured in the days just prior to the flow test
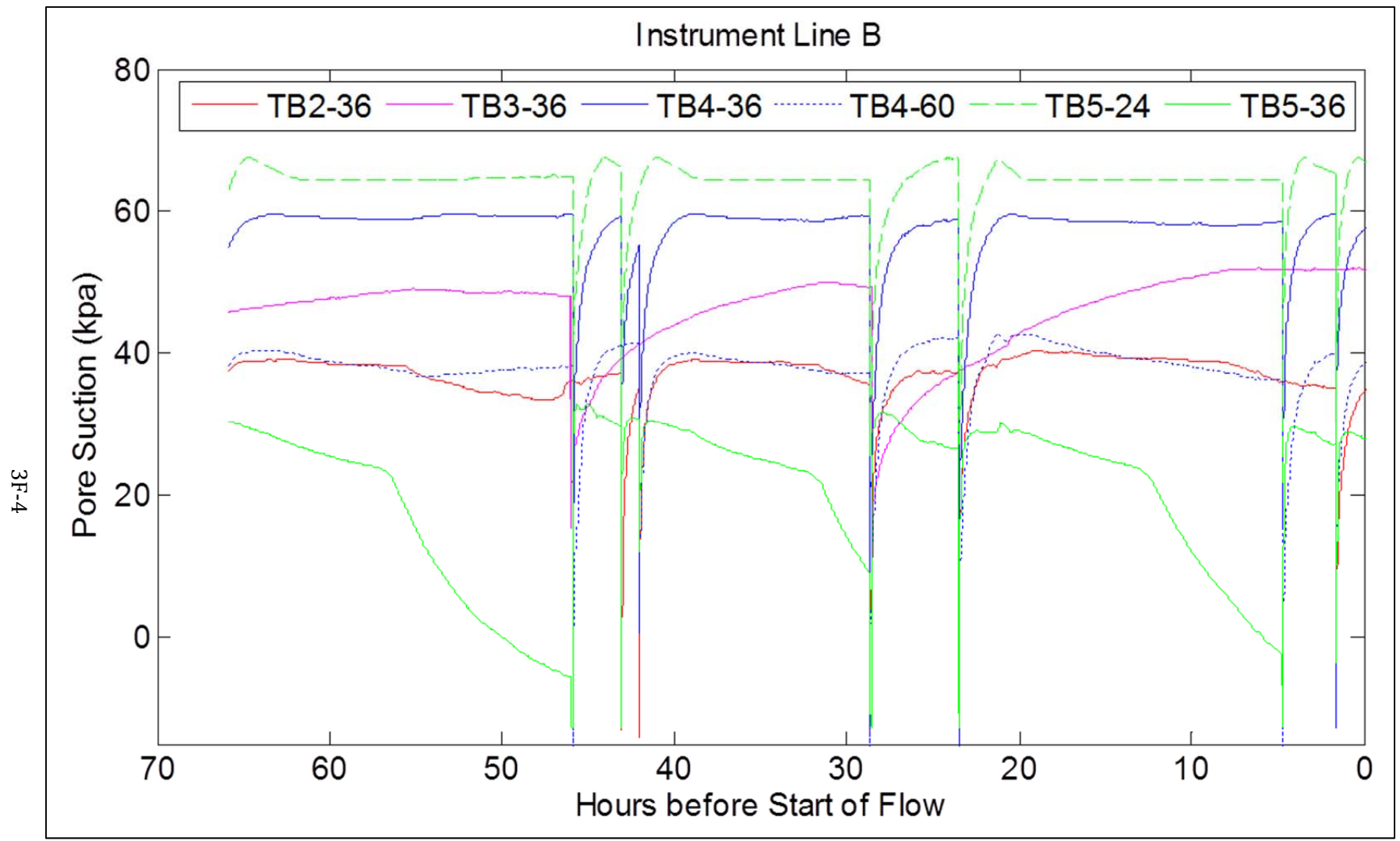
Figure 3F -3. Initial values of soil suction at instrument line B, measured in the days just prior to the flow test
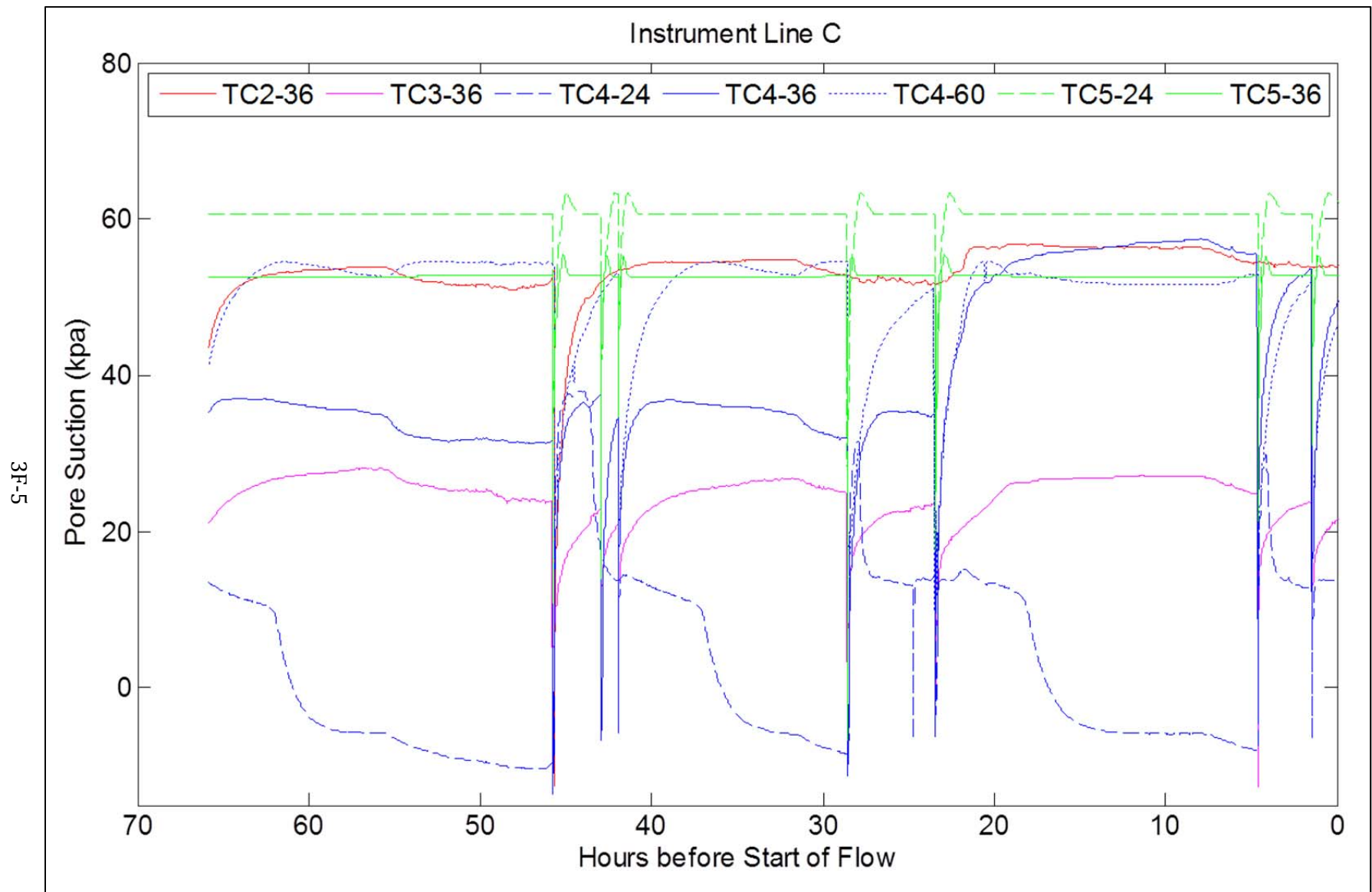
Figure 3F -4. Initial values of soil suction at instrument line C, measured in the days just prior to the flow test
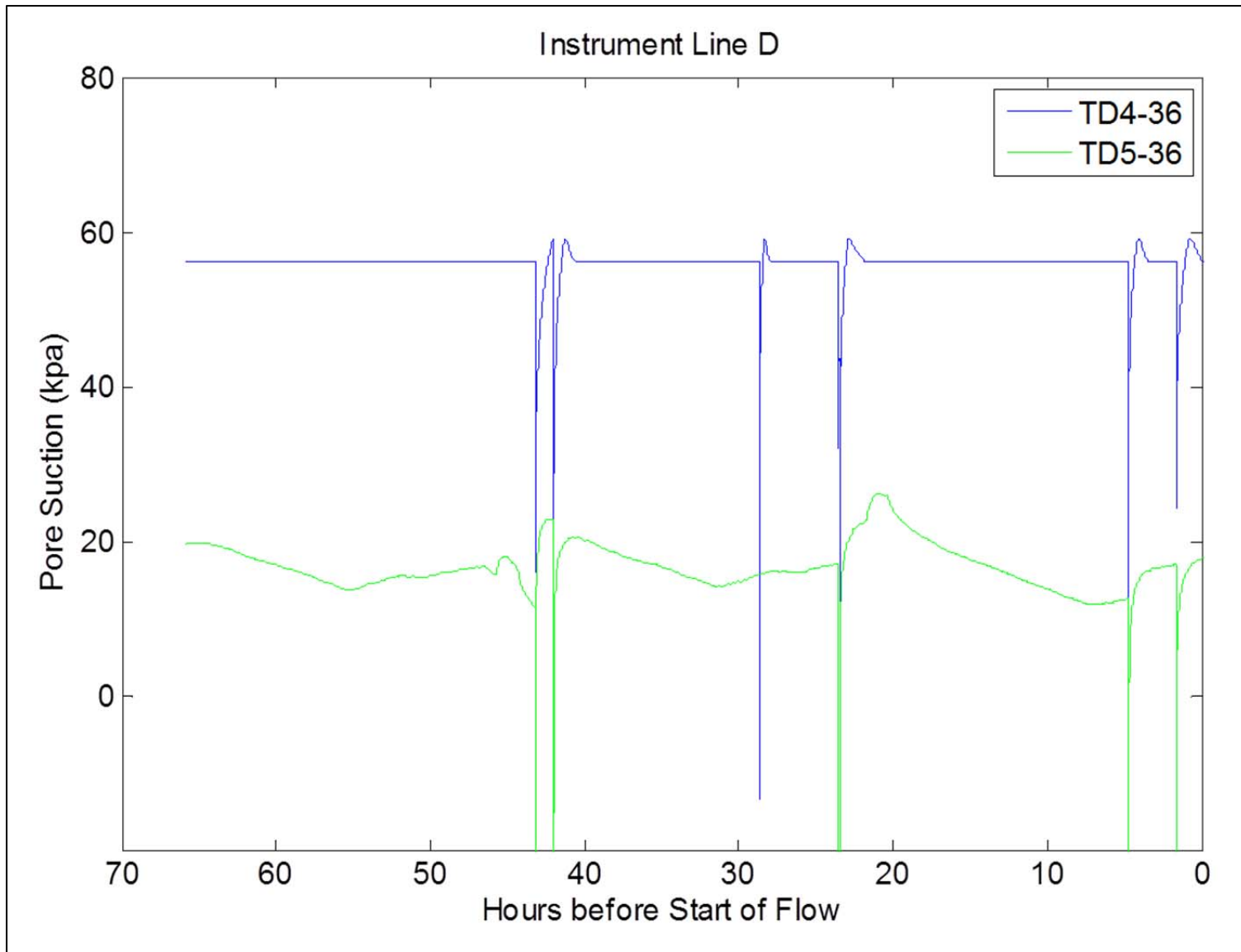
Figure 3F -5. Initial values of soil suction at instrument line D, measured in the days just prior to the flow test
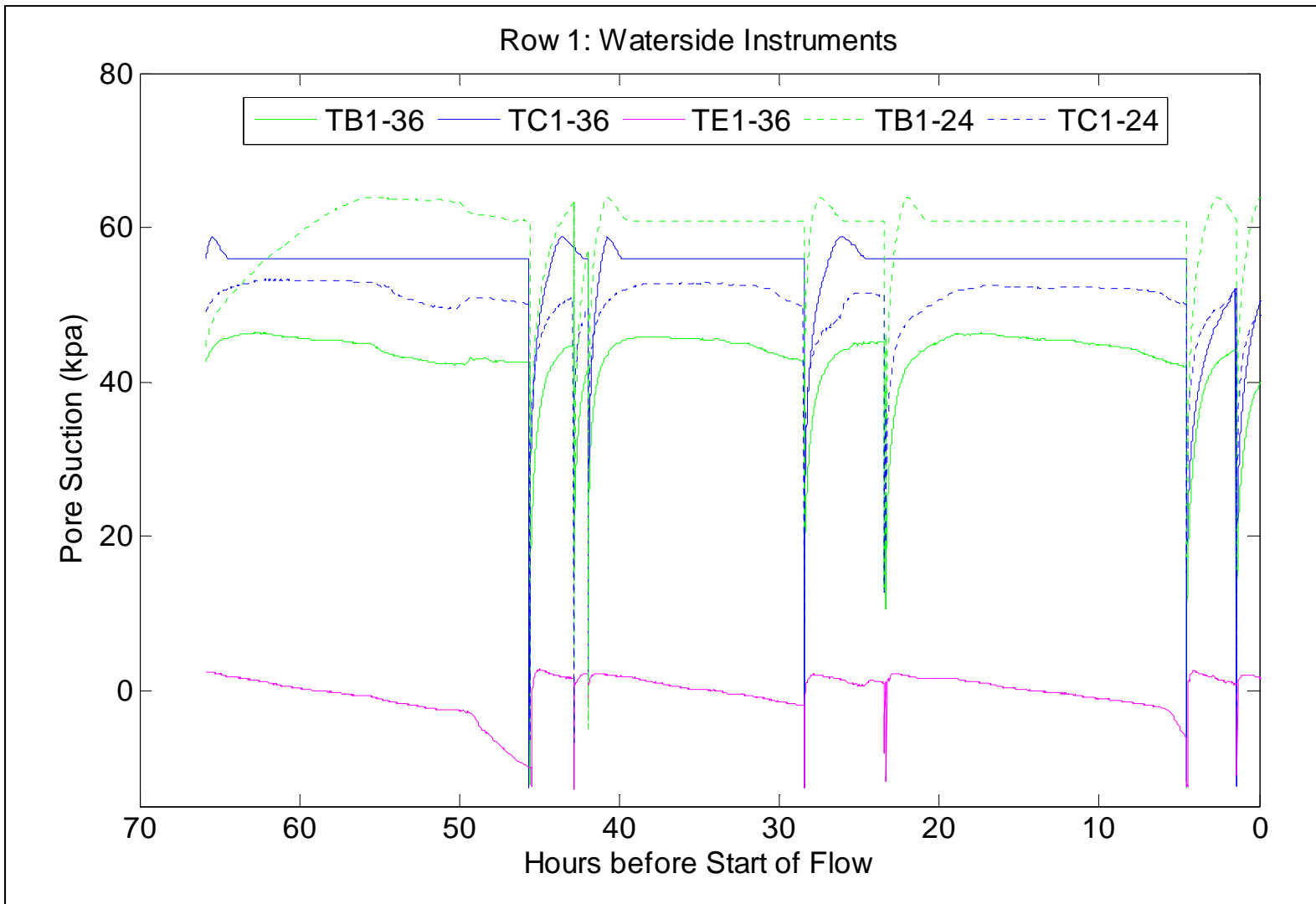
Figure 3F -6. Initial values of soil suction at waterside instruments (Row 1), measured in the days just prior to the flow test
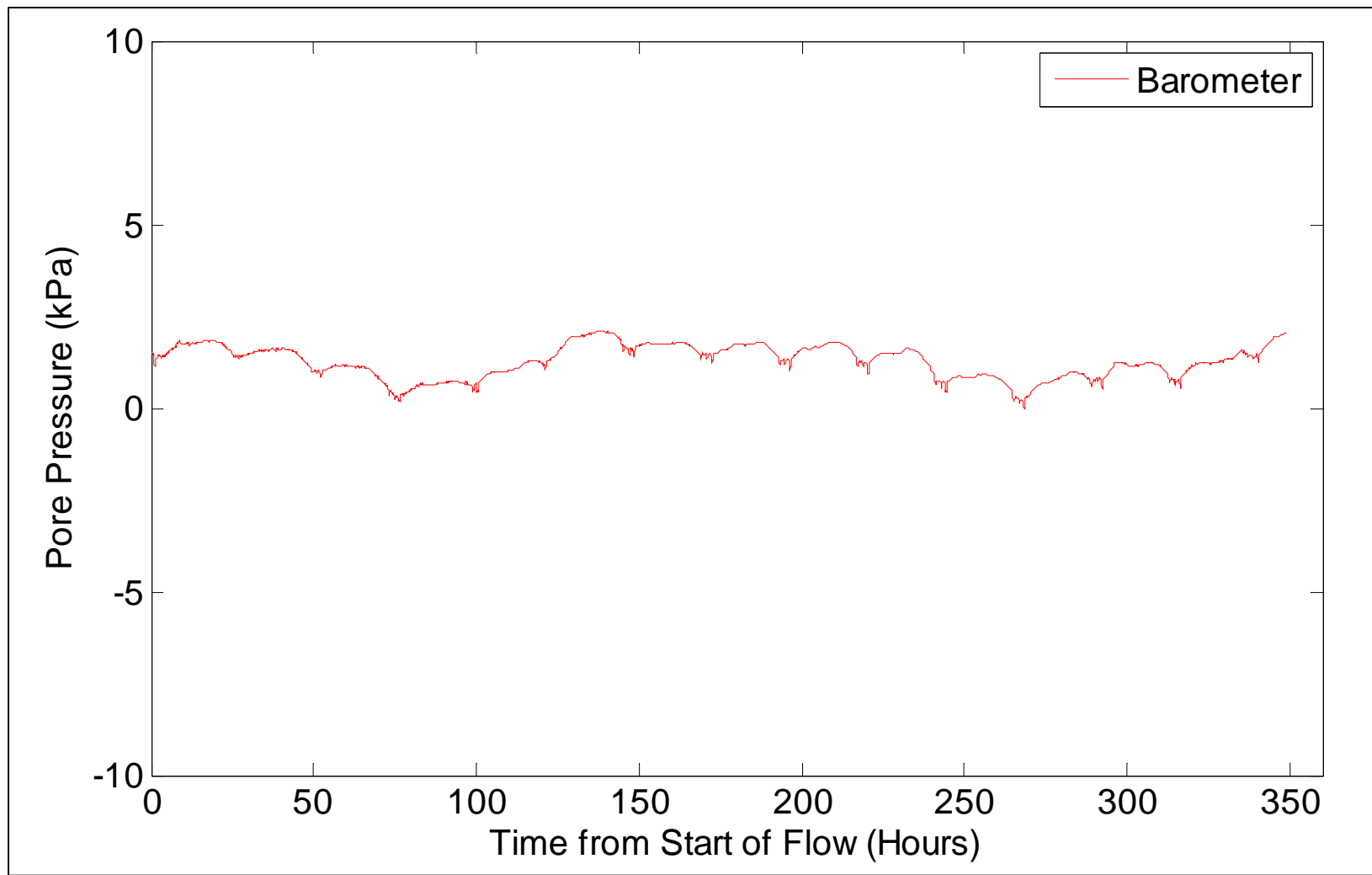
Figure 3F -7. Barometric pressures at the surface of the levee during the 10 day flow test and for 5 days afterward
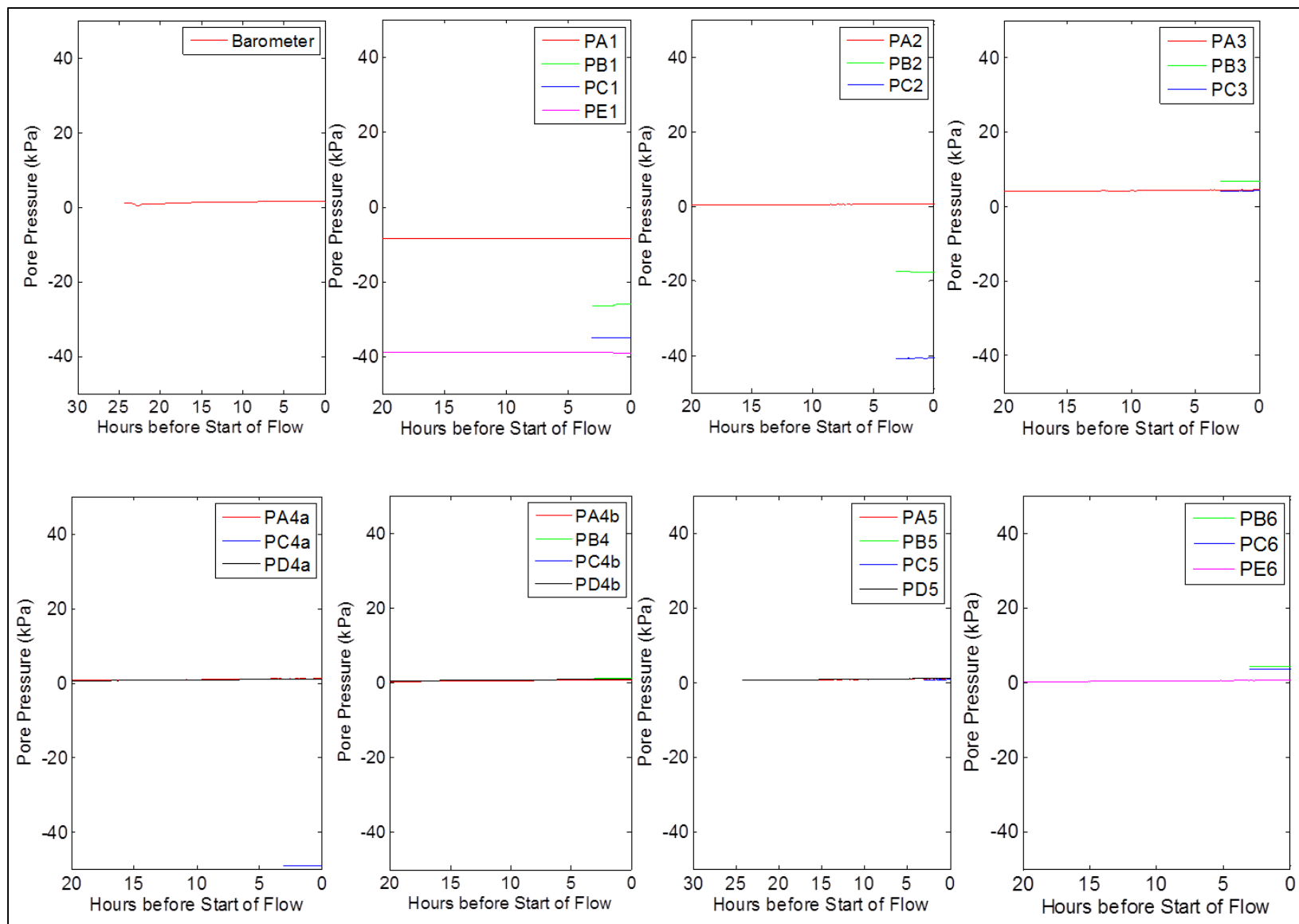
Figure 3F -8. Initial values of pore water pressure at all piezometers, measured just prior to the flow test

# APPENDIX 4A

## Root Reinforcing – Twitchell Island Test Site, Rio Vista, California

| Model | Section | Pore Pressure Condition | Root Number* | Root Embedment (ft) | Diameter (in) | Bond Stress (psf) | Tensile Strength (lbs) |
|---|---|---|---|---|---|---|---|
| Landside A | A1 | Steady State Test | 1 | 4 | 0.5 | 101 | 570 |
| | | | 2 | 6 | 0.5 | 122 | 570 |
| | | | 3 | 10 | 0.5 | 223 | 570 |
| | A2 | Steady State Test | 1 | 6 | 0.3 | 122 | 205 |
| | | | 2 | 10 | 0.5 | 223 | 570 |
| | A3 | Steady State Test | - | - | - | - | - |
| | A1 (2D) | Steady State Test No Tree | - | - | - | - | - |
| | A2 | Steady State Test No Tree | - | - | - | - | - |
| | A3 | Steady State Test No Tree | - | - | - | - | - |
| | A1 | Initial Pre-Test with Tree | 1 | 4 | 0.5 | 112 | 570 |
| | | | 2 | 6 | 0.5 | 169 | 570 |
| | | | 3 | 10 | 0.5 | 282 | 570 |
| | A2 | Initial Pre-Test with Tree | 1 | 6 | 0.3 | 169 | 205 |
| | | | 2 | 10 | 0.5 | 282 | 570 |
| | A3 | Initial Pre-Test with Tree | - | - | - | - | - |
| | A1 | Initial Pre-Test without Tree | - | - | - | - | - |
| | A2 | Initial Pre-Test without Tree | - | - | - | - | - |
| | A3 | Initial Pre-Test without Tree | - | - | - | - | - |
| | A1 | Steady State - Waterside Flood | 1 | 4 | 0.5 | 112 | 570 |
| | | | 2 | 6 | 0.5 | 169 | 570 |
| | | | 3 | 10 | 0.5 | 282 | 570 |
| | A2 | Steady State - Waterside Flood | 1 | 6 | 0.3 | 169 | 205 |
| | | | 2 | 10 | 0.5 | 282 | 570 |
| | A3 | Steady State - Waterside Flood | - | - | - | - | - |
| Landside C | C1 (2D) | Steady State Test | - | - | - | - | - |
| | C3 | Steady State Test | - | - | - | - | - |
| * Roots are numbered beginning with 1 at the shallowest embedment depth and increasing sequentially with increasing depth | | | | | | | |

| Model | Section | Pore Pressure Condition | Root Number* | Root Embedment (ft) | Diameter (in) | Bond Stress (psf) | Tensile Strength (lbs) |
|---|---|---|---|---|---|---|---|
| Waterside A | A1 | Steady State - Test | - | - | - | - | - |
| | A3 | Steady State - Test | - | - | - | - | - |
| | A1 | Steady State - Landside Flood | - | - | - | - | - |
| | A3 | Steady State - Landside Flood | - | - | - | - | - |
| Waterside B-1 | B1 | 39 Hr Transient - Test | 1 | 6 | 1 | 127 | 2280 |
| | | | 2 | 8 | 1.5 | 155 | 5130 |
| | B3 | 39 Hr Transient - Test | 1 | 6 | 1 | 127 | 2280 |
| Waterside B-2 | B1 | 39 Hr Transient - Test | 1 | 6 | 1 | 127 | 2280 |
| | | | 2 | 8 | 1.5 | 155 | 5130 |
| | B2 | 39 Hr Transient - Test | 1 | 6 | 0.75 | 127 | 1282 |
| | B3a | 39 Hr Transient - Test | 1 | 6 | 0.75 | 127 | 1282 |
| | B3b | 39 Hr Transient - Test | 1 | 6 | 0.75 | 127 | 1282 |
| | B1 - No Tree (2D) | 39 Hr Transient - Test | - | - | - | - | - |
| | B2 - No Tree | 39 Hr Transient - Test | - | - | - | - | - |
| | B3a - No Tree | 39 Hr Transient - Test | - | - | - | - | - |
| | B3b - No Tree | 39 Hr Transient - Test | - | - | - | - | - |
| Waterside BC-3 | B1 | 2 Hr Transient - Test | 1 | 6 | 1 | 169 | 2280 |
| | | | 2 | 8 | 1.5 | 226 | 5130 |
| | B2 | 2 Hr Transient - Test | 1 | 6 | 0.8 | 169 | 1459 |
| | B3 | 2 Hr Transient - Test | 1 | 6 | 0.7 | 169 | 1117 |
| | C2 | 2 Hr Transient - Test | 1 | 8 | 1 | 226 | 2280 |
| | C3 | 2 Hr Transient - Test | - | - | - | - | - |
| | B1 | 39 hrs - Test | 1 | 6 | 1 | 127 | 2280 |
| | | | 2 | 8 | 1.5 | 155 | 5130 |
| | B2 | 39 hrs - Test | 1 | 6 | 0.8 | 127 | 1459 |
| | B3 | 39 hrs - Test | 1 | 6 | 0.7 | 127 | 1117 |
| | C2 | 39 hrs - Test | 1 | 8 | 1 | 179 | 2280 |
| | C3 (2D) | 39 hrs - Test | - | - | - | - | - |
| | B1 No tree | 39 Hr Transient - Test | - | - | - | - | - |
| | B2 - No Tree | 39 Hr Transient - Test | - | - | - | - | - |
| | B3 - No Tree | 39 Hr Transient - Test | - | - | - | - | - |
| | C2 - No Tree | 39 Hr Transient - Test | - | - | - | - | - |
| | C3 - No Tree | 39 Hr Transient - Test | - | - | - | - | - |

* Roots are numbered beginning with 1 at the shallowest embedment depth and increasing sequentially with increasing depth

## Max Load Esimate Based on Root Size and Embedment

**Friction angle** 32 degrees
**Unit weight** 120 pcf
**Friction coefficient** 0.8 unitless
**Max. Tensile Stress:** 418000 psf

**Root Length** 5 ft

| Depth (ft) | Effective Overburden Stress (psf) | Bond Stress (psf) | Root Diameter (in) | | | | | | | | | | | |
|---|---|---|---|---|---|---|---|---|---|---|---|---|---|---|
| | | | 0.25 | 0.5 | 0.75 | 1 | 1.25 | 1.5 | 1.75 | 2 | 2.5 | 3 | 3.5 | 4 |
| 1 | 120 | 28.2 | 9 | 18 | 28 | 37 | 46 | 55 | 65 | 74 | 92 | 111 | 129 | 148 |
| 2 | 240 | 56.4 | 18 | 37 | 55 | 74 | 92 | 111 | 129 | 148 | 185 | 221 | 258 | 295 |
| 3 | 360 | 84.6 | 28 | 55 | 83 | 111 | 138 | 166 | 194 | 221 | 277 | 332 | 388 | 443 |
| 4 | 480 | 112.8 | 37 | 74 | 111 | 148 | 185 | 221 | 258 | 295 | 369 | 443 | 517 | 591 |
| 5 | 600 | 141.0 | 46 | 92 | 138 | 185 | 231 | 277 | 323 | 369 | 461 | 554 | 646 | 738 |
| 6 | 720 | 169.2 | 55 | 111 | 166 | 221 | 277 | 332 | 388 | 443 | 554 | 664 | 775 | 886 |
| 7 | 840 | 197.4 | 65 | 129 | 194 | 258 | 323 | 388 | 452 | 517 | 646 | 775 | 904 | 1034 |
| 8 | 960 | 225.6 | 74 | 148 | 221 | 295 | 369 | 443 | 517 | 591 | 738 | 886 | 1034 | 1181 |
| 9 | 1080 | 253.8 | 83 | 166 | 249 | 332 | 415 | 498 | 581 | 664 | 831 | 997 | 1163 | 1329 |
| 10 | 1200 | 282.0 | 92 | 185 | 277 | 369 | 461 | 554 | 646 | 738 | 923 | 1107 | 1292 | 1476 |
| 11 | 1320 | 310.2 | 102 | 203 | 305 | 406 | 508 | 609 | 711 | 812 | 1015 | 1218 | 1421 | 1624 |
| 12 | 1440 | 338.4 | 111 | 221 | 332 | 443 | 554 | 664 | 775 | 886 | 1107 | 1329 | 1550 | 1772 |
| 13 | 1560 | 366.6 | 120 | 240 | 360 | 480 | 600 | 720 | 840 | 960 | 1200 | 1440 | 1680 | 1919 |
| 14 | 1680 | 394.8 | 129 | 258 | 388 | 517 | 646 | 775 | 904 | 1034 | 1292 | 1550 | 1809 | 2067 |
| 15 | 1800 | 423.0 | 138 | 277 | 415 | 554 | 692 | 831 | 969 | 1107 | 1384 | 1661 | 1938 | 2215 |

<u>Note</u>: Root capacities reported in red are roots expected to fail in tension.

## Max Load Esimate Based on Root Size and Embedment

**Friction angle** 32 degrees
**Unit weight** 120 pcf
**Friction coefficient** 0.8 unitless
**Max. Tensile Stress:** 418000 psf

**Root Length** 10 ft

| Depth (ft) | Effective Overburden Stress (psf) | Bond Stress (psf) | Root Diameter (in) | | | | | | | | | | | |
|---|---|---|---|---|---|---|---|---|---|---|---|---|---|---|
| | | | 0.25 | 0.5 | 0.75 | 1 | 1.25 | 1.5 | 1.75 | 2 | 2.5 | 3 | 3.5 | 4 |
| 1 | 120 | 28.2 | 18 | 37 | 55 | 74 | 92 | 111 | 129 | 148 | 185 | 221 | 258 | 295 |
| 2 | 240 | 56.4 | 37 | 74 | 111 | 148 | 185 | 221 | 258 | 295 | 369 | 443 | 517 | 591 |
| 3 | 360 | 84.6 | 55 | 111 | 166 | 221 | 277 | 332 | 388 | 443 | 554 | 664 | 775 | 886 |
| 4 | 480 | 112.8 | 74 | 148 | 221 | 295 | 369 | 443 | 517 | 591 | 738 | 886 | 1034 | 1181 |
| 5 | 600 | 141.0 | 92 | 185 | 277 | 369 | 461 | 554 | 646 | 738 | 923 | 1107 | 1292 | 1476 |
| 6 | 720 | 169.2 | 111 | 221 | 332 | 443 | 554 | 664 | 775 | 886 | 1107 | 1329 | 1550 | 1772 |
| 7 | 840 | 197.4 | 129 | 258 | 388 | 517 | 646 | 775 | 904 | 1034 | 1292 | 1550 | 1809 | 2067 |
| 8 | 960 | 225.6 | <span style="color:red">142</span> | 295 | 443 | 591 | 738 | 886 | 1034 | 1181 | 1476 | 1772 | 2067 | 2362 |
| 9 | 1080 | 253.8 | <span style="color:red">142</span> | 332 | 498 | 664 | 831 | 997 | 1163 | 1329 | 1661 | 1993 | 2325 | 2658 |
| 10 | 1200 | 282.0 | <span style="color:red">142</span> | 369 | 554 | 738 | 923 | 1107 | 1292 | 1476 | 1846 | 2215 | 2584 | 2953 |
| 11 | 1320 | 310.2 | <span style="color:red">142</span> | 406 | 609 | 812 | 1015 | 1218 | 1421 | 1624 | 2030 | 2436 | 2842 | 3248 |
| 12 | 1440 | 338.4 | <span style="color:red">142</span> | 443 | 664 | 886 | 1107 | 1329 | 1550 | 1772 | 2215 | 2658 | 3101 | 3544 |
| 13 | 1560 | 366.6 | <span style="color:red">142</span> | 480 | 720 | 960 | 1200 | 1440 | 1680 | 1919 | 2399 | 2879 | 3359 | 3839 |
| 14 | 1680 | 394.8 | <span style="color:red">142</span> | 517 | 775 | 1034 | 1292 | 1550 | 1809 | 2067 | 2584 | 3101 | 3617 | 4134 |
| 15 | 1800 | 423.0 | <span style="color:red">142</span> | 554 | 831 | 1107 | 1384 | 1661 | 1938 | 2215 | 2768 | 3322 | 3876 | 4429 |

<u>Note</u>: Root capacities reported in red are roots expected to fail in tension.

## Max Load Esimate Based on Root Size and Embedment

**Friction angle**  32 degrees
**Unit weight**  120 pcf
**Friction coefficient**  0.8 unitless
**Max. Tensile Stress:**  418000 psf

Root Length 15 ft

| Depth (ft) | Effective Overburden Stress (psf) | Bond Stress (psf) | Root Diameter (in) | | | | | | | | | | | |
|---|---|---|---|---|---|---|---|---|---|---|---|---|---|---|
| | | | 0.25 | 0.5 | 0.75 | 1 | 1.25 | 1.5 | 1.75 | 2 | 2.5 | 3 | 3.5 | 4 |
| 1 | 120 | 28.2 | 28 | 55 | 83 | 111 | 138 | 166 | 194 | 221 | 277 | 332 | 388 | 443 |
| 2 | 240 | 56.4 | 55 | 111 | 166 | 221 | 277 | 332 | 388 | 443 | 554 | 664 | 775 | 886 |
| 3 | 360 | 84.6 | 83 | 166 | 249 | 332 | 415 | 498 | 581 | 664 | 831 | 997 | 1163 | 1329 |
| 4 | 480 | 112.8 | 111 | 221 | 332 | 443 | 554 | 664 | 775 | 886 | 1107 | 1329 | 1550 | 1772 |
| 5 | 600 | 141.0 | 138 | 277 | 415 | 554 | 692 | 831 | 969 | 1107 | 1384 | 1661 | 1938 | 2215 |
| 6 | 720 | 169.2 | 142 | 332 | 498 | 664 | 831 | 997 | 1163 | 1329 | 1661 | 1993 | 2325 | 2658 |
| 7 | 840 | 197.4 | 142 | 388 | 581 | 775 | 969 | 1163 | 1357 | 1550 | 1938 | 2325 | 2713 | 3101 |
| 8 | 960 | 225.6 | 142 | 443 | 664 | 886 | 1107 | 1329 | 1550 | 1772 | 2215 | 2658 | 3101 | 3544 |
| 9 | 1080 | 253.8 | 142 | 498 | 747 | 997 | 1246 | 1495 | 1744 | 1993 | 2492 | 2990 | 3488 | 3987 |
| 10 | 1200 | 282.0 | 142 | 554 | 831 | 1107 | 1384 | 1661 | 1938 | 2215 | 2768 | 3322 | 3876 | 4429 |
| 11 | 1320 | 310.2 | 142 | 570 | 914 | 1218 | 1523 | 1827 | 2132 | 2436 | 3045 | 3654 | 4263 | 4872 |
| 12 | 1440 | 338.4 | 142 | 570 | 997 | 1329 | 1661 | 1993 | 2325 | 2658 | 3322 | 3987 | 4651 | 5315 |
| 13 | 1560 | 366.6 | 142 | 570 | 1080 | 1440 | 1799 | 2159 | 2519 | 2879 | 3599 | 4319 | 5039 | 5758 |
| 14 | 1680 | 394.8 | 142 | 570 | 1163 | 1550 | 1938 | 2325 | 2713 | 3101 | 3876 | 4651 | 5426 | 6201 |
| 15 | 1800 | 423.0 | 142 | 570 | 1246 | 1661 | 2076 | 2492 | 2907 | 3322 | 4153 | 4983 | 5814 | 6644 |

Note: Root capacities reported in red are roots expected to fail in tension.

## Max Load Esimate Based on Root Size and Embedment

**Friction angle**  32 degrees
**Unit weight**  120 pcf
**Friction coefficient**  0.8 unitless
**Max. Tensile Stress:**  418000 psf

Root Length 20 ft

| Depth (ft) | Effective Overburden Stress (psf) | Bond Stress (psf) | Root Diameter (in) | | | | | | | | | | | |
|---|---|---|---|---|---|---|---|---|---|---|---|---|---|---|
| | | | 0.25 | 0.5 | 0.75 | 1 | 1.25 | 1.5 | 1.75 | 2 | 2.5 | 3 | 3.5 | 4 |
| 1 | 120 | 28.2 | 37 | 74 | 111 | 148 | 185 | 221 | 258 | 295 | 369 | 443 | 517 | 591 |
| 2 | 240 | 56.4 | 74 | 148 | 221 | 295 | 369 | 443 | 517 | 591 | 738 | 886 | 1034 | 1181 |
| 3 | 360 | 84.6 | 111 | 221 | 332 | 443 | 554 | 664 | 775 | 886 | 1107 | 1329 | 1550 | 1772 |
| 4 | 480 | 112.8 | 142 | 295 | 443 | 591 | 738 | 886 | 1034 | 1181 | 1476 | 1772 | 2067 | 2362 |
| 5 | 600 | 141.0 | 142 | 369 | 554 | 738 | 923 | 1107 | 1292 | 1476 | 1846 | 2215 | 2584 | 2953 |
| 6 | 720 | 169.2 | 142 | 443 | 664 | 886 | 1107 | 1329 | 1550 | 1772 | 2215 | 2658 | 3101 | 3544 |
| 7 | 840 | 197.4 | 142 | 517 | 775 | 1034 | 1292 | 1550 | 1809 | 2067 | 2584 | 3101 | 3617 | 4134 |
| 8 | 960 | 225.6 | 142 | 570 | 886 | 1181 | 1476 | 1772 | 2067 | 2362 | 2953 | 3544 | 4134 | 4725 |
| 9 | 1080 | 253.8 | 142 | 570 | 997 | 1329 | 1661 | 1993 | 2325 | 2658 | 3322 | 3987 | 4651 | 5315 |
| 10 | 1200 | 282.0 | 142 | 570 | 1107 | 1476 | 1846 | 2215 | 2584 | 2953 | 3691 | 4429 | 5168 | 5906 |
| 11 | 1320 | 310.2 | 142 | 570 | 1218 | 1624 | 2030 | 2436 | 2842 | 3248 | 4060 | 4872 | 5684 | 6497 |
| 12 | 1440 | 338.4 | 142 | 570 | 1282 | 1772 | 2215 | 2658 | 3101 | 3544 | 4429 | 5315 | 6201 | 7087 |
| 13 | 1560 | 366.6 | 142 | 570 | 1282 | 1919 | 2399 | 2879 | 3359 | 3839 | 4799 | 5758 | 6718 | 7678 |
| 14 | 1680 | 394.8 | 142 | 570 | 1282 | 2067 | 2584 | 3101 | 3617 | 4134 | 5168 | 6201 | 7235 | 8268 |
| 15 | 1800 | 423.0 | 142 | 570 | 1282 | 2215 | 2768 | 3322 | 3876 | 4429 | 5537 | 6644 | 7752 | 8859 |

Note: Root capacities reported in red are roots expected to fail in tension.

## Max Load Esimate Based on Root Size and Embedment

**Friction angle** 32 degrees
**Unit weight** 120 pcf
**Friction coefficient** 0.8 unitless
**Max. Tensile Stress:** 418000 psf

Root Length 25 ft

| Depth (ft) | Effective Overburden Stress (psf) | Bond Stress (psf) | Root Diameter (in) | | | | | | | | | | | |
|---|---|---|---|---|---|---|---|---|---|---|---|---|---|---|
| | | | 0.25 | 0.5 | 0.75 | 1 | 1.25 | 1.5 | 1.75 | 2 | 2.5 | 3 | 3.5 | 4 |
| 1 | 120 | 28.2 | 46 | 92 | 138 | 185 | 231 | 277 | 323 | 369 | 461 | 554 | 646 | 738 |
| 2 | 240 | 56.4 | 92 | 185 | 277 | 369 | 461 | 554 | 646 | 738 | 923 | 1107 | 1292 | 1476 |
| 3 | 360 | 84.6 | 138 | 277 | 415 | 554 | 692 | 831 | 969 | 1107 | 1384 | 1661 | 1938 | 2215 |
| 4 | 480 | 112.8 | 142 | 369 | 554 | 738 | 923 | 1107 | 1292 | 1476 | 1846 | 2215 | 2584 | 2953 |
| 5 | 600 | 141.0 | 142 | 461 | 692 | 923 | 1154 | 1384 | 1615 | 1846 | 2307 | 2768 | 3230 | 3691 |
| 6 | 720 | 169.2 | 142 | 554 | 831 | 1107 | 1384 | 1661 | 1938 | 2215 | 2768 | 3322 | 3876 | 4429 |
| 7 | 840 | 197.4 | 142 | 570 | 969 | 1292 | 1615 | 1938 | 2261 | 2584 | 3230 | 3876 | 4522 | 5168 |
| 8 | 960 | 225.6 | 142 | 570 | 1107 | 1476 | 1846 | 2215 | 2584 | 2953 | 3691 | 4429 | 5168 | 5906 |
| 9 | 1080 | 253.8 | 142 | 570 | 1246 | 1661 | 2076 | 2492 | 2907 | 3322 | 4153 | 4983 | 5814 | 6644 |
| 10 | 1200 | 282.0 | 142 | 570 | 1282 | 1846 | 2307 | 2768 | 3230 | 3691 | 4614 | 5537 | 6460 | 7382 |
| 11 | 1320 | 310.2 | 142 | 570 | 1282 | 2030 | 2538 | 3045 | 3553 | 4060 | 5075 | 6091 | 7106 | 8121 |
| 12 | 1440 | 338.4 | 142 | 570 | 1282 | 2215 | 2768 | 3322 | 3876 | 4429 | 5537 | 6644 | 7752 | 8859 |
| 13 | 1560 | 366.6 | 142 | 570 | 1282 | 2280 | 2999 | 3599 | 4199 | 4799 | 5998 | 7198 | 8398 | 9597 |
| 14 | 1680 | 394.8 | 142 | 570 | 1282 | 2280 | 3230 | 3876 | 4522 | 5168 | 6460 | 7752 | 9044 | 10335 |
| 15 | 1800 | 423.0 | 142 | 570 | 1282 | 2280 | 3461 | 4153 | 4845 | 5537 | 6921 | 8305 | 9689 | 11074 |

<u>Note</u>: Root capacities reported in red are roots expected to fail in tension.

## Max Load Esimate Based on Root Size and Embedment

**Friction angle** 32 degrees
**Unit weight** 120 pcf
**Friction coefficient** 0.8 unitless
**Max. Tensile Stress:** 418000 psf

Root Length 35 ft

| Depth (ft) | Effective Overburden Stress (psf) | Bond Stress (psf) | Root Diameter (in) | | | | | | | | | | | |
|---|---|---|---|---|---|---|---|---|---|---|---|---|---|---|
| | | | 0.25 | 0.5 | 0.75 | 1 | 1.25 | 1.5 | 1.75 | 2 | 2.5 | 3 | 3.5 | 4 |
| 1 | 120 | 28.2 | 65 | 129 | 194 | 258 | 323 | 388 | 452 | 517 | 646 | 775 | 904 | 1034 |
| 2 | 240 | 56.4 | 129 | 258 | 388 | 517 | 646 | 775 | 904 | 1034 | 1292 | 1550 | 1809 | 2067 |
| 3 | 360 | 84.6 | 142 | 388 | 581 | 775 | 969 | 1163 | 1357 | 1550 | 1938 | 2325 | 2713 | 3101 |
| 4 | 480 | 112.8 | 142 | 517 | 775 | 1034 | 1292 | 1550 | 1809 | 2067 | 2584 | 3101 | 3617 | 4134 |
| 5 | 600 | 141.0 | 142 | 570 | 969 | 1292 | 1615 | 1938 | 2261 | 2584 | 3230 | 3876 | 4522 | 5168 |
| 6 | 720 | 169.2 | 142 | 570 | 1163 | 1550 | 1938 | 2325 | 2713 | 3101 | 3876 | 4651 | 5426 | 6201 |
| 7 | 840 | 197.4 | 142 | 570 | 1282 | 1809 | 2261 | 2713 | 3165 | 3617 | 4522 | 5426 | 6330 | 7235 |
| 8 | 960 | 225.6 | 142 | 570 | 1282 | 2067 | 2584 | 3101 | 3617 | 4134 | 5168 | 6201 | 7235 | 8268 |
| 9 | 1080 | 253.8 | 142 | 570 | 1282 | 2280 | 2907 | 3488 | 4070 | 4651 | 5814 | 6976 | 8139 | 9302 |
| 10 | 1200 | 282.0 | 142 | 570 | 1282 | 2280 | 3230 | 3876 | 4522 | 5168 | 6460 | 7752 | 9044 | 10335 |
| 11 | 1320 | 310.2 | 142 | 570 | 1282 | 2280 | 3553 | 4263 | 4974 | 5684 | 7106 | 8527 | 9948 | 11369 |
| 12 | 1440 | 338.4 | 142 | 570 | 1282 | 2280 | 3562 | 4651 | 5426 | 6201 | 7752 | 9302 | 10852 | 12403 |
| 13 | 1560 | 366.6 | 142 | 570 | 1282 | 2280 | 3562 | 5039 | 5878 | 6718 | 8398 | 10077 | 11757 | 13436 |
| 14 | 1680 | 394.8 | 142 | 570 | 1282 | 2280 | 3562 | 5130 | 6330 | 7235 | 9044 | 10852 | 12661 | 14470 |
| 15 | 1800 | 423.0 | 142 | 570 | 1282 | 2280 | 3562 | 5130 | 6783 | 7752 | 9689 | 11627 | 13565 | 15503 |

<u>Note</u>: Root capacities reported in red are roots expected to fail in tension.

# APPENDIX 4B

**Slope Stability Modeling Results – Twitchell Island Test Site, Rio Vista, California**

Landside A, Steady State Conditions Without Tree

Section A1 — FS = 1.81
Section A2 — FS = 1.81
Section A3 — FS = 1.79

Landside A, Steady State Test Conditions with Tree

Section A1 — FS = 1.56
Section A2 — FS = 1.99
Section A3 — FS = 1.82
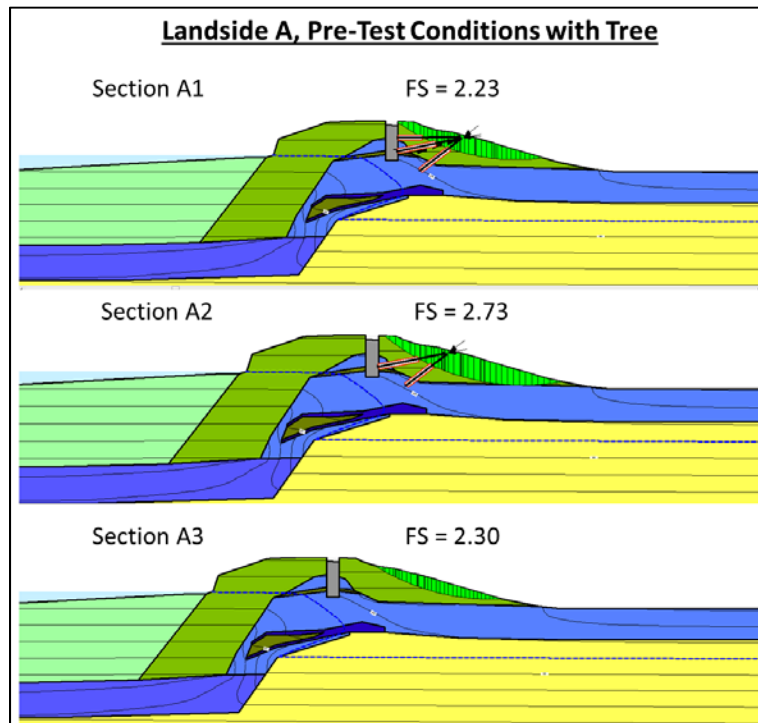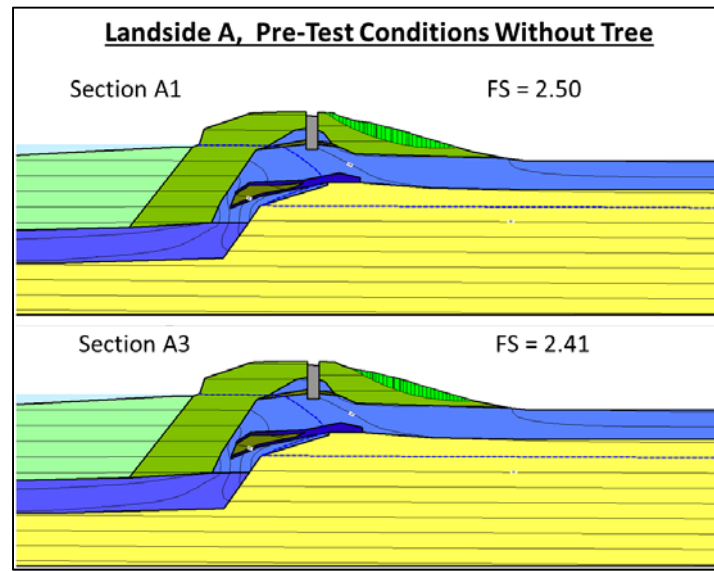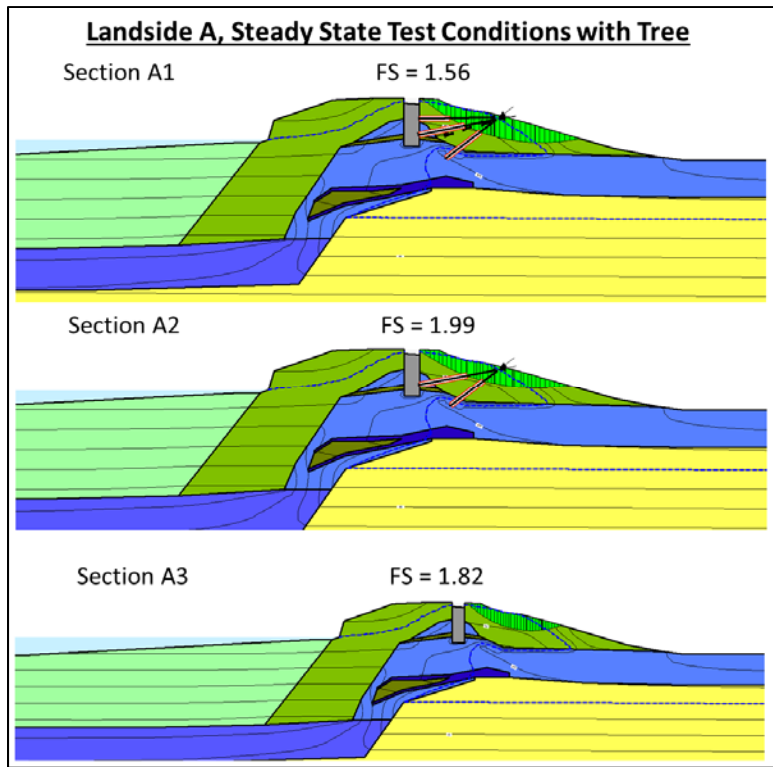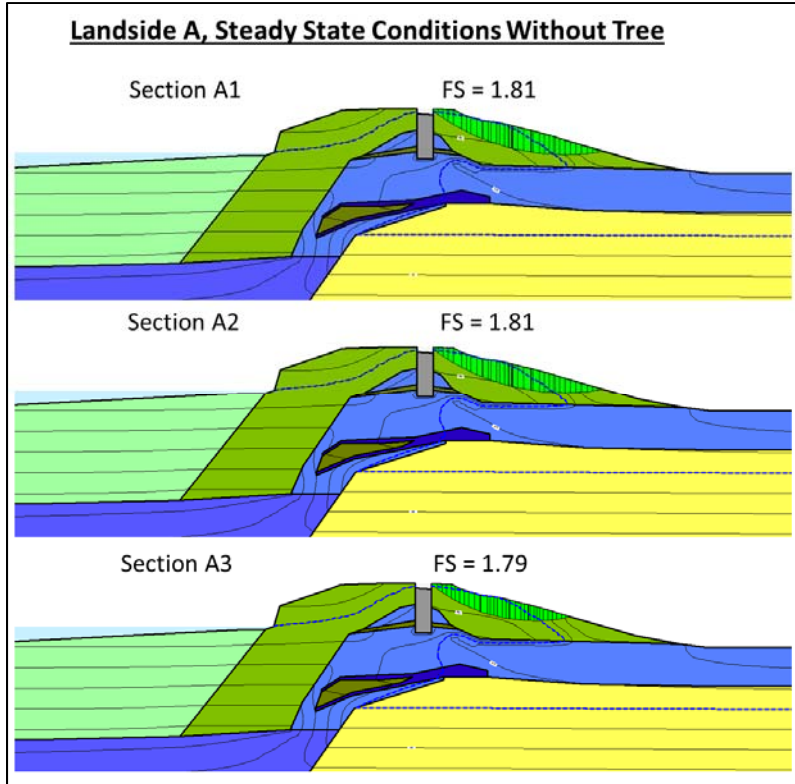
**Landside A, Steady State Waterside Flood with Tree**

Section A1 — FS = 1.89
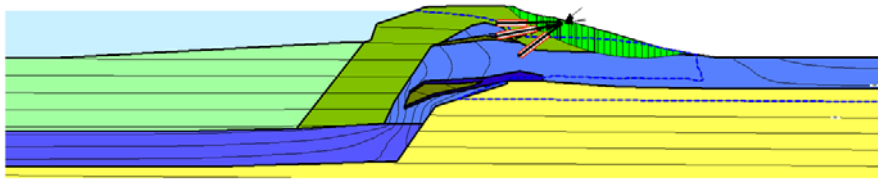
Section A2 — FS = 2.14
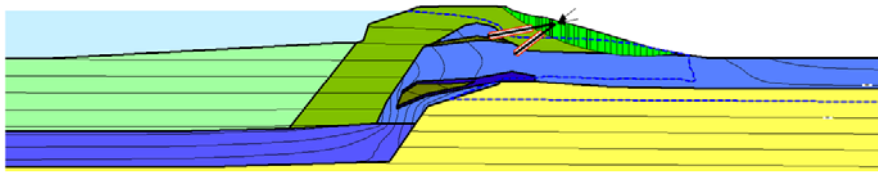
Section A3 — FS = 1.91
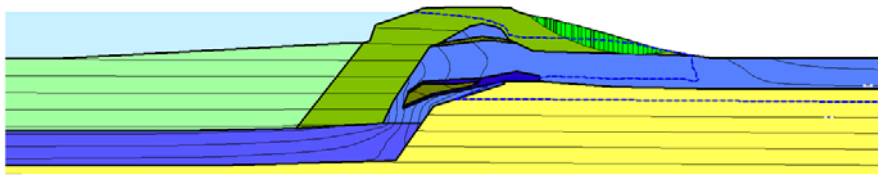


**Landside C, Steady State Test Conditions**

Section C1 — FS = 1.94
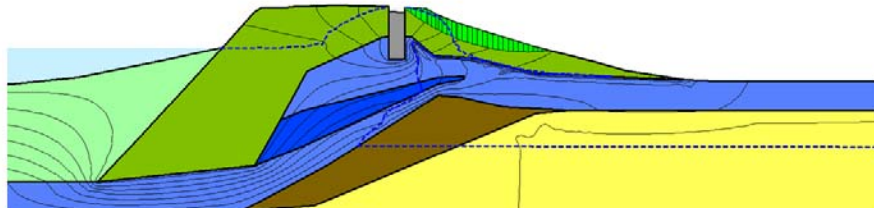
Section C3 — FS = 2.03

Waterside A Initial Pre-Test Conditions

Section A1     FS = 1.75

Section A3     Initial Pre-Test     FS = 1.61

Waterside A, Steady State Test

A1     Steady State Test     FS = 1.51

A3     Steady State Test     FS = 1.40

Waterside A, Steady State Landside Flood (crest height minus 3 ft)

A1     Steady State Landside Flood (crest minus 3 ft)     FS = 1.48

A3     Steady State Landside Flood (crest minus 3 ft)     FS = 1.36

4B-4
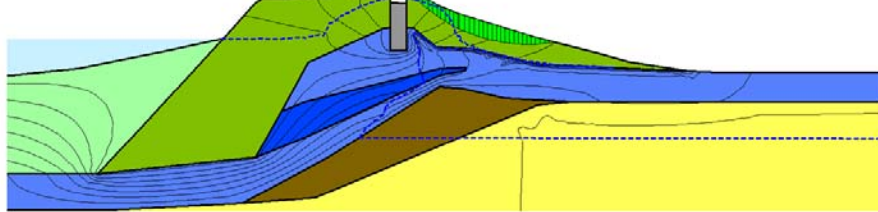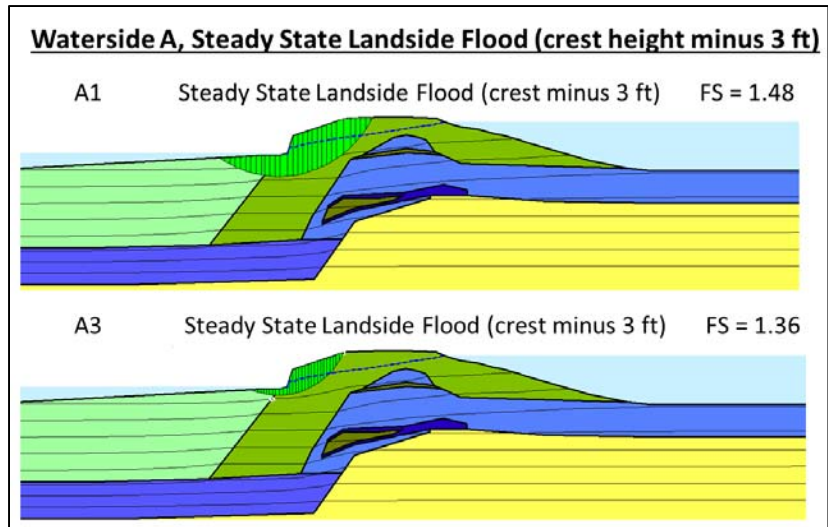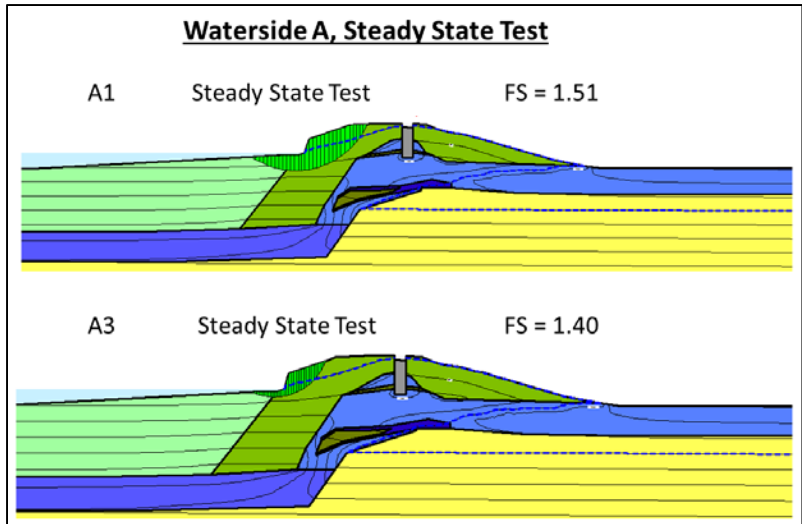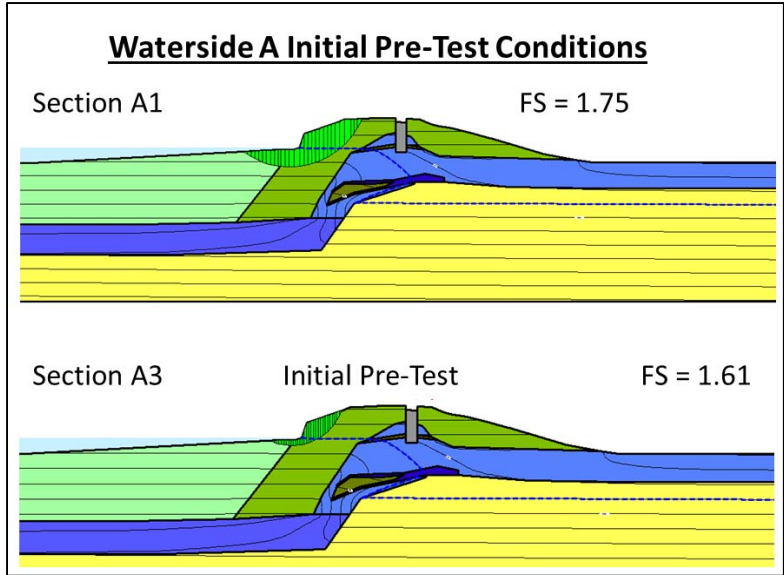
**Waterside B1 - – 39 hr Transient Test Conditions, with Tree**

Section B1      FS = 0.96
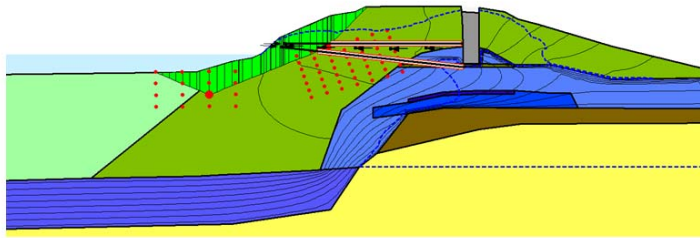
Section B3      FS = 1.50
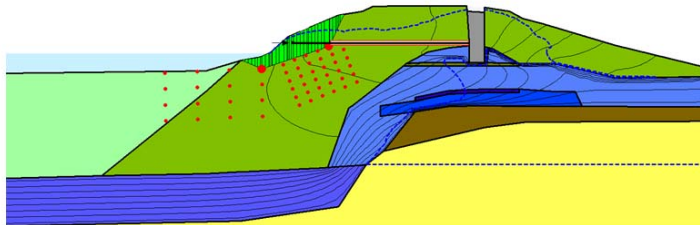


**Waterside B2 – 39 hr Transient Test Conditions, with Tree**
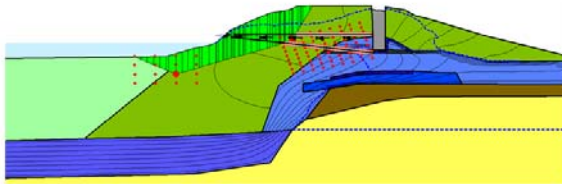
Section B1      FS = 1.05      Section B2      FS = 1.28
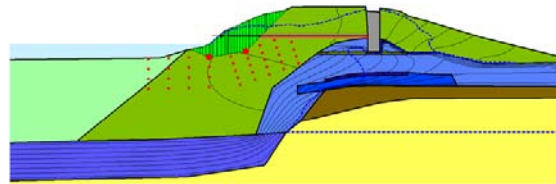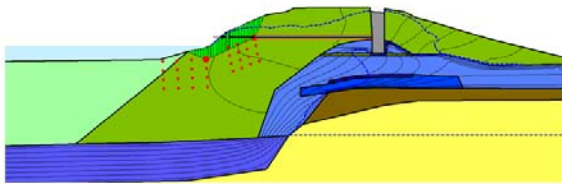
Section B3a      FS = 1.35      Section B3b      FS = 1.44
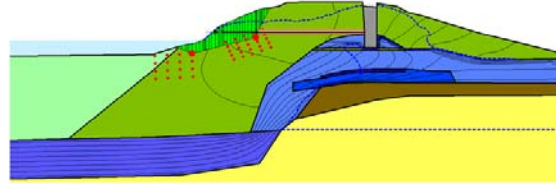
Waterside B2 – 39 hr Transient Test Conditions, Without Tree

Section B1     FS = 1.07          Section B2     FS = 1.07

Section B3a    FS = 0.96          Section B3b    FS = 0.96



Waterside BC3 – 39 hr Transient Test Conditions, with Tree

Section B1     FS = 1.12          Section B2     FS = 1.76
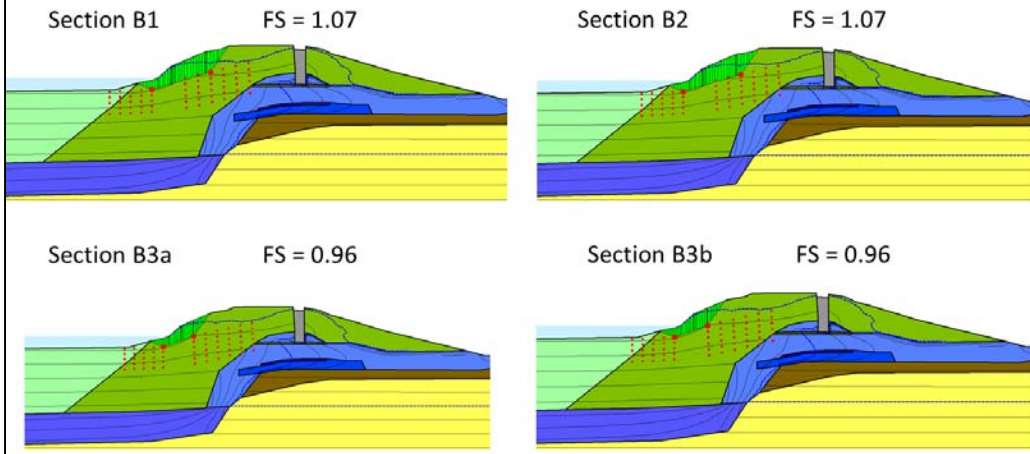
Section B3     FS = 1.28          Section C2     FS = 2.08
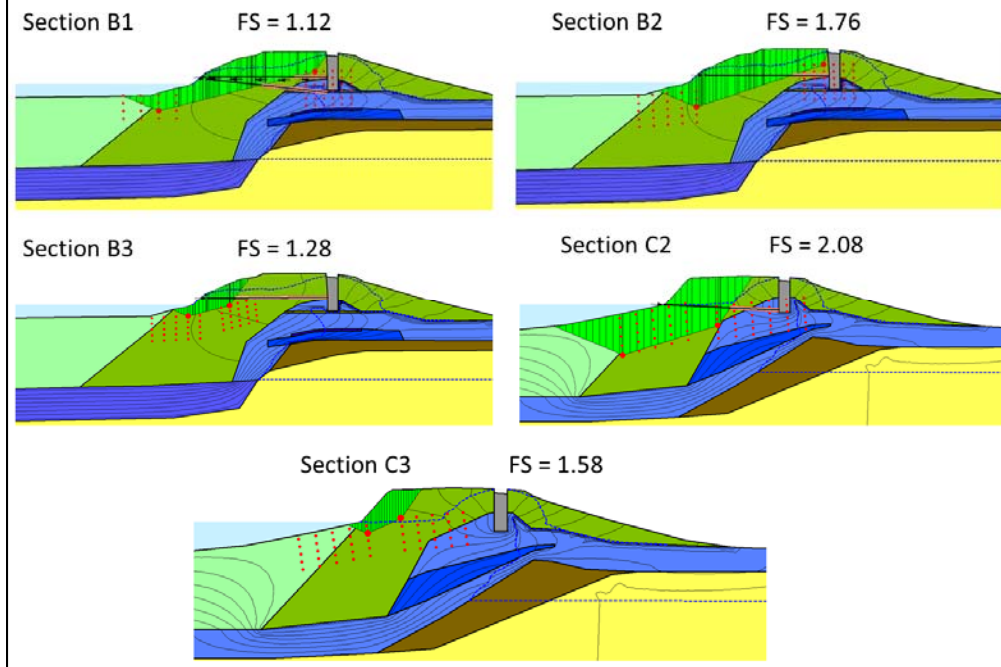
Section C3     FS = 1.58

Waterside BC3 – 2 hr Transient Test Conditions, with Tree
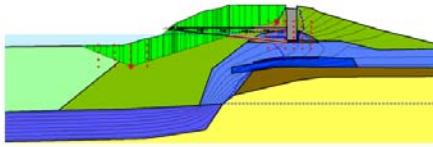
Section B1  FS = 1.36
Section B2  FS = 2.24
Section B3  FS = 2.03
Section C2  FS = 2.20
Section C3  FS = 1.64
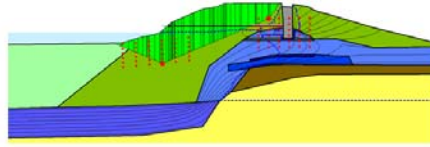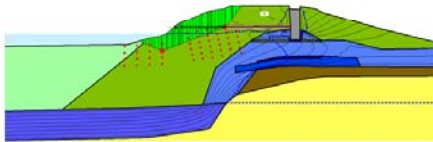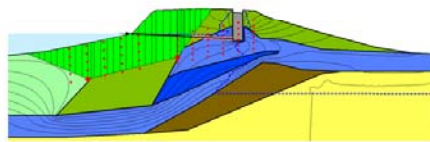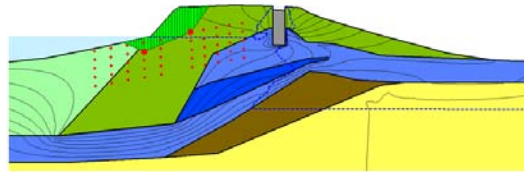


Waterside BC3 – 39 hr Transient Test Conditions, Without Tree
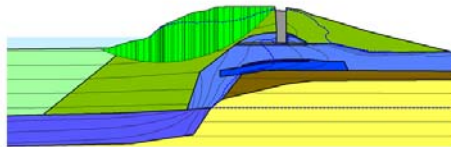
Section B1  FS = 1.69
Section B2  FS = 1.69
Section B3  FS = 0.98
Section C2  FS = 1.69
Section C3  FS = 0.98
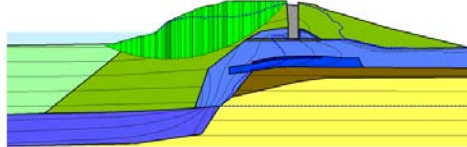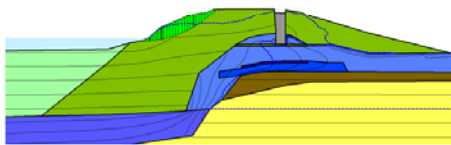
4B-7
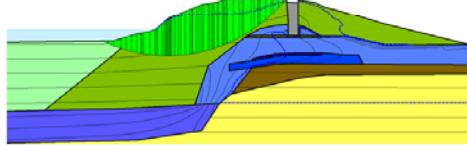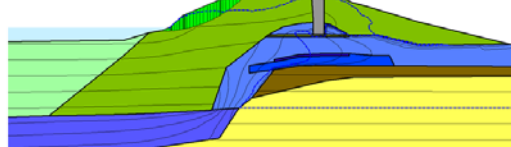
# APPENDIX 6A

## Ground motion Data

1979 Imperial Valley, Brawley Airport 225
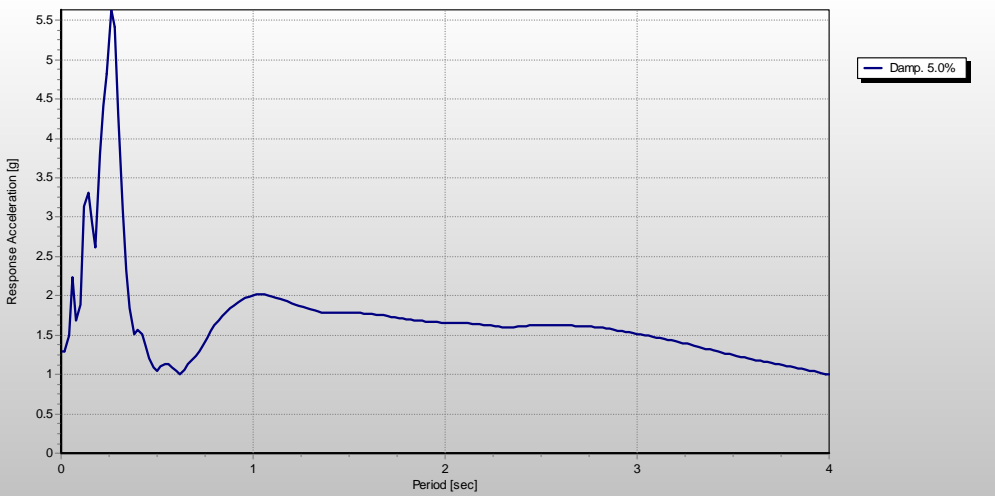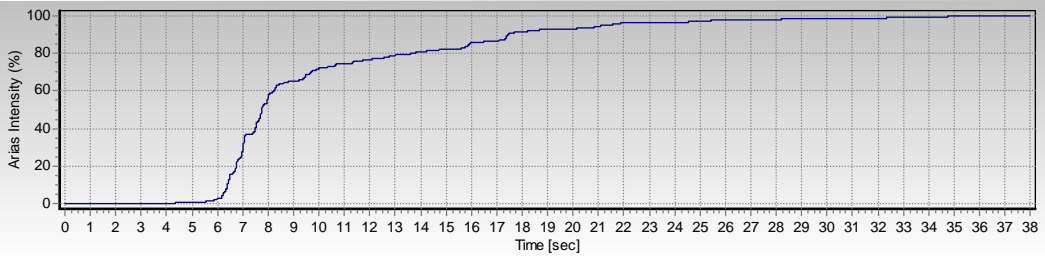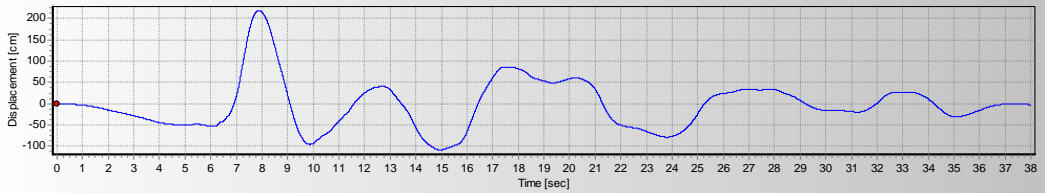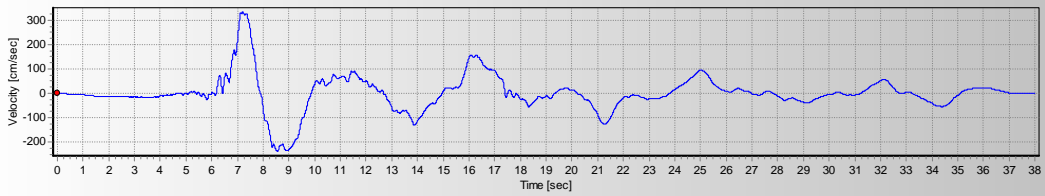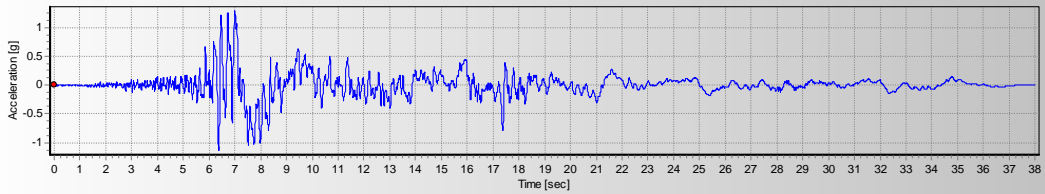
# 1994 Northridge, Sylmar – Conv Sta 052 scaled to 1.25x
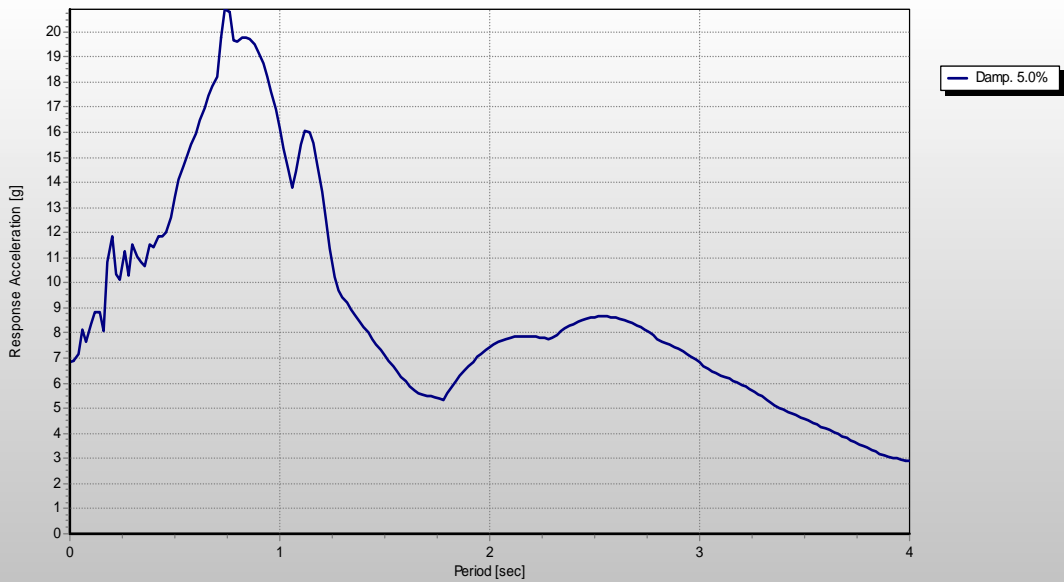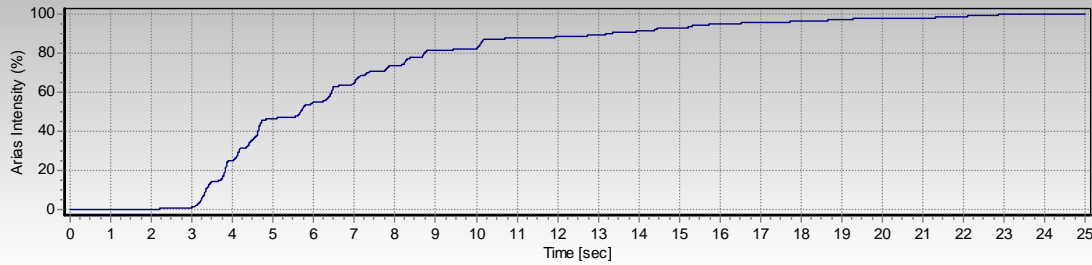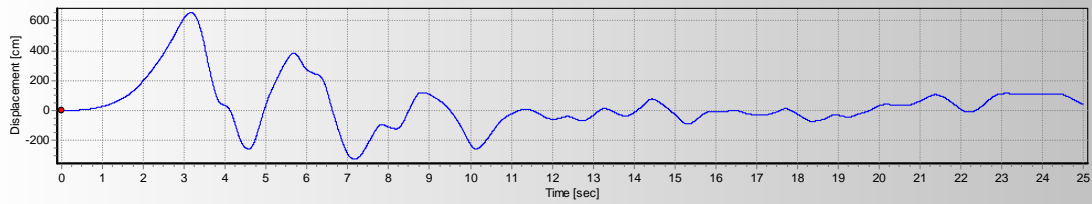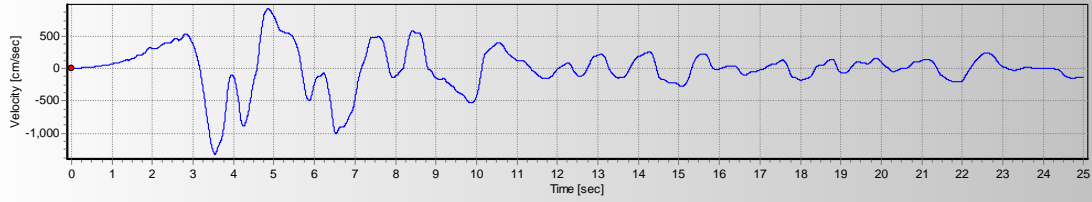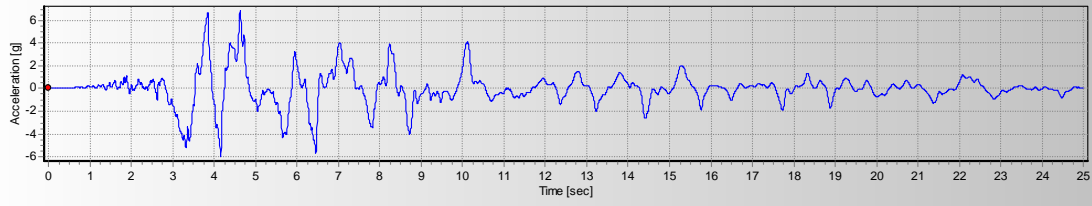
# 1987 Superstition Hills, Superstition Mountain Camera 045
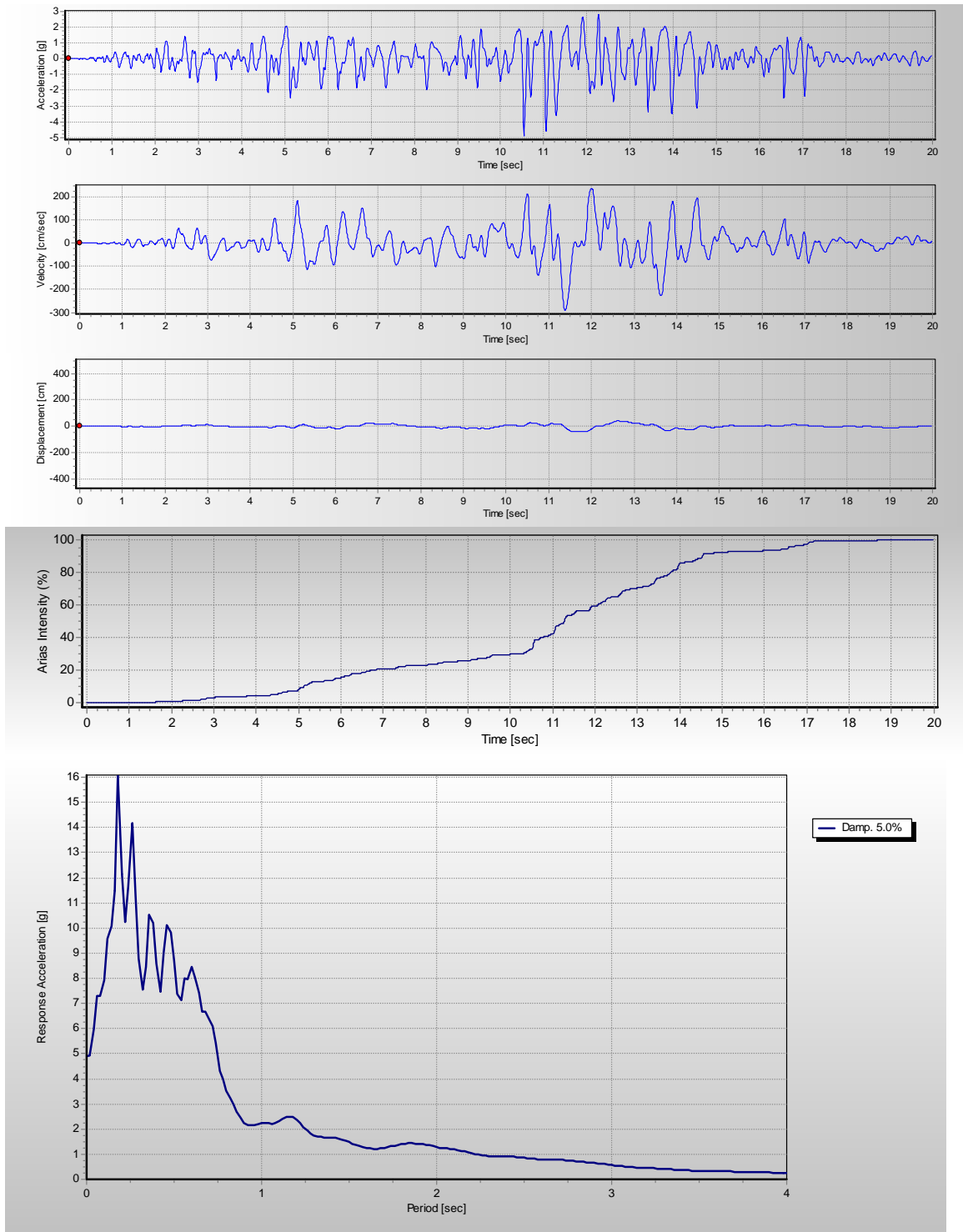
# 92 Landers, Joshua Tree 090 – Scaled by 0.75x
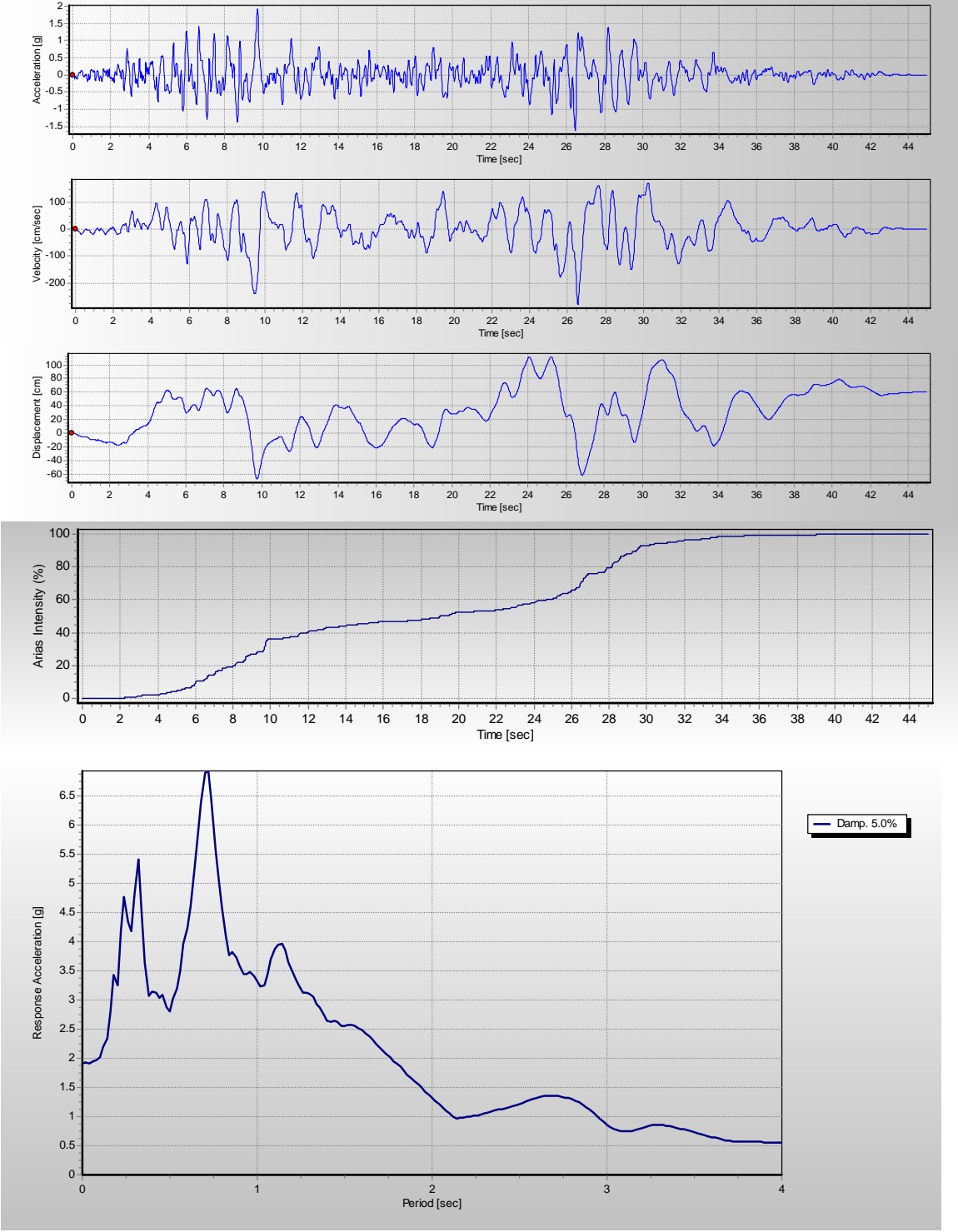
# 92 Landers, Joshua Tree 090 – Scaled by 1.0x
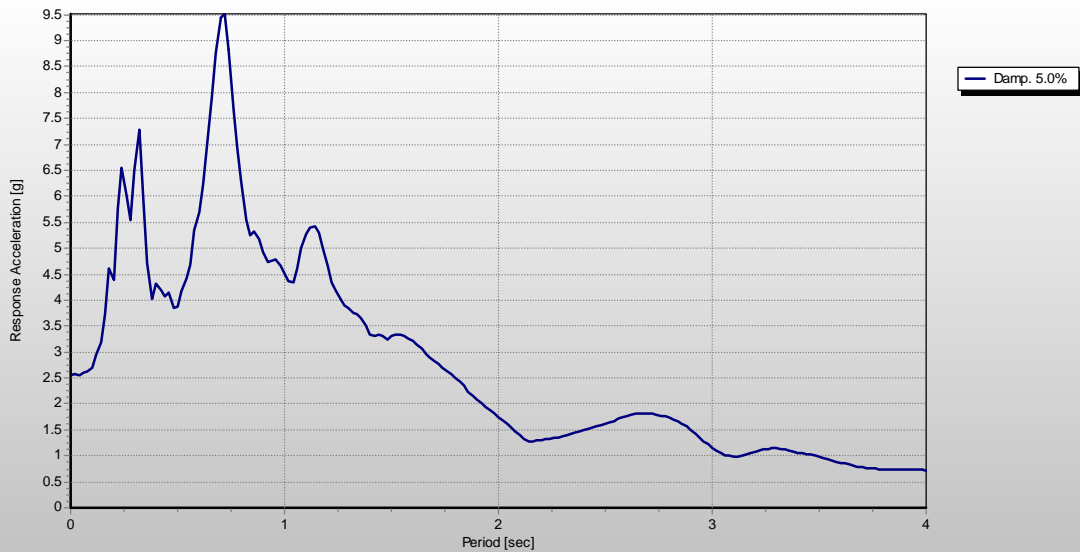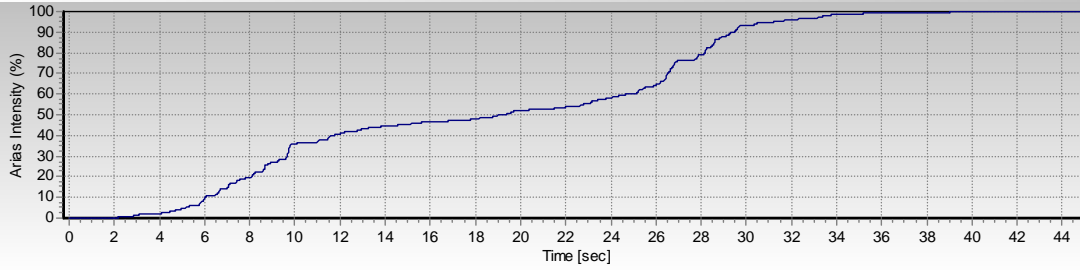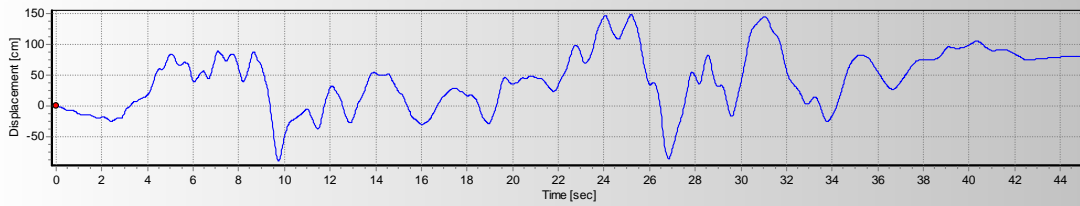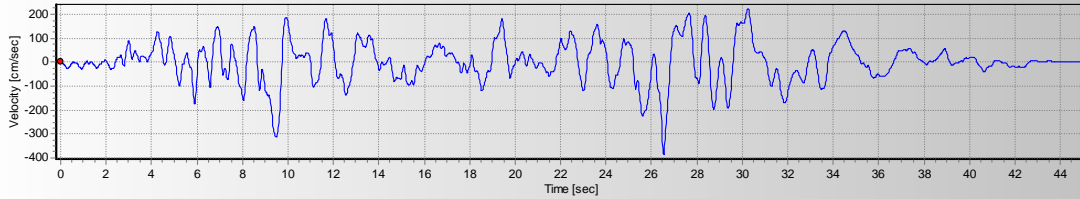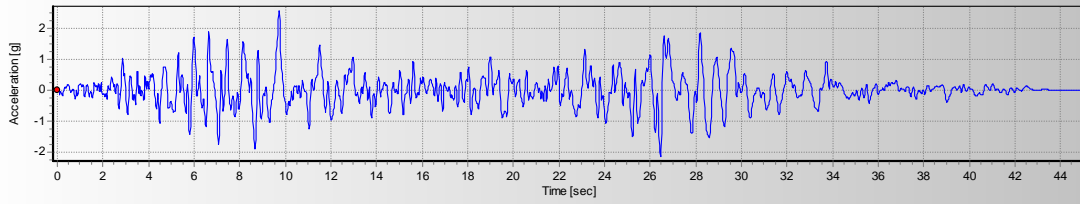
# 92 Landers, Joshua Tree 090 – Scaled by 1.5x
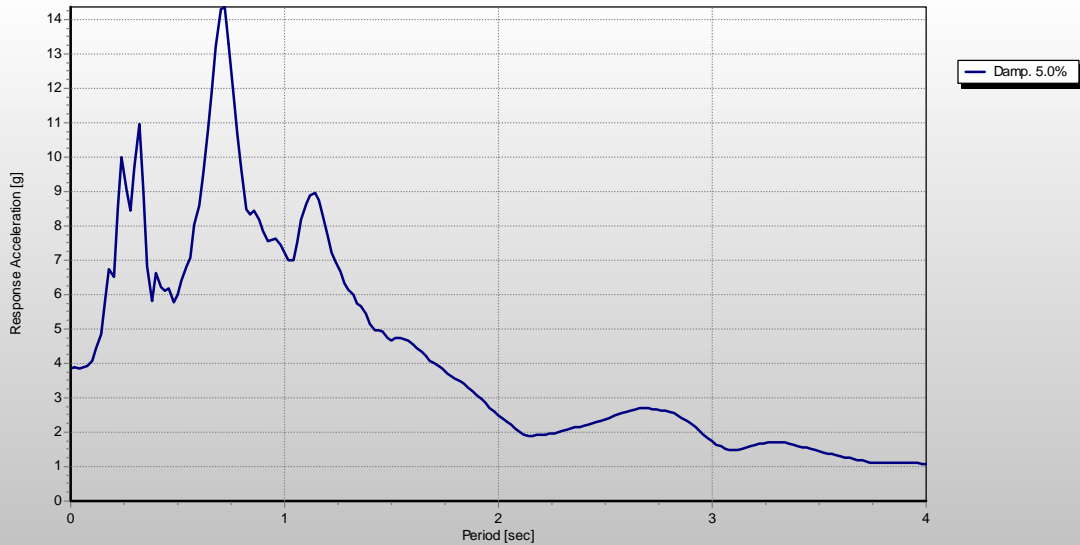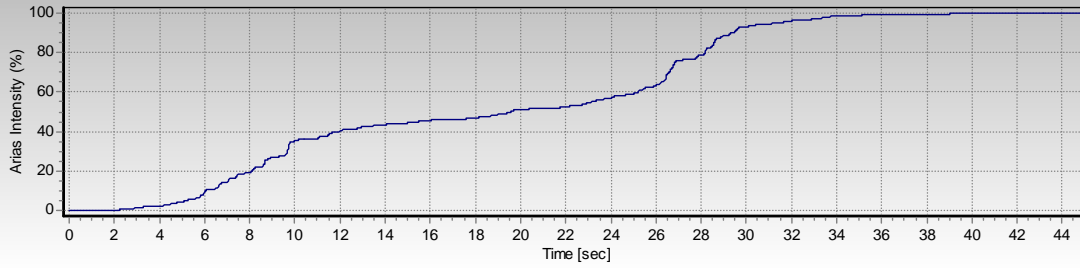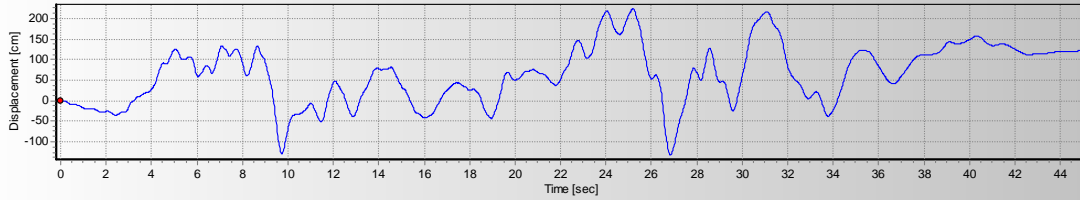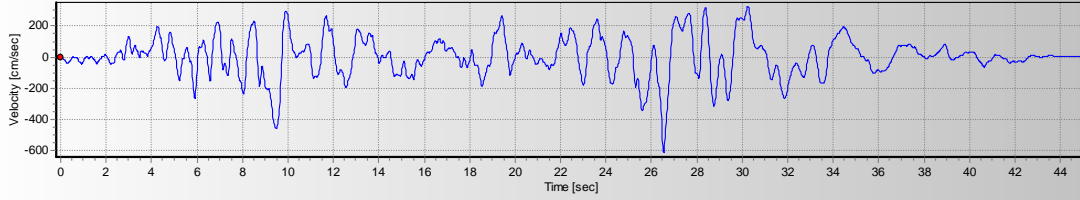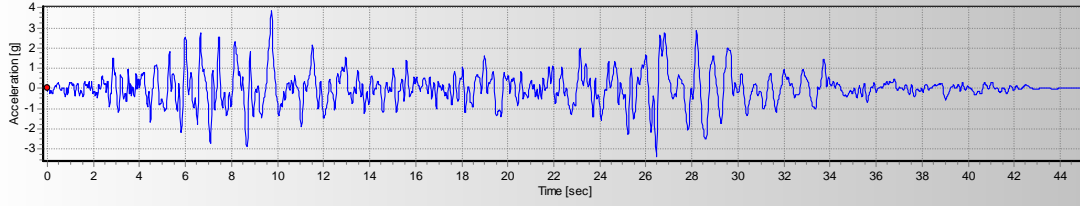
# 1992 Landers, Lucerne 260
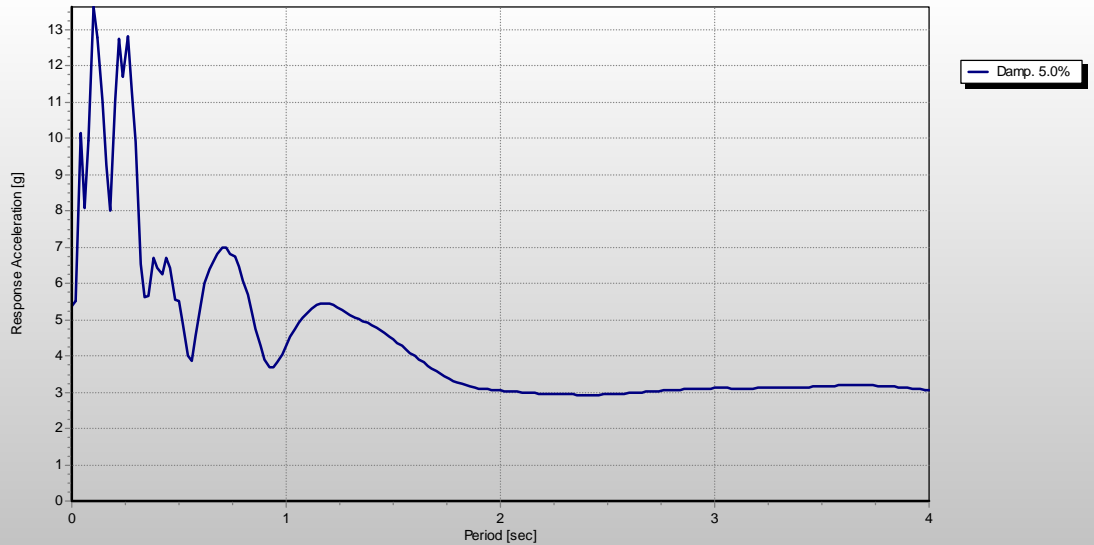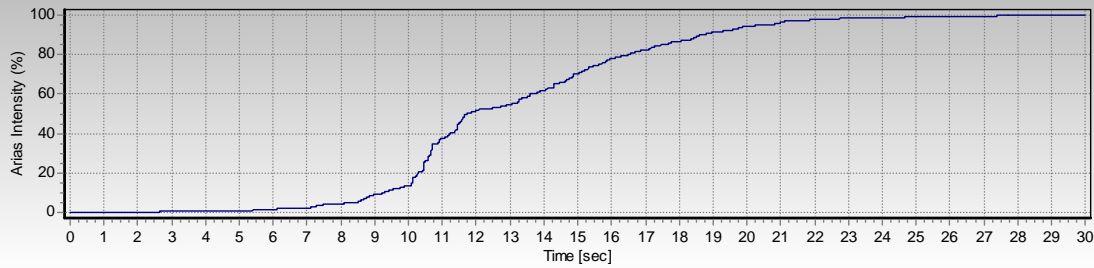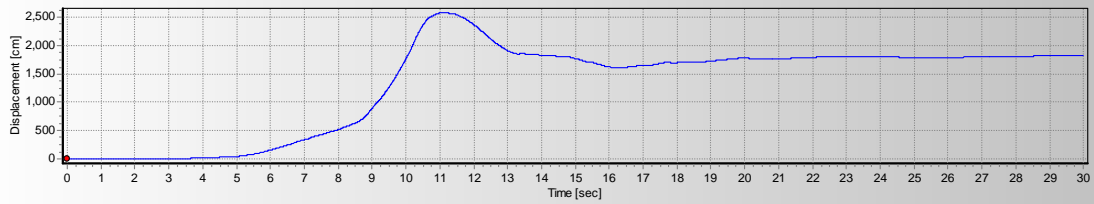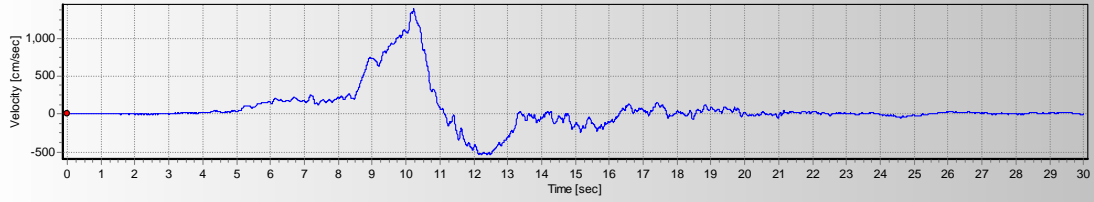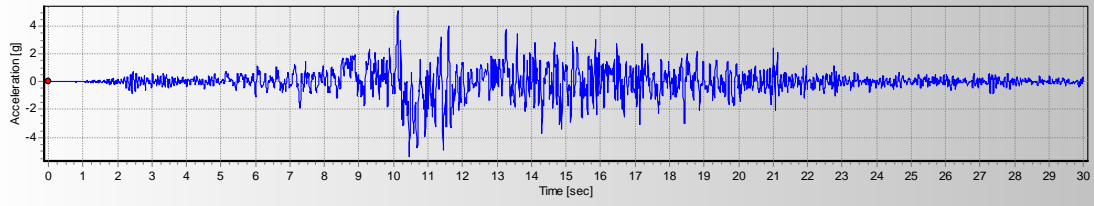
1989 Loma Prieta EQ, LGP
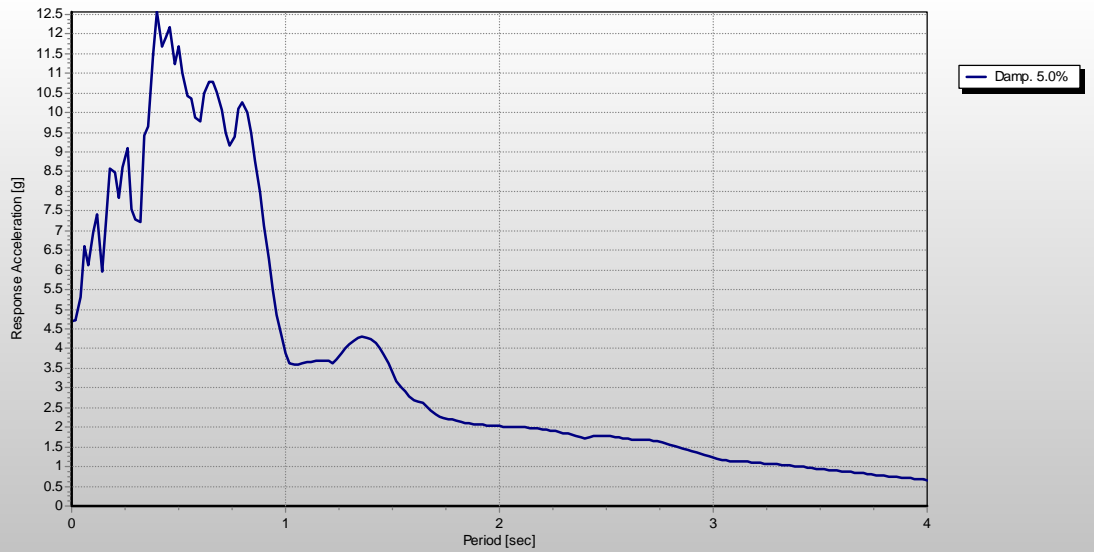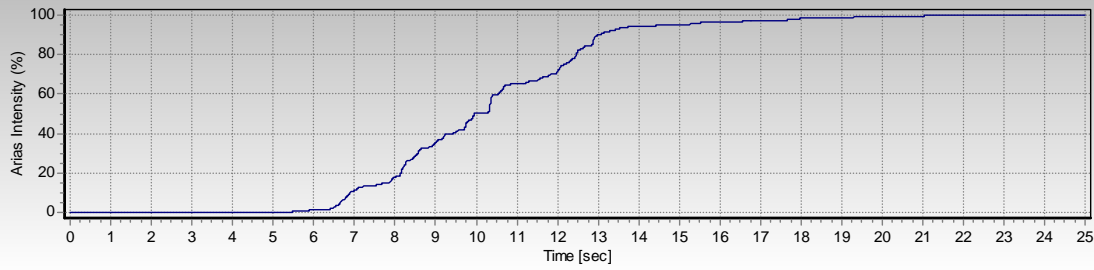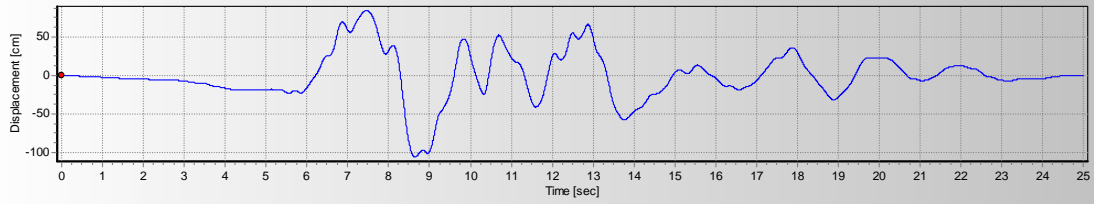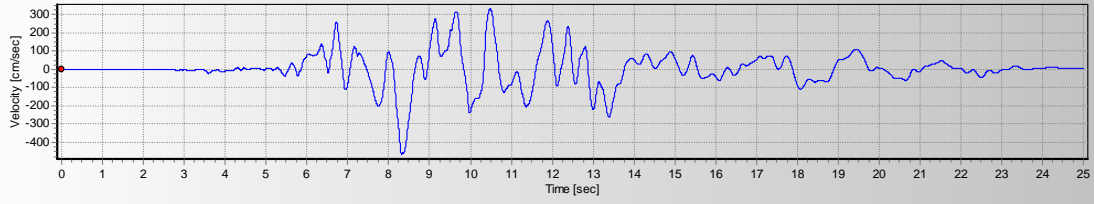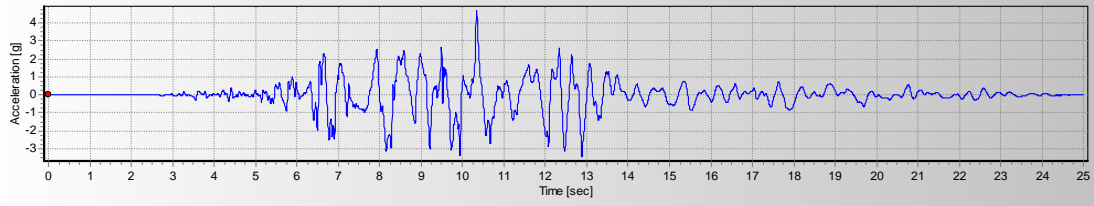
1971 San Fernando EQ, Hollywood Storage Facility,
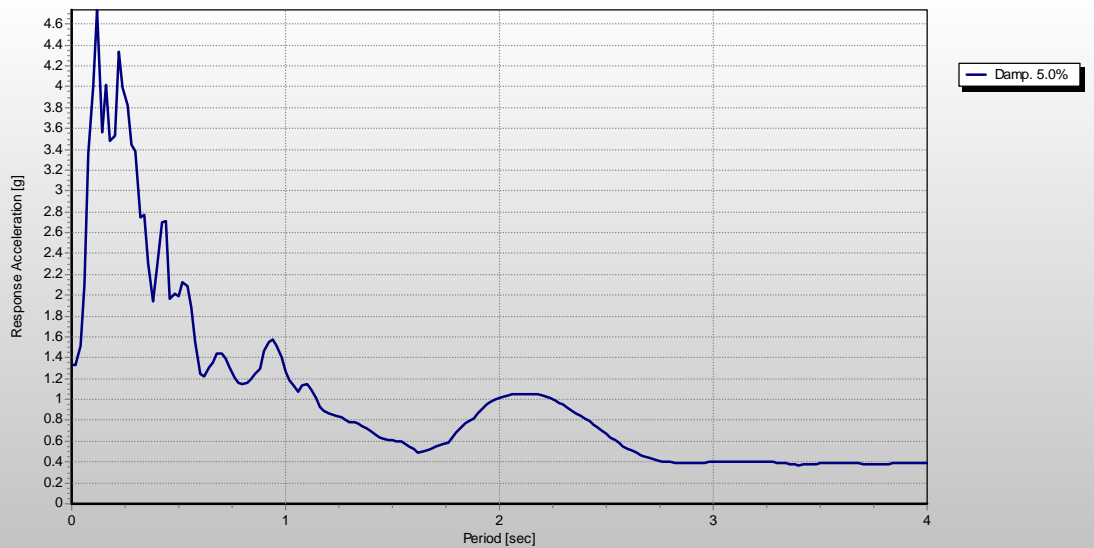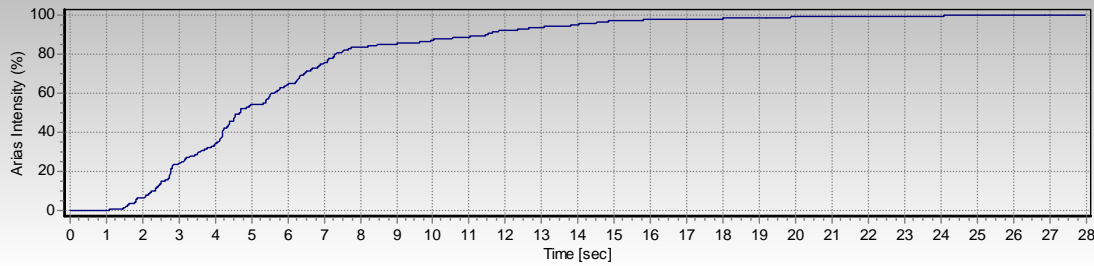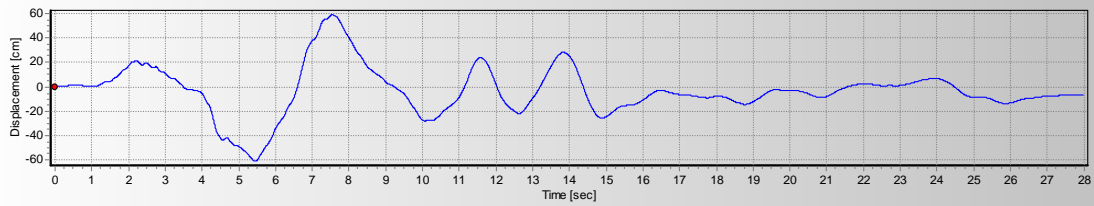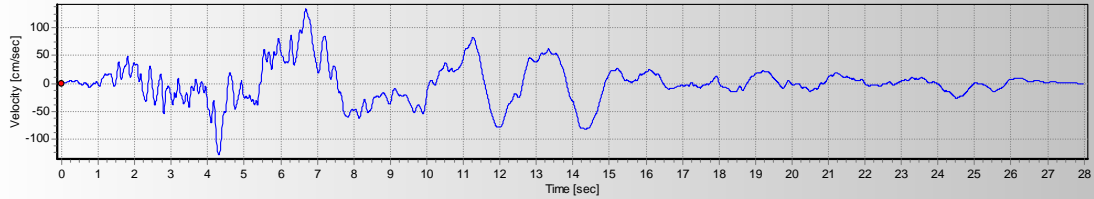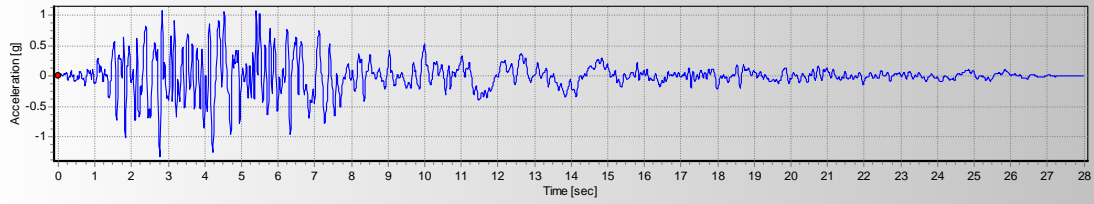
# Superstition Hills, Parachute T S
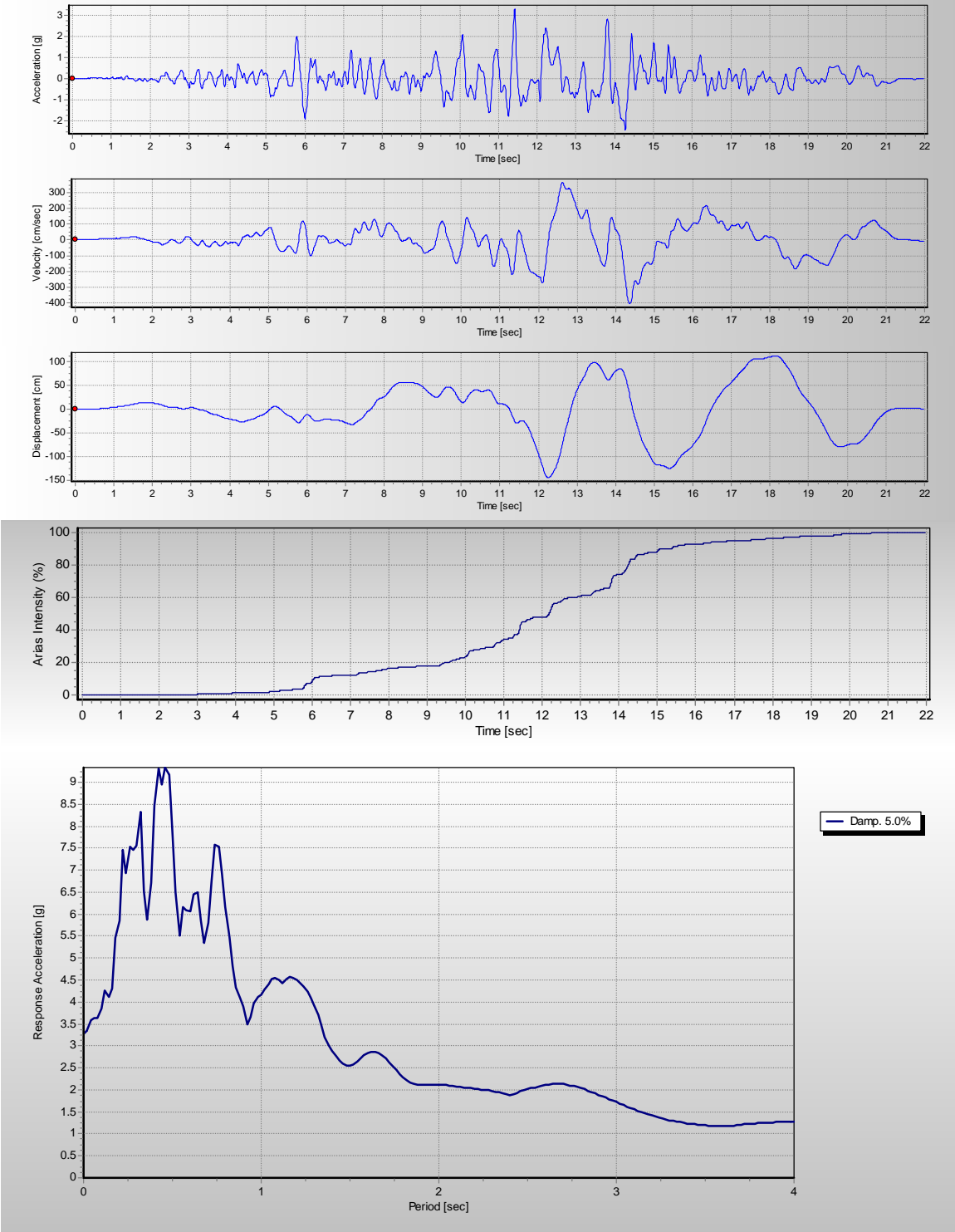
# 1994 Northridge, Rinaldi R Sta 228
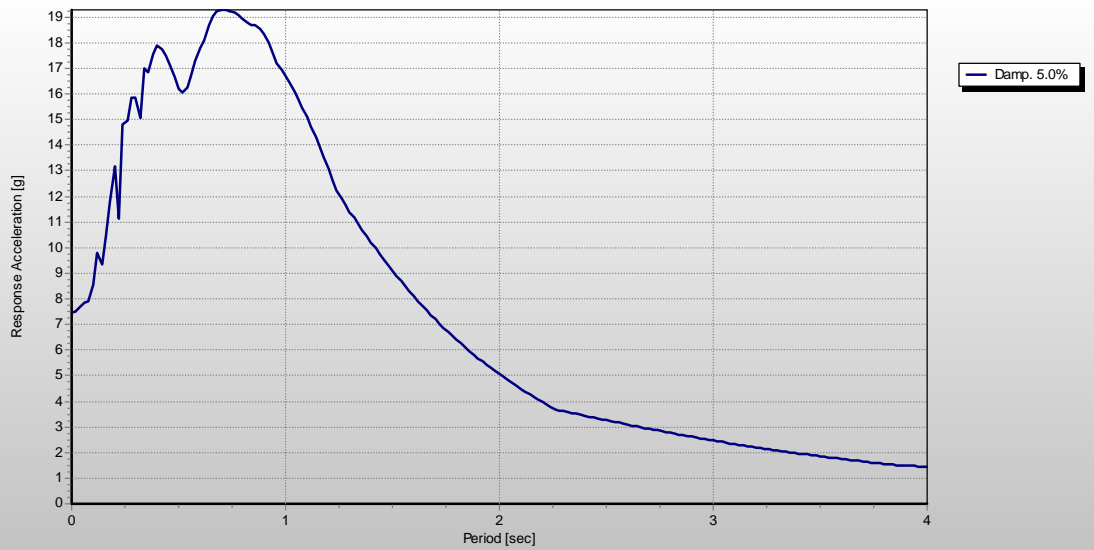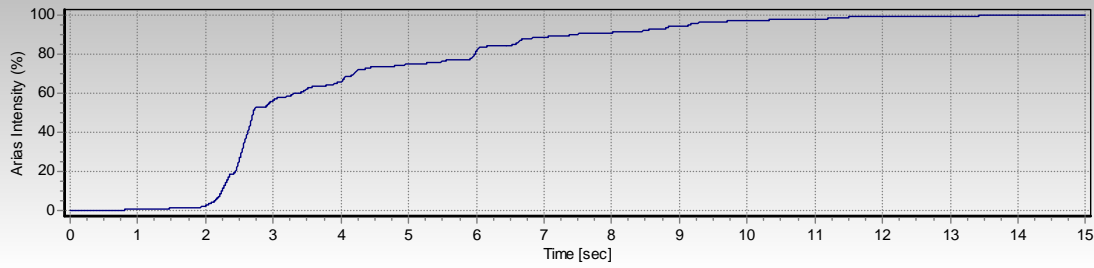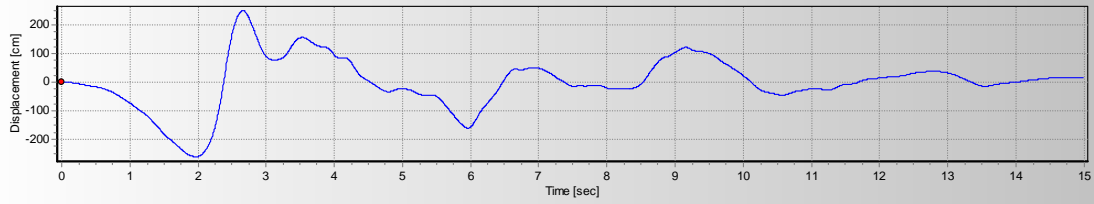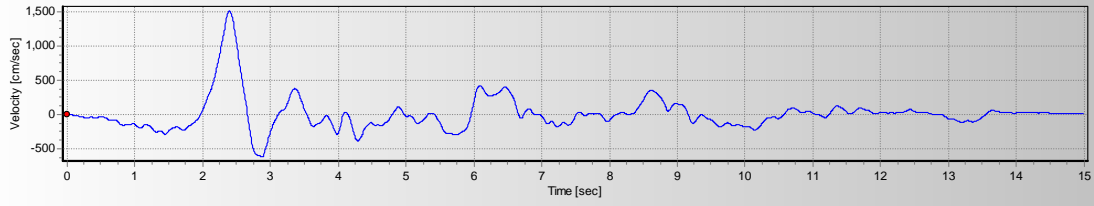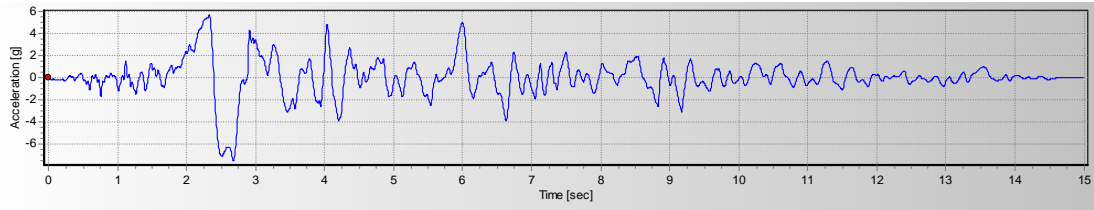
# 1994 Northridge, Sylmar – Conv Sta 052 scaled to 0.5x
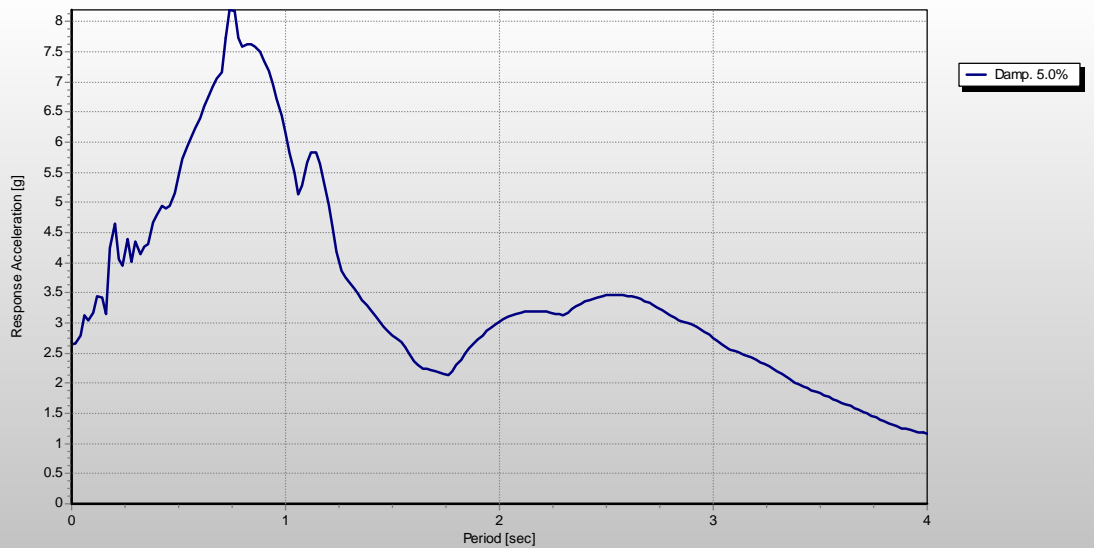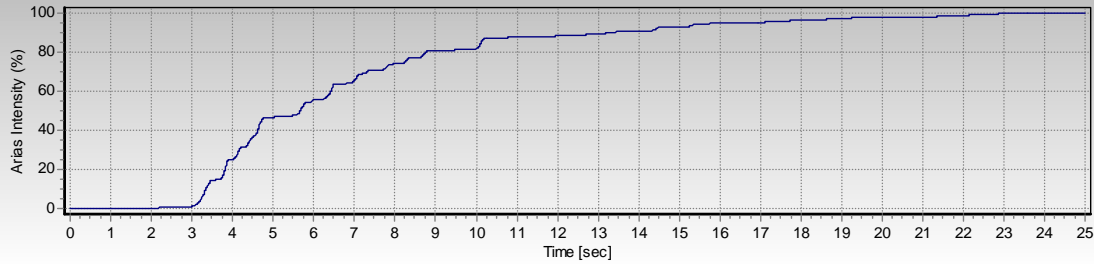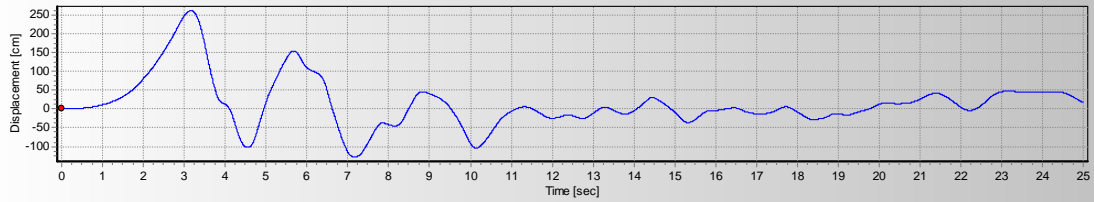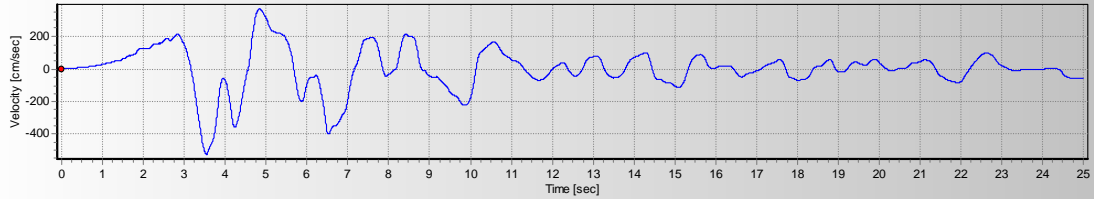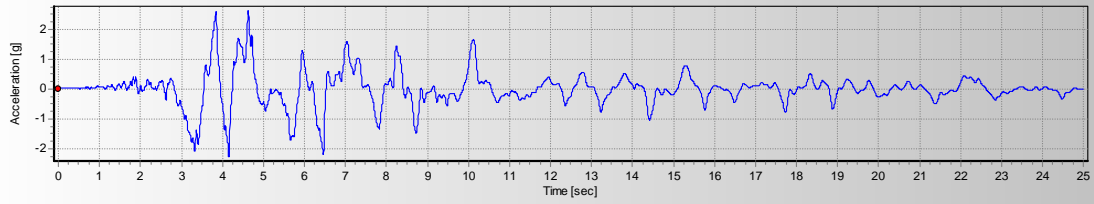
## 1994 Northridge, Sylmar – Conv Sta 052 scaled to 1.0x
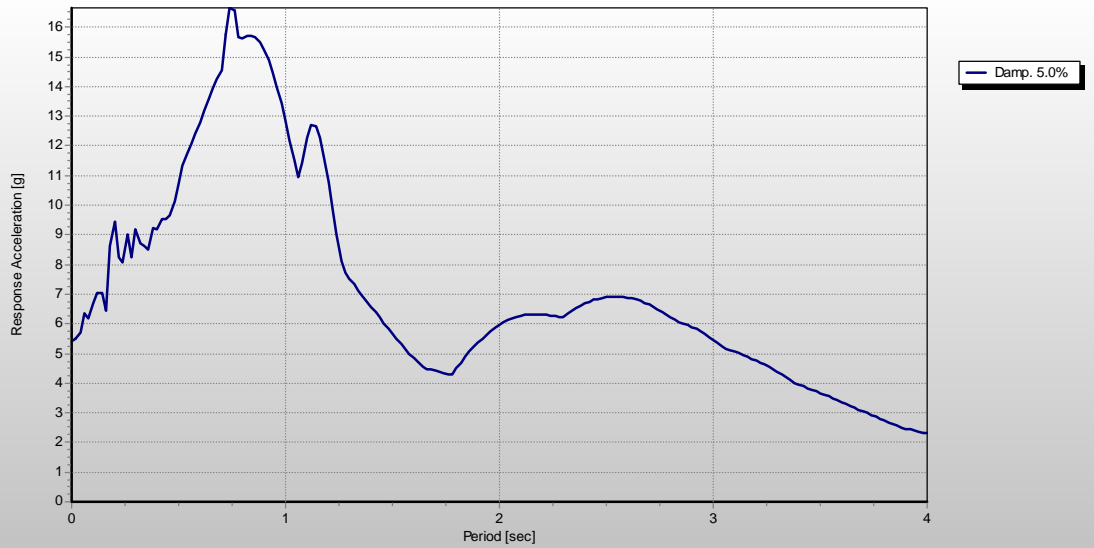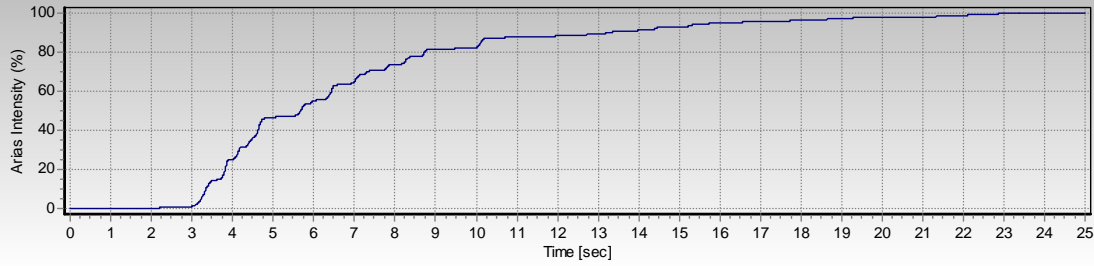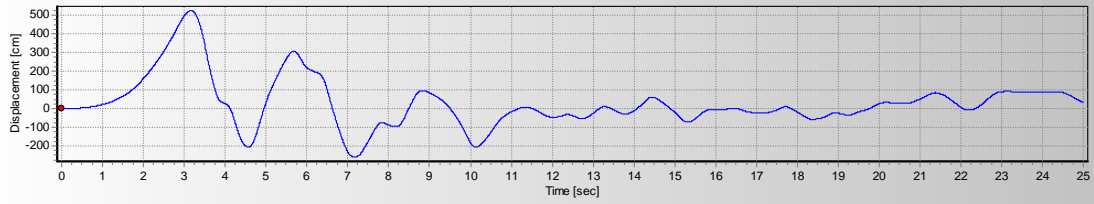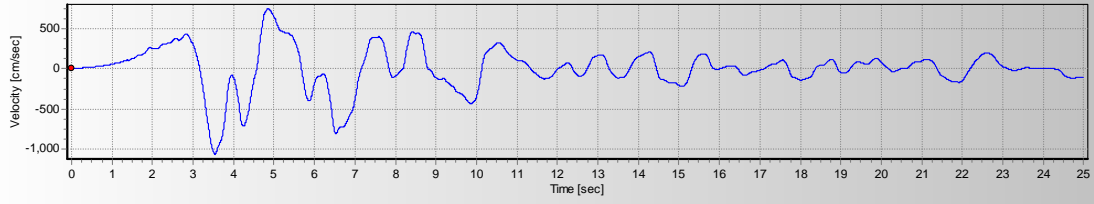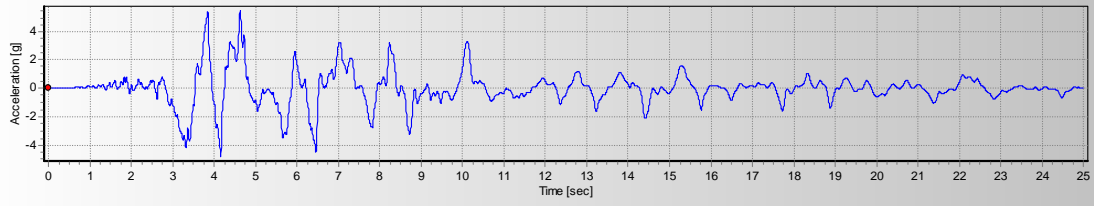
# 1994 Northridge, Sylmar – Conv Sta 052 scaled to 1.25x
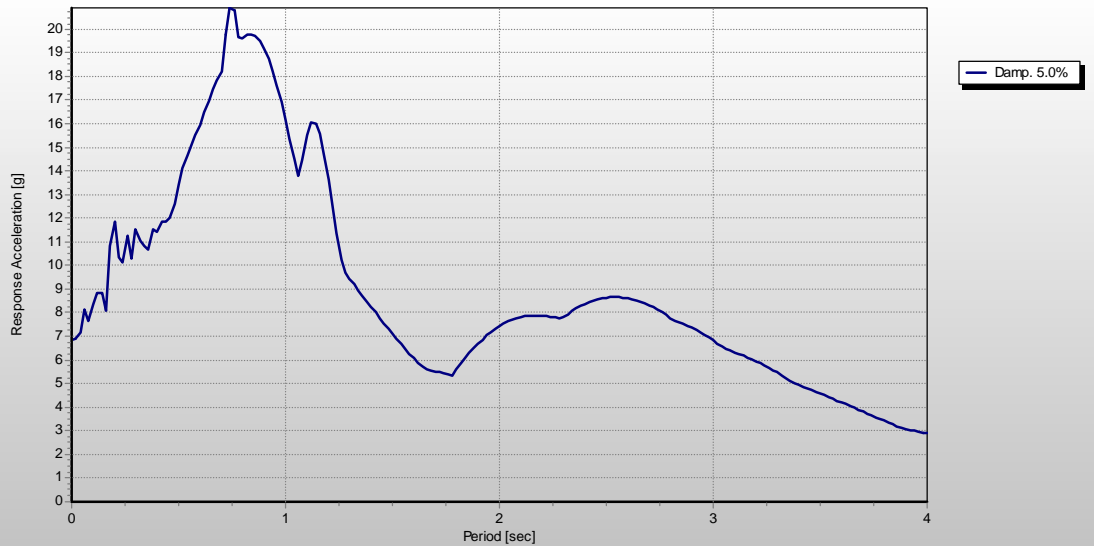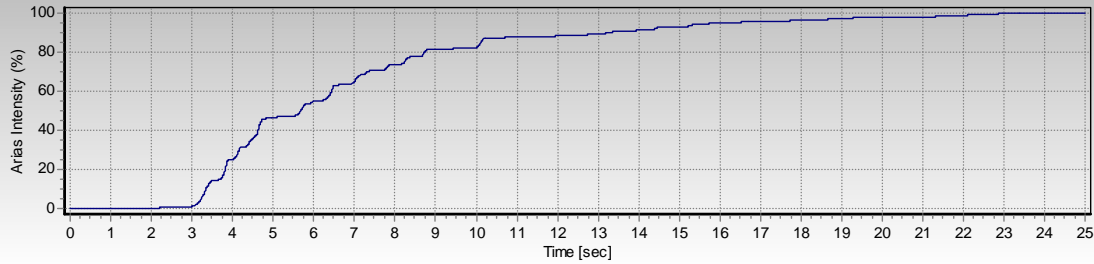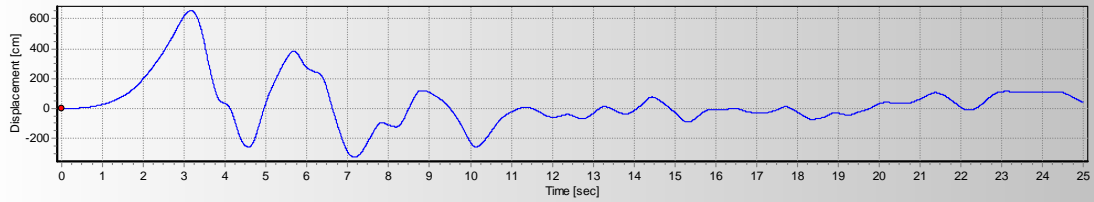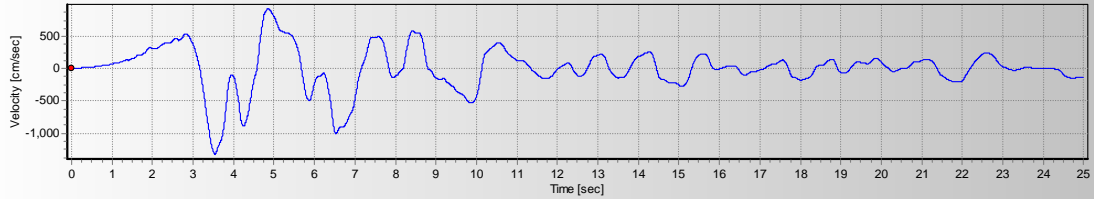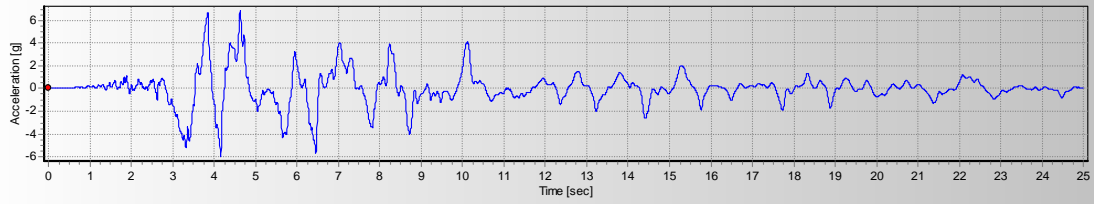
# TCU078, 1999 Chi-Chi, Taiwan Earthquake
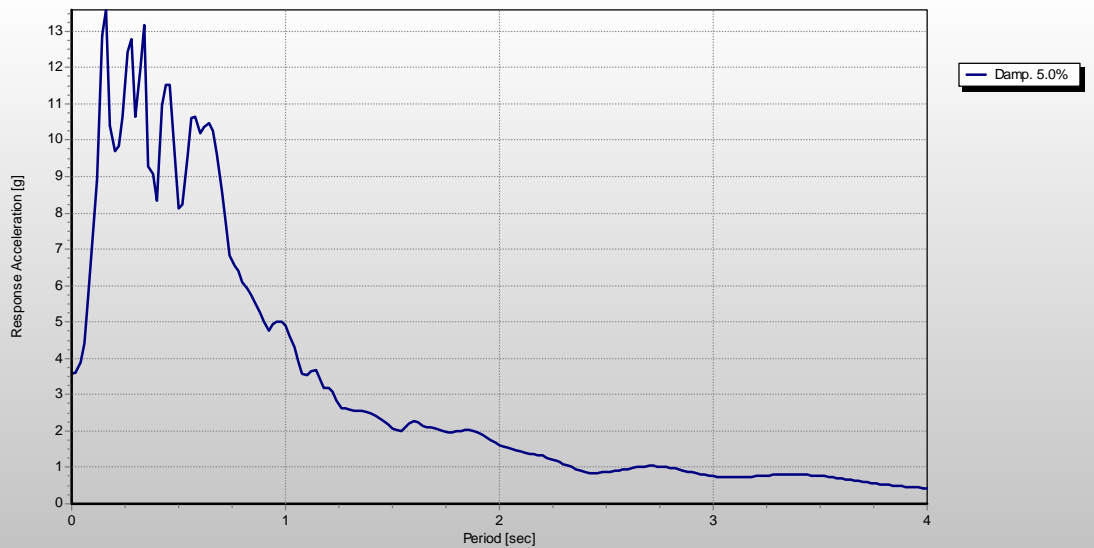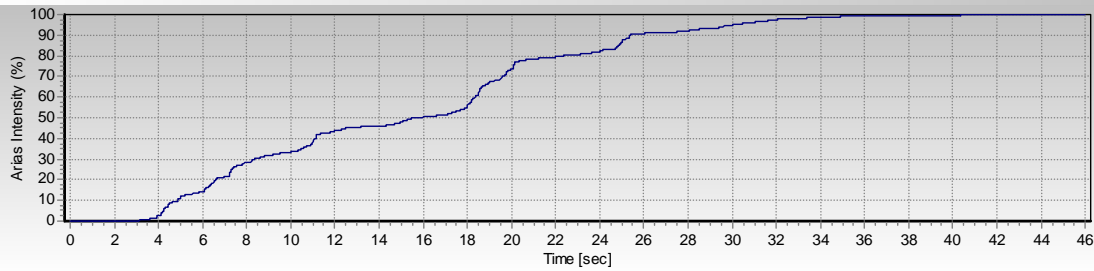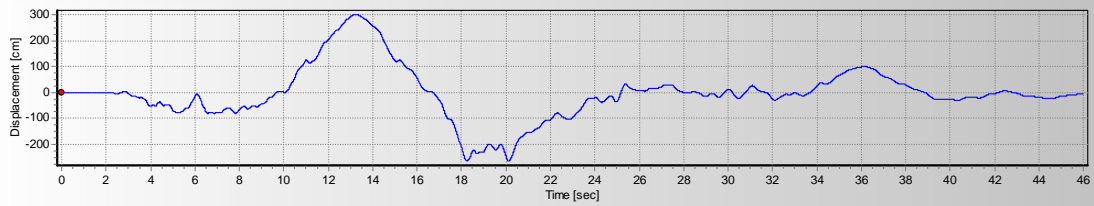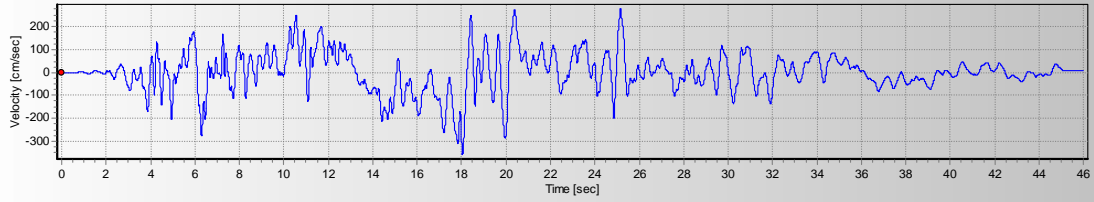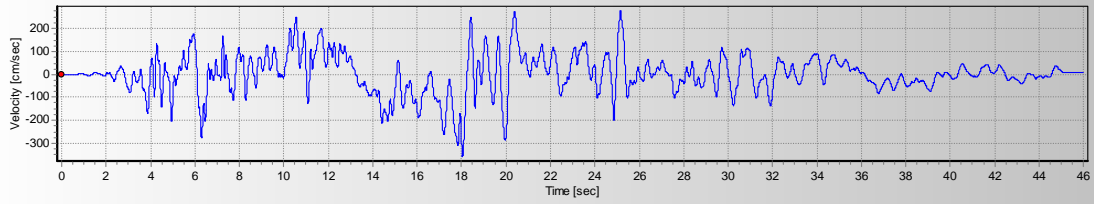
# 1994 Northridge EQ, Newhall W. Pico Canyon 046
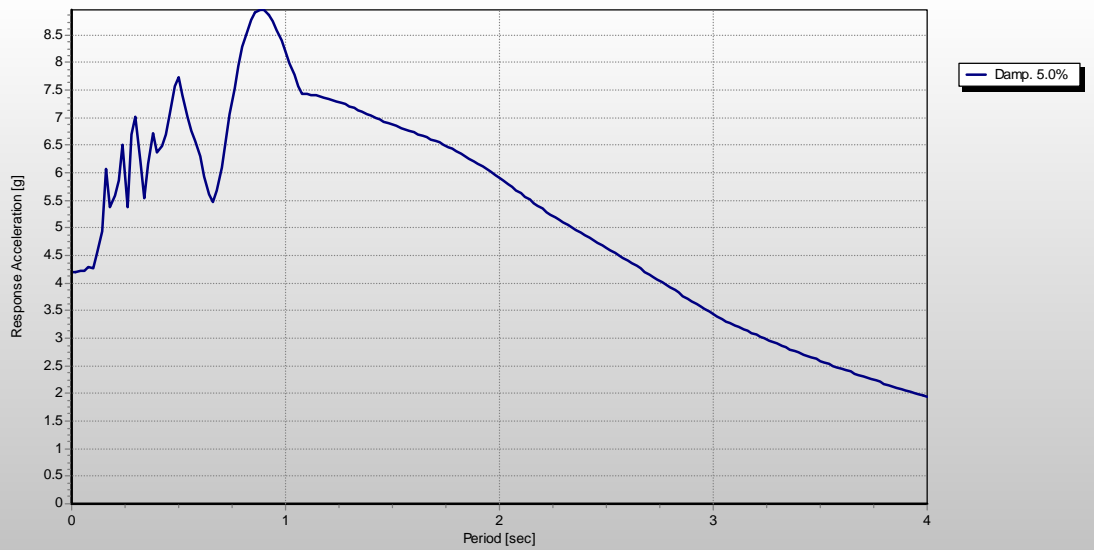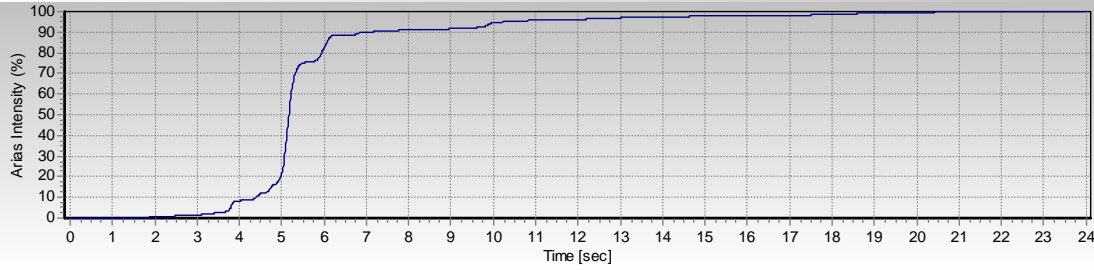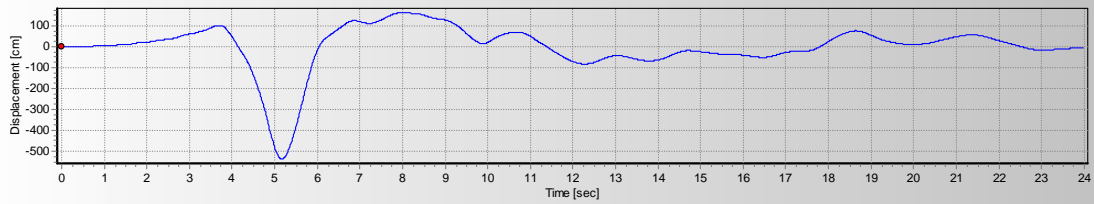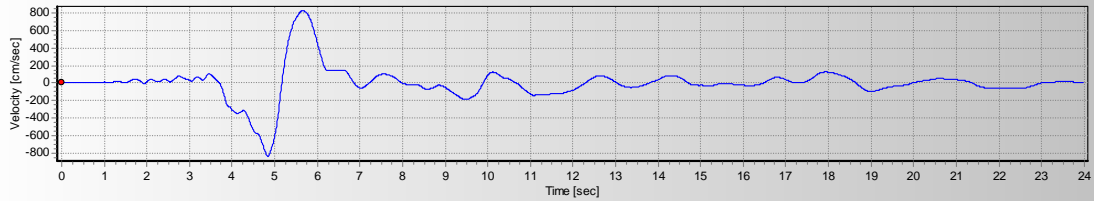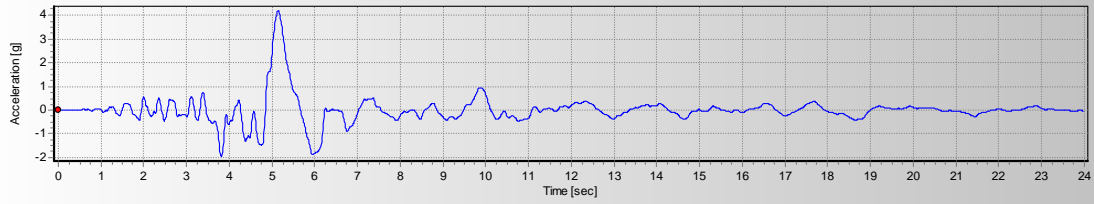
# 1989 Loma Prieta EQ, Saratoga WV Coll 270
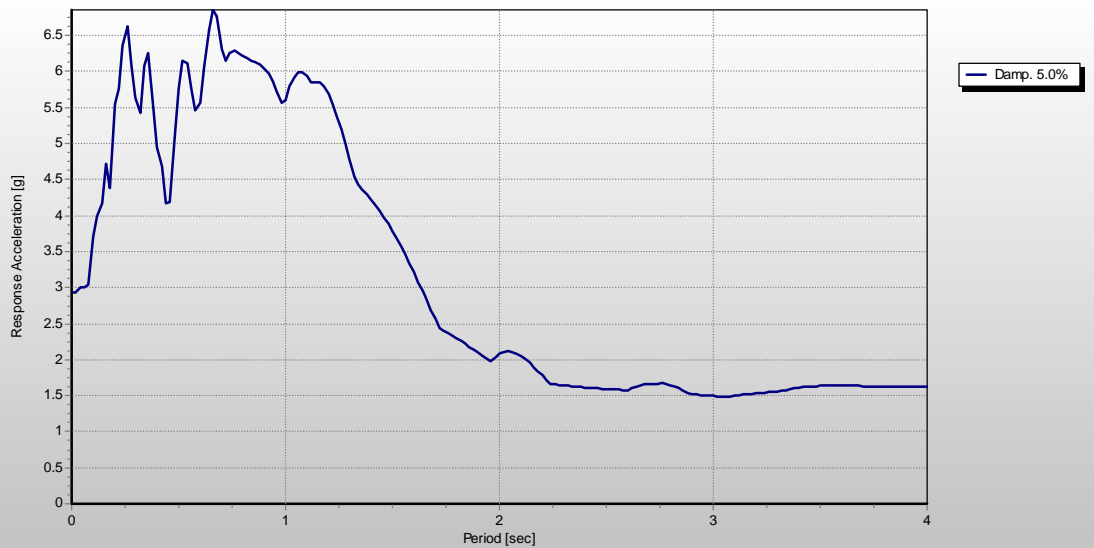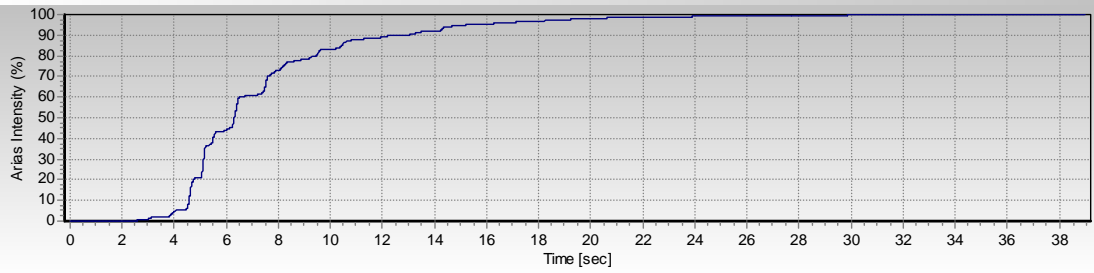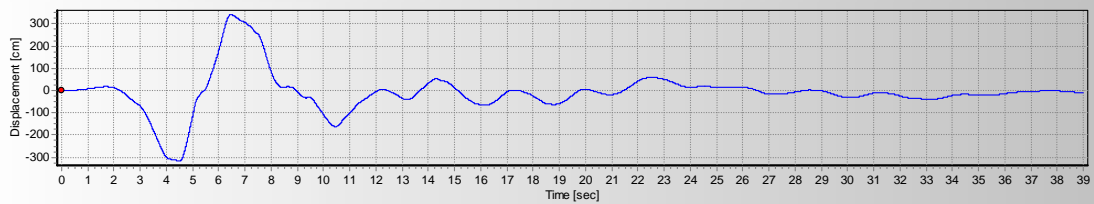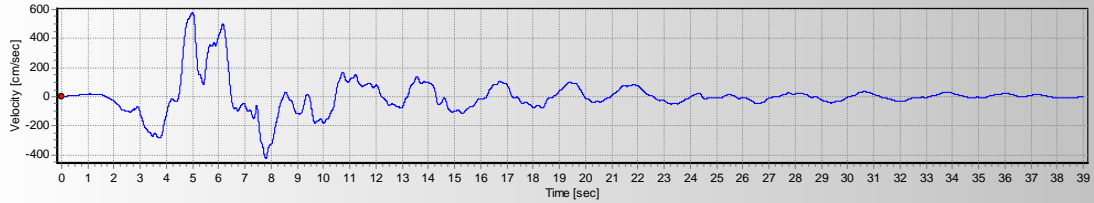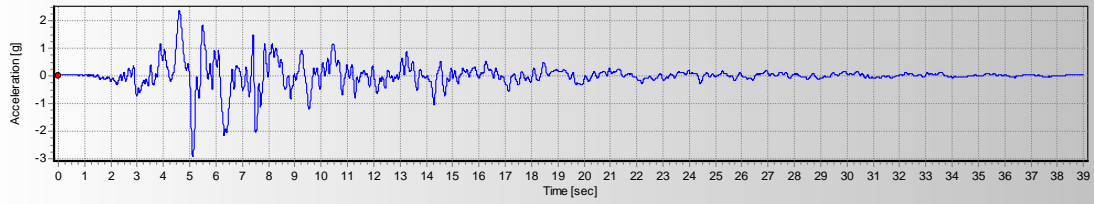
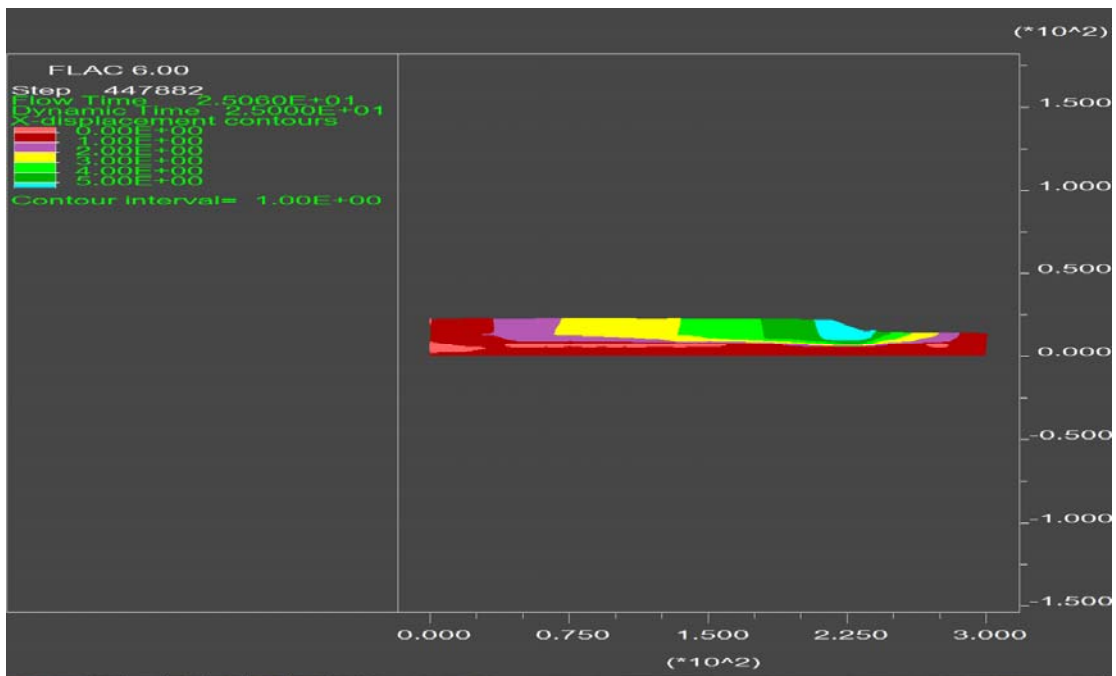# APPENDIX 6B

## Sensitivity Analysis X-Displacement Data
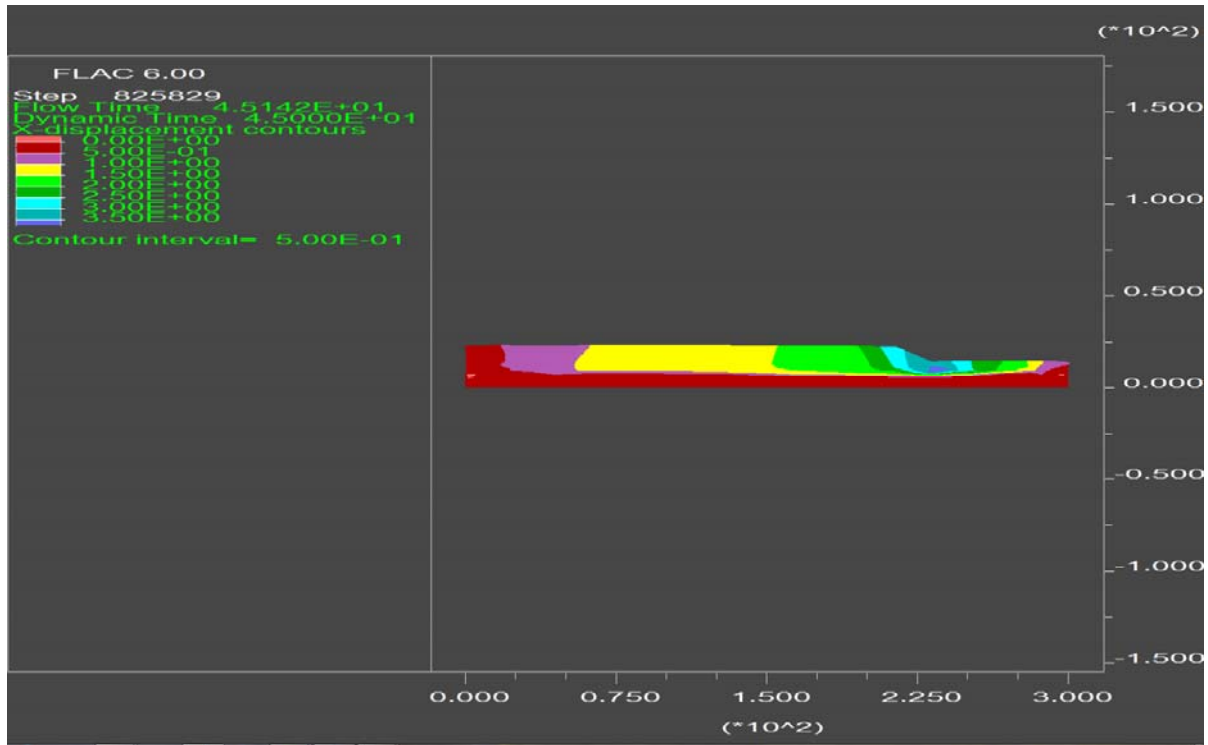


**Figure 6B-1. Contours of calculated lateral displacement (9 m embankment height, 8 meter liquefiable silt layer, clean sand corrected $(N_1)_{60\text{-cs}}$ blowcount of 8, ground motion = 92 Landers Joshua Tree 090 Scale 1.0x).**
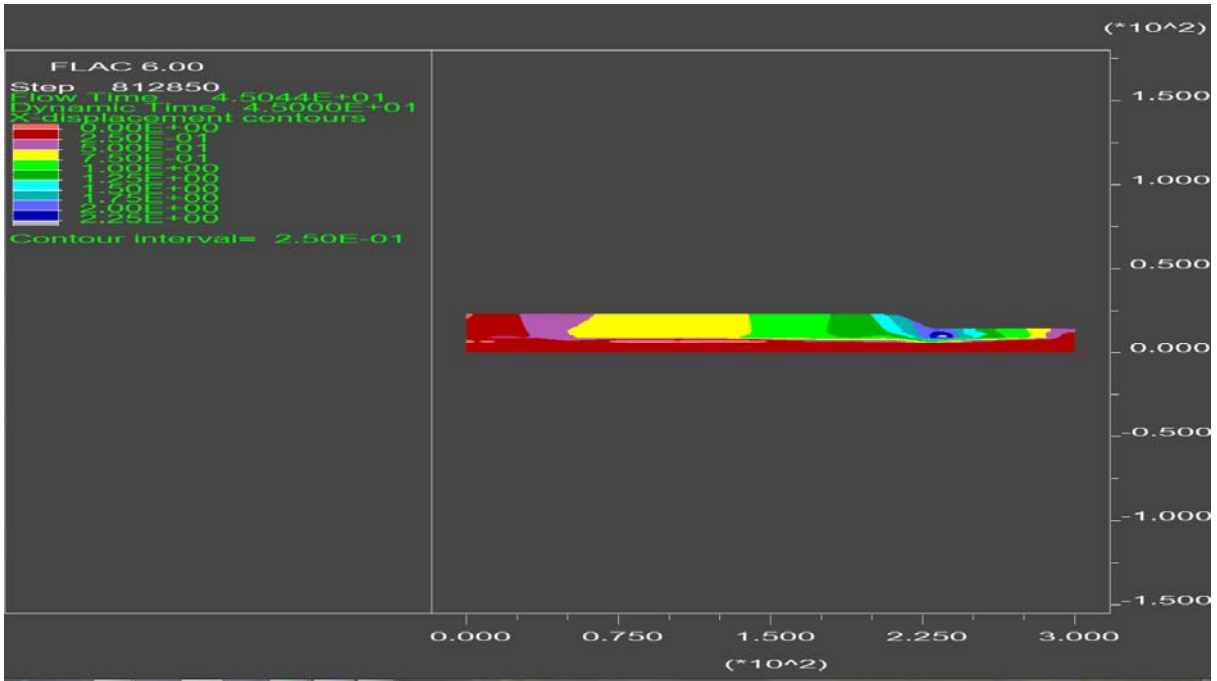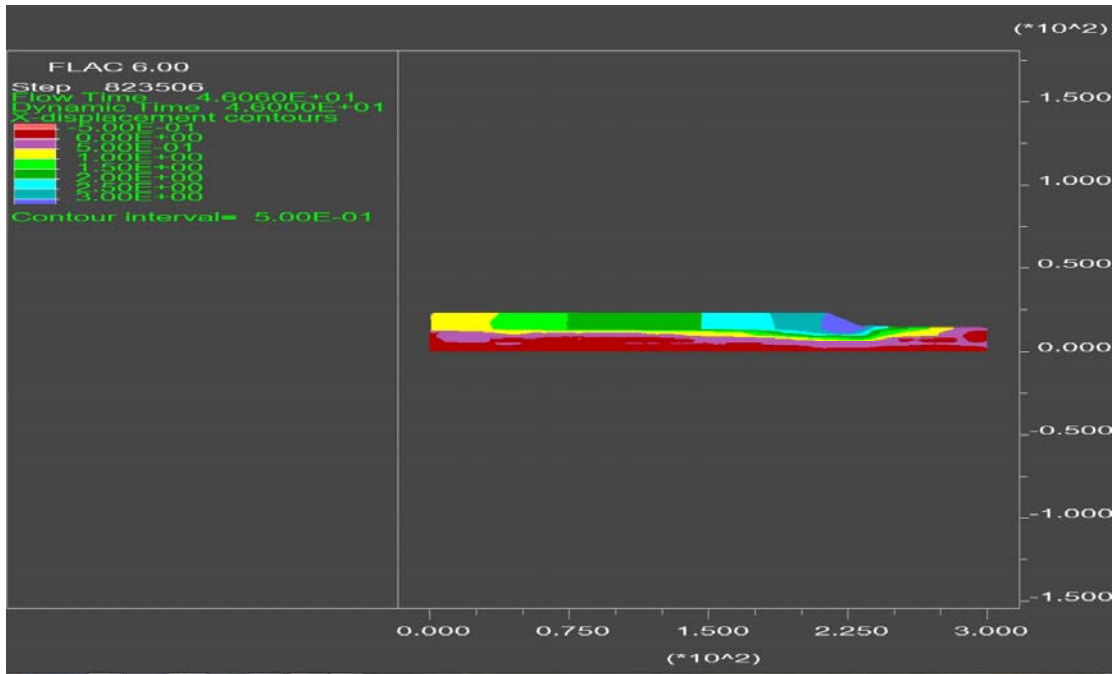
**Figure 6B-2. Contours of calculated lateral displacement (9 m embankment height, 8 meter liquefiable silt layer, clean sand corrected $(N_1)_{60\text{-cs}}$ blowcount of 15, ground motion = 92 Landers Joshua Tree 090 Scale 1.0x).**
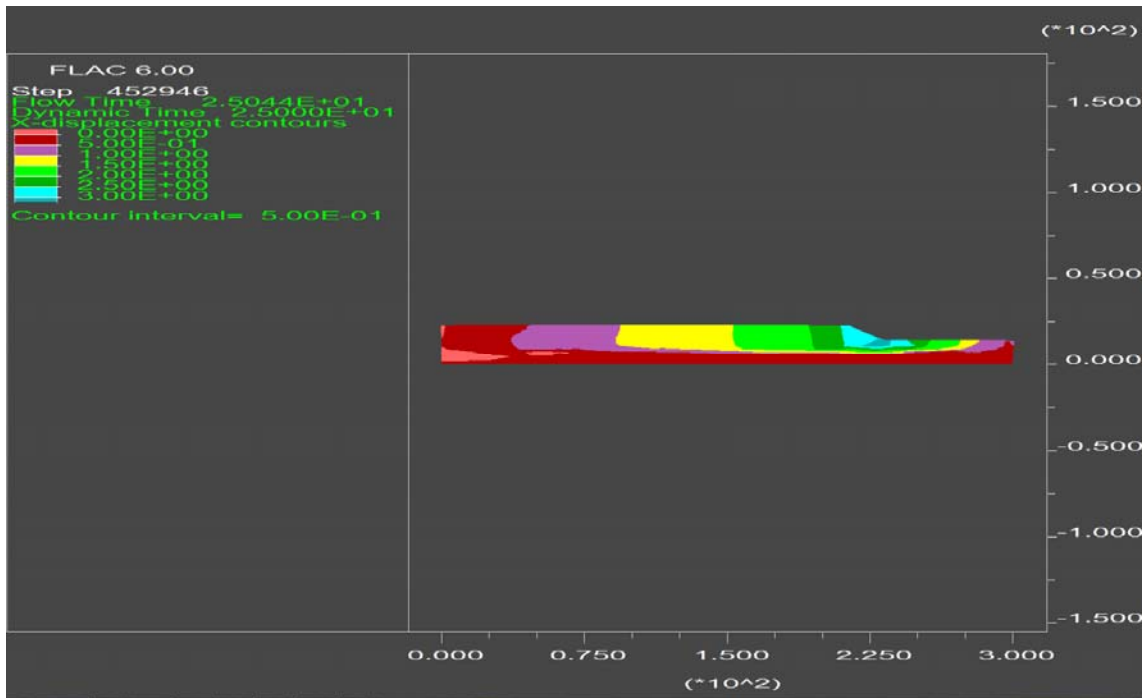


**Figure 6B-3. Contours of calculated lateral displacement (9 m embankment height, 8 meter liquefiable silt layer, clean sand corrected $(N_1)_{60\text{-cs}}$ blowcount of 15, ground motion = 94 Northridge Sylmar - Conv Sta 052 Scale 1.0x).**
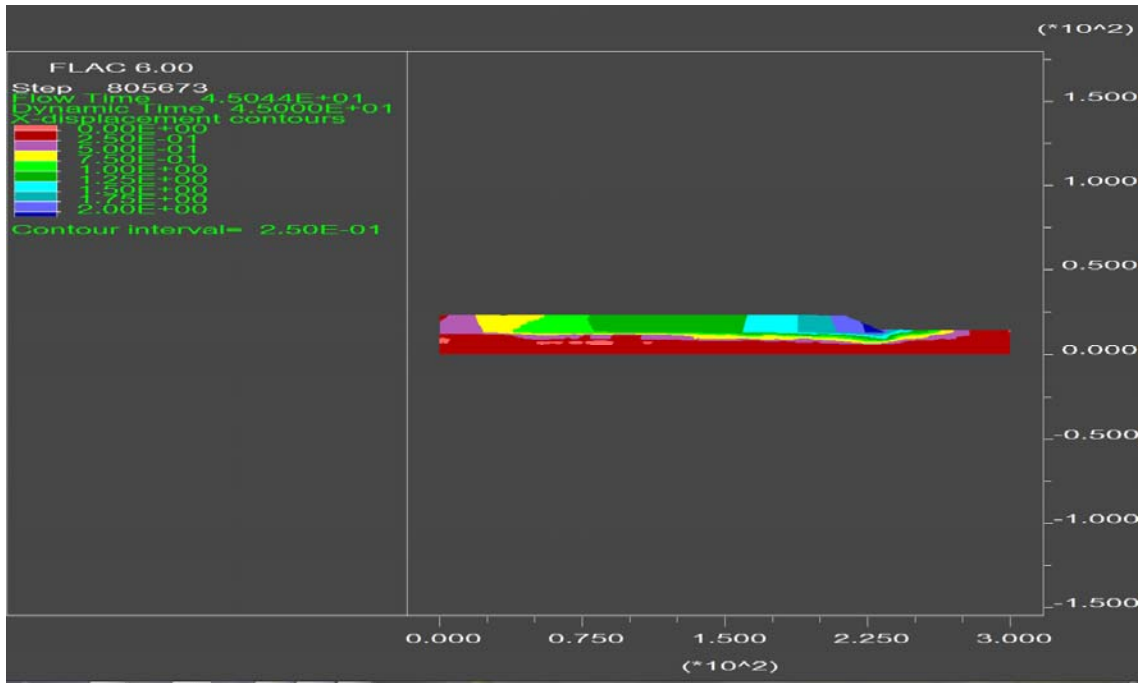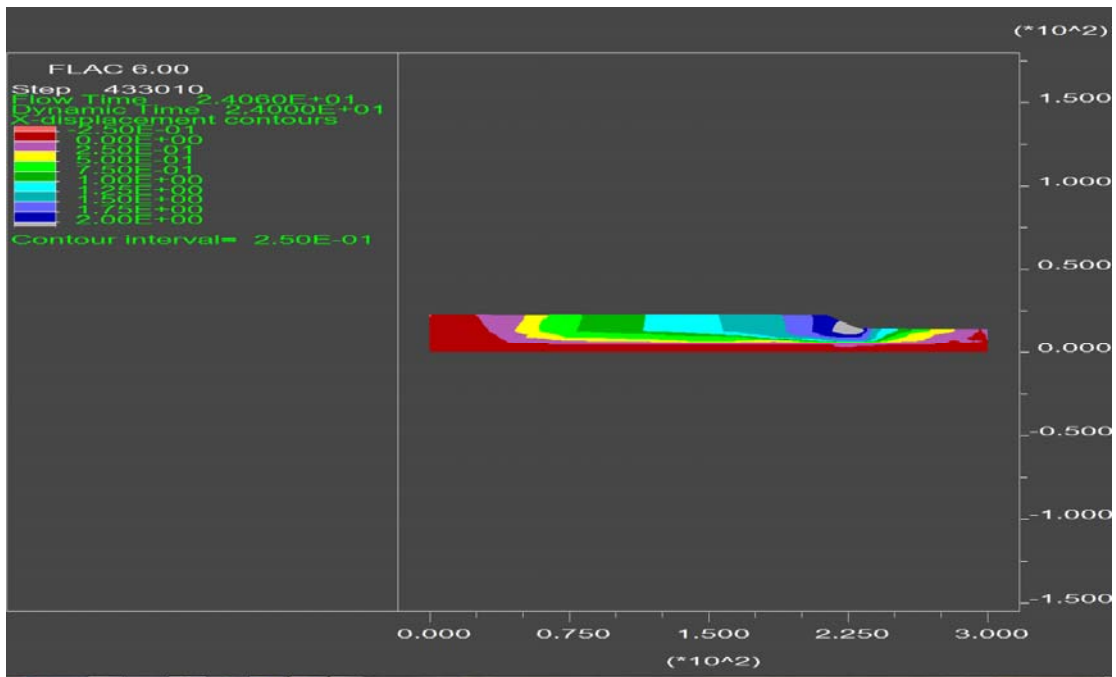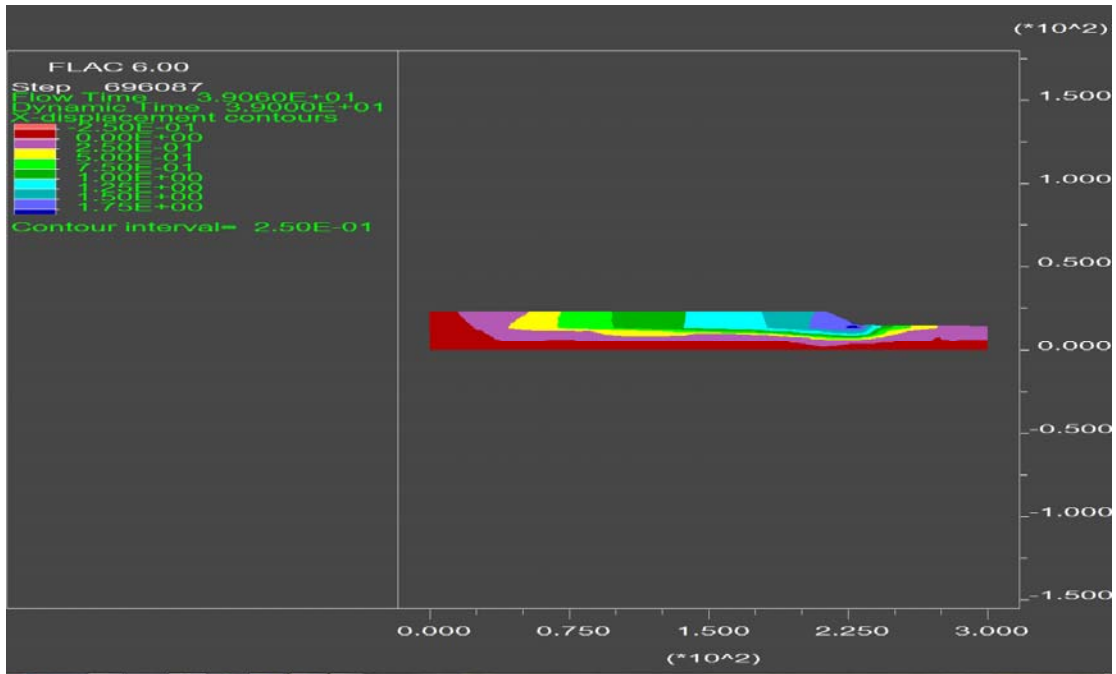
**Figure 6B-4. Contours of calculated lateral displacement (9 m embankment height, 8 meter liquefiable sand layer, corrected $(N_1)_{60}$ blowcount of 12, ground motion = 92 Landers Joshua Tree 090 Scale 1.0x).**
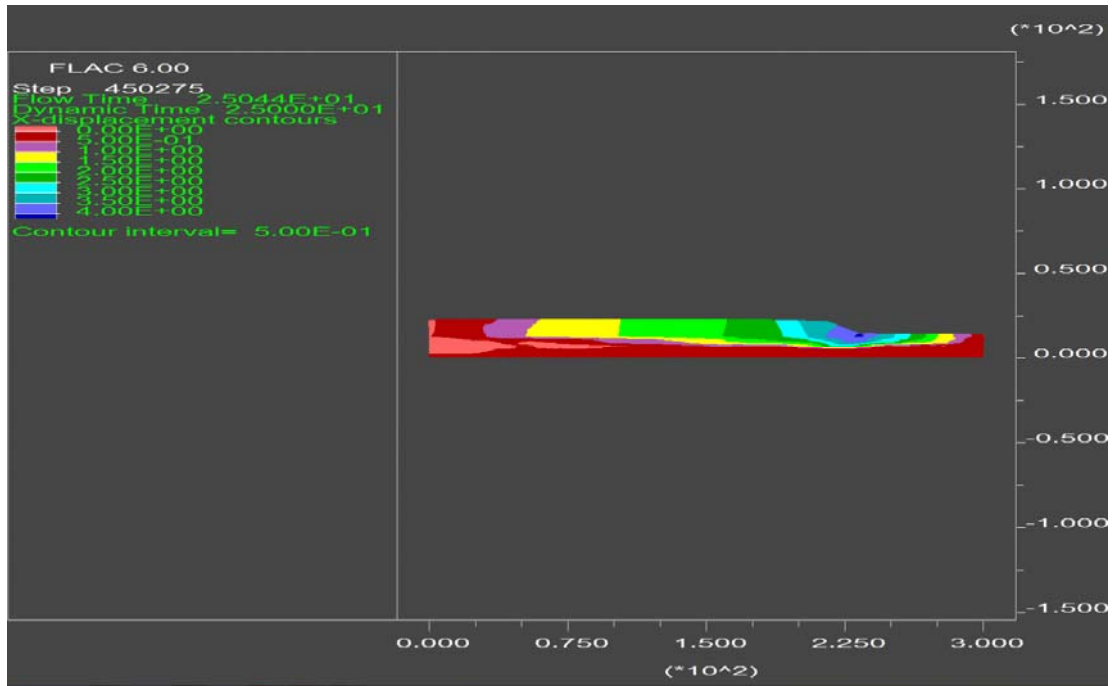


**Figure 6B-5. Contours of calculated lateral displacement (9 m embankment height, 8 meter liquefiable sand layer, corrected $(N_1)_{60}$ blowcount of 12, ground motion = 94 Northridge Sylmar - Conv Sta 052 Scale 1.0x).**
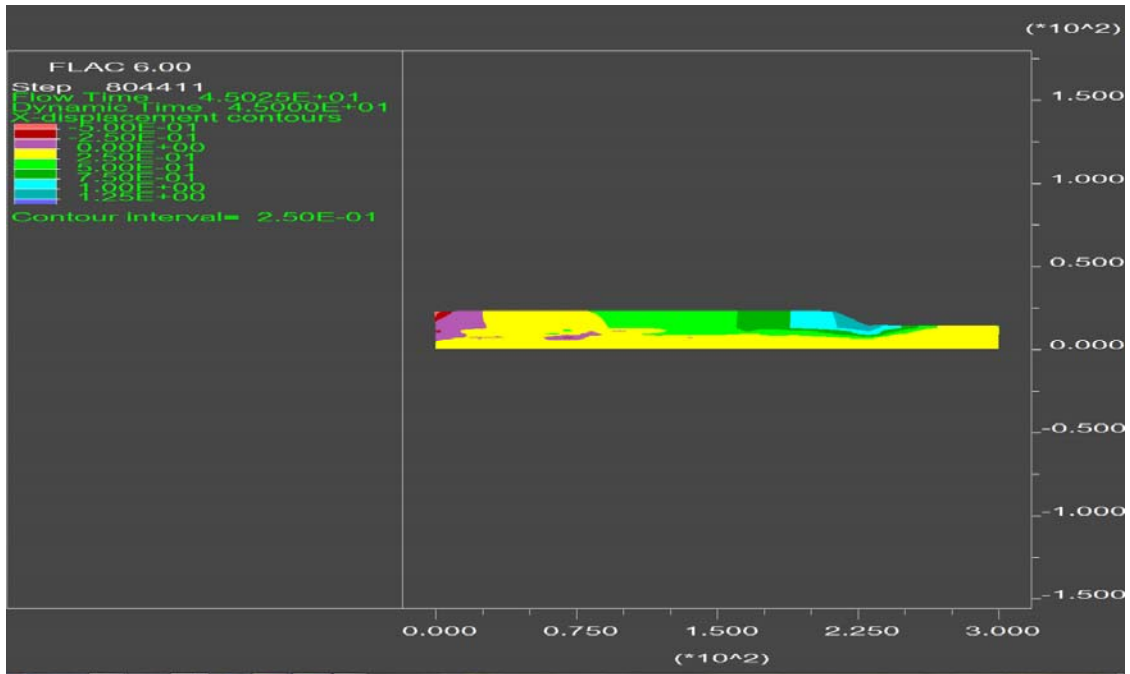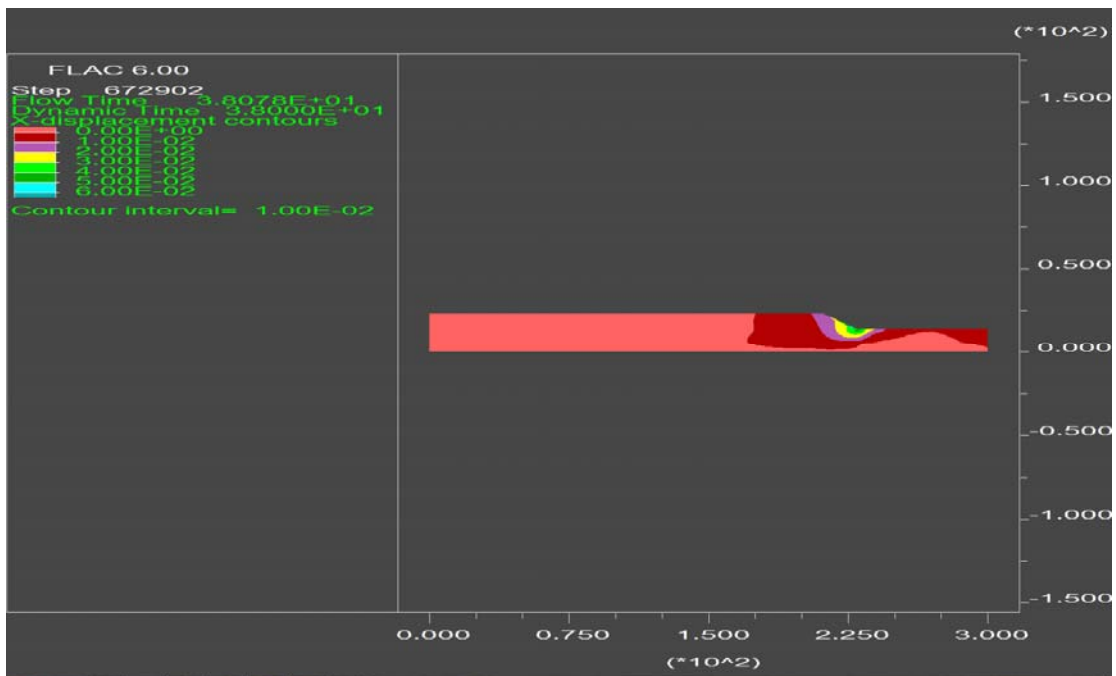
**Figure 6B-6. Contours of calculated lateral displacement (9 m embankment height, 8 meter liquefiable sand layer, corrected $(N_1)_{60}$ blowcount of 20, ground motion = 92 Landers Joshua Tree 090 Scale 1.0x).**
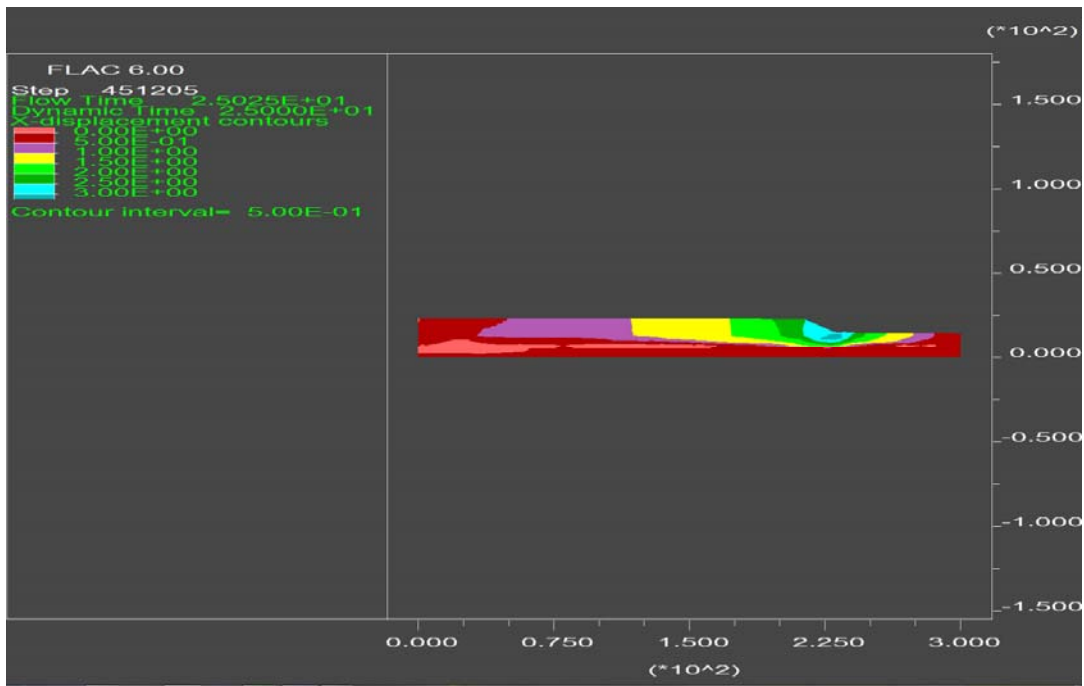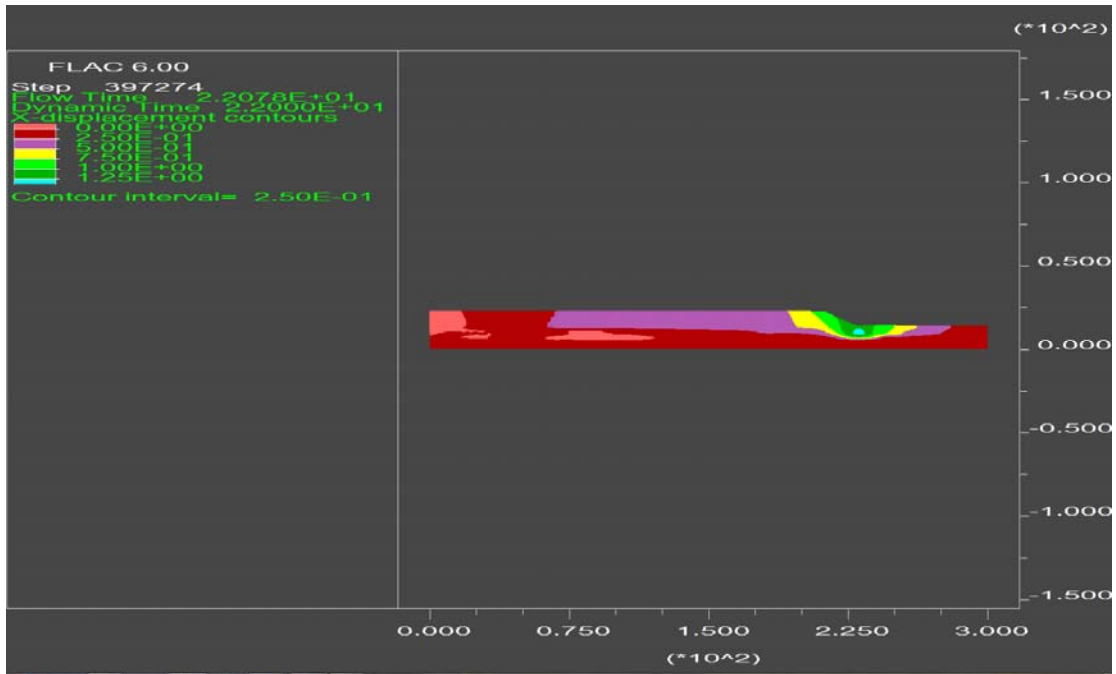


**Figure 6B-7. Contours of calculated lateral displacement (9 m embankment height, 8 meter liquefiable sand layer, corrected $(N_1)_{60}$ blowcount of 20, ground motion = 94 Northridge Sylmar - Conv Sta 052 Scale 1.0x).**
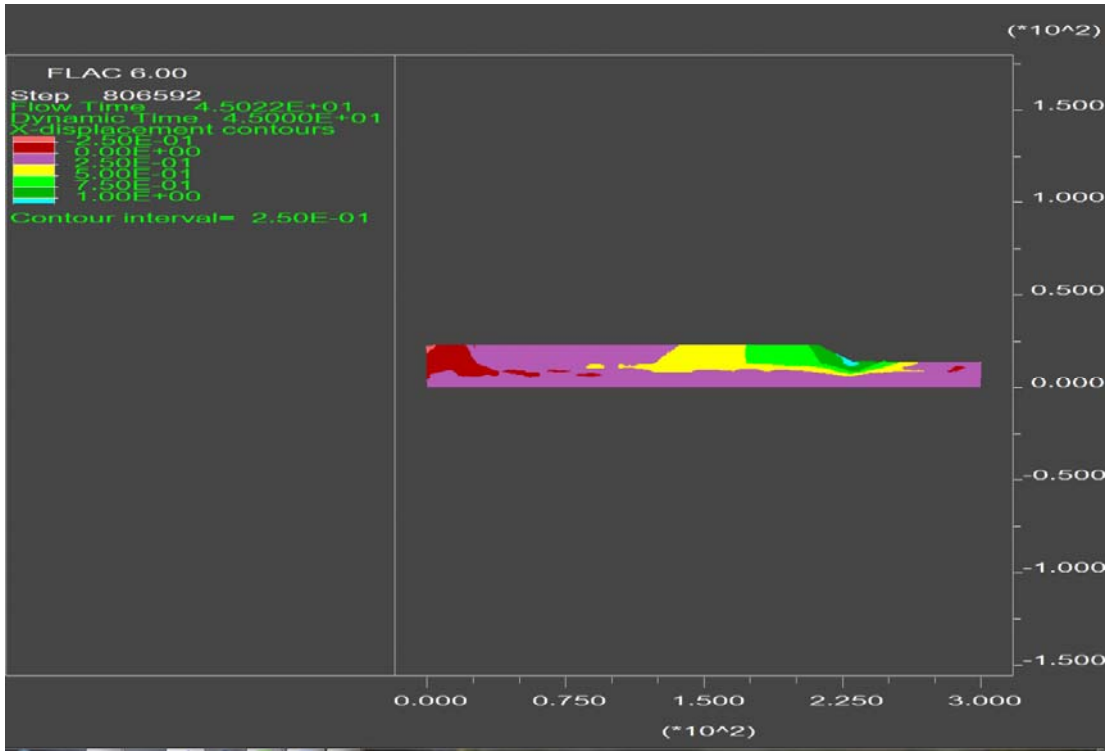
**Figure 6B-8. Contours of calculated lateral displacement (9 m embankment height, 8 meter liquefiable sand layer, corrected $(N_1)_{60}$ blowcount of 25, ground motion = 92 Landers Joshua Tree 090 Scale 1.0x).**
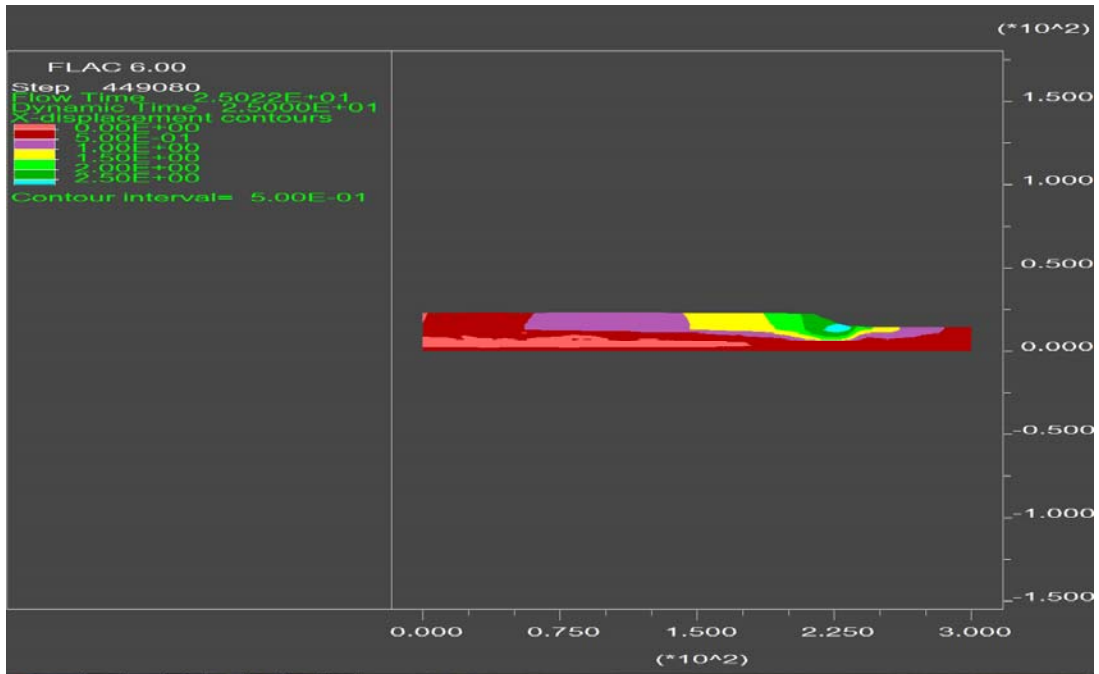


**Figure 6B-9. Contours of calculated lateral displacement (9 m embankment height, 8 meter liquefiable sand layer, corrected $(N_1)_{60}$ blowcount of 25, ground motion = 94 Northridge Sylmar - Conv Sta 052 Scale 1.0x).**
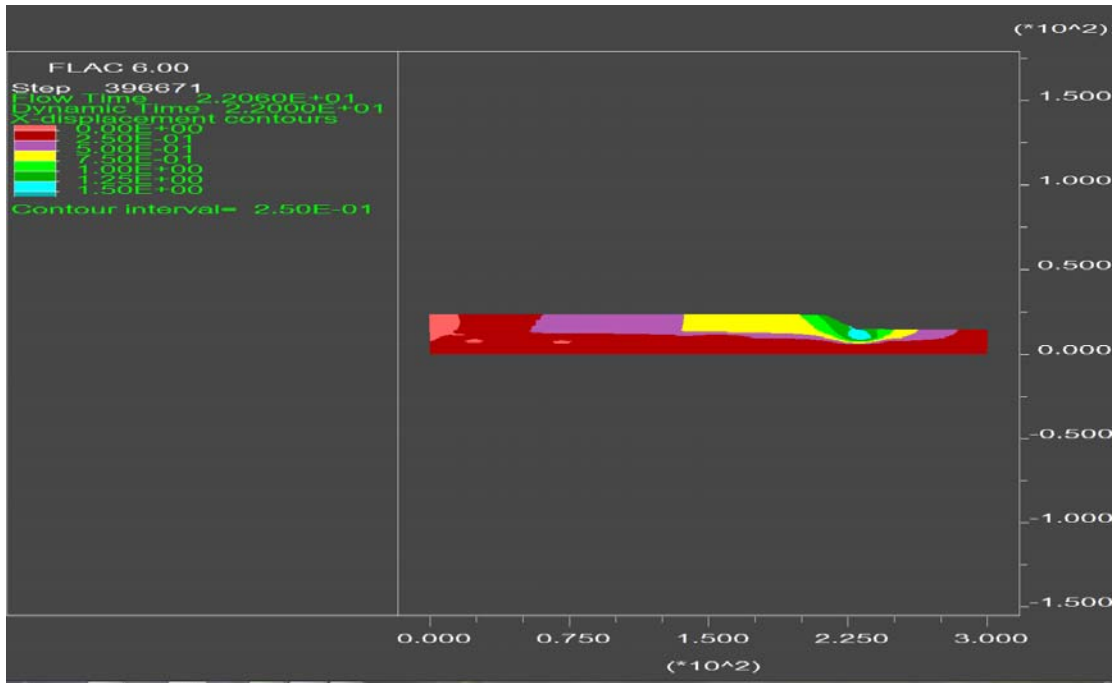
**Figure 6B-10. Contours of calculated lateral displacement (9 m embankment height, 8 meter liquefiable sand layer, corrected $(N_1)_{60}$ blowcount of 8, ground motion = 87 Superstition Hills Superstition Mtn Cam 045)**
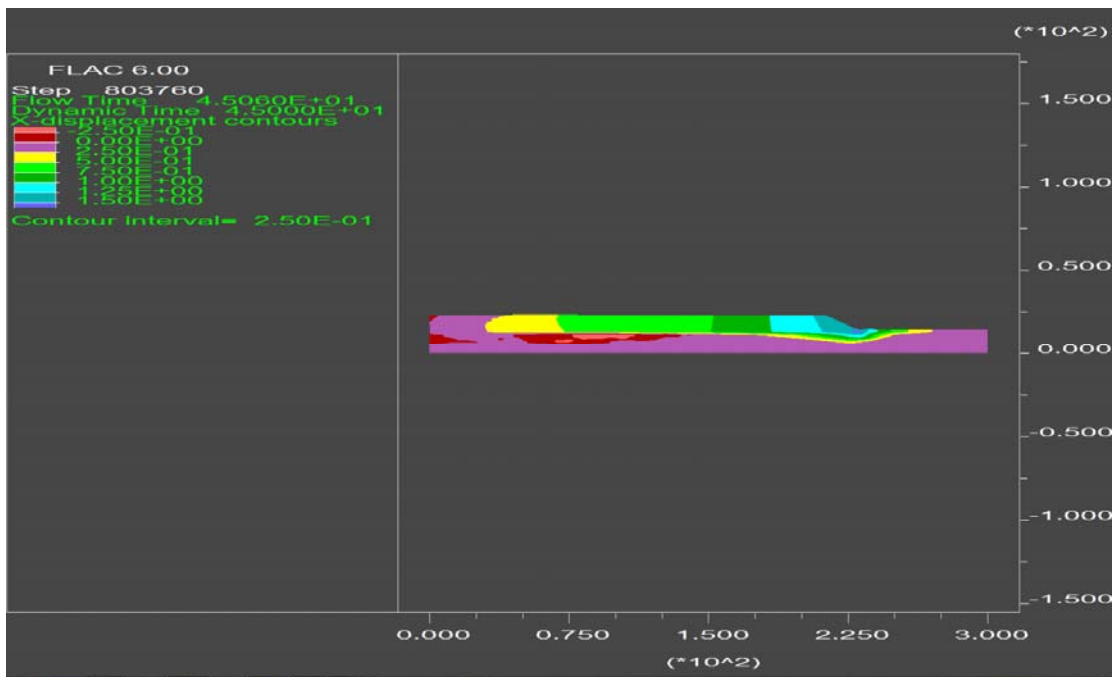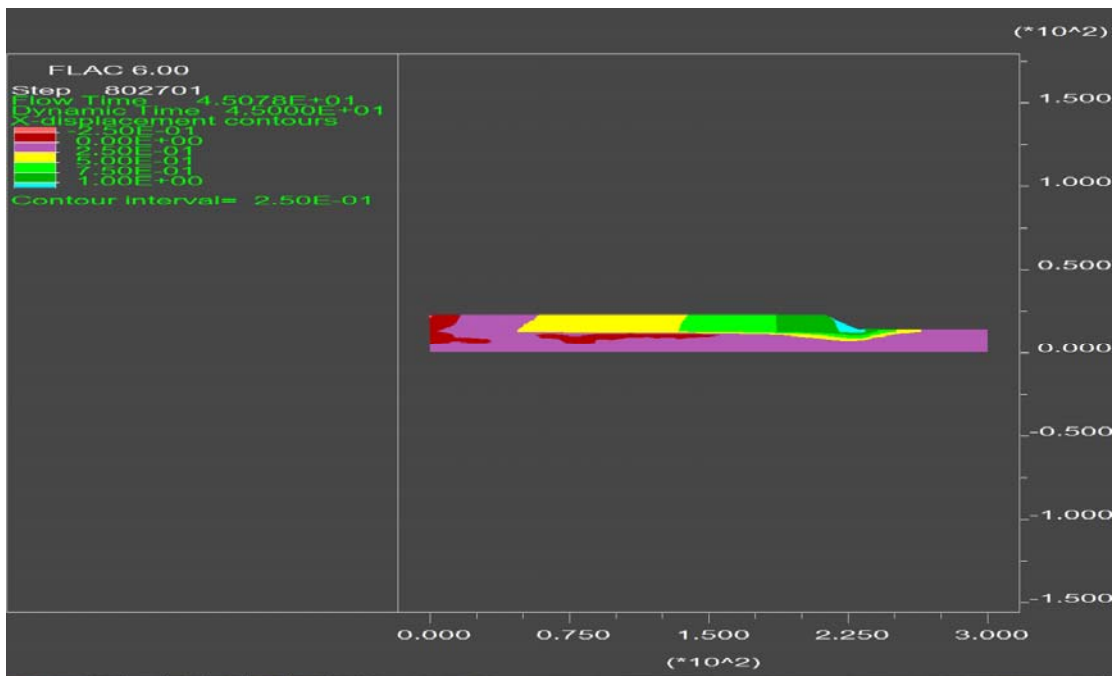


**Figure 6B-11. Contours of calculated lateral displacement (9 m embankment height, 8 meter liquefiable sand layer, corrected $(N_1)_{60}$ blowcount of 8, ground motion = 92 Landers Joshua Tree 090 Scale 0.75x).**
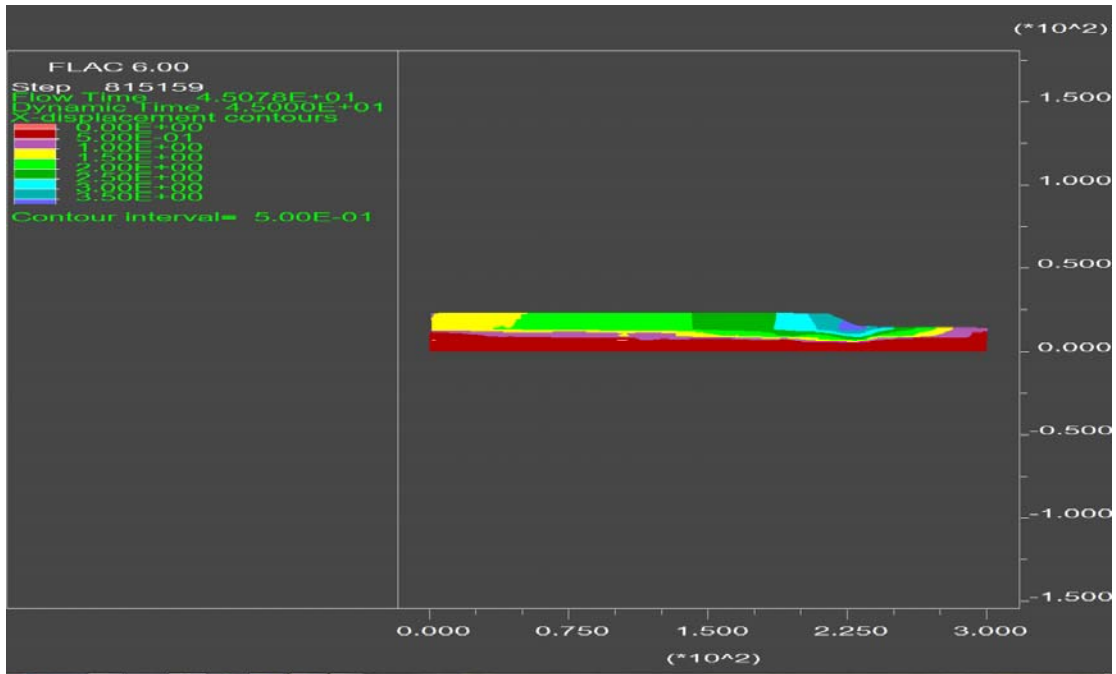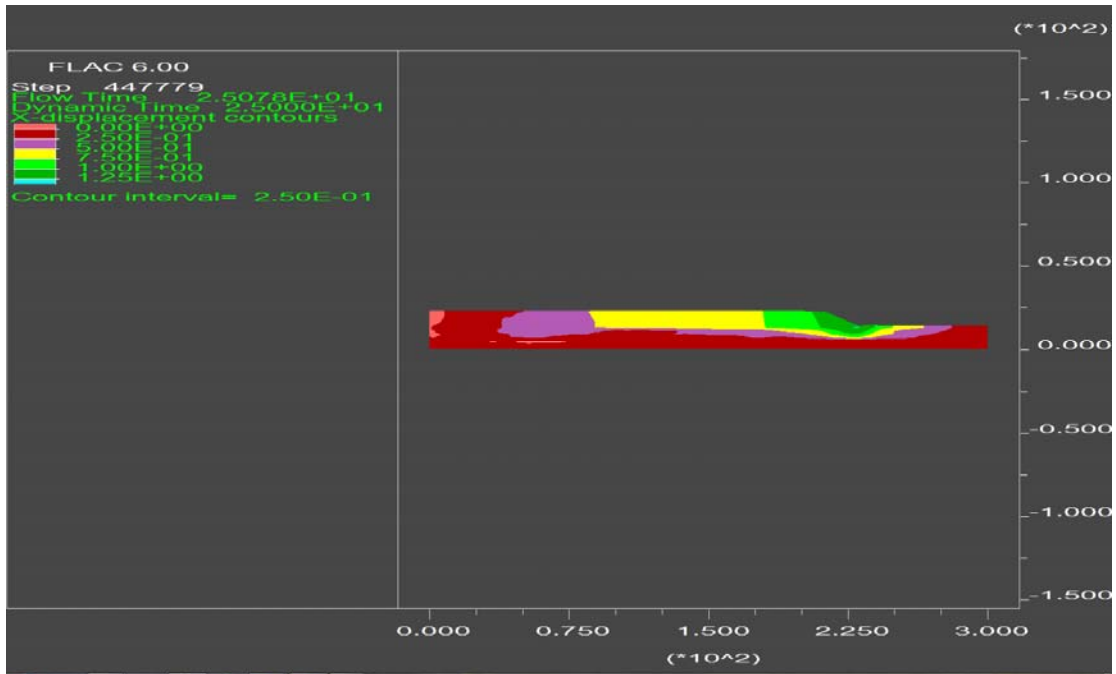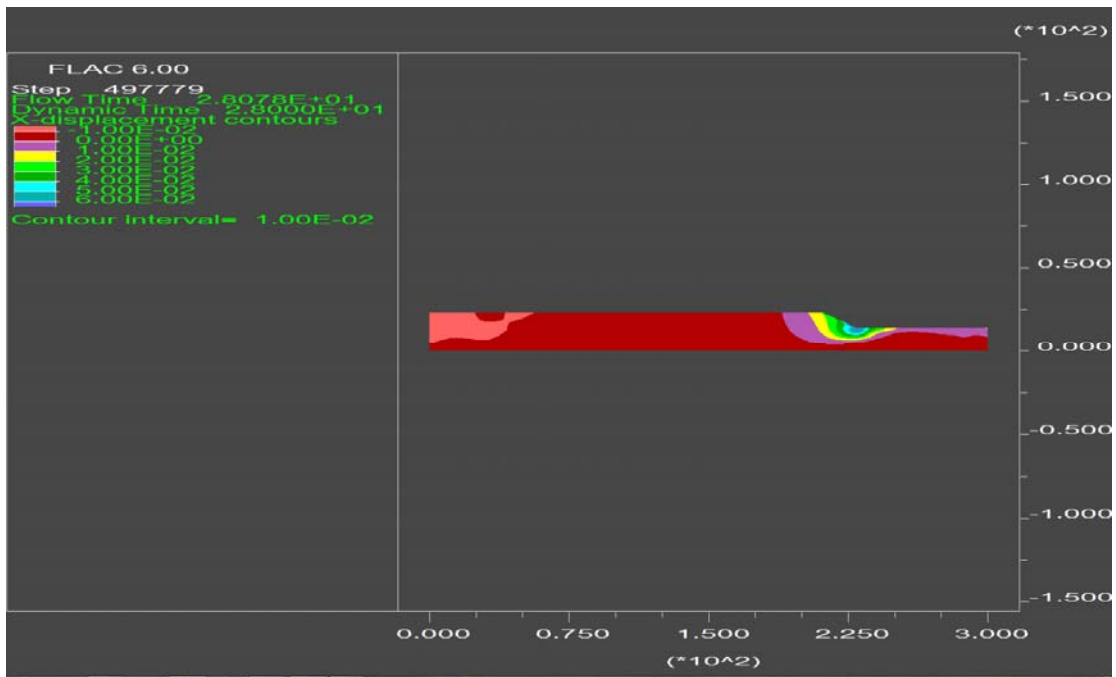
**Figure 6B-12. Contours of calculated lateral displacement (9 m embankment height, 8 meter liquefiable sand layer, corrected $(N_1)_{60}$ blowcount of 8, ground motion = 92 Landers Joshua Tree 090 Scale 1.5x).**
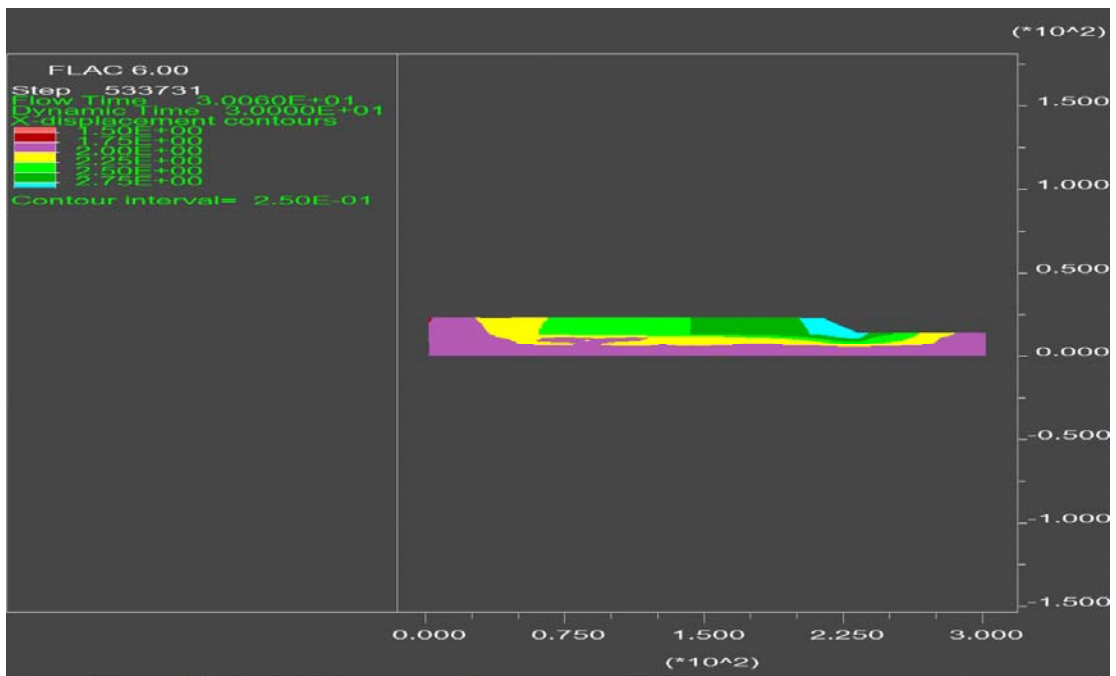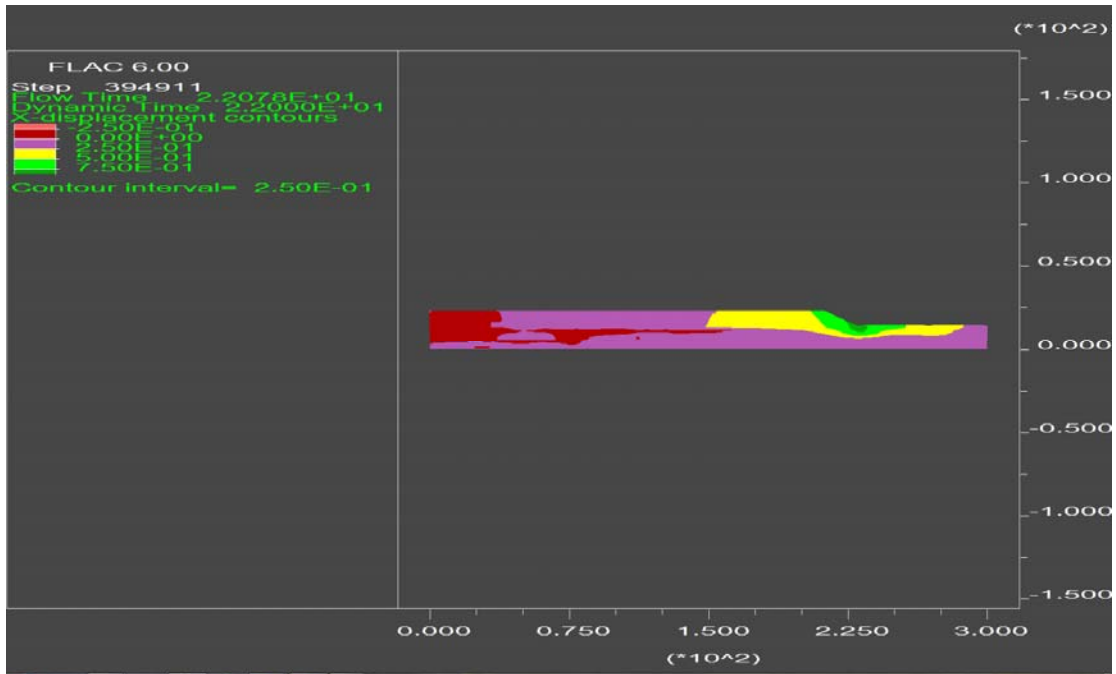


**Figure 6B-13. Contours of calculated lateral displacement (9 m embankment height, 8 meter liquefiable sand layer, corrected $(N_1)_{60}$ blowcount of 8, ground motion = 92 Landers Lucerne 260)**
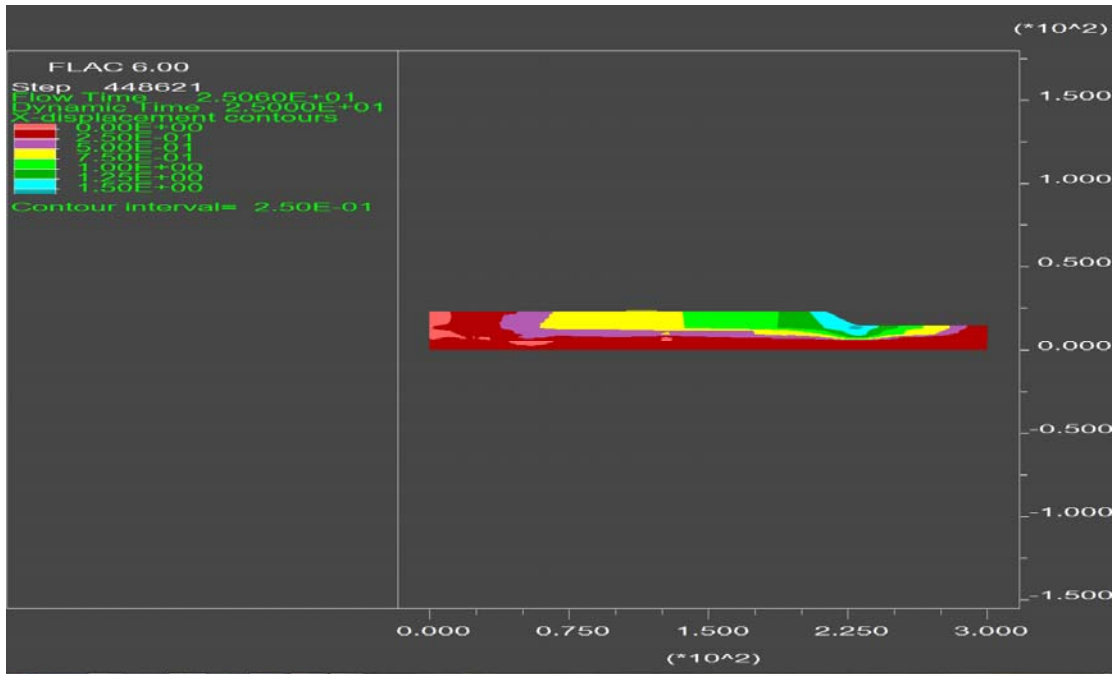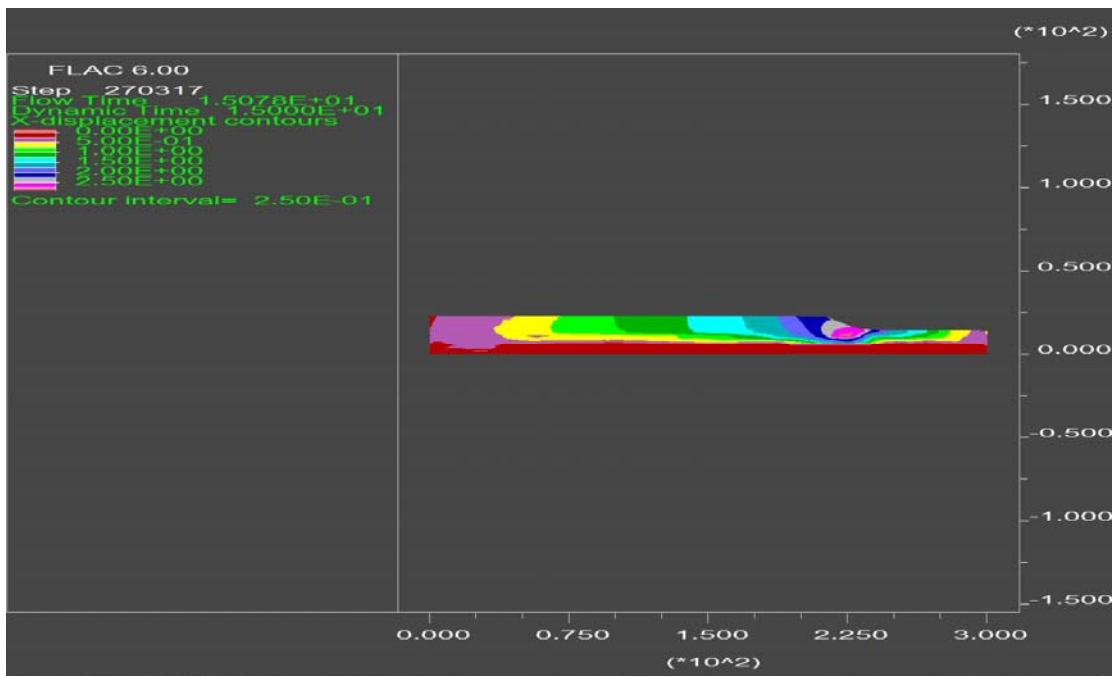
**Figure 6B-14. Contours of calculated lateral displacement (9 m embankment height, 8 meter liquefiable sand layer, corrected $(N_1)_{60}$ blowcount of 8, ground motion = 89 Loma Prieta LGPC 090)**
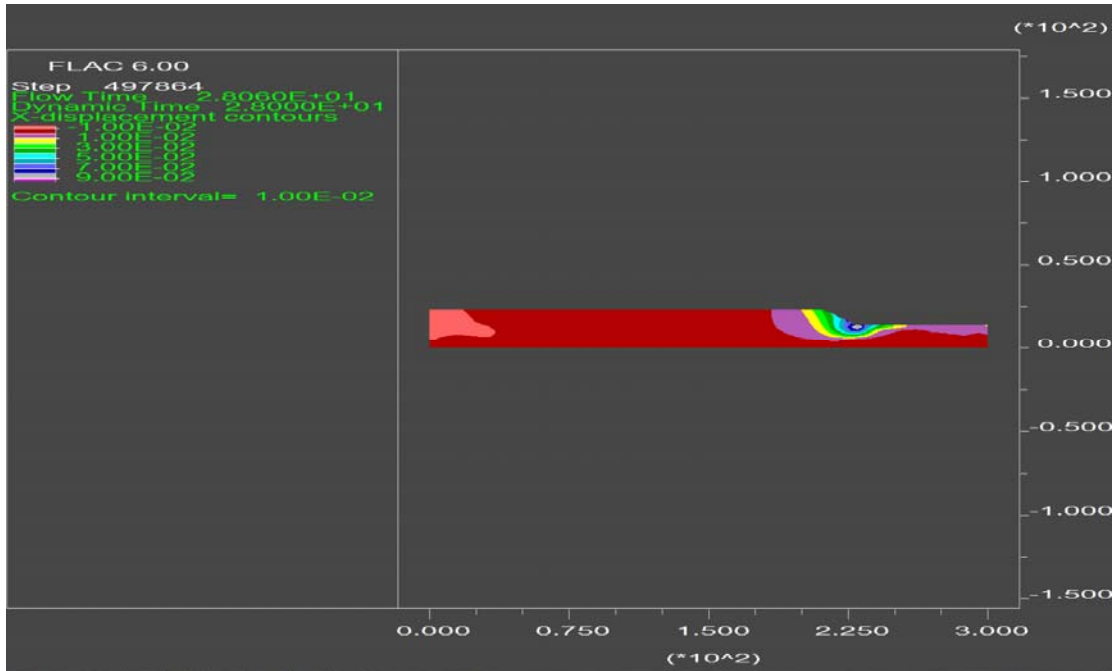


**Figure 6B-15. Contours of calculated lateral displacement (9 m embankment height, 8 meter liquefiable sand layer, corrected $(N_1)_{60}$ blowcount of 8, ground motion = 71 San Fernando LA Hollywood Stor Lot 180)**
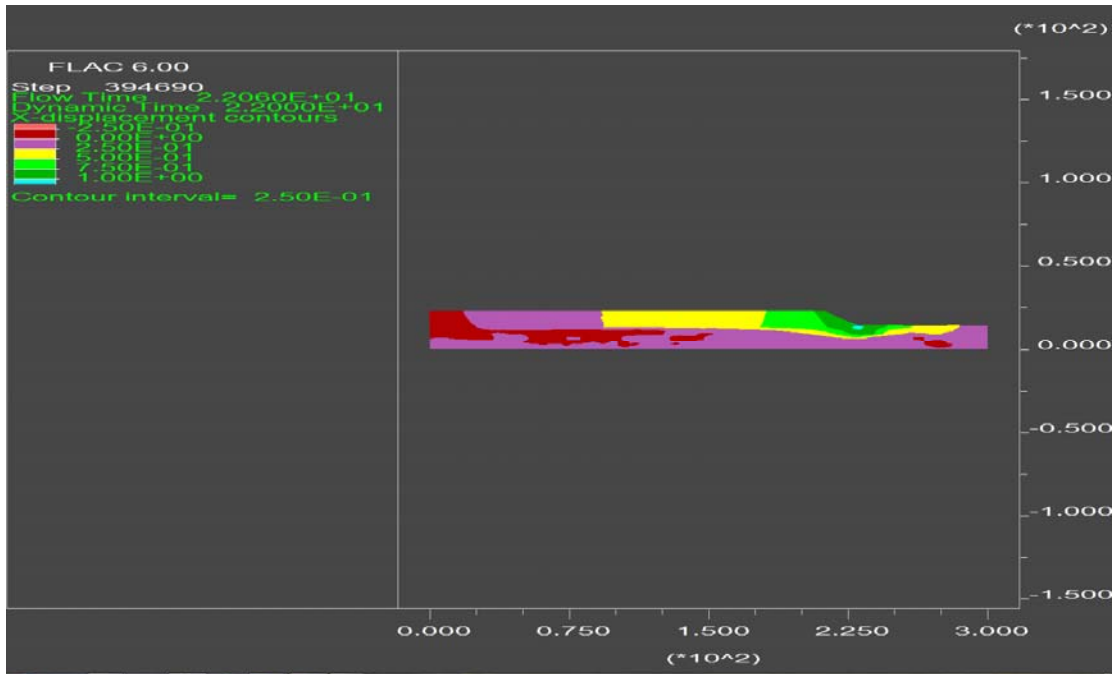
**Figure 6B-16. Contours of calculated lateral displacement (9 m embankment height, 8 meter liquefiable sand layer, corrected $(N_1)_{60}$ blowcount of 8, ground motion = 87 Superstition Hills Parachute T S 315 )**
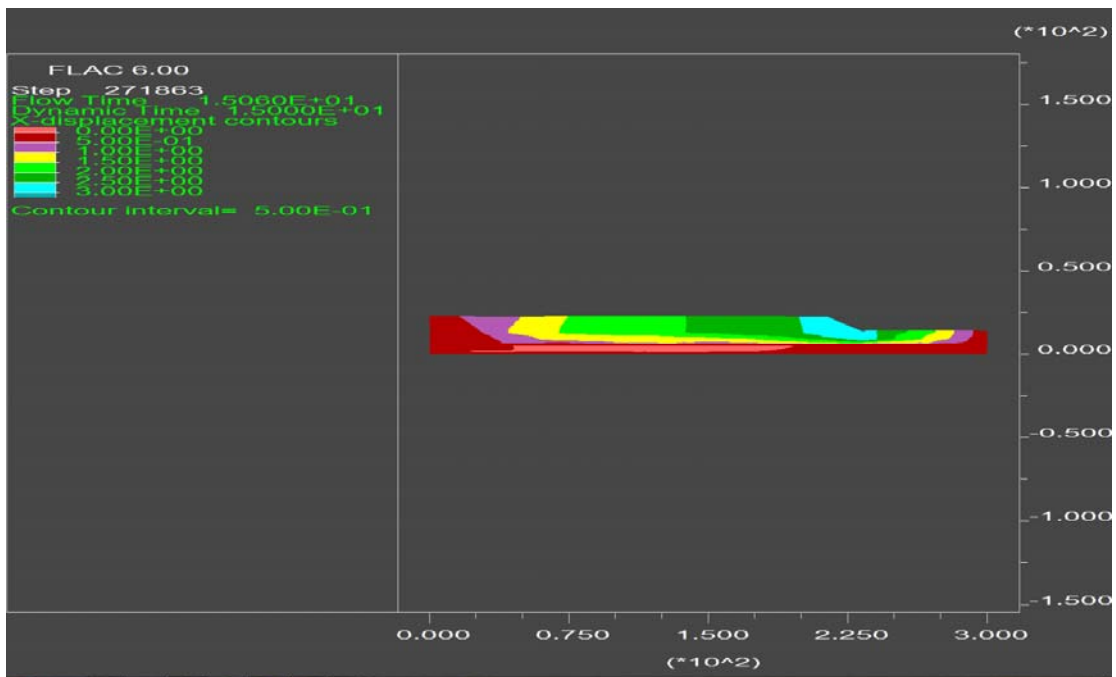


**Figure 6B-17. Contours of calculated lateral displacement (9 m embankment height, 8 meter liquefiable sand layer, corrected $(N_1)_{60}$ blowcount of 8, ground motion = 94 Northridge Rinaldi R Sta 228)**
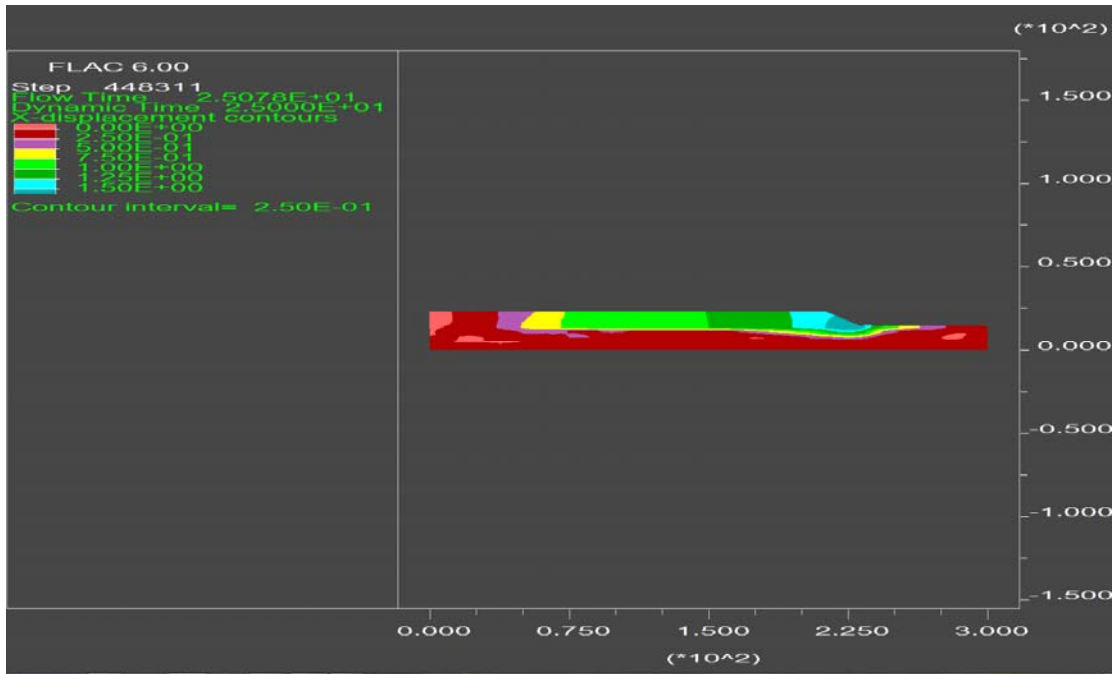
6B-9
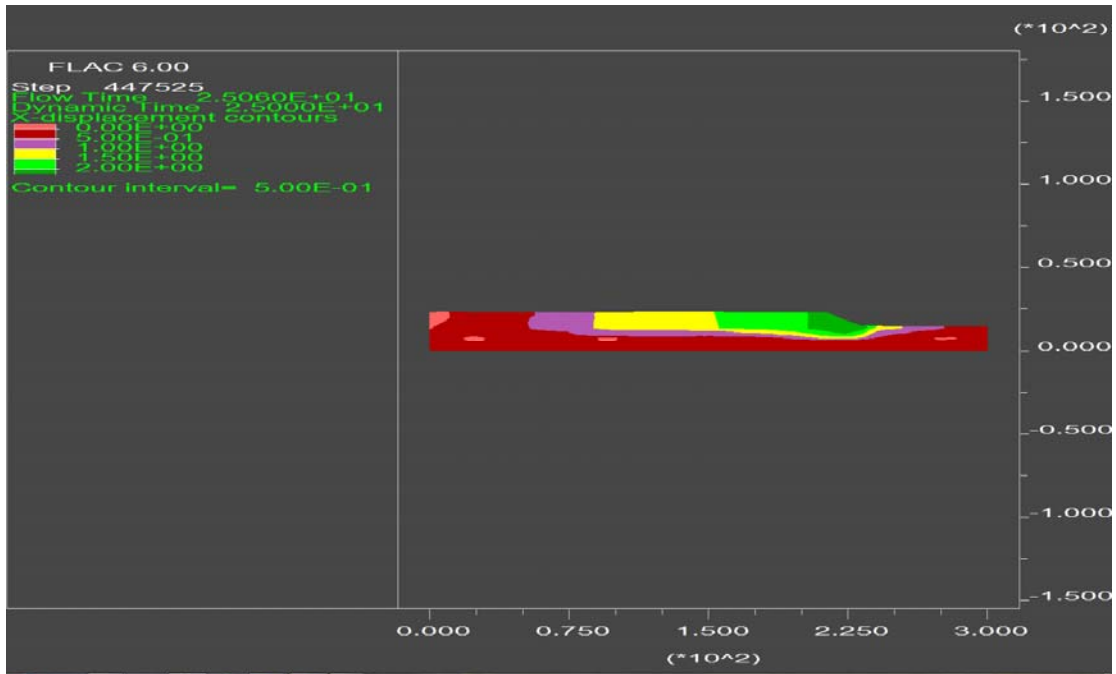
**Figure 6B-18. Contours of calculated lateral displacement (9 m embankment height, 8 meter liquefiable sand layer, corrected $(N_1)_{60}$ blowcount of 8, ground motion = 94 Northridge Sylmar - Conv Sta 052 Scale 0.5x)**
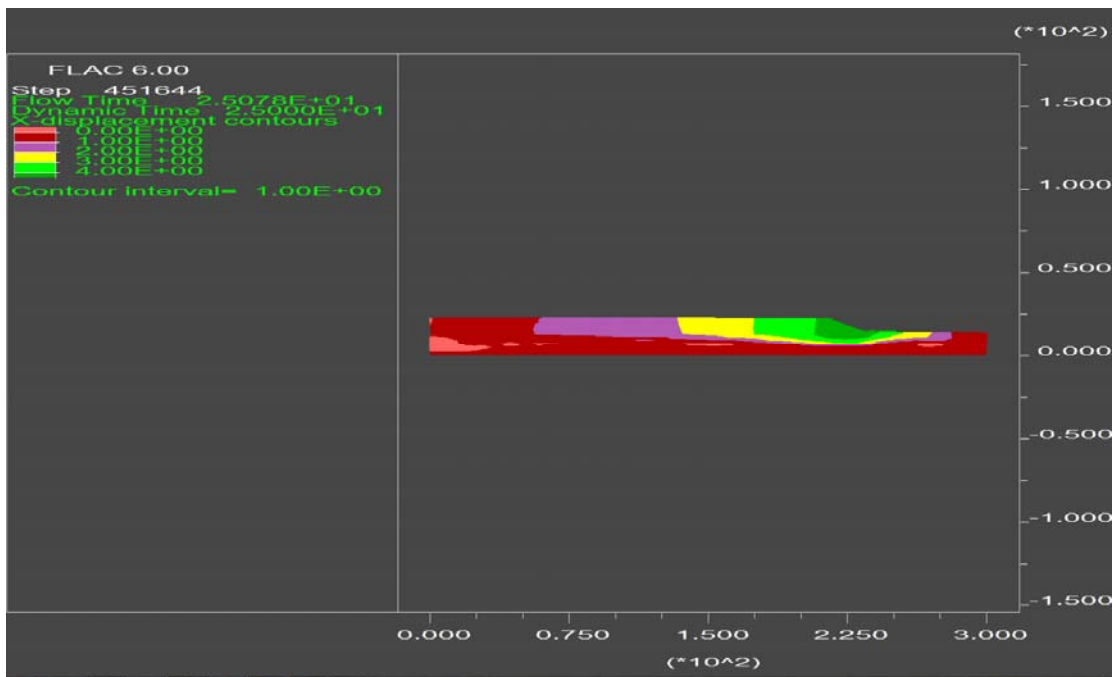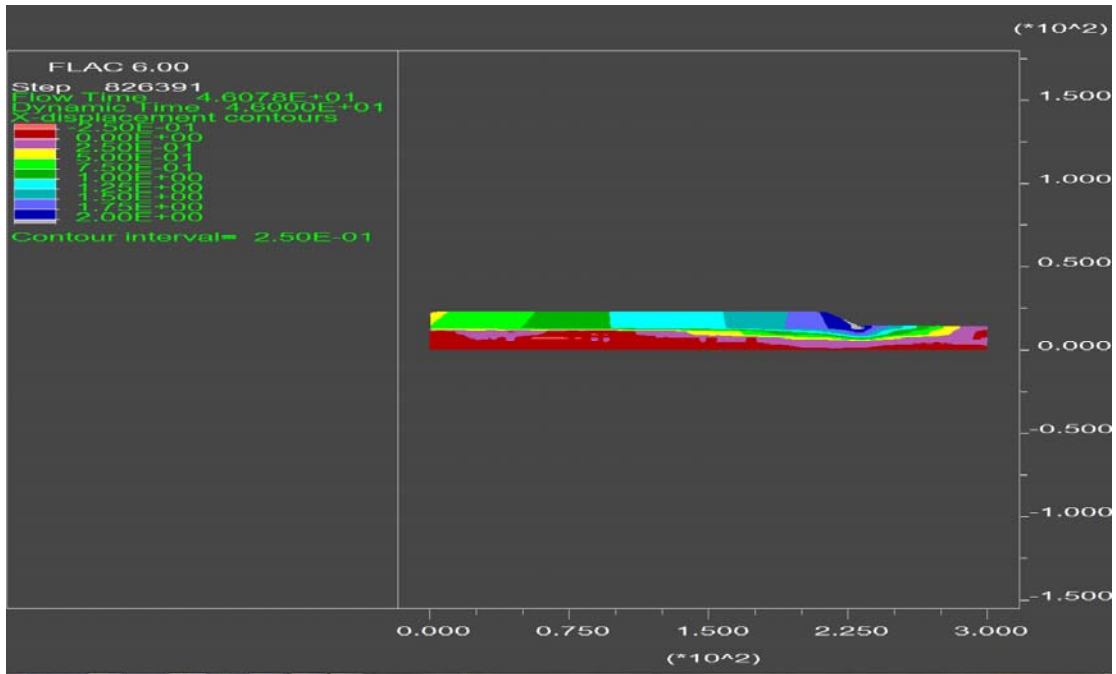


**Figure 6B-19. Contours of calculated lateral displacement (9 m embankment height, 8 meter liquefiable sand layer, corrected $(N_1)_{60}$ blowcount of 8, ground motion = 94 Northridge Sylmar - Conv Sta 052 Scale 1.25x)**

**Figure 6B-20. Contours of calculated lateral displacement (9 m embankment height, 8 meter liquefiable sand layer, corrected $(N_1)_{60}$ blowcount of 8, ground motion = 99 Chi Chi TCU078 270 (E))**
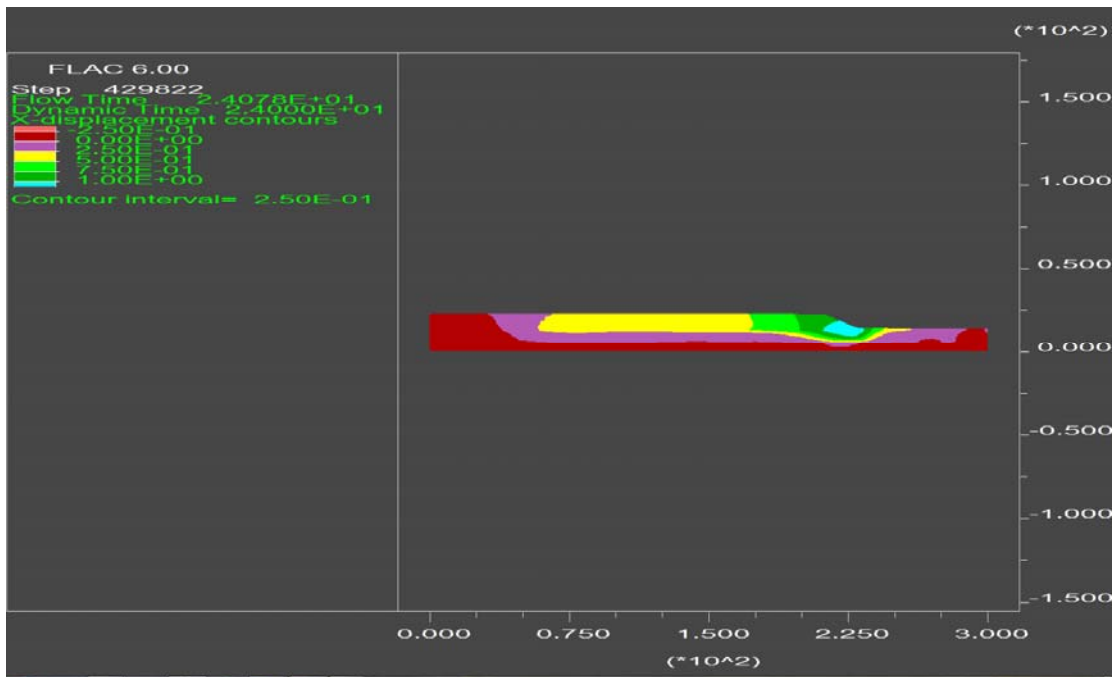


**Figure 6B-21. Contours of calculated lateral displacement (9 m embankment height, 8 meter liquefiable sand layer, corrected $(N_1)_{60}$ blowcount of 8, ground motion = 94 Northridge Newhall - W Pico Cany 046)**
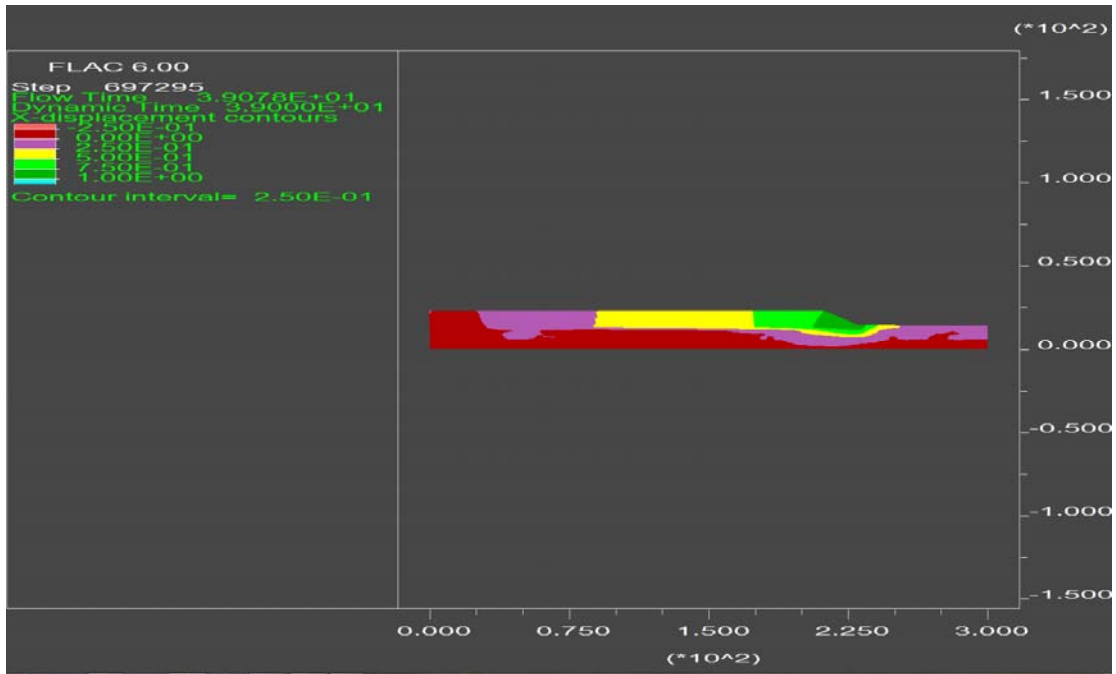
6B-11

**Figure 6B-22. Contours of calculated lateral displacement (9 m embankment height, 8 meter liquefiable sand layer, corrected $(N_1)_{60}$ blowcount of 8, ground motion = 89 Loma Prieta Saratoga WV Coll 270)**
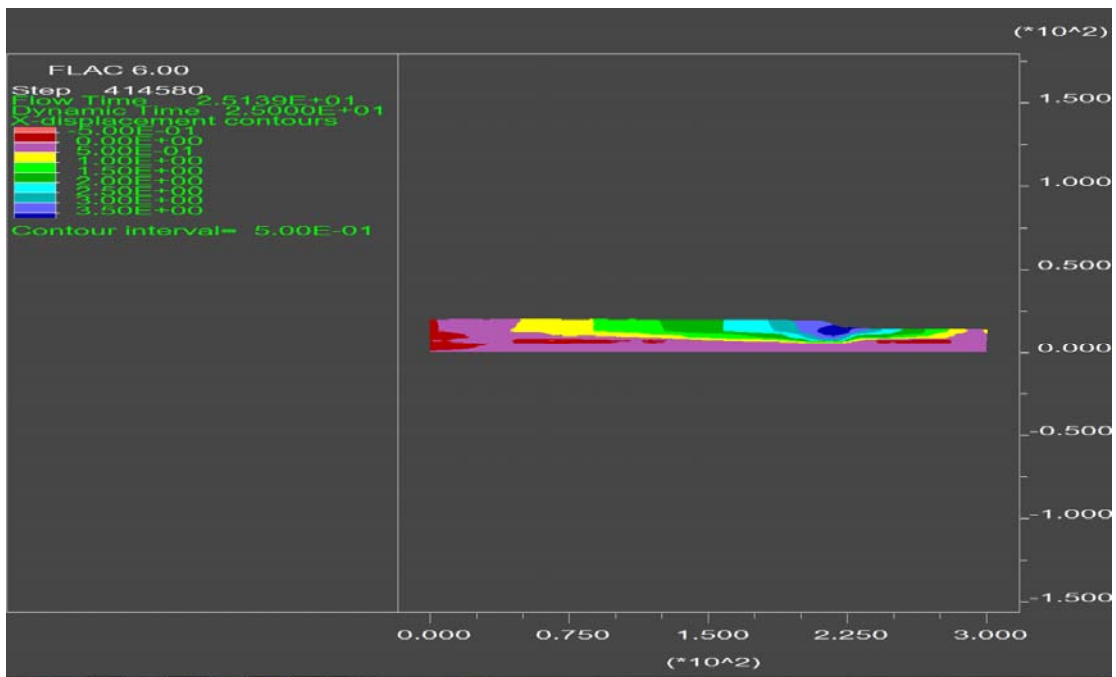


**Figure 6B-23. Contours of calculated lateral displacement (9 m embankment height, 8 meter liquefiable sand layer, corrected $(N_1)_{60}$ blowcount of 15, ground motion = 79 Imperial Valley Brawley Airport)**
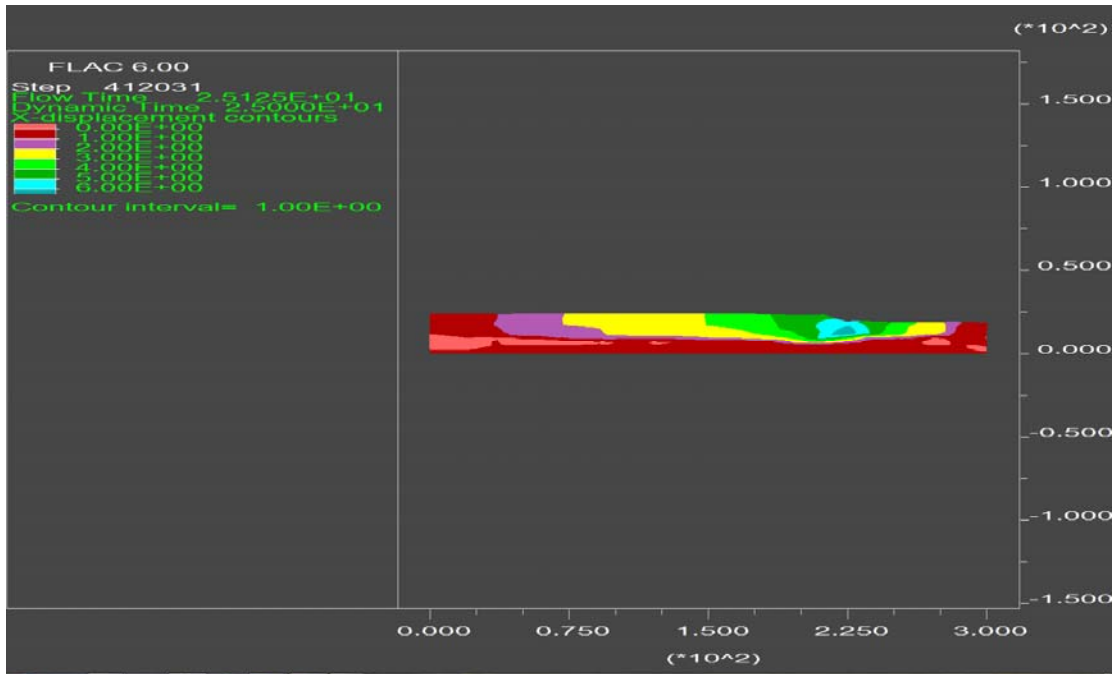
**Figure 6B-24. Contours of calculated lateral displacement (9 m embankment height, 8 meter liquefiable sand layer, corrected $(N_1)_{60}$ blowcount of 15, ground motion = 87 Superstition Hills Superstition Mtn Cam 045)**



**Figure 6B-25. Contours of calculated lateral displacement (9 m embankment height, 8 meter liquefiable sand layer, corrected $(N_1)_{60}$ blowcount of 15, ground motion = 92 Landers Joshua Tree 090 Scale 0.75x).**
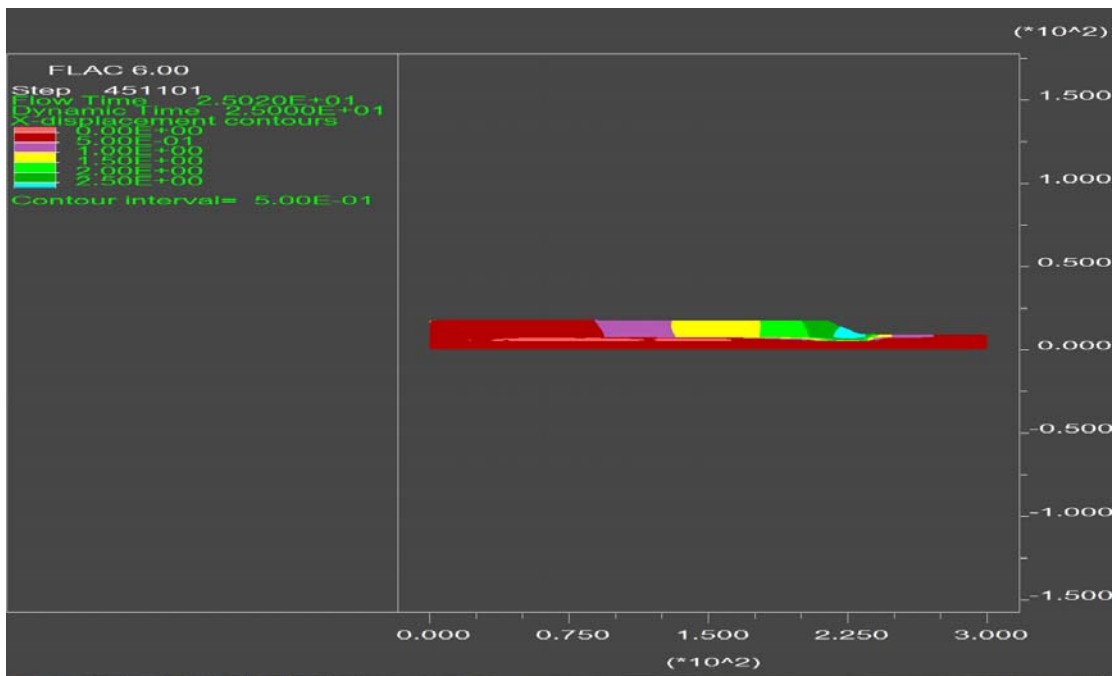
**Figure 6B-26. Contours of calculated lateral displacement (9 m embankment height, 8 meter liquefiable sand layer, corrected $(N_1)_{60}$ blowcount of 15, ground motion = 92 Landers Joshua Tree 090 Scale 1.5x).**
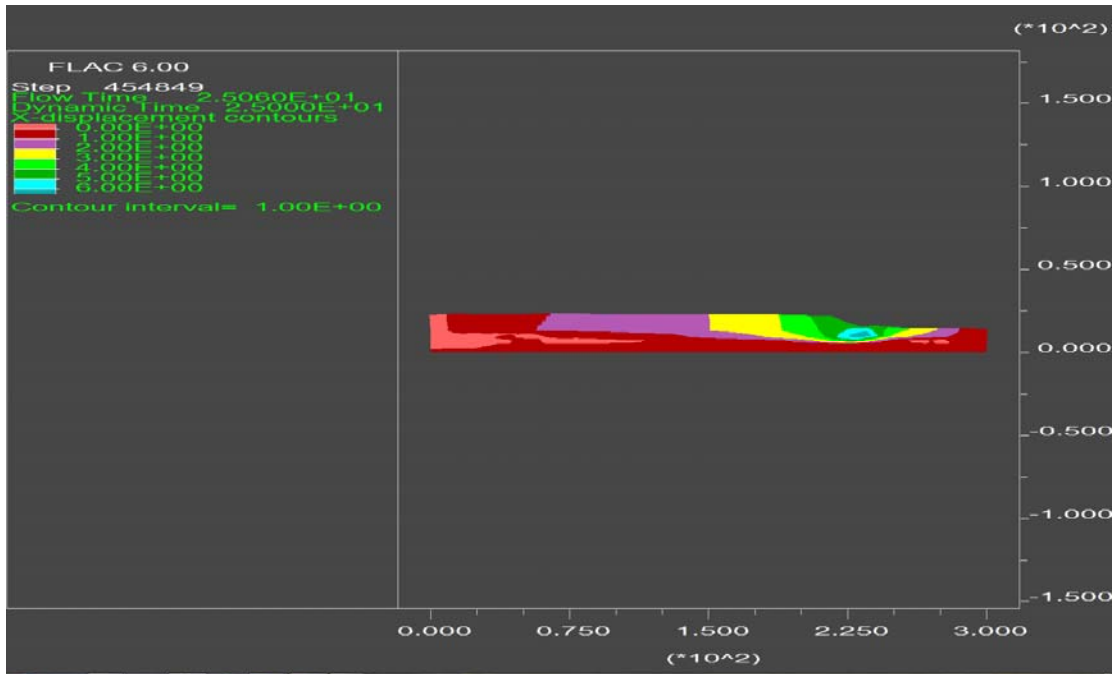


**Figure 6B-27. Contours of calculated lateral displacement (9 m embankment height, 8 meter liquefiable sand layer, corrected $(N_1)_{60}$ blowcount of 15, ground motion = 92 Landers Lucerne 260). Note that displacements shown are total displacements and include approximately 175 cm of fling step that can be subtracted out to obtain relative displacements.**
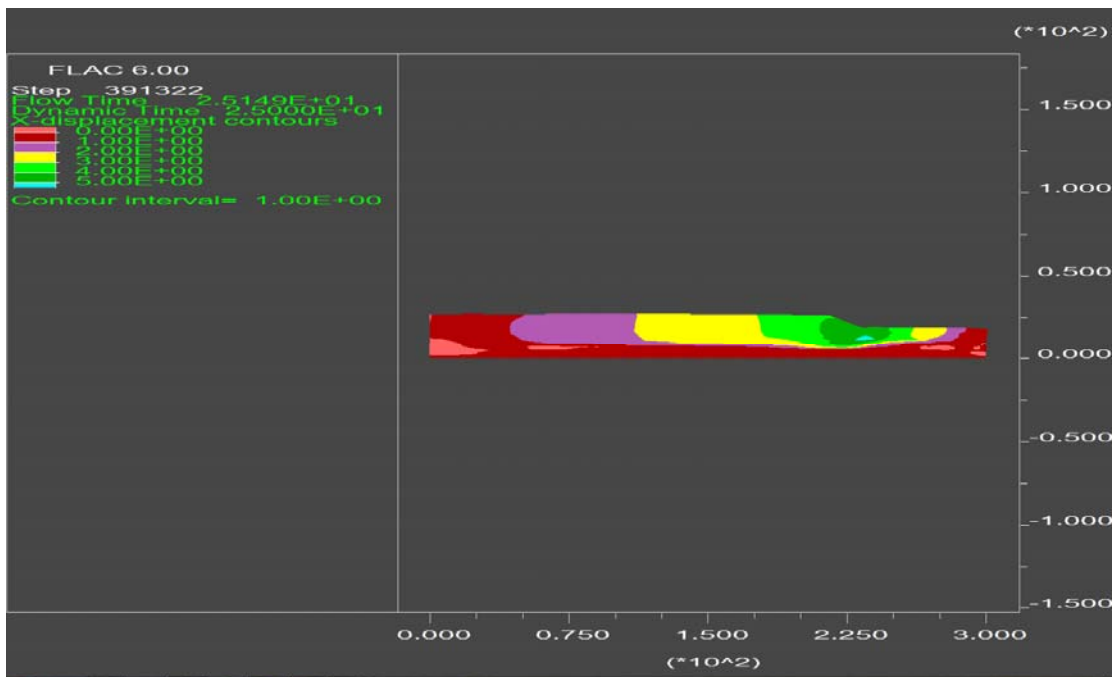
**Figure 6B-28. Contours of calculated lateral displacement (9 m embankment height, 8 meter liquefiable sand layer, corrected $(N_1)_{60}$ blowcount of 15, ground motion = 89 Loma Prieta LGPC 090)**



**Figure 6B-29. Contours of calculated lateral displacement (9 m embankment height, 8 meter liquefiable sand layer, corrected $(N_1)_{60}$ blowcount of 15, ground motion = 71 San Fernando LA Hollywood Stor Lot 180)**
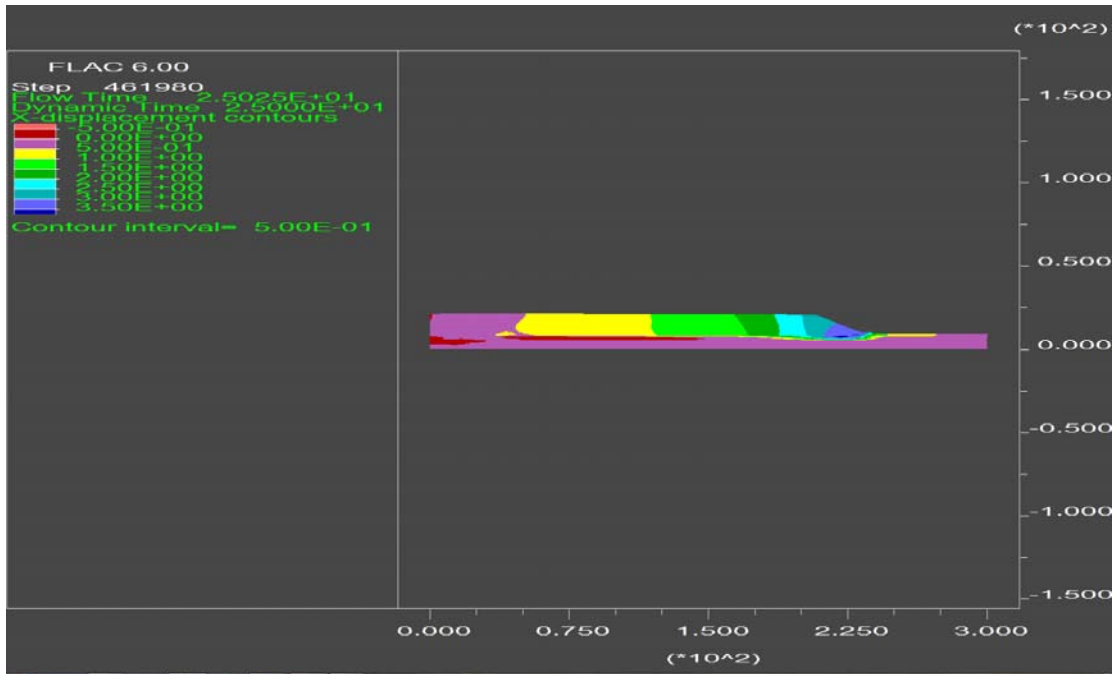
6B-15

**Figure 6B-30. Contours of calculated lateral displacement (9 m embankment height, 8 meter liquefiable sand layer, corrected $(N_1)_{60}$ blowcount of 15, ground motion = 87 Superstition Hills Parachute T S 315)**
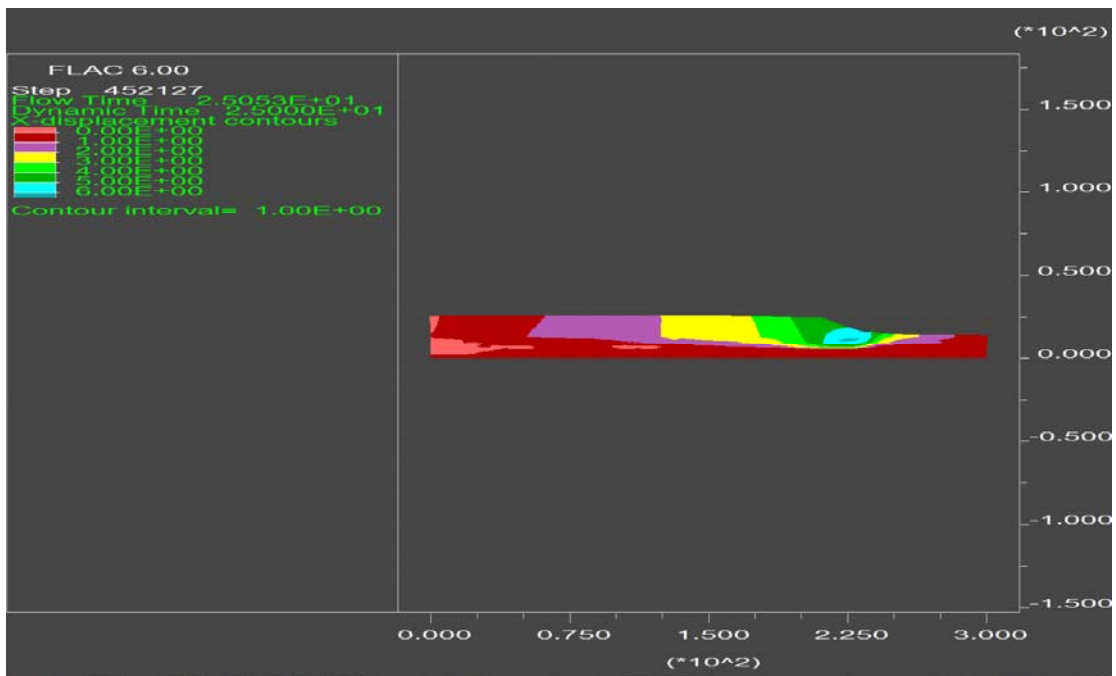


**Figure 6B-31. Contours of calculated lateral displacement (9 m embankment height, 8 meter liquefiable sand layer, corrected $(N_1)_{60}$ blowcount of 15, ground motion = 94 Northridge Rinaldi R Sta 228)**

6B-16

**Figure 6B-32.** Contours of calculated lateral displacement (9 m embankment height, 8 meter liquefiable sand layer, corrected $(N_1)_{60}$ blowcount of 15, ground motion = 94 Northridge Sylmar - Conv Sta 052 Scale 0.5x)
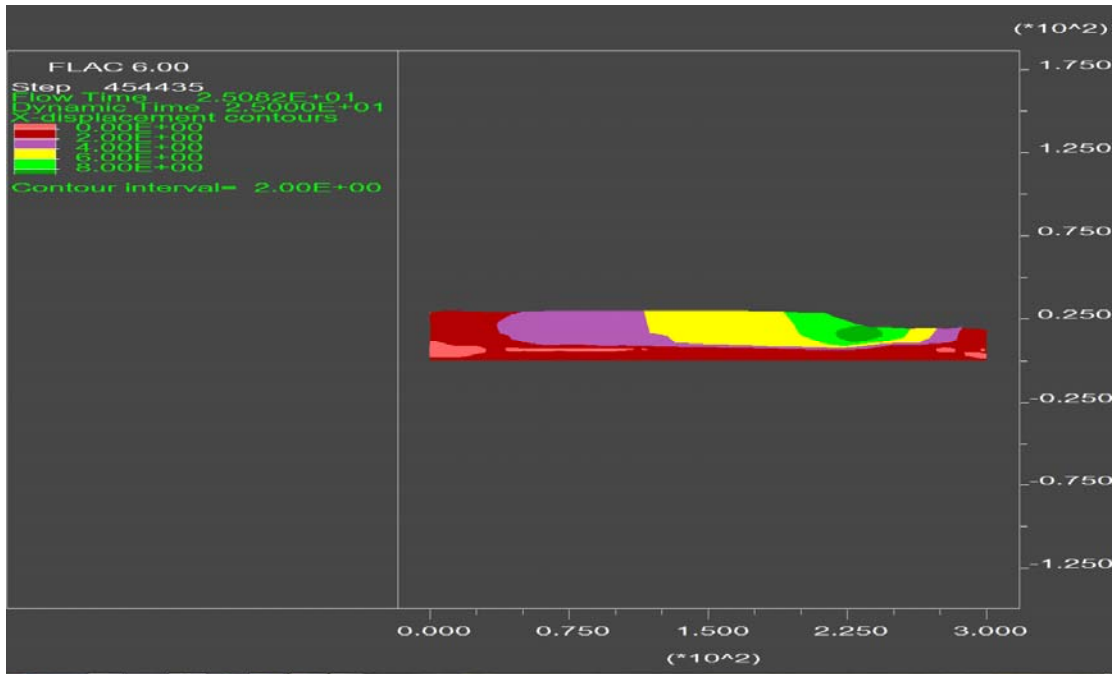


**Figure 6B-33.** Contours of calculated lateral displacement (9 m embankment height, 8 meter liquefiable sand layer, corrected $(N_1)_{60}$ blowcount of 15, ground motion = 94 Northridge Sylmar - Conv Sta 052 Scale 1.25x)
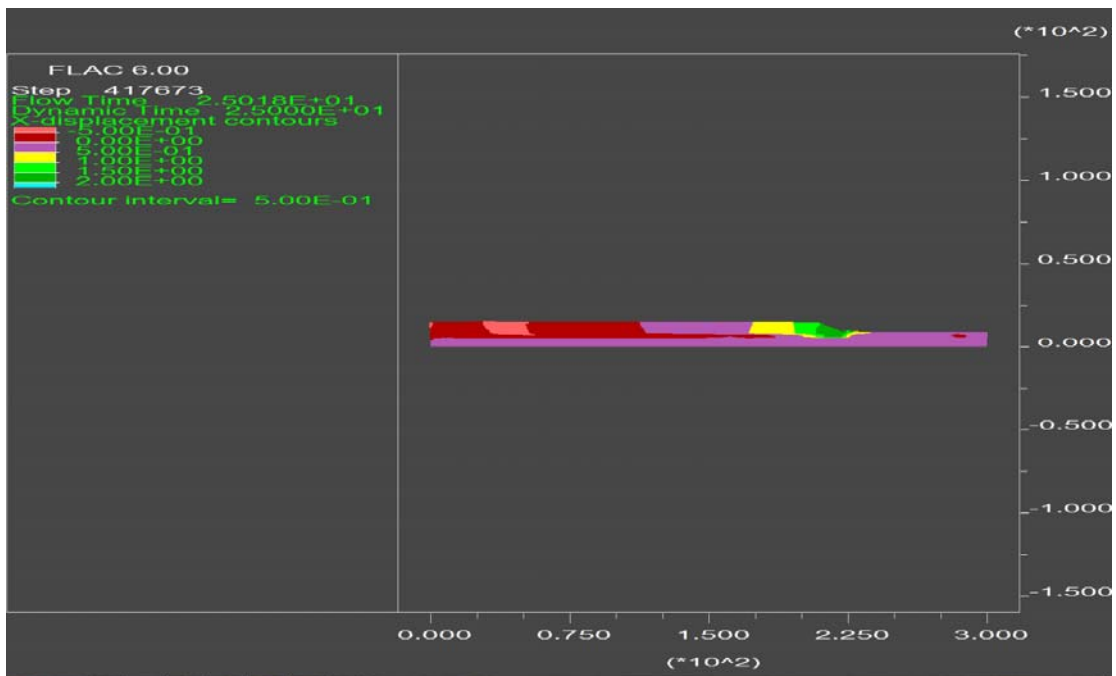
**Figure 6B-34. Contours of calculated lateral displacement (9 m embankment height, 8 meter liquefiable sand layer, corrected $(N_1)_{60}$ blowcount of 15, ground motion = 99 Chi Chi TCU078 270 (E))**



**Figure 6B-35. Contours of calculated lateral displacement (9 m embankment height, 8 meter liquefiable sand layer, corrected $(N_1)_{60}$ blowcount of 15, ground motion = 94 Northridge Newhall - W Pico Cany 046)**

**Figure 6B-36. Contours of calculated lateral displacement (9 m embankment height, 8 meter liquefiable sand layer, corrected $(N_1)_{60}$ blowcount of 15, ground motion = 89 Loma Prieta Saratoga WV Coll 270)**



**Figure 6B-37. Contours of calculated lateral displacement (6 m embankment height, 8 meter liquefiable sand layer, corrected $(N_1)_{60}$ blowcount of 8, ground motion = 94 Northridge Sylmar - Conv Sta 052 Scale 1.0x).**
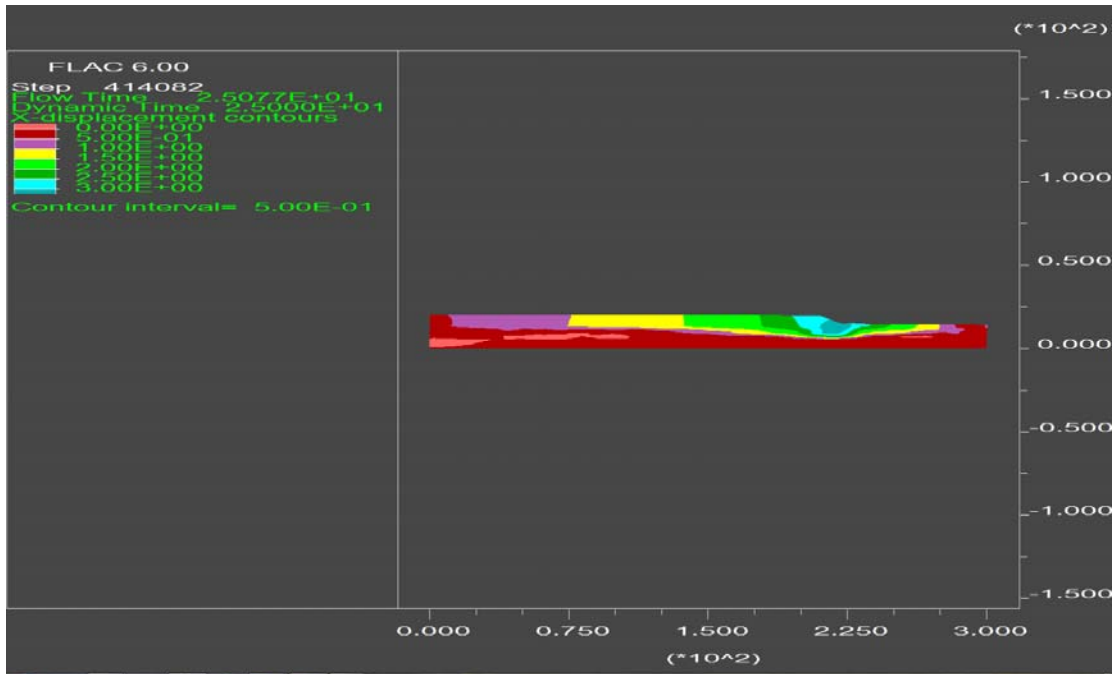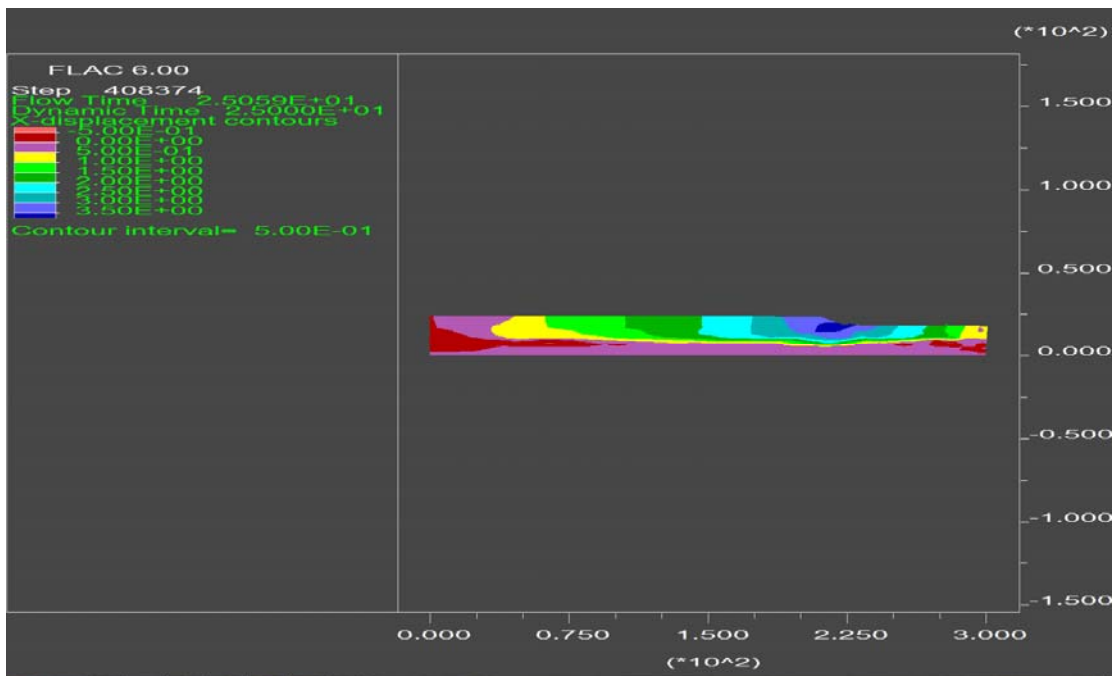
**Figure 6B-38. Contours of calculated lateral displacement (6 m embankment height, 12 meter liquefiable sand layer, corrected $(N_1)_{60}$ blowcount of 8, ground motion = 94 Northridge Sylmar - Conv Sta 052 Scale 1.0x).**
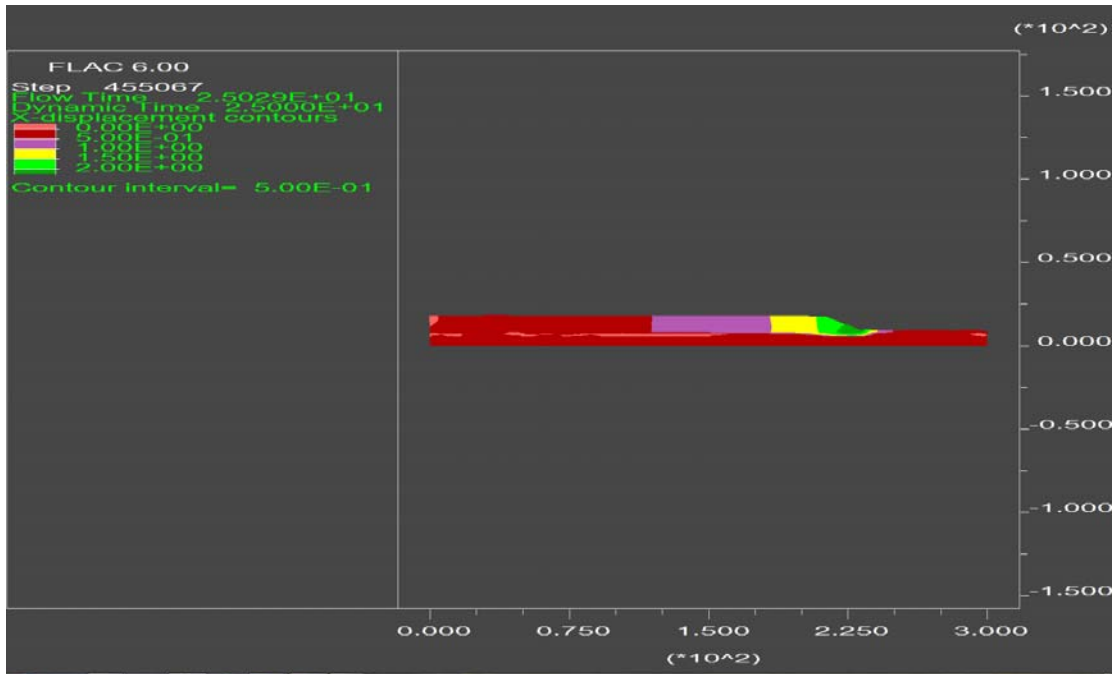


**Figure 6B-39. Contours of calculated lateral displacement (9 m embankment height, 3 meter liquefiable sand layer, corrected $(N_1)_{60}$ blowcount of 8, ground motion = 94 Northridge Sylmar - Conv Sta 052 Scale 1.0x).**
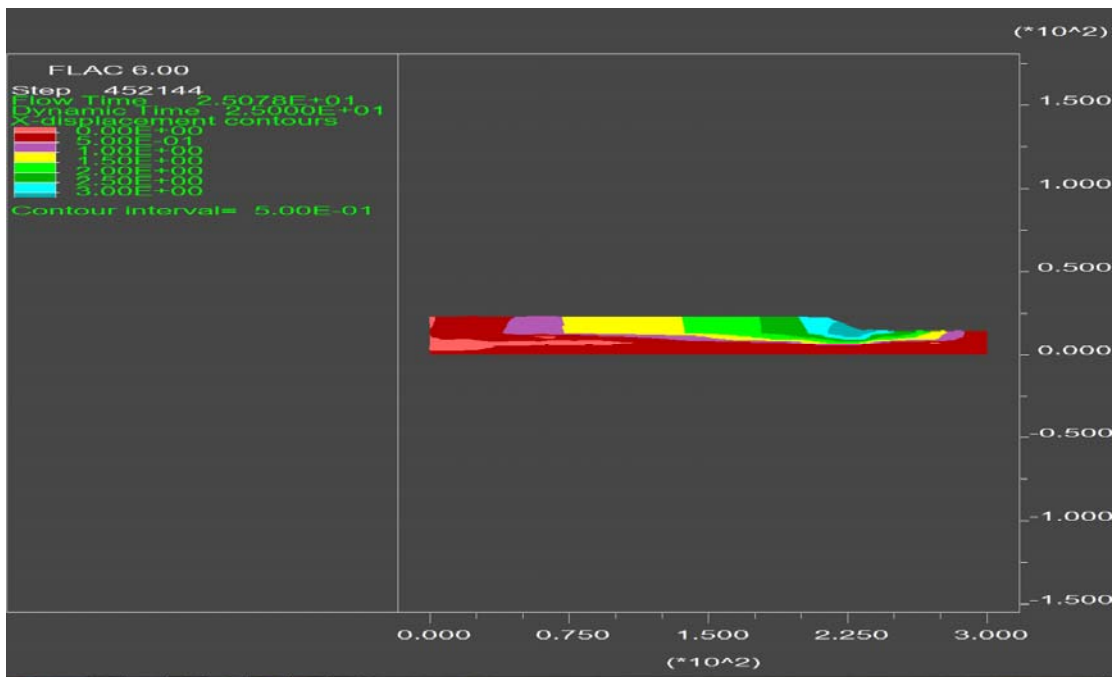
**Figure 6B-40. Contours of calculated lateral displacement (9 m embankment height, 8 meter liquefiable sand layer, corrected $(N_1)_{60}$ blowcount of 8, ground motion = 94 Northridge Sylmar - Conv Sta 052 Scale 1.0x).**
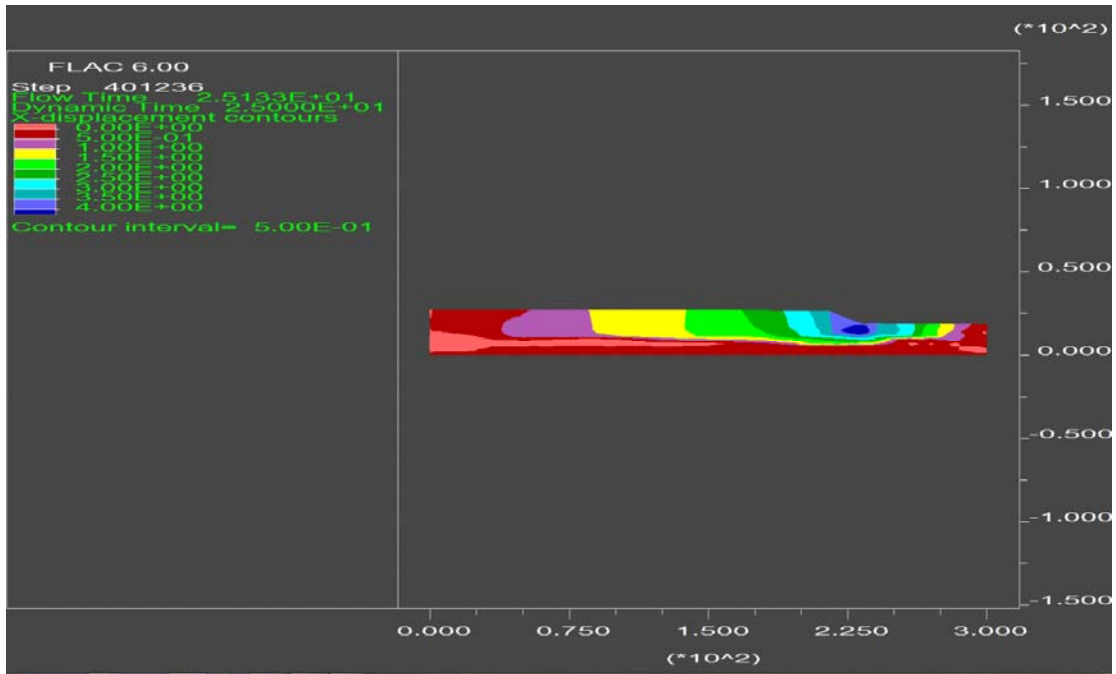


**Figure 6B-41. Contours of calculated lateral displacement (9 m embankment height, 12 meter liquefiable sand layer, corrected $(N_1)_{60}$ blowcount of 8, ground motion = 94 Northridge Sylmar - Conv Sta 052 Scale 1.0x).**

**Figure 6B-42. Contours of calculated lateral displacement (12 m embankment height, 3 meter liquefiable sand layer, corrected $(N_1)_{60}$ blowcount of 8, ground motion = 94 Northridge Sylmar - Conv Sta 052 Scale 1.0x).**
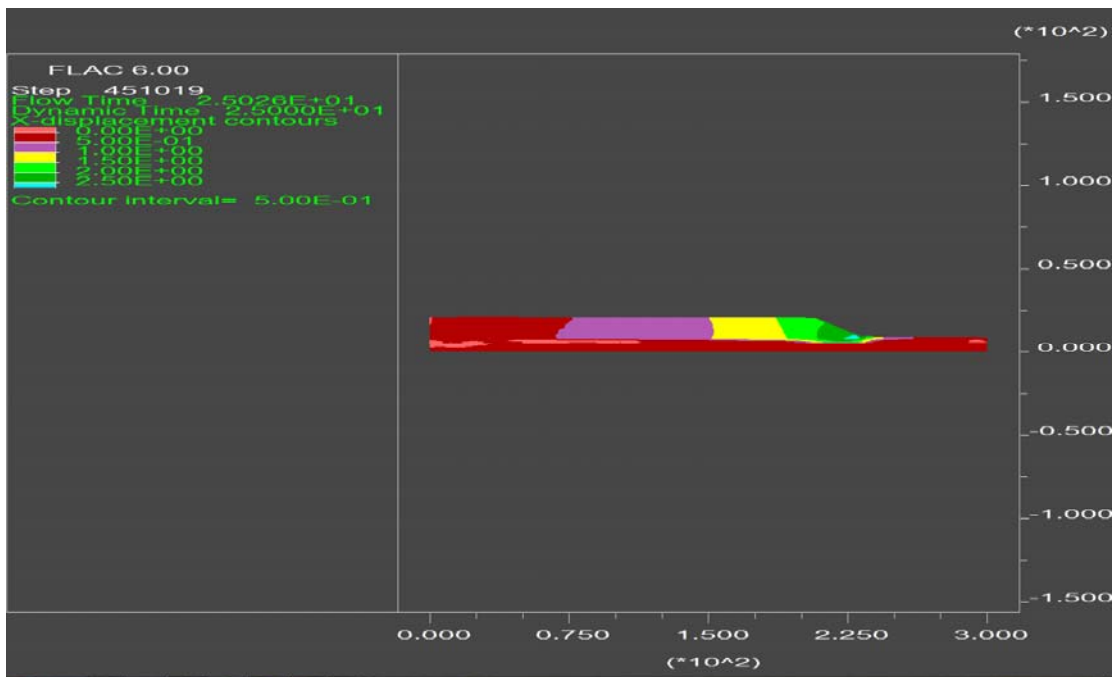


**Figure 6B-43. Contours of calculated lateral displacement (12 m embankment height, 8 meter liquefiable sand layer, corrected $(N_1)_{60}$ blowcount of 8, ground motion = 94 Northridge Sylmar - Conv Sta 052 Scale 1.0x).**

6B-22

**Figure 6B-44.** Contours of calculated lateral displacement (12 m embankment height, 12 meter liquefiable sand layer, corrected $(N_1)_{60}$ blowcount of 8, ground motion = 94 Northridge Sylmar - Conv Sta 052 Scale 1.0x).
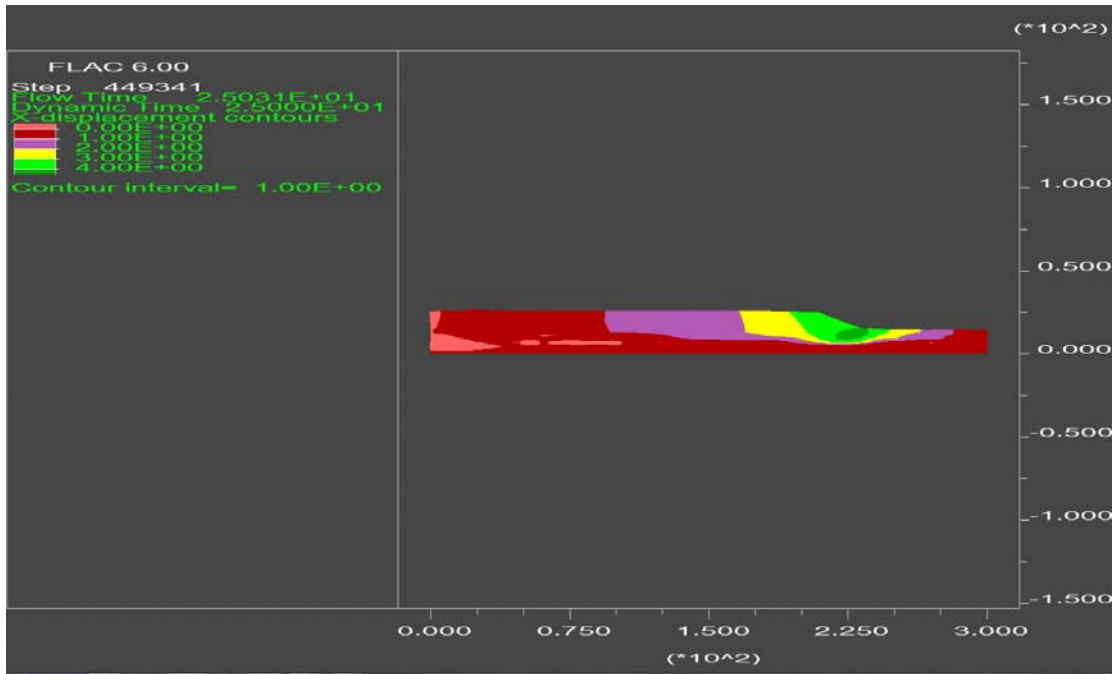


**Figure 6B-45.** Contours of calculated lateral displacement (6 m embankment height, 3 meter liquefiable sand layer, corrected $(N_1)_{60}$ blowcount of 15, ground motion = 94 Northridge Sylmar - Conv Sta 052 Scale 1.0x).
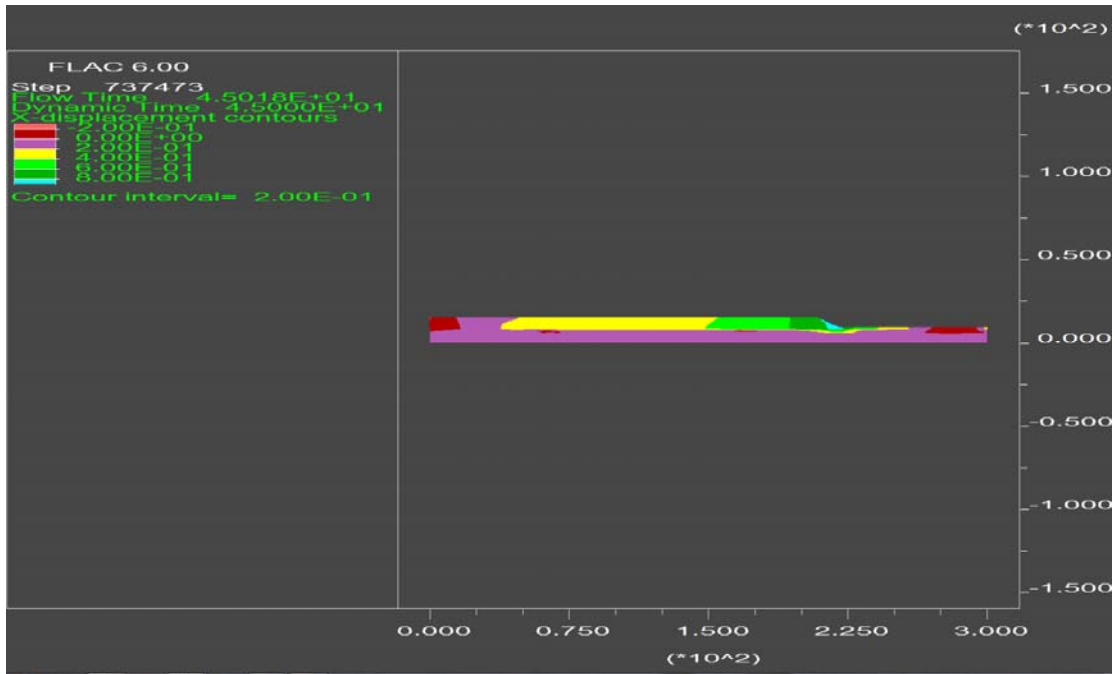
**Figure 6B-46. Contours of calculated lateral displacement (6 m embankment height, 8 meter liquefiable sand layer, corrected $(N_1)_{60}$ blowcount of 15, ground motion = 94 Northridge Sylmar - Conv Sta 052 Scale 1.0x).**
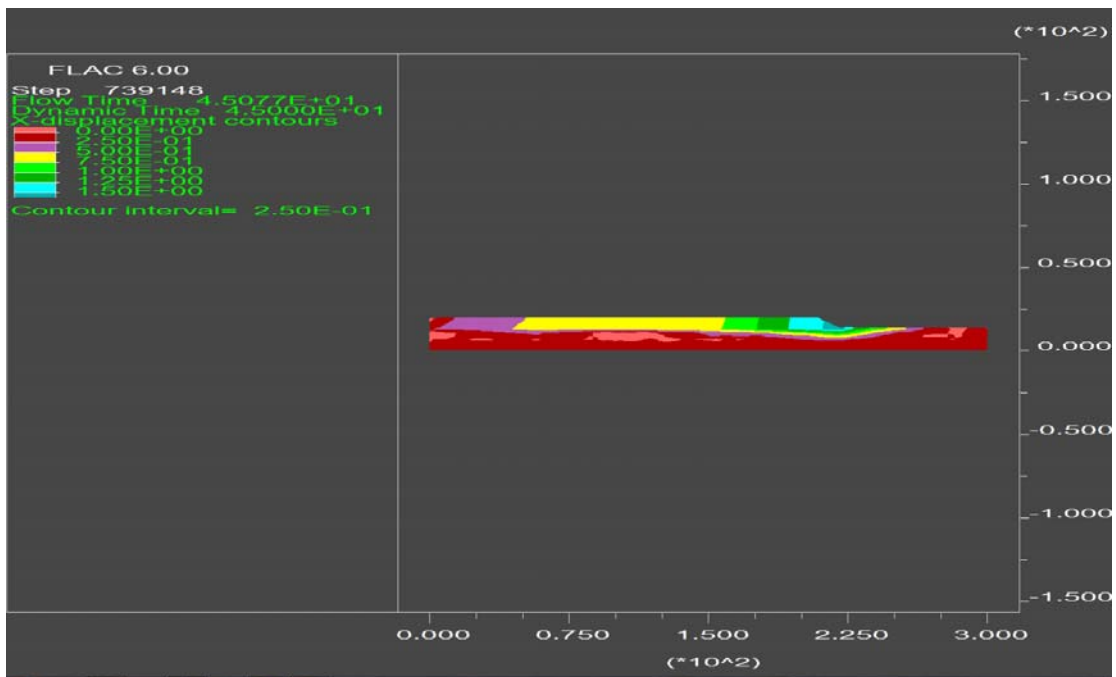


**Figure 6B-47. Contours of calculated lateral displacement (6 m embankment height, 12 meter liquefiable sand layer, corrected $(N_1)_{60}$ blowcount of 15, ground motion = 94 Northridge Sylmar - Conv Sta 052 Scale 1.0x).**
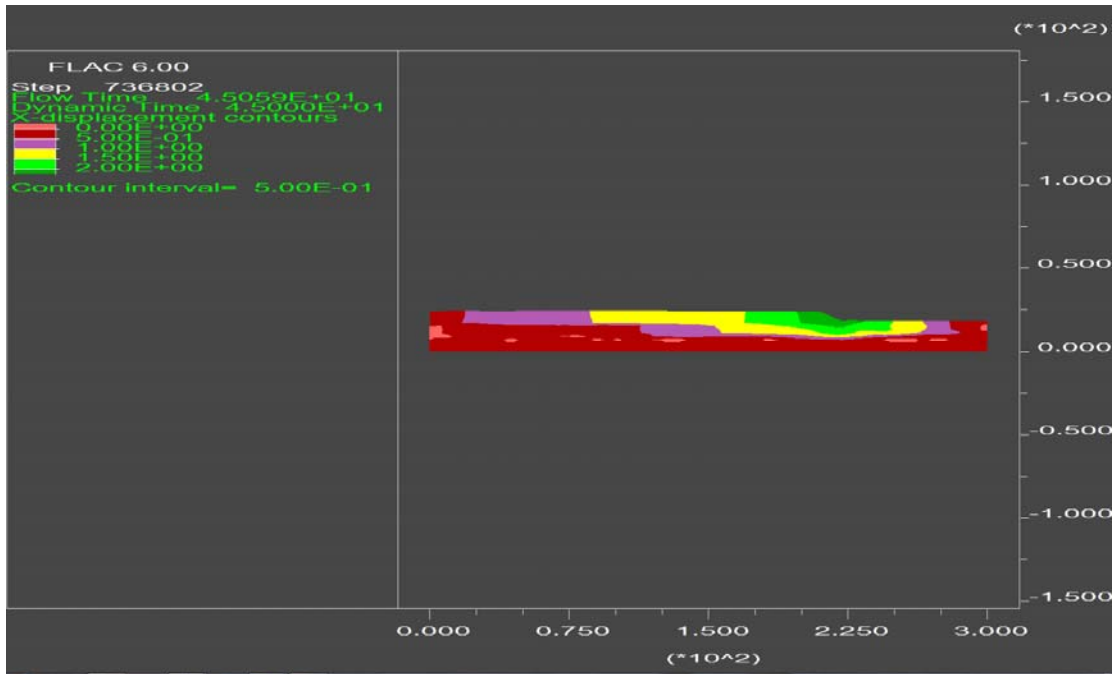
6B-24

**Figure 6B-48. Contours of calculated lateral displacement (9 m embankment height, 3 meter liquefiable sand layer, corrected $(N_1)_{60}$ blowcount of 15, ground motion = 94 Northridge Sylmar - Conv Sta 052 Scale 1.0x).**



**Figure 6B-49. Contours of calculated lateral displacement (9 m embankment height, 8 meter liquefiable sand layer, corrected $(N_1)_{60}$ blowcount of 15, ground motion = 94 Northridge Sylmar - Conv Sta 052 Scale 1.0x).**
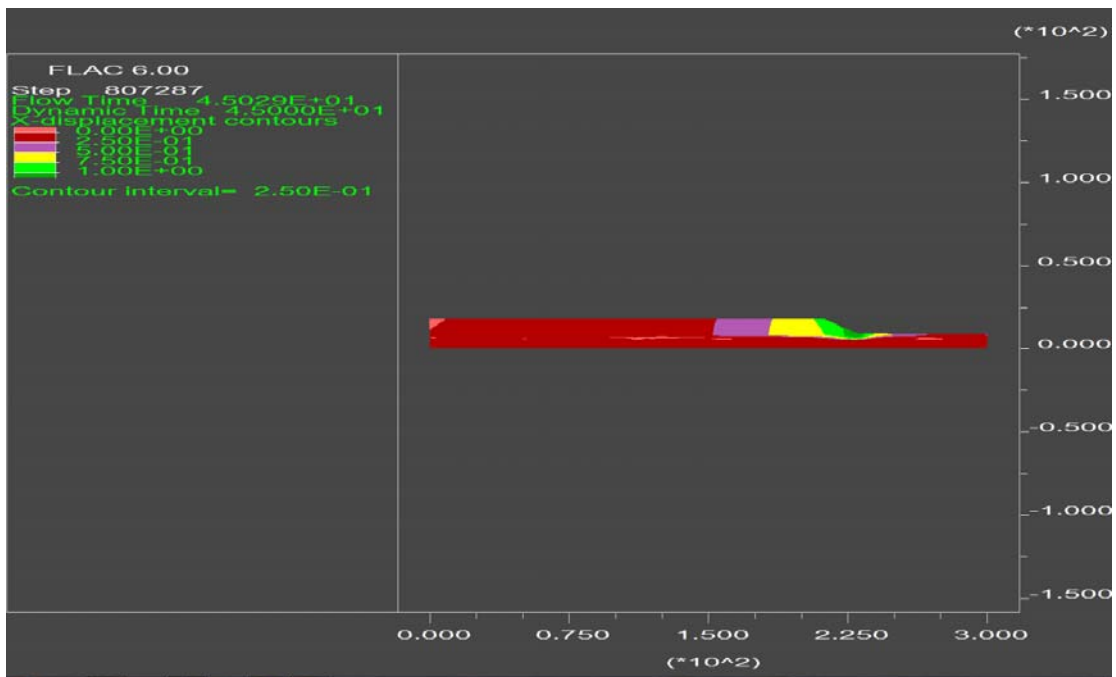
**Figure 6B-50. Contours of calculated lateral displacement (9 m embankment height, 12 meter liquefiable sand layer, corrected $(N_1)_{60}$ blowcount of 15, ground motion = 94 Northridge Sylmar - Conv Sta 052 Scale 1.0x).**



**Figure 6B-51. Contours of calculated lateral displacement (12 m embankment height, 3 meter liquefiable sand layer, corrected $(N_1)_{60}$ blowcount of 15, ground motion = 94 Northridge Sylmar - Conv Sta 052 Scale 1.0x).**

**Figure 6B-52. Contours of calculated lateral displacement (12 m embankment height, 8 meter liquefiable sand layer, corrected $(N_1)_{60}$ blowcount of 15, ground motion = 94 Northridge Sylmar - Conv Sta 052 Scale 1.0x).**

**Figure 6B-53. Contours of calculated lateral displacement (6 m embankment height, 3 meter liquefiable sand layer, corrected $(N_1)_{60}$ blowcount of 15, ground motion = 92 Landers Joshua Tree 090 Scale 1.0x).**
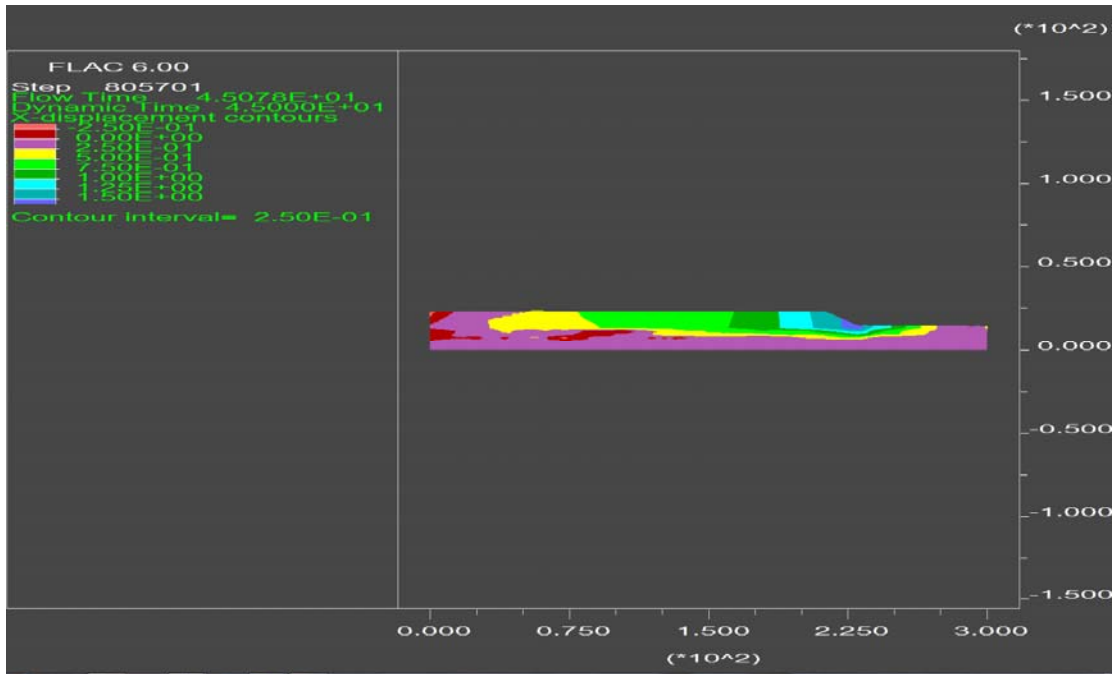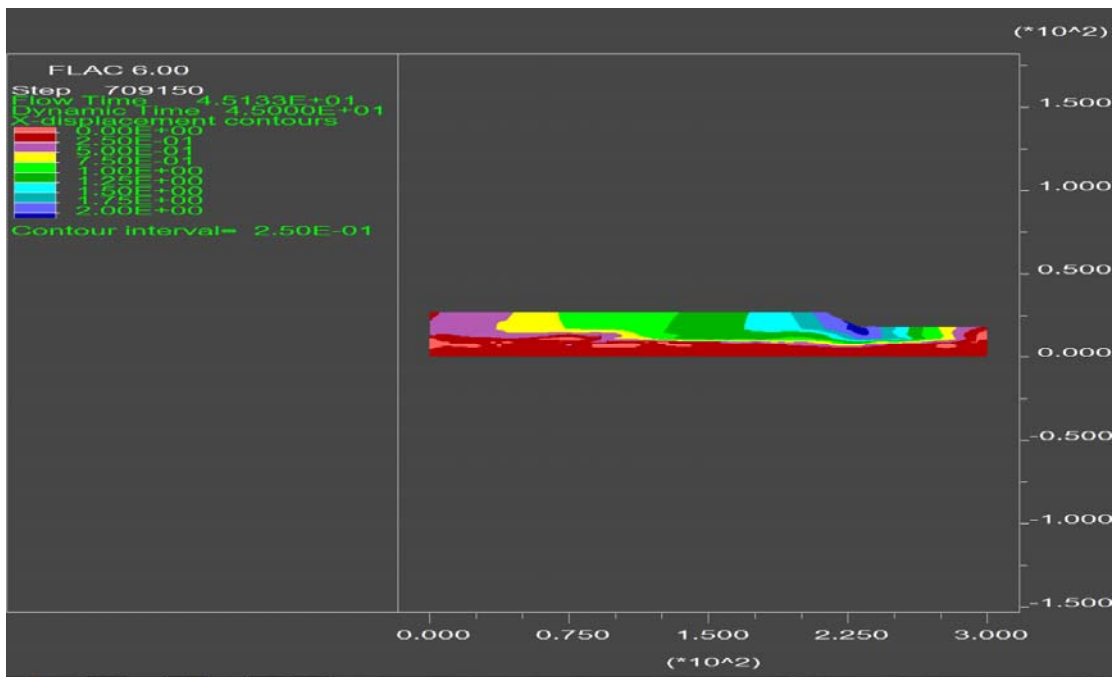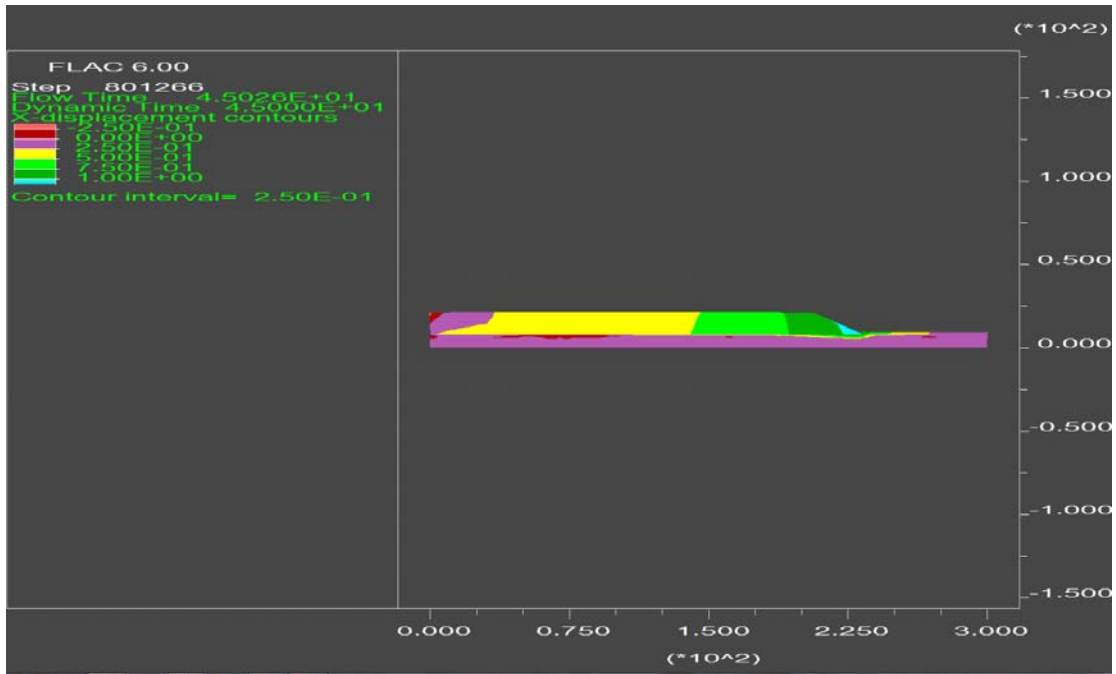


**Figure 6B-54. Contours of calculated lateral displacement (6 m embankment height, 8 meter liquefiable sand layer, corrected $(N_1)_{60}$ blowcount of 15, ground motion = 92 Landers Joshua Tree 090 Scale 1.0x).**

**Figure 6B-.55. Contours of calculated lateral displacement (6 m embankment height, 12 meter liquefiable sand layer, corrected $(N_1)_{60}$ blowcount of 15, ground motion = 92 Landers Joshua Tree 090 Scale 1.0x).**
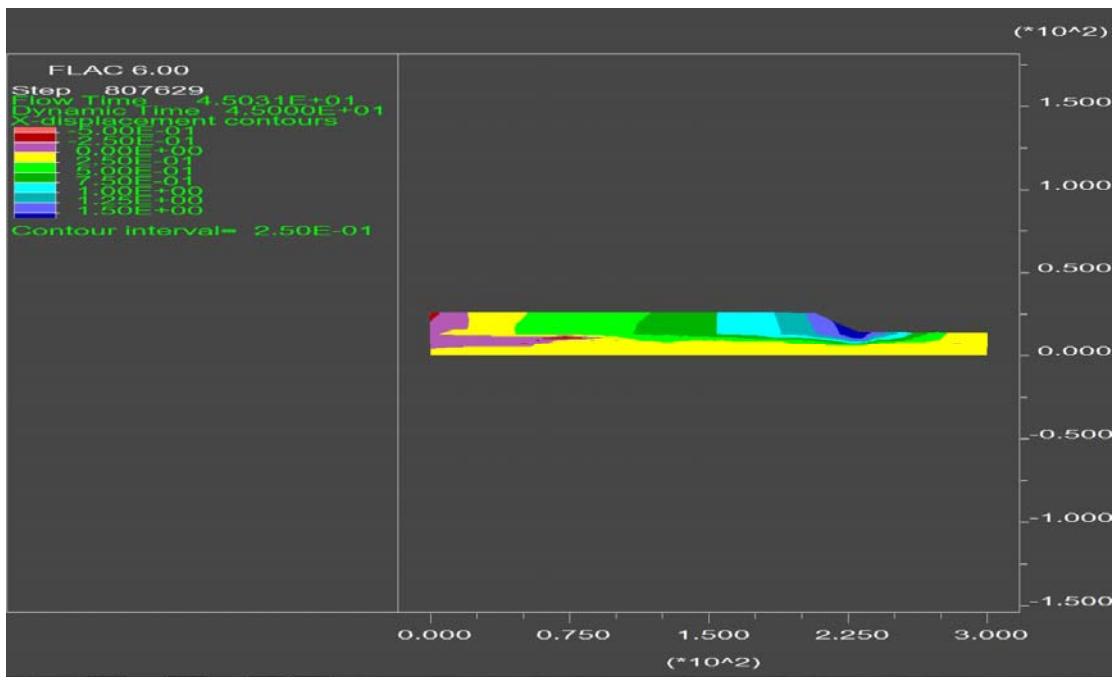


**Figure 6B-56. Contours of calculated lateral displacement (9 m embankment height, 3 meter liquefiable sand layer, corrected $(N_1)_{60}$ blowcount of 15, ground motion = 92 Landers Joshua Tree 090 Scale 1.0x).**
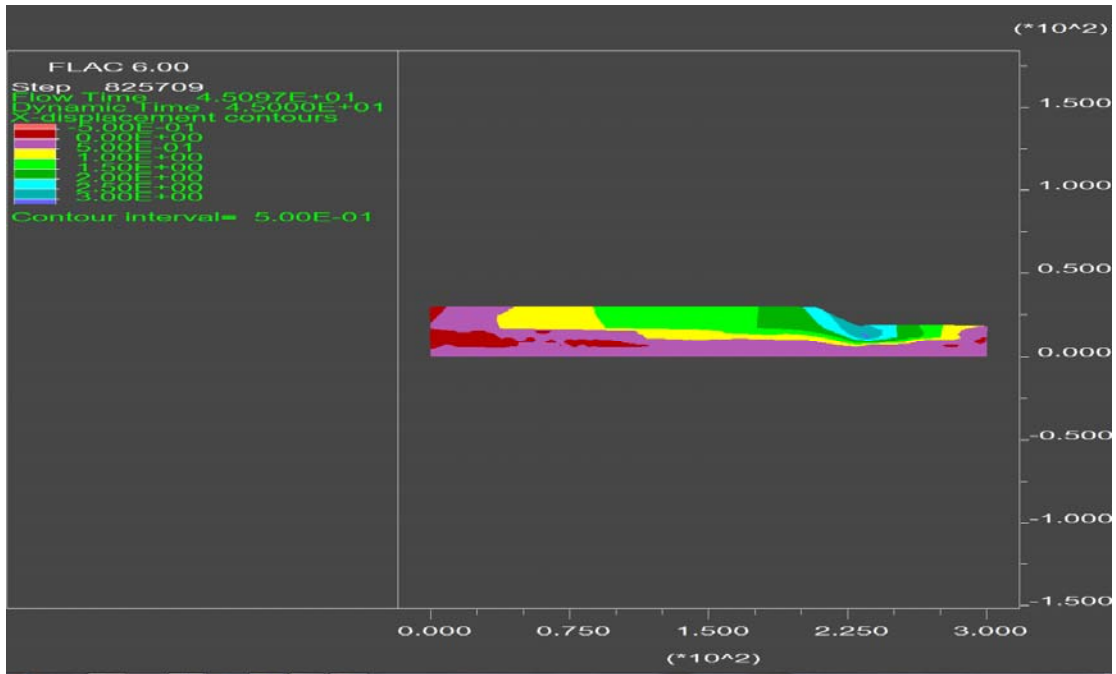
**Figure 6B-57. Contours of calculated lateral displacement (9 m embankment height, 8 meter liquefiable sand layer, corrected (N$_1$)$_{60}$ blowcount of 15, ground motion = 92 Landers Joshua Tree 090 Scale 1.0x).**



**Figure 6B-58. Contours of calculated lateral displacement (9 m embankment height, 12 meter liquefiable sand layer, corrected (N$_1$)$_{60}$ blowcount of 15, ground motion = 92 Landers Joshua Tree 090 Scale 1.0x).**
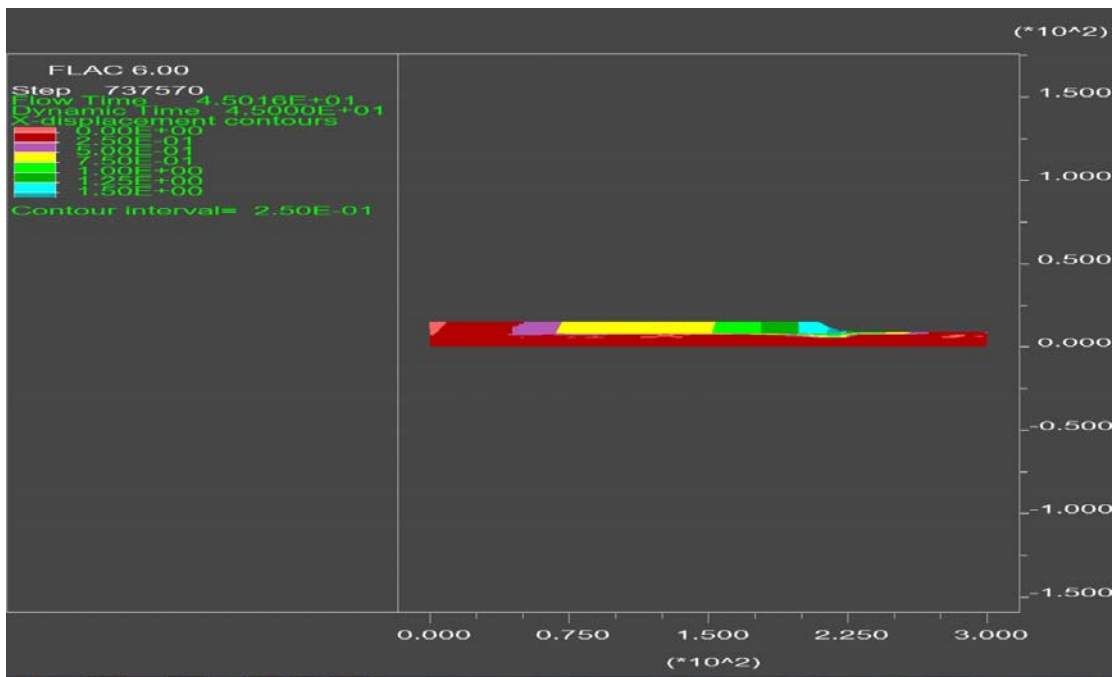
**Figure 6B-59. Contours of calculated lateral displacement (12 m embankment height, 3 meter liquefiable sand layer, corrected $(N_1)_{60}$ blowcount of 15, ground motion = 92 Landers Joshua Tree 090 Scale 1.0x).**
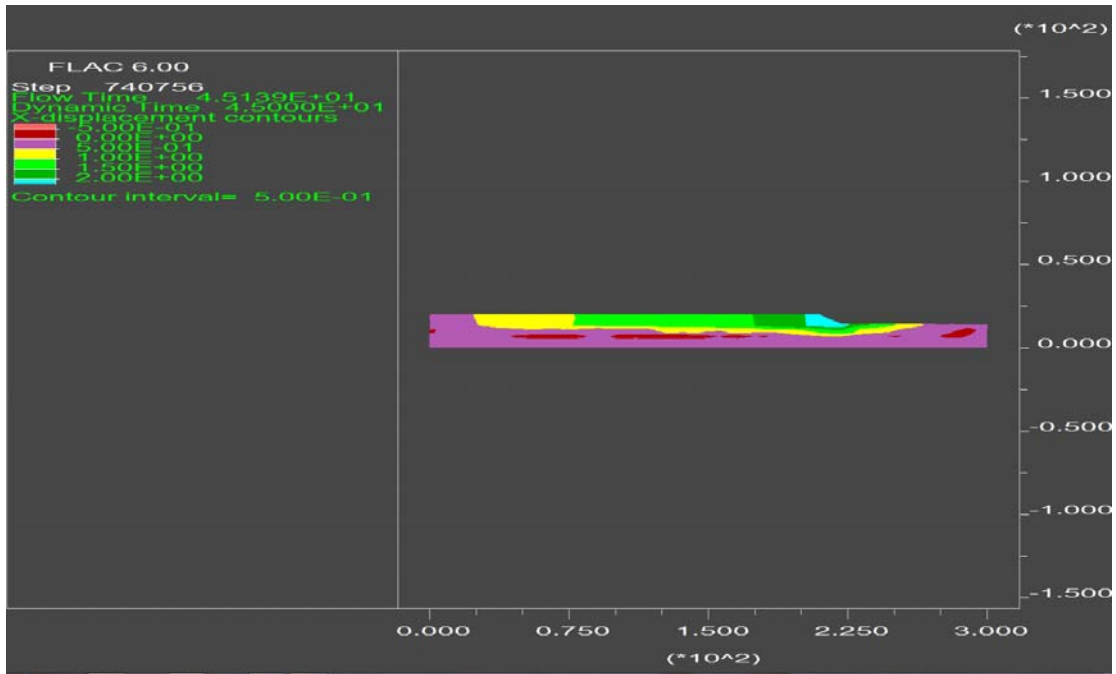


**Figure 6B-60. Contours of calculated lateral displacement (12 m embankment height, 8 meter liquefiable sand layer, corrected $(N_1)_{60}$ blowcount of 15, ground motion = 92 Landers Joshua Tree 090 Scale 1.0x).**
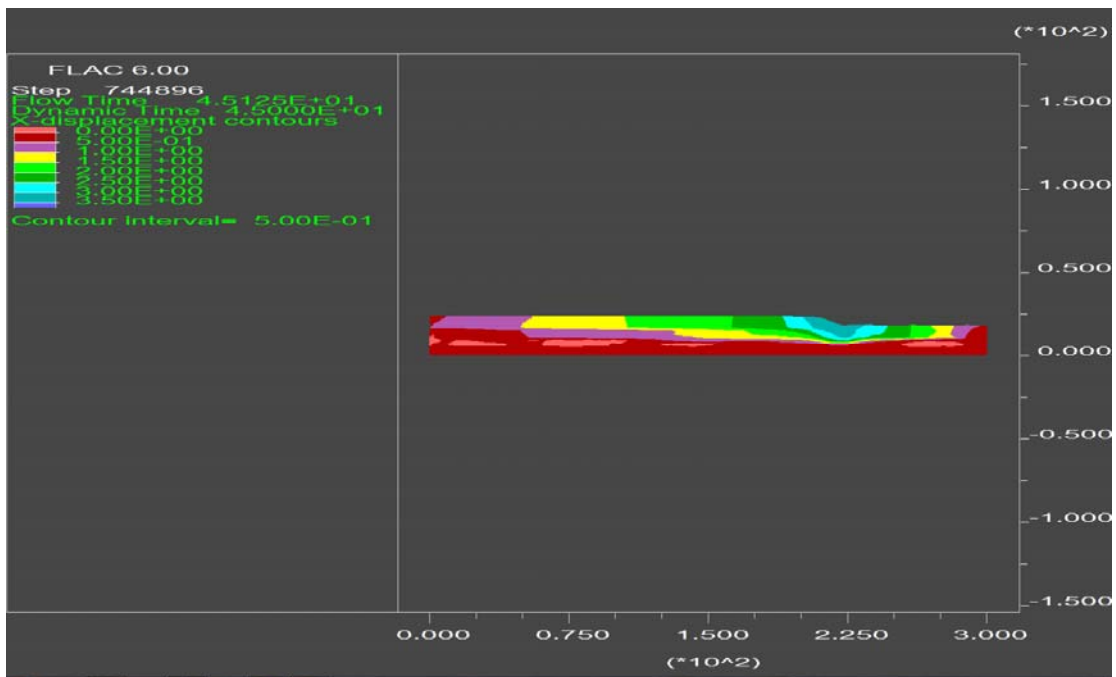
**Figure 6B-61. Contours of calculated lateral displacement (12 m embankment height, 12 meter liquefiable sand layer, corrected $(N_1)_{60}$ blowcount of 15, ground motion = 92 Landers Joshua Tree 090 Scale 1.0x).**



**Figure 6B-62. Contours of calculated lateral displacement (6 m embankment height, 3 meter liquefiable sand layer, corrected $(N_1)_{60}$ blowcount of 8, ground motion = 92 Landers Joshua Tree 090 Scale 1.0x).**
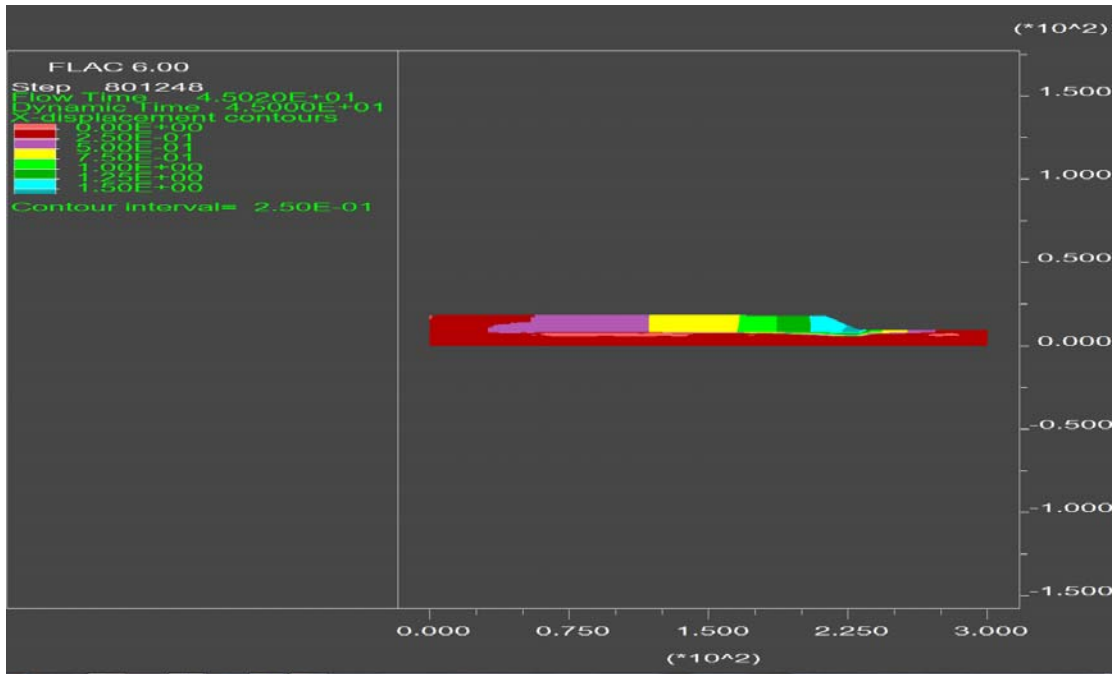
**Figure 6B-63. Contours of calculated lateral displacement (6 m embankment height, 8 meter liquefiable sand layer, corrected $(N_1)_{60}$ blowcount of 8, ground motion = 92 Landers Joshua Tree 090 Scale 1.0x).**
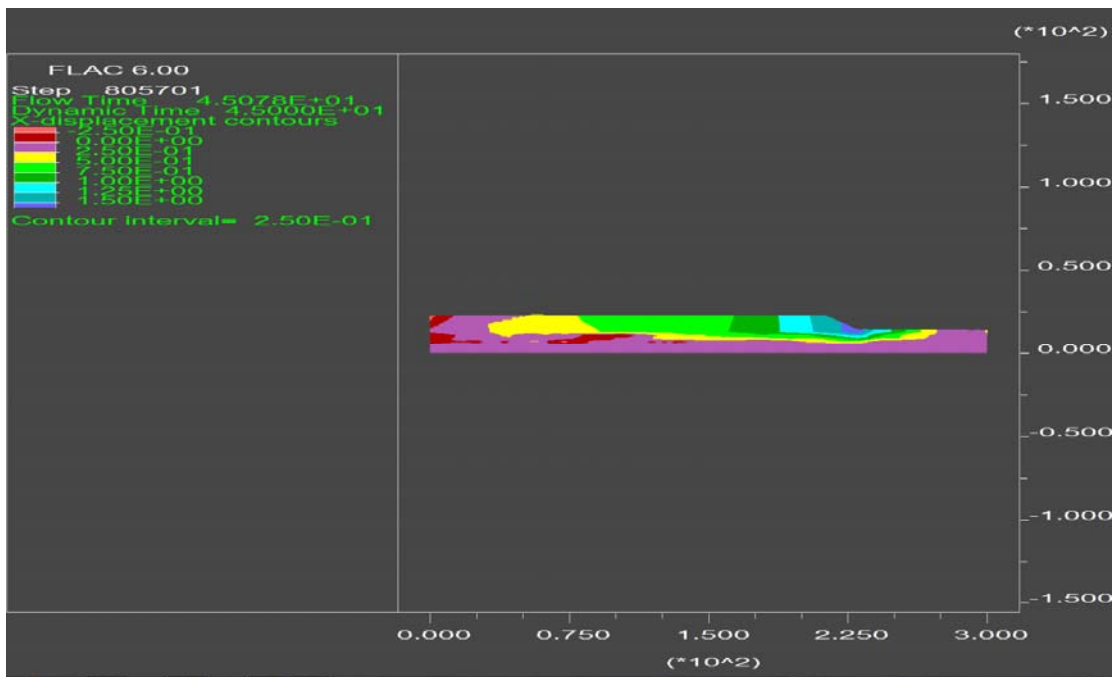


**Figure 6B-64. Contours of calculated lateral displacement (6 m embankment height, 12 meter liquefiable sand layer, corrected $(N_1)_{60}$ blowcount of 8, ground motion = 92 Landers Joshua Tree 090 Scale 1.0x).**

**Figure 6B-65. Contours of calculated lateral displacement (9 m embankment height, 3 meter liquefiable sand layer, corrected $(N_1)_{60}$ blowcount of 8, ground motion = 92 Landers Joshua Tree 090 Scale 1.0x).**
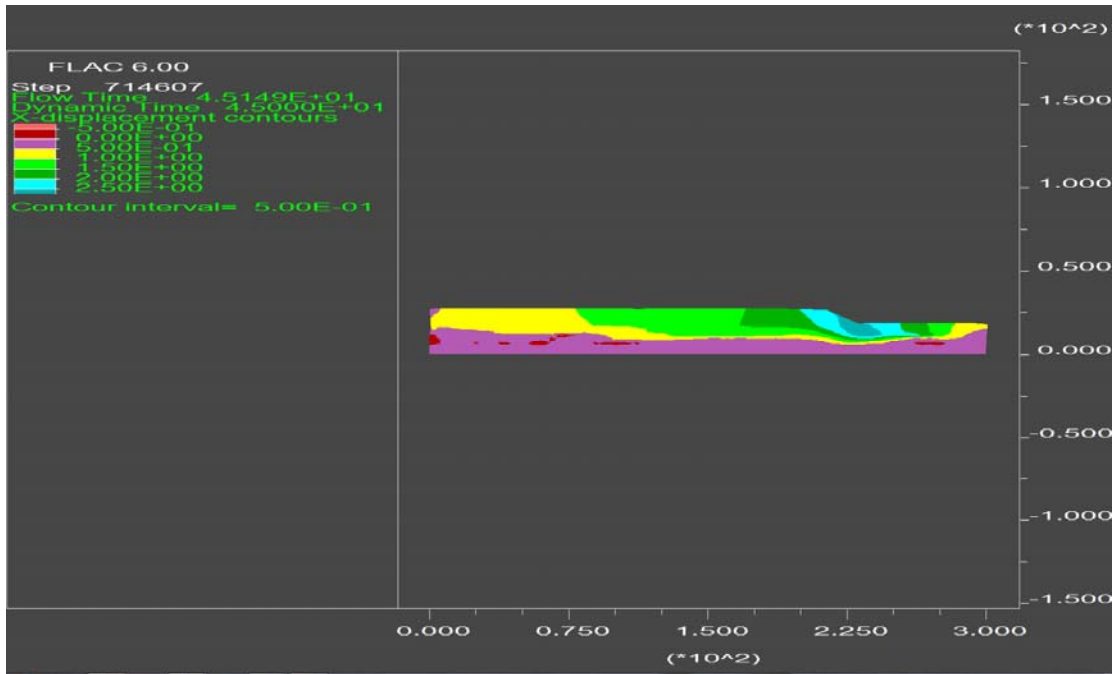


**Figure 6B-66. Contours of calculated lateral displacement (9 m embankment height, 8 meter liquefiable sand layer, corrected $(N_1)_{60}$ blowcount of 8, ground motion = 92 Landers Joshua Tree 090 Scale 1.0x).**
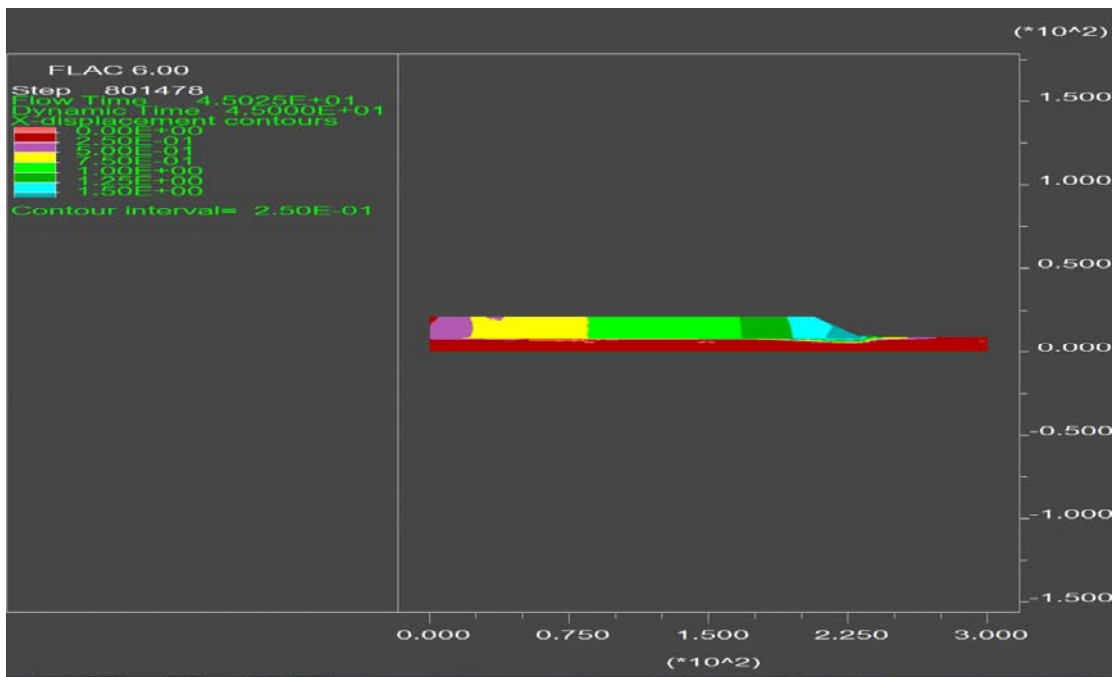
**Figure 6B-67. Contours of calculated lateral displacement (9 m embankment height, 12 meter liquefiable sand layer, corrected $(N_1)_{60}$ blowcount of 8, ground motion = 92 Landers Joshua Tree 090 Scale 1.0x).**



**Figure 6B-68. Contours of calculated lateral displacement (12 m embankment height, 3 meter liquefiable sand layer, corrected $(N_1)_{60}$ blowcount of 8, ground motion = 92 Landers Joshua Tree 090 Scale 1.0x).**
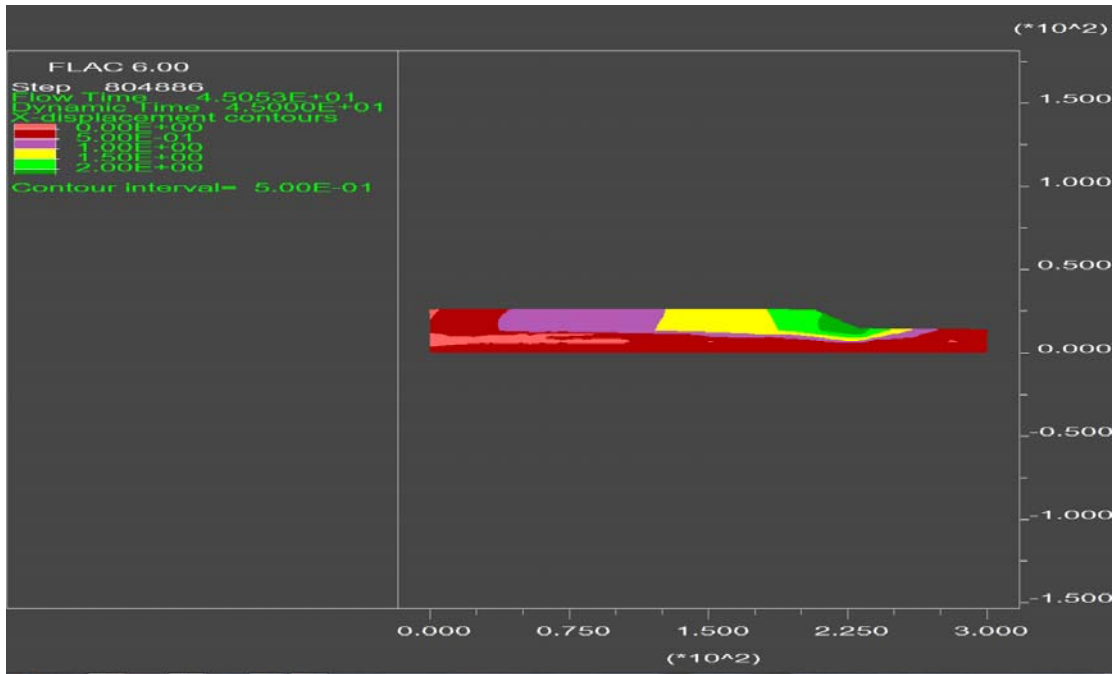
6B-35

**Figure 6B-69. Contours of calculated lateral displacement (12 m embankment height, 8 meter liquefiable sand layer, corrected $(N_1)_{60}$ blowcount of 8, ground motion = 92 Landers Joshua Tree 090 Scale 1.0x).**
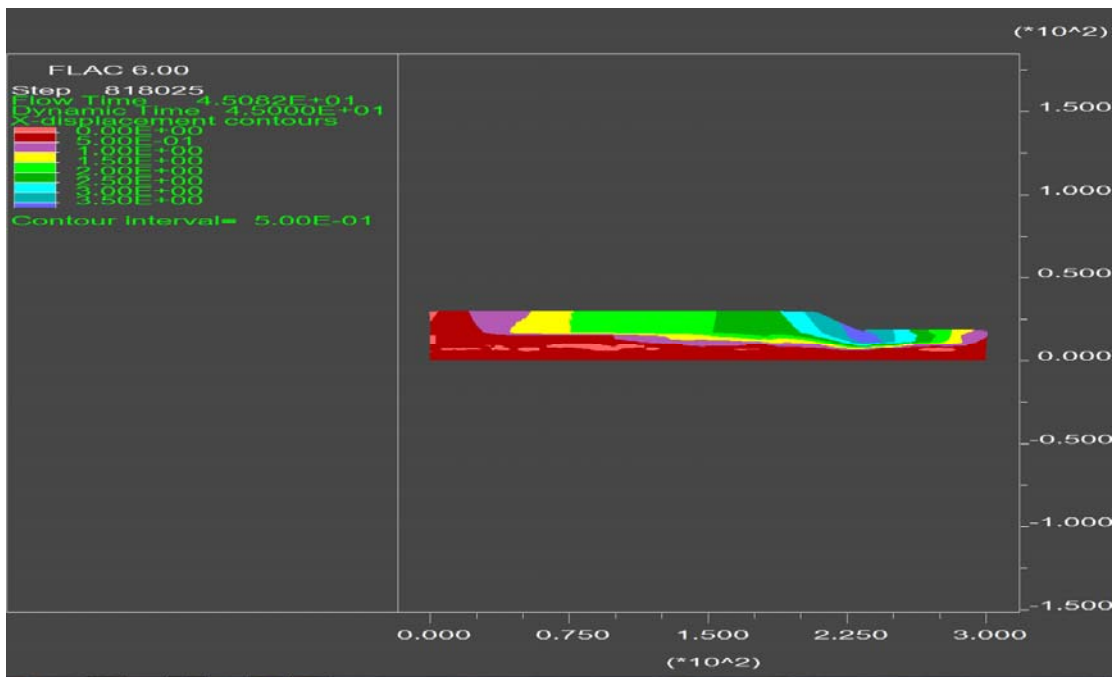


**Figure 6B-70. Contours of calculated lateral displacement (12 m embankment height, 12 meter liquefiable sand layer, corrected $(N_1)_{60}$ blowcount of 8, ground motion = 92 Landers Joshua Tree 090 Scale 1.0x).**
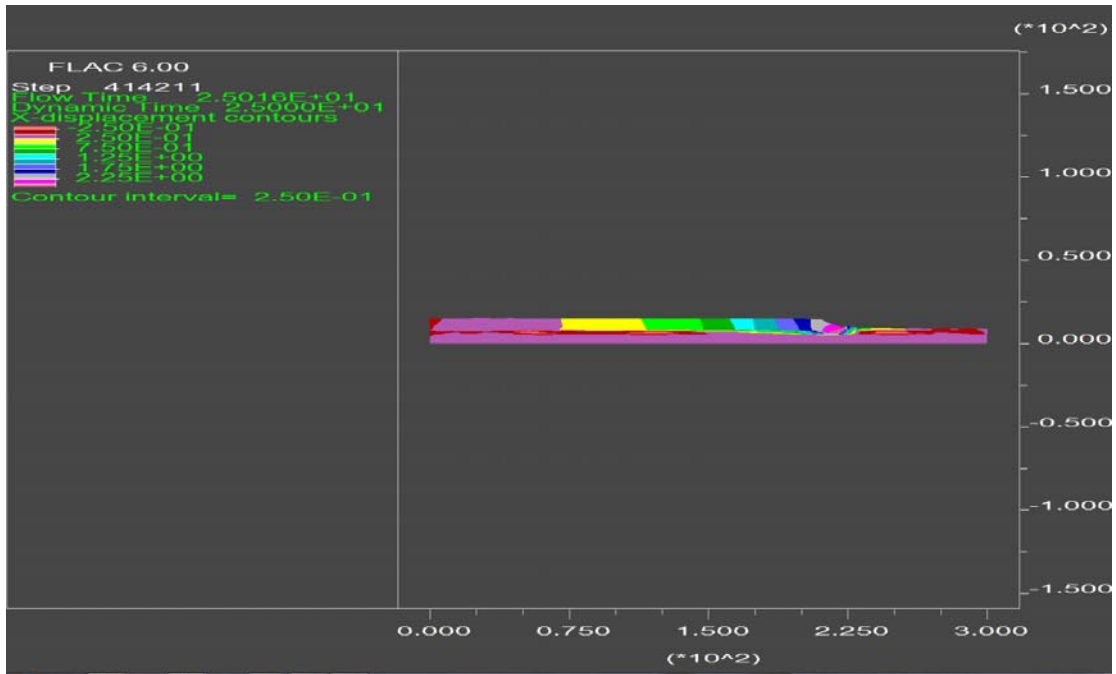
**Figure 6B-71. Contours of calculated lateral displacement (6 m embankment height, 3 meter liquefiable sand layer, corrected $(N_1)_{60}$ blowcount of 8, ground motion = 94 Northridge Sylmar - Conv Sta 052 Scale 1.0x).**